RIKEN Accelerator Progress Report 2014

vol. 48

国立研究開発法人理化学研究所　仁科加速器研究センター
RIKEN Nishina Center for Accelerator-Based Science

RIKEN Accelerator Progress Report 2014

vol. 48

国立研究開発法人理化学研究所　仁科加速器研究センター
RIKEN Nishina Center for Accelerator-Based Science
Wako, Saitama, 351-0198 JAPAN

RIKEN Accelerator Progress Report 2014 vol.48

This is an unabridged version of the 48th volume of RIKEN Accelerator Progress Report (hereinafter referred to as APR), the official annual report of the Nishina Center for Accelerator-Based Science.

A PDF version of APR can be downloaded from our website.
http://www.nishina.riken.jp/researcher/APR/index_e.html

Published by
RIKEN Nishina Center for Accelerator-Based Science
2-1 Hirosawa, Wako-shi, Saitama 351-0198 JAPAN

Director of RIKEN Nishina Center for Acclerator-Based Science
Hideto En'yo

Contact
Progress@ribf.riken.jp

RIKEN Nishina Center for Accelerator-Based Science, October 2015

PREFACE

The readers of RIKEN Accelerator Progress Report (APR) must have realized that we have stopped sending you a thick volume of papers. Instead, you now receive a compilation of the gravure and the highlights of the year with information of a web page where you can download a full set of the articles. While such change has been made to adapt to the changing times, it may make the readers of the older generation miss the good old times.

Nevertheless, when you pick up a thin booklet of the latest APR, please look into one of the highlights, "RI beam production at BigRIPS in 2014" written by N. Fukuda and his coauthors. From the impressive nuclear chart showing the history of RI beam production, you will learn that from March 2007 to December 2014, 140 new isotopes were discovered at BigRIPS, and that the production yields were measured for more than 1,000 isotopes. A total of 89 experiments have been performed so far. The Nishina Center is proud of these accomplishments and all the members who have contributed to this remarkable achievement must be applauded.

According to the BigRIPS compilation, the most popular primary beam is without a doubt uranium-238, and the close second is calcium-48. Containing 20 protons and 28 neutrons, calcium-48 is the so-called doubly magic nucleus. It is very neutron rich but its life time is 43 quintillion (10^{18}) years, much longer than the life of the universe (14 billion years). This is why there still exists natural calcium-48, but since its quantity totals only 0.18% of all the calcium, it is very expensive. Calcium-48 is our key tool to study the nuclear region called "island of inversion" and to find out where a neutron drip line for fluorine (F), neon (Ne), sodium (Na) *etc*. is. In 2014, our Ion Source Team succeeded in the calcium-48 ion production which is highly budget-friendly. As highlighted in this volume of APR as "Supply of 48Ca beam from 18-GHz ECRIS using the micro-oven" by K. Ozeki and his coauthors, the consumption of calcium-48 has been reduced by nearly a factor of 10 and the stability of the ion source has much improved. One should acknowledge that such behind the scene effort is essential for our beam performance.

Other important subject which became quite visible at the RIKEN RI Beam Factory in 2014 is nuclear chemistry. With the third event of element 113 observed in the summer of 2012, the search for 113th element was concluded which propelled us to take the next step forward, i.e. to begin search for element 119 and 120. With this shift, a long-waited research for nuclear chemistry of super-heavy elements came into full swing. There are two outstanding reports in this APR, "First chemical synthesis and investigation of $Sg(CO)_6$" by J. Even *et al.* and "Results of first online tests of small ion-surfing RF carpet gas cell at GARIS-II" by P. Schury *et al*.. The former determined that seaborgium belongs to the 6th family chemically, and the latter revealed the powerful potential of GARIS-II in its application to super heavy element chemistry when combined with the RF carpet technology developed to slow RIs down for high precision measurements. I believe super heavy chemistry has moved into an unexplored new stage of research.

The year 2014 was the landmark year for the Nishina Center in that it made a shift toward a new direction in response to the needs of today's society. We have started two governmental projects, ImPACT (Impulsing Paradigm Change through Disruptive Technologies) program titled "Reduction and Resource Recycle of High Level Radioactive Wastes with Nuclear Transmutation" and SIP (Strategic Innovation Promotion) program titled "Technology for creating next-generation forestry, agriculture and fisheries", both of which are based on our long time bottom-up efforts and activities. By initiating these governmental projects, we have declared to the society that we will give back to the community our research results.

In spite of such impressive progress made in the Nishina Center however, it was truly unfortunate that the entire JFY2014 had to be spent on complying with RIKEN's countermeasures against the STAP incident, a serious scientific misconduct that occurred at the RIKEN Center for Developmental Biology. I apologize for any inconveniences you have had to deal with. I must, however, repeat once again what I had wrote in the preface of APR2013. If any similar incident ever occurred at the Nishina Center, the Center would cease to exist. We thus declare that we will never let such an incident happen in our field.

Hideto En'yo

Director,
RIKEN Nishina Center for Accelerator-Based Science

EURICA!

~ Secrets Revealed via Decay Spectroscopy of Exotic Nuclei ~

EURICA: A state-of-the-art decay spectrometer

~ Exploring exotic nuclei with high-efficiency and high-resolution equipment ~

The RIBF in Japan, one of the world' s most powerful radioactive beam facilities, has been providing intense beams of exotic nuclei since 2007. Following the success of the first decay spectroscopy experiments in 2009, which focused on the study of neutron-rich nuclei with masses of around A = 100-117, a world-class decay project called EURICA (Euroball-RIKEN Cluster Array)† was launched owing to the efforts of 190 international collaborators. This state-of-the-art spectrometer, which consists of twelve Euroball HPGe cluster detectors (formerly GSI RISING) and the highly-segmented RIKEN β-ray detector WAS3ABi, markedly improves the performance of high-resolution decay spectroscopy of exotic nuclei with fast radioactive beams. EURICA has been in operation since 2012, and has harvested the decay properties of several hundred exotic nuclei. The lifetimes and level schemes of isotopes produced in BigRIPS can be deduced by measuring the times of flight, trajectories, and energies of the isotopes, and their subsequent β and γ rays emitted in the β-γ decay.

β-decay half-lives and nuclear astrophysics

~ How and where were the heavy elements produced in the universe? ~

The β-decay half-lives of isotopes with production rates as low as several events per day were measured using the EURICA spectrometer. In the fall of 2012, the half-lives of neutron-rich nuclei in the vicinity of ^{78}Ni (Z=28, N=50) were investigated using WAS3ABi, a device that consists of 8 layers of double-sided silicon-strip detectors (shown in the image on the right). The results are summarized in Figure 1. The systematics of the half-lives indicate a sudden decrease beyond N=50 (^{79,80}Ni) and below Z=28 (^{77}Co), thus providing robust evidence for a doubly magic ^{78}Ni.

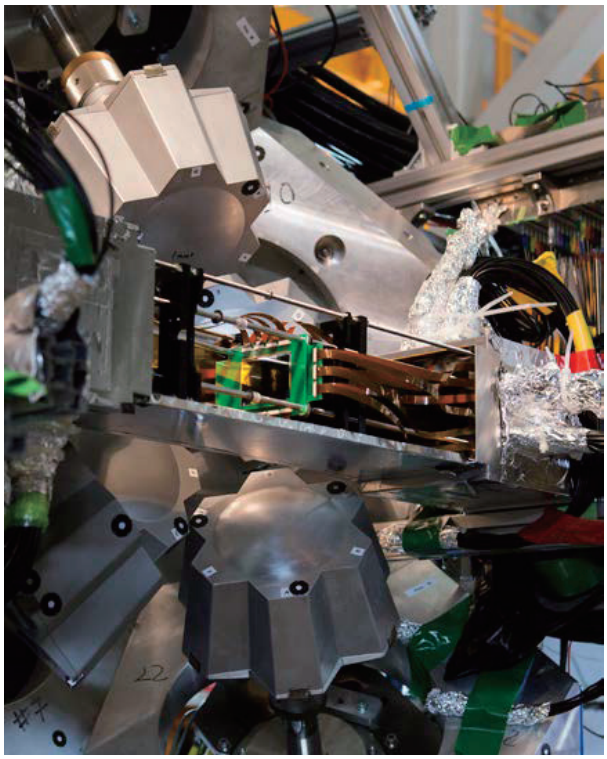

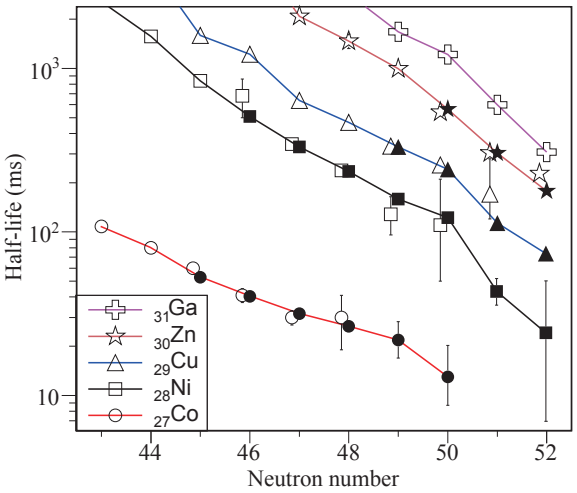

Figure 1: Experimental half-lives as a function of neutron number for the Z=27–31 isotopic chains. The filled and open symbols represent half-lives measured by EURICA and other experimental setups, respectively.

The decay properties of exotic nuclei are also key to uncovering some of the long-standing mysteries of the astrophysical rapid-neutron capture process (r-process), namely, the main astronomical site(s) and its mechanism. The r-process is a sequence of neutron-capture and β-decay processes that is known to be responsible for the synthesis of approximately half of the elements heavier than iron. Nuclear physics inputs, for example, nuclear masses (Q_β), neutron-capture rates, β-decay half-lives, and β-delayed neutron emission probabilities of very neutron-rich nuclei, are expected to play a significant role in the understanding of the mechanism and site(s) of the r-process. Figure 2 summarizes the nuclei surveyed with EURICA at the RIBF. A first attempt to study the universality of the astrophysical r-process was performed by measuring the β-decay half-lives of 110 neutron-rich nuclei around mass A=100-140, where 40 half-lives were measured for the first time. As shown in Figure 3, the reaction-network calculations of supernova nucleosynthesis with the new half-lives indicate that the (n,γ)↔(γ,n) equilibrium is still valid, and reproduces the universality of the elements with $Z > 56$.

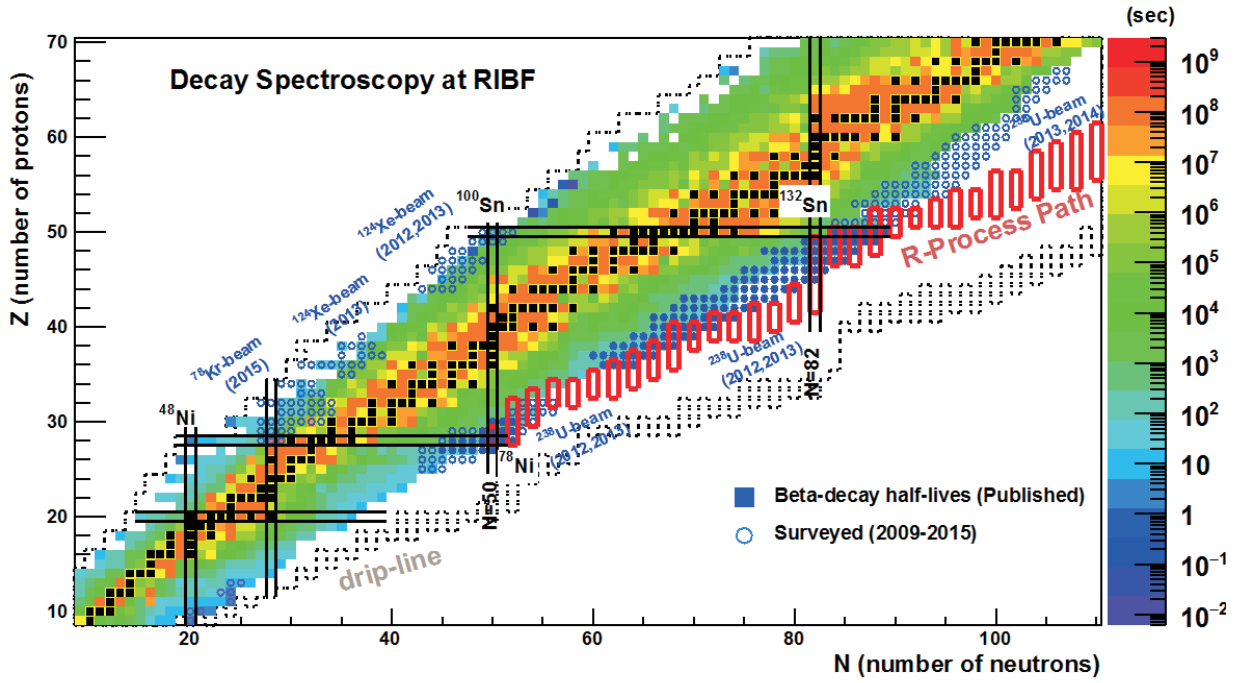

Figure 2: Summary of the nuclei surveyed with EURICA, where known half-lives are presented in color. The open circles indicate the data collected prior to the Kr beam campaign in 2015. The results are presented in S. Nishimura et al. PRL 106, 052502 (2011), Z.Y. Xu et al. PRL 113, 032505 (2014), and G. Lorusso et al. PRL 114, 192501 (2015).

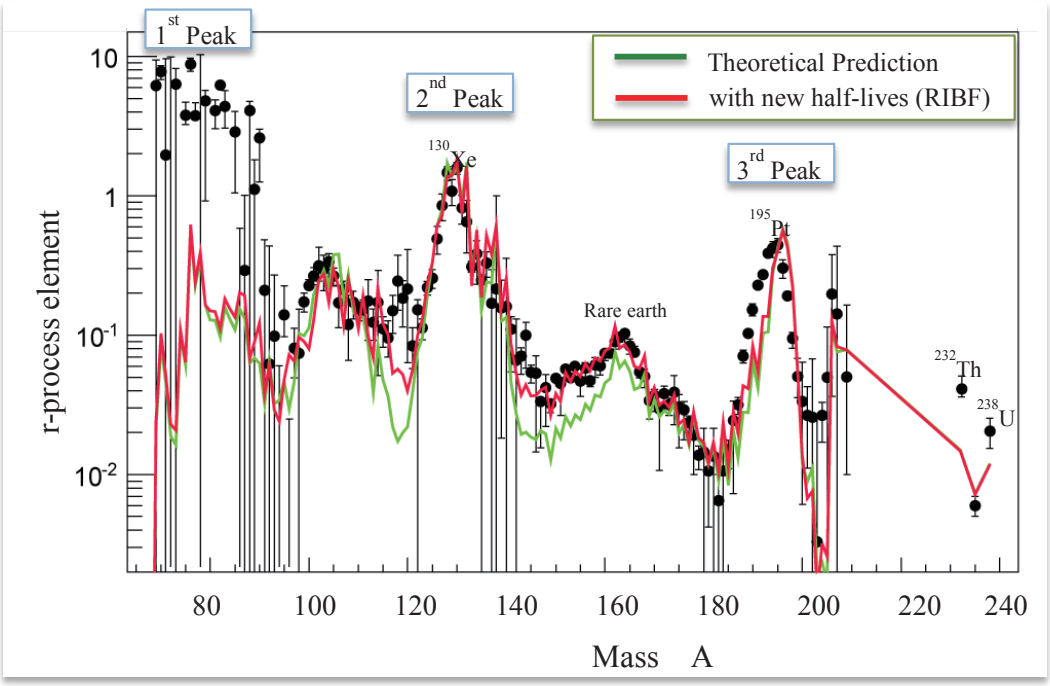

Figure 3: Abundances of r-process elements compared with estimations of reaction-network calculations of supernova nucleosynthesis.

Magicity and deformation

~ The magic numbers 28, 50, and 82, and regions far from the valley of stability ~

Understanding nuclear shell structure and its evolution toward the drip-lines is one of the major topics in nuclear structure research as well as nuclear astrophysics. One of the main goals of EURICA is to study the shell gaps around the doubly magic nuclei ^{78}Ni (Z=28, N=50), ^{132}Sn (Z=50, N=82), and ^{100}Sn (Z=50, N=50), where a possible weakening of the magicity and shell quenching effects have been discussed. Figure 4 provides a compilation of the energies of the first excited states in even-even nuclei obtained via γ rays from isomers and β-delayed γ rays from daughter nuclei. In addition, detailed level schemes were deduced for ^{116,118}Ru, ^{129}In, and ^{131}In via the β-delayed γ rays of ^{116,118}Tc, ^{129}Cd, and ^{131,132}Cd, respectively, and long-lived isomers in ^{126}Pd and ^{131}Cd were identified via internal conversion. Some of the EURICA results from 2012 are related to low-lying states in neutron-rich nuclei that contribute to the formation of the r-process peak around mass A~130. Further systematic studies on shell evolution of both neutron- and proton-rich nuclei have been conducted using β-γ spectroscopy with EURICA at the RIBF and will be reported in the future.

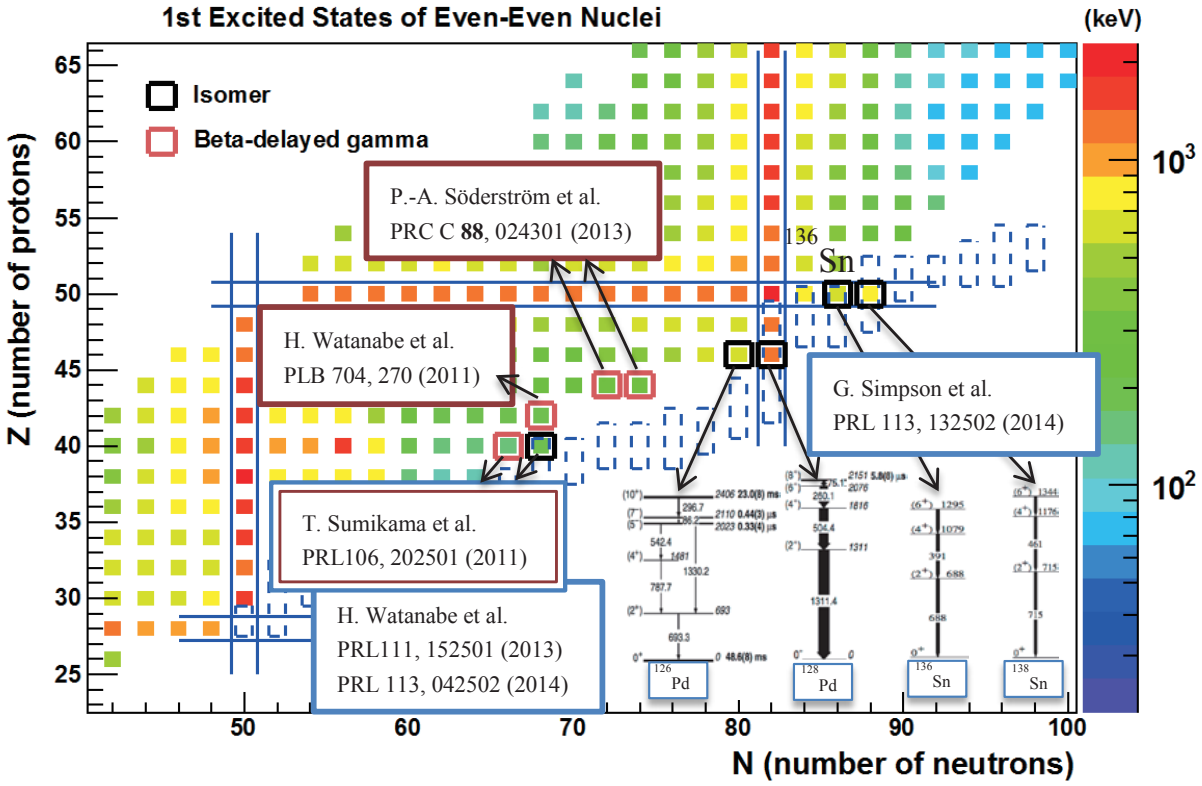

Figure 4: Overview of first excited state energies in even-even nuclei obtained via γ rays from isomers and β-delayed γ rays from daughter nuclei.

† EURICA was supported by the EUROBALL Owners Committee for the loan of the germanium detectors, and the PreSpec collaboration for the use of the readout electronics. WAS3ABi was partly funded by the Priority Centers Research Program in Korea (2009-0093817). Ten international Ph.D. students participating in the EURICA collaboration were supported by RIKEN IPA (International Program Associates).

C O N T E N T S

Ⅱ. RESEARCH ACTIVITIES I (Nuclear, Particle and Astro-Physics)

1. Nuclear Physics

2. Nuclear Physics (Theory)

3. Nuclear Data

4. Hadron Physics

5. Hadron Physics (Theory)

6. Particle Physics

7. Astrophysics and Astro-Glaciology

8. Accelerator

9. Instrumentation

3. Radiochemistry and Nuclear Chemistry

4. Radiation Chemistry and Biology

Ⅳ. OPERATION RECORDS

I. HIGHLIGHTS OF THE YEAR

<< Selection process of highlights >>

Highlights are selected by a two-step process. In the first step, a referee who reviews a manuscript decides whether she/he would recommend it as one of the highlights.
Members of the editorial board then make additional recommendations if they think an important contribution has not been recommended by the referee.

The second step involves the editor-in-chief proposing a list of highlights based on the recommendation given above to the editorial board. After discussing the scientific merits and uniqueness of the manuscripts from viewpoints of experts/non-experts, the editorial board makes the final decision.

$1p_{3/2}$ Proton-Hole State in ^{132}Sn and Shell Structure Along N=82†

J. Taprogge,[*1,*2,*3] A. Jungclaus,[*1] H. Grawe,[*4] S. Nishimura,[*2] P. Doornenbal,[*2] G. Lorusso,[*2] G.S. Simpson,[*5] P.-A. Söderström,[*2] T. Sumikama,[*6] Z.Y. Xu,[*7] H. Sakurai,[*2,*7] H.Watanabe,[*2] on behalf of the RIBF-85 and RIBF-60&62R1 collaborations

The nucleus ^{132}Sn is of particular interest for nuclear structure investigations since it is the only heavy neutron-rich doubly-magic nucleus far away from the valley of stability which is accessible for experimental studies. While ^{132}Sn as well as the neighboring Sn (Z=50) and Sb (Z=51) isotopes have been studied in detail in the past, the experimental information for nuclei in the region below ^{132}Sn is scarce. Important knowledge, e.g. with respect to the energies of the proton single-hole states in ^{132}Sn, is still missing.

In an experiment performed in December 2012 as part of the EURICA campaign at the Radioactive-Isotope Beam Factory (RIBF), the neutron-rich nuclei ^{131,132}Cd were produced by the in-flight fission of a ^{238}U beam and implanted into the active stopper WAS3ABi. The γ rays emitted following the β decay of ^{131}Cd and after β-delayed neutron emission of ^{132}Cd were detected with the EURICA array comprising 84 germanium crystals. A single γ ray with an energy of 988 keV was observed in the decays of both ^{131}Cd and ^{132}Cd. It was placed to populate the known $(1/2^-)$ β-decaying isomer in ^{131}In at an excitation energy of $E_x = 365(8)$ keV thus defining a second excited state at 1353 keV. This newly identified state is preliminary assigned to have spin and parity of $3/2^-$ and to correspond to the previously unknown $1p_{3/2}$ proton single-hole state with respect to the ^{132}Sn core. A full account of the arguments which lead to this assignment is presented in Ref. [2].

Using the newly established $1p_{3/2}$ proton single-hole energy, shell-model calculations have been performed to calculate the energies of the first excited 2^+ states and the proton gaps Δ_{2p} [defined here as $\Delta_{2p} = M(Z+2,N) + M(Z-2,N) - 2M(Z,N)$, with $M(Z,N)$ the mass of a nucleus with Z protons and N neutrons] for the N=82 isotones below ^{132}Sn as shown in Fig. 1. For comparison, Fig. 1 also shows the results of similar SM calculations performed for the N=50 isotones below ^{100}Sn, in that case in comparison with available experimental information. While for the N=50 isotonic chain typical signatures of sub-shell closures are observed at Z=38 and 40[3,4], they

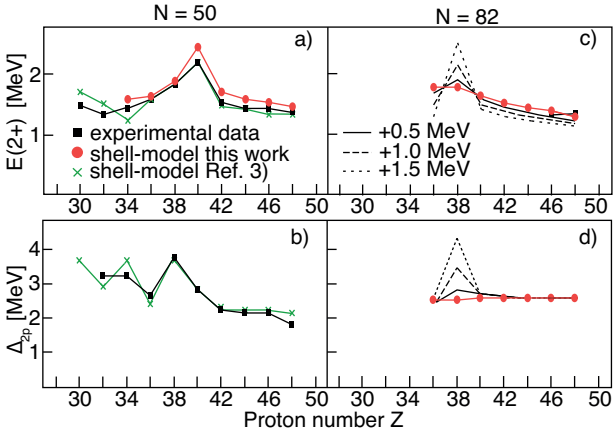

Fig. 1. a) and c): Energies of the first excited 2^+ states, E(2^+), and b) and d): proton gaps, Δ_{2p}, in the even N=50 and N=82 isotones, respectively. The black lines (solid, dashed, and dotted) in c) and d) show the results of SM calculations assuming an increase of the $1p$ splitting by 0.5, 1.0, and 1.5 MeV, respectively.

disappear for the N=82 isotones below ^{132}Sn. The disappearance of the proton sub-shell closures has its origin in the small energy gap between the $1p_{1/2}$ and the next single-particle orbital (SPO), independent of the character of the latter. Figs. 1 c) and d) show the reappearance of the sub-shell gap when increasing the energy separation between the $1p_{1/2}$ orbit and the next SPO.

Without the existence of pronounced proton sub-shell closures the N=82 isotones ^{120}Sr and ^{122}Zr should behave as mid-shell nuclei and consequently enhanced cross-shell excitations are expected to lead to a reduction of the N=82 shell gap in that region. Such a reduction would have a significant impact on r-process calculations and it is therefore concluded that preference should be given to mass models which indeed predict a reduction of the N=82 gap, such as the HFB24[5] approach.

† Condensed from the article in Phys. Rev. Lett., Vol. 112, 132501 (2014)
*1 Instituto de Estructura de la Materia, CSIC
*2 RIKEN Nishina Center
*3 Departamento de Física Teórica, Uni. Autónoma de Madrid
*4 GSI Helmholtzzentrum für Schwerionenforschung GmbH
*5 LPSC, UJF, CNRS, INPG, Grenoble
*6 Department of Physics, Tohoku University
*7 Department of Physics, University of Tokyo

References

1) J. Dobaczewski et. al., Phys. Rev. Lett. 72, 981 (1994).
2) J. Taprogge et. al., Phys. Rev. Lett. 112, 132501 (2014).
3) A. F. Lisetskiy et. al., Phys. Rev. C 70, 044314 (2004).
4) T. Fastermann et. al. Prog. Part. Nucl. Phys. 69, 85 (2013).
5) S. Goriely et. al., Phys. Rev. C 88, 024308 (2013).

Isomer decay spectroscopy of ^{164}Sm and ^{166}Gd: mid-shell collectivity around N=100†

Z. Patel,[*1,*2] P.-A. Söderström,[*1] Zs. Podolyák,[*2] P. H. Regan,[*2,*3] P. M. Walker[*2] H. Watanabe[*1,*4] E. Ideguchi[*5] G. S. Simpson[*6] H. L. Liu[*7] S. Nishimura,[*1] Q. Wu,[*8] F. R. Xu,[*8] H. Sakurai,[*1]
The RIBF-86 Collaboration and the EURICA Collaboration

The deformation of nuclei around $A = 160$ may influence the elemental abundances in the rare earth element peak. Macroscopic-microscopic calculations show a deformation maximum close to $N = 104$ and $Z = 66$ (^{170}Dy)[1]. However, these calculations seem to be contradicted by recent experimental data[2,3]. We utilise the existence of K isomers in this deformed region, to reveal the low-lying excited states in $A \approx 160$ nuclei that can provide insight into their deformation.

Neutron-rich $Z = 62, 64$ isotopes were produced by in-flight fission of a 345 A·MeV ^{238}U beam with an average beam intensity of 10 pnA incident on a ^{9}Be target at the RIBF. The secondary RI beam containing the nuclei of interest is passed through BigRIPS and the ZeroDegree spectrometers that separate and identify the beam species on an ion by ion basis, using TOF, Bρ and ΔE. The ions of interest were implanted in a stopper and the γ rays emitted following isomeric decay were detected using EURICA (Euroball-RIKEN Cluster Array): 84 HPGe crystals arranged in a 4π configuration around the stopper.

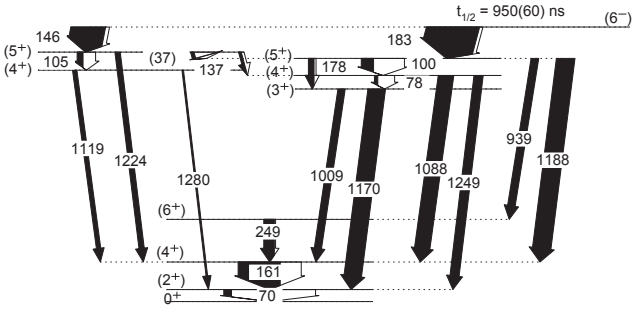

Fig. 1. Level scheme of ^{166}Gd obtained in this work.

The decay from isomeric states in ^{166}Gd and ^{164}Sm ($N = 102$) has been detected for the first time. The half-lives of the isomeric states have been measured to be 950(60) ns and 600(140) ns for ^{166}Gd and ^{164}Sm respectively. Their level schemes, seen in Figs. 1 and 2, were deduced from γ-γ coincidence analysis. Potential

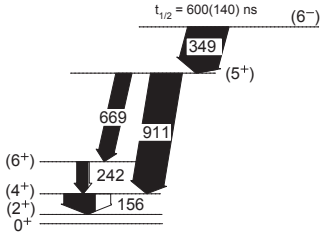

Fig. 2. Level scheme of ^{164}Sm obtained in this work.

energy surface calculations[4] with total energy minimised in $(\beta_2, \beta_4, \beta_6)$ deformation space and $\gamma = 0$ suggest a 6^- state with a 2-neutron $\nu\frac{5}{2}^-[512] \otimes \nu\frac{7}{2}^+[633]$ configuration is isomeric in both ^{166}Gd and ^{164}Sm.

A key feature of our results are the first 2^+ and 4^+ energies. The systematics of $E(2^+)$ and $E(4^+ \rightarrow 2^+)$ are shown in Fig. 3. The observed 2^+ and 4^+ energies of ^{166}Gd and ^{164}Sm are the lowest in their isotopic chains and of the $N = 102$ isotones, suggesting they are the most deformed $N = 102$ nuclei observed in this region to date. Our new points in the systematics also highlight the increase of $E(2^+)$ and $E(4^+ \rightarrow 2^+)$ at $N = 100$. This behaviour supports the appearance of a recently predicted deformed shell gap at $N = 100$[5] that will influence r-process abundance calculations.

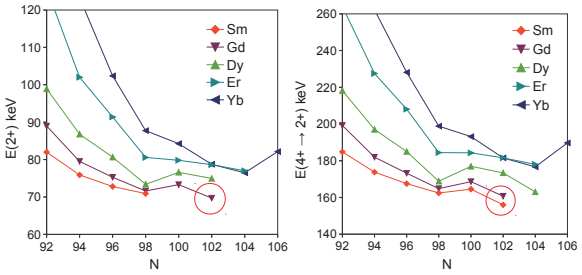

Fig. 3. Systematics of $E(2^+)$ and $E(4^+ \rightarrow 2^+)$ for Sm, Gd, Dy, Er and Yb isotopes. All data points from ENDSDF and this work.

† Condensed from the article in Phys. Rev. Lett. **113**, 262502 (2014)

*1 RIKEN Nishina Center
*2 Department of Physics, University of Surrey
*3 Radioactivity Group, National Physics Laboratory
*4 Department of Physics, Beihang University
*5 RCNP, Osaka University
*6 LPSC, UJF, CHRS, INPG, Grenoble
*7 Department of Applied Physics, Xi'an Jiaotong University
*8 School of Physics, Peking University

References

1) P. Moller *et al.*, Atomic and Nuclear Data Tables **59**, 185 (1995).
2) E. F. Jones *et al.*, Journal of Physics G **30**, L43 (2004).
3) P.-A. Söderström *et al.*, Phys. Rev. C **81**, 034310 (2010).
4) F. Xu, *et al.*, Phys. Lett. B **435**, 257 (1998).
5) S. K. Ghorui, *et al.*, Phys. Rev. C **85**, 064327 (2012).

β-Decay half-lives of ^{76,77}Co, ^{79,80}Ni and ^{81}Cu: experimental indication of doubly magic ^{78}Ni†

Z. Y. Xu,[*1,*2] S. Nishimura,[*2] G. Lorusso,[*2] F. Browne,[*3,*2] P. Doornenbal,[*2] G. Gey,[*4,*5,*2] H.-S. Jung,[*6] Z. Li,[*7] M. Niikura,[*1] P.-A. Söderström,[*2] T. Sumikama,[*8] J. Taprogge,[*9,*10,*2] Zs. Vajta,[*11,*2] H. Watanabe,[*12] J. Wu,[*7,*2] A. Yagi,[*13] K. Yoshinaga,[*14] H. Baba,[*2] S. Franchoo,[*15] T. Isobe,[*2] P. R. John,[*16] I. Kojouharov,[*17] S. Kubono,[*2] N. Kurz,[*17] I. Matea,[*15] K. Matsui,[*1] D. Mengoni,[*16] P. Morfouace,[*15] D. R. Napoli,[*18] F. Naqvi,[*19] H. Nishibata,[*13] A. Odahara,[*13] E. Şahin,[*20] H. Sakurai,[*1,*2] H. Schaffner,[*17] D. Sohler,[*11] I. G. Stefan,[*15] D. Suzuki,[*15] R. Taniuchi,[*1] and V. Werner[*19]

In order to study the nuclear shell evolution around ^{78}Ni, the β-decay half-lives of neutron-rich nuclei, i.e., ^{76,77}Co, ^{79,80}Ni and ^{81}Cu were measured for the first time. The experiment was performed as part of an EURICA campaign at the RIBF facility, RIKEN in 2012. A high-intensity ^{238}U beam was accelerated up to an energy of 345 A MeV by the RIKEN cyclotron accelerator complex before hitting a 3-mm-thick beryllium target to produce secondary beams via in-flight fission. The $^{238}U^{86+}$ beam was delivered at an average current of 5 pnA to the production target position. During the 13 days of the experiment, about 1.2×10^4 ^{78}Ni nuclei were identified and delivered to the experimental decay station at the end of the ZeroDegree spectrometer.

Figure 1 shows the experimental results (solid symbols) and the values in the literature (open symbols) as a function of the neutron number. Due to the fifth power relation between the half-life and its Q_β value, a linear relationship between $\log_{10} T_{1/2}$ and the neutron number of the parent nucleus is expected phenomenologically when Q_β evolves smoothly in an isotopic chain. In Fig. 1 this linearity is clearly visible below $N = 50$. Beyond that, a sudden reduction is seen in the $Z = 28$ isotopic chain due to the shorter half-lives of ^{79,80}Ni with reference to the systematics at $N \leq 50$. The fast β-decay processes in ^{79,80}Ni could be attributed to the neutrons outside the $N = 50$ shell, which result in higher Q_β values and β-decay rates of ^{79,80}Ni compared to that of ^{78}Ni.

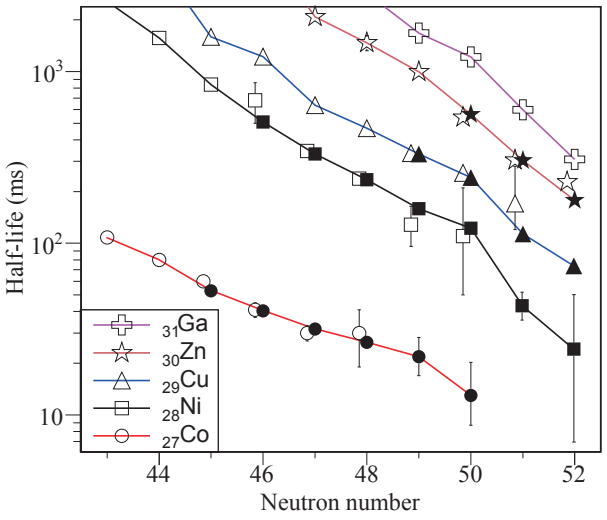

Fig. 1. Experimental half-lives as a function of neutron number for isotopes with $Z = 27 - 31$. All the solid symbols represent the half-lives determined in this work while the open symbols are the half-lives taken from the literature[1–4]. The systematic trends in the different isotopic chains are highlighted by lines connecting the data points with a smaller uncertainty.

In addition, a large gap can be noticed in Fig. 1 between the half-lives of the Co and Ni isotopes from $N = 44$ to $N = 50$. According to shell model calculations, this can be explained by the filled proton $f_{7/2}$ single particle orbit (SPO) in Ni isotopes. In this case, the proton produced in the β decay of Ni isotopes fills the $\pi f_{5/2}$ SPO above $\pi f_{7/2}$, leading to a reduction of the Q_β value and longer half-lives of Ni isotopes than those of Co isotopes. The newly measured half-lives of ^{76,77}Co follow the decreasing trend with considerable gaps relative to those of the corresponding Ni isotones, indicating an almost constant $Z = 28$ shell gap without significant quenching up to $N = 50$.

† Condensed from the article in Phys. Rev. Lett. **113**, 032505 (2014)

*1 Department of Physics, University of Tokyo
*2 RIKEN Nishina Center
*3 University of Brighton
*4 LPSC, Université Grenoble-Alpes, CNRS/IN2P3
*5 ILL, Grenoble
*6 Department of Physics, University of Notre Dame
*7 Department of Physics, Peking University
*8 Department of Physics, Tohoku University
*9 Universidad Autónoma de Madrid
*10 Instituto de Estructura de la Materia, CSIC
*11 Atomki, Debrecen
*12 IRCNPC, Beihang University
*13 Department of Physics, Osaka University
*14 Department of Physics, Tokyo University of Science
*15 Institut de Physique Nucléaire d'Orsay, IN2P3-CNRS
*16 Università di Padova and INFN Sezione di Padova
*17 GSI
*18 Istituto Nazionale di Fisica Nucleare
*19 Wright Nuclear Structure Laboratory, Yale University

References

1) NNDC database (2013), http://www.nndc.bnl.gov/;
2) C. Mazzocchi *et* al.: Phys. Lett. B **622**, 45 (2005);
3) P. Hosmer *et* al.: Phys. Rev. C **82**, 025806 (2010);
4) M. Madurga *et* al.: Phys. Rev. Lett. **109**, 112501 (2012);

Intermediate-energy Coulomb excitation of ^{104}Sn: Moderate $E2$ strength decrease approaching ^{100}Sn†

P. Doornenbal,[*1] S. Takeuchi,[*1] N. Aoi,[*2] M. Matsushita,[*3,*4] A. Obertelli,[*5] D. Steppenbeck,[*3] H. Wang,[*1,*6] L. Audirac,[*5] H. Baba,[*1] P. Bednarczyk,[*7] S. Boissinot,[*5] M. Ciemala,[*7] A. Corsi,[*5] T. Furumoto,[*8] T. Isobe,[*1] A. Jungclaus,[*9] V. Lapoux,[*5] J. Lee,[*1] K. Matsui,[*10] T. Motobayashi,[*1] D. Nishimura,[*11] S. Ota,[*3] E.C. Pollacco,[*5] H. Sakurai,[*1,*10] C. Santamaria,[*5] Y. Shiga,[*4] D. Sohler,[*12] and R. Taniuchi[*10]

In recent years, several experimental findings generated a large interest regarding the $E2$ strength pattern in the tin isotopes. While the neutron-rich isotopes with $A = 126, 128, 130$ follow the anticipated trend of smoothly decreasing $B(E2)\uparrow$ values towards the major shell closure well described by large-scale shell-model (LSSM) calculations[1,2], the proton-rich nuclei take a different path. Commencing with the stable $A = 114$ isotope a steadily growing deviation from the shell-model expectations was observed with almost constant $B(E2)\uparrow$ values for the $A = 106 - 112$ isotopes[1–3]. A first attempt for ^{104}Sn with limited statistics has recently been made[4]. The result of 0.10(4) e^2b^2 indicates a steep decrease of excitation strength in agreement with LSSM calculations. In a second measurement, a considerably larger value of 0.180(37) e^2b^2 was obtained[5]. Here, we report on the first $B(E2)\uparrow$ extraction of ^{104}Sn from absolute Coulomb excitation cross-sections at intermediate energies.

A ^{124}Xe primary beam was accelerated up to an energy of 345 MeV/nucleon and impinged on a 3 mm thick Be production target at the F0 focus of the BigRIPS fragment separator[6]. The $B\rho - \Delta E - B\rho$ method was applied to select and purify secondary beams of ^{104}Sn and ^{112}Sn in two subsequent measurements. The secondary beams were transported to the focal point F8, where a 557 mg/cm^2 thick Pb target was inserted to induce Coulomb excitation reactions. To detect γ-rays from the $2^+_1 \rightarrow 0^+_{gs}$ transitions, the reaction target was surrounded by the DALI2 array[7]. Reaction products were identified behind the reaction target by the ZeroDegree spectrometer[1].

A $B(E2)\uparrow$ value of 0.173(28) e^2b^2 was deduced for ^{104}Sn. The run with ^{112}Sn, which has a known $B(E2)\uparrow$ value, was used for feeding estimations. Our result is in agreement with the 0.180(37) e^2b^2 obtained in Ref.[5] with largely overlapping error bars, but deviates significantly from the value of 0.10(4) e^2b^2 obtained in Ref.[4]. The drop in excitation strength is much smoother than suggested in Ref.[4] and cannot be reproduced by present LSSM calculations using standard effective charges as well as proton and neutron excitation across the $N = Z = 50$ shell.

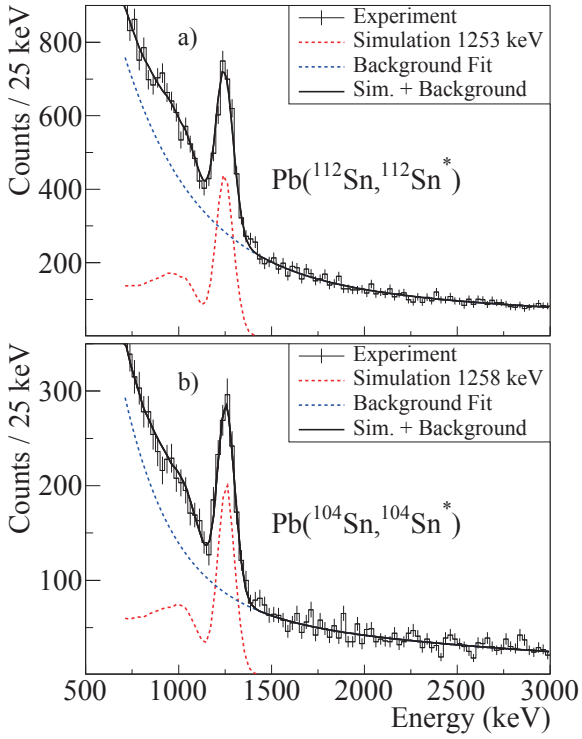

Fig. 1. Doppler corrected γ-ray spectra of ^{112}Sn (top panel a) and ^{104}Sn (bottom panel b). The observed $2^+_1 \rightarrow 0^+_{gs}$ transitions are compared to simulations.

† Condensed from the article in Phys. Rev. C 90, 061302(R) (2014).

*1 RIKEN Nishina Center
*2 Research Center for Nuclear Physics, Osaka University
*3 Center for Nuclear Study, University of Tokyo
*4 Department of Physics, Rikkyo University
*5 CEA Saclay
*6 State Key Laboratory of Nuclear Physics and Technology, Peking University
*7 Niewodniczanski Institute of Nuclear Physics, Polish Academy of Sciences
*8 National Institute of Technology, Ichinoseki College
*9 Instituto de Estructura de la Materia, CSIC
*10 Department of Physics, University of Tokyo
*11 Department of Physics, Tokyo University of Science
*12 Institute for Nuclear Research of the Hungarian Academy of Sciences

References

1) A. Banu *et al.*, Phys. Rev. C 72, 061305 (2005).
2) A. Ekström *et al.*, Phys. Rev. Lett. 101, 012502 (2008).
3) C. Vaman *et al.*, Phys. Rev. Lett. 99, 162501 (2007).
4) G. Guastalla *et al.*, Phys. Rev. Lett. 110, 172501 (2013).
5) V. Bader *et al.*, Phys. Rev. C 88, 051301(R) (2013).
6) T. Kubo *et al.*, Prog. Theor. Exp. Phys. 2012, 03C003 (2012).
7) S. Takeuchi *et al.*, Nucl. Instr. Meth. A 763, 596 (2014).

First campaign of the SEASTAR project

P. Doornenbal,[*1] A. Obertelli,[*1,*2] G. Authelet,[*1,*2] H. Baba,[*1] F. Browne,[*3] D. Calvet,[*1,*2] F. Château,[*1,*2] L.X. Chung,[*4] A. Corsi,[*1,*2] A. Delbart,[*1,*2] Zs. Dombradi,[*5] S. Franchoo,[*6] J.-M. Gheller,[*1,*2] F. Giacoppo,[*7] A. Gillibert,[*1,*2] A. Gottardo,[*6] K. Hadynska-Klek,[*7] T. Isobe,[*1] Z. Korkulu,[*5] S. Koyama,[*1,*8] Y. Kubota,[*1,*9] V. Lapoux,[*1,*2] J. Lee,[*10] M. Lettmann,[*11] C. Louchart,[*11] R. Lozeva,[*12] K. Matsui,[*1,*8] M. Matsushita,[*9] T. Miyazaki,[*1,*8] S. Momiyama,[*8] T. Motobayashi,[*1] M. Niikura,[*1,*8] S. Nishimura,[*1] L. Olivier,[*6] S. Ota,[*9] H. Otsu,[*1] Z. Patel,[*13] C. Péron,[*1,*2] A. Peyaud,[*1,*2] E.C. Pollacco,[*1,*2] J.-Y. Roussé,[*1,*2] E. Sahin,[*7] H. Sakurai,[*1,*8] C. Santamaria,[*1,*2] M. Sasano,[*1] C. Shand,[*13] Y. Shiga,[*1,*14] P.A. Söderström,[*1] G.L. Stefan,[*6] D. Steppenbeck,[*9] T. Sumikama,[*1,*15] D. Suzuki,[*6] S. Takeuchi,[*1] R. Taniuchi,[*1,*8] T. Uesaka,[*1] Zs. Vajta,[*5] H. Wang,[*1] V. Werner,[*11] J. Wu,[*1,*16] Z. Xu,[*1,*10] K. Yoneda,[*1] and the SEASTAR Collaboration

The SEASTAR (Shell Evolution And Search for Two-plus energies At the RIBF) project aims to measure systematically 2_1^+ energies of neutron-rich nuclei via in-beam γ-ray spectroscopy. Its setup combines the DALI2 γ-ray spectrometer[1)] with the MINOS setup including a liquid hydrogen target system[2)], as shown in Fig. 1, while exotic nuclei are produced with BigRIPS[3)]. In the first campaign 2_1^+ energies of ^{66}Cr, ^{70,72}Fe, and ^{78}Ni were measured with three different secondary beam settings.

A ^{238}U primary beam was accelerated to 345 MeV/nucleon and impinged on a 3-mm thick Be target at the entrance of BigRIPS. The beam intensity varied between 13 to 15 particle-nA. The spectrometer was tuned for ^{67}Mn, ^{71,73}Co, and ^{79}Cu ions to enable $(p, 2p)$ reactions and to populate 2_1^+ states in the above mentioned nuclei. Particle identification was performed with the $B\rho$-ΔE-TOF method, employing standard BigRIPS detectors. Beam energies in front of the MINOS target were around 250 MeV/nucleon, beam purities in the order of 0.1–0.3 %, and total intensities of 4 to 6 kHz.

The MINOS and DALI2 setups were installed at the F8 focus. A reaction target thickness of 102 mm was employed for all three settings. A key feature of the MINOS system was its time projection chamber, which enabled to reconstruct vertex positions of $(p, 2p)$ (and also $(p, 3p)$) reactions with an accuracy of a few mm[2)]. DALI2 was employed in its standard configuration of 186 large-volume NaI(Tl) detectors. However, MINOS was installed further upstream than reaction targets are usually employed, resulting in an azimuthal angular coverage of DALI2 between 10° and 100°.

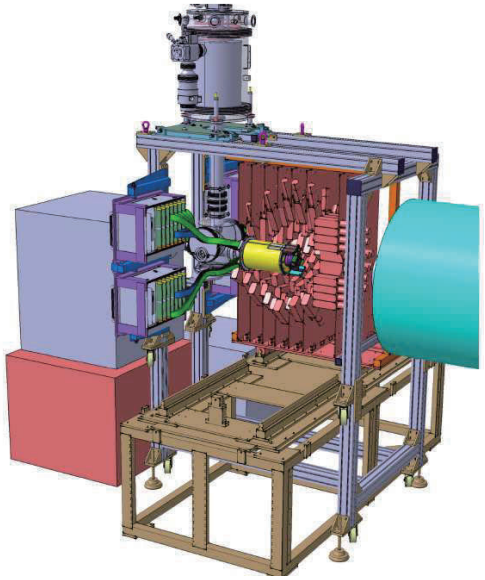

Fig. 1. Schematic view of the SEASTAR setup with the MINOS time projection chamber (yellow) mounted inside DALI2.

Reaction products were identified with the spectrometer ZeroDegree[3)], providing again particle identification via the $B\rho - \Delta E -$TOF method with standard detectors. ZeroDegree was tuned for the $(p, 2p)$ reaction channel in MINOS, resulting in total rates between 450 and 1200 Hz.

Data were collected for 7.5 days during the three settings in total, while secondary beam production with BigRIPS took 1.5 days and 1 day was used for user tuning. The 2_1^+ energies were observed on-line for the ^{66}Cr, ^{70,72}Fe, and ^{78}Ni isotopes. Currently, these data as well as many by-products are under analysis by several groups belonging to the SEASTAR collaboration.

*1 RIKEN Nishina Center
*2 CEA Saclay
*3 School of Computing Engineering and Mathematics, University of Brighton
*4 INST Hanoi
*5 MTA Atomki
*6 IPN Orsay
*7 Department of Physics, University of Oslo
*8 Department of Physics, The University of Tokyo
*9 Center for Nuclear Study, The University of Tokyo
*10 Department of Physics, The University of Hong Kong
*11 Institut für Kernphysik, TU Darmstadt
*12 IPHC Strasbourg
*13 Department of Physics, University of Surrey
*14 Department of Physics, Rikkyo University
*15 Department of Physics, Tohoku University
*16 Department of Physics, Peking University

References

1) S. Takeuchi et al.: Nucl. Instr. Meth. A 763, 596 (2014).
2) A. Obertelli et al.: Eur. Phys. J. A 50, 8 (2014).
3) T. Kubo et al.: Prog. Theor. Exp. Phys. 2012, 03C003.

Fragmentation of ^{137}Cs and ^{90}Sr on proton and deuterium

H. Wang,[*1] H. Otsu,[*1] H. Sakurai,[*1] D. Ahn,[*1] M. Aikawa,[*2] H. Baba,[*1] P. Doornenbal,[*1] T. Fukahori,[*3] N. Fukuda,[*1] T. Isobe,[*1] S. Kawakami,[*4] S. Koyama,[*5] S. Kubono,[*1] G. Lorusso,[*1] Y. Maeda,[*4] A. Makinaga,[*2] S. Momiyama,[*5] M. Niikura,[*5] Y. Shiga,[*1,*6] P.-A. Söderström,[*1] H. Suzuki,[*1] H. Takeda,[*1] S. Takeuchi,[*1] R. Taniuchi,[*1,*5] Ya. Watanabe,[*1] and Yu. Watanabe[*7]

Properties of long-lived fission products (LLFP) have been studied for decades. LLFP nuclei are highly radioactive, although they are close to the line of β stability. These fission products are also of great interest for nuclear engineering as they carry a large weight fraction in the nuclear waste from nuclear reactor systems. Transmutation of the fission products into stable or short-lived isotopes has been suggested. Aiming at investigating the LLFP transmutation, we report on the fragmentation of ^{137}Cs and ^{90}Sr on proton and deuterium in inverse kinematics.

A primary beam U was accelerated to 345 MeV/nucleon, and it bombarded a 1-mm thick Be target located at the object point of the BigRIPS fragment separator. The average beam intensity was about 12 particle nA. Two secondary beam settings were applied and optimized for the ^{137}Cs and ^{90}Sr isotopes. The energies were about 185 MeV/nucleon in front of the secondary targets for both beams. The intensities of the ^{137}Cs and ^{90}Sr beams were 1.2×10^3 and 7.1×10^3 Hz, with purities of 14% and 28%, respectively.

Three targets, 179.2 mg/cm^2 CH_2, 217.8 mg/cm^2 CD_2[1)], and 226.0 mg/cm^2 ^{12}C were used to induce the secondary reactions. Data were also collected using an empty target to obtain the contribution from the beam-line materials. Reaction products were identified by the ZeroDegree spectrometer using the TOF-$B\rho$-ΔE method. A total kinetic energy measurement was performed for identification of the charge states. In order to cover the fragments over a wide range, several settings in ZeroDegree were applied.

The isotopic distributions of the fragmentation cross sections for the ^{137}Cs and ^{90}Sr beams on proton and deuterium are shown in Figs. 1 and 2, respectively. The proton- and deuterium-induced cross sections were deduced from the CH_2 and CD_2 targets, respectively, after subtraction of the carbon contributions by the C target as well as the background contributions by the empty target run. The validation of the cross section values was around 1 mb, as determined by statistics. The results are generally reproduced by PHITS[2)], while EPAX[3)] shows some discrepancies for the multi-nucleon removal channels.

*1 RIKEN Nishina Center
*2 Faculty of Science, Hokkaido University
*3 Japan Atomic Energy Agency
*4 University of Miyazaki
*5 Department of Physics, University of Tokyo
*6 Department of Physics, Rikkyo University
*7 Kyushu University

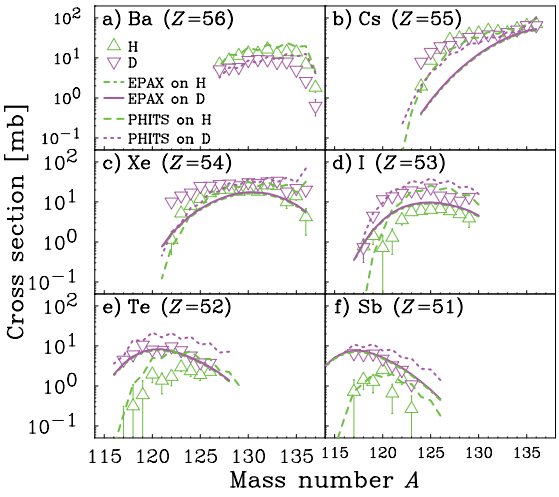

Fig. 1. Measured cross sections presented as isotope distributions for the fragments produced by ^{137}Cs on proton and deuterium. EPAX and PHITS calculations are displayed for comparison.

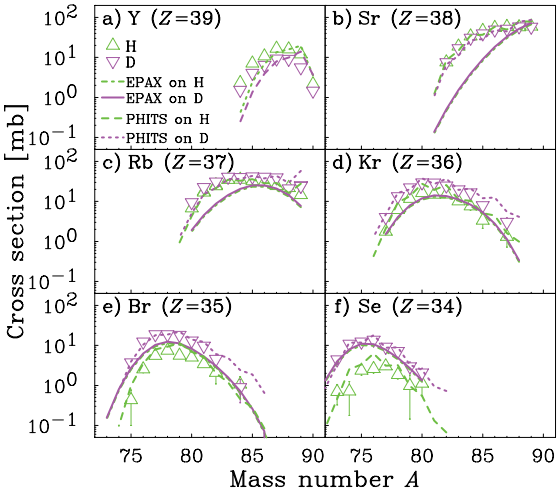

Fig. 2. Same as Fig. 1 but for ^{90}Sr

References

1) Y. Maeda et al.: Nucl. Instr. Meth. A 490, 518 (2002).
2) T. Sato et al.: J. Nucl. Sci. Technol. 50, 913 (2013).
3) K. Sümmerer and B. Blank: Phys. Rev. C 61, 034607 (2000).

Missing-mass spectroscopy of tetra-neutron system via exothermic double-charge exchange reaction ^{4}He(^{8}He,^{8}Be)4n

K. Kisamori,[*1,*2] S. Shimoura,[*2] H. Miya,[*1,*2] M. Assie,[*3] H. Baba,[*1] T. Baba,[*4] D. Beaumel,[*1,*3] M. Dozono,[*1] T. Fujii,[*1,*2] N. Fukuda,[*1] S. Go,[*1,*2] F. Hammache,[*3] E. Ideguchi,[*5] N. Inabe,[*1] M. Itoh,[*6] D. Kameda,[*1] S. Kawase,[*2] T. Kawabata,[*4] M. Kobayashi,[*2] Y. Kondo,[*1,*7] T. Kubo,[*1] Y. Kubota,[*1,*2] M. Kurata-Nishimura,[*1] C. S. Lee,[*1,*2] Y. Maeda,[*8] H. Matsubara,[*1] S. Michimasa,[*2] K. Miki,[*5] T. Nishi,[*1,*9] S, Noji,[*10] S. Ota,[*2] S. Sakaguchi,[*1,*11] H. Sakai,[*1] Y. Sasamoto,[*2] M. Sasano,[*1] H. Sato,[*1] Y. Shimizu,[*1] A. Stolz,[*10] H. Suzuki,[*1] M. Takaki,[*2] H. Takeda,[*1] S. Takeuchi,[*1] A. Tamii,[*5] L. Tang,[*2] H. Tokieda,[*2] M. Tsumura,[*4] T. Uesaka,[*1] K. Yako,[*2] Y. Yanagisawa,[*1] and R. Yokoyama[*2]

Since the report on candidates of a bound tetra-neutron system[1], multi-neutron systems in nuclei have attracted considerable attention on both the experimental and theoretical fronts. On the other hand, later theoretical studies using *ab-initio* calculations[2] have suggested that the tetra-neutron cannot exist as a bound system but possibly as a resonance system.

We performed missing-mass spectroscopy of the 4n system via the exothermic double-charge exchange reaction ^{4}He(^{8}He,^{8}Be)4n[3]. The primary goal of the experiment was to determine the energy level and its width of the 4n system. In order to produce the 4n system with a small momentum transfer of less than 20 MeV/c, a secondary beam of ^{8}He with a large internal energy was used.

The experiment was performed at the RIKEN RI Beam Factory (RIBF) using the SHARAQ spectrometer and a liquid He target system[4]. We measured the momentum of the ^{8}He beam at BigRIPS-F6 with the High-Resolution Beamline and the momenta of two alpha particles, which were the decay products of the ^{8}Be ejectile, with the SHARAQ spectrometer. The incident beam energy of ^{8}He was 186 MeV/u.

Events resulting from the ^{4}He(^{8}He,^{8}Be)4n reaction were selected. Two α particles from the ^{8}Be ejectile were detected simultaneously at the final focal plane of the SHARAQ spectrometer. Furthermore, a method to reconstruct trajectories for more than two particles under a high-intensity beam ($\sim$2 MHz) was developed [5]. In order to a obtain good signal-to-noise ratio, it was important to identify multi-particles in one bunch, which have the possibility to create the background events. These events were rejected using the Multi-Wire Drift Chamber (MWDC) at F6.

We obtained the missing-mass spectrum of a tetra-neutron system, as shown in Fig. 1. The spectrum contains 28 events including background events. The background events were estimated from the the number of events that was not identified as multi-particle in one bunch in the MWDC at F6. There were only 2.2 ± 1.0 events in the whole spectrum region, which is almost negligible compared to the selected 28 events. The excitation energy (E_{4n}) of the spectrum was calibrated using the peak position of the ^{8}Li(1^+) state and the scale of magnetic rigidity of the SHARAQ spectrometer. ^{8}Li was produced by the inverse kinematics of the (p,n) reaction of ^{8}He. The uncertainty of the energy determination accuracy was 1.25 MeV at the one sigma level. The resolution of the spectrum was 1.16 MeV at the one sigma level.

The events were concentrated in the low-excitation-energy region of $0 < E_{4n} < 2$ MeV and a continuum were observed at a region of $E_{4n} > 2$ MeV. The mean of the four events at $0 < E_{4n} < 2$ MeV was 0.83 ± 0.25 MeV. The possibility of the resonance state at the low-energy region and the shape of the continuum will be discussed in comparison with results of a theoretical calculation assuming the correlation of di-neutron clusters.

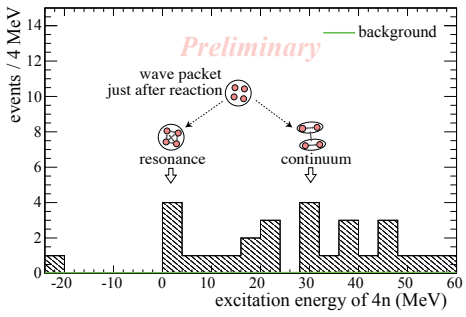

Fig. 1. Missing-mass spectrum of tetra-neutron system.

*1 RIKEN Nishina Center
*2 Center for Nuclear Study, the University of Tokyo
*3 IPN, Orsay
*4 Department of Physics, Kyoto University
*5 Research Center Nuclear Physics, Osaka University
*6 Cyclotron and Radioisotope Center, Tohoku University
*7 Department of Physics, Tokyo Institute of Technology
*8 Faculty of Engineering, University of Miyazaki
*9 Department of Physics, the University of Tokyo
*10 National Superconducting Cyclotron Laboratory, Michigan State University
*11 Faculty of Science, Kyushu University

References

1) F. Marques *et al.*: Phys. Rev. **C 65**, 044006 (2002)
2) S. Pieper: Phys. Rev. Lett. **90**, 252501 (2003)
3) K. Kisamori *et. al.*: Accelerator Progress Rep. **45** (2012)
4) M. Kurata-Nishimura *et. al.*: Accelerator Progress Rep. **46** (2013)
5) K. Kisamori *et. al.*: Accelerator Progress Rep. **46** (2013)

Laser-RF double resonance spectroscopy of $^{84-87}$Rb isotopes trapped in superfluid helium†

X.F. Yang,[*1,*2] T. Furukawa,[*1,*3] T. Wakui,[*1,*4] K. Imamura,[*1,*5] T. Fujita,[*1,*6] Y. Mitsuya,[*1,*5] M. Hayasaka,[*1,*7] Y. Ichikawa,[*1] Y. Ishibashi,[*1,*9] H. Shirai,[*1,*8] T. Suzuki,[*1,*8] Y. Ebara,[*3] A. Hatakeyama,[*10] M. Wada,[*1] T. Sonoda,[*1] Y. Ito,[*1] T. Kobayashi,[*11] S. Nishimura,[*1] M. Kurata-Nishimura,[*1] Y. Kondo,[*1,*8] K. Yoneda,[*1] H. Ueno,[*1] T. Shinozuka,[*4] T. Shimoda,[*6] K. Asahi,[*1,*8] and Y. Matsuo[*1,*12]

Laser spectroscopy measurements of various isotopes have provided a number of valuable results, such as nuclear spins, moments, and charge radii. However, to further study exotic atoms that are far from stability, higher efficiency and higher resolution are strongly required to overcome certain experimental limitations (low yield, limited beam time, large contaminations, and so on). Therefore, a new method called OROCHI was developed for laser spectroscopy measurements of radioactive isotopes (RIs) in superfluid helium (He II) using a small and controllable number of atoms.[1)] In this method, using He II as the trapping medium for the energetic ion beam and matrix for trapped atoms, we aim to systematically determine the nuclear spins and moments of RIs with a low yield. This measurement is based on the observation of Zeeman and hyperfine structures by optical pumping and the double resonance method. Recently, we have succeeded in trapping, polarization, and laser spectroscopy measurements of $^{84-87}$Rb isotopes in He II.

A general introduction to the experimental principle and method has been presented elsewhere.[2)] In this experiment, both stable ^{85,87}Rb and unstable ^{84,86}Rb energetic ions produced from the RIPS were counted accurately and implanted into He II. The number of atoms injected into He II was on the order of 10^4 pps for the current setup. Using the trapping position control system, we confirmed the precision of the trapping site (around 1 mm) of atoms in He II by detecting laser-induced fluorescence (LIF).[3)] On the basis of the trapping volume ($\pi \times 5 \times 5 \times 1$ mm^3) of atoms in He II (ion beam spot size: $\phi \approx 10$ mm), and the observation range ($5 \times 2 \times 2$ mm^3) of the LIF detection system, we estimated that more than 20% of the trapped atoms were used for laser spectroscopy measurements. From the number of injected ions and detected LIF photons, the number of detectable LIF photons from one injected atom was estimated to be approximately 0.2 - 0.3.

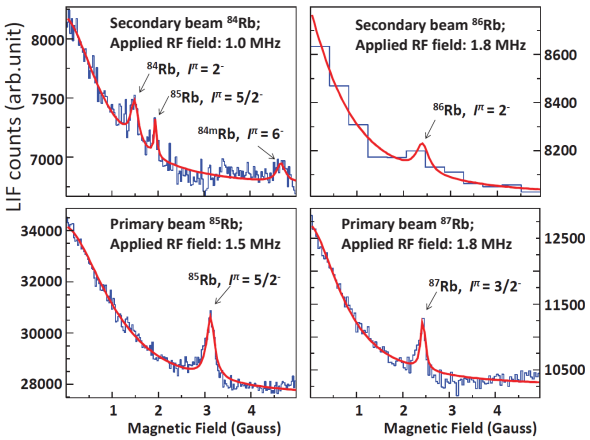

Fig. 1.: LRDR spectra of Rb isotopes trapped in He II. The red solid line is the fitting function, as described in Ref.[4)]

After the precise trapping of $^{84-87}$Rb in He II, the atoms were optically pumped and polarized with a polarized laser light. In addition, laser-RF double resonance spectra of the $^{84-87}$Rb atoms were measured by monitoring the LIF signal as a function of the scanned external magnetic field with a fixed-frequency transverse RF field applied to the atoms, as shown in Fig. 1. Relatively high spin polarization (above 40%) was achieved for the $^{84-87}$Rb isotopes,[4)] which was estimated from the difference in the LIF intensity between the linearly and circularly polarized laser. The resonance peaks provide information regarding the Zeeman splitting of atoms in a magnetic field. From these Zeeman resonance peaks, nuclear spin values for $^{84m,84-87}$Rb isotopes were determined with reasonable accuracy, after eliminating the effect of the background magnetic field.

In conclusion, we performed the effective trapping and laser spectroscopy measurements of $^{84-87}$Rb isotopes with a controllable number of atoms in He II using the newly developed method. The achievement of high trapping efficiency and high spin polarization and the determination of the nuclear spins of RIs in He II suggest the potential application of this method to the study of various exotic particles in He II.

† Condensed from the article in Phys. Rev. A **90**, 052516 (2014)

*1 RIKEN Nishina Center
*2 Nuclear and Radiation Physics Section, KU Leuven
*3 Department of Physics, Tokyo Metropolitan University
*4 Cyclotron Radioisotope Center, Tohoku University
*5 Department of Physics, Meiji University
*6 Department of Physics, Osaka University
*7 Department of Physics, Tokyo Gakugei University
*8 Department of Physics, Tokyo Institute of Technology
*9 Department of Physics, University of Tsukuba
*10 Department of Applied Physics, Tokyo University of Agriculture and Technology
*11 Laser Technology Laboratory, RIKEN
*12 Department of Advanced Sciences, Hosei University

References

1) T. Furukawa et al.: Hyp. Int. **196**, 191 (2010).
2) T. Furukawa et al.: Nucl. Instrum.Methods B **317**, 590 (2013).
3) X. Yang et al.: Nucl. Instrum.Methods B **317**, 599 (2013).
4) X. Yang et al.: Phys. Rev. A **90**, 052516 (2014).

RI beam production at BigRIPS in 2014

N. Fukuda,[*1] Y. Shimizu,[*1] H. Takeda,[*1] H. Suzuki,[*1] D.S. Ahn,[*1] N. Inabe,[*1] D. Murai,[*1,*2] K. Yoshida,[*1] H. Sato,[*1] Y. Sato,[*1] K. Kusaka,[*1] Y. Yanagisawa,[*1] M. Ohtake,[*1] D. Kameda,[*1] and T. Kubo[*1]

RI beam production at the BigRIPS fragment separator[1] in 2014 is presented. Table 1 lists the experimental programs carried out at BigRIPS in this period and the RI beams produced for each experiment.

The beam time at the RIBF started in March with the Uranium beam campaign, in which 6 experiments were performed. The long-lived fission products, ^{137}Cs and ^{90}Sr, were produced by the in-flight fission of the ^{238}U beam to investigate their nuclear-transmutation reaction[2]. Owing to their proximity to the β-stability line, we experienced difficulties in improving the purities of the isotopes of interest.

The ^{55}Ca and ^{56}Ca beams were produced by projectile fragmentation of a ^{70}Zn beam for a direct mass measurement at the SHARAQ spectrometer. A spectroscopy of deeply-bound pionic atoms was performed using the BigRIPS separator as a high-resolution spectrometer. The spring beam time ended with the ^{16}O beam experiment at the SHARAQ spectrometer.

The autumn beam time began in October with the second Uranium beam campaign, which consisted of 6 experiments. First, a machine study was conducted to study particle identification and isotope separation when producing heavier beams with an atomic number (Z) of around 80[3]. It was the first attempt at the RIBF. The ^{172}Dy and ^{170}Dy beams were delivered to the EURICA experiment. The RI-beam production around Z = 65 at BigRIPS has been pioneered in recent new-isotope-search experiments[4, 5].

The ^{48}Ca primary beam was provided with a high intensity of approximately 500 pnA. Such a high-intensity beam made it possible to search for the neutron drip line for the F, Ne, and Na isotopes.

The experiments to search for new neutron-rich isotopes were performed using the in-flight fission of a ^{238}U beam[5, 7], as shown in Table 1. A total of 28 new isotopes were identified in the preliminary analysis.

Table 1. List of the experimental programs and RI beams produced at the BigRIPS in 2014 (in chronological order).

Primary beam	Proposal No.	Course	RI beam (Primary beam)
^{238}U 345 MeV/u	NP1306-SAMURAI17	SAMURAI	^{132}Sn
	NP1306-SAMURAI14	SAMURAI	(^{238}U)
	NP1306-RIBF31R1	ZeroDegree	^{130}Cd
	DA14-01	ZeroDegree	^{137}Cs, ^{90}Sr
	DA14-02-01	BigRIPS	New isotope search (Z ~ 55—70 region)
	NP1312-RIB118	ZeroDegree	^{79}Cu, ^{73}Co, ^{67}Mn
^{70}Zn 345 MeV/u	NP1312-SHARAQ3R	SHARAQ	^{56}Ca, ^{55}Ca, ^{54}Sc
^{2}H 250 MeV/u	NP1312-RIBF54R1	BigRIPS	^{1}H, ^{3}He *(d, ^{3}He) reaction for pionic atom
^{16}O 250 MeV/u	NP1112-SHARAQ08	SHARAQ	^{1}H, (^{16}O)
^{aa238}U 345 MeV/u	MS-EXP13	BigRIPS	RI-beam production in the region of Z ~ 80
	NP1012-RIBF63	BigRIPS	^{82}Ga
	NP1012-RIBF61	ZeroDegree	^{132}Sn, ^{128}Sn
	NP1306-RIBF51R1	ZeroDegree	^{70}Ni
	DA14-02-02	BigRIPS	New isotope search (Z ~ 33 region)
	NP1112-RIBF88R1	EURICA	^{172}Dy, ^{170}Dy
^{48}Ca 345 MeV/u	NP1312-RIBF56R1	ZeroDegree	^{24}O, ^{22}O, ^{20}O
	NP1312-SAMURAI18R1	SAMURAI	^{19}B, ^{17}B, ^{14}Be, ^{11}Li
	DA14-02-03	BigRIPS	Drip line search for F, Ne, Na

*1 RIKEN Nishina Center
*2 Department of Physics, Rikkyo University

Fig. 1 shows the nuclear chart, in which all the isotopes produced at the BigRIPS from the commissioning in March 2007 to December 2014 are indicated along with the new isotopes observed at BigRIPS. The number of RI-beams produced amounted to approximately 350, and the number of new isotopes reached approximately 140. Production yields for more than 1,000 isotopes were obtained.

The number of experiments using RI beams at BigRIPS is tallied in Table 2, for various primary beams in each year. A total of 89 experiments have been performed so far.

References
1) T. Kubo: Nucl. Instr. Meth. B **204**, 97 (2003).
2) H. Wang et al.: In this report.
3) N. Inabe et al.: In this report.
4) D. Kameda et al.: RIKEN Accel. Prog. Rep. **46**, 20 (2013).
5) N. Fukuda et al.: In this report.
6) N. Inabe et al.: In this report.
7) Y. Shimizu et al.: In this report.

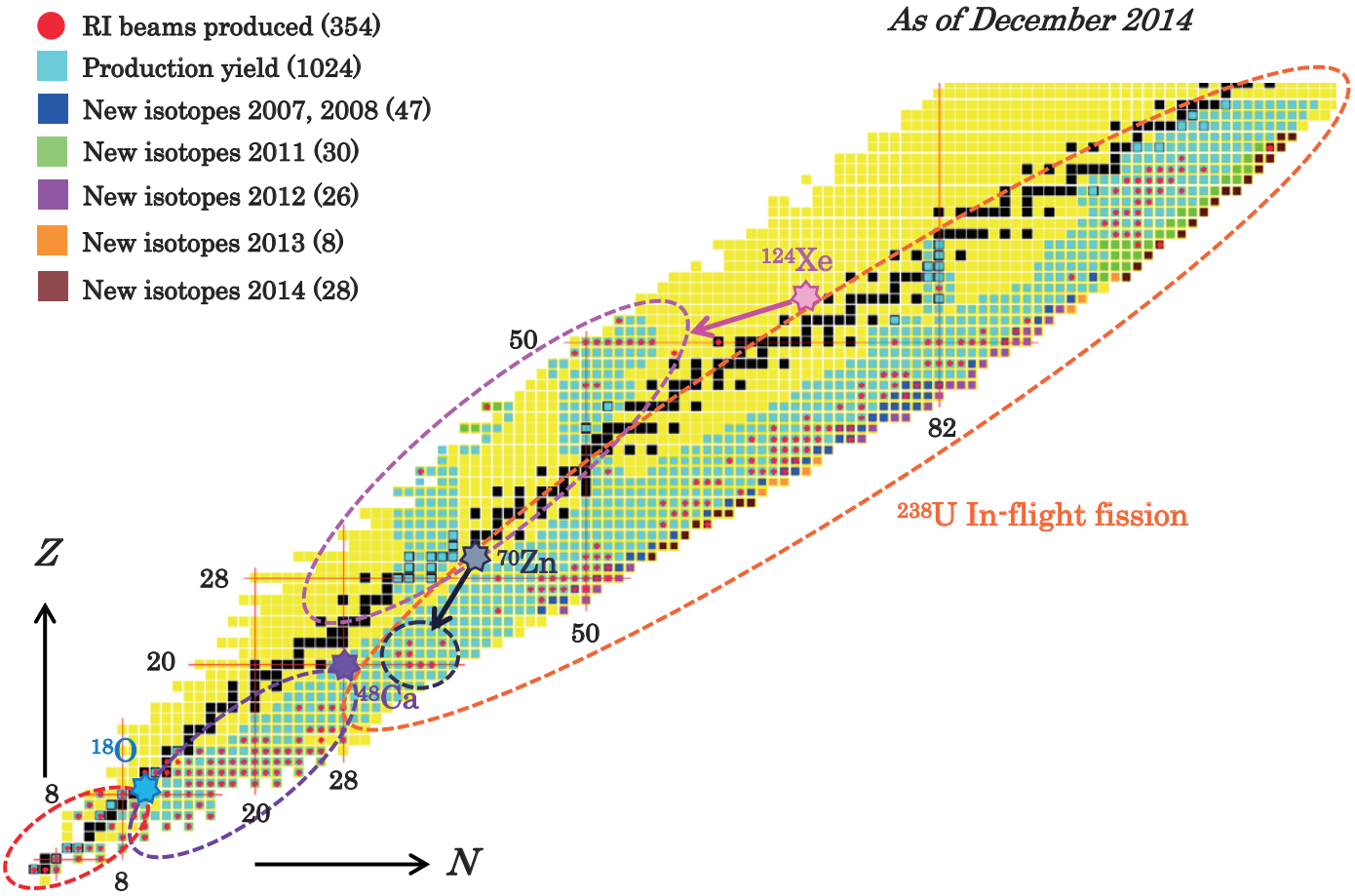

Fig. 1. RI beams produced at the BigRIPS separator from March 2007 to December 2014.

Table 2. Number of experiments using RI beams at the BigRIPS.

Year	^{238}U	^{124}Xe	^{86}Kr	^{70}Zn	^{48}Ca	^{18}O	^{16}O	^{14}N	^{4}He	^{2}H	Yearly total
‘07	4		1								5
‘08	2				4						6
‘09	3				3			3	1		10
‘10					10	1		2		1	14
‘11	4	2				2					8
‘12	6	3		1	4	6					20
‘13	4	2				3	1				9
‘14	11			1	3					1	17
Total	34	7	1	2	24	12	1	5	1	2	89

Neutron drip-line search using 48Ca beam

N. Inabe,*1 N. Fukuda,*1 H. Takeda,*1 H. Suzuki,*1 D. S. Ahn,*1 Y. Shimizu,*1 D. Murai,*2 H. Sato,*1 Y. Sato,*1
K. Kusaka,*1 Y. Yanagisawa,*1 M. Ohtake,*1 K. Yoshida,*1 H. Otsu,*1 N. Iwasa,*3 T. Nakamura,*4
O. Tarasov,*5 B. Sherrill,*5 D. Morrissey,*5 H. Geissel,*6 and T. Kubo*1

A neutron drip-line has been determined till O[1] of which mass number(A) is 24, three times the atomic number(Z). However for F, Ne and Na isotopes with A=3Z+4 were found[2]. The sudden increase in neutron numbers suggests that there might be a change in the nuclear structure of F. The drip-line search is important to investigate how many neutron number increases and determination of the drip line gives some constraints to nuclear models.

The drip-line search was performed by using the BigRIPS[3] with a 345 MeV/u ^{48}Ca beam of high intensity (> 400 particle nA). In the search, we used two settings of the BigRIPS for ^{33}F and ^{36}Ne&^{39}Na. In the two settings, magnetic rigidities before a degrader located at F1 were the same (9.385 Tm) but those after it were different. The magnetic rigidities were determined so that ^{33}F for the former and center of ^{36}Ne and ^{39}Na for the latter became a central orbit. Radioactive isotopes were produced by the 20 mm Be target. The thickness of the degrader at F1 was 15 mm. A rather thick target and degrader were used so as not to be over the maximum magnetic rigidities of both the first and second stage in the BigRIPS. Another degrader at F5 (7 mm) was used to remove light particles such as triton. Widths of momentum slits at both F1 and F5 were ±120 mm and those of both F2 and F7 slits were ±20 mm. A collimator made using iron was located upstream of F2 to remove triton, ^{6}He of long stopping ranges that could not be removed by the F2 slit. The length of the collimator for beam direction was 450 mm and the opening widths were ±35 mm at the entrance and ±20 mm at the exit. In order to study yield systematics, we measured the yields of $^{23\sim31}$F, ^{34}Ne, and ^{37}Na using the same settings of the target, degraders, and slits as the drip-line search. We also studied the secondary reaction effect in the target wherein isotope A is produced in 2 steps via a different isotope B (Here A is produced by ^{48}Ca->B->A). In this study we measured target thickness dependence (Be 5 mm, 10 mm and 20 mm) of the production yields using ^{37}Na.

Particle identification (PID) was performed by determination of Z and A/Z event by event using the ΔE-TOF-Bρ method. The ΔE was measured using four 300 μm Si stacks, the MUSIC, and plastic scintillators at F7 redundantly. TOF was measured using 2 plastic scintillators at F5 and F7. Bρ was determined by track reconstruction using positions and angles measured by PPACs located at F5 and F7. Because around Z=10, efficiency of the PPAC was not 100 %, we also measured the positions using the plastic scintillators. In the drip-line search, A/Z was determined for only the second half (from F5 to F7) in the second stage due to large contaminants at F3 (> 1 MHz), which is mainly triton.

Figure 1 shows a PID plot for the setting of the drip-line search of ^{33}F with a running time of 14.3 hours. In this measurement live time of data acquisition was 74.5 % and the intensity of ^{48}Ca beam was 415 particle nA on average. As shown in Fig. 1, ^{31}F was clearly seen but there is no event in the ^{33}F area although an expected value of ^{33}F are 20.7 counts if we assume a production cross section of ^{33}F predicted bv EPAX 2.15[4].

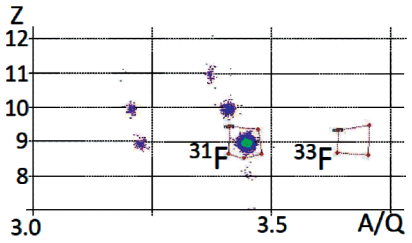

Figure 1 A/Q vs Z plot for the drip-line search of F.

Figure 2 shows the yield systematics of F isotopes with prediction of EPAX 2.15 (solid line). The measured yields are in good agreement with those of EPAX2.15.

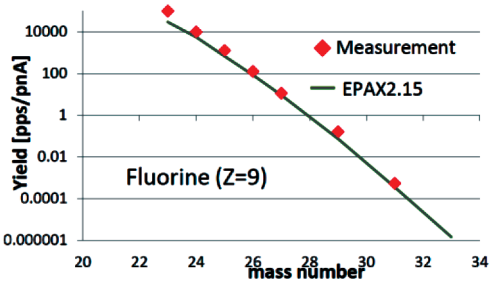

Figure 2 Yield systematic of F isotopes.

We estimated probability that ^{33}F is 0 count in the measurement by applying the expected value (20.7 counts) to the Poisson distribution. The estimated probability is 0.000000103 % and this implies that the probability that ^{33}F is unbound is 99.999999897% in this assumption. In the study of the secondary reaction effect, we did not observe a large enhancement at the thick target as expected. Detailed analysis including the ^{36}Ne&^{39}Na setting is in progress.

*1 RIKEN Nishina Center
*2 Department of Physics, Rikkyo University
*3 Department of Physics, Tokyo Institute of Technology
*4 Department of Physics, University of Tohoku
*5 Michigan State University (MSU)
*6 Gesellschaft fuer Schwerionenforshung mbH (GSI)

References

1) H. Sakurai et al: Phys. Lett. **B 448**, 180 (1999).
2) M. Notani et al: Phys. Lett. **B 542**, 49 (2002).
3) T. Kubo: Nucl. Instr. Meth. **B 204**, 97 (2003).
4) K. Sümmerer: Phys. Rew. **C 61**, 034607 (2000).

High-resolution hadronic-atom X-ray spectroscopy with superconducting transition-edge-sensor microcalorimeters

S. Okada,[*1] D.A. Bennett,[*2] C. Curceanu,[*3] W.B Doriese,[*2] J.W. Fowler,[*2] J. Gard,[*2] F.P. Gustafsson,[*4] T. Hashimoto,[*1] R.S. Hayano,[*5] J.P. Hays-Wehle,[*2] G.C. Hilton,[*2] M. Iliescu,[*3] S. Ishimoto,[*6] K. Itahashi,[*1] M. Iwasaki,[*1] K. Kuwabara,[*7] Y. Ma,[*1] J. Marton,[*8] H. Noda,[*1] G.C. O'Neil,[*2] H. Outa,[*1] C.D. Reintsema,[*2] M. Sato,[*1] D.R. Schmidt,[*2] H. Shi,[*3] K. Suzuki,[*8] T. Suzuki,[*5] D.S. Swetz,[*2] H. Tatsuno,[*2,*6] J. Uhlig,[*4] J.N. Ullom,[*2] E. Widmann,[*8] S. Yamada,[*7] and J. Zmeskal[*8] (HEATES collaboration)

Hadronic atoms provide a unique laboratory to study the strong interaction between the hadron and atomic nucleus at the low-energy limit. Effects of the strong interaction are experimentally extracted by performing characteristic X-ray-emission spectroscopy of the most tightly bound energy levels, which are most perturbed by strong forces. As for kaonic atoms, many experiments have collected data on a variety of targets[1]; however, the energy resolution of conventional semiconductor X-ray spectrometers employed in the past measurements has been insufficient to detect small spectral effects attributed to the strong interaction. As a result, the depth of the K^--nucleus potential at zero energy remains still unknown. This is closely related to the recent investigations of bound states of the kaon in the nucleus and is one of the greatest concerns in the recent strangeness nuclear physics[2].

With the aim of providing a breakthrough to the current situation, we are preparing an ultra-high resolution X-ray measurement of kaonic atoms using a novel cryogenic X-ray detector, i.e., an array of superconducting transition-edge-sensor (TES) microcalorimeters which has been recently developed at NIST[3,4]. The energy resolution is about two orders of magnitude better than that of converntional silicon drift detectors (SDDs).

To demonstrate the feasibility of the X-ray spectroscopy with TES in a hadron beam environment, we recently performed a pioneering experiment by measuring pionic carbon X rays with a 240-pixel TES array using 173 MeV/c π^- beam at the πM1 beamline of Paul Scherrer Institute. Figure 1 shows the preliminary results of (a) a correlation plot of the measured X-ray time versus energy distributions for π^- triggered events, and (b) and (c) show the projections. A sharp peak from the pionic carbon 4-3 X-ray transition was successfully observed at 6.43 keV with a clear timing correlation with the beam. The characteristic X rays of Fe Kα1 (6.404 keV) and Fe Kα2 (6.391 keV) that are uncorrelated with beam timing originate from surrounded materials that are excited using an X-ray tube. The achieved average energy resolution is 5 eV (FHWM) at 6 keV in "beam-off" condition, and 8 eV in "beam-on" condition, while the energy resolution of a SDD used as a reference in this experiment is ~165 eV as shown in Fig. 1 (d).

This demonstration is the world's first application of a TES spectrometer to the hadronic-atom X-ray spectroscopy and a key milestone toward more general use of high-resolution microcalorimeter spectrometers at charged-particle beam lines.

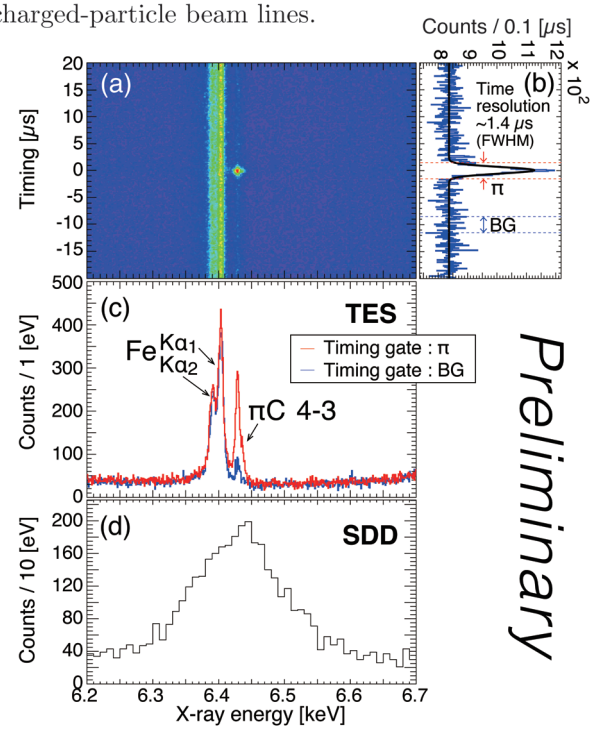

Fig. 1. Preliminary results of the measured X-ray time and energy distributions for π triggered events. (a) A correlation plot of the time difference between pion arrival and X-ray detection vs the X-ray energy measured by the TES array. (b) The projections on the time axis. (c) The projection on the energy axis. The energy spectra with two time gates, pions ("π") and background ("BG") indicated in (b), are shown. (d) An X-ray energy spectrum measured by the reference SDD.

*1 RIKEN Nishina Center
*2 National Institute of Standards and Technology (NIST)
*3 Laboratori Nazionali di Frascati dell' INFN
*4 Department of Chemical Physics, Lund University
*5 Department of Physics, University of Tokyo
*6 High Energy Accelerator Research Organization (KEK)
*7 Department of Physics, Tokyo Metropolitan University
*8 Stefan-Meyer-Institut für subatomare Physik (SMI)

References

1) C.J. Batty, E. Friedman, A. Gal: Phys. Rep. 287, 385 (1997).
2) A. Gal: Nucl. Phys. A 914, 270 (2013).
3) J.N. Ullom et al.: Appl. Phys. Lett. 87, 194103 (2005).
4) D.A. Bennett et al.: Rev. Sci. Instrum. 83, 093113 (2012).

Measurement of high-p_{T} neutral mesons with a high-energy photon trigger in ALICE

S. Yano[*1,*2] and K. Shigaki[*1]

ALICE, one of the experiments at the Large Hadron Collider (LHC) at CERN, is aimed at studying heavy-ion collisions and the properties of a deconfined state of matter, the quark-gluon plasma (QGP)[1]. High-p_{T} particle production is a powerful tool for characterizing the QGP because the interaction between its fast partons depends on the QGP transport properties. The hadron yields in heavy-ion collisions can be quantified by the nuclear modification factor (R_{AA}), which is the ratio of the particle yield in heavy-ion collisions normalized by the number of inelastic nucleon–nucleon collisions to the yield in pp collisions. Previous experiments have shown that R_{AA} at high p_{T} is significantly smaller than 1, which can be explained by the energy loss of fast partons traversing in QGP.

The ALICE experiment includes a high-resolution and high-granularity electromagnetic calorimeter called PHOS[1]. One of the main physics goals achievable by PHOS is the study of energy loss through the measurement of high-p_{T} neutral mesons (π^0 and η). Three PHOS modules are installed in the ALICE experiment, which covers azimuthal angles in the range $260^\circ < \phi < 320^\circ$ and pseudorapidity $|\eta| < 0.125$. PHOS provides a photon trigger (PHOS trigger) by requiring the measured energy to be above a threshold. The threshold was set to be 2 and 4 GeV in pp collisions at $\sqrt{s} = 8$ TeV. By using the PHOS trigger, high-p_{T} neutral mesons can be efficiently measured in the ALICE experiment. This paper discribes the analysis status of neutral-pion production measured with the PHOS trigger and minimum-bias (MB) trigger data in pp collisions. Further, neutral-pion production in pp collisions at $\sqrt{s} = 8$ TeV are compared with results for other LHC energies (0.9, 2.76 and 7 TeV)[2)3)]. In this analysis, $0.3nb^{-1}$ and $70nb^{-1}$ MB-trigger and PHOS-trigger data respectively, in pp collisions at $\sqrt{s} = 8$TeV are used.

The invariant cross-section can be calculated as

$$E\frac{d^3\sigma^{pp\to\pi^0X}}{dp^3} = \frac{1}{2\pi}\frac{1}{p_{\mathrm{T}}}\frac{\sigma_{\mathrm{MB}}}{N_{evt}}\frac{1}{\varepsilon\times Acc}\frac{1}{\mathrm{BR}}\frac{N^{\pi^0}}{\Delta y\Delta p_{\mathrm{T}}} \quad (1)$$

Here σ_{MB} is the cross-section of minimum-bias (MB), N^{π^0} is the number of reconstructed neutral pions, and Acc is the PHOS acceptance correction. N_{evt} is the number of analyzed events in the minimum-bias trigger data analysis. In case of the PHOS trigger data analysis, it is the number of analyzed PHOS trigger events times the rejection factor. In the minimum-bias trigger data analysis, ε indicates the reconstruction efficiency, whereas in the PHOS trigger data analysis, it indicates the reconstruction efficiency times the trigger efficiency for a neutral-pion meson.

The invariant cross-section of a neutral pion in pp collisions at LHC energies are shown in Fig. 1. As shown in Fig. 1, the 0.9, 2.76 and 7 TeV analyses used only minimum-bias (MB) trigger data, but the 8 TeV analysis (this analysis) used not only minimum-bias but also PHOS trigger data. The very-low p_{T} ($\sim 1\mathrm{GeV}/c$) region cross-section was measured by the Photon Conversion Method (PCM)[2] with the tracking detectors of the central burrel[1]. For the 8 TeV result, the minimum-bias and PHOS trigger data were combined to measure the very wide p_{T} range neutral-pion meson. The dashed line denotes the result fitted to Tsalis functions.

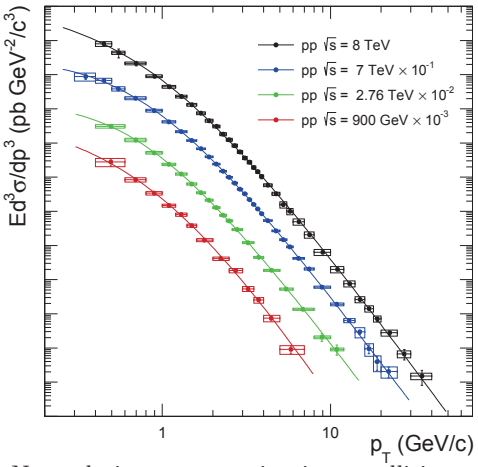

Fig. 1. Neutral-pion cross section in pp collisions at LHC energies.

By comparing the results for different LHC energies, pertubative Quantum Chromodynamics (pQCD) can be tested at LHC energies and the fragmentation function (FF) of gluon to the neutral-pion model can be restricted. Further, this comparison can help predict a neutral-pion production cross-section in pp collisions at other energies. This has not been measured yet and more precise references to study phenomena induced by AA collisions can be estimated for QGP study.

*1 Department of Physics Science, Hiroshima University
*2 RIKEN Nishina Center

References

1) The ALICE Collaboration, JINST 3, S08002 (2008).
2) The ALICE colaboration, Phys.Lett.B 717 (2012), pp. 162 - 172.
3) The ALICE colaboration, Eur. Phys. J. C (2014) 74-3108.

Transverse single-spin asymmetries in prompt photon production from proton-proton collisions†

D. Pitonyak,[*1] K. Kanazawa,[*2] Y. Koike,[*3] and A. Metz[*2]

Collinear twist-3 factorization has been used since the 1980s in order to describe transverse single-spin asymmetries A_N. For a general process $A^\uparrow B \to C\,X$, the cross section can be written as the sum of three terms depending on which non-perturbative function is kept at twist-3. For hadron production, which has been intensely studied for close to 40 years, the distribution and fragmentation contributions to the cross section cannot be disentangled, i.e., all of them are summed together in the cross section. For many years it was often assumed that the piece involving the so-called Qiu-Sterman (QS) function $G_F(x,x)$ was the main cause of A_N^π. However, this led to a so-called "sign mismatch" between the QS function and the transverse momentum dependent (TMD) Sivers function extracted from semi-inclusive deep-inelastic scattering (SIDIS)[1]. Recently we showed in [2] for the first time that the fragmentation contribution in collinear twist-3 factorization actually can describe A_N^π very well. By using a Sivers function fully consistent with SIDIS, we demonstrated that this mechanism could also resolve the sign-mismatch puzzle. Nevertheless, an independent extraction of $G_F(x,x)$, through observables like A_N^{jet} and A_N^γ, is crucial to confirm this assertion. However, one must keep in mind that for A_N^{jet} and A_N^γ other twist-3 distribution effects can enter besides the QS function. Thus, in order to have a "clean" extraction of $G_F(x,x)$, it would be ideal if these other terms were small.

Therefore, we return to the SSA in $p^\uparrow p \to \gamma X$ to see if this reaction could provide such an observable. In twist-3 collinear factorization, A_N^γ has contributions from multiparton correlators inside either the transversely polarized proton or the unpolarized proton. For this process the former has been widely discussed in the literature for both (twist-3) quark-gluon-quark[3–10] and tri-gluon[11] non-perturbative functions, which are chiral-even objects evaluated at either soft-gluon or soft-fermion poles (SGPs/SFPs). The full result for twist-3 effects on the side of the unpolarized proton is a new piece from this work and, although we refrain from showing the explicit formula for brevity, will be included in our numerical analysis. This term involves a chiral-odd quark-gluon-quark correlator $E_F(x,x)$, which is related to the TMD Boer-Mulders function.

We now focus on the phenomenology. For the SGP correlators $E_F(x,x)$ and $G_F(x,x)$ we make use of identities that relate the first to the Boer-Mulders function and the second to the Sivers function. Since at this point no information on the SFP functions is available, we assume the relation $G_F(0,x)+\widetilde{G}_F(0,x) = G_F(x,x)$. Model calculations of quark-gluon-quark correlators show that chiral-even SFP functions are much smaller as compared to the SGP one and might even vanish. Therefore, we believe that this ansatz is reasonable.

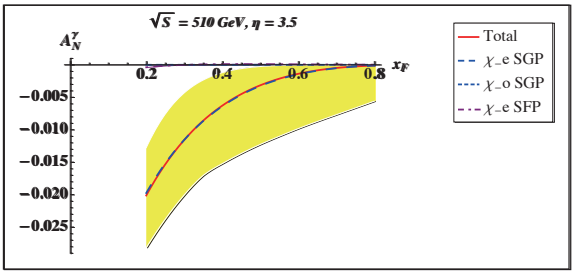

Fig. 1. A_N^γ vs. x_F at fixed $\eta = 3.5$ and $\sqrt{S} = 510\,\mathrm{GeV}$.

In Fig.1 we show an estimate of A_N^γ (along with an uncertainty band) from all these pole contributions for a set of kinematics relevant for the measurement of this observable at PHENIX and STAR. One sees that the entire effect is due to the "Sivers-type" QS mechanism. Using the Sivers function extracted from SIDIS, our results show that A_N^γ could be on the order of several (negative) percent in the forward region, providing a "clean" observable to extract of the QS function $G_F(x,x)$. In light of the "sign-mismatch" crisis involving $G_F(x,x)$ and the Sivers function[1], and the recently proposed solution to this issue that relies on the twist-3 fragmentation mechanism[2], such an extraction is of vital importance. In addition, one can obtain important information on the process dependence of the Sivers function as well as help discriminate between the Generalized Parton Model and twist-3 formalisms since the former predicts a *positive* asymmetry. Thus, measurements of this process by PHENIX and STAR are crucial.

References
1) Z.-B. Kang *et al.*, Phys. Rev. D **83**, 094001 (2011).
2) K. Kanazawa *et al.*, Phys. Rev. D **89**, 111501(R) (2014).
3) J.-w. Qiu and G. Sterman, Nucl. Phys. B **378**, 52 (1992).
4) X. Ji *et al.*, Phys. Rev. D **73**, 094017 (2006).
5) C. Kouvaris *et al.*, Phys. Rev. D **74**, 114013 (2006).
6) Y. Koike and K. Tanaka, Phys. Lett. B **646**, 232 (2007) [Erratum-ibid. B **668**, 458 (2008)].
7) K. Kanazawa and Y. Koike, Phys. Lett. B **701**, 576 (2011).
8) L. Gamberg and Z.-B. Kang, Phys. Lett. B **718**, 181 (2012).
9) K. Kanazawa and Y. Koike, Phys. Lett. B **720**, 161 (2013).
10) L. Gamberg *et al.*, Phys. Rev. Lett. **110**, 232301 (2013).
11) Y. Koike and S. Yoshida, Phys. Rev. D **85**, 034030 (2012).

† Condensed from the article in PRD **91**, 014013 (2015)

*1 RIKEN Nishina Center
*2 Department of Physics, Temple University
*3 Department of Physics, Niigata University

Entanglement entropy of de Sitter space α-vacua†

N. Iizuka,[*1] T. Noumi,[*2] and N. Ogawa[*2]

The de Sitter space is a very interesting space-time. It is a solution of Einstein equation when cosmological constant dominates, and it is related to the inflationary stage of our universe, as well as to the current stage of accelerating universe. A peculiar property of the de Sitter space is that the de Sitter invariant vacuum is not unique; it has a one-parameter family of invariant vacuum states $|\alpha\rangle$, called α-vacua[1,2].

The α-vacua give very peculiar behavior for the two point functions in the de Sitter space; the two-point functions on α-vacua between points x and y contain not only the usual short distance singularity $\delta(|x-y|)$, where $|x-y|$ is the de Sitter invariant distance between x and y, but also contain very strange singularity such as $\delta(|x-\bar{y}|)$ and $\delta(|\bar{x}-y|)$, where $\bar{x}$ and $\bar{y}$ represent the antipodal points of x and y, respectively. Since antipodal points in the de Sitter space are not physically accessible due to the separation by a horizon, one cannot have an immediate reason to discard two-point functions containing such an antipodal singularity. It is therefore unclear which vacuum should be realized in our universe. As a result, a number of studies have been done on phenomenological aspects of the α-vacua (e.g. primordial perturbations generated during inflation).

Since which vacuum one should choose is always a very important question, one is motivated to calculate physical quantities not only in a particular vacuum but also in others, and see if there is a big reason to choose or discard a particular vacuum.

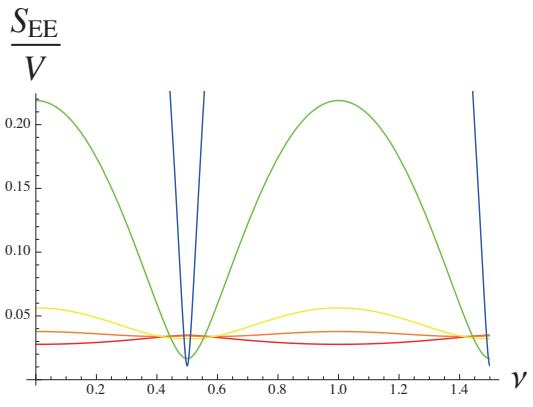

Fig. 1. Plot of S_{EE}/V against ν, for $\alpha = 0$ (red), 0.1 (orange), 0.25 (yellow), 1 (green) and 2 (blue). Notice the periodicity and reflection symmetries.

In this work, we computed the entanglement entropy in de Sitter α-vacua. By generalizing the recent calculation by Maldacena and Pimentel[3] in the Euclidean (or Bunch-Davies) vacuum for free scalar fields, we derived how entanglement entropy depends on α. The results are shown in Fig. 1 and Fig. 2.

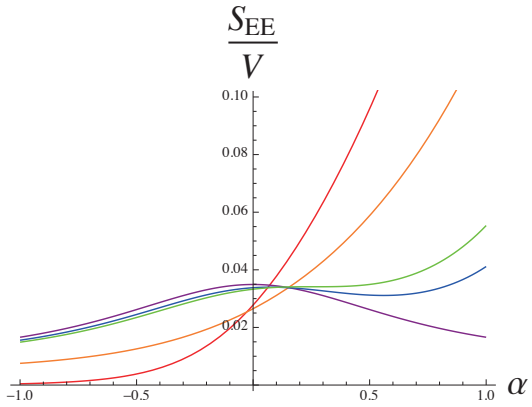

Fig. 2. Plot of S_{EE}/V against α, for $\nu = 0$ (red), 0.25 (orange), $\nu_c = 0.4062\ldots$ (green), 0.43 (blue) and 0.5 (purple).

As is seen in Fig. 2, the entanglement entropy increases significantly as we take α very large for generic values of ν. However only for $\nu = 1/2$ and $3/2$, this tendency disappears. Note that $\nu = 1/2$ is the conformal mass and $\nu = 3/2$ is massless. It is interesting to understand more physically why such a mass dependence occurs.

Our calculation is done for the free scalar field. Therefore direct comparison with the holographic calculation for the Euclidean vacuum[3] is difficult. It must be interesting to ask how the calculation of entanglement entropy on the α-vacua can be done in the strong coupling limit via holography, a la Ryu-Takayanagi formula[4]. Understanding these will hopefully shed more light on the question of which vacuum one should choose in the de Sitter space. We hope to come back to this question in near future.

References

1) E. Mottola, *Phys.Rev.* **D31** (1985) 754.
2) B. Allen, *Phys.Rev.* **D32** (1985) 3136.
3) J. Maldacena and G. L. Pimentel, *JHEP* **1302** (2013) 038, [arXiv:1210.7244].
4) S. Ryu and T. Takayanagi, *Phys.Rev.Lett.* **96** (2006) 181602, [hep-th/0603001].

† Condensed from the article arXiv:1404.7487 [hep-th].

*1 Department of Physics, Osaka University
*2 RIKEN Nishina Center

Current Reflection and Transmission at Conformal Defects: Applying BCFT to Transport Process†

T. Kimura*1,*2 and M. Murata*3

A powerful method for studying critical phenomena with conformal defects is boundary conformal field theory (BCFT). However, it has not been completely understood how BCFT describes the reflection/transmission at conformal defects. In this report, we define the reflection/transmission coefficient for conserved currents, as a natural generalization of that based on the energy-momentum tensor.[1)]

We consider two one-dimensional quantum systems connected by a junction, which can be considered as an impurity interacting with the bulk. Let us assume that the first system is in the positive domain $x > 0$, the second is in the negative $x < 0$, and they are connected at the origin as depicted in Fig. 1(a). Now we shall describe the above system in terms of BCFT. Corresponding to the two quantum systems, the BCFT picture involves two CFTs: CFT_1 and CFT_2. These CFTs are defined in the upper and lower half planes respectively as depicted in Fig. 1(b). The real axis, which divides the two CFTs, stands for the world line of the impurity, or the defect. We can reformulate this system to obtain $\mathrm{CFT}_1 \times \overline{\mathrm{CFT}}_2$ in the upper half plane thanks to the folding trick,[2)] as shown in Fig. 2. In this way, the junction of the one-dimensional quantum systems can be mapped into a CFT boundary condition.

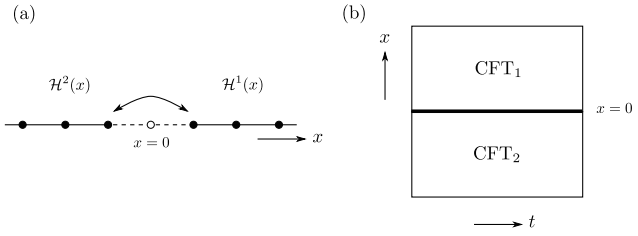

Fig. 1. From the *impurity* to the *defect*. (a) Two one-dimensional systems are connected through the impurity at $x = 0$. (b) Adding the time direction and taking the continuum limit, that system is mapped into the two-dimensional system with the defect along the line $x = 0$.

We assume that $\mathrm{CFT}_{1,2}$ have the same symmetry subalgebra $\mathcal{C}$, which is preserved at the conformal defect. For such a defect, we choose the following current gluing condition $\left(j_n^{\mathrm{tot},a} + \overline{j}_{-n}^{\mathrm{tot},a}\right)|B\rangle = 0$, where $j_n^{\mathrm{tot},a}$ takes values in the Kac–Moody algebra $\hat{\mathcal{C}}$, and $\overline{j}$ is the anti-holomorphic part. We then introduce the

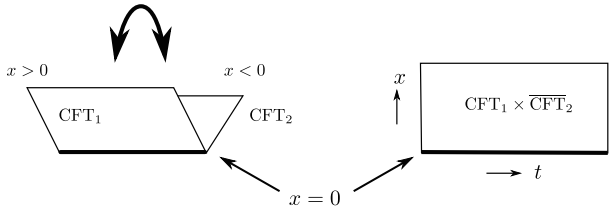

Fig. 2. From the *defect* to the *boundary*. By using the folding trick, a system with the defect is mapped into another system defined on the upper half plane with the boundary.

R-matrix based on this boundary state $|B\rangle$,

$$R[\mathcal{C}]^{ij,ab} = -\frac{\langle 0|j_1^{i,a}\overline{j}_1^{j,b}|B\rangle}{\langle 0|B\rangle}\,. \tag{1}$$

Since we have three constraints for this matrix, it has only one degree of freedom. Letting $\omega_B[\mathcal{C}]$ be

$$d^{ab}\omega_B[\mathcal{C}] = -\frac{1}{k_1k_2(k_1+k_2)}\frac{\langle 0|K_1^a\overline{K}_1^b|B\rangle}{\langle 0|B\rangle}\,, \tag{2}$$

the R-matrix is given by

$$R[\mathcal{C}] = \frac{k_1k_2}{k_1+k_2}\left(\begin{pmatrix} \frac{k_1}{k_2} & 1 \\ 1 & \frac{k_2}{k_1}\end{pmatrix} + \omega_B[\mathcal{C}]\begin{pmatrix} 1 & -1 \\ -1 & 1\end{pmatrix}\right), \tag{3}$$

where d^{ab} is the Cartan–Killing form, k_i is the level of the Kac–Moody algebra, and $K_n^a = k_2 j_n^{1,a} - k_1 j_n^{2,a}$. We can introduce the reflection and transmission coefficients based on this matrix:

$$\mathcal{R}[\mathcal{C}] = \frac{R^{11}+R^{22}}{k_1+k_2}\,, \quad \mathcal{T}[\mathcal{C}] = \frac{R^{12}+R^{12}}{k_1+k_2}\,, \tag{4}$$

which satisfy the current conservation $\mathcal{R}+\mathcal{T} = 1$. Applying this formula to the coset-type boundary state with $\mathcal{C} = su(2)$,[3)] we obtain

$$\mathcal{T}[su(2)] = \frac{2k_1k_2}{(k_1+k_2)^2}\left(1 - \frac{S_{00}^{(k_1+k_2)}S_{\rho 1}^{(k_1+k_2)}}{S_{\rho 0}^{(k_1+k_2)}S_{01}^{(k_1+k_2)}}\right), \tag{5}$$

with the modular S-matrix of $\mathrm{SU}(2)_k$ labeled by two integers, $S_{\rho\mu}^{(k)} = \sqrt{\frac{2}{k+2}}\sin\left(\frac{\pi}{k+2}(2\rho+1)(2\mu+1)\right)$.

† Condensed from the article in Nucl. Phys. **B885** 266 (2014)
*1 RIKEN Nishina Center
*2 Institut de Physique Théorique, CEA Saclay
*3 Institute of Physics, ASCR

References
1) T. Quella et al., JHEP **0704** (2007) 095.
2) M. Oshikawa, I. Affleck, Phys. Rev. Lett. **77** (1996) 2604.
3) T. Quella, V. Schomerus, JHEP **0206** (2002) 028.

Magnetic field of the slowest rotating neutron star in the symbiotic X-ray binary 4U 1954+319†

T. Enoto[*1,*2,*3], M. Sasano,[*4] S. Yamada,[*5] T. Tamagawa,[*1]
K. Makishima[*4,*6], and Suzaku 4U 1954+319 Analysis Team

Neutron stars (NSs) are not boring degenerate compact objects with a uniform face, but exhibit a large variety of observational diversities mainly due to a wide range of magnetic field (B-field, $\sim 10^4$–10^{12} T), rotation spin period ($P \sim 10^{-3}$–10^4 s), and (in some cases) mass accretion from a companion star. Binary systems with NSs are conventionally classified into high-mass X-ray binaries (HMXBs, an optical counterpart mass $M_c > 10 M_\odot$) or low-mass X-ray binaries (LMXBs, $M_c < 1$–$2 M_\odot$). The former and latter are thought to host NSs with higher and lower B-field of 10^{7-8} T and 10^{4-6} T, respectively. However, the symbiotic X-ray binary (SyXB) 4U 1954+319 was recently recognized as a rare system hosting a peculiar NS and M-type companion, and found to be the slowest rotator among known X-ray pulsars with $P \sim$5.4 h.

We performed two observations of 4U 1954+319 with the X-ray satellite *Suzaku* in 2011 (quiescent) and 2012 (flare phase), and investigated the spectral and temporal nature of this peculiar system. Although the optical counterpart is classified as a "low mass" star, its X-ray features are quite similar to a wind-fed type

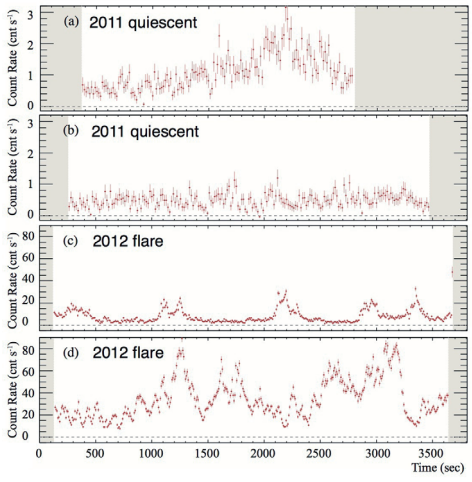

Fig. 1. The 1–10 keV X-ray count rates of 4U 1954+319 observed with X-ray CCD instruments (X-ray Imaging Spectrometer) on board the Suzaku satellite[1)], during a quiescent state (panel a and b) and an outburst (c and d) in 2011 and 2012, respectively.

† Condensed from the article in the Astrophysical Journal **786**, 127 (2014)

*1 RIKEN Nishina Center
*2 JSPS SPD Fellow
*3 NASA Goddard Space Flight Center
*4 Department of Physics, University of Tokyo
*5 Department of Physics, Tokyo Metropolitan University
*6 RIKEN MAXI Team

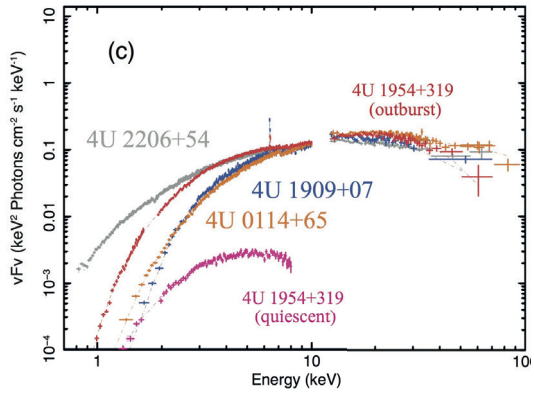

Fig. 2. Spectral comparison of 4U 1954+319 with other long period pulsars in HMXBs (modified from Enoto et al., 2014[1)]).

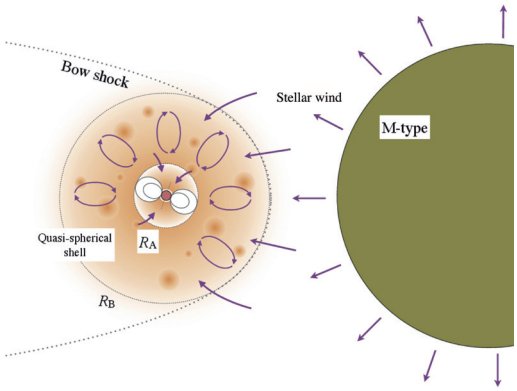

Fig. 3. Schematic view of the quasi-spherical accretion from stellar wind in the X-ray binary 4U 1954+319[1)].

HMXB system; e.g., 1) high pulsed fraction, ∼60–80%, 2) shot-like mass accretion, characterized by the log-normal distribution of the count rate (Fig.1), 3) broad-band spectral similarity to low-luminosity slowly rotating NSs in HMXBs (Fig. 2), and 4) a narrow 6.4 keV Fe-Kα line. Combined with a sign of the spin-equilibrium over a long time scale, we proposed a quasi-spherical accretion regime from a slow stellar wind from the M-type companion (Fig. 3). Even though we do not need an extremely strong B-field like magnetars, which were expected from the canonical disk-type accretion, we still need a higher B-field in the range of 10^{8-9} T as the HMXB-NSs rather than the LMXB-NSs. Our study indicates a new interesting subclass of X-ray pulsars, i.e., SyXBs, and casts a question on its evolutionary path to make such a peculiar system.

References

1) T. Enoto, M. Sasano, et al: ApJ, **786**, 127 (2014)

Short-term spectral softening of black-hole binary Swift J1753.5–0127†

A. Yoshikawa, *1*2 S. Yamada,*3 S. Nakahira,*4 M. Matsuoka,*5 H. Negoro,*6
T. Mihara,*5 and T. Tamagawa,*1

The X-ray emission from black-hole binaries (BHBs) is driven by the release of gravitational energy from accreting matter falling into a black hole (BH). The X-ray intensities are known to fluctuate for approximately weeks or months (outburst). There are two states: the low-luminosity hard (low/hard) and the high-luminosity soft (high/soft) states. The X-ray spectra of the low/hard state can be well reproduced by a power law with a photon index of 1.4–2.1.[1] The spectra of the high/soft state can be explained by optically thick thermal disk emission (accretion disk[2][3]). Transitions between the low/hard and high/soft states during the outburst have been observed in many BHBs.

The Swift J1753.5–0127 outburst was occurred on May 30 2005.[4] After the outburst, the source flux peaked on July 9 2005, and then gradually decreased for more than 9 years. Dips were observed in the 15–50 keV energy range that lasted for approximately 25 days (short-term variation). The dips are interpreted as a possible eclipse by the warped disk.[5] Observations with *MAXI*[6] revealed the increase of the intensity in the 2–4 keV energy range during the variation in 2009.[7] The increase can not be explained by the eclipse. To investigate the cause of the short-term variation, we have studied the X-ray spectrum.

For another short-term variation of the source on April 23 2012, we succeeded in tracing its spectral time evolution, as shown in Fig. 1. We overlaid the light curves for the various energy ranges normalized by the mean count rates, which were calculated by averaging over approximately 40 days. The light curves below and above 10 keV were observed using *MAXI* and *Swift*[8], respectively. The hump in the 0.7–4 keV band and the dip in the 15–50 keV band correspond to the growth and decay of the accretion disk, respectively (Fig. 1a). The X-ray spectrum observed by using the Swift-XRT[9] changed during the short-term variation (Fig. 1b). The spectrum can be fitted by the emission model of the accretion disk. The disk temperatures ($T_{\rm in}$) and energy fluxes ($F_{\rm disk}$) changed from 0.48 to 0.2 keV and from 4.8×10^{-9} to 2.2×10^{-9} erg s^{-1} cm^{-2}, respectively. The best-fit parameters show the variation of the accretion disk and the state transitions from the low/hard to high/soft state (softening) during the short-term variation. The $F_{\rm disk}$ and $T_{\rm in}$ did not obey the relationship, $F_{\rm disk} \propto {T_{\rm in}}^4$, suggesting that the structure of the accretion disk changed during the softening.

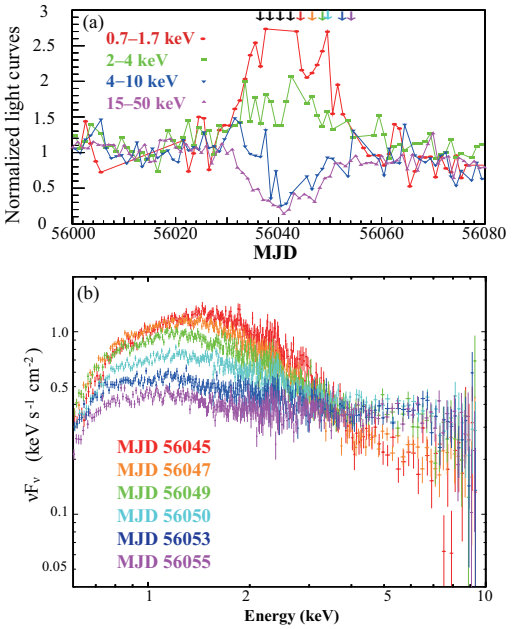

Fig. 1. (a) The light curves in energy ranges of 0.7–1.7 keV (red), 2–4 keV (green), 4–10 keV (blue), and 15–50 keV (magenta) normalized by the average value. Arrows indicate the XRT observations on MJD 56045 (red), 56047 (orange), 56049 (green), 56050 (cyan), 56053 (blue), 56055 (magenta), and the other dates (black). These colors correspond to the spectrum observed on MJD 56045, 56047, 56049, 56050, 56053, and 56055 in Fig. (b).

References
1) R. A. Remillard, & J. E. McClintock: ARA&A, 44, 49 (2006).
2) K. Mitsuda *et al.*: PASJ, 36, 741 (1984).
3) K. Makishima *et al.*: ApJ, 308, 635 (1986).
4) M. D. Palmer *et al.*: Atel #546 (2005).
5) A. W. Shaw *et al.*: MNRAS, 433, 740 (2013).
6) M. Matsuoka *et al.*: PASJ, 61, 999 (2009).
7) H. Negoro *et al.*: Atel #2341 (2009).
8) S. D. Barthelmy *et al.*: SSRv, 120, 143 (2005).
9) D. N. Burrows *et al.*: Proc. SPIE, 4140, 64 (2000).

† Condensed from the article in Publications of the Astronomical Society of Japan, 2015, 67, 1, 11

*1 High Energy Astrophysics Laboratory, RIKEN Nishina Center
*2 Department of Physics, Tokyo University of Science
*3 Department of Physics, Tokyo Metropolitan University
*4 ISS Science Project Office, ISAS, JAXA
*5 MAXI team, RIKEN
*6 Department of Physics, Nihon University

Installation of return BT line from IRC

Y. Watanabe,[*1] N. Fukunishi,[*1] M. Fujimaki,[*1] M. Komiyama,[*1] K. Kumagai,[*1] T. Maie,[*1] H.Yamasawa,[*1] S. Fukuzawa,[*2] M. Hamanaka,[*2] S. Ishikawa,[*2] K. Kobayashi,[*2] Y. Kotaka,[*2] R. Koyama,[*2] T. Nakamura,[*2] M. Nishida,[*2] M. Nishimura,[*2] J. Shibata,[*2] N. Tsukiori,[*2] and K. Yadomi[*2]

The return beam transport (BT) line from IRC to the E5 room was installed from FY2012 to FY2014 because of the biology experiments requiring a higher energy beam by a relatively heavy ion such as an Ar beam. In particular, the installed return BT line was from dipole magnet DMKR to dipole magnet DMA1, as shown in Fig. 1. The installation of the return BT line was supported by the 'Formation of Tohoku Marine Science Center' of the Ministry of Education, culture, Sports, Science and Technology, Japan. Table 1 shows the installation schedule of the return BT line. The return BT line was primarily installed in the maintenance period during every summer and winter.

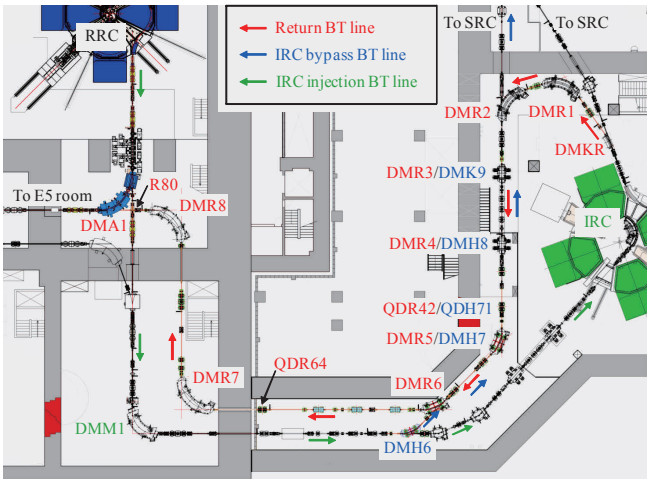

Fig. 1. Layout of the return BT line.

As preparatory works, all necessary components and works were first listed and the installation schedule was planned in FY2012. We arranged some existing components that we could use, and listed some new components that had to be produced and work that had to be done. Some quadrupole magnets, all profile monitor (PF), chambers, turbo molecular pumps (TMP) were produced in FY2012 because these components were already designed and the models chosen. A part of IRC bypass BT line and the infrastructure were modified and constructed in FY2013 before the installation of the return BT line. After temporary removal of a part of IRC bypass BT line from dipole magnet DMH6 to double quadrupole magnet QDH71, a telfer was constructed in the area from dipole magnet DMR6 to double quadrupole magnet QDR64, and some openings (holes) were made in the wall and floor in order to lay some cables in the summer of 2013. Because the old DMH6 was used as a new DMR6, the chamber and outer yokes of the old DMH6 were reversed to change the direction of flange after the dismantlement of the old DMH6, a new DMR6 was assembled, and a new DMH6 was produced. In addition, a power supply of DMKR, some stands, and ducts were produced in FY2013. Three double quadrupole magnets that were used in the old RILAC line were transferred from the E21 room to IRC room. After all magnets, stands, and chambers were carried in the area from DMR6 to QDR64, the removed IRC bypass BT line, including the new DMH6 and new DMR6, was again installed according a new line design in the winter of 2013/2014. All of the return BT line expect the IRC bypass BT line was installed in FY2014. Some quadrupole and steering magnets that were used in the old line were transferred from the E2 and E4 room to the E1 and RRC-A room, and all chambers and stands were also carried in each area. While almost all of the return BT line was installed in the summer of 2014, all cooling water piping and cables for magnets were laid, and the outer yokes of DMA1 were replaced with new ones that were fabricated such that a beam duct could be installed from the chamber R80. All faraday cups (FC), network device interface modules (N-DIM), rotary pumps (RP), gate valves (GV), stands, ducts and cables for monitors were produced by the summer of 2014, and these components were set up gradually. Finally, the operation check was smoothly done without any problem, and the first acceleration test with the Ar beam in the AVF-RRC-IRC mode using the return BT line was successfully completed in the end of January 2015.

Table 1 Installation schedule of the return BT line.

FY2012	Preparatory works and production of some quadrupole magnets, all PF, chambers, and TMP
Summer of 2013	Removal of part of the IRC bypass BT line, modification of old DMH6, construction of telpher, and boring of the wall and floor
Winter of 2013/2014	Production of new DMH6 and power supply, carrying in of some magnets and stands, laying of some cooling water piping, and installation of removed IRC bypass BT line
Summer of 2014	Installation of return BT line, except the IRC bypass BT line, laying of all cooling water piping and cables for magnets , modification of DMA1, and production of FC, N-DIM, RP, GV, and stands
Winter of 2014/2015	Set up of all PF, FC, N-DIM, vacuum pumps, laying of all cables for monitors, and finally operation check
Jan. 2015	Acceleration test with Ar beam

*1 RIKEN Nishina Center
*2 SHI Accelerator Service Ltd.

Supply of ^{48}Ca beam from 18-GHz ECRIS using the micro-oven

K. Ozeki,*1 Y. Higurashi,*1 M. Kidera,*1 and T. Nakagawa*1

In order to enhance the intensity and stability of the ^{48}Ca beam supplied from the RIKEN 18-GHz Electron Cyclotron Resonance Ion Source (ECRIS),[1] we have been conducting operational tests on a micro-oven using ^{40}Ca.[2] Owing to the cost of the material in which the ^{48}Ca isotope is highly enriched (70-80%), it is very important to reduce its consumption rate. For this purpose, we adopted the so-called "hot liner"[3-5] and studied its effect on the reduction of the consumption rate. In this study, wherein a tantalum cylinder and disk of 0.1-mm thick were installed into the ECRIS, we observed an apparent reduction of the material consumption rate by using the hot liner. Details of the results are described in Ref. 6.

The ^{48}Ca beams for a series of experiments using the micro-oven have been supplied three times until now. Each series of experiments is summarized in Table 1. The statuses of the beam supply for experiments-1, such as beam intensity and material consumption rate, are reported in Ref. 6.

Table 1. Supply of the ^{48}Ca beam using a micro-oven.

	Days	Charge	Beam course
1	Nov. to Dec. 2013	11+	GARIS, RIPS
2	Sep. to Oct. 2014	11+	GARIS, RIPS
3	Nov. to Dec. 2014	10+	BigRIPS

In the series of experiments-3, the ^{48}Ca beam produced by the present method was first supplied to the new RIBF accelerator complex. Figure 1 shows the charge distribution of the ^{48}Ca ions. The RF power fed to the ECRIS was 370 W.

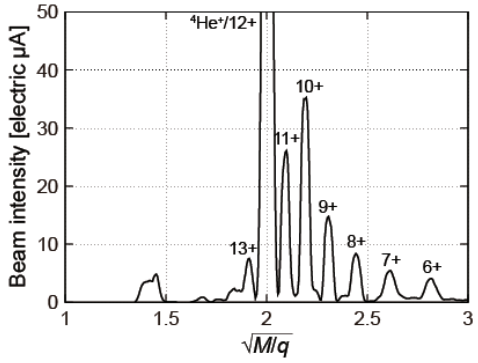

Fig. 1. Charge distribution of the ^{48}Ca ions.

The beam intensity at the exit of ECRIS and the oven current are shown in Fig. 2. The beam intensity was adjusted according to the requirements of the experiment, by changing the aperture of the slit at the exit of ECRIS. A beam intensity of ~35 electric μA with maximum slit aperture was maintained throughout the experimental duration.

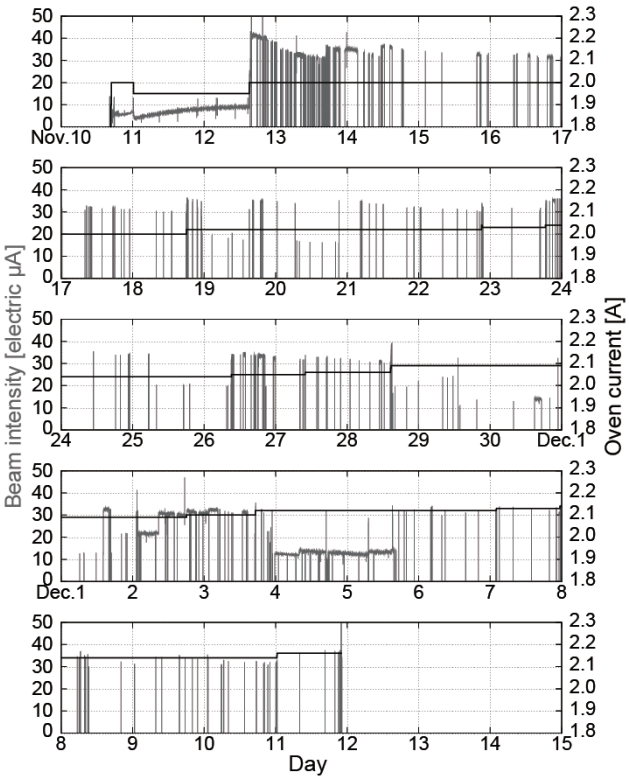

Fig. 2. Long-term supply of the ^{48}Ca beam. The beam intensity for ^{48}Ca^{10+} (gray) and the oven current (black) are shown.

The amounts of ^{48}Ca placed into the crucible and subsequently consumed were 299 mg and 98 mg, respectively. The consumption rate of ^{48}Ca was 0.13 mg/h. We succeeded in supplying stable and highly intense (twice as high compared to before, at the exit of ECRIS) beam with low material consumption rate (nearly one-tenth as low compared to before).

Previously, the peak intensity of the ^{48}Ca beam extracted from Superconducting Ring Cyclotron was 415 particle nA, but it was impractical to maintain the beam intensity at this level because of insufficient stability and high material consumption rate. The practical application of the micro-oven system realized long-term stable supply of the ^{48}Ca beam with an intensity of more than 400 particle nA to users.[7]

*1 RIKEN Nishina Center

References

1) T. Nakagawa et al.: Nucl. Instrum. Methods B **226**, 392 (2004).
2) K. Ozeki et al.: Rev. Sci. Instrum. **85**, 02A924 (2014).
3) A. Efremov et al.: Rev. Sci. Instrum. **69**, 662 (1998).
4) V. B. Kutner et al.: Rev. Sci. Instrum. **71**, 860 (2000).
5) P. Lehérissier et al.: Rev. Sci. Instrum. **73**, 558 (2002).
6) K. Ozeki et al.: Rev. Sci. Instrum. **86**, 016114 (2015).
7) http://www.nishina.riken.jp/RIBF/accelerator/tecinfo.html

Particle identification for Sn region with SAMURAI

J. Yasuda,[*1] M. Sasano,[*2] R.G.T. Zegers,[*3] H. Baba,[*2] W. Chao ,[*2] M. Dozono,[*2] N. Fukuda,[*2] N. Inabe,[*2] T. Isobe,[*2] G. Jhang,[*2,*13] D. Kamaeda,[*2] T. Kubo,[*2] M. Kurata-Nishimura,[*2] E. Milman,[*2] T. Motobayashi,[*2] H. Otsu,[*2] V. Panin, [*2] W. Powell, [*2] M. Sako, [*2] H. Sato,[*2] Y. Shimizu,[*2] L. Stuhl,[*2] H. Suzuki,[*2] T. Suwat, [*2] H. Takeda,[*2] T. Uesaka,[*2] K. Yoneda,[*2] J. Zenihiro,[*2] T. Kobayashi,[*4] T. Sumikama,[*4] T. Tako,[*4] T. Nakamura,[*5] Y. Kondo,[*5] Y. Togano,[*5] M. Shikata,[*5] J. Tsubota,[*5] K. Yako,[*6] S. Shimoura,[*6] S. Ota,[*6] S. Kawase,[*6] Y. Kubota,[*6] M. Takaki,[*6] S. Michimasa,[*6] K. Kisamori,[*6] C.S. Lee,[*6] H. Tokieda,[*6] M. Kobayashi,[*6] S. Koyama,[*7] N. Kobayashi, [*7] H. Sakai,[*8] T. Wakasa,[*1] S. Sakaguchi,[*1] A. Krasznahorkay,[*9] T. Murakami, [*10] N. Nakatsuka, [*10] M. Kaneko, [*10] Y. Matsuda, [*11] D. Mucher, [*12] S. Reichert, [*12] D. Bazin,[*3] and J.W. Lee[*13]

We performed the SAMURAI17 experiment[1] at RIKEN RIBF to study Gamow-Teller transition in ^{132}Sn by (p,n) reaction with the WINDS[2] and the SAMURAI spectrometer[3]. The SAMURAI spectrometer was used for tagging (p,n)-reaction events with the particle identification (PID) of the beam heavy fragments. The PID was performed with the TOF-$B\rho$-ΔE method. Here we report the preliminarily results on the PID.

Here, we used the ^{132}Sn beam run with empty-target cell at F13 and selected the non-reacted trigger events in order to estimate the resolution of TOF, $B\rho$ and ΔE. The beam rigidity was measured by the BigRIPS with a typical momentum resolution of $R/\sigma_R \sim 3000$.

The TOF was measured by using the plastic scintillators SBT1,2 and the HODS with flight path length $L \simeq 12.5$ m. The HODS consists of 6 plastic scintillation counters with size of 450 mm × 100 mm × 5 mm. The obtained TOF resolution is $\sigma_t = 62.1 \pm 2.7$(stat.) ps, where the statistical uncertainty is indicated. It should be noted that the non-uniformity of SBT1 thickness is as large as about 20 % which corresponds to 1 MeV/nucleon energy loss difference for 200 MeV/nucleon ^{132}Sn beam. In this analysis we gated the central position of SBT1 to estimate the TOF resolution, by using tracking information from BDC1,2[3] drift chamber which were placed between SBT1,2 and the target. In the following the resolution was estimated with the same manners.

The energy loss ΔE was measured by HODS. The ΔE is sensitive to the HODS thickness. In this experiment the non-uniformity of HODS thickness is about 10–20% for 6 counters. In order to correct the thickness dependence, we used the tracking information from FDC2[3] drift chamber which was placed after the SAMURAI spectrometer. The obtained ΔE resolution is $\sigma_{\Delta E}/\Delta E = 0.43 \pm 0.03$(stat.) %.

The rigidity was analyzed by using four drift chambers BDC1,2, FDC1 and FDC2[3]. The obtained rigidity resolution is $R/\sigma_R = 1318 \pm 27$(stat.).

Figure. 1(a) shows the PID spectrum with respect to atomic number Z and mass to charge ratio A/Q. The Z resolution is $\sigma_Z = 0.22$ corresponding to 4.6σ separation for Z=50 and 51. The A/Q resolution is $\sigma_{A/Q} = 0.14$ % for ^{132}Sn^{50+} which corresponds to 5.4σ separation.

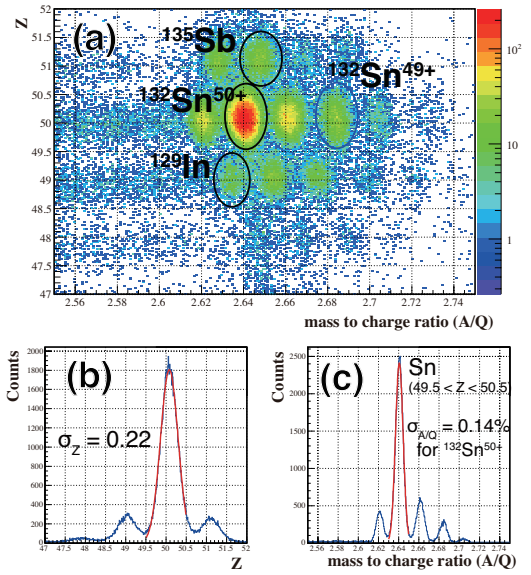

Fig. 1. (a) A SAMURAI PID spectrum with respect to Z and A/Q for non-reacted events with empty target cell. (b) Z distribution for all beam component and (c) A/Q distribution for Sn isotopes. The resolution of Z and A/Q are $\sigma_Z = 0.22$ and $\sigma_{A/Q} = 0.14\%$ for ^{132}Sn^{50+}, respectively.

*1 Department of Physics,Kyushu University
*2 RIKEN Nishina Center
*3 NSCL Michigan State University
*4 Department of Physics, Tohoku University
*5 Tokyo Institute of Technology
*6 CNS, University of Tokyo
*7 University of Tokyo
*8 ULIC, RIKEN Nishina Center
*9 MTA, Atomki
*10 Kyoto University
*11 Konan University
*12 Technical University Munich
*13 Department of Physics, Korea University

References

1) M. Sasano et al., : in this report.
2) J. Yasuda et al.,: in this report.
3) T. Kobayashi et al., Nucl. Instr. Meth. B317, 294 (2013).

Results of first online tests of small ion-surfing RF carpet gas cell at GARIS-II

P. Schury,[*1] F. Arai,[*1,*2] H. Haba,[*1] Y. Ito,[*1] I. Katayama,[*1] D. Kaji,[*1] K. Morimoto,[*1] M. Reponen,[*1] T. Sonoda,[*1] M. Wada,[*1] and H. Wollnik[*1,*3]

As part of the SLOWRI project, we have begun development of a new low-energy experimental facility, SlowSHE, for use with radioactive isotopes (RI), such as Super Heavy Elements (SHE), that are created via fusion-evaporation reactions. This new facility utilizes a small gas cell[1)] placed after the GARIS-II separator to thermalize the ions before they are transported to a multi-reflection time-of-flight mass spectrograph[2)]. A very thin mylar film (2.4 μm thick) on a rotatable frame is placed before the gas cell for use as an adjustable degrader to remove, in combination with two thin (1.1 μm and 2.4 μm thick) mylar windows, a large fraction of the ions kinetic energy. The remaining kinetic energy is removed by collisions with He gas, which the cell is pressurized with upto 100 mbar.

In this first experiment, we desired to verify the combined stopping and extraction efficiency for a variety of chemical elements using isotopes with a wide range of half-lives. We first studied stopping and extraction of the long-lived ^{205}Fr ($T_{1/2}$=3.8 s), produced via the reaction ^{169}Tm(^{40}Ar,4n)^{205}Fr.

The degrader was initially replaced with a large silicon detector array to measure the incoming rate. The α-decay rate of ^{205}Fr was calibrated against the rate of elastically scattered incoming beam near the reaction target. The detector was then replaced by the degrader and the rate of α-decay on a silicon detector placed after the gas cell was measured as a function of the degrader angle. The result, shown in Fig. 1, featured a flat plateau with efficiency peaking near 30%.

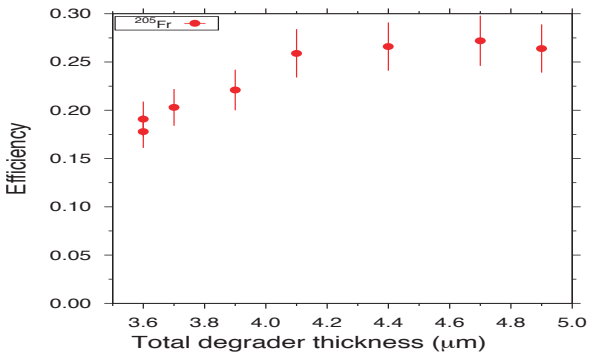

Fig. 1. Combined stopping and extraction efficiency for ^{205}Fr as a function of degrader thickness. The thickness was varied by rotating the degrader. Gas cell was operated at room temperature.

*1 RIKEN Nishina Center
*2 Department of Physics, University of Tsukuba
*3 Department of Chemistry and BioChemistry, New Mexico State University

Of perhaps greater interest was the stopping and extraction efficiency for shorter-lived isotopes. This was studied with a Tantalum target using the reactions ^{181}Ta(^{40}Ar,p4n)^{216}Th and ^{181}Ta(^{40}Ar,4n)^{217}Pa to produce species with $T_{1/2}$ of 26 ms and 3.5 ms, respectively. The α-decay spectra seen after the gas cell using a chopped beam and measuring decays during "beam off" are shown in Fig. 2. The red spectrum was measured by quickly pulsing the linac beam while the green spectrum was measured with longer period pulses. For the long period beam pulses, short-lived isotopes extracted during "beam on" decay prior to "beam off" and are suppressed.

For these beams, having higher-Z and lower energy than ^{205}Fr, the degrader was inoptimally thick. However, we were able to set lower limits on the stopping and extraction efficiencies. For the short-lived ^{216}Th, we were able to achieve ∼15% combined efficiency, while for the extremely short-lived ^{217}Pa ∼12%.

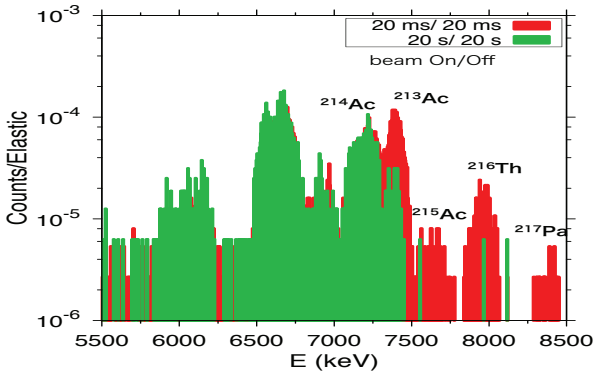

Fig. 2. α-decay spectra seen on silicon detector after the gas cell. Pulsing the linac beam with a short period, a strong suppression of short-lived isotopes was observed.

These results were obtained with the gas cell operated at room temperature; we believe that using cryogenic temperatures should provide further improvements by reducing the possibility of charge exchange with gas impurities and reducing the rate of diffusion of the ion cloud as it transits the length of the gas cell. Even with the efficiencies reported herein, it should be possible to perform precision mass measurements of even trans-Uranium isotopes with exceedingly low production rates. First such measurements are planned to take place within calendar year 2015.

References

1) F. Arai et al., this volume
2) P. Schury et al., Nuclear Instr. and Methods in Physics Research B 335 (2014) 39-53

Electron scattering spectrometer for the SCRIT project

K. Tsukada,[*1,*2] A. Enokizono,[*1,*3] K. Kurita,[*1,*3] S. Matsuo,[*1,*3] Y. Moriya,[*1,*2] T. Ohnishi,[*1] T. Suda,[*1,*2] T. Tamae,[*1,*2] M. Togasaki,[*1,*3] T. Tsuru,[*1,*2] R. Toba,[*1,*4] K. Yamada,[*1,*3] S. Yoneyama,[*1,*2] and M. Wakasugi[*1]

We have developed the magnetic spectrometer system[1], WiSES (Window-frame Spectrometer for Electron Scattering), for electron scattering on short-lived nuclei at the SCRIT electron scattering facility. The WiSES consists of a dipole magnet[2,3], FDC(Front Drift Chamber), RDC(Rear Drift Chamber)[4], plastic scintillator hodoscope, and a helium bag. Figure 1 shows a schematic view of the WiSES and SCRIT system[5]. The layer configulation of the drift chambers is XX'XX' for FDC and VV'UU'XX'VV'UU' for RDC. The gas of drift chambers are He+CH_4 (50:50) at this time. The combination of FDC and RDC enables reconstruction of the trajectory of electrons in the magnetic field and estimation of the momentum. Our goal of momentum resolution is $\delta p/p \sim 1\times10^{-3}$ for 300 MeV electron. The solid angle of the spectrometer is evaluated to be 83 msr by a simulation. The plastic scintillator hodoscope is used to generate trigger signals. A detail of the data acquisition system is reported elsewhere[6]. The helium bag made of vinyl sheets of thickness 30 μm is installed between FDC and RDC to reduce the multiple scattering of electrons.

In December 2014, a commissioning experiment was carried out to evaluate the performance of the WiSES and the luminosity monitor system[7]. A tungsten wire of diameter 50 μm was mounted in the SCRIT, and its position could be controlled remotely; this wire was used as a target. Because the differential cross section of electron elastic scattering on the tungsten target is well known, we can estimate the performance of the spectrometer by checking the reproducibility of the differential cross sections. In Fig. 2, preliminary results for the electron beam energy at 150 MeV are shown. Electrons elastically scattered from the tungsten wire are found as a peak in the vertex point and momentum distribution, and their resolutions are evaluated to be approximately 10 mm and 6×10^{-3}, respectively. These resolutions will be improved by further analysis. The obtained angular distribution is well reproduced by a simulation in which the differential cross section of the elastic scattering on the tungsten target is estimated by a DWIA calculation.

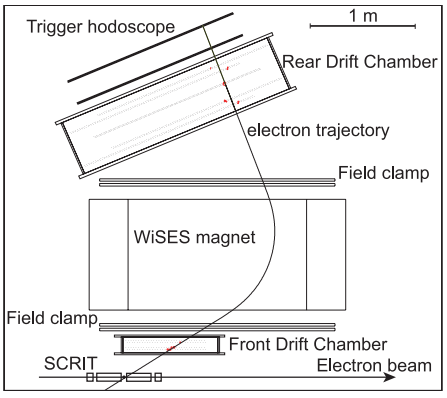

Fig. 1. Schematic view of the WiSES. A trajectory between FDC and RDC was reconstructed by a Runge-Kutta calculation. The space between FDC and RDC was filled with helium.

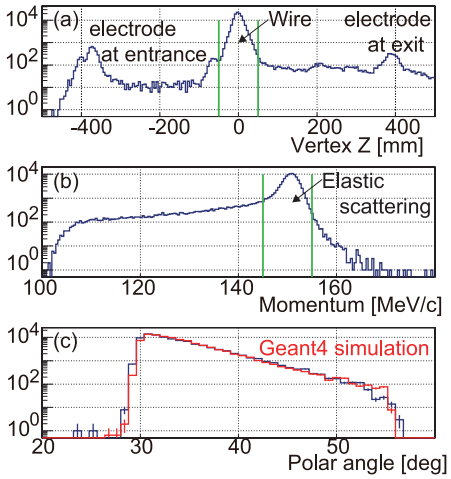

Fig. 2. Preliminary results for the electron energy at 150 MeV. (a) Vertex point distribution along the beam line. A clear peak of electrons scattered from the tungsten wire can be seen. (b) Momentum distribution of electrons from the tungsten wire. A clear peak corresponding to the elastic scattering can be seen. (c) Polar angle distribution of the elastically scattered electrons. The red line shows the simulation using the differential cross section estimated by a DWIA calculation.

*1 RIKEN Nishina Center
*2 ELPH, Tohoku University
*3 Department of Physics, Rikkyo University
*4 Department of Electrical Engineering, Nagaoka University of Technology

References

1) T. Adachi *et al.*: Accel. Prog. Rep. **45**, 144 (2012)
2) T. Suda *et al.*: Accel. Prog. Rep. **46**, 184 (2013)
3) T. Tamae *et al.*: Accel. Prog. Rep. **47**, 196 (2014)
4) S. Matsuo *et al.*: in this report.
5) M. Wakasugi *et al.*: Accel. Prog. Rep. **43**, 1 (2010)
6) A. Enokiozono *et al.*: in this report.
7) S. Yoneyama *et al.*: in this report.

Measurement of isochronism using α-source for the Rare RI Ring

Y. Abe,[*1,*2] Y. Yamaguchi,[*1] M. Wakasugi,[*1] T. Uesaka,[*1] A. Ozawa,[*2]
F. Suzaki,[*1,*3] D. Nagae,[*2] H. Miura,[*3] and T. Yamaguchi[*3]

The Rare RI Ring was constructed at the RIBF to measure the masses of nuclei pertinent to the r-process.[1] We performed an offline machine study using α-source (^{241}Am). The α-source was placed in the ring on the central orbit at the R-MD1 area after the first sector as shown in Fig. 1. First, we tried transporting the α particle in the ring and succeeded. Next, to confirm the isochronous field of the ring, we measured TOF after one revolution using two detectors. One was a carbon foil detector like a circulation detector of this ring,[2] and the other was a plastic scintillator. The carbon foil detector consisted of thin carbon foil (60 μg/cm^2 thickness) and three wired plates. A schematic view of these detectors is shown in Fig. 1. The carbon foil detector was placed in front of the source, whereas the plastic scintillator was placed behind the source to detect the α particle after one revolution. A delayed signal from the carbon foil detector was used as a stop signal of TOF, and a signal from the plastic scintillator was used as a start signal.

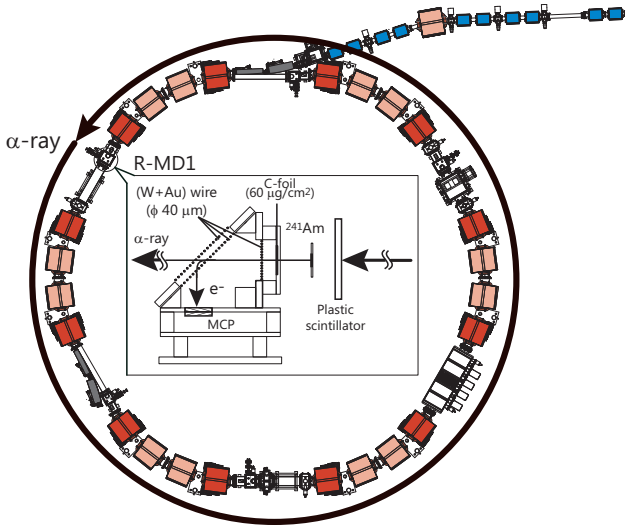

Fig. 1. Setup of α-source and detectors. The carbon foil detector was placed in front of the α-source, whereas the plastic scintillator was placed behind.

The obtained TOF was 4643.5(6) ns which corresponds to an α particle with 0.87 MeV/nucleon. This energy is equivalent to the value calculated from energy loss by the cover of the source and the carbon foil. In addtion we measured TOF while changing the radial gradient of the magnetic field using 10 trim coils.

*1 RIKEN Nishina Center
*2 Institute of Physics, University of Tsukuba
*3 Department of Physics, Saitama University

Figure 2 shows the results of measurement and simulation by MOCADI.[3] To evaluate the optimum gradient value, we fitted the results with a parabolic function. The obtained mean value of 0.207(2) is in very good agreement with the simulation result of 0.205. This shows that our isochronous field calculation was correct and an isochronous field is formed using trim coils. The final observed width had 0.61 ns standard deviation. However, the width was limited by the timing resolution of the detectors. Therefore, the achieved isochronism of the ring was less than 1.3×10^{-4}.

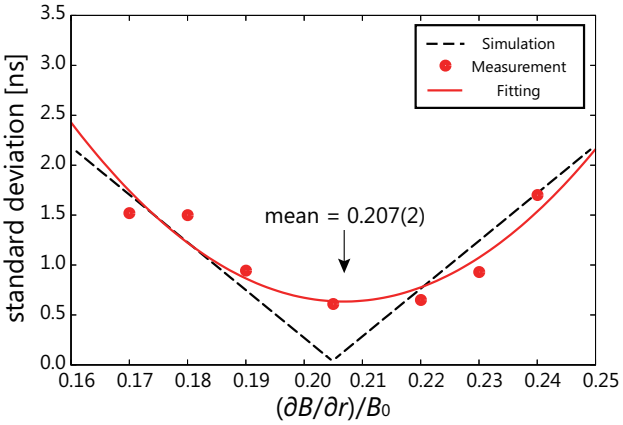

Fig. 2. Results of measurement (closed circles) and comparison with simulation (dashed line). The solid line is the result of fitting with a parabolic function.

It is seen from our results in Fig. 2 that the standard deviation was saturated. This saturation was caused by the limitation of timing resolution of the detectors.

Currently, we are testing an injection system to store the α particle from the source for several revolutions. If we can measure the TOF after several revolutions, we would be able to confirm the isochronism with higher order even though the timing resolution of the detectors is limited. Furthermore we will perform a machine study using a heavy-ion beam in the next fiscal year.

References

1) Y. Yamaguchi et al.: RIKEN Accel. Prog. Rep. 46 xiv (2013)
2) Y. Abe et al.: JPS Conf. Proc. **1**, 013059 (2014)
3) N. Iwasa et al.: Nucl. Instrum. Methods B **126**, 284 (1997)

Time-stamping system for nuclear physics experiments at RIKEN RIBF†

H. Baba,[*1] T. Ichihara,[*1] T. Ohnishi,[*1] S. Takeuchi,[*1] K. Yoshida,[*1] Y. Watanabe,[*1] S. Ota,[*2] S. Shimoura,[*2] and K. Yoshinaga[*3]

At the RIKEN RIBF, a new time-stamping system has been developed for nuclear physics experiments. The time-stamping function is implemented in a logic unit for programmable operation (LUPO)[1]. One of the remarkable features is that it can attach the time-stamp information to an existing CAMAC/VME based DAQ system in RIBF[2]. The timing resolution of the time-stamping system is 10 ns, which is sufficient to find the event correlation between separated DAQ systems. This specification enables us to merge obtained data separately on an event-by-event basis after the measurement.

The proposed time-stamping system was installed at RIKEN RIBF for use in β-decay experiments[3–6]. In these experiments, a beam line detector set, a silicon detector array, and a germanium detector array were used. Since the triggers for these detectors are independent of each other, three separate DAQ systems were used. In this report, the results for the DAQ systems for the beam line detector set (BeamDAQ) and the silicon detector array (SiDAQ) are described. The beam line detector set is triggered by RI-beams, i.e., beam events. The silicon detector array is triggered by both implanted isotopes and β rays, i.e., beam events and β-decay events. For the silicon detector array, when both SiDAQ and BeamDAQ are triggered at the same time, the event can be identified as a beam event. On the other hand, if SiDAQ is triggered but BeamDAQ is not, the event is a β-decay event. In order to determine the relationship between the number of actually generated physics events and the number of events accepted by separate DAQ systems, the combined live time was investigated. An additional DAQ system named full-event monitor was installed to acquire the time stamps of all generated triggers. By using LUPO, trigger time stamps for each DAQ system are recorded without loss. BeamDAQ and SiDAQ store detector data together with the time stamps of accepted triggers. In contrast, the full-event monitor only accumulates time-stamp values of triggers generated for BeamDAQ and SiDAQ. The combined live times for beam events and β-decay events in the silicon detector array are determined as the ratio of the number of events identified using BeamDAQ and SiDAQ and the number of triggers recorded by the full-event monitor. Table 1 lists the measured and estimated combined live times for beam and β-decay events in the silicon detector array. The real event-occurrence rate (R) is unknown if the full-event monitor is not present. However, it is possible to estimate it by comparing the observed and simulated DAQ acceptance rates (R_{acc}) when a trigger is accepted by both BeamDAQ and SiDAQ. Monte Carlo simulation was performed in order to estimate DAQ acceptance rates from a DAQ transaction time, which can be obtained using the scaler circuit in the experiment. The transaction times of BeamDAQ and SiDAQ were 210 and 108 μs, respectively. From the results of the Monte Carlo simulation, the assumed beam-event and β-decay event rates (R) are calculated to fit the observed DAQ acceptance rate (R_{acc} = 82.2 events/s). These results indicate that for beam and β-decay events, the accuracy of the Monte Carlo simulation was good. Within this simulation, the systematic error in the simulated event rates was 0.2%.

Table 1. Event rates and combined live times for beam and β decay events in the silicon detector array.

Beam events	R (events/s)	P_L (%)
Measured	87.5	94.0
Estimated	87.3	94.0
β decay events	R (events/s)	P_L (%)
Measured	368	95.3
Estimated	369	95.3

In summary, a time-stamping system has been introduced in the RIKEN RIBF. This system is particularly useful for β-decay experiments. Although the combined live time for separate DAQ systems is not straightforward to determine, it can be measured by installing a full-event monitor. It was found that Monte Carlo simulations can estimate the true event rate with a high degree of accuracy.

References
1) H. Baba et al.: RIKEN Accel. Prog. Rep. **43**, 222 (2010).
2) H. Baba et al.: Nucl. Instr. Meth. A **616**, 65 (2010).
3) H. Watanabe et al.: Phys. Lett. B **696**, 186 (2011).
4) H. Watanabe et al.: Phys. Lett. B **704**, 270 (2011).
5) S. Nishimura et al.: Phys. Rev. Lett. **106** 052502 (2011).
6) T. Sumikama et al.: Phys. Rev. Lett. **106** 202501 (2011).

† Condensed from the article in Nucl. Instr. and Meth. A 777, 75 (2015)

*1 RIKEN Nishina Center
*2 Center for Nuclear Study, University of Tokyo
*3 Tokyo University of Science

First chemical synthesis and investigation of $Sg(CO)_6$†

J. Even, [*1] A. Yakushev,[*2] Ch.E. Düllmann,[*1,*2,*3] H. Haba,[*4] M. Asai,[*5] T.K. Sato,[*5] H. Brand,[*2] A. Di Nitto,[*3] R. Eichler,[*6,*7] F.L. Fan,[*8] W. Hartmann,[*2] M. Huang,[*4] E. Jäger,[*2] D. Kaji,[*4] J. Kanaya,[*4] Y. Kaneya,[*5] J. Khuyagbaatar,[*1] B. Kindler,[*2] J.V. Kratz,[*3] J. Krier,[*2] Y. Kudou,[*4] N. Kurz,[*2] B. Lommel,[*2] S. Miyashita,[*5, *9] K. Morimoto,[*4] K. Morita,[*4, *10] M. Murakami,[*4,*11] Y. Nagame,[*5] H. Nitsche,[*12, *13] K. Ooe,[*11] Z. Qin,[*8] M. Schädel,[*5] J. Steiner,[*2] T. Sumita,[*4] M. Takeyama,[*4] K. Tanaka,[*4] A. Toyoshima,[*5] K. Tsukada,[*5] A. Türler,[* 6, *7] I. Usoltsev, [*6, *7] Y. Wakabayashi,[*4] Y. Wang,[*8] N. Wiehl,[*1, *3] S. Yamaki,[*4, *14]

Gas phase chemical studies of the superheavy elements have been limited to simple inorganic compounds so far.[1)] Due to challenging experimental conditions, access to other compound classes was limited. With the combination of physical preseparation with gas-phase chemistry techniques, parts of the experimental limitations could be overcome.[2-3)]

We succeeded in the synthesis of the first carbonyl complex of a superheavy element, namely seaborgium hexacarbonyl ($Sg(CO)_6$), at the GAs-filled Recoil Ion Separator GARIS[4)]. $Sg(CO)_6$ has been predicted to be stable[5)] and its adsorption behavior on SiO_2 surface is expected to be very similar to that of $W(CO)_6$[6)]. We therefore investigated $Sg(CO)_6$ along with $W(CO)_6$. Short-lived ^{164}W, and ~10-s ^{265}Sg were synthesized in the reactions $^{144}Sm(^{24}Mg,4n)^{164}W$ and $^{248}Cm(^{22}Ne,5n)^{265}Sg$. The evaporation residues (EVRs) were separated from the primary beam and lighter transfer products within GARIS. At the focal plane of GARIS, a recoil transfer chamber (RTC) was installed. The EVRs passed the entrance window of the RTC and were thermalized in a He / CO atmosphere (~600 mbar) in the RTC. The free single ions of W and Sg reacted with CO, forming volatile complexes[7)]. The RTC was flushed continuously, transporting volatile compounds through a 10-m long capillary to the Cryo Online Multidetector for Physics and Chemistry of the Transactinides COMPACT[8)], a thermochromatography detector array. The chromatography channel is formed by 32 pairs of silicon PIN diodes covered with a SiO_2 surface, kept at temperatures between 22 °C and -140°C. Volatile compounds adsorb at a certain temperature on the detector surface. The deposition pattern compared with Monte Carlo Simulations MCS, which allowed determining the adsorption enthalpy $-\Delta H_{ads}$. W as well as Sg were transported to COMPACT, hence, formed volatile compounds with the CO. In total 15 decay chains assigned to the decay of ^{265}Sg plus three uncorrelated fission event assigned to originate from members of the ^{265}Sg decay chain were observed under almost background free conditions at a total beam integral of $1.52 \cdot 10^{19}$. Both, the W as well as the Sg complexes deposited mainly in the last third of the detector (see Fig. 1). The W chromatograms are in agreement with former experiments reported in [3)], where the transported species was assigned to $W(CO)_6$. The Sg species shows the same adsorption behavior on SiO_2 as $W(CO)_6$, which strongly supports the assignment to $Sg(CO)_6$ [7)]. The experimental distribution and MCS are shown in Figure 1.

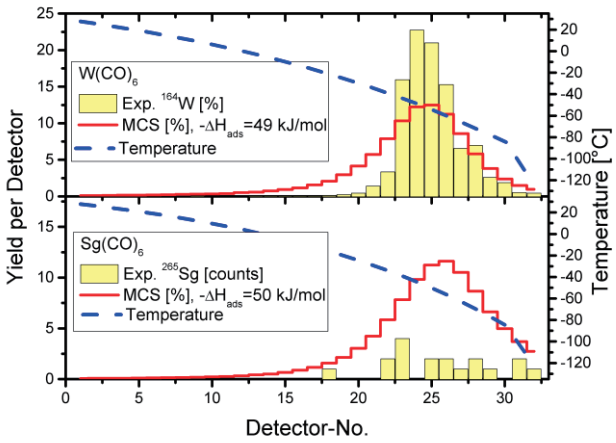

Fig. 1. Distribution of ^{164}W (upper graph) and ^{265}Sg (bottom graphic). ^{164}W was measured at 1L/min; the lower panel shows a combined chromatogram of all observed Sg events (flow rates between 1 L/min and 2.2 L/min). The black curve shows the result of the MCS (after [7]).

† Condensed from the article in Even et al. Science 345, 1491 (2014).

*1 Helmholtz-Institut Mainz.
*2 GSI Helmholtzzentrum für Schwerionenforschung GmbH.
*3 Johannes Gutenberg-Universität Mainz.
*4 Nishina Center for Accelerator-Based Science, RIKEN.
*5 Advanced Science Research Center, JAEA.
*6 University of Berne.
*7 Paul Scherrer Institute.
*8 Institute of Modern Physics Lanzhou; Chinese Academy of Sciences.
*9 Hiroshima University.
*10 Kyushu University.
*11 Niigata University.
*12 University of California, Berkeley.
*13 Lawrence Berkeley National Laboratory,.
*14 Saitama University.

References

1) A. Türler and V. Pershina: Chem. Rev. **113**, 1237 (2013).
2) Ch.E. Düllmann: Eur. Phys. J. D **45**, 75 (2007).
3) J. Even et al.: Inorg. Chem. **51**, 6431 (2012).
4) K. Morita et al.: Nucl. Instr. Meth. B **70**, 220 (1992).
5) C.S. Nash, B.E. Bursten: J. Am. Chem. Soc. **121**, 10830 (1999).
6) V. Pershina, J. Anton: J. Chem. Phys. **138**, 174301–6 (2013).
7) J. Even et al. Science **345**, 1491 (2014).
8) A. Yakushev et al., Inorg. Chem. **53**, 1624 (2014).

II. RESEARCH ACTIVITIES I
(Nuclear, Particle and Astro-Physics)

1. Nuclear Physics

Long-lived isomer in ^{126}Pd†

H. Watanabe*1,*2 for the RIBF60&62R1 Collaboration

Spectroscopic studies of ^{126}Pd have been performed at the RIBF facility. Neutron-rich nuclei below ^{132}Sn were produced using in-flight fission of a ^{238}U^{86+} beam at 345 MeV/nucleon with the intensity ranging from 7 to 12 pnA, impinging on a beryllium target with a thickness of 3 mm. The nuclei of interest were separated and identified through the BigRIPS separator and the following ZeroDegree spectrometer. A total of 5.3×10^4 ^{126}Pd fragments were implanted into a highly segmented active stopper, named WAS3ABi, which consisted of eight double-sided silicon-strip detectors (DSSSD) stacked compactly. The DSSSDs also served as detectors for electrons following β-decay and internal conversion (IC) processes. Gamma rays were detected by the EURICA array that consisted of twelve Cluster-type detectors.

The decay schemes of the isomeric states in ^{126}Pd are exhibited in Fig. 1. For ^{126}Pd, the $J^\pi = (5^-)$ and (7^-) isomers at 2023 and 2110 keV, respectively, were reported in Ref.[1]. In the present work, the γ rays below these isomers, except for the 86-keV line, have been also observed in coincidence with electrons that were associated with the prior implantation of ^{126}Pd, as demonstrated in Fig. 2(a). With gates on these γ rays, a prominent peak can be found in an electron spectrum [marked with "I" in the inset of Fig. 2(b)]; this corresponds to the conversion electrons for the 86-keV, $E2$ transition ($\alpha_T = 2.374$). In Fig. 2(b), a γ-ray at 297 keV is clearly visible in addition to the γ rays below the (5^-) isomer by gating on the 86-keV IC peak. The appearance of the 297-keV peak is emphasized by taking a γ-ray time condition earlier than electron events, as is evident from the inset of Fig. 2(a), suggesting that this new γ ray precedes the highly converted 86-keV transition. Furthermore, the 297-keV γ ray is observed in coincidence with the other γ rays in ^{126}Pd [see Fig. 2(c) as an example]. Thus, the long-lived isomer can be identified at an excitation energy of 2406 keV. A peak marked with "II" in the inset of Fig. 2(b) is expected to arise from the conversion electrons for the 297-keV transition, being most likely of an $E3$ character ($\alpha_T = 0.1197$).

The half-life ($T_{1/2}$) derived from the time distribution of the 297-keV γ ray is in agreement with that of the 693-keV one within experimental errors, as illustrated in the insets of Fig. 2(c). Similar half-lives have been observed for six other γ rays; these transitions are expected to belong to high-spin states in ^{126}Ag which are populated through the β decay of the long-lived isomer in ^{126}Pd. Therefore, the half-life is determined to be 23.0(8) ms by taking a weighted average of the respective values. Based on the observed mutual coincidence [see Fig. 2(d)] and γ-ray intensities, we propose the decay scheme from the long-lived isomer in ^{126}Pd to the high-spin states in ^{126}Ag as shown in Fig. 1.

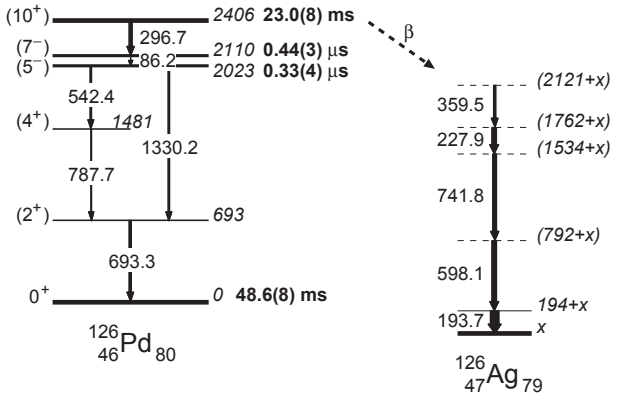

Fig. 1. Decay schemes of the $J^\pi = (10^+)$ isomer in ^{126}Pd.

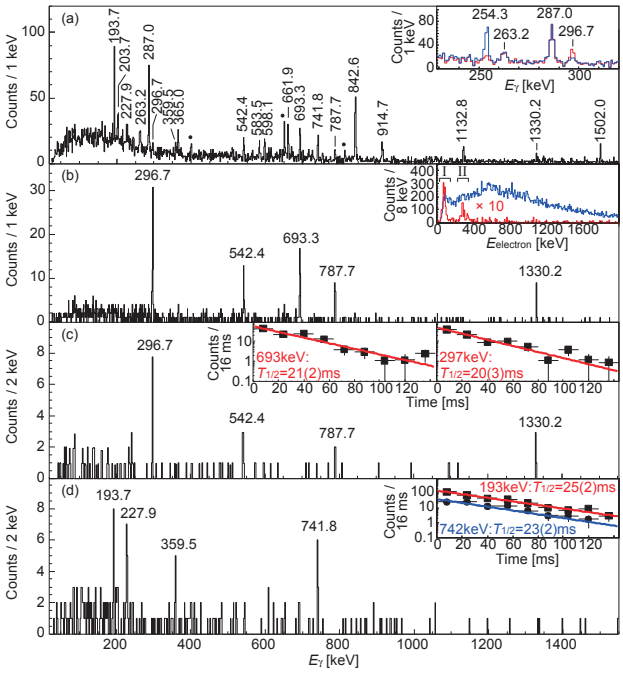

Fig. 2. Gamma-ray spectra measured with various gate conditions within 50 ms after the ^{126}Pd implantation.

† Condensed from the article in Phys. Rev. Lett. **113**, 042502 (2014)

*1 RIKEN Nishina Center
*2 IRCNPC, School of Physics and Nuclear Energy Engineering, Beihang University

References

1) H. Watanabe et al.: Phys. Rev. Lett. **111**, 152501 (2013).

Yrast 6^+ Seniority Isomers of ^{136,138}Sn†

G.S. Simpson,[*1,*2,*3] G. Gey,[*3,*4,*5] A. Jungclaus,[*6] J. Taprogge,[*6,*7,*5] S. Nishimura,[*5] K. Sieja,[*8] P. Doornenbal,[*5] G. Lorusso,[*5] H. Sakurai,[*5,*10] P.-A. Söderström,[*5] T. Sumikama,[*9] Z.Y. Xu,[*10] on behalf of the RIBF-85 collaboration

The shell model plays a key role in allowing a microscopic description of many of the properties of atomic nuclei. Its two ingredients are single-particle energies and effective nucleon-nucleon interactions. Experimental studies of semi-magic Sn nuclei beyond the doubly magic nucleus ^{132}Sn provide information that allows the neutron-neutron part of effective interactions for the $N = 82 - 126$ valence space to be tested and optimized. More generally, such studies provide a key benchmark for the methods used to construct effective interactions in a heavy-mass region far from stability. Currently there is little experimental data on the Sn isotopes beyond the $N = 82$ shell closure, which are difficult to produce and study.

Excited states in the nuclei ^{136,138}Sn have been investigated by detecting delayed γ-ray cascades using the EURICA spectrometer[1)], which was coupled to the BigRIPS separator of the RIBF facility. These exotic nuclei were produced by the in-flight fission of a 345 MeV/nucleon ^{238}U beam. Cascades containing three delayed γ rays each were observed in coincidence with identified ^{136,138}Sn ions. The spins of the isomeric states of ^{136,138}Sn were assigned as (6^+), in analogy with a very similar delayed cascade previously reported for ^{134}Sn[2)].

The energies of the excited states of ^{134,136,138}Sn have been compared to the predictions of shell-model calculations, which used state-of-the-art realistic effective interactions. These calculations used the full $N = 82 - 126$ valence space and the effective single-particle energies were the experimental ones. The experimentally determined level energies of ^{134,136,138}Sn were all well reproduced. The $B(E2; 6_1^+ \rightarrow 4_1^+)$ values were also correctly predicted for ^{134,138}Sn, though this value was more than a factor of 5 away for ^{136}Sn, as shown in Fig. 1. Three other shell-model calculations reported in the literature, using realistic and empirical effective interactions, also failed to reproduce the $B(E2; 6_1^+ \rightarrow 4_1^+)$ value for ^{136}Sn and are off by at least a factor of 2.

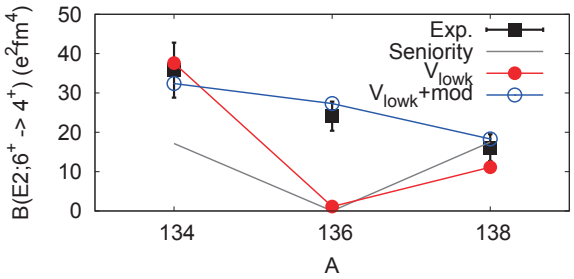

Fig. 1. Experimental (black squares) and theoretical reduced transition rates for $6_1^+ \rightarrow 4_1^+$ γ decays in $^{134-138}$Sn. The calculations used a realistic V_{low-k} interaction (red filled circles), a pairing-modified V_{low-k} interaction (blue open circles) and a pure $f_{7/2}$ seniority scheme (grey curve).

The near-constant energies of the (2_1^+), (4_1^+) and (6_1^+) states of ^{134,136,138}Sn are characteristic of dominant seniority 2 (one broken pair) excitations. The $B(E2)$ values of seniority-conserving transitions are expected to follow the shape of a symmetric positive parabola, as shown in Fig. 1. The results obtained with a realistic V_{low-k} interaction follow a similar pattern to the seniority 2 scheme. Additional shell-model calculations have been performed which allowed particle-hole excitations from the neutron $\nu 0h_{11/2}$ and proton $0g_{9/2}$ shells to the $N = 82 - 126$ and $Z = 50 - 70$ valence spaces, respectively. These allowed the influence of core polarization effects on the transition rates of the neutron-rich Sn nuclei to be examined. However, the $B(E2; 6_1^+ \rightarrow 4_1^+)$ value for ^{136}Sn was still not correctly reproduced. Reducing the energies of the $\nu 1f_{7/2}^2$ diagonal and off-diagonal matrix elements by ∼150 keV allowed the $B(E2, 6_1^+ \rightarrow 4_1^+)$ of ^{136}Sn to be correctly predicted. This shift is equivalent to a reduction in the pairing strength. The results using this pairing-modified V_{low-k} interaction are shown in Fig. 1. Similar modifications to pairing were necessary to reproduce the level schemes of ^{72,74}Ni[4)], illustrating the need for additional theoretical efforts on the construction of effective interactions.

† Condensed from the article in Phys. Rev. Lett. **113**, 132502 (2014)

*1 University of the West of Scotland
*2 SUPA
*3 LPSC, UJF, CNRS, INPG
*4 Institut Laue-Langevin
*5 RIKEN Nishina Center
*6 IEM, CSIC
*7 UAM
*8 IPHC
*9 Department of Physics, Tohoku University
*10 Department of Physics, University of Tokyo

References

1) P.A. Soderström, et al.: Nucl. Instr. Meth. B **317**, 649 (2013).
2) A. Korgul, et al.: Eur. Phys. J. A **7**, 167 (2000).
3) A. Covello, et al.: J. Phys. Conf. Ser. 267, 012019 (2011).
4) H. Grawe, et al.: Nucl. Phys. **A704**, 211 (2002).

Gamma-Spectroscopy around ^{100}Sn

D. Lubos,[*1,*2] J. Park,[*3] M. Lewitowicz,[*4] R. Gernhäuser,[*1] R. Krücken,[*3] S. Nishimura,[*2] H. Sakurai,[*5] H. Baba,[*2] B. Blank,[*6] A. Blazhev,[*7] P. Boutachkov,[*8] F. Browne,[*9,*2] I. Celikovic,[*4] P. Doornenbal,[*2] T. Faestermann,[*1] Y. Fang,[*10,*2] G. de France,[*3] N. Goel,[*8] M. Gorska,[*8] S. Ilieva,[*11] T. Isobe,[*2] A. Jungclaus,[*12] G. D. Kim,[*13] Y.-K. Kim,[*13] I. Kojouharov,[*8] M. Kowalska,[*14] N. Kurz,[*8] Z. Li,[*15] G. Lorusso,[*2] K. Moschner,[*7] I. Nishizuka,[*16,*2] Z. Patel,[*17,*2] M. M. Rajabali,[*3] S. Rice,[*17,*2] H. Schaffner,[*8] L. Sinclair,[*18,*2] P.-A. Söderström,[*2] K. Steiger,[*1] T. Sumikama,[*16] H. Watanabe,[*19] Z. Wang,[*3] J. Wu,[*12,*2] and Z. Y. Xu[*5,*2]

An experiment for studying the superallowed Gamow-Teller decay of the doubly magic nucleus ^{100}Sn was performed in June 2013 at the high-resolution separator BigRIPS of the RIBF at the RIKEN Nishina Center. A 4-mm ^{9}Be target was bombarded with a ^{124}Xe beam of 345 MeV/u at intensities up to 36.4 pnA to produce ^{100}Sn and a large cocktail[3] of its neighboring nuclei down to neutron numbers N = (Z - 2) by fragmentation. The nuclei were implanted into the WAS3ABi silicon detector that consists of 3 detectors with high granularity extended by 10 additional single-sided, seven-fold segmented detectors in a closed stack geometry to absorb the emitted β-particles at a maximum efficiency. This WAS3ABi detector was surrounded by 84 Ge- and 18 LaBr-detectors of the 4π-γ-ray spectrometer EURICA.

In order to study the branching ratios of the β-decays, derive level schemes of exotic nuclei and determine isomeric ratios as well as lifetimes of the isomers, a reliable efficiency calibration has been performed.

Owing to the special geometry of the WAS3ABi and the failure of several Ge-detectors, the calibration was performed using a $\gamma\gamma$-coincidence method. Cascading γ-transitions in ^{98}Cd, ^{94}Pd and ^{96}Pd, fed by different isomers, are available with a large number of counts. For example the delayed γ-emission in ^{98}Cd always contains a complete chain for the energies 147 keV, 198 keV, 687 keV and 1395 keV. Thus, the ratio of coincident events of a pair of transitions and the total number of events for one of them directly yields the efficiency at the corresponding energy. This method is of great advantage since the radiation, originating in the implantation region, contains the detector-specific absorption effects and it does not introduce systematic uncertainties that is usually introduced by simulation based methods. Efficiency calibrations, consistent with previous works[4], using this $\gamma\gamma$-coincidence method are shown in Fig. 1.

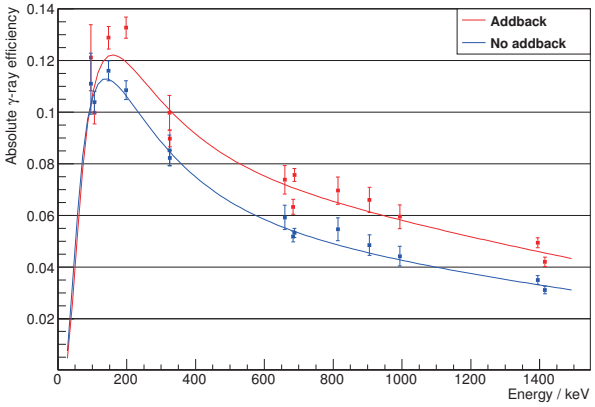

Fig. 1. Absolute γ-ray efficiency of the HPGe clusters of EURICA. γ-rays from isomers of ^{98}Cd, ^{96}Pd and ^{94}Pd, are used for the fit. Bars indicate the statistical uncertainty of the efficiencies.

In addition, greater precision of known isomer half-lives was attainable owing to high statistics in this experiment and preliminary half-lives of 8^+ and 12^+ isomers in ^{98}Cd were determined as 181^{+35}_{-25} ns and 228^{+5}_{-5} ns, respectively. This would lead to better constraints on the transition strengths for the test of modern shell models. Previously reported γ-rays in the β-decay of ^{100}Sn[1] were reproduced, allowing an unprecedented $\beta\gamma\gamma$-coincidence analysis for ^{100}In. Moreover a new high-spin isomeric state in ^{96}Cd has been observed with a half-life of about 200 ns, with a decay branch into both, the 16^+ isomer and the (10^+) state, which has a prompt decay cascade to the ground state. Further analysis is underway to finalize experimental results and compare these to large-scale shell model calculations.

*1 Physik Department E12, Technische Universität München
*2 RIKEN Nishina Center
*3 TRIUMF
*4 GANIL
*5 Department of Physics, University of Tokyo
*6 CENBG
*7 Institut für Kernphysik, Universität zu Köln
*8 GSI Darmstadt
*9 School of Comp., Eng. and Maths., Brighton University
*10 Department of Physics, Osaka University
*11 Institut für Kernphysik, TU Darmstadt
*12 IES CSIS
*13 Institute for Basic Science
*14 CERN
*15 School of Physics, Peking University
*16 Department of Physics, Tohoku University
*17 Department of Physics, Surrey University
*18 Department of Physics, University of York
*19 Department of Physics, Beihang University

References

1) C. Hinke et al.: Nature, **486**, 341 (2012).
2) B. S. Nara Singh et al.: Phys. Rev. Lett. **107**, 172502 (2011).
3) D. Lubos, RIKEN Accel. Prog. Rep.: **47** (2014)
4) K. Steiger: PhD thesis TU München (2010)

Identification of a millisecond isomeric state ^{129}Cd via the detection of internal conversion and Compton electrons†

J. Taprogge,[*1,*2,*3] A. Jungclaus,[*1] H. Grawe,[*4] S. Nishimura,[*2] P. Doornenbal,[*2] G. Lorusso,[*2] E. Nácher,[*1] G.S. Simpson,[*5] P.-A. Söderström,[*2] T. Sumikama,[*6] Z.Y. Xu,[*7] H. Sakurai,[*2,*7] H.Watanabe,[2] on behalf of the RIBF-85 and RIBF-60&62R1 collaborations

Isomeric states near nuclear shell closures are a sensitive probe to study the position of single-particle orbitals and their evolution. In the present work we have studied for the first time excited states in ^{129}Cd which decay via the emission of γ rays. The neutron-rich ^{129}Cd ions were produced at the Radioactive Isotope Beam Factory (RIBF), identified and separated in BigRIPS and then implanted in the active stopper WAS3ABi, consisting of eight closely packed DSSSD, which is surrounded by the germanium array EURICA.

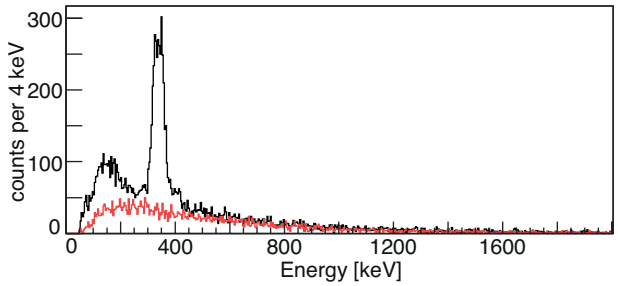

Fig. 1. Energy spectrum of the Si detector in which the ^{129}Cd ions were implanted for all decays observed in the first 10 ms (black) and from 30 to 40 ms (red) after the implantation.

Two types of events were recorded by the data acquisition system, the implantation of the ions into the active stopper WAS3ABi and their subsequent decays. In the decay of ^{129}Cd a very short-lived component in the range of a few milliseconds was observed, much shorter than the previously reported half-lives of the two β-decaying states in ^{129}Cd[1]. The inspection of the energy spectrum of the Si detector in which the ^{129}Cd ions were implanted for all decays observed in the first 10 ms after the implantation (see black curve in Fig. 1) revealed a peak structure at about 340 keV and an excess of counts below 250 keV. Those structures are not visible for decays occurring in the time interval of 30 to 40 ms after the implantation for which the smooth energy distribution expected for β decays is observed (red curve) in Fig. 1. A comparison to Monte-Carlo simulations indicated that conversion electrons and Compton electrons from transitions following the decay of a ms isomeric state in ^{129}Cd lead to the registration of decay events in the active stopper. The energies of subsequent X-rays are summed with a certain chance to the energy of the Compton electron which shifts the peak to about 340 keV. Four transitions with energies of 353, 406, 1181 and 1587 keV were observed in delayed coincidence with the implanted ^{129}Cd ions and the half-life of the new isomeric state was determined to $T_{1/2}$=3.6(2) ms from the summed time difference distributions between the observed decay events and the observation of either the 406- or 1181-keV γ rays. Furthermore, the measured intensities of both γ rays and conversion electrons were used to tentatively assign an E3 multipolarity to the primary isomeric transition with an energy of 353 keV.

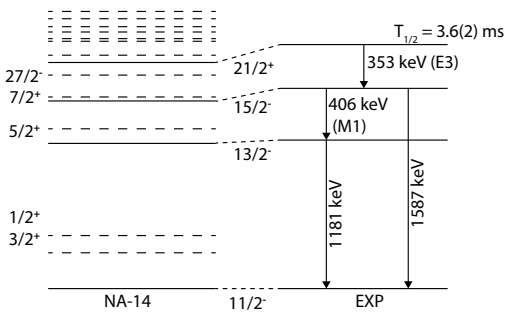

Fig. 2. Proposed decay scheme and comparison to the shell model calculations NA-14.

The deduced decay scheme is compared to shell-model calculations employing state-of-the-art realistic interactions (NA-14, same as in Ref.[2]) in Fig. 2. The dashed lines represent the predicted positions of low-lying positive parity states as well as states with positive and negative parity in the spin range $17/2 - 23/2$. None of these states is predicted to be isomeric. Based on this comparison the new state was assigned to have spin and parity $(21/2^+)$. The experimentally determined reduced transition strength of B(E3) = 0.50(3) W.u. for the $(21/2^+) \rightarrow (15/2^-)$ E3 transition is in perfect agreement with the value predicted by the SM calculations, B(E3) = 0.48 W.u..

References

1) O. Arndt *et al.*, Acta Physics Polonica B **40**, 437 (2009)
2) J. Taprogge et. al., Phys. Rev. Lett. 112, 132501 (2014).

† Condensed from the article in Phys. Lett. B, Vol. 738, 223 (2014)

*1 Instituto de Estructura de la Materia, CSIC
*2 RIKEN Nishina Center
*3 Departamento de Física Teórica, Uni. Autónoma de Madrid
*4 GSI Helmholtzzentrum für Schwerionenforschung GmbH
*5 LPSC, UJF, CNRS, INPG, Grenoble
*6 Department of Physics, Tohoku University
*7 Department of Physics, University of Tokyo

Study of shape evolution in neutron-rich Cs isotopes using β-decay spectroscopy

A. Yagi,[*1,*2] A. Odahara,[*1] R. Daido,[*1,*2] Y. Fang,[*1,*2] H. Nishibata,[*1,*2] R. Lozeva,[*3] C.-B. Moon,[*4] S. Nishimura,[*2] P. Doornenbal,[*2] G. Lorusso,[*2] P.-A. Söderström,[*2] T. Sumikama,[*5] H. Watanabe,[*6] T. Isobe,[*2] H. Baba,[*2] H. Sakurai,[*7,*2] F. Browne,[*8,*2] Z. Patel,[*9,*2] S. Rice,[*9,*2] L. Sinclair,[*10,*2] J. Wu,[*11,*2] Z.Y. Xu,[*12] R. Yokoyama,[*13] T. Kubo,[*2] N. Inabe,[*2] H. Suzuki,[*2] N. Fukuda,[*2] D. Kameda,[*2] H. Takeda,[*2] D.S. Ahn,[*2] D. Murai,[*14] F.L. Bello Garrote,[*15] J.M. Daugas,[*16] F. Didierjean,[*3] E. Ideguchi,[*17] T. Ishigaki,[*1,*2] H.S. Jung,[*18] T. Komatsubara,[*19] Y.K. Kwon,[*19] C.S. Lee,[*20] P. Lee,[*20] S. Morimoto,[*1,*2] M. Niikura,[*7,*2] I. Nishizuka,[*5] T. Shimoda,[*1] and K. Tshoo[*19]

Shape evolution in neutron-rich nuclei with the neutron number N>82 and the proton number Z>50 beyond the doubly magic ^{132}Sn nucleus have been investigated along several isotopic chains. The EURICA project[1] provides us with an opportunity to study extremely neutron-rich nuclei using β-decay and isomer-decay spectroscopy. We reported the results of the isomer-search experiment for neutron-rich Cs isotopes[2], where new isomers were found in ^{145}Cs, ^{146}Cs, ^{147}Cs, and ^{148}Cs. To understand the nuclear structure of these neutron-rich Cs isotopes in the low-spin states, we studied the β decay of neutron-rich Xe to Cs isotopes.

The neutron-rich Xe isotopes were produced through in-flight fission reaction using a 345-MeV/nucleon ^{238}U beam. Particle identification was performed using the mass-to-charge ratio (A/Q) and the atomic number deduced from the information of time-of-flight (TOF), magnetic rigidity ($B\rho$) and energy loss of fission fragments through BigRIPS and ZeroDegree Spectrometer[3]. The isotopes were implanted into a stack of five double-sided Si-strip detectors (WAS3ABi)[1]. β rays emitted from the isotopes were also detected by WAS3ABi. The parent nuclei of the β decay were identified by position correlation on the WAS3ABi between the implanted fragments and the detected β rays. γ rays emitted after the β decay were detected by the γ-ray detector array which is called EURICA[1].

*1 Department of Physics, Osaka University
*2 RIKEN Nishina Center
*3 IPHC/CNRS and University of Strasbourg
*4 Department of Display Engineering, Hoseo University
*5 Department of Physics, Tohoku University
*6 Department of Physics, Beihang University
*7 Department of Physics, University of Tokyo
*8 CEM, University of Brighton
*9 Department of Physics, University of Surry
*10 Department of Physics, University of York
*11 Department of Physics, Peking University
*12 Hong Kong University
*13 CNS, University of Tokyo
*14 Department of Physics, Rikkyo University
*15 Department of Physics, University of Oslo
*16 CEA/DAM
*17 RCNP, Osaka University
*18 Department of Physics, University of Notre Dame
*19 IBS
*20 Department of Physics, Chung-Ang University

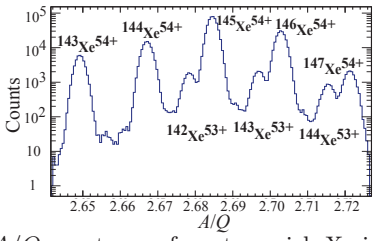

Fig. 1. A/Q spectrum of neutron-rich Xe isotopes.

Figure 1 shows a spectrum of particle identification for the Xe (Z = 54) isotopes as a function of A/Q. The fully-stripped ^{A}Xe^{54+} ions are separated from the hydrogen-like $^{A-3}$Xe^{53+} ones owing to the high A/Q resolution.

Coincidence data of β-γ and β-γ-γ with particle identification of ^{143}Xe, ^{144}Xe, ^{145}Xe, ^{146}Xe, and ^{147}Xe isotopes is analyzed. As an example, the γ-ray energy spectrum and the decay curve for the β decay of ^{145}Xe to ^{145}Cs are shown in Fig. 2. We found 11 new γ rays associated to the transitions in ^{145}Cs emitted after the β decay of ^{145}Xe. These γ-ray peaks are represented as full circles in Fig. 2. Other peaks are mostly assigned to transitions in the granddaughter ^{145}Ba nucleus. The inset in Fig. 2 shows the decay curve deduced by the time difference between the implantation of ^{145}Xe and the detection of the β rays gated on newly found 5 γ rays in ^{145}Cs. The half-life of the β decay was determined to be 197(10) ms, which is consistent with the reported one in Ref. 4. Detailed analyses are in progress.

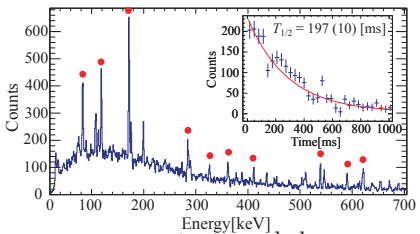

Fig. 2. γ-ray energy spectrum and decay curve of the β decay of ^{145}Xe to ^{145}Cs.

References

1) S. Nishimura et al.: Prog. Theor. Exp. Phys. **2012**, 03C006 (2012).
2) A. Yagi et al.: RIKEN Accel. Prog. Rep. **47**, 3 (2014).
3) N. Fukuda et al.: Nucl. Instrum. Methods Phys. Res. B **317**, 323 (2013).
4) U.C. Bergmann et al.: Nucl. Phys. **A714**, 21 (2003).

Shell evolution in neutron-rich Te isotopes beyond doubly magic ^{132}Sn

P. Lee,[*1] C.S. Lee,[*1] C.-B. Moon,[*2] A. Odahara,[*3] R. Lozeva,[*4] A. Yagi,[*3,*5] D.S. Ahn,[*5] H. Baba,[*5] F.L. Bello Garrote,[*15] F. Browne,[*9] R. Daido,[*3,*5] J.M. Daugas,[*5,*16] F. Didierjean, [*4] P. Doornenbal,[*5] Y. Fang,[*3] N. Fukuda,[*5] E. Ideguchi, [*17] N. Inabe,[*5] T. Ishigaki,[*3,*5] T. Isobe,[*5] H.S. Jung, [*5,*18] D. Kameda,[*5] Y.K. Kim,[*6,*19] T. Komatsubara,[*6] T. Kubo,[*5] Y.K. Kwon,[*6] G. Lorusso,[*5] S. Morimoto,[*3,*5] D. Murai,[*5,*14] M. Niikura,[*5,*8] H. Nishibata,[*3,*5] S. Nishimura,[*5] I. Nishizuka,[*5,*7] Z. Patel,[*10] S. Rice,[*10] H. Sakurai,[*5,*8] T. Shimoda,[*3] L. Sinclair,[*11] P.-A. Söderström,[*5] T. Sumikama,[*5,*7] H. Suzuki,[*5] H. Takeda,[*5] K. Tshoo,[*6] H. Watanabe,[*5,*20] J. Wu,[*5,*12] Z.Y. Xu, [*8] and R. Yokoyama [*13]

Within the context of the shell model, the nuclear structure is understood in terms of the shell orbital excitation across a large shell gap. In particular, the neutron-rich nuclei with a few valence nucleons at and near the doubly magic nuclei such as ^{132}Sn always attract attention for testing the various nuclear models in view of the rapidly changing nuclear structure with neutron numbers[1–3]. In this respect, Sb and Te isotopes, with one and two protons outside the Z=50 proton shell closure respectively, form an interesting set of nuclei to study the evolution of the nuclear structure beyond the Z=50 and N=82 shell closures. This work aims at determining the internal structures of the neutron-rich Sb and Te nuclei and observing the intrinsic nature of the nuclei such as isomerism, shape transition, and dynamic or static deformation.

The nuclei to be investigated were produced and isotope-separated with BigRIPS at the RIBF facility by the in-flight fission of a ^{238}U beam on a ^{9}Be production target at 345 MeV/nucleon. Measurements were focused on identification of $E(2^+)$ and/or $E(4^+)$ in even-even $^{138-140}$Te for investigating the ^{132}Sn core shell evolution and search for level scheme in the nuclei of interest to study the single-particle and collective features based on the β-decay level scheme. Particle identification was made by BigRIPS on the basis of the $B\rho$-ΔE-TOF method[4]. Further, subsequent β decays from the reaction products were detected after the Sb secondary beam was implanted into the active stopper, WAS^{3}ABi[5] with the EURICA array in its stopped-beam configuration[6].

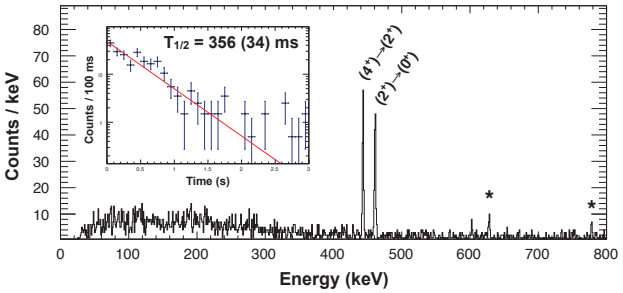

Fig. 1. Energy spectrum for β-delayed γ-decay associated with ^{138}Sb obtained by coincidence gates on lower transitions in ^{138}Te. Spectral lines marked by asterisks are newly identified γ rays in this work. The inset shows a decay curve for the β-decay of ^{138}Sb.

In the present experiment, we observed, for the first time, the β-delayed γ decay for ^{138}Sb as an example in Fig. 1. The deduced β-decay half-life for ^{138}Sb agrees well with previously reported value[7], while the half-life of ^{140}Sb needs more careful analysis to draw a conclusion. We found two new excited states above the known (4^+) state in ^{138}Te and one candidate excited state in ^{140}Te. We expect that this newly found spectroscopic information on excited states will provide crucial information on shell evolution of neutron-rich Te isotopes and pairing interaction around N=82 shell closure. Further analysis is in progress.

*1 Department of Physics, Chung-Ang University
*2 Department of Display Engineering, Hoseo University
*3 Department of Physics, Osaka University
*4 IPHC/CNRS and University of Strasbourg
*5 RIKEN Nishina Center
*6 RISP, Institute for Basic Science
*7 Department of Physics, Tohoku University
*8 Department of Physics, Tokyo University
*9 School of computing engineering and mathematics, University of Brighton
*10 Department of Physics, University of Surrey
*11 Department of Physics, University of York
*12 School of Physics, Peking University
*13 CNS, University of Tokyo
*14 Department of Physics, Rikkyo University
*15 Department of Physics, University of Oslo
*16 CEA/DAM
*17 RCNP, Osaka University
*18 Department of Physics, University of Notre Dame
*19 Department of Nuclear Engineering, Hanyang University
*20 Department of Physics, Beihang University

References

1) D. Radford et al.: Phys. Rev. Lett. **88** 222501 (2002).
2) J. Terasaki et al.: Phys. Rev. C **66** 054313 (2002).
3) F. Hoellinger et al.: Eur. Phys. J. A **6** 375 (1999).
4) N. Fukuda et al.: Nucl. Instr. Meth. B **317** 323 (2013).
5) S. Nishimura: Prog. Theor. Exp. Phys. **2001** 03C006 (2012).
6) P.-A. Söderström et al.: Nucl. Instr. Meth. Phys. B **317** 649 (2013).
7) O. Arndt et al.: Phys. Rev. C **84** 061307(R) (2011).

Decay spectroscopy of neutron-rich Z ≈ 60 isotopes

E. Ideguchi,[*1] Mn. Tanaka,[*1] R. Yokoyama,[*3] G. S. Simpson,[*2] S. Nishimura,[*4] P. Doornenbal,[*4] P.-A. Söderström,[*4] G. Lorusso,[*4] Z. Xu,[*5] J. Wu,[*4,6] T. Sumikama,[*7] N. Aoi,[*1] H. Baba,[*4] F. Bello,[*8] F. Browne,[*4,9] R. Daido,[*10] Y. Fang,[*10] N. Fukuda,[*4] G. Gey,[*2,4,11] S. Go,[*3,4] N. Inabe,[*4] T. Isobe,[*4] D. Kameda,[*4] K. Kobayashi,[*12] M. Kobayashi,[*3] T. Komatsubara,[*13] T. Kubo,[*4] I. Kuti,[*14] Z. Li,[*6] M. Matsushita,[*3] S. Michimasa,[*3] C.-B. Moon,[*15] H. Nishibata,[*10] I. Nishizuka,[*7] A. Odahara,[*10] Z. Patel,[*4,16] S. Rice,[*4,16] E. Sahin,[*8] L. Sinclair,[*4,17] H. Suzuki,[*4] H. Takeda,[*4] J. Taprogge,[*18,19] Zs. Vajta,[*14] H. Watanabe,[*20] and A. Yagi[*10]

The neutron-rich A∼150 region contains a wide variety of shape phenomena, including shape coexistence and possible static octupole and hexadecapole deformations. After the systematic studies of the excited levels of these isotopes, it was found that the nuclei beyond N = 90 or 92 in this region show characteristics of strong quadrupole deformation, such as low-energy 2^+ levels and the energy ratio of 4^+ to 2^+ levels of nearly 3.3. In addition, K isomers were systematically observed,[1] which indicates stable axial-symmetric deformation because K is a good quantum number in such nuclei and large ΔK transitions are strongly hindered.

In our studies of neutron-rich Nd isotopes through isomer spectroscopy using the EURICA spectrometer,[2] K isomers were systematically observed up to N = 100.[3] Gamma rays decaying from the isomer and those of ground-state rotational bands in low-lying levels were observed. The trend of decreasing $4^+ \rightarrow 2^+$ transition energy with increasing neutron number may indicate the development of quadrupole deformation in neutron-rich Nd isotopes.

Such development of deformation will reflect in the configuration of the ground state, and therefore, the spin and parity of neighboring odd and odd-odd nuclei will be useful for understanding the deformed structure. This can be investigated through β-γ spectroscopy.

In order to study the β decay of neutron-rich Pr isotopes, which are parent nuclei of the Nd isotope, β-γ spectroscopic measurement was performed at RIBF. The in-flight fission of ^{238}U at 345 MeV/u was employed to produce neutron-rich Pr isotopes and their neighbors. Nuclei of interest were selected and transported to the final focal plane, F11, using the BigRIPS fragment separator. These isotopes were stopped at the active stopper, WAS3ABi,[4] and β-γ spectroscopy of these isotopes was performed using the EURICA setup at F11.

Figure 1 shows a γ-ray energy spectrum after the β decay of ^{156}Pr. Gamma peaks at 67 and 155 keV are clearly identified in the spectrum, and they correspond to the previously reported $2^+ \rightarrow 0^+$ and $4^+ \rightarrow 2^+$ transitions of ^{156}Nd,[1] respectively. Based on the obtained results, we will assign the spin and parity of the parent nucleus, ^{156}Pr. In addition, γ transitions associated with the non-yrast levels of ^{156}Nd will be also investigated.

These data are currently being analyzed.

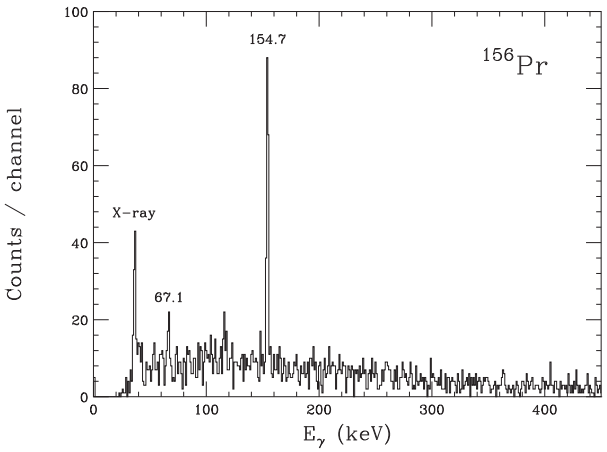

Fig. 1. Gamma-ray energy spectrum after β decay of ^{156}Pr.

References

1) G. S. Simpson *et al.*: Phys Rev. C 80, 024304 (2009).
2) S. Nishimura: Nucl. Phys. News 22, No. 3 (2012).
3) Mn. Tanaka *et al.*: RIKEN Accel. Prog. Rep. 47, xvii (2014).
4) S. Nishimura, *et al.*: RIKEN Accel. Prog. Rep. 46, 182 (2013).

*1 Research Center for Nuclear Physics, Osaka University
*2 LPSC, Université Grenoble-Alpes, CNRS/IN2P3
*3 Center for Nuclear Study, The University of Tokyo
*4 RIKEN Nishina Center
*5 Department of Physics, The University of Tokyo
*6 Peking University
*7 Department of Physics, Tohoku University
*8 University of Oslo
*9 The University of Brighton
*10 Department of Physics, Osaka University
*11 ILL
*12 Department of Physics, Rikkyo University
*13 University of Tsukuba
*14 MTA Atomki, Debrecen, Hungary
*15 Hoseo University
*16 The University of Surrey
*17 University of York
*18 Instituto de Estructura de la Materia, CSIC
*19 Universidad Autónoma de Madrid
*20 Beihang University

Investigation of octupole correlations of neutron-rich $Z \sim 56$ isotopes through β-γ spectroscopy

R. Yokoyama,[*1] E. Ideguchi,[*2] G. Simpson,[*3] Mn. Tanaka,[*2] S. Nishimura,[*4] P. Doornenbal,[*4] P.-A. Söderström,[*4] G. Lorusso,[*4] Z. Y. Xu,[*5] J. Wu,[*4,*6] T. Sumikama,[*7] N. Aoi,[*2] H. Baba,[*4] F. Bello,[*8] F. Browne,[*9,*4] R. Daido,[*10] Y. Fang,[*10] N. Fukuda,[*4] G. Gey,[*3,*4,*11] S. Go,[*1,*4] N. Inabe,[*4] T. Isobe,[*4] D. Kameda,[*4] K. Kobayashi,[*12] M. Kobayashi,[*1] T. Komatsubara,[*13] T. Kubo,[*4] I. Kuti,[*14] Z. Li,[*6] M. Matsushita,[*1] S. Michimasa,[*1] C.-B. Moon,[*15] H. Nishibata,[*10] I. Nishizuka,[*7] A. Odahara,[*10] Z. Patel,[*16,*4] S. Rice,[*16,*4] E. Sahin,[*11] L. Sinclair,[*17,*4] H. Suzuki,[*4] H. Takeda, [*4] J. Taprogge,[*18,*19] Zs. Vajta,[*14] H. Watanabe,[*20] and A. Yagi[*10]

A recent study on the existence of static octupole deformation in Ra isotopes[1] attracted much attention. The interaction between orbits with $\Delta J = \Delta L = 3$ is responsible for octupole correlations and thus the nuclei with orbits having the properties near the Fermi surface are expected to have large octupole correlations. This corresponds to Z or $N \sim 34$, 56, 88, and 134, and neutron-rich Ba isotopes ($Z = 56$, $N \sim 88$) are also expected to have large octupole correlations. The Ba isotopes have been studied and octupole bands with enhanced E1 transition rates have been discovered[2]. However, the previous study revealed that the E1 rates do not peak at $N = 88$, $^{148}Ba_{92}$ has large E1 rates comparable to as much as those of $^{144}Ba_{88}$, while $^{146}Ba_{90}$ has much smaller rates. Calculations of octupole correlation have large uncertainty and differ from each other. For example, ref[3] predicts some β_3 values in $^{150}Ba_{94}$ while ref[4] argues that the β_3 of ^{150}Ba is almost zero. Experimental investigations of neutron-rich isotopes in which no excited state is known, such as ^{150}Ba, are important to understand the strange systematics of the E1 rates of the Ba isotopes.

We performed β-γ spectroscopy on neutron-rich $Z \sim 56$ isotopes at RIBF. The neutron-rich isotopes were produced using in-flight fission of a 345MeV/nucleon ^{238}U beam. Fission fragments were identified by measuring the time-of-flight and magnetic rigidity in the second stage of BigRIPS and by measuring the energy loss by using the ion chamber at the final focal plane, F11. The secondary beam was implanted into an active stopper WAS3ABi[5], which consists of five layers of double-sided-silicon-strip detectors. The γ rays from the implanted nuclei were detected using EURICA[6], which is an array of 12-cluster Ge detectors in which each cluster consists of 7 crystals.

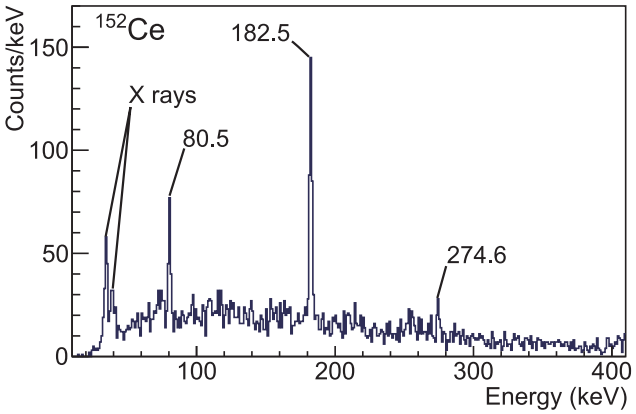

Fig. 1. Preliminary γ-ray energy spectra of the β decay from ^{152}La to ^{152}Ce. The time window is 100 ms from the ion implantation. The low-energy peaks around 34 and 39 keV are K_α and K_β X rays of Ce atoms, respectively, after the emission of conversion electrons.

Figure 1 shows the γ-ray energy and timing spectra of β-decay events after the implantation of ^{152}La. Three known γ rays were confirmed at 80.5, 182.5, and 274.6 keV; these had been reported as E2 decays from the 2^+, 4^+, and 6^+ states of the ground-state band of ^{152}Ce, respectively, by the spontaneous fission of ^{252}Cf in ref[7]. From this result for ^{152}Ce, the feasibility of the measurement and analysis has been confirmed. Analysis of Ba isotopes is in progress, and the results may help us understand the octupole correlations of nuclei.

*1 Center for Nuclear Study, The University of Tokyo
*2 Research Center for Nuclear Physics, Osaka University
*3 LPSC, Université Grenoble-Alpes, CNRS/IN2P3
*4 RIKEN Nishina Center
*5 Department of Physics, The University of Tokyo
*6 Department of Physics, Peking University
*7 Department of Physics, Tohoku University
*8 Department of Physics, University of Oslo
*9 School of Computing Engineering and Mathematics, University of Brighton
*10 Department of Physics, Osaka University
*11 ILL, Grenoble
*12 Department of Physics, Rikkyo University
*13 Department of Physics, University of Tsukuba
*14 MTA Atomki, Hungarian Academy of Science, Hungary
*15 Department of Display Engineering, Hoseo University
*16 Department of Physics, University of Surrey
*17 Department of Physics, University of York
*18 Instituto de Estructura de la Materia, CSIC
*19 Departamento de Física Teórica, Universidad Autónoma de Madrid
*20 Department of Physiscs, Beihang University

References

1) L. P. Gaffney *et. al.*: Nature 497, 199 (2013)
2) W. Urban *et. al.*: Nucl. Phys. A 613, 107 (1997)
3) P. A. Butler *et. al.*: Nucl. Phys. A 533, 249 (1991)
4) W. Nazarewicz *et. al.*: Nucl. Phys. A 429, 269 (1984)
5) S. Nishimura *et. al.*: RIKEN APR 46, 182 (2013)
6) S. Nishimura: Nucl. Phys. News 22, No.3 (2012)
7) H. J. Li *et. al.*: Phys. Rev. C 86, 067302 (2012)

Decay spectroscopy of neutron-rich rare-earth isotopes

P.-A. Söderström,[*1] P.H. Regan,[*2,*3] P. Walker,[*2] H. Watanabe,[*4,*5] J.J. Liu,[*6] P. Doornenbal,[*1] Z. Korkulu,[*7] P. Lee,[*8] G. Lorusso,[*1,*3] S. Nishimura,[*1] T. Sumikama,[*9] P. Vi,[*10] J. Wu,[*1,*11] A. Yagi,[*12] G.X. Zhang,[*5] T. Alharbi,[*13] H. Baba,[*1] F. Browne,[*14] A.M. Bruce,[*14] R. Carroll,[*2] K.Y. Chae,[*15] Zs. Dombradi,[*7] A. Estrade,[*16] N. Fukuda,[*1] C. Griffin,[*16] E. Ideguchi,[*17] N. Inabe,[*1] T. Isobe,[*1] H. Kanaoka,[*12] I. Kojouharov,[*18] F.G. Kondev,[*19] T. Kubo,[*1] S. Kubono,[*1] N. Kurz,[*18] I. Kuti,[*7] S. Lalkovski,[*2] G. Lane,[*20] E.J. Lee,[*21] G. Lotay,[*2] C.-B. Moon,[*21] I. Nishizuka,[*9] C.R. Nita,[*14,*22] A. Odahara,[*12] Z. Patel,[*2] Zs. Podolyák,[*2] O.J. Roberts,[*23] H. Sakurai,[*1,*24] H. Schaffner,[*18] C.M. Shand,[*2] H. Suzuki,[*1] H. Takeda,[*1] S. Terashima,[*5] Zs. Vajta,[*7] J.J. Valiente-Dòbon,[*25] Z.Y. Xu,[*6] and S. Yoshida[*12]

The region in the nuclear chart between $50 < Z < 82$ and $82 < N < 126$ is the largest region between traditional nuclear shells and, thus, ideal to study the evolution of collectivity and K isomerism originating from the high-j orbitals around mid-shell. Neglecting any potential sub-shell closures, the nucleus with the largest number of valence particles in this region is ^{170}Dy with proton number $Z = 66$ and neutron number $N = 104$. Accordingly it should be one of the most collective of all nuclei with $A < 208$, in its ground state. From the high degree of axial symmetry and large deformation we expect several long lived, pure K isomers. In particular, we expect a $N = 104$, $K = 6^+$ isomer in ^{170}Dy and a $N = 106$, $K = 8^-$ isomer in ^{172}Dy, similar to the $N = 102$, $K = 6^-$ isomers in ^{166}Gd and ^{164}Sm recently published[1].

A EURICA experiment was carried out in November 2014, where a 345 MeV/u ^{238}U beam impinged on a Be target and the fragments separated and identified in the BigRIPS separator and the ZeroDegree spectrometer and implanted in the WAS^{3}ABi active stopper. The experiment was carried out with two settings, 13.5 hours centering on ^{170}Dy and 45 hours centering on ^{172}Dy. The combined PID is shown in Fig. 1.

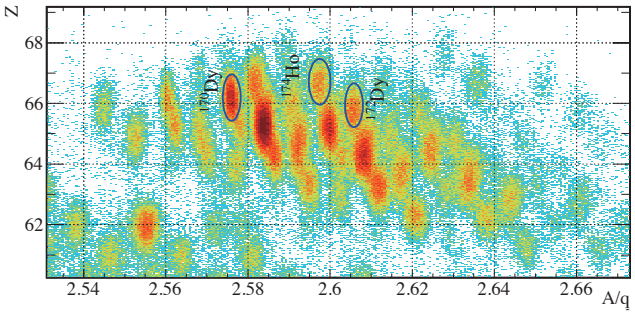

Fig. 1. Combined particle identification obtained during the two settings in the experiments.

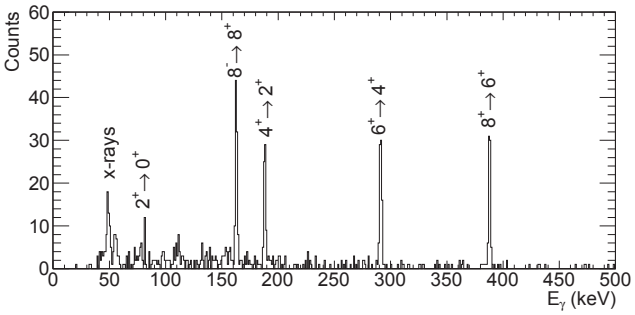

Fig. 2. Combined $\gamma\gamma$-coincidence spectrum gated on the decays from the 8^- isomer in ^{174}Er.

In Fig. 2, the decay of the known $N = 106$, $K = 8^-$ isomer in ^{174}Er[2] is shown. This shows the capabilities to measure very long lived isomers by triggering on conversion electrons in the $4^+ \rightarrow 2^+$ and $2^+ \rightarrow 0^+$ transitions, in this case populated by the β-decay of ^{174}Ho. This is not only the heaviest nucleus that has been measured in EURICA but, with a half life of 4.0 s, it is also the longest lived isomer. Besides the ^{170}Dy, ^{172}Dy, and the previously known ^{174}Er isomers, the experimental data set contains several new isomers, β-delayed γ-rays and new β-decay half-lives. All of these are currently under analysis.

*1 RIKEN Nishina Center
*2 Department of Physics, University of Surrey
*3 National Physical Laboratory, Teddington
*4 IRCNPC, Beihang University
*5 School of Physics and Nuclear Energy Engineering, Beihang University
*6 Hong Kong University
*7 INR, Hungarian Academy of Sciences
*8 Department of Physics, Chung-Ang University
*9 Department of Physics, Tohoku University
*10 Hanoi University of Science
*11 School of Physics, Peking University
*12 Department of Physics, Osaka University
*13 Department of Physics, Almajmaah University
*14 School of Computing, Engineering and Mathematics, University of Brighton
*15 Department of Physics, Sungkyunkwan University
*16 School of Physics and Astronomy, University of Edinburgh
*17 RCNP, Osaka University
*18 GSI, Darmstadt
*19 Nuclear Engineering Division, Argonne National Laboratory
*20 Department of Nuclear Physics, Australian National University
*21 Hoseo University
*22 IFIN-HH, Bucharest
*23 School of Physics, University College Dublin
*24 Department of Physics, University of Tokyo
*25 INFN-LNL, Legnaro

References

1) Z. Patel, et al.: Phys. Rev. Lett. **113**, 262502 (2014).
2) G. D. Dracoulis, et al.: Phys. Rev. C **79**, 061303 (2009).

Rotational level structure of sodium isotopes inside the "Island of Inversion" †

P. Doornenbal,[*1] H. Scheit,[*1,*2] S. Takeuchi,[*1] Y. Utsuno,[*3] N. Aoi,[*1] K. Li,[*1,2] M. Matsushita,[*1,*4] D. Steppenbeck,[*1] H. Wang,[*1,*2] H. Baba,[*1] E. Ideguchi,[*5] N. Kobayashi,[*6] Y. Kondo,[*6] J. Lee,[*1] S. Michimasa,[*5] T. Motobayashi,[*1] T. Otsuka,[*5] H. Sakurai,[*1] M. Takechi,[*1] Y. Togano,[*1] and K. Yoneda[*1]

The study of neutron-rich Ne, Na, and Mg nuclei around the breakdown of the $N = 20$ neutron magic number, an area in the Segré chart termed "Island of Inversion"[1] has provided a wealth of information on the evolution of nuclear shell structure away from the valley of β stability. Due to its location in the proximity of the neutron drip-line, accessing the "Island of Inversion" is an experimental challenge. In this paper, we report on the first γ-ray spectroscopy performed for the $N = 23, 24$ sodium isotopes ^{34,35}Na and a new transition in ^{33}Na. For the latter nucleus, previous measurements suggested that the observed two transitions originate from a $7/2^+_1 \rightarrow 5/2^+_1 \rightarrow 3/2^+_{g.s.}$ cascade and the energy ratio was found to be close to an ideal $K = 3/2$ rotational band in the strong coupling limit[2].

A ^{48}Ca beam with an average intensity of 70 particle nA was accelerated by the Superconducting Ring Cyclotron to 345 MeV/u and incident on a 15 mm thick beryllium production target. A combination of two magnetic dipoles and a 15 mm thick aluminum degrader was utilized to filter a ^{36}Mg secondary beam with the BigRIPS fragment separator[3] by applying the $B\rho - \Delta E - B\rho$ method. For further purification, a second aluminum degrader of 5 mm thickness was inserted at the dispersive focal point of the second BigRIPS stage. After passing BigRIPS, the secondary beams were incident on 2.54 g/cm^2 carbon and 2.13 g/cm^2 CH_2 (polyethylene) reaction targets, respectively. BigRIPS was operated with its full momentum acceptance of ±3% and the average intensity of ^{36}Mg was 90 particles per second. Gamma-rays emitted in coincidence with the secondary reactions were detected with the DALI2 array[4], which was composed of 186 large-volume NaI(Tl) detectors. The secondary reaction products were identified with the ZeroDegree Spectrometer[3].

In the present work, a third γ-ray transition was observed for ^{33}Na at 760(13) keV in addition to the two known ones, and forms a doublet with the $7/2^+_1 \rightarrow 5/2^+_1$ decay. For the odd-odd nucleus ^{34}Na, a single γ-ray transition was observed at 451(7) keV, while the energy spectrum of ^{35}Na exhibited transitions at 373(5) and 641(16) keV. The level structure of the odd-even sodium isotopes was found to be well described by the SDPF-M effective interaction[5].

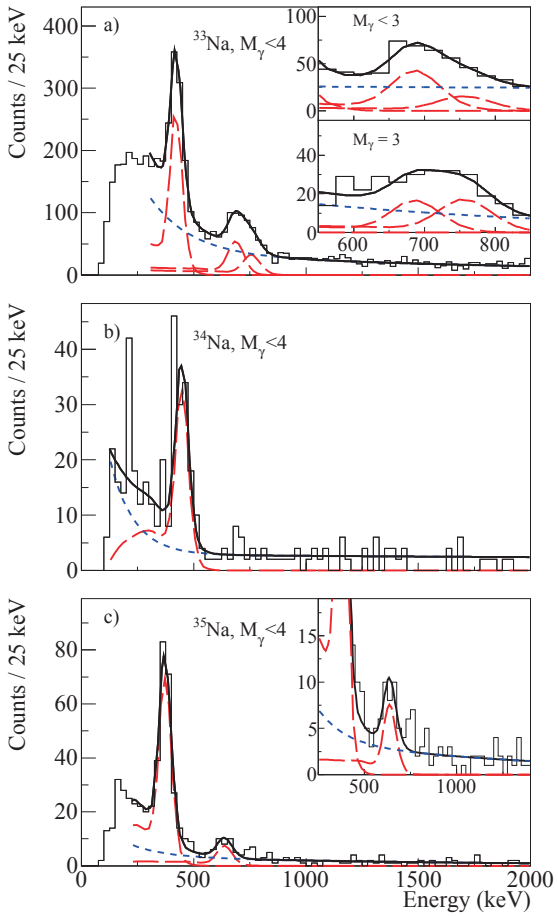

Fig. 1. Doppler corrected γ-ray spectra in coincidence with ^{33}Na a), ^{34}Na b), and ^{35}Na c). The analysis was restricted to event with aγ-ray multiplicity M_γ of less than 4.

† Condensed from the article in Prog. Theor. Exp. Phys. 2014, 053D01 (2014).

*1 RIKEN Nishina Center
*2 State Key Laboratory of Nuclear Physics and Technology, Peking University
*3 Advanced Science Research Center, Japan Atomic Energy Agency
*4 Department of Physics, Rikkyo University
*5 Center for Nuclear Study, University of Tokyo
*6 Department of Physics, Tokyo Institute of Technology

References

1) E. K. Warburton *et al.*, Phys. Rev. C 41, 1147 (1990).
2) A. Gade *et al.*, Phys. Rev. C 83, 044305 (2011).
3) T. Kubo *et al.*, Prog. Theor. Exp. Phys. 2012, 03C003 (2012).
4) S. Takeuchi *et al.*, Nucl. Instr. Meth. A 763, 596 (2014).
5) Y. Utsuno *et al.*, Phys. Rev. C 60, 054315 (1999).

In-beam γ-ray spectroscopy of ^{50}Ar

D. Steppenbeck,[*1] S. Takeuchi,[*1] N. Aoi,[*2] P. Doornenbal,[*1] M. Matsushita,[*3] H. Wang,[*1] H. Baba,[*1] S. Go,[*3] J. Lee,[*1] K. Matsui,[*4] S. Michimasa,[*3] T. Motobayashi,[*1] D. Nishimura,[*5] H. Sakurai,[*1,*4] Y. Shiga,[*6] P.-A. Söderström,[*1] T. Sumikama,[*7] R. Taniuchi,[*4] J. J. Valiente-Dobón,[*8] and K. Yoneda[*1]

Owing to the advent of intense radioactive isotope beams over recent years, it has become possible to study the structures of nuclei with large neutron-to-proton ratios using techniques including in-beam γ-ray spectroscopy and decay spectroscopy. One of the focal points of such studies has been the evolution of nuclear shell structure in exotic radioisotopes, where the nuclear 'magic' numbers in stable systems have been shown to deviate from their usual values. One such example is the onset of the new neutron magic number $N = 16$ in exotic oxygen. On the contrary, the disappearance of the standard magic number $N = 28$ has been investigated in ^{42}Si. In the neutron-rich fp shell, development of a new subshell closure at $N = 32$ has been reported in Ca[1–3], Ti[4,5], and Cr[6,7] isotones, and more recently, a sizable subshell gap at $N = 34$ was reported in ^{54}Ca[8].

In the present study, the low-lying structure of ^{50}Ar ($Z = 18$) was investigated using multi-nucleon removal reactions from a fast radioactive beam containing ^{54}Ca, ^{55}Sc, and ^{56}Ti, among other constituents, with the technique of in-beam γ-ray spectroscopy, in order to gain further insight on the magnitude of the $N = 32$ subshell closure at $Z < 20$. The secondary beam was created using projectile fragmentation of ^{70}Zn^{30+} ions at 345 MeV/u and products were identified on an event-by-event basis using the BigRIPS separator. A 10-mm-thick ^{9}Be reaction target was placed at the eighth focal plane of BigRIPS to induce nucleon removal reactions and a high efficiency γ-ray detector array[9] (DALI2) was employed to measure transitions from nuclear excited states populated by the reactions. Reaction products were identified by the ZeroDegree spectrometer; the particle identification plot for Ar isotopes is provided in Fig. 1. Data acquisition was triggered by the arrival of an ion at the end of ZeroDegree measured in coincidence with at least one γ ray in DALI2. Data were recorded to disk for offline analysis over a time period of approximately two days.

The Doppler-corrected γ-ray energy spectrum, deduced from the sum of the ^{9}Be(^{54}Ca,^{50}Ar+γ^n)X, ^{9}Be(^{55}Sc,^{50}Ar+γ^n)X, and ^{9}Be(^{56}Ti,^{50}Ar+γ^n)X multi-nucleon removal reactions ($n \geq 1$), is displayed in Fig. 2.

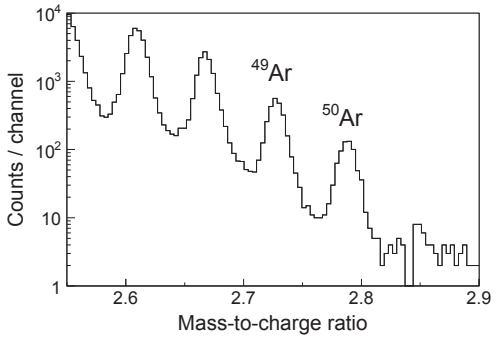

Fig. 1. Particle identification plot (A/q) for Ar isotopes measured using the ZeroDegree spectrometer.

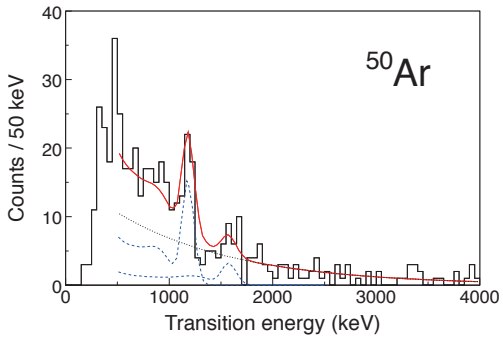

Fig. 2. (colour online) Doppler-corrected γ-ray energy spectrum for ^{50}Ar. The black dotted line and the blue dashed lines are an exponential fit to the background and GEANT4 simulations, respectively; the solid red line is the total (sum) fit.

*1 RIKEN Nishina Center
*2 RCNP, University of Osaka
*3 Center for Nuclear Study, University of Tokyo
*4 Department of Physics, University of Tokyo
*5 Department of Physics, Tokyo University of Science
*6 Department of Physics, Rikkyo University
*7 Department of Physics, Tohoku University
*8 Laboratori Nazionali di Legnaro

References

1) A. Huck et al., Phys. Rev. C **31,** 2226 (1985).
2) A. Gade et al., Phys. Rev. C **74,** 021302(R) (2006).
3) F. Wienholtz et al., Nature **498,** 346 (2013).
4) R. V. F. Janssens et al., Phys. Lett. B **546,** 55 (2002).
5) D.-C. Dinca et al., Phys. Rev. C **71,** 041302(R) (2005).
6) J. I. Prisciandaro et al., Phys. Lett. B **510,** 17 (2001).
7) A. Bürger et al., Phys. Lett. B **622,** 29 (2005).
8) D. Steppenbeck et al., Nature **502,** 207 (2013).
9) S. Takeuchi et al., Nucl. Inst. Meth. A **763,** 596 (2014).

Experimental study of isoscalar and isovector dipole resonances in neutron-rich oxygen isotopes

N. Nakatsuka,[*1,*2] H. Baba,[*2] N. Aoi,[*10] T. Aumann,[*3] R. Avigo,[*5,*14] S. R. Banerjee,[*12] A. Bracco,[*5,*14] C. Caesar,[*3] F. Camera,[*5,*14] S. Ceruti,[*5,*14] S. Chen,[*13,*2] V. Derya,[*4] P. Doornenbal,[*2] A. Giaz,[*5,*14] A. Horvat,[*3] K. Ieki,[*11] N. Imai,[*7] T. Kawabata,[*1] K. Yoneda,[*2] N. Kobayashi,[*8] Y. Kondo,[*9] S. Koyama,[*8] M. Kurata-Nishimura,[*2] S. Masuoka,[*7] M. Matsushita,[*7] S. Michimasa,[*7] B. Millon,[*5] T. Motobayashi,[*2] T. Murakami,[*1] T. Nakamura,[*9] T. Ohnishi,[*2] H. J. Ong,[*10] S. Ota,[*7] H. Otsu,[*2] T. Ozaki,[*9] A. Saito,[*9] H. Sakurai,[*2,*8] H. Scheit,[*3] F. Schindler,[*3] P. Schrock,[*3] Y. Shiga,[*11,*2] M. Shikata,[*9] S. Shimoura,[*7] D. Steppenbeck,[*2] T. Sumikama,[*6] I. Syndikus,[*3] H. Takeda,[*2] S. Takeuchi,[*2] A. Tamii,[*10] R. Taniuchi,[*8] Y. Togano,[*9] J. Tscheuschner,[*3] J. Tsubota,[*9] H. Wang,[*2] O. Wieland,[*5] K. Wimmer,[*8] Y. Yamaguchi,[*7] and J. Zenihiro[*2]

Giant resonance is one of the most important phenomena for understanding quantum many-body systems. Neutron-rich nuclei are predicted to have exotic giant resonances due to their smaller neutron separation energy and excess neutrons. One of the exotic giant resonances in neutron-rich nuclei is a dipole resonance found at excitation energies lower than 10 MeV[1]. The nature of these resonances is of great interest. One of the method to understand the nature of these resonances is to investigate if they are iso-vector or iso-scalar resonances. In order to study the relationship between iso-vector and iso-scalar dipole resonances in neutron-rich oxygen isotopes, we performed an experiment at RIBF and measure the dipole resonances of the neutron-rich nuclei ^{20}O, ^{22}O, and ^{24}O. These beams were produced via projectile fragmentation of a 345MeV/nucleon ^{48}Ca beam on ^{9}Be targets with mass thicknesses of 2.8 g/cm^2, 2.8 g/cm^2, and 2.2 g/cm^2. Γ rays from the excited beam particles were detected with large volume $LaBr_3$ crystals from INFN Milano[2] in combination with DALI2[3]. Two different targets, 5 g/cm^2 Au for coulomb excitation and 300 mg/cm^3 liquid helium for inelastic α particle scattering, were used to obtain the iso-vector and iso-scaler dipole strengths respectively.

A preliminary particle identification (PID) plot of Z versus A/Z for the ^{24}O beam is shown in Fig. 1. PID was performed by the Bρ-ΔE-TOF technique using the BigRIPS. The $B\rho$ information was reconstructed from the time difference between the left- and right-hand sides of the plastic scintillator installed at the dispersive focal plane. The achieved purity of ^{20}O, ^{22}O, and ^{24}O was 73%, 66%, and 51%, respectively. PID of the outgoing beams was performed by the same Bρ-ΔE-TOF technique using the ZD spectrometer. Low-pressure multi-wire drift chambers[4] were used to measure Bρ of the outgoing beams. Figure 2 shows a preliminary PID plot of Z versus A/Z for the outgoing beam where an ^{24}O beam is on a Au target. The reaction products are clearly observed. The analysis of γ rays is in progress.

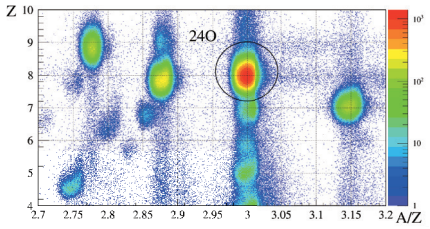

Fig. 1. PID plot of the ^{24}O beam setting

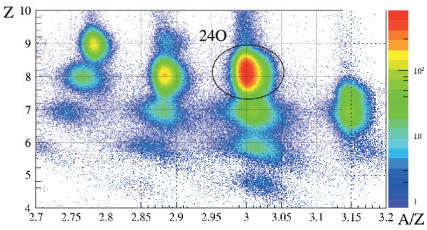

Fig. 2. PID plot of the ^{24}O beam and the Au target setting on ZD spectrometer

*1 Department of Physics, Kyoto University
*2 RIKEN Nishina Center
*3 Institut für Kernphysik, Technische Universität Darmstadt
*4 Institut für Kernphysik, Universität zu Köln
*5 Istituto Nazionale di Fisica Nucleare Milan
*6 Department of Physics, Tohoku University
*7 Center for Nuclear Study, The University of Tokyo
*8 Department of Physics, The University of Tokyo
*9 Department of Physics, Tokyo Institute of Technology
*10 Research Center for Nuclear Physics, Osaka University
*11 Department of Physics, Rikkyo University
*12 Variable Energy Cyclotron Centre, The Indian Department of Atomic Energy
*13 School of Physics, Peking University
*14 University of Milan

References

1) V. Derya et al. J. Phys. Conf. Ser. 366, 012012 (2012)
2) A. Giaz et al. Nucl. Instrum. Methods Phys. Res., Sec. A **729**, 910 (2013)
3) S. Takeuchi et al. Nucl. Instrum. Methods Phys. Res., Sec. A **763**, 596 (2014)
4) H. Miya et al. Nucl. Instrum. Methods Phys. Res., Sec. B **317**, 701 (2013)

Study of the pygmy-dipole resonances of ^{132}Sn and ^{128}Sn in inelastic α-scattering

J. Tscheuschner,[*1,*2] T. Aumann,[*1] D. S. Ahn,[*2] R. Avigo,[*3,*4] H. Baba,[*2] K. Boretzky,[*5] A. Bracco,[*3,*4] C. Caesar,[*5] A. Camera,[*3,*4] S. Chen,[*2,*6] V. Derya,[*7] P. Doornenbal,[*2] J. Endres,[*7] N. Fukuda,[*2] U. Garg,[*8] A. Giaz,[*3,*4] M. N. Harakeh,[*9] M. Heil,[*5] A. Horvat,[*1] K. Ieki,[*10] N. Imai,[*11] N. Inabe,[*2] N. Kalantar-Nayestanaki,[*9] N. Kobayashi,[*11] Y. Kondo,[*12] S. Koyama,[*11] T. Kubo,[*2] I. Martel,[*13] M. Matsushita,[*14] B. Million,[*15] T. Motobayashi,[*2] T. Nakamura,[*12] N. Nakatsuka,[*2,*16] M. Nishimura,[*2] S. Nishimura,[*2] S. Ota,[*14] H. Otsu,[*2] T. Ozaki,[*12] M. Petri,[*1] R. Reifarth,[*17] D. Rossi,[*18] A. Saito,[*12] H. Sakurai,[*2,*11] D. Savran,[*5] H. Scheit,[*1] F. Schindler,[*1] P. Schrock,[*1] D. Semmler,[*1] Y. Shiga,[*2,*10] M. Shikata,[*12] Y. Shimizu,[*2] H. Simon,[*5] D. Steppenbeck,[*2] H. Suzuki,[*2] T. Sumikama,[*19] D. Symochko,[*1] I. Syndikus,[*1] H. Takeda,[*2] S. Takeuchi,[*2] R. Taniuchi,[*11] Y. Togano,[*12] J. Tsubota,[*12] H. Wang,[*2] O. Wieland,[*3] K. Yoneda,[*2] J. Zenihiro,[*2] and A. Zilges[*7]

Pygmy-dipole resonance is commonly considered as a dipole mode of the nucleus related to a vibration of excess neutrons against a core. As such, it should be related to the neutron richness of the nucleus as well as its neutron-skin thickness. So far, the experimental information on this low-lying dipole mode is astonishingly scarce, even for stable nuclei[1]. One interesting open question is the isospin character of the low-lying dipole strength. In an experiment with the stable ^{124}Sn isotope[2], it has been concluded that a large fraction of the pygmy strength is of isoscalar character, however significant differences in the strength distribution compared with photoexcitation have been observed.

In November 2014, the isoscalar mode of the pygmy-dipole resonances in ^{128}Sn and ^{132}Sn isotopes were measured in inelastic α-scattering at RIKEN. The isotopes of interest were produced with a high-intensity primary ^{238}U beam of 345 MeV/u impinging on a beryllium target. The resulting secondary beam with an energy of approximately 200 MeV/u was directed towards the liquid helium target with a thickness of approximately 300 mg/cm^2. The γ-rays, which are ejected at the target position, have been measured by 8 large-volume 3.5"×8"$LaBr_3$:Ce crystals from Hector INFN Milano[3] and 95 large-volume NaI(Ti) DALI2[4] crystals. These crystals surrounded the target chamber to achieve a high geometric acceptance.

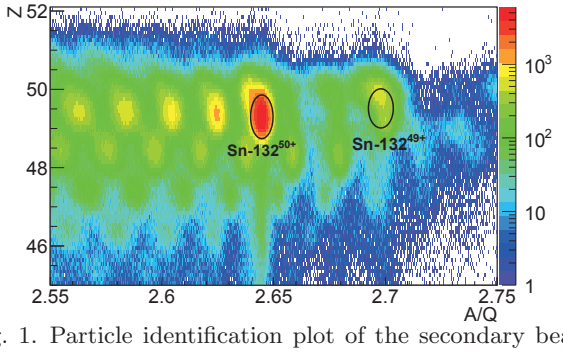

Fig. 1. Particle identification plot of the secondary beam after the liquid Helium target, gated on incoming ^{132}Sn ions determined using the ZeroDegree spectrometer.

As a first step of the analysis, the preliminary particle identification (PID) plot of Z versus A/Q can be determined by a combination of the measured energy loss, magnetic rigidity, and the time-of-flight using the BigRIPS and the ZeroDegree spectrometer[5]. As a result, beam purity was dertermined to be 18% for ^{128}Sn and 26% for ^{132}Sn. As an example, the resulting PID for the outgoing particles for the ^{132}Sn experiment is shown in Fig. 1. In the plot, different charge states for ^{132}Sn can be observed. However, the ^{129}Sn^{49+}-state has to be considered, because it has a similar A/Q-value as the fully stripped ^{132}Sn ion ($A/Q(^{129}\mathrm{Sn}^{49+})$=2.633 and $A/Q(^{132}\mathrm{Sn}^{50+})$=2.640). The pygmy-dipole resonances can be identified by the correlation of the identified particles to the corresponding γ-rays. Finally, the strength of the isoscalar pygmy-dipole resonances can be determined. In addition, experiments already performed at GSI Darmstadt with the R^{3}B setup will profit, because with the result of this experiment, the isovector part of the resonance can be separated from the isoscalar part.

*1 Institut für Kernphysik, TU Darmstadt
*2 RIKEN Nishina Center
*3 INFN sezione di Milano
*4 Dipartimento di Fisica, Universita degli studi di Milano
*5 GSI Helmholtzzentrum Darmstadt
*6 School of Physics, Peking University
*7 Institute für Kernphysik, Universität zu Köln
*8 Department of Physics, University of Notre Dame
*9 KVI-CART Groningen
*10 Department of Physics, Rikkyo University
*11 Department of Physics, University of Tokyo
*12 Department of Physics, Tokyo Institut of Technoloy
*13 Departamento de Fisica Aplicada, Universidad de Huelva
*14 Center for Nuclear Research, University of Tokyo
*15 VECC India
*16 Department of Physics, Kyoto University
*17 Institut für Kernphysik, Goethe Universität Frankfurt
*18 National Supercoducting Cyclotron Laboratory, Michigan State University
*19 Department of Physics, Tohoku University

References

1) D. Savran et al.: Prog. Part. Nucl. Phys. **70**, p.210 (2013).
2) J. Endres et al.: Phys. Rev. Lett. **105**, 212503 (2010).
3) A. Giaz et al.: NIM A**729**, 910 (2013).
4) S. Takeuchi et al.: NIM A **763**, 596 (2014).
5) T. Kubo et al.: Prog. Theor. Exp. Phys. 03C003 (2012).

Coulomb excitation of ^{130}Cd

H. Wang,[*1] N. Aoi,[*2] P. Doornenbal,[*1] S. Takeuchi,[*1] M. Matsushita,[*3] Y. Shiga,[*1,*4] D. Steppenbeck,[*3] R. Taniuchi,[*1,*5] R. Avigo,[*6] H. Baba,[*1] C. Bauer,[*7] Z. Dombradi,[*8] Z. Elekes,[*8] E. Ideguchi,[*2] T. Isobe,[*1] A. Jungclaus,[*9] J. Lee,[*1] H. Liu,[*1,*10] S. Momiyama,[*5] T. Motobayashi,[*1] K. Nacher,[*9] M. Niikura,[*5] S. Nishimura,[*1] A. Obertelli,[*11] H. Otsu,[*1] H. Sakurai,[*1] C. Santamaria,[*11] P.-A. Söderström,[*1] T. Sumikama,[*12] J. Taprogge,[*9] Z. Vajta,[*8] J. Wu,[*1,*10] Z. Xu,[*1] T. Yamamoto,[*2] and K. Yoneda[*1]

The properties of the nuclei beyond ^{132}Sn have drawn considerable attention recently because this doubly magic nucleus lies far away the line of β stability. The evolution of the $N = 82$ shell gap to the "south" of ^{132}Sn has been discussed in several studies[1,2]. For nuclear astrophysics, it has been suggested that the $N = 82$ shell closure affects the r-process abundance distribution around mass $A \approx 130$[2]. However, for the $N = 82$ magicity in the Cd ($Z = 48$) isotopes, the mass and the spectroscopy measurements show contradictory results. The Q_β value of ^{130}Cd was better reproduced by a mass model assuming a quenched shell gap[3]. However, a good shell closure was suggested from the first 2^+ state as the excitation energy of 1.3 MeV[4] is close to those in other even-even $N = 82$ isotones. In order to investigate the magic character of $N = 82$ in ^{130}Cd, we measured the reduced transition possibility ($B(E2)$) via the Coulomb excitation.

The secondary beams were produced from an in-flight fission reaction of a U primary beam at 345 MeV/nucleon incident on a 3-mm-thick Be target located at the object point of the BigRIPS fragment separator[5]. The average beam intensity was about 10 particle nA. The fission products around ^{130}Cd were selected and purified by employing two wedge-shaped aluminum energy degraders with thicknesses of 8 and 2 mm, respectively, located at the dispersive foci. The momentum acceptance of BigRIPS was set to 5%. The secondary beam was identified event-by-event via the TOF – $B\rho - \Delta E$ method using standard BigRIPS detectors. Figure 1 shows a two-dimensional plot of Z versus A/Q for the secondary beam in BigRIPS. The intensity of the ^{130}Cd beam was 15 counts/s with a purity of 1.3%. The beam energy was about 160 MeV/nucleon before the secondary target.

A 1-mm-thick Bi target was used to induce Coulomb excitation reactions. De-excitation γ rays were detected by the DALI2 spectrometer[6], which surrounded the secondary target. Reaction residues were collected and analyzed by the ZeroDegree spectrometer[5]. The spectrometer was optimized for the transportation of ^{130}Cd. Particle identification was performed again using the TOF – $B\rho - \Delta E$ method, as in BigRIPS. In addition, a $LaBr_3$(Ce) scintillation detector (Saint-Gobain BrilLanCe^{TM}380) located downstream of the ionization chamber was used for the total kinetic energy measurement.

The analysis for the $B(E2)$ value is currently in progress.

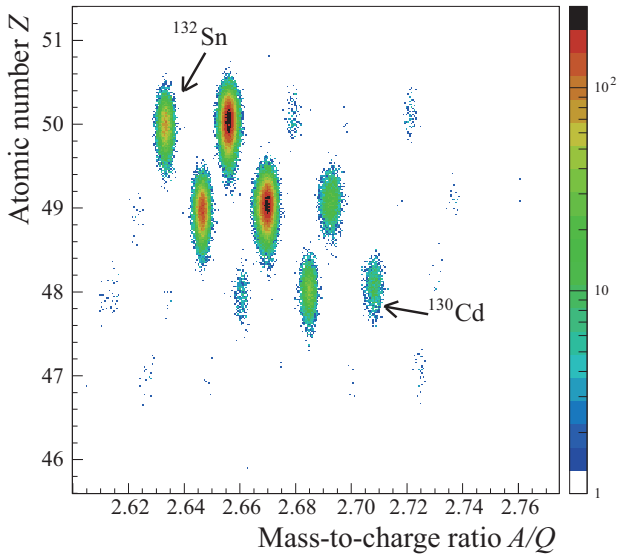

Fig. 1. Particle identification plot of the secondary beams in BigRIPS.

*1 RIKEN Nishina Center
*2 RCNP, Osaka University
*3 CNS, University of Tokyo
*4 Department of Physics, Rikkyo University
*5 Department of Physics, University of Tokyo
*6 INFN, Italy
*7 TU Darmstadt, Germany
*8 Institute for Nuclear Research, Hungary
*9 Instituto de Estructura de la Materia, CSIC
*10 School of Physics and State Key Laboratory of Nulcear Physics and Technology, Peking University
*11 CEA Saclay, France
*12 Department of Physics, Tohoku University

References

1) J. Dobaczewski et al.: Phys. Rev. Lett. 72, 981 (1994).
2) B. Pfeiffer et al.: Nucl. Phys. A 693, 282 (2001).
3) I. Dillmann et al.: Phys. Rev. Lett. 91, 162503 (2003).
4) A. Jungclaus et al.: Phys. Rev. Lett. 99, 132501 (2007).
5) T. Kubo et al.: Prog. Theor. Exp. Phys. 2012, 03C003 (2012).
6) S. Takeuchi et al.: Nucl. Instr. Meth. A 763, 596 (2014).

Search of E1 strength around threshold in ^{70}Ni†

R. Avigo,[*1,*2] O. Wieland,[*1] A. Bracco,[*1,*2] F. Camera,[*1,*2] H. Baba,[*3] N. Nakatsuka,[*4] P. Doornenbal,[*3] Y. Togano,[*5] J. Tscheuschner,[*6] T. Aumann,[*6] G. Benzoni,[*1] N. Blasi,[*1] K. Boretzky,[*7] S. Brambilla,[*1] S. Ceruti,[*1,*2] S. Chen,[*8] F.C.L. Crespi,[*1,*2] N. Fukuda,[*3] A. Giaz,[*1,*2] K. Ieki,[*9] N. Kobayashi,[*10] Y. Kondo,[*5] S. Koyama,[*10] T. Kubo,[*3] S. Leoni,[*1,*2] M. Matsushita,[*11] B. Million,[*1] A.I. Morales,[*1,*2] T. Motobayashi,[*3] T. Nakamura,[*5] M. Nishimura,[*3] S. Nishimura,[*3] H. Otsu,[*3] T. Ozaki,[*5] L. Pellegri,[*1,*2] A. Saito,[*5] H. Sakurai,[*3] H. Scheit,[*6] P. Schrock,[*6] Y. Shiga,[*3] M. Shikata,[*5] D. Steppenbeck,[*3] T. Sumikama,[*12] S. Takeuchi,[*3] R. Taniuchi,[*10] J. Tsubota,[*5] H. Wang,[*3] and K. Yoneda[*3]

The structure and nature of the E1 strength distribution around the separation energy depends mainly on the neutron excess. Some information in stable nuclei has been obtained in the past but only very few data are available for exotic neutron rich nuclei using mainly Coulomb excitation techniques[1) and references therein].

There is an ongoing discussion on the possibility of extracting information on the neutron skin from the pygmy resonance strength[2)]. This quantity can be related to the isospin-dependent part of the nuclear equation of state (EOS) which in turn has relevant implications for the description of neutron stars. Furthermore, the presence of a strength with E1 character close to the particle threshold has important astrophysical implications in explosive nucleosynthesis scenarios.

In order to understand better the characteristics of this pygmy dipole strength it is important to study an isotopic chain of a nucleus with increasing neutron number. As the pygmy dipole strength distribution in ^{68}Ni around the threshold has recently been studied[1,2,3)], a new high intensity and high resolution experiment was performed on ^{70}Ni at RIKEN Radioactive Isotope Beam Factory (RIBF) in November 2014.

A ^{238}U primary beam was accelerated up to an energy of 345 *A*MeV and made to impinge on a thick rotating Be production target. In BigRIPS[4)] the Bρ-ΔE- Bρ method was applied to select and purify a secondary beam of ^{70}Ni (30 kcps with 40% purity at a beam energy of 260 *A*MeV). The ^{70}Ni isotope was incident on a 2 g/cm^2 thick gold secondary target. Reaction residues from the secondary target were identified using the ZeroDegree Spectrometer. Scattering angles were determined using parallel plate avalanche counters.

To detect gamma rays from the decay of different nuclear levels the reaction target was surrounded by a combination of the DALI2 array[5)] (consisting of 96 NaI(TI) crystals) and 8 large volume 3.5'' x 8'' $LaBr_3$:Ce detectors[6)] mounted at 30° in the forward direction. These latter detectors have a high efficiency, excellent energy resolution for high energy gamma rays and very good time resolution.

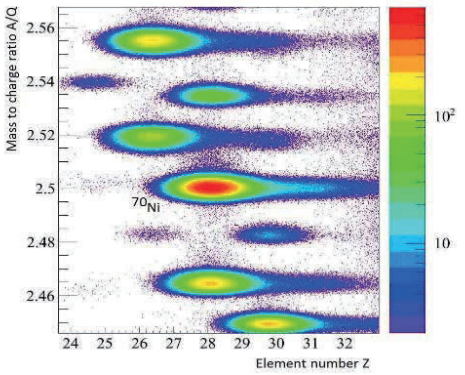

Fig. 1. Particle identification plot (Bρ-ΔE- B TOF) of the secondary beam in front of the Au reaction target. The ^{70}Ni isotopes are labeled.

Fig. 1 shows the particle identification plot taken during the experiment can be seen. The data are under analysis. The first preliminary outcome will be the 2+ state strength of ^{70}Ni. This known $2^+ \rightarrow 0^+_{gs}$ E2 transition strength will be taken as a benchmark for the determination of the unknown E1 transitions strengths below and above the threshold. Presently high energy gamma ray events in the $LaBr_3$:Ce detectors and add back spectra in DALI2 are being analyzed. The determination of the E1 strength distribution of the measured ^{70}Ni and the subsequent analysis of the relation between strength and neutron skin together with the data of the measured ^{68}Ni will give a better and important contribution to the understanding of the features of the pygmy dipole strength.

† Experiment NP1306 -RIBF51R1, November 2014

*1 INFN sezione di Milano
*2 University of Milano
*3 RIKEN Nishina Center
*4 Kyoto University
*5 Department of Physics, Tokyo Institute of Technology
*6 TU Darmstadt
*7 GSI Darmstadt
*8 Peking University
*9 Rikkyo University
*10 University of Tokyo
*11 CNS, University of Tokyo
*12 Tohoku University

References

1) O. Wieland et al. PRL **102,** 092502 (2009).
2) A. Carbone et al. Phys. Rev. C **81** 041301(R) (2010).
3) D. Rossi et al. PRL **111**, 242503 (2013).
4) T. Kubo et al. Prog. Theor. Exp. Phys. 03C003 (2012).
5) S. Takeuchi et al. NIM A**763**, 596 (2014).
6) A. Giaz et al. NIM A**729,** 910 (2013).

Structure at and beyond the dripline in the vicinity of the N=14 and 16 sub-shell closures

S. Leblond,[*1] Y. Kondo,[*2] J. Gibelin,[*1] F. M. Marqués,[*1] T. Nakamura,[*2] N. A. Orr,[*1] S. Ogoshi,[*2] R. Minakata,[*2] R. Tanaka,[*2] N. L. Achouri,[*1] T. Aumann,[*3] H. Baba,[*4] F. Delaunay,[*1] P. Doornenbal,[*4] N. Fukuda,[*4] J. W. Hwang,[*5] N. Inabe,[*4] T. Isobe,[*4] D. Kameda,[*4] D. Kanno,[*2] S. Kim,[*5] N. Kobayashi,[*2] T. Kobayashi,[*6] T. Kubo,[*4] J. Lee,[*4] T. Motobayashi,[*4] D. Murai,[*7] T. Murakami,[*8] K. Muto,[*6] T. Nakashima,[*2] N. Nakatsuka,[*8] A. Navin,[*9] S. Nishi,[*2] H. Otsu,[*4] H. Sato,[*4] Y. Satou,[*5] Y. Shimizu,[*4] H. Suzuki,[*4] K. Takahashi,[*6] H. Takeda,[*4] S. Takeuchi,[*4] Y. Togano,[*10] A. G. Tuff,[*11] M. Vandebrouck,[*12] and K. Yoneda[*4]

The structure of the neutron-rich nuclei in the vicinity of the N=14 and 16 sub-shell closures have attracted considerable interest in recent years. In particular, ^{19}B and ^{22}C represent the heaviest canidate two-neutron halo systems[1–3] whilst also spanning N=14 and 16 below doubly-magic ^{22,24}O. In terms of the most neutron-rich oxygen isotopes, the behaviour beyond ^{24}O, with the ultimate goal of investigating ^{28}O, has taken on renewed interest in the light of recent improvements in sophisticated structure modelling[4,5]. The present report describes the status of the analysis of data acquired during a series of three experiments, undertaken with these goals in mind, as part of the initial phase of operation of the SAMURAI spectrometer[6] coupled to the large area neutron array NEBULA[7] and DALI2[8] NaI array.

One of the systems of particular interest in terms of modelling ^{22}C and the evolution of the $\nu 2s_{1/2}$ and $\nu 1d_{5/2}$ levels is ^{21}C[9], the unbound sub-system of Borromean ^{22}C. In the present work we have attemped to populate ^{21}C via both neutron and proton removal from ^{22}C and ^{22}N respectively, whereby it is expected that the different valence neutron configurations of the projectile ground states should result in the population of correspondingly different final states. Figure 1 shows the reconstructed ^{20}C+n invariant mass (or decay energy) spectra for the two reactions. As may be seen, the selectivety of the two reactions is markedly different, with neutron removal from ^{22}C exhibiting in particular a rather narrow structure close to 1.5 MeV. We note that in comparison to the featureless, but very limited statistics spectrum of Ref.[10], the proton removal from ^{22}N shows here a very pronounced structure at around 1 MeV.

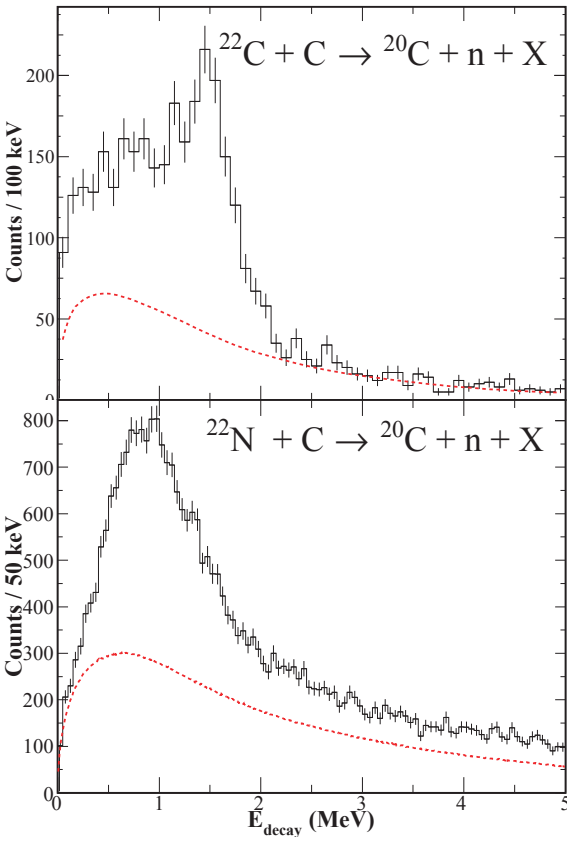

Fig. 1. Preliminary results for the ^{20}C+n decay energy spectra obtained for neutron (upper) and proton (lower panel) removal reactions at 240 MeV/nucleon. The dotted line, normalised at high decay energy, represents an event-mixed estimate of the corresponding uncorrelated distribution.

The further analysis of these preliminary results is currently underway, including the extraction of the ^{20}C+n momentum distribution for the neutron removal channel, which will shed light on the angular momentum of the removed neutron and hence the character of the corresponding ^{21}C states. Analysis of the data acquired for two-proton removal from ^{23}O is also in progress with the initial results exhibiting a decay

*1 LPC-Caen, ENSICAEN, Université de Caen, CNRS/IN2P3
*2 Department of Physics, Tokyo Institute of Technology
*3 Institut für Kernphysik, Technische Universität Darmstadt
*4 RIKEN Nishina Center
*5 Department of Physics and Astronomy, Seoul National University
*6 Department of Physics, Tohoku University
*7 Departiment of Physics, Rikkyo University
*8 Department of Physics, Kyoto University
*9 GANIL, CEA/DSM-CNRS/IN2P3
*10 ExtreMe Matter Institute (EMMI) and Research Division, GSI
*11 Department of Physics, University of York
*12 Institut de Physique Nucléaire, Université Paris-Sud, IN2P3-CNRS, Orsay

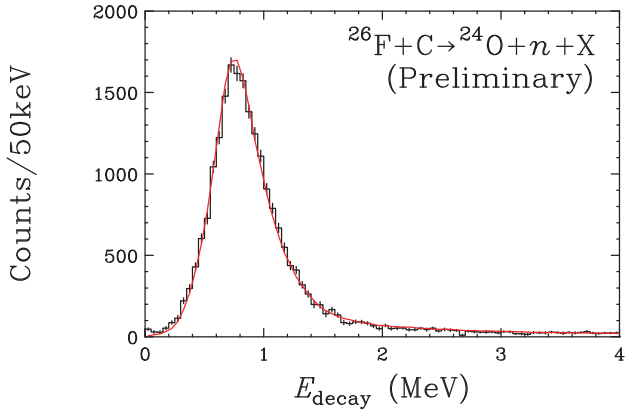

Fig. 2. Preliminary results for the ^{24}O+n relative energy spectrum obtained for proton removal from ^{26}F at 212 MeV/nucleon. The solid curve shows the results of a fit assuming a single resonance (see text)

Beam	Energy (MeV/nucleon)	$\Delta P/P$ (%)	Intensity (kpps/100pnA)
^{27}F	241	±3	1.0
^{28}Ne	212	±3	29
^{26}F	212	±0.6	2.5
^{27}Ne	240	±0.6	14

Table 1. Intensities, in terms of the ^{48}Ca primary beam (354 MeV/nucleon) intensity (pnA), for the secondary beams employed to investigate ^{25,26}O. The momentum aecceptance of the BigRIPS separator is noted in each case as is the mean secondary beam energy.

energy spectrum similar to that observed in single-proton removal from ^{22}N.

Data was also acquired for reactions of ^{19}B and ^{22}C beams on a Pb target with the goal of deducing the E1 strength functions for the two-neutron dissociation channel. This should enable further constraints to be placed on the halo structure of both nuclei as well as insight into the halo neutron spatial configurations[11]. The analysis of the data is on going, with very preliminary results indicating that both nuclei exhibit considerable near threshold strength.

In the case of the heavy oxygen isotopes, the analysis of the data obtained for proton removal from a ^{26}F beam to populate ^{25}O is in its final stages. Figure 2 shows the preliminary results obtained for the ^{24}O+n decay energy spectrum, including a comparison with the best fit results for an ℓ=2 resonance. A resonance energy of 0.75 MeV and width of 0.09 MeV have been estimated, which are in line with the results of earlier studies undertaken elsewhere employing the same reaction[12,13].

Work is currently proceeding to finalise the analysis of the data acquired for single-proton removal from ^{27}F to populate ^{26}O. To date the ^{24}O+2n decay energy spectrum has been successfully reconstructed after implementation of neutron cross talk rejection procedures based on kinematic conditions. The spectrum exhibits a feature at around 1.3 MeV, which represents the first observation of an excited (presumably 2^+) state in ^{26}O, together with a very sharp peak at threshold corresponding to the ground state[13,14]. A detailed analysis is being performed to determine the characteristics (energies and widths) of both states. The considerably higher statistics obtained in the present work should allow for a much more precise determination of the ground state energy. In the near future the data acquired for the two-proton removal from ^{27,28}Ne will also be exploited in the hope of providing further insight into the structure of ^{25,26}O.

We note that in an earlier report[15], intensities were quoted for the secondary beams employed for the investigation of ^{25,26}O. For reference, for future experiments, Table 1 lists updated determinations of the intensities.

The work described here relating to the investigation of ^{21}C forms part of the PhD thesis of S. Leblond (LPC-Caen).

References

1) K. Tanaka *et al.*: Phys. Rev. Lett. **104**, 062701 (2010).
2) N. Kobayashi *et al.*: Phys. Rev. **C83**, 054604 (2012).
3) L. Gaudefroy *et al.*: Phys. Rev. Lett. **109**, 20503 (2012).
4) T. Otsuka *et al.*: Phys. Rev. Lett. **105**, 032501 (2010).
5) G.R. Jansen *et al.*: Phys. Rev. Lett. **108**, 242501 (2012).
6) T. Kobayashi *et al.*: Nucl. Instr. Meth. B **317**, 294 (2013).
7) Y. Kondo *et al.*: RIKEN Accel. Prog. Rep. **45**, 131 (2012); http://be.nucl.ap.titech.ac.jp/~nebula
8) S. Takeuchi *et al.*: Nucl. Instr. Meth. B **A763**, 596 (2014).
9) G. Jansen *et al.*: Phys. Rev. Lett. **113**, 142502 (2014).
10) S. Mosby *et al.*: Nucl. Phys. **A909**, 69 (2013).
11) T. Nakamura *et al.*: Phys. Rev. Lett. **96**, 252502 (2006).
12) C.R. Hoffman *et al.*: Phys. Rev. Lett. **100**, 152502 (2008).
13) C. Caeser *et al.*: Phys. Rev. **C88**, 034313 (2013).
14) E. Lunderberg *et al.*: Phys. Rev. Lett. **108**, 142503 (2012).
15) Y. Kondo *et al.*: RIKEN Accel. Prog. Rep. **46**, 6 (2013).

Study of neutron-unbound states of ^{19}C at SAMURAI

J.W. Hwang,[*1,*2] Y. Satou,[*1] S. Kim,[*1,*2] N. A. Orr,[*3] T. Nakamura,[*4,*2] Y. Kondo,[*4,*2] N. L. Achouri,[*3] T. Aumann,[*5] H. Baba,[*2] F. Delaunay,[*3] P. Doornenbal,[*2] N. Fukuda,[*2] J. Gibelin,[*3] N. Inabe,[*2] T. Isobe,[*2] D. Kameda,[*2] D. Kanno,[*4,*2] N. Kobayashi,[*4,*2] T. Kobayashi,[*6,*2] T. Kubo,[*2] S. Leblond,[*3] J. Lee,[*2] F. M. Marques,[*3] R. Minakata,[*4,*2] T. Motobayashi,[*2] D. Murai,[*7] T. Murakami,[*8] K. Muto,[*6] N. Nakatsuka,[*8] T. Nakashima,[*4,*2] A. Navin,[*9] S. Nishi,[*4,*2] S. Ogoshi,[*4,*2] H. Otsu,[*2] H. Sato,[*2] Y. Shimizu,[*2] H. Suzuki,[*2] K. Takahashi,[*6] H. Takeda,[*2] S. Takeuchi,[*2] R. Tanaka,[*4,*2] Y. Togano,[*10,*13] A. G. Tuff,[*11] M. Vandebrouck,[*12] and K. Yoneda[*2]

The neutron-unbound region of the nuclear level structure has been investigated extensively in recent years, especially for nuclei near the neutron drip line. In this report, we provide the result of the experiment to study neutron-unbound states in ^{19}C by usin a one-neutron knockout reaction. The report contains the outcome of the succeeding research following the report in the previous year.[1)]

The experiment was performed at the RIBF facility. A ^{20}C secondary beam at 280 MeV/nucleon separated by BigRIPS impinged on a 1.8 g/cm^2-thick carbon target. Neutron-unbound states of ^{19}C produced by one-neutron knockout decays into a ^{18}C ion and a neutron. ^{18}C was identified and its momentum was measured using the SAMURAI spectrometer[2)] with the help of its experimental appratus. Arrays of plastic scintillators for neutron detection (NEBULA) were used to measure the momenta of decay neutrons.[3)] The experimental setup is identical to that of Ref.[4)].

A preliminary relative energy spectrum for the system of $^{18}\mathrm{C}+n$ is shown in Fig. 1 with the result of fitting analysis. Acceptance was corrected for considering the effect of the geometry of the detector system, which was estimated using a Monte-Carlo simulation. Error bars are statistical ones. Briet-Wigner shape functions were used as response functions generated using a simulation code taking the detector resolution into account. The background consists of a Boltzmann-type distribution for non-resonant continuum and a distribution for uncorrelated $^{18}\mathrm{C}+n$ pairs reconstructed using the event mixing technique. A different scale from 0.5 MeV is taken in the y-axis be-

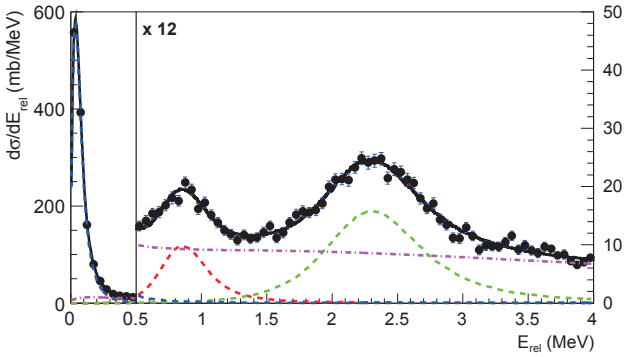

Fig. 1. Preliminary relative energy spectrum for the system of $^{18}\mathrm{C}+n$ (filled circles). The black solid line is the result of the fit; the dashed lines are for the two resonances; the dot-dashed line is the assumed background. (see details in the text)

cause of the significant threshold resonance. Three resonances were observed at $E_{\mathrm{rel}} = 36\pm1$ keV, 0.84 ± 0.02 MeV and 2.33 ± 0.01 MeV, corresponding to the states of $E_x = 0.62(9)$ MeV, 1.42(9) MeV, and 2.91(9) MeV, respectively, based on the formula: $E_x = E_{\mathrm{rel}} + S_n$, where S_n is the one-neutron separation energy of ^{19}C (0.58(9) MeV[5)]). Note that all values are preliminary. While the first and second resonances are consistent with the $5/2^+_1$ and $5/2^+_2$ states reported by the knockout experiment[6)] and the inelastic scattering measurement[7)], respectively, the third one was observed for the first time in the present study. A next step of analysis is planned to obtain the parallel momentum distribution of the knockout residue to investigate spins and parities of the observed states.

*1 Department of Physics and Astronomy, Seoul National University
*2 RIKEN Nishina Center
*3 LPC-Caen, ENSICAEN, Université de Caen, CNRS/IN2P3
*4 Department of Physics, Tokyo Institute of Technology
*5 Institut für Kernphysik, Technische Universität Darmstadt
*6 Department of Physics, Tohoku University
*7 Department of Physics, Rikkyo University
*8 Department of Physics, Kyoto University
*9 GANIL, CEA/DSM-CNRS/IN2P3
*10 ExtreMe Matter Institute (EMMI) and Research Division, GSI
*11 Department of Physics, University of York
*12 Institut de Physique Nucléaire, Université Paris-Sud, IN2P3-CNRS
*13 Present address:Department of Physics, Tokyo Institute of Technology

References

1) J. W. Hwang et al.: RIKEN Accel. Prog. Rep. **47**, xix (2014).
2) T. Kobayashi et al.: Nucl. Instr. Meth. B **317**, 294 (2013).
3) Y. Kondo et al.: RIKEN Accel. Prog. Rep. **45**, 131 (2012).
4) Y. Kondo et al.: RIKEN Accel. Prog. Rep. **46**, 6 (2013).
5) M. Wang et al: Chin. Phys. C **36**, 1603 (2012).
6) M. Thoennessen et al.: Nucl. Phys. A **912**, 1 (2013).
7) Y. Satou et al.: Phys. Lett. B **660**, 320 (2008)

Measurement of unbound states in ^{17}C at SAMURAI

S. Kim,[*1,*2] Y. Satou,[*1] J.W. Hwang,[*1,*2] T. Nakamura,[*2,*3] N. A. Orr,[*4] Y. Kondo,[*2,*3] J. Gibelin,[*4] N. Kobayashi,[*2,*3] R. Tanaka,[*2,*3] R. Minakata,[*2,*3] S. Ogoshi,[*2,*3] S. Nishi,[*2,*3] D. Kanno,[*2,*3] T. Nakashima,[*2,*3] N. L. Achouri,[*4] T. Aumann,[*5] H. Baba,[*2] F. Delaunay,[*4] P. Doornenbal,[*2] N. Fukuda,[*2] N. Inabe,[*2] T. Isobe,[*2] D. Kameda,[*2] T. Kobayashi,[*6,*2] T. Kubo,[*2] S. Leblond,[*4] J. Lee,[*2] F. M. Marqués,[*4] T. Motobayashi,[*2] D. Murai,[*7] T. Murakami,[*8] K. Muto,[*6] N. Nakatsuka,[*8] A. Navin,[*9] H. Otsu,[*2] H. Sato,[*2] Y. Shimizu,[*2] H. Suzuki,[*2] K. Takahashi,[*6] H. Takeda,[*2] S. Takeuchi,[*2] Y. Togano,[*10,*13] A. G. Tuff,[*11] M. Vandebrouck,[*12] and K. Yoneda[*2]

To study unbound states in ^{17}C above the neutron separation energy of 0.735(18) MeV[1], an experiment was performed at RIBF during the first physics run of the SAMURAI spectrometer[2]. The unbound states of ^{17}C were produced using the one-neutron knockout reaction of ^{18}C. The ^{18}C beam was provided by BigRIPS. The beam intensity was typically 2300 pps with the energy of 250 MeV/nucleon under the momentum acceptance of ±3%. Particle identification of the beam was carried out by employing the $B\rho$-TOF-ΔE method with a mass resolution of $A/\Delta A = 770$ at 1 sigma. The unbound states of ^{17}C populated by one-neutron knockout of ^{18}C on a carbon reaction target with a thickness of 1.8 g/cm^2 immediately decays into a ^{16}C fragment and a neutron. The particle identification of this fragment was also carried out using the $B\rho$-TOF-ΔE method with a mass resolution of $A/\Delta A = 250$ at 1 sigma. The identification of the states of the ^{16}C fragment subsequent to the decay was carried out on the basis of γ-n coincidence. The de-excitation γ-rays in ^{16}C were detected by a γ-ray detector array DALI2[3], while neutrons were detected by the neutorn detector array NEBULA consisting of neutron detectors (NEUT) and charged-particle veto detectors (VETO). For NEUT, the timing resolution was 270 ps in a flight length of approximately 11 m.

The relative energy ($E_{\rm rel}$) of ^{17}C was reconstructed using the momentum vectors of the ^{16}C fragment and the neutron. To determine the positions of the resonances, responses were generated using a Monte Carlo simulation that considers the beam characteristics, reaction mechanism, and detector resolutions. From the simulation, the $E_{\rm rel}$ resolution was evaluated as $\Delta E_{\rm rel} = 0.4\sqrt{E_{\rm rel}}$ MeV in FWHM.

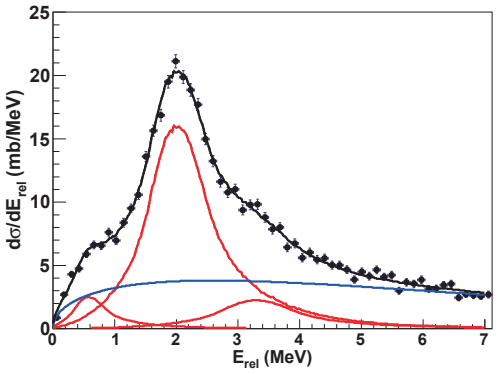

Fig. 1. Preliminary spectrum of the relative energy of ^{17}C. The black solid line represents the result of the overall fit by three responses (red solid lines) and a Maxwellian background (a blue solid line).

A preliminary result of the fitting to the experimental spectrum with three responses and a Maxwellian background is shown in Fig. 1 where resonances at $E_{\rm rel} = 0.58(3)$, 2.01(2), and 3.30(6) MeV are observed. In this measurement, the resonance at $E_{\rm rel} = 0.58(3)$ exhibited a correlation with a gamma line at 1.72(12) MeV, which corresponds to the 2^+ state of ^{16}C[4]. Consequently, the three resonances correspond to excited states at 3.04(12), 2.75(3), and 4.04(6) MeV. The excited states at 2.75(3) and 4.04(6) MeV are likely to correspond to the states at 2.71(2) and 3.93(2) MeV, respectively, which have been observed in the β-delayed neutron measurement[5]. Further analysis involving a comparison with Glauber model calculations is in progress to investigate the orbital angular momentum and spin-parity of the observed resonances.

*1 Department of Physics and Astronomy, Seoul National University
*2 RIKEN Nishina Center
*3 Department of Physics, Tokyo Institute of Technology
*4 LPC-Caen, ENSICAEN, Université de Caen, CNRS/IN2P3
*5 Institut für Kernphysik, Technische Universität Darmstadt
*6 Department of Physics, Tohoku University
*7 Department of Physics, Rikkyo University
*8 Department of Physics, Kyoto University
*9 GANIL, CEA/DSM-CNRS/IN2P3
*10 ExtreMe Matter Institute (EMMI) and Research Division, GSI
*11 Department of Physics, University of York
*12 Institut de Physique Nucléaire, Université Paris-Sud, IN2P3-CNRS
*13 Department of Physics, Tokyo Institute of Technology

References

1) M. Wang, G. Audi, A. H. Wapstra, F. G. Kondev, M. MacCormick, X. Xu, and B. Pfeiffer: Chin. Phys. C 36, 1603 (2012).
2) T. Kobayashi et al.: Nucl. Instrum. Methods Phys. Res. B 317, 294 (2013).
3) S. Takeuchi et al.: Nucl. Instrum. Methods Phys. Res. A 763, 596 (2014).
4) D. R. Tilley et al.: Nucl. Phys. A 564, 1 (1993).
5) H. Ueno et al.: Phys. Rev. C 87, 034316 (2013).

Detailed analysis of tracking detectors for SAMURAI08 experiment

S. Koyama,[*1,*2] H. Otsu,[*2] for SAMURAI08 collaboration

We performed an experiment at SAMURAI to search for α-cluster levels in ^{16}C.[1] The levels were populated by bombarding a ^{16}C secondary beam on a liquid He target. The excitation energies were reconstructed from the invariant mass of the $^{16}C^{*} \rightarrow {}^{12}\mathrm{Be} + {}^{4}\mathrm{He}$ decay channel by measuring their four momenta. The four momenta were deduced from timing measurements and the tracking of drift chambers (DCs). For these DCs, the tracking efficiency and position resolution depend on the energy loss in the detector, which depends on the element number (Z) of penetrating fragments. In order to determine the four momenta accurately, the parameters for tracking should be separately optimized for each Z.

Figure 1 shows a particle identification (PID) plot of reaction products measured using the plastic scintillator array HODF and HODP.[2] Note that 1 scintillator out of 32 of the array on which the secondary beam directly hits with an intensity of 2×10^5 is excluded.

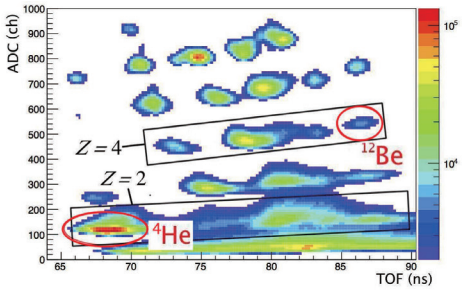

Fig. 1. PID plot of reaction products. The vertical axis shows the mean light output and the horizontal axis shows the time of flight (TOF) between the plastic scintillator placed upstream of the target and HODF and HODP.

DCs consist of more than 3 planes with different kinds of wire orientations. FDC2,[2] which was placed downstream of the SAMURAI magnet[2] (B = 2.3 T at the center), has 6 X (vertical, 0°), 4 U (+30°) and 4 V (−30°) planes. The drift length on each plane is measured and the trajectories of fragments for one axial direction, $x = a_0 + a_1 z$, are reconstructed by fitting a linear function, where x is the position orthogonal to the beam line, a_0 and a_1 are linear fitting parameters and z is the position along the beam line. The x positions of fragments in the k-th plane of a DC x_k are deduced from the time-to-digital converter (TDC) spectrum with a space-time conversion (STC) function, which converts time information to drift length. The STC function is first obtained by integrating the TDC spectrum and is corrected in response to the result of tracking. Figure 2 (a) shows the two STC functions optimized for $Z = 2$ and $Z = 4$ fragments. The difference between the two functions is clear. The residue r_k is defined as $r_k = x_k - x'_k$, where $x'_k = a_0 + a_1 z_k$ and z_k is the z position of the k-th plane. Figs. 2 (b) and (c) show how $x_k - r_k$ correlation changes when a different STC function is applied for tracking. The positions are well reconstructed when the optimized STC function is applied (Fig. 2 (b)) while they systematically deviate from the case in which an inappropriate STC function is applied (Fig. 2 (b)).

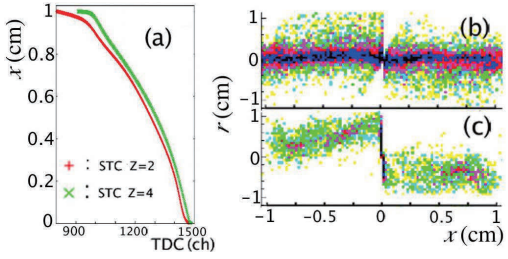

Fig. 2. (a) The optimized STC functions for $Z = 2$ (red) and $Z = 4$ (green) fragments. (b) $x_k - r_k$ correlation with the optimized STC function. (c) $x_k - r_k$ correlation with an unoptimized STC function.

The position resolution of the k-th plane of a DC Δx_k can be evaluated using the standard deviation of the residue of the plane Δr_k as follows:

$$\Delta r_k = \sqrt{1 - \frac{S_{zz} - 2S_z z_k + S_1 z_k^2}{D}}\,\Delta x, \qquad (1)$$

where $S_1 = \sum_k 1, S_z = \sum_k z_k, S_{zz} = \sum_k z_k^2$, and $D = S_1 S_{zz} - S_z^2$. It is assumed that Δx_k has the same value Δx in the same wire-oriented planes of a DC to deduce Eq. 1. Table 1 summarizes the position resolutions of X, U, and V planes with the optimized STC function for each Z. The position resolution of FDC2 is 120 μm[2] for $Z = 6$. Note that the value of the high voltage (2.4 kV) is not optimized for one Z to measure fragments with different Z in this experiment.

Table 1. Resolution of each plane of FDC2

Wire orientation	Resolution (μm) $Z = 2$	Resolution (μm) $Z = 4$
X	342	309
U	255	195
V	257	199

*1 Department of Physics, University of Tokyo
*2 RIKEN Nishina Center

References

1) H. Otsu et. al.: RIKEN Accel. Prog. Rep. 47, xx (2014).
2) T. Kobayashi et. al.: Nucl. Instrum. Meth. B 317 (2013).

Fission Barrier Studies of Neutron-Rich Nuclei via the (p,2p) Reaction: Status of NP1306-SAMURAI-14 Experiment

D. Mücher,[*1,*2] S. Reichert,[*1,*2] M. Sako,[*2] M. Sasano,[*2] A. Andreyev,[*3] T. Aumann,[*4] H. Baba,[*2] M. Böhmer,[*1] M. Dozono,[*5] N. Fukuda,[*2] R. Gernhäuser,[*1] W. F. Henning,[*6] K. Hirose,[*3] N. Inabe,[*2] D. Kameda,[*2] N. Kobayashi,[*2] T. Kobayashi,[*7] Y. Kondo,[*8] T. Kubo,[*2] Y. Kubota,[*2,*5] R. Lang,[*1] L. Maier,[*1] Y. Matsuda,[*9] S. Mitsuoka,[*4] T. Motobayashi,[*2] T. Nakamura,[*8] N. Nakatsuka,[*9] S. Nishimura,[*2] I. Nishinaka,[*3] K. Nishio,[*3] R. Orlandi,[*3] H. Otsu,[*2] V. Panin,[*2] S. Sakaguchi,[*2] H. Sato,[*2] Y. Shimizu,[*2] L. Stuhl,[*2] T. Sumikama,[*2] H. Suzuki,[*2] H. Takeda,[*2] Y. Togano,[*2] T. Uesaka,[*2] J. Yasuda,[*2] K. Yoneda,[*2] and J. Zenihiro[*2]

The aim of NP1306-SAMURAI-14 is to experimentally determine fission barrier heights in neutron-rich nuclei "north east" of doubly-magic ^{208}Pb using RIB's at RI Beam Factory (RIBF) at RIKEN. The results will drastically improve our experimental knowledge on fission barriers away from stability which is poor at present. Neutron-rich nuclei around Z $\approx$ 82 and N $>$ 126 are good subjects to be studied because the isospin dependence of fission barriers in those nuclei are quite controversial: The Rotating Liquid Drop Model predicts an increase of barrier heights with neutron number, while modern, more microscopic fission models make completely different and, depending on the model, quite varying behaviors (see e.g.[1] and references therein). The behavior of fission barriers towards neutron-rich nuclei has a direct impact on the r-process[2], which is believed to produce about half of the stable heavy elements in the universe.

The basic idea is to use the quasifree (p,2p) reaction in inverse kinematics to excite the nuclei of interest. Heavy neutron-rich nuclei provided at the RI Beam Factory bombard a hydrogen target and measurements of proton four-momenta tells us an excitation energy of the neutron-rich isotopes. In case that fission takes place, the two fission fragments are detected and analyzed with the large-acceptance SAMURAI spectrometer[3]. This allows to extract a threshold energy for the fission process.

For this experiment, heavy secondary beams must be produced from a primary ^{238}U beam and identified using BigRIPS. This is a difficult task as the secondary fragments after the production target have very similar A/Q ratios compared to the primary beam, which has to be stopped in the beam dump after the D1 magnet. A first test was performed from the BigRIPS team in autumn 2014 to produce neutron-rich Polonium (Z=84) nuclei (N. Inabe et al. in the present volume of this APR).

In April 2014, we performed a one day test at the SAMURAI setup using a stable ^{238}U beam. The experimental setup was basically identical to the one used for experiment NP1306-SAMURAI-17 (M. Sasano in the present volume of this APR). To keep the beam intensity below $5 \cdot 10^4$ pps in the SAMURAI area, the ^{238}U beam was produced as a secondary beam, using a 5 mm Be production target. The best setting was found by choosing the Q=87+ charge state after the target, followed by a Q=90+ charge state after a thin aluminum degrader. In this way, 40 kHz beam rate after BigRIPS was achieved using 0.75 pnA primary beam intensity. The beam purity was better then 98 %. The beam hit a 1 cm liquid hydrogen target. A multiplicity trigger of the WINDS array (see reports of the present volume of the APR) was used to trigger on possible (p,2p) events close to the target. These data are currently analyzed by S. Reichert. Indeed, based on time-of-flight and QDC information, coincident protons follow the expected kinematics of quasi-free scattering. However, in order to achieve the desired missing mass resolution, a new high-resolution proton-detection system is currently under development in collaboration of the TU Munich and RIKEN. The status of the development of this setup can be found in the report of S. Reichert et al. in the present volume of this APR.

The test experiment also gives first results about the response and performance of various detectors of the SAMURAI setup on high-Z beams. The mass and charge resolution for the identification of fission fragments is currently analyzed by M. Sako (see report in the present volume of this APR). Furthermore the data allow us to study the tracking efficiency of coincident fission fragments. A first analysis about the identification of fission fragments using the FDC1 detector was done by S. Reichert (see report in the present volume of this APR).

*1 Physics Department E12, Technical University Munich
*2 RIKEN Nishina Center
*3 ASRC JAEA
*4 IKP, Technical University Darmstadt
*5 Center for Nuclear Studies, University of Tokyo
*6 Physics Devision, Argonne National Laboratory
*7 Department of Physics, Tohoku University
*8 Department of Physics, Tokyo Institute of Technology
*9 Department of Physics, Kyoto University

References

1) P. Moeller et al.: Phys. Rev. C **79**, 064304 (2009).
2) G. Martinez-Pinedo et al.: Prog. Part. Nucl. Phys. 59 (2007) 199-205.
3) T. Kobayashi et al.: Nucl. Inst. Meth. B 317, 294-304(2013).

Identification of fission fragments from tracks measured by the FDC1

S. Reichert,[*1,*2] M. Sako,[*2] M. Sasano,[*2] D. Mücher,[*1,*2] A. Andreyev,[*3] T. Aumann,[*4] H. Baba,[*2] M. Böhmer,[*1] M. Dozono,[*5] N. Fukuda,[*2] R. Gernhäuser,[*1] W. F. Henning,[*6] K. Hirose,[*3] N. Inabe,[*2] D. Kameda,[*2] N. Kobayashi,[*2] T. Kobayashi,[*7] Y. Kondo,[*8] T. Kubo,[*2] Y. Kubota,[*2,*5] R. Lang,[*1] L. Maier,[*1] Y. Matsuda,[*9] S. Mitsuoka,[*4] T. Motobayashi,[*2] T. Nakamura,[*8] N. Nakatsuka,[*9] S. Nishimura,[*2] I. Nishinaka,[*3] K. Nishio,[*3] R. Orlandi,[*3] H. Otsu,[*2] V. Panin,[*2] S. Sakaguchi,[*2] H. Sato,[*2] Y. Shimizu,[*2] L. Stuhl,[*2] T. Sumikama,[*2] H. Suzuki,[*2] H. Takeda,[*2] Y. Togano,[*2] T. Uesaka,[*2] J. Yasuda,[*2] K. Yoneda,[*2] and J. Zenihiro[*2]

The purpose of the experiment NP1306-SAMURAI14 is to characterize parameters of fission of neutron rich heavy nuclei, like the fission barrier heights and the fragment distributions. As a first step, we performed in April 2014 a 24-hour beamtime experiment using ^{238}U as primary beam at 250 MeV/u and an intensity of 5×10^4 pps. A liquid hydrogen target in the setup of NP1306-SAMURAI17 was used as a secondary target.

In this report we present a method to identify fission fragments by the forward drift chamber 1 (FDC1) which is positioned upstream in front of the SAMURAI spectrometer. In the beam direction, the FDC1 has 14 layers. For each layer the positions of the particles passing the active volume are determined. The most likely trajectory is defined as the composition of the available positions in all layers which has the smallest χ^2. When two fission fragments are incident, there are two possible positions for all the layers and their tracks are given by the two smallest χ^2 values.

In Fig. 1 we show examples of trajectories through the 14 layers in beam axis of the FDC1. In Fig. 1(a) the number of possible positions of the particles in each layer is one. Hence the track corresponds to a beam-like particle, showing no fission reaction is induced. The situation in Fig. 1(b) is totally different where each layer has two entries and two tracks with a large gap can be reconstructed. Such events are interpreted as two particles crossing the FDC1 at the same time.

For these cases the distance b between their intersection points and the first layer of the FDC1 in beam direction is obtained by

$$b = \frac{a_1 + a_2}{tan\theta_1 + tan\theta_2} \quad (1)$$

where $\theta_{1/2}$ are the angles of the two fission fragments 1 and 2 in respect to the beam axis and $a_{1/2}$ are defined as their most probable intersection point with the first layer of the FDC1.

The results for two 1/2 h runs with each with the

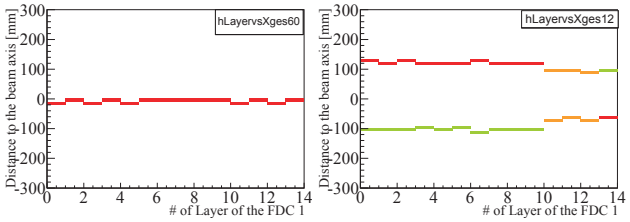

Fig. 1. Online plot of typical tracks observed in the FDC1

filled target or with the empty one are shown in Fig. 2(a) and (b). In both cases the maximum of the very broad peak is in good agreement with the real distance to the target of 2215 mm. The sharp peak at $b \approx$ 4600 mm also appears in both spectra but it is not yet understood. The peak in the case of the empty run can be considered as interactions of the beam with the target foil. The main and important difference is the number of events which drops down from over 100.000 to ∼5000 entries removing the liquid hydrogen from the target.

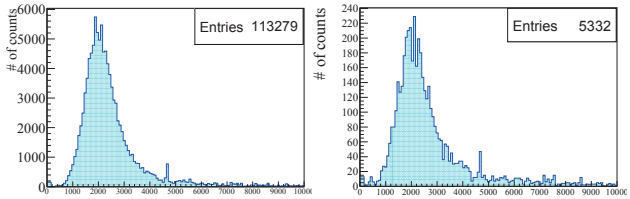

Fig. 2. Intersection point of two tracks of the FDC1 in respect to the beam axis. (a) is the result where the target was mounted, in (b) there was no liquid hydrogen between the target foils.

This method seems promising for a fast and reliable way to identify fission stemming from reactions inside the target. However the uncertainty in the reconstructed vertex position b is very large, $\sigma \sim 600$ mm. In the future this might be improved, e.g., by including the position of the incoming beam by the beam drift chambers. A precise beam position and incident angle is also needed for determining the A/Q value of the fission fragments in the downstream part of the SAMURAI spectrometer.

*1 Technical University Munich
*2 RIKEN Nishina Center
*3 ASRC JAEA
*4 Technical University Darmstadt
*5 Center for Nuclear Studies, University of Tokyo
*6 ANL
*7 Tohoku University
*8 Tokyo Institute of Technology
*9 Kyoto University

Analysis status of the experiment on fission associated with the (p,2p) reaction with ^{238}U beam

M. Sako,[*1] S. Reichert,[*1,*2] M. Sasano,[*1] D. Mücher,[*2] A. Andreyev,[*3] T. Aumann,[*4] H. Baba,[*1] M. Böhmer,[*2] M. Dozono,[*5] N. Fukuda,[*1] R. Gernhäeuser,[*2] W. F. Henning,[*6] K. Hirose,[*3] N. Inabe,[*1] D. Kameda,[*1] N. Kobayashi,[*1] T. Kobayashi,[*7] Y. Kondo,[*8] T. Kubo,[*1] Y. Kubota,[*1,*5] R. Lang,[*2] L. Meier,[*2] Y. Matsuda,[*9] S. Mitsuoka,[*4] T. Motobayashi,[*1] T. Nakamura,[*8] N. Nakatsuka,[*1,*9] S. Nishimura,[*1] I. Nishinaka,[*3] K. Nishio,[*3] R. Orlandi,[*3] H. Otsu,[*1] V. Panin,[*1] S. Sakaguchi,[*7] H. Sato,[*1] Y. Shimizu,[*1] L. Stuhl,[*1] T. Sumikama,[*1] H. Suzuki,[*1] H. Takeda,[*1] Y. Togano,[*8] T. Uesaka,[*1] J. Yasuda,[*1,*10] K. Yoneda,[*1] and J. Zenihiro[*1]

Our experimental program NP1306-SAMURAI14[1] is the first attempt to determine fission barrier height for neutron-rich heavy nuclei such as ^{212}Bi or ^{213}Po. In this experiment, we use missing mass spectroscopy to determine the excitation energy of the fissioning nucleus produced by the (p,2p) reaction in combination with the SAMURAI spectrometer.

In this report, we show preliminary results of data analysis for the test experiment performed using a primary ^{238}U beam with a typical intensity of 5×10^4 pps and at a beam energy of 250A MeV.Liquid hydrogen with a 10-mm thickness was used as the secondary target to study the proton induced (p,2p) reaction.

Figure 1(a) shows the layout of the experimental setup in the downstream part of the SAMURAI spectrometer[2,3]: the forward drift chamber 2 (FDC2), the ion chamber for fragment (ICF), the hodoscope (HODS), and the total energy detector (TED). HODS has seven slats of plastic scintillators. Here, we label the slats with IDs from 0 (lower rigidity side) to 6 (higher rigidity side). TED is an array of 8 × 4 CsI crystals, labeled from 0 to 7 corresponding to HODS for the second row from the bottom side.

Figure 1(b) shows the energy deposition for the slat ID = 1 in HODS without any constraint on the HODS multiplicity, while Fig. 1(c) is constrained by multiplicity = 2. A peak around 3000 ch in Fig. 1(b) corresponds to ^{238}U beam, which disappears with the multiplicity gate. A bump structure around 1000 ch corresponds to fission fragments in Fig. 1(c).

Figure 2 shows two-dimensional histograms of the ΔE-E correlation for fission fragments. Slats ID = 1 (left) and 6 (right) in HODS are selected for ΔE, while the crustal ID = 1 and 6 are selected for total E. The multiplicity gate is applied to Fig. 2 (b) and (d). The test experiment was successful to measure the fission fragments associated with the (p,2p) reaction.

*1 RIKEN Nishina Center
*2 Technical University Munich
*3 ASRC JAEA
*4 Technical University Darmstadt
*5 Center for Nuclear Studies, University of Tokyo
*6 ANL
*7 Tohoku University
*8 Tokyo Institute of Technology
*9 Department of Physics,Kyoto University
*10 Department of Physics,Kyushu University

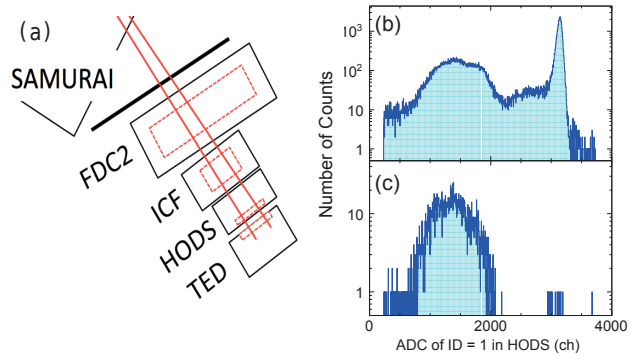

Fig. 1. (a)Layout of the experimental setup of the SAMURAI downstream detectors. The energy deposition (ADC) of slat ID = 1 in the HODS without (b) and with (c) multiplicity gate for slat ID = 1 and 6.

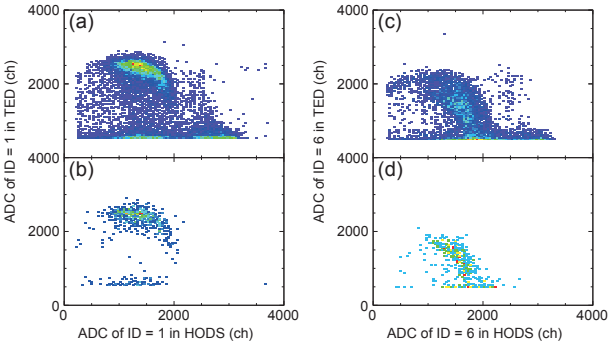

Fig. 2. ΔE-E correlation for each fission fragment with ADC between the TED and HODS with slat ID = 1 (left) and 6 (right) without (top) and with (bottom) the multiplicity gate.

Further analysis will be performed to establish the identification of mass and charge number for each fission fragment.

References

1) D. Mücher, M. Sasano, M. Sako et al.: Proposal RIBF NP-PAC- 12 Fission Barrier Studies of Neutron-Rich Nuclei via the (p,2p) Reaction (2013).
2) T. Kobayashi et al.: Nucl. Instr. Meth. B 317, 294, (2013).
3) SAMURAI Magnet and Detectors: http://ribf.riken.jp/SAMURAI/index.php?ChargedParticleDetector

Study of Neutron-Proton Correlations & 3N Forces in ^{12}C

H. N. Liu,[*1,*2] J. Lee,[*1,*3] H. Otsu,[*1] Y. Kondo,[*4] S. Takeuchi,[*1] Y. Togano,[*4] H. Baba,[*1] N. Chiga,[*5] P. Doornenbal,[*1] N. Fukuda,[*1] J. Gibelin,[*6] J. Hwang,[*7] T. Isobe,[*1] T. Kawabata,[*8] N. Kobayashi,[*9] T. Kobayashi,[*5] K. Kusaka,[*1] S. Leblond,[*6] Y. Matsuda,[*8,*13] M. Matsushita,[*10] R. Minakata,[*4] T. Motobayashi,[*1] T. Murakami,[*5] K. Muto,[*5] T. Nakamura,[*4] N. Nakatsuka,[*8] A. Navin,[*11] M. Nishimura,[*1] S. Ogoshi,[*4] J. Ohnishi,[*1] S. Sakaguchi,[*12] H. Sakurai,[*1] M. Sasano,[*1] H. Sato,[*1] Y. Satou,[*7] K. Sekiguchi,[*5] Y. Shimizu,[*1] T. Sumikama,[*5] Y. Wada,[*5] K. Yoneda,[*1] and J. Zenihiro[*1]

The study of neutron-proton (np) correlations in nuclei is very important to understand the nuclear structure. Direct two-nucleon knockout reactions offer a powerful tool for quantitative measurements of the n-p correlations in $N = Z$ nuclei.[1,2] The measured inclusive two-nucleon knockout cross sections[3,4] show significant enhancement of np ($T = 0$ & 1) over nn and pp ($T = 1$) correlations in ^{12}C. The shell-model calculation for the two-nucleon overlaps within the p shell can reproduce the inclusive cross sections for like-nucleon pair removal, but underestimates the np-pair removal cross section by approximately a factor of two.[1] This discrepancy implies insufficient description of the $T = 0$ np interactions in the shell-model wave functions. A recent calculation using the no-core shell model that exploits modern chiral effective field theory NN+3N interactions[2] suggests that the final-state-exclusive np-knockout cross sections from ^{12}C to the $T = 0$ states can provide an immediate test of the np correlations (particularly in their $T = 0$ component) and three-nucleon forces. To investigate the nature of these forces, we therefore measured γ-residue coincidence to extract the final-state-exclusive np- and pp-removal cross sections from ^{12}C to ^{10}B and ^{10}Be.

The experiment was carried out at RIBF. The secondary ^{12}C beam (presently not available as the primary beam for SRC-use experiments) was produced by fragmentation of an ^{18}O primary beam at 250 MeV/u using a 5-mm thick Be target. The ions of interest were selected using the BigRIPS fragment separator[5] by measuring the energy loss (ΔE) and time of flight (TOF) with plastic scintillators at the intermediate foci F3 and F13. The incident angle and position of the beam on a 1.879-g/cm^2 thick Be target were determined by two drift chambers, BDC1 and BDC2. The target was surrounded by the DALI2 γ-ray spectrometer.[6] One hundred and fifty-nine crystals of DALI2 were employed with an azimuthal angular coverage from 25° to 154°. The mid-target energy of ^{12}C was approximately 190 MeV/u. Reaction products were transported to the SAMURAI spectrometer[7] and identified with the $B\rho$-ΔE-TOF method. The magnetic rigidity $B\rho$ was determined from the measured positions at the forward drift chambers, FDC1 and FDC2. ΔE and TOF were measured by using the plastic scintillator hodoscopes, HODF and HODP. Fig. 1 shows the particle identification of reaction residues. It should be noted that the reaction channels of interest were measured simultaneously because of the large acceptance of SAMURAI.

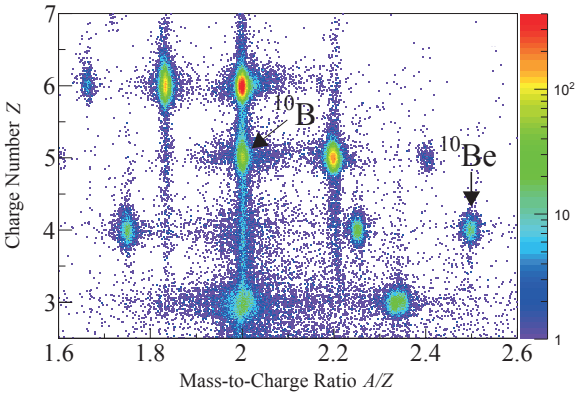

Fig. 1. Particle identification after the secondary target.

The preliminary ratio of inclusive np- to pp-removal cross sections was obtained, which is consistent with the previous result within errors.[3] Currently, the γ-ray spectrum analysis is ongoing. Further, the partial cross sections will be extracted.

*1 RIKEN Nishina Center
*2 School of Physics and State Key Laboratory of Nuclear Physics and Technology, Peking University
*3 Department of Physics, The University of Hong Kong
*4 Department of Physics, Tokyo Institute of Technology
*5 Department of Physics, Tohoku University
*6 LPC, Caen
*7 Department of Physics, Seoul National University
*8 Department of Physics, Kyoto University
*9 Department of Physics, The University of Tokyo
*10 CNS, The University of Tokyo
*11 GANIL, CEA/DSM-CNRS/IN2P3
*12 Department of Physics, Kyushu University
*13 CYRIC, Tohoku University

References

1) E. Simpson and J. A. Tostevin: Phys. Rev. C **83**, 014605 (2011).
2) E. Simpson et al.: Phys. Rev. C **86**, 054609 (2012).
3) J. M. Kidd et al.: Phys. Rev. C **37**, 2613 (1988).
4) D. L. Olson et al.: Phys. Rev. C **28**, 1602 (1983).
5) T. Kubo et al.: Prog. Theor. Exp. Phys. **2012**, 03C003 (2012).
6) S. Takeuchi et al.: Nucl. Instr. Meth. A **763**, 596 (2014).
7) T. Kobayashi et al.: Nucl. Instr. Meth. B **317**, 294 (2013).

Measurement of the ^{132}Sn(p,n) reaction at 270 MeV/nucleon

M. Sasano,[*1] J. Yasuda,[*2] R.G.T. Zegers,[*3] H. Baba,[*1] W. Chao,[*1] M. Dozono,[*1] N. Fukuda,[*1] N. Inabe,[*1] T. Isobe,[*1] G. Jhang,[*1,13] D. Kamaeda,[*1] T. Kubo,[*1] M. Kurata-Nishimura,[*1] E. Milman,[*1] T. Motobayashi,[*1] H. Otsu,[*1] V. Panin, [*1] W. Powell, [*1] M. Sako, [*1] H. Sato,[*1] Y. Shimizu,[*1] L. Stuhl,[*1] H. Suzuki,[*1] T. Suwat, [*1] H. Takeda,[*1] T. Uesaka,[*1] K. Yoneda,[*1] J. Zenihiro,[*1] T. Kobayashi,[*4] T. Sumikama,[*4] T. Tako,[*4] T. Nakamura,[*5] Y. Kondo,[*5] Y. Togano,[*5] M. Shikata,[*5] J. Tsubota,[*5] K. Yako,[*6] S. Shimoura,[*6] S. Ota,[*6] S. Kawase,[*6] Y. Kubota,[*6] M. Takaki,[*6] S. Michimasa,[*6] K. Kisamori,[*6] C.S. Lee,[*6] H. Tokieda,[*6] M. Kobayashi,[*6] S. Koyama,[*7] N. Kobayashi, [*7] H. Sakai,[*8] T. Wakasa,[*2] S. Sakaguchi,[*2] A. Krasznahorkay,[*9] T. Murakami, [*10] N. Nakatsuka, [*10] M. Kaneko, [*10] Y. Matsuda, [*11] D. Mucher, [*12] S. Reichert, [*12] D. Bazin,[*3] and J.W. Lee[*13]

Among the collective modes[1], the Gamow-Teller (GT) giant resonance is an interesting excitation mode. It is a $0\hbar\omega$ excitation characterized by the quantum-number changes of orbital angular momentum ($\Delta L = 0$), spin ($\Delta S = 1$), and isospin ($\Delta T = 1$), and induced by the transition operator $\sigma\tau$. In the stable nuclei in medium or heavier mass regions ($A > 50$), the collectivity in this mode exhibits the GT giant resonance (GTGR), which gives information that is critically important for understanding the isovector part of the effective nucleon-nucleon interaction[2] and the symmetry potential of the equation of the state[3].

The goal of the NP1306-SAMURAI17 experiment performed in Spring 2014 was to extract the GT and spin-dipole (SD) transition strengths over a wide excitation range covering their giant resonances on the key doubly magic nucleus ^{132}Sn via the charge-exchange (p,n) reaction at 270 MeV/nucleon in inverse kinematics. This is an essential step toward establishing comprehensive theoretical models for nuclei situated between ^{78}Ni and ^{208}Pb; at the same time, this is a milestone for extending the research on various phenomena in stable nuclei such as GT quenching, and nuclear weak processes of astrophysical interest, to the neutron-rich region far from the beta stability. An experimental technique based on the missing mass spectrocopy[4,5] was employed to reconstruct the excitation energy spectra for the reaction.

In the experiment, a secondary beam of ^{132}Sn at 270 MeV/nucleon was produced through an abrasion-fission reaction with a 345 MeV/nucleon primary beam of ^{238}U. The resulting cocktail beam had a total intensity of 1.4×10^4 pps, containing ^{132}Sn with a purity of 45%. The particle identification (PID) was performed on an event-by-event basis by measuring the energy loss in the ionization chamber at the F7 focal plane, and the magnetic rigidity and the time of flight of the beam particles in the BigRIPS spectrometer.

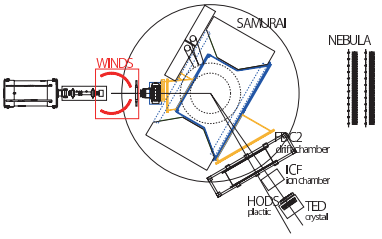

Fig. 1. Top view of the experimental setup around the SAMURAI spectrometer.

Figure 1 shows a top view of the experimental setup around the SAMURAI spectrometer[6]. The secondary beam was impinged on a liquid hydrogen target[7] before the entrance of the SAMURAI magnet. The recoil neutrons were detected by using the Wide-angle Inverse-kinematics Neutron Detectors for SHARAQ (WINDS) surrounding the target. The PID of the reaction residues was performed with the SAMURAI spectrometer and the decay neutrons from the residues were detected with the NEBULA. Detailed reports on the WINDS setup, the PID analysis in the SAMURAI spectrometer, and the NEBULA DAQ based on a fast clear mode are given in other reports in the current volume of the APR. The analysis is in progress. In preliminary results, the kinetic curves corresponding to the (p,n) reaction are clearly observed; this indicates that the experiment worked as planned.

*1 RIKEN Nishina Center
*2 Department of Physics,Kyushu University
*3 NSCL Michigan State University
*4 Department of Physics, Tohoku University
*5 Tokyo Institute of Technology
*6 CNS, University of Tokyo
*7 University of Tokyo
*8 ULIC, RIKEN Nishina Center
*9 MTA, Atomki, Debrecen, Hungary
*10 Kyoto University
*11 Konan University
*12 Technical University Munich
*13 Department of Physics, Korea University

References

1) M. N. Harakeh and A. M. van der Woude: Giant Resonances (Oxford University Press, Oxford, 2001).
2) S. Fracasso and G. Colo: Phys. Rev. C 72, 064310 (2005).
3) P. Danielewicz: Nucl. Phys. A 727, 233 (2003).
4) M. Sasano et al.: Phys. Rev. Lett. 107, 202501 (2011).
5) M. Sasano et al.: Phys. Rev. C 86, 034324 (2012).
6) T. Kobayashi et al.: Nucl. Inst. Meth. B 317, 294-304 (2013).
7) M. Kurata-Nishimura et al.: RIKEN Accel. Prog. Rep. 45, 122 (2012).

Experimental study on neutron-neutron correlation in Borromean nuclei via the (p, pn) reaction at intermediate energy with the SAMURAI spectrometer

Y. Kubota,[*1,*2] A. Corsi,[*3] G. Authelet,[*3] H. Baba,[*2] C. Caesar,[*4] D. Calvet,[*3] A. Delbart,[*3] M. Dozono,[*1] J. Feng,[*5] F. Flavigny,[*6] J.-M. Gheller,[*3] J. Gibelin,[*7] A. Gillibert,[*3] K. Hasegawa,[*8] T. Isobe,[*2] Y. Kanaya,[*9] S. Kawakami,[*9] D. Kim,[*10] Y. Kiyokawa,[*1] M. Kobayashi,[*1] N. Kobayashi,[*11] T. Kobayashi,[*8] Y. Kondo,[*12] Z. Korkulu,[*13] S. Koyama,[*11] V. Lapoux,[*3] Y. Maeda,[*9] F. M. Marqués,[*7] T. Motobayashi,[*2] T. Miyazaki,[*11] T. Nakamura,[*12] N. Nakatsuka,[*14,*2] Y. Nishio,[*15] A. Obertelli,[*3] A. Ohkura,[*15] N. A. Orr,[*7] S. Ota,[*1] H. Otsu,[*2] T. Ozaki,[*12] V. Panin,[*2] S. Paschalis,[*4] E. C. Pollacco,[*3] S. Reichert,[*16] J.-Y. Roussé,[*3] A. Saito,[*12] S. Sakaguchi,[*15] M. Sako,[*2] C. Santamaria,[*3] M. Sasano,[*2] H. Sato,[*2] M. Shikata,[*12] Y. Shimizu,[*2] Y. Shindo,[*15] L. Stuhl,[*2] T. Sumikama,[*8] M. Tabata,[*15] Y. Togano,[*12] J. Tsubota,[*12] T. Uesaka,[*2] Z. Yang,[*5] J. Yasuda,[*15] K. Yoneda,[*2] and J. Zenihiro[*2]

Dineutron correlation is one of the symbolic phenomena expected to appear in neutron drip-line nuclei. It has been studied using different approaches, such as the transfer reaction and the break up reaction. However, currently available data seem to be insufficient to study the neutron-neutron correlation in terms of (i) the decomposition of high-angular-momentum components, (ii) the extraction of a core excitation, (iii) and the effect of final state interactions (FSIs).[1] In this study, (i) the MINOS[2] was used for higher luminosity, (ii) γ rays were detected to tag the core excitation, (iii) and the quasi-free (p, pn) reaction was employed to minimize the FSI.

The experiment was performed at RIBF. Secondary beams were produced and separated by the BigRIPS, by projectile fragmentation of a ^{48}Ca primary beam at 345 MeV/nucleon with a typical intensity of 400 particle nA in a 20-mm or a 30-mm thick Be target. They were detected and identified using plastic scintillators at the focal planes F3, F5, F7, and F13 and multi-wire drift chambers (MWDCs) at F13 (BDC). The sufficient number of beam particles required, which are large enough as indicated, is listed in Table 1. The ratio of ^{3}H in the beam at F13 was typically 14%.

Figure 1 shows a schematic view of the experimental setup. The reaction point in a 15-cm thick liquid hydrogen target was determined from the tracks of charged particles reconstructed from signals from the MINOS TPC and the BDC. The momenta of decay neutrons, a knocked-out neutron, and a recoil proton were determined respectively by the NEBULA,[3] the WINDS,[4] and a recoil proton detector (RPD) setup consisting of an MWDC and a plastic scintillator array. The charged fragments were identified and momentum analyzed by the SAMURAI spectrometer[5] using the two MWDCs (FDC1 and FDC2) followed by the hodoscopes (HODF and HODP). γ rays emitted from the excited core were detected by the DALI2.[6]

Table 1. Number of beam particles on the target. $\Delta p/p$ denotes the momentum acceptance of the BigRIPS.

Beam	Energy [MeV/nucleon]	$\Delta p/p$ [%]	Number of beam particles Required	Obtained
^{11}Li	246	3.2	9.5×10^{9}	1.6×10^{10}
^{14}Be	265	3.2	1.8×10^{9}	2.3×10^{9}
^{17}B	277	3.2	8.6×10^{7}	1.6×10^{9}
^{19}B	224	3.2	4.3×10^{7}	9.8×10^{6}

Data analysis is currently in progress.

We thank the staff of accelerators and BigRIPS for their effort and support. The theoretical support and discussion provided by Y. Kikuchi and K. Ogata are highly appreciated.

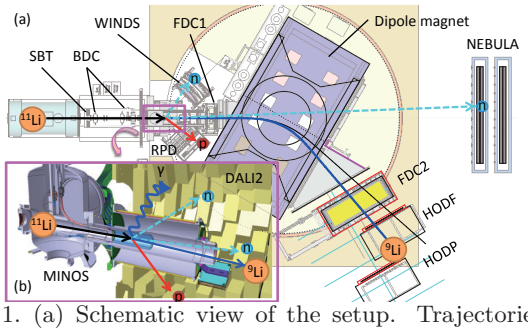

Fig. 1. (a) Schematic view of the setup. Trajectories of particles are shown by arrows. (b) Schematic view of the MINOS surrounded by the DALI2.

*1 Center for Nuclear Study, University of Tokyo
*2 RIKEN Nishina Center
*3 CEA, Saclay
*4 Department of Physics, Technische Universität Darmstadt
*5 Department of Physics, Peking University
*6 IPN Orsay
*7 LPC Caen
*8 Department of Physics, Tohoku University
*9 Department of Applied Physics, University of Miyazaki
*10 Department of Physics, Ehwa Womans University
*11 Department of Physics, University of Tokyo
*12 Department of Physics, Tokyo Institute of Technology
*13 MTA Atomki
*14 Department of Physics, Kyoto University
*15 Department of Physics, Kyushu University
*16 Department of Physics, Technische Universität München

References

1) Y. Kikuchi *et al.*: Phys. Rev. C**87**, 034606 (2013).
2) A. Obertelli *et al.*: Eur. Phys. Jour. A**50**, 8 (2014).
3) Y. Kondo *et al.*: RIKEN Accel. Prog. Rep. **45**, 131 (2012).
4) K. Yako *et al.*: RIKEN Accel. Prog. Rep. **45**, 137 (2012).
5) T. Kobayashi *et al.*: Nucl. Instr. Meth. B**317**, 294 (2013).
6) S. Takeuchi *et al.*: Nucl. Instr. Meth. A**763**, 596 (2014).

Simulations for experimental studies of breakup reactions on neutron-deficient isotopes relevant to the astrophysical *rp*-process

V. Panin,[*1] K. Yoneda,[*1] T. Uesaka,[*1] M. Kurokawa,[*1] T. Motobayashi,[*1] H. Otsu,[*1] Z. Elekes,[*2] A. Saastamoinen,[*3] and B. C. Rasco[*4]

Our experimental program aims to investigate explosive nucleosynthesis in the *rp*-process occurring in type I X-ray bursts related to the most frequent type of stellar explosions in the Galaxy[1)]. Indispensable experimental information related to resonant structures in most sensitive proton-capture reactions with extremely neutron-deficient isotopes will result in the advancement of the existing X-ray burst models by providing a reliable nuclear-data input[2)]. A particular focus of this research is to obtain spectroscopic information about proton-unbound excited states in ^{66}Se and ^{58}Zn, which are expected to be involved in the breakout from the waiting-point nuclei ^{64}Ge and ^{56}Ni through the sequential two-proton capture[3)]. Single-neutron removal reactions from ^{67}Se and ^{59}Zn at 250 MeV/nucleon beam energy will be deployed to populate the states above one- and two-proton separation energy in ^{66}Se and ^{58}Zn, respectively. Proton decay in-flight of these highly excited states will then be measured in complete kinematics using High-Resolution (HR) 90° mode of the SAMURAI magnetic spectrometer[4)] in combination with the existing tracking systems and the custom-designed Si-strip detectors for simultaneous detection and tracking of heavy ions and protons.

The conceptual design of the setup was examined by detailed Geant4 simulations, aiming to achieve an experimental resolution of about 100 keV (sigma) for a single resonance and a total detection efficiency of at least 20%. The multidimensional parameterization and fit algorithm was developed to reconstruct the total momentum of every particle and eventually the proton-fragment relative energy E_{rel} in their rest frame. Compromising the resulting E_{rel} resolution, detection efficiency, and construction cost, an appropriate experimental configuration was worked out after systematical variation of the setup parameters such as the geometry and location of the tracking detectors, target thickness, magnetic field strength, *etc.* In addition, specific simulations were performed to study the effect of δ-electrons on the measurements by the Si trackers. In particular, the interference with a proton signal is studied together with various options to suppress this effect by placing compact kick-off magnets between the Si-trackers, by adjusting the relative distance between the detectors, and/or by track discrimination using track information in the proton-tracking system after the magnet. Based on these studies, the minimum requirements for the design of a vacuum chamber for the Si trackers (*i.e.*, its size, position relative to the target, and internal locations of the detectors) were specified and the following conclusions were drawn:

(1) The HR-mode is suitable for the heavy-ion-proton (HI-p) experiments with beam energies ranging from 200 to 250 MeV/nucleon.
(2) The value of acceptance×efficiency in the HR-mode can be comparable to that of the standard "Day one" configuration (≃40% for one-proton decay with E_{rel}=1 MeV and beam energy of 250 MeV/nucleon).
(3) The HR-mode provides a better mass (momentum) resolution (≃1/1500) for heavy ions.
(4) The momentum resolution for protons and E_{rel} resolution can be determined mainly by the straggling in the target and by the position resolutions of the proton-tracking detectors.
(5) E_{rel} resolution (sigma) of approximately 100 keV can be achieved at E_{rel}=1 MeV along with the beam energies between 200 and 250 MeV/nucleon.

These results together with the LISE++ simulations were used in the experimental proposal that was reviewed and approved by the 14th NP-PAC in June 2014. In a similar way, feasibility studies and experimental optimizations were performed for other potential HI-p experiments involving one- and two-proton breakup of ^{9}C, ^{28}S, ^{32}Ar, ^{34}Ca, ^{35}K, ^{36}K and ^{36}Ca. A common setup configuration for all HI-p experiments was figured out and presented by the collaborators in the 15th NP-PAC. Thus, we intend to perform a total of four HI-p experiments in the next two years, ideally as campaign-type measurements, which will provide a wealth of experimental data that can significantly enrich our knowledge and understanding of nucleosynthesis in type I X-ray bursts.

*1 RIKEN Nishina Center
*2 Institute for Nuclear Research, MTA Atomki
*3 Cyclotron Institute, Texas A&M University
*4 Department of Physics and Astronomy, Louisiana State University

References
1) S. E. Woosley and R. E. Taam: Nature, Vol. 263 (1976), 101-103
2) A. Parikh, J. Jose, G. Sala, and C. Iliadis: Prog. Par. and Nucl. Phys., Vol. 69 (2013), 225-223
3) O. Forstner *et al.*: Phys. Rev. C, Vol. 64 (2001), 045801
4) T. Kobayashi *et al.*: Nucl. Inst. Meth. B 317 (2013), 294-304

Future plan to study light nuclei near the neutron drip line via charge-exchange (p,n) reactions in inverse kinematics

L. Stuhl,[*1] M. Sasano,[*1] D. Ahn,[*1] H. Baba,[*1] W. Chao,[*2] M. Csatlós,[*3] Zs. Dombrádi,[*3] M. Dozono,[*4] N. Fukuda,[*1] B. Hong,[*5] N. Inabe,[*1] T. Isobe,[*1] G. Jhang,[*5] M. Kaneko,[*6] S. Kawase,[*4] K. Kisamori,[*4] M. Kobayashi,[*4] N. Kobayashi,[*7] T. Kobayashi,[*8] Y. Kondo,[*9] Z. Korkulu,[*1] S. Koyama,[*7] A. Krasznahorkay,[*3] T. Kubo,[*1] Y. Kubota,[*1,*4] C. S. Lee,[*1,*4] Y. Matsuda,[*10] S. Michimasa,[*4] E. Milman,[*11] T. Motobayashi,[*1] T. Murakami,[*6] S. Naimi,[*1] T. Nakamura,[*9] N. Nakatsuka,[*6] M. Niikura,[*7] M. Kurata-Nishimura,[*1] A. Ohkura,[*12] S. Ota,[*4] H. Otsu,[*1] V. Panin,[*1] S. Reichert[*13] S. Sakaguchi,[*12] H. Sakai,[*1] M. Sako,[*1] H. Sakurai,[*7] H. Sato,[*1] Y. Satou,[*14] M. Shikata,[*9] Y. Shimizu,[*1] S. Shimoura,[*4] Y. Shindo,[*12] H. Suzuki,[*1] M. Tabata,[*12] M. Takaki,[*4] H. Takeda,[*1] J. Timár,[*3] Y. Togano,[*9] H. Tokieda,[*4] J. Tsubota,[*9] T. Uesaka,[*1] Zs. Vajta,[*3] T. Wakasa,[*12] K. Yako,[*4] J. Yasuda,[*12] K. Yoneda[*1] and J. Zenihiro[*1]

We plan to investigate the isovector response of ^{11}Li and ^{14}Be nuclei near the neutron drip line. The variation of spin-isospin residual interaction and the effect of spatial distribution of neutron skin or halo on spin-isospin responses will be studied using charge-exchange (p,n) reactions, at intermediate energies (260-280 MeV/nucleon) in inverse kinematics. The Gamow-Teller (GT) and spin-dipole (SD) transitions including their giant resonances will be measured. Experimentally, the (p,n) reactions at intermediate beam energies can selectively excite GT states up to high excitation energies in the final nucleus. There is a close proportionality between the cross-sections at 0° and the transition strengths B(GT) in these reactions[1]. Therefore, the (p,n) reactions provide a powerful method to study the B(GT) distributions.

An experimental approach to study the variation of the spin-isospin collectivity is the energy difference between the GT giant resonance (GTGR) and isobaric analog state (IAS) over a wide range of (N-Z)/A. Measurements on stable nuclei show that the GTGR is a few MeV higher than the IAS. This difference gives access to spin-isospin residual interaction strength. However, it is expected to differ at high (N-Z)/A[2,3]. According to predictions for (N-Z)/A values greater than 0.3, the GTGR energy decreases below the IAS energy. It is a compelling interest to obtain new experimental data on nuclei with high (N-Z)/A along the neutron drip line to clarify how the spin-isospin residual interaction strength changes and whether it is related also to the skin or halo structures. With only two pioneer experiments[4,5] this effect is not well studied and further experimental data are needed.

A new experimental technique developed at NSCL, MSU[6,7] will be applied to measure the (p,n) reaction in inverse kinematics which enables us to achieve a high luminosity using a thick target without losing the information on the recoil neutron momentum necessary for the missing mass reconstruction. The setup using BigRIPS, WINDS (Wide-angle Inverse-kinematics Neutron Detectors for SHARAQ) and the SAMURAI spectrometer together with a 10-mm thick liquid hydrogen target will allow us to extract the GT and SD transition strengths from the low-lying region up to 40 MeV excitation energies. The use of the SAMURAI is crucial for covering all decay channels simultaneously and for obtaining conclusive data on the GT strengths of the nuclei of interest.

By using WINDS placed at a distance of 1 m (1.25 m) from the target position both on left and right (top and bottom) sides with respect to the beam line, we detect recoil neutrons from the (p,n) reaction. From the measured neutron TOF and recoil angle, the excitation energy and center-of-mass scattering angle can be deduced. The reaction products will be momentum-analyzed by the SAMURAI spectrometer. The particle identification for the reaction residues will be made using the TOF and energy loss information measured by hodoscopes (HODF, HODP). The energy loss information will be complementary used. The NEBULA detector will be used for tagging the neutron decay of the reaction products.

Our proposal has been presented at the 15th Program Advisory Committee for Nuclear Physics experiments at RI Beam Factory (NP-PAC). The NP-PAC approved 5 days of beam time.

*1 RIKEN Nishina Center
*2 School of Physics, Peking University
*3 MTA Atomki, Debrecen, Hungary
*4 CNS, University of Tokyo
*5 Department of Physics, Korea University
*6 Division of Physics and Astronomy, Kyoto University
*7 Department of Physics, University of Tokyo
*8 Department of Physics, Tohoku University
*9 Department of Physics, Tokyo Institute of Technology
*10 Department of Physics, Konan University
*11 Department of Physics, Kyungpook National University
*12 Department of Physics, Kyushu University
*13 Department of Physics, Technical University Munich
*14 Dept. of Physics and Astronomy, Seoul National University

References

1) T. D. Taddeucci et al.: Nucl. Phys. A **469**, 125 (1987).
2) C. Gaarde: Nucl. Phys. A **396**, 127 (1983).
3) H. Sagawa et al.: Phys. Lett. B **303** 215 (1993).
4) M. Kobayashi et al.: JPS Conf. Proc. **1**, 013034 (2014).
5) H. Sakai et al.: In preparation.
6) M. Sasano et al.: Phys. Rev. Lett. **107**, 202501 (2011).
7) M. Sasano et al.: Phys. Rev. C **86**, 034324 (2012).

Spin-dipole response of ^{4}He by using (^{8}He, ^{8}Li(1$^+$))

H. Miya,[*1] S. Shimoura,[*1] K. Kisamori,[*1,*2] M. Assié,[*3] H. Baba,[*2] T. Baba,[*4] D. Beaumel,[*3] M. Dozono,[*1] T. Fujii,[*2] N. Fukuda,[*2] S. Go,[*1] F. Hammache,[*3] E. Ideguchi,[*5] N. Inabe,[*2] M. Itoh,[*6] D. Kameda,[*2] S. Kawase,[*1] T. Kawabata,[*4] M. Kobayashi,[*1] Y. Kondo,[*7] T. Kubo,[*2] Y. Kubota,[*1,*2] C. S. Lee,[*1,*2] Y. Maeda,[*8] H. Matsubara,[*9] S. Michimasa,[*1] K. Miki,[*5] T. Nishi,[*10] M. Kurata-Nishimura,[*2] S. Ota,[*1] H. Sakai,[*2] S. Sakaguchi,[*11] M. Sasano,[*2] H. Sato,[*2] Y. Shimizu,[*2] H. Suzuki,[*2] A. Stolz,[*12] M. Takaki,[*1] H. Takeda,[*2] S. Takeuchi,[*2] A. Tamii,[*5] H. Tokieda,[*1] M. Tsumura,[*4] T. Uesaka,[*2] K. Yako,[*1] Y. Yanagisawa[*2] and R. Yokoyama[*1]

The spin dipole (SD) (Δ S = Δ L =1) of spin-isospin responses is connected with the tensor correlation in nuclei. Especially, on a double-closed nucleus, the SD excitation contribution is large because of the nucleon configuration. The SD excitation function was measured on ^{4}He which is the lightest double-closed nucleus. This is important for the study of supernova nucleosynthesis with the neutrino-nucleus reaction[1].

We coducted the exothermic charge-exchange (CE) reaction of ^{4}He(^{8}He, ^{8}Li(1$^+$))^{4}H. CE reactions are powerful tools to study the spin-isospin responses. The spin-flip transition of ^{8}He(0$^+$) $\rightarrow$ ^{8}Li(1$^+$) can be identified by measuring the de-excited γ-rays (E$_\gamma$=0.98 MeV) from the first 1$^+$ state of ^{8}Li. The beam energy region of 100–300 MeV/nucleon is suitable for the study of the spin-isospin responses[2].

The experiment was performed at the RIKEN RIBF facility by using BigRIPS[3], the high-Resolution beamline[4], and the SHARAQ spectrometer[5]. The ^{8}He beam, which was produced via a projectile-fragmentation reaction with an ^{18}O beam and ^{9}Be target, was transported to the secondary target position at an intensity of 2 MHz. We used the liquid-^{4}He target[6] with a thickness of 120 mg/cm^2. In order to determine the excitation energy using missing mass method, the momenta of ^{8}He and ^{8}Li at an energy of 190 MeV/nucleon were measured at the beamline and SHARAQ within the low-pressure multi-wire drift chamber (LP-MWDC) [7] and cathode readout drift chamber[8]. The γ-ray detector array DALI2[9] was placed around the target position to measure the 0.98 MeV γ-ray.

Figure 1 shows the missing mass spectrum of the (^{8}He,^{8}Li) reaction (black line). The contribution of both the ^{4}He target and hydrogen is included in this spectrum. The region around 10 MeV and −17 MeV shows the ^{4}He $\rightarrow^4$ H and ^{1}H $\rightarrow$ n reactions, respectively. The ^{1}H $\rightarrow$ n reaction originates at the plastic scintilator installed at the upstream of the target. The amount of contamination (red line) was estimated by using the energy loss of the LP-MWDC placed between the scintilator and the target. Thus, the ^{4}He(^{8}He, ^{8}Li)^{4}H reaction was obtained.

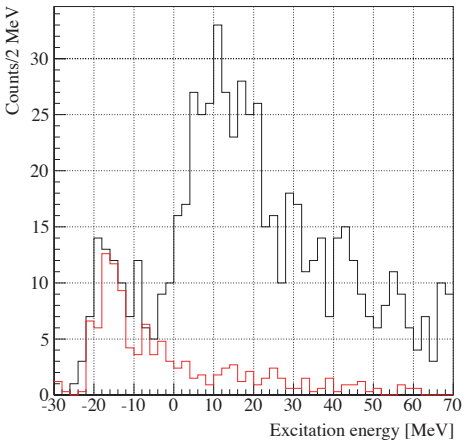

Fig. 1. Excitation energy distribution of ^{4}H obtained using missing mass method. The red line shows the background estimated from the contamination of the excitation energy distribution.

Further analysis to obtain the angular distribution and double differential cross-sections is now in progress to obtain the isovector SD strength of ^{4}He.

*1 Center for Nuclear Study, The University of Tokyo
*2 RIKEN Nishina Center
*3 Institut de Physique Nucléaire, Orsay
*4 Department of Physics, Kyoto University
*5 Research Center Nuclear Physics, Osaka University
*6 Cyclotron and Radioisotope Center, Tohoku University
*7 Department of physics, Tokyo Institute of Technology
*8 Department of Applied Physics, University of Miyazaki
*9 National Institute of Radiological Sciences
*10 Department of physics, The University of Tokyo
*11 Department of Physics, Kyushu University
*12 National Superconducting Cyclotron Laboratory, Michigan State University

References

1) T. Suzuki *et al.* Phys. Rev. C **74**, 034307 (2006).
2) W. G. Love and M. A. Franey: Phys. Rev. C **24**, 1073 (1981).
3) T. Kubo *et al.*: Nucl. Instr. Meth. B **204**, 97-113 (2003).
4) T. Kawabata *et al.*: Nucl. Instr. Meth. B **266**, 4201-4204 (2008).
5) S. Michimasa *et al.*: Nucl. Instr. Meth. B **317**, 305-310 (2013).
6) H. Ryuto *et al*: Nucl. Instr. Meth. A 555, 1-5 (2005).
7) H. Miya *et al.*: Nucl. Instr. Meth. B **317**, 701-704 (2013).
8) K. Kisamori *et al.*: CNS Ann. Rep. 2011 (2013).
9) T. Takeuchi *et al.*: Nucl. Instr. Meth. A **763**, 1-8 (2014).

Spectroscopy of Single-Particle States in Oxygen Isotopes via $^{A}\mathrm{O}(\vec{p}, 2p)$ Reaction with Polarized Protons

S. Kawase,[*1] T. L. Tang,[*1] T. Uesaka,[*2] D. Beaumel[*2,*3] M. Dozono,[*2] T. Fujii,[*1,*2] T. Fukunaga,[*2,*4] N. Fukuda,[*2] A. Galindo-Uribarri,[*5] S. H. Hwang,[*6] N. Inabe,[*2] D. Kameda,[*2] T. Kawahara,[*2,*7] W. Kim,[*6] K. Kisamori,[*1,*2] M. Kobayashi,[*1] T. Kubo,[*2] Y. Kubota,[*1,*2] K. Kusaka,[*2] C. S. Lee,[*1,*2] Y. Maeda,[*8] H. Matsubara,[*2] S. Michimasa,[*1] H. Miya,[*1*2] T. Noro,[*2,*4] A. Obertelli,[*9] S. Ota,[*1] E. Padilla-Rodal,[*10] S. Sakaguchi,[*2,*4] H. Sakai,[*2] M. Sasano,[*2] S. Shimoura,[*1] S. S. Stepanyan,[*6] H. Suzuki,[*2] M. Takaki,[*1,*2] H. Takeda,[*2] H. Tokieda,[*1] T. Wakasa,[*2,*4] T. Wakui,[*2,*11] K. Yako,[*1] Y. Yanagisawa,[*2] J. Yasuda,[*2,*4] R. Yokoyama,[*1,*2] K. Yoshida,[*2] and J. Zenihiro[*2] for the SHARAQ04 collaboration

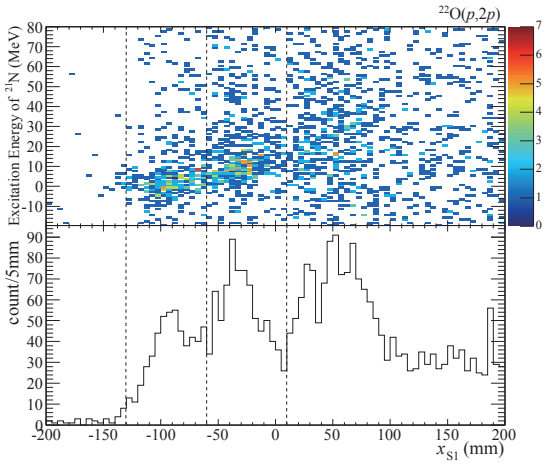

Fig. 1. Correlation between the excitation energy of ^{21}N and x_{S1}.

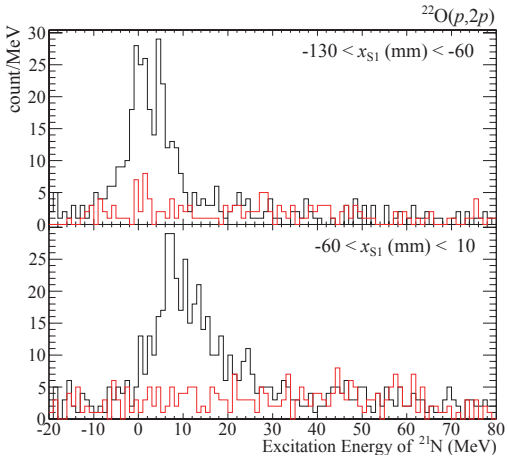

Fig. 2. Excitation energy spectrum for $^{22}\mathrm{O}(p, 2p)$ for each x_{S1} region. The red lines show the background estimated from the $2p$ coincidence events occurred in the carbon target.

We performed $^{14,22-24}\mathrm{O}(\vec{p}, 2p)$ reaction measurements (SHARAQ04 experiment) with a polarized proton target at RIBF to measure single-particle spectra and to determine spin-orbit splitting of 1p proton single-particle orbits in $^{14,22-24}$O as a function of their neutron number. For the experimental setup, see ref.[1]. In this report, current status of the analysis for ^{22}O(p,2p) is described.

The $(p, 2p)$ reaction was identified via the particle identifications of incident nuclei and two scattered protons. Particles were identified via the Time-of-Flight(TOF)-ΔE method on an event-by-event basis. Then the proton separation energy of the incident nuclei and the excitation energy of the residual nuclei were calculated from scattering angles and TOF of scattered protons.

Position of the residual nuclei and TOF from the target are also measured at a focal plane S1 at the downstream of the reaction point for the identification of the residual particle in order to improve the S/N ratio and to separate the excited states of ^{21}N. Figure 1 shows the correlation between the excitation energy and the position of the residual nuclei at the S1 focal plane (x_{S1}) after applying a TOF gate. At S1, particles with larger $B\rho$ come to the smaller x_{S1} region. There are two clear loci in the x_{S1} region of $(-130, -60)$ and $(-60, 10)$. The former corresponding to ^{21}N and the latter should be ^{19}N or ^{20}N generated through the neutron emission of ^{21}N. It will be clarified by $B\rho$ analysis.

Figure 2 shows the excitation energy spectra of ^{21}N for different x_{S1} regions. The red lines show the background originated from the carbon contamination of the polarized target and obtained from the measurement with a carbon target. At least two discrete states are observed in these plots.

The cross sections, spectroscopic factors, and the spin-polarization observables such as the vector analyzing power are expected to be obtained through subsequent analyses in the near future.

*1 Center for Nuclear Study (CNS), University of Tokyo
*2 RIKEN Nishina Center
*3 Institut de Physique Nucléaire d'Orsay
*4 Department of Physics, Kyushu University
*5 Oak Ridge National Laboratory
*6 Department of Physics, Kyungpook National University
*7 Department of Physics, Toho University
*8 Department of Applied Physics, University of Miyazaki
*9 CEA Saclay
*10 Instituto de Ciencias Nucleares, Universidad Nacional Autónoma de México
*11 CYRIC, Tohoku University

References

1) S. Kawase *et al.*: RIKEN Accel. Prog. Rep., **46**, 30 (2013)

Status on residual analysis of SHARAQ04 experiment

T. L. Tang,[*1] S. Kawase,[*1] T. Uesaka,[*2] D. Beaumel,[*2,*3] M. Dozono,[*2] T. Fujii,[*1,*2] N. Fukuda,[*2] T. Fukunaga,[*2,*4] A. Galindo-Uribarri,[*5] S. H. Hwang,[*6] N. Inabe,[*2] D Kameda,[*2] T. Kawahara,[*2,*7] W. Y. Kim,[*6] K. Kisamori,[*1,*2] M. Kobayashi,[*1] T. Kubo,[*2] Y. Kubota,[*1,*2] K. Kusaka,[*2] C. S. Lee,[*1] Y. Maeda,[*8] H. Matsubara,[*2] S. Michimasa,[*1] H. Miya,[*1,*2] T. Noro,[*2,*4] A. Obertelli,[*9] S. Ota,[*1] E. Padilla-Rodal,[*10] S. Sakaguchi,[*2,*4] H. Sakai,[*2] M. Sasano,[*2] S. Shimoura,[*1] S. S. Stepanyan,[*6] H. Suzuki,[*2] M. Takaki,[*1,*2] H. Takeda,[*2] H. Tokieda,[*1] T. Wakasa,[*2,*4] T. Wakui,[*2,*11] K. Yako,[*1] Y. Yanagisawa,[*2] J. Yasuda,[*2,*4] R. Yokoyama,[*1,*2], K. Yoshida,[*2] and J. Zenihiro,[*2] for SHARAQ04 collaboration

Proton knockout reaction on radioactive fluorine and oxygen isotopes was performed in SHARAQ04 experiment at RIBF, RIKEN Nishina Center. The analyses on ^{14}O and ^{22}O have been reported by S. Kawase et al.[1, 2]. The identification of residual nuclei at downstream (S1 focal plane of the SHARAQ spectrometer[3]) serves an important role in identifying the reaction channel and separating the strengths in the excitation energy spectrum. The objective of the present analysis is particle identification via Z vs A/Q plot. We will explain the conversion from the energy loss (ΔE) vs time-of-flight (TOF) plot to the Z vs A/Q plot.

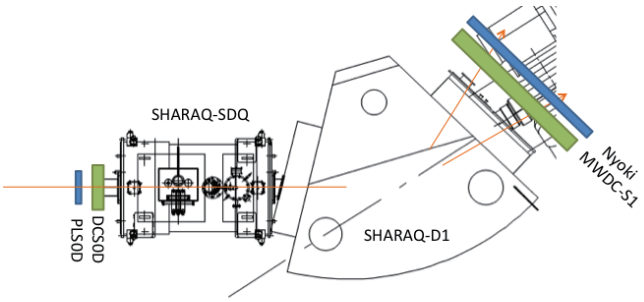

Fig. 1. Experimental setup before S1 focal plane of SHARAQ spectrometer.

Figure 1 shows the experimental setup for downstream. The TOF was measured by an array of 14 identical plastic scintillators (5 mm X 50 mm X 85 mm), named Nyoki, with a plastic scintillator (PLS0D) located in the entrance of the SDQ magnet as start timing. Each scintillator of Nyoki was labeled from 0 to 13. The even ID scintillators were 10 mm downstream from odd ID. There was 5 mm overlap between adjacent IDs. The energy loss of each Nyoki's scintillator was calibrated with the energy loss in PLS0D. The positions of the residual nuclei were measured by an MWDC at the exit of the D1 magnet. The flight-length was then calculated by using the position at S1. The velocities of the residual nuclei were calculated from the flight length and the TOF.

*1 Center of Nuclear Study (CNS), University of Tokyo
*2 RIKEN Nishina Center
*3 Institut de Physique Nucléaire d'Orsay
*4 Department of Physics, Kyushu University
*5 Oak Ridge National Laboratory
*6 Department of Physics, Kyungpook National University
*7 Department of Physics, Toho University
*8 Department of Applied Physics, University of Miyazaki
*9 CEA Saclay
*10 Instituto de Ciencias Nucleares, Universidad Nacional Autónoma de México
*11 CYRIC, Tohoku University

The conversion from ΔE-TOF to Z-A/Q is based on the following equations,

$$Z = \beta \sqrt{\frac{L}{g + h\,L}}, \tag{1}$$

$$\frac{A}{Q} = \left(\frac{c}{u}\right)\frac{1}{\gamma\beta}\left(B_\rho\right)_{D1}\left(1 + \frac{x}{(x|\delta)}\right), \tag{2}$$

where β and γ are the Lorentz factors of residual nuclei; L is the light output of Nyoki; g and h are the parameters from the Birks formula[4], which correct the non-linearity of light-output and energy loss; c is the speed of light in vacuum; u is the atomic mass unit; $(B_\rho)_{D1}$ is the magnetic rigidity of the D1 magnet (6.5269 Tm); x is the x-position on MWDC-S1; and $(x|\delta)$ is the dispersion at the S1 focal plane.

Figure 2 shows the Z vs A/Q plots for the beam without reaction. The left plot is from downstream and the right plot is from upstream. The accuracy and resolution of both Z and A/Q in the downstream plot are bad compared with those in the upstream plot. The resolution of Z is 0.3 in the downstream plot, while it is 0.1 for the upstream plot. The resolution of A/Q is 0.1 for the downstream plot, and it is 0.01 for the upstream plot.

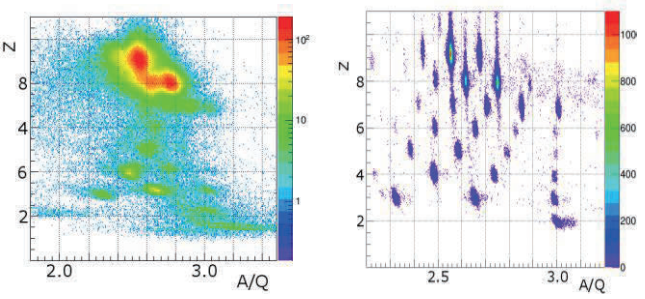

Fig. 2. Z vs A/Q plots under beam trigger; (left) downstream; (right) upstream.

The analysis is still in progress. We are focusing on improving the accuracy and resolution by 1) better estimation of the parameters such as g, h, and $(x|\delta)$; 2) better calculation on flight-length; and 3) better tracking of SMWDC-S1.

References

1) S. Kawase *et al.*: RIKEN Accel. Prog. Rep. 46 (2013) 30.
2) S. Kawase *et al.*: in this report.
3) T. Uesaka *et al.*: Nucl. Inst. Meth. Phys. B 266 (2008) 4218.
4) W. R. Leo: Techniques for Nuclear and Particle Physics Experiments (Springer-Verlag, Berlin, 1994), P 168.

Parity-transfer reaction for study of spin-dipole 0^- mode

M. Dozono,[*1] K. Fujita,[*2] N. Fukuda,[*3] M. Ichimura,[*3] N. Inabe,[*3] S. Kawase,[*1] K. Kisamori,[*1] Y. Kiyokawa,[*1] K. Kobayashi,[*4] M. Kobayashi,[*1] T. Kubo,[*3] Y. Kubota,[*1] C. S. Lee,[*1] M. Matsushita,[*1] S. Michimasa,[*1] H. Miya,[*1] A. Ohkura,[*2] S. Ota,[*1] H. Sagawa,[*1,*5] S. Sakaguchi,[*2] H. Sakai,[*3] M. Sasano,[*3] S. Shimoura,[*1] Y. Shindo,[*2] L. Stuhl,[*3] H. Suzuki,[*3] H. Tabata,[*2] M. Takaki,[*1] H. Takeda,[*3] H. Tokieda,[*1] T. Uesaka,[*3] T. Wakasa,[*2] K. Yako,[*1] M. Yamagami,[*5] Y. Yanagisawa,[*3] J. Yasuda,[*2] R. Yokoyama,[*1] K. Yoshida,[*3] and J. Zenihiro[*3]

The spin-dipole (SD) 0^- excitation has recently attracted theoretical attention owing to its strong relevance in the tensor correlations in nuclei. For example, self-consistent HF+RPA calculations in Ref.[1] predict that the tensor correlations produce a strong hardening (shifting toward higher excitation energy) effect on the 0^- resonance. It is also predicted that the effect is sensitive to the magnitude of the tensor strength. Thus experimental data of the SD 0^- distribution enable us to examine the tensor correlation effects quantitatively. Despite this importance, experimental information on 0^- states is limited because of the lack of the experimental tools suitable for 0^- studies.

We propose a new probe, the parity-transfer $(^{16}\mathrm{O}, ^{16}\mathrm{F}(0^-, \mathrm{g.s.}))$ reaction, for 0^- studies[2]. The parity-transfer reaction selectively excites unnatural-parity states for a 0^+ target nucleus, which is an advantage over the other reactions used thus far. In order to establish the parity-transfer reaction as a new tool for 0^- studies, we measured the $^{12}\mathrm{C}(^{16}\mathrm{O}, ^{16}\mathrm{F}(0^-, \mathrm{g.s.}))^{12}\mathrm{B}$ reaction. We demonstrate the effectiveness of this reaction by identifying the known 0^- state at E_x = 9.3 MeV in ^{12}B.

The experiment was performed at the RIKEN RI Beam Factory (RIBF) by using the SHARAQ spectrometer and the high-resolution beam line. Figure 1 shows a schematic layout of the experimental setup. A primary ^{16}O beam at 250 MeV/nucleon and 10^7 pps from the superconducting RING cyclotron (SRC) was transported to the S0 target position. The beam line to the spectrometer was set up for dispersion-matched transport. We used a segmented plastic scintillation detector as an active ^{12}C target. This detector consisted of 16 plastic scintillators with a size of 30 mm × 5 mm × 1 mm, and it was used to determine the x-position of the beam on the target. The outgoing $^{15}\mathrm{O} + p$ particles produced by the decay of ^{16}F were measured in coincidence. The particles were momentum analyzed by using the SHARAQ spectrometer. The ^{15}O particles were detected with two low-pressure multi-wire drift chambers (LP-MWDCs) at the S2 focal plane, while the protons were detected with two MWDCs at the S1 focal plane.

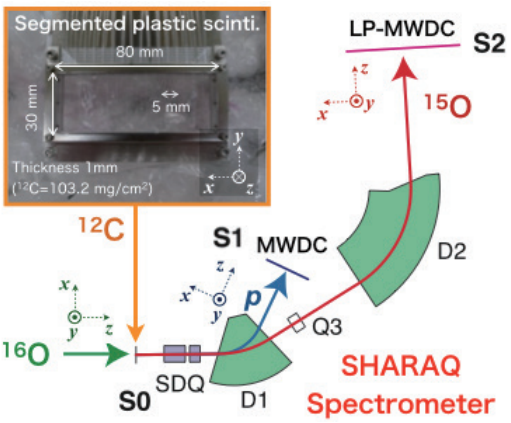

Fig. 1. Schematic layout of the experimental setup.

We reconstructed the relative energy E_{rel} between the ^{15}O and the proton. A preliminary result is shown in Fig. 2. The obtained E_{rel} resolution was 150 keV in FWHM at E_{rel} = 535 keV, and the 0^- ground state of ^{16}F was clearly separated from other excited states. In order to identify the $^{12}\mathrm{B}(0^-, 9.3\ \mathrm{MeV})$ state, data analysis for obtaining the $^{12}\mathrm{C}(^{16}\mathrm{O}, ^{16}\mathrm{F}(0^-, \mathrm{g.s.}))$ spectrum and its angular distributions is in progress.

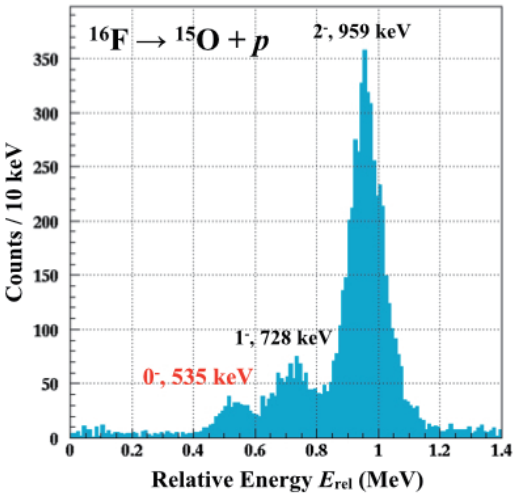

Fig. 2. Preliminary result of the relative energy between the ^{15}O nucleus and the proton from the decay of ^{16}F.

*1 Center for Nuclear Study, University of Tokyo
*2 Department of Physics, Kyushu University
*3 RIKEN Nishina Center
*4 Rikkyo University
*5 Center for Mathematics and Physics, University of Aizu

References

1) H. Sagawa and G. Colò: Prog. Part. Nucl. Phys. **76**, 76 (2014).
2) M. Dozono *et al.*: RIKEN Accel. Prog. Rep. **45**, 10 (2012).

Direct mass measurements of neutron-rich Ca isotopes beyond $N = 34$

M. Kobayashi,[*1] S. Michimasa,[*1] Y. Kiyokawa,[*1] H. Baba,[*2] G.P.A. Berg,[*3] M. Dozono,[*1] N. Fukuda,[*2] T. Furuno,[*4] E. Ideguchi,[*5] N. Inabe,[*2] T. Kawabata,[*4] S. Kawase,[*1] K. Kisamori,[*1,*2] K. Kobayashi,[*6] T. Kubo,[*2] Y. Kubota,[*1,*2] C.S. Lee,[*1,*2] M. Matsushita,[*1] H. Miya,[*1] A. Mizukami,[*7] H. Nagakura,[*6] D. Nishimura,[*7] H. Oikawa,[*7] S. Ota,[*1] H. Sakai,[*2] S. Shimoura,[*1] A. Stolz,[*8] H. Suzuki,[*2] M. Takaki,[*1] H. Takeda,[*2] S. Takeuchi,[*2] H. Tokieda,[*1] T. Uesaka,[*2] K. Yako,[*1] Y. Yamaguchi,[*6] Y. Yanagisawa,[*2] R. Yokoyama,[*1] and K. Yoshida[*2]

The shell evolution in nuclei far from stability is one of the main subjects of nuclear physics. Nuclear mass is one of the most fundamental quantity providing information on the shell structure. The neutron numbers of 32 and 34 have been suggested to be candidates of new magic numbers in the Ca isotopes[1]. Recently the masses of ^{53}Ca and ^{54}Ca were measured, and the shell closure at $N = 32$ was established[2]. The present work aims at studying the nuclear shell evolution at $N = 32$, 34 by direct mass measurements of neutron-rich nuclei in the vicinity of ^{54}Ca.

The experiment was performed at the RIKEN RI Beam Factory (RIBF). The masses were measured directly by the TOF-$B\rho$ method. Neutron-rich isotopes were produced by fragmentation of a ^{70}Zn primary beam at 345 MeV/nucleon in a ^{9}Be target. The fragments were separated by BigRIPS, and transported in the High Resolution Beam Line to the SHARAQ spectrometer. The beam line and SHARAQ were operated in the dispersion matching mode allowing a momentum resolution of 1/14700.

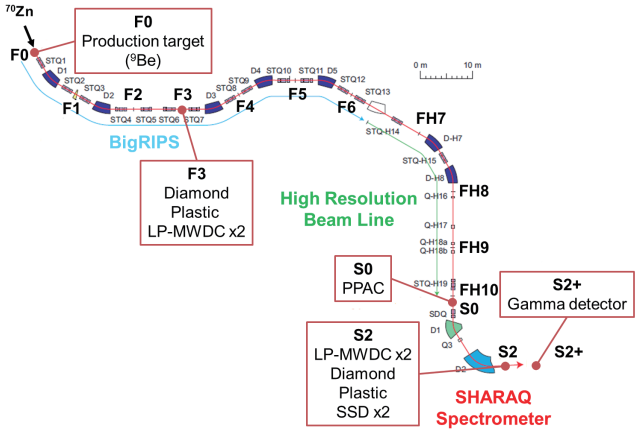

Fig. 1. Schematic view of the beamline and the detectors used in the experiment.

A schematic view of the beamline with the detectors used in the experiment is shown in Fig. 1. The TOF was measured with newly developed diamond detectors[3] installed at BigRIPS-F3 and the final focal plane of SHARAQ (S2). The flight path length between F3 and S2 is 105 m along the central ray. We installed two low pressure multi-wire drift chambers (LP-MWDCs)[4] at both F3 and S2 to correct the flight pass lengths using the tracking information on an event-by-event basis. The $B\rho$ value was measured by a parallel plate avalanche counter (PPAC) located at the target position of SHARAQ (S0). At S2, we mounted two silicon strip detectors for identification of the atomic numbers of the fragments. To identify the isomers, which leads to a systematic shift towards higher masses, we placed a plastic stopper downstream of S2 and a γ-detector array consisting of 2 Ge clover and 16 NaI(Tl) detectors. Details of this system can be found in Ref.[5].

Figure 2 shows the preliminary particle identification of the secondary beams. The total yield of ^{55}Ca was on the order of several thousands. Many species of reference nuclei over a broad range of A and Z were observed, which were used in the mass calibration. Further analysis is in progress.

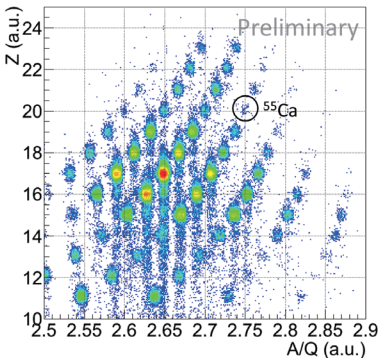

Fig. 2. Particle identification of the secondary beams.

*1 Center for Nuclear Study, University of Tokyo
*2 RIKEN Nishina Center
*3 Department of Physics, University of Notre Dame
*4 Department of Physics, Kyoto University
*5 RCNP, Osaka University
*6 Department of Physics, Rikkyo University
*7 Department of Physics, Tokyo University of Science
*8 NSCL, Michigan State University

References

1) T. Otsuka *et al.*: Phys. Rev. Lett. **87** 082502 (2001).
2) F. Wienholtz *et al.*: Nature **498** 349 (2013).
3) S. Michimasa *et al.*: Nucl. Instr. Meth. B **317** 305 (2013).
4) H. Miya *et al.*: Nucl. Instr. Meth. B **317** 317 (2013).
5) Y. Kiyokawa *et al.*: in this report.

Gamma-ray detector array for isomer tagging at SHARAQ

Y. Kiyokawa,[*1] S. Michimasa,[*1] M. Kobayashi,[*1] R. Yokoyama,[*1] D. Nishimura,[*2] S. Ota,[*1] A. Mizukami,[*2] H. Oikawa,[*2] K. Kobayashi,[*3] H. Baba,[*4] G.P.A. Berg,[*5] M. Dozono,[*1] N. Fukuda,[*4] T. Furuno,[*6] E. Ideguchi,[*7] N. Inabe,[*4] T. Kawabata,[*6] S. Kawase,[*1] K. Kisamori,[*1,*4] T. Kubo,[*4] Y. Kubota,[*1,*4] C.S. Lee,[*1] M. Matsushita,[*1] H. Miya,[*1] H. Nagakura,[*3] H. Sakai,[*4] S. Shimoura,[*1] A. Stolz,[*8] H. Suzuki,[*4] M. Takaki,[*1] H. Takeda,[*4] S. Takeuchi,[*4] H. Tokieda,[*1] T. Uesaka,[*4] K. Yako,[*1] Y. Yamaguchi,[*3] Y. Yanagisawa,[*4] and K. Yoshida[*4]

Mass measurement of neutron-rich short-lived nuclei was performed by employing the TOF-Bρ technique at the RIKEN RI Beam Factory(RIBF). A beam of ^{70}Zn at 345MeV/nucleon bombarded a ^{9}Be target to produce neutron-rich nuclei with atomic numbers (Z) ranging from 10 (Ne) to 23 (V) and A/Q from 2.5 to 2.9. Nuclei of interest were separated and particle identified on an event-by-event basis by using the BigRIPS separator coupled with the SHARAQ spectrometer. Details of this experiment can be found in Ref.[1].

Herein, we report on an isomer tagging gamma-ray detector array to assist in particle identification.Furthermore the array was used to search for new isomeric states. Figure 1 shows a schematic view of the γ-ray detector array, installed in the air downstream of the final focal plane (S2) of the SHARAQ spectrometer. The array consisted of 2 clover-type HPGe detectors, each surrounded with 8 NaI(Tl) scintillators. A 20-mm-thick plastic scintillator was placed as an active beam stopper for Sc isotopes at the center of the detector array. An 12-mm-thick aluminum degrader was installed upstream to adjust the stopping range of the nuclei of interest. A veto scintillator was installed downstream of the γ-ray detector array to reject the events where the nuclei penetrated the stopper. The dynamic range of HPGe and NaI(Tl) detectors covers γ-rays up to 3 MeV. The energy resolution of the HPGe [NaI(Tl)] detectors was about 3.8 keV [60 keV] at 1333 keV [662 keV] in FWHM and full-energy peak efficiencies were 0.6% [9.7%] for 1.2-MeV γ rays. The decay time window for gamma-ray spectra was set to 100 ns – 15 μs after the particles arrived at S2. The data acquisition (DAQ) system for the γ-ray detector array was separate from the one for the mass measurement and ran with single triggers from HPGe or NaI(Tl) detectors. For making an event correlation between the two DAQs used for isomer tagging and for particle identification, a common time stamp was recorded in both DAQ systems.

Figure 2 shows the delayed γ-ray spectra measured by HPGe in (a) ^{50}K and (b) ^{43}S used for the particle identification. The energies of the observed gamma rays were consistent with those of previous works, Refs.[2),3)].

Further analysis for the identification of new isomeric states and isomeric ratios is in progress.

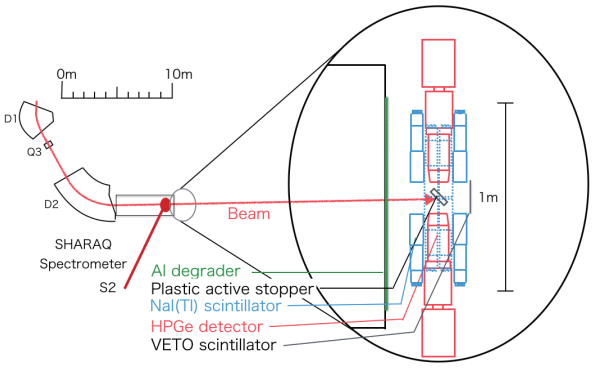

Fig. 1. Schematic view of the isomer tagging system downstream of the final focal plane of SHARAQ(S2).

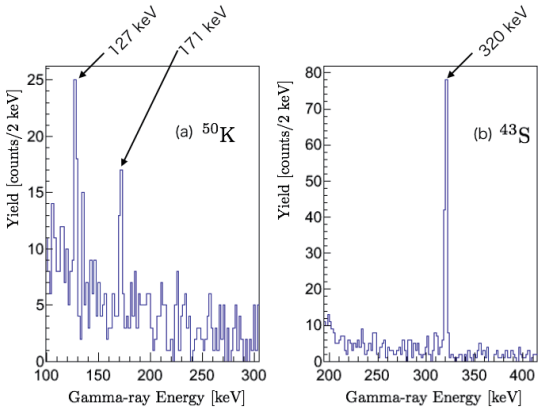

Fig. 2. Delayed γ-ray spectra measured by HPGe in (a) ^{50}K and (b) ^{43}S used for the particle identification.

*1 Center for Nuclear Study, University of Tokyo
*2 Tokyo University of Science
*3 Rikkyo University
*4 RIKEN Nishina Center
*5 University of Notre Dame
*6 Department of Physics, Kyoto University
*7 RCNP, Osaka University
*8 NSCL, Michigan State University

References

1) M. Kobayashi *et al.*: in this report.
2) J.M. Daugas *et al.*: Phys. Rev. C. **81** (2010) 034304.
3) L. Gaudefroy *et al.*: Phys. Rev. Lett. **102** (2009) 092501.

Quadrupole collectivity in island-of-inversion nuclei ^{28,30}Ne and ^{34,36}Mg†

S. Michimasa,[*1] Y. Yanagisawa,[*2] K. Inafuku,[*3] N. Aoi,[*4] Z. Elekes,[*5] Zs. Fülöp,[*5] Y. Ichikawa,[*2] N. Iwasa,[*3] K. Kurita,[*6] M. Kurokawa,[*2] T. Machida,[*6] T. Motobayashi,[*2] T. Nakamura,[*7] T. Nakabayashi,[*7] M. Notani,[*8] H. J. Ong,[*4] T. K. Onishi,[*9] H. Otsu,[*2] H. Sakurai,[*2,*9] M. Shinohara,[*7] T. Sumikama,[*3] S. Takeuchi,[*2] K. Tanaka,[*2] Y. Togano,[*7] K. Yamada,[*2] M. Yamaguchi,[*2] and K. Yoneda[*2]

We report here on the in-beam γ-ray spectroscopy in very neutron-rich even-even nuclei of ^{28,30}Ne and ^{34,36}Mg by proton inelastic scattering using a liquid hydrogen target in inverse kinematics. The ^{30}Ne nucleus has a conventional magic number of 20, and ^{36}Mg is located in the middle of the shell closures of $N = 20$ and 28. The ^{30}Ne and ^{36}Mg are closer to the neutron drip line than the nuclei belonging to the so-called "island of inversion (IOI)". We have studied the evolution of quadrupole deformation on the side with more neutrons and less protons than IOI. The report is a condensed version of our published paper[1].

The experiment was performed using the RIPS beamline at the RI Beam Factory. A radioactive secondary beam, containing neutron-rich nuclei ^{32,34,36}Mg and ^{28,30}Ne, was produced by fragmentation reactions from 63-MeV/nucleon ^{48}Ca. Details of the experimental setup around the secondary target and beam conditions are provided in Ref.[1].

The angle-integrated cross sections for population of the 2^+_1 states were obtained from the yields of the $2^+_1 \rightarrow 0^+_1$ transitions with γ-detection multiplicity equal to one. The spectra are shown in Figs. 3–6, 8 in Ref.[1]. The deduced cross sections and deformation lengths are summarized in Table 1.

The present results extended the measurements of quadrupole collectivity along Ne and Mg isotopic chains by providing deformation lengths with improved accuracies for ^{28,30}Ne, ^{34}Mg and a new measurement for ^{36}Mg. The systematic trends of the deformation lengths are displayed in Fig. 1(a) and (b). The filled and open circles indicate the deformation lengths deduced in the present work and those that have been estimated from the previous results using the WP09 potential[2], respectively. The thin black and thick orange error bars represent statistical and systematic errors, respectively. The squares indicate previous results of Coulomb excitation experiments.

Figures 1(a) and (b) also display several theoretical results that can be compared to the experimental results. The solid-blue and dashed-red lines are predictions by AMPGCM[3] and the shell model with the SDPF-M effective interaction[4], respectively. The shell model calculations in a $0\hbar\omega$ model space are shown by the green dotted[5] and orange dotted[6] lines. For Mg isotopes, the AMPGCM and SDPF-M calculations, which implement configuration mixing around $N = 20$, reproduce the systematic trend of experimental deformation lengths in a satisfactory manner. In addition, they agree with the trend for the Ne isotopic chain, although they both systematically overestimate the experimental values.

Table 1. Angle-integrated cross sections for the 2^+_1 states and deduced deformation lengths in ^{28,30}Ne and ^{32,34,36}Mg.

Nucleus	$\sigma(2^+_1)$ (mb)	$\delta_{(p,p')}$ (fm)
^{28}Ne	23(2)	1.33 ± 0.06 (stat) ± 0.05 (syst)
^{30}Ne	37(4)	$1.59^{+0.08}_{-0.09}$ (stat) ± 0.07 (syst)
^{32}Mg	40^{+9}_{-8}	1.85 ± 0.20 (stat) ± 0.08 (syst)
^{34}Mg	63(5)	$2.30^{+0.09}_{-0.10}$ (stat) ± 0.16 (syst)
^{36}Mg	47(8)	$1.90^{+0.16}_{-0.17}$ (stat) ± 0.16 (syst)

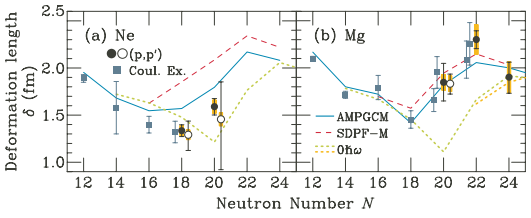

Fig. 1. Systematics of deformation lengths around the IOI region. Panels (a) and (b) show deformation lengths of Ne and Mg isotopes, respectively. Details are described in the text.

† Condensed from the article in Phys. Rev. C **89**, 054307 (2014).

*1 Center for Nuclear Study, University of Tokyo
*2 RIKEN Nishina Center
*3 Department of Physics, Tohoku University
*4 RCNP, Osaka University
*5 ATOMKI
*6 Department of Physics, Rikkyo University
*7 Department of Physics, Tokyo Institute of Technology
*8 Argonne National Laboratory
*9 Department of Physics, University of Tokyo

References

1) S. Michimasa *et al.*, Phys. Rev. C **89** (2014) 054307.
2) S.P. Weppner *et al.*, Phys. Rev. C **80** (2009) 034608.
3) R.R. Rodríguez-Guzmán *et al.*, Eur. Phys. J. A **17** (2003) 37; Nucl. Phys. A **709** (2002) 201; Phys. Lett. B **474** (2000) 15.
4) Y. Utsuno *et al.*, Rhys. Rev. C **60** (1999) 054315.
5) E. Caurier *et al.*, Rhys. Rev. C **58** (1998) 2033.
6) F. Nowacki and A. Poves, Phys. Rev. C **79** (2009) 014310.

Study of nuclear structure in proton-rich carbon isotopes

T. Miyazaki,[*1,*2] H. Otsu,[*2] E. Yu. Nikolskii,[*2,*5] Y. Shiga,[*2,*3] M. Kurata-Nishimura,[*2] S. Takeuchi,[*2] Y. Satou,[*4] M. Kurokawa,[*2] H. Baba,[*2] G. Lorusso,[*2] T. Isobe,[*2] M. Niikura,[*1] E. A. Kuzmin,[*2,*5] A. A. Korsheninnikov,[*2,*5] A. A. Ogloblin,[*2,*5] S. A. Krupko,[*6] M. S. Golovkov,[*6] A. A. Bezbakh,[*6] R. S. Slepnev,[*6] A. S. Fomichev,[*6] S. I. Sidorchuk,[*6] A. V. Gorshkov,[*6] A. G. Knyazev,[*6] P. Papka,[*7] H. J. Ong,[*8] S. Kim,[*4] J. W. Hwang,[*4] S. Choi,[*4] H. Chae,[*4] E. Kim,[*4] Y. H. Kim,[*4] D. Lubos,[*2,*9] D. Beaumel,[*2,*10] P. A. Söderström,[*2] S. Sakaguchi,[*11] S. Kubono,[*2] A. K. Perrevoort,[*2] E. Milman,[*2] S. Chebotaryov,[*2] W. Powell,[*2] T. Motobayashi,[*2] K. Yoneda,[*2] and H. Sakurai[*1,*2]

The structures of the proton-rich carbon isotopes ^{8}C and ^{9}C were studied by the neutron transfer ^{10}C(p,t) and ^{10}C(p,d) reactions, respectively. The experiment was aimed at measuring the unknown excited states in ^{8}C, which had not been achieved in the previous studies[1–4] and identifying the decay property of the unbound first excited state in ^{9}C.

The experiment was performed in 2013 at the RIKEN RIPS facility[5]. A ^{10}C secondary beam at 51 AMeV was impinged on the hydrogen gas target system (CRYPTA)[6,7]. Recoilied tritons and deuterons were identified by using the ΔE-E method, with the help of the Dubna telescope consisting of an annular double-sided strip silicon detector and 16 CsI(Tl) scintillators. The reaction residues were identified by the ΔE-E method using a four-plastic-scintillator array at 0 degree[8].

The excitation energy spectrum of ^{8}C after subtracting the background is shown in Fig. 1. The ground state of ^{8}C was observed. The deduced mass excess of the ^{8}C nucleus was 34.9(1.1) MeV, which is consistent with the values reported in previous works[1–4]. The differential cross-section of the ^{10}C$(p,t)^{8}$C$_{\mathrm{g.s.}}$ reaction will be analyzed in order to deduce the transferred angular momentum in the reaction.

The background-subtracted excitation energy spectrum of ^{9}C is shown in Fig. 2. The known ground and first excited states in ^{9}C were observed. The deduced excitation energy of the first excited state in ^{9}C was 2.4(5) MeV, which is consistent with the value obtained in the previous experiment[9]. By tagging the residual nucleus separated by the detectors at 0 degree, the decay paths of the first excited states in ^{9}C will be determined.

In summary, the ground state of ^{8}C and the ground and first excited states of ^{9}C were observed by using the ^{10}C(p,t) and ^{10}C(p,d) reactions, respectively. Their excitation energies were consistent with the previous results. In future studies, observation of the excited states in ^{8}C with higher statistics, better energy resolution, and higher S/N ratio is expected.

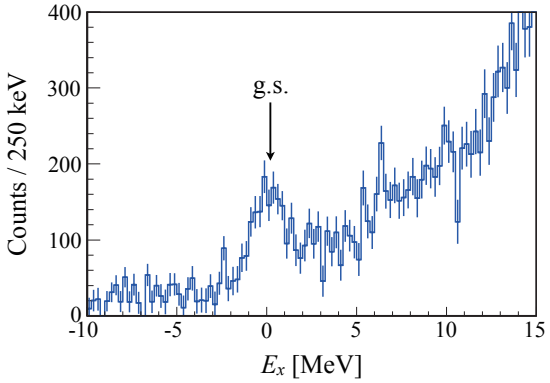

Fig. 1. The excitation energy spectrum of ^{8}C.

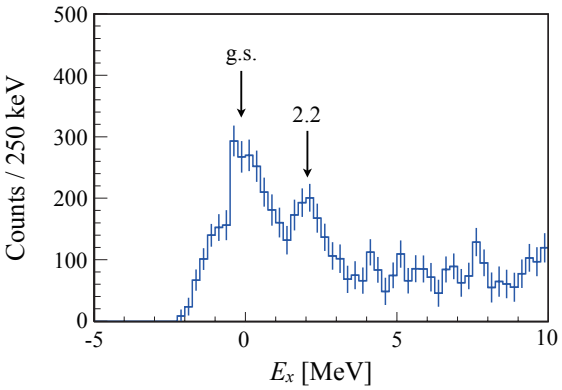

Fig. 2. The excitation energy spectrum of ^{9}C.

*1 Department of Physics, The University of Tokyo
*2 RIKEN Nishina Center
*3 Department of Physics, Rikkyo University
*4 Department of Physics, Seoul National University
*5 National Research Centre "Kurchatov Institute"
*6 Flerov Laboratory of Nuclear Reactions, Joint Institute for Nuclear Research
*7 Department of Physics, Stellenbosch University
*8 Research Center for Nuclear Physics, Osaka University
*9 Technische Universität München
*10 Institut de Physique Nucléaire d'Orsay, IN2P3/CNRS
*11 Department of Physics, Kyushu University

References

1) R. G. H. Robertson *et al.*: Phys. Rev. Lett. 32, 1207 (1974).
2) R. E. Tribble *et al.*: Phys. Rev. C 13, 50 (1976).
3) R. G. H. Robertson *et al.*: Phys. Rev. C 13, 1018 (1976).
4) R. J. Charity *et al.*: Phys. Rev. C 84, 014320 (2011).
5) T. Kubo *et al.*: Nucl. Instrum. Methods B 70, 309 (1992).
6) H. Ryuto *et al.*: Nucl. Instrum. Methods. A 555, 1 (2005).
7) M. Kurata-Nishimura *et al.*: RIKEN Accel. Prog. Rep. 46, 165 (2013).
8) T. Miyazaki *et al.*: RIKEN Accel. Prog. Rep. 47, 23 (2014).
9) W. Benenson and E. Kashy: Phys. Rev. C 10, 2633 (1974).

Triton contamination in the ^{10}C secondary beam produced by RIPS

T. Miyazaki,[*1] H. Otsu,[*2] M. Niikura,[*1*2] for DA13-03-01 collaboration

We have performed missing mass spectroscopy on ^{8}C to measure its excited states populated by the two-neutron transfer reaction from ^{10}C, ^{10}C$(p,t)^{8}$C, in an inverse kinematics.[1,2] In this experiment, an unexpected triton contamination was found to occur in a proton-rich ^{10}C secondary beam produced and separated by the RIKEN Projectile-fragment Separator (RIPS).[3]

The ^{10}C secondary beam was produced by the projectile-fragmentation of a ^{12}C beam with an energy of 70 MeV/nucleon impinging on a 94.2-mg/cm^2-thick ^{9}Be production target. The secondary beam was first separated by its magnetic rigidity ($B\rho$) using the first dipole magnet (D1) and a slit at the dispersive focal plane (F1) of the RIPS. A wedge-shaped aluminum degrader of 321-mg/cm^2 thickness was placed at F1 for further selection of the beam through analysis of its $B\rho$ using the second dipole magnet (D2) and a slit at the achromatic focus (F2). The widths of the F1 and F2 slits were adjusted to ±24 mm and ±5 mm, and magnetic rigidities of D1 and D2 were set to 1.9858 Tm and 1.8262 Tm, respectively. We expected to obtain nearly pure ^{10}C beam using this RIPS setting.

The secondary ^{10}C beam was injected into a cryogenic H_2 gas target (CRYPTA)[4] to induce the (p,t) reaction. The recoil tritons were detected with a Dubna telescope consisting of an annular double-sided strip silicon detector followed by cesium iodide scintillators. The telescope was installed downstream of the CRYPTA target. The excitation energy of the proton-unbound ^{8}C nucleus of was reconstructed by measuring the scattering angle and the total kinetic energy (TKE) of the recoil tritons.

Figure 1 shows the TKE spectra of tritons detected with the Dubna telescope. The solid line represents the TKE spectrum measured with the H_2 gas target (target run) and the shaded histogram represents that without the target (empty run) normalized by the beam intensity. The peak at 55 MeV ($G_{\mathrm{g.s.}}$), which is found only in the target run, corresponds to the ground state of ^{8}C produced by the two-neutron transfer reaction. The mass excess of the ground state of ^{8}C deduced from this peak is consistent with previous studies.[5–8] Hence, the peak at 48 MeV (G_0) should not originate from the (p,t) reaction.

To identify the origin of the G_0 peak, the position of the detected triton on the Dubna telescope is plotted by gating on G_0 and $G_{\mathrm{g.s.}}$ as shown in Fig. 2 (a) and (b), respectively. While tritons produced by the transfer reaction were found to distribute through the

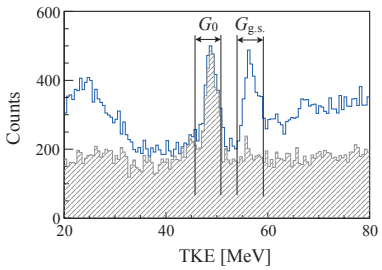

Fig. 1. Total kinetic energy of tritons measured with the Dubna telescope in the target run (solid line) and empty run (shaded)

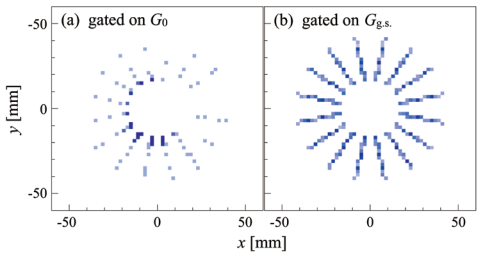

Fig. 2. Hit position of tritons on the Dubna telescope gated on the TKE spectra of G_0 (a) and $G_{\mathrm{g.s.}}$ (b).

entire region of the Dubna telescope, tritons in G_0 were detected only at the inner rings of the telescope. In addition, the TKE of tritons having $B\rho$ of D2 is 52 MeV, which is close to the measured TKE of G_0. Therefore, we concluded that a triton contaminant was present in the proton-rich ^{10}C secondary beam.

In the present experiment, data acquisition was triggered by timing signals of the plastic scintillator placed upstream of the target ($\mathrm{Pl}_{\mathrm{F3}}$) coincident with the Dubna telescope. Since the threshold of $\mathrm{Pl}_{\mathrm{F3}}$ was set to be much higher than the energy loss for the tritons, the triton contaminants on the Dubna telescope were obtained as an accidental-coincidence events and the count rate of the tritons could not be estimated. The contaminants were removed by gating on the prompt timing of the Dubna telescope for further analysis.

In conclusion, we observed the unexpected triton contaminant in the proton-rich ^{10}C secondary beam, even though a large A/Q difference exists between ^{10}C and triton.

*1 Department of Physics, the University of Tokyo.
*2 RIKEN Nishina Center.

References

1) T. Miyazaki et al.: RIKEN Acc. Prog. Rep. **47**, 23 (2014).
2) T. Miyazaki et al.: RIKEN Acc. Prog. Rep. 2014.
3) T. Kubo et al.: Nucl. Instrum. Methods B **70**, 309 (1992).
4) H. Ryuto et al.: Nucl. Instrum. Methods. A **555**, 1 (2005).
5) R.G.H. Robertson et al.: Phys. Rev. Lett. **32**, 1207 (1974).
6) R.E. Tribble et al.: Phys. Rev. C **13**, 50 (1976).
7) R.G.H. Robertson et al.: Phys. Rev. C **13**, 1018 (1976).
8) R.J. Charity et al.: Phys. Rev. C **84**, 014320 (2011).

β-NMR measurement of ^{41}S

Y. Ichikawa,[*1] Y. Ohtomo,[*1,*2] Y. Ishibashi,[*1,*3] T. Suzuki,[*2] T. Sato,[*2] K. Imamura,[*1,*4] T. Fujita,[*5] T. Furukawa,[*6] K. Asahi,[*2] T. Egami,[*7] C. Funayama,[*2] M. Hayasaka,[*8] C. Hirao,[*2] S. Kojima,[*2] T. Komine,[*2] M. Matsumoto,[*8] Y. Sakamoto,[*2] A. Takamine,[*9] D. Tominaga,[*7] H. Yamazaki,[*1] and H. Ueno[*1]

The erosion of $N = 28$ shell gap has been suggested from several spectroscopic experimental data.[1–4] In particular, the ^{43}S nucleus is of considerable interest because shape coexistence is expected to occur, which is key to understanding the evolution of shell gaps far from stability. The isomeric state of ^{43}S at 320 keV is suggested to have a shape close to spherical with a spin-parity of $7/2^-$,[5,6] but both the spin-parity and deformed parameter of the ground state have not been determined directly. To investigate the mechanics leading to such an anomalous nuclear structure, we aim to measure the ground-state nuclear moment of ^{41,43}S. First, μ of ^{41}S was measured using the β-ray detected nuclear magnetic resonance (β-NMR) method,[7] combined with a technique to produce spin-polarized RI beams.[8]

The experiment was carried out at the RIPS facility at RIBF. The RI beam of ^{41}S was produced by the fragmentation of a primary beam of ^{48}Ca at an energy of $E = 63$ MeV/nucleon on a primary target of ^{9}Be with a thickness of 0.52 mm. The typical intensity of the ^{48}Ca beam at the target was 200 pnA. To realize the spin polarization in ^{41}S, an emission angle of $\theta_F > 1^\circ$ and a momentum window of $p_F = p_0 \times (1.015 \pm 0.025)$ were selected, where p_0 represents the central momentum of the fragment ^{41}S. Under this condition, the particle identification of the secondary beam was performed on an event-by-event basis with information regarding time of flight (TOF) and energy loss (ΔE) as shown in Fig. 1. The beam was pulsed with durations of beam-on and beam-off periods of 2.9 s and 2.9 s, equally.

The ^{41}S beam was then transported to the final focal plane and implanted into a stopper crystal of CaS with which $AP = -0.14\%$ was observed previously,[9] where A and P denote the asymmetry parameter for the β-ray emission and the degree of polarization of ^{41}S, respectively. The CaS stopper was mounted between the poles of a dipole magnet that produces an external magnetic field of $B_0 = 0.5$ T. β rays emitted from the stopper were detected using plastic scintillator telescopes located above and below the stopper. An oscillating radio-frequency field B_1 was applied perpendicular to B_0 using a pair of coils. The frequency of B_1 was swept over a certain region, and spin reversal occurred when the region included the Larmor frequency. The spin reversal was detected through the change of the up/down ratio R of the β-ray counts at the two telescopes. Because the range within which the g-factor of ^{41}S is predicted theoretically is quite wide, a fast switching system for changing the tank-circuit frequency[10] was used. In this experiment, the g-factor search was conducted in the region where $0.2 < g < 0.8$. The results of the NMR measurements are under analysis.

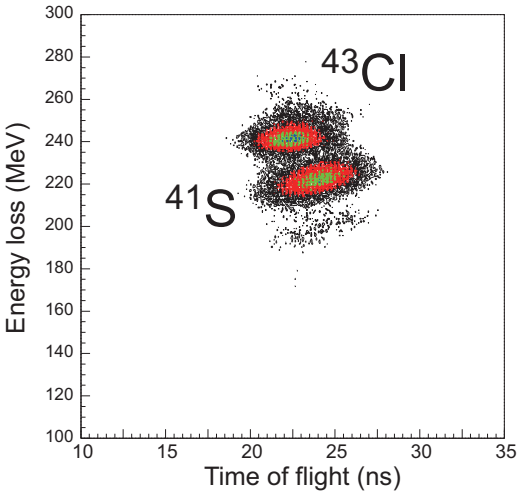

Fig. 1. Particle identification of ^{41}S. The horizontal and vertical axes represent TOF between the plastic scintillators at F2 and F3, and ΔE taken at the silicon detector at F2, respectively.

*1 RIKEN Nishina Center
*2 Department of Physics, Tokyo Institute of Technology
*3 Department of Physics, University of Tsukuba
*4 Department of Physics, Meiji University
*5 Department of Physics, Osaka University
*6 Department of Physics, Tokyo Metropolitan University
*7 Department of Physics, Hosei University
*8 Department of Physics, Tokyo Gakugei University
*9 Department of Physics, Aoyama Gakuin University

References

1) R. W. Ibbotson et al.: Phys. Rev. C **59**, 642 (1999).
2) F. Sarazin et al.: Phys. Rev. Lett. **84**, 5062 (2000).
3) Zs. Dombrádi et al.: Nucl. Phys. **A727**, 195 (2003).
4) S. Grévy et al.: Eur. Phys. J. **A 25**, 111 (2005).
5) L. Gaudefroy et al.: Phys. Rev. Lett. **102**, 092501 (2009).
6) R. Chevrier et al.: Phys. Rev. Lett. **108**, 162501 (2012).
7) K. Sugimoto et al.: J. Phys. Soc. Jpn. **21**, 213 (1966).
8) K. Asahi et al.: Phys. Lett. B **251**, 488 (1990).
9) H. Shirai et al.: RIKEN Accel. Prog. Rep. **47**, in print.
10) N. Yoshida et al.: Nucl. Instrum. Meth. B **317**, 705 (2013).

β-NMR measurement in coincidence with β-delayed γ rays of ^{41}S

Y. Ichikawa,[*1] Y. Ohtomo,[*1,*2] Y. Ishibashi,[*1,*3] T. Suzuki,[*2] T. Sato,[*2] K. Imamura,[*1,*4] T. Fujita,[*5] T. Furukawa,[*6] K. Asahi,[*2] T. Egami,[*7] C. Funayama,[*2] M. Hayasaka,[*8] C. Hirao,[*2] S. Kojima,[*2] T. Komine,[*2] M. Matsumoto,[*8] Y. Sakamoto,[*2] A. Takamine,[*9] D. Tominaga,[*7] H. Yamazaki,[*1] and H. Ueno[*1]

We aim to measure the magnetic moment of the ground-state ^{41}S, by combining the technique to produce spin-polarized RI beams[1] and the method of β-ray-detected nuclear magnetic resonance (β-NMR). In the previous experiment, the spin polarization realized in the ^{41}S beams implanted in a CaS crystal was measured to be $AP = -0.14(4)\%$[2] using the adiabatic field rotation (AFR) device[3]. Since the AP value is the product of the asymmetry parameter A for the β-ray emission and the degree of polarization P of ^{41}S, the small AP value may be attributed to a cancellation of A when various β-decay branches are mixed. Indeed, the decay scheme of ^{41}S has not been established other than the observation of several β-delayed γ rays[4]. In order to avoid a possible cancellation of the A parameter, we have attempted to perform the β-NMR measurement in coincidence with the β-delayed γ rays, along with the normal β-NMR measurement[5].

The experiment was carried out at the RIPS at RIBF. The beam production of ^{41}S and experimental setup are common to the normal β-NMR measurement[5]. The β-delayed γ rays emitted from ^{41}S in the CaS crystal located at the center of poles of the dipole magnet were detected with two Ge detectors set at a distance of 20 cm from the crystal. Each Ge detector has a relative efficiency of 35%. The data acquisition was system triggered by a γ-hit event defined by a logical OR of signals from the Ge detectors.

In this experiment, we have observed 3 β delayed γ rays of ^{41}S with large yields, with energies of 131, 554 and 761, as shown in Fig. 1 (a), (b) and (c), respectively. To confirm the origin of these γ rays, the half lives associated with these γ rays were deduced from the decay curve spectra synchronized with the beam pulsing: 2.9 s for beam-on and 2.9 s for beam-off. Figure 2 shows the decay-curve spectra for the 131-keV γ ray in the beam-off period. The decay-curve was fitted to an exponential function on a constant background, and then, the half life was preliminarily determined to be 1.99(5) s, which is in good agreement with the previous value[4], and the origin was confirmed to be ^{41}S. Further analysis to obtain the NMR spectra in coincidence with these γ rays is in progress.

*1 RIKEN Nishina Center
*2 Department of Physics, Tokyo Institute of Technology
*3 Department of Physics, University of Tsukuba
*4 Department of Physics, Meiji University
*5 Department of Physics, Osaka University
*6 Department of Physics, Tokyo Metropolitan University
*7 Department of Physics, Hosei University
*8 Department of Physics, Tokyo Gakugei University
*9 Department of Physics, Aoyama Gakuin University

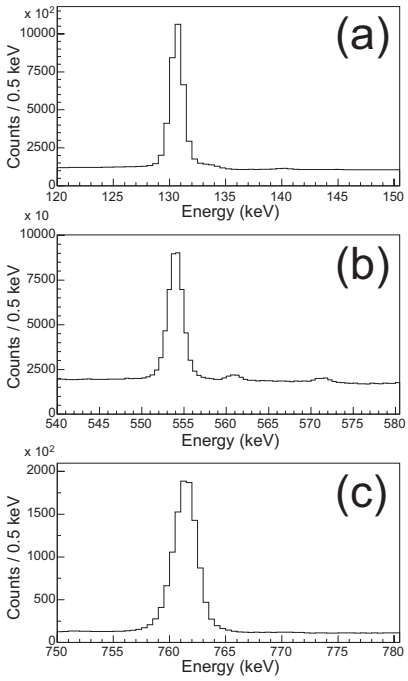

Fig. 1. β-delayed γ rays of ^{41}S with energy of (a) 131 keV, (b) 554 keV and (c) 761 keV.

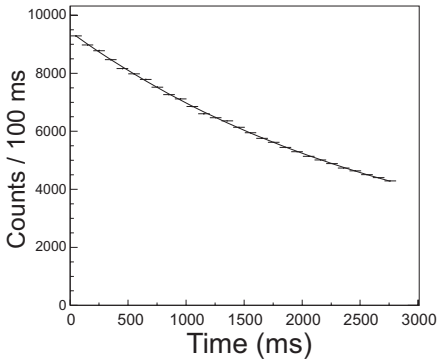

Fig. 2. Decay-curve spectrum for 131-keV γ ray. The half life was preliminarily determined to be 1.99(5) s.

References

1) K. Asahi et al.: Phys. Lett. B **251**, 488 (1990).
2) H. Shirai et al.: RIKEN Accel. Prog. Rep. **47**, 39 (2014).
3) Y. Ishibashi et al.: Nucl. Instrum. Meth. B **317**, 714 (2013).
4) J. A. Winger et al.: AIP Conf. Proc. **455**, 606 (1998).
5) Y. Ichikawa et al.: RIKEN Accel. Prog. Rep. **48** (in this report).

Interaction of ^{8}B, unstable and loosely bound, with ^{208}Pb: scattering and breakup

C. Signorini,[*1] A. Boiano,[*2] C. Boiano,[*3] C. Manea,[*4] M. Mazzocco,[*4] C. Parascandolo,[*2] D. Pierroutsakou,[*2] A.M. Sánchez-Benítez,[*5] E. Strano,[*4] D. Torresi,[*4] M. La Commara,[*2] H. Yamaguchi,[*6] D. Kahl,[*6] Y. Hirayama,[*7] H. Ishiyama,[*7] N. Imai,[*6,*7] N. Iwasa,[*8] S.C. Jeong,[*7,*13] S. Kimura,[*7] Y.H. Kim,[*7] S. Kubono,[*6,*9] H. Miyatake,[*7] M. Mukai,[*7] T. Nakao,[*7] Y. Sakaguchi,[*6] T. Teranishi,[*10] Y. Wakabayashi,[*9] Y.X. Watanabe,[*7] C.J. Lin,[*11] H.M. Jia,[*11] L. Yang,[*11] and Y.Y. Yang[*12]

The main motivation of this experiment was to investigate of the reaction dynamics induced by the radioactive ion-beam ^{8}B, extremely loosely bound with S_p =137keV, at Coulomb barrier energy: i.e., reaction cross section deduced from elastic scattering, as well as the transfer and/or breakup processes. The ^{8}B beam, provided by the CRIB facility, was produced via the inverse kinematics reaction ^{3}He(^{6}Li, n)^{8}B. The primary ^{6}Li beam intensity ranged from 1 to 3 eμA, resulting in a ^{8}B intensity of ~10^{4} Hz, with an energy of 50±1 MeV. The ^{6}Li ion source had to be retuned twice owing to the total consumption of the lithium material. This resulted in a beamtime loss of two days, allowing us to accumulate statistics for four days beamtime on target. As expected, the ^{8}B beam was contaminated by ^{7}Be, via the ^{3}He(^{6}Li,pn)^{7}Be reaction, by ^{3}He, recoiling from the ^{3}He material of the production gas target, and by some ^{6}Li halo (originating from the primary beam, that was around 10^{8} times more intense than the secondary one); thus, the ^{8}B beam purity achieved was approximately 20%. The contaminations were not problematic since each beam species was identified via a time of flight technique. The light charged particles produced in the reaction were detected and identified with six ΔE-E telescopes, consisting of 40–50 μm + 300 μm double sided silicon strip detectors. The detectors were arranged symmetrically around the target at a distance of pproximately 11 cm. All the detectors with the related electronics were brought from Italy, INFN[1]. For the E-detectors we utilized for the first time, ASIC digital electronics, whereas we used for the ΔE detectors low-noise electronics; these electronics were also fully developed in Italy[2,3]. The charged particles identified were ^{8}B, ^{7}Be, ^{6}Li, ^{4}He, ^{3}He, and protons (Fig. #1), confirming our preliminary estimates: namely, the existence of a consistent

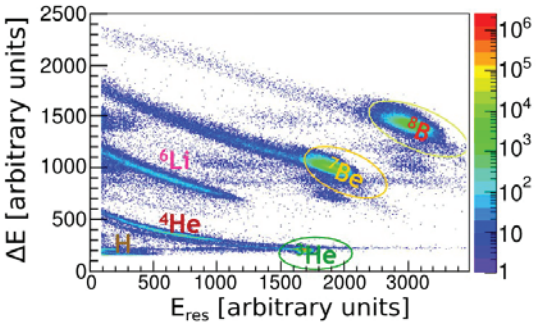

Fig. 1. ΔE-E_{res} identification of the different ions produced in the scattering of the cocktail ^{8}B-^{7}Be-^{3}He beam onto a ^{208}Pb target.

amount of transfer (p transferred with ^{7}Be out) and breakup processes (→^{7}Be+p, and possible subsequent ^{7}Be breakup →^{3}He+^{4}He). Preliminary data from the angular distribution of the ^{8}B elastic scattering confirm our expectations of a strong absorption occurring in the ^{8}B-induced reactions.

In all the runs we were able to verify the good capabilities of the homemade electronics[2,3] for identifying the various ions detected by the ΔE silicon via the built-in risetime detection. Fig. #2 shows a typical spectrum: signal rise time vs. ΔE, with the related ion identification.

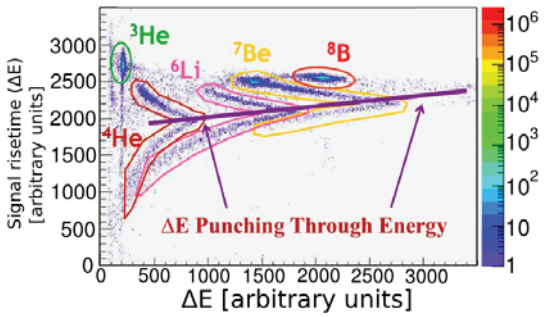

Fig. 2. Performances of the homemade electronics of the thin ΔE detectors. The measurement of the risetime signal vs. the energy loss allows for clear ion identification.

[*1] INFN, LNL, Legnaro
[*2] Department. of Physics and INFN, Napoli
[*3] INFN-Sezione di Milano
[*4] Dept. of Physics and Astronomy and INFN, Padova
[*5] University of Lisbon, Nuclear Physics Centre
[*6] CNS University of Tokyo, RIKEN
[*7] KEK
[*8] Department of Physics, Tohoku University
[*9] RIKEN Nishina Center
[*10] Department of Physics, Kyushu University
[*11] China Institute of Atomic Energy
[*12] Institute of Modern Physics, Chinese Academy of Sciences
[*13] Institute for Basic Science

References

1) E.Strano et al., Nucl. Instr. and Meth. **B317**(2013)657
2) C.Boiano et al.; IEEE Nucl.Science Symposium and Medical Imaging Conference. (NSS/MIC)14-34(2012)865
3) C. Boiano et al.; IEEE Nucl.Science Symposium, Conference Records 1-173(2009)1399.

First production of ^{10}Be beam at CRIB and ^{10}Be+α resonant elastic scattering

H. Yamaguchi,[*1] D. Kahl,[*1] S. Hayakawa,[*1] Y. Sakaguchi,[*1] and T. Nakao,[*2] for CRIB collaboration

α-cluster states are known to occur in many nuclei, including isotopes of the carbon nucleus. Among the α-cluster states, linear-chain cluster states have been considered as exotic and of interest for a long time. Although there have been many theoretical investigations, no clear experimental evidence has been obtained for such states thus far.

By performing an antisymmetrized molecular dynamics (AMD) calculation, Suhara and En'yo[1,2] obtained a band (0^+_5, 2^+_6, 4^+_6) that could be explained as linear-chain cluster levels of ^{14}C. It was predicted that these levels appear a few MeV or more above the ^{10}B+α threshold, unlike the prolate bands in the study of Oertzen et al.[3] The investigation[2] shows that the AMD wave function has a configuration in which two α particles and two neutrons are located close to each other, while the remaining α particle is relatively faraway. This implies that states having such a linear-chain configuration could be accessed from the ^{10}Be+α channel.

The aims of the present work are 1) to search for a linear-chain configuration via ^{10}Be+α resonant scattering, and 2) to determine the resonant parameters of the high excited states (13-18 MeV) of ^{14}C, which are still mostly unknown, in order to elucidate on the cluster-band structure. The experimental method is similar to that used in previous studies.[4,5]

The study was conducted at the low-energy radioactive-isotope (RI) beam separator CRIB. The ^{10}Be beam at CRIB was first produced on January 17-19, 2014. Using a 5.57 MeV/u primary ^{11}B beam from the AVF cyclotron and a 500-Torr cryogenic deuterium target, ^{10}Be particles were produced via the ^{11}B(d, ^{3}He)^{10}Be reaction in inverse kinematics. The 4^+ charge state was selected using the D1 dipole magnet of CRIB. The produced ^{10}Be^{4+} beam was contaminated with a small amount of ^{10}B^{4+}, which was mostly excluded by inserting a 0.7 μm-thick Mylar film as a charge stripper at the F1 focal plane. The highest ^{10}Be beam production rate was 2×10^4 pps at the final focal plane (F3). The beam energy was 3.51 MeV/u before reaching parallel-plate avalanche counters (PPACs) installed for the beam monitoring.

We also performed a test measurement of α resonant scattering using a chamber filled with helium gas at 760 Torr, which served as the target for elastic scattering. The chamber had a window covered with a 25 μm-thick Mylar film at the beam entrance. A pair of silicon detectors, which had thicknesses of 20 μm and 480 μm, were placed in the gas-filled chamber, consisting of a "ΔE-E" telescope. The telescope was located at 482 mm from the Mylar entrance window, exactly in the direction of the beam axis. The energy of the beam degraded and the beam was stopped by the thick gas target and α particles originating from elastic scatterings reached the telescope. The energy spectrum of the α particles exhibited several peaks, as shown in Fig. 1. In principle, α-cluster like resonances including theoretically predicted ones should be observed as peaks in the present measurement. In particular, two distinct peaks that likely correspond to resonances in ^{14}C are observed at excitation energies of 14.3 MeV and 16 MeV; however, the resonant features of those are yet to be investigated. The peak at the highest energy of approximately 17 MeV could be due to background events arising from impurities in the ^{10}Be beam and should be eliminated in the main run.

In summary, we successfully produced a ^{10}Be beam at CRIB for the first time and also showed that the resonant scattering measurement is feasible. The actual measurement for 7.5 days will be performed in 2015.

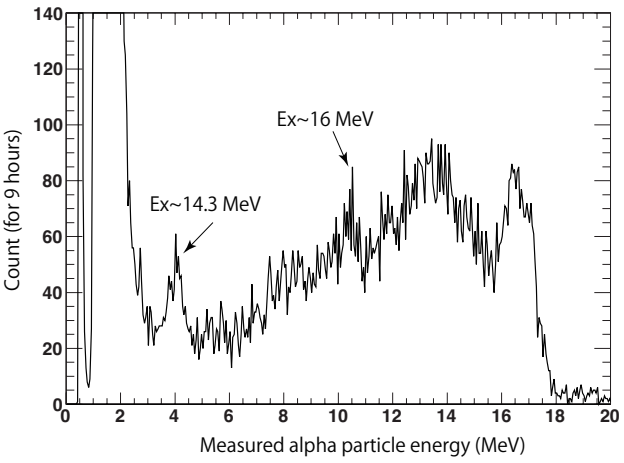

Fig. 1. Energy spectrum of α particles. The data were accumulated for 9 hours.

*1 Center for Nuclear Study, University of Tokyo
*2 Advanced Science Research Center, Japan Atomic Energy Agency

References

1) T. Suhara and Y. Kanada-En'yo: Phys. Rev. C **82**, 044301 (2010).
2) T. Suhara and Y. Kanada-En'yo: Phys. Rev. C **84**, 024328 (2011).
3) W. Oertzen, et al.: Eur. Phys. J. **A21**, 193 (2004).
4) H. Yamaguchi et al.: Phys. Rev. C **83**, 034306 (2011).
5) H. Yamaguchi et al.: Phys. Rev. C **87**, 034303 (2013).

Investigation of the waiting point ^{22}Mg in the rp-process

N. N. Duy,[*1,*2] L. H. Khiem,[*2] S. Kubono,[*3] H. Yamaguchi,[*4] D. Kahl,[*4] and N. K. Uyen[*5]

Nucleosynthesis in stars occurs via several reaction chains, including a combination of the (α,p)-process, (p,γ)-process, and β^+-decay. A nucleus is a waiting point if the (α,p) or (p,γ) reaction rate is so low that the nuclear processing has to wait for β^+-decay. Since the nucleosynthesis grows to the ^{22}Mg nucleus via the following reaction chains, $^{14}O(\alpha,p)(p,\gamma)^{18}Ne(\alpha,p)(p,\gamma)^{22}Mg$-$(\alpha,p)(p,\gamma)^{26}Si(\alpha,p)(p,\gamma)^{30}S(\alpha,p)(p,\gamma)^{34}Ar(\alpha,p)(p,\gamma)^{38}K$, there are three possible ways by which the reactions can proceed through ^{22}Mg: $^{22}Mg(\beta^+)^{22}Na$, $^{22}Mg(\alpha,p)^{25}Al$, and $^{22}Mg(p,\gamma)^{23}Al$. Because of the small Q-value (Q = 0.125 MeV) of the *(p,γ)*-reaction, it is thought that the photodisintergration of ^{23}Al prevents a significant part of the flow through this reaction. In addition, at high-temperature condition, i.e., T_9 = 1 – 10 GK, the $^{22}Mg(\alpha,p)^{25}Al$ reaction was thought to be dominant. If the reaction rate of $^{22}Mg(\alpha,p)^{25}Al$ is lower than the rate of beta decay, the nucleosynthesis must await the decay from ^{22}Mg, and subsequently, the ^{22}Mg nucleus becomes a waiting point. To investigate the potential waiting of ^{22}Mg, we measured the ^{22}Mg+α reaction and determined the resonance states[1] of ^{26}Si that are used to calculate the reaction rate of $^{22}Mg(\alpha,p)^{25}Al$ under such stellar conditions. According to the results of a previous work,[2] we could estimate the rate of the (α,p)-process, (p,γ)-process, and β^+-decay in ^{22}Mg.

The reaction rate of $^{22}Mg(\alpha,p)^{25}Al$ was determined by using the resonance states of ^{26}Si obtained from alpha scattering in the ^{22}Mg+α experiment. The calculation was performed by using following expression:

$$N_A\langle\sigma v\rangle_{tot} = 8.08\times10^{-9}\left(\mu T_6\right)^{-3/2}\sum_i(\omega\gamma)_i\exp\left(-\frac{11605E_i}{T_6}\right) \quad (1)$$

where μ, (ωγ), E_i, and T_6 are reduced mass, resonance strength, resonance states, and temperature in million Kelvin, respectively. The resonance strength was calculated by assuming that of the proton occupied 10% of the total width. As shown in Fig. 1, the rates of the (α,p) reaction corresponding to the first resonance is the highest. The reaction rate is low under concerned stellar conditions, with a value in the range of 10^{-30} – 10^{-7}. The speed of the (α,p) reaction, which depends on the abundance of isotopes in the stellar environment, and that of beta decay were obtained from the following equations:

$$R_{\alpha p} = \left(\rho X_\alpha / m_\alpha\right) N_A\langle\sigma v\rangle_{\alpha p} \quad (2)$$

$$R_{\beta+} = \ln 2 / T_{1/2}, \quad (3)$$

where ρ, X_a, $N_A\langle\sigma v\rangle$, m_a, and $T_{1/2}$ are the density of the materials in the stellar environment, abundance of ^{4}He, rate of the (α,p) reaction, mass of ^{4}He, and half-life of ^{22}Mg. According to the rates obtained in the previous work,[2] we could determine the speed of the (p,γ) reaction. The results show that in the temperature range of T_9 = 1 – 10 GK, the (p,γ) reaction is the dominant. Table 1 compares the three processes.

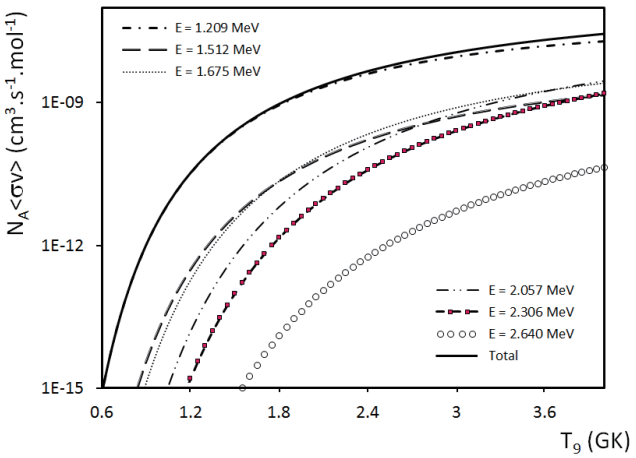

Fig. 1. Rates of the reaction $^{22}Mg(\alpha,p)^{25}Al$ calculated by using the resonance states of ^{26}Si via alpha scattering of ^{22}Mg.

Table 1. Speed of the reactions and beta decay

T_9 (GK)	$R_{\alpha p}$ (reaction/s)	$R_{p\gamma}$ (reaction/s)	$R_{\beta+}$ (decay/s)
1.0	2.99E-06	7.80E+03	0.1789
1.5	1.79E-04	2.47E+04	0.1789
2.0	1.26E-03	4.92E+04	0.1789
2.5	3.90E-03	7.80E+04	0.1789
10	7.50E-02	----	0.1789

Since the speed of the (p,γ) reaction is much higher than that of the others, it does not wait for beta decay. Therefore, under the conditions of X-ray burst and Type-II supernovae, the ^{22}Mg nucleus does not act as a waiting point. Subsequently, beta decay does not occur. Once the beta decay is skipped, the ^{22}Na unstable isotope which decays beta-plus (β+) to the excited state of ^{22}Ne, which de-excites to ground state by emitting gamma rays with energy of 1.275 MeV, cannot be formed. Therefore, such gamma rays have not been observed by satellites up to date. In addition, the ^{22}Ne/^{20}Ne ratio changes, which is one of the causes of the Ne-E problem.

*1 Department of Physics, Dong Nai University.
*2 Institute of Physics, Vietnam Academy of Science and Technology.
*3 RIKEN Nishina Center.
*4 Center for Nuclear Study, The University of Tokyo.
*5 Department of Physics, HCM University of Technology and Education.

References

1) N. N. Duy et al: RIKEN Accel. Prog. Rep. 47, 43 (2015).
2) J. J. He et al: Phys. Rev. C 76, 1 (2007).

Production of Lv isotope in the hot fusion reaction of ^{248}Cm+^{48}Ca at E^*=38.4 MeV

D. Kaji,[*1] K. Morita,[*1,*2] K. Morimoto,[*1] C. Berner,[*1,*3] H. Haba,[*1] Y. Komori,[*1] M. Murakami,[*1,*4] Y. Narikiyo,[*1,*2] M. Takeyama,[*1,*5] K. Tanaka,[*1,*6] T. Tanaka,[*1,*2] Y. Wakabayashi,[*1] and S. Yamaki[*1,*7]

In 2013, a gas-filled recoil ion separator (GARIS) was employed to study the production of Lv (Livermorium, Z=116) isotopes in the hot fusion reaction of ^{248}Cm+^{48}Ca at the excitation energy of compound nucleus E^*=41.5 MeV[1]. As a result, five correlated decay chains were observed. On the basis of the assignments of the precedent studies[2–4], two of the events were attributed to the decays of ^{293}Lv (3n), and three of them were assigned to the decays of ^{292}Lv (4n). With the aim of clear identification of these nuclides, we started to measure the excitation function in the reaction of ^{248}Cm+^{48}Ca → ^{296}Lv*.

The experimental setup was almost the same as that used in our previous work[1] using ^{48}Ca^{11+} beam with 261.6 MeV. In this work, the ^{248}Cm target was irradiated with a 258 MeV ^{48}Ca^{11+} beam from RIKEN heavy-ion linear accelerator RILAC. Total beam dose was 5.0×10^{18} during a net irradiation time of 14.2 days. The average beam intensity on the target was 0.68 particle μA. The reaction products were separated in-flight from projectiles and other by-products using GARIS, and then they were guided into the focal plane detection system after they passed through the time-of-flight (TOF) detector[5]. The separator was filled with He gas at 73 Pa. Magnetic rigidity for measuring the Lv isotope was set to be 2.174 Tm. Then, the typical trigger rate at the focal plane was 58 cps at 0.89 particle μA.

Seventy-three events, which were anti-coincided with TOF detectors, with energies above 100 MeV were observed. Two events among their fission events were found to be correlated with preceding α-particles and implanted evaporation residue (ER). Observed decay chains are shown in Fig. 1. The first chain, which was observed on September 22, 2014, consists of three consecutive α-decays followed by SF. Decay properties of all nuclides in the first chain agree well with those of the decay chain from ^{293}Lv reported in early works[2–4]. The second chain consists of two consecutive α-decays followed by SF. Assuming the first α originating from ^{293}Lv is not detected in the second chain, the chain looks the same as the first series because decay properties of two α and SF in the second chain agree well with those of α_2 and α_3 followed by SF in the first one. However, the missing probability is estimated to be 0.3% by considering the dead time for data acquisition and counting rate of the FPD. By the low missing probability, we can not conclude whether the second chain is from ^{293}Lv or the other nuclide that is provided directly (and emitted the 9.71 MeV α-particle).

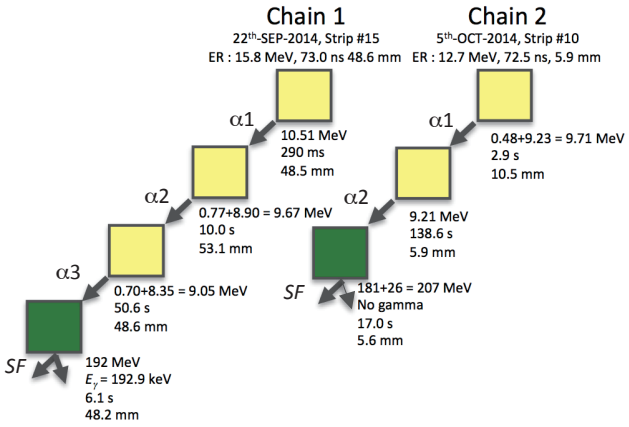

Fig. 1. Observed decay chains. Strip number, kinetic energy, TOF, and position of ER are given as well as decay energy and time, and position for each α-decay and/or SF.

The cross-section was deduced to be $0.9^{+2.1}_{-0.7}$ pb for 3n evaporation channel assuming the transmission of GARIS to be 35%. The cross section agrees well with the previously reported value of $1.1^{+1.7}_{-0.7}$ pb at E^*=40.9 MeV[2,3]. On the other hand, we did not observe the decay chain originating from 4n. The cross-section limit was 1.64 pb for 4n although the reported value is $3.3^{+2.5}_{-1.4}$ pb.

For further understanding from the reaction mechanism, we will measure the excitation function at an energy higher than 41.5 MeV.

References

1) K. Morita et al.: RIKEN Accel. Prog. Rep. 47, (2014).
2) Yu. Ts. Oganessian et al.: JINR preprint, E7-2004-160, p.1 (2004).
3) Yu. Ts. Oganessian et al.: Phys. Rev. C70, p.064609 (2000).
4) S. Hofmann et al.: Eur. Phys. J. A48, p.62 (2012).
5) D. Kaji et al.: RIKEN Accel. Prog. Rep. 47, (2014).

*1 RIKEN Nishina Center
*2 Department of Physics, Kyushu University
*3 Faculty of Physics, Technical University Munich
*4 Graduate School of Science and Technology, Niigata University
*5 Department of Physics, Yamagata University
*6 Graduate School of Science, Tokyo University of Science
*7 Department of Physics, Saitama University

Production of ^{215}U and ^{216}U and attempt to produce ^{219}Np and ^{220}Pu

Y. Wakabayashi,[*1] K. Morimoto,[*1] D. Kaji,[*1] H. Haba,[*1] M. Takeyama,[*1,*2] S. Yamaki,[*1,*3] K. Tanaka,[*1,*4] K. Nishio,[*5] M. Asai,[*5] Y. Komori,[*1] M. Murakami,[*1,*6] T. Tanaka,[*7] A. Yoneda,[*1] and K. Morita[*1,*7]

Theory[1] predicts that nuclei with $N = 126$ exist up to Fm ($Z = 100$) because of the fission barrier arising from the ground-state shell effect. The heaviest $N = 126$ nuclei reported so far is ^{218}U ($Z = 92$). In this program to study nuclei with $N = 126$, we attempt to produce heavier nuclei such as ^{220}Pu. In previous experiments, a new isotope ^{216}U, which is the daughter nucleus of ^{220}Pu and ^{215}U, were observed[2].

We performed an experiment at the RIKEN Linear Accelerator (RILAC) facility. We used ^{82}Kr ion as an incident beam and $^{136,137,138}BaCO_3$, $^{Nat}La_2O_3$, and $^{Nat}CeO_2$ as targets to study the ^{82}Kr + ^{136,137,138}Ba, ^{139}La, and ^{140}Ce reactions. Each target material was prepared by sputtering on 0.8–1.1-μm-thick aluminum foils so as to achieve a thickness of 300–500 μg/cm^2, and it was also covered with 40 μg/cm^2 of aluminum.The ^{82}Kr beams with energies of 365, 381 and 386 MeV were used to bombard these target foils mounted on a rotating target.

Evaporation residues (ERs) were separated from the beam particles and other products using a gas-filled recoil ion separator (GARIS), and they were implanted into a position-sensitive strip detector (PSD; 58 × 58 mm^2). The PSD was boxed in four Si detectors (SSD) to catch α particles escaping from the PSD. Two timing detectors were set in front of the PSD to measure the time-of-flight (TOF) of the ERs. Time information was also used to distinguish between the α-decay events in the PSD and the recoil implantations. A Ge-detector was placed 6 mm behind the PSD to measure the γ-rays coinciding with the α-decays. The isotopes were identified by using an α-decay chain with known α-decay properties of the descendants and the position correlations between the implanted ERs in the PSD and the subsequent α-decays.

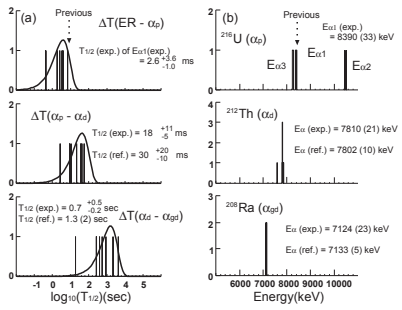

Fig. 1. α-decay time (a) and energy (b) spectra for ^{216}U. The previous results are indicated by dotted arrows. Each ΔT indicates the time difference between each decay generation (α_p, α_d, and α_{gd}). The labeled energies $E_{\alpha1}$, $E_{\alpha2}$, and $E_{\alpha3}$ for ^{216}U are specified. Observed α-decay energies and half-lives are written with reported ones except for ^{216}U.

*1 RIKEN Nishina Center
*2 Department of Physics, Yamagata University
*3 Department of Physics, Saitama University
*4 Tokyo University of Science
*5 Japan Atomic Energy Agency
*6 Department of Chemistry, Niigata University
*7 Department of Physics, Kyushu University

In this experiment, we confirmed the production of ^{215}U and ^{216}U by observing one chain and six chains, respectively, including the candidates of new transitions. For the decay chains of ^{216}U, the α-decay energies and decay times are shown in Fig. 1. These decay events and cross sections are summarized in Table 1, and we labeled the decay energies with $E_{\alpha1}$, $E_{\alpha2}$, and $E_{\alpha3}$ temporarily. For a new transition, $E_{\alpha2}$ of ^{216}U may be a transition from isomer-state in ^{216}U to ground-state in ^{212}Th as well as an isomer state of ^{218}U with the α-decay energy of 10678 keV[3]. In the attempt to produce ^{219}Np and ^{220}Pu using the ^{82}Kr + ^{139}La and ^{140}Ce reactions, cross section upper limits of 28 pb and 46 pb, respectively, were obtained. Further discussion, such as the interpretation of new transitions, is ongoing.

Table 1. α-decay events of ^{215}U and ^{216}U. The time and position difference between the implanted ERs and the α-decay are ΔT and ΔX, respectively. E_b represents the ^{82}Kr beam energy at the center of the target.

	E_α (keV)	ΔT (ms)	$\lvert\Delta X\rvert$ (mm)	Reaction (E_b) & Cross section
^{216}U	8408[2]	6.98	0.2	^{137}Ba+^{82}Kr (366)
($E_{\alpha1}$)	8371	3.95	0.2	$\rightarrow$ ^{216}U + 3n
	8379*	0.43	0.5	22^{+14}_{-9} pb
^{216}U	10518	2.50	0.2	
($E_{\alpha2}$)	10459*	0.43	2.3	
^{216}U	8254	1.81	0.1	^{136}Ba+^{82}Kr (350)
($E_{\alpha3}$)	8265*	3.40	0.2	$\rightarrow$ ^{216}U + 2n
				58^{+77}_{-38} pb
^{215}U	8436[2]	5.82	1.0	^{136}Ba+^{82}Kr (373)
($E_{\alpha1}$)				$\rightarrow$ ^{215}U + 3n
^{215}U	8230[2]	0.64	0.4	31^{+28}_{-18} pb
($E_{\alpha2}$)	8283	2.10	0.2	

* Sum energy of PSD and SSD.

References

1) H. Koura: Prog. Theor. Exp. Phys. 2014, 113D02 (2014).
2) Y. Wakabayashi et al.: RIKEN Accel. Prog. Rep. vol.47, xxii (2014).
3) A.P. Leppänen et al.: Eur. Phys. J. A25, Supplement 1, 183 (2005).

Search for new isotopes in the region around Z = 33 using the in-flight fission of a ^{238}U beam at 345 MeV/nucleon

Y. Shimizu,[*1] T. Kubo,[*1] N. Inabe,[*1] D.S. Ahn,[*1] N. Fukuda,[*1] K. Kusaka,[*1] D. Murai,[*1,*2] M. Ohtake,[*1] H. Suzuki,[*1] H. Takeda,[*1] Y. Yanagisawa,[*1] K. Yoshida,[*1] Y. Hirayama,[*3] Y. Ichikawa,[*1] N. Imai,[*4] T. Isobe,[*1] N. Iwasa,[*5] S.C. Jeong[*3] D. Kim,[*6] E.H. Kim,[*6] H. Miyatake,[*3] M. Mukai,[*3] H. Otsu,[*1] H. Sato,[*1] T. Sonoda,[*1] and A. Yagi[*7]

A new isotope search experiment in the neutron-rich region around $Z = 33$ was performed in November 2014, aiming to expand the frontier of accessible neutron-rich exotic nuclei. In this experiment, the nuclei of interest were produced by the in-flight fission of a 345 MeV/nucleon ^{238}U beam colliding with a 4.00-mm-thick Be target. The primary beam intensity was 10.8 particle nA on average. Fission fragments were separated and identified using the superconducting in-flight separator BigRIPS[1]. In order to separate and purify the RI beams, two wedge-shaped energy degraders were placed at the F1 and F5 dispersive foci. The typical counting rate at the F3 and F7 achromatic foci were 30.1 kHz and 1.88 kHz, respectively. Table 1 summarizes the experimental conditions.

Table 1. Summary of the experimental conditions.

Target (mm)	Be 4.00
Bρ [a] (Tm)	8.087
Degrader at F1 (mm)	Al 2.82
Degrader at F5 (mm)	Al 2.99
F1 slit (mm)	+64.2 / −64.2
F2 slit (mm)	+20.0 / −12.0
F5 slit (mm)	+120.0 / −120.0
F7 slit (mm)	+15.0 / −15.0
Central particle	^{94}As
Irradiation time (h)	97.3
Live time of DAQ (%)	66.1
Trigger rate (kHz)	1.24
Total dose	2.35×10^{16}

[a] The values from the magnetic fields of the first dipole magnet.

Particle identification (PID) was performed using the ΔE-TOF-$B\rho$ method in which the energy loss (ΔE), time of flight (TOF), and magnetic rigidity ($B\rho$) were measured to allow the event-by-event determination of atomic number Z and mass-to-charge ratio A/Q of fragments[2]. The PID was confirmed by measuring the delayed γ-rays emitted from short-lived isomers, such as ^{95}Kr and ^{94}Br, by using two clover-type high-purity germanium detectors placed at the F7 achromatic focus; this technique is called isomer tagging.

*1 RIKEN Nishina Center
*2 Department of Physics, Rikkyo University
*3 High Energy Accelerator Research Organization (KEK)
*4 Center for Nuclear Study (CNS), University of Tokyo
*5 Department of Physics, Tohoku University
*6 Institute for Basic Science (IBS)
*7 Department of Physics, Osaka University

Figure 1 shows a two-dimensional PID plot of Z versus A/Q. The solid red line indicates the limit of previously identified isotopes. The relative root mean square (rms) Z resolution and the relative rms A/Q resolution achieved were typically 0.57% and 0.055%, respectively. We can see some candidates for new isotopes such as ^{93}As, ^{96}Se, and ^{99}Br.

Detailed analysis is currently in progress.

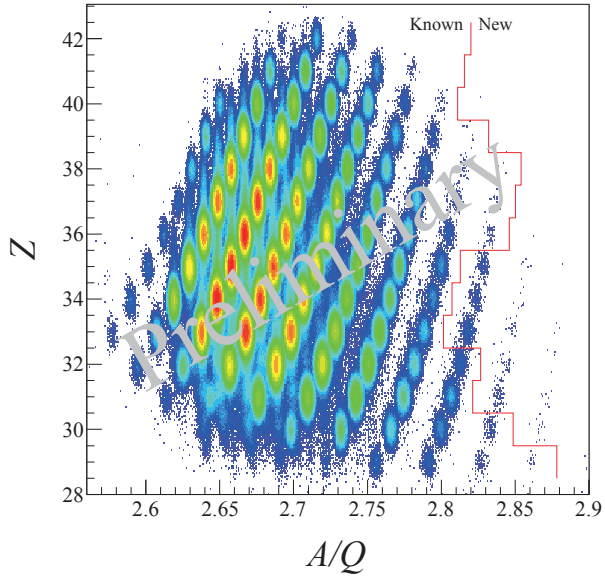

Fig. 1. Two-dimensional PID plot of Z versus A/Q. Red line indicates the limit of known isotopes.

References

1) T. Kubo et al.: Nucl. Instr. Meth. B **204**, 97 (2003).
2) N. Fukuda et al.: Nucl. Instr. Meth. B **317**, 323 (2013).

Search for new neutron-rich isotopes with $Z \sim 55$–70 using a 345 MeV/nucleon ^{238}U beam

N. Fukuda,[*1] N. Inabe,[*1] D. Kameda,[*1] H. Suzuki,[*1] H. Takeda,[*1] D.S. Ahn,[*1] D. Murai,[*1,*2] K. Yoshida,[*1] K. Kusaka,[*1] Y. Yanagisawa,[*1] M. Ohtake,[*1] Y. Shimizu,[*1] Y. Sato,[*1] H. Sato,[*1] H. Otsu,[*1] H. Baba,[*1] G. Lorusso,[*1] P.-A. Söderström,[*1] T. Isobe,[*1] N. Imai,[*3] M. Mukai,[*1,*4] S. Kimura,[*4] H. Miyatake,[*4] N. Iwasa,[*5] A. Yagi,[*6] R. Yokoyama,[*3] O.B. Tarasov,[*7] H. Geissel,[*8] and T. Kubo[*1]

Since the commissioning of the BigRIPS separator[1] in 2007, an extensive search for new isotopes has been conducted to expand the region of accessible exotic nuclei. By the end of 2013, about 100 new neutron-rich isotopes had been observed using the in-flight fission of a ^{238}U beam[2–4], and 4 new neutron-deficient nuclei had been observed by the projectile fragmentation of a ^{124}Xe beam[5]. In April 2014, we searched for new neutron-rich isotopes with the atomic number $Z \sim 55$–70 for the second time since the 2011 experiment[3], with an increased beam intensity.

The neutron-rich isotopes were produced by the in-flight fission of a ^{238}U beam at 345 MeV/nucleon. The maximum beam intensity was approximately 12.5 pnA. The fission fragments were collected and separated with the BigRIPS. The experimental conditions are summarized in Table1. We adopted two different $B\rho$ settings of the separator, each targeting new isotopes around ^{161}Pr (Pr setting) and ^{180}Er (Er setting). The settings were determined using the measured cross sections[6] and the detailed simulations with the code LISE++[7].

Table 1. Summary of the experimental conditions.

Setting	Pr setting	Er setting
Production target	Be 4.0 mm	Be 6.9 mm
Isotope tuned	^{161}Pr	^{180}Er[a)]
$B\rho$ of D1	7.527 Tm	6.311 Tm
Degrader at F1	Al 1.4 mm	Al 0.98 mm
Degrader at F5	Al 1.4 mm	Al 0.96 mm
F1 slit	±64.2 mm	+32.1/−42.8 mm
F2 slit	+10/−3 mm	+4/−3 mm
F5 slit	±120 mm	±120 mm
F7 slit	±25 mm	±25 mm
Average intensity	12.6 pnA	3.39 pnA
Running time	54.6 h	44.2 h
Total dose of ^{238}U	1.55×10^{16} particles	3.36×10^{15} particles

[a)] Hydrogen-like ($Q = 67$) ions were chosen in the first half of the first stage of BigRIPS.

*1 RIKEN Nishina Center
*2 Department of Physics, Rikkyo University
*3 Center for Nuclear Study, University of Tokyo
*4 High Energy Accelerator Research Organization (KEK)
*5 Department of Physics, Tohoku University
*6 Department of Physics, Osaka University
*7 NSCL, Michigan State University
*8 GSI

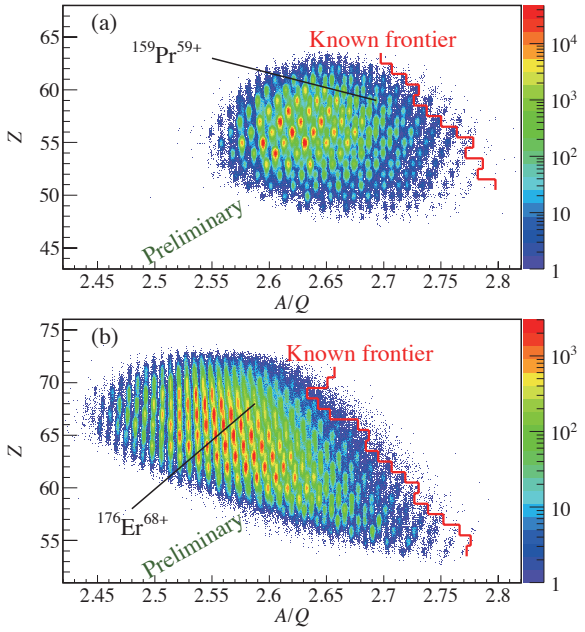

Fig. 1. Z versus A/Q particle identification plots obtained in the Pr (a) and Er (b) settings. The known frontiers are indicated by the red lines.

Particle identification (PID) was based on the TOF-$B\rho$-ΔE method to deduce Z and the mass-to-charge ratio (A/Q)[8]. The preliminary PID plots of Z versus A/Q are shown in Fig.1. The relative root mean square A/Q and Z resolutions are typically 0.037% and 0.45%, respectively, for the ^{161}Pr setting, and 0.047% and 0.88%, respectively, for the ^{180}Er setting. A total of 18 new isotopes have preliminarily been identified ranging from $Z = 56$ to 69. Further analysis is currently in progress.

References

1) T. Kubo: Nucl. Instr. Meth. B **204**, 97 (2003).
2) T. Ohnishi et al.: J. Phys. Soc. Jpn. **79**, 073201 (2010).
3) D. Kameda et al.: RIKEN Accel. Prog. Rep. **46**, 20 (2013).
4) Y. Shimizu et al.: RIKEN Accel. Prog. Rep. **47**, 47 (2014).
5) H. Suzuki et al.: Nucl. Instr. Meth. B **317**, 756 (2013).
6) D. Kameda et al.: RIKEN Accel. Prog. Rep. **47**, viii (2014).
7) O.B. Tarasov and D. Bazin: Nucl. Instr. Meth. B **266**, 4657 (2008).
8) N. Fukuda et al.: Nucl. Instr. Meth. B **317**, 323 (2013).

Study of particle identification and RI beam separation for the Z~80 region using projectile fragmentation of ^{238}U

N. Inabe,*[1] N. Fukuda,*[1] H. Takeda,*[1] H. Suzuki,*[1] Y. Shimizu,*[1] D. Murai,*[2] D. S. Ahn,*[1] H. Sato,*[1] Y. Sato, *[1] K. Kusaka,*[1] Y. Yanagisawa,*[1] M. Ohtake,*[1] K. Yoshida,*[1] M. Sako,*[1] N. Imai,*[3] S. Kimura,*[3] M. Mukai,*[3] H. Miyatake,*[3] N. Iwasa,*[4] and T. Kubo*[1]

An atomic number of Z~80 produced through a projectile fragmentation of ^{238}U is the next area for RI beam production at the BigRIPS.[1)] In this area, charge-state distributions are broad, which causes some problems for production concerned with both particle identification (PID) and isotope separation. To study this effect, we performed a test experiment to produce RI beams of high Z.

The test experiment was carried out using a 345 MeV/u ^{238}U beam. To study PID, RI beams were produced by the ^{238}U beam in low counting rates of ~2 x10^5 pps so as to make PID easy by sometimes mixing the ^{238}U primary beam of the charge state 92+ at F1. The production target was 5.79-mm-thick Be and the magnetic rigidity (Bρ) of the first dipole D1 was 6.001 Tm. Degraders were not used at F1 and F5. The F1 slits were set to produce a momentum byte in the range between -3% and 0.1% when the primary beam was not mixed and between -3% and 0.5 % when mixing it. The PID was performed by determining Z and A/Q on an event-by-event basis using the ΔE-TOF-Bρ method. ΔE was measured by MUSIC at F7 and TOF was measured using two plastic scintillators at F3 and F7. Bρ was determined by track reconstruction using positions and angles measured by PPACs located at F3, F5, and F7. Total kinetic energy (TKE) was also measured using by NaI at F7 to determine A.

Figure 1a and b show the PID spectra of A/Q vs. Z for Z > 30 and Z > 85, respectively. We can see not only projectile fragments but also fission fragments below Z~70 in Fig. 1a. Fig. 1c shows the similar plot as Fig. 1b when primary beams are mixed. We can clearly see four charge states of ^{238}U, which are produced by changing the charge state from 92+ in the scintillator at F3. Resolutions of Z are 0.58 % for Z~90 and 0.41 % for Z~50. The worse resolution in the high-Z area might be attributed to charge state straggling, which broadens energy loss spectra when passing through a detector with some charge states.

We performed the PID of U isotopes. Fig. 2 shows an A/Q spectrum of U produced by cutting with Z= 92±0.3. We identified the main peaks of A/Q > 2.55 but could not assign those of low A/Q because of overlap with isotopes of Z=91. The resolution of A/Q is 0.05%. We tried to examine whether other small peaks exist in large peaks, for example, $^{233}U^{89+}$ in the $^{236}U^{90+}$ peak but we could not determine this because of the quenching of the TKE counter.

In order to study isotope separation, we produced RI beam of which the central orbit was $^{226}Bi^{82+}$ with the 7-mm-thick Be target. Bρ of the first dipole was 6.13 Tm. The degrader at F1 of 0.3 mm and momentum acceptance of ±3% were used to produce many types of isotopes at the same time such as a search for new isotopes. The isotopes were not well-separated in this experiment owing to large unexpected contaminants of fission fragments with Z~60 and high counting rates of ~100 kHz/pnA. These phenomena have not been predicted by the simulation.

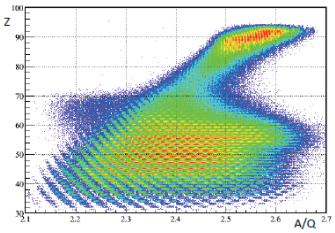

Fig. 1a Z vs. A/Q plot (Z>30)

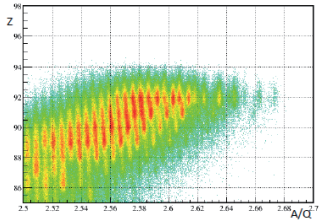

Fig. 1b Z vs. A/Q plot (Z>85)

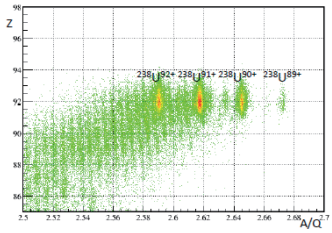

Fig. 1c Z vs. A/Q plot on mixing with the primary beam.

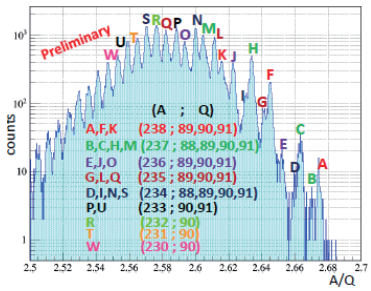

Fig.2 A/Q spectrum of U isotopes

Reference

1) T. Kubo: Nucl. Instr. Meth. **B 204**, 97 (2003).

*1 RIKEN Nishina Center
*2 Department of Physics, Rikkyo University
*3 KEK
*4 Department of Physics, University of Tohoku

Production cross section measurements of radioactive isotopes produced from a ^{124}Xe beam at 345 MeV/u by the BigRIPS separator

H. Suzuki,[*1] N. Fukuda,[*1] H. Takeda,[*1] D. Kameda,[*1] Y. Shimizu,[*1] D.S. Ahn,[*1] D. Murai,[*1,*2] H. Sato,[*1] K. Yoshida,[*1] K. Kusaka,[*1] Y. Yanagisawa,[*1] M. Ohtake,[*1] Y. Sato,[*1] N. Inabe,[*1] and T. Kubo[*1]

We have measured the production rates and the production cross sections for a variety of radioactive isotopes (RIs), which were produced from a ^{124}Xe beam at an energy of 345 MeV/u using the BigRIPS separator.[1] Proton-rich isotopes with atomic numbers $Z = 34-52$ were produced by the projectile fragmentation of the beam on a 4-mm thick Be production-target. The particle identification of RIs was based on the TOF-$B\rho$-ΔE method.[2]

The production cross sections were deduced from the measured production rates and the transmission efficiency in the BigRIPS separator, which was simulated with the LISE^{++} code.[3] In the LISE^{++} simulation, the parametrization for momentum distribution was adjusted, because the exponential tails in the low-momentum regions fell off faster than those in the LISE^{++} calculation with the original parametrization for the 345-MeV/u ^{124}Xe + Be reaction.[4]

Figure 1 shows the production cross sections of RIs obtained in three experiments, including our first ^{124}Xe-beam experiment[4] with predictions of the EPAX empirical cross-section formulae. The type of symbols represents the experiment from which the data were obtained. The filled symbols indicate that the distribution peak is located inside the slit opening at each focus, while the open symbols indicate that the peak is located outside the opening. The deduced cross sections of the same isotopes obtained in different settings / experiments were fairly consistent with each other, even though some isotopes were accepted only their low-momentum tails in the separator. This indicates the reliability of our measurements and simulations with LISE^{++}.

The solid and dashed lines in Fig. 1 show the cross sections predicted from the empirical formulae EPAX3.1a[5] and EPAX2.15,[6] respectively. EPAX3.1a predicts the cross sections better than EPAX2.15, which overestimates them. The measured cross sections of RIs with a wide range of Z are fairly well reproduced by EPAX3.1a, although some isotopes show systematic discrepancies in the highly neutron-deficient region. For ^{100}Sn, our experimental cross section at 345 MeV/u is approximately 1/6 of that predicted by EPAX3.1a. Further, the discrepancy becomes significant in the large Z region.

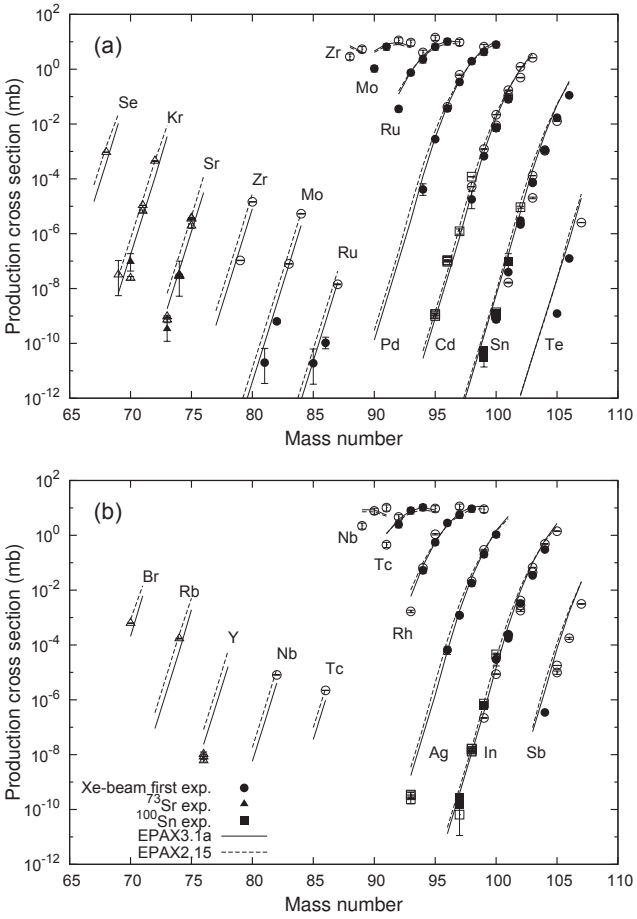

Fig. 1. Production cross sections of RIs produced in the ^{124}Xe + Be reaction at 345 MeV/u with the predictions of EPAX parametrization. (a) Results for even-Z isotopes. (b) Results for odd-Z isotopes.

*1 RIKEN Nishina Center
*2 Department of Physics, Rikkyo University

References

1) T. Kubo: Nucl. Instrum. Meth. Phys. Res. **B 204**, 97 (2003).
2) N. Fukuda et al.: Nucl. Instrum. Meth. Phys. Res. **B 317**, 323 (2013).
3) O. B. Tarasov and D. Bazin: LISE^{++} site, http://lise.nscl.edu, Michigan State University.
4) H. Suzuki et al.: Nucl. Instrum. Meth. Phys. Res. **B 317**, 756 (2013).
5) K. Sümmer: Phys. Rev. C **86**, 014601 (2012).
6) K. Sümmer and B. Blank: Phys. Rev. C **61**, 034607 (2000).

Production cross section measurements for fragments of ^{70}Zn beam

D. S. Ahn,[*1] H. Suzuki,[*1] N. Fukuda,[*1] H. Takeda,[*1] Y. Shimizu,[*1] D. Murai,[*1,*2] K. Yoshida,[*1] D. Kameda,[*1] H. Sato,[*1] Y. Sato,[*1] Y. Yanagisawa,[*1] K. Kusaka,[*1] M. Ohtake,[*1] N. Inabe,[*1] and T. Kubo[*1]

We measured the production yields and production cross sections of radioactive isotopes (RIs) in the neutron-rich region with the atomic number $Z = 16 \sim 24$ produced from an ^{70}Zn beam at an energy of 345 MeV/nucleon by using the BigRIPS separator[1]. Neutron-rich RIs were produced through projectile fragmentation on a 10-mm Be target, and the particle identification (PID) of RIs was performed using the TOF-Bρ-ΔE method. The energy loss (ΔE) was measured using an ion chamber at F7. The time-of-flight (TOF) between F3 and F7 was measured using plastic scintillators and the trajectory was measured at F3, F5, and F7 by using Parallel Plate Avalanche Counters(PPACs).

The Bρ of BigRIPS was set to the rigidity corresponding to the center of the momentum distribution of ^{56}Ca, and the PID was confirmed by the isomers of ^{56}Sc and ^{59}Ti. The experimental conditions for ^{56}Ca setting are listed in Table 1. Figure 1 is a PID plot showing the relation between the atomic number (Z) and mass-to-charge ratio (A/Q). Background events were eliminated by the correlations among phase-space profiles by using the PPAC, pulse-height, and timing signals from the plastic scintillators; reaction loss events in the ionization chamber; pile-up events using plastic scintillators and the ionization chamber; particle trajectories between two different foci; and charge state change at F5.

Table 1. Experimental conditions.

Center particle	^{56}Ca
Target	Be 10 mm
F1 degrader	Al 3 mm
F5 degrader	Al 5 mm
Bρ01	7.349 Tm
Momentum acceptance	± 3%

The production cross sections were obtained using the transmission efficiency calculated using LISE++ code[3] and production yields. In Figure 2, the red circles represent the experimental result of RIs produced from the ^{70}Zn beam. The solid and dashed lines in Fig. 2 represent the production cross sections calculated with empirical formulae EPAX3.1a[4] and EPAX2.15[5], respectively. EPAX3 is proposed as the universal empirical formula, and it shows better agreement with experimental data for the most neutron-rich fragments than EPAX2 does. Overall, our experimental measurements of cross sections are in good agreement with the EPAX parameterizations. The production cross sections are consistent with EPAX2.15 for $Z < 20$ and with EPAX3.1a for $Z > 20$.

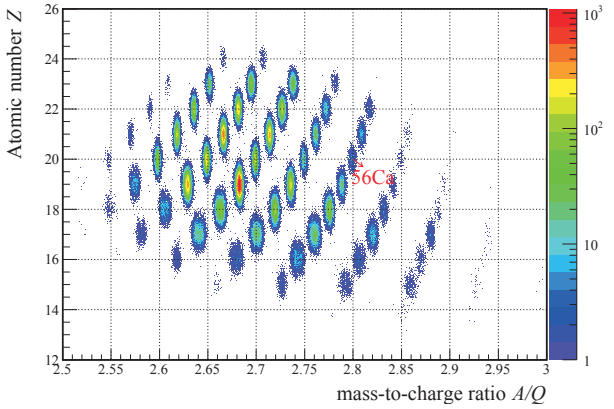

Fig. 1. Particle identification plot of atomic number Z versus mass-to-charge ratio A/Q for projectile fragmentation in the reaction of ^{70}Zn + Be at an energy of 345 MeV/nucleon.

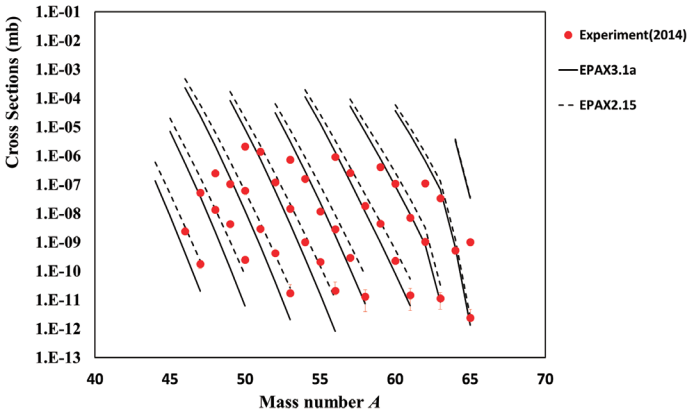

Fig. 2. Production cross section for fragments of the ^{70}Zn beam. The solid and dashed lines represent EPAX parameterizations, and the red circles represent experimental results.

*1 RIKEN Nishina Center
*2 Department of Physics, Rikkyo University

References
1) T. Kubo et al.: Nucl. Instrum. Meth. Phys. Res. **B 204**, 97 (2003).
2) N. Fukuda et al.: Nucl. Instrum. Meth. Phys. Res. **B 317**, 323 (2013).
3) O. B. Tarasov et al.: http://lise.nscl.msu.edu
4) K. Sümmer: Phys. Rev. C **86**, 014601 (2012).
5) K. Sümmer and B. Blank: Phys. Rev. C **61**, 034607 (2000).

On-line test of rotating magnetic field system for β-NMR method

Y. Ishibashi,[*1,*2] D. Nagae,[*1] Y. Abe,[*1,*2] Y.E. Ichikawa,[*1] K. Sawahata,[*1] A. Ozawa,[*1] and H. Ueno[*2]

The β-ray detected nuclear magnetic resonance (β-NMR) method[1] is an efficient method to measure the nuclear magnetic (μ) moment of unstable nuclei. The absolute value of μ moments are measured for various nuclei by using β-NMR. However, the sign of μ moments are rarely measured in experiment. In the β-NMR method, a linear oscillating magnetic field (RF), which can be a superposition of a right- and left-rotating RF, is applied to invert the direction of spin polarization. Thus, only the absolute value of μ moments is estimated from the applied frequency of the linear RF. Therefore, to determine the sign of a μ moment, applying a rotating RF is necessary. A rotating RF system has been under development[2,3] to determine the sign of a μ moment by using the β-NMR method. The rotating magnetic field is obtained using two Helmholtz-like coils with axes crossed at right angles. The experimental apparatus to produce the rotating RF is shown in Fig. 1, and a detailed description is given in Ref. 2 and 3.

In the present work, the performance of the system was studied with spin-polarized ^{20}F ($I^\pi = 2^+$, $T_{1/2}$ = 11.163 s, $\mu(^{20}\mathrm{F}) = +2.09335(9)\ \mu_N$) nuclei at the Research Center for Nuclear Physics, Osaka University. A spin-polarized ^{20}F nucleus was produced in the $^{19}\mathrm{F}(\vec{d}, \mathrm{p})^{20}\mathrm{F}$ reaction. In this reaction, the polarization of the beam particles is transferred to each nucleus. The $\vec{d}$ beam was produced using a polarized ion source[4], and accelerated at E/A = 10 MeV using the AVF cyclotron. The polarized beams were impinged on a CaF_2 crystal (0.5 mm^t) to produce the polarized ^{20}F. The crystal was placed at the center of the β-NMR apparatus (See Fig. 1.) at room temperature with a static magnetic field B_0 = 500 mT applied.

The β-rays emitted from ^{20}F nuclei were detected with plastic scintillator telescopes located above and below the crystal. The up/down ratio R of the β-ray counts is written as $R_0 \approx a(1+A_\beta P)/(1-A_\beta P)$, where a denotes a constant factor representing asymmetries in counter solid angles and efficiencies and A_β and P denote the β-ray asymmetry parameter and the degree of spin-polarization, respectively. A rotating RF perpendicular to B_0 is applied to ^{20}F by using the two pairs of coils. If the frequency and direction of the rotating RF correspond to the resonance values, the direction of the spin polarization is inverted ($P \to -P$) by the NMR. Thus, the up/down ratio is changed as $R \approx a(1-A_\beta P)/(1+A_\beta P)$. When the polarization is altered because of the resonant spin change, a change appears in the ratio R_0/R. The β-ray asymmetry $A_\beta P$ is written as $A_\beta P = \sqrt{(R_0/R)} - 1/\sqrt{(R_0/R)} + 1$.

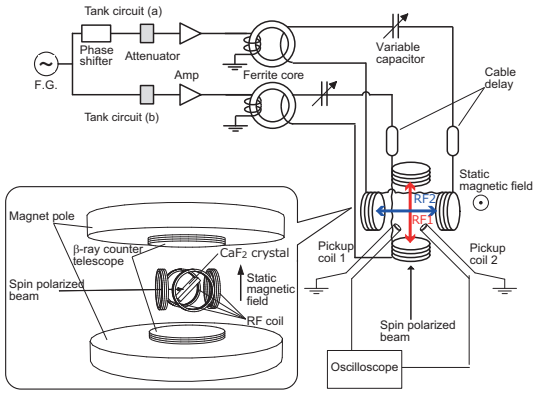

Fig. 1. Block diagram of the RF system for the rotating magnetic field and a schematic layout of the β-NMR setup.

The $\vec{d}$ beam was pulsed with beam-on and beam-off periods of 16 s and 22.02 s, respectively. In the beam-off period of a cycle, RF was applied for the first 10 ms. Subsequently, the β-rays were counted for 22 s, and in the last 10 ms of the beam-off period RF was applied again to restore the spin direction. First, we measured R_0 without RF and then, we measured R with RF. This cycle was repeated until the required measurement statistics were attained.

In this experiment, we first measured a μ moment by using β-NMR applied to the linear RF using tank circuit (a); then, measured it using another one. Figure 2 shows obtained $A_\beta P$ values. Next, we attempted to measure the sign of $\mu(^{20}\mathrm{F})$ by applying a rotating RF. Analysis of the results is in progress.

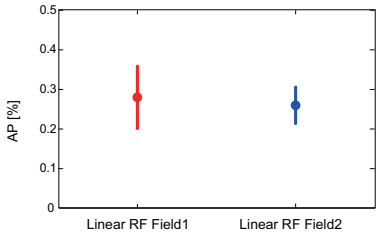

Fig. 2. Obtained $A_\beta P$ value of ^{20}F with applied linear RF field.

*1 Institute of Physics, Univ. of Tsukuba
*2 RIKEN Nishina Center

References
1) K. Sugimoto et al.: J. Phys. Soc. Jpn. 21, 213 (1966)
2) T. Niwa et al.: UTTAC 81, 5 (2012)
3) D. Nagae et al.: Hype. Int. 220, 65 (2013)
4) K. Hatanaka et al.: Nucl. Instr. and Meth. 217, 397 (1983)

Probing the critical behavior in the evolution of GDR width at very low temperatures in A ∼ 100 mass region†

B. Dey,[*1] D. Mondal,[*1] D. Pandit,[*1] S. Mukhopadhyay,[*1] S. Pal,[*1] S. Bhattacharya,[*2] A. De,[*3] K. Banerjee,[*1] N. Dinh Dang,[*4] N. Quang Hung,[*5] and S.R. Banerjee[*1]

Although a wealth of data exists on the angular momentum dependence of width of giant dipole resonance (GDR) in different mass regions, the measurement of the GDR width at low temperatures ($T < 1$ MeV) is rather scarce due to the experimental difficulties in populating the nuclei at low excitation energies. The present work aims at providing systematic experimental data on the GDR width, specifically, at this very low temperature region. It is also our endeavor to systematically assess the different theoretical models and understand the complete nature of the damping mechanism as a function of T inside the atomic nucleus.

The increase of the GDR width as a function of T is described reasonably well within the Phonon Damping Model (PDM)[1]. The GDR damping mechanism is caused by coupling of the GDR to noncollective particle-hole (ph) and particle-particle (pp) [hole-hole (hh)] configurations. The coupling to the various ph configurations leads to the quantal width (exists even at $T = 0$), whereas the thermal width arises owing to the coupling to pp and hh configurations which appear at $T > 0$ because of the distortion of the Fermi surface. Thermal pairing since is also included, since in finite systems it does not collapse at the temperature of the superfluid-normal phase transition in infinite systems, but decreases monotonically as T increases. The macroscopic Thermal Shape Fluctuation Model (TSFM)[2,3], on the other hand, is based on the fact that large-amplitude thermal fluctuations of the nuclear shape play an important role in describing the increase of the GDR width as a function of T. The TSFM, however, cannot explain the T dependence below 1.5 MeV in different mass regions. Recently, by modifying the phenomenological parameterization (pTSFM)[3], a new fitting formula, called the Critical Temperature included Fluctuation Model (CTFM), was proposed[4], which gives a good description of the GDR width behavior for both T and J in the entire mass region.

In this work, a systematic measurement of the apparent GDR width has been carried out in the unexplored region ($T = 0.8 - 1.5$ MeV) for ^{97}Tc using alpha induced fusion reactions. This is the first measurement of the GDR width at finite temperature in A ∼ 100 mass region both above and below the critical point and can be effectively used to verify the existing theoretical models. The experiments were performed at the Variable Energy Cyclotron Centre (VECC), Kolkata. A self supporting 1 mg/cm^2 thick ^{93}Nb target was bombarded with alpha beams produced by the K-130 cyclotron. Four different beam energies of 28, 35, 42 and 50 MeV were used to form the compound nucleus (CN) ^{97}Tc at the excitation energies of 29.3, 36, 43 and 50.4 MeV, respectively. The high energy γ-rays from the decay of ^{97}Tc were detected using the high energy photon spectrometer LAMBDA.

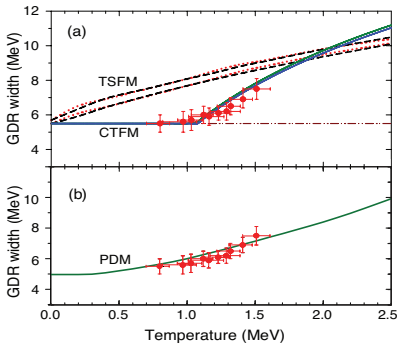

Fig. 1. (a) GDR width as a function of temperature. Symbols are experimental data. The TSFM calculations with shell effect (dotted lines) and without it (dashed lines) are shown for $J = 0\hbar$ (lower) and $J = 30\hbar$ (upper). Continuous lines are the CTFM predictions for $J = 10\hbar$ (lower) and $J = 20\hbar$ (upper). (b) The solid line shows the result of PDM calculations, performed at $J = 0$ by using the single-particle energies obtained within the deformed Woods-Saxon potentials with the deformation parameter $\beta = 0.134$, and including exact canonical-ensemble thermal pairing gaps for neutrons and protons.

The data have been compared with the TSFM, CTFM and PDM. Interestingly, the CTFM and PDM give the similar results and agree with the data, whereas the TSFM differs significantly even after incorporating the shell effects (Fig. 1).

† Condensed from the article in Phys. Lett. B **731**, 92 (2014)
*1 Variable Energy Cyclotron Center, Kolkata
*2 Department of Physics, Barasat Govt. College, Kolkata
*3 Department of Physics, Raniganj Girls' College, Kolkata
*4 RIKEN Nishina Center
*5 School of Engineering, Tan Tao University

References

1) N. Dinh Dang and A. Arima, Phys. Rev. Lett. **80**, 4145 (1998), Nucl. Phys. A **636**, 427 (1998); N. Dinh Dang, Phys. Rev. C **85**, 2023 (2012); N. Dinh Dang and N. Quang Hung, Phys. Rev. C 86, 044333 (2012).
2) W. E. Ormand et al., Phys. Rev. Lett. **77** 607 (1996).
3) D. Kusnezov et al., Phys. Rev. Lett. **81**, 542 (1998).
4) Deepak Pandit et al., Phys. Lett. B **713**, 434 (2012).

2. Nuclear Physics (Theory)

Hoyle band and α condensation in ^{12}C

Y. Funaki*1

The Hoyle state, the second $J^\pi = 0^+$ state at 7.65 MeV in ^{12}C, is a typical example of cluster states and had a long history since it was predicted by F. Hoyle and subsequently observed by Cook *et al.* as a key state in the synthesis of ^{12}C in stellar evolution. In the last decade, the aspects of the α condensate, in which α clusters occupy an identical S-orbit, has attracted great interest since the so-called Tohsaki-Horiuchi-Schuck-Röpke (THSR) wave function[1], which has the 3α condensate character, was shown to be equivalent to the Hoyle state wave function obtained by solving the equations of the full 3α resonating group method (RGM) or generator coordinate method (GCM)[2]. In addition to the Hoyle state, the nature of the other positive-parity excited states were recently highlighted by many experiments[3–6].

In this report, we investigate the structures of the positive parity excited states above the 3α threshold by using an extended version of the THSR wave function, which includes the 3α condensate and ^{8}Be + α asymptotic configurations, with a treatment of resonances[7]. In particular, we focus on the structures of the "Hoyle band" states as well as the 2_2^+[3–5] and 4_2^+[6] states, which were recently observed above the Hoyle state, in addition to the structures of the 0_3^+ and 0_4^+ states, which were also quite recently identified in experiment[3].

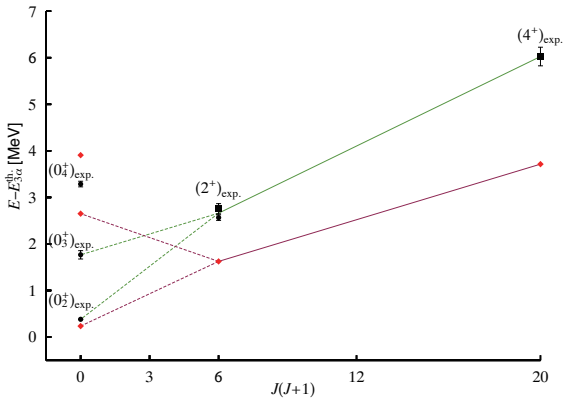

Fig. 1. The observed energy levels for the 0_3^+, 0_4^+, and 2_2^+ states in Ref.[3], and the 2_2^+[5] and 4_2^+[6] states are denoted by black circles and black squares, respectively. The calculated energy levels for the five states are denoted by red diamonds.

In Fig. 1, the calculated energy levels are plotted as a function of $J(J+1)$, together with the experimental data. We can observe that the 0_2^+, 2_2^+, and 4_2^+ states roughly follow a $J(J+1)$ trajectory both in theory and experiment, which gives a support to the rotational picture. In fact, we found the very strong $E2$ transitions inside the Hoyle band $B(E2; 4_2^+ \to 2_2^+) = 591$ e^2fm^4 and $B(E2; 2_2^+ \to 0_2^+) = 295$ e^2fm^4.

On the other hand, the $J^\pi = 0^+$ band head in experiment seems to be fragmented into the Hoyle state and the 0_3^+ state, and the calculated levels also have a similar tendency concerning the $B(E2)$ transition from the 2_2^+ state, the Hoyle state being located slightly below and the 0_3^+ state slightly above the $J(J+1)$ line. Accordingly, the transition between the 2_2^+ and 0_3^+ states is also very strong $B(E2; 2_2^+ \to 0_3^+) = 104$ e^2fm^4.

This suggests that the Hoyle band, especially in what concerns the 0^+ band-head state, cannot be considered a simple rotational band. This results from the fact that the 3α condensate structure in the Hoyle state is not the same as the usual ^{8}Be$(0^+) + \alpha$ rotation, in which the remaining α cluster orbits outside the ^{8}Be core. Namely, in the Hoyle state, the remaining α cluster also orbits inside the ^{8}Be core, and independent 3α-cluster motion in an identical $0S$-orbit is realized. Consequently, the Hoyle state gains extra binding energy, and hence its energy position is considered to be pushed below the $J(J+1)$ line, as shown in Fig. 1. The same effect is also argued to occur in the study of ^{16}O[8,9], in which the 4α condensate is identified as a "complete condensate" and the ^{12}C$(0_2^+) + \alpha$ state as a "local condensate". Because of the existence of the "complete condensate", a higher 0^+ excited state, which is shown to have a prominent ^{8}Be$(0^+) + \alpha$ structure[7,10] with the remaining α cluster orbiting outside the ^{8}Be core, appears as a higher nodal state, the 0_3^+ state excited from the Hoyle state with a very strong monopole transition strength calculated to be $M(E0; 0_2^+ \to 0_3^+) = 35$ fm^2.

*1 RIKEN Nishina Center

References

1) A. Tohsaki et al. Phys. Rev. Lett. **87**, 192501 (2001).
2) Y. Funaki et al. Phys. Rev. C **67**, 051306(R) (2003).
3) M. Itoh et al. Nucl. Phys. A **738**, 268 (2004); M. Itoh et al. Phys. Rev. C **84**, 054308 (2011).
4) M. Freer et al. Phys. Rev. C **80**, 041303(R) (2009).
5) W. R. Zimmerman et al. Phys. Rev. Lett. **110**, 152502 (2013).
6) M. Freer et al. Phys. Rev. C **83**, 034314 (2011).
7) Y. Funaki arXiv: 1408.5855.
8) S. Ohkubo and Y. Hirabayashi Phys. Lett. B **684**, 127 (2010).
9) Y. Funaki et al. Prog. Theor. Phys. Supple. **196**, 439 (2012).
10) C. Kurokawa and K. Katō Phys. Rev. C **71**, 021301 (2005); Nucl. Phys. A **792**, 87 (2007).

Energy and mass-number dependence of hadron-nucleus total reaction cross sections†

A. Kohama,[*1] K. Iida,[*1,*2] and K. Oyamatsu[*1,*3]

The size of an atomic nucleus is one of the most fundamental quantities that characterize the bulk properties of nuclei. It is well known for β stable nuclei in the ground state thanks to systematic measurements of electron and proton elastic differential cross sections. This helps clarify the equation of state of nuclear matter near the saturation point.[1)]

In this work, we systematically analyze nuclear reaction data that are sensitive to nuclear size, namely, proton-nucleus total reaction cross sections $\sigma_R(p+A)$ and differential elastic cross sections, using a phenomenological black-sphere (BS) approximation of nuclei that we are developing. In this framework, the radius of the black sphere "a" is found to be a useful length scale that simultaneously accounts for the observed $\sigma_R(p+A)$ and first diffraction peak in the proton elastic differential cross section. This framework is expected to be applicable to any kind of projectile that is strongly attenuated in the nucleus. On the basis of a cross-section formula constructed within this framework (BS cross-section formula)[2)] as function of the target mass number A and the proton incident energy T_p, we find that a less familiar $A^{1/6}$ dependence of σ_R plays a crucial role in describing the T_p dependence.

In order to illustrate the A dependence of σ_R, in Fig. 1, we compare the values of the BS cross-section formula with those obtained by using the square-well potential of the same radius "a" within the eikonal approximation for the cases of $^{\rm natu.}$C and Pb. By noting that a very well scales as $A^{1/3}$, we examine the difference in the A dependence between the two expressions. As a result of expansion in A, the leading term is proportional to $A^{2/3}$, while the subleading term is proportional to $A^{1/3}$ multiplied by an A dependent exponential suppression factor in the eikonal approximation, which causes a different T_p dependence from the solid curve in each panel of Fig. 1. This difference results from the $A^{1/6}$ dependence in σ_R.

By comparing the solid curves in the upper and lower panels of Fig. 1, one can see the relatively weaker T_p dependence for the case of Pb. The cross section itself grows proportional to $\sim A^{2/3}$, while the T_p-dependent term is proportional to $\sim A^{1/6}$, leading to $O(A^{-1/2})$ corrections to the $O(A^{2/3})$ term. Thus, the relative change in the cross section by T_p is suppressed. This is the reason why the slope toward a lower T_p becomes steeper for the case of C than that of Pb. The latest empirical values of σ_R [4)] apparently support the presence of the $O(A^{1/6})$ correction term in σ_R.

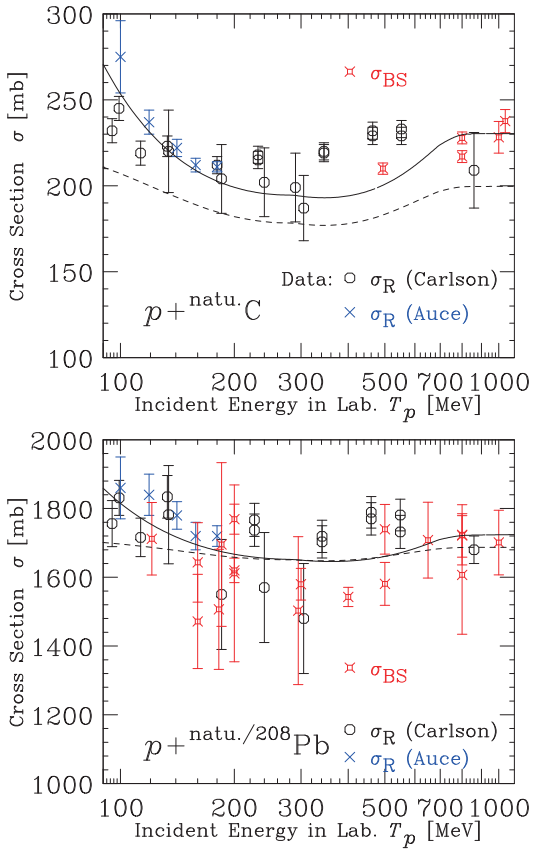

Fig. 1. Comparison of the BS cross-section formula (solid curve) with the eikonal approximation based on the square-well potential (dashed curve) for $\sigma_R(p+^{\rm natu.}{\rm C})$ (upper) and $\sigma_R(p+^{\rm natu./208}$ Pb) (lower) as a function of T_p. We adopt both the BS radius at 800 MeV and the square-well radius as 2.70 fm for carbon and 7.40 fm for lead. The values of $\sigma_{\rm BS}$ ($\equiv \pi a^2$), which are represented by squares with crosses, are obtained from the measured peak angle of the first diffraction maximum of the proton elastic scattering. They are consistent with the measured σ_R (○[3)], ×[4)]).

A part of this work was already reported in Ref.[5].

† Condensed from the article in arXiv: 1411.7737

*1 RIKEN Nishina Center
*2 Depart. of Natural Science, Kochi University
*3 Depart. of Human Informatics, Aichi Shukutoku University

References
1) K. Oyamatsu *et al.*: Prog. Theor. Phys. **109**, 631 (2003).
2) K. Iida *et al.*: J. Phys. Soc. Japan **76**, 044201 (2007).
3) R. F. Carlson: At. Data Nucl. Data Tables **63**, 93 (1996).
4) A. Auce *et al.*: Phys. Rev. C **71**, 064606 (2005).
5) A. Kohama *et al.*: RIKEN Accel. Prog. **43**, 59 (2009).

Systematic calculation of $T = 1$ triplets with proton–neutron mixed energy density functionals

K. Sato,[*1] J. Dobaczewski,[*2,*3,*4] T. Nakatsukasa,[*1,*5] and W. Satuła[*2,*4]

We performed a systematic calculation for $T = 1$ isobaric analog states (IASs) based on energy density functionals (EDFs) including proton-neutron (p-n) mixing. Recently, we developed a new model to calculate IASs on the basis of the Skyrme EDFs that include arbitrary mixing between protons and neutrons[1]. In this framework, single-particle states are generalized as superpositions of proton and neutron components. In connection with this extension of single particles, density functionals are also extened to those with mixing between protons and neutrons[2]. In this work, we consider an extension of EDFs including p-n mixing only in the particle-hole (p-h) channel, with both the rotational and isospin symmetries conserved. Our ultimate goal, however, is to develop a consistent symmetry-unrestricted EDF approach including p-n mixing both in the p-h and pairing channels.

We developed a code for the p-n mixing calculation by extending the code "HFODD,"[3] which solves the nuclear Skyrme–Hartree–Fock(–Bogolyubov) problem by using the Cartesian deformed harmonic-oscillator basis. In this p-n mixing calculation, we perform isocranking calculation by adding the isocranking term to the Hamiltonian: $\hat{h}' = \hat{h} - \vec{\lambda}\cdot\vec{\hat{t}}$. Here, $\vec{\hat{t}}$ is the isospin operator. The isocranking term is analogous to that used in the standard tilted-axis-cranking calculations for high-spin states. By adjusting the isocranking frequency $\vec{\lambda}$, we can control the size and direction of the isospin of the system.

In Ref. 1), we developed an efficient method for determining the isocranking frequency and successfully applied the isocranking model to the IASs in even-even $A = 40 - 56$ and odd-odd $A = 14$ isobars. Thus, we demonstrated that the p-n mixed single-reference EDF approach is capable of quantitatively describing the isobaric analog excited states. Among the results in Ref. 1), that of odd-odd $T = 1$ IASs is of particular interest (See Fig. 4 in Ref. 1)). We calculated the energies of the $I = 0^+, T = 1$ triplet of states in the $A = 14$ isobars, ^{14}C, ^{14}N, and ^{14}O by using the SkM* EDF. We found that there is asymmetry between the energy differences $|E(T_z = 0) - E(T_z = -1)|$ and $|E(T_z = 0) - E(T_z = 1)|$, which may be related to charge asymmetry and independence of the NN interaction. To investigate this point, in this study, we performed a systematic calculation of the $T = 1$ triplets in $A = 4n + 2$ nuclei. We calculated the triple energy difference (TED)[4] $2E(T_z = 0) - E(T_z = 1) - E(T_z = -1)$ with several Skyrme parameter sets. In this model, while the $T_z = \pm 1$ IASs are obtained with the standard Hartree-Fock calculation without p-n mixing, the $T_z = 0$ IAS is calculated using the isocranking model and is described by a single time-even Slater determinant consisting of p-n mixed single particles.

Figure 1 shows examples of the results of the calculation. We plot the deviation of the calculated TEDs from the experimental data in the $A = 14 - 58$ region. The TEDs in the $T = 1$ triplets calculated with the SLy4, SIII, and SkM* parameter sets are shown. One can see a systematic underestimation of the TEDs in Fig. 1. In this calculation, we used isoscalar EDFs, which are invariant under rotation in isospin space, plus the Coulomb energy functional. This systematic deviation may imply that we need to extend functionals further to include isospin breaking terms. We already started performing a calculation including the isospin breaking interaction, which will be reported elsewhere.

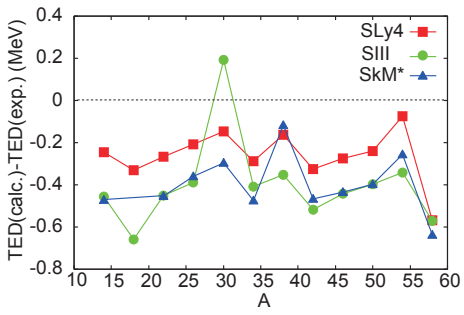

Fig. 1. Deviation of the calculated triple energy difference from the experimental data[5], TED(calc.)-TED(exp.), for the $T = 1$ triplets in $A = 14 - 58$ nuclei. The TEDs calculated with SLy4, SIII, and SkM* are plotted.

*1 RIKEN Nishina Center
*2 Institute of Theoretical Physics, Faculty of Physics,University of Warsaw
*3 Department of Physics, University of Jyväskylä
*4 Helsinki Institute of Physics, University of Helsinki
*5 Center for Computational Sciences, University of Tsukuba

References
1) K. Sato et al.: Phys. Rev. C **86**, 061301(R) (2013).
2) E. Perlińska et al.: Phys. Rev. C **69**, 014316 (2004).
3) N. Schunck et al.: Comput. Phys. Commun. **183**, 166 (2012); J. Dobaczewski et al. (unpublished).
4) W. Satuła et al.: Acta. Phys. Pol. B **45** 167 (2014).
5) National Nuclear Data Center, Brookhaven National Laboratory, http://www.nndc.bnl.gov/.

Correlated two-neutron emission in decay of unbound nucleus ^{26}O†

K. Hagino*1 and H. Sagawa*2,*3

We study the two-neutron decay of the unbound ^{26}O nucleus with a three-body model assuming an inert ^{24}O core and two valence neutrons. In order to describe the decay properties of the neutron unbound nucleus, we take into account the couplings to the contiuum by using the Green's function technique.

In the experiment of Ref.[1], the ^{26}O nucleus was produced in a single proton-knockout reaction from a secondary ^{27}F beam. Therefore, we first construct the ground state of ^{27}F with a three-body model, assuming the ^{25}F+n+n structure. We then assume a sudden proton removal; that is, the ^{25}F core changes to ^{24}O keeping the configuration for the n+n subsystem of ^{26}O to be the same as that in the ground state of ^{27}F. This initial state, Ψ_i, is then evolved with the Hamiltonian for the three-body ^{24}O+n+n system for the two-neutron decay.

We consider two three-body Hamiltonians, one for the initial state ^{25}F+n+n and the other for the final state ^{24}O+n+n. For both cases, we use the Hamiltonian

$$H = \hat{h}_{nC}(1) + \hat{h}_{nC}(2) + v(1,2) + \frac{\vec{p}_1 \cdot \vec{p}_2}{A_c m}, \qquad (1)$$

where A_c is the mass number of the core nucleus, m is the nucleon mass, and $\hat{h}_{nC}$ is the single-particle (s.p.) Hamiltonian for a valence neutron interacting with the core. We use a contact interaction between the valence neutrons. See ref.[2] for details of the parameters of Eq. (1) and the contact interaciton between the neutrons.

With the initial wave function from the three-body model, the decay energy spectrum can be computed as[3]

$$\frac{dP}{dE} = \frac{1}{\pi}\Im\langle\Psi_i|G(E)|\Psi_i\rangle, \qquad (2)$$

with $G(E) = G_0(E) - G_0(E)v(1 + G_0(E)v)^{-1}G_0(E)$, where $\Im$ denotes the imaginary part. $G(E)$ is the perturbed Green's function, while $G_0(E)$ is the unperturbed Green's function given by

$$G_0(E) = \sum_{1,2} \frac{|(j_1 j_2)^{(0^+)}\rangle\langle(j_1 j_2)^{(0^+)}|}{e_1 + e_2 - E - i\eta}, \qquad (3)$$

where the sum includes all independent two-particle states coupled to the total angular momentum $J = 0$ with positive parity, as described by the three-body Hamiltonian for ^{24}O+n+n.

Figure 1 shows the decay energy spectrum obtained with Eq. (2). The solid line shows the correlated spectrum, in which the final–state nn interaction is fully taken into account, while the dotted line shows the result without the final–state nn interaction. The latter corresponds to the term $G_0(E)$ in $G(E)$. Without the final–state nn interaction, the two valence neutrons in ^{26}O occupy the s.p. resonance state of $1d_{3/2}$ at 770 keV, and the peak in the decay energy spectrum appears at twice this energy. When the final–state nn interaction is taken into account, the peak is drastically shifted towards a lower energy and appears at 0.14 MeV, in good agreement with the experimental data. The figure also shows with the dashed line the result obtained by including only the $(d_{3/2}d_{3/2})^{(0^+)}$ configurations in the unperturbed Green's function of Eq. (3). This corresponds to the case without the dineutron correlation in the final state, as the dineutron correlation is caused by an admixture of several configurations with different parities. The dineutron correlation shifts the peak position further down, making the peak appear at an energy close to the threshold, as shown by the solid line.

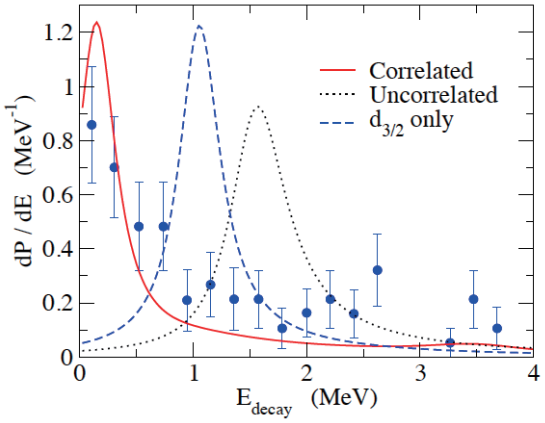

Fig. 1. (Color online) Decay energy spectrum for the two-neutron emission decay of ^{26}O. The solid line shows the result with the full inclusion of the final–state neutron-neutron (nn) interaction, while the dotted line shows the result without the final–state nn interaction. The dashed line is obtained by including only the $(d_{3/2}d_{3/2})^{(0^+)}$ configurations in the unperturbed Green's function of Eq. (3). The theoretical curves are drawn with a finite width of 0.21 MeV, which is the same as the experimental energy resolution. The experimental data are taken from Ref.[1].

We discuss the role of neutron-neutron correlation in the decay probability as well as in the energy and the angular distributions of the emitted neutrons in Ref.[2]

† Condensed from the article in Phys. Rev. C **89**, 014331(2014)

*1 Department of Physics, Tohoku University
*2 RIKEN Nishina Center
*3 Center for Mathematics and Physics, University of Aizu

References
1) E.Lunderberg *et al.*,Phys.Rev.Lett.**108**,142503 (21012).
2) K.Hagino and H.Sagawa, Phys.Rev.C**89**,014331(2014).
3) H.Esbensen and G.F.Bertsch, Nucl.Phys.**A542**, 310(1992).

Three-body model calculation of the 2^+ state in ^{26}O†

K. Hagino*1,*2 and H. Sagawa*3,*4

We discuss the 2^+ state of ^{26}O using a three-body model of an ^{24}O+n+n system with full account of the continuum. The decay energy spectrum for a given angular momentum I can be evaluated as

$$\frac{dP_I}{dE} = \sum_k |\langle \Psi_k^{(I)} | \Phi_{\rm ref}^{(I)} \rangle|^2 \, \delta(E - E_k), \qquad (1)$$

where $\Psi_k^{(I)}$ is a solution of the three-body model Hamiltonian with angular momentum I and energy E_k, and $\Phi_{\rm ref}^{(I)}$ is the wave function for a reference state with the same angular momentum. For a reference state we use the uncorrelated state of ^{27}F with the neutron $|[1d_{3/2} \otimes 1d_{3/2}]^{(IM)}\rangle$ configuration, which is dominant in the ground state of ^{27}F.

With a contact interaction, the continuum effects on the decay energy spectrum can be taken into account in terms of the Green's function. Notice that Eq. (1) can be expressed as

$$\begin{aligned} \frac{dP_I}{dE} &= -\frac{1}{\pi} \Im \sum_k \langle \Phi_{\rm ref}^{(I)} | \Psi_k^{(I)} \rangle \frac{1}{E_k - E - i\eta} \langle \Psi_k^{(I)} | \Phi_{\rm ref}^{(I)} \rangle, \\ &\equiv -\frac{1}{\pi} \Im \langle \Phi_{\rm ref}^{(I)} | G^{(I)}(E) | \Phi_{\rm ref}^{(I)} \rangle, \end{aligned} \qquad (2)$$

where $\Im$ denotes the imaginary part and η is an infinitesimal number and $G^{(I)}(E)$ is the correlated Greens's function. The correlated Greens's function will be constructed using the unperturbed Green's function.

The upper panel of Fig. 1 shows the decay energy spectrum of ^{26}O for $I = 0$ (dashed line) and I=2 (solid line). For presentation purposes, we set η in Eq. (2) to be a finite value, i.e., $\eta = 0.21$ MeV[1]. For comparison, we also show the spectrum for the uncorrelated case with a dotted line, which gives the same spectrum both for $I = 0$ and $I = 2$. For the uncorrelated case, the spectrum has a peak at $E = 1.54$ MeV, which is twice the single-particle resonance energy, 0.77 MeV. With the pairing interaction between the valence neutrons, the peak energy shifts towards lower energies. The energy shift ΔE is larger in $I = 0$ than in $I = 2$, i.e. , the peak in the spectrum appears at $E = 0.148$ MeV ($\Delta E = -1.392$ MeV) for $I = 0$ and at $E = 1.354$ MeV ($\Delta E = -0.186$ MeV) for $I = 2$.

We have shown that the 2^+ state appears at approximately $E = 1.35$ MeV. This 2^+ energy is close to, but slightly smaller than, the unperturbed energy, $E = 1.54$ MeV, and thus the energy shift from the unperturbed energy is much smaller than the energy shift for the 0^+ state. We have argued that this is a typical spectrum well understood by the single-j model with the pairing residual interaction. Many shell model calculations such as the ab initio[3] and USDA and USDB[4] calculations have predicted the excitation energy of the 2^+ state in ^{26}O in the opposite trend, i.e., they have predicted a higher energy than the unperturbed energy. The energy of the 2^+ state needs to be urgently confirmed experimentally[5] in order to clarify the validity of nuclear models and effective interactions in nuclei on and beyond the neutron drip-line.

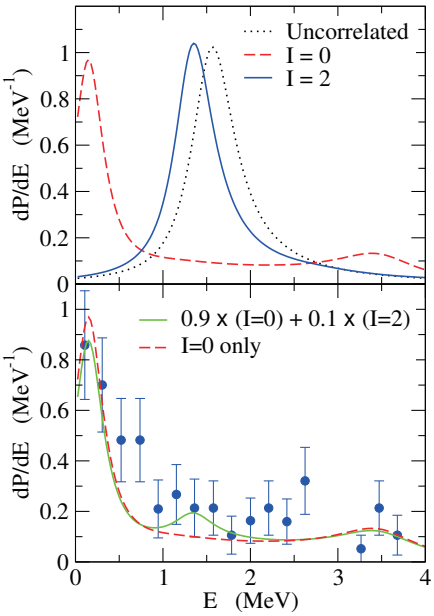

Fig. 1. (upper panel) The decay energy spectrum for the two-neutron emission decay of ^{26}O. The dashed and solid lines represent the 0^+ and 2^+ states, respectively. The dotted line shows the uncorrelated spectrum obtained by ignoring the interaction between the valence neutrons. (lower panel) The decay energy spectrum obtained by superposing the $I = 0$ and $I = 2$ components. The dashed line is the decay energy spectrum for the pure $I = 0$ configuration. The experimental data, normalized to the unit area, are taken from Ref.[2].

† Condensed from the article in Phys. Rev. C **90**, 027303(2014)

*1 Department of Physics, Tohoku University
*2 Research Center for Electron Photon Science, Tohoku University
*3 RIKEN Nishina Center
*4 Center for Mathematics and Physics, University of Aizu

References
1) K.Hagino and H.Sagawa, Phys.Rev.C**89**,014331(2014).
2) E.Lunderberg *et al.*, Phys.Rev.Lett.**108**, 142503(21012).
3) C.Caesar *et al.*, Phys. Rev. C**88**, 034313 (2013).
4) B.A.Brown and W.A.Richter, Phys.Rev.C**74**,034315(2006).
5) Y.Kondo and T.Nakamura, private communications.

Proton-neutron pairing vibrations in ^{40}Ca: Precursory soft mode of the isoscalar spin-triplet pairing condensation†

K. Yoshida*1

The pairing correlation plays a central role in low-energy nuclear phenomena. The correlation is so strong that the fluctuations of the pairing gap around its zero equilibrium value develop in nuclei near the closed shell, and the systems get deformed eventually in gauge space when more nucleons are added. The collective pairing vibration emerging in the closed-shell nuclei is thus associated with the occurrence of the pairing condensation.

It is in the isovector and spin-singlet ($T = 1, S = 0$) channel that the pairing correlation has been extensively studied. With the advent of the radioactive-isotope beam technology, heavy proton-rich nuclei along the $N = Z$ line have received considerable attention. The isoscalar and spin-triplet ($T = 0, S = 1$) pairing correlation is expected to be visible in $N \sim Z$ nuclei because the shell structures around the Fermi levels of both neutrons and protons are similar to each other and the spatial overlap between the neutron and proton single-particle wave functions would be large to form a proton-neutron (pn) Cooper pair[1]. Because of the strongly attractive pn interaction in the $^3S_1$ channel, the possible $T = 0$ pairing condensate has been discussed theoretically in heavy $N \sim Z$ nuclei[2–4].

I investigate the possibility of a collective $T = 0$ pn-pairing vibrational mode in the "normal" phase where the $T = 0$ pairing gaps are zero. The pn pair excitations are described microscopically based on the nuclear energy-density functional (EDF) method. More precisely, the pn-pairing vibrational modes are obtained out of the solutions of the pn particle-particle random-phase approximation (ppRPA) equation, and are described as elementary modes of excitation generated by two-body interactions acting between a proton and a neutron. Then, I show that the strongly collective $T = 0$ pn-pairing vibrational mode emerges when the interaction is switched on.

Figure 1 shows the strength distributions for the monopole ($L = 0$) pn-pair-addition and removal transfer $|\langle Z \pm 1, N \mp 1; \lambda | \hat{P}^{\dagger}_{T,S}(\hat{P}_{T,S}) | Z, N \rangle|^2$ as functions of the RPA frequency ω_λ in ^{40}Ca. In the present calculation, the SGII interaction is used for the particle-hole (ph) channel. For the pp channel, the density-dependent contact interactions are employed. The pairing strength in the $T = 1$ channel is fixed as $V_0^{(T=1)} = -390$ MeV fm^3. The pairing strength in the $T = 0$ channel is given as $V_0^{(T=0)} = f \times V_0^{(T=1)}$.

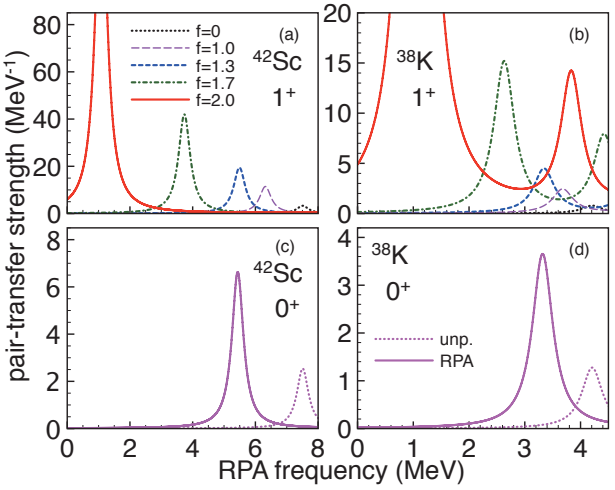

Fig. 1. Monopole pn pair-addition strengths of ^{40}Ca → ^{42}Sc and pair-removal strengths of ^{40}Ca → ^{38}K in the $J^\pi = 1^+, T = 0$ [(a), (b)] and $J^\pi = 0^+, T = 1$ [(c), (d)] states smeared with a width of 0.1 MeV. For the $(J, T) = (1, 0)$ channel, the strengths obtained with factors $f = 0, 1.0, 1.3, 1.7$, and 2.0 are shown. For the $(J, T) = (0, 1)$ channel, the unperturbed single-particle transition strengths are also shown by a dotted line.

Factor f is changed to see the effect of the interaction in the $T = 0$ channel.

It is clearly visible that the RPA frequency of the $T = 0$ pn-pairing vibrational mode becomes lower on increasing the pairing strength f. The pairing collectivity generated is sensitive to the shell structure as well as to the interactions. The critical strength is found to be $f_c = 2.04$. A rapid lowering of the RPA frequency seen here indicates the occurrence of true vacuum giving the $T = 0$ pairing gaps $\boldsymbol{\Delta} \equiv \langle \hat{P}_{T=0,S=1} \rangle \neq 0$ in the limit of the strong pairing interaction $f > f_c$. Another direct measure of the collectivity is the pn transfer strength. One can also see an exponential enhancement in the transition strengths when approaching the critical strength f_c. Therefore the 1^+ state in ^{38}K and ^{42}Sc can be considered as a precursory soft mode of the $T = 0$, $S = 1$ pairing condensation.

References

1) A. L. Goodman: Phys. Rev. C 58, R3051 (1998).
2) W. Satuła and R. Wyss: Phys. Lett. B 393, 1 (1997).
3) A. L. Goodman: Phys. Rev. C 60, 014311 (1999).
4) G. F. Bertsch and Y. Luo: Phys. Rev. C 81, 064320 (2010).

† Condensed from the article in Phys. Rev. C 90, 031303(R) (2014)

*1 Graduate School of Science and Technology, Niigata University

Study of low-frequency negative-parity vibrational excitations of superdeformed rotational band in ^{40}Ca using cranked Skyrme-RPA calculations

M. Yamagami [*1] and K. Matsuyanagi[*2]

An atomic nucleus is a unique quantum system. A nucleus exists in various modes with diverse shapes and collective motions by adding only a small percentage of the total binding energy. The diversity also increases with additional isospin and angular momentum.

^{40}Ca is a representative nucleus: the ground state is spherical with a spherical magic number $N = Z = 20$; however a superdeformed (SD) band built on the excited 0^+ state at 5.2 MeV was found.[1] The large octupole collectivity can be expected in the SD state associated with the SD shell structure that consists of approximately an equal number of positive- and negative-parity levels.

The description of diverse nuclear phenomena through a single theoretical framework is a challenging subject. Toward this direction, we have developed the first computer code of the cranked random phase approximation with Skyrme density functional (cranked Skyrme-RPA). Using this code, once the Skyrme density functional is fixed, we can calculate consistently the ground state as well as the rotational and vibrational excitations in nuclei across the nuclear chart.

We adopt the single-particle Hamiltonian with the triaxially deformed potential that uniformly rotates about the x-axis with a rotational frequency ω_{rot}; $h' = h - \omega_{rot} j_x$. The Skyrme SLy4 interaction is employed for h. Two discrete symmetries, the parity and rotation about the x-axis at the angle π, are imposed on the single-particle wave functions. The wave functions are represented through Fourier-series expansion in order to effectively treat the configurations involving unbound single-particle states.

We solve the RPA equation in the matrix form with a residual interaction derived from the Skyrme force through the Landau-Migdal approximation. The octupole transition operators $O^{(\xi,\zeta)}_{3K}$ can be classified by the z-component K of its angular momentum and the x (z) - signature ξ (ζ) $= \pm 1$ representing the symmetry of rotation about the x (z) - axis. The Coriolis coupling mixes the different K and ζ modes. The excitations can be classified into two types by ξ.

We study the low-frequency negative-parity vibrational excitations of the SD rotational band in ^{40}Ca. The upper part of Fig. 1 shows the six vibrational states with $\xi = -1$ for vibrational energy $E_{vib} < 5$ MeV. The isoscalar octupole transition strength B(IS : O_3) changes as a function of ω_{rot}, and the maximum value for each vibrational state exceeds 50 Weisskopf units (W.u.) within the region from $\omega_{rot} = 0$ to 1.6 MeV/$\hbar$.

The vibrational energy of the first excitation decreases as a function of ω_{rot}. The B(IS : O_3) value is 66.5 W.u. at $\omega_{rot} = 0.4$ MeV/$\hbar$ and then decreases slowly. This ω_{rot} dependence is associated with the rotational alignment of [440]1/2 particle states: This effect reduces the SD shell gap at N (Z) = 20 by 42.4 (40.4) percent while ω_{rot} changes from 0 to 1.5 MeV/$\hbar$. The B(IS : O_3) value is dominated by the $\zeta = +1$ component B(IS : $O_3^{(\zeta=+1)}$) consisting of $O_{31}^{(-1,+1)}$ and $O_{33}^{(-1,+1)}$ operators.

It is quite interesting to investigate what will happen if ω_{rot} is increased further; however we could not obtain reliable RPA solutions. A better method for eliminating the spurious center of mass component may be required. Nevertheless, it seems reasonable to assume that the above discussion will continue: the vibrational energy will decrease further and cross the yrast line. This may indicate an instability of the SD shape, leading to a transition to a non-axial reflection-asymmetric shape.

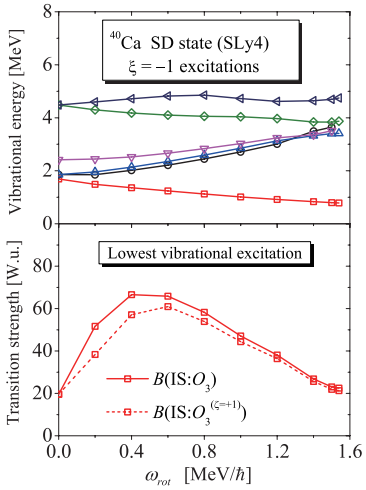

Fig. 1. (Upper) The vibrational energies of negative-parity excitations with $\xi = -1$ of the SD state in ^{40}Ca are shown as a function of ω_{rot}. (Lower) The B(IS : O_3) and B(IS : $O_3^{(\zeta=+1)}$) of the lowest vibrational excitation.

*1 Department of Computer Science and Engineering, University of Aizu
*2 RIKEN Nishina Center

References
1) E. Ideguchi et al.: Prog. Theor. Phys. Suppl. **196**, 427 (2012).

Self-consistent Hartree-Fock and RPA Green's function method for monopole response of neutron-rich Ni isotopes†

I. Hamamoto*1,*2 and H. Sagawa*1,*3

We discuss low-energy monopole strength of Ni isotopes using the self-consistent Hartree-Fock calculation and the RPA Green's function method with Skyrme interactions. This study is strongly motivated by a recent observation of monopole strength by inelastic alpha scattering at $50A$ MeV on the unstable nucleus ^{68}Ni.[1)] The observation of soft monopole mode is reported at 12.9 ± 1.0 MeV, in addition to the isoscalar giant monopole resonance (ISGMR), for which the centroid is placed at 21.1 ± 1.9 MeV. To study the properties of low-energy monopole strength, the continuum effect must be properly taken into account in the theoretical calculations. Therefore, we perform the self-consistent HF+RPA calculations with the Skyrme interactions in coordinate system. The strength distributions $S(E)$ are obtained from the imaginary part of the RPA Green function, G_{RPA}, as

$$S(E) = \sum_n |< n \mid Q \mid 0 >|^2 \, \delta(E - E_n)$$
$$= \frac{1}{\pi} Im\, Tr(Q^\dagger(\vec{r})\, G_{RPA}(\vec{r}, \vec{r'}; E)\, Q(\vec{r'})) \quad (1)$$

where Q expresses one-body operators

$$Q^{\lambda=0,\,\tau=0} = \frac{1}{\sqrt{4\pi}} \sum_i r_i^2 \quad (2)$$

for isoscalar monopole strength. The calculated results are shown in Fig. 1. Note that the widths of all responses are due to the coupling to the continuum without any smearing factor. It is concluded that sharp monopole peaks with width on the order of 1 MeV can hardly be expected for ^{68}Ni in the low energy region below 20 MeV. Instead, a broad shoulder of monopole strength consisting of neutron excitations to non-resonant one-particle states (called threshold strength) with relatively low angular momenta (ℓ, j) is obtained in the continuum energy region above the particle threshold, which is considerably lower than that of the isoscalar giant monopole resonance. In the monopole excitations of ^{68}Ni there are no unperturbed particle-hole states below 20 MeV, in which the particle is placed in either a bound or a resonant state. It is emphasized that in the theoretical estimation a proper treatment of the continuum is extremely important.

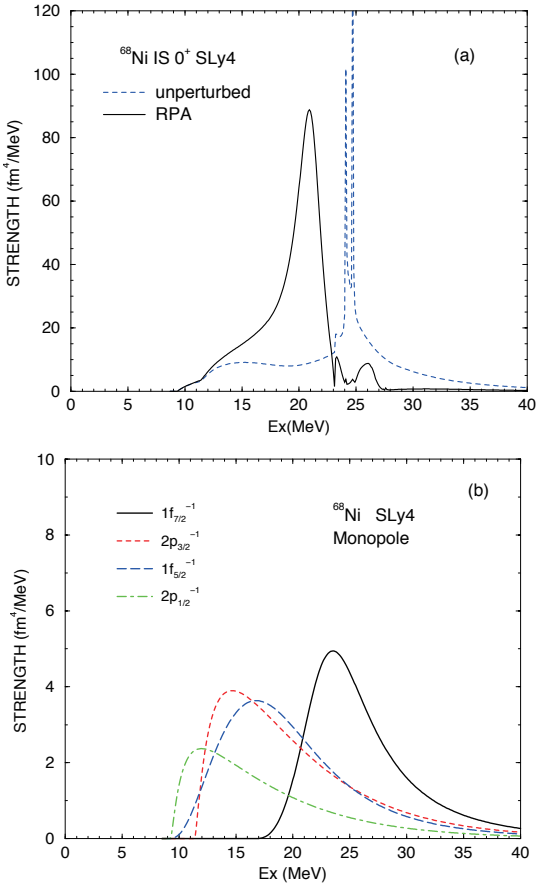

Fig. 1. (Color online) Monopole strength function (1) of ^{68}Ni . (a) Unperturbed monopole strength and isoscalar monopole RPA strength. The RPA strength denoted by the solid curve includes all strengths due to the coupling between bound and unbound states in RPA. In the unperturbed response, the p-h strengths, in which both particle and hole orbits are bound, are not included. The energies of those unperturbed p-h excitations are the $1d_{5/2} \rightarrow 2d_{5/2}$ excitation at 27.60 MeV for neutrons and the excitations of $1p_{3/2} \rightarrow 2p_{3/2}$ at 27.58 MeV and $1p_{1/2} \rightarrow 2p_{1/2}$ at 27.46 MeV for protons. In addition, the proton excitation at 27.3 MeV from the bound $1d_{5/2}$ orbit to the one-particle resonant $2d_{5/2}$ orbit has such a narrow width that the strength is not plotted. The narrow peaks at 24.1 and 24.7 MeV in the unperturbed strength curve are the proton $2s_{1/2} \rightarrow s_{1/2}$ and $1d_{3/2} \rightarrow 2d_{3/2}$ excitations, respectively. (b) Unperturbed neutron threshold strengths, which contribute to the total unperturbed strength below the energy of ISGMR in Fig. 1a, are shown for respective occupied hole orbits.

† Condensed from the article in Phys. Rev. C **90**, 031302(R)(2014)

*1 RIKEN Nishina Center
*2 Division of Mathematical Physics, Lund Institute of Technology at the University of Lund
*3 Center for Mathematics and Physics, University of Aizu

References

1) M.Vandebrouck et al., Phys.Rev.Lett. **113**,032504(2014).

Origin of fusion hindrance in heavy systems

K. Washiyama*1

In fusion reactions in heavy systems whose charge product $Z_P Z_T$ is larger than 1600, it has been observed[1] that the formation of a compound nucleus is strongly hindered around the Coulomb barrier energy, compared with $Z_P Z_T < 1600$ systems. In such heavy systems, an additional energy is needed to achieve fusion, which is called the extra-push energy.[2] The most probable reason behind the fusion hindrance phenomenon is the occurrence of the quasi-fission process, which involves reseparation without the formation of a compound nucleus after two nuclei touch each other, in heavy systems. A macroscopic fluctuation–dissipation model using a Langevin equation has been developed[3] to analyze quasi-fission and fusion dynamics especially in the synthesis of superheavy elements. Recently, the quasi-fission process was analyzed using the microscopic time-dependent Hartree-Fock (TDHF) model.[4]

The aim of this study is to analyze in detail the origin of fusion hindrance in heavy systems by using the microscopic TDHF model. To this end, we employ our method[5] to extract nucleus–nucleus potential and one-body energy dissipation from the relative motion of colliding nuclei to internal degrees of freedom in the entrance channel of fusion reactions from TDHF evolutions. We reported in Ref.[6] that the nucleus–nucleus potential extracted from TDHF in the $^{96}\mathrm{Zr}+^{124}\mathrm{Sn}$ system monotonically increases as the relative distance decreases, and that the potential shows no ordinary barrier. In this report, we present results of our systematic study for fusion in heavy systems and discuss a possible origin of fusion hindrance.

First, we perform systematic calculations for estimating the extra-push energy by TDHF for several heavy systems. We define the extra-push energy using TDHF as the difference between the fusion threshold energy and the potential barrier obtained from the frozen density approximation, $E_{\mathrm{extra}} = E_{\mathrm{thres}} - V_{\mathrm{FD}}$. The frozen density potential is estimated while keeping the projectile and target densities frozen to their respective ground-state densities. We confirm that the obtained extra-push energies agree well with those deduced from experimental observations. Then, we extract the nucleus–nucleus potential $V(R)$ and friction coefficient $\gamma(R)$ as a function of the relative distance between two nuclei R for those systems. We find that the property of the extracted potentials is similar to that in the $^{96}\mathrm{Zr}+^{124}\mathrm{Sn}$ system,[6] i.e., monotonic increase and no barrier structure in the potential. Finally, we analyze the fusion hindrance in heavy systems. We extract $V(R)$ and $\gamma(R)$ at the fusion threshold energy. We stop the extraction at R_{min} where the remaining kinetic energy reduces as much as possible in the TDHF simulations. At R_{min}, we can identify the extra-push energy as a sum of the remaining kinetic energy, accumulated dissipation energy estimated from $\gamma(R)$[5], and increase in potential due to the frozen density barrier, denoted by $\Delta V = V(R_{\mathrm{min}}) - V_{\mathrm{FD}}$. In Fig. 1, the increase in potential ΔV and dissipated energy E_{diss} are plotted for the $^{100}\mathrm{Mo}+^{92,100}\mathrm{Mo}$, $^{104}\mathrm{Ru}$, $^{110}\mathrm{Pd}$ (left panel) and $^{96}\mathrm{Zr}+^{124,132}\mathrm{Sn}$, $^{136}\mathrm{Xe}$ (right panel) systems. It is clear that the contribution from the increase in potential to the extra-push energy is larger than that from the dissipated energy. From this finding, we conclude that the dynamical increase in potential energy is the main contribution to the extra-push energy.

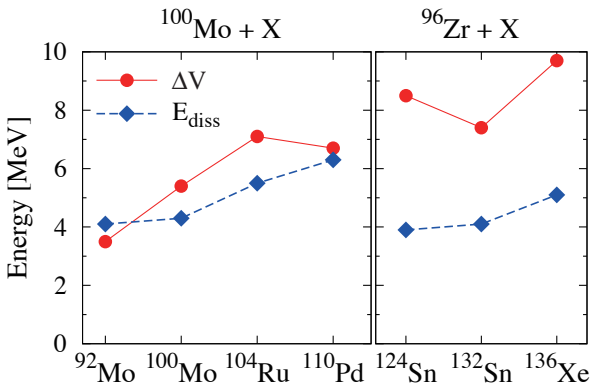

Fig. 1. Increase in potential ΔV (red circle) and accumulated dissipation energy E_{diss} (blue diamond) for the $^{100}\mathrm{Mo}+^{92,100}\mathrm{Mo}$, $^{104}\mathrm{Ru}$, $^{110}\mathrm{Pd}$ and $^{96}\mathrm{Zr}+^{124,132}\mathrm{Sn}$, $^{136}\mathrm{Xe}$ systems.

References
1) C.-C. Sahm et al.: Nucl. Phys. A **441**, 316 (1985).
2) W. J. Swiatecki: Nucl. Phys. A **376**, 275 (1982).
3) Y. Aritomo, K. Hagino, K. Nishio, and S. Chiba: Phys. Rev. C **85**, 044614 (2012).
4) C. Simenel: Eur. Phys. J. A **48**, 152 (2012); L. Guo and T. Nakatsukasa: EPJ Web Conf. **38**, 09003 (2012); V. E. Oberacker, A. S. Umar, and C. Simenel, Phys. Rev. C **90**, 054605 (2014).
5) K. Washiyama and D. Lacroix: Phys. Rev. C **78**, 024610 (2008); K. Washiyama, D. Lacroix and S. Ayik: Phys. Rev. C **79**, 024609 (2009).
6) K. Washiyama: RIKEN Accel. Prog. Rep. **47**, 67 (2013).

*1 RIKEN Nishina Center

Pairing effect in thermal shape fluctuation model on the width of giant dipole resonance†

A.K. Rhine Kumar,*1 P. Arumugam,*1 and N. Dinh Dang*2

The study of nuclear properties at high temperature, spin and isospin has gained much of interest in recent times. Apart from these extremes, there are still some unexplored regimes of hot nuclei. The properties of nuclei at very low temperatures and the phase transitions associated with that belong to such area where conclusive experimental results are scarce. At such low temperatures, the shell (quantal) and pairing effects are quite active though being modified by thermal effects. In hot nuclei, thermal fluctuations are expected to be large since the nucleus is a tiny finite system. Thermal shape fluctuations and fluctuations in the pairing field are the dominating fluctuations and have been so far studied separately within different models. Both of these fluctuations are expected to be present at low temperatures. However, the interplay between them has not been investigated so far. The present work addresses this subject and we study the influence of this interplay on the experimental observables, namely the width of giant dipole resonance (GDR). The thermal shape fluctuation model (TSFM), which is often used by experimentalists, describes the increase of the GDR width with temperature by averaging the GDR cross section over all the quadrupole shapes. However this model is known to largely overestimate the GDR width in open-shell nuclei at low temperatures. The success of a proper pairing approach[1,2] suggests the necessity of including pairing correlations to cure this shortcoming of the TSFM. This is done in the present work.

We employ the thermal shape fluctuation model built on Nilsson-Strutinsky calculations[3] with a macroscopic approach to GDR and examine the inclusion of the fluctuations in the pairing field. The nuclear shapes are related to the GDR observables using a model comprising an anisotropic harmonic oscillator potential with separable dipole-dipole interaction. In this formalism the GDR Hamiltonian can be written as $H = H_{osc} + \eta\ D^\dagger D\ + \chi\ P^\dagger P$, where H_{osc} stands for the anisotropic harmonic oscillator hamiltonian, the parameter η characterizes the isovector component of the neutron and proton average field and χ denotes the strength of the pairing interaction. The pairing interaction changes the oscillator frequencies $[\omega_\nu^{osc}(\nu = x, y, z)]$ resulting in the new set of frequencies $\omega_\nu = \omega_\nu^{osc} - \chi\omega^P$, where $\omega^P = \left(\frac{Z\Delta_P + N\Delta_N}{Z+N}\right)^2$ with χ having the units of MeV^{-1}. Alternatively, the role of pairing is to renormalize the dipole-dipole interaction strength such that, $\eta = \eta_0 - \chi_0\sqrt{T}\omega^P$, with χ_0 having the units of MeV$^{-5/2}$. The effective GDR cross-sections is calculated by averaging all the cross-sections obtained from thermal fluctuations of quadrupole shapes by using the formula for the expectation value of an observable $\mathcal{O}$ as $\langle\mathcal{O}\rangle_{\beta,\gamma,\Delta_P,\Delta_N} = \int \mathcal{O}W(T,\beta,\gamma,\Delta_P,\Delta_N)\mathcal{D}[\alpha] / \int W(T,\beta,\gamma,\Delta_P,\Delta_N)\mathcal{D}[\alpha]$ with $W(T,\beta,\gamma,\Delta_P,\Delta_N) = \exp[-F(T;\beta,\gamma,\Delta_P,\Delta_N)/T]$, $\mathcal{D}[\alpha] = \beta^4|\sin 3\gamma|\, d\beta\, d\gamma\ d\Delta_P\ d\Delta_N$. The total free energy (F_{TOT}) at a fixed deformation is calculated using the expression $F_{TOT} = E_{LDM} + \sum_{p,n}\delta F$. The liquid-drop energy (E_{LDM}) is calculated by summing up the Coulomb and surface energies corresponding to a triaxially deformed shape defined by the deformation parameters β and γ. The shell correction (δF) is obtained with exact temperature dependence using the single-particle energies given by the triaxial Nilsson model.

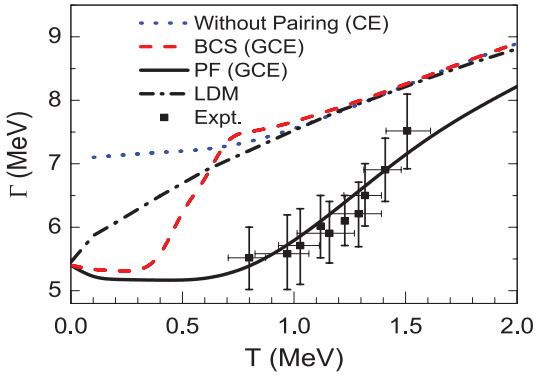

Fig. 1. (Color online) GDR width for ^{97}Tc, calculated within the liquid drop model (LDM), without pairing, including BCS pairing and pairing fluctuations, as a function of temperature in comparison with experimental data[2].

The results of our calculations for ^{97}Tc, ^{120}Sn and ^{208}Pb demonstrate that the TSFM can be quite successful if the shell effects (with explicit temperature dependence) and the pairing ones are properly incorporated in the free energy (See Fig. 1).

† Condensed from the article in Phys. Rev. C. **90**, 044308 (2014)

*1 Department of Physics, Indian Institute of Technology Roorkee, Uttarakhand
*2 RIKEN Nishina Center

References

1) N. Dinh Dang, A. Arima, Phys. Rev C **68**, 044303 (2003); N. Dinh Dang, N. Quang Hung, Phys. Rev C **86**, 044333 (2012).
2) B. Dey, et al, Phys. Lett. B **731**, 92 (2014).
3) P. Arumugam, G. Shanmugam, S. K. Patra, Phys. Rev. C **69**, 054313 (2004).

Shell-model study of Gamow-Teller transition from ^{100}Sn

M. Honma,[*1] T. Otsuka,[*2,*3,*4] T. Mizusaki,[5] Y. Utsuno,[*6] N. Shimizu,[*3] and M. Hjorth-Jensen[*4,*7]

In the previous report[1)], we presented the results of shell-model calculations with an effective interaction determined for the use around ^{100}Sn. We adopted the model space consisting of four orbits $1p_{1/2}$, $0g_{9/2}$, $1d_{5/2}$ and $0g_{7/2}$ assuming a hypothetical "core" $^{76}_{38}$Sr$_{38}$. Starting with a G-matrix interaction,[2)] the Hamiltonian parameters were modified by iterative fits to experimental energy data. The shell-model results reasonably described the systematics of energy levels and electromagnetic transitions for nuclei around ^{100}Sn.

As a next step, we report on the Gamow-Teller (GT) transition from ^{100}Sn using the same shell-model framework. Since ^{100}Sn is a doubly-magic, jj-closed $N = Z$ nucleus, some similarity to ^{56}Ni is expected. In the case of ^{56}Ni, the GT transition is dominated by the $\pi f_{7/2} \rightarrow \nu f_{5/2}$ excitation, and in the extreme single-particle picture the final state is described by a 1p-1h configuration on top of the closed ^{56}Ni core. However, according to the realistic shell-model calculations, the GT strengths are distributed over many states due to the configuration mixing. We have reported[3)] that the "double-peak" structure in the strength distribution becomes significant after including 4p-4h components. Therefore it is interesting to examine whether the similar structure could be seen in the case of ^{100}Sn.

Since the GT transition from ^{100}Sn should be dominated by the $\pi g_{9/2} \rightarrow \nu g_{7/2}$ excitation, we can expect a reasonable description in the present model space. At the price of the lack of some (possibly minor) components such as the $\pi d_{5/2} \rightarrow \nu d_{3/2}$, the present model space allows us to take into account the effects of sufficiently many np-nh configurations. The calculated GT strength distribution is shown in Fig.1. Although we don't see clear "double-peak" structure in this case even at the t=5 truncation level, the splitting of the strength becomes significant as more and more particle-hole configurations are included.

In the recent β-decay experiment of ^{100}Sn[4)], a possible "superallowed" GT transition corresponding to B(GT)=$7.6^{+2.2}_{-2.5}$ was observed. The analysis was made under the assumption that the GT decay goes into the single final 1^+ state of ^{100}In. This assumption was supported by large-scale shell-model calculations in the gds model space, which predict the concentration of a large part (69%) of the GT strengths on the lowest 1^+ state. In the present calculation, the GT decay goes mainly into the lowest three states, and the 1^+_3 state carries the largest strength as shown in Fig.1 (B(GT)=2.8 including the standard quenching factor of 0.74). Further analysis is desired for clarifying the GT strength distribution and the corresponding closed-core structure.

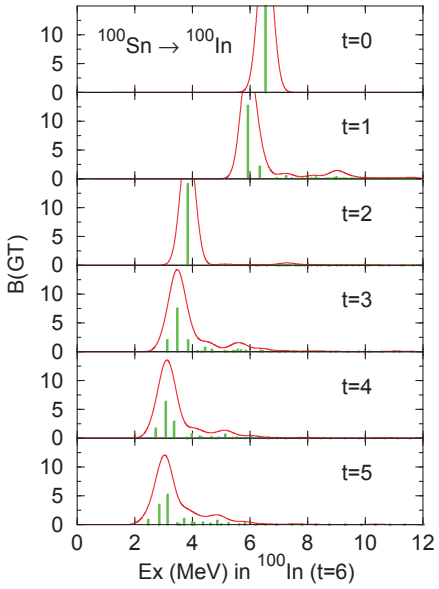

Fig. 1. The GT transition strength from ^{100}Sn calculated by the shell model varying the truncation order t, which stands for the number of nucleons allowed to excite from the lower orbits ($p_{1/2}$, $g_{9/2}$) to the higher orbits ($d_{5/2}$, $g_{7/2}$). The discrete strengths indicated by thick vertical bars are obtained by the prescription in Ref.[5)] through 100 Lanczos iterations, and they are folded by Gaussian of σ=0.5MeV as shown with a smooth curve. No quenching factor is considered for the purpose of comparison. The shell-model results are obtained by using the efficient code MSHELL64[6)].

*1 Center for Mathematics and Physics, University of Aizu
*2 Department of Physics, University of Tokyo
*3 Center for Nuclear Study, University of Tokyo
*4 National Superconducting Cyclotron Laboratory, Michigan State University
*5 Institute of Natural Sciences, Senshu University
*6 Advanced Science Research Center, Japan Atomic Energy Agency
*7 Department of Physics and Center of Mathematics for Applications, University of Oslo

References

1) M. Honma *et al.*: RIKEN Accel. Prog. Rep. **47**, in press.
2) M. Hjorth-Jensen *et al.*: Phys. Rep. **261**, 125 (1995).
3) M. Honma *et al.*: RIKEN Accel. Prog. Rep. **46**, 45 (2012).
4) C. B. Hinke *et al.*: Nature **486**, 341 (2012).
5) R. R. Whitehead: in *Moment Methods in Many Fermion Systems*, edited by B. J. Dalton et al. (Plenum, New York, 1980), p. 235.
6) T. Mizusaki *et al.*: MSHELL64 code (unpublished).

Reentrance phenomenon of superfluid pairing in hot rotating nuclei

N. Quang Hung,[*1] N. Dinh Dang,[*2] B.K. Agrawal,[*3] V.M. Datar,[*4] A. Mitra,[*4] and D.R. Chakrabarty[*4]

When a nucleus rotates (total angular momentum J and/or rotational frequency ω are not zero), the nucleon (proton and neutron) pairs located around the Fermi surface will scatter to the empty levels nearby and lead to the decreasing of pairing correlation. When the J or ω is sufficiently high, i.e., equal to the critical value J_c or ω_c, the scattered nucleons completely block the single-particle levels around the Fermi surface. Consequently, pairing correlation disappears. However, when J is slightly higher than J_c (or $\omega \geq \omega_c$), the increase of temperature T will relax the particles scattered around the Fermi surface and causes some levels become partially unoccupied, making them available for scattered pairs. As a result, the pairing correlation reappears at some critical value T_1. As T goes higher, e.g., at $T_2 > T_1$, the newly created pairs will be eventually broken down again. This phenomenon is called the pairing reentrance. The recently developed FTBCS1 theory that includes the effect due to quasiparticle-number fluctuations in the pairing field and angular momentum z projection at $T \neq 0$ has predicted the pairing reentrance effect in some realistic nuclei[1]. The shell-model Monte Carlo calculations have suggested that the pairing reentrance effect can be observed in the nuclear level density in a form of a local maximum at low T (or excitation energy E^*) and high J (or ω). Recently, an enhancement of level density of ^{104}Pd at low E^* and high J has been experimentally reported[2]. In this work we try to see whether the enhancement observed in the extracted level density of ^{104}Pd is an experimental evidence of pairing reentrance phenomenon in atomic nuclei.

The FTBCS1 equations at finite temperature and angular momentum are derived based on the variational method to minimize the expectation value of the pairing Hamiltonian $H = \sum_k \epsilon_k (a^\dagger_{+k} a_{+k} + a^\dagger_{-k} a_{-k}) - G \sum_{kk'} a^\dagger_k a^\dagger_{-k} a_{-k'} a_{k'} - \lambda \hat{N} - \omega \hat{M}$, in the grand-canonical ensemble. This Hamiltonian describes a system rotating about the symmetry axis, which is chosen to coincide with its z component. The particle-number operator $\hat{N}$ and the z projection $\hat{M}$ of the total angular momentum $\hat{J}$ (which coincides with $\hat{M}$ for spherical nuclei) are defined as $\hat{N} = \sum_k (a^\dagger_{+k} a_{+k} + a^\dagger_{-k} a_{-k})$, $\hat{M} = \sum_k m_k (a^\dagger_{+k} a_{+k} - a^\dagger_{-k} a_{-k})$, where $a^\dagger_{\pm k}(a_{\pm k})$ are the creation (annihilation) operators of a particle in the k-th deformed state, whereas ϵ_k, λ, and ω are respectively the single-particle energies, chemical potential, and rotational frequency. The FTBCS1 equation for the pairing gap has the final form as $\Delta_k = \Delta + \delta\Delta_k$, where $\Delta = G \sum_{k'} u_{k'} v_{k'} (1 - n^+_{k'} - n^-_{k'})$, $\delta\Delta_k = G\delta\mathcal{N}^2_k u_k v_k / (1 - n^+_k - n^-_k)$, with u_k, v_k, and n_k being the Bogolyubov' u, v coefficients and quasiparticle occupation numbers, respectively. The total level density $\rho(\mathcal{E}, J)$ is calculated as $\rho(\mathcal{E}, J) = \rho(\mathcal{E}, M = J) - \rho(\mathcal{E}, M = J + 1)$, where $\rho(\mathcal{E}, M)$ is obtained by using the inverse Laplace transformation of the grand partition function.

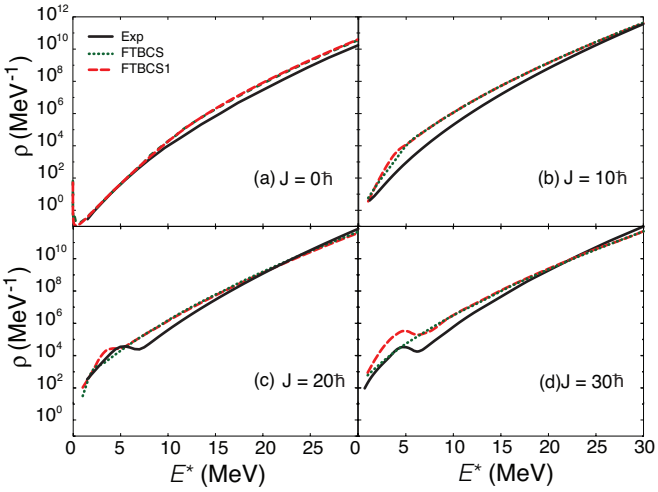

Fig. 1. (Color online) Total level densities for ^{104}Pd as function of E^* obtained within at the quadrupole deformation parameter $\beta_2 = 0.276$ at several J. The dotted and dashed lines stand for the FTBCS and FTBCS1 results, respectively. The solid lines are the experimentally extracted level densities

Because of quasiparticle number fluctuations, the FTBCS1 gaps decrease monotonically with increasing excitation energy E^* and do not collapse at $E^* = E^*_c$ as in the case of the FTBCS. Within the FTBCS1, the pairing reentrance is seen very clearly at $J = 20\hbar$ for neutrons and at $J = 30\hbar$ for protons. Consequently, there appear local enhancements in the FTBCS1 level densities at around $2 < E^* < 5$ MeV at these two values of J(Fig. 1). The FTBCS1 level densities agree fairly well with the experimental data at all J values considered in present work.

*1 School of engineering, Tan Tao University, Long An
*2 RIKEN Nishina Center
*3 Theory Division, Saha Institute of Nuclear Physics, Kolkata
*4 Nuclear Physics Division, Bhabha Atomic Research Center, Mumbai

References

1) N.D. Dang and N.Q. Hung, Phys. Rev. C **77**), 064315 (2008); N.Q. Hung and N.D. Dang, Phys. Rev. C **78**, 064315 (2008), Phys. Rev. C **84**, 054324 (2011).
2) A. Mitra *et al.*, J. Phys. G **36**, 095103 (2009); A. Mitra *et al.*, EPJ Web of Converences **2**, 04004 (2010); V. Datar, A. Mitra, and D.R. Chakrabarty, unpublished.

Giant dipole resonance in highly excited nuclei†

N. Dinh Dang*1

The present work summarizes the achievements of the Phonon Damping Model (PDM)[1] in the description of the the GDR width and shape at finite temperature T and angular momentum J. The GDR parameters predicted by the PDM and experimentally extracted are also used to calculate the shear viscosity of finite hot nuclei.

The PDM's Hamiltonian consists of the independent single-particle (quasiparticle) field, GDR phonon field, and the coupling between them. The Woods-Saxon potentials at $T = 0$ are used to obtain the single-particle energies ϵ_k. The GDR width $\Gamma(T)$ is a sum: $\Gamma(T) = \Gamma_{\rm Q} + \Gamma_{\rm T}$ of the quantal width, $\Gamma_{\rm Q}$, and thermal width, $\Gamma_{\rm T}$. In the presence of superfluid pairing, the quantal and thermal widths are $\Gamma_{\rm Q} = 2\gamma_Q(E_{GDR}) = 2\pi F_1^2 \sum_{ph}[u_{ph}^{(+)}]^2(1 - n_p - n_h)\delta[E_{\rm GDR} - E_p - E_h]$, and $\Gamma_{\rm T} = 2\gamma_T(E_{GDR}) = 2\pi F_2^2 \sum_{s>s'}[v_{ss'}^{(-)}]^2(n_{s'} - n_s)\delta[E_{\rm GDR} - E_s + E_{s'}]$, where $u_{ph}^{(+)} = u_p v_h + u_h v_p$, $v_{ss'}^{(-)} = u_s u_{s'} - v_s v_{s'}$ $(ss' = pp', hh')$ with the coefficients of Bogolyubov's transformation u_k and v_k, quasiparticle energies $E_k \equiv \sqrt{(\epsilon_k - \lambda)^2 + \Delta^2}$, superfluid pairing gap Δ, and quasiparticle occupations numbers $n_k = [\exp(E_k/T) + 1]^{-1}$. F_1 is chosen so that Γ_Q at $T = 0$ is equal to GDR's width at $T = 0$; F_2 is chosen so that, with varying T, the GDR energy E_{GDR} does not change significantly. E_{GDR} is the solution of $E_{GDR} - \omega_q - P_q(E_{GDR}) = 0$, where ω_q is the energy of the GDR phonon before the coupling between the phonon and single-particle mean fields is switched on, and $P_q(\omega)$ is the polarization operator owing to this coupling. In numerical calculations the representation $\delta(x) = \lim_{\varepsilon\to 0} \varepsilon/[\pi(x^2 + \varepsilon^2)]$ is used for the δ-function with $\epsilon = 0.5$ MeV.

In the verification of the condition for applying hydrodynamics to nuclear system, the quantum mechanical uncertainty principle requires a finite viscosity for any thermal fluid. It has been conjectured that the ratio η/s of shear viscosity η to the entropy volume density s is bounded at the lower end for all fluids, namely the value $\eta/s = \hbar/(4\pi k_B)$ is the universal lower bound (KSS bound or unit). From the viewpoint of collective theories, one of the fundamental explanations for the giant resonance damping is the friction term (or viscosity) of the neutron and proton fluids. The exact expression for the shear viscosity $\eta(T)$ in terms of the GDR's parameters at zero and finite T was obtained as $\eta(T) = \eta(0)[\Gamma(T)/\Gamma(0)]\{E_{GDR}(0)^2 + [\Gamma(0)/2]^2\}/\{E_{GDR}(T)^2 + [\Gamma(T)/2]^2\}$. The predictions

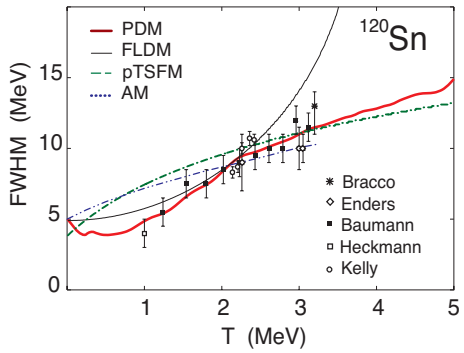

Fig. 1. GDR width for ^{120}Sn predicted by the PDM, phenomenological thermal shape fluctuations (pTSFM), adiabatic (AM), and Fermi liquid drop (FLDM) models as functions of T in comparison with experimental data in tin regions.

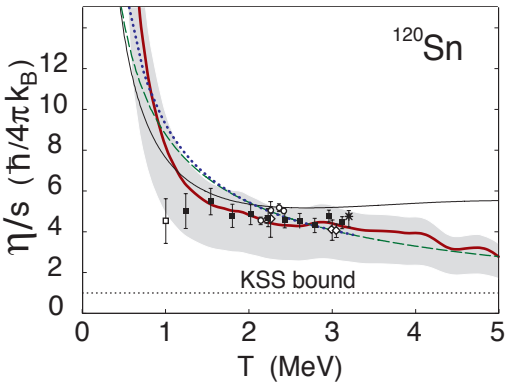

Fig. 2. The ratio η/s as a function of T for nuclei in the tin region. The gray areas are the PDM predictions by using $0.6u \le \eta(0) \le 1.2u$ with $u = 10^{-23}$ Mev s fm^{-3}.

for the GDR width and the ratio η/s by the PDM, pTSFM, AM, and FLDM for ^{120}Sn are plotted as functions of T in Figs. 1 and 2 in comparison with the empirical results. The latter are extracted from the experimental systematics for GDR in tin region making use this exact expression. It is seen that the predictions by the PDM have the best overall agreement with the empirical results. Based on these results and on a model-independent estimation, it is concluded that η/s for medium and heavy nuclei at $T = 5$ MeV is in between (1.3 - 4.0) KSS units.

References

1) N. Dinh Dang and A. Arima, Phys. Rev. Lett. **80**, 4145 (1998); Nucl. Phys. A **636**, 427 (1998); Phys. Rev. C **68**, 044303 (2003).

† Condensed from the article in EPS Web of Conferences **66**, 02024 (2014)

*1 RIKEN Nishina Center

Theoretical analysis of ^{132}Xe by generator coordinate method

N. Yoshinaga,[*1,*3] K. Higashiyama,[*2] and E. Teruya [*1]

Xe, Ba, and Ce nuclei in the mass $A \sim 130$ region exhibit γ-instability in low-lying states, which is characterized by energy staggering of the even-odd spin states in the quasi-γ band and by some forbidden transition rates between the yrast and quasi-γ bands. The energy levels and decay properties of the low-lying states were discussed in the framework of the interacting boson model[1], where quadrupole collective excitations are described in terms of the angular momenta zero (s) and two (d) bosons.

Another characteristic feature of even-even nuclei is the irregular level sequence in the yrast band, i.e., the backbending phenomenon, which is interpreted as band crossing between the ground-state band and the s band originating from the alignment of two neutrons in $0h_{11/2}$ orbitals. Sudden decreases in the level spacing and the $E2$ transition rates are observed around the states of spin 10. Recently, full-fledged shell-model calculations have been performed for the even-even, odd-mass and doubly-odd nuclei in this mass region[2]. The shell-model calculations well reproduce the experimental energy levels and electromagnetic transition rates.

In the present study, we apply the quantum-number-projected generator coordinate method (GCM) to ^{132}Xe under the same interaction used in the previous shell model studies[2]. All the five orbitals, $0g_{7/2}$, $1d_{5/2}$, $1d_{3/2}$, $0h_{11/2}$ and $2s_{1/2}$, in the major shell of $50 \le N(Z) \le 82$ are considered, and valence neutrons (protons) are treated as holes (particles).

In the present scheme, spins of the neutron and proton systems (I_ν and I_π) are projected separately, and the total spin is constructed by angular momentum coupling. To generate functions for the GCM in a neutron or proton system ($\tau = \nu$ or π), we employ the Nilsson BCS intrinsic states $\left|\Phi_\tau(\beta,\gamma)\right\rangle$, where β and γ indicate axial and triaxial quadrupole deformations, respectively. The ρth GCM wave function with angular momentum I_τ in neutron or proton space is given by

$$\left|\Psi^{(\tau)}_{I_\tau M_\tau \rho}\right\rangle = \sum_i \sum_{K_\tau=-I_\tau}^{I_\tau} \mathcal{F}^{I_\tau i}_{K_\tau \rho} \hat{P}^{I_\tau}_{M_\tau K_\tau} \hat{P}_{N_\tau} \left|\Phi_\tau(\beta_i,\gamma_i)\right\rangle, \qquad (1)$$

where $\hat{P}^{I_\tau}_{M_\tau K_\tau}$ is the spin projection operator, $\hat{P}_{N_\tau}$ is the particle-number projection operator, $\mathcal{F}^{I_\tau i}_{K_\tau \rho}$ is the weight function to be determined by solving the Hill-Wheeler equation, and i stands for a representative point with deformation (β,γ). Then, the wave function

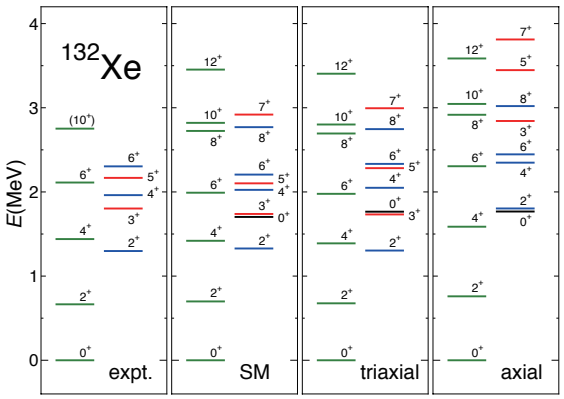

Fig. 1. Comparison of the experimental energy levels (expt.) with the shell-model (SM) results, those in the triaxial GCM (triaxial), and those in the axial GCM (axial).

for an even-even nucleus can be written as

$$\left|\Psi_{IM}(I_\nu \rho I_\pi \sigma)\right\rangle = \left[\left|\Psi^{(\nu)}_{I_\nu \rho}\right\rangle \otimes \left|\Psi^{(\pi)}_{I_\pi \sigma}\right\rangle\right]^{(I)}_M, \qquad (2)$$

where I is the total spin and M is its projection. GCM calculations are carried out for two cases: (i) triaxial deformations (9 points) with $\beta = 0.10$, 0.20, 0.30, $\gamma = 10°$, 30°, 50°; (ii) only axial deformations (49 points) with $\beta = 0.00$, 0.02, 0.04, $\cdots$, 0.48 and $\gamma = 0°$, 60°. In Fig. 1, experimental energy levels are compared with the shell-model results, and those in the GCM. In both cases of triaxial and axial deformations, the GCM well reproduces the experimental energy levels of the even-spin yrast band and those obtained by the shell model. In the case of other excited states, the GCM calculations performed by assuming triaxial deformation are in good agreement with the shell model results, especially for the 2^+_2, 3^+_1, 4^+_2, and 5^+_1 states, which are members of the γ-band. However, energy levels calculated by assuming only axial deformation for the 3^+_1, 5^+_1, and 7^+_1 states are much higher than those calculated using the shell model. Apparently, the description of the 2^+_2, 3^+_1, 4^+_2, and 5^+_1 states is not satisfactory when assuming only the axially symmetric shape. The triaxial components play an essential role in the description of these states.

*1 Department of Physics, Saitama University
*2 Department of Physics, Chiba Institute of Technology
*3 RIKEN Nishina Center

References

1) F. Iachello and A. Arima: *The Interacting Boson Model*, (Cambridge University Press, Cambridge, England, 1987).
2) E. Teruya, N. Yoshinaga, K. Higashiyama, and A. Odahara, to be published.

Tops-on-top model applied to TSD bands in ^{164}Lu†

K. Sugawara-Tanabe,[*1,*2] K. Tanabe,[*1,*3] and N. Yoshinaga[*3]

The top-on-top model with moments of inertia (MoI) dependent on angular-momentum (I) works quite well in describing triaxial strongly deformed (TSD) bands in odd-mass nuclei.[1–3] In this paper, the top-on-top model is extended to the tops-on-top model for an odd-odd nucleus ^{164}Lu, in which one proton and one neutron in each single-j orbital are coupled to the triaxial rotor.

Both positive- and negative- parity TSD bands in ^{164}Lu are well reproduced by taking account of attenuation factors in the Coriolis interaction, which includes the effect of the partially filled single-j shell. In order to observe the effect of the attenuation factor, we compared numerical results with and without the attenuation factor and confirmed its importance for the excitation energies relative to the reference, i.e., $E^* - aI(I+1)$ with $a = 0.0075$ MeV.[4,5]

For a pure-rotor case without single-particle potentials, an explicit algebraic formula for the TSD band levels is obtained. The level is classified by three quantum numbers $(n_\alpha, n_\beta, n_\gamma)$, where n_α is related to the rotor wobbling quantum number, and n_β and n_γ to the precession quantum numbers for a proton and a neutron. Under the condition of D_2-invariance,[6] three quantum numbers take limited integers depending on the value of $I - j_1 - j_2$ and $n_\alpha - n_\beta - n_\gamma$. As an example, we assume $j_1 = j_2 = 13/2$, and compare the energy eigenvalues from this boson model with the result obtained from the exact diagonalization of the rotor Hamiltonian in Fig. 1 for odd number I where $I - j_1 - j_2$ is even. In this case n_β and n_γ appear as the combination $n_\mathrm{p} = n_\beta + n_\gamma$. The yrast has quantum numbers $(0,0)$ and the yrare $(0,2)_3$. On the other hand, for even number I where $I - j_1 - j_2$ is odd, the yrast has quantum numbers $(1,0)$ and the yrare $(2,1)_2$. The boson model reproduces the exact results in good accuracy.

It is easy to derive the stability condition for a pure-rotor case. We found that there is no wobbling around the axis with the intermediate MoI. The wobbling motion exists only around the axis with the maximum or minimum MoI, which agrees with the result in classical mechanics.[7] Consequently, we can state that there is no stable rotation around the axis with the intermediate MoI, and that stable rotational motion exists only around the axis with the maximum or minimum MoI.

The difference in quantum numbers between the yrast and yrare TSD bands in ^{164}Lu, in which single-particle potentials are included, is confirmed by direct estimation of spin alignments. It is confirmed that the yrast TSD band with even $I-j_1-j_2$ has quantum numbers $(n_\alpha, n_\beta, n_\gamma)$=(0,0,0), while the yrare TSD band with odd $I - j_1 - j_2$ has (1,0,0).

The electromagnetic transition rates of $B(M1)$ are reduced by a factor of 1/20 because the signs of g-factors of a proton and a neutron are different in comparison with the odd-A case, while the electromagnetic transition rates of $B(E2)$ are in the same order but reduced by a factor of 1/2. These reductions of electromagnetic transition rates will make the observation of TSD bands in even-even nuclei difficult.

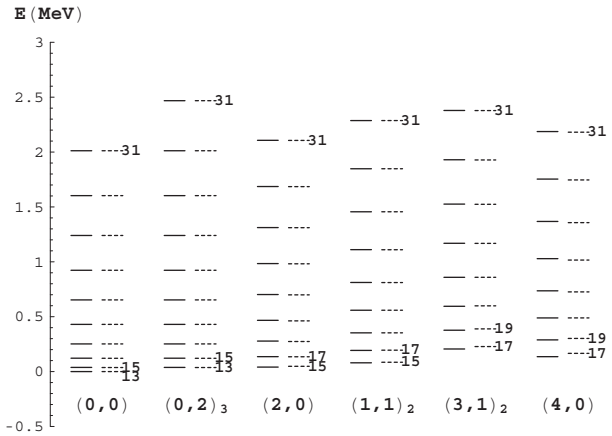

Fig. 1. Comparison of the energy levels of odd spin I ($13 \le I \le 31$) between the boson model (solid lines) and the exact result (dashed lines). Quantum numbers and degeneracy of levels $(n_\mathrm{p}+1)$ are given by $(n_\alpha, n_\mathrm{p})_{n_\mathrm{p}+1}$ below each rotational band. Angular momentum values are assigned to the lowest two levels and the highest level in the right-hand side of each band.

References
1) K. Tanabe and K. Sugawara-Tanabe: Phys. Rev. C **73**, 034305 (2006).
2) K. Tanabe and K. Sugawara-Tanabe: Phys. Rev. C **77**, 064318 (2008).
3) K. Sugawara-Tanabe and K. Tanabe: Phys. Rev. C **82**, 051303(R) (2010).
4) S. Törmänen et al.: Phys. Lett. B **454**, 8 (1999).
5) P. Bringel et al.: Phys. Rev. C **75**, 044306 (2007).
6) A. Bohr: Mat. Fys. Medd. Dan. Vidensk. Selsk. **26**, no. 14 (1952).
7) L. D. Landau and E. M. Lifshitz: *Mechanics* (Butterworth-Heinemann, Oxford, 1976), 3rd ed., Sect. 37.

† Condensed from the article in Prog. Theor. Exp. Phys., Vol.2014, 063D01 (2014)

*1 RIKEN Nishina Center
*2 Otsuma Women's University
*3 Department of Physics, Saitama University

Recent progress and open issues on pseudospin and spin symmetries†

H. Z. Liang,[*1] J. Meng,[*1,*2] and S.-G. Zhou[*3]

Pseudospin symmetry (PSS)[1,2] was introduced to explain the near degeneracy between pairs of nuclear single-particle states with the quantum numbers $(n-1, l+2, j=l+3/2)$ and $(n, l, j=l+1/2)$. They are regarded as pseudospin doublets by defining the quantum numbers $(\tilde{n}=n-1, \tilde{l}=l+1, j=\tilde{l}\pm 1/2)$, as illustrated in Fig. 1.

This observation raised a fascinating question whether such near degeneracy is accidental (a degeneracy not explained by an obvious symmetry) or due to symmetry breaking (more descriptively hidden symmetry). Since PSS was recognized as a relativistic symmetry in the 1990s,[3] many special features, including the spin symmetry (SS) for anti-nucleons,[4] and many new concepts have been introduced in relevant studies, which led to several exciting discoveries during the past decade.

In this review article,† we intended to systematically provide a comprehensive overview on the recent progress. The PSS and SS in various systems and potentials were discussed based on the following aspects:

- From stable nuclei to exotic nuclei
- From non-confining to confining potentials
- From local to non-local potentials
- From central to tensor potentials
- From bound states to resonant states
- From nucleon spectra to anti-nucleon spectra
- From nucleon spectra to hyperon spectra
- From spherical nuclei to deformed nuclei

Then, three of the open issues in this field were selected and discussed in detail, i.e., the perturbative nature of PSS, the puzzle of intruder states, and the supersymmetric (SUSY) representation of PSS.

For the perturbative nature of PSS, we emphasized that the symmetry breaking behaves perturbatively depending on whether an appropriate symmetry limit is chosen and an appropriate symmetry-breaking term is identified. As long as an appropriate symmetry limit is chosen, the nature of PSS is indeed perturbative.[5]

For the puzzle of intruder states, we showed several different features about this puzzle, i.e., the bound states in the non-confining or confining potentials, the bound and resonant states identified by the zeros of Jost function,[6] a continuous transformation between SS and PSS, and the SUSY transformation of the PSS scheme. By doing so a number of "contradicting" results in the literature for the spin (pseudospin) partners have been clarified explicitly.

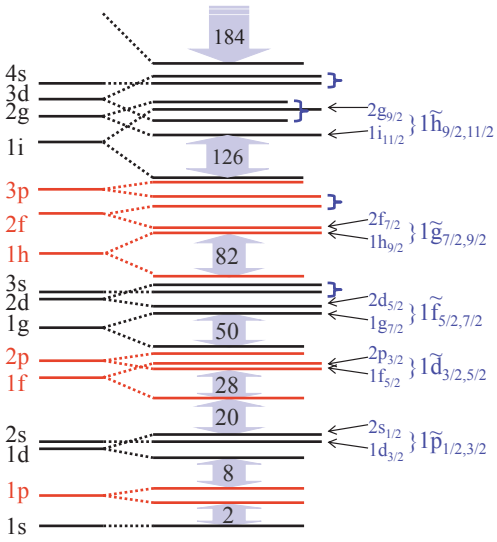

Fig. 1. Schematic nuclear single-particle spectrum. Pairs of single-particle states in braces are defined as the pseudospin doublets.

For the SUSY representation of PSS, we pointed out one of the promising ways for understanding the PSS and its symmetry breaking, by combining the similarity renormalization group, the SUSY quantum mechanics, and the perturbation theory.[7] Meanwhile, application of the SUSY technique directly to the Dirac equations, which have non-trivial scalar and vector potentials, remains an interesting and open proposition.

Another important issue is the experimental signals of these symmetries. So far, several nuclear structure phenomena have been interpreted directly or implicitly by the PSS, including nuclear superdeformed configurations, identical bands, quantized alignment, and pseudospin partner bands. The relevance of PSS in the structure of halo nuclei and superheavy nuclei was also pointed out. More experimental evidences for PSS are highly desired for future studies.

† Condensed from the article in Phys. Rep. **570**, 1 (2015)
*1 RIKEN Nishina Center
*2 School of Physics, Peking University
*3 Institute of Theoretical Physics, Chinese Academy of Sciences

References

1) A. Arima, M. Harvey, and K. Shimizu: Phys. Lett. B **30**, 517 (1969).
2) K. Hecht and A. Adler: Nucl. Phys. A **137**, 129 (1969).
3) J. N. Ginocchio: Phys. Rev. Lett. **78**, 436 (1997).
4) S.-G. Zhou, J. Meng, and P. Ring: Phys. Rev. Lett. **91**, 262501 (2003).
5) H. Z. Liang et al.: Phys. Rev. C **83**, 041301(R) (2011).
6) B.-N. Lu, E.-G. Zhou, and S.-G. Zhou: Phys. Rev. Lett. **109**, 072501 (2012); Phys. Rev. C **88**, 024323 (2013).
7) H. Z. Liang et al.: Phys. Rev. C **87**, 014334 (2013).

Nuclear moment of inertia in super-normal phase transition region†

K. Tanabe*1,*2 and K. Sugawara-Tanabe*1,*3

The purpose of this paper is to derive the analytic expression for the angular momentum (I) dependence of the moment of inertia (MoI) from the microscopic many-body theory both for even-even and odd-mass nuclei. The I-dependence of MoI has been proved to be essential in simulating triaxial, strongly deformed (TSD) bands in a series of papers.[1–4)]

We adapt the approximation developed for the gap (Δ) dependence of the ratio of MoI (J) to the rigid-body value (J^{rig}).[5,6)] It assumes that only large matrix elements of single-particle angular momentum of $(j_x)_{\alpha\beta}$ contribute to J with a common excitation energy of $\delta(=\varepsilon_\beta - \varepsilon_\alpha)$, where ε_α denotes the single-particle energy of the level α. We apply this approximation to the gap equation including the Coriolis antipairing (CAP) effect[7)] through the second-order perturbation to the cranking term.[8,9)]

When Δ is larger than half of the single-particle level distance d, we can apply a definite integral for the gap equation with the CAP effect. When Δ is smaller than half of d, we propose the finite sum method with the picket-fence approximation for the level distribution. In this case, it is proved that Δ never tends to zero, and there is no sharp phase transition from the superconducting state to the normal state. Neglecting the higher order in $2\Delta/\delta$ for the case $\Delta < d/2$ (finite sum method), we express MoI as an analytic function of I.

In Fig. 1, we compare the approximate solution between even-even and odd-mass nuclei as functions of I measured from the band-head angular momentum I_0. Usually, $I_0 = 0$ for even-even nucleus, while $I_0 \neq 0$ for odd-mass nucleus, for example, $I_0 = 13/2$ for the TSD yrast band in ^{163}Lu.[10)] We choose the single-particle energy for a valence nucleon as $\varepsilon_\ell = 0.6$ MeV above the Fermi surface, and the initial pairing gap at $I=I_0$ for odd mass as 0.6 MeV, smaller than 0.8 MeV for even-even nucleus (blocking effect). The blocking effect reduces the starting value of Δ and increases that of the MoI. In odd-mass case, there is a term that correlates the single-particle state of ℓ with α through $(j_x)^2_{\alpha\ell}$. The matrix element of $(j_x)^2_{\alpha\ell}$ is chosen to be 12 for $\varepsilon_\alpha > \varepsilon_\ell$ and 10 for $\varepsilon_\alpha < \varepsilon_\ell$. The other parameters are the same as those for the even-even case. We have started both approximate solutions with $\Delta = 0.15$ MeV corresponding to $I-I_0 \sim 15$, while $d = 0.4$ MeV.

As is seen in Fig. 1, the main difference between even-even (dashed line) and odd-mass (solid line) nuclei is from the blocking effect. Then, both curves increase gradually, and approach the value 1. The MoI of odd-mass case is chosen to be slightly larger than that of the even-even case. The curves become convex upward before they reach to rigid-body values. This upward convexity is also necessary for explaining the energy sequence of TSD bands.[4)] For the case of $\Delta \geq d/2$ (definite integral), J goes to J^{rig} around $I-I_0 \sim 17$ or 18 (sharp phase transition). Even in this case, odd-mass nuclei show an upward convexity before the phase transition at $I=17 \sim 18$. Because of larger I_0, the slow phase transition occurs at larger I for odd-mass nuclei than for even-even nuclei.

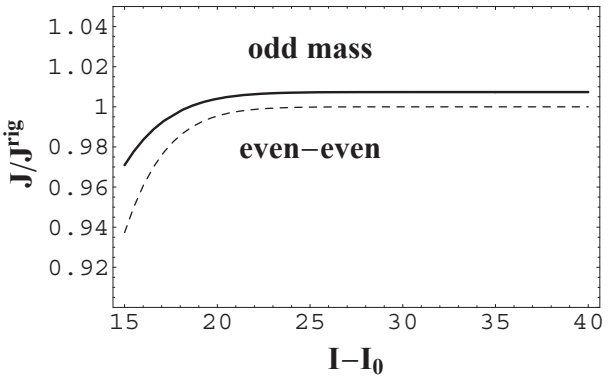

Fig. 1. Comparison of the ratio J/J^{rig} in the approximate sum method as functions of $I-I_0$ for even-even (dashed line) and odd-mass (solid line) nuclei.

References
1) K. Tanabe and K. Sugawara-Tanabe: Phys. Rev. C **73**, 034305 (2006).
2) K. Tanabe and K. Sugawara-Tanabe: Phys. Rev. C **77**, 064318 (2008).
3) K. Sugawara-Tanabe and K. Tanabe: Phys. Rev. C **82**, 051303(R) (2010).
4) K. Sugawara-Tanabe, K. Tanabe and N. Yoshinaga: Prog. Theor. Exp. Phys. **2014**, 063D01 (2014).
5) A. Bohr and B. R. Mottelson: *Nuclear Structure* (Benjamin, Reading, MA, 1975), Vol. II.
6) D. Bengtsson and J. Helgessen: Lecture notes in a summer school at Oak Ridge (1991).
7) B. R. Mottelson and J. G. Valatin: Phys. Rev. Lett. **5**, 511 (1960).
8) M. Sano and M. Wakai: Nucl. Phys. **67**, 481 (1965).
9) K. Sugawara: Prog. Theor. Phys. **35**, 44 (1966).
10) S. W. Ødegård *et al.*: Phys. Rev. Lett. **86**, 5866 (2001).

† Condensed from the article in Phys. Rev. C, Vol. 91, 034328 (2015)

*1 RIKEN Nishina Center
*2 Department of Physics, Saitama University
*3 Otsuma Women's University

Joint project for large-scale nuclear structure calculations in 2014

N. Shimizu,[*1] T. Otsuka, [*1,*2] T. Togashi,[*1] N. Tsunoda,[*2] and Y. Utsuno[*1,*3]

A joint project for large-scale nuclear structure calculations has been promoted since the year 2002 based on a collaboration agreement between the RIKEN Accelerator Research Facility (currently RIKEN Nishina Center) and the Center for Nuclear Study, the University of Tokyo. Currently, we maintain 16 PC servers with Intel CPUs for large-scale nuclear shell-model calculations. One of the servers has 40 CPU cores and 1TB main memory. Based on this project, we performed shell-model calculations of the various nuclides which had been measured at the RIKEN RI Beam Factory, such as ^{31}Ne, ^{33}Mg, and ^{50}Ar under collaborations with many experimentalists.[1] Since the results of these collaborations are presented in other reports, here we introduce four theoretical achievements of this project in 2014: development of a shell-model code, shell-model analyses of the isomeric states of ^{43,44}S and high-spin states of neutron-rich Cr, Fe isotopes, and an application of the extended Kuo-Krenciglowa (EKK) method in understanding the island of inversion.

We developed a new code, named "KSHELL" for large-scale shell-model calculations on state-of-the-art supercomputers[2]. In nuclear shell-model calculations, we solve an eigenvalue problem of the Hamiltonian matrix, whose dimension tends to be huge, by including many-body correlations fully inside the model space. The newly developed code enables us to solve this eigenvalue problem by using many CPU cores efficiently.

We have investigated the structure of exotic nuclei in the $N \sim 28$ region, which attracts much attention in experimental studies using RIBF. In our most recent work[3], we focus on the nature of exotic isomeric states in neutron-rich S isotopes, in particular strongly hindered $E2$ decay from 4_1^+ and 2_1^+ in ^{44}S[4]. This study is based on shell-model calculations using the SDPF-MU interaction[5] which was developed in this joint project. In order to extract intrinsic states from the shell model, we carry out the variation after angular-momentum projection (AM-VAP). The AM-VAP calculation shows that the 4_1^+ level is dominated by a $K = 4$ intrinsic state and that this is the origin of the strong $E2$ hindrance. The 4_1^+ level in ^{44}S is the lightest high-K isomer among the ones ever identified in the $A \sim 100$, $A \sim 130$, $A \sim 180$, and $A \sim 250$ regions.

We have performed large-scale shell model calculations for natural- and unnatural-parity states in Cr and Fe isotopes with $N \leq 35$[6]. Unnatural positive-parity states in odd-mass Cr and Fe nuclei with $N \leq 35$ were observed experimentally from low-lying energy levels to high-spin ones. These states are dominated by one-particle one-hole excitation across the $N = 40$ shell gap. The model space of our calculation is composed of fp-shell + $0g_{9/2}$ + $1d_{5/2}$ orbits with the truncation allowing $1\hbar\omega$ excitation of a neutron. It effectively describes and predicts the energy levels up to the high-spin states. The effective single-particle energies of $\nu 0g_{9/2}$ in Cr and Fe isotopes are rather constant in the region with $N \leq 35$. This indicates that the sharp drop of the $9/2_1^+$ levels in this mass region, which is discussed as an indication of the evolution of $\nu 0g_{9/2}$, is explained by the Fermi surface approaching the $\nu 0g_{9/2}$ orbit with the increase of neutron number.

Investigation of the neutron-rich nuclei starting from the fundamental nuclear force has been accomplished by the newly constructed EKK method[7]. To construct the effective interaction for the shell model starting from the nuclear force, we usually utilize the many-body perturbation theory, but the standard perturbation theory ends up with a series of divergences when applied to a large shell-model space, for example, the model space spanned by two major shells. The EKK method avoids a divergence with a re-summation of the perturbative series and makes it possible to construct the effective interaction for more than one major shell. We constructed the effective interaction for the $sdpf$-shell, starting from the N3LO interaction with the EKK method. The contribution from the three-body force is also added as effective two-body interactions. We found that this interaction consistently describes the ground state energies and low-lying levels of even-even nuclei (O, Ne, Mg, Si isotopes). In particular, the disappearance of the $N = 20$ gap of Ne, Mg isotopes and the restoration of the $N = 20$ gap of Si and S isotopes are well described.

*1 Center for Nuclear Study, University of Tokyo
*2 Department of Physics, University of Tokyo
*3 Japan Atomic Energy Agency

References

1) T. Nakamura et al.: Phys. Rev. Lett. **112**, 142501 (2014).
2) N. Shimizu, arXiv:1310.5431 [nucl-th].
3) Y. Utsuno, N. Shimizu, T. Otsuka, T. Yoshida, and Y. Tsunoda: Phys. Rev. Lett. **114**, 032501 (2015).
4) D. Gonzalez et al.: Phys. Rev. C **83**, 061305(R) (2011).
5) Y. Utsuno, T. Otsuka, B. A. Brown, M. Honma, T. Mizusaki, and N. Shimizu: Phys. Rev. C **86**, 051301(R) (2012).
6) T. Togashi, N. Shimizu, Y. Utsuno, T. Otsuka, and M. Honma: Phys. Rev. C **91**, 024320 (2015).
7) N. Tsunoda, K. Takayanagi, M. H.-Jensen, and T. Otsuka: Phys. Rev. C **89**, 024313 (2014).

3. Nuclear Data

Development of a new EXFOR editor system

A. Sarsembayeva,[*1,*2] S. Imai,[*1,*2] S. Ebata,[*1,*2] M. Chiba,[*3] K. Katō,[*1] N. Otuka,[*4,*5] and M. Aikawa[*1]

The International Network of the Nuclear Reaction Data Centers (NRDC)[1] is a worldwide network of nuclear data centers organized under the auspices of the International Atomic Energy Agency (IAEA). NRDC was established to collect experimental data from all over the world, initially addressing the data needs of the fission reactor industry.

The present aim of the NRDC is to encompass all types of nuclear reaction data, including neutron- and charged particle-induced data, as well as photonuclear data. Such data are required for many nuclear applications such as accelerator-driven systems, fusion reactors, nuclear medicine, materials analysis, environmental monitoring, and basic research[2]. Since the early 80s, the Nuclear Reaction Data Centre of Hokkaido University (JCPRG, formerly Japan Charged-Particle Nuclear Reaction Data Group)[3] an active member of the NRDC.

Under the NRDC, experimental nuclear reaction data are compiled in a unified format EXFOR (EXchange FORmat) and stored in the library[4]. EXFOR is the main source of experimental nuclear reaction data and covers results published as early as in the 1930s[2].

In order to make EXFOR compilation easy, various editor systems have been developed within the NRDC community. ANDEX[5] developed by IAEA-NDS (Vienna) and ERES by CNDC (Beijing)[6] are such systems developed in the 1990s. An EXFOR editor developed by CNPD (Sarov) in 2000s is currently used by many EXFOR compilers. In JCPRG, a web-based nuclear data input system HENDEL (Hyper Editor for Nuclear Data Exchange Libraries) was developed for the compilation of experimental nuclear reaction data in EXFOR and NRDF formats[7]. The latter is the original database in JCPRG and is being used as a standard compilation editor system at JCPRG since 2001[8]. For the beginners of EXFOR compilation, the HENDEL system is very useful because it requires only an elementary knowledge of EXFOR. It is now also used by young EXFOR compilers in Kazakhstan and Mongolia. While the current HENDEL system is well designed to create outputs in both NRDF and EXFOR formats, some extra input forms for the creation of NRDF outputs could be rather confusing for foreign compilers. Therefore, development of HENDEL specialized for EXFOR outputs is of our interest.

Recently, we have started to develop a new HENDEL system using the Java programming language for a stand-alone application type. Java is platform independent and an object-oriented programming language. Note that EXFOR compilers emphasized in a recent EXFOR compilation workshop (6-10 Oct. 2014, Vienna) that it is important to develop an OS-independent EXFOR editor system[9].

We adopt Java Swing API for building a GUI (graphical user interface) application. A main page of the new HENDEL editor under development is shown in Fig.#1. Contents of the editor will be organized in a Tree format. The contents of the editor consist: Bibliography, information commonly applied to all data sets of the EXFOR entry (Subentry 001), and information applied to each data set of the EXFOR entry independently (Subentry 002, 003,..). The Bibliography section consists of Title, Author, Affiliation, and Reference. One of the new improvements in this editor is that the Affiliation and Reference part in the Bibliographic section can be multiplied by "+" button, as shown in Fig. 1.

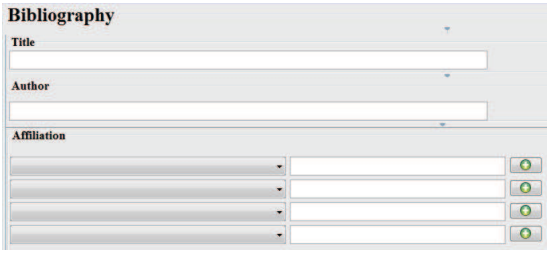

Fig. 1. Bibliography section of a Java-based Hendel system.

In the current stage, the design of the user interface and inclusion of utilities (e.g., checking tools) have been completed.

References

1) N. Otuka (ed.): Report INDC(NDS)-0401 Rev.6, IAEA (2014).
2) H. Henriksson et al.: Proc. Int. Conf. on Nucl. Data Sci. Tech., (Nice, 2007), p. 737.
3) Nuclear Reaction Data Centre, `http://www.jcprg.org`, 2015/04/27.
4) N. Otuka et al.: Nucl. Data Sheets 120 (2014) 272.
5) V. Osolio: Report IAEA-NDS-0101, IAEA (1991).
6) Li Shubing et al.: Report IAEA-NDS-0151, IAEA (1994).
7) Web-based Editor for Nuclear Data, `http://www.jcprg.org/hendel/`, 2015/04/27.
8) N. Otuka et al.: Report INDC(NDS)-0434, IAEA (2002), p. 144.
9) V. Semkova, B. Pritychenko (eds.): Report INDC(NDS)-0672, IAEA (2015).

*1 Faculty of Science, Hokkaido University
*2 Meme Media Laboratory, Hokkaido University
*3 Sapporo-Gakuin University
*4 Nuclear Data Section, International Atomic Energy Agency
*5 RIKEN Nishina Center

Thick-target yields derived from inverse kinematics toward transmutation

S. Imai,[*1] M. Aikawa,[*2] and S. Ebata[*1]

Nuclear transmutation of long-lived fission products (LLFP) into stable and short-lived isotopes is considered as an important technique for reducing nuclear wastes in nuclear power plants[1]. Thick-target yields (TTY) on radioactive targets are fundamental and key information for establishing such a technique, although experiments on such radioactive targets suffer from high radioactivity. Recent progress in experimental techniques now allow the utilization of beams composed of radioactive isotopes (RI) including LLFP. In fact, an experiment has been performed at RIBF to obtain cross section data relating to ^{90}Sr and ^{137}Cs[2]. Unstable nuclei of astrophysical interests have also been applied to obtain cross sections deduced from the thick-target method of elastic scattering[3].

We therefore suggest an estimation method for the TTY on a radioactive target based on inverse kinematics. In the case that the projectile is stopped inside the thick target, the TTY denoted by Y is obtained by the integration value of cross-section σ and density ρ of the target, up to the projectile penetration length. While the energy decrease of the projectile is described by the stopping power $S(E) = -\frac{dE}{d(\rho x)}$ at a certain point x, the TTY can be expressed as:

$$Y(\epsilon_{\rm in}) = \frac{N_{\mathcal{A}} A_P}{A_T} \int_0^{\epsilon_{\rm in}} \sigma(\epsilon) \frac{1}{S(\epsilon)} d\epsilon, \tag{1}$$

which leads to:

$$\frac{dY(\epsilon)}{d\epsilon} = \frac{N_{\mathcal{A}} A_P}{A_T} \sigma(\epsilon) \frac{1}{S(\epsilon)}, \tag{2}$$

where the Avogadro constant $N_{\mathcal{A}}$, the mass number of the target A_T, the energy per nucleon $\epsilon = E/A_{\rm P}$ with the mass number of the projectile $A_{\rm P}$ and its incident energy $\epsilon_{\rm in}$ are used. In this report, we call this system the forward kinematics and its TTY $Y_{\rm for}$.

The inverse kinematics with an RI beam suggests that by swapping roles of the radioactive target and incident particle, we can obtain the TTY of the inverse kinematics system denoted by $Y_{\rm inv}$. The ratio of the TTYs between differential yields, $R(\epsilon)$, at the same energy ϵ is given by:

$$R(\epsilon) \equiv \frac{dY_{\rm for}(\epsilon)}{dY_{\rm inv}(\epsilon)} = \frac{A_P^2}{A_T^2} \frac{S_{\rm inv}(\epsilon)}{S_{\rm for}(\epsilon)}. \tag{3}$$

Since the $\sigma(\epsilon)$ of both systems are the same and are canceled out in the ratio, the TTY $Y_{\rm for}$ ($Y_{\rm inv}$) can be estimated without cross-section if we know $Y_{\rm inv}$ ($Y_{\rm for}$). Note that the stopping powers $S_{\rm for}$ and $S_{\rm inv}$ can be computed by SRIM 2008 code[4].

*1 Meme Media Laboratory, Hokkaido University
*2 Faculty of Science, Hokkaido University

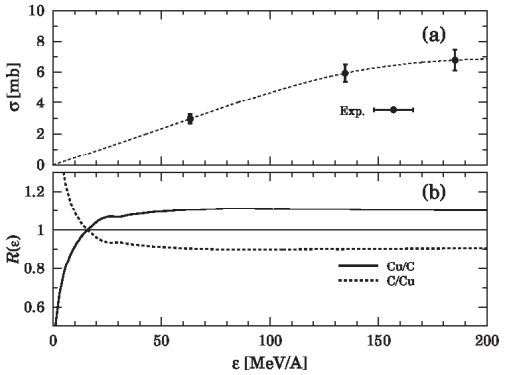

Fig. 1. Cross-section of $^{\rm nat}$Cu(^{12}C,X)^{24}Na with experimental data[5] with spline fitting in (a), and the evaluated ratio $R(\epsilon)$ by SRIM 2008[4] in (b) as functions of ϵ.

Table 1. TTY $Y_{\rm for}$ at two incident energies evaluated from Eq. (4) taking $R \simeq 1.1$ and from Eq. (1).

$Y_{\rm for}(\epsilon_{\rm in})$	40 MeV	100 MeV
From Eq. (4)	0.94×10^{-5}	0.113×10^{-3}
From Eq. (1)	0.91×10^{-5}	0.114×10^{-3}

We show the example of $^{\rm nat}$Cu(^{12}C, X)^{24}Na[5]. In order to calculate $Y_{\rm for}$ and $Y_{\rm inv}$ using Eq. (1), the cross-section $\sigma(\epsilon)$ and stopping power $S(\epsilon)$ should be known (see in Fig. 1). $R(\epsilon)$ shown in Fig. 1 (b) converges at a constant value at a high energy of more than 50 MeV/A. This simple behavior of $R(\epsilon)$ at a high energy and small $\sigma(\epsilon)$ at a low energy allows us to use a more convenient conversion method as:

$$Y_{\rm for}(\epsilon_{\rm in}) \simeq \tilde{R}\, Y_{\rm inv}(\epsilon_{\rm in}), \tag{4}$$

where $\tilde{R}$ is a constant value of $R(\epsilon)$ at the high energy. Indeed, these are in good agreement with values derived from Eq. (1) (Table 1).

This conversion method will be applied to radioactive isotopes, such as ^{137}Cs, and used to search suitable projectiles for transmutation of LLFP.

References

1) W. S. Yang et al.: Nucl. Sci. Eng. 146, 291 (2004).
2) H. Wang et al.: In this report.
3) H. S. Jung et al.: Phys. Rev. **C90**, 035805 (2014).
4) J. F. Ziegler, J. P. Biersack and M. D. Ziegler: *SRIM: the Stopping and Range of Ions in Matter*, http://www.srim.org.
5) H. Yashima *et al.*: Phys. Rev. **C66**, 044607 (2002).

Compilation of nuclear reaction data from the RIBF

D. Ichinkhorloo,[*1] M. Aikawa,[*2] S. Ebata,[*1] N. Furutachi,[*3] S. Imai,[*1] K. Katō,[*2] A. Makinaga,[*4] M. Odsuren,[*5] N. Otuka,[*6,*7] A. Sarsembayeva,[*1] and B. Zhou[*1]

Nuclear reaction data, such as cross sections, angular and energy distributions of secondary particles, and resonance parameters, are required to be compiled into a database for their users for a large variety of applications and research fields. A nuclear reaction database that fulfils this requirement is the EXFOR library, which is maintained by the International Atomic Energy Agency (IAEA) and the International Network of Nuclear Reaction Data Centres (NRDC). The NRDC members are involved in data compilation and software development for nuclear data users. Each member is responsible for compiling data about neutrons, charged particles, and photon-induced reactions. This responsibility is assigned to members according to area where the experimental facility to obtain data is located.

One of the NRDC members is the Hokkaido University Nuclear Reaction Data Centre (JCPRG).[1)] JCPRG covers nuclear reaction data except neutron-induced data obtained in Japan and contributes about 10% of charged-particle nuclear reaction data in the EXFOR library.[2)] At the JCPRG, the compiled nuclear reaction data are stored in two databases, NRDF and EXFOR libraries, simultaneously. The former is the original database of JCPRG and the latter is the collaborative one among the NRDC. Both databases are available and searchable online on the JCPRG website.

In addition to the NRDC, we have also collaborated with the RIKEN Nishina Center for data compilation from January 2010 to March 2014. The purpose of this collabotation is to increase the availability of nuclear reaction data produced at the RIBF. The compiled data produced at the RIBF are translated into EXFOR format and available online for the benefit of nuclear data users. In this article, we report on our activities in 2014 concerning the compilation of experimental nuclear reaction data from the RIBF.

In 2014, we compiled 28 new papers, data of which were obtained in Japan. 14 of them contain RIBF data and match the compilation scope of the EXFOR library. 10 papers were published in 2013 and 2014 and their compilation reflects recent activities of the RIBF. On the contrary, the remaining 4 papers were published before 2009 and compiled for completeness of data published by the RIBF. Especially, 2 papers are written in Chinese and were published in 2005 and 2006. All data are accessible by the accession numbers listed in Table 1. For higher quality of the contents, numerical data are requested from the corresponding authors of the compiled papers. Most of the compiled RIBF data in 2014 are provided by the authors. Such additional information is also available with the list of compiled RIBF data on the JCPRG website.

Table 1. Entry numbers with references compiled from the RIBF data in 2014

Entries	E2398[3)]	E2399[4)]	E2439[5)]
	E2440[6)]	E2442[7)]	E2443[8)]
	E2444[9)]	E2448[10)]	E2450[11)]
	E2451[12)]	E2455[13)]	E2456[14)]
	E2457[15)]	E2458[16)]	
Total		14	

During the four-year fruitful collaboration, we could establish a good procedure to compile new publications. Therefore, most of recent experimental nuclear reaction data from the RIBF have successfully been compiled in the EXFOR library. As a next step, we are focusing on the improvement of the completeness and usability of the data produced at the RIBF. In addition, we are developing a new data format using XML technology. The new format will allow us to communicate with experimentalists for proofreading compiled information.

*1 Meme Media Laboratory, Hokkaido University
*2 Faculty of Science, Hokkaido University
*3 Faculty of Engineering, Hokkaido University
*4 Graduate School of Medicine, Hokkaido University
*5 Nuclear Research Center, National University of Mongolia
*6 RIKEN Nishina Center
*7 NDS, IAEA

References
1) http://www.jcprg.org/
2) http://www.jcprg.org/exfor/
3) N. Iwasa et al.: Phys. Rev. C **78**, 024306 (2008).
4) Z. Elekes et al.: Phys. Rev. C **79**, 011302 (2009).
5) M. U. Khandaker et al.: Nucl. Instrum. Methods Phys. Res., Sect. B **316**, 33 (2013).
6) S. J. Jin et al.: Phys. Rev. C **88**, 035801 (2013).
7) G. L. Zhang et al.: High Energy Physics and Nuclear Physics, **29**, 940 (2005) (in Chinese).
8) D. Y. Pang et al.: High Energy Physics and Nuclear Physics, **30**, 22 (2006) (in Chinese).
9) L. Audirac et al.: Phys. Rev. C **88**, 041602 (2013).
10) Y. Satou et al.: Phys. Lett. B **728**, 462 (2014).
11) H. Haba et al.: Phys. Rev. C **89**, 024618 (2014).
12) T. Nakamura et al.: Phys. Rev. Lett. **112**, 142501 (2014).
13) A. Ozawa et al.: Phys. Rev. C **89**, 044602 (2014).
14) S. Michimasa et al.: Phys. Rev. C **89**, 054307 (2014).
15) M. U. Khandaker et al.: Nucl. Instrum. Methods Phys. Res., Sect. B **335**, 8 (2014).
16) N. Kobayashi et al.: Phys. Rev. Lett. **112**, 242501 (2014).

4. Hadron Physics

Performance improvement of PHENIX MUID

S. Han,[*1,*2] S. Caussin,[*1,*3] I. Nakagawa,[*1] and the PHENIX collaboration

PHENIX Muon Identifier, MUID, is one of the PHENIX detectors. It has north and south arms, and each arm consists of 5 layers of alternating energy absorbers and low-resolution ionization chambers. The chamber is composed of many bunches of larocci tubes.[1)]

During the RHIC-Run 13, the efficiency of the MUID dropped to less than down under 60% under conditions of high beam luminosity, as shown in Fig. 1. The high voltage supply system is implemented with 400 M Ω current-limiting resistors, and thus, the voltage is sagged at the tube as a function the drawing current, which results in the efficiency drop. The latest performance of MUID indicated a possible degradation of the efficiency from what was observed at the early stage of MUID operation a decade ago.

In order to update the performance, we executed the high voltage(HV) scan in July 2014. The resulting efficiency curve as a function of HV values demonstrated that the current operation voltage (4400V) is almost the edge of the plateau curve and an additional current draw immediately leads to a substantial efficiency drop, as shown in Fig. 2. Overall, more than 50% of the HV chains showed degraded efficiency performance as compared to that observed in 2004. All these phenomena signify that the plateau of the MUID became narrower than observed initially. Thus, it is obvious that an improvement of the MUID performance is required before starting the RHIC-Run 16. We aim to measure Drell-Yan using a high luminosity beam at a collision energy of 500GeV. The MUID efficiency is a topic of much concern because detection efficiency affects on square for this measurement.

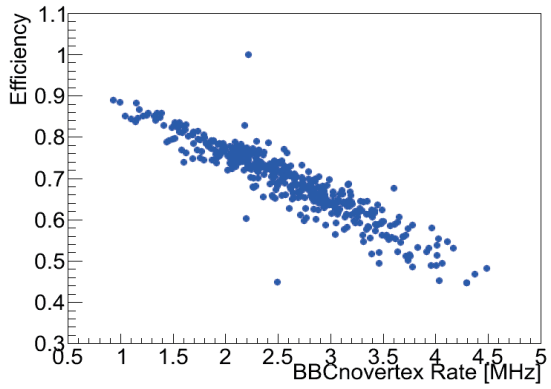

Fig. 1. Efficiency drop with an increase in BBC novertex rate. BBC is the beam luminosity monitoring device.

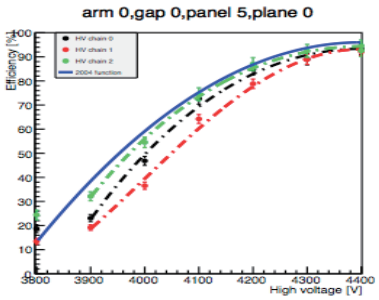

Fig. 2. Efficiency versus high voltage for south arm gap 0, panel 5, plane 0. New data (green, black, red points) indicate a steeper drop than the efficiency turn on curve (blue solid line) observed in 2004.

One of the ways to improve the aforesaid situation is to reconsider the operating HV condition, i.e., if a higher voltage can be set away from the edge of the plateau. To define the current plateau region, we explored the higher voltage region and evaluated hit rates vs HV values, as shown in Fig. 3.

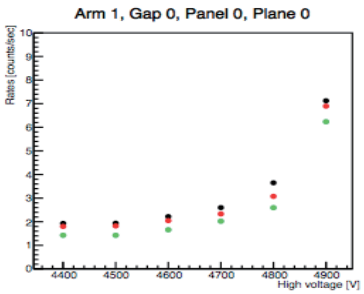

Fig. 3. Hits per sec graph range of 4400V to 4900V at north arm gap 0, panel 0, plane 0.

Fig. 3. shows the result of the scan up to 4900V. It is obvious that the operation voltage should not be pushed over 4600V, because a plateau region is created from 4400V to 4600V.

The observed plateau runs up to 4550 - 4600V depending on the HV chain. The results obtained thus far indicate that the MUID can be operated at a higher voltage of +100V to +200V with a relatively small increase in the noise hit rates. HV optimization is currently in progress.

*1 RIKEN Nishina Center
*2 Ewha Womans University
*3 ENSICAEN

References

1) J. Murata et al.: Nucl.Instrum.Meth. A500 (2003)
2) W. Anderson et al.: Mar 2011. 51pp. arXiv:1103.4277

PHENIX Run13 Local Polarimetry

M. Kim[*1,*2] for the PHENIX collaboration

One of the most important goals of the PHENIX experiment at the Relativistic Heavy Ion Collider (RHIC) is to study the proton spin structure by measuring spin asymmetries during particle production. The Run13 PHENIX experiment collided longitudinally polarized protons at $\sqrt{s} = 510$ GeV. Helicity asymmetry measurements of various probes from the experiment are ongoing.

RHIC is capable of running polarized proton beams, and each beam polarization P is measured by RHIC polarimeters using left-right asymmetry in elastic scattering in the Coulomb Nuclear Interference (CNI) region. Since the stable beam polarization direction in the RHIC rings is vertical, the beam polarization direction is kept vertical in RHIC except in experimental halls. For each ring, Spin Rotators, which consist of superconducting helical dipole magnets, rotate the beam polarization direction the 90 degrees at the entrance and the exit of the PHENIX experimental hall.

Since beam polarization may not purely be longitudinal at the experimental hall, we require measurements of transverse and longitudinal component of P ($P_\perp$, $P_\parallel$) at the experimental hall, which is local polarimetry, as they introduce systematic error. Local polarimetry is especially important in A_{LL} measurements for studying gluon polarization in a proton since A_{LL} is very small, and $P_\perp$ has potential to introduce significant error.

PHENIX Local Polarimetry uses large transverse single spin asymmetry (left-right asymmetry) A_N of forward neutron production. Left-right asymmetry originates from the interference between spin flip and non-flip amplitudes. One Pion Exchange (OPE) models describe the production cross section of forward neutron reasonably well, but the pion exchange amplitude is fully spin flip.[1] Theoretical study is still ongoing.

PHENIX Local Polarimeter measures energies and trajectories of forward neutrons. The local polarimeter consists of Zero Degree Calorimeters (ZDCs), and Shower Max Detectors (SMDs). ZDC consists of W-Cu alloys and PMMA (polymethyl methacrylate) based optical fibers, and collects Cherenkov photons produced by charged secondary particles from neutron showers. SMD is an X-Y plastic scintillator strip hodoscope. It is located between the 1st and 2nd ZDC modules, where the approximate hadronic shower is maximum. X-Y position of a neutron is reconstructed by using shower profile on SMD. Those detectors are located 1800 cm away from the collision point, and cover 10 cm x 10 cm of a transverse plane at each zero degree area.

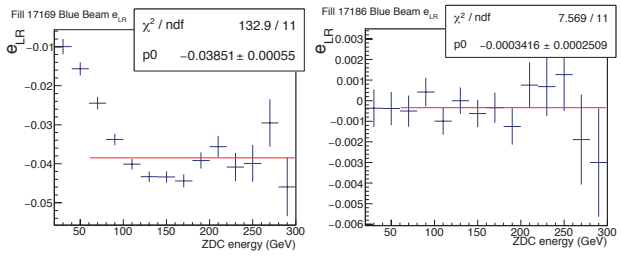

Fig. 1. Observed asymmetry in transverse fill (left), in longitudinal fill (right). The red lines are constant fittings.

The observed left-right asymmetry e_N of forward neutron production is defined as $e_N = P_\perp A_N^{\rm Eff}$, where $A_N^{\rm Eff} = f_{\rm smear} A_N$. $f_{\rm smear}$ is the smearing effect, correlated to the neutron energy-dependent position resolution[1]. $f_{\rm smear}$ is assumed to be constant during the Run13 experiment.We measure $A_N^{\rm Eff}$ at transversely polarized proton beam collisions, where $P_\perp = P$ so that it is measured by RHIC polarimeters. After that, we measure e_N with the local polarimeter to obtain $P_\perp$ of longitudinally polarized beams.

Fig.1 shows e_N plots. The left (right) plot shows e_N of transversely (longitudinally) polarized proton beam collisions.

As a final result, $\frac{P_\perp^Y}{P^Y}\frac{P_\perp^B}{P^B}$ is $\sim O(10^{-3})$ and $\frac{P_\parallel^Y}{P^Y}\frac{P_\parallel^B}{P^B}$ is ≈ 0.999 in the Run13 experiment. The measured double helicity asymmetry becomes

$$A_{LL}^{\rm Measured} \approx \frac{1}{P^Y}\frac{1}{P^B}(P_\parallel^Y P_\parallel^B A_{LL} + P_\perp^Y P_\perp^B A_{TT}) \quad (1)$$

$$\approx 0.999 A_{LL} + O(10^{-3}) A_{TT} \quad (2)$$

where Y and B represent two colliding beams, and A_{TT} is the double transverse spin asymmetry. This analysis suppressed the systematic error of A_{TT} term to $O(10^{-3})$. A_{LL} measurements have been done up to $O(10^{-4})$ so far[2], and $O(10^{-3})A_{TT}$ is orders of magnitude smaller than 10^{-4}.[3] Therefore, $P_\perp$ does not significantly contribute to systematic error in A_{LL} measurements in Run13.

References
1) A. Adare et al.: Phys. Rev. D 88, 032006 (2013)
2) A. Adare et al.:Phys. Rev. D 90, 012007 (2014)
3) K. Boyle: AIP Conf. Proc. 915,335 (2007)

*1 RIKEN Nishina Center
*2 Department of Physics and Astronomy, Seoul National University

Hadronic backgrounds pattern study for $W^{\pm} \rightarrow \mu^{\pm}$ analysis in PHENIX

C. Kim,[*1,*2] Y. Goto,[*2] S. Caussin,[*2,*3] S. Han,[*2,*4] M. Kim,[*2,*5] T. Moon,[*2,*6] T. Murakami,[*7] J. Murata,[*8] T. Nagashima,[*2,*8] I. Nakagawa,[*2] S. Park,[*2,*5] R. Seidl,[*2] W. Saito,[*2,*8] K. Tanida,[*2,*5] and I. Yoon[*2,*5]

The ongoing $W^{\pm} \rightarrow l^{\pm}$ analysis at PHENIX aims to precisely constrain the sea quark spin contribution to the proton spin of 1/2. The main observable of this analysis is single longitudinal spin asymmetry among muons (A_L), which directly decayed from W boson[1)].

To measure the desired asymmetry precisely S/BG needs to be estimated as accurately as possible. However, observing a distinct Jacobian peak in $W^{\pm} \rightarrow \mu^{\pm}$ is not expected due to the large momentum and charge smearing in the muon reconstruction in addition to dominant backgrounds from various sources. As a result, conventional S/BG estimation is not available; thus, we use a partially indirect method based on likelihood to the W (Wness), which is calculated by using NLO level signal Monte Carlo (MC) and data itself.

In an actual S/BG estimation, we perform an unbinned maximum likelihood fit (UMLF) by using six probability density functions (PDFs) from a pair of kinematic variables (η (pseudorapidity) and $dw23$ (reduced azimuthal bending)) and three processes (signal, muonic BG, and hadronic BG).

Among these PDFs, the hadronic BG process is modeled from the data itself owing to the difficulty in hadronic MC production. To obtain the expected hadronic distribution among the final muon candidates, we modeled each kinematic variable's distribution from the BG dominant region in the data ($0.1 <$ Wness < 0.9), and then extrapolated it into the signal dominant region (Wness > 0.9). For the validity of the method, each variable's distribution along Wness should be understood precisely. However, as there exists a serious Wness dependence of $dw23$ (Fig. 1) unlike η, a specific pattern study was required to reflect its shape along Wness.

A typical $dw23$ in a certain Wness range (ex. $0.1 <$ Wness < 0.2) can be described by a stack of two Gaussians. To understand its development along Wness, we collected $dw23$ over a certain Wness range, performed a fit using two Gaussians, and then parameterized each Gaussian's parameters (maximum, center, and FWHM) along Wness. Then we fed it back during the hadronic BG $dw23$ modeling process as explained above.

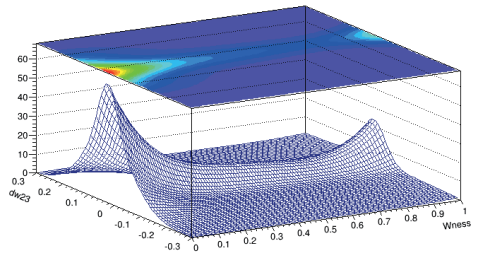

Fig. 1. An example of dw23 vs. Wness.

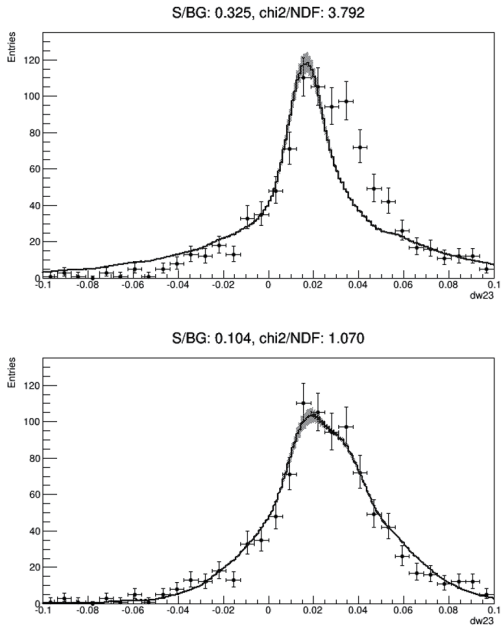

Fig. 2. Comparison between fit results before (top) and after (bottom) the pattern study for $W^{+} \rightarrow \mu^{+}$ measured in the North muon arm. The gray-hatched area of the solid line indicates the uncertainty of the final PDF itself.

Figure 2 shows the results of a 2D UMLF projection onto $dw23$ in the final sample before and after the pattern study. A noticeable improvement was observed in the fit's χ^2, and we plan to apply the pattern study in $W^{\pm} \rightarrow \mu^{\pm}$ analysis for both the 2012 and 2013 datasets.

*1 Department of Physics, Korea University
*2 RIKEN Nishina Center
*3 Department of Physics, ENSICAEN
*4 Department of Physics, Ewha Womans Univeristy
*5 Department of Physics, Seoul National University
*6 Department of Physics, Yonsei University
*7 Department of Physics, Kyoto University
*8 Department of Physics, Rikkyo University

References

1) H. Oide et al: RIKEN Accel. Prog. Rep. 46 xviii

W→ μ parity violating asymmetries from the 2013 running period in the PHENIX experiment

R. Seidl*1 for the PHENIX collaboration

During the 2013 data taking period 277 pb^{-1} of longitudinally polarized proton collision data at a center of mass energy of 510 GeV were accumulated with an average beam polarization of 53% per beam at the PHENIX experiment at RHIC. This data corresponds to the largest data sample available for the polarized W data analysis. In order to access the sea quark polarization in the nucleon real W boson production is an elegant way. The parity violation of the weak interaction directly selects the helicity of the quarks and anti-quarks and the charge of the produced W boson selects the quark and anti-quark flavors. For example the W^- gets produced by a left-handed d quark and a right-handed anti-u quark. While the u and d quark helicities are already reasonably well known the sea quark helicities are only very poorly determined and the question whether the polarized light sea is symmetric or not has been predicted rather differently in various nucleon models. The analysis of W decay muons in the forward and backward muon arm detectors of PHENIX is not as straightforward as at central rapidities as there is no clean W decay signature such as a Jacobian peak at half the W mass. Also a large number of background sources exist such as heavy flavor decay muons and hadrons decaying within the tracking volume mimicking a high momentum muon as previously reported. With the help of kinematically different variables for signal and backgrounds candidate events were pre-selected by a likelihood ratio where only high signal likelihood events were kept. Then the relative signal and background contributions were fit by a maximum unbinned likelihood fit. From those preliminary $pp \to W^{\pm}X$ cross sections were extracted which turned out to be consistent with NLO predictions, see Fig. 1. After correcting the raw single spin asymmetries for beam polarization and dilution by background the preliminary results[6] for the single spin asymmetries were obtained as seen in Fig. 2. The results are in good agreement with the parameterizations and will eventually be used in future iterations of the global helicity fits to all the existing deep inelastic scattering and proton-proton collision data. The 2013 PHENIX W results are currently being prepared for publication and it is expected to reduce the systematic uncertainties which are dominated by the uncertainties on the signal to background ratio still.

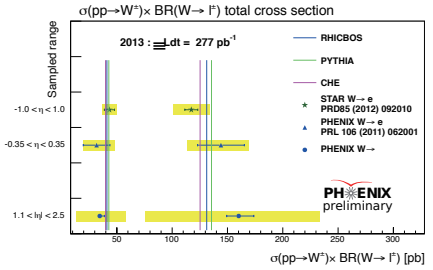

Fig. 1. Total $pp \to W^{\pm}X \times BR(W \to l)$ cross sections for forward muon and previously published $W \to e$ results by PHENIX[1] and STAR[2] as well as predictions by Pythia[3], CHE[4] and RHICBOS[5].

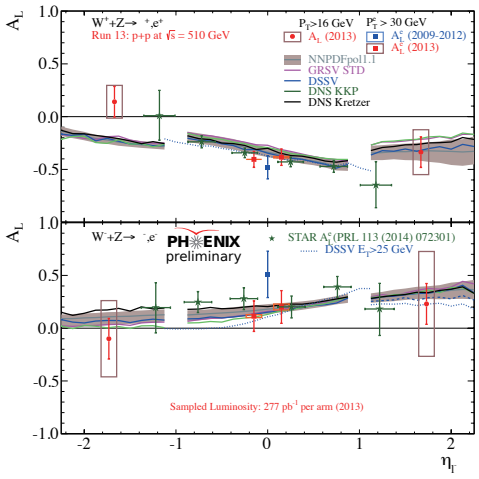

Fig. 2. Single spin asymmetries of W+Z decay leptons as a function of lepton rapidity. The preliminary PHENIX electron and muon results from the 2013 data taking period (red) and the published STAR electron results from 2012 (green)[7] are shown as well as various helicity parameterizations.

*1 RIKEN Nishina Center

References

1) A. Adare *et al.* [PHENIX Collaboration], Phys. Rev. Lett. **106** (2011) 062001
2) L. Adamczyk *et al.* [STAR Collaboration], Phys. Rev. D **85** (2012) 092010
3) T. Sjostrand*et al.* Comput. Phys. Commun. **135** (2001) 238
4) D. de Florian and W. Vogelsang, Phys. Rev. D **81** (2010) 094020
5) P. M. Nadolsky and C. P. Yuan, Nucl. Phys. B **666** (2003) 31
6) F. Giordano [PHENIX Collabortion], to appear in JPCS (Spin 2014 proceedings).
7) L. Adamczyk *et al.* [STAR Collaboration], Phys. Rev. Lett. **113** (2014) 072301

Neutral pion double helicity asymmetry†

K. Boyle*1

A major goal of the RHIC Spin program is to determine the gluon spin distribution in the proton. The quark spin contribution to the proton spin ($\Delta\Sigma$) is only about 25%[1], and so the remaining spin must be carried by the gluon spin (ΔG), or by the gluon and quark orbital angular momentum (L_q and L_g, respectively):

$$S_p = \frac{1}{2} = \frac{1}{2}\Delta\Sigma + \Delta G + L_q + L_g \quad (1)$$

written in units of $\hbar$.

At RHIC, ΔG can be probed directly through measurements of the double helicity asymmetry in polarized $p+p$ collisions, in this case for neutral pions:

$$A_{LL} = \frac{1}{P_B P_Y}\frac{N_{++} - RN_{+-}}{N_{++} + RN_{+-}} \quad (2)$$

where P_B and P_Y are the polarizations of the two proton rings at RHIC, N is the yield of neutral pions, π^0, $++$ and $+-$ indicate same and opposite helicity combinations of the two beam helicities, and R is the relative luminosity, defined as $R = L_{++}/L+-$, which is required to normalize differences in the luminosity L between RHIC proton bunches.

In 2009, RHIC PHENIX recorded 14 pb^{-1} with an average polarization of 56%. The π^0 A_{LL} was measured, and found to be consistent with previous results. The combined results from 2005[2], 2006[3] and 2009[4] are plotted in Fig. 1. The systematic uncertainty from relative luminosity in 2009 was larger than in previous years, and for the lowest π^0 transverse momentum, p_T, was larger than the statistical uncertainties.

The combined data set are shown in Fig. 1 and Fig. 2 compared to several theoretical expectations based on fits to the world polarized scattering data. In the case of[1], the RHIC 2005 and 2006 π^0 data are also included. In fits that do not use RHIC data, such as GRSV[5], LSS[6] and BB[7], there is large uncertainty in ΔG and therefore in the expected π^0 A_{LL}. Fits including some RHIC data, such as DSSV[1] and NNPDF[8] find a smaller range of possible ΔG. These data therefore offer significant constraint on ΔG. Recently, the RHIC 2009 data have been included in an updated version of DSSV[9], and indicate that the gluon spin contribution to the proton spin is about the same size as that of the quarks.

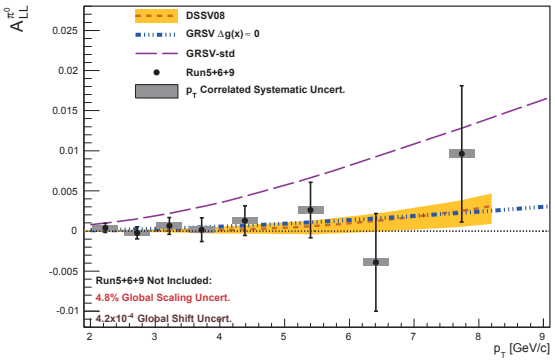

Fig. 1. Results for π^0 A_{LL} vs. p_T from the combined 2005, 2006 and 2009 PHENIX data sets. The data are compared with several theoretical expectations.

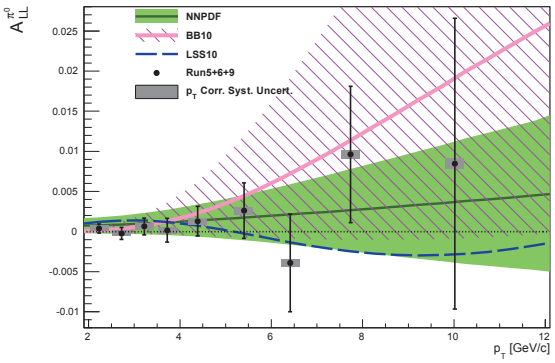

Fig. 2. Results for π^0 A_{LL} vs. p_T from the combined 2005, 2006 and 2009 PHENIX data sets. The data are compared with several theoretical expectations.

References

1) D. de Florian, R. Sassot, M. Stratmann and W. Vogelsang, Phys. Rev. D **80**, 034030 (2009).
2) A. Adare *et al.* [PHENIX Collaboration], Phys. Rev. D **76**, 051106 (2007).
3) A. Adare *et al.* [PHENIX Collaboration], Phys. Rev. Lett. **103**, 012003 (2009).
4) A. Adare *et al.* [PHENIX Collaboration], Phys. Rev. D **90**, no. 1, 012007 (2014).
5) M. Gluck, E. Reya, M. Stratmann and W. Vogelsang, Phys. Rev. D **63**, 094005 (2001).
6) E. Leader, A. V. Sidorov and D. B. Stamenov, Phys. Rev. D **82**, 114018 (2010).
7) J. Blumlein and H. Bottcher, Nucl. Phys. B **841**, 205 (2010).
8) R. D. Ball *et al.* [The NNPDF Collaboration], Nucl. Phys. B **874**, 36 (2013).
9) D. de Florian, R. Sassot, M. Stratmann and W. Vogelsang, Phys. Rev. Lett. **113**, 012001 (2014).

† Condensed from the article in Phys. Rev. D **90**, no. 1, 012007 (2014)

*1 RIKEN BNL Research Center

Preliminary results of $A_{LL}^{\pi^0}$ measurement at $\sqrt{s} = 510$ GeV at mid-rapidity through a PHENIX experiment

I. Yoon*1,*2 for the PHENIX collaboration

One of the important functions of the relativistic heavy ion collider (RHIC) longitudinally polarized proton program is to constrain the gluon-spin component of the proton (ΔG) by measuring the double helicity asymmetry (A_{LL}) of π^0 and jet production. Based on the results of deep inelastic scattering experiments, the quark-spin component of proton is only $0.330 \pm 0.011(Theo.) \pm 0.025(Exp.) \pm 0.028(Evol.)$.[1] The remaining spin might be carried by gluons or orbital momentum. However, ΔG has not been measured in detail as yet.[2]

The measurement of A_{LL} for π^0 production ($A_{LL}^{\pi^0}$) at $\sqrt{s} = 200$ GeV has been successfully published and has contributed to constraining ΔG.[3] To explore the lower Bjorken x region, where dominant uncertainty remains, longitudinally polarized proton-proton collisions in 2013 (Run13) were successfully carried out with increased energy, i.e. $\sqrt{s} = 510$ GeV. Because of the increased energy, the measurement at $\sqrt{s} = 510$ GeV can reach a lower x range, $0.01 < x$, while the previous measurement could reach only $0.02 < x$. The measurement at $\sqrt{s} = 510$ GeV is ongoing and preliminary results have been released.

$A_{LL}^{\pi^0}$ can be defined in terms of differences in cross-sections as

$$A_{LL}^{\pi^0} = \frac{d\Delta\sigma^{\pi^0}}{d\sigma^{\pi^0}} = \frac{d\sigma_{++}^{\pi^0} - d\sigma_{+-}^{\pi^0}}{d\sigma_{++}^{\pi^0} + d\sigma_{+-}^{\pi^0}} \quad (1)$$

where $\sigma_{++(+-)}$ stands for π^0 cross-section with the same(opposite) helicity proton collisions. Because σ^{π^0} can be described by the parton distribution function, the partonic reaction cross-section and fragmentation function and most of π^0s are from quark-gluon or gluon-gluon scattering at mid-rapidity region, gluon helicity distribution (Δg) is accessible by measuring $A_{LL}^{\pi^0}$. This description is verified by comparing the π^0 cross-section between theoretical and experimental data.

Equation 1 can be rewritten in terms of experimental observables as

$$A_{LL} = \frac{1}{P_B P_Y} \frac{N_{++} - RN_{+-}}{N_{++} + RN_{+-}}, R = \frac{L_{++}}{L_{+-}} \quad (2)$$

where $P_{B(Y)}$ is the polarization of RHIC's "Blue (Yellow)" beam, $N_{++(+-)}$ is the yield of the π^0 candidate from the same (opposite) helicity collisions, and R is the relative luminosity of the same and opposite helicity collisions.

*1 RIKEN Nishina Center
*2 Seoul National University

As the collision rate increases in Run13, the effect of multiple collisions on one beam crossing becomes sizable. The effect of multiple collisions is fully taken into account for the relative luminosity measurement. Luminosity miscount by the finite resolution of the vertex width of luminosity detector is also considered. The uncertainty of the relative luminosity is a dominant systematic uncertainty of the measurement.

To reduce the combinatorial background in diphoton invariant distribution, several cuts are applied. Hits by a charged track, hadron, and previous crossings are rejected. To evaluate A_{LL} for the remaining background, A_{LL} of the background is also measured and is subtracted to obtain physical asymmetry.

Fig. 1 shows preliminary results of $A_{LL}^{\pi^0}$ measurement at $\sqrt{s} = 510$ GeV. The result covers 2 GeV/c $< P_T <$ 20 GeV/c ($0.008 < x_T < 0.08$, where $x_T = 2P_T/\sqrt{s}$). The DSSV14 theory curve is shown and it agrees with experimental data within uncertainty. The measurement at $\sqrt{s} = 200$ GeV is also shown for comparison. Larger asymmetry is observed at higher collision energy.

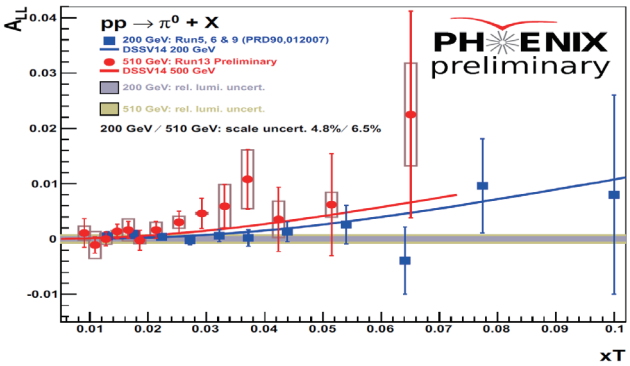

Fig. 1. Preliminary result of $A_{LL}^{\pi^0}$ measurement at $\sqrt{s} =$ 510 (red line) and comparison with $A_{LL}^{\pi^0}$ at $\sqrt{s} = 200$ GeV[3] (blue line). DSSV14 theory curves[2] are shown. The grey and yellow bands indicate systematic uncertainty due to the uncertainty of relative luminosity. Global-scale uncertainty due to systematic uncertainty of polarization is not shown. Open boxes denote point-to-point systematic uncertainty.

Further analysis is ongoing to obtain the final result.

References

1) A. Airapetian et al.: Phys. Rev. D **75**, 012007 (2007).
2) D. de Florian, R. Sassot, M. Stratmann and W. Vogelsang: Phys. Rev. Lett. **113**. 012001 (2014).
3) A. Adare et al.: Phys. Rev. D **90**, 012007 (2014).

Cross section and asymmetry measurement of very forward neutral particle production at RHIC

Y. Goto*1 for the RHICf Collaboration

Although air shower observations at the surface of the earth have been carried out to understand the origin of the ultrahigh energy cosmic rays, these observations have uncertainties in the interpretation of the observed data from the present phenomenological nuclear collision models. The LHCf experiment has been performed at LHC for understanding cosmic ray generation from the collider experiment data[1–3]. Precision measurements of the very forward particle production in the collider experiments improve the understanding of particle production processes in the nuclear collisions, and largely affect the interpretation of the observed data and the origin of the cosmic rays.

A large 10% single transverse-spin asymmetry (SSA) in neutron production from transversely polarized proton collisions was found at RHIC in 2002[4]. This provides an important clue to study elementary processes in air shower generation because the large SSA indicates that there are dominant contributions from processes that strongly interfere with each other. Because the SSA measurement of neutron production provides interference measurement with one pion exchange with a spin flip, it is sensitive to a meson exchange without spin flip[5]. Although the SSA of very forward neutrons at collision energies of 62 GeV, 200 GeV, and 500 GeV was measured at RHIC, the transverse-momentum resolution of the data was limited.

We will perform a new collider experiment at RHIC, the so called RHICf experiment, which uses a LHCf detector (which is called the RHICf detector) with a high resolution and wide coverage of transverse-momentum measurements in order to improve the studies performed at RHIC and LHC. RHIC is a dedicated machine for QCD physics and it allows flexible operation to achieve our physics goals. In the RHICf experiment, we will have an improved transverse-momentum resolution using the RHICf detector. The LHCf experiment has measured very forward neutral particle cross section at collision energies of 0.9 TeV and 7 TeV. We will obtain precision measurements of very forward neutral particles (neutron, photon, neutral pion) at a collision energy of 510 GeV at RHIC. These data of various collision energies will provide an understanding of air shower generation and the limitations in the origin of the ultrahigh energy cosmic rays.

The RHICf detector will be located in front of the Zero-Degree Calorimeter (ZDC) in the north side, 18 m from the PHENIX collision point. In this area, all charged particles are swept out by the last dipole magnet for colliding beams at RHIC, and only neutral particles are detected. The RHICf detector consists of two sampling EM (electromagnetic) calorimeters with 44 interaction-length tungsten, 16 layers of scintillators, and 8 layers of silicon strip detectors; one with 25 mm × 25 mm and another with 32 mm × 32 mm cross sectional area. The ZDC detector is a sampling hadron calorimeter composed of Cu-W alloy absorbers with PMMA (Polymethyl methacrylate)-based optical fibers. The detection, identification, and energy measurement of photons and neutrons are performed using EM and hadron calorimeters. A schematic view of the RHICf detector installation and the structure of the calorimeter are shown in Fig. 1.

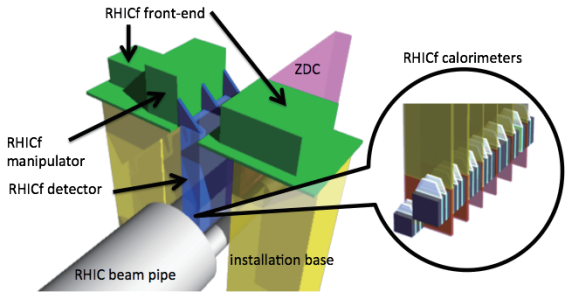

Fig. 1. Schematic view of the RHICf detector installation and the structure of the calorimeter.

We have proposed to perform a dedicated run for 1 week in 2016 with 510 GeV polarized proton collisions[6], and we are preparing for it. In the dedicated RHICf run, we will use the normal accelerator condition of the RHIC, except the beta function value at the PHENIX collision point, $\beta^* = 10$ m, in order to obtain parallel beam collisions. We need 12 h to achieve sufficient luminosity for cross section measurements of photons, neutrons, and neutral pions including the transverse-momentum scan. The SSA can be measured with the same data set with higher statistics than the measurements in the past.

*1 RIKEN Nishina Center

References
1) O. Adriani *et al.*, Phys. Lett. B 715, 298 (2012).
2) O. Adriani *et al.*, Phys. Rev. D 86, 092001 (2012).
3) O. Adriani *et al.*, Phys. Lett. B 703, 128 (2011).
4) Y. Fukao, M. Togawa *et al.*, Phys. Lett. B 650, 325 (2007).
5) B. Z. Kopeliovich, I. K. Potashnikova, I. Schmidt and J. Soffer, Phys. Rev. D 84, 114012 (2011).
6) Y. Itow *et al.* [RHICf Collaboration], arXiv:1409.4860 [physics.ins-det].

Fragmentation function measurements in Belle

R. Seidl,[*1] F. Giordano,[*2] M. Leitgab,[*2] A. Vossen,[*3] H. Li,[*3] W. Jacobs,[*3] N. Kobayashi,[*4] M. Grosse-Perdekamp,[*2] A. Ogawa,[*1] C. Hulse[*5] and G. Schnell[*5,*6]

Fragmentation functions allow us to study the process of nearly free partons fragmenting into final state hadrons as they also exist in visible matter. While the theory of the strong interaction, QCD, is generally accepted as the force governing all hadronic matter around us, only high energy processes are directly calculable. Parton distribution functions as well as fragmentation functions need to be obtained by experiment. Of particular interest is, how a parton of a certain flavor fragments into certain types of hadrons, how initial parton spin gets translated into the distribution of final state hadrons and how transvserse momentum is generated relative to the initial parton. In the Belle experiment one can study these aspects well since the underlying process of electron-positron annihilation provides a clean initial state without any hadrons to study the emerging final state hadrons. However, normally the quark flavor is not directly accessible as both a quark and an antiquark are created and at least for light flavors (u, d and s quarks) tagging techniques are not reliable. A first way around this limitation was already performed in the Collins type analysis[1)] where two charged pions in opposite hemispheres were studied. Having two hadrons in opposite hemispheres mostly ensures, that one hadron was fragmentating from the quark and another from the antiquark. The ratio of same over opposite charges then revealed the differences of favored and disfavored polarized and un-polarized fragmenation functions. This method was extended for pion-kaon and kaon-kaon combinations to obtain sensitivity of the strange quark Collins functions as well as disfavored u,d quark to kaon Collins fragmentation functions. Preliminary results have been obtained in 2014[2)] as shown in Fig. 1 and are expected to be published soon.

Furthermore the unpolarized fragmentation functions $D^h_{1,q}(z,s)$ can be studied in a similar way and first results have been prepared for all combinations of charged pions and kaons either in opposite hemispheres or also the same for comparison. Here, $z = 2E_h/\sqrt{s}$ is the fractional energy the hadron h carries relative to the initial parton q and $\sqrt{s}$ is the center of mass energy. In the thus obtained cross sections as a function of fractional energy z the ratios between same and opposite sign pion pairs in opposite hemispheres essentially provide the ratio of dis-favored over favored

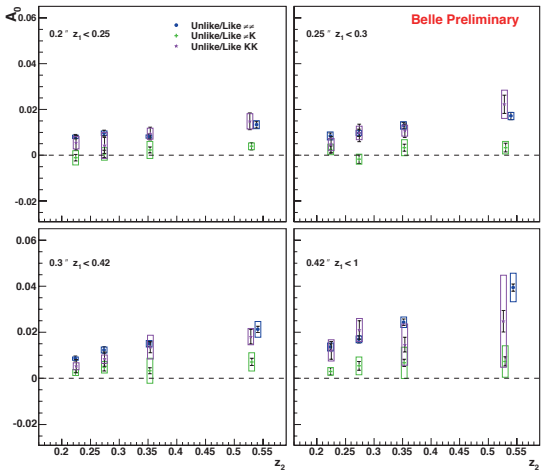

Fig. 1. Collins type azimuthal moments as a fucntion of fractional energy z_2 in bins of fractional energy z_1 for opposite sign over same sign pion pairs (blue), πK (green) and kaon pairs (purple).

fragmentation from u,d quarks to pions. Favored fragmentation relates to fragmentation into a hadron with valence content the same as the initial parton (ie u to $\pi^+ = |u\overline{d}\rangle$) and dis-favored fragmentation with valence content not the same (ie d to π^+). First results have been obtained and are expected to be shown as preliminary results and be published soon. The expected precision is such, that even the ratios at fractional hadron energies z above 0.8 have still reasonably small uncertainties.

In addition an analysis of transverse momenta of one hadron relative to a second hadron is ongoing which should help improve the rather large uncertainties and assumptions of any transvserse momentum dependent distribution and fragmentation functions. These are needed for the analysis of quark transversity and Sivers function data of semi-inclusive deep inelastic scattering and hadron collision experiments. These explicit transvserse momentum dependent measurements are also expected to obtain preliminary status this year.

*1 RIKEN Nishina Center
*2 Physics department, University of Illinois
*3 Physics department, University of Indiana
*4 Department of Physics, Tokyo Institute of Technology
*5 Department of Physics, University of the Basque Country
*6 Ikerbasque

References

1) R. Seidl *et al.* [Belle Collaboration], Phys. Rev. Lett. **96**, 232002 (2006). R. Seidl *et al.* [Belle Collaboration], Phys. Rev. D **78**, 032011 (2008), [Erratum-ibid. D **86**, 039905 (2012)]. A. Vossen *et al.* [Belle Collaboration], Phys. Rev. Lett. **107**, 072004 (2011).
2) F. Giordano [Belle Collaboration], PoS DIS **2014**, 212 (2014).

Measurement of direct photon azimuthal anisotropy in $\sqrt{s_{NN}}$=200GeV Au+Au collisions in RHIC-PHENIX experiment

S. Mizuno[*1,*2] for the PHENIX collaboration

High-energy heavy-ion collision experiments have been carried out since 2000 at the Relativistic Heavy Ion Collider (RHIC), to study the properties of quark-gluon plasma (QGP). Direct photons are defined as all photons except for those coming from hadron decays. Photons do not strongly interact with the medium. Furthermore, they are emitted from various sources, such as initial hard scattering, jet fragmentation, and thermal radiation, during all stages of collisions. Thus, direct photon is a powerful tool to study QGP.

Direct photon p_T spectra have been measured via a calorimeter method[1], virtual photon method[2], and conversion photon method[3]. It is found that the p_T spectra of Au+Au collisions include an additional exponential p_T spectra compared to those of p+p collisions scaled by the number of binary collisions. The effective temperature is obtained from the inverse slope of the exponential p_T spectra, it is approximately 240 MeV. It is found that photons mainly originate from a very hot medium in the early stage of collisions, since the kinetic freeze-out temperature obtained is approximately 100 MeV.

Azimuthal anisotropy is defined as the relative amplitude of anisotropic azimuthal distribution with respect to the event plane. To quantify the anisotropy, Fourier series is used for the azimuthal distribution of the number of emitted particles.

$$dN/d\phi = N_0[1 + \sum 2v_n \cos\{n(\phi - \Psi_n)\}], \quad (1)$$

$$v_n = \langle \cos\{n(\phi - \Psi_n\}\rangle, \quad (2)$$

where ϕ is the azimuthal angle of photons, and v_n and Ψ_n are the strength and event plane of the n^{th}-order harmonic azimuthal anisotropy, respectively. The mechanism of azimuthal anisotropy has been studied, and it is understood that it strongly depends on the initial geometry shape. The photon emission angle is expected to depend on the photon sources and initial geometry of the participant shape: thermal photons have $v_2 > 0$, photons fragmented from a jet have $v_2 > 0$, and prompt photons have zero v_2,. Direct photon v_2 is measured[4] to identify the photon sources. It is found that the strength of direct photon v_2 at around 2 GeV/c is comparable to that of hadron v_2. Because photons are emitted during all stages of collisions, emitted photons should include photons emitted from the medium, which is not yet expanded. This is why direct photon v_2 was predicted to be smaller than hadron v_2 in many theoretical models. Since a photon has large v_2, the results suggest that photons in the low p_T region are mainly generated from in the late stage of collisions.

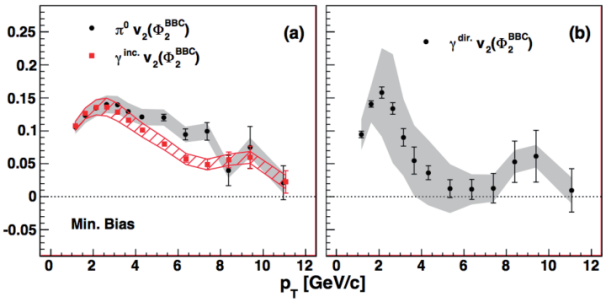

Fig. 1. (Left) v_2 as a function of p_T of a neutral pion (black) and inclusive photon (red). (Right) v_2 as a function of p_T of a direct photon[4].

There is a discrepancy called "photon puzzle". There are no models to explain both the results simultaneously. In order to constrain the photon production mechanism, the third-order azimuthal anisotropy v_3 is measured. Figure 2 shows direct photon v_3 for $p_T < 4$ GeV/c. It is found that the strength of direct photon v_3 is comparable to that of hadron v_3. It shows a similar trend to direct photon v_2. It can be interpreted that photons emitted in the late stage of collisions are dominant in the low p_T region. These results would be helpful for understanding the photon puzzle.

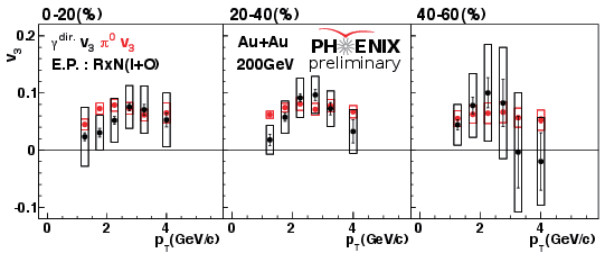

Fig. 2. v_3 as a function of p_T of a neutral pion (red) and direct photon (black) by 20% centrality steps from 0 to 60%.

*1 University of Tsukuba
*2 RIKEN Nishina Center

References
1) S.S. Adler et al.: P.R.L. 94, 232301 (2005)
2) A. Adare et al.: P.R.L. 104, 132301 (2010)
3) A. Adare et al.: arXiv:1405.3940 [nucl-ex] (2014)
4) A. Adare et al.: P.R.L. 109, 122302 (2012)

Charged hadron elliptic and triangular flow in Cu+Au at $\sqrt{s_{NN}} = 200$GeV

H.Nakagomi[*1,*2] for the PHENIX collaboration

Quark-gluon-plasma(QGP) is considered to be a hot and dense nuclear matter which is a phase of matter in quantum chromodynamics. A QGP was created by colliding nuclei at the Relativistic Heavy Ion Collider(RHIC) .

One of the strong evidence to prove the formation of QGP is that the low momentum particle production is anisotropic. Azimuthal anisotropy originates from initial spatial geometry. For low momentum particles, anisotropic collective flow is considered to result from the hydrodynamic expansion of QGP. Further the strength of azimuthal anisotropic flow has been used to determine the specific viscosity over entropy ratio(η/s) of QGP and the initial spatial condition by comparing it with the theoretical model. Thus measuring the azimuthal anisotropic flow is a good method to investigate the bulk property of QGP and the space time expansion mechanism.

The produced particle distribution is expressed as a Fourier expansion series as follows

$$\frac{dN}{d\phi} \propto 1 + \sum_{n=1} 2v_n \cos(n(\phi - \Psi_n)) \quad (1)$$

where $v_n = \langle\cos(n(\phi - \Psi_n))\rangle$ n(1,2,3,4,,,) corresponds to the strength of anisotropic flow, ϕ is the azimuthal angle of the produced particle, Ψ_n is the n_{th} order event plane that is the average of all emitted particles angles. So far the 2_{nd} order flow harmonic v_2 which is called elliptic flow has been studied in symmetric systems such as Au+Au, the 3_{rd} order flow harmonic v_3 which is called triangular flow was not predicted to exist because initial geometry was considered to be symmetric. However recently, a large v_3 was measured at RHIC. The v_3 is assumed to have originated from the initial spatial fluctuation.

In 2012, a Cu+Au collision was performed at RHIC. In Cu+Au collisions, the initial spatial geometry is asymmetric. The pressure gradient is predicted to be different for the Au and Cu sides. Thus the different expansion at the Au and Cu sides will lead to the asymmetric emission of particles. The v_n in the Cu+Au collision could help determine η/s and the initial spatial condition.

Figure 1 ilustrates the N_{part} dependence of v_2 and v_3 for three collision systems. The system size dependence of v_2 is clearly seen. The v_2 values in Cu+Au collisions are between those in Au+Au and Cu+Cu data sets and v_2 in all systems increases as N_{part} decreases, the difference of v_2 values between the different systems reduce with a decreasing N_{part}. The N_{part} dependencies of v_2 and v_3 could be expected from those of 2_{nd} and 3_{rd} order initial spatial anisotropies(ϵ_2 and ϵ_3). The ϵ_2 and ϵ_3 are calculated using a Glauber Monte Carlo simulation. Figure 2 ilustrates comparison between v_2 and v_3 as a function of p_T with event-by-event hydrodynamical calculation with η/s for 20-30 % centrality bin. In this hydrodynamical calculation, Glauber Monte Carlo simulations are employed as the initial spatial condition and $4\pi/s = 1$ or $4\pi/s = 2$ is used. The hydrodynamical calculation with $4\pi/s = 1$ has better agreement with v_2 and v_3 at low p_T than $4\pi/s = 2$, whereas at high p_T hydrodynamical calculation with $4\pi/s = 2$ has better agreement with v_2 and v_3 than $4\pi/s = 1$.

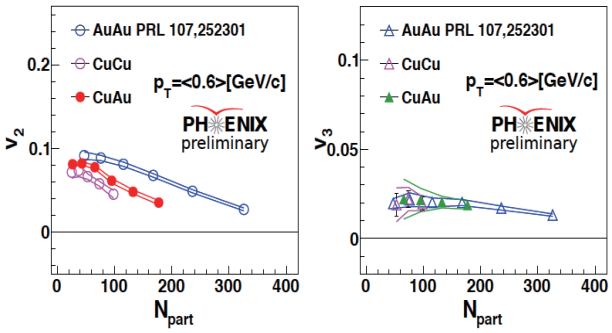

Fig. 1. Comparison of v_2 and v_3 as a function of N_{part} for four centrality bins in Au+Au, Cu+Cu and Cu+Au

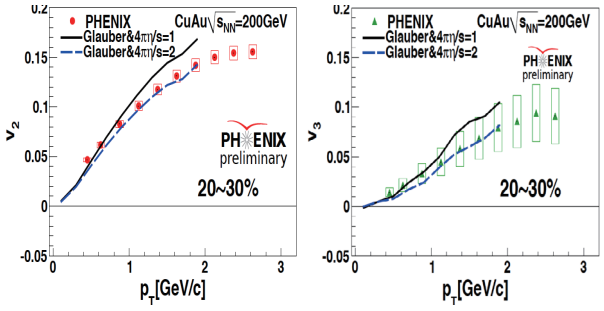

Fig. 2. v_2 and v_3 as a function of p_T for 20-30% centrality bin. Comparison of PHENIX experimental data points and hydrodynamical calculation

*1 RIKEN Nishina Center
*2 Graduate School of Pure and Applied Sciences University of Tsukuba

References

1) A. Adare et al (PHENIX Collaboration), Phys. Rev. Lett. 107 252301 (2011)
2) M. R. Haque, M. Nasim, B. Mohanty, Phys. Rev. C 84, 067901 (2011)
3) Bozek Phys. Lett. B717, 287(2012)

Commissioning and operation of silicon vertex detector for PHENIX experiment in RHIC Run-14

M. Kurosawa,[*1] Y. Akiba,[*1] H. Asano,[*2] J. Bryshawskyj,[*3] T. Hachiya,[*1] M. Lentz,[*4] B. Miljko,[*5] T. Moon,[*1] H. Nakagomi,[*6] R. Nouicer,[*4] C. Pancake,[*7] P. Stankus,[*5] T. Sumita,[*1] A. Taketani,[*1] M. Wysocki,[*5] and the PHENIX VTX group

The PHENIX experiment aims to elucidate the spin structure of nucleons and the property of the hot and dense matter at the Relativistic Heavy Ion Collider (RHIC). A silicon vertex detector (VTX) was successfully installed in 2010 as a key element in the spin and, hot and dense matter physics. The VTX comprises a four-layer barrel detector built from two inner silicon pixel detectors and two outer silicon strip detectors. As mentioned in our previous report, the silicon pixel detectors were repaired and the active area of VTX was improved from 60% to 90% before Run-14[1]. This report presents the results of the commissioning and the performance of silicon pixel detectors in Run-14.

The silicon sensor module is an assembly of a silicon pixel sensor and four readout chips bump-bonded to the sensor with soldering bumps. Most of the dead area 10% results from the defects of soldering bumps caused by a thermal stress during operation. The pixel response at the boundary between the active and the dead areas is unstable, and those pixels become noisy because they have high resistivity caused by a week electrical connection. The main tasks in the commissioning stage are the determination of the threshold level and mask of noise pixels for all readout chips for minimizing fake hits.

Figure 1 shows the threshold dependence of a hit event rate for a readout chip. The threshold is represented as a DAC value. The higher the DAC value, the lower the number of electrons. The average of the optimized threshold for all readout chips was 180, which correspons to 3,700 electrons. The average was substantially low compared with that for the 14,000 electrons of Minimum Ionizing Particle (MIP).

Pedestal data was taken with a random trigger to detect noise pixels. The location of noise pixels were determined by detecting pixels that have a high hit rate. Since the noise level is dependent on the threshold level, a threshold and noise scan were iterated several times. Figure 1 shows the plot after removing pixels that have high hit rate. Approximately 0.03% of all pixels were masked and the probability of the noise-hit per event was reduced to 10^{-5}.

Figure 2 illustrates a performance plot that shows the correlation of the z vertex between beam-beam counter (BBC) and VTX. The BBC is a Cherenkov counter and determines the z vertex with a precision of 5 mm. The position resolution of VTX is less than 80 μm at over 1 GeV/c[2]. The width of the plot depends on the resolution of the BBC.

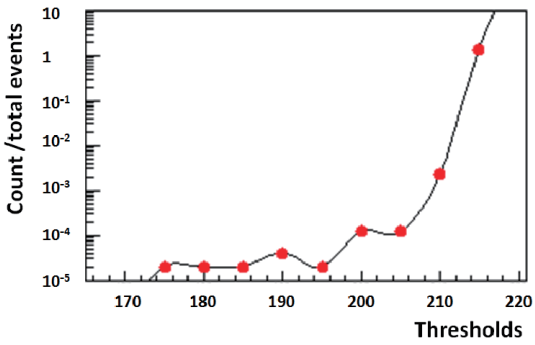

Fig. 1. Relationship between the threshold and the count/total event.

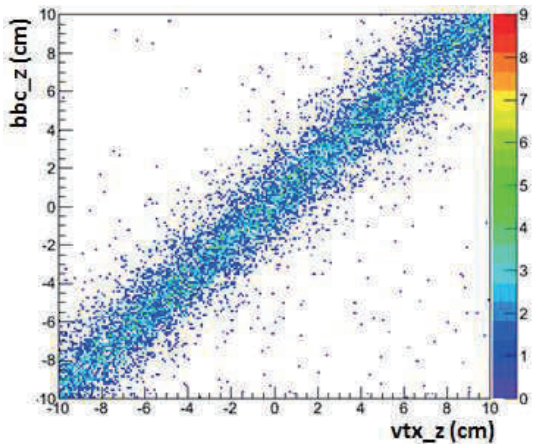

Fig. 2. Scatter plot of the z vertex position for BBC and VTX.

The 200 GeV Au+Au collision run was started in March and it ended in the middle of June. The VTX took about 20 billion events of physics data keeping the active area of 90% without any serious issues during this period.

*1 RIKEN Nishina Center
*2 Department of Physics, Kyoto Univ.
*3 Department of Physics, City Univ. of New York
*4 Brookhaven National Laboratory
*5 Oak Ridge National Laboratory
*6 Department of Physics, Tsukuba Univ.
*7 Department of Physics, Stony Brook University

References

1) M. Kurosawa et al.: RIKEN Accel. Prog. Rep. 47, 228 (2013)
2) T. Moon et al.: In this report.

Alignment of the PHENIX Silicon Vertex Tracker (VTX) in the 2014 RUN

T. Moon,[*1,*2] A. Adare,[*3] Y. Akiba,[*1] H. Asano,[*1,*4] S. Bathe,[*1] J. Bryslawskyj,[*5] T. Koblesky,[*3] T. Hachiya,[*1] M. Kurosawa,[*1] D. Mcglinchey,[*3] H. Nakagomi,[*1,*6] R. Nouicer,[*1] T. Rinn,[*7] Z. Rowan,[*5] T. Sumita,[*1] A. Taketani,[*1] and the PHENIX VTX group

During the 2014 run, PHENIX has recorded a large number (∼20B) of events with the PHENIX silicon vertex tracker (VTX)[1),2)] and the Foward VTX (FVTX) combined. This dataset is also the best quality dataset of VTX since it was installed in 2011.

The VTX is located close to the interaction point of the two incoming particles. It consists of four coaxial cylindrical layers, with radii between 2.63 and 16.69 cm, covering the pseudo-rapidity range $|\eta| < 1.2$ and azimuthal angle $\Delta\phi \sim 2\pi$. The two innermost layers consist of silicon pixel sensors, and the two outermost layers are made of silicon strip-pixel sensors.

The VTX is designed to reconstruct primary and secondary vertices with a resolution better than $100\mu m$ for $p_T > 1\mathrm{GeV}/c$ as well as to significantly improve tracking performance in conjunction with other detectors, particulary the drift chamber (DC). The VTX, thus, is necessary for charm and bottom separation, and for direct measurement of D^0 meson using a distance of closest approach (DCA) of the reconstructed track from the primary vertex position.

In reality, the actual installed detector position cannot be measured by our high-precision surveys. Thus there exists a relatively large mis-alignment that will significantly degrade the resolution of the measurement.

Alternatively, the mis-alignment can be improved through the track-to-hit based alignment via software. The ideal geometry of the VTX for pixel and strip-pixel is first known by measurements of sensor positions in surveys and the design positions, respectively. The position of (hits on) the sensor is represented in a VTX coordinate system. On the other hand, the track for the alignmemt is reconstructed by the DC in a global (DC) reference coordinate system regardless of the VTX, and it is projected to the primary vertex. The relative postion between the VTX and the DC is determined by measuring a beam center in each coordinate system and then (hits on) the sensor, and the track projection is represented in the global reference coordinate system. Residual (distance between the tracks and the measured hit on the sensor plane) is used to evaluate the mis-alignment in the VTX geometry as input for the next iteration. The mis-alignment is minimized as the residual becomes 0. This procedure is iterated until convergence is reached.

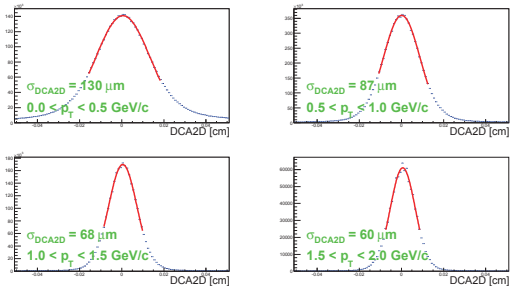

Fig. 1. DCA distributions in X-Y plane as a p_T after the alignment

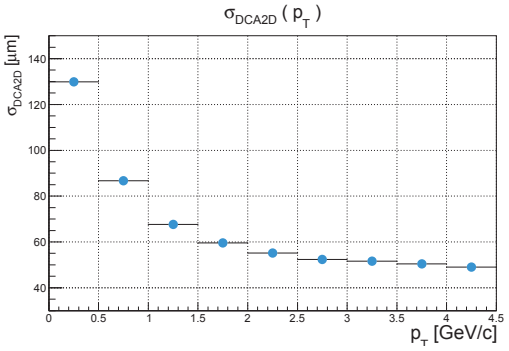

Fig. 2. Resolution of DCA in X-Y plane as a function of p_T after the alignment

The VTX alignment in the 2014 run has been successfully completed as stated above. The final results are shown in Fig. 1 and Fig. 2, which indicate DCA distributions and resolution as a function of p_T in X-Y plane after the alignment. It should be noted that deterioration of the resolution in the low p_T region ($p_T < 1\mathrm{GeV}/c$) is attributed mainly to backgrounds and multiple scattering.

We have achieved DCA resoultion of $< 70\mu m$ for $1\mathrm{GeV}/c$ of p_T, which enables precise investigation of charm and bottom physics in both the $p+p$ and Au+Au collision systems with the PHENIX detector at RHIC.

*1 RIKEN Nishina Center
*2 Department of Physics, Yonsei University
*3 Department of Physics, University of Colorado, Boulder
*4 Department of Physics, Kyoto University
*5 Department of Physics, Baruch Colleage, CUNY
*6 Department of Physics, Univ. of Tsukuba
*7 Department of Physics, Iowa State University

References

1) A. Taketani et al. [PHENIX Collaboration], Nucl. Instrum. Meth. A. **623**, 374, (2010).
2) T. Hachiya et al.: RIKEN Accel. Prog. Rep. **44**, 179 (2011).

Distance of closest approach analysis with VTX at RHIC-PHENIX

H. Asano,[*1,*2] A. Adare,[*3] Y. Akiba,[*2] S. Bathe,[*4,*2] J. Bryslawskyj,[*4] T. Hachiya,[*2] T. Koblesky,[*3] M. Kurosawa,[*2] D. McGlinchey,[*3] T. Moon,[*7,*2] H. Nakagomi,[*10,*2] R. Nouicer,[*11,*2] T. Rinn[*8] Z. Rowan,[*4] T. Sumita,[*2] A. Taketani,[*2] and the PHENIX VTX group

Heavy quark production is being studied via a PHENIX experiment by measuring of electrons from semi-leptonic decays of hadrons containing charm and bottom quarks. A large suppression and strong elliptic flow of single electron heavy flavor has been observed in Au+Au collisions at $\sqrt{s} = 200$ GeV[1]. In past measurement, PHENIX was unable to distinguish electrons from charm and bottom quarks.

In order to understand the medium effects in more detail, the Silicon Vertex Tracker (VTX) was developed and installed in year 2011 in the RHIC-PHENIX experiment. The VTX can measure charm and bottom separately using the distance of closest approach (DCA) to the primary vertex. After the preliminary result of the fraction of $b \to e/(b \to e+c \to e)$ in Au+Au collision was reported[2], we improved the DCA analysis to obtain the final result.

(i) In the high multiplicity environment, hits on the VTX can be associated with uncorrelated tracks. They are one of the main sources of background of DCA distribution. We studied the chi-square distribution of track fitting using real data and a Monte Carlo simulation. We determined the threshold of the chi-square value of tracks to reject random association candidates as much as possible. The real tracks are expected to be removed around 5% from the simulation study.

(ii) Electrons from photon conversion and Dalitz decay of neutral mesons are also the background source in the electron DCA measurement. We identify e^+, e^- pairs by VTX and removed these pairs from the DCA distribution. The tagging efficiency of the conversion and the Dalitz decay are estimated thorough the simulation. The yield of the remaining electrons and the shape of the DCA distribution from conversions and Dalitz decays are also estimated using the past measurement data[1] and the simulation.

(iii) Electrons from J/ψ and Kaon also cause small background noise. The yield of these electrons and the shape of DCA distribution are estimated using the past measurement data and the simulation.

After completing the study, we decomposed electron DCA distribution. In Fig. 1, the shape of each component is obtained through the simulation and each component is overlaid on the DCA distribution of real data. Currently, the ratio of charm and bottom quarks are based on theoretical prediction. The fraction of each DCA background (conversion, Dalitz, Kaon, J/ψ...) is obtained from (ii) and (iii). The sum of those DCA distribution values describes the shape of the electron DCA distribution in real data very well.

To obtain the precise ratio of $b \to e/(b \to e+c \to e)$ as a function of transverse momentum and momentum distribution of parent mesons (D and B mesons) from DCA measurement, an invariant yield of heavy flavor electrons and DCA distribution are being analyzed simultaneously. The results will be published soon.

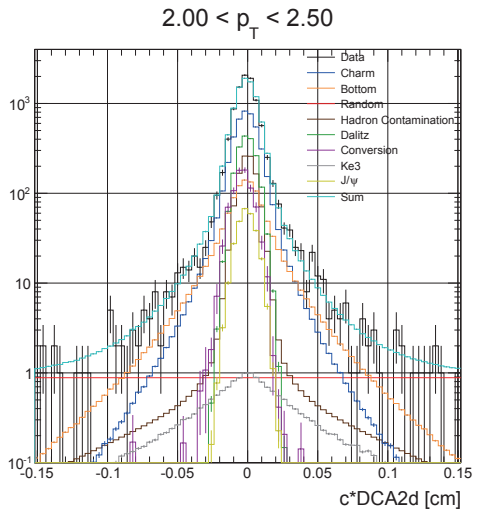

Fig. 1. Electron DCA distribution at 2.0-2.5 GeV/c. Charm (blue) and bottom (yellow) are signal. The other components are backgrounds. The sum of the signals and backgrounds (light blue) obtained through the simulation is consistent with data (black).

*1 Department of Physics, Kyoto University
*2 RIKEN Nishina Center
*3 Department of Physics, University of Colorado Boulder
*4 Department of Physics, City University of New York
*5 Department of Physics, Yonsei University
*6 Graduate School of Pure and Applied Sciences, University of Tsukuba
*7 Brookhaven National Laboratory
*8 Department of Physics and Astronomy, Iowa State University

References
1) A. Adare et al. Phys.Rev., C84:044905, (2011).
2) R. Nouicer et al. Nucl.Phys., A904-905 (2013) 647c-652c

Current status of bottom and charm measurements using VTX at RHIC-PHENIX

T. Hachiya,[*1] A. Adare,[*2] Y. Akiba,[*1] H. Asano,[*1,*3] S. Bathe,[*1,*4] J. Bryslawskeyj,[*4] T. Koblesky,[*2] M. Kurosawa,[*1] D. Mcglinchey,[*1] T. Moon,[*1,*5] H. Nakagomi,[*1,*6] R. Nouicer,[*7] T. Rinn,[*8] Z. Rowan,[*4] T. Sumita,[*1] and A. Taketani[*1]

One of the most noteworthy results at RHIC was the strong suppression of inclusive open heavy quarks (bottoms and charms) at high p_T in central Au+Au collisions[1]. It was expected that heavy quarks would be less suppressed due to their large mass. However, the results showed that the suppression was comparably strong with pions. In order to study the suppression in detail, we developed a silicon vertex tracker (VTX) at PHENIX. VTX can measure bottom and charm separately using the distance of closest approach (DCA) to the primary vertex.

We reported the preliminary result of the fraction of $(b \to e)/(b \to e + c \to e)$ using VTX in Au+Au collisions[2]. Numerous improvements of the analysis for the final result are underway. Here, we have listed a few of these improvements:

(1) Rejecting photon conversions and Dalitz decays:
Photon conversions and Dalitz decays of light neutral mesons are the main background sources in single electron measurement. Electron pairs from the backgrounds are generated with small opening angles and the pair makes correlated hits in VTX. Therefore, VTX can significantly reject the backgrounds by requiring pair-wise hits in VTX. On the other hand, heavy flavor electrons ($b \to e$ and $c \to e$) rarely make the correlated hits. Figure 1 shows the fraction of heavy flavor electrons to inclusive electrons. The open and closed circles correspond to the result before and after VTX installation, respectively. This plot indicates that VTX could reject the background effectively and provide a good signal to noise ratio.

(2) Unfolding of DCA distribution:
We developed an unfolding method to decompose bottom and charm contributions[3]. The method is a Bayesian approach using the Markov chain Monte Carlo sampler[4]. Using this method, the bottom and charm yields are obtained by fitting both the DCA and the p_T distribution of heavy flavor electrons simultaneously. The DCA shape is correlated with the p_T distribution of the parent B and D mesons because the DCA is determined by the convolution of two effects: the decay length of the parent particle and the decay p_T kick relative to the parent momentum. As a consistency test, we verified if the known input can be reproduced using a simulation[3].

(3) Detector efficiency:
The detector efficiency was determined by full GEANT simulation with the actual dead map. The raw p_T spectrum of heavy flavor electrons was corrected using the efficiency, and the corrected spectrum is consistent with the published data[5]

(4) DCA smearing by random association
The DCA shape is smeared and modified by the random association of electron tracks with VTX. The smearing effect was studied by embedding simulated electron tracks into real events. Then, we found that the unphysically large DCA tail in the data was explained by the smearing effect.

The current analysis of Au+Au data will be completed for publication soon. We took 20 billion Au+Au data in year 2014, which is 20 times larger statistics. This new dataset will be analyzed. The alignment calibration of the dataset was completed[6] and the data production was started.

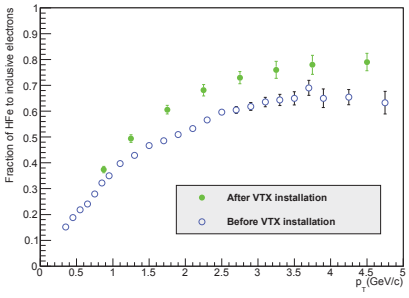

Fig. 1. Fraction of heavy flavor electrons to inclusive electrons before (closed) and after (open) the VTX installation.

*1 RIKEN Nishina Center
*2 Department of Physics, University of Colorado, Boulder
*3 Department of Physics, Kyoto University
*4 Department of Natural Science, Baruch College, CUNY
*5 Department of Physics, Yonsei University
*6 Department of Physics, University of Tsukuba
*7 Brookhaven National Laboratory
*8 Department of Physics, Iowa State University

References

1) A. Adare et al: Phy. Rev. Lett. **98**, 172301 (2007).
2) R. Akimoto et al.: RIKEN Accel. Prog. Rep. 46, 60 (2013).
3) A. Adare et al.: Quark Matter 2014 poster.
4) G. Choudalakis.: arXiv:1201.4612v4
5) H. Asano at al.: In this report.
6) T. Moon at al.: In this report.

Development of the FVTX high multiplicity trigger system for the PHENIX experiment

T. Nagashima,[*1,*2] Y. Fukushima,[*1,*2] S. Hasegawa,[*3] I. Nakagawa,[*1] W. Saito,[*1,*2]
and the PHENIX FVTX group

Protons and neutrons, which are the components of familiar substances, are composed of quarks and gluons that bind quarks together. Immediately following the big bang, under extremely high-density and high-temperature conditions, quarks and gluons are considered to escape from the boundary of nucleons. This liquid-like state is called Quark Gluon Plasma (QGP).

The PHENIX group investigates the behavior of matter in such a high-density and high-temperature state produced by collision using Relativistic Heavy Ion Collider (RHIC). In particular, in Au+Au and Pb+Pb collisions, the particle angular correlation exhibits a similar azimuthal pattern throughout the wide range of the rapidity region, referred to as "ridge." The ridge correlation is considered as a consequence of the hydrodynamic flow of products, and it is interpreted as a characteristic of QGP. Certain experiments at the LHC have recently reported that the ridge was observed especially in high-multiplicity events in small colliding systems, such as p+p.[1)] Similar ridge phenomena were observed in d+Au and He3+Au at RHIC. However, they have not yet been observed in p+p.

Previous experiments demonstrated high-multiplicity events are the key to observe the ridge in p+p collisions. In PHENIX, the Forward Silicon Vertex Detector (FVTX) is suitable to select such high-multiplicity events since it is the tracker closest to the vertex point. The FVTX trigger design is shown in Fig. 1. The trigger signal is generated on FPGAs implemented on FVTX readout electronics,[2)] Front End Module (FEM) and FEM Interface Board (FEM-IB). Using the feature that each FEM corresponds to an azimuthal slice of the FVTX sensor, each FEM judges whether there is any track, following which the FEM-IB counts the number of track flag sent from the FEM, and finally the FVTX trigger fires when the number of track is greater than that of our interest.

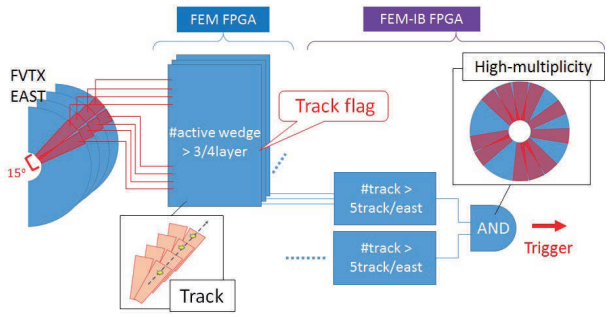

Fig. 1. FVTX trigger design based on the FPGA logic implemented on the readout electronics

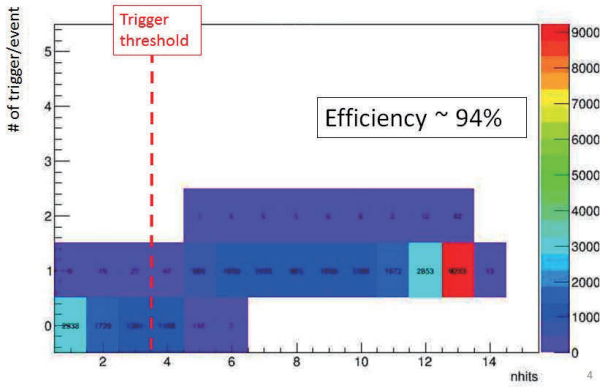

Fig. 2. Correlation between the number of hits and the trigger state

The trigger algorithm in the FEM FPGA was tested through evaluation of the process efficiency depending on the number of hits on the detector. The hits were generated by using a calibration pulse that injects typically 13 strips per detector per event. Fig. 2 shows the correlation between the number of hits per event measured from offline data analysis and the trigger state; the vertical axis shows the trigger flag at an FEM that is supposed to give 1 for the events where the number of hits is greater than the threshold. The efficiency, defined as the number of trigger events divided by the number of events with more hits than the trigger threshold, was 94%, and a few fake triggers were observed.

New serial line cables for FEM - FEM-IB communication were installed in the trigger system, and their signal transmission test was performed. Performance was monitored by scanning the signal rate, and the cables exhibited good performance up to a trigger rate of 4.7 MHz. The timing of the trigger signal was tuned with GL1. It was found that GL1 does not recognize the trigger signal depending on timing. It is adjusted using the BBC trigger signal, which is already used as a trigger.

*1 RIKEN Nishina Center
*2 Department of Physics, Rikkyo University
*3 J-Parc

References

1) V. Khachatryan et al.: CMS Collaboration, JHEP 1009 (2010) 091
2) arXiv:1311.3594v2 [physics.ins-det] 14 Feb. 2014

Study of direct photon polarization to shed on strong magnetic field in heavy ion collisions at PHENIX†

T. Hoshino*1,*2

A strong magnetic field is expected to be created in non-central heavy-ion collisions. This field is created by the effect of both of the collision participants and spectators. The field direction is perpendicular to the collision reaction plane. The magnitude of the field created in the collisions at BNL-RHIC top energy is estimated to reach as high as 10^{14} teslas. If the magnitude of the magnetic field in heavy-ion collisions is compared with the QED critical magnetic field ($B_c = m_e^2/e = 4\times10^9$ teslas) and the surface of magnetars (10^{11} teslas), the field magnitude is much higher in heavy ion collisions. The field magnitude is decreased rapidly but keeps the magnitude above the critical field of an electron for about 3 fm/c.

Creation of a strong magnetic field in heavy ion collisions was first expected in 1976[1]. The strong magnetic field in heavy ion collisions has recently attracted the interest of researchers in theories and experiments in recent years for the following reasons. First, the magnetic field can reach beyond the critical field and interesting phenomena such as Chiral magnetic effects and non-linear QED effects can appear in such a strong field. Second, quark-gluon plasma (QGP) is expected to be created in a strong magnetic field thus the evolution of the plasma may have an effect by the strong magnetic field. The state of the initial stage is another topic of recent interest. Measuring the effect of the field should be the key to understanding the initial stage.

Chiral magnetic effect is measured by experiments using charged particle asymmetry with respect to the reaction plane which is reported by STAR and ALICE experiments[2)3)]. However the field has not yet been directly detected by experiments. If the effects of the magnetic field can be detected, we can directly access to the initial stage of collisions. Electro-magnetic particles are a clean probe for accessing the initial stage because they are not affected by the strong interaction.

Dilepton production rate in an external magnetic field is calculated using a photon vacuum polarization tensor, and the production rate depends on the direction of the field. The production rate is higher in perpendicular direction to the field than that parallel to the field.

Dilepton polarization is also measured to understand the production mechanism of quarkonia. The PHENIX experiment measured J/ψ polarization with dielectron [4)]. While the physics motivation and mechanism are different between the measurement of quarkonia and virtual photon polarization, we are now using the same parametrization with that analysis.

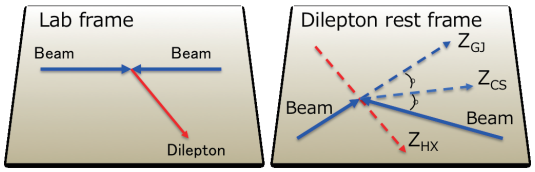

Fig. 1. Definitions of polarization axis

$$\frac{dN}{d\cos(\theta)} \propto 1 + \lambda\cos(\theta) \tag{1}$$

where θ is the angle between the positive lepton in a dilepton rest frame and a certain polarization axis, and λ is the polarization parameter; if λ is positive (negative), polarization is transverse (longitudinal).

Three definitions of polarization frames are usually used. In the helicity (HX) frame, the axis is the dilepton momentum in the laboratory frame. In the Collins-Soper (CS) frame, the axis is the bisector between two beams in the dilepton rest frame. In the Gottfried-Jackson (GJ) frame, the axis is the direction of the beam in the dilepton rest frame.

We use the data set of Au+Au and p+p at 200 GeV/nucleon pair collected in 2004 and 2006, respectively. The PHENIX experiment has excellent electron identification capabilities and has succeeded in measurement of direct virtual photons.

The direct virtual photon is the probe and π^0 and η Dalitz decay electrons are candidates of control probes because they are from a later stage of the collisions. Polarization measurement in $p+p$ collisions can also act as a control probe since a field is not created in the collisions.

We are measuring polarization with the following mass regions, $0.12 < M_{ee} < 0.3$ (containing virtual photon) and $M_{ee} < 0.12$ GeV/c^2 (π^0 Dalitz decay dominant). The acceptance effect is included in the $\cos(\theta)$ distribution. Thus we need to correct the effect with simulation. Since the simulation does not contain the effect of the magnetic field, we can estimate the effect. We are now estimating the acceptance effect with single particle simulations.

*1 RIKEN Nishina Center
*2 Department of Physical Science, Hiroshima University

References
1) B.Muller et al.: Phys. Rev. Lett. 36, 517 (1976)
2) B. I. Abelev et al., Phy. Rev. Lett. 103, 251601 (2009)
3) B. Avelev et at., Phys. Rev. Lett. 110, 012301 (2013)
4) A. Adare et. al., Phys. Rev. D 82, 012001 (2010)

Measurement of dielectron production in $\sqrt{s_{NN}} = 5.02$ TeV p-Pb collisions by using the ALICE detector

S. Hayashi,[*1,*2] H. Hamagaki,[*2] and T. Gunji[*2]

Heavy quark (charm and bottom quarks) measurements in heavy ion collisions provide key information on the properties of the deconfined matter, the quark gluon plasma (QGP). Since heavy quarks are produced via gluon fusion, gluon splitting, and flavor excitation, cold nuclear matter effects (CNM) cannot be negligible[1]. In p-Pb collisions at the Large Hadron Collider (LHC), correlations between electrons from heavy flavor decays and charged hadrons in p-Pb collisions show the correlations in rapidity space, which may be due to the gluon saturation or collective expansion of the system[2]. In the electron-positron pair (dielectron) mass spectrum, dielectrons from semi-leptonic decays of heavy quarks are dominant at $m_{ee} > 1$ GeV/c^2 and can be affected by CNM effects. The Transition Radiation Detector (TRD) in ALICE provides online electron trigger[3]. ALICE recorded 1.4 nb^{-1} with the TRD trigger in p-Pb collisions in 2012-2013, which is 20 times larger statistics than the minimum bias data (0.067nb^{-1}).

In the ALICE detector, charged tracks are reconstructed by the Inner Tracking System (ITS) and the Time Projection Chamber (TPC)[4]. Electrons are identified by dE/dx in the TPC and hadrons are rejected by a time-of-flight (ToF) detector. To extract the raw dielectron spectrum, the background is estimated using the same event like-sign pairs corrected by the relative acceptance difference between unlike-sign and like-sign pairs, which is evaluated using an event-mixing technique[5]. Pair acceptance and detection efficiency are evaluated with the fast Monte Carlo simulation. First, the single electron efficiency is obtained from the full Monte Carlo calculation using the DPMJET event generator and GEANT3 simulations. Pair efficiency is extracted by the product of the single electron efficiency. Dielectrons from light meson decays ($\pi^0, \eta, \rho, \omega, \eta^{'}, \phi$) are generated from EXODUS according to the measured charged pion spectrum in p-Pb collisions and m_T scaling. For heavy quarks contribution, dielectrons are generated using PYTHIA with the parametrization tuned for the NLO calculation[6]. Figure 1 shows the pair efficiency as a function of invariant mass, where circles and boxes correspond to the pair reconstruction efficiency and TRD trigger efficiency for pairs, respectively. The single electron trigger efficiency is calculated as the number of triggered electrons divided by the number of minimum bias electron samples. TRD trigger efficiency for pairs is extracted according to Eq 1 .

$$\epsilon_{trig}^{pair}(m_{ee}, p_T^{ee}) = 1-[1-\epsilon_{trig}^{single}(p_{T_1})][1-\epsilon_{trig}^{single}(p_{T_2})] \quad (1)$$

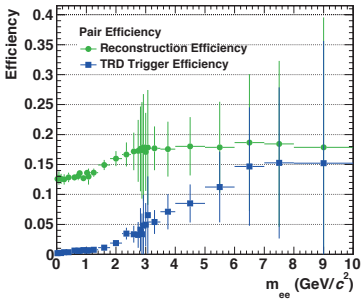

Fig. 1. p_T integrated pair efficiency as a function of invariant mass. Circles and boxes correspond to the pair reconstruction efficiency and TRD trigger efficiency for pairs, respectively.

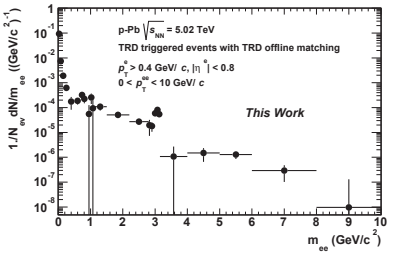

Fig. 2. Corrected dielectron yield per inelastic p-Pb collision as a function of invariant mass.

Figure 2 shows the inclusive invariant yield of dielectrons as a function of invariant mass. The next step is to take into account the azimuthal angle and rapidity dependence of the single electron efficiency in the pair and trigger efficiency calculations. After the invariant yield is extracted, $c\bar{c}$ and $b\bar{b}$ cross-sections will be extracted and compared with the theoretical models to understand the dielectron production in p-Pb collisions.

References

1) H. Fujii, K. Watanabe, NPA 920, 78-93 (2013).
2) E. Pereira de Oliveira Filho, arXiv:1404.3983v2 (2013) NPA in press..
3) J. Klein, NIMA 706 23-28 (2013).
4) F. Carminati *et al.*, J. Phys. G: Nucl. Part. Phys. 30 1517 1763 (2004).
5) S. Hayashi *et al.*, CNS Ann. Rep., 2012 (2014)
6) M. Mangano, *et al.*, Nucl. Phys. B373, 295 (1992)

*1 RIKEN Nishina Center
*2 Center for Nuclear Study, Graduate School of Science, the University of Tokyo

Measurement of neutral pion v_2 in Pb-Pb collisions at $\sqrt{s_{NN}} = 2.76$ TeV by the ALICE experiment

T. Tsuji,[*1,*2] H. Hamagaki,[*2] T. Gunji,[*2] for the ALICE collaboration

In central Pb-Pb collisions at $\sqrt{s_{NN}} = 2.76$ TeV at the Large Hadron Collider (LHC) in CERN, the yield of particles at high transverse momentum (p_T) is observed to be strongly suppressed as compared with the expected yield from p+p collisions scaled by the average number of the binary collisions. This suppression is explained by the energy loss of hard scattered partons in the medium created in heavy ion collisions. This suppression is called jet quenching. This suppression is quantified by the nuclear modification factor (R_{AA}), which is the ratio of the yield in Pb-Pb collisions to the yield in p-p collisions scaled by the nuclear thickness function $\langle T_{AA} \rangle$ as follows:

$$R_{AA}(p_T) = \frac{1}{< T_{AA} >} \frac{d^2N_{AA}/dp_T dy}{d^2\sigma_{pp}/dp_T dy}.$$

$R_{AA}(p_T)$ is well described by many models that employ different approaches for the calculation of parton energy loss. For a better understanding of the energy loss mechanisms, measurement of the path length dependence of the energy loss is crucial.[1] Since the path length is highly correlated with the azimuthal angle with respect to the reaction plane ($\Delta\phi$), R_{AA} is measured as a function of ($\Delta\phi$).

The $R_{AA}(p_T, cent, \Delta\phi)$ is expressed as

$$R_{AA}(p_T, cent, \Delta\phi) = F(\Delta\phi, p_T) \cdot R_{AA}(p_T, cent),$$

where $F(\Delta\phi, p_T)$ is the ratio of the relative yield as given by

$$F(\Delta\phi, p_T) = \frac{N(\Delta\phi, p_T)}{\int d\phi N(\Delta\phi, p_T)},$$

and $N(\Delta\phi, p_T)$ can be expressed in terms of a Fourier expansion with $\Delta\phi$.

$$N(\Delta\phi, p_T) \propto 1 + 2\sum_{n=1}^{\inf}(v_n \cos(n\Delta\phi)),$$

where v_n is the magnitude of the n-th order harmonic. The second harmonic, v_2, represents the strength of elliptic azimuthal anisotropy. Since high p_T particles are dominated by the jet fragmentation, the v_2 of jets is induced by the path length dependence of the energy loss.

The v_2 is obtained by fitting the azimuthal angular distribution of π^0 with

$$N(\Delta\phi, p_T) = N(1 + 2v_2 \cos(2\Delta\phi)).$$

*1 RIKEN Nishina Center
*2 Center for Nuclear Study, Graduate School of Science, University of Tokyo

π^0's are identified by the invariant mass between two photons with a Photon Spectrometer (PHOS).[2] Figure 1 shows the v_2 of π^0 values as a function of

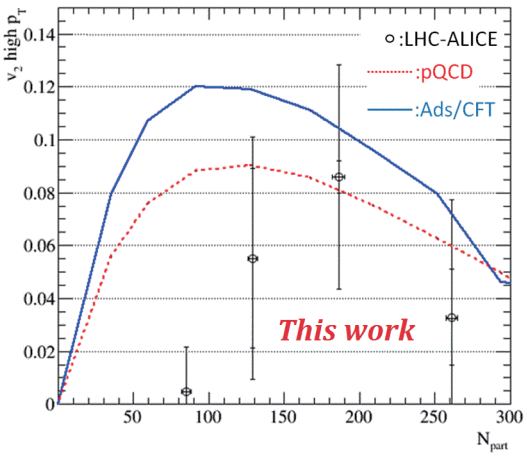

Fig. 1. v_2 of π^0 values as a function of N_{part}. The data points represent v_2 of π^0 measured by the LHC-ALICE experiment. Solid and dashed lines indicate model calculations using pQCD and Ads/CFT, respectively.

N_{part} at 6 GeV $< p_T <$ 20 GeV. The analysis is performed by using semi-central triggered data recorded in 2011 Pb-Pb collisions. Solid and dashed lines represent model calculations from pQCD-based (weakly coupled medium) and AdS/CFT-based (strongly coupled medium) energy loss models, respectively. In this plot, the v_2 of π^0 values shows the same tendency as the v_2 values of the charged particles qualitatively.[3] Comparison of the model calculations and experimental results for v_2 of π^0 is currently in progress.

References

1) A. Majumber: J. Phys. G. Nucl. Part. Phys. 34, S377 (2007).
2) K. Aamodt et al., for the ALICE Collaboration: JINST 3, S08002 (2008).
3) B. Abelev et al., for the ALICE Collaboration: Phys. Lett. B719, 18-28 (2013).

Long-range correlation in p-Pb collisions at $\sqrt{s_{NN}}$=5.02 TeV with the ALICE detector

Y. Sekiguchi,[*1,*2] H. Hamagaki,[*2] and T. Gunji[*2]

Measuring of the correlations in particle production in the azimuthal angular space and rapidity space is very useful for investigating the underlying mechanism and dynamics of particle production in high-energy nucleus-nucleus collisions. The long-range correlations in the rapidity space in near-side angular pairs in dihadron correlations was first observed in Au-Au collisions at $\sqrt{s_{NN}}$= 200 GeV at RHIC.[1,2] This long-range correlation was derived from the collective expansion of the initial geometry fluctuations. Unexpectedly, a similar structure has also been observed in high-multiplicity p-p collisions at $\sqrt{s}$=7 TeV with the LHC-CMS experiment.[3] The high-density gluon fields in a small x of nucleus and the collision of two high-density gluon sheets can explain the long-range correlation.[4] It is very interesting to study the correlation in p-Pb collisions since the initial gluon density and magnitude of the collective expansion are very different from those in other collision systems (pp and Pb-Pb).

A Large Ion Collider Experiment (ALICE) is dedicated to understand the state of matter as it existed shortly after the Big Bang, called Quark Gluon Plasma (QGP). The main subsystems in the ALICE for the study are the inner tracking system (ITS), time projection chamber (TPC), and time of flight (TOF). The ITS consists of 6 layers of silicon detectors for vertex finding and tracking. The TPC is the main tracking detector and is used for particle identification by measuring the specific energy loss dE/dx. The TOF is used to identify particles by measuring the time of flight. They have a common acceptance $|\eta|$ <0.9.

The correlation function as a function of $\Delta\eta$ and $\Delta\phi$ between two charged particles is defined as:

$$\frac{1}{N_{trig}}\frac{d^2N_{asso}}{d\Delta\eta d\Delta\phi} = \frac{S(\Delta\eta,\Delta\phi)}{B(\Delta\eta,\Delta\phi)} \quad (1)$$

where this correlation function is studied for different p_T intervals and different event classes according to the event multiplicity, and N_{trig} is the total number of triggered particles in the event class and $p_{T,trig}$ interval. The signal distribution $S(\Delta\eta,\Delta\phi) = 1/N_{trig}d^2N_{same}/d\Delta\eta d\Delta\phi$ is the associated yield per trigger particle for particle pairs from the same event. The background distribution $B(\Delta\eta,\Delta\phi) = \alpha 1/N_{trig}d^2N_{mixed}/d\Delta\eta d\Delta\phi$ corrects for pair acceptance, pair efficiency, and uncorrelated pairs. It is constructed by correlating the trigger particle in one event with the associated particles from other events in the same event multiplicity class. The α factor is chosen so that it is unity for pairs at $(\Delta\eta,\Delta\phi) = (0,0)$. The correlation function in peripheral collisions (low-multiplicity event class) is subtracted from that in central collisions (high-multiplicity event class) to remove the auto-correlations from jets. Figure 1 shows the associated yield per trigger particle in 0-20% event class subtracted by 60-100% event class with 1<$p_{T,trig}$, $p_{T,asso}$ <2 GeV. The projection onto $\Delta\phi$ averaged over 0.8< $|\Delta\eta|$ <1.6 on the near side and $|\eta|$ <1.6 on the away side is shown in Fig. 2. The double ridge structure is observed.

Measurements of the correlation functions by tagging identified hadrons and strange baryons are ongoing to evaluate the collectivity in p-Pb collisions and the initial state effects.

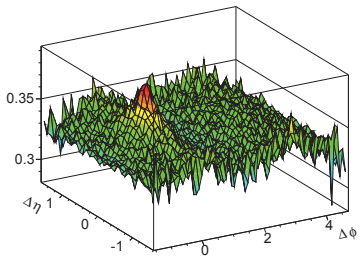

Fig. 1. Associated yield per trigger partile in 0-20% event class subtracted by 60-100% event class with 1<$p_{T,trig}$, $p_{T,asso}$ <2 GeV

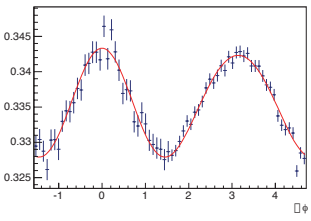

Fig. 2. Projection onto $\Delta\eta$ averaged over 0.8< $|\eta|$ <1.6 on the near side and $|\eta|$ < 1.6 on the away side

*1 RIKEN Nishina Center
*2 Center for Nuclear Study, the University of Tokyo

References

1) STAR Collaboration, Phys. Rev. C80 (2009) 064912
2) PHOBOS Collaboration, Phys. Rev. Lett. 104 (2010) 062301
3) CMS Collaboration, JHEP 09 (2010) 091
4) K. Duslingand and R. Venugopalan, Phys, Rev, D 87 (2013) 054014

Azimuthal distributions of jets with respect to high-p_T neutral pion triggers in pp collisions at $\sqrt{s}$ = 7 TeV and PbPb collisions at $\sqrt{s_{NN}}$ = 2.76 TeV from ALICE

D. Watanabe[*1,*2] and T.Chujo[*2]

Jet measurements play a critical role in probing the hot and high energy density matter created in heavy ion collisions. Energy loss of patrons can be studied by measuring changes in the jet structure during jet suppression.

In general, the energy loss of recoil jets and leading jets depends on the path length in the medium. For example, jet pairs with a large energy asymmetry in the final states can be from the surface of the medium. While leading jets escape the medium from the surface, recoil jets traverse in the medium with loss to its energy. We can use this surface bias to obtain deeper insight into the properties of the medium. The stronger the surface bias, the greater is the path length in the dense medium of the recoiling jet at the opposite azimuth. By measuring the full jets in the recoil side rather than measuring high-p_T leading hadrons, we can perform a more comprehensive and direct study of jet interactions with the medium.[1)]

In this paper, we report the jet azimuthal distribution with neutral pion trigger in pp collisions at $\sqrt{s}$ = 7 TeV and PbPb collisions at $\sqrt{s_{NN}}$ = 2.76 TeV from LHC-ALICE. The ALICE detector was built to exploit the unique physics potential of nucleus-nucleus interactions at the LHC.[2)] This analysis used the central tracking devices, ITS and TPC, for charged particle track measurements, and the electromagnetic calorimeter EMCal for π^0 measurements.

This analysis used the shower shape and cluster splitting method[3)] to identify high p_T π^0. Using this method, high p_T π^0 around 40 GeV/c can be identified with a signal-to-noise ratio of 90 %.

Jets are reconstructed with the anti-k_T jet algorithm of the FastJet[4)] package combining charged tracks measured in the central tracking devices and a cone size parameter of R = 0.4. The contribution of underlying events is subtracted from the reconstructed jets using the average background momentum method.

Figure.1 and 2 show the azimuthal correlation between trigger π^0 and jet in pp and PbPb collisions, respectively, with three different trigger π^0 regions and two different associated jet p_T thresholds. Two clear jet peaks are observed, indicating that high p_T production is corelated with jet production. Both near and away-side widths decrease with increasing p_T of the trigger π^0. The decrease is stronger for the away-side correlation width. As the next step, we plan to study the path length dependence by selecting different trigger $\pi^0 p_T$ in the ratio of the per-trigger yield (I_{AA}).

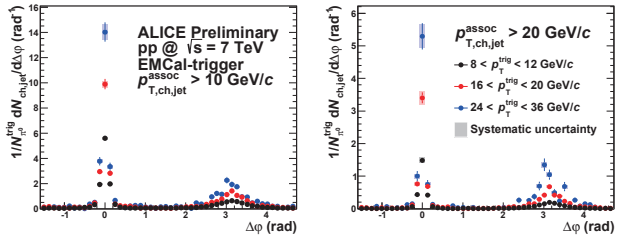

Fig. 1. π^0-jet azimuthal correlations in pp collisions at $\sqrt{s}$ = 7 TeV normalized by number of trigger π^0 for trigger π^0 regions $8 < p_T^{trig} < 12$ GeV/c, $16 < p_T^{trig} < 20$ GeV/c, $24 < p_T^{trig} < 36$ GeV/c, and associated jet thresholds $p_T^{asso} > 10$, 20 GeV/c

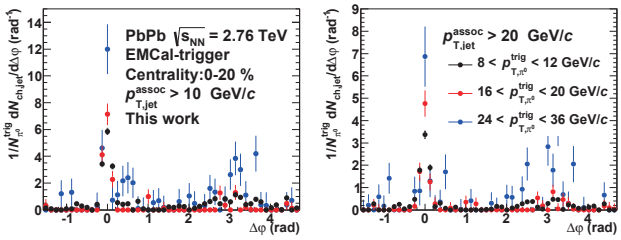

Fig. 2. π^0-jet azimuthal correlations in PbPb collsions at $\sqrt{s_{NN}}$ = 2.76 TeV normalized by number of trigger π^0. Trigger $\pi^0 p_T$ regions and associated jet p_T thresholds are same as Fig.1.

*1 RIKEN Nishina Center
*2 University of Tsukuba

References

1) ALICE collaboration, An Addendum to the EMCal Technical Design Report (DCAL), CERN-LHCC-2010-011
2) ALICE collaboration, Performance of the ALICE Experiment at the CERN LHC, arXiv:1402.4476v2
3) ALICE collaboration, X. ZHU, Analysis of the π^0-Charged Hadron Correlations Using ALICE EMCAL, https://indico.cern.ch/event/181055/session/37/contribution/451
4) M. Cacciari, G. P. Salam, G. Soyez et al.: CERN-PH-TH/2011-297

Study of ion backflow with 2GEMs + MICROMEGAS for the ALICE-TPC upgrade

K. Terasaki,[*1,*2] H. Hamagaki,[*2] and T. Gunji[*2]

ALICE is a dedicated experiment to study Quark Gluon Plasma (QGP), a hot and dense Quantum chromodynamics (QCD) medium, via heavy ion collisions at LHC. The ALICE Time Projection Chamber (ALICE-TPC),[1] which is the main device in the central barrel for tracking and particle identification of charged particles, consists of a 90 m^3 cylinder filled with $Ne/CO_2/N_2$ (90/10/5).

Secondary ions generated in an electron-avalanche process in the TPC return to the drift space, known as "Ion Backflow (IBF)." Because IBF distorts the electric field in the drift space, its reduction is essential to achieve good performance of the TPC. A gating grid system is widely employed to reduce IBF; however, it limits the data acquisition rate to the order of kilohertz. The rate of heavy-ion collisions at the LHC will be 50 kHz from 2019. The ALICE-TPC will be upgraded to read out the data of Pb-Pb collisions continuously, which requires IBF and energy resolution for ^{55}Fe to be less than 1.0% and 12%, respectively, at a gain of 2000 for Ne-based gas mixtures.[2]

The performance of quadruple GEM stacks as a readout chamber is being investigated for this upgrade. In addition, investigations with 2GEMs + MICROMEGAS are being carried out. The MICRO-MEsh-GAeous Structure (MICROMEGAS)[3] has a micromesh $\sim$ 100 μm above a readout. Electrons are multiplied through application of a potential difference between the mesh and the readout ($\Delta V_{\rm MM}$). Secondary ions are absorbed efficiently on the mesh when the electric field above the mesh is considerably smaller (by a factor of 100) than that below the mesh.

A schematic of the measurement setup with 2GEMs + MICROMEGAS is shown in Fig. 1. Our MICROMEGAS has a 400 LPI (Lines Per Inch) mesh located 128 μm above 120 readout pads (8×10 mm^2) and the current from all the readout pads is summed up. Two 50 μm-thick GEMs are placed above MICROMEGAS. IBF is defined as $I_{\rm c}/I_{\rm a}$, where $I_{\rm c}$ and $I_{\rm a}$ are the current at the cathode plane and that at the anode pads, respectively. Gain is calculated as $I_{\rm a}/(N_{\rm seed} \times R \times e)$, where $N_{\rm seed}$, R, and e are the number of seed electrons for ^{55}Fe in Ne gas, the rate of X-ray from ^{55}Fe, and the charge of an electron, respectively.

The correlation between energy resolution and IBF for Ne/CO_2 (90/10) and $Ne/CO_2/N_2$ (90/10/5) with different voltage setups is shown in Fig. 2. Different

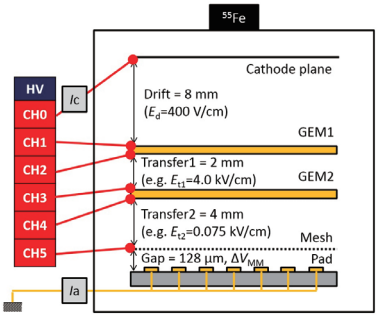

Fig. 1. A schematic of measurement setup with 2GEMs + MICROMEGAS.

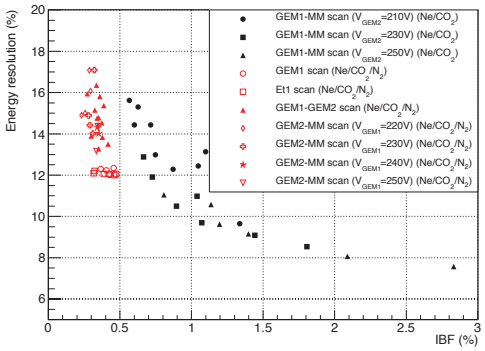

Fig. 2. Energy resolution as a function of IBF for Ne/CO_2 (black) and $Ne/CO_2/N_2$ (red).

measurements are indicated by different markers; for example, the GEM1-MM scan represents the points corresponding to variations of both $\Delta V_{\rm GEM1}$ and $\Delta V_{\rm MM}$ to maintain the gain of 2000. It shows that certain points meet the requirement for Ne/CO_2 (90/10) and IBF is less than 0.5% at an energy resolution of $\sim$ 12% for $Ne/CO_2/N_2$ (90/10/5). Additional nitrogen leads to better IBF because a larger potential difference is required to achieve the gain of 2000 and subsequently the field ratio of MICROMEGAS decreases. The evaluation for $Ne/CO_2/N_2$ (90/10/5) at a better energy resolution (and worse IBF) is in progress. Eventually, the performance of a MICROMEGAS that has a 780 LPI micromesh and 90 μm gap will be evaluated.

*1 RIKEN Nishina Center
*2 Center for Nuclear Study, Graduate School of Science, University of Tokyo

References

1) CERN-LHCC-2000-001 (2000).
2) CERN-LHCC-2013-020 (2013).
3) Y. Giomataris et al.: Nucl. Instr. and Meth. **A 376**, 29 (1996).

Search for dark photons from neutral meson decays in $p+p$ and d+Au collisions at $\sqrt{s_{NN}}$=200 GeV†

Y. Akiba*1 and Y. Yamaguchi*2,*3 for PHENIX Collaboration

The standard model (SM) of particle physics provides unprecedented numerical accuracy for quantities such as the anomalous magnetic moment of the electron $(g-2)_e$. Hence, measurements that lie outside SM predictions warrant a special investigation. One such result is the measured value of $(g-2)_\mu$, which deviates from SM calculations by 3.6σ. An intriguing explanation for this discrepancy has been proposed by adding a "dark photon"[1]. This possibility has recently gained more relevance because it provides a simultaneous explanation of various beyond-the-standard-model phenomena in addition to $(g-2)_\mu$. These includes the positron excess observed by PAMELLA, FERMI, and AMS-2 satellite experiments.

A simple formulation of the dark sector postulates a "dark photon" U of mass m_U that mixes with the QED photon via the "kinetic coupling" term in the Lagrangian

$$\mathcal{L}_{\rm mix} = -\frac{\varepsilon}{2} F^{\rm QED}_{\mu\nu} F^{\mu\nu}_{\rm dark},$$

where ε parameterizes the mixing strength. Dark photons can then mix with the QED photon through all processes that involves QED photons.

The PHENIX experiment searched for possible decays of π^0, $\eta \to \gamma U$, $U \to e^+e^-$ by examining the invariant mass m_{ee} of e^+e^- pairs in a large sample of Dalitz decays, $\pi^0, \eta \to \gamma e^+e^-$ for $30 < m_U < 90$ MeV/c^2 in the dark photon parameter space. The weak coupling of the dark photon with the QED photon implies that the natural width of the dark photon is very narrow. Thus if the dark photon mass is in this range, a clear dark photon signal should appear as a narrow peak in the e^+e^- mass spectrum.

We used the data set of $p+p$ collisions in the 2006 and 2009 runs and d+Au collisions in the 2008 run, at $\sqrt{s_{NN}} = 200$ GeV, but did not find any significant signal. Thus, we set the upper limit on the mixing parameter ε^2 as a function of the dark photon mass m_U.

Fig.1 shows the limits determined by the PHENIX along with the 90% confidence level (CL) limits from other experiments and the 2σ upper limit theoretically calculated from $(g-2)_e$. The band indicates the range of parameters that would allow the dark photon to explain the $(g-2)_\mu$ anomalies with 90% CL. The PHENIX experiment limits exclude the values of

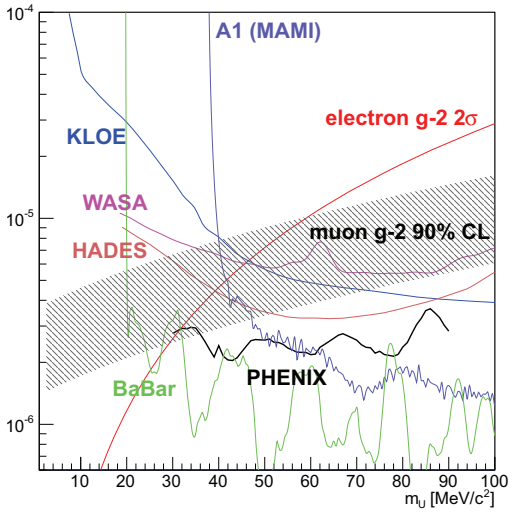

Fig. 1. A compilation of the limits of the U^γ mixing parameter, showing the PHENIX results, together with other experiments and the band indicating the range of mass and coupling parameters favored by the $(g-2)_\mu$ anomaly at 90% CL. Also shown is the 2σ upper limit obtained from $(g-2)_e$.

the coupling favored by the $(g-2)_\mu$ anomaly above $m_U > 36$ MeV/c^2. Recently, BaBar reported stricter limits from a search of the reaction $e^+e^- \to \gamma U, U \to l^+l^-$, excluding values of the preferred $(g-2)_\mu$ region for $m_U > 32$ MeV/c^2[2]. As a result, nearly all the available parameter space that would allow the dark photon to explain the $(g-2)_\mu$ results are ruled out at 90% CL by independent experiments. The entire parameter space to explain the $(g-2)_\mu$ anomaly by the dark photon can be excluded at 85% CL by the PHENIX data alone. The level of compatibility between our data and the coupling strength favored for the $(g-2)_\mu$ anomaly is 10% with a statistical test.

In summary, the PHENIX results set limits for the coupling of a dark photon to the QED photon over the mass range $30 < m_U < 90$ MeV/c^2. Combining with the BaBar results, the dark photon is ruled out at 90% CL as an explanation for the $(g-2)_\mu$ anomaly for $m_U > 32$ MeV/c^2, leaving only a small remaining part of the parameter space in the region $29 < m_U < 32$ MeV/c^2.

† Condensed from the article in Phys. Rev. C91:031901(R)(2015)

*1 RIKEN Nishina Center
*2 CNS, University of Tokyo
*3 Stony Brook University

References

1) P. Fayet, Phys. Rev. D**75**:115017(2007).
2) J. Lees et al. (BaBar Collaboration), Phys. Rev. Lett.**113**:201801 (2014).

Progress in probing flavor asymmetry of antiquarks in protons in the E906/SeaQuest experiment at Fermilab

K. Nagai,[*1] Y. Goto,[*2] Y. Miyachi,[*3] S. Miyasaka,[*1] K. Nakano,[*1] S. Nara,[*3] S. Sawada,[*2,*4] T.-A. Shibata[*1,*2]
for the E906/SeaQuest Collaboration

E906/SeaQuest is a Drell–Yan experiment at Fermi National Accelerator Laboratory (Fermilab). SeaQuest aims to measure the flavor asymmetry of antiquarks ($\bar{d}/\bar{u}$) in protons at large Bjorken x more accurately than the E866 experiment, which is the Drell–Yan experiment conducted previously at Fermilab.[1)] The flavor asymmetry is derived from the ratio of the Drell–Yan cross sections in proton-proton (pp) and proton-deuteron (pd) reactions, as shown below:

$$\frac{\sigma^{pd}}{2\sigma^{pp}} \sim \frac{1}{2}\left[1+\frac{\bar{d}}{\bar{u}}\right]. \quad (1)$$

We use a 120-GeV proton beam extracted from Fermilab Main Injector and liquid hydrogen and deuterium as targets. Carbon, iron, and tungsten are also used as targets for measuring nuclear effects on the parton distribution. The Drell–Yan process creates a $\mu^+\mu^-$ pair, and therefore the muons are measured to count the number of Drell–Yan events. SeaQuest acquired data for 10 months in 2013 and 2014 (called "Run 2").

Data acquired over two months of the data were analyzed as an initial step. Results of the analyzed data and prospects are discussed in this report.

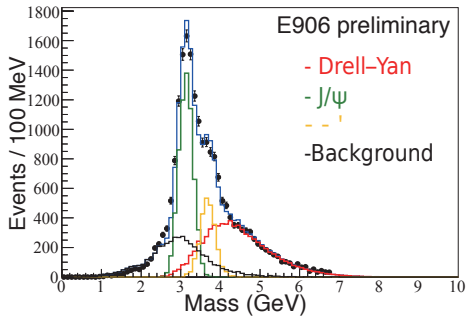

Fig. 1. Reconstructed di-muon mass distribution with all the targets (black points). It is fitted with four components (red, green, yellow, and black lines).

We succeeded in reconstructing the mass distribution of di-muons with all the targets as shown in Fig. 1. The mass distribution was fitted with four components, Drell–Yan events, J/ψ events, ψ' events, and random backgrounds. The distribution shapes of the Drell–Yan, J/ψ, and ψ' events were simulated, while that of random backgrounds was estimated using real data. The experimental data ware fitted reasonably well to simulated events and estimated backgrounds, which suggests the detectors and the algorithm of di-muon reconstruction work as expected. The Drell–Yan events were selected with a di-muon cut-off mass of 4.2 GeV. We evaluated the cross-section ratio using the yields of the Drell–Yan events in the pp and pd interactions. The flavor asymmetry ($\bar{d}/\bar{u}$) was derived from the cross-section ratio using Eq. 1. The magnitude and systematic error of $\bar{d}/\bar{u}$ are currently being evaluated. Thus, Fig. 2 shows only the statistical errors of $\bar{d}/\bar{u}$

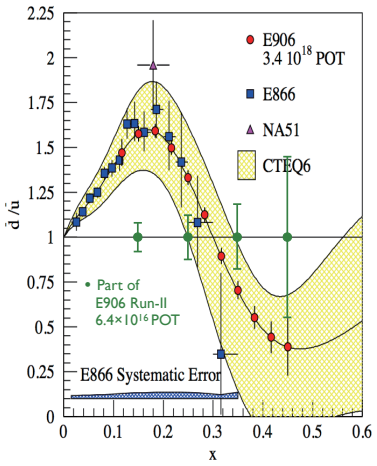

Fig. 2. Plot of $\bar{d}/\bar{u}$ vs Bjorken x obtained by E866 (blue points), and the size of statistical errors expected in the SeaQuest experiment (red points) and that obtained using the analyzed data (green points).

using the analyzed data, together with the previous measurement results. The amount of analyzed data at small x is approximately the same as that of the E866 data.

We started acquiring another set of data for two years in November 2014. After data acquisition, we will obtain 20 times more statistics than the set of data we analyzed. The result that will be obtained using in the SeaQuest experiment will considerably improve the understanding of the internal structure of protons.

*1 Graduate School of Science and Engineering, Tokyo Institute of Technology
*2 RIKEN Nishina Center
*3 Faculty of Science, Yamagata University
*4 Institute of Particle and Nuclear Studies, KEK

References

1) E.A. Hawker et al.: E866/NuSea, Phys. Rev. Lett. 80, 3715 (1998)

Results of the K^-pp bound-state search in J-PARC E15[1st]

T. Hashimoto,[*1] K. Itahashi,[*1] M. Iwasaki,[*1] Y. Ma,[*1]H. Ohnishi,[*1] S. Okada,[*1] H. Outa,[*1] F. Sakuma,[*1] M. Sato,[*1] M. Tokuda,[*1] and Q. Zhang,[*1] for the J-PARC E15 collaboration

The interaction between a nucleon and an anti-kaon ($\bar{K}$), the lightest hadron with a strange quark, is one of the keys to understanding meson-baryon interactions in low energy quantum chromodynamics (QCD) incorporating three flavors in the nuclear system. Precise measurements of elementary $\bar{K}N$ interactions and investigations of $\bar{K}$-nuclear bound systems ($\bar{K}$ nuclei) are currently hot topics. The K^-pp state, a bound system of a negative kaon and two protons, is theoretically considered the simplest $\bar{K}$ nucleus,[1)] and thus it has attracted special interest. We are searching for the K^-pp bound state by using an in-flight reaction as the J-PARC E15 experiment.[2)] The first physics data acquisition (E15^{1st}) was performed in May 2013, with 5×10^9 kaons at 1 GeV/c on a liquid ^{3}He target.

Figure 1 shows the obtained semi-inclusive neutron spectrum at $\theta_n^{lab} = 0°$.[3)] Here, we detected the neutron by using a plastic scintillator array $\sim$ 15 m away from the target. To reconstruct the reaction vertex for the time-of-flight measurement, at least one charged track is required in a cylindrical detector system (CDS) surrounding the target. The K^0-tagged spectrum, shown in the inset of Fig. 1, is attributed to the charge-exchange $K^-p \to K_s^0 n$ reaction, and demonstrates that the detector resolution and the missing-mass scale are well understood.

The observed yield in the deeply bound region, corresponding to K^-pp binding energies larger than 80 MeV, was in good agreement with the evaluated backgrounds originating from 1) accidental hits and neutral particles other than neutrons, 2) reactions on the target cell, and 3) neutrons produced via charged Σ decay. In this mass region, upper limits on the production cross section of a bound state were evaluated, assuming a $K^-pp \to \Lambda p$ isotropic decay. They were determined to be 30-270 μb/sr, depending on the mass and the decay width. The upper limits obtained are much smaller than the theoretical calculation.[4)] The ratios of the upper limits to cross sections of the quasi-elastic channels are (0.5–5)% (quasi-elastic) and (0.3–3)% (charge exchange). These ratios are rather small compared to the sticking probability of the usual hypernucleus formation. On the other hand, a significant excess was observed around the K^-pp binding threshold. However, in spite of the observed large yield corresponding to $\sim$ 1 mb/sr, structures suggested in theoretical spectral functions[4,5)] cannot be identified from only the semi-inclusive measurement.

We also analyzed the Λp events detected using the CDS to investigate the K^-pp decay. A Λ was reconstructed from a $\pi^- p$ pair detected using the CDS to be almost free from the background. Missing-neutron events were identified by the ^{3}He$(K^-, \Lambda p)X$ missing mass, with $\sim$ 20% $\Sigma^0 p$-event contamination ($\Sigma^0 \to \Lambda\gamma$). The preliminary Λp invariant-mass spectrum, obtained with $\sim$ 10 MeV/c^2 resolution, consists of a flat component widely distributed in the three-body phase space and an enhancement around the threshold. The threshold structure mainly originates from events with a low-momentum transfer, and it might be evidence for the K^-pp bound state.

In 2015, we plan to conduct the 2nd-stage physics run with 10 times the number of beam-kaons in the 1st stage, as well as calibration runs with hydrogen and deuteron targets. With the new data set, we will further investigate the structure around the K^-pp binding threshold.

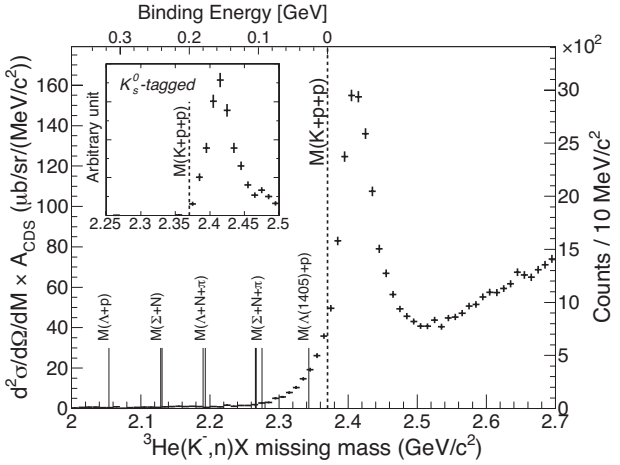

Fig. 1. ^{3}He$(K^-, n)X$ semi-inclusive missing-mass distribution at $\theta_n^{lab} = 0°$[3)]. A_{CDS} denotes the charged-tagging acceptance of the CDS. The inset shows the K_s^0-tagged spectrum.

References

1) T. Yamazaki and Y. Akaishi: Phys. Lett. B **535** (2002) 70.
2) M. Iwasaki et al.: J-PARC proposal P15, "A search for deeply-bound kaonic nuclear states by in-flight ^{3}He(K^-, n) reaction" (2005).
3) T. Hashimoto et al.: arXiv:1408.5637 (2014).
4) T. Koike and T. Harada: Phys. Rev. C **80** (2009) 055208.
5) J. Yamagata-Sekihara, D. Jido, H. Nagahiro, and S. Hirenzaki: Phys. Rev. C **80** (2009) 045204.

*1 RIKEN Nishina Center

Measurement of the proton Zemach radius from the hyperfine splitting energy in ground-state muonic hydrogen

M. Sato,[*1] S. Aikawa,[*2] K. Ishida,[*1] M. Iwasaki,[*1,*2] S. Kanda,[*3] Y. Ma,[*1] Y. Matsuda,[*4] T. Matsuzaki,[*1] K. Midorikawa,[*5] Y. Oishi,[*1] S. Okada,[*1] N. Saito,[*5] A. Takamine,[*6] K. Tanaka,[*1,*4] H. Ueno,[*1] and S. Wada[*5]

Studies of the proton electromagnetic structure have recently attracted great interest stimulated by *the proton radius puzzle*, which is a 7σ discrepancy in the proton charge radius determined using two different methods. One is a traditional determination method using $e-p$ scattering and the atomic hydrogen spectroscopies as compiled in CODATA[1]. The other is a method of laser spectroscopy of the Lamb shift in muonic hydrogen[2]. To understand this inconsistency between "electronic" and "muonic" methods, there are several hypotheses including physics beyond the Standard Model. However, none of them are conclusive, and the puzzle is still an unsettled question.

Since the proton charge radius is defined only from the electric distribution in the proton, it is a curious question as to how we can determine the magnetic distribution of a proton probed with muons, which may become a clue to solve the puzzle. Therefore, we focus on the proton Zemach radius, which contains information on both the charge and magnetic-moment distributions in the proton. The proton Zemach radius, R_Z, is expressed as

$$R_Z = \int d^3\mathbf{r}|\mathbf{r}| \int d^3\mathbf{r}' \rho_E(\mathbf{r}')\rho_M(\mathbf{r}-\mathbf{r}'),$$

where ρ_E and ρ_M denote spatial distributions of the charge and magnetic moment of the proton, respectively. This Zemach radius can be determined from the hyperfine splitting energy of a hydrogen-like atom. Thus, we determine the proton Zemach radius from the laser spectroscopy of the hyperfine splitting energy of muonic hydrogen.

The experimental principle is as follows. When negative muons are stopped in hydrogen, they form muonic hydrogen atoms and are quickly deexcited to the ground state. Its energy level is split into hyperfine sublevels by the spin combination of the proton and muon: the spin singlet (F = 0) and the triplet (F = 1) states. The splitting energy is ∼0.183 eV, which corresponds to a mid-infrared frequency of 44.2 THz and wavelength of 6.78 μm. We will measure this energy through a laser spectroscopy. To search for the resonance frequency, the spatial asymmetry of spin-polarized muon decays is used. To populate the spin polarization in F = 1, we use a circularly polarized laser. A specific F = 1 state is selectively excited because of the conservation of the total angular momentum. The electrons from polarized muon decays are detected to find the decay asymmetry during the laser frequency scan.

A conceptual drawing of the experimental setup is shown in Fig. 1. Negative muons with momenta of 40 MeV/c are stopped in a gas hydrogen target. The density of the hydrogen gas is optimized to be 0.01% of LHD (liquid hydrogen density) to suppress the collisional quench process, which is a deexcitation from F = 1 to F = 0 through a collision with a neighboring atoms. The mid-infrared laser is injected from the side of the target ∼ 1 μs after the stopped μ^- timing. The laser power is a key issue to achieve sufficient polarization through a laser-induced excitation. The laser system is under development in RIKEN[3], and the achievable laser performance is a power of 40 mJ and bandwidth of 50 MHz with a repetition rate of 50 Hz. For further enhancing the effective laser power by multiple reflection, a multi-pass cavity consisting of two mirrors facing each other is installed in the hydrogen target, as schematically illustrated in the figure. The mirror reflectivity is assumed to be 99.95% and the resulting polarization is ∼16%.

The yield estimation and a feasibility study of the present measurement are nearing completion. A beam study with negative muons in RIKEN-RAL is scheduled for the next fiscal year.

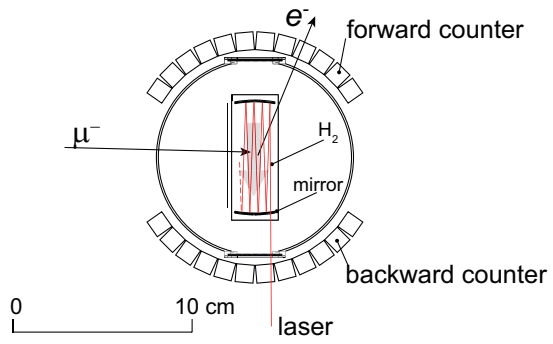

Fig. 1. Conceptual drawing of the experimental setup.

*1 RIKEN Nishina Center
*2 Department of Physics, Tokyo Institute of Technology
*3 Department of Physics, The University of Tokyo
*4 Graduate School of Arts and Science, The University of Tokyo
*5 RIKEN Center for Advanced Photonics
*6 Department of Physics and Mathematics, Aoyama Gakuin University

References
1) P. J. Mohr, B. N. Taylor, D. B. Newell: Rev. Mod. Phys. **84**, 1527 (2012).
2) R. Pohl et al.: Nature **466**, 213 (2010).
3) N. Saito et al.: Proc. of SPIE, Vol. 8526, 852605 (2012).

5. Hadron Physics (Theory)

Strong enhancement of jet-medium coupling in the quark-gluon plasma near transition temperature†

J. Liao*1,*2

A new, deconfined form of QCD matter known as the quark-gluon plasma is created in relativistic heavy ion collisions. In such collisions, highly energetic jets provide unique probe of the quark-gluon plasma properties. The observable quantifying jet energy loss is the nuclear modification factor, R_{AA} as well as its azimuthal anisotropy characterized by its second harmonic coefficient v_2. Both RHIC and LHC measurements have shown a sizable v_2 in the high p_t region.

Recently the temperature dependence of jet-medium coupling, which may be quantified by the so-called jet transport coefficient $\hat{q}(T)$, has attracted significant interest. As was first found in[1], the geometric anisotropy v_2 at high p_t is particularly sensitive to such temperature dependence, and a simultaneous description of high p_T R_{AA} and v_2 at RHIC requires a strong enhancement of jet-medium coupling in the near-T_c region. Furthermore, the near-T_c enhancement predicts a visible reduction of average opaqueness of the fireball from RHIC to LHC which was confirmed by analyzing how the R_{AA} evolves with beam energy[2,3]. Therefore phenomenologically there are robust evidences for such near-T_c enhancement, while a precise theoretical determination of such nontrivial T-dependence has not been known owing to the highly nonperturbative dynamics in the near-T_c regime.

One important approach for strongly coupled quark-gluon plasma is to use holographic QCD models. It is particularly important to introduce non-conformal physics that is most prominent around T_c. By constructing such a model[4], we have found that: 1) there are strong non-conformal, non-perturbative dynamics going on in the near-T_c region; 2) such dynamics leads to non-monotonic behavior in QGP thermodynamics as shown by the strong near-T_c peak of trace anomaly (which is well modeled by holography); 3) the same dynamics leads to non-monotonic behavior in QGP transport properties and in particular strong near-T_c enhancement of jet-medium coupling $\hat{q}/T^3$ (see Fig.1).

More recently we have developed a new jet quenching framework, CUJET3.0[5], that is shown to account well for both high p_T single inclusive hadron suppression R_{AA} and its azimuthal anisotropy v_2 at both RHIC and the LHC energies. CUJET3.0 model includes two new nonperturbative effects in the QCD transition temperature range $T \sim 140 - 250$ MeV: (1) the Polyakov loop suppression of color-electric scattering and (2) the enhancement of scattering due to emergent magnetic monopoles near T_c. We find that the CUJET3.0 jet transport parameter $\hat{q}(E,T)/T^3$ peaks near T_c and has very strong nonconformal E and T dependence up to $T \sim 400$ MeV. Extrapolating down to $E = 2$ GeV, we find a striking new connection between bulk perfect fluidity with $\eta/s \sim 0.1$ near T_c and high p_T high T perturbative jet quenching.

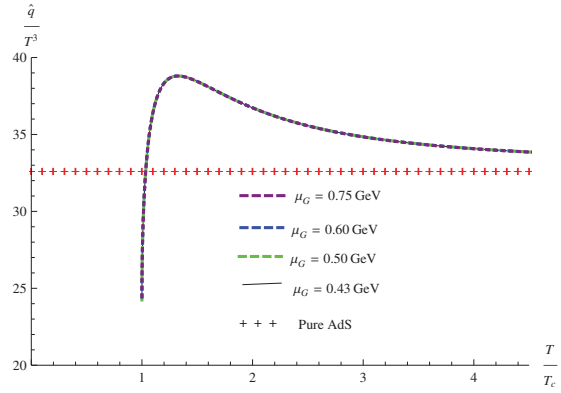

Fig. 1. Temperature dependence of jet-medium coupling from a non-conformal holographic QCD model[4].

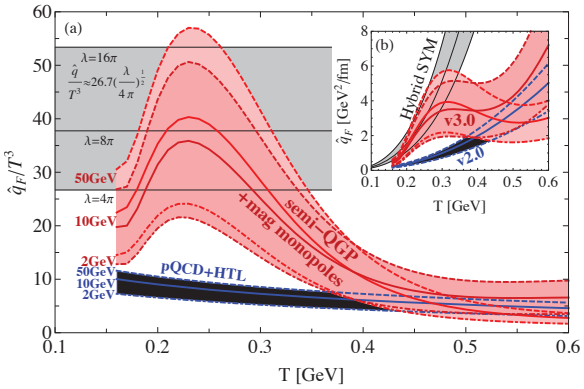

Fig. 2. Temperature dependence of jet-medium coupling from the CUJET3.0 model[5].

References
1) J. Liao and E. Shuryak, Phys. Rev. Lett. **102**, 202302 (2009).
2) X. Zhang and J. Liao, Phys. Rev. C **89**, no. 1, 014907 (2014).
3) X. Zhang and J. Liao, Phys. Rev. C **87**, 044910 (2013).
4) D. Li, J. Liao and M. Huang, Phys. Rev. D **89**, no. 12, 126006 (2014).
5) J. Xu, J. Liao and M. Gyulassy, arXiv:1411.3673 [hep-ph].

† Condensed from the articles in Phys. Rev. D. **89**, 126006 (2014) and in arXiv:1411.3673.

*1 Physics Department and Center for Exploration of Energy and Matter, Indiana University
*2 RIKEN Nishina Center

Magnetic moments of light nuclei from lattice QCD†

S. Beane,[*1] E. Chang,[*2] S. Cohen,[*2] W. Detmold,[*3] H. Lin,[*1] K. Orginos,[*4] A. Parreno,[*5] M. Savage,[*2] and B. Tiburzi[*6]

The structure and dynamics of nuclei have been extensively probed using electromagnetic interactions. Magnetic moments historically helped support a picture of light nuclei as collections of weakly interacting nucleons, which led to the phenomenologically successful shell-model description of nuclei. At a fundamental level, however, nuclei are bound states of the quark and gluon degrees of freedom of QCD. Nuclear forces emerge from QCD as a consequence of confinement and chiral symmetry breaking. Yet, nuclei are not simply collections of quarks and gluons determined by global quantum numbers; rather, nuclei have the structure of interacting nucleons, and this feature remains to be understood at a deep level. Knowledge of the quark structure of nuclei, moreover, is required to turn nuclei into laboratories for probing fundamental symmetries, and pushing the limits of the Standard Model.

We have computed magnetic moments of the lightest few nuclei using lattice QCD. These calculations, the first of their kind, have been performed at unphysical light-quark masses. All three light-quark masses in our computation were set equal to the physical strange quark mass. At this $SU(3)$ flavor-symmetric point, the resulting pion mass is $m_\pi \approx 800\,\mathtt{MeV}$. Further details of the lattice action and gauge configurations are found in Ref.[2]. To compute magnetic moments, $U(1)_{\mathcal{Q}}$ gauge links giving rise to a uniform magnetic field were post multiplied onto each QCD gauge field. While quenching sea quark electric charges is an approximation, there are no contributions to magnetic moments resulting from coupling the magnetic field to sea quarks in our computation This fact owes to the three degenerate quark flavors with their non-singlet electric charge matrix, $\mathcal{Q} = e\,\mathtt{diag}\left(+\frac{2}{3}, -\frac{1}{3}, -\frac{1}{3}\right)$. Sub-percent QED effects, however, have been neglected in our computation. The combined gauge fields were used to compute up and down (≡ strange) quark propagators, which were then contracted to form the required nuclear correlation functions using the techniques of Ref.[3]. Finally nuclear correlation functions were projected onto spin components with respect to the direction of the magnetic field.

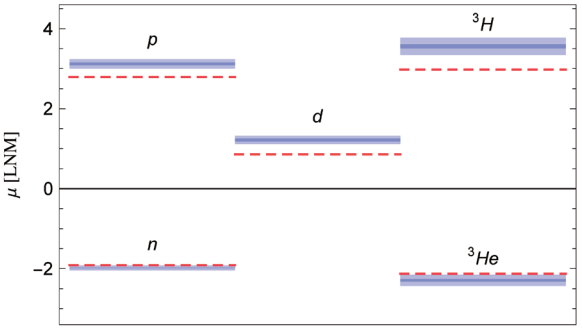

Fig. 1. Nuclear magnetic moments computed using lattice QCD at the $SU(3)$ flavor-symmetric point[1]. Results in lattice nuclear magnetons [LNM] (blue bands) are remarkably close to experimentally measured moments in physical nuclear magnetons (dashed red lines). Despite deep binding found at this unphysically large quark mass, magnetic moments of light nuclei are close to those predicted from simple shell-model configurations.

The ground-state energy of a non-relativistic hadron having mass M, and charge Qe is given by

$$E(\vec{B}) = M + \frac{e}{2M}|Q\vec{B}| - \vec{\mu}\cdot\vec{B} + \mathcal{O}(B^2). \qquad (1)$$

The field-dependent terms appearing above are due to the lowest Landau level and Zeeman interaction, which is proportional to the hadron's magnetic moment, μ. To isolate magnetic moments with good statistical precision, the long Euclidean-time limit of correlator ratios was utilized. For a spin-half hadron, e.g., we consider the ratio

$$\mathcal{R}^{(B)}(\tau) = \frac{C^{(B)}_\uparrow(\tau)}{C^{(B)}_\downarrow(\tau)} \Big/ \frac{C^{(0)}_\uparrow(\tau)}{C^{(0)}_\downarrow(\tau)} \sim e^{-2\mu|B|\tau}, \qquad (2)$$

as a function of the applied magnetic field. Extracted magnetic moments are shown in Fig. 1 in lattice nuclear magnetons, i.e. units of $\frac{e}{2M_N}$, where M_N is the lattice nucleon mass, $M_N \approx 1.6\,\mathtt{GeV}$. When scaled in this fashion, results are remarkably close to experimental values. In particular, evidence for shell-model configurations suggests that this property of nuclei may extend over a broad range of quark masses.

† Condensed from Reference[1]

*1 Dept. of Physics, University of Washington, Seattle
*2 Dept. of Physics, University of Washington, Seattle; and Institute for Nuclear Theory, Seattle
*3 Center for Theoretical Physics, MIT, Cambridge
*4 Dept. of Physics, College of William and Mary, Williamsburg; and JLab, Newport News
*5 Dept. d'Estructura i Constituents de la Matèria (ICC), Universitat de Barcelona
*6 Dept. of Physics, The City College of New York (CUNY); and RIKEN–BNL Research Center

References

1) S. R. Beane, E. Chang, S. Cohen, W. Detmold, H.-W. Lin, K. Orginos, A. Parreno, M. J. Savage, and B. C. Tiburzi, Phys. Rev. Lett. **113**, 252001 (2014).
2) S. R. Beane *et al.* (NPLQCD Collaboration), Phys. Rev. D **87**, 034506 (2013), arXiv:1206.5219 [hep-lat].
3) W. Detmold and K. Orginos, Phys. Rev. D **87**, 114512 (2013), arXiv:1207.1452 [hep-lat].

Nucleon structure in lattice QCD near physical mass

S. Ohta[*1,*2,*3] for RBC and UKQCD Collaborations

The RIKEN-BNL-Columbia (RBC) collaboration continue numerical lattice-QCD investigations of nucleon structure[1–6]. Here, I report results obtained from ensembles[7–9] generated jointly with the UKQCD collaboration near the physical pion mass. In these ensembles the strange quark mass is set very close to its physical value while the degenerate up and down quark is varied toward the physical mass, resulting in pion mass ranging from about 420 to 170 MeV. Isovector observables such as vector- and axialvector-current form factors and some low moments of structure functions are calculated.

The isovector axial charge, g_A, is about the most important observable concerning nucleon structure. It determines the neutron life and pion-nucleon interaction through the celebrated Goldberger-Treiman relation. And as such it determines nuclear abundance and much of nuclear physics. Lattice-QCD calculations have experienced difficulty reproducing this quantity: they generally underestimate the experimental value of 1.2723(23)[10]. Our latest results do not escape this problem, as summarized in Fig. 1: About 10% deficit

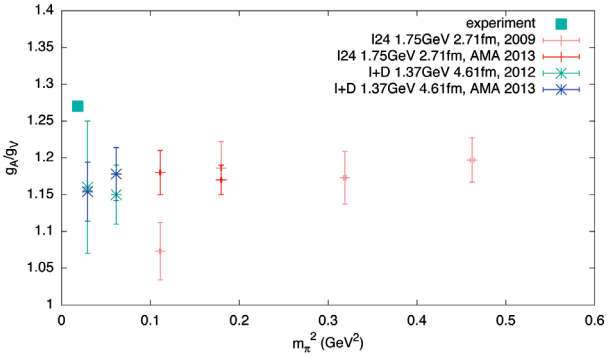

Fig. 1. The ratio, g_A/g_V, of isovector axia chargel, g_A, to isovector vector charge, g_V, calculated in our recent lattice-QCD ensembles plotted against calculated pion mass squared, m_π^2 [6]

is persistent across the mass range investigated, and possibly worsens toward the physical mass.

Much of our efforts during the past year were concentrated in understanding this[11], starting with the long-range autocorrelation observed at the lightest-mass ensemble at pion mass $m_\pi = 170$ MeV. This ensemble is at the smallest finite-size scaling parameter, $m_\pi L = 3.9$, where L is the linear extent of the lattice volume. That weaker but similar auto-correlation was seen at heavier mass, $m_\pi = 330$ MeV, with the second smallest finite-size scaling parameter, $m_\pi L = 4.6$, but not at a lighter mass of 250 MeV with larger $m_\pi L = 5.8$, hints this autocorrelation may be related to too small lattice volume.

We found weaker but similar autocorrelation in isovector transversity, $\langle 1 \rangle_{\delta u - \delta d}$, that differs by only one extra Dirac γ matrix factor from the axialvector current. This, together with the axial charge observation, suggests the virtual pion cloud around the nucleon may not be well contained within the lattice volume. The other observables, including the isovector vector-current form factors and isovector quark momentum fraction, $\langle x \rangle_{u-d}$, and isovector quark helicity fraction, $\langle x \rangle_{\Delta u - \Delta d}$ do not show such autocorrelation at any mass.

A possible cause for such a long-range autocorrelation is interference from the gauge-field topology that is known to have long autocorrelation. However the axial charge and topological charge are not found to be correlated[11].

We also looked at how the axial charge fluctuates spatially by dividing the volume into halves with lower and higher $x-$, $y-$, or $z-$coordinates[11]: we found that it fluctuates rather wildly.

At the pion mass of about 170 MeV the virtual pion cloud around the nucleon may not be well contained in our lattice box with linear extent of about 4.5 fm.

*1 Institute of Particle and Nuclear Studies, KEK
*2 Department of Particle and Nuclear Physics, SOKENDAI
*3 RIKEN BNL Research Center, BNL

References

1) H. -W. Lin, et al., Phys. Rev. D **78**, 014505 (2008) arXiv:0802.0863 [hep-lat].
2) T. Yamazaki et al., Phys. Rev. Lett. **100**, 171602 (2008) arXiv:0801.4016 [hep-lat].
3) T. Yamazaki, et al., Phys. Rev. D **79**, 114505 (2009) arXiv:0904.2039 [hep-lat].
4) Y. Aoki, et al., Phys. Rev. D **82**, 014501 (2010) arXiv:1003.3387 [hep-lat].
5) M. Lin, PoS LATTICE **2013**, 275 (2014) arXiv:1401.1476 [hep-lat].
6) S. Ohta, PoS LATTICE **2013**, 274 (2014) arXiv:1309.7942 [hep-lat].
7) C. Allton et al. , Phys. Rev. D **78**, 114509 (2008) arXiv:0804.0473 [hep-lat].
8) Y. Aoki et al., Phys. Rev. D **83**, 074508 (2011) arXiv:1011.0892 [hep-lat].
9) R. Arthur et al., Phys. Rev. D **87**, 094514 (2013) arXiv:1208.4412 [hep-lat].
10) K.A. Olive *et al.* (Particle Data Group), Chin. Phys. C, **38**, 090001 (2014).
11) S. Ohta, PoS LATTICE **2014**, 134 arXiv:1410.8353 [hep-lat].

Holographic heavy-quark symmetry†

K. Hashimoto,[*1,*2] N. Ogawa,[*1] and Y. Yamaguchi[*1]

Hadrons containing heavy quarks, i.e., charm and bottom quarks, have attracted much interest in hadron and nuclear physics. Accelerator experiments have found rich spectra of heavy hadrons for conventional states, three-quark baryons and quark-antiquark mesons, and exotic hadrons having complex structures such as multiquark states and hadronic composite states[1]. Various structures of heavy hadrons are generated by the nature of internal quark potentials and/or hadron-hadron interactions which result from fundamental phenomena of quantum chromodynamics (QCD).

In heavy quark sectors, a new symmetry that has not been appeared in the light-quark sector is expected to be important. It is called heavy-quark spin symmetry[2], and it emerges because of the suppression of the spin-dependent interaction between quarks, which is inversely proportional to quark masses. This symmetry leads to a specific feature: mass degeneracy of heavy hadrons having different spins. In the case of mesons, we find small mass splittings between spin-0 pseudo-scalar mesons and spin-1 vector mesons in experimental results, e.g., the mass splitting of BB^* ($\sim$45 MeV) in the bottom-quark sector is much smaller than that of KK^* ($\sim$ 400 MeV) in the strange-quark sector. The symmetry also affects decays and productions of heavy hadrons with different spins. Hence, the heavy-quark spin symmetry plays a significant role in heavy-hadron spectroscopy.

The spectra of heavy hadrons have been studied using various theoretical approaches, such as the quark model and lattice QCD. In addition, we found that the gauge/gravity correspondence[3] is a promising approach because it provides powerful methods to deal with strongly coupled theories.

The gauge/gravity correspondence has been applied to investigate hadron spectra by introducing dynamical quarks described by excitations on probe D-branes. For example, $\mathcal{N} = 2$ hypermultiplet flavors (= quark multiplets) added to $\mathcal{N} = 4$ SU(N_c) super Yang-Mills theory are realized by introducing N_f probe D7-branes on the $\mathrm{AdS}_5 \times \mathrm{S}^5$ background (generated by N_c D3-branes) on the gravity side[4]. In this model, the quarks are given as fundamental strings stretched between D3- and D7-branes. The masses of pseudo-scalar and vector mesons are obtained as fluctuations of the scalar and vector fields on the flavor D-branes[4].

In the gauge theory holding supersymmetry, however, both pseudo-scalar and vector mesons are members of the same multiplet, and the masses are completely degenerate regardless of the value of the quark mass. Even when the supersymmetry is broken by finite temperature, Shark-Schwartz compactification, etc, the supersymmetry is recovered in the heavy-quark limit (i.e., in the UV limit) in most of the top-down models. Hence, the presence of the heavy-quark spin symmetry has not been obvious in the gauge/gravity duality. In order to determine whether the heavy-quark spin symmetry exists, we need to investigate meson mass degeneracies in theories that are non-supersymmetric even in the UV region.

In this study, we propose a semi-bottom-up, deformed D3-D7 model. The background geometry is deformed from the conventional $\mathrm{AdS}_5 \times \mathrm{S}^5$ and obtained as

$$ds^2_{str} = r^{2\alpha}\eta_{\mu\nu}dx^\mu dx^\nu + R^2 r^{-2\beta}\left(\frac{dr^2}{r^2} + r^{2\delta}d\Omega_5^2\right), \quad (1)$$

$$e^\phi = g_0 r^{-4\gamma}, \quad (2)$$

in the string frame, where R corresponds to the radius of AdS_5, $d\Omega_5^2$ represents the metric of S^5, and ϕ is the dilaton. Here r is the non-dimensional coordinate. The background geometry is given in the UV leading form and generally holds no supersymmetry or conformal symmetry. We introduce 4 deformation parameters $(\alpha, \beta, \delta, \gamma)$ for the background, but they are constrained by several conditions so that the theory would have physically reasonable properties. The standard D3 background corresponds to $(\alpha, \beta, \delta, \gamma) = (1, 0, 0, 0)$. We investigate the spectra of the pseudo-scalar and vector quarkonia at the limit $m_Q \to \infty$, computed as the fluctuations of the fields on the flavor D7-brane placed on this background.

We observed a slight mass difference between pseudo-scalar and vector quarkonia, which is at most $\simeq 1.5\%$, even in the non-supersymmetric analysis. The mass degeneracy is found in not only ground states but also excited states.

References
1) N. Brambilla, S. Eidelman, B. K. Heltsley, R. Vogt, G. T. Bodwin, E. Eichten, A. D. Frawley and A. B. Meyer et al.: Eur. Phys. J. C **71**, 1534 (2011).
2) A. V. Manohar and M. B. Wise: Camb. Monogr. Part. Phys. Nucl. Phys. Cosmol. **10**, 1-191 (2000).
3) J. M. Maldacena: Int. J. Theor. Phys. **38**, 1113 (1999) [Adv. Theor. Math. Phys. **2**, 231 (1998)].
4) A. Karch and E. Katz: JHEP **0206**, 043 (2002).
5) M. Kruczenski, D. Mateos, R. C. Myers, and D. J. Winters: JHEP **0307**, 049 (2003).

† Condensed from the article in arXiv:1412.5590 [hep-th]

*1 RIKEN Nishina Center
*2 Department of Physics, Osaka University

Possibility of ferromagnetic neutron matter†

K. Hashimoto*1,*2

Ferromagnetic order in nature always attracts interest for study as it manifests microscopic structure of matter and materials. Among observed magnetic fields in nature, perhaps the strongest stable magnetic field is on the surface of magnetars, which goes up to 10^{15} [G] and more. The mechanism for generating such a strong field is yet to be uncovered, and it is natural to resort the origin to the high density of neutrons of which the neutron stars consist. In fact, after the discovery of pulsars, the possibility of ferromagnetism at neutron stars was proposed. However, numerical simulations of neutron matter with realistic inter-nucleon potentials have not shown the ferromagnetic phase. So the possibility of the ferromagnetic phase at high density neutron matter, if exists in nature, waits for a new mechanism of the spontaneous magnetization.

In this paper, we study the possibility of the ferromagnetic phase at high density of neutrons, by using the simplest but general chiral effective action. Low energy dynamics of neutrons is governed by the chirally symmetric interactions through pions and the spin-magnetic coupling with magnetic fields. Our model consists of dense neutrons coupled with neutral pions and magnetic fields, together with the chiral anomaly term. These are indispensable ingredients, and we will see the outcome for the magnetic phase from this minimal model.

The reason for choosing the neutral pion is simply for the realization of the ferromagnetism, as other pion condensations such as charged pion condensation have not been shown to exhibit a ferromagnetism. In addition, with a neutral pion condensation of the form $\Pi_0(x) \propto \sin \boldsymbol{k} \cdot \boldsymbol{x}$, a neutron lattice is formed with an alternating layer structure (ALS)[1], then the neutron spins cancel each other, and macroscopic magnetization would not emerge. In this paper, instead, we analyze a neutral pion condensation of the different form $\Pi_0(x) = \boldsymbol{q}\cdot\boldsymbol{x}$ following Dautry and Neyman[2], and generalize the study to include magnetic fields and QCD anomaly.

Our study is motivated by the earlier work[3] in which, together with M. Eto and T. Hatsuda, the author proposed a mechanism for a ferromagnetic phase at high density of neutrons. The mechanism utilizes a neutral pion domain wall coupled to the magnetic field through the QCD chiral anomaly. A spontaneous magnetization was shown in[3] in the approximation of a single wall and one-loop neutrons. In this paper, we generalize the idea, and study in the simplest chiral model the Fermi energy of the dense neutrons and its back-reaction due to the pion condensation and the magnetic fields. A successive array of the domain walls can be approximated by the linear pion condensation of Dautry and Neyman.

Let us summarize what we find in this paper.

- Toy model of neutral fermions.
  First we provide a toy model of a neutral fermion with a Zeeman coupling to magnetic fields. Under the assumption of the spatial homogeneity, we calculate the energy density of the ferromagnetic phase and show that it is favored compared to the ordinary fermion matter.
- Simplest chiral model and ferromagnetic order.
  The toy model of the neutral fermions is the essential part of the chiral model of neutrons and pions. We analyze the simplest chiral effective model of dense neutrons and neutral pions, together with the magnetic field coupling and the QCD anomaly. We find that the neutral pion condensation of form proposed by Dautry and Neyman is precisely in the same place as the magnetization, under the assumption of the spatial homogeneity. The energy density of the ferromagnetic-pion-condensation phase is lower than the ordinary neutron matter at high density around $\rho > 5\rho_0$ where ρ_0 is The generated magnetic field is ~ 40 [MeV] $\sim \mathcal{O}(10^{17})$[G].
- Comparison to ALS.
  We compare our energy density with that of the inhomogeneous ALS phase (which does not exhibit a magnetization), and find that the ALS phase is favored. The energy gain of the ALS is by several times greater than that of our ferromagnetic phase.
- Axial vector meson condensation.
  To seek for the possibility of the ferromagnetism, we look at the *axial vector meson condensation* accompanied by our model. Indeed, any axial vector meson plays the same role as the neutral pions, and the axial vector meson condensation further reduces the energy density of the ferromagnetic phase significantly.

References

1) R. Tamagaki and T. Takatsuka, Prog. Theor. Phys. **56**, 1340 (1976).
2) F. Dautry and E. M. Nyman, Nucl. Phys. A **319**, 323 (1979).
3) M. Eto, K. Hashimoto and T. Hatsuda, Phys. Rev. D **88**, 081701 (2013) [arXiv:1209.4814 [hep-ph]].

† Condensed from the article in arXiv:1412.6960

*1 RIKEN Nishina Center
*2 Department of Physics, Osaka University

Pion and Kaon form factors in the NJL model

Y. Ninomiya,[*1] W. Bentz,[*1,*2] and I. C. Cloët[*3]

In this work we study the dressed quark mass dependence of the pion and kaon electromagnetic form factors at the quark level using the Nambu-Jona-Lasinio (NJL) model, which is a powerful chiral effective quark model of QCD[1]. We choose the proper-time regularization scheme and introduce an infrared cut-off as in previous studies[2,3] in order to include one important aspect of quark confinement. In the calculation there is one free model parameter, which we take as the dressed light quark (u and d) mass M. The constituent quark model suggests that M is about 0.3–0.4 GeV, and it is often fixed as 0.4 GeV in NJL model calculations. However, in this work we show that the description of the pion and kaon form factors, as well as other physical quantities, are sensitive to the dressed light quark mass, and can be greatly improved if the dressed light quark mass is taken to be $M \simeq 0.25$ GeV.

We first explore the quark condensates $\langle \bar{q}q \rangle$, the kaon decay constant f_K, and the light (m) and strange (m_s) current quark masses using various values of the dressed quark mass. Our results for these quantities are shown in Table I. It is revealed that our results for the three ratios m_s/m, f_K/f_π and $\langle \bar{s}s \rangle / \langle \bar{\ell}\ell \rangle$ are in excellent agreement with recent experimental analyses and lattice QCD calculations, if the mass of the dressed light quark is approximately $M \simeq 0.25$ GeV. Therefore, it is interesting to study the pion and kaon form factors for the case where M is assumed to be smaller than the usually adopted values.

Figs. 1 and 2 show our calculated results for the pion and kaon form factors for the case $M = 0.25$ GeV. In each figure the dotted line denotes the result when the quark-photon vertex is treated as point-like (bare); the dash-dotted line includes effects from the pion cloud; and the dashed line is the full result which also includes the vector mesons contributions to the quark-photon vertex. The solid line shows the monopole functions which are determined so as to reproduce the empirical charge radii. From these figures it is clear that the data and the monopole functions can be reproduced very well by choosing $M \simeq 0.25$ GeV and including both the pion cloud and vector meson contributions. Such good agreement can not be attained for the case of $M \simeq 0.4$ GeV.

Table 1. Results for the current quark masses, kaon decay constant and quark condensates, for various values of the dressed light quark mass M. Masses and f_K are in units of GeV, and quark condensates in units of GeV^3. The model parameters are chosen to reproduce $f_\pi = 0.093$ GeV, $m_\pi = 0.14$ GeV and $m_K = 0.49$ GeV.

M	m	m_s	f_K	$\langle \bar{\ell}\ell \rangle$	$\langle \bar{s}s \rangle$
0.20	0.0041	0.131	0.128	$-(0.275)^3$	$-(0.329)^3$
0.25	0.0086	0.227	0.110	$-(0.214)^3$	$-(0.224)^3$
0.30	0.0123	0.293	0.010	$-(0.190)^3$	$-(0.180)^3$
0.35	0.0150	0.331	0.094	$-(0.177)^3$	$-(0.159)^3$
0.40	0.0168	0.357	0.091	$-(0.170)^3$	$-(0.148)^3$

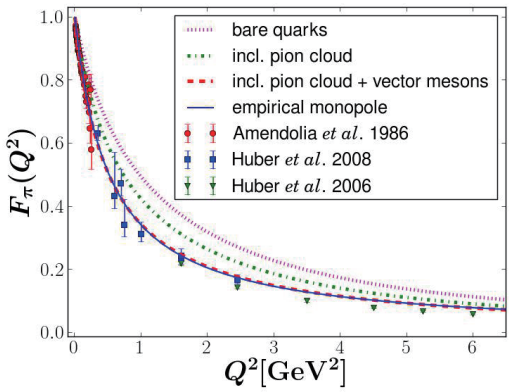

Fig. 1. Pion form factor for the case $M = 0.25$ GeV.

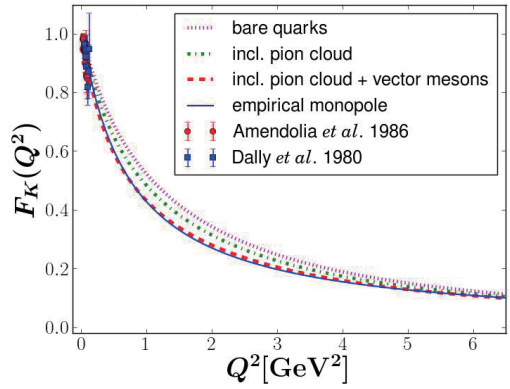

Fig. 2. Kaon form factor for the case $M = 0.25$ GeV.

W.B. acknowledges support by the Grant in Aid for Scientific Research (Kakenhi) of the Japanese Ministry of Education, Culture, Sports, Science and Technology, project no. 20168769.

References

1) T. Hatsuda and T. Kunihiro, Phys. Rept. **247**, 221 (1994).
2) W. Bentz and A. W. Thomas, Nucl. Phys. A **696**, 138 (2001).
3) I. C. Cloët, W. Bentz and A. W. Thomas, Phys. Lett. B **621**, 246 (2005).

† Condensed from an article by Y. Ninomiya *et al.*, Phys. Rev. C **91**, 025202 (2015).

*1 Department of Physics, School of Science, Tokai University
*2 RIKEN Nishina Center
*3 Physics Division, Argonne National Laboratory

Chiral Magnetic and Vortical Effects at Weak Coupling

H. -U. Yee[*1,*2]

Chiral magnetic and vortical effects are parity-odd transport phenomena in the hydrodynamics of a plasma of chiral massless fermions, which are macroscopic manifestations of the underlying microscopic chiral anomaly. For the plasma of a single right-handed Weyl fermion, the chiral magnetic effect dictates a current along an applied external magnetic field $\vec{B}$ as $\vec{J} = \frac{\mu}{4\pi^2}\vec{B}$ where μ is the chemical potential, and in the case of chiral vortical effect, the vorticity of fluid $\vec{\omega} = (1/2)\vec{\nabla} \times \vec{v}$ plays a role similar to the magnetic field, $\vec{J} = (\mu^2 + \pi^2 T^2/3)\vec{\omega}$. These effects are robust due to the topological nature of chiral anomaly, and should persist both in weak and strong coupling limits. Demonstrating the expected universality of these phenomena in weak and strong coupling limits is an interesting and non-trivial test of the topological nature of chiral anomaly. While the strong coupling limit provided by AdS/CFT correspondence has successfully confirmed the universality of these effects, the weak coupling picture, albeit more intuitive, contains more subtleties that need to be carefully taken into accounts.

In general, one can define the chiral magnetic conductivity[1] $\sigma_\chi(\omega, k)$ by $\vec{J} = \sigma_\chi(\omega, k)\vec{B}(\omega, k)$ where (ω, k) are frequency and longitudinal momentum of the in-homogeneous time-dependent magnetic field $\vec{B}(\omega, k)$. One expects the zero frequency-momentum limit of $\sigma_\chi(\omega, k)$ to reproduce the topologically robust result of chiral magnetic effect, $\lim_{k\to 0}\lim_{\omega\to 0}\sigma_\chi(\omega, k) = \frac{\mu}{4\pi^2}$. In the interaction-free limit, both diagrammatic[1] and kinetic[2] approaches give a result for $\sigma_\chi(\omega, k)$ such that $\lim_{k\to 0}\lim_{\omega\to 0}\sigma_\chi(\omega, k) \neq \lim_{\omega\to 0}\lim_{k\to 0}\sigma_\chi(\omega, k) = \frac{1}{3}\cdot\frac{\mu}{4\pi^2}$, while a hydrodynamic argument indicates that there should not be such a difference between the two limits[3]. Since hydrodynamic regime exists only in an interacting theory, it is natural to study this issue in an interacting theory going beyond the non-interacting limit. In Ref.[3] we showed in both kinetic and diagrammatic approaches that the above difference between two limits disappears in the presence of relaxation dynamics caused by interactions, confirming the expectation from the hydrodynamics argument.

It is interesting to understand how chiral magnetic and vortical effects arise in the quasi-particle picture of kinetic theory of chiral fermions. The essential ingredient that is responsible for chiral anomaly is the Berry's curvature in momentum space[4,5], $\vec{b} = \vec{\nabla}_p \times \mathcal{A}_p = \vec{p}/2|\vec{p}|^3$, where $\mathcal{A}_p$ is the Berry's connection of momentum-dependent chiral spinors. We showed in Ref.[6] that the quasi-particle energy in the presence of magnetic field is dictated to be $\epsilon(\vec{p}) = |\vec{p}| - \vec{B}\cdot\vec{p}/2|\vec{p}|^2$ by Lorentz invariance where the second term is a spin-magnetic moment interaction. This term brings about several interesting consequences. Since the equilibrium distribution is $f^{eq}(\vec{p}) = 1/(\exp[\beta\epsilon(\vec{p})] + 1)$ the distribution becomes distorted by the magnetic field, which causes a net current along the magnetic field. This effect turns out to explain 1/3 of the full chiral magnetic effect. On the other hand, the equation of motions of quasi-particles with the Berry's curvature is given by[5] $\sqrt{G}\dot{\vec{x}} = \partial\epsilon/\partial\vec{p} + (\vec{b}\cdot\partial\epsilon/\partial\vec{p})\vec{B}$ where $\sqrt{G} = 1 + \vec{b}\cdot\vec{B}$ is the modified phase space density. The second term proportional to $\vec{B}$ induces a net current along the magnetic field even with spherically symmetric equilibrium distribution. This contribution gives the rest 2/3 of the full chiral magnetic effect.

Interestingly, a similar feature also exists in the chiral vortical effect[6]. With the fluid vorticity $\vec{\omega}$, a detailed valance in the Boltzmann equation with conservation of angular momentum $\vec{L} = \vec{x}\times\vec{p} + (1/2)\vec{p}/|\vec{p}|$, where the second term is the spin angular momentum, dictates the equilibrium distribution to be $f^{eq} = 1/(\exp[\beta(\epsilon - \frac{\vec{\omega}\cdot\vec{p}}{2|\vec{p}|})] + 1)$, which induces a net current proportional to $\vec{\omega}$: the result comprises 1/3 of the full chiral vortical effect. From the spin-magnetic moment interaction term in the energy, $-\vec{B}\cdot\vec{p}/2|\vec{p}|^2$, one can obtain a contribution to the current by the variation of the quasi-particle action with respect to eternal gauge potential, the result of which takes a form $\Delta\vec{J} = \int d^3\vec{p}/(2\pi)^3\,(\vec{\nabla}f\times\vec{p}/(2|\vec{p}|^2))$. With distribution function $f = f^{eq}(\epsilon - \vec{v}\cdot\vec{p})$, the resulting current along $\vec{\omega}$ constitutes the rest 2/3 of the chiral vortical effect.

In space-time dimensions higher than four, there are generalizations of chiral magnetic and vortical effects. A weak coupling computation of them in real-time formalism was performed in Ref.[7], which successfully confirmed the hydrodynamics prediction in Ref.[8]

*1 Department of Physics, University of Illinois, Chicago
*2 RIKEN Nishina Center

References

1) D. E. Kharzeev and H. J. Warringa, Phys. Rev. D **80**, 034028 (2009).
2) D. T. Son and N. Yamamoto, Phys. Rev. D **87**, no. 8, 085016 (2013).
3) D. Satow and H. U. Yee, Phys. Rev. D **90**, 014027 (2014).
4) D. T. Son and N. Yamamoto, Phys. Rev. Lett. **109**, 181602 (2012).
5) M. A. Stephanov and Y. Yin, Phys. Rev. Lett. **109**, 162001 (2012).
6) J. Y. Chen, D. T. Son, M. A. Stephanov, H. U. Yee and Y. Yin, Phys. Rev. Lett. **113**, no. 18, 182302 (2014).
7) H. U. Yee, Phys. Rev. D **90**, 065021 (2014).
8) D. E. Kharzeev and H. U. Yee, Phys. Rev. D **84**, 045025 (2011).

Collinear parton splitting for early thermalization and chemical equilibration in heavy-ion collisions

A. Monnai*1 and B. Müller*2,*3

High-energy heavy-ion collisions at the BNL Relativistic Heavy Ion Collider (RHIC) and CERN Large Hadron Collider (LHC) are the gateway to the early universe, where quarks and gluons are deconfined from hadrons. The strong elliptic flow observed suggests that the system is thermally equilibrated within a very short time $\tau_{\rm th} = 0.5$-1 fm/c, at which point relativistic hydrodynamics becomes a valid description of the bulk medium. The mechanism that leads to the early equilibration, on the other hand, is still not well known. A theoretical explication of the formation of a QCD droplet is of high importance in collider physics.

In this work, we propose a phenomenological description of the local early equilibration based on collinear parton splitting and recombination[1]. Equilibration of a heavy-ion system requires (i) thermalization, (ii) chemical equilibration, and (iii) isotropization since the colliding nuclei are described as the color glass condensate where gluons are saturated up to the typical momentum $p \simeq Q_s$[2]. Collinear splitting introduces two low-momentum partons from a high-momentum incident parton. This is suitable for the description of the first two types of equilibration because the thermal distribution has a relatively large number of low-momentum partons. The processes we consider are (a) splitting of a gluon into two gluons, (b) gluon emission by quarks and (c) quark-antiquark pair production. Momentum fraction in a splitting is governed by the parton splitting functions[3]. The rate of splitting in a dimensional analysis is given as $\Gamma \simeq \alpha_s^{1/2}(\hat{q}/p)^{1/2}$, where α_s is the QCD coupling and $\hat{q}$ is the transport coefficient for momentum diffusion. The recombination processes are introduced phenomenologically; hence, the equations of motion for the quark and the gluon phase-space distributions satisfy the second law of thermodynamics. The effects of elastic scattering, which creates off-shell partons, are encoded in the model via the Focker-Planck equation. The detailed expressions of the equations of motion can be found here[1].

We perform numerical estimations with a non-expanding (1+1)-dimensional geometry to investigate the qualitative properties of the equilibration model. Figure 1 shows the gluon distribution of a pure gluon system before and after time-evolution. The effective degrees of freedom are included in the definition of the phase-space distribution. Here, the initial condition is a color-glass-like one where $f^g(p=0) \simeq 1/\alpha_s$ and $Q_s \simeq 2$ GeV. The system almost thermalizes at 0.8 fm/c when the initial time is 0.2 fm/c. Next, we consider the case when $N_f = 3$ and obtain the gluon and the quark distributions shown in Fig. 2. Here, the system approaches the thermalized state rather quickly, but the effective numbers of degrees of freedom remain far from those in equilibrium owing to the slowness of the quark chemical equilibration process. For the current parameter settings, the typical time required for chemical equilibration is estimated as $\tau_{\rm chem} \simeq 2$ fm/c. The results imply that collinear parton splitting and recombination play an important role in the early-time dynamics of heavy-ion collisions, and the quark-gluon plasma at the onset of hydrodynamic evolution can be gluon-rich.

Future prospects include improvement of the model parameters and development of a (3+1)-dimensional numerical model for quantitative description of isotropization in such QCD systems.

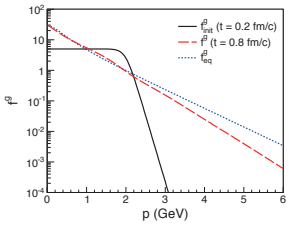

Fig. 1. Gluon distribution before and after the time-evolution compared with that in equilibrium.

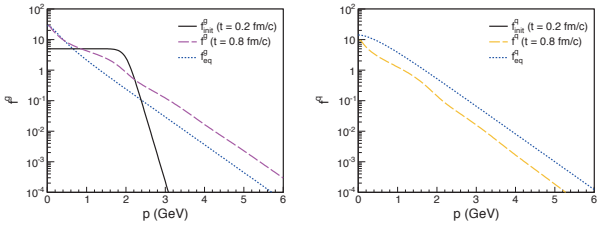

Fig. 2. (Left panel) Gluon and (right panel) quark distributions before and after the time-evolution compared with those in equilibrium.

*1 RIKEN Nishina Center
*2 Physics Department, Duke University
*3 Brookhaven National Laboratory

References
1) A. Monnai and B. Müller: arXiv:1403.7310 [hep-ph].
2) L. D. McLerran and R. Venugopalan: Phys. Rev. D **49**, 2233 (1994); D **49**, 3352 (1994).
3) G. Altarelli and G. Parisi: Nucl. Phys. B **126**, 298 (1977).

Chemical equilibration of QCD medium for photon v_2 puzzle

A. Monnai*1

Discovery of the quark-gluon plasma (QGP), a deconfined phase of QCD, at BNL Relativistic Heavy Ion Collider and CERN Large Hadron Collider is a milestone in hadron physics. The produced medium is considered to be strongly coupled because the momentum anisotropy in hadronic spectra is large enough to validate hydrodynamic description. This is quantified by elliptic flow v_2 defined as a Fourier expansion coefficient of the yield N:

$$\frac{dN}{d\phi} = \frac{N}{2\pi}[1 + 2\sum_{n=1} v_n \cos(\phi - \Psi_n)], \tag{1}$$

where ϕ is the azimuthal angle in momentum space and Ψ_n is the n-th harmonic event plane. On the other hand, direct photon v_2 is found to be a few times larger than hydrodynamic predictions,[1,2] which is recognized as the "photon v_2 puzzle." Of direct photons, thermal photons from the QGP medium are the dominant source of anisotropy because prompt photons from initial hard processes do not have it intrinsically.

In this work, I have considered the effects of chemical equilibration in the QGP on thermal photon v_2.[3] A heavy-ion system before the collision is described as the color glass condensate, a state of saturated gluons. Several early equilibration models indicate that chemical equilibration is slower than thermalization.[4] This implies that the quark number at the onset of hydrodynamic evolution is smaller than that under equilibrium. Since photons are coupled to quarks, late chemical equilibration suppresses the emission of thermal photons in the early stages where flow anisotropy is still small. Consequently, thermal photon v_2 can become effectively large owing to the contribution from later times.

I have developed a new (2+1)-dimensional ideal hydrodynamic model and coupled it to the rate equations for the parton number densities. The number changing processes are (a) $g \leftrightarrow gg$, (b) $g \leftrightarrow q\bar{q}$, and (c) $q(\bar{q}) \leftrightarrow gq(g\bar{q})$. Here, the vanishing net baryon number limit is considered. The relaxation equations are:

$$\partial_\mu N_q^\mu = 2r_b n_g - 2r_b \frac{n_g^{\rm eq}}{(n_q^{\rm eq})^2} n_q^2, \tag{2}$$

$$\partial_\mu N_g^\mu = (r_a - r_b) n_g - r_a \frac{1}{n_g^{\rm eq}} n_g^2 + r_b \frac{n_g^{\rm eq}}{(n_q^{\rm eq})^2} n_q^2 + r_c n_q - r_c \frac{1}{n_g^{\rm eq}} n_q n_g, \tag{3}$$

where r_a, r_b, and r_c are the reaction rates. Since pair production is the only quark numbe-changing process, chemical equilibration time would be given by $\tau_{\rm chem} = 1/r_b$. Here, the rates are parametrized as $r_i = c_i T$. The equation of state is a hyperbolic interpolation of those for hadron and parton gases with $N_f = 2$. The thermal photon emission rate is also derived from those for the hadron and QGP phases.

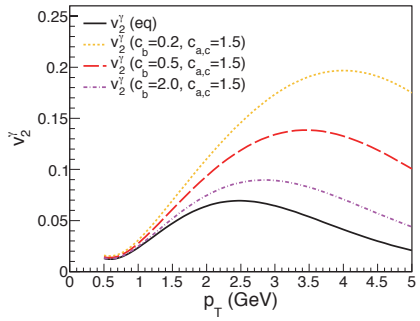

Fig. 1. Thermal photon v_2 with different quark chemical equilibration rates.

Figure 1 shows the elliptic flow of thermal photons for Au-Au collisions at $\sqrt{s_{NN}} = 200$ GeV with the impact parameter $b = 7$ fm. The chemical reaction parameters are chosen as $c_b = 0.2, 0.5$, and 2.0, where $c_{a,c} = 1.5$. Thermal photon v_2 can be visibly enhanced by late quark chemical equilibration. For the suggested chemical equilibration time $\tau_{\rm chem} = 2$ fm,[4] $c_b = 0.5$ follows from $T \sim 0.2$ GeV. The dependences on the gluon number-changing processes characterized with r_a and r_c are found to be small as expected. The particle spectrum of thermal photons is not affected much by chemical non-equilibrium with the current parameter settings. This implies that late quark chemical equilibration is important to explain the photon v_2 problem. It should be noted that the mechanism can also be an explanation to the large photon v_3 recently observed in the experiments.

Future prospects include the introduction of a dynamical equation of state, improved initial conditions, and chemical equilibration rates. Effects of viscosities would also be important in quantitative discussion because thermal photons are sensitive to early-time fluid dynamics where off-equilibrium corrections are large because photons can pass through the QCD medium.

† Condensed from the article in Phys. Rev. C **90**, 021901(R) (2014)

*1 RIKEN Nishina Center

References

1) A. Adare *et al.* [PHENIX Collaboration]: Phys. Rev. Lett. **109**, 122302 (2012).
2) D. Lohner [ALICE Collaboration]: J. Phys. Conf. Ser. **446**, 012028 (2013).
3) A. Monnai: Phys. Rev. C **90**, 021901 (2014).
4) A. Monnai and B. Müller: arXiv:1403.7310 [hep-ph].

Refraction of light in the quark-gluon plasma

A. Monnai*1

Electromagnetic probes in high-energy heavy-ion collisions provide us with important information on the quark-gluon plasma (QGP) because experimental data indicate that the hot medium is color opaque but electromagnetically transparent. An important discovery regarding such probes is the excessive yield of direct photon elliptic (v_2) and triangular flow (v_3).[1] Direct photons consist of prompt photons created in the initial hard processes and thermal photons emitted from the medium. Flow harmonics is defined as a Fourier expansion coefficient of particle spectra in the azimuthal angle and is induced by geometrical anisotropy in the system via medium interaction. Since hadronic flow harmonics follows hydrodynamic description and is considered as an evidence for the existence of a strongly coupled medium, quantitative understanding of the direct photon flow harmonics is an important issue in heavy-ion phenomenology.

I have investigated the effect of refraction on prompt photons by the QGP medium in the transverse plane (Fig. 1).[2] The emission rate for prompt photons is derived from p-p collision data.[3] The path of a ray in a medium with the refractive index n is given as $d^2x/d\tau^2 = (1/2)dn^2/dx$ according to Fermat's principle. The dynamical evolution of an inhomogeneous medium should be considered, because the typical lifetime and size of the system are comparable. Here, I use a (2+1)-dimensional ideal hydrodynamic model with Monte-Carlo Glauber initial conditions and a lattice QCD equation of state. The initial time is 0.4 fm/c and the freeze-out temperature is 0.15 GeV. The temperature and frequency dependence of the refractive index is parametrized as $n^2(T,\omega) = 1-\omega_p^2/\omega^2$, where the plasma frequency is parametrized as $\omega_p^2 = a^2T^2$. In the high-temperature limit, $\omega_p^2 \sim m_D^2 \sim e^2T^2$ is obtained using the Debye mass m_D. This implies $a^2 \sim 10^{-1}$ since $e^2 = 4\pi\alpha_{\rm EM}$. The frequency ω is Doppler-shifted from the original frequency as $\omega = \omega_0/\gamma(1+\beta\cos\Delta\phi)$, where $\Delta\phi$ is the angle between the flow and the direction of a ray. It should be noted that the phase velocity in the QGP medium, $v_{\rm ph} = 1/n$, exceeds the speed of light, but causality is not violated because the group velocity remains smaller than unity. When $n^2 < 0$, the medium does not bend a ray but partially absorbs it.

The elliptic flow of prompt photons is shown in Fig. 2. When there is no refraction, the quantity vanishes. For non-unity refractive indices, on the other hand, positive v_2 is observed above plasma frequencies. The magnitude, however, is not large enough to account for the large photon v_2 found in collider experiments. Below the plasma frequency, the high-temperature region near the center of the medium becomes semitransparent and suppresses photons traveling horizontally, leading to negative v_2. Once the entire system becomes translucent at low momentum, v_2 again becomes positive because photons have better chance of moving out of the medium in the direction of the minor axis. This implies that the QGP plasma frequency can be constrained from measurements. The absorptive behavior has not been found in photon p_T spectra above 0.5 GeV at RHIC and 1 GeV at LHC.[4] Here, the former condition is more stringent and the maximum refraction parameter allowed is $a^2 \sim$ 1-2. Higher-order harmonics, v_3-v_5, are found to be positive but small. Note that the above argument depends on the choice of refractive index. Numerical analyses with different indices and introduction of thermal photons will be performed in the future.

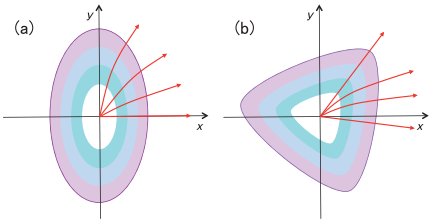

Fig. 1. Schematic of medium refraction for (a) elliptic flow and (b) triangular flow.

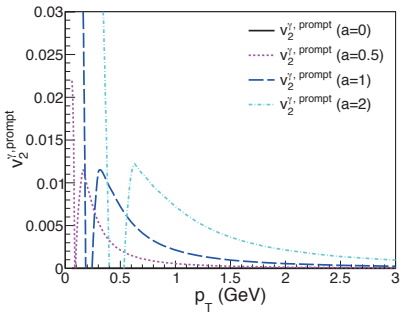

Fig. 2. Differential elliptic flow of prompt photons for different refraction parameters.

*1 RIKEN Nishina Center

References
1) A. Adare *et al.* [PHENIX Collaboration]: Phys. Rev. Lett. **109**, 122302 (2012).
2) A. Monnai: arXiv:1408.1410 [nucl-th].
3) S. Turbide, R. Rapp and C. Gale: Phys. Rev. C **69**, 014903 (2004).
4) A. Adare *et al.* [PHENIX Collaboration]: arXiv:1405.3940 [nucl-ex].

Transverse single-spin asymmetries in proton-proton collisions and the role of twist-3 fragmentation†

D. Pitonyak,[*1] K. Kanazawa,[*2] Y. Koike,[*3] and A. Metz[*2]

The field of transverse single-spin asymmetries (SSAs) in hard semi-inclusive processes began close to 40 years ago at FermiLab. People noticed early on that the collinear parton model cannot generate the large effects that were found. It was then pointed out that SSAs for single-particle production in hadronic collisions are genuine twist-3 observables for which, in particular, collinear 3-parton correlations have to be taken into account. This formalism later on was worked out in more detail and applied to SSAs in processes like light hadron production in proton-proton collisions, $p^\uparrow p \to hX$. Here we focus on SSAs in such reactions, which have been complemented by many experiments, including those at RHIC.

For quite some time it was believed that effects inside the transversely polarized proton dominate the transverse SSA in $p^\uparrow p \to hX$ (typically denoted by A_N)[1–4]. In particular, the so-called Qiu-Sterman function T_F was thought to be the main non-perturbative object that generates this observable. T_F can be related to the transverse-momentum dependent (TMD) Sivers parton density $f_{1T}^\perp$. Because of this relation, one can extract T_F from data on either A_N or on the Sivers transverse SSA in semi-inclusive deep-inelastic scattering (SIDIS) A_{SIDIS}^{Siv}. It therefore came as a major surprise when an attempt failed to simultaneously explain both A_N and A_{SIDIS}^{Siv} — the two extractions for T_F actually differ in sign[5], a puzzle that has become known as the "sign mismatch".

At this point one may start to question the dominance of T_F. In fact, data on the neutron target transverse SSA in inclusive DIS[6] seem to support this point of view[7]. Therefore, we study here the potential role of fragmentation effects, whose analytical result in the twist-3 formalism was first worked out in [8]. It involves the non-perturbative functions $\hat{H}$, $\hat{H}_{FU}^{\Im}$, and H, where the first is related to the TMD Collins function and the third can be written in terms of the other two.

In Fig. 1 we show our results from fitting the collinear 3-parton fragmentation correlator $\hat{H}_{FU}^{\Im}$ to data for $A_N^{\pi^0}$ from STAR[9–11] and $A_N^{\pi^\pm}$ from BRAHMS[12]. Our fit describes the data very well; moreover, one can see without $\hat{H}_{FU}^{\Im}$, one cannot obtain the rise in A_N at large x_F that is characteristic of the data. Therefore, we have demonstrated for the first time that twist-3 factorization actually can describe high-energy RHIC data for A_N^π if one takes the fragmentation contribution into account. This work also allows us to potentially resolve the sign-mismatch crisis since one does not need T_F to describe the data. Since in the twist-3 approach part of A_N can be fixed by spin/azimuthal asymmetries in SIDIS and in $e^+e^- \to h_1h_2X$, we have shown that at present a simultaneous description of all those observables is possible.

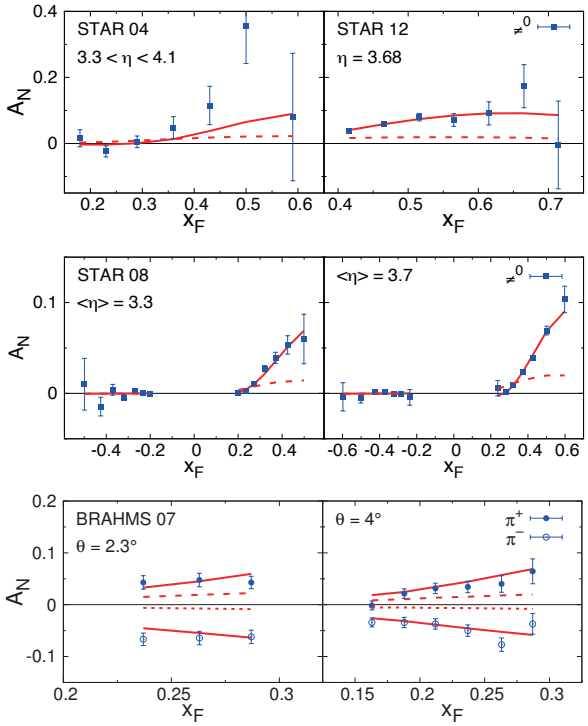

Fig. 1. Fit results for $A_N^{\pi^0}$ and $A_N^{\pi^\pm}$. The dashed line (dotted line in the case of π^-) means $\hat{H}_{FU}^{\Im}$ switched off.

† Condensed from the article in PRD **89**, 111501(R) (2014)
*1 RIKEN Nishina Center
*2 Department of Physics, Temple University
*3 Department of Physics, Niigata University

References
1) J.-w. Qiu and G. Sterman, Phys. Rev. D **59**, 014004 (1999).
2) C. Kouvaris *et al.*, Phys. Rev. D **74**, 114013 (2006).
3) Y. Koike and T. Tomita, Phys. Lett. B **675**, 181 (2009).
4) K. Kanazawa and Y. Koike, Phys. Rev. D **82**, 034009 (2010); Phys. Rev. D **83**, 114024 (2011).
5) Z.-B. Kang *et al.*, Phys. Rev. D **83**, 094001 (2011).
6) J. Katich, Phys. Rev. Lett. **113**, 022502 (2014).
7) A. Metz *et al.*, Phys. Rev. D **86**, 094039 (2012).
8) A. Metz and D. Pitonyak, Phys. Lett. B **723**, 365 (2013).
9) J. Adams *et al.* [STAR Collaboration], Phys. Rev. Lett. **92**, 171801 (2004).
10) B. I. Abelev *et al.* [STAR Collaboration], Phys. Rev. Lett. **101**, 222001 (2008).
11) L. Adamczyk *et al.* [STAR Collaboration], Phys. Rev. D **86**, 051101 (2012).
12) J. H. Lee *et al.* [BRAHMS Collaboration], AIP Conf. Proc. **915**, 533 (2007).

Left-right spin asymmetries in lepton-nucleon collisions†

D. Pitonyak,[*1] L. Gamberg,[*2] Z.-B. Kang,[*3] A. Metz,[*4] and A. Prokudin[*5]

The field of transverse single-spin asymmetries (SSAs) in hard semi-inclusive processes began close to 40 years ago when large effects were found at FermiLab that could not be generated within the collinear parton model. Here we focus on the left-right azimuthal asymmetry that can be defined in single-inclusive leptoproduction of hadrons if the nucleon is transversely polarized, $\ell N^\uparrow \to hX$. This asymmetry is similar to the transverse single-spin asymmetry A_N that occurs in $p^\uparrow p \to h\,X$, which has been intensely studied at RHIC. Recently, the HERMES Collaboration[1)] and the Jefferson Lab Hall A Collaboration[2)] reported the first ever measurements of A_N in lepton-nucleon scattering. In general, one may expect that A_N in this reaction could give new insight into the underlying mechanism of A_N in hadronic collisions that is the subject of longstanding discussions.

We compute A_N for $\ell N^\uparrow \to hX$ in collinear factorization, where one can have twist-3 effects in the transversely polarized nucleon or in the unpolarized outgoing hadron. The former involves the so-called Qiu-Sterman function F_{FT} — a specific quark-gluon-quark correlator that has an intimate connection with the transverse momentum dependent (TMD) Sivers function $f_{1T}^\perp$, while the latter arises from parton fragmentation, specifically through the functions $\hat{H}$, H, and $\hat{H}_{FU}^{\Im}$, where the first is related to the TMD Collins function. Both of these mechanisms have been studied in $p^\uparrow p \to h\,X$ within collinear factorization, e.g., in [3–6)]. Note that $\ell N^\uparrow \to hX$ has also been computed in the so-called Generalized Parton Model (GPM) (most recently in [7)]), which uses TMD parton correlation functions.

We will estimate A_N based on leading-order formulas, which we refrain from showing here explicitly for brevity, and study the contributions from the distribution term involving F_{FT}, and the fragmentation term involving $\hat{H}$, H, and $\hat{H}_{FU}^{\Im}$. It is important to realize that for the process at hand, $\ell\,N \to h\,X$, only the hadron transverse momentum $P_{h\perp}$ can serve as the hard scale. Here we give a sample of our results, namely some for HERMES and an EIC. In Fig. 1 we plot (in the top panel) A_N as a function of $x_F^{\rm H} = -x_F$ for π^+ production with $1 < P_{h\perp} < 2.2$ GeV ($\langle P_{h\perp}\rangle \simeq 1$ GeV) for lepton-proton collisions at HERMES energy $\sqrt{S} = 7.25$ GeV. Also shown (in the bottom panel) is our prediction for π^0 production at EIC energy

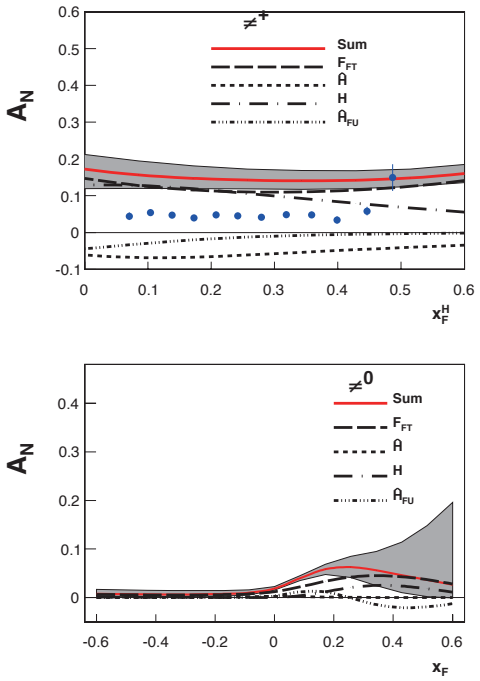

Fig. 1. A_N as a function of $x_F^H = -x_F$ for π^+ at HERMES kinematics (top), and a prediction for A_N as function of x_F for π^0 at EIC kinematics (bottom).

$\sqrt{S} = 63$ GeV and $P_{h\perp} = 3$ GeV. Note that for $p^\uparrow p \to \pi\,X$ in the forward region ($x_F > 0$) very large values for A_N have been observed. We find that a non-zero A_N is predicted in this region at an EIC.

We see that our theoretical estimates for A_N agree with the HERMES results in sign and roughly in shape, but in terms of magnitude they are typically above the data. Such a discrepancy cannot be considered a failure of the collinear twist-3 formalism, but rather shows the need for for a next-to-leading order calculation, especially in the region of lower $P_{h\perp}$. It will also be important to better constrain the 3-parton fragmentation correlator $\hat{H}_{FU}^{\Im}$ through measurements, e.g., of $A_N^{\pi^-}$, which might allow one to test the recent extraction of $\hat{H}_{FU}^{\Im}$ that can play a crucial role in A_N in pp collisions[6)], and to discriminate between the GPM and the twist-3 frameworks.

† Condensed from the article in PRD **90**, 074012 (2014)
*1 RIKEN Nishina Center
*2 Division of Science, Penn State University–Berks
*3 Theoretical Division, Los Alamos National Lab
*4 Department of Physics, Temple University
*5 Jefferson Lab

References

1) A. Airapetian *et al.* [HERMES Collaboration], Phys. Lett. B **728**, 183 (2014).
2) K. Allada *et al.* [Jefferson Lab Hall A Collaboration], Phys. Rev. C **89**, 042201 (2014).
3) J.-w. Qiu and G. Sterman, Phys. Rev. D **59**, 014004 (1999).
4) C. Kouvaris *et al.*, Phys. Rev. D **74**, 114013 (2006).
5) A. Metz and D. Pitonyak, Phys. Lett. B **723**, 365 (2013).
6) K. Kanazawa *et al.*, Phys. Rev. D **89**, 111501(R) (2014).
7) M. Anselmino *et al.*, Phys. Rev. D **89**, 114026 (2014).

Twist-3 double-spin asymmetries in lepton-nucleon collisions†

D. Pitonyak,[*1] K. Kanazawa,[*2] A. Metz,[*2] and M. Schlegel[*3]

Hadrons, the strongly interacting particles that comprise almost all of the visible matter in the universe, have been shown to possess a complex inner-structure that goes beyond a simple quark picture. For example, experimental results in the 1970s on transverse single-spin asymmetries (SSAs) revealed the crucial role that quark-gluon-quark correlations could play in hadrons. This is a consequence of the fact that such observables are twist-3 effects. Much work over the last 40 years has been performed in the study of transverse SSAs from both the experimental and theoretical sides. In addition, one also has twist-3 double-spin asymmetries (DSAs), namely those where one particle is longitudinally polarized and the other is transversely polarized. We will denote these by A_{LT}. The classic process for which this effect has been analyzed is A_{LT} in inclusive deep-inelastic lepton-nucleon scattering (DIS). In that case the entire result can be written in terms of the collinear twist-3 function $g_T(x)$. Furthermore, this asymmetry has been studied in the Drell-Yan process involving two incoming polarized hadrons[1–4]; in inclusive lepton production from W-boson decay in proton-proton scattering[5]; for jet production in lepton-nucleon collisions[6]; and for direct photon production[7], jet/hadron production[8], and D-meson production[9] in nucleon-nucleon collisions.

Here we consider the reaction $\vec{\ell} N^{\uparrow} \to h X$, where one can have twist-3 contributions from both the distribution (incoming nucleon) and the fragmentation (outgoing hadron) sides. The leading-order (LO) analytical formulas for these terms are new results from this work, but we refrain from showing them explicitly for brevity. Based on this computation we will give numerical estimates for $\vec{e} N^{\uparrow} \to \pi X$, where $N = p, n$. We will only look at the distribution piece, where we need LO input for the non-perturbative functions $D_1(z)$ (unpolarized fragmentation function), $\tilde{g}(x)$ ("worm-gear"-type function), $g_T(x)$, and $g_1(x)$ (helicity distribution), where $\tilde{g}(x)$ is the least known of these functions and has gained quite some interest over the years.

Since we have little information on $\tilde{g}(x)$, we look at two scenarios: i) using the approximate relation $\tilde{g}(x) \approx -f_{1T}^{\perp(1)}(x)$, where $f_{1T}^{\perp}$ is the Sivers function; and ii) using a Wandzura-Wilczek (WW)-type approximation $\tilde{g}(x) \approx x \int_x^1 \frac{dy}{y} g_1(y)$, which was also used elsewhere in the literature and holds relatively well in certain models. In both cases for $g_T(x)$ we use the WW approximation, $g_T(x) \approx \int_x^1 \frac{dy}{y} g_1(y)$. In Fig. 1 we show a sample of our results, namely for HERMES and JLab6, where finalized data is expected soon from both groups.

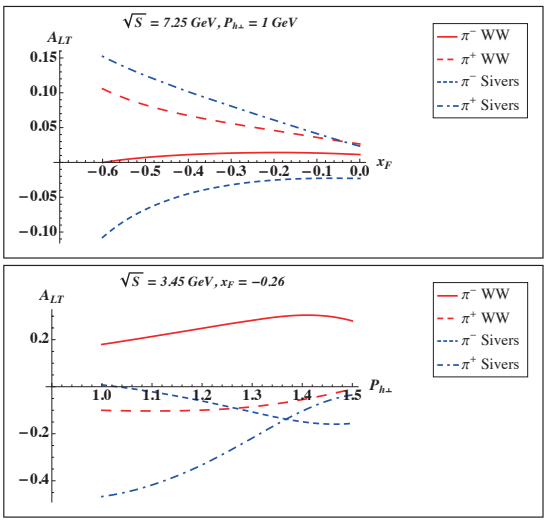

Fig. 1. A_{LT} vs. x_F for HERMES (top) and A_{LT} vs. $P_{h\perp}$ for JLab6 (bottom), where $x_F = 2P_{hz}/\sqrt{S}$ with P_{hz} ($P_{h\perp}$) the hadron's longitudinal (transverse) momentum.

We see from our plots that the "Sivers" input and "Wandzura-Wilczek" input can give quite different results due to the different behavior of $\tilde{g}(x)$. Thus, even a qualitative comparison of our predictions with experiment could help distinguish between the Sivers and WW scenarios. Moreover, if the magnitude of the data is in line with our results, one could have direct access to the "worm-gear"-type function $\tilde{g}(x)$, which has received some attention recently. If the magnitude is not in agreement, this observable could give insight into the importance of quark-gluon-quark correlations in the nucleon and/or twist-3 fragmentation effects in unpolarized hadrons. However, one always has to keep in mind the potential large impact of next-to-leading order terms. In general, we found the best chance to measure a nonzero asymmetry is at HERMES, JLab, and COMPASS, as the high center-of-mass energy of an EIC leads to a very small effect. We expect this conclusion to be rather robust.

† Condensed from the article arXiv:1411.6459 submitted to PLB
*1 RIKEN Nishina Center
*2 Department of Physics, Temple University
*3 Institute for Theoretical Physics, Tübingen University

References

1) R. L. Jaffe and X. D. Ji, Phys. Rev. Lett. **67**, 552 (1991); Nucl. Phys. B **375**, 527 (1992).
2) R. D. Tangerman and P. J. Mulders, hep-ph/9408305.
3) Y. Koike *et al.*, Phys. Lett. B **668**, 286 (2008).
4) Z. Lu and I. Schmidt, Phys. Rev. D **84**, 114004 (2011).
5) A. Metz and J. Zhou, Phys. Lett. B **700**, 11 (2011).
6) Z.-B. Kang *et al.*, Phys. Rev. D **84**, 034046 (2011).
7) Z.-T. Liang *et al.*, Phys. Lett. B **712**, 235 (2012).
8) A. Metz *et al.*, Phys. Rev. D **86**, 114020 (2012).
9) Y. Hatta *et al.*, Phys. Rev. D **88**, 014037 (2013).

Strong binding and shrinkage of single and double $\bar{K}$ nuclear systems (K^-pp, K^-ppn, K^-K^-p and K^-K^-pp) predicted by Faddeev-Yakubovsky calculations

S. Maeda,[*1] Y. Akaishi,[*2,*3] and T. Yamazaki[*2,*4]

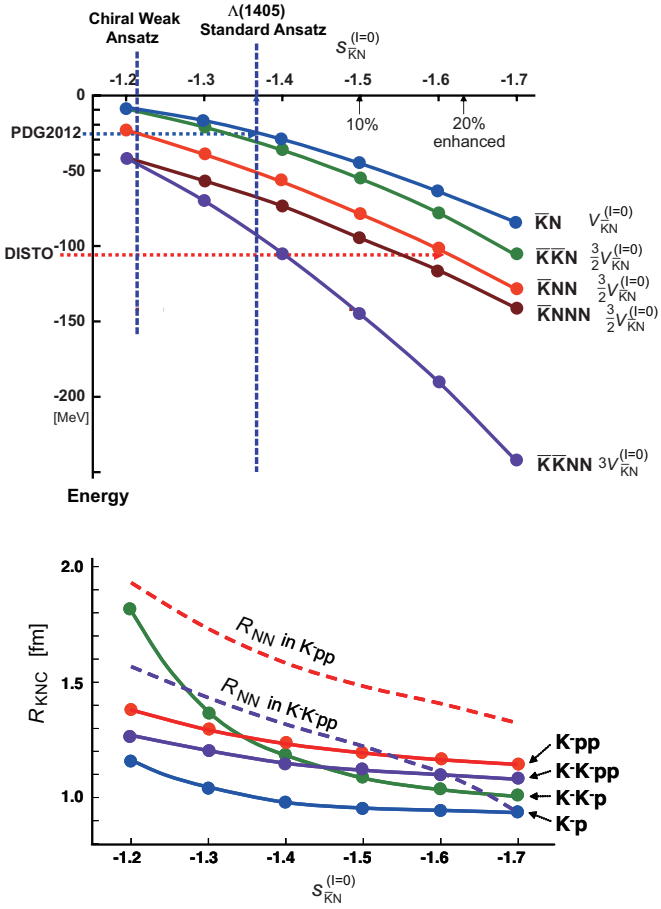

Fig. 1. Global view of the calculated bound-state energies (upper) and sizes (lower), $R_{\rm KNC}$ and R_{NN} of $\bar{K}$ nuclear clusters as functions of the $\bar{K}N$ interaction strength, $s_{\bar{K}N}^{(I=0)}$, which is normalized so as to be -1 at the binding threshold. The zones of the standard "Λ(1405) ansatz" ($s=-1.37$) and the "Chiral" ansatz ($s=-1.22$) are shown by vertical broken lines. The experimental value of the mass of K^-pp as observed by DISTO[7] is shown by a horizontal broken line, where a relativistic correction for the binding energy around 10 MeV is not taken into account.

Non-relativistic Faddeev and Faddeev-Yakubovsky calculations were made for K^-pp, K^-ppn, K^-K^-p and K^-K^-pp kaonic nuclear clusters, where the quasi bound states were treated as bound states by employing real separable potential models for the K^--K^- and the K^--nucleon interactions as well as for the nucleon-nucleon interaction[1].

The binding energies and spatial shrinkages of these states, obtained for various values of the $\bar{K}N$ interaction, were found to increase rapidly with the $\bar{K}N$ interaction strength. Their behaviors are shown in a reference diagram, Fig. 1, where possible changes by varying the $\bar{K}N$ interaction in the dense nuclear medium are given. Using the Λ(1405) ansatz with a PDG mass of 1405 MeV/c^2 for K^-p, the following ground-state binding energies together with the wave functions were obtained: 51.5 MeV (K^-pp), 69 MeV (K^-ppn), 30.4 MeV (K^-K^-p) and 93 MeV (K^-K^-pp), which are in good agreement with previous results of variational calculation based on the Akaishi-Yamazaki coupled-channel potential[2–5]. The K^-K^-pp state has a significantly increased density where the two nucleons are located very close to each other, in spite of the inner NN repulsion. Relativistic corrections on the calculated non-relativistic results indicate substantial lowering of the bound-state masses, especially of K^-K^-pp, toward the kaon condensation regime. The fact that the recently observed binding energy of K^-pp[7] is much larger (by a factor of 2) than the originally predicted one may infer an enhancement of the $\bar{K}N$ interaction in dense nuclei by about 25%, possibly due to chiral symmetry restoration. In this respect some qualitative accounts are given based on "clearing QCD vacuum" model of Brown, Kubodera and Rho.[8]

*1 Department of Agro-Environmental Science, Obihiro University of Agriculture and Veterinary Medicine.
*2 RIKEN Nishina Center
*3 College of Science and Technology, Nihon University
*4 Department of Physics, University of Tokyo

References

1) See full description: S. Maeda, Y. Akaishi and T. Yamazaki, Proc. Jpn. Acad. Ser. B **89** (2013) 418.
2) Y. Akaishi and T. Yamazaki, Phys. Rev. C **65** (2002) 044005.
3) T. Yamazaki and Y. Akaishi: Phys. Lett. B **535** (2002) 70.
4) T. Yamazaki, A. Doté and Y. Akaishi, Phys. Lett. B **587** (2004) 167.
5) T. Yamazaki and Y. Akaishi, Phys. Rev. C **76** (2007) 045201.
6) M. Agnello *et al.*, Phys. Rev. Lett. **94** (2005) 212303.
7) T. Yamazaki *et al.*, Phys. Rev. Lett. **104** (2010) 132502.
8) G.E. Brown, K. Kubodera and M. Rho, Phys. Lett. B **192** (1987) 273.

New way to produce dense double-antikaonic dibaryon system, K^-K^-pp, through $\Lambda(1405)$-doorway sticking in $p+p$ collisions

M. Hassanvand,[*1,*2] Y. Akaishi,[*1,*3] and T. Yamazaki[*1,*4]

A recent successful observation of a dense and deeply bound $\bar{K}$ nuclear system, K^-pp, in the $p+p \to K^+ + K^-pp$ reaction in a DISTO experiment[1] indicates that the double-$\bar{K}$ dibaryon, K^-K^-pp, which was predicted to be a dense nuclear system[2,3], can also be formed in $p+p$ collisions.

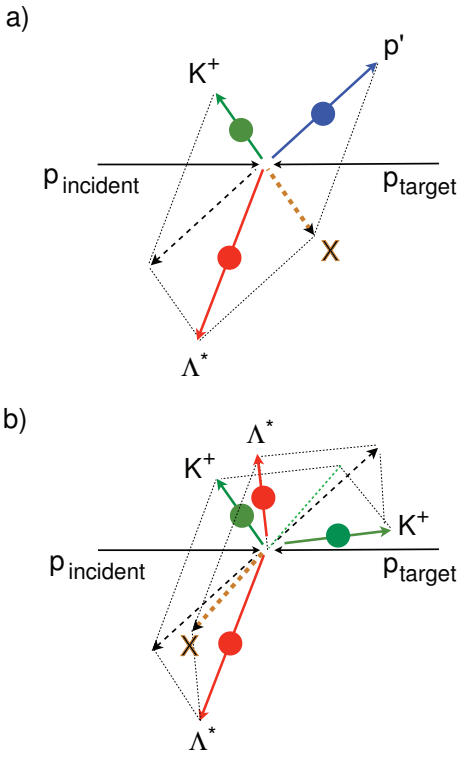

Fig. 1. Reaction diagrams in the center-of-mass system of pp collisions. a) For $pp \to K^+ + K^-pp$ and b) for $pp \to K^+ + K^+ + K^-K^-pp$. The $\Lambda(1405)$ resonance particle as a doorway is indicated by Λ^*.

We have formulated and calculated the differential cross section for the formation of the simplest double-$\bar{K}$ nuclear cluster system, K^-K^-pp, in the reaction process

$$p+p \to K^+ + K^+ + \Lambda^* + \Lambda^*,$$
$$\to K^+ + K^+ + K^-K^-pp,$$
$$\to K^+ + K^+ + \Lambda + \Lambda,$$

where Λ^* is a quasi-bound K^-p state corresponding to the $\Lambda(1405)$ resonance[4,5]. From a comprehensive study of the calculated effects of the binding and density of K^-K^-pp on the cross section, we find that the bound-state peak of K^-K^-pp dominates over the spectrum when and only when the system is dense. This is understood as the two Λ^* doorway particles interact immediately within a short distance, assisted by a large momentum transfer (~ 1.8 GeV/c) and a short collision length (~ 0.3 fm), which helps to enlarge the $\Lambda^* - \Lambda^*$ sticking into a dense K^-K^-pp system. See details in Ref.[4,5]. This mechanism is similar to that for a single $\bar{K}$ cluster (K^-pp) formation[6,7], which has just been proven by the DISTO experiment.

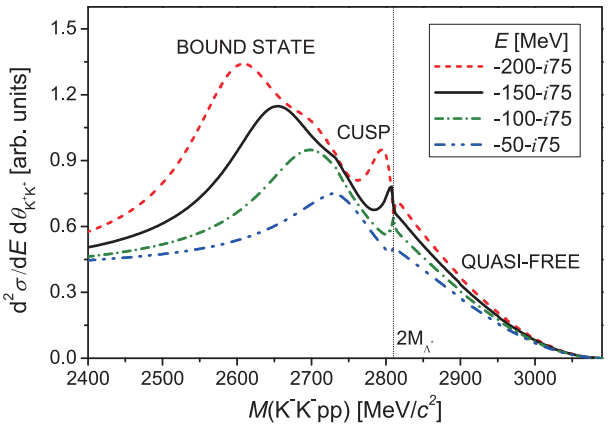

Fig. 2. (Color online) Differential cross sections for various bound-state energies, E, of the K^-K^-pp system for T_p = 7.0 GeV, Γ = 150 MeV, b = 0.3 fm and θ_{12} = 180.

*1 RIKEN Nishina Center
*2 Department of Physics, Isfahan University of Technology
*3 College of Science and Technology, Nihon University
*4 Department of Physics, University of Tokyo

References
1) T. Yamazaki *et al.*, Phys. Rev. Lett. **104** (2010) 132502.
2) T. Yamazaki, A. Doté and Y. Akaishi, Phys. Lett. B **587** (2004) 167.
3) S. Maeda, Y. Akaishi and T. Yamazaki, Proc. Jpn. Acad. Ser. B **89** (2013) 418.
4) T. Yamazaki, Y. Akaishi and M. Hassanvand, Proc. Jpn. Acad. Ser. B **87** (2011) 362.
5) M. Hassanvand, Y. Akaishi and T. Yamazaki, Phys. Rev. C **84** (2011) 015207.
6) T. Yamazaki and Y. Akaishi, Proc. Jpn. Acad. Ser. B **83** (2007) 144.
7) T. Yamazaki and Y. Akaishi, Phys. Rev. C **76** (2007) 045201.

Theoretical analysis of $\Lambda(1405) \rightarrow (\Sigma\pi)^0$ mass spectra produced in $p + p \rightarrow p + \Lambda(1405) + K^+$ reactions

M. Hassanvand,[*1,*2] S. Z. Kalantari,[*2] Y. Akaishi,[*1,*3] and T. Yamazaki [*1,*4]

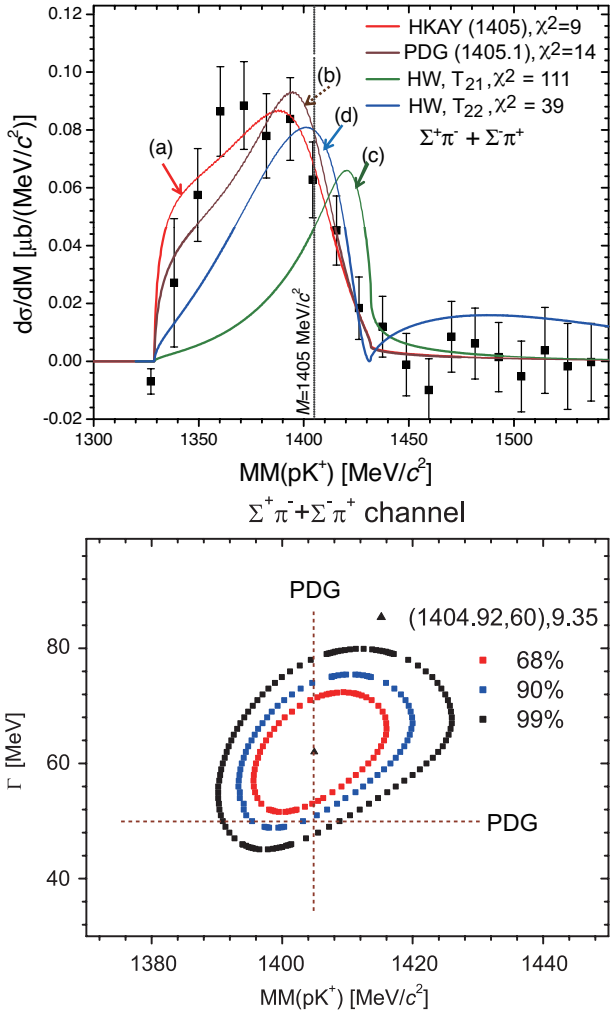

Fig. 1. (Color online) (Upper) Comparison of HADES data ($\Sigma^+\pi^- + \Sigma^-\pi^+$, closed squares) at $T_p = 3.50$ GeV[?)] with best-fit theoretical spectral functions $S(x)$. a) Best-fit HKAY curves (with $\chi^2 = 9.5$, $M = 1405^{+11}_{-9}$ MeV/c^2 and $\Gamma = 62 \pm 10$ MeV). b) AY model with the PDG parameters (with $\chi^2 = 14$, $M = 1405.1^{+1.3}_{-1.0}$ MeV/c^2 and $\Gamma = 50$ MeV[6)]). The *Chiral* model using HW's T_{21} (with $\chi^2 = 111$, c)) and T_{22} (with $\chi^2 = 40$, d)). (Lower) Confidence level contours from χ^2 fitting of the HADES data of $\Sigma^+\pi^- + \Sigma^-\pi^+$ at $T_p = 3.50$ GeV. The PDG12 values are also shown.

We formulated the $\Lambda(1405)$ (abbreviated as Λ^*) $\rightarrow (\Sigma\pi)^0$ invariant-mass spectra produced in $p + p \rightarrow p + \Lambda^* + K^+$ reactions, in which both the incident channel for a quasi-bound K^-p state and its decay process to $(\Sigma\pi)^0$ were taken into account realistically[1)]. We calculated $M(\Sigma\pi)$ spectral shapes for various theoretical models for Λ^*. They are asymmetric and skewed, and were compared with recent experimental data of HADES[2)]. The nearly isotropic proton distribution observed in DISTO[3)] and HADES is ascribed to a short collision length in the production of Λ^*, which justifies the high sticking mechanism of Λ^* and the participating proton into K^-pp[4)].

In the present work we formulate the spectral shape of the $(\Sigma\pi)^0$ mass to provide theoretical guides to analyze experimental data of $(\Sigma\pi)^0$ mass spectra from the above reaction. We take into account both the formation and the decay processes of Λ^* in pp reactions realistically, following our $\bar{K}N - \Sigma\pi$ coupled-channel formalism[5)]. In this way, we derive the general form of the spectral function, which is not symmetric, but skewed with respect to the pole position. Then, we analyzed $(\Sigma^{+-}\pi^{-+})^0$ spectra from HADES at $T_p = 3.50$ GeV[2)], and obtained: $M(\Lambda^*) = 1405^{+11}_{-9}$MeV/$c^2$ and $\Gamma = 62 \pm 10$ MeV, where the interference effects of the $\bar{K}N$-$\Sigma\pi$ resonance with I= 0 and 1 $\Sigma\pi$ continuum are considered. Whereas the HADES spectrum shows a very broad peak centered around 1385 MeV/c^2, significantly lower lying than 1405 MeV/c^2, we have clarified that it is due to kinematical distortion. The present result on M and Γ is in good agreement with the PDG12 and PDG14 values[6)]. The Hyodo-Weise (HW) spectra[7)], shown as the curves (c) and (d) in the figure, do not account for the experimental spectrum.

*1 RIKEN Nishina Center
*2 Department of Physics, Isfahan University of Technology
*3 College of Science and Technology, Nihon University
*4 Department of Physics, University of Tokyo

References

1) M. Hassanvand, S.Z. Kalantari, Y. Akaishi and T. Yamazaki, Phys. Rev. C **87**, 055202 (2013); Phys. Rev. C **88**, 019905(E) (2013).
2) G. Agakishiev *et al.* (HADES collaboration), Phys. Rev. **C 87**, 025201 (2013).
3) T. Yamazaki *et al.*, Phys. Rev. Lett. **104** (2010) 132502; P. Kienle *et al.*, Eur. Phys. J. A **48** (2012) 183.
4) T. Yamazaki and Y. Akaishi, Phys. Rev. C **76** (2007) 045201.
5) Y. Akaishi, Khin Swe Myint and T. Yamazaki, Proc. Jpn. Acad. **B 84**, (2008) 264.
6) Particle Data Group 2012, J. Beringer *et al.*, Phys. Rev. **D 86** (2012) 010001; Particle Data Group 2014, K.A. Olive *et al.*, Chin. Phys. **C 38**, 090001 (2014).
7) T. Hyodo and W. Weise, Phys. Rev. **C 77**, 035204 (2008).

6. Particle Physics

$h^0 \to c\bar{c}$ as a test case for quark flavor violation in the MSSM†

A. Bartl,[*1] H. Eberl,[*2] E. Ginina,[*2] K. Hidaka,[*3,*4] and W. Majerotto[*2]

It is very important to determine if the SM (Standard Model)-like Higgs boson discovered at the LHC (Large Hadron Collider) in 2012[1,2] is the SM Higgs boson or the Higgs boson of New Physics. This is the most important issue in the present particle physics world. In this report based on our paper[3], we study the possibility that it is the lightest Higgs boson h^0 of the Minimal Supersymmetric Standard Model (MSSM), by focusing on the width of the decay $h^0 \to c\bar{c}$. We compute the decay width at a full one-loop level in the $\overline{DR}$ renormalization scheme in the MSSM with nonminimal Quark Flavor Violation (QFV).

We take our reference QFV scenario as shown in Table 1 in Ref.[3]. The main features of the scenario are: (i) it contains large $\tilde{c} - \tilde{t}$ (scharm-stop) mixings and large QFV trilinear couplings of squark-squark Higgs boson, and (ii) it satisfies the strong constraints on QFV from the B meson data, where scharm [stop] is the supersymmetry (SUSY) partner of the charm [top] quark. In this scenario, the lightest up-type squarks $\tilde{u}_1$ and $\tilde{u}_2$ are strong mixtures of $\tilde{c}_{L/R}$ - $\tilde{t}_{L/R}$, and the trilinear couplings ($\tilde{c}_L$ - $\tilde{t}_R$ - h^0, $\tilde{c}_R$ - $\tilde{t}_L$ - h^0, $\tilde{t}_L$ - $\tilde{t}_R$ - h^0 couplings) are large; therefore, $\tilde{u}_{1,2} - \tilde{u}_{1,2} - h^0$ couplings are large. This leads to an enhancement of the $\tilde{u}_{1,2}$ - $\tilde{u}_{1,2}$ - $\tilde{g}$ -loop vertex correction to the decay amplitude of $h^0 \to c\bar{c}$ shown in Fig. 1, where $\tilde{g}$ is a gluino, which is a hypothetical supersymmetric partner of a gluon. Thus, this results in a large deviation of the MSSM prediction for the decay width $\Gamma(h^0 \to c\bar{c})$ from the SM prediction.

In Fig. 2, we show the contour plot of the deviation of the MSSM prediction from the SM prediction $\Gamma^{SM}(h^0 \to c\bar{c})$ = 0.118 MeV in the δ_{23}^{uRR} - δ_{23}^{uLR} plane, where δ_{23}^{uRR} and δ_{23}^{uLR} are the $\tilde{c}_R$ - $\tilde{t}_R$ and $\tilde{c}_L$ - $\tilde{t}_R$ mixing parameters, respectively. We see that the MSSM prediction is very sensitive to the QFV parameters δ_{23}^{uRR} and δ_{23}^{uLR}, and that the deviation of the MSSM prediction from the SM prediction can be very large (as large as ~ 35%). We have found that the MSSM prediction becomes nearly equal to the SM prediction if we switch off all the QFV parameters in our reference QFV scenario.

The observation of any significant deviation of the decay width from its SM prediction indicates new physics beyond the SM. It is important to estimate the theoretical and experimental uncertainties of the width reliably in order to confirm such a deviation. The relative error of the SM width is estimated to be ~ 6%[4]. The relative error of the MSSM width is estimated to be ~ 6%[3]. As seen in Fig. 2, the deviation of the MSSM width from the SM width can be as large as ~ 35%. Such a large deviation can be observed at a future e^+e^- collider ILC (International Linear Collider) with a CM energy 500 GeV and an integrated luminosity of 1600 fb^{-1}, where the expected experimental error of the width is ~ 3%[5]. A measurement of the width at LHC is a hard task because of the difficulties in charm-tagging.

In this report, we have shown that the full one-loop corrected decay width $\Gamma(h^0 \to c\bar{c})$ is very sensitive to the QFV parameters in the MSSM. In a scenario with large $\tilde{c} - \tilde{t}$ mixings, the width can differ up to ~ 35% from its SM value. After estimating the uncertainties of the width, we conclude that an observation of these MSSM QFV effects is possible at ILC. Therefore, we have a good opportunity to discover the QFV SUSY effect in this decay $h^0 \to c\bar{c}$ at ILC.

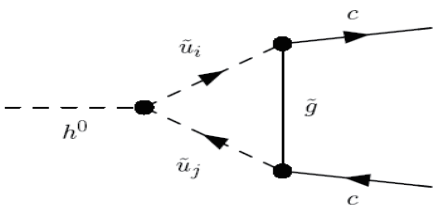

Fig. 1. Gluino-loop vertex correction to $h^0 \to c\bar{c}$.

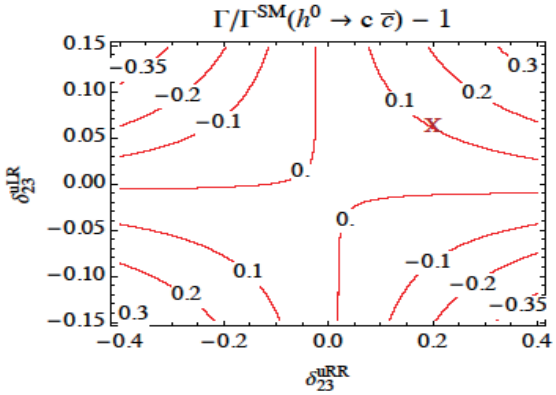

Fig. 2. Contour plot of the deviation of the full one-loop level MSSM width $\Gamma(h^0 \to c\bar{c})$ from the SM width $\Gamma^{SM}(h^0 \to c\bar{c})$ for our reference QFV scenario.

References

1) G. Aad et al.: Phys. Lett. B 716, 1 (2012).
2) S. Chatrchyan et al.: Phys. Lett. B 716, 30 (2012).
3) A. Bartl et al.: Phys. Rev. D 91, 015007 (2015).
4) L. G. Almeida et al.: Phys. Rev. D 89, 033006 (2014).
5) J. Tian and K. Fujii: Proc. EPS-HEP 2013, Stockholm, Sweden, PoS(EPS-HEP2013)316 [arXiv:1311.6528 [hep-ph]].

† Condensed from the article in Phys. Rev. D 91, 015007 (2015)

*1 Institute for Physics, University of Vienna
*2 Institute for High Energy Physics, OEAW, Vienna
*3 Department of Physics, Tokyo Gakugei University
*4 RIKEN Nishina Center

Update on lattice QCD calculation of neutral B meson mixing in static limit of b quark

T. Ishikawa,[*1] Y. Aoki,[*2,*1] T. Izubuchi,[*3,*1] C. Lehner,[*3] and A. Soni,[*3] for RBC Collaboration

The Cabibbo–Kobayashi–Maskawa (CKM) matrix is a key part of elementary particle physics, and constraints on the elements V_{ts} and V_{td} can be obtained from $B^0 - \overline{B^0}$ mixing, where highly nonperturbative hadronic weak matrix elements play an essential role. We perform simulations on this subject using static heavy quark as the treatment of b quark.[1)2)] The final values of B meson decay constants and mixing matrix elements and ξ parameter in the static b quark limit are summarized as

$$f_B = 218.8(6.5)_{\rm stat}(16.1)_{\rm sys}\ [\rm MeV], \quad (1)$$

$$f_{B_s} = 263.5(4.8)_{\rm stat}(18.7)_{\rm sys}\ [\rm MeV], \quad (2)$$

$$f_{B_s}/f_B = 1.193(20)_{\rm stat}(35)_{\rm sys}, \quad (3)$$

$$f_B\sqrt{\hat{B}_B} = 240(15)_{\rm stat}(17)_{\rm sys}\ [\rm MeV], \quad (4)$$

$$f_{B_s}\sqrt{\hat{B}_{B_s}} = 290(09)_{\rm stat}(20)_{\rm sys}\ [\rm MeV], \quad (5)$$

$$\xi = 1.208(41)_{\rm stat}(44)_{\rm sys}, \quad (6)$$

where statistical (stat) and systematic (sys) errors are given. In Fig. 1, the error budget is presented. Among the uncertainties presented in Fig. 1, a large portion of the error consists of statistical error, chiral extrapolation uncertainty, and renormalization uncertainty; it is thus important to reduce them to obtain more reliable results.

The first step in improving the current results is reducing the statistical errors using the All-Mode-Averaging (AMA) technique.[3)] This involves locating many source points in the measurement but using an approximation in obtaining quark propagators to greatly reduce computational cost. We show the preliminary results of the AMA calculation in Fig. 2 and compare them with the current results (without AMA). Although the AMA calculation is still ongoing, the presented error reduction is quite encouraging.

The systematic uncertainties involve chiral extrapolation and renormalization error. For the chiral extrapolation, we are currently focusing our effort on physical pion simulation, where we use RBC/UKQCD's 2+1 flavor $48^3 \times 96$ domain-wall fermion ensemble. By this calculation, most of the chiral extrapolation uncertainty is removed. Currently, the renormalization error is large for non-ratio quantities because only one-loop perturbation is employed. We are, however, investigating a possibility of nonperturbative method for the matching using RI/MOM scheme and coordinate space method,[4)] where removing power divergence is essential to the existence of the static heavy quark.

*1 RIKEN Nishina Center
*2 Nagoya University, KMI
*3 Brookhaven National Laboratory

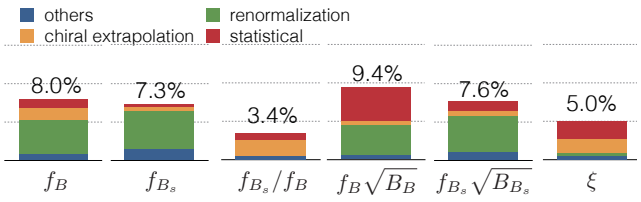

Fig. 1. Error budget for final quantities. The height of the bars indicates total error, whereas the relative size of the colors is determined by squared errors.[1)]

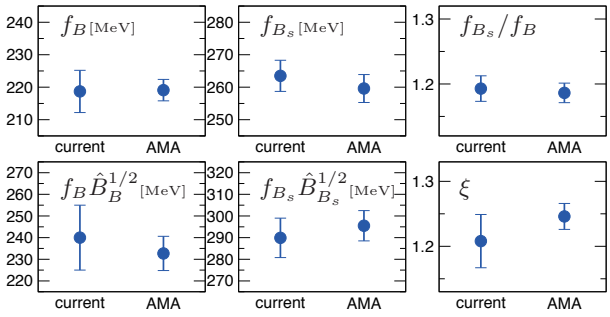

Fig. 2. Comparison of chiral and continuum extrapolated physical quantities between current and AMA results. The error denotes only statistical one.

Although the static limit is a good approximation for b quark, it is known to have $O(\Lambda_{\rm QCD}/m_b) \sim 10\%$ uncertainty. To obtain precise results, we need to remove or reduce this uncertainty systematically. The heavy quark expansion of a heavy-light quantity $\Phi_{\rm hl}$, which has a finite asymptotic limit as $m_Q \to \infty$, is written as

$$\Phi_{\rm hl}(1/m_Q) = \Phi_{\rm hl}(0)\exp\left[\sum_{p=1}^{\infty}\gamma_p\left(\frac{\Lambda_{\rm QCD}}{m_Q}\right)^p\right], \quad (7)$$

where m_Q is the heavy quark mass, which is heavier than the QCD scale $\Lambda_{\rm QCD}$. Our project finally includes simulations in light quark mass region (typically c quark mass region) for obtaining expansion parameters γ_ps. Combining the static result with the lighter quark mass enables us to obtain results with much less uncertainty, where our static limit results play a crucial role as a valuable "anchor point".

References

1) Y. Aoki et al.: arXiv:1406.6192 [hep-lat].
2) T. Ishikawa et al.: PoS LATTICE **2013**, 410 (2014).
3) T. Blum et al.: Phys. Rev. D **88**, 094503 (2013).
4) K. Cichy et al.: Nucl. Phys. B **865**, 268 (2012).

Progress toward an *ab initio*, Standard Model calculation of direct CP-violation in K-decays

C. Kelly*1 for the RBC and UKQCD collaborations

Recent theoretical and computational advances in the field of lattice QCD have opened the door to an *ab initio* determination of ϵ', the measure of direct CP-violation in Standard Model $K \to \pi\pi$ decays. New sources of direct CP-violation are required to explain the observed matter-antimatter asymmetry in the Universe, and ϵ' is particularly sensitive to the contributions introduced by many Beyond the Standard Model theories. A comparison of the Standard Model value to the precisely measured experimental number may therefore provide evidence of new physics.

In $K \to \pi\pi$ decays, the final $\pi\pi$ state can have either isospin $I = 2$ or 0 and ϵ' manifests as a difference in the complex phases of the corresponding amplitudes, A_2 and A_0 respectively: $\epsilon' \propto \left(\frac{\mathrm{Im}A_2}{\mathrm{Re}A_2} - \frac{\mathrm{Im}A_0}{\mathrm{Re}A_0}\right)$.

The RBC and UKQCD collaborations have successfully performed calculations of A_2 with 10% total errors[1)], and only A_0 remains to be determined. This is significantly more difficult than A_2, firstly because the $\pi\pi$ state can mix with the vacuum, leading to disconnected diagrams in which the two pions annihilate and are recreated at a later time. Such diagrams are typically extremely noisy and require advanced techniques such as all-to-all (A2A) propagators. The second difficulty is in creating a $\pi\pi$ state that is degenerate with the kaon such that the decay occurs with physical kinematics. This requires the pions to be moving, necessitating the use of G-parity spatial boundary conditions[2)] (GPBC) to control the statistical noise.

Efficient use of GPBC and A2A introduces a large number of computational challenges that must be overcome. To this end, we developed parallel code highly optimized for the IBM Blue Gene/Q machines at BNL, ANL and Edinburgh University and have, to date, generated $\mathcal{O}(100)$ independent measurements of the $K \to \pi\pi$ amplitude. The measurements were performed on a custom generated ensemble with a $(4.6\ \mathrm{fm})^3$ lattice volume and a relatively coarse 0.143 fm lattice spacing. We use a three-flavor chiral action with degenerate up and down quarks and a physical strange quark.

With our chosen lattice parameters we obtain a measured pion mass of $m_\pi = 142.4(1.3)$ MeV and a kaon mass of $m_K = 489.9(2.4)$ MeV, very close to their physical values of 135 MeV and 495 MeV respectively. We use GPBC in all three spatial directions and obtain a $\pi\pi$ energy of $E_{\pi\pi} = 524(45)$ MeV, which agrees with the kaon mass within errors, suggesting a near-physical decay.

In Fig. 1 we plot the contributions to A_0 from the Q_2 and Q_6 operators, which respectively dominate $\mathrm{Re}A_0$ and $\mathrm{Im}A_0$. Here we use a $K \to \pi\pi$ time separation of 12, and fit to the plateau between $t = 4$–8; outside of this region the signal is contaminated by excited states. Our analysis also includes measurements with $K \to \pi\pi$ time separations of 10 and 14. Preliminary results from our current, somewhat limited, data set suggest a ∼50% statistical error on our result for $\mathrm{Re}A_0$ and ∼40% for $\mathrm{Im}A_0$. The error is almost completely dominated by the disconnected diagrams, despite our use of A2A methods, and can only be resolved with more statistics. We anticipate doubling the statistics within the next 6 months.

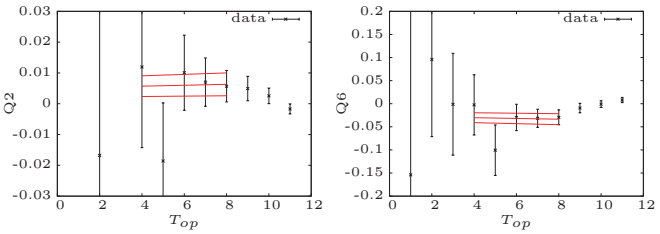

Fig. 1.: Lattice time dependence of Q_2 and Q_6, the dominant contributions to $\mathrm{Re}A_0$ and $\mathrm{Im}A_0$ respectively. The fit is shown in red.

The systematic errors on our results are dominated by the discretization error and the error on the Wilson coefficients. The former arises because the measurement is performed on a single, coarse lattice, and is expected to be $\mathcal{O}(20\%)$; in future calculations this can be removed by performing a continuum extrapolation over results computed at different lattice spacings. The Wilson coefficients are involved because we match the low-energy lattice calculation to the three-flavor Weak effective theory where the charm has been integrated out perturbatively; as the charm is comparatively light, it is not clear how reliable this is. We intend to study this by comparing A_0 computed using cheaper lattice calculations with stationary pions and both three and four dynamical flavors. Ultimately we intend to repeat the calculation with a dynamical charm quark.

References

1) T. Blum, P. A. Boyle, N. H. Christ, J. Frison, N. Garron, T. Janowski, C. Jung and C. Kelly et al., Phys. Rev. D **91** (2015) 7, 074502 [arXiv:1502.00263 [hep-lat]].
2) C. Kelly, PoS LATTICE **2012**, 130 (2012).

*1 RIKEN Nishina Center, Brookhaven National Laboratory

Collisional Energy Loss in Semi-Quark Gluon Plasma†

S. Lin,*1 R. D. Pisarski,*1,*2 and V. V. Skokov*3

Quantum chromodynamics (QCD) above the deconfinement temperature T_c is in quark gluon plasma (QGP) phase. The QGP produced in the relativistic heavy ion collider (RHIC) and large hadron collider (LHC) remains in a temperature window $T_c \sim 2T_c$ for much of its lifetime. This is a regime where high-temperature perturbation theory becomes inappropriate. The regime is called semi-QGP, which is characterized by a non-trivial Polyakov loop. A matrix model with background color charges $A_0^{\rm cl} = i/g\,{\rm diag}(-Q, 0, Q)$ has been proposed to describe the physics in the regime[1]. The background color charges can be viewed as imaginary chemical potentials for quarks and gluons, which effectively suppress their number density as compared to high-temperature QGP. In this letter, we considered how the suppression of quark and gluon number density affects heavy-quark collisional energy loss in semi-QGP.

It is known that heavy quarks lose their energy by Coulomb scattering and Compton scattering, in which heavy quarks scatter off gluons and a light quarks respectively. Both processes contribute to total energy loss. The presence of background color charges suppresses light quark and gluon number densities differently, resulting in different suppression factors for energy loss corresponding to the two processes. For Coulomb scattering, we found that the energy loss per unit length, to the leading logarithmic order, is given by a Q-dependent factor $S^{\rm qk}(Q)$ times the energy loss at $Q = 0$:

$$\left.\frac{dE}{dx}\right|_Q^{\rm qk} = S^{\rm qk}(Q)\ \left.\frac{dE}{dx}\right|_{Q=0}^{\rm qk}. \tag{1}$$

The energy loss, to the leading logarithmic order, at $Q = 0$ is as follows[2]:

$$\left.\frac{dE}{dx}\right|_{Q=0}^{\rm qk} = \frac{2}{9}\,\pi\,\alpha_{\rm s}^2\,T^2\,N_f\,\ln\left(\frac{ET}{m_D^2}\right), \tag{2}$$

where N_f and $\alpha_{\rm s}$ are respectively the number of light quark flavors and strong coupling constant. m_D is the gluon Debye mass. $S^{\rm qk}(Q)$ is the infinite sum of traces of the Wilson loop $\mathbb{L} \equiv \mathcal{P}e^{ig\int_0^{1/T} d\tau A_0^{cl}}$:

$$S^{\rm qk}(Q) = \frac{4}{\pi^2}\sum_{n=1}^{\infty}\frac{(-)^{n+1}}{n^2}\,{\rm tr}\,\mathbb{L}^n\,. \tag{3}$$

The energy loss from Compton scattering also factorizes to a Q dependent factor and the energy loss at $Q = 0$ to leading logarithmic order.

$$\left.\frac{dE}{dx}\right|_Q^{\rm gl} = S^{\rm gl}(Q)\ \left.\frac{dE}{dx}\right|_{Q=0}^{\rm gl}. \tag{4}$$

The energy loss at $Q = 0$ can be expressed as follows[2]:

$$\left.\frac{dE}{dx}\right|_{Q=0}^{\rm gl} = \pi\,\alpha_{\rm s}^2\,T^2\left(\frac{4}{3}\ln\left(\frac{ET}{m_D^2}\right) + \frac{8}{27}\ln\left(\frac{ET}{M^2}\right)\right), \tag{5}$$

where M is the mass of heavy quark. $S^{\rm gl}(Q)$ again involves an infinite sum of traces of the Wilson loop

$$S^{\rm gl}(Q) = \frac{1}{8}\left(\frac{6}{\pi^2}\sum_{n=1}^{\infty}\frac{|{\rm tr}\,\mathbb{L}^n|^2}{n^2} - 1\right). \tag{6}$$

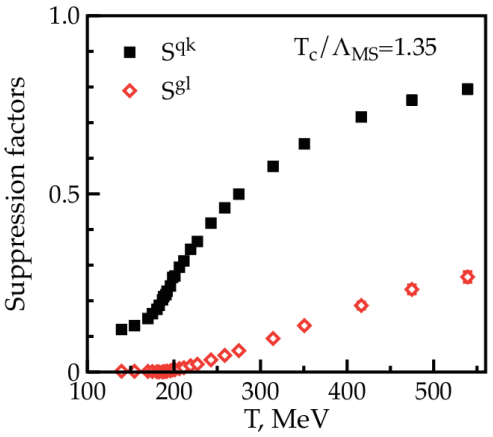

Fig. 1. Suppression factors for Coulomb scattering $S^{\rm qk}$ and Compton scattering $S^{\rm gl}$.

The suppression factors $S^{\rm qk}(Q)$ and $S^{\rm gl}(Q)$ are both functions of temperature through Q, whose temperature dependence is extracted from results of lattice simulation on Polyakov loop. Fig. 1 shows the plots of $S^{\rm qk}(Q)$ and $S^{\rm gl}(Q)$ versus T. We found that Coulomb scattering and Compton scattering are significant suppressed as QGP approaches T_c from temperature above T_c. It is also noteworthy that the suppression is much greater for Compton scattering than for Coulomb scattering.

† Condensed from the article in Phys. Lett. B, Vol.730, 236 (2014)

*1 RIKEN Nishina Center
*2 Department of Physics, Brookhaven National Laboratory
*3 Department of Physics, Western Michigan University

References

1) A. Dumitru, Y. Guo, Y. Hidaka, C. P. K. Altes and R. D. Pisarski, Phys. Rev. D **83**, 034022 (2011) [arXiv:1011.3820 [hep-ph]].
2) S. Peigne and A. Peshier, Phys. Rev. D **77**, 114017 (2008).

Entropic destruction of heavy quarkonium in non-Abelian plasma from the holographic correspondence†

K. Hashimoto*1,*2 and D. E. Kharzeev*3

The studies of heavy quarkonium at finite temperature are expected to advance the understanding of QCD plasma and to clarify the nature of the deconfinement transition. It was originally proposed[1] to use the quarkonium suppression in heavy ion collisions as a way to detect the Debye screening in the quark-gluon plasma. The subsequent experimental studies of quarkonium production at different energies however revealed a puzzle – the charmonium suppression observed at RHIC (lower energy density) appeared stronger than at LHC (larger energy density). This is in contrast to both the Debye screening scenario[1] and the thermal activation through the impact of gluons. One possible solution to this puzzle is the recombination of the produced charm quarks into charmonia.

However, recently it was argued[2] that an anomalously strong suppression of charmonium near the deconfinement transition can be a consequence of the nature of deconfinement. The argument put forward in Ref.2 was based on the lattice QCD results indicating a large amount of entropy associated with the heavy quark-antiquark pair placed in the quark-gluon plasma. This entropy S was found on the lattice to grow as a function of the distance L between the quark and antiquark. The proposal of[2] is that this entropy should thus lead to the emergent entropic force

$$F = T\,\frac{\partial S}{\partial L}, \tag{1}$$

where T is the temperature of the plasma. It has been found that the balance of the attractive force from the internal interaction and the repulsive entropic force indicates a strong suppression of charmonium states near the deconfinement transition. The leading role of the entropic force in the deconfinement transition itself has been conjectured, as well as a possible link of the observed peak in the entropy near the deconfinement transition to the "long string" condensation.

In this paper, we investigate the microscopic origin of the entropy associated with the heavy quark pair in non-Abelian plasma using the holographic correspondence (the AdS/CFT correspondence). We conclude that the narrow and strong peak in the entropy associated with the heavy quark pair near the transition temperature is indeed related to the nature of deconfinement, and in holographic description originates from the entropy of a long fundamental string at the bottom of the confining geometry which would be absorbed into a black hole horizon after a deconfinement transition. It is absent in the conformal $\mathcal{N} = 4$ supersymmetric Yang-Mills theory, but emerges in a confining Yang-Mills theory obtained by compactification of the fifth dimension. On the boundary, this entropy has to be attributed to long-range, delocalized excitations entangled with the heavy quark pair that can indeed be described as the "long string".

The origin of this peak in the holographic description is intriguing – it arises because the heavy quark pair acts as an eyewitness of the black hole formation in the confining (at low temperatures) bulk geometry. This process of black hole formation is the dual holographic representation of the deconfinement transition on the boundary. From this viewpoint, the entropy associated with the quark-antiquark pair is the right quantity to detect the temperature at which the deconfinement occurs.

We also study the entropic force in holographic setup of strongly coupled gauge theories. It turns out that the entropic force associated with the distribution of the quarks is at a sub-leading order in the strong coupling expansion in terms of the 'tHooft coupling constant, while the entropic force of the QCD string is comparable to the quark-antiquark force. However a reasonable evaluation of the sub-leading term shows that the Einstein entropic force increases such that the critical distance of the quark pair to be destructed entropically is shortened.

Our proposal of using the entropy associated with the heavy quark-antiquark pair to detect the deconfinement transition is somewhat similar to the idea of using the entanglement entropy as an order parameter of deconfinement. The difference is that the order parameter discussed in is the von Neumann entanglement entropy of a spatial region with a boundary, while we consider the Gibbs entropy. In terms of the boundary theory, the entropy of the quark-antiquark pair likely emerges from the entanglement of a "long string" connecting the quark and antiquark with the rest of the system. It would be interesting to clarify this issue further as it may improve our understanding of both deconfinement and confinement.

† Condensed from the article in Phys. Rev. **D90**, 125012 (2014)

*1 RIKEN Nishina Center
*2 Department of Physics, Osaka University
*3 Department of Physics and Astronomy, Stony Brook University

References

1) T. Matsui and H. Satz, Phys. Lett. B **178**, 416 (1986).
2) D. E. Kharzeev, Phys. Rev. D **90**, 074007 (2014) [arXiv:1409.2496 [hep-ph]].
3) K. Hashimoto and T. Oka, JHEP **1310**, 116 (2013) [arXiv:1307.7423].

Magnetic instability in AdS/CFT : Schwinger effect and Euler-Heisenberg Lagrangian of Supersymmetric QCD†

K. Hashimoto,[*1,*3] T. Oka,[*2] and A. Sonoda[*3]

The renowned Schwinger effect[1]creation process of electron-positron pairs in strong electric fields, is a big challenge in the field of non-linear quantum field theory. Although the Schwinger limit $E \sim m_e^2$ has not been reached by the direct experiments such as strong lasers, similar effective setups in materials are actively investigated. Theoretical foundation of the Schwinger effect was to evaluate the imaginary part of the effective action of QED under a constant electromagnetic field, the Euler-Heisenberg Lagrangian[2] which dates back to 1936. The Euler-Heisenberg Lagrangian is a generating function of nonlinear electromagnetic responses of the vacuum. In its expression, the electric field couples to the magnetic field in a complicated and nonlinear manner, and the total effective Lagrangian is a starting point in the research of strong fields in QED, including the non-perturbative Schwinger effect.

In our previous paper[3], two of the present authors derived an Euler-Heisenberg Lagrangian for a supersymmetric QCD in the strong coupling limit, by using the AdS/CFT correspondence but the Maxwell electric field) is applied, a quark antiquark pair is created. The nontrivial part is the gluon interaction at strong coupling in QCD. The quarks are confined, and between the quark and the antiquark a confining force (a QCD string) is present to bind them. If the electric field is strong enough, the quarks are liberated. This truly nonperturbative process is of importance, not only because it can be a realistic phenomenon occurring in the universe, but also because it may be a touchstone for understanding the quark confinement.

There are at least two cases in which the QCD Schwinger effect may play an important role: First, the heavy ion collision experiment, and second, magnetars (neutron stars with a very strong magnetic field). In the heavy ion collisions, very strong electric fields are generated by the the electric current induced by heavy ions passing by each other. Since the magnetic field is time dependent, there appears strong electric field as well, and it may be related to the formation of the quark gluon plasma. On the other hand, magnetars are known to be the most dense place in the universe, and the strong magnetic field accompanied by some electric field can occur and affect the core structure of the stars, possibly having a quark phase inside. In these examples, the understanding of QCD and Schwinger effect in strong electric and magnetic fields can be tested by experiments/observations and serves as a playground at which we can test our theoretical knowledge on strongly coupled quantum field theories.

The result of Ref.[3] is summarized as follows; The Euler-Heisenberg Lagrangian of strongly coupled $\mathcal{N} = 2$ supersymmetric QCD at large N_c limit was calculated in the presence of a constant electric field using the AdS/CFT correspondence. Its imaginary part explicitly evaluated is found to agree with large electric field expansion of the Schwinger effect of $\mathcal{N} = 2$ supersymmetric QED (once the QCD string tension is replaced by the electron mass). However, there, only the electric field was considered. In this paper, we include the full dependence of the magnetic field, which is important as is obvious from the physical situations explained above.

Here we summarize the finding of the present paper:

- We obtain the Euler-Heisenberg Lagrangian of the $\mathcal{N} = 2$ supersymmetric QCD in a constant electromagnetic field, at strong coupling and large N_c limit.
- We evaluate the imaginary part of the Euler-Heisenberg Lagrangian, and find that the rate of the quark antiquark creation diverges at zero temperature for massless quarks.
- The divergent rate can be regularized, i.e., the vacuum is unstable but the lifetime becomes finite, by either introducing finite temperature or a quark mass.
- We compute the real part of the Euler-Heisenberg Lagrangian, and show the disappearance of Cotton-Mouton effect in an expansion with the electromagnetic field.
- The imaginary part of the Euler-Heisenberg Lagrangian for a small quark mass is shown to coincide with that of $\mathcal{N} = 2$ supersymmetric QED, at the leading order in electron mass. The agreement is found also for the real parts responsible for the Cotton-Mouton effect.

References
1) J. S. Schwinger, Phys. Rev. **82**, 664 (1951).
2) W. Heisenberg and H. Euler, Z. Phys. **98**, 714 (1936)
3) K. Hashimoto and T. Oka, JHEP **1310**, 116 (2013) [arXiv:1307.7423].

† Condensed from the article in JHEP **1406** (2014) 085

*1 RIKEN Nishina Center
*2 Department of Applied Physics, University of Tokyo
*3 Department of Physics, Osaka University

Turbulent meson condensation in quark deconfinement†

K. Hashimoto,[*1,*2] S. Kinoshita,[*3] K. Murata,[*4] and T. Oka[*5]

Quark confinement is one of the most fundamental and challenging problems in elementary particle physics, left unsolved. Although quantum chromodynamics (QCD) is the fundamental field theory describing quarks and gluons, their clear understanding is limited to the deconfined phase at high energy or high temperature limits due to the asymptotic freedom. We may benefit from employing a more natural description of the zero temperature hadron vacuum. A dual viewpoint of quark confinement in terms of the "fundamental" degrees of freedom at zero temperature - mesons, is a plausible option.

The mesons appear in families: they are categorized by their spin/flavor quantum numbers, as well as a resonant excitation level n giving a resonance tower such as $\rho(770), \rho(1450), \rho(1700), \rho(1900), \cdots$. In this Letter we find a novel behavior of the higher meson resonances, *i.e.*, mesons with large n. In the confined phase, when the deconfined phase is approached, we observe *condensation of higher mesons*. In this state, macroscopic number of the higher meson resonances, with a characteristic distribution, are excited. The condensed mesons have the same quantum number as the vacuum. The analysis is done via the anti-de Sitter space (AdS)/conformal field theory (CFT) correspondence, one of the most reliable tools to study strongly-coupled gauge theories. By shifting our viewpoint from quark-gluon to meson degrees of freedom, we gain a simple and universal understanding of the confinement/deconfinement transition, with a bonus of solving mysteries in black holes physics through the AdS/CFT.

The system we study is the $\mathcal{N} = 2$ supersymmetric $SU(N_c)$ QCD which allows the simplest AdS/CFT treatment. The deconfinement transition is induced by external electric fields. In static fields, the confined phase becomes unstable in electric fields stronger than the Schwinger limit $E = E_{\rm Sch}$ beyond which quarks are liberated from the confining force. We find that this instability is accompanied by the condensation of higher mesons. A striking feature is revealed for the case of an electric field quench: The kick from the quench triggers a domino-like energy transfer from low to high resonant meson modes. This leads to a dynamical deconfinement transition[1] even below the Schwinger limit. The transfer we find resembles that of turbulence in classical hydrodynamics as higher modes participate; thus we call it a "turbulent meson condensation" and suggest it being responsible for deconfinement. See Fig.1.

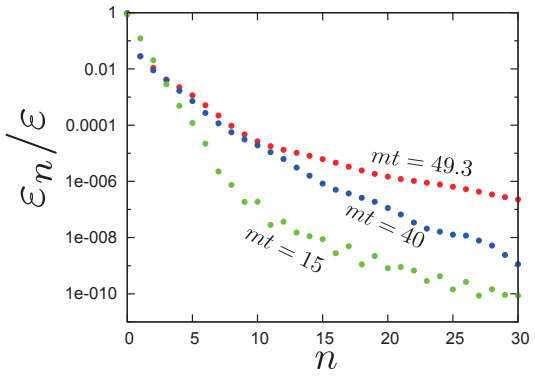

Fig. 1. Turbulent behavior of mesons toward deconfinement. The horizontal axis is the meson resonance level n, and the vertical axis is the meson energy. m is the quark mass, and t is time measured after the electric field quench. It shows a power-law behavior turned from an exponential behavior, which is a turbulence.

We remind that the $\mathcal{N} = 2$ theory is a toy model: The meson sector is confined and has a discrete spectrum while the gluon sector is conformal and is always deconfined. Here, we concentrate on the deconfinement of heavy quarks and not the gluons. Note that the mesons with low spins in this theory are described by a confining potential and an effective QCD string exists, whereby we define our "quark confinement".

The higher meson resonances are naturally interpreted as long QCD strings, therefore our finding is consistent with interpreting deconfinement as condensation of QCD strings[2]. Under the condensation, a quark can propagate away from its partner antiquark by reconnecting the bond QCD string with the background condensed strings. The gravity dual of the deconfined phase is with a black hole, so given the relation with long fundamental strings, our result may shed light on the issue of quantum black holes; In particular, our time-dependent analysis gives a singularity formation on the flavor D-brane in AdS, a probe-brane version of the Bizon-Rostworowski turbulent instability in AdS geometries[3].

References
1) K. Hashimoto, S. Kinoshita, K. Murata and T. Oka, arXiv:1407.0798 [hep-th].
2) A. M. Polyakov, Phys. Lett. B **72**, 477 (1978).
3) P. Bizon and A. Rostworowski, Phys. Rev. Lett. **107**, 031102 (2011) [arXiv:1104.3702 [gr-qc]].

† Condensed from the article in arXiv:1408.6293

*1 RIKEN Nishina Center
*2 Department of Physics, Osaka University
*3 Osaka City University Advanced Mathematical Institute
*4 Keio University
*5 Department of Applied Physics, University of Tokyo

Meson turbulence at quark deconfinement from AdS/CFT†

K. Hashimoto,[*1,*2] S. Kinoshita,[*3] K. Murata,[*4] and T. Oka[*5]

How the quarks are confined at the vacuum of quantum chromodynamics (QCD) is one of the most fundamental questions in the standard model of particle physics. We would like to find a universal feature of the deconfinement. To understand the nature of the quark confinement, we need a proper observable which exhibits a universal behavior irrespective of how we break the confinement. In this paper, we propose a universal behavior of resonant mesons and name it *meson turbulence*.

Following our previous paper[1)], we find that a particular behavior of resonant mesons (excited states of mesons) can be an indicator of the deconfinement. The meson turbulence is a power-law scaling of the resonant meson condensations. For the the resonant meson level n ($n = 0, 1, 2, \cdots$), the condensation of the meson $\langle c_n(x,t)\rangle$ with its mass ω_n causes the n-th meson energy ε_n scaling as $(\omega_n)^\alpha$ with a constant power α. This coefficient α will be unique for a given theory, and does not depend on how one breaks the confinement. In particular, for the theory which we analyze in this paper, that is $\mathcal{N} = 2$ supersymmetric QCD with $\mathcal{N} = 4$ supersymmetric Yang-Mills as its gluon sector at large N_c at strong coupling, the universal power-law scaling parameter α is found to be

$$\langle \varepsilon_n \rangle \propto (\omega_n)^\alpha, \quad \alpha = -5\,. \tag{1}$$

where ε_n is the energy of the n-th meson resonance. Normally, for example at a finite temperature, the energy stored at the n-th level of the resonant meson should be a thermal distribution, $\varepsilon_n \propto \exp[-\omega_n/T]$. The thermal distribution is Maxwell-Boltzmann statistics, in which the higher (more massive) meson modes are exponentially suppressed. However, we conjecture that this standard exponential suppression will be replaced by a power-law near any kind of the deconfinement transitions. If we think of the meson resonant level n as a kind of internal momentum, then the energy flow to higher n can be regarded as a so-called weak turbulence. This is why we call the phenomenon meson turbulence, and the level n can be indeed regarded as a momentum in holographic direction in the AdS/CFT correspondence.

The reason we came to the universal power behavior is quite simple. We combined two well-known things,

- Mesons are excitations of an open QCD string.

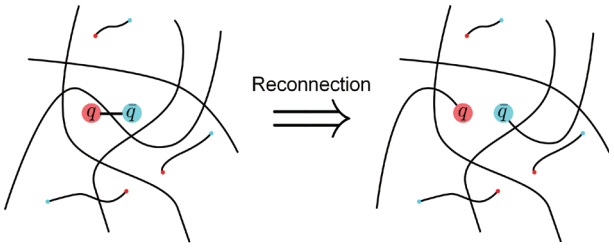

Fig. 1. A schematic picture of the deconfinement phase as condensation of QCD strings. Left: we add a meson (a pair of a quark and an anti-quark connected by a QCD string) to the system. Right: due to the background condensed QCD strings, the QCD string can be reconnected, and the quark can freely propagate away from the anti-quark.

- Deconfinement phase is described by a condensation of long strings.

Combining these two leads us to the conjecture that *the deconfinement of quarks is indicated by a condensation of higher meson resonances*. More precisely, we claim that *the condensation should be turbulent*: the higher mode condensation is not suppressed exponentially but behaves with a power-law.

We shall investigate various deconfining transitions in this paper, to check the universality of our conjecture of the meson turbulence. First, we work with a static case. A nonzero electric field is a good example since a strong electric field can make the quark-antiquark pair dissociate. Then we investigate time-dependent setup. The virtue of the AdS/CFT correspondence is that time-dependent analysis is possible, as opposed to lattice simulations of QCD. To demonstrate the universality of the meson turbulence, we work in two examples: (1) electric-field quench, and (2) quark-mass quench. In all cases, we find numerically the meson turbulence and the universal power law with the power $\alpha = -5$.

The universality we found in this paper strongly indicates that the meson turbulence is a universal phenomena which is independent of how one breaks the confinement.

References

1) K. Hashimoto, S. Kinoshita, K. Murata and T. Oka, arXiv:1408.6293 [hep-th].

† Condensed from the article in arXiv:1412.4964

*1 RIKEN Nishina Center
*2 Department of Physics, Osaka University
*3 Osaka City University Advanced Mathematical Institute
*4 Keio University
*5 Department of Applied Physics, University of Tokyo

Electromagnetic instability in holographic QCD†

K. Hashimoto,[*1,*3] T. Oka,[*2] and A. Sonoda[*3]

Schwinger effect[2] is one of the most interesting phenomena in particle physics. This is a phenomenon that a pair creation of charged particles occur under an external field such as an electromagnetic field. Schwinger obtained the creation rate of an electron positron pair by evaluating the imaginary part of Euler-Heisenberg Lagrangian[1], which is an effective Lagrangian for a constant electric field. This rate Γ is derived as $\Gamma \sim \exp\left(-\pi m_e^2/eE\right)$ to leading order and has a form with a negative power in the gauge coupling e. So the Scwinger effect is a non-perturbative effect. Here, m_e is the electron mass and E is an electric field. A critical electric field necessary energy for the electron positron pair creation is $E_{\rm cr} \sim m_e^2 c^3/e\hbar$, and the strength is about 10^{18} [V/m]. So, it is a phenomenon which shows up only under strong electromagnetic fields.

Recently, we have seen advance in research on a strong electromagnetic field in both theoretical and experimental aspects of hadron physics. At the heavy ion collision in RHIC and LHC, it is expected that a strong magnetic field is generated by a collision of charged particles accelerated at about the speed of light.

Within the AdS/CFT framework, the quark pair creation rate in the strongly coupled $\mathcal{N} = 4$ supersymmetric Yang-Mills theory was obtained in[3]. On the other hand, two of the present authors obtained the vacuum decay rate, which can be identified as the creation rate of quark-antiquark pairs, in $\mathcal{N} = 2$ supersymmetric QCD(SQCD) by using a different method[4] in AdS/CFT correspondence: *the imaginary part of the probe D-brane action.* D3-D7 brane system corresponds to $\mathcal{N} = 4$ supersymmetric $SU(N_c)$ Yang-Mills theory including an $\mathcal{N} = 2$ hypermultiplet in the fundamental representation of the $SU(N_c)$ gauge group. They obtained the creation rate of the quark antiquark in the $\mathcal{N} = 2$ SQCD under a constant electric field by evaluating the imaginary part of the D7-brane action. Then, the present authors evaluated the imaginary part of the D7-brane action including not only a constant electric field but also a constant magnetic field and obtained the creation rate of the quarks and antiquarks in the $\mathcal{N} = 2$ SQCD[5].

We summarize the properties of the creation rate in both electric and magnetic fields obtained in[5] for $\mathcal{N} = 2$ SQCD as follows. We derived the Euler-Heisenberg Lagrangian for a constant electromagnetic field in $\mathcal{N} = 2$ SQCD at large N_c and at strong coupling. Then, we obtained the creation rate of the quarks and antiquarks by evaluating the imaginary part of the Lagrangian. We found that the creation rate diverges at a zero temperature in the massless quark limit while it becomes finite when we introduce a nonzero temperature. The divergence of the creation rate is influenced not only by a constant electric field but also by a constant magnetic field. The results in SQCD showed similarities with the creation rate of the electron positron pair in $\mathcal{N} = 2$ supersymmetric QED(SQED) in constant electromagnetic field.

In this paper, we study the quark antiquark pair creation in *non-supersymmetric* QCD at large N_c at strong coupling, and the imaginary part of D8-brane action in a constant electromagnetic field. The holographic models are the Sakai-Sugimoto model[6] and its deformed version. Our findings in this paper are as follows:

- We derive the Euler-Heisenberg Lagrangian for confining gauge theories: the Sakai-Sugimoto model and the deformed Sakai-Sugimoto model. We obtain the creation rate of the quark antiquark pair under the electromagnetic field, by evaluating the imaginary part of the D-brane actions.
- The imaginary part is found to increase with the magnetic field parallel to the electric field, while it decreases with the magnetic field perpendicular to the electric field. So the vacuum instability strongly depends on the direction of the applied magnetic field relative to the electric field.
- We obtain a critical value of the electric field, i.e., the Schwinger limit, by using the condition that the D-brane action has the imaginary part. In the case of the Sakai-Sugimoto model, the critical electric field corresponds to a QCD string tension between a quark and an antiquark.

As for the first part among above, a result with only an electric field was reported in Ref. 7). We analyze generic electric and magnetic fields in this paper.

References
1) J. S. Schwinger, Phys. Rev. **82** (1951) 664.
2) W. Heisenberg and H. Euler, Z. Phys. **98** (1936) 714 [physics/0605038].
3) G. W. Semenoff and K. Zarembo, Phys. Rev. Lett. **107** (2011) 171601 [arXiv:1109.2920 [hep-th]].
4) K. Hashimoto and T. Oka, JHEP **1310**, 116 (2013) [arXiv:1307.7423].
5) K. Hashimoto, T. Oka and A. Sonoda, JHEP **1406** (2014) 085 [arXiv:1403.6336 [hep-th]].
6) T. Sakai and S. Sugimoto, Prog. Theor. Phys. **113** (2005) 843 [hep-th/0412141].
7) K. Y. Kim, S. J. Sin and I. Zahed, JHEP **0807**, 096 (2008) [arXiv:0803.0318 [hep-th]].

† Condensed from the article in arXiv:1412.4254

*1 RIKEN Nishina Center
*2 Department of Applied Physics, University of Tokyo
*3 Department of Physics, Osaka University

Electric Field Quench in AdS/CFT†

K. Hashimoto,[*1,*2] S. Kinoshita,[*3] K. Murata,[*4] and T. Oka[*5]

In this paper, we analyze response of the strongly coupled gauge theory against an electric field quench, by using the AdS/CFT correspondence. The system is $\mathcal{N} = 2$ supersymmetric QCD with $\mathcal{N} = 4$ super Yang-Mills as a gluon sector, and has a confining spectrum for the meson sector (while the gluon sector is always deconfined). We turn on the electric field in a time-dependent manner, and find that the system develops to a deconfinement phase of mesons.

We study time-dependent behavior of various observables such as electric current carried by the quarks and the quark condensate. We define the thermalization time scale and the deconfinement time in terms of the gravity dual side: the thermalization is with the Hawking temperature, and the deconfinement is with the strong redshift.

Among our findings, the most interesting is the fact that the deconfinement transition of the mesons occurs even with a small electric field once it is applied time-dependently. In the static electric field, there exists a critical value of the electric field beyond which the electric current flows and the system is deconfined. In our time-dependent quench, if the quench is made sufficiently fast, even with a final electric field which is smaller than the critical value, the system goes to a deconfinement phase — there appears a strong red shift region in the gravity dual.

In the dual gravity picture, this phenomena can be understood as the D-brane version of the weakly turbulent AdS instability. The wave packet on the D-brane is getting sharp as time increases and, eventually, collapses into the naked singularity. Accordingly, we also found a curious behavior of the deconfinement time — the time scale when a strong redshift region appears on the D7-brane. The deconfinement time takes only discrete values.

Furthermore, the potential implication of the present study of nonequilibrium dynamics in QCD to strongly correlated electron system is suggestive. Then, it is tempting to speculate that the formation of naked singularity explained in the previous section is an indication of the "meson Mott transition", i.e., the QCD version of the exciton Mott transition. We plot a schematic phase diagram obtained by this analogy in Fig. 1 with three regions (i), (ii), and (iii).

(i) Confinement phase with coherent oscillation. When the field is weak, the system is always in the confinement phase. However, when the ramp speed is fast (small ΔV), the field induces a coherent oscillation of vacuum polarization due to meson excitation.

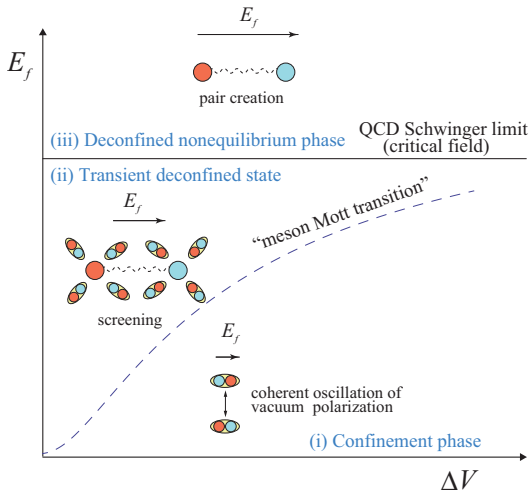

Fig. 1. Schematic "dynamical phase diagram" of states realized in the present study by a static electric field E_f following an initial ramp (parametrized by the time parameter ΔV). See text for details.

(ii) Transient deconfined phase ("meson Mott transition"). This is the speculated "meson Mott transition" regime. When the meson amplitude becomes large, the confinement force becomes relatively weak due to screening. The quarks become liberated and deconfinement takes place in the meson (quark) sector.

(iii) Deconfined nonequilibrium phase above QCD Schwinger limit. When the electric field is stronger than the confining strength (= QCD Schwinger limit), the confinement phase becomes unstable against direct pair creation of quark and anti-quarks.[1)]. This state is a static nonequilibrium phase with finite current.

In summary, by studying the dynamics of supersymmetric QCD in strong electric fields, we observed many interesting, and universal nonequilibrium physics. Our finding implies similarities between possible formation mechanism of quark gluon plasma in heavy ion collision experiments to laser induced phase transitions in condensed matter, which helps us understand the physics more deeply.

† Condensed from the article in JHEP **1409** (2014) 126
*1 RIKEN Nishina Center
*2 Department of Physics, Osaka University
*3 Osaka City University Advanced Mathematical Institute
*4 Keio University
*5 Department of Applied Physics, University of Tokyo

References

1) K. Hashimoto and T. Oka, JHEP **1310**, 116 (2013) [arXiv:1307.7423].

Holographic entanglement and causal shadow in the time-dependent Janus black hole†

Y. Nakaguchi,[*1,*2] N. Ogawa,[*3] and T. Ugajin[*4]

The relation between entanglement and the black hole interior has been attracting attention recently. For eternal AdS black holes, some interior information is captured by the entanglement entropy of an interval on the dual theory, i.e. a thermofield doubled CFT[1)].

In some kinds of black holes, the interior appears even more difficult to access since they have "causal shadow" regions inside. In this work, we consider one such black hole, called the three-dimensional time-dependent Janus black hole[2)],

$$ds^2 = L^2\left[dy^2 + \frac{r_0^2}{\tilde{g}(y)^2\cosh^2 r_0 t}(-dt^2+d\theta^2)\right],$$
$$\tilde{g}(y) = \sqrt{\frac{2}{1+\sqrt{1-2\gamma^2}\cosh 2y}}, \qquad (1)$$

where γ is a deformation parameter from the BTZ black hole. This is a solution of the Einstein-scalar theory and it corresponds to a pair of two entangled 2D CFTs, whose coupling constants are different from each other.

This geometry has a horizontally extended Penrose diagram as shown in Fig. 1. The remarkable property of this geometry is the existence of a so-called "causal shadow region," which is causally inaccessible from both boundaries.

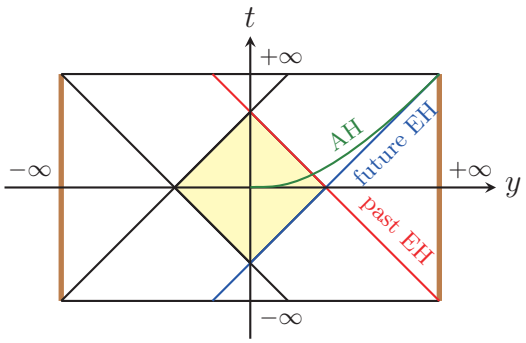

Fig. 1. Penrose diagram of the 3D time-dependent Janus black hole. The causal shadow is painted yellow. The apparent horizons (green line) in the time slices τ = const. are located inside the future event horizon.

We studied the time-evolution of the same entanglement entropy in this system in a holographic manner, by using the Ryu-Takayanagi formula. As in the BTZ black hole, there are two candidate extremal surfaces in the bulk, whose area gives the entanglement entropy. One of the extremal surfaces, which we call the connected surface, connects two asymptotic boundaries and probes the black hole interior. The other extremal surface, which we call the disconnected surface, localizes near each of the asymptotic boundaries.

In the Janus black hole, when the deformation from the BTZ black hole is not so large, we found a similar behavior but with the critical time t_c shorter than that of the BTZ black hole. Roughly speaking, this is because the deformation makes the wormhole region longer and results in a longer connected surface. The results for the time evolution of the entanglement entropy of each phase are plotted in Fig. 2.

In addition, we also found that with a sufficiently large deformation, the disconnected surface is always dominant, and that the holographic entanglement entropy is already proportional to the size of the subsystem from the initial time. This means that the entanglement entropy of this subsystem does not probe the black hole interior.

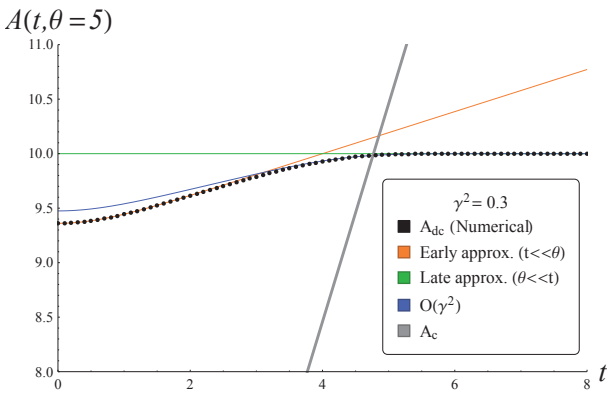

Fig. 2. The time t dependence of the extremal surface area A for a subsystem $\theta = 5$, in the disconnected phase (black dotted line, numerically obtained) and in the connected phase (gray line).

† Condensed from the article arXiv:1412.8600 [hep-th].

*1 Institute for the Physics and Mathematics of the Universe, University of Tokyo
*2 Department of Physics, University of Tokyo
*3 RIKEN Nishina Center
*4 Kavli Institute for Theoretical Physics, University of California

References

1) T. Hartman and J. Maldacena, *JHEP* **1305** (2013) 014, [arXiv:1303.1080].
2) D. Bak, M. Gutperle, and S. Hirano, *JHEP* **0702** (2007) 068, [hep-th/0701108].
3) D. Bak, M. Gutperle, and A. Karch, *JHEP* **0712** (2007) 034, [arXiv:0708.3691].

Radion stabilization in the presence of Wilson line phase†

Y. Abe,[*1] T. Inami,[*2*3] Y. Kawamura,[*1] and Y. Koyama[*4]

In a higher-dimensional gravity theory, a scalar field ϕ called "radion" appears in the extra-dimensional graviton components, and its vacuum expectation value is related to the size of the extra space. The stabilization of the radius is crucial for the solution to the hierarchy problem in the Randall-Sundrum model[1] and inflation based on the radion[2]. The stabilization is realized by the quantum effects of a graviton and fermions in a 5D model $M_4 \times S^1$[3].

In a higher-dimensional gauge theory, the extra-dimensional components of gauge bosons are massless at the tree level because of gauge invariance, and their zero modes become dynamical degrees of freedom called the Wilson line phases θ and are stabilized by quantum corrections[4]. There is a possibility that realistic gauge symmetries including the standard model ones survive after the stabilization of the Wilson line phases. The Wilson line phase receives finite radiative corrections in its mass and can play the role of the Higgs boson[5], providing a solution to the gauge hierarchy problem. An inflation model has been proposed based on the idea that the Wilson line phase becomes the inflaton[6].

We investigate how the Wilson line phase and the Casimir energy from various bulk fields are involved in the stabilization of the radion in a different setup. Particularly, we study the stabilization of the extra-dimensional radius of S^1 in the presence of a Wilson line phase of the extra $U(1)$ gauge symmetry in 5D space-time with a flat background metric and without branes, by using the effective potential V for ϕ and θ at the one-loop level.

Our model consists of the 5D graviton $\hat{g}_{MN}$, a $U(1)$ gauge boson B_M, c_1 charged fermions ψ_i ($i = 1, \cdots, c_1$), and c_2 $U(1)$ neutral fermions η_l ($l = 1, \cdots, c_2$). We take $M^4 \times S^1$ as the background 5D space-time and impose periodic boundary conditions on every field. We obtain the one-loop potential

$$V(\phi,\theta) = -\frac{6}{\pi^2}\frac{1}{\phi^2 L^4}\zeta(5) + c_2\frac{3}{\pi^2}\frac{1}{\phi^2 L^4}\left[\mathrm{Li}_5(e^{-L\mu\phi^{1/3}}) + L\mu\phi^{1/3}\mathrm{Li}_4(e^{-L\mu\phi^{1/3}}) + \frac{1}{3}L^2\mu^2\phi^{2/3}\mathrm{Li}_3(e^{-L\mu\phi^{1/3}})\right]$$
$$+c_1\frac{3}{\pi^2}\frac{1}{\phi^2 L^4}\mathrm{Re}\left[\mathrm{Li}_5(e^{-Lm\phi^{1/3}}e^{i\theta}) + Lm\phi^{1/3}\mathrm{Li}_4(e^{-Lm\phi^{1/3}}e^{i\theta}) + \frac{1}{3}L^2m^2\phi^{2/3}\mathrm{Li}_3(e^{-Lm\phi^{1/3}}e^{i\theta})\right], \quad (1)$$

where L, m and μ are the compactification circumference, the mass of the charged fermions and the neutral fermions, respectively.

The potential has a finite minimum in the presence of neutral fermions the number c_2 of which is larger than c_1+2 and the radion is stabilized at a certain finite value of ϕ. A typical shape of $V(\phi,\theta)$ is depicted in Fig. 1. From this figure, we see that the true minimum of the potential is located on the line $\theta = \pi$. The values of ϕ and the potential at the minimum depend on the parameters m, μ and L. Their values do not drastically modify the shape of the potential drastically.

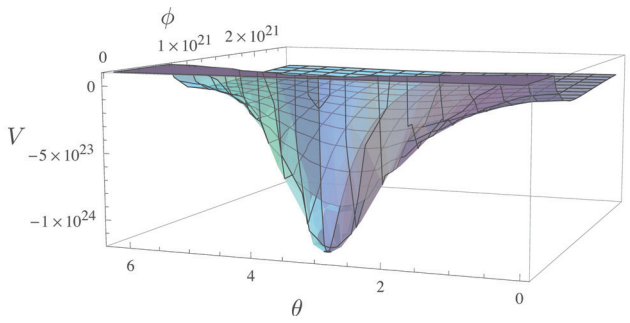

Fig. 1. The potential $V(\phi,\theta)$ with $c_1 = 1$, $c_2 = 4$, $m = 1\times10^{10}$GeV, $\mu = 1\times10^{10}$GeV and $L = 3\times10^{-17}$GeV^{-1}.

In this work, we investigated the behavior of the potential for both large and small values of the radion and found that the potential does not have a finite minimum in the case with only charged fermions as matter fields. The radion stabilization is realized in the presence of neutral fermions whose number is larger than the number of charged ones by two.

The remaining subject is the application of our potential $V(\phi,\theta)$ to an inflation model. By identifing the extra-dimensional scalar component of the 5D gauge field and/or the scalar component of the 5D metric as the inflaton, we examine whether the potential reproduces realistic inflation parameters. The radion properties differ from thoset of the Wilson line phase.

† Condensed from the article in PTEP **2014** 7, 073B04(2014).
*1 Department of Physics, Shinshu University
*2 RIKEN Nishina Center
*3 Department of Physics, National Taiwan University
*4 Department of Physics, National Tsing Hua University

References

1) L. Randall and R. Sundrum: Phys .Rev. Lett. **83**, 3370 (1999).
2) A. Mazumdar: Phys. Lett. B**469**, 55 (1999).
3) Y. Fukazawa, T. Inami, and Y. Koyama: Prog. Theor. Exp. Phys. **2013** 021B01 (2013).
4) Y. Hosotani: Phys. Lett. B**126**, 309 (1983).
5) H. Hatanaka, T. Inami, and C.S. Lim: Mod. Phys. Lett. A**13**, 2601 (1998).
6) N. Arkani-Hamed, H.-C. Cheng, P. Creminelli, and L. Randall: Phys. Rev. Lett. **90**, 221302 (2003).

Is cosmological constant screened in Liouville gravity with matter?

T. Inami,[*1,*2] Y. Koyama,[*3] Y. Nakayama,[*4] and M. Suzuki[*5,*6]

Recent observation of dark energy in our universe has led to the conviction that the cosmological constant Λ has an infinitesimal positive value. It means that our space-time is de Sitter (dS) space with the Hubble constant H being $\sqrt{\Lambda}$. It has been proposed that the strong infrared (IR) divergence property of quantum corrections on dS space may explain the smallness of Λ in our current universe (so called cosmological constant problem). The Einstein equation describes the relation between the space-time Ricci tensor $R_{\mu\nu}$ and the energy momentum (EM) tensor $T_{\mu\nu}$ due to the presence of matter. In vacuum, where $T_{\mu\nu}$ is proportional to the metric, the Einstein equation takes the form

$$R_{\mu\nu} - \frac{1}{2}g_{\mu\nu}R + g_{\mu\nu}\Lambda_{\rm eff} = 0,\ \Lambda_{\rm eff} = \Lambda - \frac{\kappa}{D}T_\rho{}^\rho, \quad (1)$$

where R is the scalar curvature, $\kappa = 8\pi G$ with G being Newton's constant. The vacuum contribution of $T_{\mu\nu}$ is now combined with Λ to define the effective cosmological constant $\Lambda_{\rm eff}$.

In view of this expression, we may wonder if a large value of $T_{\mu\nu}$ cancels the large value of Λ, yielding a very small value of $\Lambda_{\rm eff}$ that we observe today.[1)] We study this question in 2-dimensional (2D) Liouville gravity.

We are interested in the dS solution of Liouville gravity, which can describe the interaction between scaler field and gravity. The 2D cosmological constant has two components: the coupling of the Liouville potential and the trace of the EM tensor. By using Weyl transformation to 2D metric $g_{\mu\nu}(g_{\mu\nu} = e^{2\phi}\hat{g}_{\mu\nu})$, we obtain the equation,

$$\begin{aligned} &S_{L+{\rm mat}}[\Phi,\phi] \\ &= -\int d^2x\sqrt{-\hat{g}}\left[\frac{1}{4\pi b^2}\hat{g}^{\mu\nu}\partial_\mu\Phi\partial_\nu\Phi + \frac{Q}{4\pi b}\hat{R}\Phi\right. \\ &\quad \left. + \frac{\Lambda}{\kappa}e^{2\Phi} + \frac{1}{2}\hat{g}^{\mu\nu}\partial_\mu\phi\partial_\nu\phi + e^{2\Phi}V(\phi)\right]. \end{aligned} \quad (2)$$

The first three terms are Liouville gravity. At this point, it is important to note that the negative value of Λ corresponds to dS space in Liouville gravity.

As a concrete matter Lagrangian, we have studied a massless scalar field theory with $\lambda\phi^4$ interaction minimally coupled to Liouville gravity.

$$\mathcal{L} = -\frac{1}{2}g^{\mu\nu}\partial_\mu\phi\partial_\nu\phi\sqrt{-g} - \frac{1}{4!}\lambda\phi^4\sqrt{-g} + \Delta\mathcal{L}, \quad (3)$$

*1 RIKEN Nishina Center
*2 Department of Physics, National Taiwan University
*3 Department of Physics, National Tsing-Hua University
*4 Walter Burke Institute for Theoretical Physics, California Institute of Technology
*5 Department of Physics, Shizuoka University
*6 Department of Information Science and Technology, Graduate School of Science and Technology, Shizuoka University

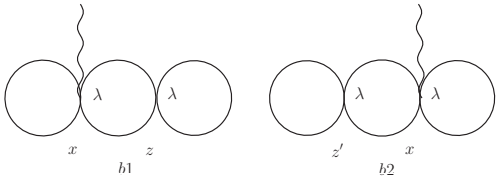

Fig. 1. Part of λ^2-order corrections to the EM tensor $T_{\mu\nu}$.

where $\Delta\mathcal{L}$ consists of counter-terms. In dS space, the massless scalar propagator contains IR divergence in the long wavelength limit and the IR logarithm appears because the cutoff regularization of the IR divergence. Based on the in-in formalism, [2-4)] we have computed the VEV of the EM tensor to the order of λ^2.

$$\begin{aligned} \Lambda_{\rm eff} \sim\ &\Lambda + (\text{Weyl anomaly}) + \frac{\kappa\lambda}{32\pi^2}\ln^2 a(\eta) \\ &+ \frac{1}{8\pi}\frac{\kappa\lambda^2}{(4\pi)^2H^2}\ln^4 a(\eta), \end{aligned} \quad (4)$$

where $a = -\frac{1}{H\eta}$ is the scale factor and $\eta = -\frac{1}{H}e^{-Ht}$ is conformal time. The resulting VEV has time dependence through the IR logarithms, and as a consequence, the effective cosmological constant shows the screening effect at late time such that the absolute value decreases with time. This should be in contrast with the situations where $D > 2$, in which the cosmological constant is anti-screened in the $\lambda\phi^4$ theory.[5)]

To claim that the observed dS breaking effects are physical, we need to find whether they may be eliminated from the local counter-terms. Here, we discuss rather unfamiliar time-dependent IR counter-terms. This possibility plays a crucial role to understand the (in)equivalence between the Sine-Gordon model and the massive Thirring model in dS space. We are indeed able to recover the dS invariance by adding time-dependent IR counter-terms to the naive perturbative computations using the dS breaking propagator. Within the perturbation theory we have studied, however, a similar mechanism does not seem to be workable in $\lambda\phi^4$ theory. This fact supports the claim that the observed screening mechanism of the cosmological constant should be physical. This sensitive issue will be further discussed in our future publication.

References

1) J. Polchinski: hep-th/0603249.
2) J. S. Schwinger: J. Math. Phys. **2**, 407 (1961).
3) L. V. Keldysh: Zh. Eksp. Teor. Fiz. **47**, 1515 (1964) [Sov. Phys. JETP **20**, 1018 (1965)].
4) S. Weinberg: Phys. Rev. D **72**, 043514 (2005).
5) V. K. Onemli and R. P. Woodard: Class. Quant. Grav. **19**, 4607 (2002).

Effective Higgs interactions of composite dark matter†

E. T. Neil*1,*2 for the LSD Collaboration

The recent discovery of the Higgs boson has placed significant and direct constraints on models which predict new physics near the electroweak scale. At the same time, recent dark matter direct-detection experiments have greatly improved their sensitivity, pushing into the region of parameter space where dark matter interacts with the standard model through exchange of a Higgs boson.

These new constraints are particularly interesting in the context of composite dark matter models (e.g.[1]). In such a model, the lightest stable bound state of a strongly-coupled gauge sector provides a dark matter candidate. Although the bound state itself must be net electroweak neutral due to direct-detection experimental constraints, its constituents may carry electroweak charges; the resulting interactions with the standard model in the early universe can explain the observed dark matter abundance, while scattering from present-day direct detection experiments is through suppressed higher-dimensional operators[2].

If the dark gauge interaction spontaneously breaks a continuous symmetry, then some of the bound states will be massless Nambu-Goldstone bosons, which are ruled out by experiment if they are electroweak charged. A realistic composite dark matter model thus requires a mechanism for mass generation of the constituents. In most models the constituents are fermions, and they can be given mass through the Higgs mechanism; depending on the assignment of charges, "vector-like" mass terms may also be allowed[3]. The Higgs couplings required for mass generation are directly constrained by direct-detection experiment, in terms of the Higgs coupling of the dark matter bound state itself.

We consider for concreteness a model consisting of an SU(4) dark gauge force, and a set of degenerate fermions m_f carrying electric charge $Q = \pm 1/2$. The dark matter candidate is a neutral baryon-like bound state of four such fermions, and has total mass m_B. The coupling of the Higgs boson to this baryon-like state is given by the formula

$$g_{h,B} = \frac{m_B}{v}\left(\sum_f \frac{v}{m_f}\left.\frac{\partial m_f(h)}{\partial h}\right|_{h=v}\right) f_f^{(B)} \qquad (1)$$

where $v = 246$ GeV is the vacuum expectation value of the Higgs field. The factor $f_f^{(B)}$ contains the scalar matrix element of the fermions inside the baryon-like state, $\langle B|\bar{f}f|B\rangle$. This matrix element can be extracted using the Feynman-Hellmann theorem from the slope of the baryon mass, $\partial m_B/\partial m_f$; this is a non-perturbative quantity, and is calculated using lattice simulations of the SU(4) theory. We find $0.15 \lesssim f_f^{(B)} \lesssim 0.34$ in the range of fermion masses simulated.

Finally, the term in parentheses,

$$\alpha = \frac{v}{m_f}\left.\frac{\partial m_f(h)}{\partial h}\right|_{h=v}, \qquad (2)$$

is entirely model-dependent, and parameterizes the fraction of the fermion mass m_f which is generated due to the Higgs mechanism; if there are no "vector-like" mass terms, then $\alpha = 1$. The current upper bound on α in this model, based on our lattice calculation of $f_f^{(B)}$ and the latest experimental results from LUX[4], is shown in Fig. 1. For the entire range of models considered, this constraint is significantly less than 1, indicating that generation of m_f in this model requires more than the Higgs mechanism alone.

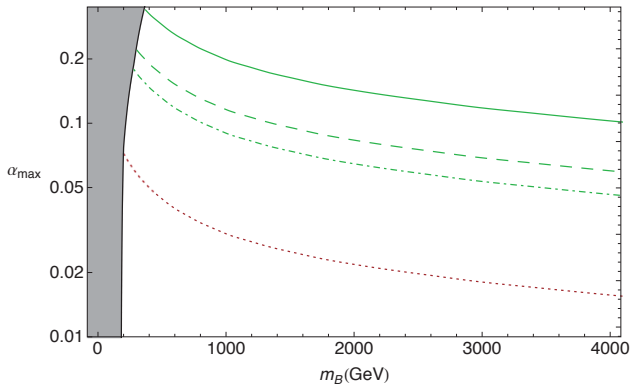

Fig. 1. From[3], upper bound on the effective Higgs coupling α based on three lattice simulations at various values of the fermion mass (green curves) and in the heavy quark limit (red dotted curve). The filled region on the left shows values of m_B ruled out by experimental bounds on light charged particles from LEP.

References
1) G. D. Kribs, T. S. Roy, J. Terning, and K. M. Zurek, Phys. Rev. **D81** (2010) 095001
2) T. Appelquist et al. (LSD Collaboration): Phys. Rev. **D88** (2013), 014502
3) T. Appelquist et al. (LSD Collaboration): Phys. Rev. **D89** (2014), 094508
4) D. S. Akerib et al. (LUX Collaboration): Phys. Rev. Lett. **112** (2014) 9, 091303

† Condensed from the article in Phys. Rev. **D89**, 094508 (2014)

*1 RIKEN Nishina Center
*2 Department of Physics, University of Colorado, Boulder

Effective field theory for spacetime symmetry breaking†

Y. Hidaka,[*1] T. Noumi,[*1] and G. Shiu[*2,*3]

Symmetry and its spontaneous breaking play an important role in various areas of physics. In particular, the low-energy effective field theory (EFT) based on the underlying symmetry structures provides a powerful framework for understanding the low-energy dynamics in the symmetry broken phase.

For internal symmetry breaking in Lorentz invariant systems, the EFT based on coset construction had been established in 1960's[1,2]. When a global symmetry group G is broken to a residual symmetry group H, the corresponding Nambu-Goldstone (NG) fields $\pi(x)$ are introduced as the coordinates of the coset space G/H and the general effective action can be constructed from the Maurer-Cartan one form,

$$J_\mu = \Omega^{-1}\partial_\mu\Omega \quad \text{with} \quad \Omega(x) = e^{\pi(x)} \in G/H\,. \qquad (1)$$

Such a coset construction was also extended to spacetime symmetry breaking[3,4] accompanied by the inverse Higgs constraints[5] and has been applied to various systems. Although the coset construction captures certain aspects of spacetime symmetry breaking, its understanding seems incomplete compared to the internal symmetry case.

For example, a naive counting of broken spacetime symmetries based on the global symmetry picture contains redundant fields and causes a wrong counting of NG modes. For conformal symmetry breaking, it is known that the inverse Higgs constraints compensate such a mismatch of NG mode counting. It is also argued recently that the inverse Higgs constraints eliminate not only the redundant fields but also the massive modes, which nonlinearly transform under the broken symmetries (see, e.g.,[6–8]). In addition to the massless modes, such massive modes associated with the symmetry breaking can be relevant in the construction of phenomenological models (e.g. massive fields with a Hubble scale mass are nonnegligible in cosmology).

In this work, we discussed the effective field theory for spacetime symmetry breaking from the local symmetry point of view. By gauging spacetime symmetries, the identification of NG fields and the construction of the effective action are performed based on the breaking pattern of diffeomorphism, local Lorentz, and (an)isotropic Weyl symmetries as well as the internal symmetries including possible central extensions in nonrelativistic systems. Such a local picture distinguishes, e.g., whether the symmetry breaking condensations have spins and provides a correct identification of the physical NG fields, while the standard coset construction based on global symmetry breaking does not. We illustrated that the local picture becomes important in particular when we take into account massive modes associated with symmetry breaking, whose masses are not necessarily high.

We also revisited the coset construction for spacetime symmetry breaking. Based on the relation between the Maurer-Cartan one form and connections for spacetime symmetries, we classify the physical meanings of the inverse Higgs constraints by the coordinate dimension of broken symmetries. Inverse Higgs constraints for spacetime symmetries with a higher dimension remove the redundant NG fields, whereas those for dimensionless symmetries can be further classified by the local symmetry breaking pattern.

We are now working on several applications of our approaches for spacetime symmetry breaking. For example, there are some recent discussions that inhomogeneous chiral condensations may appear in the QCD phase diagram. Using our EFT framework, we discuss the dispersion relation of the NG field in such a phase. Another ongoing application is inflation. We are e.g. trying to classify the source of primordial gravitational waves (which potentially affect the B-mode polarization of cosmic microwave backgrounds) by the symmetry breaking point of view. We hope to report those applications in near future.

References
1) S. R. Coleman, J. Wess and B. Zumino, Phys. Rev. **177**, 2239 (1969).
2) C. G. Callan, Jr., S. R. Coleman, J. Wess and B. Zumino, Phys. Rev. **177**, 2247 (1969).
3) D. V. Volkov, Sov. J. Part. Nucl. **4**, 3 (1973) .
4) V. I. Ogievetsky, Proc. of X-th Winter School of Theoretical Physics in Karpacz **1**, 117 (1974).
5) E. A. Ivanov and V. I. Ogievetsky, Teor. Mat. Fiz. **25**, 164 (1975).
6) A. Nicolis, R. Penco, F. Piazza and R. A. Rosen, JHEP **1311**, 055 (2013) [arXiv:1306.1240 [hep-th]].
7) S. Endlich, A. Nicolis and R. Penco, Phys. Rev. D **89**, no. 6, 065006 (2014) [arXiv:1311.6491 [hep-th]].
8) T. Brauner and H. Watanabe, Phys. Rev. D **89**, no. 8, 085004 (2014) [arXiv:1401.5596 [hep-ph]].

† Condensed from the article in arXiv:1412.5601.

*1 RIKEN Nishina Center
*2 Department of Physics, University of Wisconsin, Madison
*3 Center for Fundamental Physics and Institute for Advanced Study, Hong Kong University of Science and Technology

Dynamical breaking of shift-symmetry in supergravity-based inflation†

A. Mazumdar,[*1] T. Noumi,[*2] and M. Yamaguchi[*3]

The observations of the cosmic microwave background (CMB) temperature anisotropies[1,2] now strongly support the occurrence of primordial inflation in the early Universe. The observed temperature anisotropy can be well fitted by the primordial perturbations generated during inflation and the anti-correlation of the temperature (T) and E-mode polarization at large angular scale suggests that the primordial perturbations have been stretched on superhorizon scales[1,2]. In addition, very recently, BICEP2 reported the detection of the primordial tensor perturbations through the B-mode polarization as[3]

$$r = 0.20^{+0.07}_{-0.05}\ (68\%\text{CL}), \tag{1}$$

where r is the tensor-to-scalar ratio. To explain this large tensor-to-scalar ratio is challenging for cosmology and particle physics because of the Lyth bound[4]: one would expect a super-Planckian excursion of the inflaton field in order to generate large r.

Generally speaking, the super-Planckian excursion of the inflaton is problematic from the effective field theory (EFT) point of view. In particular, within string theory there are many scales, the string scale, M_s, the compactification scale, M_c and the derived 4 dimensional Planck scale, with a spectrum, $M_s \leq M_c \leq M_p$. Beyond M_s there are quantum corrections not only to the inflaton potential but also to the inflaton kinetic term which can lead to various complications. Even if we assume that we have only one fundamental scale, such as M_p, there are many issues pertaining to the validity of an EFT when the field's VEV goes beyond M_p. In principle, a gauge singlet inflaton can couple to many degrees of freedom, including the Standard Model and the hidden sector degrees of freedom. Typically, the individual inflaton's couplings to matter has to be smaller than 10^{-3} to maintain the flatness of the inflaton potential and also to match the density perturbations created during inflation.

In spite of all these challenges, we wish to ask the question - whether can we explain *at least* a such small inflaton couplings to matter, and large inflaton's VEV during inflation within an EFT approach by invoking some symmetry such as *shift-symmetry*, $\phi \to \phi' = \phi + c$, where ϕ is the inflaton and c is a constant. Within EFT, one has to ensure that the inflaton's and *all other field's* kinetic terms are small, and here we simply assume so in some patch of the Universe just to be within the EFT regime. Such a *shift-symmetry* has been for the first time introduced in the context of chaotic inflation in supergravity (SUGRA)[5,6]. However, based on the same token if *shift-symmetry* remains unbroken inflation would never occur in our patch of the universe. The *shift-symmetry* has to be broken, but in such a way that the breaking remains *soft*, which could be understood via some dynamics of the fields. A hard breaking can be introduced[5,6], but the predictions can be lost or one has to resort to some anthropic arguments.

The purpose of this work is to illustrate a concrete model of dynamical shift symmetry breaking. We showed that it is indeed possible to break the *shift-symmetry* dynamically within 4 dimensional supergravity prior to a long phase of inflation. Thanks to the *shift-symmetry*, the leading contribution to the inflaton potential is free from the dangerous exponential factor even after its breaking, which is the main obstacle to realizing the super-Planckian inflation in supergravity. In our simple mode, the resulting effective inflaton potential schematically takes the form $V_{\rm eff}(\phi_{\rm inf}) \sim \cos\dfrac{\phi_{\rm inf}}{\mu}$ with μ being the dynamical symmetry breaking scale. This potential can induce an inflationary epoch with the inflaton excursion $\Delta\phi_{\rm inf} \sim \mu$. Unfortunately, in this model, it is difficult to realize the super-Planckian inflation $\Delta\phi_{\rm inf} > M_p$ as long as the dynamical symmetry breaking scale μ is sub-Planckian. We hope to extend our simple model to realize the super-Planckian inflation, in near future.

References

1) G. Hinshaw *et al.* [WMAP Collaboration], arXiv:1212.5226 [astro-ph.CO].
2) P. A. R. Ade *et al.* [Planck Collaboration], arXiv:1303.5082 [astro-ph.CO].
3) P. A. R. Ade *et al.* [BICEP2 Collaboration], arXiv:1403.3985 [astro-ph.CO].
4) D. H. Lyth, Phys. Rev. Lett. **78**, 1861 (1997) [hep-ph/9606387].
5) M. Kawasaki, M. Yamaguchi and T. Yanagida, Phys. Rev. Lett. **85**, 3572 (2000) [arXiv:hep-ph/0004243].
6) M. Kawasaki, M. Yamaguchi and T. Yanagida, Phys. Rev. D **63**, 103514 (2001) [arXiv:hep-ph/0011104].

† Condensed from the article in Phys.Rev. D90 (2014) 043519.

*1 Physics Department, Lancaster University
*2 RIKEN Nishina Center
*3 Department of Physics, Tokyo Institute of Technology

Non-Gaussianities of primordial perturbations and tensor sound speed†

T. Noumi*1 and M. Yamaguchi*2

Inflation is now widely accepted as a paradigm of early Universe to explain the origin of the primordial perturbations as well as to solve the horizon and the flatness problems of the standard big-bang cosmology. The current observational data such as the cosmic microwave background (CMB) anisotropies support almost scale-invariant, adiabatic, and Gaussian primordial curvature fluctuations as predicted by inflation. While the paradigm itself is well established and widely accepted, its detailed dynamics, e.g. the identification of an inflaton, its kinetic and potential structure, and its gravitational coupling, are still unknown.

The non-Gaussianities of primordial curvature perturbations are powerful tools to give such informations. For example, it is well-known that the equilateral type of bispectrum of primordial curvature perturbations is enhanced by the inverse of their sound speed squared [1,2]. The null observation of the equilateral type by the Planck satellite, characterized as $f_{\rm NL}^{\rm equil} = 42 \pm 75$ (68% CL)[3], yields stringent constraints on the sound speed of the curvature perturbations as $c_s \geq 0.02$ (95% CL)[3].

Inflation generates not only primordial curvature perturbations but also primordial tensor perturbations [4]. Very recently, it was reported that primordial tensor perturbations have been found and the tensor-to-scalar ratio r is given by $r = 0.20^{+0.07}_{-0.05}$ (68% CL)[5], though it is constrained as $r < 0.11$(95% CL) in the Planck results[6]. Their amplitude directly determines the energy scale of inflation, so it is estimated as $V^{1/4} \simeq 2.2 \times 10^{16}$ GeV given $r \simeq 0.2$[5] and $P_\zeta \simeq 2.2 \times 10^{-9}$[6]. If we go beyond the powerspectrum, it is known that the bispectra of primordial tensor perturbations enable us to probe the gravitational coupling of the inflaton field[7]. Such a non-trivial gravitational coupling easily modifies the sound speed of primordial tensor perturbations, c_γ, and it can significantly deviate from unity[8]. Then, one may wonder if the small sound velocity of primordial tensor perturbations can enhance their non-Gaussianities as in the case of the curvature perturbations. In this work, we addressed this issue.

The relation between the sound speed and the non-Gaussianities of primordial curvature perturbations can be clearly understood by use of the effective field theory (EFT) approach to inflation[9]. Inflation can be characterized by the breakdown of time-diffeomorphism invariance due to the time-dependent cosmological background and the general action for inflation can be constructed based on this symmetry breaking structure. The primordial curvature perturbation can be identified with the Goldstone mode π associated with the breaking of time-diffeomorphism invariance. The symmetry arguments require that modification of the sound speed c_s induces non-negligible cubic interactions of the Goldstone mode π, and hence the sound speed and the bispectrum of the curvature perturbations are directly related.

In this work, we investigated the relation between the sound speed of tensor perturbations and the bispectrum of primordial perturbations, based on the EFT approach. We first identified what kind of operators can modify the tensor sound speed. Then, we clarify which type of non-Gaussianity arises associated with the modification and can be used as a probe for the tensor sound speed. We found that the tensor sound speed is not directly related to tensor bispectra, in contrast to the scalar sound speed case. We also discussed primordial trispectra as a possible probe of tensor sound speed.

References

1) D. Seery and J. E. Lidsey, JCAP **0506**, 003 (2005) [astro-ph/0503692].
2) X. Chen, M. -x. Huang, S. Kachru and G. Shiu, JCAP **0701**, 002 (2007) [hep-th/0605045].
3) P. A. R. Ade *et al.* [Planck Collaboration], arXiv:1303.5084 [astro-ph.CO].
4) A. A. Starobinsky, JETP Lett. **30**, 682 (1979) [Pisma Zh. Eksp. Teor. Fiz. **30**, 719 (1979)].
5) P. A. R. Ade *et al.* [BICEP2 Collaboration], arXiv:1403.3985 [astro-ph.CO].
6) P. A. R. Ade *et al.* [Planck Collaboration], arXiv:1303.5082 [astro-ph.CO].
7) X. Gao, T. Kobayashi, M. Yamaguchi and J. 'i. Yokoyama, Phys. Rev. Lett. **107**, 211301 (2011) [arXiv:1108.3513 [astro-ph.CO]].
8) T. Kobayashi, M. Yamaguchi and J. 'i. Yokoyama, Prog. Theor. Phys. **126**, 511 (2011) [arXiv:1105.5723 [hep-th]].
9) C. Cheung, P. Creminelli, A. L. Fitzpatrick, J. Kaplan and L. Senatore, JHEP **0803**, 014 (2008) [arXiv:0709.0293 [hep-th]].

† Condensed from the article in arXiv:1403.6065.

*1 RIKEN Nishina Center
*2 Department of Physics, Tokyo Institute of Technology

Spin operator and entanglement in quantum field theory†

K. Fujikawa,*1 C.H. Oh,*2 and C. Zhang*2

Entanglement is studied in the framework of Dyson's S-matrix theory in relativistic quantum field theory, which leads to a natural definition of entangled states of a particle-antiparticle pair and the spin operator from a Noether current. As an explicit example, the decay of a massive pseudo-scalar particle into an electron-positron pair is analyzed. Two spin operators are extracted from the Noether current. The Wigner spin operator characterizes spin states at the rest frame of each fermion and, although not measurable in the laboratory, gives rise to a straightforward generalization of the low energy analysis of entanglement to the ultra-relativistic domain. In contrast, if one adopts a (modified) Dirac spin operator, the entanglement measured using spin correlation becomes maximal near the threshold of the decay, while the entanglement is replaced by the classical correlation for the ultra-relativistic electron-positron pair by analogy to the case of neutrinos, for which a hidden-variables-type description is possible. Entanglement in this sense depends on the energy scale involved. Chiral symmetry which is fundamental in particle physics differentiates the spin angular momentum and the magnetic moment. The use of weak interaction, which can measure helicity, is suggested in the analysis of entanglement at high energies instead of a Stern-Gerlach apparatus, which is known to be useless for the electron. A difference between the electron spin at high energies and the photon linear polarization is also noted.

We formulate the entanglement in the framework of relativistic quantum field theory, or more precisely, in the S-matrix theory defined by Dyson.[1] In the S-matrix theory, we treat only asymptotic states that contain particles far apart from each other.

We consider the decay of a very massive pseudoscalar particle P into an electron-positron pair by an interaction Hamiltonian, $H_I(t) = g\int d^3x : P(x)\bar{\psi}(x)i\gamma_5\psi(x) :$ with a coupling constant g. The Dyson formula for the S-matrix gives the state $\Psi = -ig\int d^4x : P(x)\bar{\psi}(x)i\gamma_5\psi(x) : |P(\vec{0})\rangle$, where we assume a small g. We then obtain for the fixed momentum direction of the electron,

$$\Psi(\vec{p}) \equiv \frac{1}{\sqrt{2}}[a^\dagger(\vec{p},s)b^\dagger(-\vec{p},-s) + a^\dagger(\vec{p},-s)b^\dagger(-\vec{p},s)]|0\rangle.$$

This shows a way to prepare a desired state in the framework of local and causal relativistic field theory. All the properties of the asymptotic state are accounted for in the framework which is consistent with locality, causality and the uncertainty principle; in particular, it is important to recognize that we integrate over the entire Minkowski space in defining Ψ; that is, we have no information about when and where the particle decayed.

Spin Operator

The conserved angular momentum operator (Noether charge) of the Dirac action is given by $\hat{\vec{J}} = \int d^3x : \psi^\dagger(x)[\vec{L}+\vec{S}]\psi(x) :$, which is written as

$$\begin{aligned}
&\int d^3p \sum_{s,s'} \frac{1}{2}\{\xi(s')^\dagger\vec{\sigma}\xi(s)a^\dagger(\vec{p},s')a(\vec{p},s) \\
&\qquad -\xi^\dagger(-s)\vec{\sigma}\xi(-s')b^\dagger(\vec{p},s')b(\vec{p},s)\} \\
&+\int d^3p \sum_{s}\{a^\dagger(\vec{p},s)\left(\vec{L}a(\vec{p},s)\right) \\
&\qquad +b^\dagger(\vec{p},s)\left(\vec{L}b(\vec{p},s)\right)\}.
\end{aligned}$$

The first term is called the Wigner spin operator, which is not directly measured in the laboratory. We instead define the (modified) Dirac spin operator

$$\begin{aligned}
&\hat{\vec{S}}(\vec{p}) \\
&\equiv \sum_{s,s'}\{[\frac{1}{2}\frac{m}{E}\xi^\dagger(s')\vec{\sigma}_T\xi(s) + \frac{1}{2}\hat{p}\xi^\dagger(s')(\vec{\sigma}\cdot\hat{p})\xi(s)] \\
&\quad \times a^\dagger(\vec{p},s')a(\vec{p},s) \\
&-[\frac{1}{2}\frac{m}{E}\xi^\dagger(-s)\vec{\sigma}_T\xi(-s') + \frac{1}{2}\hat{p}\xi^\dagger(-s)(\vec{\sigma}\cdot\hat{p})\xi(-s')] \\
&\quad \times b^\dagger(-\vec{p},s')b(-\vec{p},s)\},
\end{aligned}$$

which is close to what is measured in the laboratory. A salient feature of this spin is that it appraoches the helicity state proportional to the momentum direction $\hat{p}$ for $E \to \infty$. That is, the spin correlation at high energies becomes similar to the correlation of neutrinos. The spin correlation of two neutrinos, which can have only two states $h = \pm$, does not define the entanglement in the conventional sense. That is, the high energy electron states behave like classical particles, which show the correlation but not entanglement. This transition to helicity states may be measured using weak interactions.[2]

References
1) F. J. Dyson: Phys. Rev. **75**, 1736 (1949).
2) K. Fujikawa and R. Shrock: Phys. Rev. Lett. **45**, 963 (1980).

† Condensed from the article in Phys. Rev. D. 90, 025028 (2014).

*1 RIKEN Nishina Center
*2 Center for Quantum technologies, National University of Singapore,

Linearity of quantum probability measure and Hardy's model†

K. Fujikawa,*1 C.H. Oh,*2 and C. Zhang*2

Hardy proposed a characterization of entanglement that does not use inequalities by EPR-type arguments. It is however disturbing that his scheme, which is intended as a measure of entanglement, completely fails for the maximally entangled case.[1)]

The local hidden-variables model in $d = 4 = 2 \times 2$ dimensions of the Hilbert space is defined by[2)]

$$\langle\psi|\mathbf{a}\cdot\sigma\otimes\mathbf{b}\cdot\sigma|\psi\rangle = \int_\Lambda \rho(\lambda)d\lambda a(\psi,\lambda)b(\psi,\lambda), \quad (1)$$

where $\mathbf{a}$ and $\mathbf{b}$ are 3-dimensional unit vectors, σ stands for the Pauli matrix, and $a(\psi,\lambda)$ and $b(\psi,\lambda)$ are dichotomic variables assuming the eigenvalues ±1 of $\mathbf{a}\cdot\sigma$ and $\mathbf{b}\cdot\sigma$, respectively. One can show that this local hidden-variables model does not satisfy the linearity of the quantum mechanical probability measure in the sense $\langle\psi|\mathbf{a}\cdot\sigma\otimes\mathbf{b}\cdot\sigma|\psi\rangle + \langle\psi|\mathbf{a}\cdot\sigma\otimes\mathbf{b}'\cdot\sigma|\psi\rangle = \langle\psi|\mathbf{a}\cdot\sigma\otimes(\mathbf{b}+\mathbf{b}')\cdot\sigma|\psi\rangle$ for non-collinear $\mathbf{b}$ and $\mathbf{b}'$. If the linearity of the probability measure is strictly imposed, which is tantamount to asking that the non-contextual hidden-variables model in $d = 4$ gives the CHSH inequality $|\langle B\rangle| \le 2$ uniquely,[3)] it is shown that the hidden-variables model can describe only separable quantum mechanical states[4)]

$$\langle\psi|\mathbf{a}\cdot\sigma\otimes\mathbf{b}\cdot\sigma|\psi\rangle = \int \rho_1(\lambda_1)d\lambda_1 a(\psi,\lambda_1) \times \int \rho_2(\lambda_2)d\lambda_2 b(\psi,\lambda_2). \quad (2)$$

In this case, it is shown that Hardy's model becomes trivial. Although Hardy's paradox is interesting as an experimental test of local realism, its mathematical basis is less solid than hitherto assumed.

Hardy's model

Hardy defines the projection operators[1)]

$$\hat{U}_i = |u_i\rangle\langle u_i|, \quad \hat{D}_i = |d_i\rangle\langle d_i|, \quad (3)$$

with $i = 1, 2$, and

$$|u_i\rangle = \frac{1}{\sqrt{\alpha+\beta}}[\beta^{1/2}|+\rangle_i + \alpha^{1/2}|-\rangle_i],$$
$$|d_i\rangle = \frac{1}{\sqrt{\alpha^3+\beta^3}}[\beta^{3/2}|+\rangle_i - \alpha^{3/2}|-\rangle_i] \quad (4)$$

for the entangled state $|\psi\rangle = \alpha|+\rangle_1|+\rangle_2 - \beta|-\rangle_1|-\rangle_2$ with $\alpha^2+\beta^2 = 1$.

He then shows the relations

$$\frac{\langle\psi|D_1U_2D_1|\psi\rangle}{\langle\psi|D_1|\psi\rangle} = 1, \quad (5)$$
$$\frac{\langle\psi|D_2U_1D_2|\psi\rangle}{\langle\psi|D_2|\psi\rangle} = 1, \quad (6)$$
$$\frac{\langle\psi|D_1D_2D_1|\psi\rangle}{\langle\psi|D_1|\psi\rangle} = 1 - \frac{\alpha\beta}{(1-\alpha\beta)}, \quad (7)$$
$$\langle\psi|U_1U_2|\psi\rangle = 0, \quad (8)$$

with $0 < \alpha\beta \le 1/2$.

In the hidden-variables model, the projection operators are assigned their eigenvalues; for example, $D_1(\psi,\lambda) = 1$ or 0, depending on the hidden-variable λ. Relation (7) implies $\int d\lambda\rho(\lambda)D_1(\psi,\lambda)D_2(\psi,\lambda) \neq 0$ for $0 < \alpha\beta < 1/2$ and thus

$$D_1(\psi,\lambda) = 1 \text{ and } D_2(\psi,\lambda) = 1 \quad (9)$$

for *some* λ, while (8) implies $\int d\lambda\rho(\lambda)U_1(\psi,\lambda)U_2(\psi,\lambda) = 0$ and thus

$$U_1(\psi,\lambda)U_2(\psi,\lambda) = 0 \quad (10)$$

for all λ. On the other hand relations (5) and (6) imply

$$D_1(\psi,\lambda) = 1 \Rightarrow U_2(\psi,\lambda) = 1,$$
$$D_2(\psi,\lambda) = 1 \Rightarrow U_1(\psi,\lambda) = 1, \quad (11)$$

respectively, where $\Rightarrow$ means "inevitably implies".

For the entangled state with $0 < \alpha\beta < 1/2$ except for $\alpha\beta = 1/2$, which implies the maximum entanglement, the relations (9)-(11) are inconsistent.[1)] This is called Hardy's paradox, which shows the inconsistency of local realism with entanglement except for the maximally entangled case without referring to inequality.

On the other hand, for a pure state, Bell's theorem $|\langle B\rangle| \le 2$ with $B = \mathbf{a}\cdot\sigma\otimes(\mathbf{b}+\mathbf{b}')\cdot\sigma + \mathbf{a}'\cdot\sigma\otimes(\mathbf{b}-\mathbf{b}')\cdot\sigma$ for any $\mathbf{a}$, $\mathbf{a}'$, $\mathbf{b}$, and $\mathbf{b}'$ implies[5)] relation (2), namely, the separable state. The separable state in Hardy's model, which is consistent with local realism, imlies $\alpha = 1$ and $\beta = 0$, for example, for which $|\psi\rangle = |+\rangle_1|+\rangle_2$ while $\hat{U}_i = |-\rangle_{ii}\langle-|$ and $\hat{D}_i = |-\rangle_{ii}\langle-|$. In this case,

$$\langle U_1\rangle = \langle U_2\rangle = \langle D_1\rangle = \langle D_2\rangle = 0, \quad (12)$$

and all the correlations vanish; thus, Hardy's model becomes mathematically trivial. Hardy's model is inconsistent with local realism by construction.

† Condensed from the article in Int. J. Mod. Phys. A29, 1450017 (2014).

*1 RIKEN Nishina Center
*2 Center for Quantum Technologies, National University of Singapore

References

1) L. Hardy: Phys. Rev. Lett. **71**, 1665 (1993).
2) J. S. Bell: Physics **1**, 195 (1965).
3) J. F. Clauser, M. A. Horne, A. Shimony, R. A. Holt: Phys. Rev. Lett. **23**, 888 (1969).
4) K. Fujikawa: Prog. Theor. Phys. **127**, 975 (2012).
5) N. Gisin: Phys. Lett. A**154**, 201 (1991).

SSD and the infinite circumference limit of CFT†

T. Tada*1

Among all the Virasoro generators of Conformal Field Theory (CFT), three of them, L_0, L_1 and L_{-1}, form a subalgebra that is isomorphic to $sl(2,\mathbb{R})$ and corresponds to the global conformal transformation. The Casimir operator of the subalgebra can be expressed as

$$C_2 = L_0^2 - L_+^2 - L_-^2, \tag{1}$$

where

$$L_+ = \frac{L_1 + L_{-1}}{2} \ , \ L_- = \frac{L_1 - L_{-1}}{2i}. \tag{2}$$

In analogy with the 2+1 dimensional Lorentz transformation, the space spanned by L_0, L_+ and L_- is apparently divided into three distinctive regions. The first region is the "time-like" region that contains L_0 and small perturbations around it. Any vector within this region can be transformed to L_0 upto some numerical multiplication, by the global conformal transformatiom or the $sl(2,\mathbb{R})$. This is actually the region one would have in mind, when one demanded the invariance of the vacuum on the basis of the physical equivalence for the states connected by the global conformal transformation. The second is the "space-like" region, which contains the linear combination of L_+ and L_-. The region between these two is the last one, and could be called the "light-cone" region. This region is represented by either $L_0 - L_+$ or $L_0 - L_-$.

If one further invokes the analogy with the Lorentz geometry, the "time-like" region corresponds to the "massive" representation. Since one observes the spectrum of L_0 in this region, the "mass" in this case should be the inverse of the circumference, or the finite scale of CFT[1,2]. Then, it is natural to induce that the "light-cone" region corresponds to the "massless" representation and the infinite circumference. In this letter, we will argue that if one takes the generator in the "light-cone" region, say $L_0 - L_+$ (plus anti-holomorphic part $\bar{L}_0 - \bar{L}_+$, to be exact), as a Hamiltonian, one can obtain a CFT with the infinite circumference.

Should we adopt a generator that corresponds to $L_0 - L_+$ as a Hamiltonian, we can define the following conserved charges:

$$\mathcal{L}_\kappa \equiv \frac{1}{2\pi i} \oint^{t=const.} dz(-\frac{1}{2}(z-1)^2) e^{\frac{2\kappa}{z-1}} T(z), \tag{3}$$

where $T(z) = T_{zz}(z)$ is the energy momentum tensor of the original CFT. Note that for $\kappa = 0$

$$\mathcal{L}_0 = \frac{1}{2\pi i} \oint^{t=const.} dz(-\frac{1}{2}(z-1)^2) T(z)$$

$$= L_0 - \frac{L_1 + L_{-1}}{2}. \tag{4}$$

One can further calculate the commutation relations among the charges defined above using the operator product expansion of the energy momentum tensor

$$T(z)T(w) \sim \frac{c/2}{(z-w)^4} + \frac{2T(w)}{(z-w)^2} + \frac{\partial_w T(w)}{z-w} + \cdots. \tag{5}$$

The result reads

$$[\mathcal{L}_\kappa, \mathcal{L}_{\kappa'}] = (\kappa - \kappa')\mathcal{L}_{\kappa+\kappa'} + \frac{c}{12}\kappa^3 \delta(\kappa + \kappa'). \tag{6}$$

We have thus obtained the continuous Virasoro algebra with the central charge c, establishing that we have the theory that exhibits the continuous spectrum. This is consistent with the argument presented at the beginning.

This also nicely explains the feature observed in the phenomena called sine-square deformation (SSD) at least for the case that involves CFT. It was found [3–6] that a certain class of quantum systems, systems with closed and open boundary conditions, have identical vacua provided that the coupling constants of the open-boundary system are modulated in a specific way. In particular, SSD works for two-dimensional conformal field theories and it's implications for string theory were discussed by the present author[7,8]. SSD for CFT adopts exactly (4) as the (holomorphic part of) Hamiltonian. At that time, it had been somewhat enigmatic that these two systems with different boundary conditions share the same vacuum state, but this can be explained through the discovery of the continuous spectrum for the SSD system. Because the continuous spectrum suggest that SSD system has an infinitely large space, the distinction between the open and closed condition at the ends that located at infinitely away, is no longer physically relevant.

*1 RIKEN Nishina Center

References

1) A. A. Belavin, A. M. Polyakov and A. B. Zamolodchikov: Nucl. Phys. B **241**, 333 (1984).
2) J. L. Cardy: J. Phys. A **17**, L385 (1984).
3) A. Gendiar, R. Krcmar and T. Nishino: Prog. Theor. Phys. **122** (2009) 953; *ibid.* **123** (2010) 393.
4) H. Katsura: J. Phys. A **45**, 115003 (2012)
5) H. Katsura: J. Phys. A: Math. Theor. **44** (2011) 252001.
6) I. Maruyama, H. Katsura and T. Hikihara, Phys. Rev. **B 84** (2011) 165132.
7) T. Tada: *Proceedings of the 12th Asia Pacific Physics Conference* JPS Conf. Proc. 1, 013003 (2014) .
8) T. Tada: Mod. Phys. Lett. A **30**, 1550092 (2015).

Towards U($N|M$) knot invariant from ABJM theory

B. Eynard[*1,*2] and T. Kimura[*1,*3]

The knot invariant can be realized using the Wilson loop operator in Chern–Simons gauge theory. Especially for the invariant for unknot and torus knot, there exists an integral representation analogous to the U(N) symmetric matrix model. Recently it was pointed out that the partition function of ABJM theory on S^3 can be written as a supermatrix integral.[1] From this point of view, it is natural to explore a possibile connection between the ABJM Wilson loop and a knot invariant.

The ABJM partition function is written as follows,

$$\mathcal{Z} = \frac{1}{N!^2}\int [dx]^N [dy]^N \det_{1\le i,j\le N}\left(\frac{1}{2\cosh\frac{x_i-y_j}{2}}\right)^2, \tag{1}$$

where $[dx] = \frac{dx}{2\pi}\, e^{-\frac{1}{2g_s}x^2}$ and $[dy] = \frac{dx}{2\pi}\, e^{\frac{1}{2g_s}y^2}$ with the string coupling constant $g_s = 2\pi i/k$. In this expression the Wilson loop operator in the representation R is given by the corresponding character of U($N|N$) group, $W_R \to \mathrm{Str}_R\, U(x;y)$ with the holonomy matrix $U(x;y) = \mathrm{diag}(e^{x_1},\cdots,e^{x_N},-e^{y_1},\cdots,-e^{y_N})$. When the partition λ, corresponding to the representation R, satisfies $\Lambda_{N+1} > N$, this character is decomposed into that for SU(N) which is written in terms of the Schur function,

$$\mathrm{Str}_R\, U(x;y) = s_\mu(e^x)\, s_\nu(e^y) \prod_{i,j=1}^{N}(e^{x_i}-e^{y_j}), \tag{2}$$

where $\mu_i^t = \lambda_{i+N}^t$ and $\nu_i^t = \lambda_{i+N}$. We consider this case in particular. Thus the integral representation for the unknot Wilson loop in ABJM theory is now written

$$\begin{aligned}&\Big\langle W_R(K_{\mathrm{unknot}})\Big\rangle \\ &= \int [dx]^N [dy]^N \det\left(\frac{1}{2\cosh\frac{x_i-y_j}{2}}\right)\prod_{i=1}^{N} e^{x_i\xi_i+y_i\eta_i}\end{aligned} \tag{3}$$

with $\xi_i = \lambda_i - i + 1/2$, $\eta_i = \lambda_i^t - i + 1/2$. We can compute this integral by applying the Fourier transform formula $1/\cosh w = \int \frac{dz}{\pi} e^{2iwz/\pi}/\cosh z$,

$$\begin{aligned}\Big\langle W_R(K_{\mathrm{unknot}})\Big\rangle &= k^{-N} q^{\frac{1}{2}(C_2(\mu)-C_2(\nu))} \\ &\times \det_{1\le i,j\le N}\left(\frac{1}{q^{\frac{1}{2}(\xi_i+\eta_j)}+q^{-\frac{1}{2}(\xi_i+\eta_j)}}\right),\end{aligned} \tag{4}$$

where the parameter is defined as $q = e^{g_s}$ and $C_2(\lambda) = \sum_{i=1}^{\infty}\left(\left(\lambda_i - i + \frac{1}{2}\right)^2 - \left(-i+\frac{1}{2}\right)^2\right)$ is the second Casimir operator, corresponding to the framing factor. This shows that the U($N|N$) character average is factorized into that for U(1|1) theory. This kind of property is called Giambelli compatibility.[2]

In order to see the connection to the ordinary knot invariant in U(N) from the determinantal expression (4), it is convenient to rewrite as follows,

$$\begin{aligned}&k^{-N} q^{\frac{1}{2}(C_2(\mu)-C_2(\nu))} \prod_{i,j=1}^{N}\left(q^{\frac{1}{2}(\xi_i+\eta_j)}+q^{-\frac{1}{2}(\xi_i+\eta_j)}\right)^{-1} \\ &\times \prod_{i<j}^{N}\left(q^{\frac{1}{2}(\xi_i-\xi_j)}-q^{-\frac{1}{2}(\xi_i-\xi_j)}\right)\left(q^{\frac{1}{2}(\eta_i-\eta_j)}-q^{-\frac{1}{2}(\eta_i-\eta_j)}\right).\end{aligned} \tag{5}$$

The last two factors coincide with the Wilson loop average in U(N) theory, which is given by the quantum dimension of the representation R, up to the normalization constant.

The integral formula shown above can be generalized to the situation for the torus knot, which is labeled by two coprime integers (P,Q). In this case the partition function is slightly modified

$$\begin{aligned}\mathcal{Z}_{(P,Q)} &= \frac{1}{N!^2}\int [dx]^N [dy]^N \\ &\times \det_{1\le i,j\le N}\left(\frac{1}{2\cosh\frac{x_i-y_j}{2P}}\right)\det_{1\le i,j\le N}\left(\frac{1}{2\cosh\frac{x_i-y_j}{2Q}}\right).\end{aligned} \tag{6}$$

We can show this torus knot partition function is just given by the symplectic transform of the original unknot partition function. Thus it can be shown that they are related in a simple way, $\mathcal{Z}_{(P,Q)} = (PQ)^N \mathcal{Z}_{(1,1)}$. Since there exists the U($N|N$) character, written in terms of the Schur function, $s_\lambda(u^Q;v^Q) = \sum_\mu c^\mu_{\lambda,Q} s_\mu(u;v)$, as well as the ordinary U(N) theory, finally the torus knot Wilson loop average can be expressed as a linear combination of that for the fractionally framed unknot,

$$\Big\langle W_R(K_{P,Q})\Big\rangle = \sum_V c^V_{R,Q}\Big\langle W_R(K_{1,f})\Big\rangle \tag{7}$$

with the framing number $f = Q/P$. This is just a supersymmetric version of the Rosso–Jones formula for the torus knot invariant.[3]

*1 Institut de Physique Théorique, CEA Saclay
*2 CRM, Université de Montréal
*3 RIKEN Nishina Center

References
1) A. Kapustin et al, JHEP **1003** (2010) 089.
2) A. Borodin et al, Adv. Appl. Math. **37** (2006) 209.
3) M. Rosso, V. Jones, J. Knot Th. Ram. **2** (1993) 97.

Duality and integrability of supermatrix model with external source†

T. Kimura*1,*2

In quantum field theory, in order to compute correlation functions, it is convenient to introduce the generating function by adding an extra source term. Such a generating function is defined in the sense of path integral, and thus it is quite difficult to compute in general. However, in the matrix model, just a zero dimensional theory, a number of methods for computation are established, which are also applicable to the model with the external source. In this report we generalize the duality of the matrix model with the external source with a characteristic polynomial, which was originally found in the Gaussian matrix model,[1] to the supermatrix model with an arbitrary matrix potential.

The correlation function of the characteristic polynomial in the supermatrix model, which we study here, is given by

$$\Psi_{N,M;p,q}\left(\{a_i\}_{i=1}^N,\{b_j\}_{j=1}^M;\{\lambda_\alpha\}_{\alpha=1}^p,\{\mu_\beta\}_{\beta=1}^q\right) = \int dZ\, e^{-\frac{1}{\hbar}\operatorname{Str} W(Z)+\operatorname{Str} ZC}\frac{\prod_{\alpha=1}^p \operatorname{Sdet}(\lambda_\alpha - Z)}{\prod_{\beta=1}^q \operatorname{Sdet}(\mu_\beta - Z)} \quad (1)$$

where Z is a size $N+M$ Hermitian supermatrix, and the external source is $C=\operatorname{diag}(a_1,\dots,a_N,b_1,\dots,b_M)$. This formula includes several useful situations, e.g., the ordinary characteristic polynomial average ($M=q=0$), the average of inverses ($M=p=0$), and the ratio average ($M=0$). Therefore it provides a master formula for the characteristic polynomial average in various matrix models.

The matrix measure in the integral is invariant under the supergroup transformation, $dZ=d(UZU^{-1})$ with $U\in \mathrm{U}(N|M)$, which is expressed in terms of eigenvalues, $dZ=\Delta_{N,M}(x;y)^2\,d^Nx\,d^My\,dU$. Here the Jacobian is given by the Cauchy determinant,

$$\Delta_{N,M}(x;y)=\frac{\prod_{i<j}^N(x_i-x_j)\prod_{i<j}^M(y_i-y_j)}{\prod_{i,j}^{N,M}(x_i-y_j)}. \quad (2)$$

Then, to compute the intgral, we now introduce the Harish-Chandra–Itzykson–Zuber formula for the supergroup $\mathrm{U}(N|M)$[2–4]

$$\int_{\mathrm{U}(N|M)} dU\, e^{\operatorname{Str} ZUCU^{-1}} = \frac{\det e^{x_ia_i}\,\det e^{-y_ib_j}}{\Delta_{N,M}(x;y)\Delta_{N,M}(a;b)}. \quad (3)$$

Applying this formula, we obtain the following expression for the matrix integral in terms of eigenvalues

$$\Psi_{N,M;p,q}=\int\prod_{i,j}^{N,M}dx_i\,dy_j\,e^{-\frac{1}{\hbar}W(x_i)+\frac{1}{\hbar}W(y_j)+x_ia_i-y_jb_j} \times\frac{\Delta_{N+p,M+q}(x,\lambda;y,\mu)}{\Delta_{N,M}(a;b)\Delta_{p,q}(\lambda;\mu)}. \quad (4)$$

Since the Cauchy determinant can be written as a determinant

$$\Delta_{N,M}(x;y)=\det\begin{pmatrix} x_i^{k-1}\\ (x_i-y_j)^{-1}\end{pmatrix} \quad (5)$$

with $i=1,\dots,N$, $j=1,\dots,M$, $k=1,\dots,N-M$, if $N\geq M$, we obtain the determinanal formula for the characteristic polynomial average

$$\Psi_{N,M;p,q}\left(\{a_i\}_{i=1}^N,\{b_j\}_{j=1}^M;\{\lambda_\alpha\}_{\alpha=1}^p,\{\mu_\beta\}_{\beta=1}^q\right) = \frac{1}{\Delta_{N,M}(a;b)\Delta_{p,q}(\lambda;\mu)}\det\begin{pmatrix} Q_{k-1}(a_i) & P_{k-1}(\lambda_\alpha)\\ R(a_i;b_j) & S_{\mathrm{R}}(\lambda_\alpha;b_j)\\ S_{\mathrm{L}}(a_i;\mu_\beta) & \tilde R_{\lambda_\alpha;\mu_\beta}\end{pmatrix}, \quad (6)$$

where we have introduced auxiliary functions:

$$P_{i-1}(x)=x^{i-1},\quad \tilde R(x;y)=\frac{1}{x-y}, \quad (7)$$

$$Q_{i-1}(a)=\int dx\,P_{i-1}(x)\,e^{-\frac{1}{\hbar}W(x)+xa}, \quad (8)$$

$$R(a;b)=\int dxdy\,\tilde R(x;y)\,e^{-\frac{1}{\hbar}(W(x)-W(y))+xa-yb}, \quad (9)$$

$$S_{\mathrm{L}}(a;\mu)=\int dx\frac{1}{x-\mu}e^{-\frac{1}{\hbar}W(x)+xa}, \quad (10)$$

$$S_{\mathrm{L}}(\lambda;b)=\int dy\frac{1}{\lambda-y}e^{\frac{1}{\hbar}W(y)-yb}. \quad (11)$$

The formula (6) actually shows a duality between the external source and the characteristic polynomial, which is just given by Laplace (Fourier) transforms,

$$\Psi_{N,M;p,q}\left(\{a_i\}_{i=1}^N,\{b_j\}_{j=1}^M;\{\lambda_\alpha\}_{\alpha=1}^p,\{\mu_\beta\}_{\beta=1}^q\right) \overset{\text{F.T.}}{=} \Psi_{p,q;N,M}\left(\{\lambda_\alpha\}_{\alpha=1}^p,\{\mu_\beta\}_{\beta=1}^q;\{a_i\}_{i=1}^N,\{b_j\}_{j=1}^M\right). \quad (12)$$

This is because the auxiliary functions transform to each other through the Fourier transformation: $P_{i-1}(x)\leftrightarrow Q_{i-1}(a)$, $R(x;y)\leftrightarrow\tilde R(a;b)$, $S_{\mathrm{L}}(\lambda;b)\leftrightarrow S_{\mathrm{R}}(a;\mu)$.

† Condensed from the article in PTEP **2014** 123A01 (2014)
*1 RIKEN Nishina Center
*2 Institut de Physique Théorique, CEA Saclay

References
1) E. Brézin, S. Hikami, Comm. Math. Phys. **214** (2000) 11.
2) T. Guhr, J. Math. Phys. **32** (1991) 32.
3) J. Alfaro et al., J. Math. Phys. **36** (1995) 3085.
4) T. Guhr, Comm. Math. Phys. **176** (1996) 555.

Bulk angular momentum and Hall viscosity in chiral superconductors†

A. Shitade*1 and T. Kimura*2,*3

Chiral superfluids and superconductors (SCs) are exotic states whose time-reversal symmetry is spontaneously broken and Cooper pairs carry nonzero angular momentum (AM). There is a long-standing problem on the AM in chiral ℓ-wave SCs, the so-called intrinsic AM paradox, which is summarized as $L_z = \hbar m N_0/2 \times (\Delta_0/E_\mathrm{F})^\gamma$, where $|m| \leq \ell$, N_0, Δ_0, E_F, γ are the magnetic quantum number, the total number of electrons, the gap strength, the Fermi energy, and the exponent characterizing the dependence on the SC gap. $\gamma = 0$ is the most natural if all electrons from Cooper pairs with the AM $\ell_z = \hbar m$. On the other hand, $\gamma = 1$ is intuitively plausible if a electrons near the Fermi surface from Cooper pairs.[1] One of the obstacle is that the physical quantities involving the position operator are ill defined in periodic systems, and we have to manage an inevitable divergence in the bulk limit. An interesting clue to the AM is the Hall viscosity (HV), which has been intensively discussed in the context of the quantum Hall effect. The important relation $\eta_\mathrm{H} = \hbar N_0 \bar{s}/2$ holds in general gapped systems at zero temperature,[2] in which the orbital spin $\bar{s}$ is equal to $\frac{\ell}{2}$ in chiral ℓ-wave SCs. In this report, we derive the Berry-phase formulas for the AM and the Hall viscosity (HV) to apply to chiral SCs in two and three dimensions, which allow us to deal with the bulk systems.

We examine an angular velocity from the gauge-theoretical viewpoint. Now that the system is rotated, we have to deal with a theory in a curved spacetime. We use the Cartan formalism, consisting of two gauge potentials, a vielbein and a spin connection. Since we are now interested in the orbital AM, we do not consider the spin connection corresponding to the internal AM for simplicity. A vielbein ${h^a}_\mu$ is a gauge potential corresponding to local spacetime translations, while a spin connection is that corresponding to local Lorentz transformations. The spatial component of a vielbein is related to a displacement vector. Since a vielbein is a gauge potential, it induces a field strength called torsion,

$$ {T^l}_{j0} = \partial_j {h^l}_0 - \partial_0 {h^l}_j \,, \quad {T^l}_{ij} = \partial_i {h^l}_j - \partial_j {h^l}_i \,. \tag{1} $$

The former is "electric." The first term describes an angular velocity if l and j are antisymmetric, while the second term describes a strain-rate tensor if symmetric. On the other hand, the latter is "magnetic" characterizing edge and screw dislocations in crystals.

Based on this formalism, we derive the momentum polarization, at zero temperature in a gapped fermion system,

$$ {P_k}^i = \sum_n^{\mathrm{occ}} \int \frac{d^d\pi}{(2\pi\hbar)^d} \pi_k A^i_{n\vec{\pi}} \,, \tag{2} $$

where $\vec{\pi}$ is the momentum, the summation is taken over the occupied states, the Berry connection is given by $A^i_{n\vec{\pi}} = i\hbar \langle u_{n\vec{\pi}} | \partial_{\pi_i} u_{n\vec{\pi}} \rangle$, and $u_{n\vec{\pi}}$ is the Bloch eigenstate. Then the AM is obtained by the antisymmetric part of the momentum polarization,

$$ L_k = \epsilon_{ijk} P^{ji} = \sum_n^{\mathrm{occ}} \int \frac{d^d\pi}{(2\pi\hbar)^d} \epsilon_{ijk} A^i_{n\vec{\pi}} \pi^j \,. \tag{3} $$

Since the Berry connection is regarded as the expectation value of the position operator in the Wannier basis, this Berry-phase formula really indicates $\vec{\ell} = \vec{x} \times \vec{p}$ in the momentum space.

Here we define the nonsymmetric viscosity by ${\eta_k}^i{}_l{}^j = \partial {T_k}^i / \partial \left(-T^l_{j0}\right)$. As well as the AM formula, we obtain

$$ {\eta_k}^i{}_l{}^j = \frac{1}{\hbar} \epsilon^{ijm} \sum_n^{\mathrm{occ}} \int \frac{d^d\pi}{(2\pi\hbar)^d} \pi_k \pi_l \Omega_{n\vec{\pi}_m} f_{n\vec{\pi}} \,, \tag{4} $$

where $f_{n\vec{\pi}} = f(\epsilon_{n\vec{\pi}} - \mu)$ is the Fermi distribution function and the Berry curvature is defined by $\Omega_{n\vec{\pi}k} = i\hbar^2 \epsilon_{ijk} \left\langle \partial_{\pi_i} u_{n\vec{\pi}} | \partial_{\pi_j} u_{n\vec{\pi}} \right\rangle$. The proper HV is obtained as its symmetric part. Especially in two dimensions, the antisymmetric part yields

$$ \eta_\mathrm{H} = \frac{1}{4\hbar} \sum_n \int \frac{d^2\pi}{(2\pi\hbar)^2} \vec{\pi}^2 \Omega_{n\vec{\pi}z} f_{n\vec{\pi}} \,. \tag{5} $$

These expressions are quite analogous to that for the Hall conductivity, corresponding to the charge transport. The integrand just differs in the factor of $\vec{\pi}$.

By applying these formulas to the Bogoliubov–de Gennes system, we obtain the AM for gapped chiral SCs at zero temperature

$$ L_z = -\hbar \sum_{\vec{k}} (\vec{A}_{\vec{k}} \times \vec{k})_z = \hbar m N_0/2 \,, \tag{6} $$

which is consistent with $\gamma = 0$, and shows the relation to the HV, $L_z = 2\eta_\mathrm{H}$. See, for example, for the recent microscopic studies suggesting $\gamma = 0$.[3]

† Condensed from the article in Phys. Rev. **B90** 134510 (2014)
*1 Department of Physics, Kyoto University
*2 Institut de Physique Théorique, CEA Saclay
*3 RIKEN Nishina Center

References
1) A. J. Leggett, Rev. Mod. Phys. **47** (1975) 331.
2) N. Read, Phys. Rev. **B79** (2009) 045308.
3) Y. Tsutsumi, K. Machida, Phys. Rev. **B85** (2012) 100506.

7. Astrophysics and Astro-Glaciology

Insights from Antarctica on volcanic forcing during the Common Era†

M. Sigl,[*1] J. R. McConnell,[*1,*2] M. Toohey,[*3] M. Curran,[*4] S. B. Das,[*5] R. Edwards,[*6] E. Isaksson,[*7] K. Kawamura,[*2,*8] S. Kipfstuhl,[*9] K. Krüger,[*3,*10] L. Layman,[*1] O. J. Maselli,[*1] Y. Motizuki,[*11] H. Motoyama,[*2] D. R. Pasteris,[*1] and M. Severi[*12]

Assessments of climate sensitivity to projected greenhouse gas concentrations underpin environmental policy decisions, with such assessments often based on model simulations of climate during recent centuries and millennia[1)-3)]. These simulations depend critically on accurate records of past aerosol forcing from global-scale volcanic eruptions, reconstructed from measurements of sulphate deposition in ice cores[4)-6)]. Non-uniform transport and deposition of volcanic fallout mean that multiple records from a wide array of ice cores must be combined to create accurate reconstructions. Here we re-evaluated the record of volcanic sulphate deposition using a much more extensive array of Antarctic ice cores. In our new reconstruction, many additional records have been added and dating of previously published records corrected through precise synchronization to the annually dated West Antarctic Ice Sheet Divide ice core[7)], improving and extending the record throughout the Common Era. Whereas agreement with existing reconstructions is excellent after 1500, we found a substantially different history of volcanic aerosol deposition before 1500; for example, global aerosol forcing values from some of the largest eruptions (for example, 1257 and 1458) previously were overestimated by 20–30% and others underestimated by 20–50%.

References

1) G. A. Schmidt et al.: J. Quat. Sci. 25, 7 9 (2010)..
2) G. C. Hegerl, et al.: Nature 440, 1029 (2006).
3) IPCC Summary for Policymakers in Climate Change 2007: The Physical Science Basis (eds Solomon, S. et al.) (Cambridge Univ. Press, 2007).
4) G. A. Schmidt, et al.: Geoscientific Model Dev. 5, 185 (2012).
5) T. J. Crowley, & M. B. Unterman: Earth Syst. Sci. Data 5, 187 (2013).
6) C. C.Gao et al.: J. Geophys. Res. 113, D23111 (2008).
7) M. Sigl, et al.: J. Geophys. Res. 118, 1151 (2013).

† Condensed from the article in Nature Climate Change 4, 693–697 (2014)

*1 Desert Research Institute
*2 National Institute of Polar Research
*3 GEOMAR Helmholtz Centre for Ocean Research Kiel
*4 Australian Antarctic Division and Antarctic Climate and Ecosystems
*5 Woods Hole Oceanographic Institution
*6 Department of Imaging and Applied Physics, Curtin University
*7 Norwegian Polar Institute
*8 Department of Biogeochemistry, JAMSTEC
*9 Alfred Wegener Institute, Helmholtz Centre for Polar and Marine Research
*10 University of Oslo
*11 RIKEN Nishina Center
*12 Department of Chemistry 'Ugo Schi', University of Florence

Variation in chemical composition induced by solar energetic particle events in the middle atmosphere

Y. Nakai,[*1] Y. Motizuki,[*1] M. Maruyama,[*1] H. Akiyoshi,[*1,*2] and T. Imamura[*2]

Recently, the influences of super solar flares on the earth environment have been extensively investigated. One of the areas of focus in such investigations is the change of chemical composition in the terrestrial atmosphere induced by energetic particles generated in the super solar flares. The bombardment of solar energetic particles (SEPs) to the atmosphere is called an SEP event, where a large amount of X-rays, gamma-rays, protons, and heavier ions from the surface of the sun intrude the terrestrial atmosphere. In particular, high-energy protons come down into the stratosphere and induce dissociation of nitrogen molecules followed by an increase of odd nitrogen oxides (NOx) and reactive odd nitrogen species (NOy). Consequently, the increase of NOx and NOy affects the ozone concentration over a period longer than SEP events.

We have performed simulations to investigate variation in chemical composition in SEP events by solving a large number of rate equations for the concentrations of chemical species in air.[1)] We adopt 77 chemical species including ions and about 480 chemical reactions (ionic reaction processes, neutral reactions, photolysis, etc.) in the present simulation. A large number of ionic processes, including recombination in the stratosphere, were treated for the first time, to the best of our knowledge. No transport processes are taken into account. This model is referred to as the Box-model hereafter. We carried out calculations using commercial software for solving complex chemical reaction systems (FACSIMILE, MCPA Software Ltd).

In order to estimate the yields of prompt products by the SEP protons, we used the G-values (amount of products per absorbed energy of 100 eV) investigated by radiolysis studies[2,3)], based on the assumption that the prompt product yields are determined only by the energy deposit of the SEP protons in air. The prompt products are assumed to be charged products (positive atomic ions, positive molecular ions, and electrons) and neutral products (ground-state and the metastable atoms) generated from nitrogen and oxygen molecules in air. The energy deposit was estimated using the calculations of ion-pair creation by the SEP protons[4)]. During an SEP event, both the photochemical reactions induced by the UV and visible radiation from the sun and the reactions induced by the SEP protons are considered in the simulation. The variation in chemical composition in an SEP event is estimated as the difference between the result obtained through simulation including the radiolysis processes due to the SEP protons and that obtained under consideration of only photochemical reactions using the same initial condition.

*1 RIKEN Nishina Center
*2 National Institute for Environmental Studies

Figure 1 shows a tentative result of the variation in the ozone concentration at the 50 km altitude in the northern polar region for the SEP event in October-November 2003. The energy deposit in the SEP event continued for six days. A sharp decrease of the ozone concentration is observed immediately after the SEP event starts. On the third day of the event, when the energy deposit also reaches the maximum, the decrease of the concentration reaches the maximum and increases back gradually after that. The ozone concentration does not completely recover and remains depleted for a few weeks or more. This depletion of the ozone presumably corresponds to a very slow recovery of the NOx concentrations. The NOx concentration begins to increase when an SEP event starts. It continues to increase for four days and is almost maintained constant after the SEP event. The depletion of ozone is thought to continue after the SEP event since the ozone is consumed in the catalytic reaction cycle involving NOx, e.g., $NO+O_3 \rightarrow NO_2+O_2$.

In the near future, we will investigate the global and long-term influence of SEP events on the atmospheric chemical composition. In our approach, we will estimate short-term variations during an SEP event using our Box-model, and the estimated variations will then be input into a three-dimensional (3D) chemical climate model (CCM)[5)] as instantaneous perturbation of the chemical composition. This is because the transport of chemical species treated in 3D is essential for investigating the global and long-term influence.

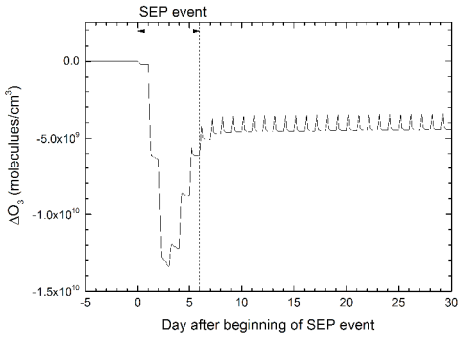

Figure 1. Tentative result for the variation in the ozone concentration at the 50km altitude caused by SEP (see text).

References

1) For the early-stage model: K. Sekiguchi *et al*., RIKEN Accel. Prog. Rep. **46**, 124 (2013).
2) C. Willis and A. W. Boyd, Int. J. Radiat. Phys. Chem. 8, 71 (1976).
3) H. Mätzing, Adv. Chem. Phys. LXXX, 315 (1991).
4) C.H. Jackman *et al.*, Atmos. Chem. Phys. **8**, 765 (2008).
5) H. Akiyoshi *et al*., J. Geophys. Res. 114, D3, 16 (2009).

Measurements of nitrogen isotope ratios in samples with very low nitrate concentrations from the Dome Fuji ice core (Antarctica) drilled in 2010

Y. Motizuki,[*1] S. Okamoto,[*1, *2] K. Takahashi,[*1] Y. Nakai,[*1] A. Makabe,[*3, *4] K. Koba,[*3] and H. Motoyama[*5]

Nitrate (NO_3^-) in ice core samples is known to provide a variety of information on past and present atmospheric conditions. For instance, NO_3^- data for samples from the Talos Dome ice core (Antarctica) exhibited a highly significant relationship with cosmic ray fluxes.[1] In addition, several research groups[2),3)] have measured the $\delta^{15}N$ of NO_3^- in surface snow in Antarctica to quantify the extent of isotopic fractionation due to photolytic processes after precipitation. However, there is little information available about the depth profiles of the $\delta^{15}N$ of NO_3^- in ice core samples from Antarctica.

Our goal was to precisely analyze the $\delta^{15}N$ and $\delta^{18}O$ of NO_3^- in ice cores to clarify the history of solar activity and cosmic events. However, it is difficult to measure the $\delta^{15}N$ and $\delta^{18}O$ of NO_3^- in Antarctic ice cores because the NO_3^- concentrations are low (typically <0.4 μmol/L), and the available sample volume is limited. In this study, as a feasibility study, we used a denitrifier method[4] to perform highly sensitive measurements of the $\delta^{15}N$ of NO_3^- in samples from the DFS10 ice core, which was drilled in 2010, 7 km south of Dome Fuji Station (DFS), to obtain a profile of the $\delta^{15}N$ of NO_3^-. The NO_3^- concentration in the core was approximately 0.35 μmol/L. In what follows, we will introduce the outline of the results for 70 samples collected from the ice core of depths of Dome Fuji at 3.3–7.6 m. The sampling procedure was the same as that described by Motizuki *et al.* (2014)[5] for the ice core drilled at Dome Fuji in 2001. We assume that these samples correspond to approximately the time interval from AD 1900 to 1960. Each sample segment cut from the ice core corresponds to a time interval of approximately 0.7–1.0 year. A 10 mL aliquot of each sample was used; NO_3^- in the sample water was quantitatively converted to N_2O by the denitrifying bacteria, *Pseudomonas aureofaciens*, which lack N_2O reductase. The isotopic composition of the N_2O gas produced by the bacteria was measured using a mass spectrometer (IsoPrime100) with a purge-and-trap introduction system. The isotope ratios were referenced to the internationally recognized standards USGS32, USGS34, and USGS35 provided by IAEA (International Atomic Energy Agency). Nitrate concentrations were analyzed by ion chromatography (ICS2000) with error limits of 2 or 3%. The amount of nitrogen used for the analysis ranged from 2.1 to 4.8 nmol. $\delta^{15}N$ ranged from 144.8 to 332.0‰ and the maximum error was ± 2.5‰. The high, positive $\delta^{15}N$ values obtained in the study were therefore attributed to a post-depositional effect on NO_3^-. Figure 1 shows the depth profiles of NO_3^- concentrations and $\delta^{15}N$ values. Despite the lack of any correlation between NO_3^- concentrations and $\delta^{15}N$ values, their depth profiles appear to be related for several depth intervals. For example, both profiles are convex in the depth intervals 3.3–4.0 and 5.5–6.0 m. It has been reported that NO_3^- concentration decreases as $\delta^{15}N$ values increases near the surface of snow because of photolysis in the surface snow (vide supra).[2] There was no negative correlation between NO_3^- concentration and $\delta^{15}N$ values for our ice core samples, which indicates that the variations of $\delta^{15}N$ and NO_3^- concentration in ice core samples below 3 m do not reflect post-depositional fractionation of nitrogen isotopes. Instead, the depth profiles of $\delta^{15}N$ and NO_3^- concentration likely preserve the corresponding variations in the original precipitation.

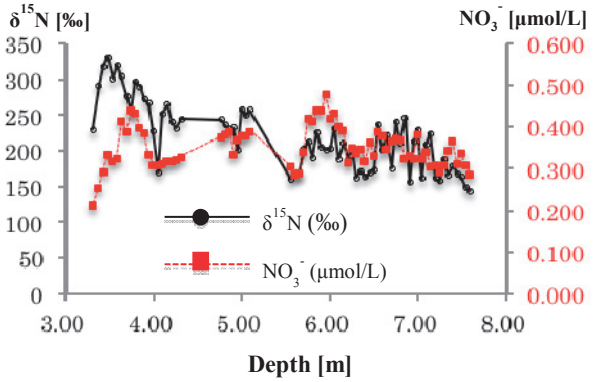

Fig. 1 The depth profiles of $\delta^{15}N$ and NO_3^- concentration.

We intend to continue the measurements of nitrogen and oxygen isotopes in NO_3^- for samples collected from deeper in the ice core. We expect that the depth profiles of nitrogen and oxygen isotopes will reflect the variations in the chemical and physical characteristics of past precipitation, indicate the origin of the NO_3^- production in the stratosphere, and provide important information that will help elucidate the history of solar activity and cosmic events.

*1 RIKEN Nishina Center
*2 National Institute for Environmental Studies
*3 Tokyo University of Agriculture and Technology
*4 JAMSTEC
*5 National Institute of Polar Research

References

1) R. Traversi et al.: Solar Phys. **208**, 237 (2012).
2) T. Blunier et al.: Geophys. Res. Lett. **32**, L13501 (2005).
3) M. Frey et al.:Atmos. Chem. Phys. **9**, 8681 (2009).
4) M. MacIlvin and L. Casciotti: Anal. Chem. **83**, 4905 (2011).
5) Y. Motizuki et al.: Cryosphere Discuss. **8**, 769 (2014).

X-ray and Optical/UV Correlation Studies of Active Galactic Nuclei

H. Noda,[*1] and T. Minezaki,[*2] on behalf of the AGN Optical–X-ray Monitoring Collaboration

Almost all galaxies in the universe are considered to harbor, at their center, a supermassive Black Hole (BH) with a mass of $\sim 10^{5-10}$ $M_\odot$, where $M_\odot$ is Solar mass. In Active Galactic Nuclei (AGNs), a considerable amount gas accretes onto the BH, and multi wavelength signals, including optical, UV, and X-ray, are generated with bolometric luminosity of $\sim 10^{40-46}$ erg s^{-1}. The X-ray is presumably generated, via inverse comptonization in high-temperature electron clouds (coronae) formed near the BH, while the optical/UV emissions via black body processes of an optically thick and geometrically thin accretion disk extending out to farther radii from the BH. Although a combination of the accretion disk and coronae has been known as "the central engine" creating a large amount of energy in AGNs, its properties including geometries, physical conditions, and heating mechanisms are still unclear.

Applying a timing method[1] to *Suzaku*[2] data of an AGN called NGC 3227, we found that a Hard Primary Component (HPC) dominated X-ray emission in the faint phase, while a Broad-band Primary Component (BPC) appeared in addition to the HPC in the bright phase (Fig. 1a). This demonstrates that at least two X-ray emitting regions with distinct properties exist near a BH, and one emitting the HPC is always visible, while the other radiating the BPC shows up only when the amount of accreting gas is large[3]. However, the geometries of the HPC and BPC creating regions can be hardly identified with only the X-ray information.

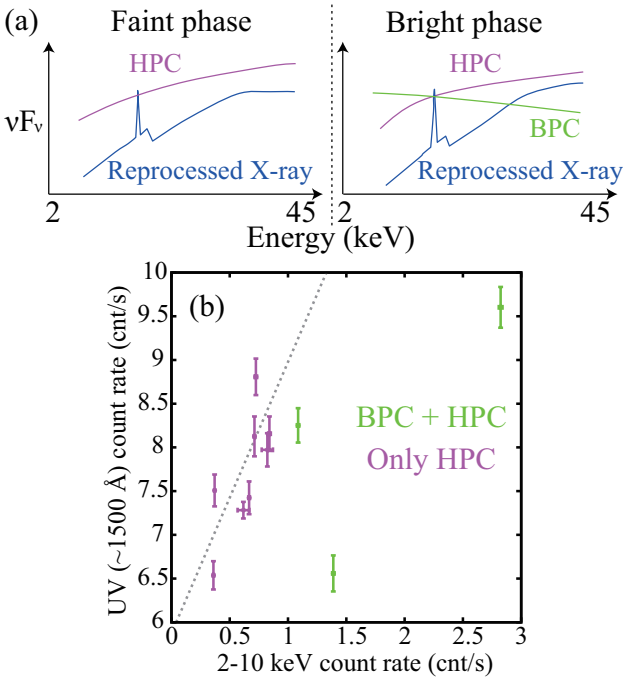

Fig. 1. (a) Spectral components of NGC 3227 in the faint (left) and bright (right) phase[3]. (b) A plot between fluxes in the 2–10 keV and UV bands. Systematic errors of the *Swift* detectors were not included in the errors.

*1 RIKEN Nishina Center
*2 Institute of Astronomy, School of Science, The University of Tokyo

To study the geometries, we focus on correlations between the fluxes of primary X-ray and optical/UV, because a better correlation possibly reflects a stronger geometrical connection of an X-ray radiating region with the accretion disk. In 2013–2014, we performed optical and X-ray simultaneous monitoring on an AGN called NGC 3516 with *Suzaku* and five Japanese ground-based telescopes. As a result, a significant correlation was discovered between fluxes of HPC and the optical signals. The result will be discussed elsewhere.

Optical–UV data derived by *Swift*[4] are useful as well. Almost all *Suzaku* observations of NGC 3227[3] were simultaneously followed up by *Swift*; therefore X-ray flux in the faint and bright phase, identified by *Suzaku* (Fig. 1a), can be individually compared with those in optical/UV. First, we extracted UV count rates from a 5"-radius circle centering at the nucleus on UV images obtained with the UVW2 filter. Next, we extracted 2–10 keV count rates from the *Suzaku* and *Swift* datasets derived at the same time as the UV images. Figure 1(b) shows a count-count plot between the UV and X-ray count rates with different colors between the faint (purple) and bright (green) phases. When we fitted the faint-phase plots (Fig. 1b purple) with a linear function, including systematic errors of 3% into the UV count rates, the fit almost succeeded with $\chi^2/\nu = 13.4/6$. However, in fitting all the plots (Fig. 1b purple plus green) again with a linear function, after including the 3% systematic errors into the UV count rates, the result degraded giving $\chi^2/\nu = 61.5/9$. This might indicate that the HPC flux is strongly correlated with UV, while the BPC flux is little correlated.

Because the HPC was found to deeply relate with black body photons from the accretion disk, it may come from an hot accretion flow, and if so, the faint phase corresponds to the low/hard state[5]. On the other hand, the origin of the BPC still remains unclear, because it did not appear for long enough in the previous observations of NGC 3516 and NGC 3227. To examine the bright phase in detail, we perform another X-ray and optical monitoring with *Suzaku*, and the systematic analyses of AGN data in the *Swift* archive.

References

1) H. Noda et al.: ApJ, 771, 100 (2013)
2) K. Mitsuda et al.: PASJ, 59, 1 (2007)
3) H. Noda et al.: ApJ, 794, 2 (2014)
4) N. Gehrels et al.: ApJ, 611, 1005 (2004)
5) F. Yuan & R. Narayan: ARAA, **52**, 529 (2014)

Time-variable Fe K emission lines from accreting white dwarf binaries

T. Yuasa*1

Accretion of gas from a normal star in a binary system onto a compact star liberates a vast amount of gravitational potential energy. This often results in heating of the gas and high-energy electromagnetic radiation. By observing the emission, properties of the compact star can be studied because the emission occurs from regions close to the star.

We have been studying the mass-accreting white dwarf system that is considered to be an important candidate of type Ia supernovae. In particular, our focus has been on measuring the mass of a white dwarf in a binary system by modeling of X-ray spectra of heated gas. For details of the modeling and initial results, see our previous publication (Yuasa et al. 2010).

To further improve the accuracy of the mass measurement, it is crucial to understand the geometry and profiles of density, temperature, and bulk velocity of the X-ray emitting plasma. In April 2014, we were awarded a 180k-second observation of the magnetic accreting white dwarf V1223 Sgr by using the Japanese Suzaku X-ray telescope. The aim of the observation is to assess the geometry assumed in the model calculation based on precise measurement of time variation of Doppler energy shifts and intensities of the Fe atomic lines after the previous marginal report (Hayashi et al. 2011).

After the standard data selection, we obtained high-photon-statistics spectrum as presented in Fig. 1. To disentangle Doppler energy shifts of lines caused by in-falling bulk velocity of the X-ray emitting gas and other effects such as white dwarf spin and subsequent line-of-sight viewing angle variation, we performed phase resolved spectral fitting by splitting the total observation time into four phase bins with a period of 754 s (corresponding to the spin period of the white dwarf in V1223 Sgr). No statistically significant time variation was observed for the centroid energies of the lines, in contrast to the previous report (Hayashi et al. 2011), due to long-term degradation of the energy resolution of the instrument. On the other hand, as shown in Fig. 2, the line intensities varied over spin phases although statistical fitting errors are still large due to phase resolving (resulting shorter integration time per phase bin).

These time variations can be interpreted to be caused by the resonance-trapping beaming effect (Terada et al. 2001) where the optical thickness of the X-ray emitting hot plasma becomes greater than unity only for resonance line photons and trapped within the plasma while continuum photons exit the plasma region almost freely (i.e. the plasma is optically thin for continuum photons). In this scheme, the optical thickness is sensitive to the plasma density, the geometrical shape, and the white dwarf mass. Therefore, we are continuing to perform detailed analyses and comparison with Monte Carlo radiation transfer simulation results to utilize this resonance-beaming feature as an alternative constraint for measuring the white dwarf mass and related physical quantities of the binary system such as the mass accretion rate.

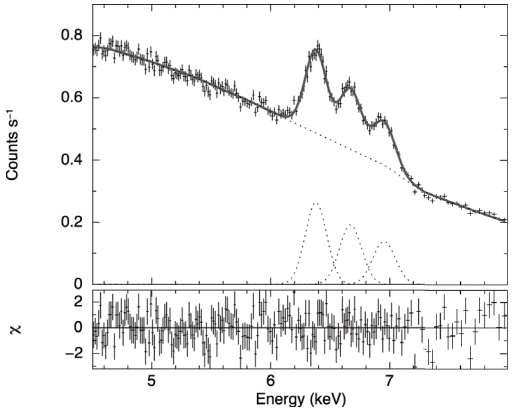

Fig. 1. Time-average X-ray CCD spectrum of V1223 Sgr. Thermal bremsstrahlung continuum and three atomic emission lines from neutral Fe (6.4 keV) and highly ionized Fe ions (6.7 and 6.9 keV).

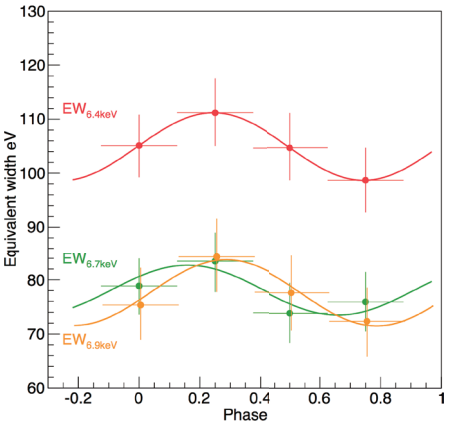

Fig. 2. Crosses are intensities of the three Fe emission lines over white dwarf spin phases (ordinate presents the equivalent width, which is a measure of the line intensity). Solid curves are the best-fit sinusoidal functions.

References

1) Yuasa T., et al. 2010, A&A, 520, A25
2) Hayashi T., et al. 2011, PASJ, 63, 739
3) Terada Y., et al. 2001, MNRAS, 328, 112

*1 RIKEN Nishina Center

Spectral and Temporal Approach to Physics of Neutron Stars

T. Enoto,[*1,*2,*3] T. Tamagawa,[*1] T. Kitaguchi,[*1,*4] A. T. Hayato,[*1] T. Yuasa,[*1]
W. B. Iwakiri,[*1] H. Noda,[*1] A. Yoshikawa,[*1] Y. Takeuchi,[*1] M. Kubota,[*1] and K. Nishida[*1]

Astronomical observations of neutron stars provide us an unique approach to investigate the fundamental physics under extreme condition. Degenerate matter inside neutron stars exceeds the nuclear density, and the equation of state of high density matter is observationally constrained via measurements of stellar mass and radius. Neutron stars are also characterized by strong gravity (gravitational redshift $z \sim 0.2$), fast rotation (up to $P \sim 1$ ms), and strong magnetic field ($B \sim 10^8$ T). Recent progress of X-ray observations further indicates an strongly magnetized subclass of neutron stars, called magnetars[1]. There are accumulating evidence for 2–3 orders of magnitude higher magnetic field than that of canonical neutron stars, with peculiar flare and burst activities interpreted as dissipation of the magnetic energy[2]. Neutron stars are, thus, an ideal laboratory in our universe[3].

We are now about to enter the age of precise astrophysical measurement of neutron stars. The ASTRO-H X-ray observatory[4], expected to be launched in 2015, will realize a ultra-high spectral resolution of $\triangle E \sim 7$ eV in the ∼0.3–10 keV band (cf., ∼130 eV FHWM at 6 keV of the X-ray CCD onboard *Suzaku*). This will enable us to search for a proton cyclotron feature as direct evidence for the strong field and for a gravitationally-redshifted absorption feature to determine the equation of state of neutron stars. One year after the ASTRO-H, the Neutron star Interior Composition Explorer (NICER)[5] will be attached to the International Space Station (ISS). The NICER project will provide us unprecedented high-timing resolution data of neutron stars with very large photon statistics, and is expected to reveal the equation of state of neutron stars. In addition to these spectral and temporal improvements, polarization is expected to open a new observational window of the X-ray astronomy. The Gravity and Extreme Magnetism Small Explorer (GEMS)[6], the first polarization-dedicated X-ray satellite, was re-proposed in 2014 with a new name.

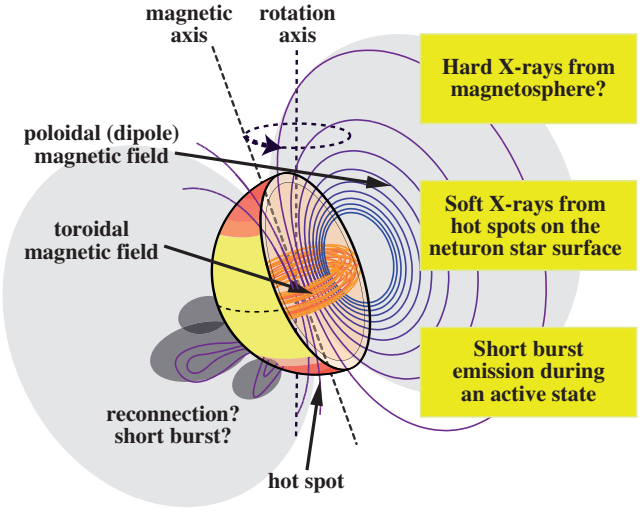

Fig. 1. Schematic view of a magnetar, a subclass of neutron stars with extremely strong magnetic field.

Prior to the ASTRO-H launch, we have started investigations of scientific topics and possible candidates of observations, and published it as the ASTRO-H White Paper[7]. Hard X-ray from magnetars is listed as one of the good candidates of ASTRO-H[8]. We are also preparing the handbook for the high spectral data handling, called the "Cookbook". As international cooperation for future missions, we have also collaborated with the NICER and X-ray polarimeter groups at NASA Goddard Space Flight Center, mainly contributing to calibration of the NICER X-ray mirror and developments of the X-ray polarimeter[9]. As our collaborative relationship grows, FUture Cooperation is a Key element for the Spectral and Temporal Approach to Physics for neutron stars.

In 2014, we reported a signature of the toroidal field embedded in the magnetar interior[10] from 4U 0142+61 (see Fig 1), and also studied how neutrino emission coupled with the toroidal field affects spin evolution of neutron stars[11]. We studied the magnetic field and accretion mechanism of the slowest rotating X-ray pulsar, 4U 1954+319[12], and iron line emission from the prototypical X-ray pulsar, Herculis X-1 (Her X-1)[13].

*1 RIKEN Nishina Center
*2 JSPS SPD Fellow
*3 NASA Goddard Space Flight Center
*4 Department of Physical Science, Hiroshima University

References
1) C. Thompson et al: MNRAS, **275**, 255 (1995)
2) T. Enoto et al.: PASJ, **62**, 475 (2010)
3) A. S. Burrows et al: PNAS, **111**, 2409 (2014)
4) T. Takahashi, K. Mitsuda, R. Kelley, et al: Proc. of the SPIE, **8443**, 84431Z (2012)
5) K. C. Gendreau, Z. Arzoumanian, & T. Okajima: Proc. of the SPIE, **8443**, 844313 (2012)
6) K. Jahoda: Proc. of the SPIE, **7732**, 77320W (2010)
7) S. Kitamoto, T. Enoto, S. Safi-Harb, et al: arXiv:1412.1165 (2014)
8) T. Enoto et al: ApJ, **722**, L162 (2010)
9) T. Enoto et al: Proc. of the SPIE, **9144**, 91444M (2014)
10) K. Makishima, T. Enoto, J. S. Hiraga, et al: Phys. Rev. Lett., **112**, 171102 (2014)
11) Y. Suwa, & T. Enoto: MNRAS, **443**, 3586 (2014)
12) T. Enoto et al: ApJ, **786**, 127 (2014)
13) F. Asami, T. Enoto, et al: PASJ, **66**, 44 (2014)

Timing analysis of solar flares in hard X-ray and soft γ-ray bands measured by the Suzaku Wide-band All-sky Monitor

W.B. Iwakiri,[*1] on behalf of Suzaku WAM team

Hard X-ray and γ-ray observations have proved to be a powerful tool to for studying the physics of particle acceleration and transfer in solar flares. These high-energy photons are often observed in X class flares defined by the GOES satellite. The origin of emission is thought to be the thick-target bremsstrahlung of high energy particles accelerated by magnetic reconnection. Previous observations have revealed that the arrival times of hard X-ray photons (20 - 200 keV) depend on their energy[1]. The energy-dependent time delays can be explained through the trap plus precipitation model[1]. First, the model suggests that electrons accelerated by magnetic reconnection are injected into a magnetic loop and trapped (magnetic mirror trap). Next, the trapped electrons escape the loop by pitch-angle scattering and precipitate to the chromosphere. As a result, hard X-ray photons are produced by thick-target bremsstrahlung. If Coulomb collisions represent the dominant pitch angle scattering for trapped electrons, the collisional deflection time τ can be represented as[2]

$$\tau(E) \propto E^{1.5}. \quad (1)$$

In this progress report, we performed a timing analysis of the Sept 24 2011 solar flare observed by the Wide-band All-sky Monitor (WAM)[3] onboard Japanese fifth X-ray satellite *Suzaku* from 80 keV to 7 MeV.

The WAM consists of four lateral walls composed of bismuth germanium oxide $Bi_4Ge_3O_{12}$ (BGO) crystals. The event data are recorded with a 1-s time resolution in the 55 energy band. The WAM has a large effective area that reaches 400 cm^2 at 1 MeV. This is the largest area in among currently working γ-ray spectrometers on-board astronomical satellites. Therefore, WAM is suitable for hard X-ray and soft γ-ray observation of solar flares[4]. Figure 1 shows the energy-resolved time profiles of the solar flare on Sept 24 2011 observed by WAM. The lightcurves show that the main peak has shifted progressively later at the higher energy band.

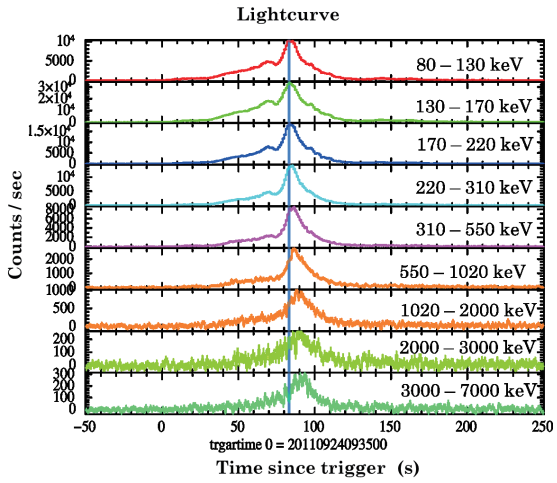

Fig. 1. Background-subtracted lightcurves of solar flare triggered on Sept 24 2011 09:35:00 UT observed by Suzaku-WAM in nine energy bands.

In order to evaluate the time lag quantitatively, we measured the delay using a cross correlation technique between the 80 - 130 keV lightcurve and the other eight energy-resolved lightcurves (130 - 7000 keV band). Before the analysis, we used a low-pass filter for each lightcurve by running an average of 10 bins (the time bin size is 1 s) to exclude the higher frequency component, because the observed fast structures are caused by the difference of electron time-of-flight from directly precipitating electrons[1]. The derived time delays as a function of energy are shown in Fig.2. The results show the energy dependence of the time delays are clearly changed around 1000 keV. In the lower energy band, the relation is roughly consistent with $E^{1.5}$, which is predicted by the pitch angle scattering of Coulomb collision[2]. On the other hand, above 1000 keV, the relation becomes more flat. If we fit the results using the broken power-law model and the power-law index of the lower energy is fixed at 1.5, the derived index of the higher energy band is 0.253±0.008 with a cutoff energy of 598±9 keV (the errors are 90% confidence). The estimation of systematic errors caused by a pile up effect is currently in progress.

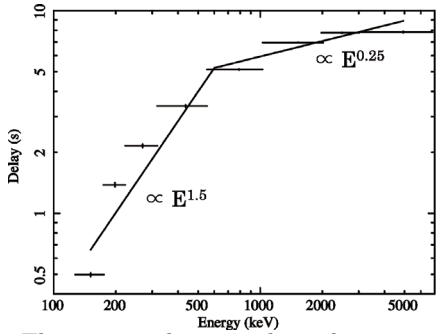

Fig. 2. The measured energy-dependent time delay of the Sept 24 2011 flare using the cross correlation method.

*1 RIKEN Nishina Center

References
1) M. J. Aschwanden et al: ApJ, 487, 936 (1997)
2) D. B. Melrose, & J. C. Brown: MNRAS, 176, 15 (1976)
3) K.Yamaoka et al: PASJ, 61, 35 (2009)
4) A.Endo et al: PASJ, 62, 1341 (2010)

Spurious shear from tree-rings on LSST CCD

Y. Okura,[*1,*2], A. Plazas,[*3,*4], M. May[*3] and T. Tamagawa[*1]

Charge-COupled Device(CCD) detectors in observational instruments are composed of a silicon layer, which changes photons from astronomical objects into electrons. The electron signal is amplified and contains information about the objects. Impurity gradients in the silicon that originate when it is grown produce transverse electric fields that bend the electron path. The bending creates flux modulation, position displacement and shape distortion of objects. The tree-ring effect is caused by circularly symmetric impurity gradients in the silicon wafer., which induce flux modulation, position displacement, and shape distortion of the observed astronomical objects. The tree-ring effect in some recent observational instruments (DES[a] , HSC[b]) are smaller than the pixel scale, inducing small changes in object images. Future high precision cosmology by the LSST[c] needs high precision measurement of astronomical objects. One of the methods for studying cosmology is the measurement of weak lensing shear (Schneider et al., 2006[1]), which changes the shape of the image of objects from a large scale structure (cosmic shear). Statistics of the cosmic shear depend on the cosmological parameters, which characterize the initial state and future of the Universe. However, the tree-ring effect causes systematic error in the measurement because it changes the shape of images (Plazas et al., 2014[2]). We studied the impact of the tree-ring effect on the LSST test CCDs for high-precision cosmology.

We are the first to quantify the tree-ring effect on the LSST prototype sensors. We used flat images that contain data taken with uniform illumination where concentric flux modulation (tree rings) can be observed. We found the center of the tree-ring effect near the corner of the CCD (Fig. 1) and measured teh one-dimensional profile by averaging by angle (blackline in Fig. 2). If the flux modulation or position displacement are concentric, shape distortion(spurious shear) can be obtained (Okura et al in preparation) as

$$\gamma_{rad}^{TR}(r) \approx -\frac{1}{2} f(r), \qquad (1)$$

where $f(r)$ and $\gamma_{rad}^{TR}(r)$ are the profiles of flux modulation and spurious shear, respectively. We show the measured spurious shear in Figure 2, and the blue line indicates the measured spurious shear. As typical scale of the spurious shear is 0.005%, it is much smaller than the cosmic shear which has typical scale of approximately 1-2 %.

Next, we calculated the two-point correlation of the spurious shear because, in cosmological analysis, we calculate the two-point correlation of the cosmic shear for obtaining the statistics of the cosmic shear. Figure 3 shows the two-point correlation of the spurious shear in the field of view of LSST (189 CCDs, 60000 × 60000 pixels) with a sampleing scale of 50 pixels. The typical scale of the correlation is approximately 10^{-13}, which is much smaller than the two-point correlation of the cosmic shear(10^{-6}). Therefore, the tree-ring effect on the LSST CCDs will not degrade the constraining of the cosmological parameters.

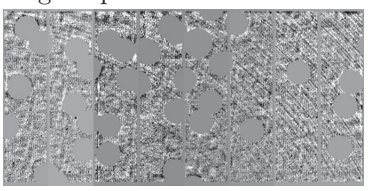

Fig. 1. Tree-ring pattern on the LSST CCD

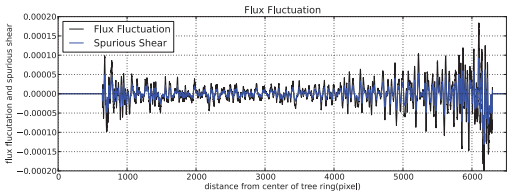

Fig. 2. One-dimensional profile of the flux modulation (black) and spurious shear (blue) caused by the tree-ring effect on the LSST CCD.

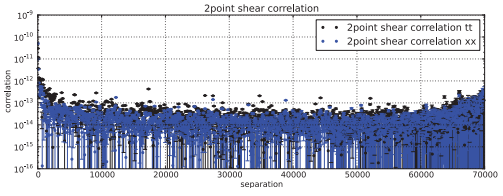

Fig. 3. Absolute values of two-point spurious shear correlation caused by the tree-ring effect on the FOV of the LSST CCD. Black points indicate parallel correlation, and blue points indicate cross correlation with 50-pixels sampling. Non-absolute values oscillated about zero.

*1 RIKEN Nishina Center
*2 RIKEN BNL Research Center
*3 Brookhaven National Laboratory
*4 Jet Propulsion Laboratory
a) http://www.darkenergysurvey.org
b) http://www.naoj.org/Projects/HSC/HSCProject.html
c) http://www.lsst.org

References

1) P. Schneider., Part 1: Introduction to gravitational lensing and cosmology, Springer-Verlag Berlin Heidelberg, (2006)
2) A. A. Plazas, G. M. Bernstein, E. S. Sheldon, PASP, Volume 126, issue 942, (2014) pp.750-760

Performance test of TPC Polarimeter for cosmic X-ray sources at BNL NSLS-1

W.B. Iwakiri,[*1] K. Black,[*2] T. Kitaguchi,[*1] J. Hill,[*2] K. Jahoda,[*2] T. Enoto,[*1,*2] T. Tamagawa,[*1,*3] Y. Takeuchi,[*1,*3] M. Kubota,[*1,*3] H. Marlowe,[*4] R.Cole,[*4] K. Nishida,[*1,*3] and A.Hayato[*1]

Cosmic X-ray polarimetry is believed to be a powerful measurement technique for studying the physics in extreme environments such as strong gravitational fields and magnetic fields in the universe. However, soft X-ray polarization has not succeeded so far except for a few detections in the 1970's [1]. To study such an unexploited field, NASA and RIKEN have been developing an X-ray polarimeter that employs the Time Projection Chamber (TPC) technique[2]. In this progress report, we discuss the performance test of a TPC polarimeter with a new Read Out Board (ROB) design[3].

When an incident X-ray interacts with a gas atom, a photoelectron is ejected preferentially in the direction of the electric field vector of the incident photon according to a cosine^2 probability distribution. Thus, we can determine the polarization degree and the phase by obtaining a track image and initial direction of the photoelectron. A schematic view of TPC polarimeter is shown in Fig 1. To ensure high efficiency for the polarization signal, the charge detection plane of the TPC polarimeter consists of the Gas Electron Multiplier (GEM) designed by RIKEN[4] mounted over strip anodes parallel to the incident X-rays. Two-dimensional images of photoelectron are created using a one-dimensional strip readout and by timing the arrival of charge[2]. For a small satellite mission of cosmic X-ray polarimetry, we have proposed two different ROB designs. One design uses two gold-plated titanium frames with "tongue in groove" to secure the strips under tension[3]. The performance of the polarimeter using this type of ROB has been verified and meets all mission requirements[5]. To reduce cost and risk by further simplifying the assembly more, the other design one has used epoxy adhesives to hold the strips under tension to the lower frame.

We carried out the performance test for the polarimeter at the Brookhaven National Laboratory (BNL) Synchrotron Light Source-1 facility in September 2014. The polarimeter was filled with 190 torr dimethyl ether (DME). To make the pixels of the track image square-shaped, the electrical drift region was selected as 196 V/cm, which is the drift velocity equal to the 121 μm divided by the 50 ns sampling time. The transfer field between the GEM and the ROB was selected as 660 V/cm considering the collection efficiency of the charge. The detector was irradiated with liner-polarized monochromatic X-rays at eight energy bands. The total number of the events is 5×10^4 for individual measurement. Further, to calibrate the polarimeter, we also acquired 2.7 keV unpolarized events.

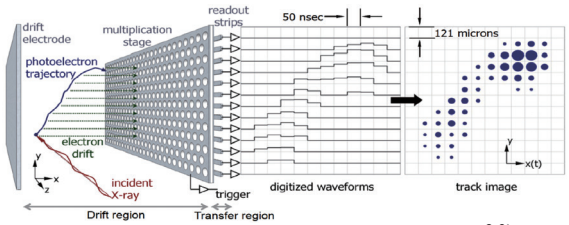

Fig. 1. Schematic view of the TPC polarimeter[2,3]

Fig.2 shows the derived modulation curves for three energy bands and the 2.7 keV unpolarized data at 8 mm from GEM, which corresponds to the detector optical axis. The results have subtracted the pedestal and common mode noise and deconvolved the electronics response. The S/N achieved 5 σ levels. To correct the asymmetry caused by the difference of the drift velocity between the drift and the transfer region, the results are corrected using Gaussian convolution in the time axis. The Gaussian σ value is 46 μm which is optimized using the 2.7 keV unpolaraized data[5]. As an indicator of the polarization sensitivity, we introduce a modulation factor μ , which is defined as

$$\mu = (f_{max} - f_{min}) / (f_{max} + f_{min}),$$

where f_{max} and f_{min} are maximum and minimum values of the modulation curve, respectively. The derived modulation factors of 2.7 keV, 4.5 keV, and 6.4 keV are 21.3±0.6%, 37.9±0.6%, and 46.6±0.6%, respectively. The results are consistent with previous ROB design[5] and meet the measurement requirement. The estimation of the systematic error for the detector position is still under discussion.

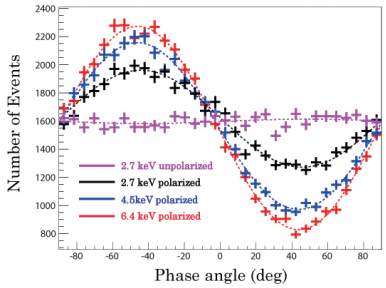

Fig. 2. Modulation at three energy bands measured at BNL using TPC polarimeter.

*1 RIKEN Nishina Center
*2 NASA Goddard Space Flight Center
*3 Department of Physics, Tokyo University of Science
*4 Department of Physics and Astronomy, University of Iowa

References
1) M.C.Weisskopf et al: ApJL, 220, L117 (1978)
2) K. Black et al: NIMPA, 581, 755 (2007)
3) J. Hill et al: Proc. of the SPIE, 9144 , 91441N (2014)
4) T. Tamagawa et al: NIMPA, 608, 390 (2009)
5) T. Enoto et al: Proc. of the SPIE, 9144, 91444M (2014)

Fabrication of a TPC X-ray Polarimeter and Preliminary Testing with the Synchrotron Radiation Light Source at Spring-8

A. Hayato,[*1] T. Tamagawa,[*1] T. Kitaguchi,[*1,*2] E. Teruaki,[*1,*3] W. B. Iwakiri,[*1]
Y. Takeuchi,[*1,*4] M. Kubota,[*1,*4] and K. Nishida[*1,*2]

X-ray polarimetry is expected to provide unique information about stars, such as strong gravitational fields around black holes. However, it is far behind in technology in comparison to radio/optical polarimetry, and the observation of Crab nebula by OSO-8 satellite 40 years ago has been the only detection of X-ray polarization among astronomical objects[1]. NASA and RIKEN have been developing the X-ray polarimeter using the time projection chamber (TPC) technique with the sensitivity 10 times greater than the OSO-8 polarimeter, for the Gravity and Extreme Magnetism Small explorer (GEMS), an X-ray polarization telescope mission[a]. Although we have already built the flight model[2], a detailed study is still needed in order to fully understand the characteristics of the TPC polarimeter. We therefore fabricated an in-house TPC polarimeter at RIKEN (RIKEN polarimeter) for tests in various situations. In this report, we present a brief overview and the basic performance of the RIKEN polarimeter.

The TPC polarimeter is a gas-based detector with sensitivity in the energy range of $2-10$ keV. The polarimeter can image a photoelectron and reconstruct its initial direction, where the azimuth angle distribution depends on the linear polarization degree/angle of the incoming X-ray[3].

The design of the RIKEN polarimeter is originally based upon the GEMS polarimeter[4], although handy materials (e.g., bare aluminum instead of copper-tungsten or gold-plated aluminum) are used for easier machining. Another modification is that we adopted the Scalable Readout System (SRS), manufactured by CERN/RD51, instead of a custom-made ASIC as the strip readout. A SRS consists of APV25(s) with a sampling rate of 40 MHz, ADC card(s), and a Front-End Card. Figure 1 shows the photoelectron track taken by the RIKEN polarimeter.

What we actually measure with the polarimeter is a modulation curve, an azimuth angle distribution of the photoelectron. The modulation factor μ is derived from $(f_{max}-f_{min})/(f_{max}+f_{min})$, where f_{max} and f_{min} are the maximum and minimum counts in the curve. The modulation factor of the polarimeter μ_{pol}, which represents the sensitivity of polarimetry, is defined as μ which should be measured with a 100% polarized source. The first step of our study is to determine μ_{pol} of the RIKEN polarimeter.

We performed two experiments: (a) to measure μ with highly (∼85%) polarized source at BL32B2 SPring-8, and (b) to confirm the flat modulation with unpolarized line emission produced by an X-ray generator. We took measurements at 4.5, 5.5, 6.4, 7.0, and 7.5 keV for (a) and 4.5 and 6.4 keV for (b), although we focus on only the result of the 4.5 keV data here.

Figure 2(a) shows the modulation curve taken with the well-collimated (200×200 μm^2) 4.5-keV polarized X-ray at the middle height of the active volume, and (b) shows that with the 4.5-keV unpolarized X-ray under the same condition. The obtained μ_{pol} at 4.5 keV is $0.3\times0.85/p_{beam}$, where p_{beam} is the polarization degree of the X-ray beam, while the observed flat modulation is 0.00 ± 0.02. Meanwhile, the determination accuracy for the polarization angle is about 4° at a certain drift height. A detailed comparison with the GEMS polarimeter and other performance studies (e.g., detector angle dependency for the sensitivity) are in progress.

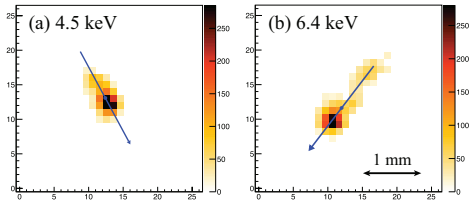

Fig. 1. Charge-weighted photoelectron track image taken by the RIKEN polarimeter with a 6.4-keV X-ray, together with a reconstructed angle with the blue arrow.

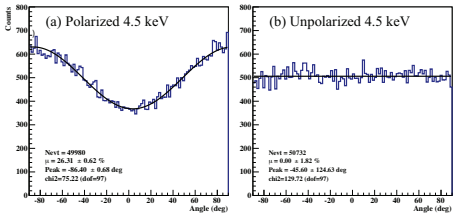

Fig. 2. Modulation curve for 4.5 keV (a) polarized X-ray and (b) unpolarized X-ray taken with the TPC polarimeter.

*1 RIKEN Nishina Center
*2 Department of Physics, Hiroshima University
*3 NASA Goddard Space Flight Center
*4 Department of Physics, Tokyo University of Science
a) GEMS was canceled in 2012 regarding the cost.

References

1) M. C. Weisskopf et al.: ApJ, **208**, L125 (1976).
2) J. E. Hill et al.: Proc. SPIE, **8433**, 84331Q (2012).
3) K. Black et al.: NIMPA, **581**, 755 (2007).
4) T. Enoto et al.: Proc. SPIE, **9144**, 91444M (2014).

Measurement of X-ray beam polarization of BL32B2 at SPring-8 using a Compton polarimeter

M. Kubota,[*1,*2] T. Kitaguchi,[*1] A. Hayato,[*1] W. Iwakiri,[*1] T. Enoto,[*1,*3] K. Nishida,[*1,*2] Y. Takeuchi,[*1,*2] A. Yoshikawa,[*1,*2] and T. Tamagawa[*1]

We develop a photoelectric tracking gas detector using a time projection chamber technique for a cosmic X-ray polarimetry[1]. To calibrate the X-ray polarimeter at a synchrotron facility, the polarization degree of the incident X-ray beam should be known. In order to measure the beam polarization, we build a Compton polarimeter based on the X-ray scattering processes, where the angular distribution of the scattered X-rays is sensitive to the polarization direction of the incident X-rays. The Compton polarimeter can accurately measure the beam polarization owing to its high analyzing power. We use the Compton polarimeter to measure the beam polarization of the BL32B2 beamline at the SPring-8 synchrotron facility where the gas X-ray polarimeter is verified.

Figure 1 shows the schematic view of the experimental setup. The Compton polarimeter consists of a cylindrical Be scatterer and two X-ray detectors, i.e., a Si sensor and a CdTe sensor, that face each other across the scatterer. Each detector is located 1 cm away from the Be scatterer and has a diameter of 4 mm and an effective length of 4 mm. Incident X-rays from left to right, as shown in Fig. 1, are scattered by the Be cylinder and then detected by these sensors. As the detectors rotate around the scatterer through a rotation stage, the count rates modulate with the minimum rate in the direction of the electric field vector (i.e., the polarization direction) of the incident X-rays and the maximum rate perpendicular to the vector. The count rate shows a sinusoidal curve as a function of the rotation angle (modulation curve). The polarization degree of the incident X-rays is derived from the modulation curve. We measure the polarization degree of the incident X-rays at 4.5, 6.4, and 8.0 keV.

Figure 2 shows the modulation curve for 4.5 keV X-rays. The data points are fitted by a sinusoidal model with a constant offset: $f(\theta) = a * \cos(2 * (\theta - b)) + c$, where θ is the rotation angle. The free parameters a, b, and c represent the amplitude, polarization direction, and offset, respectively. The observed beam polarization degree, $\mu_{\rm obs}$, is calculated using the equation: $\mu_{\rm obs} = a/c$. We define zero degree in the detector coordinate system when the Si detector is on top. In order to reduce the systematic error caused by beam misalignment, we calculate the average of the count rates obtained from two angles 180 degrees apart from each other. To calculate the beam polarization, P, we need to know the modulation factor, $M_{\rm sim}$, which is 100% for a perfect polarimeter and 0% for an insensitive detector. We estimate it using the Geant4 Monte Carlo toolkit[2]. The obtained parameters, $\mu_{\rm obs}$, $M_{\rm sim}$, and P, are listed in Table 1. The beam polarization degrees at 4.5, 6.4, and 8.0 keV are estimated to be $75.9 \pm 0.1\%$, $77.1 \pm 0.2\%$, and $77.0 \pm 0.1\%$, respectively.

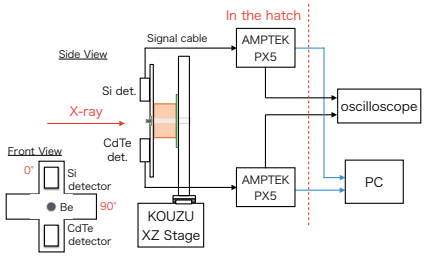

Fig. 1. Experimental setup to measure the synchrotron X-ray beam polarization. The two X-ray detectors are the AMPTEK XR100CR Si detector and the XR100T CdTe detector.

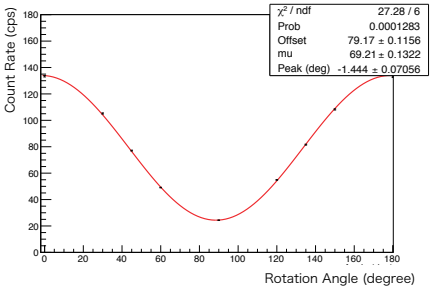

Fig. 2. Modulation curve of polarized X-rays with an energy of 4.5 keV. The red line indicates the best-fit model.

Table 1. Summary of the observed modulation ($\mu_{\rm obs}$), simulated modulation factor ($M_{\rm sim}$), and beam polarization (P)

E (keV)	$\mu_{\rm obs}$ (%)	$M_{\rm sim}$ (%)	P (%)
4.5	69.2 ± 0.1	91.21 ± 0.10	75.9 ± 0.1
6.4	70.6 ± 0.2	91.62 ± 0.05	77.1 ± 0.2
8.0	72.1 ± 0.1	93.67 ± 0.02	77.0 ± 0.1

*1 RIKEN Nishina Center
*2 Department of Physics, Tokyo University of Science
*3 NASA/GSFC

References
1) K. Black et al: NIM A, 581, 755 (2007)
2) S. Agostinelli, et al: NIM A, 506, 250 (2003)

Performance test of Modulated X-ray Source using UV-LED and Channel Electron Multiplier

W.B. Iwakiri,[*1] K. Gendreau,[*2] A. Hayato[*1] Y. Takeuchi,[*1,*3] K. Nishida,[*1,*3] M. Kubota,[*1,*3] and T. Tamagawa[*1]

A Modulated X-ray Source (MXS) with Channel Electron Multiplier (CEM) developed by NASA is a newtype of X-ray generator that uses UV-LED[1]. MXS has many advantages compared with radioactive sources or X-ray generators that require hot filaments. For example, the timing of the X-ray output can be controlled using the modulated LED. Moreover, electronic amplification by CEM leads to the generation of short X-ray pulses (tens of nanosecond). These advantages make the calibration of an X-ray detector considerably easy. For example, we can determine the drift velocity of an electron in a gas using high-precision X-ray photon emission timing. It is important to calibrate an X-ray polarimeter using the Time Projection Chamber technique[2]. In this progress report, we show the performance of MXS with CEM.

A basic layout of MXS with CEM is shown in Fig 1. When an UV-photon emitted from an LED hits a photocathode, the photon converts to a photoelectron. The photoelectron is accelerated onto a target through a potential difference and it produces an X-ray. In fact, the modulation of the LED provides modulated photoelectron and it leads to the generation of modulated X-rays eventually. The X-ray spectrum can be controlled by choosing the target material and the acceralating potential. To amplify the photoelectron, i.e., to obtain a high X-ray flux, CEM is set between a photocathod and the target. Figure 2 shows the MXS made at RIKEN. The assembly is based on the SUS304 cuboid that is 67×34×34 mm. We adopted MgO as the photocathode and Ti as the target.

To verify the performance of the MXS quantitatively, first, we checked the output X-ray flux. The pressure in the MXS is set at 10^{-7} torr with pumping. The voltage of the CEM and target are set as −2.25 kV and 10 kV, respectively. The frequency of the input pulse is fixed at 10 kHz. We used a Si detector, AMPTEK XR100CR, to evaluate the output X-ray. Figure 3 (left) shows the relation between the width of the input pulse with 10 kHz for the LED and the output X-ray flux. The results show that these two parameter have a linear relationship. When the width of the input pulse is 500 ns, the observed X-ray flux is 4000 counts/s/msr.

Next, we evaluate the duration of the output X-ray pulse using a Time-to-Digital Converter (TDC). We measured the time interval between the leading time of input pulse for LED (used as the start signal of the TDC) and the arrival time of the output X-ray photon (used as the stop signal of the TDC). Figure 3 (right) shows the derived TDC histogram at 5 different widths of the input pulse (50, 100, 200, 400, and 600 ns). The bin size of the histograms are 62.5 ns. The width of each histogram corresponds to the pulse width of the output X-rays. It means that the MXS output is controlled by choosing the input pulse, and we can provide a X-ray photon when needed at precisely known times. To reduce the cost and size, currently, we are developing a new MXS using a carbon nanotube instead of LED and CEM.

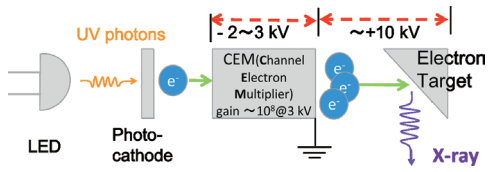

Fig. 1. Schematic view of MXS with CEM.

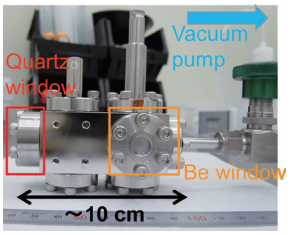

Fig. 2. MXS with CEM developed by our group.

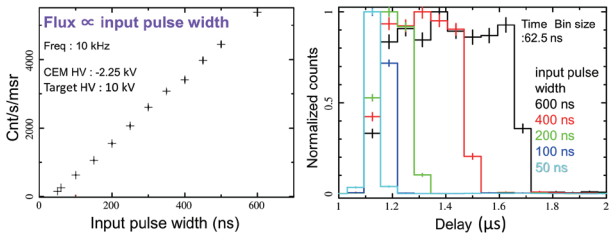

Fig. 3. Left : Output X-ray flux as a function of the width of input pulse for the LED (the frequency of the input pulse is fixed at 10 kHz). Right : TDC histogram at five different input pulse widths. The start and stop signal are the input pulse and the arrival timing of the output X-ray, respectively.

*1 RIKEN Nishina Center
*2 NASA Goddard Space Flight Center
*3 Department of Physics,Tokyo University of Science

References

1) K.Gendreau et al: Proc. of the SPIE, 8443, 84434V (2012)
2) K.Black et al: Proc. of the SPIE, 7732, 77320X (2010)

Property of LCP-GEM in pure dimethyl ether at low pressures†

Y. Takeuchi,[*1,*2] T. Tamagawa,[*1,*2] T. Kitaguchi,[*1] S. Yamada,[*1] W. Iwakiri,[*1] F. Asami,[*1,*2] A.Yoshikawa,[*1,*2] K. Kaneko,[*1,*2] T. Enoto,[*1,*3] A. Hayato,[*1] T.Kohmura,[*4] and the GEMS/XACT team

We developed a photoelectric X-ray polarimeter onboard X-ray advanced concepts testbed (XACT) sounding rocket, the first dedicated NASA rocket mission for high sensitivity observation of cosmic X-ray polarization.[1,2] The polarimeter uses a time projection chamber technique to obtain the distribution of photoelectron emissions from which the polarization of the incident X-rays can be measured. A key device of the polarimeter is a 100-μm-thick gas electron multiplier (GEM) foil with a copper-clad liquid crystal polymer insulator (LCP-GEM),[3,4] which amplifies the signal that keeps the track image of photoelectrons. The required gain of the LCP-GEM for the polarimeter is 3,000 without discharge. Fine photoelectron track images are essential for a highly sensitive measurement of X-ray polarization. By extending the track length using a low-pressure gas, high-resolution photoelectron track images can be obtained. On the other hand, the low-pressure gas decreases the X-ray detection efficiency of the polarimeter. We anticipate that the optimum gas pressure of pure dimethyl ether (DME) is 50−150 Torr by considering the trade-off between the detected count rate and the modulation factor.[1] However, LCP-GEMs have never been operated below 190 Torr in DME gas. Under such low gas pressures, discharge is one of the most significant risks to the successful operation of GEMs. To explore this unknown regime, we performed a systematic investigation of the gain properties of a 100-μm-thick LCP-GEM in DME at low pressures for the first time.

We developed a prototype gas-chamber detector, which possesses the same geometry as the flight model of XACT. By irradiating the chamber with 6.4 keV X-rays, we obtained the spectrum from the readout pad and fitted it with a Gaussian model. An energy resolution of approximately 20% at the FWHM was achieved. The highest gain under stable operation at 190 Torr was 2×10^4 at d$V_{\rm GEM}$= 560 V, while that at 20 Torr was approximately 300 at d$V_{\rm GEM}$= 470 V. Above 50 Torr, the highest gain exceeded 3000, which meets our requirements for the XACT polarimeter. The gain curves could be reproduced by exponential functions; however, a change of slope with pressure was observed. In addition, we determined the real GEM gain derived from the sum of charge amounts induced in the readout pad and GEM anode using the same data set. The real gain represents the amplification degree of electron drifting in the GEM hole, while the effective gain is the real gain multiplied by the amplified electron collection efficiency of the readout pad.[5] The real gain is approximately twice the effective one because the charge amount of the GEM anode is almost the same as that of the readout pad.[6] The highest gain at 190 Torr is 4×10^4, while that at 20 Torr is around 600. These real gain curves also show deviation from an exponential function.

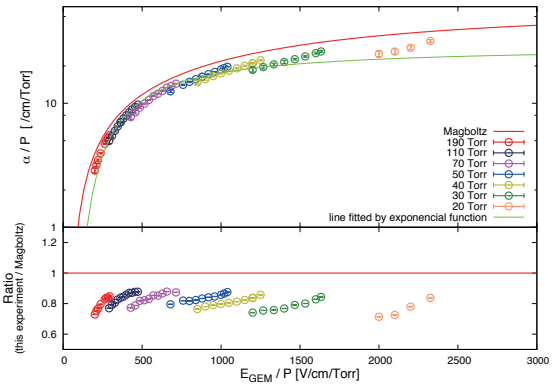

Fig. 1. Top: Comparison between the measured α and the α simulated by Magboltz[7] with 1σ errorbars.Bottom: Ratio of α obtained in this experiment to that obtained with Magboltz calculation.

To comprehensively characterize the gain variations with different gas pressures and GEM voltages, we derived the first Townsend coefficient, α. Fig. 1 shows the observed α as a function of $E_{\rm GEM}/P$ superposed with the results of Magboltz calculations.[7] $E_{\rm GEM}$ is the electric field applied to the GEM. The data points can be roughly reproduced by an exponential function, although they show deviation from it in the higher $E_{\rm GEM}/P$ range. This is because the DME ions gain sufficient kinetic energy from such a strong electric field to ionize the DME gas and emit additional electrons that are amplified in the GEM hole. The measured α values were approximately 80% of ones derived from Magboltz calculations, which suggests that the length over which the number of electrons were amplified in the GEM hole was different from the GEM thickness but close to 80 μm.

References
1) K. Gendreau et al.: Proc. SPIE, **8443** 84434V-1 (2012)
2) J.K. Black et al.: NIM, **A581** 755 (2007)
3) T. Tamagawa et al.: NIM, **A560** 418 (2006)
4) T. Tamagawa et al.: NIM, **A608** 390 (2009)
5) J. Benlloch et al.: NIM, **A419** 410 (1998)
6) Y. Takeuchi et al.: JINST, **7 C03042** (2012)
7) S.F. Biagi: NIM, **A421** 234 (1999)

† Condensed from the article in JINST 9 C01002 (2014)

*1 RIKEN Nishina Center
*2 Department of Physics, Tokyo University of Science
*3 NASA/GSFC
*4 Department of Mechanical Engineering, Kogakuin University

Measurement of the electron drift velocity in DME gas

M. Kubota,[*1,*2] T. Kitaguchi,[*1] A. Hayato,[*1] W. Iwakiri,[*1] T. Enoto,[*1,*3] K. Nishida,[*1,*2] Y. Takeuchi,[*1,*2] A. Yoshikawa,[*1,*2] and T. Tamagawa[*1]

We have developed a photoelectric tracking type gas X-ray polarimeter using a time projection chamber technique for cosmic X-ray polarimetry.[1)] We select dimethyl ether (DME) as target gas of the polarimeter because the electron drift velocity in DME is relatively slow. The polarimeter chamber, filled with DME gas under a pressure of 190 Torr, consists of three components: drift plane, gas electron multiplier (GEM), and readout strips. When an X-ray interacts with a DME gas atom, a photoelectron is ejected in a direction according to a cosine probability distribution aligned with the electric field vector of the incident X-ray. Secondary electrons produced by photoelectron ionization are drawn by the electric field to the GEM, amplified by a factor ∼3000 with the strong electric field in the GEM hole, and then collected by readout strips. The 2-d image of the photoelectron track created by the readout strip position and timing enables measurement of the polarization degree of incident X-rays. In order to square the pixel size of the 2-d image, the electron drift velocity is optimized to be 0.242 cm/μs, which is derived from a strip pitch of 121 μm over a sampling rate of 50 ns. Thus, we accurately measure the electron drift velocity in DME gas under a pressure of 190 Torr as a function of applied electric filed.

Figure 1 shows a schematic view of experimental setup. We generated X-rays with a modulated X-ray source (MXS), whose X-ray radiation can be controlled by a switching LED[2)] with a pulse generator. Generated X-rays were collimated and directed parallel to the GEM foil. The drift distance of electrons to the GEM foil changed by moving it up and down the chamber using the Sigma Koki Z-stage. We measured the time interval between the leading edge of the pulse, which turned on the LED, and a discriminator signal created by charges induced on the GEM cathode. The drift velocity can be determined by dividing the X-ray beam position difference by the time interval difference. Figure 2 shows time interval as a function of stage position. The drift velocity was calculated by the slope of this plot.

The observed drift velocities, $v_{\rm obs}$, at various electric field are listed in Table 1. The drift velocities are determined with an accuracy of $< 0.5\%$, and are consistent with the Magboltz prediction[3)], $v_{\rm sim}$, under the DME gas condition of 190 Torr and 25°C. We determined that the electric field, where the drift velocity is 0.242 cm/μs, is 196.3 V/cm by interpolating the observed values. Reproducibility of the results should be checked in further experiments.

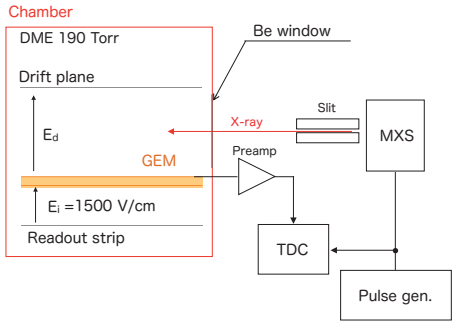

Fig. 1. Experimental setup to measure the electron drift velocity in DME gas.

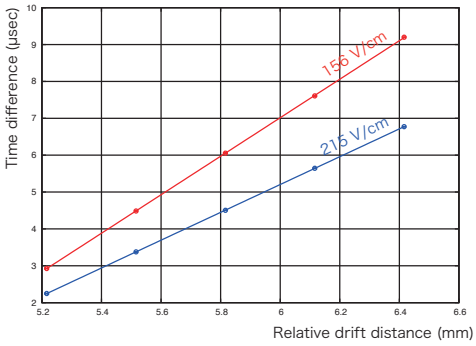

Fig. 2. Time difference as a function of stage position. The drift velocity is calculated by the slope of this plot.

Table 1. Comparison of simulated drift velocity and measured velocity.

E_d (V cm^{-1})	$v_{\rm obs}$ (cm μs^{-1})	$v_{\rm sim}$ (cm μs^{-1})
156	0.1918(6)	0.1916(2)
176	0.2161(10)	0.2158(2)
186	0.2291(8)	0.2285(3)
196	0.2405(8)	0.2411(3)
205	0.2525(9)	0.2532(3)
215	0.2650(8)	0.2651(3)

*1 RIKEN Nishina Center
*2 Department of Physics, Tokyo University of Science
*3 NASA/GSFC

References
1) K. Black et al: NIMPA, 581, 755 (2007).
2) Keith Gendreau et al: Proc. of the SPIE, 8443, 84434V (2012).
3) S.F. Biagi: Nucl. Instr. and Meth. A 283, 716 (1989).

Measures for Micro Meteoroids and Orbital Debris in Cooler Driver Harnesses of the Soft X-ray Spectrometer onboard ASTRO-H

H. Noda[*1] and T. Tamagawa[*1] on behalf of the SXS team

The Soft X-ray Spectrometer (SXS)[1] onboard the 6th Japanese X-ray satellite ASTRO-H[2] covers an 0.3–12 keV band with an unprecedentedly high energy resolution of 7 eV (the target value is 4 eV). The performance of X-ray spectroscopy is achieved using micro-calorimeter technology at a low temperature of $\sim$ 50mK, which is maintained through the following cooling chain. Stirling coolers, called Shield Coolers (SCs) and Pre-Coolers (PCs), decrease the temperature from $\sim$ 290K to $\sim$ 20K, and subsequently, a Joule-Thomson cooler (JT) further decreases the temperature to $\sim$ 4.5K. Then, the temperature is cooled down to $\sim$ 1.2K with superfluid helium and/or an Adiabatic Demagnetization Refrigerator (ADR), and finally the temperature is reduced to $\sim$ 50mK using two-stage ADRs at the front end of the chain.

Electric power derived by a satellite bus is supplied to SCs, PCs, and the JT via cooler drivers named SC Driver (SCD), PC Driver (PCD), and JT Driver (JTD), respectively[1]. The cryo-coolers and cooler drivers are connected by multiple harnesses, and the numbers of particularly important harnesses for driving the cryo-coolers are 4 in SCD, 4 in PCD, and 2 in JTD (10 in total). Because a part of the dewar surface is placed in front of a window of the satellite panel (Fig. 1[2]), the harnesses are partly exposed to space, and hence, Micro Meteoroids and Orbital Debris (MMODs) of various sizes can collide with the harnesses. If one of the important harnesses is destroyed because of collision with an MMOD, the cooling chain fails to work as required, significantly degrading the SXS performance. Thus, the design needs to satisfy the requirement that the number of MMODs passing through an important harness per year must be lower than 0.1. In the present document, we roughly estimate the probabilities with 1-digit accuracy in cases with and without a Kevlar measure[3], and we determine whether the requirement can be satisfied.

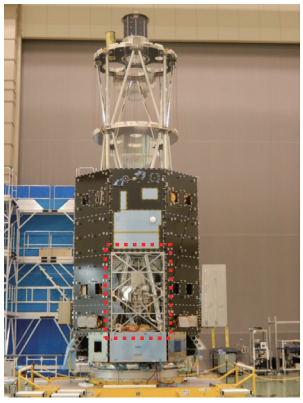

Fig. 1. Flight model of the *ASTRO-H* satellite body in a vibration test, including the engineering model of the SXS dewar[2] on the inside. The red dotted square shows a window at the satellite panel, through which the harnesses are exposed to the space and MMODs can enter.

The probability that a harness is penetrated by an MMOD can be estimated by multiplying an area exposed to space, a solid angle against space, and flux of MMODs. In each harness, the part exposed to space commonly has a length of $\sim$ 2 m and a solid angle of $\sim 0.5\pi$ against space, while the sum of widths of important parts driving the cryo-coolers is $\sim$ 1–3 mm (for simplicity, we hereafter employ a width of 3 mm for all the harnesses). According to a debris flux model, MASTER2009[4], developed by the European Space Agency (ESA), the MMOD flux drastically changes with their sizes. Because the critical MMOD size is determined as the smallest diameter penetrating a harness, the flux depends on the toughness of the harnesses. According to the JAXA space debris protection manual[3], the critical MMOD size for a commonly used harness cable is $\sim$ 0.2 mm, while that for the same cable covered by a 1-layer Kevlar fiber is calculated to be $\sim$ 0.4 mm. Therefore, the MMOD fluxes can be determined to be $\sim$ 10 and $\sim$ 1 collisions/m^2/year for harnesses without and with the 1-layer Kevlar coverage, respectively.

We calculated the probabilities that one of the important harnesses is penetrated per year. The case without Kevlar coverage has the probability

$$10 \text{ pieces} \times 2 \text{ m} \times 0.003 \text{ m} \times \frac{0.5\pi}{2\pi} \times 10 \text{ collisions/m}^2\text{/year} \approx 0.2 \text{ collisions/year},$$

while the probability for the case with the 1-layer Kevlar fiber decreases to

$$10 \text{ pieces} \times 2 \text{ m} \times 0.003 \text{ m} \times \frac{0.5\pi}{2\pi} \times 1 \text{ collisions/m}^2\text{/year} \approx 0.02 \text{ collisions/year}.$$

Thus, we successfully confirmed that the design with the 1-layer Kevlar fiber coverage is effective to satisfy the requirement, and we have employed the measures for all the SCD, PCD, and JTD important harnesses.

*1 RIKEN Nishina Center

References
1) K. Mitsuda et al. SPIE **7732**, 773211 (2010)
2) T. Takahashi et al. SPIE, **9144**, 914425 (2014)
3) JAXA space debris protection manual, 2009, JERG-2-144-HB001
4) ESA MASTER: http://www.master-model.de

8. Accelerator

Emittance measurements for RIKEN 28 GHZ SC-ECRIS†

Y. Higurashi,[*1] J. Ohnishi,[*1] K. Ozeki,[*1] and T. Nakagawa[*1]

During the last several years, we have been working on increasing the intensity of highly charged uranium (U) ion beams and we have produced intense beams (≈180 eμA for U^{35+} and ≈230 eμA for U^{33+}) using the sputtering method [1]. It is obvious that the emittance of highly charged U ion beams should be sufficiently smaller than the acceptance of the accelerators of the RIKEN RIBF for safe acceleration. Therefore, to minimize the extent of emittance for intense beams of U ions, we intensively studied the effect of the ion source parameters on the emittance. If the magnetic field distribution affects the ion dynamics and the trajectory of the extracted beams, [2] it may also affect the emittance of highly charged heavy ions.

Emittance was measured using an emittance monitor, which consists of a movable thin slit and wires (beam profile monitor).

The root mean square (rms) emittance is defined as

$$\varepsilon_{x-rms} = \sqrt{\langle x^2\rangle\langle x'^2\rangle - \langle xx'\rangle^2}$$
$$\varepsilon_{y-rms} = \sqrt{\langle y^2\rangle\langle y'^2\rangle - \langle yy'\rangle^2} \quad (1)$$

In these equations, the averages of the phase-space coordinates of position (x, y) and divergence (x', y') are weighted by the beam intensity [3].

To investigate the magnetic field distribution effect, we measured the emittance for various magnetic field distributions with 18- and 28-GHz microwaves.

The magnitude of maximum mirror magnetic field strength at the beam extraction side (B_{ext}) was changed from ≈1.8 T to ≈1.4 T, while keeping the other magnetic field strengths constant (B_{injti}≈3.1 T, B_{min}≈0.65 T and B_r≈1.8 T) for investigating the B_{ext} effect with 28-GHz microwaves. The RF power and the extraction voltage were ≈1.5 kW and 22 kV, respectively. Figure 1 shows the normalized rms y-emittance as a function of B_{ext}. The emittance drastically changed from ≈0.07 to ≈0.17 π mm mrad as B_{ext} decreased from ≈1.4 T to ≈1.8 T. The beam intensity also depended on B_{ext}. It changed from ≈60 eμA to 40 eμA as B_{ext} decreased from ≈1.8 T to ≈1.4 T. In this figure, open circles denote the averaged emittance for various drain currents (2.5-4.5 mA), which is proportional to the extraction current. The error bars (emittance spread ≈0.015 π mm mrad) are the standard deviations.

The magnitude of B_{inj} was changed from ≈1.5 T to 3.1 T, while keeping the other magnetic field strengths constant (B_{ext} ≈1.45 T, and B_{min} ≈0.65 T, B_r ≈1.8 T) for investigating the B_{inj} effect. Figure 2 shows the results for rms y-emittance. The emittance increased from ≈0.09 to ≈0.17 π mm mrad as B_{inj} increased.

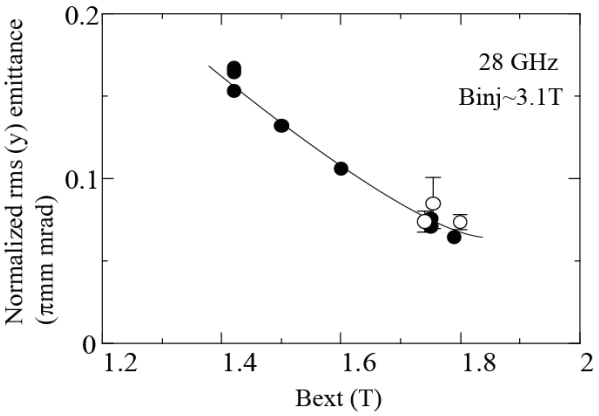

Fig. 1. Normalized rms y-emittance as a function of B_{ext}.

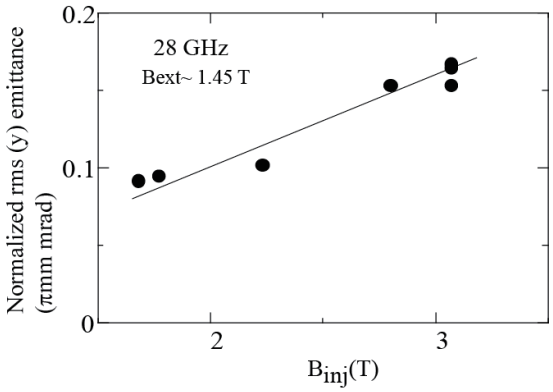

Fig. 2. Normalized rms y-emittance as a function of B_{inj} with 28-GHz microwaves, for B_{ext} ≈1.45 T.

We measured the emittance of U^{35+} ions for various ion source conditions. The extent of emittance was independent of the drain current and extraction electrode position. On the other hand, it strongly depended on the magnetic field distributions. The study of the B_{inj} effect may yield some novel information, implying that the emittance of U^{35+} ions is not influenced by the extraction conditions, but rather by the ion dynamics in the plasma modified by B_{inj}. On the other hand, for less heavy ions such as Xe, Kr, and O ions, preliminary experimental results did not show any strong effects of the magnetic field distributions as for U^{35+} ion beams. The magnetic field distribution may affect only highly charged very heavy ions. Additional research is required to understand these phenomena.

References

1) Y. Higurashi et al.: Rev. Sci. Instrum. 85 02A953 (2014).
2) P. Spaedtke et al.: Proc of 18th Int. Workshop on ECR ion sources, Chicago, USA, 2008, http://www.jacow.org, P. 213.
3) I. G. Brown: The Physics and Technology of Ion Sources. (Wiley, New York, 1989, p. 94).

†Condensed from the proceedingw of ECRIS 2014, 21st International Workshop on ECR Ion Sources August, 24-28,Nizhny Novgorod, Russia

*1 RIKEN Nishina Center

Supply of ^{70}Zn beam from 18-GHz ECRIS using the micro-oven

K. Ozeki,[*1] Y. Higurashi,[*1] and T. Nakagawa[*1]

In the 18-GHz electron cyclotron resonance ion source (ECRIS)[1], we have achieved the practical use of the micro-oven to supply high-intensity and stable ^{48}Ca beams for a long term.[2-4] In the process of the operational tests, we found that the temperature of our oven could be increased up to about 1000°C without damaging the oven. At that temperature, the vapor pressure of ZnO is expected to reach a level high enough to extract the Zn beam with adequate intensity. Therefore, we conducted the supply test of Zn beam using the micro-oven.

In contrast to the Ca beam, in which the Al powder is mixed to the CaO powder to reduce CaO, only the powder of ZnO was placed in the crucible because the vapor pressure of ZnO is sufficiently high. The hot liner[5], which plays an important role in reducing the material consumption rate when supplying the ^{48}Ca beam, is not used when supplying the ^{70}Zn beam because even if the oven current is increased, the beam intensity hits a peak at an inadequate level when installing the hot liner into the ECRIS.

When increasing the oven current gradually, the water evaporated first. By increasing the oven current, the production of the Zn beam was observed at the oven current lower than that at which the Ca beam was produced. This production seems to be due to the metallic Zn existing slightly in ZnO. The production of the Zn beam at this oven current was terminated after a short time. By further increasing the oven current, the production of the Zn beam was observed again at the oven current higher than that at which the Ca beam was produced.

The $^{70}Zn^{15+}$ beam produced by the micro-oven was first supplied for the experiment at the RIBF, from May to June 2014. The beam intensity at the exit of ECRIS and the oven current are shown in Fig. 1. As an example, the power applied to the oven for the oven current of 2.45 A (May 16 to May 19) is estimated to be 39 W. The RF power fed to the ECRIS was 550 W. During the experiment, the sudden increases in pressure in the ECRIS, followed by either the increase in beam intensity or runaway of the ECRIS, occurred several times. These phenomena seem to be due to the grain size of the ZnO (in this experiment, the material was prepared by chipping sintered ZnO rod. The grain size was up to about 1 mm in diameter). Assuming that a grain had a metallic Zn core and a ZnO shell, the inner pressure of the grain increases. The shell becomes thinner with the evaporation of ZnO and cracks at some point to cause a sudden increase in pressure in the ECRIS. This instability problem seems to be prevented by chipping the grains as fine as possible.

Because there was a break period ("CGS failure" in Fig. 1), the material was replaced just to be safe. The statuses of beam supply before and after the break are summarized in Table 1. The consumption rate all through the experiment was 0.14 mg/h.

Table 1. Status of beam supply.

	Before	After
Beam intensity [electric μA]	30	33
Amount of ZnO placed in the crucible [mg]	1007	835
Amount of ZnO consumed [mg]	59	22
Consumption rate of ZnO [mg/h]	0.16	0.10

The vapor pressures among Ca, Zn, and ZnO are in the following order: Zn > Ca > ZnO. In order to evaporate ZnO, an oven temperature higher than that for Ca is required. But after being decomposed into Zn and O by the plasma, a vapor pressure higher than that of Ca is obtained. Sufficiently low consumption rate without the hot liner seems to stem from the above relation of vapor pressures.

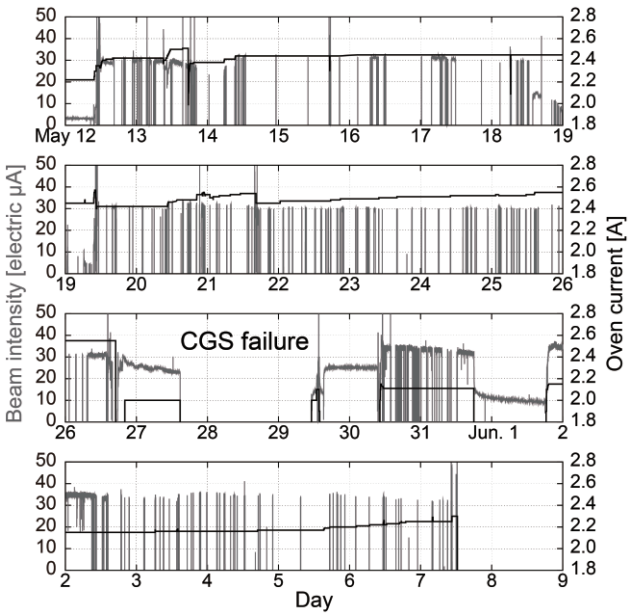

Fig. 1. Long-term supply of the ^{70}Zn beam for the experiment at the RIBF. The beam intensity for $^{70}Zn^{15+}$ (gray) and the oven current (black) are shown.

References

1) T. Nakagawa et al.: Nucl. Instrum. Methods B **226**, 392 (2004).
2) K. Ozeki et al.: RIKEN Accel. Prog. Rep. **46**, 128 (2013).
3) K. Ozeki et al.: Rev. Sci. Instrum. **85**, 02A924 (2014).
4) K. Ozeki et al.: Rev. Sci. Instrum. (*to be published*).
5) A. Efremov et al.: Rev. Sci. Instrum. **69**, 662 (1998).

*1 RIKEN Nishina Center

Current status of the RIKEN 18-GHz superconducting ECR ion source

T. Nagatomo,[*1] K. Kobayashi,[*2] M. Nishimura,[*2] T. Kageyama,[*1] Y. Kotaka,[*2,*3] Y. Ohshiro,[*3] V. Tzoganis,[*1,*4] O. Kamigaito,[*1] and T. Nakagawa[*1]

The RIKEN 18-GHz superconducting electron cyclotron resonance ion source (18-GHz SC-ECRIS) provides comparatively light ions to the RIKEN AVF cyclotron[1], which is used as an injector at the RI Beam Factory (RIBF) as well as for investigations in low-energy nuclear physics, material sciences, and biological irradiations and RI productions for commercial use. The 18-GHz SC-ECRIS was designed as a liquid-He-free system, and similar ion sources were constructed at the end of the 1990s[2]. The SC-ECRIS consists of four superconducting solenoid coils and a permanent Nd-B-Fe hexapole magnet, which generate the so-called minimum-B magnetic mirror geometry. A high-power 18-GHz microwave ($\sim$ 500 W) is used to heat up the electrons in the plasma, so that highly charged heavy ions can be produced. The superconducting solenoid coils whose filaments are made of Nb-Ti alloy are cooled with a 4.2-K Gifford-McMahon (GM) refrigerator (0.7 W). In addition, the high-T_c superconducting current leads are cooled with another 20-K GM (4 W).

Last summer, these coils could not be cooled below 100 K after 21 days of cooling. This happened just after the annual maintenance of the cryostat systems, and so, we suspected that the thermal insulation surrounding the solenoid coils might be degraded. That is why the whole set of the solenoid coils and the vacuum insulation including the cryostat systems have been replaced with another set that was used in the past and was held in reserve. The replacement was carried out last October, following which the super-conducting coils could successfully be cooled to 4 K.

The permanent hexapole magnet had a length of 350 mm and an outer diameter of 199 mm. The hexapole magnet has been replaced with a larger one with an outer diameter of 210 mm so that the radial magnetic field increases from 1.0 T to 1.1 T at the magnet pole face to enhance the plasma confinement for the 18-GHz operation.

The klystron power amplifier (KPA), which was used to generate the high-power 18-GHz microwave, also showed degradation over time. Moreover, the output power was unstable, which directly led to fluctuation of the extracted beam intensity. That is why we have introduced a traveling-wave tube amplifier (TWTA) instead of the KPA even though the maximum output power of the TWTA (750 W) is half of that of the KPA. As a result of this replacement, new remote control functions and additional interlocks to protect the ion source were appended to the existing remote operating system.

The beam emittance extracted from the 18-GHz SC-ECRIS does not seem to be well matched with the acceptance of the low energy beam transport (LEBT) system of the AVF cyclotron. Transverse emittances are crucial parameters and can be optimized by matching the emittance with the acceptance of the LEBT. Moreover, decoupling any inter-plane correlation in the transverse 4D emittance is important to increase the beam brightness[3]. At present, no device to measure the emittance is installed in the beam line following the 18-GHz SC-ECRIS. Because of a spatial limitation to install a new device, we have started to develop a compact emittance meter based on the pepper-pot method[4]. The prototype emittance meter was installed behind the analyzing magnet. As the first step, we have obtained an image of beam spots of 6.52-keV p^+ ($\sim$ 80 $e\mu$A) as shown in Fig. 1. The transverse r.m.s emittances were measured to be about 40 mm mrad. Further developments and investigations are in progress to establish the emittance meter which can be applied for diagnostics of the low-energy highly charged heavy-ion beam extracted from ECR ion sources.

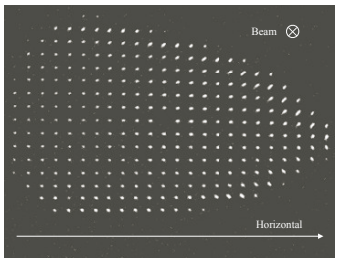

Fig. 1. An image of beam spots obtained using the prototype pepper-pot emittance meter.

*1 RIKEN Nishina Center
*2 SHI Accelerator Service Ltd.
*3 CNS, The University of Tokyo
*4 Department of physics, University of Liverpool

References
1) S. Kohara et al.: Nucl. Instrum. and Meth. A, **526** (2004), p. 230.
2) T. Kurita et al.: Rev. Sci. Instrum. **71** (2000), p. 909
3) C. Xiao et al.: Phys. Rev. STAB, **16** (2013), 044201
4) H.R. Kremers et al.: Rev. Sci. Instrum. **84** (2013), 025117

Acceleration test of ^{235}U

K. Ozeki,[*1] Y. Higurashi,[*1] T. Nagatomo,[*1] and O. Kamigaito[*1]

Transmutation of long-lived fission products included in the radioactive waste into short-lived or stable nuclei is one of the fundamental issues for future nuclear energy. In order to design a reasonable process for transmutation, fundamental data on nuclear reactions, such as the neutron capture cross section over a wide energy range, are crucial. Acceleration of such radioactive nuclei would help in obtaining the fundamental data through nuclear reaction studies using radioactive beams.

The biggest obstacle in the acceleration of such nuclei is their high radioactivity, which limits the available amount of radioactive material in an ion source. The solution to this problem is to mix a very small amount (several tenths of micrograms) with the usual ion source materials, and accelerate them by pilot-beam acceleration. In this machine study, the feasibility of pilot-beam acceleration was investigated for ^{235}U, which is included in natural uranium (natural abundance of 0.7204%), using ^{238}U as the pilot beam. As shown in Fig. 1, the ^{235}U isotope is present in such minute quantities that it is impossible to be identified by the analyzing system of the RIKEN 28-GHz Superconducting Electron Cyclotron Resonance Ion Source (28-GHz SC-ECRIS).[1)]

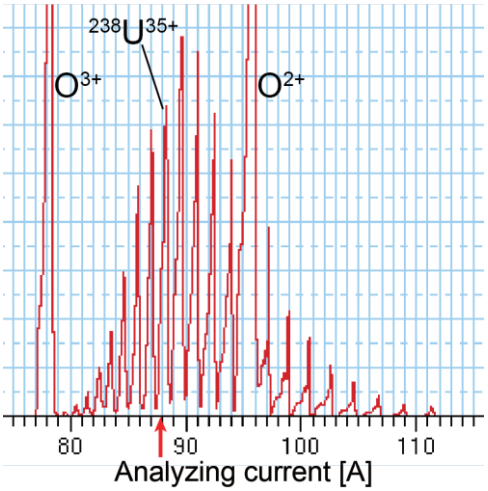

Fig. 1. Charge distribution of the uranium ions with a slit aperture of ±0.1 mm. ^{235}U ions are expected to appear at the position indicated by the red arrow, but they cannot be identified.

As the first step of the machine study, the $^{238}U^{35+}$ beam, which was used as a pilot beam, was extracted from the RIKEN Ring Cyclotron (RRC).[2)] Next, the aperture of the slit installed at the exit of the 28-GHz SC-ECRIS (SL-U10) was decreased, and the excitation current of the analyzing magnet of the 28-GHz SC-ECRIS was swept. Then, a small peak speculated to be due to $^{235}U^{35+}$ was identified by the profile monitor installed at downstream of SL-U10 (PF-U10b). The extraction voltage of the 28-GHz SC-ECRIS and acceleration voltage of the RIKEN Linear Accelerator 2 (RILAC2)[3)] were multiplied by 235/238 to extract and accelerate the particles comprising the peak. The $^{235}U^{35+}$ beam was successfully observed downstream of the RILAC2 (B61).

Since the $^{235}U^{35+}$ beam with an intensity of several electric nA was observed with the main differential probe (MDP) moved to the injection region, we tried to accelerate $^{235}U^{35+}$ by tuning only the phase of RF and the excitation current of the main coils of the RRC, while keeping the signal of the MDP as constant as possible. However, because of our insufficient tuning skill, it was difficult to go beyond the radii of 2 m; hence, we gave up this acceleration procedure.

Therefore, the SL-U10 was fully opened. A beam intensity of about 100 electric nA was observed with the MDP, which was enough to obtain the signal from the phase probe (PP). By tuning the isochronism, we achieved acceleration of the $^{235}U^{35+}$ beam in the RRC. The turn pattern of the circulating $^{235}U^{35+}$ beam measured by the MDP is shown in Fig. 2. The extraction efficiency was about 75%.

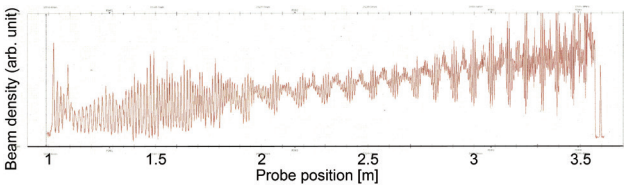

Fig. 2. Turn pattern of the circulating $^{235}U^{35+}$ beam in the RRC.

Besides our insufficient operational ability, the difficulty in the acceleration test mentioned above stemmed from the fundamental fact that isochronism cannot be achieved by changing only the main coil current. The magnetic field calculation revealed that several trim-coil currents should be changed over a wide range to accommodate the mass difference of more than 1% of the uranium ions. In our subsequent study, we plan to accelerate $^{234}U^{35+}$ by using $^{235}U^{35+}$ as the pilot beam, based on an accurate magnetic field calculation.

References

1) T. Nakagawa et al.: Rev. Sci. Instrum. **81**, 02A320 (2010).
2) H. Kamitsubo: Cyclotrons'86, 17 (1986).
3) O. Kamigaito et al.: Proc. of PASJ2-LAM31, 502 (2006).

[*1] RIKEN Nishina Center

Modification of septum electrode for RRC-EDC

K. Yamada,[*1] S. Ishikawa,[*2] T. Nakamura,[*2] M. Nishida,[*2] and H. Okuno[*1]

Electric deflection channel (EDC) is an important device to extract the circling ion beam in a cyclotron by using high-static electric field up to 10 MV/m. The circling beam and the extracting beam in the cyclotron are separated by a septum electrode, which is a thin ground electrode of the EDC and only the extracting beam is affected by the electric field and deflected. Because major beam loss in the cyclotron occurs on the septum electrode, the heat load restricts the maximum beam intensity accelerated by the cyclotron. Especially for the uranium beam acceleration at the RIBF, turn separation of the circling beam in the RIKEN ring cyclotron (RRC) is about 7 mm due to the low acceleration voltage and the short stopping range of ions in a material causes melting of the septum electrode, as happened in fiscal year 2012. Therefore, a new septum electrode for the RRC-EDC was introduced in order to improve the heat-load durability of the beam loss.

We fabricated the septum electrode with a V-cut entrance as shown in Fig. 1. The septum electrode was made of oxygen-free copper and divided into two pieces, the entrance side and the remainder, to facilitate the replacement of the damaged entrance side. Thickness of the beam-pass area on the septum electrode was 0.8 mm for the entrance side, 1.6 mm for the central part, and 5 mm for the exit. The cooling water pipes between the two pieces were connected by a VCR[1)] tube fitting. Ten points of E-type thermocouple devices were mounted on the septum electrode for thermal interlock.

Figure 2 shows the results of the 3D heat transfer calculation for the original and the new septum electrode assuming turbulent forced convective heat transfer by cooling water. The range of both plots is from 0 °C to 1100 °C. For the original septum electrode, which is a simple flat plate, the maximum temperature was about 850 °C assuming 4.0 mm(height)×0.8 mm(thickness)×0.05 mm(range) uniform distribution of 300 W heat load at the entrance, and assuming the heat transfer coefficient of 20000 W/(m^2·K) on the inside of cooling water pipe. On the other hand, the maximum temperature was reduced to 670 °C for the new septum electrode assuming 500 W uniform heat load for the same dimensions and same heat transfer coefficient. For both cases, the peripheral temperature was set to 25 °C. The original septum electrode was replaced by the new one, and the old driving motors for the RRC-EDC were also changed to new stepping motors. The modified RRC-EDC was used for the machine time from the winter of 2013, including the RIBF experiment. No failure was found on the new septum electrode with about 4.5 kW of $^{238}U^{35+}$ beam and 1.6 kW of ^{48}Ca beam.

In order to extend the capability for further intensity growth, we have started to develop a mass-less septum electrode by arranging numerous thin tungsten ribbons. A test piece of a 50-μm-thick tungsten ribbon was irradiated by varying the intensity of $^{238}U^{35+}$ beam with an energy of 10.7 MeV/u provided by the RRC in November 2014 to investigate the melting boundary. The tungsten ribbon melted at an intensity of about 50μA. The result will be compared with the heat transfer calculation and the prototype septum electrode will be fabricated.

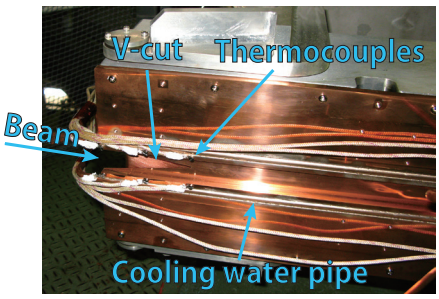

Fig. 1. New septum electrode with a V-cut entrance.

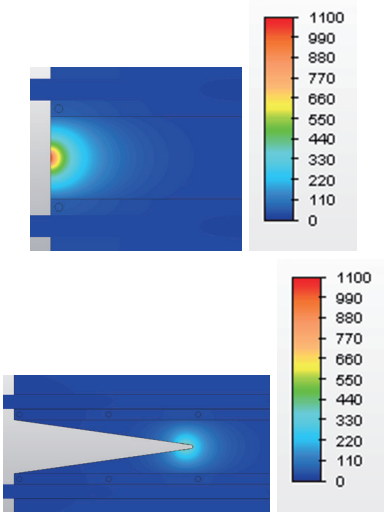

Fig. 2. Results of the 3D heat transfer calculation around the beam entrance side for the original (upper panel) and the new (lower panel) septum electrode.

*1 RIKEN Nishina Center
*2 SHI Accelerator Service Ltd.

References

1) Product of Swagelok Co.

Construction of new amplifiers for RILAC†

K. Suda,[*1] E. Ikezawa,[*1] N. Sakamoto,[*1] K. Yamada[*1] Y. Touch,[*2] T. Ohki,[*3] K. Oyamada,[*3] K. Kaneko,[*3] M. Tamura,[*3] H. Yamauchi,[*3] A. Yusa,[*3] and O. Kamigaito[*1]

RILAC consists of six variable frequency cavities (tanks) constructed in 1978[1]. The first amplifier was constructed in 1977 as a prototype for tank #1. Five other amplifiers were constructed the next year. The #5 and #6 amplifiers were upgraded in 1999 for experiments super heavy element synthesis. Three final-stage plate DC power supply (plate PS) were upgraded at the same time; one PS supplies DC voltage to two amplifiers.

In recent years, several issues related to amplifiers #1 to #4 were encountered, such as water leaks from cooling pipes and damages to the socket for the tetrode caused by insufficient contact. The contact between the socket and tetrode is shallow and a careful alignment is necessary. In particular, the design of the #1 amplifier was the oldest, so it became difficult to maintain it. Therefore, the amplifier #1 was upgraded in FY 2013 along with #2, because the plate PS was common for #1 and #2, and its control system had to be upgraded at the same time.

The new amplifier, as well as those for #5 and #6 are based on a tetrode RS2042SK coupled with a RS2012CJ from THALES/SIEMENS with a grounded grid circuit, that were originally designed for RRC[2]. The maximum RF signal of 0.01 W (10 dBm, 18 to 40 MHz) is amplified by pre-, driver- and, final-stage amplifiers up to 150 kW. In 14 years of operation of the RILAC #5 and #6, we have experienced several parasitic modes, which might damage the tank and/or the amplifier itself. One is caused by a coupled oscillation between the 99-MHz G1-G2 resonance of RS2042SK and the output circuit including a feeder line to the tank. The other example is the 7th harmonic mode observed in RILAC #5. In order to avoid such parasitic modes, a 50 kW dummy load was installed at a plate stub.

In a factory, matching conditions for input and output circuits of driver- and final-stage amplifiers were measured and/or tuned. (1) The gain of the input circuit for a driver amplifier called as "All Pass Network" was measured and confirmed to be sufficient. (2) An input circuit for the final amplifier was tuned by a vacuum variable capacitor (INCAP) and a movable shorting stub located at a cathode input. The following was performed after installation in an accelerator hall: (3) An output impedance of the final amplifier was matched by changing a plate stub and a capacitor (OUTCAP). Details are described in Ref.[3].

*1 RIKEN Nishina Center
*2 Sumitomo Heavy Industries
*3 SHI Accelerator Service Ltd.

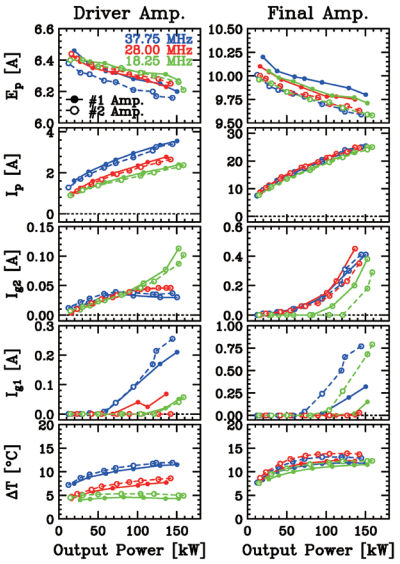

Fig. 1. Result of dummy load tests for two amplifiers (#1, #2). Voltages of plate (E_p), currents of plate (I_p), screen (I_{g2}) and control grids (I_{g1}), and the increase in temperatures of the cooling water (ΔT) for the driver and final amplifiers are shown.

The old amplifiers were removed in December 2013, and the new ones were installed in January 2014. Dummy load and power tests were performed in February 2014. In dummy load tests, a water-cooled 250 kW dummy load was connected to the output of the amplifier. It succeeded in obtaining an output power of 150 kW at three frequencies (Fig. 1). Then, load tests were performed at 36.5 MHz. The required acceleration voltages of RILAC #1 and #2 were successfully obtained. Beam service using the new amplifiers started on schedule on March 10th, 2014. A few problems occurred during operations. One was the leakage of cooling water from a rf power feeder of #1[4]. This was partly due to heating at the output flange of the amplifier. The parameters of the amplifier were tuned, so that the temperature of the flange decreased. The other problem was that an automatic tuning control system stopped its sequence abnormally. This happened in both amplifiers in some cases since May 2014. The PLC program was corrected in October 2014.

References

1) M. Odera et al., Nucl. Instrum. and Methods, 227, 187 (1984).
2) T. Fujisawa et al., Sci. Papers I.P.C.R. 80 (1985).
3) K. Suda et al., Proc. of LINAC14, MOPP12, 339 (2015).
4) E. Ikezawa et al., In this report.

Magnet system for a new beam transport line from IRC to E5 experimental room

K. Kumagai,[*1] N. Fukunishi,[*1] and S. Fukuzawa[*2]

We constructed a new beam transport line to provide high-energy beams accelerated by the IRC to the E5 experimental room in the Nishina building for biological experiments. The magnet system of the beam transport line was designed on the basis of the following factors: (1) For economic reasons, magnet power supplies were not produced, and existing power supplies were used by switching. (2) The new transport beam line was connected to the second half of the existing RRC to the E5 beam line. (3) As a part of the new beam transport line uses the existing IRC bypass beam line in the opposite direction, the beam line optics was designed to reduce the number of magnets that require polarity change. (4) In order to be able to switch a large number of magnets or magnet polarity with a simple procedure, nineteen switches assembled in two control panels were laid out in one place.

Figure 1 shows the layout of the new beam transport line. The magnet power supplies were prepared in the following way:

•The DAKR magnet (1500 A-26 V) used the old DC power supply previously used for the fRC-MIC2. As this power supply could operate at various currents and voltages, it was installed in front of the RRC room so that it could be utilized as a spare of the several power supplies for the RRC when it was not used for the DAKR.

•The polarity switches were added to the power supplies for DMR3, DMR4, and DMR5 dipole magnets on the bypass beam line.

•Three dipole magnets, DMR6, DMR7, and DMR8, were connected in series and excited by the old fRC main power supply removed in 2012 for the enhancement of the fRC.[1] The auxiliary power supplies built into the power supply were used for fine adjustment of the magnetic field of individual magnets. The transistor banks in the auxiliary power supplies had to be modified to match the output power of each magnet.

•As the maximum current (300 A) of the existing power supply for the DMD5 dipole magnet immediately before entering the E5 room was insufficient, the 420 A-150 V power supply for RIPS-Q11 was used by switching.

•Fourteen new quadrupole magnets used the power supplies for quadrupole magnets on the IRC-SRC transport line by switching. The cables from the power supplies were wired to the magnets on the new beam transport line and the IRC-SRC transport line through load switching panels.

•The first steering magnet right after the IRC named STR00 used the power supply for STK01 on the IRC-SRC transport line by switching.

•All magnets on the new beam line except STR00 used the dedicated 10 A-60 V power supplies controlled by a Linux-based PLC named F3RP61.

Boring for the wiring through experimental vaults and relocation of the power supplies were completed in 2013. Wiring and an operation test of the power supplies were performed in the summer of 2014. In December 2014, the polarity check and excitation test for the all magnets were performed. In January 2015, we planned to carry out the commissioning of the new transport line using the 160MeV/u ^{40}Ar beam.

At present, the switching of the dipole and quadrupole magnets and their polarity is performed manually. In FY2015, we plan to operate switching automatically using buttons.

References

1) K.Kumagai et al.: RIKEN Accel. Prog. Rep. 46, 132 (2012).

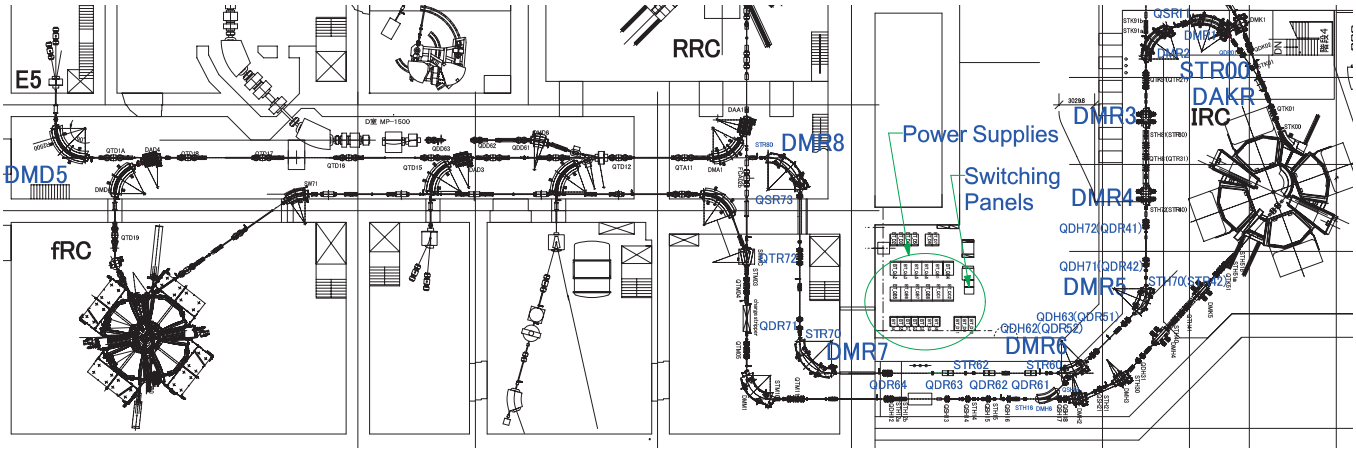

Fig. 1. Layout of the new beam transport line from IRC to E5.

*1 RIKEN Nishina Center
*2 SHI Accelerator Service Ltd.

Improved-flatness beryllium disk stripper for uranium acceleration at RIKEN RIBF

H. Hasebe,[*1] H. Okuno,[*1] H. Kuboki,[*1] H. Imao,[*1] N. Fukunishi,[*1] M. Kase,[*1] and O. Kamigaito[*1]

We have successfully provided a stable uranium beam during long-term operation in November 2012 (totally 1.18 × 10^{18} particles in 37 days) using a rotating beryllium disk stripper with a thickness of 0.1 mm as the second stripper. The number of irradiating particles and disk conditions are summarized in Table 1 along with those of other disks described below. This first used Be disk is denoted as Disk 1 in the Table. However, emittance growth due to the nonflatness of the disk exceeded the accepted levels for subsequent cyclotrons (IRC, SRC)[1].

To realize flatter disks, we prepared a Be disk subjected to diamond polishing (Disk 2) in March 2013[2]. Also, disk thickness was reduced from 0.1 mm to 0.085 mm, which was suited for the IRC injection energy. Therefore, transmission efficiencies of the IRC and SRC were improved. The Be disk was still usable even after the totally 9.29 × 10^{17} U-particle irradiation during the 30-day beam time operation[3].

Disk 2 was used again for the U beam time in March 2014. The lifetime of this disk ended and was determined to be additional 21 days (Fig. 1: Right). The total number of U beam particles was 1.68 × 10^{18} during 51 days (including 30 days in 2013) as written in Table 1. Many cracks were observed along the beam irradiation traces.

The Be disk was replaced with a new one (Disk 3), which was identical to Disk 2 (0.085-mm-thick, diamond polished), for the remaining beam time. Irradiation with an additional 8.83 × 10^{17} U particles was carried out in 17 days. Beam transmission efficiency was improved, but since the thermal load to the disk was increased from 90 W to 230 W because of the increased beam intensity, the disk was greatly deformed. The difference in the deformation is shown in Fig. 1 (Right: Disk 2, Left: Disk 3).

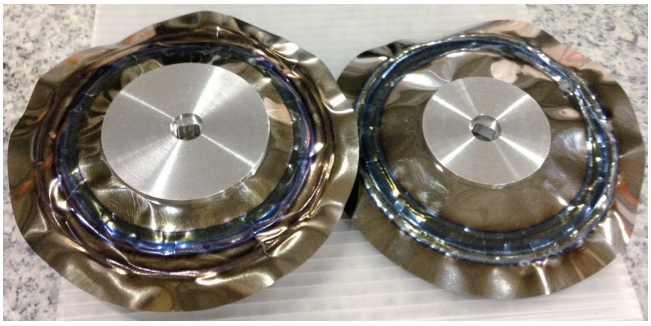

Fig. 1. Polished Be disks after irradiation (Right: Disk 2, Left: Disk 3).

*1 RIKEN Nishina Center

Table 1. Summary of four Be disk used.

	Irradiation current Total beam particle	Days	State
Be Disk 1 Not polish 0.1-mm thick	4 - 5 eμA 1.18x10^{18}	37	Many cracks Still usable Slight beam fluctuation
Be Disk 2 Diamond polish 0.085-mm thick	4 - 12 eμA 1.68x10^{18}	51 (30+21)	Distortion and Many cracks Not usable Slight beam fluctuation
Be Disk 3 Diamond polish 0.085-mm thick	12 eμA 8.83x10^{17}	17	Distortion, Slightly cracked Still usable No beam fluctuation
Be Disk 4 Diamond polish 0.085-mm thick Φ110mm Special processing	8 eμA 9x10^{17}	20	Slightly Distorted No crack Still usable No beam fluctuation

In October 2014, we introduced the Be disk with a special design[2] (Disk 4) to reduce the thermal deformation. Due to this improvement, this Be disk survived after the U beam time with approximately 9 × 10^{17} U-particle irradiation in 20 days. Main changes were as follows: 1) The outer diameter of the disk was 110 mm (from 120 mm), 2) 12 areas with cuts existed around the disk circumference, 3) the disk holder was made of copper (from aluminum) with an outer diameter of 65 mm, and 4) 12 holes with 2-mm diameter existed around the holder. Beam availability was further improved by the suppression of the beam fluctuation. The conditions of U beam irradiation are listed in Table 1 (Disk4). This Be disk is still usable and exhibits no problem. Figure 2 shows the special-design Be disk: (left) new and (right) after usage.

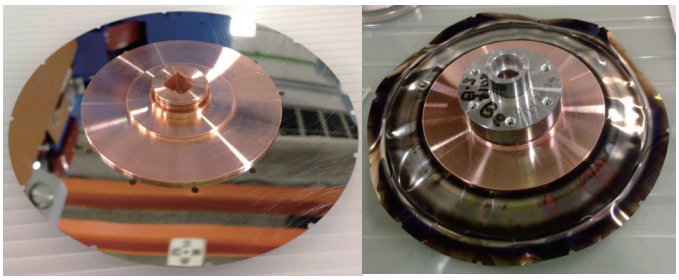

(a) (b)

Fig. 2. (a) New specially designed Be disk and (b) after irradiation. Deformation was moderated.

References

1) H. Hasebe et al., RIKEN Accel. Prog. Rep. **46**, 133 (2013).
2) PASCAL CO., LTD.
URL: http://www.pascal-co-ltd.co.jp/home.html
3) H. Hasebe et al., RIKEN Accel. Prog. Rep. **47**, 144 (2014).

Thinning effect of gas strippers for high-intensity very heavy ion beams

H. Imao,[*1] H. Okuno,[*1] H. Kuboki,[*1] O. Kamigaito,[*1] H. Hasebe,[*1] R. Koyama,[*1*2] and M. Kase[*1]

Intensity upgrade of very heavy ions beams, such as U and Xe beams, is one of the main concerns at the RIKEN Radioactive Isotope Beam Factory (RIBF). In the acceleration of the very heavy ion beams, the possible output intensities have been limited mainly by the lifetime problem of the carbon foil strippers. In previous years, the realization of gas strippers was an important breakthrough for the intensity upgrade of very heavy ion beams[1,2]. In order to achieve higher intensities of very heavy ion beams, we must understand the application limit of the gas stripper. Density reduction of the gas along the trajectories of the beams, caused by the heat load (thinning effect), is a factor determines the application limit of the gas stripper. To validate the thinning effect at the present intensities, we measured the velocities of the uranium beams after the stripper as a function of the beam intensities.

In the measurements, $^{238}U^{35+}$ beams up to 1-particle μA at 10.8 MeV/u were injected into the helium gas stripper placed after the RIKEN ring cyclotron. The arrival time of the beams before and after the stripper were measured using the phase probe. The measured time difference ($\propto$ gas density and gas temperature) depends on the output beam current, as shown in Fig. 1, where the beam current is changed with the duty of a beam chopper. For the higher beam current, the velocities of the output beams are higher because of gas density reduction due to higher heat deposition. The saturation of the time difference depends on the chopping frequency f, as shown in Fig. 1. The beam structure for the chopping frequency f is also shown in Fig. 1. A simplified differential equation for the temperature rise T is given as $dT/dt = Q/C - c_p\dot{m}/C$, where Q is the heat load of the beams, C is the heat capacity of helium, c_p is the specific heat of helium for constant pressure and $\dot{m}$ is the mass flow rate. At Q=0 (timing of beam off), the temperature reduces with the time constant $\tau = C/c_p\dot{m} = M/\dot{m}$. The saturation also depends on $\dot{m}$ in the beam region.

Figure 2 shows the dependence of the temperature rise of the helium gas stripper on the beam current. The chopping frequency was fixed with 1 kHz in these measurements. Although the temperature rise depends slightly on the beam profile, all measured values were lower than those expected from the calculations (dotted line) with flow-3D (computational fluid dynamics simulation software). A possible explanation may be some suppression mechanisms of heat on helium due to vacuum ultraviolet light emission from the excited helium atoms and molecules or energetic delta electrons emission.

In summary, we clearly observed the thinning effect of helium gas stripper by 1-particle μA uranium beams. Our results have important implications for lower heating efficiencies obtained with some suppression mechanisms.

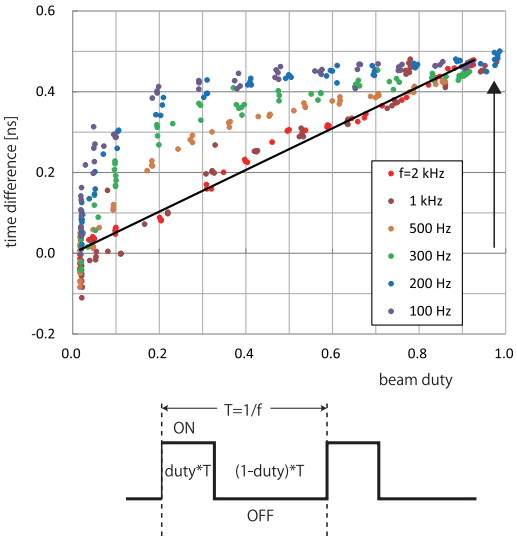

Fig. 1. The dependence of the arrival time difference on the beam duty for various chopping frequencies (up) and the beam structure of the chopped beam (down).

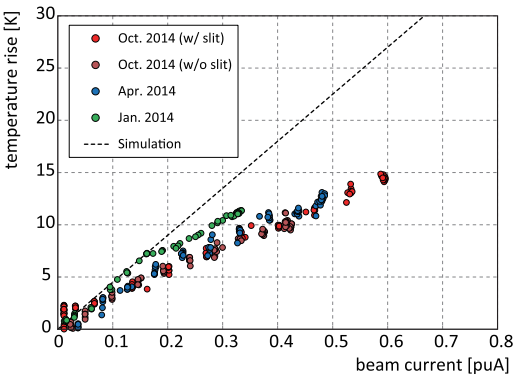

Fig. 2. Dependence of the temperature rise of helium on the beam current. Dotted line indicates the calculated values.

*1 RIKEN Nishina Center
*2 SHI Accelerator Service Ltd.

References
1) H. Imao et al., IPAC 2013, Shanghai (2013).
2) H. Imao et al., IPAC 2014, Dresden (2013).

Control and monitoring system of gas strippers

R. Koyama*1,*2 and H. Imao*1

We report on the control and monitoring system of a gas stripper, a new RIBF charge stripper using a gas target. A gas stripper has been developed as an alternative to a traditional carbon-foil stripper for increasing the intensity in very heavy ion beams such as uranium or xenon beams at the RIBF. A recirculating helium gas stripper[1] and an air stripper[2] are installed at the A02 site after the RRC and at the M04 site after the fRC (GS-A02 and GS-M04), respectively.

The schematic block diagram of their control and monitoring system is shown in Fig. 1.

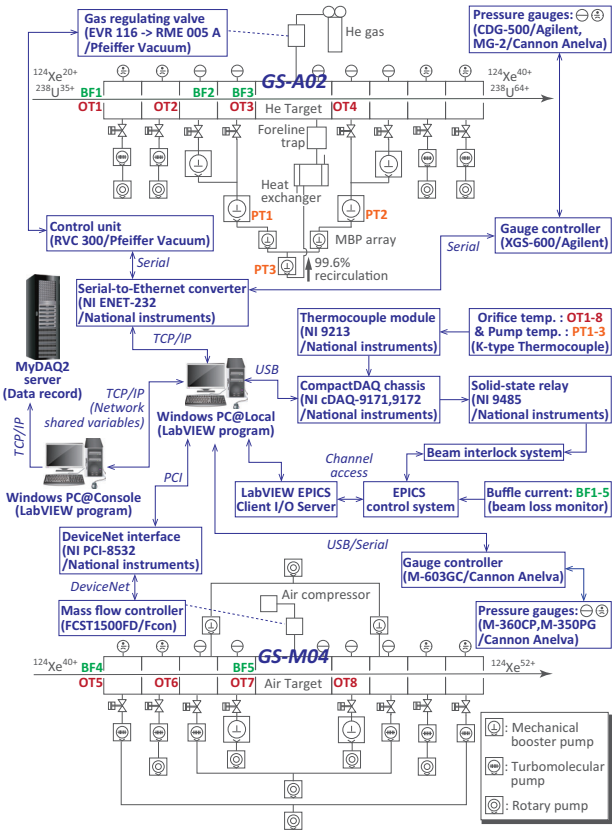

Fig. 1. Schematic block diagram of control and monitoring system for gas strippers.

We developed a user-friendly GUI program using the LabVIEW for the system, which includes the following:

- Remote control of the pressure and/or flow rate of the target gas
- Monitoring of the pressure of each differentially pumped section
- Monitoring of buffle current BF1–BF5 (beam loss monitor) via the EPICS control system[3,4]
- Monitoring of the temperature of orifices OT1–OT8 and mechanical booster pumps PT1–PT3
- Signal output to the beam interlock system in response to the monitoring value via the NI CompactDAQ
- Data recording to the MyDAQ2 system[3]

The developed system allows us to remotely optimize the target pressure of gas strippers with the assistance of the online beam monitoring system[5]. Figure 2 shows the correlation among the target pressure of GS-A02, beam timing, and beam intensity nondestructively observed by a phase probe (PP).

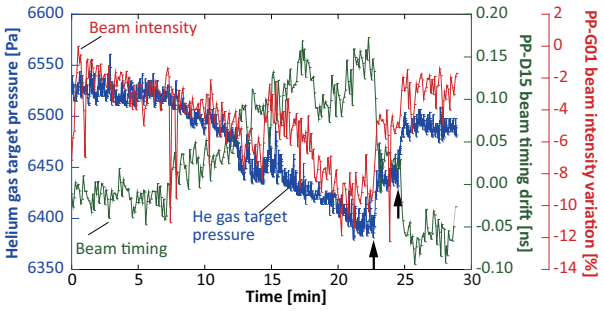

Fig. 2. Correlation among target pressure of GS-A02, beam timing, and beam intensity observed by the phase probe.

In this case, the beam timing at PP-D15 (31 m downstream of the GS-A02) gradually varied owing to the energy loss reduction in the GS-A02 as its target pressure decreased[6], resulting in a ∼10% decrease in beam intensity at PP-G01 (5 m downstream of the SRC). The beam intensity was recovered by twice fine controlling the target pressure by observing the beam monitoring system, as indicated by the arrows in Fig. 2. The pressure should be regulated with ±1% accuracy by the control unit, however, it got out-of-control at the end of the machine time, so we speculate that its accuracy was reduced owing to irradiation damage to the regulating valve EVR 116 near the GS-A02 in the RRC vault. EVR 116 has been replaced with radiation-proof RME 005 A.

*1 RIKEN Nishina Center
*2 SHI Accelerator Service Ltd.

References

1) H. Imao et al.: Proc. of IPAC2013, Shanghai, China, May 2013, THPWO038, p.3851 (2013).
2) H. Imao et al.: Proc. of IPAC2014, Dresden, Germany, Jun. 2014, THPME067, p.3388 (2014).
3) M. Komiyama et al.: Proc. of ICALEPCS2011, Grenoble, France, Oct. 2011, MOPKN005, p.90 (2011).
4) R. Koyama et al.: RIKEN APR **46**, 135 (2013).
5) R. Koyama et al.: Nucl. Instr. Meth. A **729**, (2013) 788.
6) H. Imao et al.: in this proceedings.

Beam Energy and Longitudinal Beam Profile Measurement System at the RIBF†

T. Watanabe,[*1] M. Fujimaki,[*1] N. Fukunishi,[*1] H. Imao,[*1] O. Kamigaito,[*1] M. Kase,[*1] M. Komiyama,[*1] N. Sakamoto,[*1] K. Suda,[*1] M. Wakasugi,[*1] and K. Yamada[*1]

Monitors with plastic scintillators as sensors (scintillation monitors) were fabricated to measure the energy and longitudinal profiles of heavy-ion beams at the RIKEN RI beam factory (RIBF). Six pairs of two scintillation monitors installed in the transport lines were used to measure the particle time-of-flight (TOF) between the paired monitors to determine the acceleration energy of the heavy-ion beams. The energy of the beam can be calculated from the measured TOF. In addition, five scintillation monitors were installed to measure the longitudinal profiles of the heavy-ion beams. Longitudinal beam profiles were obtained by using a time-to-digital converter (TDC), which digitizes the detected signals from the scintillator and the RF clock signal. Recently, to help users operate the system more easily, a new embedded processor with a higher-performance CPU has been introduced, and a new user interface has been constructed using the LabVIEW program.

For data acquisition and control of the scintillation monitors, we developed a ccompactPCI system that uses a Windows-based PC[1]. Signals from the detectors are amplified and converted to logic pulses by a constant-fraction discriminator. The TDC digitizes this pulse along with the RF clock and stores the events into the memory of the TDC. The TDC (TC890) has two memory banks based on a so-called ping-pong memory architecture that enables data readout while the module continues to acquire events. When a bank is ready to be read, an interrupt is generated, and the readout starts in the direct memory access mode.

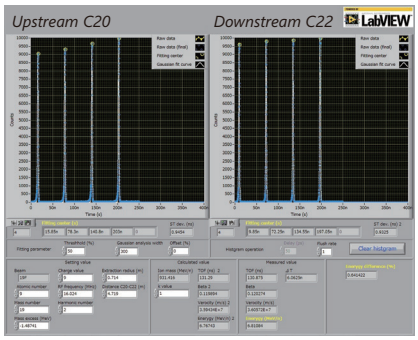

Fig. 1. Longitudinal profiles the $^{19}F^{9+}$ beam measured at C20 (upstream) and C22 (downstream) in the AVF cyclotron beam transport line as displayed on the graphical user interface.

† Condensed from the proceedings in 5th International Particle Accelerator Conference (IPAC'14)

*1 RIKEN Nishina Center

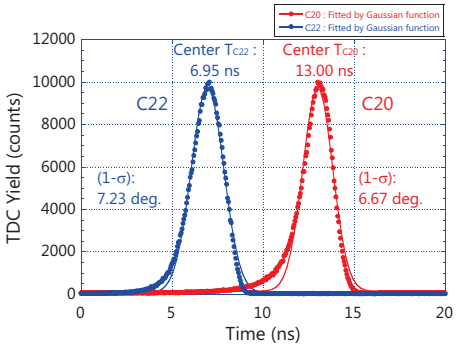

Fig. 2. Gaussian functions fit to the rightmost beam profiles at C20 and C22 in Fig. 1.

The programs for the data acquisition, control, and for showing results are written in LabVIEW (Windows7). The PCs are connected to a laptop in the main control room located 100 m from the Riken ring cyclotron (RRC) hall via Ethernet and remote desktop connection. The EPICS system controls insertion of the monitor into the beam line or its retraction from the beam line and it monitors these statuses.

We measured the energy of a $^{19}F^{9+}$ beam accelerated by the AVF cyclotron by using the TOF method. The $^{19}F^{7+}$ beam was used to produce element 105, ^{262}Db from a target of ^{248}Cm[2]. Because the sequential double pulse resolution was 15 ns, the $^{19}F^{9+}$ beam was attenuated to be under 1 M s^{-1} using beam attenuators. The longitudinal profile of the $^{19}F^{9+}$ beam was measured at C20 (upstream) and C22 (downstream) in the AVF cyclotron beam transport line were displayed on the graphical user interface as shown in Fig. 1. The rightmost longitudinal profiles obtained at C20 and C22 in Fig. 1 are expanded and plotted in Fig. 2. By fitting the profiles in Fig. 2 with Gaussian functions, we determined the center times T_{C20} and T_{C22} of the profiles and the longitudinal phase widths (1-σ), as shown in Fig. 2. The beam kinetic energy (T_{TOF}) obtained by measuring the TOF was 6.81 MeV/u. In addition, the beam kinetic energy ($T_{B\rho}$) can be determined by the magnetic field of the bending magnet that bends the $^{19}F^{9+}$ beam because the field was already known as a function of the exciting current. In this measurement, the hysteresis effect was not taken into account. The kinematic energy $T_{B\rho}$ was determined to be 6.80 MeV/u. These energies are in good agreement, with a difference between T_{TOF} and $T_{B\rho}$ of 0.1%.

References

1) T. Watanabe et al.: RIKEN Accel. Rep. **43**, 135 (2010).
2) M. Murakami et al.: RIKEN Accel. Rep. **47**, 265 (2014).

Maintenance and development of the RIBF control system

M. Komiyama,[*1] A. Uchiyama,[*1] M. Fujimaki,[*1] K. Kumagai,[*1]
N. Fukunishi,[*1] M. Hamanaka,[*2] and T. Nakamura[*2]

We report on the maintenance work and development of the RIBF control system, which include addressing a problem experienced with a beam interlock system (BIS),[1] upgrades for two types of control boards used for magnet power supplies and an extension of the control system to install a new beam transport line.

The RIBF control system consists of two parts according to the development of RIBF. One of them is used for the old facility, once called the RIKEN Accelerator Research Facility (RARF), which started its operation in 1986. The other is the new facility that started its operation in 2006. A BIS was developed to protect the hardware of the RIBF accelerator complex from unallowable beam losses for high-power heavy ion beams. The BIS is composed mainly of Melsec PLCs[2] that process many interlock signals, such as failure signals sent from rf systems used in our cyclotrons, magnet power supplies, and vacuum gate valves in beam transport lines, within 1ms. At the RIBF facility, there are two sets of BIS working for the old facility and the new facility as well as the control system. In 2014, we experienced for the first time a serious problem in which several interlock conditions were changed without any command inputs. After careful investigations, the cause of this malfunction, a failure of the CPU module used in the BIS, was rectified by replacing the existing CPU module with a spare one. Because the hardware used in the BIS is aging and the trigger of this malfunction is unclear, we prepared spare CPU modules in preparation for similar troubles in the future; this would be effective in reducing downtimes during RIBF operation.

The second topic is upgrades for the Network-I/O (NIO) system. The NIO is a commercially available control system manufactured by Hitachi Zosen Corporation. It is widely used to control many magnet power supplies used in the new facility and a part of the old facility. The NIO system consists of several types of controllers. The NIO-S board is directly attached to a magnet power supply and controls it according to a signal from an upper-level control system. About 500 NIO-S boards are used in RIBF. The NIO-C board works as a master board of NIO-S boards and is designed to run in VME computing machines. The NIO-C and the NIO-S are connected by an optical cable through a branch board. The existing NIO system has been working stably but production of the present NIO-S board was terminated because some parts are unavailable today. Therefore, we developed a successor of the existing NIO-S board in 2013 and this year we ran its performance tests. This successor was designed to be compatible with the existing NIO-S board but the performance tests revealed that some types of magnet power supplies cannot be controlled by the successor because the widths of some output pulses produced by the successor are slightly different from those given by the existing one. Currently, finding a solution to stably control these magnet power supplies is under consideration.

On the other hand, production of the NIO-C has also been completed for the same reason as in the case of NIO-S. Hence, we should also develop a successor board of the present NIO-C. Its R&D started in 2014. The specifications required for the new board are essentially the same as for the existing one, but we decided to design the new board to run in a control system constructed by PLC modules instead of the VME computing environment currently used, in order to achieve cost reduction and functional scalability. We started the design of its prototype in 2014, which is scheduled to be delivered in March 2015. Software developments required for the successor board are scheduled in 2015, where some new features will be added.

The third topic is extension of the control system to cover a new beam transport line now under construction, aiming at increasing the available beam energies in the existing beam irradiation port dedicated to biological experiments. The new beam line transports a beam extracted from the intermediate stage ring cyclotron (IRC) to the E5 experimental vault (hereafter, IRC-E5 BL). The control system for the IRC-E5 BL is constructed as a natural extension of the existing control system of the RIBF accelerator complex by adding the new components used in the IRC-E5 BL to the existing control system because no new types of components are installed in the IRC-E5 BL. Magnet power supplies are controlled by the NIO system and F3RP61,[3] which is a Linux-based PLC-CPU module manufactured by Yokogawa Electric Corporation, on which EPICS programs can be executed. Vacuum systems and beam diagnostic devices such as beam profile monitors are controlled using in-house controllers' Network Device Interface Module (N-DIM[4]) as well as the other beam transport lines of the RIBF accelerator complex. Regarding the beam interlock signals of the IRC-E5 BL, we incorporate them into BIS. Beam commissioning is scheduled in January 2015.

*1 RIKEN Nishina Center
*2 SHI Accelerator Service Ltd.

References

1) M. Kobayashi-Komiyama et al.: RIKEN Accel. Prog. Rep. 39, 239 (2006)
2)http://www.mitsubishielectric.co.jp/fa/products/cnt/plcq/items/
3) http://www.yokogawa.co.jp/rtos/Products/rtos-prdcpu9-ja.htm
4) M. Fujimaki et al.: RIKEN Accel. Prog. Rep. 37, 279 (2004)

Development of new operational log system for RIBF operation

A. Uchiyama,[*1] M. Komiyama,[*1] and N. Fukunishi[*1]

The operational log system is one of the electric log systems for recording and viewing the accelerator operation time and contents of an operated device. Zlog (Zope-based log system)[1] developed by KEK was utilized as the operational log system for the RIKEN RIBF control system. Zope is an open-source Web server and Web application framework written in Python programming language.[2] Using the Web application, information on accelerator operation is designated by a character string on Web browsers. However, the displayed string character on the Web browser will be complex for accelerator operators because many parameters are changed in accelerator operation, though the Web-based system has many advantages. For smoother accelerator operation, an ergonomically designed operational log system is required. Additionally, it is not always easy to set the many monitored parameters for Zlog without omission, because the user must code with Python programming language for one monitored parameter in the case of the Zlog system. Therefore, we developed a new operational log system for RIBF control system.

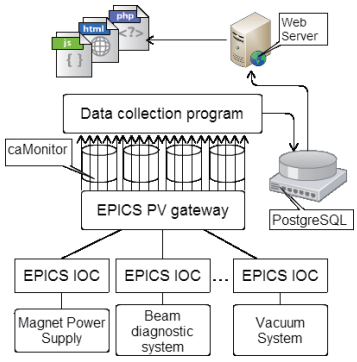

Fig. 1. Outline of the new operational log system.

In addition to the Zlog system, the PostgreSQL-based database, which is one of the major relational databases, is adopted for recording logs in the new operational log system. In order to ensure compatibility with Zlog, the new operational log system uses the same database table configuration as in Zlog. The system chart of new operational log system is shown in Fig.1. The RIBF control system consists of a distributed control system constructed using the Experimental Physics and Industrial Control System (EPICS).[3] Therefore, the feature to store the data into the database is developed on the basis of caMonitor, which is an event driven program using EPICS channel access (CA) protocol.

When the monitored operation status, such as the DAC value of a magnet power supply, is changed, the status is stored as operational information into the database. As one of the features, the monitor program acquires the event signal via the EPICS PV gateway[4] because EPICS input/output controllers (IOCs) require much system resources when a large number of caMonitors are connected to EPICS IOCs. In order to construct a Web application as the user interface for providing operational information, the Apache Web server and Bootstrap Web framework[5], are used by the system. Therefore, it is possible to provide operational logs with a variety of rich GUI components.

As of now, the operational log system has been working for accelerator operation by monitoring approximately 3,000 points as the EPICS record without any serious problem since November 2013. As an example, the user interface of the operational log for magnet power supplies is shown in Fig. 2. The operational log is displayed by using a character string and line chart on a Web browser (Firefox). In the near future, we will update the system for improving the usability to fully satisfy the requirements of users.

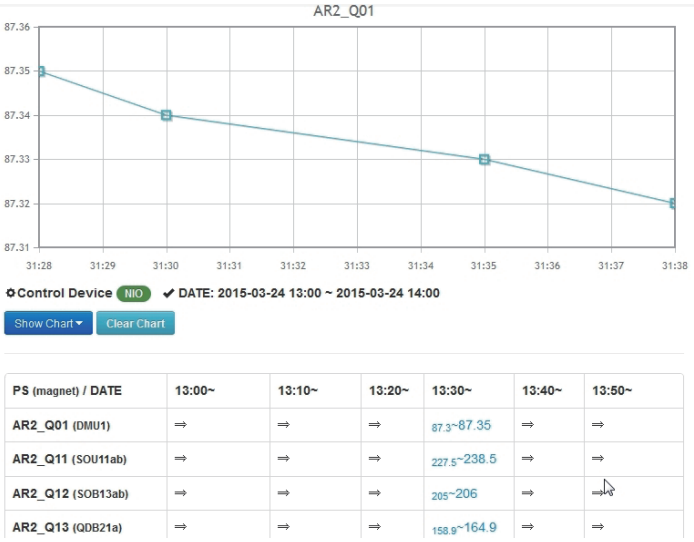

Fig. 2. User interface showing operational log for magnet power supply.

*1 RIKEN Nishina Center

References
1) K. Yoshii et al.: Proc. ICALEPCS07, (2007), p. 299.
2) http://www.zope.org/
3) M. Komiyama et al.: RIKEN Accel. Prog. Rep. 47.
4) K. Evans. Proc. ICALEPCS2005, (2005), PO1.033-6.
5) http://getbootstrap.com/

Commissioning of the Laser Ion Source for RHIC EBIS †

M. Okamura *1,*2 and T. Kanesue *1

The electron beam ion Source (EBIS)-based heavy ion preinjector (RHIC-EBIS) served for RHIC and NASA Space Radiation Laboratory (NSRL) at Brookhaven National Laboratory (BNL)[1]. The NSRL is a facility that simulates the effect of galactic cosmic radiation (GCR), which consists of highly energetic heavy ions of various kinds in space. The RHIC-EBIS is required to provide fast switching between heavy-ion species for this purpose. A new laser ion source (LIS), named "LION," is funded by NASA to expanding the range of ion species available for fast switching. Fast switching can be accomplished by switching the laser-irradiation position on different target materials[2,3].

LION consists of a high-power pulsed laser, a target chamber, a 3-m-long plasma drift region with a solenoid magnet, and an extraction chamber. The ion extraction voltage may be up to 40 kV. The laser is equipped with two identical Q-switched Nd:YAG laser oscillators (850 mJ/6 ns at FWHM, 1062 nm wavelength). A built-in laser combiner merges the two laser beams into one laser path to aim at the same position. The laser is focused on a solid state target plate. The laser spot on the target is 5 mm in diameter. Different laser energies in the range 500 ~ 700 mJ is used depending on the species to achieve singly charged ions. In a target chamber, several targets are held on a tungsten target holder, as shown in Fig.1, which is mounted on an x-y linear stage. The stage allows the laser to irradiate different positions on different target materials. The solenoid magnet is used to reduce the diverging angle of the expanding plasma. The typical magnetic field to be used is only several Gauss. With this drift length, an ion beam with a pulse width of a few hundred microseconds is achieved.

The commissioning of the beam was started on March 7, 2014 with an Fe target. LION was isolated from the EBIS beam line to prevent RHIC gold run as a precaution. The platform voltage was set to 12 kV for the first beam test. The Fe beam extracted from the LION was very close to what we expected. No breakdown caused by the generated plasma was observed.

From March 14, the operation mode of EBIS was adjusted for LION. The transport line and the EBIS injection timing were investigated to capture ions. The first beam extracted from the EBIS was observed on March 16.

On March 26, the first beam at the NSRL target room was observed with a Ta beam. The beam intensity was sufficiently high for an NSRL run. Hence, we decided to use the LION for an NSRL run.

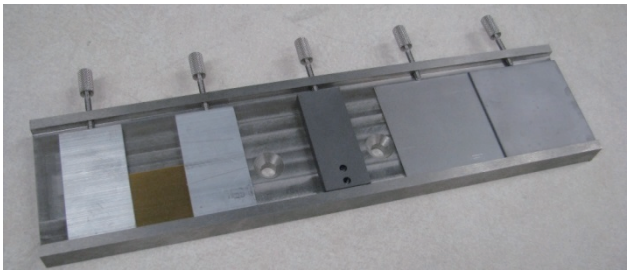

Fig. 1 Target holder with Au, C, Fe, and Ta targets from left to right. Aluminium plates are used to hold the Au target.

The user operation with LION was started from March 27, and it was very successful. Since then, LION has provided most of beams for NSRL. This is beyond our initial plan to use the LIS for several days for commissioning. After all, C, Si, Ti, Fe, Ta, and Au beams are provided for NSRL user runs.

As predicted, lighter species show less tolerance of the number of shots on a single spot to maintain long-term stability. The target scan step of 0.1 mm / 80 s was used for C while 0.1 mm / 540 s was used for Fe. These numbers are conservative and should be investigated further for efficient use of target materials.

The EBIS injection efficiency and the EBIS setting had been improved continuously. Since June 3, LION with a platform voltage of 18 kV started to provide Au beams for RHIC instead of providing beams for NSRL. Until the end of the run, LIS has been working continuously. The target scan step for the Au target was set at 0.5 mm / 20 s. The target was 1-mm thick with 25 mm x 25 mm area, and the target consumed approximately 50% of its life.

LION was used to provide C, Si, Ti, Fe, Ta, and Au beams for NSRL and RHIC user operation. This is the first LIS for low-charge-state ion production to be combined with an EBIS-type heavy-ion source for long term user operation.

References

1) J. Alessi et al., New York, 2011, p. 1966 (2011)
2) T. Kanesue et al., Rev. Sci. Instrum., 79, 02B102 (2008)
3) K. Kondo et al., Rev. Sci. Instrum., 81, 02A511 (2010)

† Condensed from the article in Proceeding of IPAC2014 (2000)

*1 Collider-Accelerator Department, BNL
*2 RIKEN Nishina Center

NISHINA RIBF water-cooling system 2014

T. Maie,[*1] K. Kusaka,[*1] M. Ohtake,[*1] Y. Watanabe,[*1] E. Ikezawa,[*1] M. Kase,[*1]
M. Oshima,[*2] H. Shiraki,[*2] K. Kobayashi,[*3] and J. Shibata [*3]

1. Operation condition

In the fiscal year 2014, the Nishina and RIBF water-cooling installation was operated for one hundred and fifty days and five months, respectively. These operation periods correspond to the scheduled beam service time of RIBF, which is five months. In addition, Nishina's cooling installation was used not only for the full RIBF operation but also for the AVF standalone operation, RILAC + RRC operations, RILAC2+ RRC operations, and AVF + RRC operations. During FY2014, there were no severe problems that caused beam service interruption for the Nishina and RIBF cooling water system. However, mind problems were often encountered, these are reported here.

2. Trouble report

Water leakage in the cooling system was a problem, particularly water leakage from a connection part of the flange portion and coupler in the cooling laying of the pipes. Another problem is the deterioration due to aging of the slack and the flange packing of the bolt by the vibration of the coolant pump, electrolytic corrosion, corrosion of the cooling plumbing is important. However, with the cooling facilities at the Nishina center, a water leakage sensor is attached to the outside of the accelerator and a beam line, the point of the cooling plumbing and, regardless of the whole stop, a member of driving of the accelerator discovers it easily while driving and comes to be able to cope. Other problems, include issues with the inverter, pressure gauge, and flowmeter, as well as problems with the packing of the coolant pump and damage of the mechanical seal; control is the main problem that occurred in 2014. In some cases, damage to the motor of the cooling tower fan occurred at snowy weight by the snow. Other factors affecting cooling facilities other than the above-mentioned problems include a affected by cooling facilities than a stop of steam and the cold water supplied from rolling blackouts and the cogeneration in the place. SRC and the Big RIPS He-refrigerator do not become if they do not always cool off, and it is necessary for pro-backup, to change the power supply and coolant beforehand to prevent one from being affected by a blackout and suspension of the water supply, which 2-3 times occurs in a year.

3. New establishment, improvement

Even during periodical maintenance, etc. when the accelerator is stopped, the RIBF cooling facilities have various new establishments and show, improved construction. It is built the cooling facilities for return beam lines as a representative thing by new construction sequentially from the year before last; As an example of the improved construction, I improved the cooling plumbing for the ability for cooling reinforcement pro-IRC and SRC exc. cooling and cooling reinforcement of SRC-MDC1 sequentially from last year.

4. Summary

I intend to minimize the problems associated with cooling facilities in future, while aiming for stable cooling facilities without problems, and suggesting the enforcement of effective maintenance, and undertaking premeditated deterioration measures.

References

1) T. Maie et al.: RIKEN APR .47
2) Y. Watanabe et al.: RIKEN APR .48

*1 RIKEN Nishina Center
*2 Nippon Kucho Service Co., Ltd
*3 SHI Accelerator Service Co., Ltd

Charge State Selective Ion Beam Acceleration Using the RFQ Linac

Y. Fuwa,[*1,*2] S. Ikeda,[*1,*3] T. Kanesue,[*4] M. Okamura,[*4] and Y. Iwashita[*5]

In the field of Heavy ion beam Inertial Fusion (HIF) [1], one of the promising ion species as the driver beam is Bi^{2+}. Considering a scenario based on the RF accelerator, a laser ion source with the Direct Plasma Injection Scheme (DPIS)[2] has the advantage to provide high-intensity heavy ion beams[3]. Ion charge states produced by laser ion sources has distribution[4]. With DPIS, all charge states of ions can be injected into an RFQ linac. However, in the case of Bi^{2+} production, Bi^{1+} and Bi^{3+} would also be injected. These unnecessary ions would waste RF power and/or cause unexpected radioactivation. Thus, charge-state-selective acceleration using the RFQ linac is desired. In this study, a scheme to achieve charge-state-selective ion beam acceleration is discussed.

In the case of accelerating ions with a charge state q and a mass number A different from the desired particle with q_0 and A_0, the condition for stable acceleration is described as below[5]:

$$\frac{q}{A}\cos(\phi_s) = \frac{q_0}{A_0}\cos(\phi_{s0}), \tag{1}$$

where ϕ_s is the synchronous phase of a particle with charge-to-mass ratio q/A, and ϕ_{s0} is that of the desired particle. Then, the condition of capture for the case of $A = A_0$ is

$$0 < \frac{q_0}{q}\cos(\phi_{s0}) < 1. \tag{2}$$

Usually, the synchronous phase of the the desired particle in the accelerating section of the RFQ linac is approximately $-30°$. Therefore, by choosing Bi^{2+} as the desired particle ($q_0 = 2$), Bi^{1+} ($q = 1$) has no stable phase and would not be accelerated, while unwanted Bi^{3+} will be accelerated. The results of a particle tracking simulation show that more than 30% of Bi^{3+} are captured and accelerated by a conventionally designed RFQ for Bi^{2+}.

One of the solutions to accelerate only Bi^{2+} is the following scheme: 1) The ions are injected into the RFQ with different momentums depending on charge state q. Using this initial momentum difference between Bi^{2+} and Bi^{3+}, these ions can be pre-bunched separately in the longitudinal phase space. 2) The modulation or acceleration voltage is raised when Bi^{2+} ions are in the acceleration phase and Bi^{3+} ions are in the deceleration phase, and Bi^{2+} ions would gain energy while Bi^{3+} ions would be decelerated. 3) Due to the energy difference between Bi^{2+} and Bi^{3+}, only Bi^{2+} ions would be captured in the RF bucket and be stably accelerated. To realize this scheme, we varied cell lengths in the bunching section. An example of the sequence of the designed cell parameters is shown in Fig. 1. Fig. 2 shows the particle tracking simulation results with the cell parameters shown in Fig. 1. The capture rate of Bi^{3+} could be suppressed by up to 3 %.

*1 RIKEN Nishina Center
*2 Graduate School of Science, Kyoto University
*3 Interdisciplinary Graduate School of Science and Engineering
*4 Collider Accelerator Department, Brookhaven National Laboratory
*5 Institute for Chemical Research, Kyoto University

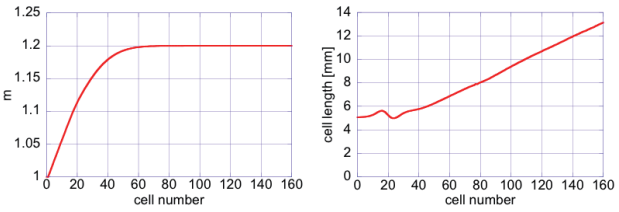

Fig. 1. Applied cell parameters versus cell number.

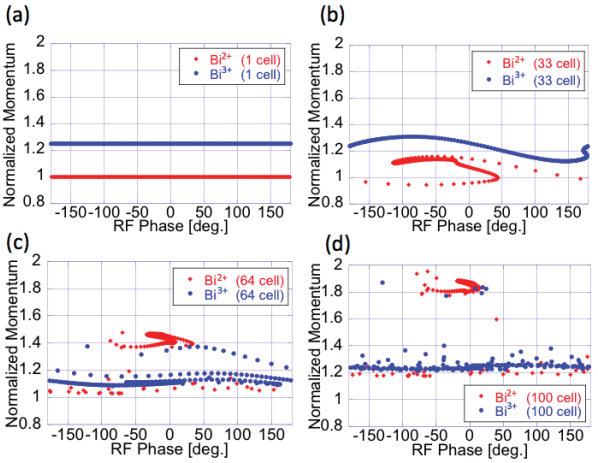

Fig. 2. Result of longitudinal phase space distribution. Red: Bi^{2+}, Blue: Bi^{3+}. The ordinate axis shows momentum normalized to Bi^{2+} initial momentum. The abscissa shows RF phase. (a) Initial distribution, (b) after pre-bunching, (c) after capturing Bi^{2+}, (d) after acceleration.

References

1) R. Burke, Nucl. Instrum. Methods Phys. Res., Sect. A 733 (2014) 158
2) M. Okamura et al., Rev. Sci. Instrum., 79 (2008) 02B314.
3) M. Okamura et al., Nucl. Instrum. Methods Phys. Res., Sect. A 733 (2014) 97.
4) K. Kondo et al., Rev. Sci. Instrum. 81, (2010) 02A511.
5) P. N. Ostroumov et al., Phys. Rev. ST Accel. Beams 3, 030101 (2000).

Investigation of the effect of solenoidal magnetic field on Fe plasma flux for application to laser ion source

S. Ikeda,[*1,*2] M. Okamura,[*3] and K. Horioka[*2]

Laser ablation plasma has been studied as a highly charged ion source for nuclear physics experiments[1] and as a high flux ion source for heavy ion inertial fusion,[2] and it is used as an ion source at Brookhaven National Laboratory[3]. In a typical configuration of the source, plasma flux at an extractor varies as a function of time. The time-dependent flux results in the changes in the ion beam current and its optics within a beam pulse. To prevent the changes, we propose to apply a pulsed magnetic field. Enhancement of the flux after passing through a static solenoidal magnetic field was observed[4]. The enhancement depended on the magnetic intensity. Therefore, if we apply the fast-rising magnetic field in accordance with the transient flux level of the plasma, we will be able to make the flux level flat.

To predict the optimal pulsed magnetic field, we first investigated the effect of a static magnetic field that was driven by quasi-stationary current during the plasma passing through the coil. We scanned a biased ion probe detecting plasma flux transversely or normal to the plasma drifting direction by applying a magnetic field.

Figure 1 is a brief schematic diagram of the experimental setup. A Nd:YAG laser irradiated an iron target with a pulse width of 6 ns and intensity of 4.0×10^8 W/cm^2. At this irradiation level, the laser mainly produces singly charged ions in the chamber evacuated to 4×10^{-4} Pa. The coil was driven by a pulse circuit. During the plasma passing through the coil, the decrease in magnetic flux density was less than 10 % and we can regard the magnetic field as almost constant during the interaction. A 2-mm-diameter aperture and

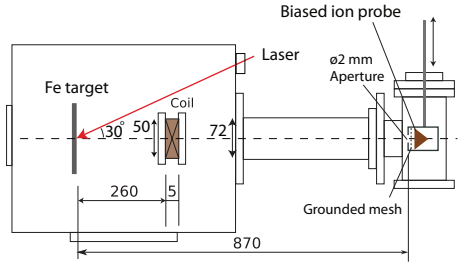

Fig. 1. Schematic of experimental setup for transverse scan of ion flux distribution

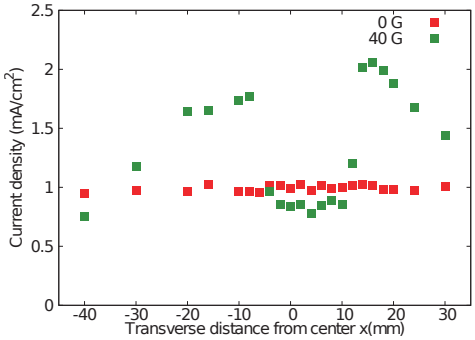

Fig. 2. Transverse flux distribution with and without magnetic field

a metal mesh whose transparency was 90.3 %, were grounded and placed in front of the probe.

Figure 2 shows the transverse distribution of plasma flux whose longitudinal velocity v_z is 14 mm/μs at 870 mm away from the target. v_z was estimated by division of the distance by the time of flight. Horizontal axis is the distance x from the center axis. Each point is an average of 3 data. The red squares are data with no magnetic field and green ones are in the presence of magnetic field. The magnetic flux density at the center of the coil is estimated to be 40 G using a simulation code(OPERA). When the magnetic field was applied, two peaks and decrease in the flux near the center axis were observed. The formation of two peaks around $x =$ -15 and 20 mm means that the plasma collected around the radius. The collection indicates that the magnetic field had focusing force that increases nonlinearly with increasing x. On the other hand, the decrease in the flux around the center ($x = 0$ mm) may mean that the magnetic field does not converge the plasma within a certain value of x. The difference in the magnetic field effect on the plasma with respect to x may result from the shape of the magnetic field. We need to investigate this difference in order to increase the ion flux with minimum emittance growth. The discussion of the enhancement mechanism will help optimize the parameters of pulsed magnetic field.

*1 RIKEN Nishina Center
*2 Interdisciplinary Graduate School of Science and Engineering, Tokyo Institute of Technology
*3 Collider Accelerator Department, Brookhaven National Laboratory

References

1) P. Fournier et al.: Nucl. Instrum. Meth. A, **71**, 924 (2000).
2) J. W. Kwan, IEEE Trans. Plasma Sci. IEEE Nucl. Plasma Sci. Soc., **33**, 1901 (2005).
3) T. Kanesue et al.: *Proceedings of IPAC2014, Dresden, Germany*, p 1890 (2014).
4) J. Wolowski et al.: Laser Part. Beams, **20**, 113 (2002).

9. Instrumentation

Operational status of the superconducting SAMURAI magnet

H. Sato,[*1] K. Kusaka,[*1] M. Ohtake,[*1] and T. Kubo[*1]

The first cooling down of the superconducting SAMURAI magnet[1] was done by TOSHIBA in April 2011, and we had maintained the operation of the cryogenic systems of the magnet. However, the magnet was warmed up in September 2013 in order to save the operation time of the cryocoolers[2]. Therefore, the magnet was cooled down again in February 2014 for the coming experiments. The cooling operation was performed by ourselves in order to save the cost.

Firstly, the pumping of the vacuum vessels of the cryostats was started. We waited for 8 days until the vacuum level reached 2×10^{-5} Torr. Secondly, the cooling-down procedure was started. The temperature of each point in the cryostat, excluding the coil, was monitored by thermometers. The temperature of the coil was monitored by measuring the resistance of the coil using the correlation shown in Fig. 1. Although the temperature below 9 K cannot be measured with this method, there is no problem for the cooling-down operation because the temperature of the coil vessel is also monitored.

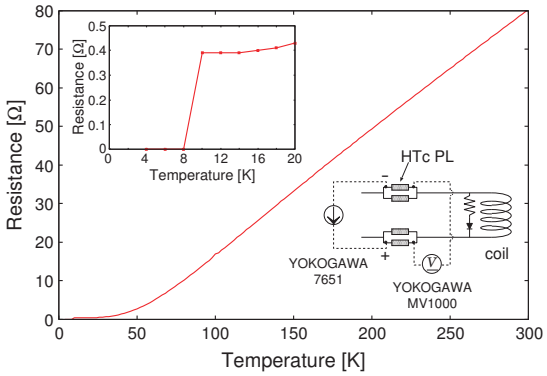

Fig. 1. Correlation between resistance and temperature of the superconducting coil. The upper and lower insets are an enlarged graph of below 20 K and a schematic diagram of the measurement of the resistance, respectively.

Figure 2 shows the trend of the temperature, pressure in the helium vessels, and liquid helium level. It took one month to complete the cooling-down operation, and 7,125 L of liquid nitrogen (LN_2) and 3,145 L of liquid helium (LHe) were used in total.

The graph of the lower coil exposes our inexperience of the cooling of the magnet. This led to imperfect removal of LN_2, resulting in the dissipation of LHe. However, we gathered technical know-how during the cooling-down procedure of the lower coil. (1) The cooling-down speed during LN_2 transfer should be around 10 K/h. (2) Special care must be taken when checking the residual LN_2. (3) The pressure of gaseous He should be 0.03–0.05 MPa when pushing and removing LN_2. (4) The coil vessels should be evacuated to be −99 kPaG before replacing the residual gaseous N_2 in the coil vessels with gaseous He. It takes about 30 min. (5) The position of the transfer tube in the service port is very important in order to transfer LHe without loss. (6) The pressure of gaseous He should be 0.03–0.05 MPa, and that of the LHe Dewar should be 0.028–0.034 MPa (4–5 psi) when transferring LHe. These were successfully applied to the cooling of the upper coil. In our next operation, the period of the cooling down will be shortened, and the amount of LN_2 and LHe will be reduced with the experience gained in this study.

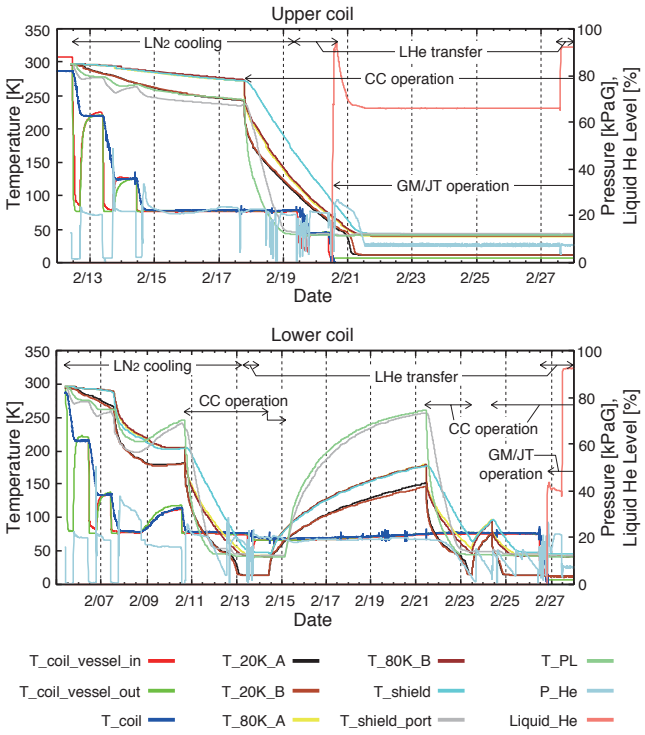

Fig. 2. Trend graph of the upper and lower coil during the cooling. T_ means the temperature of each part[1]. P_He means the pressure in the helium vessel. Liquid_He means the LHe level (100%≈240 L). The notation "CC" means 20 K, 80 K, PL cryocoolers, and "GM/JT" the GM/JT cryocoolers[1].

*1 RIKEN Nishina Center

References

1) H. Sato et al.: IEEE Trans. Appl. Supercond. **23**, 4500308 (2013).
2) H. Sato et al.: RIKEN Accl. Prog. Rep. **47**, 173 (2014).

Preparation status of the $(p, 2p)$ fission experiment with the SAMURAI spectrometer

S. Reichert,[*1,*2] M. Sako,[*2] M. Sasano,[*2] D. Mücher,[*1,*2] A. Andreyev,[*3] T. Aumann,[*4] H. Baba,[*2] M. Böhmer,[*1] M. Dozono,[*5] N. Fukuda,[*2] R. Gernhäuser,[*1] W. F. Henning,[*6] K. Hirose,[*3] N. Inabe,[*2] D. Kameda,[*2] N. Kobayashi,[*2] T. Kobayashi,[*7] Y. Kondo,[*8] T. Kubo,[*2] Y. Kubota,[*2,*5] R. Lang,[*1] L. Maier,[*1] Y. Matsuda,[*9] S. Mitsuoka,[*4] T. Motobayashi,[*2] T. Nakamura,[*8] N. Nakatsuka,[*9] S. Nishimura,[*2] I. Nishinaka,[*3] K. Nishio,[*3] R. Orlandi,[*3] H. Otsu,[*2] V. Panin,[*2] S. Sakaguchi,[*2] H. Sato,[*2] Y. Shimizu,[*2] L. Stuhl,[*2] T. Sumikama,[*2] H. Suzuki,[*2] H. Takeda,[*2] Y. Togano,[*2] T. Uesaka,[*2] J. Yasuda,[*2] K. Yoneda,[*2] and J. Zenihiro[*2]

The experiment NP-1306-Samurai14 is the first attempt at determining fission barrier heights for unstable nuclei like ^{212}Bi or ^{213}Po[1]. For this the missing mass spectroscopy of the two protons from the $(p, 2p)$ reaction in inverse kinematics provides a suitable method of determining the threshold for the fission barrier height unambiguously and directly. We report on the development status of the experimental setup for measuring the $(p, 2p)$ reaction using the heaviest projectiles.

The goal for the resolution power of the setup is to achieve an energy resolution of σ=1 MeV for the reconstructed excitation energy. The systematic uncertainty in the reconstructed missing energy should be less than 0.1 MeV. To realize this goal we need to measure the opening angle and energies of two emitted protons with resolutions of $\sigma_{\theta_{op}} < 3$ mrad and $\sigma_{E_p}/E_p < 2\%$.

The design of the $(p, 2p)$ setup is schematically shown in Fig. 1. The setup consists of a vacuum chamber containing a liquid hydrogen target and three layers of single-sided detectors on two arms with respect to the beam line. The reaction point and the emission angles of emitted protons are determined by the silicon detectors in connection with the beam trackers of the standard SAMURAI setup, BDC1 and BDC2. The setup has additional plastic scintillation detectors at a distance of 1.6 m from the target and outside the vacuum chamber to measure the time of flight (TOF) of protons in order to determine their kinetic energies.

We prepare two types of silicon detectors with the same dimensions of 51 × 78 mm; the first type (type A) is segmented to 768 strips parallel to the short side with a 100 μm pitch, whereas the other type (type B) has 498 strips parallel to the long side with the same pitch size as type A.

The three layers in one arm are structured in this way: The closest one to the target is type A, from which two sets of type A and B detectors are placed at a center distance of 10 cm to fit the solid angle coverage. They are mounted in parallel with the beam line as shown by the red lines in Fig. 1, aligning the shorter side of the detector vertically.

The type A and B detectors are used to determine horizontal and vertical positions of proton tracks, respectively. To meet the requirements on the opening angle and proton energy measurements, the thicknesses of the detectors must be thin as long as the signal-to-noise ratio in the charge readout of each strip allows a clear detection of protons. We aim at using 50 μm silicon detectors for the innermost layer and 100 μm ones for the others, to satisfy the requirements. At the end of 2014, 100 μm ones were ordered. A readout system based on the highly integrated APV25 chips[2] is currently set up for full system tests.

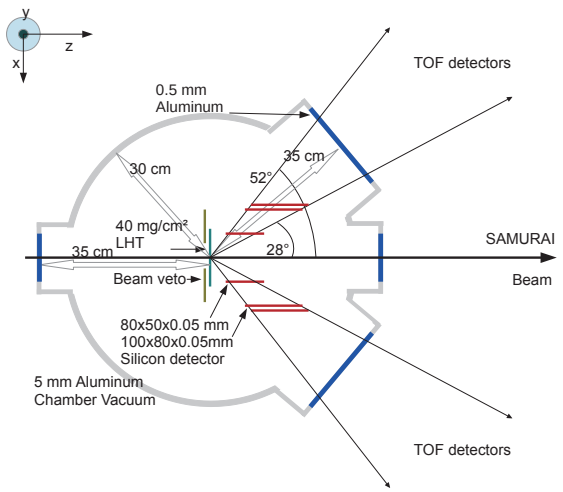

Fig. 1. Target chamber (top view) including three layers of one-dimensional silicon strip detectors on each side.

*1 Technical University Munich
*2 RIKEN Nishina Center
*3 ASRC JAEA
*4 Technical University Darmstadt
*5 Center for Nuclear Studies, University of Tokyo
*6 ANL
*7 Tohoku University
*8 Tokyo Institute of Technology
*9 Kyoto University

References

1) D. Muecher et al.: Proposal RIBF NP-PAC-12 *Fission Barrier Studies of Neutron-Rich Nuclei via the (p,2p) Reaction* (2013).
2) J. Lawrence et al.: *User Guide Version 2.2 for the APV25-S1* (2001).

Slow neutron detector WINDS for (p, n) reaction in inverse kinematics with SAMURAI

J. Yasuda,[*1] M. Sasano,[*2] R.G.T. Zegers,[*3] H. Baba,[*2] W. Chao ,[*2] M. Dozono,[*2] N. Fukuda,[*2] N. Inabe,[*2] T. Isobe,[*2] G. Jhang,[*2,*13] D. Kameda,[*2] T. Kubo,[*2] M. Kurata-Nishimura,[*2] E. Milman,[*2] T. Motobayashi,[*2] H. Otsu,[*2] V. Panin, [*2] W. Powell, [*2] M. Sako, [*2] H. Sato,[*2] Y. Shimizu,[*2] L. Stuhl,[*2] H. Suzuki,[*2] T. Suwat, [*2] H. Takeda,[*2] T. Uesaka,[*2] K. Yoneda,[*2] J. Zenihiro,[*2] T. Kobayashi,[*4] T. Sumikama,[*4] T. Tako,[*4] T. Nakamura,[*5] Y. Kondo,[*5] Y. Togano,[*5] M. Shikata,[*5] J. Tsubota,[*5] K. Yako,[*6] S. Shimoura,[*6] S. Ota,[*6] S. Kawase,[*6] Y. Kubota,[*6] M. Takaki,[*6] S. Michimasa,[*6] K. Kisamori,[*6] C.S. Lee,[*6] H. Tokieda,[*6] M. Kobayashi,[*6] S. Koyama,[*7] N. Kobayashi, [*7] H. Sakai,[*8] T. Wakasa,[*1] S. Sakaguchi,[*1] A. Krasznahorkay,[*9] T. Murakami, [*10] N. Nakatsuka, [*10] M. Kaneko, [*10] Y. Matsuda, [*11] D. Mucher, [*12] S. Reichert, [*12] D. Bazin,[*3] and J.W. Lee[*13]

In April 2014, we performed the SAMURAI17 experiment[1] at RIKEN RIBF to study Gamow-Teller transition on ^{132}Sn by using (p, n) reaction with the Wide-angle Inverse-kinematics Neutron Detectors for SHARAQ (WINDS)[2] and the SAMURAI spectrometer.

Figure 1 shows a schematic view of the experimental setup around the target. The secondary beam was transported to a 10 mm thick liquid hydrogen target, which was surrounded by the WINDS to detect recoil neutrons. From the measured neutron time-of-flight (TOF) and recoil angle, the excitation energy and center-of-mass scattering angle are determined.

The WINDS consists of 61 plastic scintillators with sizes of $600 \times 100 \times 30$ mm^3. In this experiment 12 scintillators of the ELENS[3] with sizes of $1000 \times 45 \times 10$ mm^3 were also installed. The left and right walls with respect to the beam line covered the angular region from 20 to 122 degrees with 5 degree steps. Top and bottom walls covered the angular region from 16 to 74 degrees with 3.5 degree steps. Each detector is placed such that the 30-mm-wide (WINDS) or 10-mm-wide (ELENS) plane is oriented to the target direction and placed at a distance of 900 mm (1200 mm) from the target for left and right (top and bottom) walls.

The charge signal from each PMT is digitized by a CAEN V792 QDC. The timing signal is processed by a leading-edge discriminator (LeCroy 4413) and digitized by CAEN V1190 TDC. In order to maintain a low threshold of neutron detection, the PMT voltage is kept to be as high as possible, typically -2700V and -2500V for H7195 and H7415. The threshold for light output in the scintillator was set to be 70 keV proton energy.

The timing resolution of WINDS bar was estimated by using prompt γ ray from the liquid hydrogen target. The timing reference was taken from the plastic scintillators SBT1,2 whose timing resolution is typically 40 ps in FWHM. The observed peak width of the prompt γ ray was 800 ps in FWHM which is most due to the timing resolution of WINDS. This timing resolution corresponds to energy resolution of $\Delta E/E = 11\%$.

The neutron-detection efficiency depends on the energy of neutrons as well as the threshold on light output. The typical efficiency with a threshold of 60 keV$_{ee}$ was estimated by using the Monte Calro code of MCNP[4], and it varied from 40% at 0.6 MeV neutron to 20% at 4 MeV neutron. The efficiency calibration was performed by locating a neutron source of ^{252}Cf at the target position with a NE213 liquid scintillator whose absolute efficiency as well as energy and threshold dependence are well known. The data analysis is currently in progress.

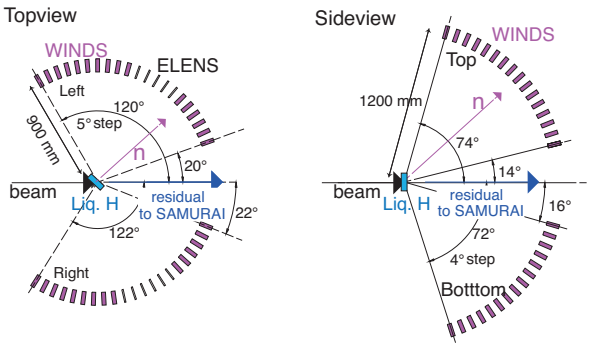

Fig. 1. A schematic view of the WINDS setup.

*1 Department of Physics,Kyushu University
*2 RIKEN Nishina Center
*3 NSCL Michigan State University
*4 Department of Physics, Tohoku University
*5 Tokyo Institute of Technology
*6 CNS, University of Tokyo
*7 University of Tokyo
*8 ULIC, RIKEN Nishina Center
*9 MTA, Atomki
*10 Kyoto University
*11 Konan University
*12 Technical University Munich
*13 Department of Physics, Korea University

References

1) M. Sasano *et al.*,: in this report.
2) K. Yako *et al.*, RIKEN Accel. Prog. Rep **45**, 137 (2012).
3) L. Stuhl *et al.*, Nucl. Instr. Meth. A 736, 1 (2014).
4) Monte Carlo NParticle Transport Code System, MCNP5-1.60 and MCNPX-2.7.0.

Integration of GET system for SπRIT-TPC

T. Isobe,[*1] M. Kurata-Nishimura,[*1] H. Baba,[*1] N. Nakatsuka,[*2] T. Murakami,[*2] W.G. Lynch,[*3] J. Barney,[*3] J. Estee,[*3] S. Tangwancharoen,[*3] G. Jhang,[*4] W. Powell,[*5] and Y. Ayyad,[*6] for the SπRIT Collaboration

A Time Projection Chamber (TPC) has been produced as the main detector of the SAMURAI-SπRIT project for the study of the nuclear equation of state using heavy ion collision experiments[1]. As the readout system for the SπRIT-TPC, we have integrated the Generic Electronics for TPC (GET) system[2], which was developed mainly by a France and USA collaboration[3]. For the integration of GET electronics, development of interfaces in terms of both hardware and software are necessary.

Since the GET system was developed for general usage, the interface of the GET electronics to a TPC depends on the specifications of each detector, such as connector types and the signal characteristics of the detector, and this interface has to be developed for each project. We call such an interface a ZAP board, which serves as an adapting connector between the GET electronics and the TPC, as well as providing protection for the electronics. Thus GET electronics can be mounted on any TPC by just making the ZAP board. There are several requirements for designing the ZAP board. In the case of SπRIT-TPC, the board was designed to fit in the space on the TPC which is supposed to be installed in the SAMURAI chamber, to reduce the noise in order to increase the dynamic range, and to reduce the distortion of gain among the different channels. It is especially important to reduce noise since it strongly affects the electrical treatments of a signal. Here the electrical treatments of each signal are: 1. hit pattern register which is made by the discriminator on each signal after the pre-amplification, 2. internal trigger which is made with the hit pattern register, and 3. zero-suppression of digitized signal. The quality of the internal trigger strongly depends on noise level, which is strongly affected by the design of the ZAP board.

To satisfy our requirements, prototypes of several types of interface boards were made and the above requirements were checked quantitatively by using the minimum GET system composed of CoBo+AsAd+ZAP boards. The AsAd board is for the amplification and digitization of an analog signal[3]. The AsAd must be installed near the TPC in order to reduce noise. The CoBo board is for handling the trigger, controlling the AsAd and managing data[3].

To fit the AsAd board on the SπRIT-TPC within the limited vertical space of ∼17 cm, a prototype flexible ZAP made of a thin Cu plate (10 μm) and polymide (12.5 μm) was first made. The noise level of the flexible board, which can be estimated through RMS of pedestal, is not small. This is most likely due to the large capacitor made by the noise shield and signal line (50∼100 pF/ch). The capacitance of each signal line can be roughly calculated as a plane parallel plate capacitor. Ultimately it was decided to use a ZAP board made of conventional rigid electric board which has a short signal line and small capacitor on each signal line of 10∼20 pF/ch. The achieved noise level is 4 ADC under the configuration of a dynamic range of 12 bit, 120 fC and a shaping time of 233 nsec. It can be reduced to be 2∼3 ADC after the subtraction of a fixed noise pattern (FPN) line which is not connected to TPC pads. Without this ZAP, the GET electronics exhibit and average noise level of 3 ADC. This noise level is small enough for the SπRIT experiment, and so the production of ZAP has started and the mounting of GET electronics on the TPC is ongoing.

The user of the GET system is not only responsible for the interface to their TPC, but they must also integrate or develop the DAQ. For the SπRIT project, NARVAL[4] is planned to be employed as the DAQ system. By employing NARVAL, large amounts of data of more than 100 MByte/sec from SπRIT-TPC can be handled. The development of an interface to send data from Babirl to NARVAL is being developed so that raw data from Babirl can be merged with data from GET system by using NARVAL.

We have performed a test experiment using the GET system on another TPC with the final ZAP at HIMAC during November 2014. NARVAL was not used in this test experiment. The analysis result of the test experiment is reported by G. Jhang in this APR. In the test experiment, we took benchmark test data of the GET system. We read out 756 channels with a sampling rate of 25 MHz and 256 time buckets. A partial readout mode using the hit pattern register was used to increase the data acquisition rate as much as possible. A data acquisition rate of 600 Hz and a data rate of 1 GByte/min were achieved, which is sufficient for the first experiment of SπRIT project.

*1 RIKEN Nishina Center
*2 Department of Physics, Kyoto University
*3 National Superconducting Cyclotron Laboratory, Michigan State University
*4 Department of Physics, Korea University
*5 Department of Physics, University of Liverpool
*6 Research Center for Nuclear Physics, Osaka University

References

1) S. Rebecca et al.: Physics Procedia **37**, 1799 (2012).
2) T. Isobe et al.: RIKEN Accel. Prog. Rep. **46**, 151 (2014).
3) E. Pollacco et al.: Physics Procedia **37**, 1799 (2012).
4) X. Grave.: Proc. 14th IEEE NPSS RT Conf, 65(2005).

Performance evaluation of GET readout electronics for heavy ion collision experiments at RIBF

G. Jhang,[*1,*2] T. Isobe,[*2] M. Kurata-Nishimura,[*2] T. Murakami,[*3] M. B. Tsang,[*4] S. Hasegawa,[*5] K. Hosomi,[*5] S. Hwang,[*5] H. Sugimura,[*5] J. Brzychczyk,[*6] B. Hong,[*1] P. Lasko,[*6] J. Lukasik,[*7] W. G. Lynch,[*4] P. Pawlowski,[*7] Z. Sosin,[*6] and S. Tangwancharoen[*4] for the SπRIT Collaboration

GET(Generic Electronics for TPCs)[1] will be used as the front-end readout electronics for the newly constructed SπRIT-TPC(SAMURAI pion Reconstruction Ion-Tracker Time Projection Chamber)[2]. The GET electronics has been recently developed by the GET collaboration for the particle and nuclear physics experiments and its performance is yet to be evaluated. We performed a test experiment at the Heavy Ion Medical Accelerator in Chiba(HIMAC) facility using the BRAHMS-TPC(TPM1)[3] to evaluate the performance of the GET electronics. The TPC has the multi-wire configuration similar to the SπRIT-TPC: anode wires for signal multiplication, gating grid wires to reduce the background noise.

We used 300 AMeV ^{132}Xe beam with 500 mg/cm^2 CsI target surrounded with the multiplicity trigger array of 60 scintillator plastics. To evaluate the resolution in both wire and drift directions, in the first setup the BRAHMS-TPC(TPM1) was placed at 60 degrees off the beam axis and we took data with different sampling rate of 5, 10, 25, 50, 100 and 200 MHz and shaping time of 70, 232, 502 and 1014 ns. Due to breakdown of the μ-TCA power supply, only one AsAd board(256 channels) is used in this configuration.

In the second setup the BRAHMS-TPC(TPM1) was located at 0 deg. We replaced the broken power supply and took data with three AsAd boards(768 channels) controlled by a full CoBo(Control Board for 4 AsAd boards). We tested the gating grid drivers with beam intensities varying from 10^2 to 10^5 pps. We placed five 3 mm thick Al plates in front of the TPC to stop the beam and heavy fragments so that only the light charged particles with $Z < 3$ can reach the TPC at the intensity 10^4 and 10^6 pps. Finally, with beam intensity 10^4 and 10^5 pps we took data under the SπRIT-TPC experimental condition: sampling rate of 25 MHz, shaping time of 232 ns, 256 time buckets(10.24 μs), and zero suppression mode.

Figure 1 shows the preliminary result in the first setup. The resolution is presented as a function of the layer numbers, where one layer means a row of 96 pads perpendicular to the beam axis and the BRAHMS-TPC has 12 layers. To obtain the resolution we selected three successive layers and calculated the difference between the hit position on the middle layer and the average position of hits on the first and the third layers assuming that the resolution of each pad is the same as δx. For example, $x = 0$ means the resolution is calculated with the layer number 0, 1, and 2 by accumulating $x_1 - (x_0 + x_2)/2$ values for all events. By the error propagation the RMS value of the distribution, σ, and the resolution, δx, have the relation: $\sigma = \sqrt{3/2}\delta x$.

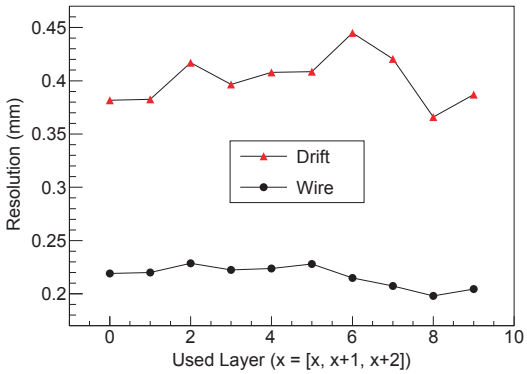

Fig. 1. Resolution of the wire and drift direction as a function of the layer number x, which is the first layer number among three layers.

Table 1. Resolution from two collaborations

Collaboration	Direction	
	wire (μm)	drift (μm)
BRAHMS	310	427
SπRIT	217±10	401±22

Comparison between the result from both collaborations is summarized in Table 1. Our result is better because the GET electronics is 12 bit ADC while the BRAHMS collaboration used 10 bit ADC.

Further analyses in the second setup are ongoing.

*1 Department of Physics, Korea University
*2 RIKEN Nishina Center
*3 Department of Physics, Kyoto University
*4 National Superconducting Cyclotron Laboratory and Department of physics and Astronomy, Michigan State University
*5 Advanced Science Research Center, Japan Atomic Energy Agency
*6 Jagiellonian University
*7 Institute of Nuclear Physics PAN

References

1) E. Pollacco *et al.*: Physics Procedia **37** (2012) 1799.
2) R. Shane *et al.*: Nucl. Instr. and Meth. A **784** (2015) 512.
3) M. Adamczyk *et al.*: Nucl. Instr. and Meth. A **499** (2003) 437.

Status of SπRIT-TPC

M. Kurata-Nishimura,[*1] R. Shane,[*2] A. McIntosh,[*3] T. Isobe,[*1] J. Barney,[*2] J. Estee,[*2] G. Jhang,[*1*4] W. Powell,[*5] W.G. Lynch,[*2] M.B. Tsang,[*2] T. Murakami,[*6] S. Tangwancharoen,[*2] S.J. Yennello ,[*3] for SπRIT-TPC collaboration

The SAMURAI Pion-Reconstruction and Ion-Tracker Time-Projection Chamber (SπRIT-TPC)[1] was constructed at Michigan State University and transferred to RIKEN RIBF-SAMURAI in February 2014. The main aim of this project is to constrain the symmetry energy term in the nuclear-matter equation of state (EoS) at supra-saturation density. The SπRIT-TPC is capable measuring the momentum of pions and light particles emitted in heavy nuclear collisions, such as ^{132}Sn + ^{112}Sn at beam energies of hundreds of MeV/nucleon.

In summer 2014, an installation procedure for the SπRIT-TPC into the SAMURAI magnet chamber was developed and verified. The SπRIT-TPC is designed to maximize the coverage in the SAMURAI magnet chamber. The internal height of SAMURAI chamber is designed to be 800 mm. Bolts, covered by 25 mm high caps, surround the magnet pole on top and bottom to prevent the chamber from crushing due to the pressure difference when the chamber is under vacuum. On the other hand, the design height of the SπRIT-TPC is 742 mm and thus there is a very small margin of error for installing it into the SAMURAI chamber. Thus the confirmation of the installation is one of the most important issues in this project. Also confirmation of safe operation in the magnetic field is critical.

The setup for installation of the SπRIT-TPC in the chamber is shown in Fig.1. In this figure, the SAMURAI magnet was oriented at 30 degrees, it is most common experimental configuration. However, the SpiRIT TPC was designed to sit inside the SAMURAI magnet chamber when it is oriented at zero degree. To test the installation procedure without expending a lot of resources to reconfigure the SAMURAI magnet, the SπRIT-TPC was inserted from one half side of the exit window with the oblique angle. Rails placed in the chamber extended toward the downstream window where additional rails were located on tables. The SπRIT-TPC was set on a slider which moves along rails with negligible friction. It was able to be pushed and pulled in the chamber using dual hydraulic jacks. When the SπRIT-TPC was installed inside the chamber, it was raised up about 25 mm to the beam height. Installing and dismounting the SπRIT-TPC was completed in about 20 minutes.

An operational test in the magnetic field was also performed. Before hand, all magnetic material items on the SπRIT-TPC were removed. The read out electronics described in Ref.[2] were set up. Finally, charged particle tracks of cosmic rays and beta source were detected in a magnetic field ranging from 0.1 to 0.5 T. Figure 2 shows a part of a helical track produced by a cosmic ray was observed within the detection area read out by one AsAd electronics board.

Furthermore, a remote controlled target ladder was mounted inside the TPC-enclosure. The target position is determined by reading the voltage drop between the fixed and movable contacts on a resistive strip.

The overall geometry and position of the field cage and the target ladder relative to the enclosure were measured using photogrammetry[2]. The deviation from the design value was evaluated as less than 200 μm.

In summary, significant progress on the preparation for the SπRIT-TPC experiment has been achieved.

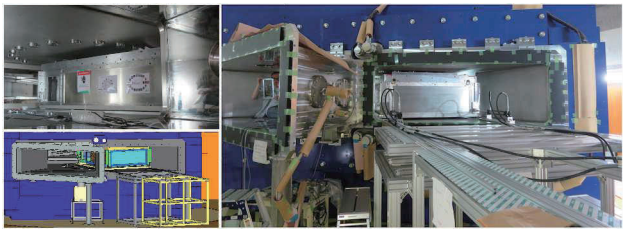

Fig. 1. Picture of the SπRIT-TPC inserted into the SAMURAI chamber. Left top: picture in the chamber. Left bottom: schematic view of the installation method.

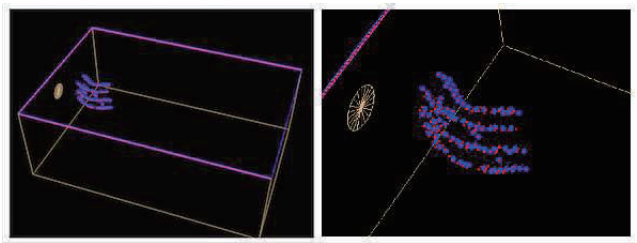

Fig. 2. Event display for a cosmic ray detected by the SπRIT-TPC in the SAMURAI magnet at 0.3 T. Enlarged view of the track is on the right.

*1 RIKEN Nishina Center
*2 National Superconducting Cyclotron Laboratory and Department of Physics and Astronomy, Michigan State University
*3 Cyclotron Institute, Texas A&M University
*4 Department of Physics, Korea Universtiy
*5 Department of Physics, University of Liverpool
*6 Department of Physics, Kyoto University

References

1) R. Shane at al.: Nucl. Instr. Meth. A **784** (2015) 513.
2) http://www.geodetic.com/products/systems/v-stars-s.aspx
3) T. Isobe et al.: in this report.

Test of prototype crystals of the γ-ray detector CATANA

Y. Togano,[*1,*2] M. Shikata,[*1] T. Ozaki,[*1] Y. Kondo,[*1,*2] and T. Nakamura[*1,*2]

The γ-ray detector CATANA (**CA**esium iodide array for γ-ray **T**ransitions in **A**tomic **N**uclei at high isospin **A**symmetry) has been developed to measure γ ray associated with highly excited states like the pygmy dipole resonance and/or giant dipole resonance. CATANA will be used with SAMURAI at RIBF.[1] The excitation energy will be reconstructed by combining the invariant mass of the reaction products measured by SAMURAI and γ-ray energies from CATANA.

The CATANA array consists of CsI(Na) crystals and has between 10 and 15 cm thickness. The crystals are housed in 0.5-mm-thick aluminum boxes. The photosensors for the scintillation light from the crystals are the photo multiplier tubes (PMTs) R580 and R11265 from Hamamatsu Photonics. A detailed description of CATANA can be found in ref.[2].

The position dependence of light collection efficiency can be significant for the crystals of CATANA, because the crystals have relatively large volumes. We have tested the position dependence of the light collection efficiency of the prototype CsI(Na) crystals by using γ rays from ^{137}Cs, ^{22}Na, and ^{60}Co sources. The geometry of the tested crystals is shown in Fig. 1. To evaluate the position dependence, the collimated γ rays irradiated the crystals from a direction perpendicular to the $x-z$ plane defined in Fig. 1. The collimator was a 10 cm thick lead with a 1-cm-diameter hole. The test was performed for two crystals from different companies. The two crystals have almost identical geometry. We tentatively name the two crystals as A and B in this report. Figure 2 shows the typical response of the crystals A and B to the uncollimated 511 and 1275 keV γ rays from ^{22}Na. Crystal A has a better energy resolution than crystal B. The position dependence of the light collection efficiency along crystal length z of the crystals A and B to the γ rays from ^{22}Na is shown in Fig. 3. The light output of the crystal B is larger at larger z. This tendency is due to the optical focusing caused by the reflection of lights at the polished surface of crystal B[3]. To obtain a better position dependence and energy resolution, changes in the reflectivity of the crystal A surfaces were realized by roughening the crystal surfaces.

The fabrication of the CsI(Na) crystals for CATANA will start in spring 2015, and finish in late 2015.

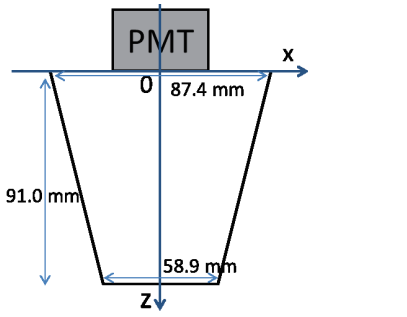

Fig. 1. Geometry of the tested prototype crystals. The definition of the axis in the test is also shown. PMT was attached to the top of the crystals.

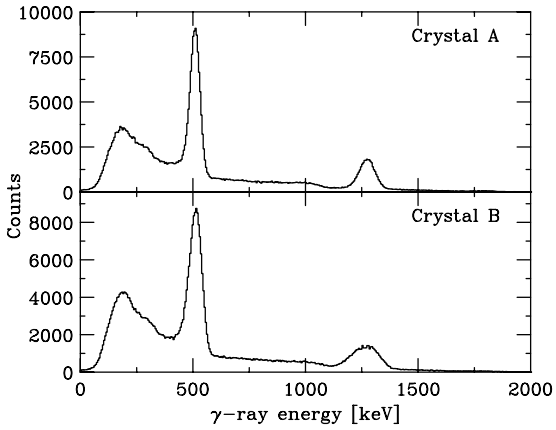

Fig. 2. Typical response of the crystals to the ^{22}Na source.

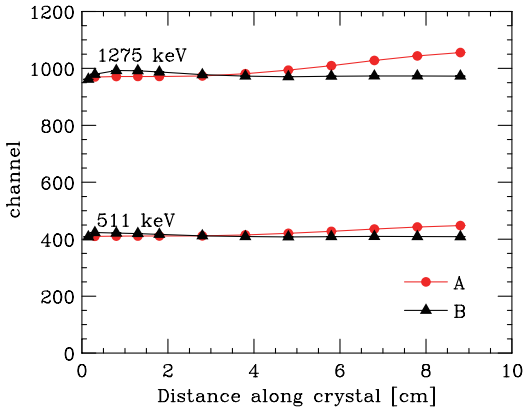

Fig. 3. Position dependence of the light collection efficiency for the crystals A (red) and B (black) along the crystal length z. Crystal B shows larger position dependence of the light collection efficiency.

*1 Department of Physics, Tokyo Institute of Technology
*2 RIKEN Nishina Center

References

1) T. Kobayashi et al.: Ncul. Instrum. and Meth. B **317**, 294 (2013).
2) Y. Togano et al.: RIKEN Accel. Prog. Rep. **47**, 179 (2014).
3) J. Bea et al.: Nucl. Instrum. and Meth. A **350**, 184 (1994).

Isotope separation with new ion-optics mode

H. Takeda,[*1] T. Kubo,[*1] N. Fukuda,[*1] H. Suzuki,[*1] N. Inabe,[*1] and H. Geissel[*2]

Two-stage structure is an important feature of the in-flight fragment separator BigRIPS.[1)] The first stage, which consists of two dipoles (D1 and D2) and four superconducting triplet quadrupoles (STQs) (STQ1-4), is located between the production target F0 and achromatic focus F2 with the momentum dispersive focus F1. The second stage, which consists of four dipoles (D3-D6) and eight STQs (STQ7-14), is located between the achromatic foci F3 and F7 with the momentum dispersive foci F4, F5, and F6. The stage between F2 and F3, which consists of two STQs (STQ5-6), acts as a matching section. Rare-isotope (RI) beam is produced and separated in the first stage with an energy-loss degrader at F1, and particle identification and momentum analysis are performed in the second stage.[1,2)] Another energy-loss degrader placed at F5 is often effective when unwanted isotopes are transmitted as a result of the charge state change or the secondary reaction in the first degrader at F1. The thicknesses and shapes of the degraders at F1 and F5 are chosen so as to optimize the RI beam according to the experimental requirements.

The two stages act independently and their isotopic separation power can be added or subtracted, depending on the experimental condition. When the separation powers of the two stages are subtracted, the horizontal spatial distance of the separated isotopes becomes small at the final focus F7. Adding the isotopic separation powers of the two stages would increase the horizontal spatial distance. Because widths also increase, improvement of the final resolving power will depend on the experimental condition.

The ion-optical solution for adding the separation power can be realized by having either one or three foci in the matching section F2-F3, which have two foci (F2 and F3) in the standard mode. At least one focus in the standard mode is abandoned in the former case. It is not desirable because both F2 and F3 are important for slits and diagnostics of the RI beam. Therefore, here we present the solution having three foci.

Figure 1 shows the horizontal (X) and vertical (Y) tracks of the beam from F0 to F7 obtained from the solution of the first-order ion-optical calculation. In this solution, ion-optical conditions of the two stages (F0-F2 and F3-F7) are the same as the ones in the standard mode. Only the matching section F2-F3 is modified to have an additional focus in the X direction at the midpoint "F2.5" between F2 and F3, while the beam is not focused in the Y direction at F2.5 to reduce excitation

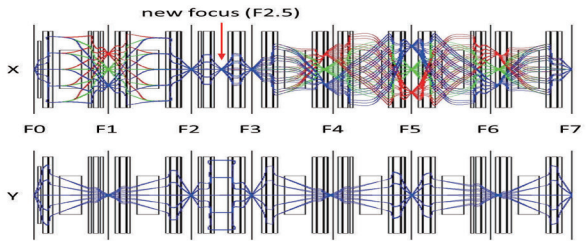

Fig. 1. Horizontal (X) and vertical (Y) tracks of the beam in the new mode.

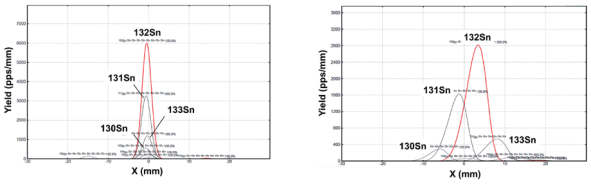

Fig. 2. Comparison of tin isotope distribution at F7 between the standard mode (left) and new mode (right) simulated with LISE^{++}.

currents of STQ5 and STQ6. Reversing the polarity of all quadrupoles of the two STQs is also necessary to reduce the currents. The maximum magnetic rigidity ($B\rho$) of 8.7 Tm is achieved in this solution. The value is almost the same as the maximum $B\rho$ of the second stage (8.8 Tm). There is a trade-off between achieving high $B\rho$ and large acceptance.

Figure 2 shows an example of horizontal distributions of tin isotopes at F7, simulated by LISE^{++}, in a ^{238}U + Be 4 mm reaction at 345 MeV/nucleon using 3 mm- and 2.2-mm-thick aluminum degraders at F1 and F5, respectively. The spectrometer is tuned for ^{132}Sn with D1 $B\rho = 7.49$ Tm. The left and right panels show the results in the standard and new modes, respectively. In the standard mode, all isotopes accumulate in the center ($X = 0$) because of the subtraction of the separation power. In contrast, the isotope separation is improved in the new mode.

Note that the difference between the two modes is small for separation of isotones because they often collect at approximately the same position at F2. Altering the combination of energy and degrader thickness is required for isotone separation.

A machine study for the new ion-optical mode proposed here had been scheduled in November 2014, but was cancelled. We expect to perform this study in the next year.

*1 RIKEN Nishina Center
*2 GSI Helmholtzzentrum für Schwerionenforschung GmbH

References

1) T. Kubo: Nucl. Instr. Meth. **B204**, 97 (2003), T. Kubo et al.: Prog. Theor. Exp. Phys. **2012**, 03C003 (2012).
2) N. Fukuda et al.: Nucl. Instr. Meth. **B317**, 323 (2013).

A NaI(Tl) detector array for measurements of γ rays from fast radioactive isotope beams †

S. Takeuchi,[*1] T. Motobayashi,[*1] Y. Togano,[*2] M. Matsushita,[*3] N. Aoi,[*4] K. Demichi,[*5] H. Hasegawa,[*5] and H. Murakami[*1]

The recent development of fast radioactive ion (RI) beams requires a new type of γ-ray detector array for in-beam spectroscopic studies. Experiments are performed in inverse kinematics by using fast RI beams with a high velocity of $v/c \simeq 0.3 - 0.6$ that causes a large Doppler shift for γ rays emitted. In order to extract the transition energy in the rest frame of the projectile, precise measurements of emission angles of γ rays as well as a good intrinsic energy resolution are required. Another requirement for γ-ray detection is high efficiency, because the secondary-beam intensity for nuclei far from stability is typically low. The RIKEN RIBF provides the world's highest intensity exotic beams to study unstable nuclei. To capitalize on the performance of RIBF, we have constructed a new γ-ray detector array called DALI2 (Detector Array for Low Intensity radiation 2) for in-beam γ-ray spectroscopy experiments.

The design of the DALI2 array follows a concept similar to the original array DALI[1,2], which was developed for experiments at the old facility at RIKEN that provides light exotic beams with $v/c \simeq 0.3$. In experiments performed at the new RIBF facility providing higher-velocity exotic beams with $v/c \simeq 0.6$, the performance of DALI is not optimized. Therefore, DALI2 was designed to fulfill the required conditions for experiments performed at the RIBF facility by improving the angular resolution and the detection efficiency. In order to compromise on requirements such as intrinsic resolution, detection efficiency, and cost, we adopted NaI(Tl) as the detector material. The DALI2 array consists of a large number of detectors, 160-186, which, depending on the experimental conditions, are at various distances from the target. As shown in Fig. 1, the detectors are arranged to form twelve layers that are set perpendicularly to the beam axis, and a detector matrix covers the forward angles. Each layer consists of 6-14 detectors and the forward matrix consists of 64 detectors. In this standard configuration, DALI2 can cover a polar angle between 15° and 160°.

The performance of DALI2 was examined by using measurements with standard γ sources and by performing the Monte Carlo simulations with the GEANT3 code[3]. Simulations reproduce measurements well, including results obtained by in-beam experiments. A typical full-energy-photopeak resolution of 10% (FWHM) and 20% efficiency are achieved for 1-MeV γ rays emitted from moving nuclei with $v/c \simeq 0.6$ without applying add-back analysis. This resolution is satisfactory for spectroscopy of low-lying states in even-even nuclei. The high efficiency enables γ-γ coincidence measurements even for beam intensity as low as 1 Hz. The DALI2 array has been applied successfully to a variety of experiments at the old RIKEN facility and more recently at the new RIBF facility. This will be used in many more experiments to study nuclear structures of exotic nuclei at RIBF. For further spectroscopic studies of heavy or odd-mass nuclei, the SHOGUN array with superior energy resolution is planned[4].

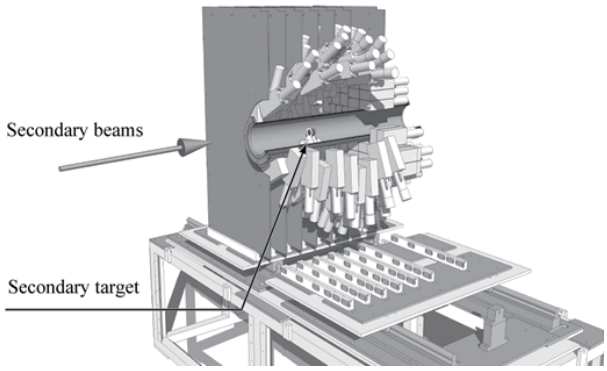

Fig. 1. Schematic view of DALI2 in its standard configuration consisting of 186 NaI(Tl) crystals.

References

1) T. Motobayashi *et al.*: Phys. Lett. B **346**, 9 (1995).
2) T. Nishio *et al.*: RIKEN Accel. Prog. Rep. **29**, 184 (1996).
3) GEANT3, CERN Program Library Long Writeup W5013, 1993.
4) P. Doornenbal *et al.*: RIKEN Accel. Prog. Rep. **42**, 182 (2009).

† Condensed from the article in Nucl. Instrum. and Methods in Phys. Res. Sect. A, **763**, 596 (2014)

*1 RIKEN Nishina Center
*2 Department of Physics, Tokyo Institute of Technology
*3 CNS, University of Tokyo
*4 RCNP, Osaka University
*5 Department of Physics, Rikkyo University

Development of a total-kinetic-energy counter for high-rate experiments at ZeroDegree spectrometer

R. Taniuchi,[*1,*2] H. Wang,[*2] N. Aoi,[*3] H. Baba,[*2] S. Koyama,[*1,*2] M. Kurokawa,[*2] M. Matsushita,[*4] S. Momiyama,[*1,*2] M. Niikura,[*1] Y. Shiga,[*2,*5] and S. Takeuchi[*2]

A total-kinetic-energy (TKE) counter for particle identification at the ZeroDegree (ZD) spectrometer was tested in 2014. The detector is aimed at the discrimination of not fully stripped ions for the mass region $A \gtrsim 100$. For example in the case of ^{136}Sn (RIBF31), the mass-to-charge ratios (A/Q) of ^{133}Sn^{49+} and ^{136}Sn^{50+} are similar and the resolution of A/Q obtained by the TOF−Bρ−ΔE method is not sufficient to separate them. In order to separate the fully stripped ions from the neighboring charge-state contaminants, the TKE counter is required to have the mass resolution of 1% (FWHM).

Considering the beams with high counting rate (∼100 kcps), the counter should have a short decay time and radiation resistance. For this purpose, a ø3″ LaBr$_3$(Ce) scintillator[a] with a 0.5-mm^t aluminum housing is prepared[b]. It is mounted downstream of the F11 multiple sampling ionization chamber (MUSIC). In previous studies[1–3], the feasibility of charge-state identification using this scintillator was tested. The mass resolution was not as good as 1% (FWHM). Simultaneously, a quenching phenomenon was observed [3], namely, the light yield per energy deposition of the incident beam decreased as a function of Z. To obtain higher resolution, the degree of the quenching phenomenon should be known for the optimization of the amplification factor of the light readout.

In 2014, two types of light readouts were tested. For the first case (tested in the experiments RIBF31R1 and DA14-01-01), five PIN-photodiodes (S3204-08, HPK) were aligned on the downstream surface of the scintillator[4]. For the second setting (tested in the experiments RIBF61, RIBF51R1 and RIBF56R1), the readout consisting of a ø3″ PMT (R6091HA, HPK) and a tapered-type divider (E5859, HPK) were coupled with the scintillator. In this report, the result of the second setting is discussed.

During three experiments, the amplitudes of the signal of the PMT were measured using an oscilloscope with several high-voltage (HV) settings. The ZD spectrometer were set for ^{132}Sn (20.8 GeV), ^{70}Ni (15.2 GeV), and ^{22}O (5.21 GeV)[c], for the respective

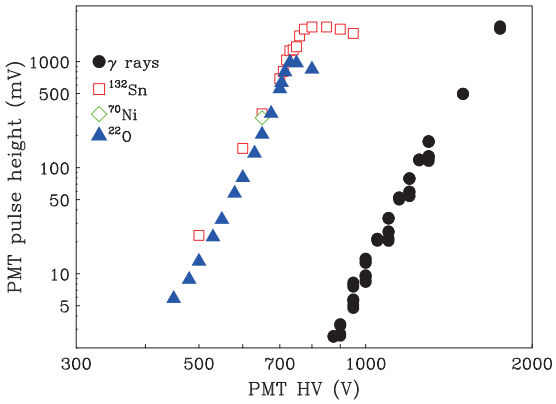

Fig. 1. Amplitude of the PMT output with several HVs for each ZD spectrometer settings.

Table 1. Signal amplitudes per unit energy.

Particle	Amplitude (mV/GeV)	Quenching factor[d]
γ/δ-ray	124	1
^{22}O	40	0.32
^{70}Ni	19	0.16
^{132}Sn	15	0.13

experiments. Figure 1 shows the signal amplitudes as a function of applied HV for different isotopes. For reference, data of γ-ray calibration before and after the experiment with ^{22}Na, ^{60}Co and ^{137}Cs sources are also plotted. They are normalized by the energy of the γ-ray, namely, the amplitudes per 1 MeV.

For the ^{132}Sn and ^{22}O settings, owing to the frequent implantation rate (∼40-100 kcps) and high light yield, the PMT output was saturated with overcurrent of the divider circuit when the HV value was above 700 V. On the other hand, the slopes below 700 V are similar to the one of γ-ray. This ensures that the PMT has linearity even for the lower operation voltage.

By extrapolating the γ-ray results to the lower-voltage region, the light yield of the scintillator is compared with heavy ions. The values in the center column of Table 1 are the signal amplitudes per the kinetic energies when the HV is set at 650 V. The quenching phenomena of the light yield are observed obviously.

According to this result, optimum gain of the PMT can be discussed. A new divider circuit designed from this result will be tested in 2015.

References

1) Yuta Hara, Master thesis, Rikkyo University, 2010.
2) Riyato Kambayashi, Master thesis, Rikkyo University, 2011.
3) Kota Kobayashi, Master thesis, Rikkyo university, 2012.
4) He Wang *et al.*, *in print.*

*1 Department of Physics, the University of Tokyo
*2 RIKEN Nishina Center
*3 Research Center for Nuclear Physics, University of Osaka
*4 Center for Nuclear Study, the University of Tokyo
*5 Department of Physics, Rikkyo University

a) Saint-Gobain BrilLanCe^{TM} 380
b) LaBr$_3$(Ce) is known to have a light decay time around 16 ns.
c) The kinetic energies of heavy ions are deduced from the $B\rho$ values of the last dipole of ZD spectrometer.
d) the ratio of the signal amplitudes per energies of heavy ions to that of γ-ray.

Low-pressure MWDC system for ESPRI experiment

Y. Matsuda,[*1,*2] J. Zenihiro,[*2] W. Chao,[*2,*3] H. Sakaguchi,[*2,*4] J. Tanaka,[*4] M. Tsumura,[*2,*5] and N. Nakatsuka[*2,*5]

Elastic scattering of protons with RI beams (ESPRI) has been used to study the ground-state properties of unstable nuclei[1]. In order to achieve good energy resolution in the experiment, position and angular resolutions of 100 μm and 0.1 mrad are required at a position of the solid hydrogen target. The typical energy and intensity of the beam are 200-300 MeV/nucleon and 10^{5-6} particles per second (pps), respectively. This report describes a multi wire drift chamber (MWDC) system newly constructed for this purpose.

Figure 1 shows a schematic layout of the system, and Table 1 shows the specification of the MWDC. Two MWDCs are installed inside a vacuum chamber at a distance of 1 m. Through the SHV connectors, negative potentials are applied to the cathode planes and the potential wires against the anode wires. Signals from the anode wires are converted into LVDS signals by the ASDs (GND, GNA-210), and fed to multihit TDCs.

The chamber including the MWDCs, with volume of about 25 L, is filled with 100% quench gas (CH_4, C_2H_6, i-C_4H_{10}) at low pressures to reduce multiple scattering of the beam. Figure 2 shows a schematic diagram of the gas handler system. The pressure of the gas is controlled with a pressure controller (MKS, 640B), and measured with two vacuum gauges (INFICON, CDG025D-X3). The flow rate is adjusted with a metering valve (Swagelok, SS-4MG / SS-4L).

Basic characteristics of the system were evaluated with a ^{132}Xe beam at HIMAC. Figure 3 shows the detection efficiency as a function of the bias voltage when i-C_4H_{10} (99.5%) was used at 6666 Pa. Definition of symbols in Fig. 3 is the same as in Ref. 3. The flow rate was about 100 cc/min at 1 atm to maintain the purity of more than 99%. The efficiency reached 100% without any electric discharge. In addition, position resolution for each plane was about 60 μm (rms).

In summary, we constructed a low-pressure MWDC system. By using the ^{132}Xe beam and the i-C_4H_{10} gas, basic characteristics were evaluated for the beam intensities of 10^{3-4} pps. We will further study these quantities for the beam intensities of 10^{5-6} pps.

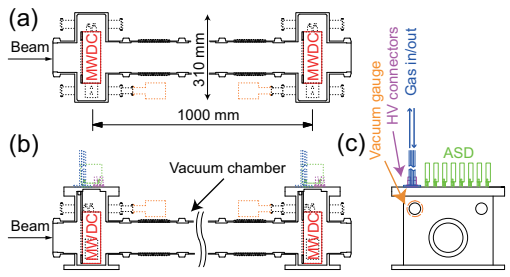

Fig. 1. Schematic layout of the MWDC system: (a) vertical sectional, (b) cross sectional, (c) front views.

Table 1. Specification of each MWDC. The design was based on the MWDC for SAMURAI[2].

Configuration	X-X'-Y-Y'-X-X'-Y-Y'
Effective area	77.5 mm(X) × 77.5 mm(Y)
Drift length	2.5 mm (Anode-Potential)
Gap	$4.8^{+0.0}_{-0.1}$ mm (Cathode-Cathode)
Anode wire	W-Re / Au (Diameter: 16 μm)
Potential wire	Al / Au (Diameter: 80 μm)
Cathode foil	Kapton / Al (Thickness: 7.5 μm)
Window foil	Aramid (Thickness: 4 μm)

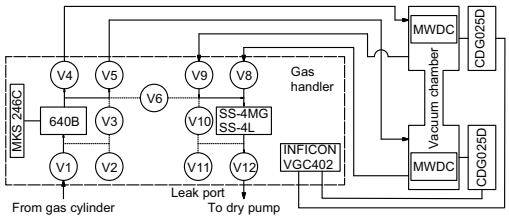

Fig. 2. Schematic diagram of the gas handler system.

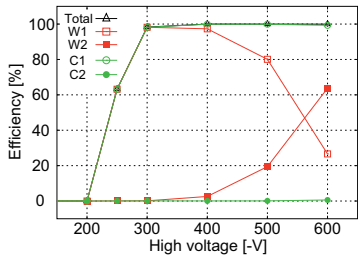

Fig. 3. Detection efficiency for the 200 MeV/nucleon Xe beam. The beam intensity was 6×10^3 particles per pulse (pulse width 1 s). The threshold voltages of the ASDs were -20 mV. Definition of the symbols is the same as in Ref. 3.

*1 Department of Physics, Konan University
*2 RIKEN Nishina Center
*3 Department of Physics, Peking University
*4 RCNP, Osaka University
*5 Department of Physics, Kyoto University

References

1) Y. Matsuda et al.: Phys. Rev. C 87, 034614 (2013).
2) T. Kobayashi et al.: Nucl. Instr. and Meth. B 317, 294 (2013).
3) Y. Matsuda et al.: Nucl. Instr. and Meth. A 670, 25 (2012).

NiGIRI: Identification of n, p, d, t, ^{3,4}He, ^{6,7}Li, and γ-rays†

H. Matsuzawa,[*1,*2] S. Nishimura,[*2] T. Isobe,[*2] G. Lorusso,[*2] M. Kurata-Nishimura,[*2] and K. Ieki[*1]

The azimuthal angle correlation of neutrons and charged particles with respect to the reaction plane in heavy-ion collisions is expected to provide essential information on the equation of state (EOS) of high density nuclear matter in supernovae and neutron star. A new scintillation detector NiGIRI (Neutron, ion, and γ-ray Identification for Radioactive Isotope beam), comprises two types of PMTs (Hamamatsu H11265-200, R8520-20-12) attached on both sides of a plastic scintillator EJ299-33 ($30\times55\times127$ mm^3), is designed to measure the positions and energies of neutrons ($\geq$ 100 keV) and charged particles ($\pi^{\pm}$, p, d, t, ^{3,4}He, ^{6,7}Li, ..) with pulse-shape discrimination (PSD) capability[1–3].

A feasiblity study of the NiGIRI detectors was performed using ^{132}Xe + CsI collisions at energies of 400 AMeV at HIMAC. The energies and positions of charged particles were reconstructed and identified using the correlations of energy losses (ΔE), timings, and PSDs among the different layers of NiGIRI detectors. Sixty four signals (32 NiGIRI detectors x 2 PMTs), recorded with a synchronized wave-dump mode of four flash ADC modules (CAEN V1730B; 500 MHz with 14 bits), were analyzed to deduce the integrated charge, timing, and PSD offline.

Figure 1 demonstrates the particle identification of low energy p, d, t, ^{3,4}He, and ^{6,7}Li in the energy correlation of the 1st layer of NiGIRI (E) and a charged-particle veto plastic scintillator (CPV: 2 mm^t; ΔE). The punch-through charged particles with higher energy were identified using up to 8 layers of NiGIRI detectors.

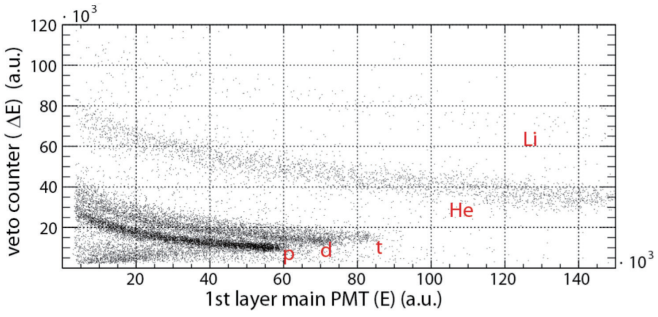

Fig. 1. Correlation between the veto counter (ΔE) and 1st layer (E).

Particle identification of neutrons was tested using the PSD, which is the ratio of the total charge-integral (gate width = 385 ns) and tail charge-integral (gate width = 360 ns; delay = 24 ns) of each PMT signal. The energy dependences of the PSD for charged-particles (Fig. 2a: events with CPV signal) and neutral particles (Fig. 2b: events with no CPV signal) show separation of particles among (p-d-t)-(He)-(Li) and (γ)-(n), respectively. The energies of these ions can be deduced using the time-of-flight (TOF) between the CsI target and the NiGIRI detectors, which is also useful for the consistency check with the energy losses in the NiGIRI detectors. $\pi^{\pm}$ production can also be studied by tagging stopped π decays in wave-dump signals of the last NiGIRI detector.

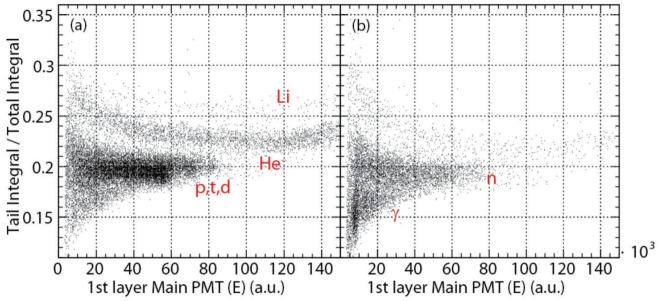

Fig. 2. PSD of the 1st layer main PMT of charged particles (a) and neutrons and γ-rays (b). Charged particle after CP veto in (b) is simply due to insufficient coverage of the NiGIRI detector.

Figure 3 shows the proto-type NiGIRI arrays arranged with full azimuthal coverage. Upgraded NiGIR detectors will be applied at RIBF to study the neutron-proton differencial flow at target rapidity in neutron-rich nucleus collisions, where reaction plane will be determined by measuring the squeeze-out out-of-plane flow in mid-rapidity region.

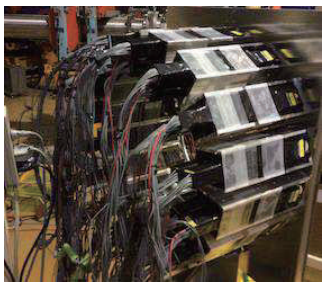

Fig. 3. Thirty two NiGIRI detectors (16 arrays x 2 layers) arranged at target rapidity for multiplicity measurement.

*1 Department of Physics, Rikkyo Univ.
*2 RIKEN Nishina Center

References

1) S.A. Pozzi et al.; Nucl. Instr. Meth. A **723**, 19-23 (2013)
2) S. Nyibule et al.; Nucl. Instr. Meth. A **728**, 36-39 (2013)
3) H. Matsuzawa et al.; RIKEN Accel. Prog. Rep. **47** (2015)

Proposal of novel delayed-neutron branching ratio measurements using MRTOF

M. Wada,[*1] P. Schury,[*1] and Y. Ito,[*1]

The astrophysical r-process plays important roles in synthesis of heavy elements in the universe[1]. The r-process pathway is dominantly determined by the neutron separation energies of neutron-rich nuclei and the abundance of the elements strongly depends on the half-life of the nuclei in the pathway. In addition to these two dominant nuclear properties, the delayed neutron emission probabilities (P_n) and the neutron capture cross sections (σ_n) contribute partially to the element abundance. The cross section does not contribute during equilibrium, but strongly affects the freeze-out stage. However, direct neutron capture cross sections of very neutron rich nuclei is so far very difficult to determine experimentally[2]. During freeze-out, the β-decay path towards stability is defined by P_n. Although almost all nuclei in the r-process pathway have non-negligibly finite P_n, only a limited number of them are experimentally determined.

So far the experimental P_n values have been determined by a limited variety of methods: direct detection of delayed-neutron by ^{3}He gas counters, detection of recoil ions in an ion trap[3], and radiochemical identification of daughter nuclei. We propose a novel method using a gas catcher cell and a multi-reflection time-of-flight mass spectrograph (MRTOF-MS). The principle is the same as the radiochemical method. All daughter nuclides are identified and the yields are compared to determine P_n. In the radiochemical method, characteristic γ-rays and their branching ratios are needed to obtain the yields, however, they are often unknown in such very neutron rich nuclei. In the new method, we identify the daughters and remaining precursor ions by the MRTOF-MS. Figure 1 shows a schematic drawing of the experimental setup. The injected precursor nuclear ions are first thermalized in the gas catcher and decay in the cell. The decay products are also thermalized in the cell and then extracted from the cell using an rf-carpet and transport to the MRTOF-MS. The recoil products are identified by the mass spectrograph. Figure 2 shows a schematic mass spectrum for the case of ^{94}Br. Note that remaining precursor and β decay recoil, single neutron decay recoil, two neutron decay recoil and their daughters (grand daughters of the precursor) are all identified in a single spectrum. It is especially important that the isobaric pair of the precursor and the β-decay product (without neutron emission) can be clearly separated. Such simultaneous detection of multiple atomic mass numbers along with separation of isobaric ions is a unique feature of MRTOF-MS[4]. It is difficult to achieve such capabilities in any other type of separator. The β-delayed neutron decay probabilities can be obtained:

$$P_n = N(A-1)/N_0, \quad (1)$$

$$P_{2n} = N(A-2)/N_0, \quad (2)$$

$$N_0 = N^\star(A) + N(A-1) + N(A-2), \quad (3)$$

where $N(A-x)$ is the sum of x-neutron branch, $N^\star(A)$ is β-decay recoil and daughters excluding the remaining precursor, and N_0 corresponds to the total β-decay number.

Thus obtained P_{xn} have ambiguities due to mixing of the daughter's P_{xn}. However, this can be corrected by an independent measurement using the daughter as a precursor. Moreover, for astrophysical applications, the final mass distribution from a single precursor is the required data. Another possible uncertainty can be attributed to the decay in MRTOF, however, this fraction can be evaluated if the lifetimes are known. In case a cocktail RI beam is provided, one can still determine P_n by solving a linear algebra of the final distributions of isotopes in a few different but known distributions of the cocktail beams.

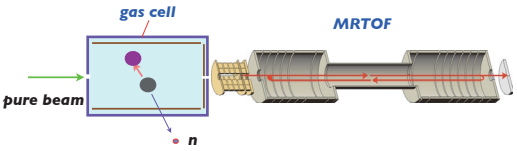

Fig. 1. Sketch of setup for P_n measurement with MRTOF

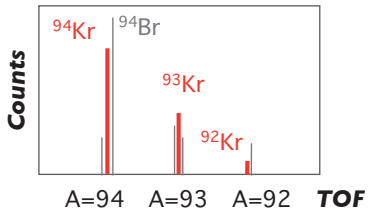

Fig. 2. Schematic time of flight spectrum showing the precursor ^{94}Br, β-decay daughter ^{94}Kr, delayed single neutron decay recoil ^{93}Kr, delayed two neutron decay recoil ^{92}Kr and their daughters.

*1 RIKEN Nishina Center

References
1) E. Burbidge et al, Rev. Mod. Phys., 29 (1957) 547.
2) T. Yamazaki et al., Nucl. Inst. Meth. A325 (1993) 489.
3) Y. M. Yee et al., Phys. Rev. Lett. 110 (2013) 092501.
4) P. Schury et al., Int. J. Mass Spectrom., 359 (2014) 19.

Advanced development of GARIS-II using He-H_2 mixture as a filled gas toward the study of superheavy element

D. Kaji,[*1] K. Morimoto,[*1] H. Haba,[*1] Y. Wakabayashi,[*1] M. Takeyama,[*1,*2] S. Yamaki,[*1,*3] K. Tanaka,[*1,*4] and K. Morita[*1,*5]

Performance of a gas-filled recoil ion separator (GARIS-II) has been investigated using various asymmetric fusion reactions[1–5]. The studies have indicated that the separator has a large transmission under a low-background condition in comparison with GARIS and that the separation of unwanted particles is improved using He-H_2 mixture as a filled gas. The low-background condition is very important for identifying superheavy elements (SHE) produced with a low cross section of pb-order. Therefore, the usefulness of He-H_2 mixture as a filled gas toward the study of SHE was investigated further in this work. As a typical example, results for ^{214}Th, which was produced via the reaction of ^{197}Au(^{23}Na,6n), are given here.

The reaction products of ^{214}Th were separated in-flight from projectiles and other by-products using GARIS-II, and then they were guided into a double sided silicon detector after passing through a time-of-flight detector[1–3]. The separator was filled with He-H_2 mixture gases with various H_2 mixing ratios (0, 10, 20, and 36%). The gas pressure was maintained 47 Pa.

The yields of ^{214}Th, which was assigned from an α-transition of 7.678 MeV, were measured by varying the fraction of H_2 composition from 0 to 36% as shown in Fig. 1. Each yield is plotted against the magnetic rigidity $B\rho$. The optimum $B\rho$ value was determined by fitting to the data points using a Gaussian function. The optimum $B\rho$ value was shifted from 1.711 to 1.821 Tm by increasing the mixing ratio of H_2 from 0 to 36%, and the yields of ^{214}Th were enhanced 1.43 times.

The shift of the optimum $B\rho$ value implies that the equilibrium charge state $\overline{q}$ of recoil ions moving in a filled gas becomes small. The $\overline{q}$, which was deduced from the optimum $B\rho$ values, are plotted against the mixing ratio of H_2 in Fig. 2. The $\overline{q}$ was decreased with increasing H_2 composition. The $\overline{q}$ in pure H_2 can be estimated to be 3.58 using empirical systematics, which was obtained using a Dubna gas-filled recoil separator DGFRS[6]. Interpolated values of $\overline{q}$ between 4.28 and 3.58 in the case of pure He and H_2 are indicated as a broken line in Fig. 2. The interpolation well agrees with the obtained $\overline{q}$ values using various mixing ratios within an error bar. On the other hand, the transmission is improved with increasing the mixing ratio of H_2, although the width parameter $\Delta B\rho/B\rho$ becomes slightly worse from 8.4% to 9.4%. To establish a suitable condition to study SHE using the He-H_2 mixture, further investigation is in-progress.

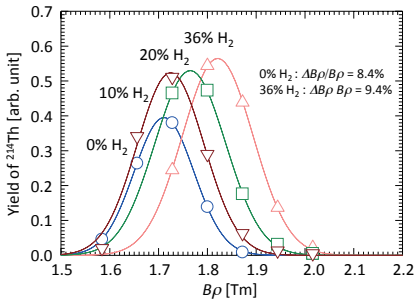

Fig. 1. Yield curve of ^{214}Th as a function of magnetic rigidity for various He-H_2 mixture gases (○:pure He, ▽:10% H_2, □:20% H_2, △:36% H_2). Each solid curve is a Gaussian function fitted to data points.

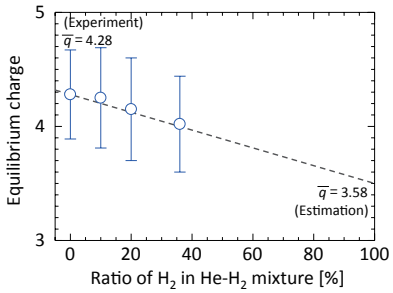

Fig. 2. Equilibrium charge state of ^{214}Th ions moving in a He-H_2 mixture. Interpolation between experimentally obtained $\overline{q}$ of 4.28 and estimated $\overline{q}$ of 3.58 from DGFRS's work[6] is indicated as a broken line.

*1 RIKEN Nishina Center
*2 Department of Physics, Yamagata University
*3 Graduate School of Science, Tokyo University of Science
*4 Department of Physics, Saitama University
*5 Department of Physics, Kyushu University

References

1) D. Kaji et al.: J. Radioanal. Nucl. Chem. 303, p.1523 (2015).
2) D. Kaji et al.: JPS Conf. Proc. 1, p.013051 (2014).
3) D. Kaji et al.: Nucl. Instrum. Methods B 317, p.311 (2013).
4) D. Kaji et al.: RIKEN Accel. Prog. Rep 47, (2014) [In print].
5) D. Kaji et al.: RIKEN Accel. Prog. Rep 46, p.189 (2013).
6) Yu. Ts. Oganessian et al.: Phys. Rev. C64, p.064309 (2001).

Pulse shape analysis for short-lived decay of superheavy elements

S. Yamaki,[*1,*2] K. Morimoto,[*1] D. Kaji,[*1] Y. Wakabayashi,[*1] M. Takeyama,[*1,*3] K. Tanaka,[*1,*4] H. Baba,[*1] T. Yamaguchi,[*2] T. Suzuki,[*2] and K. Morita[*1,*5]

In heavy or superheavy element research, it is important to know the α decay energies and half-lives of the nuclei to confirm that objective nuclei have been formed. The α decay half-lives of these nuclei are very short (0.1-1 μs) for heavier Z according to some theoretical calculations. However in the traditional system, the combination of a shaping amplifier and PH-ADC cannot separate sequential events within 1 μs. To measure the α decay properties of such short-lived nuclei, a digital data acquisition system with flash-ADC was implemented in the GARIS-II[1] read-out system. In the new system, waveforms from a preamplifier are directly registered with flash-ADC SIS3301 to avoid the summing phenomena caused by pileup in the shaping amplifier. Figure 1 shows the PH-ADC read-out and flash-ADC read-out systems. The DAQ systems for the PH-ADC and flash-ADC are operated independently. Separately obtained data are synchronized by the LUPO time-stamp module.

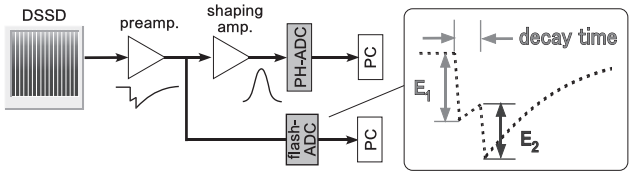

Fig. 1. The setup of PH-ADC and flash-ADC read-out systems.

In a recent study, a pulse shape analysis (PSA) algorithm for the waveforms from the GARIS-II read-out system was developed[2]. PSA was tested using off-line tests. ^{241}Am α was implanted in a Si PIN photodiode (Hamamatsu S3204) and the signal was preamplified by the Clear Pulse 579. The sampling rate was 100 MHz. Some pileup events occurred when the α source was set close to the detector. Figure 2(a) shows an example of a pileup pulse. In order to distinguish pileup events from single events, the weighted mean in time over threshold (MTOT) method for the differentiated waveforms was developed and applied. MTOT is defined as:

$$\mathrm{MTOT} = \frac{\sum_{t=0}^{t_m} t w_t}{\sum_{t=0}^{t_m} w_t} - T, \quad w_t = \begin{cases} 1 & (v_t \le v_{th}) \\ 0 & (v_t > v_{th}) \end{cases}, \quad (1)$$

where t is the time, t_m is the sampling period (800 clock), v_t is the voltage, v_{th} is the voltage threshold, and T is the minimum t when $w_t = 1$. Figure 2(b) shows a histogram of the MTOT. The peak that corresponds to single events is seen around 17 clock (= 170 ns). The larger MTOT events from this peak correspond to pileup ones. For example the MTOT for the waveform in Fig.2(a) is calculated as $(\sum_{t=83}^{116} t + \sum_{t=273}^{305} t)/(\sum_{t=83}^{116} + \sum_{t=273}^{305}) - 83 = 109.8$ (> 17). Therefore, this event is treated as a pileup one.

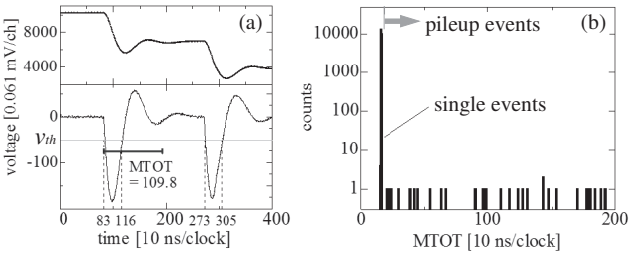

Fig. 2. (a) An example of a pileup pulse (upper panel) and its differential (lower panel). (b) MTOT histogram when ^{241}Am α was implanted in the PIN diode.

In the second stage, template fitting for each pulse was performed[3]. The template was made by averaging 10000 ^{241}Am α waveforms for each channel. The fitting function is given as:

$$f(t) = A[0] \cdot template(t - A[1]) + baseline, \quad (2)$$

where the free parameters ($A[i]$; $i = 0, 1$) represent the pulse height and time offset. The baseline is an average of the data from $t = 0$ to the start of the pulse. For a single pulse, an energy resolution of 25 keV (FWHM) for 5486 keV α was obtained, while a resolution of 20 keV was obtained using the original PH-ADC system. In addition the shortest time interval between sequential events identified by PSA was 349 ns (Fig. 3). The energies of the first and second pulses were 5494 keV and 5444 keV, respectively. Further development of PSA is now underway.

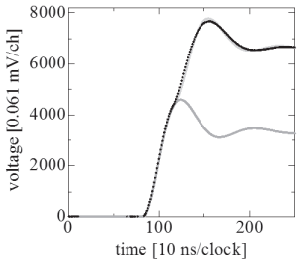

Fig. 3. Pileup pulse (dotted line) and fitting of this event (solid line). From this fitting, the time interval between two events was determined to be 349 ns.

*1 RIKEN Nishina Center
*2 Department of Physics, Saitama Univ.
*3 Graduate School of Science and Engineering, Yamagata Univ.
*4 Faculty of Science and Technology, Tokyo Univ. of Science
*5 Department of Physics, Kyusyu Univ.

References

1) D. Kaji et al.: Nucl. Instr. and Meth. **B 317**, 311 (2013).
2) S. Yamaki et al.: Proc. ARIS2014 in print.
3) S.N. Liddick et al.: Nucl. Instr. and Meth. **A 669**, 70 (2012).

Performance of ion surfing rf-carpet for high-energy RI beam gas catcher

F. Arai,[*1,*2] Y. Ito,[*2] I. Katayama,[*2] M. Reponen,[*2] P. Schury,[*2] T. Sonoda,[*2] M. Wada,[*2] and H. Wollink[*2,*3]

High-energy radioactive isotopes have been used in ion trap-based precision experiments after being stopped in a large gas cell. The stopped ions of these isotopes can be extracted from the large gas cell as a low-energy ion beam. To transport and extract these ions quickly and efficiently, electric fields are required to guide them. In this respect, an rf-carpet (RFC) method utilizing a dc potential gradient is a standard technique.[1)] However, such a method is restricted to longer half-life isotopes because of the transport time owing to the upper limit on the dc gradient that can be supported before electric discharges occur in the large gas cell. To study short half-life isotopes, an RFC featuring faster transport is required. Recently, a hybrid technique wherein the dc gradient is replaced by a traveling potential wave was proposed, called ion surfing.[2)]

Recently, we have demonstrated the transport and extraction of K^+ ions using a circular RFC in 20 mbar of He gas pressure.[3)] However, in a practical gas cell, the gas pressure is higher by one order of magnitude.

In this study, the transport and extraction of K^+ and Cs^+ ions with the ion surfing method were tested in high pressure He gas using a 100 mm cylinder electrode to create a push electric field E_{push} and a circular RFC of 80 mm diameter. In addition, we compared the effect of an RFC of a fine pitch with one of a rough pitch. The fine pitch RFC consists of 0.08 mm wide ring electrodes with 0.16 mm pitch and 0.32 mm diameter orifice, whereas the rough pitch RFC consists of 0.16 mm wide ring electrodes with 0.32 mm pitch and 0.64 mm diameter orifice.

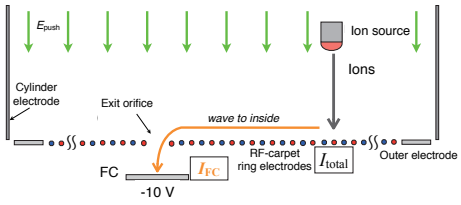

Fig. 1. Sketch of the transport and extraction efficiency measurement scheme. An rf frequency of 9.3 MHz and rf amplitude of 104 V_{pp} are typical operating conditions.

Figure 1 illustrates the scheme used to test the efficiency of this method. The study required measuring two ion currents: the current reaching the RFC electrodes (with rf off), I_{RFC} and the ion current reaching a Faraday Cup (FC), I_{FC}. The FC was biased at −10 V to pull ions out from the extraction orifice.

We define the combined transport and extraction efficiency as $I_{\mathrm{FC}}/I_{\mathrm{RFC}}$. Figure 2 shows the efficiency for K^+ and Cs^+ ions with the fine pitch RFC and the rough pitch RFC as functions of the He gas pressure P_{He}. Above a maximum pressure, the efficiency decreases with increasing pressure because the effective repelling force decreases because of stronger damping effect at high He gas pressures; the push electric field then exceeds the effective repelling field of the RFC causing ions to hit the RFC. The efficiency for Cs^+ is always higher than for K^+ because the effective repelling force scales with the mass-to-charge ratio. The fine pitch RFC is more efficient than the rough pitch RFC at higher He gas pressures. This indicates that the effective repelling force is stronger for finer pitch at higher He gas pressures.

We obtained an ion collection efficiency up to nearly 100% within a wide range of He gas pressures. To allow operation at higher P_{He}, a larger effective repelling force is needed.

We applied the ion surfing RFC to a superheavy element gas cell. The results are presented elsewhere in this journal[4)].

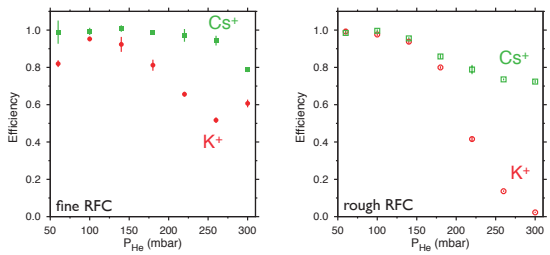

Fig. 2. The efficiency of K^+ and Cs^+ ions as a function of the He gas pressure P_{He} with fine RFC (left) and rough RFC (right).

*1 Department of Physics, University of Tsukuba
*2 RIKEN Nishina Center
*3 Department of Chemistry and Biochemistry, New Mexico State University

References
1) M. Wada et al.: Nucl. Instr. Meth. B204, 570 (2003).
2) G. Bollen: Int. J. Mass Spectrom. 299, 131 (2011).
3) F. Arai et al.: Int. J. Mass Spectrom. 362,56 (2014).
4) P. Schury et al.: In this report.

Evaluation of effects of a large energy deposition on Deuterium gaseous active target for a high-intensity ion beam injection

C.S. Lee,[*1,*2] S. Ota,[*1] M. Takaki,[*1] Y. Kiyokawa,[*1] Y.N. Watanabe,[*2,*3] H. Tokieda,[*1] and J. Zenihiro[*2]

A deuterium gaseous active target, CNS Active Target (CAT)[1,2], has been under development for measuring the Isoscalar Giant Monopole Resonance (ISGMR) in unstable nuclei via the (d, d') reaction. In order to extract the ISGMR component by using the multipole decomposition analysis, a wide angular coverage of the distribution of the differential cross-section is required. The CAT consists of GEM-TPC and Si detectors. In the center-of-mass frame, the scattering angular region of recoil particle of $\theta_{\rm CM}$ around 2 degrees was covered by the GEM-TPC, while the region of $\theta_{\rm CM} \geq 5$ degrees was covered by the Si detectors. In the previous experiment[2] at HIMAC using a ^{132}Xe beam with a high intensity of around 1 MHz at 115-MeV/u incident energy, we experienced instabilities of the CAT; a sudden jump of the current value of the field cage and a fluctuation of the baseline of Si signals were observed. The instabilities can be considered as the effect of high energy-loss density in the active gas target caused by a heavy ion beam. For evaluating of such effect, we bombarded the CAT with a very intense 3-MeV proton (H^+) beam provided by a pelletron in RIKEN. In this paper, the experiment and the results are reported.

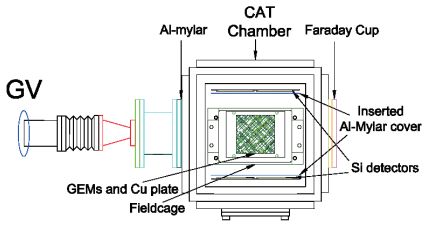

Fig. 1. A schematic view of the setup at pelletron, RIKEN.

Figure 1 shows a schematic view of the experimental setup. The CAT was connected to the exit of the pelletron beam port with a 12-μm-thick Al-mylar foil. An Al flange of the chamber at the exit of the CAT was used as a Faraday Cup (FC). A copper plate was employed to collect the charges multiplied by three thick GEMs (THGEMs) for evaluating the effective gas gain. The current outputs of the FC and the Cu plate were measured using picoammeters (ADVANTEST TR8641). The voltage and current values of each high-voltage supply were recorded using a multimeter (KEITHLEY 2701). Four Si detectors with an effective area of 9×9 cm^2 and thickness of 0.5 mm were surrounding the field cage. The Si signals were amplified using a preamplifier (mesytec MPR-32) and read out using an oscilloscope. The energy of the H^+ beam was 3 MeV, and its intensity was varied from 1 to 60 pA. The GEM-TPC was operated at an effective gas gain of about 60 in 0.4-atm H_2.

Baseline fluctuations were observed in the signals of the Si detectors for a beam intensity of 20-pA, as shown in the left panel in Fig. 2. This beam condition provides an energy-loss density equivalent to a ^{132}Xe beam with an intensity of 1.2 MHz and energy 115 MeV/u. The fluctuation disappeared, when, with the same beam condition, a 10-μm-thick Al-mylar foil was placed in front of each Si detector. Therefore, we understand that the fluctuation is possibly due to radioactive noise. At 60-pA 3-MeV H^+ beam injection, the fluctuations became smaller.

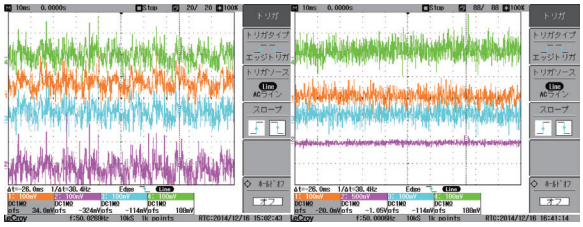

Fig. 2. Preamplifier outputs of Si detectors for a 20-pA 3-MeV H^+ beam injection without Al-mylar foil cover (left) and with Al-mylar foil cover (right).

Figure 3 shows the variation of current in the Cu plate and field cage during the 20-pA 3-MeV H^+ beam injection. The current of the field cage increased by 4-5 μA immediately after the injection of the high-intensity beam and gradually increased during the beam irradiation. This may be explained by the effect of the initial ions from the beam and the ion back flow (IBF) from the THGEMs. Although the field cage had tripped (the current limit was 1 mA) several times, a sudden jump of the current value seldom happened. This may be caused by the difference between a heavy-ion and a light-ion, such as δ-ray creation. The effect of δ-rays on both Si detectors with Al-mylar covers and the GEM-TPC will be evaluated by using a high-intensity heavy-ion beam in the near future.

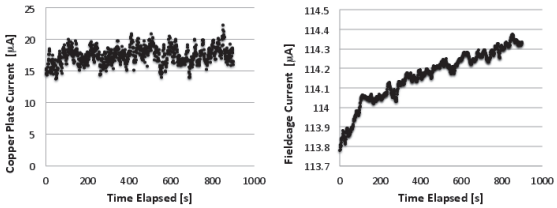

Fig. 3. Current variation of the Cu plate (left) and the field cage (right) during a 20-pA 3-MeV H^+ injection.

References

1) S. Ota et al.: CNS Annual Report **2011**, CNS-REP-90 (2013) 70-71.
2) S. Ota et al.: CNS Annual Report **2013**, CNS-REP-93 (2015) 49-50.

*1 Center for Nuclear Study, The University of Tokyo
*2 RIKEN Nishina Center
*3 Department of Physics, The University of Tokyo

Design of a thin-film polarized proton target system for low-energy RI beam experiments

E. Milman,[*1,*3] S. Sakaguchi,[*2] S. Chebotaryov, [*1,*3] W. Kim,[*3] K. Tateishi,[*1] and T. Uesaka [*1]

The search for unknown resonances of unbound ^{10}N via ^{9}C+p elastic resonant scattering is proposed. Theoretically, four broad and overlapping low-lying ^{10}N resonances that may not be clearly identifiable in the ^{9}C+p excitation function are expected.The vector analyzing power is measured to determine these broad resonances[1]. The level information obtained in the experiment is useful for discussing resonances in ^{10}Li since ^{10}N and ^{10}Li are mirror nuclei that are expected to have a similar structure. The ^{10}Li structure provides us with valuable information for constructing the three-body model of the borromean ^{11}Li nucleus.

A polarized target is required for the measurement of the analyzing power. A polarized proton solid target for low-energy beam experiments[2] has been designed based on an existing system for intermediate energies [3]. In the target, proton polarization is obtained by transferring the electron polarization of photo-excited triplet state of pentacene to protons of p-terphenyl. Polarization transfer is done by microwave irradiation that satisfies the condition that the Rabi frequency of electron spin is matched to the Larmor frequency of the proton[2].

We select a magnetic field strength of 0.2 T. This value is a tradeoff between the magnitude of proton polarization and magnetic field effect for the trajectory of recoil particles. At this field strength, the resonance frequency of electron spins is ∼4.8 GHz and the proton resonance frequency is ∼8.5 MHz.

For the detection of low-energy recoil protons emitted with respect to ±22.5° where the analyzing power is expected to be the largest, the microwave resonator must be sufficiently short to avoid interference with the trajectory of scattered protons.A three-loop two-gap resonator[4] (LGR) was chosen as the microwave resonator, as shown in Fig. 1 (Left). Its structure allows us to sufficiently shorten the resonator and to implement NMR coil close to the resonator without affecting its performance[4].

We conducted a simulation of the LGR using the electromagnetic field simulation software CST Microwave Studio. In the simulation, the LGR was placed inside a brass shield to reduce microwave radiation losses, as shown in Fig. 1 (Right). The shield was designed to allow beam particles and recoil protons to pass through the resonator freely. The LGR was excited by an antenna placed close to one of edge loops.

The resonance frequency of LGR and the strength of the oscillating microwave field were simulated at 1-W incident power. The power required for optimal polarization transfer was evaluated. Simulations were performed for different central loop diameters. We found that the resonator with 18-mm diameter and 5-mm length was the tradeoff between the target size and required incident power of 20 W.

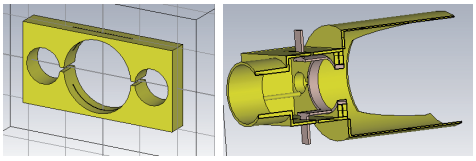

Fig. 1. Three-loop two-gap resonator (LGR) (Left). LGR placed in the shield (Right).

The thickness of the target was chosen to be 110 μm to cover the range of the ^{9}C beam with an energy of 5.6 MeV/nucleon. A novel thin crystal production method is proposed. In this method, the crystal prepared by the Bridgmann method is placed in a vacuum tube and heated. The crystal sublimates and its thickness slowly decreases. The sublimation speed is controlled by the heater temperature. A test sample prepared by the sublimation method is shown in Fig. 2.The sample thickness is approximately 700 μm.

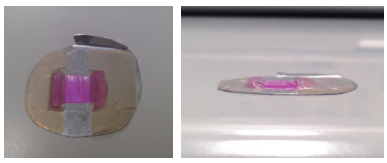

Fig. 2. Sample prepared by the sublimation method.

In conclusion, the microwave resonator was designed for the thin-film polarized proton target at 0.2 T. The sublimation method was proposed to produce thin crystals. In the next fiscal year, the resonator will be built and tested. A thin crystal with a thickness of approximately ∼100 μm will be produced by the sublimation method.

*1 RIKEN Nishina Center
*2 Department of Physics, Kyushu University
*3 Department of Physics, Kyungpook National University

References

1) T. Teranishi, S. Sakaguchi, T. Uesaka et al.: AIP Conf. Proc. **1525**, 552 (2013).
2) S. Sakaguchi et al.: Nucl. Instrum. Methods Phys. Res. B **317**, 679 (2013).
3) T. Uesaka et al.: Nucl. Instrum. Methods Phys. Res. A **526**, 186 (2004).
4) R. L. Wood, W. Froncisz, J. S. Hyde: J. Magn. Reson. **58**, 243 (1984).

Kinetic parameters of photo-excited triplet state of pentacene determined by dynamic nuclear polarization

T. Kawahara,[*1,*2] S. Sakaguchi,[*1,*3] K. Tateishi,[*1] T. L. Tang,[*4] and T. Uesaka[*1]

A polarized proton target prepared by dynamic nuclear polarization (DNP) techniques, which is a means of transferring electron spin polarization to nuclei by microwave irradiation, has been extensively used in particle and nuclear physics experiments.[1)] However, in these studies, DNP is carried out at a cryogenic temperature of <4.2K and in a high magnetic field of several Tesla. On the other hand, DNP using photo-excited triplet states (Triplet-DNP) can produce high nuclear spin polarization without such equipment, by using the non-equilibrated electron spin polarization in the lowest photo-excited triplet state generated by laser irradiation.[2)]

In this paper, we determined kinetic parameters of the triplet electron spin of pentacene, which is mainly used as a polarizing agent in Triplet-DNP, to optimize the polarization transfer sequence for maximizing the polarization of the target. Although the polarization of the triplet electrons is initially higher than 70%, it decreases as a function of time after the optical excitation. There are two processes relevant to this phenomenon: one is the decay from the triplet state to the ground state, while the other is the relaxation to the thermal equilibrium in the triplet state. The time constants are referred to as lifetimes (τ_i, i=+1, 0, -1: i represents the sublevels in the triplet state) and spin-lattice relaxation time (T_1).

We determined the time constants of pentacene doped into p-terphenyl in 0.3 T and at room temperature, based on the NMR signal intensities of proton spins enhanced by Triplet-DNP. A continuous-wave Ar-ion laser pulsed by an optical chopper is used for optical excitation. We first measured the delay-time (the timing of microwave irradiation for polarization transfer) dependence (Fig. 1(a)). Analysis using only this data revealed a difficulty in separating the contributions of τ_i and T_1. We thus utilized the pulse-structure (the duty and the repetition rate of laser pulse) dependence data as additional information (Fig. 1(b)). The combined analysis of these data allowed us to separate the contributions of the parameters. The values of τ_0 and $\tau_\pm$ were determined to be 22.3 $\mu s^{+3.0\ \mu s}_{-1.5\ \mu s}$ and 88 $\mu s^{+13\ \mu s}_{-19\ \mu s}$, respectively (Fig. 1(c)). The value of T_1 was found to be longer than 300 μs. It was also found that the proton signal enhancement is limited at a high repetition rate owing to the partial cancellation of the electron spin polarization by the remaining population produced by the preceding laser pulses.

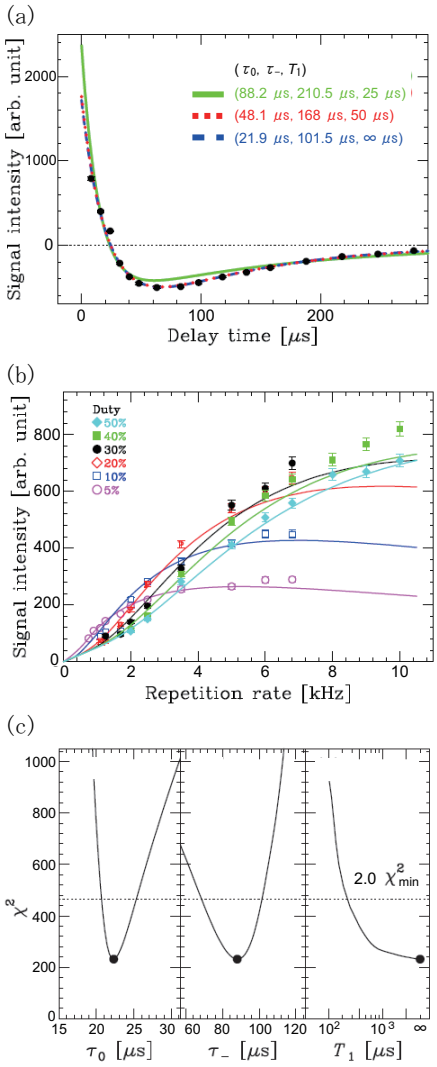

Fig. 1. (a) the delay-time dependence of the NMR signal intensities of proton spins enhanced by Triplet-DNP. (b) the pulse-structure (the duty and the repetition rate of laser pulse) dependence of the signal intensities. (c) Variation of the chi square values of τ_0, τ_-, and T_1.

† Condensed from the article in J. Phys. Soc. Jpn. **84**, 044005 (2015)

*1 RIKEN Nishina Center
*2 Department of Physics, Toho University
*3 Department of Physics, Kyushu University
*4 Center for Nuclear Study, University of Tokyo

References

1) D. G. Crabb and W. Meyer: Annu. Rev. Nucl. Part. Sci. **47** 67 (1997).
2) T.Wakui et al.: Nucl. Instrum. Methods Phys. Res. Sect. A **550** 521 (2005).

Development of single-crystal CVD diamond detector for time-of-flight measurements

Y. Sato,[*1] T. Shimaoka,[*2] M. Kobayashi,[*3] M. Takaki,[*3] H. Miya,[*3] M. Matsushita,[*3] S. Michimasa,[*3] K. Yako,[*3] S. Shimoura,[*3] M. Tsubota,[*2] J. H. Kaneko,[*2] H. Murakami,[*1] H. Sato,[*1] K. Yoshida,[*1] T. Kubo[*1]

Production and identification techniques for radioactive isotope (RI) beams are important for nuclear physics experiments involving exotic nuclei that are very unstable. RI beams are generally produced as secondary beams from high-energy heavy-ion reactions using in-flight fragment separators. In these devices, a charged-particle detector with a fast response and high radiation hardness is required to measure the time of flight (TOF) of ions for identifying the RI beams in high-dose environments.

Diamond is one of the most promising materials for fabricating a charged-particle detector for performing accurate timing measurements under high-intensity beam conditions. Fast signals for superior timing resolution can be obtained because of the high breakdown electrical field strength and high carrier saturation velocities of the diamond crystal. Additionally, high radiation hardness to large charged-particle fluxes can be expected because of the higher displacement energy of diamond.

In this study, we fabricated a single-crystal (sc) chemical-vapor-deposited (CVD) diamond detector and evaluated the intrinsic timing resolution of the detector. Figure 1 shows the block diagram of the electronic circuit used for evaluating the timing resolution. Two diamond detectors were placed in the E7B beam line at the RIKEN accelerator facility. The detectors were fabricated using an sc-diamond of approximately 4×4 mm^2. In brief, the detector has a layer structure of Pt/sc-diamond/Ti/Au. The thickness of the diamond crystals are 90 μm and 139 μm for the front-side and rear-side of the detector, respectively.

8.6 MeV/nucleon-^{7}Li beams penetrated two diamond detectors. The pulses induced from the detector were read out using a broadband amplifier with an analog bandwidth of 1 MHz–2 GHz (CIVIDEC C2 Broadband Amplifier). The amplifier signals were processed with a leading edge discriminator, a time-to-amplitude-converter (TAC), and 8 k-multi-channel analyzer (MCA) for TOF measurement. The timing resolution of the measurement system was estimated to be 7.8 ps (σ) using a constant time difference generated by the fast-pulser signal and cables.

Figure 2 shows the measured TOF spectrum. The width of the peak was estimated to be 45 ps (σ). The intrinsic timing resolution of the detector was evaluated by dividing the width of the peak by $\sqrt{2}$ and subtracting the timing resolution of the measurement system. Here, the same performance of the two detectors was assumed. The intrinsic timing resolution was estimated to be 31 ps (σ).

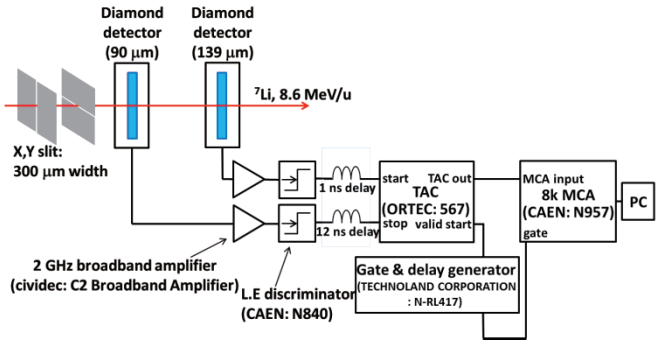

Fig. 1: Block diagram of the electronic circuit used in the TOF measurement. The start signal and stop signal were created by output signals from the rear-side and the front-side detector, respectively. The bias supply is left out. The time offset of ~11 ns was created using cables. L.E. discriminator: leading edge discriminator, TAC: time-to-amplitude-converter, MCA: multi-channel analyzer

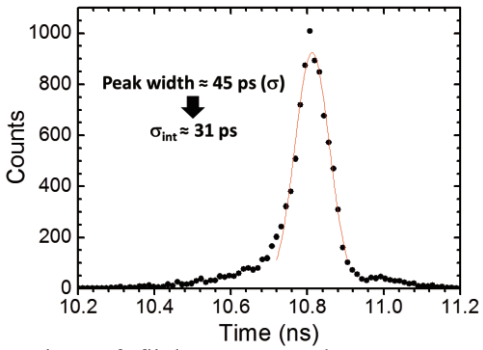

Fig. 2: Time of flight spectrum between two diamond detectors. The intrinsic timing resolution (σ_{int}) was evaluated using distribution of the peak (45 ps (σ)) and the timing resolution of the measurement system (7.8 ps (σ)).

This value is superior to the values reported by GSI: 57 ps and 39 ps for 600 MeV/nucleon-^{58}Ni and 1 GeV/nucleon-^{238}U, respectively[1,2]. On the other hand, NSCL/MSU achieved a resolution of ~15 ps for 87 MeV/nucleon-^{78}Kr[3].

In a future study, we will attempt to fabricate a charged-particle detector using a higher quality sc-diamond and evaluate the intrinsic timing resolution. On the other hand, the use of a large size sc-CVD diamond (20 mm×20 mm) was considered to fabricate the process for manufacturing, large size detector.

References

1) E. Berdermann, et al.: Nuclear Physics B **78**, 533 (1999).
2) E. Berdermann, et al.: XXXVI Int. Winter Meeting on Nucl. Physics, Bormio 1998.
3) A. Stolz, et al.: Diam. Relat. Mater., **15**, 807 (2006).

[*1] RIKEN Nishina Center
[*2] Graduate School of Engineering, Hokkaido University
[*3] Center for Nuclear Study, University of Tokyo

Efficient excitation of photo-excited triplet electrons of pentacene for dynamic nuclear polarization

K. Tateishi,[*1] T. Tsukihana,[*2] Y. Urata,[*2] S. Wada,[*2] and T. Uesaka[*1]

Dynamic Nuclear Polarization (DNP) has been successfully applied to a polarized target. DNP is a methods of transferring spin polarization from electrons to nuclei with microwave irradiation. However, as long as electron spins in thermal equilibrium are used as a polarizing agent, cryogenic temperatures of approximately 4.2 K will be required for hyperpolarization in the order of 10% even under strong magnetic fields of several Tesla.[1)] One approach for overcoming the limitation is to use non-thermalized electron spins as a polarizing agent instead.

DNP using the photo-excited triplet-electron spin of pentacene[2)] requires neither a cryogenic system nor a superconducting magnet, but a laser for creating hyperpolarized electron spins. There are four important requirements in the light source: wavelength, pulse width, repetition rate, and output power. The wavelength affects the excitation efficiency from the ground state to the excited singlet state. The pulse width influences the transition efficiency from the excited singlet state to the triplet state. The repetition rate is related the initial buildup rate of ^{1}H spin polarization. The output power is determined by the number of excited electrons, i.e., the sample volume.

To this end, a new laser system is developed, which is constructed using two neodymium-doped yttrium aluminum garnet (YAG) lasers with wavelengths of 1064 nm and 1319 nm and a LiB_3O_5 crystal for sum-frequency generation (Fig. 1). [3)] The wavelength, pulse width, repetition rate, and output power are 589 nm, 126 ns, 3 kHz, and 1 W, respectively. We developed oscillators independently using laser diode pumped YAG crystals. The acousto-optic Q-switch (A/O Q-sw) was chosen to generate light pulses because of the high repetition frequency. The pulse width can be varied by adjusting the input current of the laser diode, and in this experiment we used final output pulse widths of 84 and 126 ns. In order to generate 589-nm light, the infrared lights were overlapped at the LiB_3O_5 crystal. Finally, residual infrared lights were separated by visible-coated mirrors.

Using a single crystal of *p*-terphenyl doped with deuterated pentacene[4)], we carried out the DNP experiments in 0.35 T and at 300 K with laser pulses of 84 ns and 126 ns. The maximum polarization of a 84 ns laser pulse is 16% with a repetition rate of 400 Hz. The maximum polarization of the 126 ns laser pulse is 22% with a repetition rate of 600 Hz. The optimal repetition rate was different because the excited electrons play not only the role of a polarized agent but also that of a relaxation source. When the repetition rate was increased, the initial buildup rate increases, but the paramagmetism acceralates spin-lattice relaxation of ^{1}H spins. The final achievable polarization is determined by the balance of these two effects. Furthermore, to obtain higher ^{1}H spin polarization, our results indicated that a longer laser pulse width to increase the initial buildup rate or a higher external magnetic field to decrease the spin-lattice relaxation of ^{1}H spins is necessary.

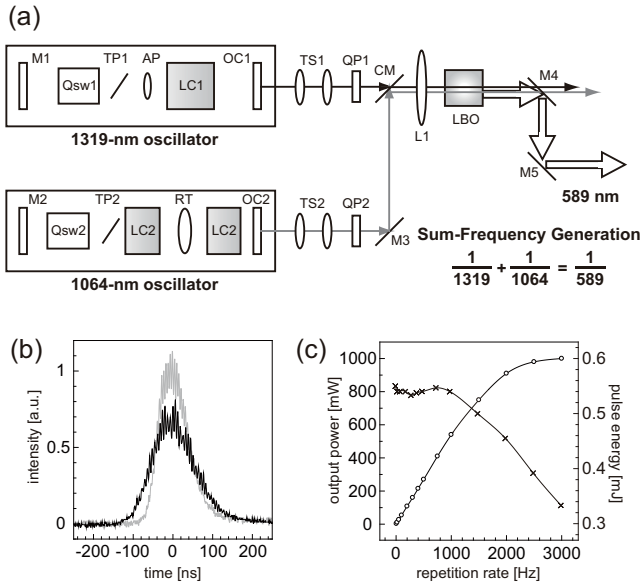

Fig. 1. (a) Schematic view of 589-nm laser constructed with two Nd-doped YAG lasers with wavelengths of 1064 nm and 1319 nm and a LiB_3O_5 crystal for sum-frequency generation. M1,M2: Oscillator mirror; Qsw1,Qsw2: A/O Qsw; TP1,TP2: Thin Plate; LCP,LC2: Laser Chamber; RT: Rotator; OC1,OC2: Output coupler; AP: Aperture; TS1,TS2: Telescope; QP1,QP2: Quarter-wave plate; CM: Combiner mirror; L1:Lens; M3,M4,M5: Mirror; LBO: LiB_3O_5 crystal. (b) Pulse shape. (c) Output power (circles) and pulse energy (crosses) as a function of repetition rate.

*1 RIKEN Nishina Center
*2 RIKEN Center for Advanced Photonics

References
1) T. Maly *et al.*: J. Chem. Phys. **128** 052211 (2008).
2) K. Takeda: *Triplet State Dynamic Nuclear Polarization* (VDM Verlag, 2009).
3) N. Saito *et al.*: Opt. Lett. **32** 1965 (2007).
4) K. Tateishi *et al.*: Proc. Natl. Acad. Sci. USA **111** 7527 (2014).

Realization of ^{1}H spin polarization of 40% at room temperature

K. Tateishi,[*1] T. Tsukihana,[*2] Y. Urata,[*2] S. Wada,[*2] and T. Uesaka[*1]

Dynamic Nuclear Polarization (DNP) is a means of transferring spin polarization from electrons to nuclei. As a method for enhancing bulk nuclear spin polarization, DNP has been successfully applied to areas ranging from fundamental physics to materials science, biology, and medical science. The conventional DNP, which is used radical as a polarizing agent, is carried out in the strong magnetic field and at cryogenic temperature (e.g. 3.35 T and 1.4 K) to polarize electron spins in the order of 10%.[1)] One approach for overcoming the limitation of the experimental conditions is to use non-thermalized electron spins instead. DNP with electron spins in the photo-excited triplet state (triplet-DNP) can achieve hyperpolarization independent of the magnetic field strength and temperature.[2)] We employed pentacene as a polarizing agent, which has an electron spin polarization of 73%, and *p*-terphenyl as a host material because of its stability at room temperature and large pentacene capacity.

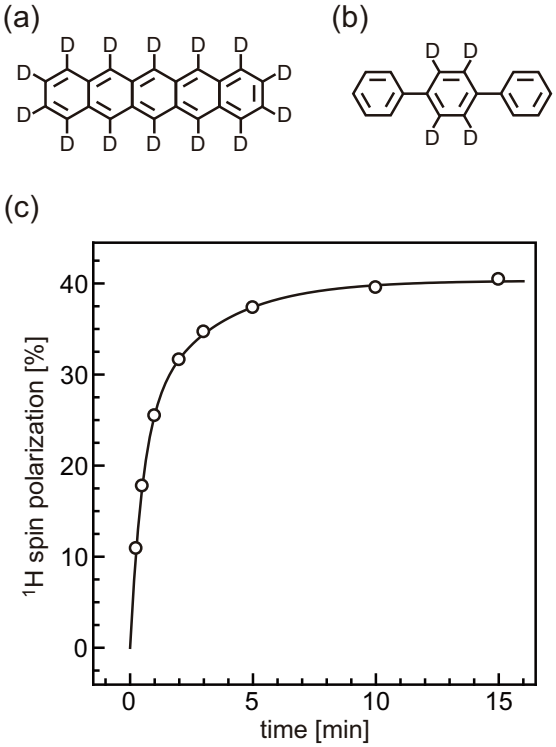

Fig. 1. (a) pentacene-d_{14}. (b) *p*-terphenyl-2',3',5',6'-d_4. (c) Polarization buildup curve. The polarizations were estimated by comparing the intensities of the hyperpolarized signals and the thermal intensities in 0.6 T at room temperature.

*1 RIKEN Nishina Center
*2 RIKEN Center for Advanced Photonics

In this study, we focused on realizing the highest ^{1}H spin polarization at *room temperature*. The finally achievable nuclear spin polarization with triplet-DNP is determined by the balance between the spin-lattice relaxation time of the nuclear spin (^{1}H in this report) and the speed of the polarization transfer.

In order to suppress the spin-lattice relaxation time[3)] , we used pentacene-d_{14} as the polarizing agent (Fig. 1(a)). The triplet electrons played the role of a polarizing agent as well as contributed to ^{1}H spin-lattice relaxation through a perturbation of the local field of the ^{1}H spins in the vicinity. In addition, we synthesized *p*-terphenyl-2',3',5',6'-d_4 (Fig. 1(b)). The ^{1}H spin-lattice relaxation in *p*-terphenyl-h_{14} was mainly due to the pendulum motion of the central benzene ring, which modulates the local dipolar field of the ^{1}H spins in and near the central ring.[4)]

A high-repetition-rate laser system was developed to increase the speed of polarization transfer, and it consists of two Neodymium-doped Yttrium Aluminum Garnet (YAG) lasers with wavelengths of 1064 nm and 1319 nm and LiB_3O_5 crystal for sum-frequency generation.[5)] The wavelength, pulse width, repetition rate, and output power were 589 nm, 126 ns, 3 kHz, and 1 W, respectively.

Using a single crystal of *p*-terphenyl-d_4 doped with pentacene-d_{14} and the new laser, we conducted the triplet-DNP in 0.65 T and at room temperature. The buildup curve is shown in Fig. 1(c). 40% of ^{1}H spin polarization was obtained in 15 minutes, which corresponded to the 20,000-fold enhancement under the same conditions.

Hyperpolarization techniques using photo-excited triplet electrons can be used to simplify DNP experiments. The NMR sensitivity of samples that prefer ambient temperatures can be boosted significantly.[3)] Bulk nuclear hyperpolarization in such low magnetic fields is also desirable to achieve the polarized target for RI beams[6)] and the polarized filter for neutron beams.[7)]

References

1) J. H. Ardenkjaer-Larsen et al.: Proc. Natl. Acad. Sci. USA **100** 0158 (2003).
2) K. Takeda: *Triplet State Dynamic Nuclear Polarization* (VDM Verlag, 2009).
3) K. Tateishi et al.: Proc. Natl. Acad. Sci. USA **111** 7527 (2014).
4) K. Kahda et al.: J. Phys. Soc. Jpn. **51** 3936 (1982).
5) N. Saito et al.: Opt. Lett. **32** 1965 (2007).
6) T. Uesaka et al.: Phys. Rev. C 82 021602(R) (2010).
7) M. Haag et al.: Nucl. Instrum. Methods Phys. Res., Sect. A 678 91 (2012).

Production of spin polarization of atoms in superfluid helium using a pulsed Ti: sapphire laser

M. Hayasaka,[*1,*2] T. Furukawa,[*3] H. Tomita,[*4] T. Takamatsu,[*4] K. Imamura,[*2,*5] T. Fujita,[*6] T. Kobayashi,[*7] H. Uematsu,[*1] H. Ueno,[*2] and Y. Matsuo[*8]

We are developing a new laser spectroscopic technique "OROCHI" to determine nuclear spins and moments of RI atoms. In this technique, superfluid helium (He II) is used as a material for trapping short-lived RI atoms. We utilize optical pumping to produce atomic spin polarization, and laser - radio frequency (RF) /microwave double resonance method to investigate Zeeman and hyperfine splittings of the RI atoms, respectively. In He II spin polarization can be maintained for a long time (>2 s in the case of Cs),[1] which enables us to produce a high degree of spin polarization. As for optical pumping, CW lasers are generally used to produce spin polarization. High-repetition-rate pulsed lasers can be superior in producing spin polarization owing to the large pumping rate. Using pulsed lasers, we expect to produce spin polarization efficiently for various atomic species that have not been spin-polarized yet. We here report on the production of spin polarization and RF resonance of Rb atoms in He II using a tunable pulsed Ti: sapphire (Ti: Sa) laser operated at 1-3 kHz.

We have constructed a pulsed Ti: Sa laser with a z-shaped cavity[2] originally developed at Mainz University (see Fig. 1). The Ti: Sa laser can lase in wide range of wavelength from 670 to 1050 nm[3] and UV output can be easily obtained by second harmonic generation. The Ti: Sa crystal is pumped by a second harmonic output of a Nd: YLF laser. The laser cavity contains four mirrors for light of wavelength ranging from 750 to 850 nm. The tunable range of wavelength using a birefringent filter is 749-790 nm. For the Rb experiment, the laser is tuned to the excitation wavelength of Rb atoms in He II (780 nm)[4]. At this wavelength the achieved output power is >150 mW at 1 kHz, and >200 mW at 2 and 3 kHz.

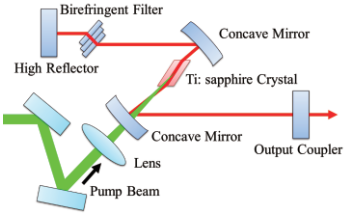

Fig. 1. Schematic diagram of the Ti: sapphire laser layout

*1 Department of Physics, Tokyo Gakugei University
*2 RIKEN Nishina Center
*3 Department of Physics, Tokyo Metropolitan University
*4 Department of Quantum Engineering, Nagoya University
*5 Department of Physics, Meiji University
*6 Department of Physics, Osaka University
*7 RIKEN Center for Advanced Photonics
*8 Department of Advanced Sciences, Hosei University

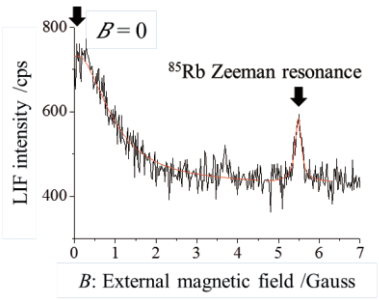

Fig. 2. RF resonance of ^{85}Rb obtained by applying RF frequency of 2.35 MHz. We can see the resonance peak at B = 5.4(9) Gauss and peak of LIF intensity with no spin polarization at B = 0 Gauss. The repetition rate of the pulsed laser was 3 kHz and the output power was 7.5 mW.

Using this pulsed Ti: Sa laser, we conducted experiments for Rb atoms in He II with optical pumping and laser-RF double resonance method.

Figure. 2 shows laser induced fluorescence (LIF) signal from Rb atom by the magnetic field swept from 0 to 7 Gauss. At B = 0, the LIF intensity was larger than that with magnetic field because spin polarization of atoms was not conserved. With increasing external magnetic field, the LIF intensity decreased due to the increase in spin polarization. When the RF frequency is in resonance with Zeeman splittings, the spin polarization was decreased and then LIF intensity was increased. In Fig. 2, we can see the RF resonance of the ^{85}Rb Zeeman transitions in He II. These results reveal that the produced spin polarization using pulsed laser was sufficient to observe RF resonance clearly. In the case of using pulsed lasers under 10 mW at 1 to 3 kHz repetition rate, we could produce comparable spin polarization to the CW laser experiment[4] and observe RF resonance.

In the future, we plan to use the pulsed Ti: Sa laser for optical pumping of atomic species that have not yet been spin-polarized and develop a technique to produce spin polarization of various atoms. The excitation wavelength of In atoms is 370 nm in He II[5]. We expect to produce spin polarization of In atoms using a second harmonic generation of the pulsed Ti: Sa laser.

References

1) T. Furukawa et al.: Phys. Rev. Lett. **96**, 095301 (2006)
2) J. Yi et al.: Jpn. J. Appl. Phys. **42**, 5066-5070 (2003)
3) K. Muramatsu.: Master Dissertation, Nagoya University (2011)
4) T. Furukawa.: Doctor Dissertation, Osaka University (2007)
5) Y. Kato. Master Dissertation, Meiji University (2012)

Microwave system development of enlarged spin-polarized proton target for RI beam experiments

S. Chebotaryov, [*1,*3] S. Sakaguchi, [*1,*2] T. Kawahara, [*1] W. Kim, [*3] E. Milman, [*1,*3] K. Tateishi, [*1] and T. Uesaka [*1]

A spin-polarized proton target provides opportunities to observe spin-dependent interactions in unstable nuclei. The center for Nuclear Study, University of Tokyo and RIKEN groups have developed a spin-polarized proton target system that is applicable to RI beam experiments.[1] The method of generating spin polarization employed in the target system is based on the cross-polarization technique,[2] where the polarization of an electron system is transferred to protons in the presence of a rotating magnetic field. The rotating field is generated as a standing electromagnetic wave using a microwave resonator.

Recently, the target system was upgraded to accomodate a target sample with a larger diameter (24 mm) compared with the diameter before (14 mm). This upgrade was carried out to increase the fraction of beam particles accepted by the target and to decrease the rate of background events from the target holder. One of the problems expected with this upgrade is that the standing electromagnetic wave in a large resonator is generally weaker than that in a small one, which might prevent us from producing a sufficiently strong field required for achieving optimal polarization conditions and attaining a high spin polarization.

To facilitate polarization transfer using the cross-polarization technique, electron and proton systems have to be coupled in order for spin-exchange interaction to occur. The coupling condition $\hbar\omega_e = \hbar\omega_I$ is known as the "Hartmann–Hahn condition"[3]. Here, ω_e is the electron effective Larmor frequency in an external microwave magnetic field H_1, and ω_I is the proton Larmor frequency. The electron effective Larmor frequency is proportional to the amplitude of H_1, $\omega_e \propto H_1$, and therefore ω_e can be adjusted to match the proton Larmor frequency. In the experiment, ω_e is tuned by changing the H_1 field amplitude, which in turn is proportional to the square root of the input power supplied to the system, $H_1 \propto \sqrt{P_{MW}}$.

In the test we performed previously,[4] it was found that the amplitude of the oscillating magnetic field was not sufficiently high to fulfill the Hartmann–Hahn condition. To address this problem, a redesign of the loop-gap resonator (LGR) has been attempted. LGR is the device responsible for generating a microwave field with power P_{MW} provided from an RF amplifier. It is made of a sheet of CuFlon material, which consists of a copper metal clad on both sides of a thin Teflon sheet. The CuFlon sheet is rolled around a holder to form a cylindrical resonator.[5] Our estimation shows that there is a possibility to increase the efficiency of the resonator by increasing the thickness of its copper plates from 4.4 to 36 μm, as thicker plates better suppress radiation losses due to the skin effect.

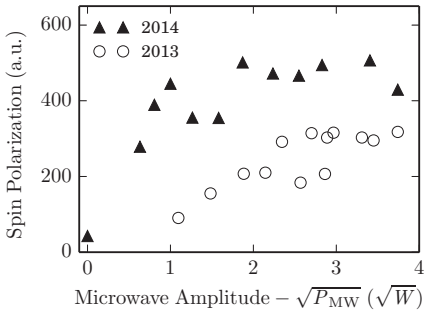

Fig. 1. Dependence of proton spin polarization signal intensity on the square root of the applied microwave power.

In Fig. 1, the closed triangles represent results of the present test carried out with LGR whose copper plates are 36 μm thick. It can be seen that saturation is reached at approximately 2.0 $\sqrt{W}$ of input power where the polarization stops increasing despite the increasing input power. The presence of saturation indicates that the Hartmann–Hahn condition was fulfilled, i.e., the polarization of electrons was fully transferred to the protons. In Fig. 1 the hollow circles indicate the results of the test carried out using LGR whose coppers plates are 4.4 μm thick. Here, the signal intensity rises across the entire region of powers applied, which means that the condition was satisfied only partially.

In summary, we designed LGR with thicker copper plates and performed test with it. The results of the test are promising – the Hartmann–Hahn condition is satisfied at reasonable microwave powers, which means that the newly constructed LGR should be suitable for application with enlarged target samples.

*1 RIKEN Nishina Center
*2 Department of Physics, Kyushu University
*3 Department of Physics, Kyungpook National University

References

1) T. Wakui et al.: Nucl. Instr. Meth. Phys. Res. A 550, 521 (2005).
2) A. Henstra et al.: Chem. Phys. Lett. 165, 6 (1990).
3) S. Hartmann, E. Hahn: Phys. Rev. 128, 2042 (1962).
4) S. Chebotaryov: in RIKEN Accelerator Progress Report Vol. 47, 187 (2013).
5) T. Barnard et al.: J. Magn. Reson., Ser A 120, 72 (1996).

The off-line adjustment of the parasitic production of low-energy RI-beam system for installation in BigRIPS

T. Sonoda,[*1] M. Wada,[*1] I. Katayama,[*1] N. Fukuda,[*1] H. Iimura,[*2] N. Inabe,[*1] T. Kubo,[*1] K. Kusaka,[*1] H. Takeda,[*1] H. Suzuki,[*1] M. Reponen,[*1] M. Wakasugi,[*1] K. Yoshida[*1] and SLOWRI collaborations

The construction of a low-energy RI-beam facility SLOWRI[1] began in 2013. The parasitic low-energy RI-beam production system (PALIS)[2] in SLOWRI was successfully manufactured in 2014. The preliminary installation of PALIS in the second focal plane chamber (F2) in BigRIPS was demonstrated. The performance evaluation of PALIS by off-line experiments is in progress.

We will restore unused RI-beams by installing a small gas cell in the F2 chamber in BigRIPS. This will provide parasitic low-energy RI-beams for various precision experiments whenever BigRIPS experiments are in operation. In order to realize the parasitic beam production, there should be no interference from PALIS in terms of BigRIPS beam tuning, detector operation and replacement, vacuum level, etc. This year we confirmed the following items whether there is no mechanical interference due to the installation of PALIS in the F2 chamber. The first item was the fitting check between the F2 chamber and PALIS which is integrated with the F2 chamber's roof[3]. Position reproducibility was ensured by using locating guide pins equipped in PALIS. PALIS, whose weights approximately 1100 kg, was carefully moved by a floor-operated crane and placed on the F2 chamber within <1.0 mm reproducibility without any trouble. The second item was the applicability for the replacement of detectors used for BigRIPS beam tuning without taking PALIS away. There are three detectors, i.e., two PPACs and one plastic scintillator inside the F2 chamber, they need to be occasionally replaced for maintenance. By using two maintenance windows equipped in PALIS, we confirmed that these detectors were able to be put in or out. The third item was the vacuum level for the F2 chamber together with PALIS. After several hours of pumping, the pressure in the F2 chamber was 10^{-4} Pa, the same as in conventional operation. Fig. 1 shows the photographs during the installation test of PALIS in the F2 chamber in BigRIPS.

The off-line experiment was started for the performance evaluation of PALIS. A new differential pumping method was implemented in PALIS from the result of a prototype system[4]. The differential pumping region is devided into four sections. The capability of differential pumping was verified; a pressure difference from approximately 10^5 Pa argon or helium in the gas cell down to 10^{-4} Pa in the final section was achieved, while using a 2 mm diameter gas cell exit hole.

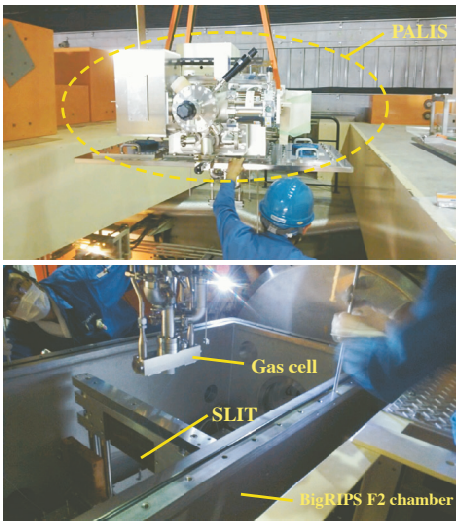

Fig. 1. The upper photo shows the entire PALIS integrated with the F2 chamber's roof. The lower photo is the gas cell part in PALIS.

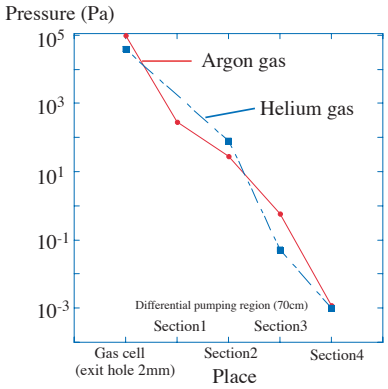

Fig. 2. Capability of differential pumping in PALIS.

We plan to start on-line commissioning experiments in 2015.

References

1) M. Wada et al., Hyp. Int. 199 (2011) 269.
2) T. Sonoda et al. APS Conf. Proc. 1104 (2009) 132.
3) T. Sonoda et al. ARIS2014 proceedings to be published.
4) T. Sonoda *et al.*: Nucl. Inst. and Meth. B295 1(2013).

*1 RIKEN Nishina Center
*2 Japan Atomic Energy Agency

Current status of the gas cell ion beam cooler-buncher at SLOWRI

Y. Ito,[*1] F. Arai,[*1,*2] I. Katayama,[*1] M. Reponen,[*1] P. Schury,[*1] T. Sonoda,[*1] M. Wada,[*1] and H. Wollnik[*1,*3]

Conversion of a continuous ion beam to a pulsed ion beam will be an essential process for various precision experiments at the SLOWRI facility[1]. Continuous ion beams from SLOWRI gas cells can be stopped and provided as low-emittance pulsed ion beams with a gas cell ion beam cooler-buncher (GCCB)[2]. The GCCB consists of a gas cell with an RF carpet (RFC), an RF quadrupole ion guide, and a flat trap[3]. Ion beams of energy as high as 30 keV will be injected into a low-pressure He gas cell, and then decelerated and thermalized solely by gas collisions. The ions will then be efficiently transported by the RFC and the RFQ ion guide to the flat trap, and then bunched and cooled.

In this process, there was a concern regarding the performance of the RF carpet at such unusually low pressure – as low as 2 mbar. Simulations indicated that a rough-pitch RFC could transport ions more efficiently than a fine-pitch RFC[4]. The transport and extraction efficiency was investigated experimentally using an RFC with a pitch of 0.32 mm and an exit hole with a diameter of 0.64 mm with K^+ ions. Here the pitch was twice as large as the fine-pitch RFC used in high pressure gas cells. The experimental parameters were optimized to achieve a high efficiency (described in Fig. 1), which is defined as the ratio of the ion current leaving the exit hole measured by a Faraday cup placed after the RFC to the ion current measured on the RFC electrodes when the RF and AF voltages are turned off.

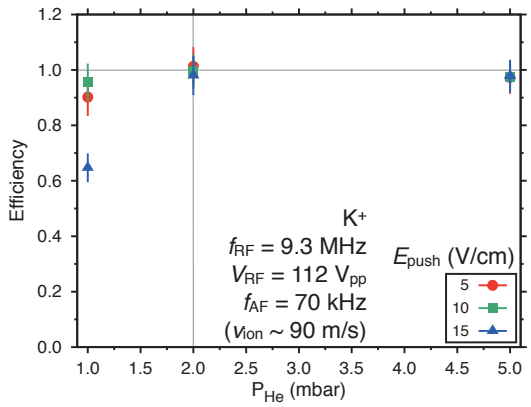

Fig. 1. Transport and extraction efficiency as a function of the He gas pressure for several E_{push} values.

As shown in Fig. 1, at He gas pressures higher than 2 mbar, efficiencies of ≈100% were obtained for a wide range of push electric field strengths. For an even lower gas pressure, such as 1 mbar, the efficiency slightly decreased; efficiencies of more than 60% were achieved even with the highest push electric field strengths. Compared to the efficiency of 22% seen with a fine-pitch RFC at 5 mbar, a rougher pitch can be expected to make the GCCB highly efficient.

Another concern was the injection of a 30 keV beam into the gas cell. The gas cell has no window to transport the low-energy ion beam, and thus all elements can be injected into the gas cell. However the incoming beam might be scattered due to the leak gas around the entrance. As a complementary idea, we are considering using nm-thick windows for the entrance. One option is a SiN membrane and the other is a Acetylcellulose membrane. The minimum thicknesses of SiN and Acetylcellulose membranes are 10 nm with 5×5 mm^2 area and 10 nm with ∼10 mm diameter, respectively. The ranges for both windows were calculated by the SRIM code as shown in Fig. 2. In both cases, the ranges at 30 keV for the elements as heavy as Cs are larger than the minimum thicknesses, indicating that ions can penetrate the windows. Because the residual ion energy after the window will be much lower than the windowless case, the size of the gas cell can be much smaller, i.e., total length of <100 mm.

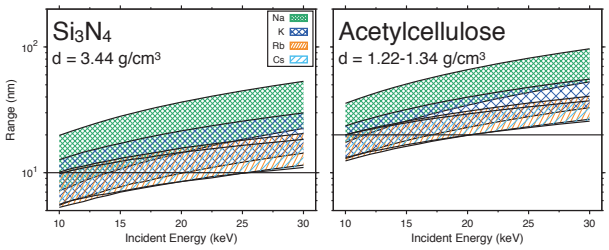

Fig. 2. Ranges as a function of the incident energy of an incoming ion beam for several elements with both SiN and Acetylcellulose membranes. The bands describe the range straggling in $\pm 1\sigma$ and the dashed lines indicate the minimum thicknesses for each material.

A performance test of these windows, i.e., a stress test for the pressure difference and the heat cycle between the room temperature and cryogenic temperature, will be performed soon. Using a 30 keV ion beam of stable nuclei, the overall efficiency of the GCCB with and without a window will be evaluated in FY2015.

*1 RIKEN Nishina Center
*2 Department of Physics University of Tsukuba
*3 Department of Chemistry and Biochemistry, New Mexico State University

References

1) M. Wada et al., Nucl. Instr. Meth. B **204**, 570 (2003)
2) Y. Ito et al., JPS Conf. Proc. **6** (2015) (in press)
3) Y. Ito et al., Nucl. Instr. Meth. B **317**, 544 (2013)
4) Y. Ito et al., RIKEN Accl. Prog. Rep. **47**, 205 (2013)

SCRIT luminosity monitor

S. Yoneyama,[*1,*2] A. Enokizono,[*1,*3] K. Kurita,[*1,*3] S. Matsuo,[*1,*3] Y. Moriya,[*1,*2] T. Ohnishi,[*1] T. Suda,[*1,*2] T. Tamae,[*1,*2] R. Toba,[*1,*4] M. Togasaki,[*1,*3] K. Tsukada,[*1,*2] T. Tsuru,[*1,*2] M. Wakasugi,[*1] and K. Yamada [*1,*3]

A luminosity monitor has been newly constructed and installed at the SCRIT electron scattering facility[1,2]. This monitor measures the number of bremsstrahlung photons produced by collisions between an electron beam and the target short-lived nuclei trapped in the SCRIT device. Using known a bremsstrahlung cross section, one can determine the collision luminosity on-line.

The monitor consists of a position detector and a calorimeter as shown in Fig. 1. The position detector measures the spatial distribution of the bremsstrahlung photons, and the calorimeter measures their energies. The position detector consists of two identical X- and Y-detectors, each of which has 16 optically isolated scintillating fibers of 3 × 3 mm^2 cross section. The scintillating fibers are coupled to a 4 × 4 multi-anode photomultiplier. The calorimeter consists of seven optically isolated pure-CsI crystals, each of which is 20 cm long with a hexagonal cross section with 4 cm sides.

In order to define the angular acceptance of the detector for the bremsstrahlung process, a large Pb block, 300 (h) x 300 (w) x 50 (t) mm^3, with a hole of 50 mm ϕ is placed in front of the monitor for collimation of bremsstrahlung photons. Note that the bremsstrahlung photons enters the center crystal of the calorimeter. The luminosity monitor is placed ∼670 cm downstream from the center of the SCRIT device.

Figure 2 shows the spatial distributions of bremsstrahlung photons, whose energy is larger than 50 MeV. The stored electron beam energies were 150 and 300 MeV, and typical stored currents were 250 mA for both energies.

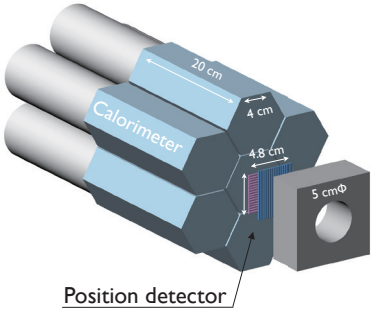

Fig. 1. Bremsstrahlung Luminosity Monitor.

Non-identical shapes observed for X and Y distributions should be attributed to the asymmetric material distributions of the storage ring along the beam axis, where the bremsstrahlung photons travel through. GEANT4 simulations are performed by taking the material distributions precisely into account as possibly, and the simulation results are found to reproduce the measured spatial distributions reasonably well. In addition, the measured energy distributions of the bremsstrahlung is also well accounted for by the simulation. Assuming that the trapped residual gases are purely oxygen, the collision luminosities are determined as L = 2.34 ± 0.09 cm^{-2}s^{-1} and 17.2 ± 0.69 cm^{-2}s^{-1}, respectively[3].

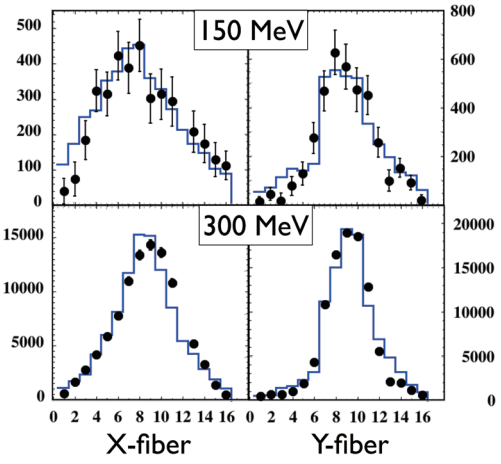

Fig. 2. X and Y distributions for E_e = 150 and 300 MeV

During the luminosity measurements mentioned above, elastically scattered electrons from the trapped residual gases were measured simultaneously using a newly installed high-resolution large-acceptance magnetic spectrometer, WiSES (Window-frame Spectrometer for Electron Scattering)[4]. As the elastic scattering cross section for oxygen is also well known, the collision luminosity will be independently determined from the elastic scattering events soon, and the results should be compared with that determined by the luminosity monitor.

*1 RIKEN Nishina Center
*2 ELPH, Tohoku University
*3 Department of Physics, Rikkyo University
*4 Department of Electrical Engineering, Nagaoka University of Technology

References

1) M. Wakasugi *et al.* Nucl. Instrum. and Method **B317**, (2013) 668.
2) T. Suda *et al.* Prog. Theor. Exp. Phys. **03C008**, (2012)
3) S. Yoneyama, Master thesis (in Japanese), (2014) Tohoku University.
4) K. Tsukada *et al.*, in this report.

Study of the performance of the SCRIT rear drift chamber

S. Matsuo,[*1,*2] A. Enokizono,[*1,*2] K. Kurita,[*1,*2] Y. Moriya,[*2,*3] T. Suda,[*2,*3] T. Tamae,[*2,*3] K. Tsukada,[*2,*3] T. Tsuru,[*2,*3] and S. Yoneyama[*2,*3]

The SCRIT electron spectrometer called WiSES (Window-frame Spectrometer for Electron Scattering) consists of a dipole magnet, front and rear drift chambers (FDC and RDC, respectively), a helium bag to reduce multiple scattering and plastic scintillators for event triggering. To obtain charge density distributions of unstable nuclei, the angular distributions of differential cross sections have to be precisely measured using elastic electron scattering. Thus, the WiSES is required to achieve a good momentum resolution ($\Delta p/p \approx 10^{-3}$) for a wide momentum range[1)], and the position resolution of the RDC is required to be ∼150 μm to achieve the momentum resolution. A newly developed electronics module (RAINER) is employed to read data for the RDC[2)]. In this article, we report performances of the RDC and RAINERs, which were examined using a tungsten wire target experiment in December 2014[3)].

Since the RDC and RAINERs are installed very close to the RF power source for the electron storage ring, the background noise effect must be carefully investigated. Although the RF noise test has been performed using a small prototype DC with RP1212 (an old version of RAINER) which showed a good performance[4)], the actual RF effect on the RDC is still uncertain. Therefore, we repeated the same RF noise test using the RDC and RAINERs prior to the wire target experiment. As shown in Fig. 1 (a), the noise level was found to be slightly larger than that observed in the previous report but still less than ∼800 mV in the worse case. Fig. 1 (b) shows the comparison of noise counts between the RF off and on cases as a function of the threshold voltage (V_{th}) for the ASD chip in RAINER. There is basically no difference in the noise rate for the RF on/off conditions at $V_{th} > 800$ mV, and the rate reduces to zero for $V_{th} > 2200$ mV. For the wire target experiment, V_{th} is set to 1500 mV, where the noise rate is still much smaller than the event rate (a few hundred hertz) and such a low-rate random background could be eliminated in the tracking.

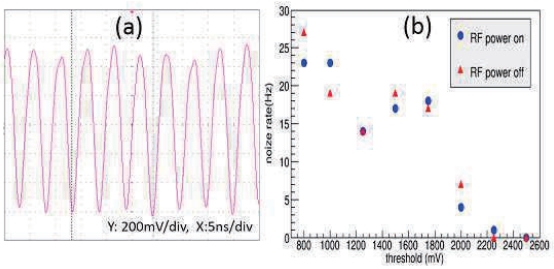

Fig. 1. (a) RF noise level measured at the ASD chip in the RAINER card. (b) Noise count rates as a function of V_{th} with/without RF power.

The RDC consists of 10 layers as VV′UU′XX′VV′UU′ and the tracking is performed using the following iterative algorithm. First, the U and V planes are determined using the hit position information for every four layers. Here, the initial hit position in each cell is calculated using TDC and a roughly estimated $x - t$ (space-time) calibration parameter. Second, a track is determined by combining the V/U planes and the hit positions in the remaining two X layers by minimizing χ^2/ndf. Then, the residual distributions between the initial hit positions and the track intersection on the layer planes and the $x - t$ calibration parameters are re-evaluated for each layer. The procedure is iterated (typically 4-5 times) until the widths of the residual distributions converge to the minima. The position resolution and efficiency per layer of the RDC were determined from the wire-target experimental data. Fig. 2 shows the converged residual distribution for a given V layer without the hit information of the layer. The rms was found to be ∼200 μm.

In summary, we conducted a wire target experiment for SCRIT WiSES and obtained calibration parameters for the RDC. Some efforts to improve the tracking algorithm are underway by tuning the calibration parameters to obtain a better position resolution.

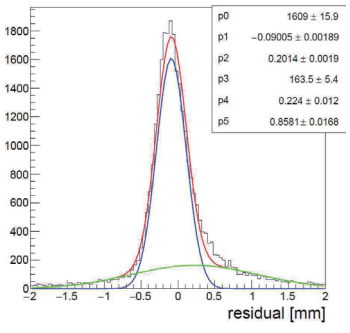

Fig. 2. Residual distribution of a V layer of the RDC

*1 Department of Physics, Rikkyo University
*2 RIKEN Nishina Center
*3 Research Center for Electron-Photon Science, Tohoku University

References

1) T. Suda *et al.*: Prog. Theor. Exp. Phys. 03C, 008 (2012)
2) A. Enokizono *et al.*: in this progress report.
3) K. Tsukada *et al.*: in this progress report.
4) S. Matsuo *et al.*: Accel. Prog. Rep. 47, 198 (2014)

Current status of RI beam production at electron-beam-driven RI separator for SCRIT (ERIS)

T. Ohnishi,[*1] S. Ichikawa,[*1] M. Togasaki,[*1,*2] K. Kurita,[*1,*2] and M. Wakasugi[*1]

ERIS (electron-beam-driven RI separator for SCRIT [1]) consists of an RI generator, a FEBIAD-type ion source, and an RI separator. The photofission of uranium driven by an electron beam is used for RI production in ERIS. Details of ERIS were reported in Ref. 2. During the present year, we improved the release efficiency including the efficiency of release from the production target and that of transport from the target to the ionization chamber. In this paper, we report improvements and the present status of ERIS.

One of the improvements is the stable supply of a 1-mm uranium carbide target disk. Using a 1-mm target disk, the efficiency of release from the production target is expected to increase, because the total surface area of target disks becomes larger than in the case of 2-mm target disks used in the previous test[3]. Uranium carbide is obtained by the carbothermal reduction of uranium oxide in presence of carbon. Details of constructing the target were presented in Ref. 3. In order to construct a thin disk, the careful selection of the graphite grain size is required for the process of constructing a disk from graphite powder. Furthermore, the uranium-oxide-coated graphite powder is also needed to construct a disk without a binder. These requirements are aimed at reducing the vacancy inside the disk and the crack at the edge of the disk. The obtained disk was approximately 1 mm in a thickness and 18 mm in a diameter. In total, 23 disks were prepared. The total amount of uranium was about 15 g, and the average mass concentration of uranium in the disk was estimated as 3.4 g/cm^3.

Another improvement involved strengthening the heat shield. In particluar, the heat shield of the transfer tube located between the target and the ionization chamber was increased in order to ensure no cold spots were present.

After these improvements, the uranium-carbide disks were irradiated with an electron beam accelerated to 150 MeV. The electron beam power was nearly 10 W. Tantalum disks with a thickness of 5 mm and a diameter of 20 mm were inserted in front of the production target to increase the production of γ rays. The temperature of the target and the transfer tube was approximately 2000 °C. The produced RIs were accelerated to 20 kV and mass-separated by the analyzing magnet. They were identified by the measurement of γ rays corresponding to the decay of the RIs using a Ge detector.

Figure 1 shows the rate of Sn and Xe isotopes at the Ge detector. These rates are estimated from the observed γ-ray yield using the efficiency of the Ge detector and the half-life of each isotope. The overall efficiency is the ratio of the observed rate to the expected production rate inside the target. This efficiency includes the efficiency of release from the target, ionization in the ion source, and efficiency of transport from the ion source to the detector. The overall efficiency of stable xenon with a calibrated gas flow was also measured during the experiment. Because stable xenon was introduced into the ionization chamber through a gas inlet, the measured overall efficiency of stable xenon includes only ionization and transport efficiencies. In the case of tin isotopes, the same ionization and transport efficiency as those of xenon can be used, which is supported by the results at ALTO[4]. As a result, the release efficiency of xenon and tin isotopes can be estimated. Table 1 shows the summary of rate and efficiency in the case of ^{137}Xe and ^{132}Sn. Compared with the previous results[3], the release efficiencies of ^{137}Xe and ^{132}Sn become almost nine and six times larger, respectively. Furthermore, the overall efficiency of ^{132}Sn at ERIS is achieved at same level as ALTO[4]. Further studies are in progress in order to realize the electron elastic scattering experiment with RI.

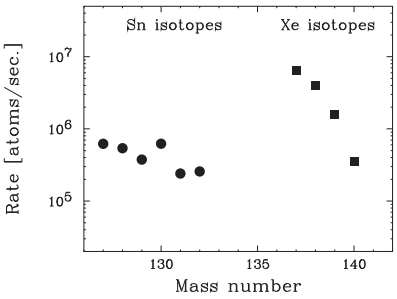

Fig. 1. Rate of Sn and Xe isotopes at the particle identification detector at ERIS. The electron beam power was almost 10 W. Total amount of uranium is 15g.

Table 1. Summary of rate and efficiency with 10-W beam

	^{137}Xe	^{132}Sn
Observed rate (atoms/s)	6.4×10^6	2.6×10^5
Expected rate (atoms/s)	7.5×10^7	1.3×10^7
Overall efficiency	8.4%	2.1%
Overall efficiency of stable xenon	14%	15%
Release efficiency	61%	14%

*1 RIKEN Nishina Center
*2 Department of Physics, Rikkyo University

References
1) M. Wakasugi et. al: Nucl. Instr. Meth. B**317**, 668(2013).
2) T. Ohnishi et. al: Nucl. Instr. Meth. B**317**, 357(2013).
3) T. Ohnishi et. al: RIKEN Accel. Prog. Rep. **47**, ?(2014).
4) M. Cheikh Mhamed et. al: Nucl. Instr. Meth. B**266**, 4092(2008).

Development of the readout system for SCRIT WiSES

A. Enokizono,[*1,*2] H. Baba,[*2] Y. Haki,[*3] K. Kurita,[*1,*2] S. Matsuo,[*1,*2] Y. Moriya,[*2,*4] T. Suda,[*2,*4] T. Tamae,[*2,*4] K. Tsukada,[*2,*4] T. Tsuru[*2,*4] and S. Yoneyama[*2,*4]

WiSES (Window-frame Spectrometer for Electron Scattering) has been developed for SCRIT experiments in order to achieve the world's first measurement of the detailed structures of unstable nuclei using electron elastic scattering[1]. A detailed description of the WiSES apparatus is reported elsewhere[2]. One of the key components of WiSES is the Rear Drift Chamber (RDC) and the readout module (RAINER). In December 2014, all WiSES components including RDC and RAINERs have been installed for a wire target experiment, and the performance has been measured[3)4)]. In this report, the setup of RDC and the WiSES readout system for the wire target experiment is described.

RDC has a volume of 274 cm x 36 cm x 78 cm and consists of 10 layers as UU′VV′XX′UU′VV′ made out of 1002 sense wires (20 μm Au-W) and 3026 field wires (80 μm Au-Al). Each drift cell has a hexagonal shape with each side measuring 1 cm, and He + CH_4 (50:50) gas is used with an operation voltage of 2.95 kV. During the performance measurement and burn-in test for a year, 2 field wires of the U and V layers had a high current problem and have been replaced. We have found no hot/dead channel and experienced no HV trip throughout the wire target experiment.

Figure 1 shows RAINER which is a general multipurpose readout card (15 cm x 20 cm) manufactured by REPIC and is capable of processing ADC and TDC for 64 independent channels. TDC is counted by FPGA with the timing resolution of ∼1 ns with an 8 μs ring buffer. One of the advantages of using RAINER is the reduction of analog background noises by digitizing the signal at FPGA and the data is sent on TCP. This is beneficial for RDC which is installed near SCRIT SR2's RF power source. An RF noise test has been performed and reported elsewhere[4]. 16 cards are mounted on RDC to read all 1002 channels and the data is sent to a DAQ PC via Ethernet cables with a Gigabit switching hub. It has two data write modes, i.e. RAW mode and zero suppression mode to help in speeding up the DAQ rate.

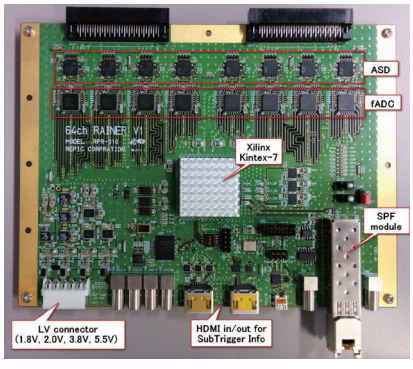

Fig. 1. RAINER card

As shown in Figure 2, two plastic scintillators are installed for triggering events and veto scintillators are also placed to remove cosmic events and background from the SR2 ring. TDC data for FDC are obtained with AMT-VME and the data is sent to the same DAQ PC as one for RAINERs. RIBFDAQ[5] (Babirl and ANAROOT) are used as the DAQ and online monitoring softwares. 16 RAINER data and VME data are taken by independent 17 processes using only one DAQ PC including the event builder. The DAQ performance test shows that there is no event loss up to a few kHz in the zero suppression mode. This is sufficient considering our trigger rate which is typically a few hundreds Hz including backgrounds.

In summary, SCRIT WiSES and the readout system have been developed and operated smoothly for the wire target experiment, except for a few minor issues. More studies and improvements of the DAQ system are underway toward the first electron-^{132}Sn scattering experiment at SCRIT in 2015.

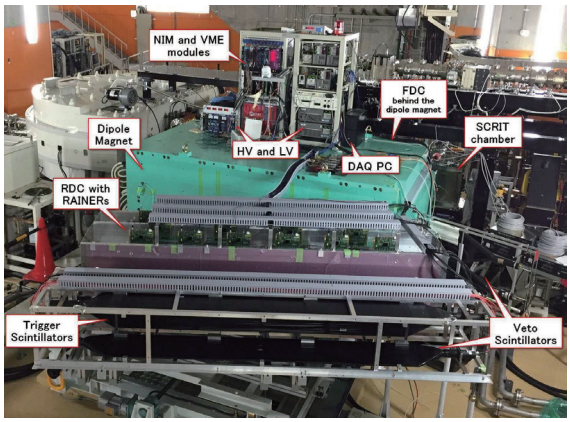

Fig. 2. Appearance of WiSES setup at SCRIT experiment.

*1 Department of Physics, Rikkyo University
*2 RIKEN Nishina Center
*3 REPIC Corporation
*4 Research Center for Electron-Photon Science, Tohoku University

References

1) M. Wakasugi *et al.*: NIM **B317**, 668 (2013).
2) T. Suda *et al.*: Prog. Theor. Exp. Phys. **03C008** (2012).
3) K. Tsukada *et al.*: in this progress report.
4) S. Matsuo *et al.*: in this progress report.
5) H. Baba *et al.*: NIM **A616**, 65 (2010).

New fast-kicker system for Rare RI Ring

Y. Yamaguchi,[*1] H. Miura,[*1,*2] Y. Abe,[*1,*3] and M. Wakasugi[*1]

We are developing a new fast-kicker system for Rare RI Ring. Figure 1 shows the block diagram of the new fast-kicker system. It primarily consists of a thyratron

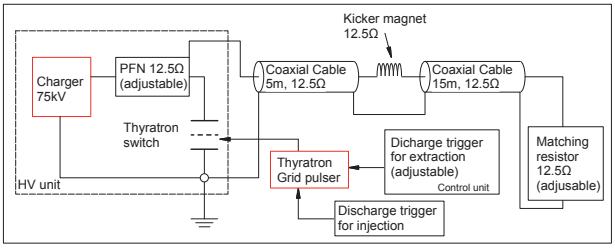

Fig. 1. Block diagram of the new fast-kicker system.

switch, a charger coupled with a pulse forming network (PFN), a kicker magnet, a matching resistor, and a control section of the discharge trigger. The thyratron is a deuterium-filled three-gap ceramic CX1171, which was assembled by e2v technologies. The kicker magnet is a distributed constant type magnet with a characteristic impedance of 12.5 Ω. We use a new substrate of the thyratron grid pulser on the basis of a previous feasibility study[1)] to shorten the response time. In addition, we adopt a fast-charger named the hybrid charging system[2)] to reduce the recharging time.

The new substrate of the thyratron grid pulser is mainly composed of four FET drivers, four MOSFETs, and four pulse transformers (PTs). Here, the response time refers to the interval between the time of input of the discharge trigger signal and the time of 10 % of the thyratron current output. The response time steadies at around 250 ns when the charging voltage becomes 25 kV or more.

The hybrid charging system, which consists of a main charging part and a sub-charging part, is indispensable for extracting a particle from the ring in 700 μs using the same kicker magnet. The main charge (90 %) is achieved in about 0.1 ms using a double forward converter composed of IGBTs and a PT. After the main charging process is completed, the sub-charging process is immediately started. The sub-charge is completed within 0.1 ms using a high-frequency (500 kHz) resonant circuit and a PT. In addition, a high-precision voltage divider, which connects to the sub-part coupled with a comparator, can be maintained at a constant charging voltage level within the range of fluctuation of less than ± 1 %. Figure 2 indicates an example of the PFN charging waveform for injection/extraction.

*1 RIKEN Nishina Center
*2 Department of Physics, Saitama University
*3 Institute of Physics, University of Tsukuba

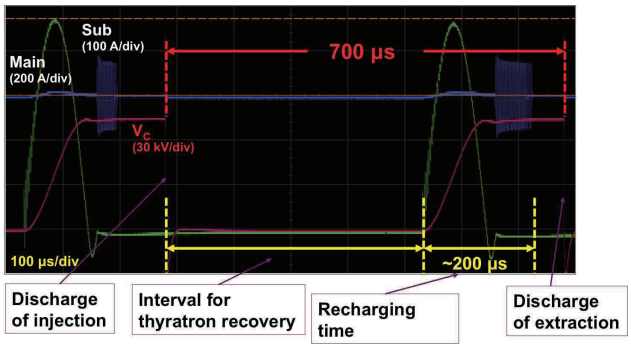

Fig. 2. PFN charging waveform for injection/extraction.

We fabricated a prototype twin kicker magnet to investigate the magnetic field by using a single-turn long search coil. Figure 3 shows the waveform of the magnetic field. Owing to the faster response time,

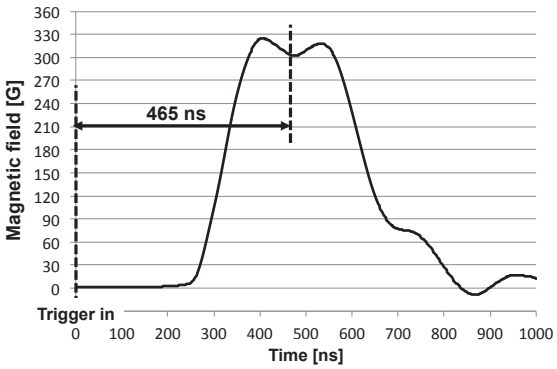

Fig. 3. Waveform of the magnetic field at the charging voltage Vc = 25 kV.

the propagation time from a trigger signal input to the power supply until the flattop center of the kicker magnetic field is about 465 ns. On the other hand, the shape of the flat-top part and the tail-part of the waveform does not satisfy our requirements. The fluctuation of the flat-top, which is defined as ±80 ns of the flat-top center, should be maintained at less than ±3%, and we want to restrict it to less than 0 ± 1% for the region after 355 ns (for 200 MeV/u) from the flat-top center. Therefore, we are trying to reduce the disturbance of the waveform.

References

1) Y. Yamaguchi et al.: RIKEN Accel. Prog. Rep. **44**, 157 (2011).
2) Y. Yamaguchi et al.: RIKEN Accel. Prog. Rep. **46**, 166 (2013).

Status of the resonant Schottky pick-up for the Rare RI Ring project

F. Suzaki,[*1,*2] Y. Abe,[*1,*3] S. Naimi,[*1] A. Ozawa,[*3] T. Suzuki,[*2] T. Uesaka,[*1] M. Wakasugi,[*1] K. Yamada,[*1] T. Yamaguchi,[*2] Y. Yamaguchi,[*1] J. Zenihiro,[*1] and Rare-RI Ring collaboration

Precise mass measurements of rare RI make a substantial contribution to the study of nucleosynthesis and nuclear structure. Rare RI Ring is an isochronous storage ring for precision mass measurements of rare RI [1,2]. The Rare RI Ring allows us to determine masses with a precision of 10^{-6}. For such high precision measurement, it is essential to maintain the isochronous condition at 10^{-6}. We are interested in neutron-rich nuclei that have short lifetimes and low production rates. To measure such nuclei, we adopted the individual injection technique, in which a single particle is injected to the ring and stored.

Resonant Schottky pick-up is a beam diagnostic device which can detect non-destructively the signal from a particle passing through the resonant cavity at the resonance frequency, $f_{\rm res}$. With the resonant Schottky pick-up we acquire revolution frequencies of nuclei circulating in the ring. The distribution of the revolution frequency corresponds to the distribution of the momentum of nuclei. We adopted the resonant Schottky pick-up as a monitor for tuning the isochronous field in the ring. Similar resonant Schottky pick-ups have been used for the same purpose at GSI[3] in Germany and IMP[4] in China.

We performed the offline performance test of the resonant cavity with a network analyzer[5]. From the measurements, $f_{\rm res} = 171.43$ MHz, shunt impedance $R_{\rm sh} = 161$ kΩ, unloaded quality factor $Q_0 = 1880$, and $R_{\rm sh}/Q_0 = 86$ Ω were obtained. With results of the offline test, the output signal power corresponding to a single ion with charge q at resonance[3] is estimated to be $P = q^2 \times 2.7 \times 10^{-21}$ W and the power of thermal noise $P_{\rm noise}$ is estimated to be 7.1×10^{-19} W. For $q \geq 17$, the signal from a single particle could be detected by the present Schottky pick-up.

We have started new offline test to investigate the sensitivity of the resonant Schottky pick-up. We developed a test system using the electron beam generated by an electron gun. Figure 1 shows the schematic view of the setup. We used a Ta filament cathode. A grid is connected to a function generator. With the output coupler, we detect the induced electromagnetic wave inside the resonant cavity at the resonance frequency. Usually, we obtain a DC electron beam when thermal electrons are accelerated. However, the DC electron beam does not induce the alternative electromagnetic field in the resonant cavity. Therefore, we add a frequency modulation at the desired frequency and amplitude into the grid. The modulated frequency is set to the resonance frequency. This simulates the ion circulation in the storage ring at the frequency. Changing the amplitude of the modulation controls the ion beam current. Therefore, we quantitatively evaluate the sensitivity of the resonant Schottky pick-up. The results of the test will be reported in coming publications.

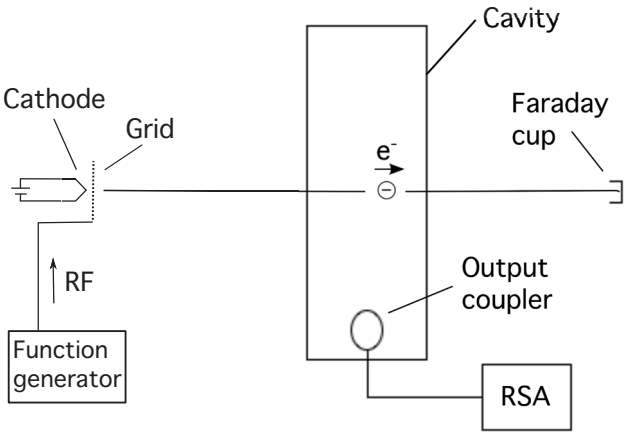

Fig. 1. Schematic view of the offline test using an electron beam. To induce an alternative electromagnetic field inside the resonant cavity, we use the grid to modulate the DC electron beam at the resonance frequency. Therefore alternative electromagnetic fields are induced by electrons passing through the resonant cavity. We detect the induced signals with a real time spectrum analyzer (RSA).

References
1) Y. Yamaguchi et al.: Nucl. Instrum. Methods. Phys. Res. B 317 (2013) 629.
2) A. Ozawa et al.: Prog. Theor. Exp. Phys. 2012 Issue 1 (2012) 03C009.
3) F. Nolden et al.: Nucl. Instrum. Methods. Phys. Res. A 659 (2011) 69.
4) J. X. Wu et al.: Nucl. Instrum. Methods. Phys. Res. B 317 (2013) 623.
5) F. Suzaki et al.: JPS. Conf. Proc. (ARIS2014) *in press.*

*1 RIKEN Nishina Center
*2 Department of Physics, Saitama University
*3 Institute of Physics, University of Tsukuba

Extraction of multi-nucleon transfer reaction products in ^{136}Xe and ^{198}Pt systems

Y. Hirayama,[*1] H. Ishiyama,[*1] S.C. Jeong,[*1] H. Miyatake,[*1] M. Oyaizu,[*1] Y.X. Watanabe,[*1] N. Imai,[*2] M. Mukai,[*3] S. Kimura,[*3] Y.H. Kim,[*4] M. Wada,[*5] T. Sonoda,[*5] P. Van Duppen,[*6] Yu. Kudryavtsev,[*6] and M. Huyse[*6]

We have developed the KEK Isotope Separation System (KISS) to study the β-decay properties of the neutron-rich isotopes with neutron numbers around $N = 126$ for astrophysics research[1–3]. In the KISS, a gas cell filled with argon gas at a pressure of 50 kPa, in which nuclei produced by multi-nucleon transfer reactions are to be stopped and collected, is essential equipment for selectively extracting the isotope of interest by using a resonant ionization technique. Using the elastic events of ^{198}Pt in the ^{136}Xe beam and ^{198}Pt target system, we evaluated the absolute extraction efficiency and beam purity of the KISS gas cell system. We successfully measured the lifetime of the unstable nucleus of ^{199}Pt extracted from the KISS.

We performed on-line tests using the ^{136}Xe beam with an energy of 10.75 MeV/nucleon and a maximum intensity of 20 pnA. The ^{136}Xe beam was directed onto the ^{198}Pt target placed in the gas cell, and was stopped at a tungsten beam dumper after passing through the gas cell. The thermalized and neutralized ^{198,199}Pt atoms of the reaction products were re-ionized in the gas cell, and the ions were extracted and detected after mass separation by using a Channeltron detector for ion counting. The lifetime of ^{199}Pt was measured by using β-ray telescopes newly installed at the E3 experimental hall[4].

We successfully extracted laser-ionized ^{198}Pt atoms emitted from the target by elastic scattering. However, the ^{198}Pt ions formed molecular ions such as $^{198}PtH_2$, $^{198}PtH_2O$, and $^{198}PtAr_2$ with the intensity ratio of 1, 1, and 6, respectively, relative to the intensity of ^{198}Pt ions. Figure 1 shows the measured extraction efficiency of the $^{198}PtAr_2$ molecular ions ($A = 278$) as a function of the primary beam intensity. The extraction efficiency was defined as a ratio of the number of $^{198}PtAr_2$ ions detected to the number of ^{198}Pt atoms emitted from the target by elastic scattering (17 barn). The measured efficiency of about 0.20% was observed to be independent of the primary beam intensity, as shown in Fig. 1, owing to the bend structure of the gas cell. The obtained beam purity was $> 99.7\%$ at the maximum primary beam intensity of 20 pnA.

After the extraction of ^{198}Pt, we extracted laser-ionized ^{199}Pt ($t_{1/2} = 30.8(2)$ min) atoms that mainly formed $^{199}PtAr_2$ molecular ions like ^{198}Pt did. Figure 2 shows the measured lifetime when $^{199}PtAr_2$ molecular ions are used. The measured lifetime $t_{1/2} = 33(4)$ min was in good agreement with the reported value. Thus, the molecular formation does not affect the lifetime measurement of unstable nuclei.

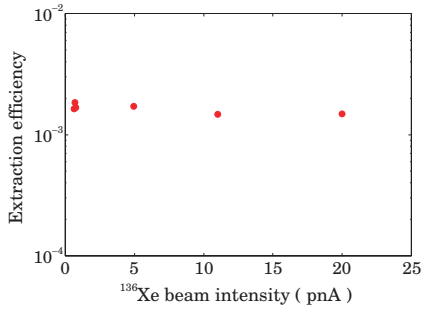

Fig. 1. Extraction efficiency of $^{198}PtAr_2$ molecular ions measured as a function of the ^{136}Xe beam intensity.

Considering the production rates of nuclei around $N = 126$ calculated by the GRAZING code[1], we can measure 12 new lifetimes with an efficiency of 0.1%, beam purity of $> 99.7\%$, and a primary beam intensity of 20 pnA. To extend this study to more neutron-rich nuclei, we have been developing a new sextupole ion guide with a large angular acceptance for increasing the extraction efficiency.

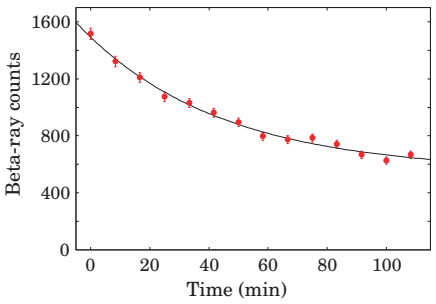

Fig. 2. Lifetime measurement of ^{199}Pt.

*1 Institute of Particle and Nuclear Studies (IPNS), High Energy Accelerator Research Organization (KEK)
*2 Center for Nuclear Study, University of Tokyo
*3 Department of Physics, University of Tsukuba
*4 Department of Physics, Seoul National University
*5 RIKEN Nishina Center
*6 Instituut voor Kern-en Stralingsfysica, KU Leuven

References

1) S.C. Jeong et al.: KEK Report 2010-2.
2) Y. Hirayama et al.: RIKEN Accel. Prog. Rep. **44** (2011) 25; **45** (2012) 152; **46** (2013) 176; **47** (2015).
3) H. Ishiyama et al.: RIKEN Accel. Prog. Rep. **45** (2012) 151.
4) S. Kimura et al.: reported in this RIKEN Accel. Prog. Rep. **48**.

Detector system for the KEK isotope separation system

S. Kimura,[*1] H. Ishiyama,[*2] N. Imai,[*3] S.C. Jeong,[*2] H. Miyatake,[*2] Y. Hirayama,[*2] Y.X. Watanabe,[*2] M. Oyaizu,[*2] M. Mukai,[*1] Y.H. Kim,[*4] and A. Ozawa[*1]

The KISS has been developed to study the β-decay properties of neutron-rich nuclei around neutron number N = 126 which determine the r-process path and form the third peak of the elemental abundance (A$\sim$195).[1,2] The detector system of the KISS requires high detection efficiency for low-energy β-rays because the nuclei of interest have small Q-value around 2 MeV. In addition, the system should be operated in a low-background environment because of the low production rates of these nuclei. Although the tolerable count rate of the background depends on the production rates, our ultimate goal is to set around several tens of counts per day, allowing access to these nuclei.

The detector system of the KISS consists of β-ray telescopes, Ge detectors, and a tape transport system. A schematic view of the detector system is shown in Fig. 1. For particle identification, three Ge detectors are employed to detect K-X rays emitted from the nuclei of interest. To efficiently count low-energy β-rays with low background, the β-ray telescopes are composed of three double-layered thin plastic scintillators; the thicknesses of the first and second layers are 0.5 mm and 1 mm, respectively. The solid angle of the β-ray telescopes is 90% of 4π.

The β-ray telescopes worked as designed. The energy spectra of the scintillators were in good agreement with Geant4 simulations. A comparison of energy deposit in the first layer between the simulation and the measured result is shown in Fig. 2. The measured efficiency of the β-ray telescopes for low-energy β-rays emitted from a ^{90}Sr/^{90}Y source was 55.4(15)% with an energy threshold of 20 keVee for the first layer and 30 keVee for the second layer.

The background rate of the β-ray telescopes was measured to be 5 cps. The origins of the background were considered to be cosmic rays and electrons scattered by γ-rays from natural activities. Initially, to reduce the cosmic rays, a veto counter system was installed, which consisted of plastic scintillators. The configuration of the plastic scintillators was designed based on the Geant4 simulation, and the designed value of the veto efficiency was 92% for 1 GeV muon. The veto counter reduced the previous background rate by 1.1 cps. In addition, to reduce the room background of γ-rays from natural activities, we installed

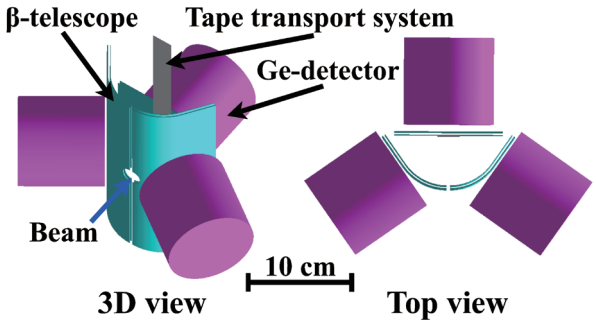

Fig. 1. Schematic view of the detector system.

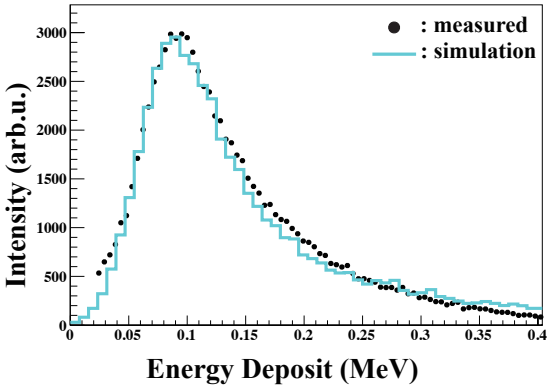

Fig. 2. Energy deposit distribution of the first layer for β-rays from the ^{90}Sr/^{90}Y source.

shields with low-activity Pb blocks and reduced the background rate by 2.4 cps. Finally, by raising the energy threshold of the second layer to 70 keVee without significant sacrifice of the detection efficiency for β-rays of interest, we reduced the background rate by 0.3 cps. In total, we reduced the background rate to 1.2 cps from 5 cps.

The main component of this background rate is environmental γ-rays and accidental coincidence rate in an extra active area of the scintillators. We will replace the present telescopes with new ones consisting of gas counters and thin plastic scintillators. Gas counters will be constructed with a small amount of materials to reduce the Compton scattering of γ-rays.

*1 Department of Physics, University of Tsukuba
*2 Institute of Particle and Nuclear Studies (IPNS), High Energy Accelerator Research Organization (KEK)
*3 Center for Nuclear Study, University of Tokyo
*4 Department of Physics, Seoul National University

References

1) S. C. Jeong et al.: KEK Report 2010-2.
2) Y. Hirayama et al.: In this report.

Q-value resolution improvements in the spectroscopy of deeply bound pionic atoms using BigRIPS

T. Nishi,[*1,*2] D. Ahn,[*2] G.P.A. Berg,[*2,*3] M. Dozono,[*2] D. Etoh,[*2,*4] H. Fujioka,[*2,*5] N. Fukuda,[*2] N. Fukunishi,[*2] H. Geissel,[*2,*6] E. Haettner,[*2,*6] T. Hashimoto,[*2] R.S. Hayano,[*1] S. Hirenzaki,[*2,*7] H. Horii,[*1,*2] N. Ikeno,[*4,*8] N. Inabe,[*2] K. Itahashi,[*2] M. Iwasaki,[*2] D. Kameda,[*2] S. Kawase,[*9] K. Kisamori,[*2,*9] Y. Kiyokawa,[*9] T. Kubo,[*2] K. Kusaka,[*2] M. Matsushita,[*9] S. Michimasa,[*9] G. Mishima,[*1,*2] H. Miya,[*2] D. Murai,[*2] H. Nagahiro,[*7] M. Niikura,[*1,*2] S. Ota,[*9] N. Sakamoto,[*2] K. Sekiguchi,[*2,*4] H. Suzuki,[*2] K. Suzuki,[*2,*10] M. Takaki,[*9] H. Takeda,[*2] Y.K. Tanaka,[*1,*2] T. Uesaka,[*2] Y. Wada,[*2,*4] Y.N. Watanabe,[*1,*2] H. Weick,[*2,*6] H. Yamakami,[*2,*5] Y. Yanagisawa[*2] and K. Yoshida[*2]

In June 2014, we performed missing-mass spectroscopy on the deeply bound pionic atoms to measure their binding energies and widths.[1,2] The Q values of the ^{122,117}Sn(d,^{3}He) reactions were measured using BigRIPS near the π^- emission threshold. We succeeded in accumulating a sufficient number of events and achieved the best Q-value resolution in the spectroscopy of the Sn(d,^{3}He) reaction thus far. In this paper, we report how we achieved the resolution.

We improved two aspects. First, the emittance and momentum spread of the primary beam were reduced by optimizing accelerator parameters. Second, the optics of the beam-transfer line was adjusted to realize optimum dispersion matching. Here, the "beam-transfer line" indicates the beam line from the exit of SRC to the F0 focal plane in BigRIPS.

The emittance and momentum spread were monitored using the beam position and angle at the achromatic focal plane F3 and the dispersive focal plane F5 in BigRIPS. According to these measurements, the voltage and phase of the flat top cavity of SRC, the phase of the RF of RRC, and the voltage of the rebuncher were optimized. We also optimized the phase slit inside and the double slits downstream of the AVF cyclotron. After optimization, we achieved an emittance of 0.2 × 2.0 πmm·mrad (horizontal) and a momentum spread of 0.027% (σ), which are dramatic improvements from those achieved in the pilot experiment: an emittance of 0.7 × 3.0 πmm·mrad and momentum spread of 0.04% (σ).

To adjust the dispersion at F0, a new method was developed using position information at the F3 and F5 focal planes. In our experiment, we developed new ion optics with finite dispersion at F0 to realize the dispersion-matching condition.[3] However, there are no high-precision position/angle detectors in the beam-transfer line to tune the optics. In the new method, the momentum deviation of the particle and the position at F0 can be deduced through position measurements at F3 and F5 using the following equations:

$$x_0 = x_3/(x|x)_{03},$$
$$\delta = (x_5 - (x|x)_{35}x_3)/(x|\delta)_{35}.$$

Here, x_0, x_3, and x_5 are the positions at the F0, F3, and F5 focal planes in BigRIPS, respectively. $(x|x)_{03}$ and $(x|x)_{35}$ are the magnifications from F0 to F3 and from F3 to F5, respectively. $(x|\delta)$ represents dispersion. Because of achromatic transport from F0 to F3, $(x|\delta)_{03}$ is assumed to be 0. These transfer matrix elements of BigRIPS were measured in advance by setting the optics of the beam-transfer line to the standard mode, in which the F0 focal plane was achromatic. Figure 1 shows the 2D plot of the deduced δ and x_0. By using this method, we could measure and improve the new optics in the beam-transfer line.

As a result, we succeeded in improving the Q-value resolution. The peaks in the online spectrum of the present experiment were clearly narrower than those of similar past experiments. The precise analysis is in progress.

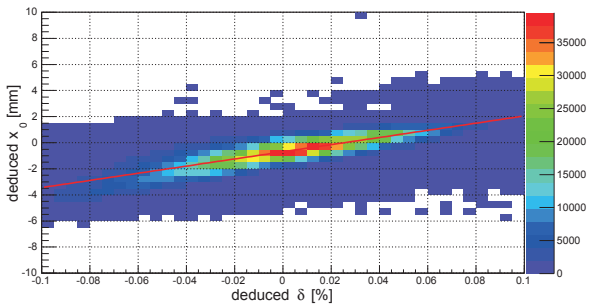

Fig. 1. Scatter plot of x_0 versus δ deduced from x_3 and x_5. The slope corresponds to the dispersion at F0.

*1 Department of Physics, University of Tokyo
*2 RIKEN, Nishina Center
*3 JINA and Department of Physics, University of Notre Dame
*4 Department of Physics, Tohoku University
*5 Department of Physics, Kyoto University
*6 GSI Helmholtzzentrum für Schwerionenforschung GmbH
*7 Department of Physics, Nara Women's University
*8 YITP, Kyoto University
*9 CNS, University of Tokyo
*10 Stefan Meyer Institute, Austrian Academy of Sciences

References

1) K. Itahashi et al.: *RIBF Proposal* **No.054** (2008).
2) K. Itahashi et al.: *RIBF Proposal* **No.054R1** (2013).
3) T. Nishi et al.: Nucl. Instrum. Methods. in Phys. Res. B 317 290-293 (2013).

Development of D_2 gas-filled drift chamber for spectroscopy measurements of pionic atoms in inverse kinematics

Y. N. Watanabe,[*1,*2] H. Fujioka,[*1,*3] R. S. Hayano,[*2] K. Itahashi,[*1] T. Nishi[*1,*2] and Y. K. Tanaka[*1,*2]

We report the development of a D_2 gas-filled drift chamber for spectroscopy measurements of pionic atoms. We plan to perform missing-mass spectroscopy measurements of deeply bound pionic atoms in inverse kinematics of the (d,^{3}He) reaction. We will employ a D_2 gas-filled multi-wire drift chamber (MWDC) as an active target in a magnetic field of $\sim$ 1 T. A heavy ion beam is injected into the chamber inside which the reaction occurs. The reaction angle and the energy of forward scattered ^{3}He are measured using the MWDC and silicon strip detectors, which are installed inside the MWDC. The energy of the ^{3}He is approximately 60 MeV. The feasibility of the measurements was investigated through simulations in a previous study.[1)] According to the results of the simulations, a position resolution of 500 μm and enough gain to measure 60 MeV ^{3}He are required for the MWDC.

To check the performance of the D_2 gas-filled MWDC, we fabricated a prototype of the detector. For the MWDC, hexagonal wire geometry, in which a sense wire is surrounded by six potential wires, is adopted. The side length of the hexagon is 6 mm. The MWDC consists of 10 planes, five of which are tilted (two U planes at 18° and three V planes at -18° as shown in Fig. 1) to measure the vertical position of charged particles. The outer cells serve as guard wires against chamber walls to eliminate field deformation.

Figure 2 shows the measurement setup. Inside the MWDC, an α source (^{241}Am, 4.3 kBq) was placed and a silicon strip detector (12 strips, 37.5 × 50 mm^2, 300 μm thick) was installed on the opposite side. The trigger was initiated by the signal of the silicon detector and the timing of the MWDC signal was recorded using a TDC. In this measurement, the chamber was filled with 1 atm H_2 gas instead of D_2 gas as the first step.

Tracking analysis was performed and position resolution was evaluated when a HV of -1420 V was applied to the potential wires. The α-ray detection efficiency was higher than 99% for all planes except for the first one. Figure 1 shows a typical event display. The drift length in each cell is expressed as a circle and the hit strip in the silicon strip detector is painted black. The track was successfully reconstructed as indicated by the red line in Fig. 1. The position resolution of the planes with vertical and tilted wires was evaluated to be 100 – 150 μm and 100 – 250 μm. The resolution is sufficient for the experiment if the magnetic field does not deteriorate the resolution considerably.

*1 RIKEN Nishina Center
*2 Department of Physics, University of Tokyo
*3 Department of Physics, Kyoto University

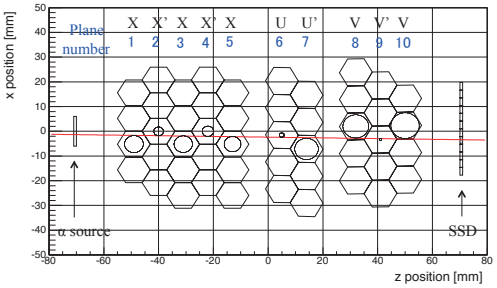

Fig. 1. An example of an event display. There are potential wires on the vertices and sense wires at the center of the hexagons. The circles represent the drift length for each wire and the straight line is the deduced track.

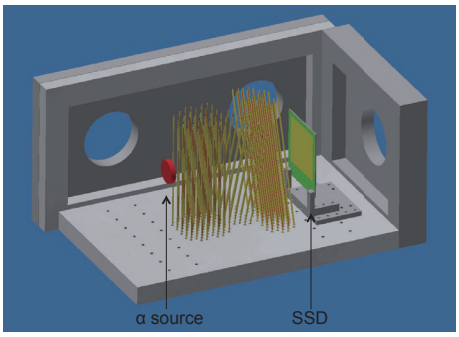

Fig. 2. A schematic drawing of the measurement setup. An α source was placed in front of the first plane and a silicon detector was placed on the opposite side.

In the measurement, we observed the position dependence, i.e., the plane dependence of gas gain. In the fifth – eighth planes, facing blank regions, the gas gain was more than five times larger than that in the other planes when HV was -1420 V. This was due to the geometrical configuration of the wires, and it was qualitatively confirmed through Garfield[2)] calculations that the electric field strength in these planes was effectively 5% higher. Geiger-mode behavior in these planes caused a rapid increase of current and made it difficult to apply higher voltage. We found that extra guard wires were needed facing the blank regions. Under the current condition, the detection efficiency for 60 MeV ^{3}He in the low-gain planes was estimated to be less than 20%.

As the next step, we will improve gain uniformity by applying discrete voltage to each plane.

References

1) K. Okochi et al.: Accel. Prog. Rep. **46**, 79 (2013).
2) R. Veenhof: Garfield, (http://garfield.web.cern.ch/garfield)

Radiation monitoring in the RIBF using ionization chamber

M. Nakamura,*1 K. Yamada,*1 A. Uchiyama,*1 H. Okuno,*1 and M. Kase*1

In recent years, we have attempted to monitor radiation due to beam loss in the RIBF by using self-made ionization chambers (ICs)[1),2),3)] However, in the course of RIBF operations, a part of $^{238}U^{86+}$ ion beam accelerated at 345 MeV/nucleon struck the septum electrode of the electrostatic deflection channel (EDC) of RRC and the septum was damaged in December 2012. To avoid such serious damages, the part of septum where the ion beams can easily irradiate was cut off and molded to the "V-shaped" edge and many thermocouples (TCs) were set at the surface of the septum. Before the septum was damaged by the irradiation of ion beams and the consequent rise in temperature, these signals are input to BIS. However, the response time of these TCs are estimated in the order of few seconds. Furthermore, such results showed that the septum was damaged only when a part of the $^{238}U^{86+}$ beam hit the septum within 10^{-1} to 1 s. Hence, a faster signal for BIS with a response time of at least of the order of 10^{-1} s is required. On the other hand, the response time of IC can be estimated to the order of 10^{1} ms. The response time of the whole BIS is about 1～max. 25 ms. Accordingly, we can obtain the response time to the order of 10^{-1} s when the alarm signal from IC is used for BIS. Hence, we investigated to introduce the alarm signal from IC around the EDC of RRC into BIS in the case of $^{238}U^{86+}$ ion beam acceleration.

Usually, we input the alarm signal from IC near the EDC of SRC to BIS after the "calibration experiments"[1,2)]. In these experiments, the ion beams were attenuated from 1/100 to 1/10 and irradiated to the EDC for a fairly short time and IC voltages were measured. From these results, we can estimate the alarm levels of IC to BIS. However, it can be very dangerous to irradiate heavy-ion beams to the EDC of RRC because of a sudden increase in the temperature of the septum. Therefore, we can consider the alarm levels of IC from the signals of TCs set at the septum. When the temperature difference between the TC set at the upper part of the septum with the TC set at the beam-exit side of the septum (defined as "the maximum value of septum temperature rising") becomes 10℃, the alarm signal is input to BIS. Hence, we have compared the maximum value of septum temperature rising with the signal of IC set near the EDC of RRC in the machine time of the $^{238}U^{86+}$ beam. The result is shown in fig. 1. The data showed little dispersion and the calibration curve in fig. 1 can be drawn. From this curve, we can recognize that the voltage of IC became about 1.4 V when the maximum temperature rising of EDC reached 10℃, shown as red dotted line in fig. 1. Then we can decide the alarm level of IC for BIS for the $^{238}U^{86+}$ ion beam.

*1 RIKEN Nishina Center

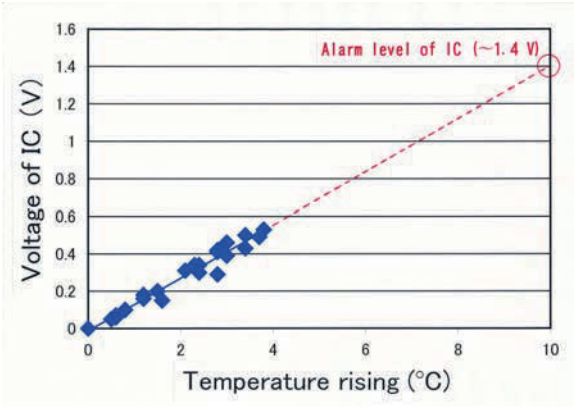

Fig. 1 Correlation of IC voltage and maximum value of septum temperature rising

We have input the alarm signal to BIS from April 28 to May 12 and from October 16 to November 14, 2014 when the $^{238}U^{86+}$ ion was accelerated at 345 MeV/nucleon. On May 5, the BIS by the alarm signal from IC acted and stopped the operations of RIBF. Fig. 2 shows the IC signal from May 5, 0:00 to 9:00. At 5:45, the signal suddenly rose up to 6.4 V and the alarm signal was sent to BIS. We could confirm that this signal reached BIS faster than the alarm signals from TCs set at EDC. After this signal, any alarm from IC did not reach BIS in the machine time of the $^{238}U^{86+}$ beam in 2014. The cause of this unusual signal shown in fig. 2 is unknown. In any case, as described above, we could confirm that the faster alarm signal to BIS can be input from the IC near the EDC of RRC. Thus, we investigated to input the alarm signal from IC in RRC to BIS each time heavy ions are accelerated, such as $^{238}U^{86+}$.

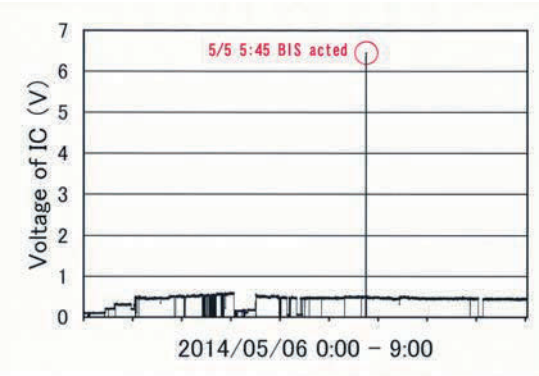

Fig. 2 Signal from the IC near EDC of RRC

References

1) M. Nakamura et al.: RIKEN Accel. Prog. Rep. 44, 293 (2011)
2) M. Nakamura et al.: RIKEN Accel. Prog. Rep. 45, 228 (2012)
3) M. Nakamura et al.: RIKEN Accel. Prog. Rep. 47, 310 (2014)

Measurement of activation around the He gas stripper at RIBF

A. Akashio,[*1] K. Tanaka,[*1] and H. Imao[*1]

The activation of the He gas stripper setup caused by a uranium beam was evaluated. There are several types of gas and solid stripper setup in RIBF, and a stripper setup is selected for the beam nuclide, such as uranium, xenon, and calcium. The He gas stripper setup has been developed for uranium beam acceleration at RIBF. [1] The stripper setups are often exchanged with other types to change the beam nuclide of the RIBF accelerator. The radiation exposure caused by the residual dose during the exchange and maintenance works is a serious issue. Thus, evaluating the residual dose and studying the origin of the dose are important to improve future setups. This evaluation is also applicable for the shielding design of future facilities.

In this study, the activation method was applied for the He gas stripper irradiated by a uranium beam. During the machine operation in the autumn of 2014, the samples were placed both inside and outside the stripper chamber. After uranium beam irradiation, the γ rays emitted from the samples were measured using a Ge detector.

The energy of the uranium beam on the stripper was 10.75 A MeV and the beam intensity in operation was 1200 particle nA. The beam irradiated for one month. The He gas pressure was 7 kPa, and the gas thickness was approximately 50 cm which corresponds to 0.7 mg/cm^2. The sample materials were aluminum and bismuth. The aluminum sample is made of the same material as the gas stripper chamber. Bismuth is a useful element for neutron measurement. Radioactive isotopes of bismuth are generated by neutron irradiation, and the generated isotope nuclides depend on the neutron energy because of the threshold energy of the reactions, as listed in table 1.

Some of the aluminum samples were set in the gas stripper chamber where the He gas pressure was highest. The distance between the nearest sample and the uranium beam was 47.25 mm. The samples placed inside the stripper chamber were hit by the nuclei of the fission products of the uranium beam. The other aluminum samples set outside the striper chamber are sensitive to the neutron only because the fission products stop in the chamber wall and do not reach outside. Thus, the aluminum samples are the benchmark of the neutron activation of aluminum chamber itself. The bismuth samples are set with the aluminum samples outside the chamber to obtain the neutron energy on the aluminum samples.

Figure 1 shows the measured γ-ray spectrum obtained from the aluminum sample set inside the chamber after cooling for 13.5 days. Table 2 lists the identified nuclides with short half lives. Typical nuclides of the fission products from the ^{238}U beam were observed. γ ray peaks from long-lived nuclides were not observed yet in the spectrum owing to the high background γ rays from the short-lived nuclides. γ-ray peaks of aluminum itself, such as ^{24}Na with a 15 hour half life, were not found.

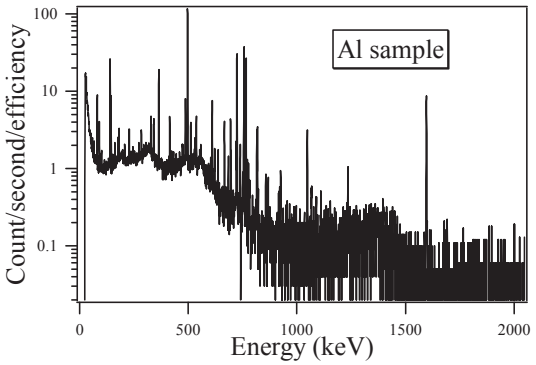

Fig. 1. Typical γ ray spectrum of the Al sample set in the gas stripper chamber. Many energy peaks caused by radioactive isotopes generated from the fission of ^{238}U were observed.

Table 1 lists the observed bismuth isotopes in the natural ^{209}Bi samples that were set outside the stripper chamber. The result suggests that the energy of irradiated neutrons on the bismuth samples was up to 22.55 MeV, since γ rays from the ^{205}Bi nucleus, which have a threshold energy of 28.6 MeV, were not detected.

After cooling the samples for a long time and background levels become low, γ rays from the long-lived nuclides will be detected. The result will be compared with a Monte Carlo simulation result to evaluate radiation issues in the future.

Table 1. Threshold of neutron energy corresponding to the production of radioactive bismuth isotopes observed in this study.

Nuclide	Half life	Reaction	Threshold
^{207}Bi	31.6 year	^{209}Bi(n,3n)^{207}Bi	14.12
^{206}Bi	6.4 day	^{209}Bi(n,4n)^{206}Bi	22.55

Table 2. Typical radioactive nuclei observed in the aluminum sample inside the stripper chamber.

Nuclide	Half life	Nuclide	Half life
^{95}Zr	64 day	^{136}Cs	13 day
^{95}Nb	35 day	^{140}Ba	13 day
^{99}Mo	2.8 day	^{140}La	1.7 day
^{99m}Tc	6.0 hour	^{141}Ce	32.6 day
^{103}Ru	39 day	^{147}Nd	11 day
^{131}I	8.0 day		

References

1) H. Imao et al.: Proc. of IPAC2013, Shanghai, China, May 2013 THPWO038, p.3851 (2013).

*1 RIKEN Nishina Center

Beam preparation for fee-based utilization of a 70-MeV/A Kr-beam

T. Kambara*1 and A. Yoshida*1

In October 2014, RIKEN provided a 70 MeV/A Kr beam from the RIKEN Ring Cyclotron (RRC) to private companies as the first fee-based utilization.[1] Since the customers required irradiations in an atmosphere with a uniform flux distribution over a large area and specified linear energy transfer (LET), we developed the following system at the E5A beam line and successfully delivered desired beams to the customers.

The uniform beam-flux distribution was achieved with wobbler magnets and a scatterer foil. A pair of 60-Hz wobbler magnets deflected the beam from the RRC vertically and horizontally so that the beam center traced a circle. At about 68 cm downstream, the beam passed through a scatterer (48-μm thick Au foil), where multiple scattering brought about a lateral velocity distribution. At about 392 cm downstream from the scatterer, the beam passed to the atmosphere through an 8-cm diameter and 75-μm thick polyimide (Kapton) vacuum-separation window.

In the atmosphere part of the beam path, we used an energy degrader and several detectors to control the LET and measure the beam characteristics. Figure 1 shows the configuration. After the window, there were an ionization chamber (IC: Applied Engineering Inc., AE-1341S) and a 0.5-mm thick plastic scintillator for measuring the total beam intensity. The IC had a 5-cm diameter window that determined the beam size downstream. An adjustable energy degrader (Wood-Bell Co. Ltd.) followed to control the LET, where the beam energy was adjusted by inserting up to eight Al foils with 8-cm diameter and thicknesses of 12.8, 23.8, 48.6, 100.2, 100.8, 196.4, 486.0, and 975.4 μm. We can insert any combination of the foils by using a remote-control pneumatic system to set the LET almost continuously. After the degrader, two sets of $\Delta E + E$ Si-detector stacks were mounted on a motor-driven linear slider; the detectors can be not only placed at the center of the beam path but also horizontally moved across the beam for measuring the beam-flux distribution. The customer samples were placed at about 10 cm downstream from the Si detectors.

Beam scanning with the Si detectors revealed that the beam flux was uniform within ±1.8 % over a diameter of about 35 mm. Another measurement with a GAFCHROMIC-film irradiation showed that the local deviation of the dose was within ±5 %.

For the beam-intensity measurements, the scintillator counted the ions from nearly-zero intensity to about 2.5×10^5 ions/s and the IC was available from 400 to 2.5×10^6 ions/s.

We adjusted and verified the LET at the sample in the following way: Increasing the thicknesses of the degrader foils, we measured the beam energy by using the Si detectors until the beam was totally stopped. Then we compared the thickness-energy relation to SRIM calculations[2] and obtained the stopping power in the sample as a function of the degrader thickness, with a correction for the energy loss in the atmosphere between the Si detector and the sample. We considered the stopping power as the LET.

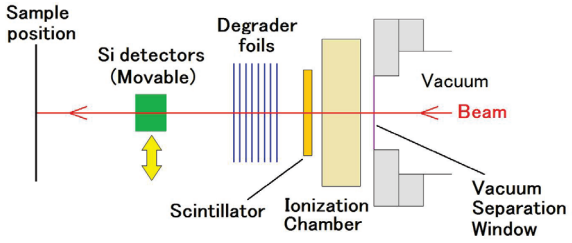

Fig. 1. Setup of Kr-beam irradiation after the window.

Figure 2 shows the relation between the LETs of ^{40}Ar, ^{84}Kr, and ^{132}Xe ions at the surface of Si and their ranges in the material. The 70-MeV/A ^{84}Kr beam from the RRC has the maximum energy of 43 MeV/A at the irradiation position, which corresponds to an LET between 13.2 and 40.9 MeV/(mg/cm^2); the solid line in Fig. 2 indicates this region. In addition, if we use 95-MeV/A ^{40}Ar and 26-MeV/A ^{132}Xe beams accelerated by the RRC, an LET from 2.3 to 69 MeV/(mg/cm^2) is available at the same beam line.

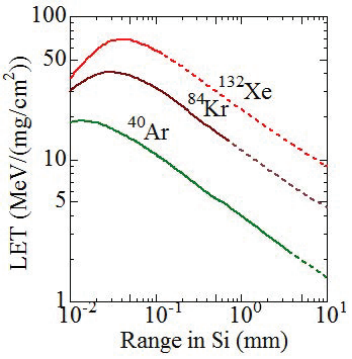

Fig. 2. LETs of ^{40}Ar, ^{84}Kr, and ^{132}Xe ions at the surface of Si as functions of their ranges. The solid lines correspond to the ions accelerated by the RRC and extracted to the atmosphere.

*1 RIKEN Nishina Center

References
1) A. Yoshida et al.: In this report.
2) J. F. Ziegler: http://www.srim.org.

Implantation of ^{7}Be and ^{22}Na beams for wear diagnostics application

A. Yoshida,[*1] T. Kambara,[*1] H. Takeichi,[*1] H. Yamaguchi,[*2] T. Nakao,[*2] D. Kahl,[*2] R. Uemoto,[*3] and N.Takahashi[*4]

To develop a method for wear diagnostics of industrial material using RI beams,[1,2] intense beams of ^{7}Be ($T_{1/2}$ = 53 days) and ^{22}Na ($T_{1/2}$ = 2.6 years) provided by CRIB were implanted in the surface of machine parts. Here we describe the generation and characterization of the RI beams.

The ^{7}Be beam was produced via H(^{7}Li,^{7}Be)n reaction. A beam of 5.7 MeV/A $^{7}Li^{2+}$ with an average intensity of 1.7 particle μA (pμA) was introduced to CRIB and passed through a cryogenic H_2 gas target at a pressure of 760 Torr and cooled by liquid N_2 to 90 K. The produced $^{7}Be^{4+}$ beam was introduced to a dedicated vacuum chamber at the F2 focal plane. A position-sensitive Si detector (PSD, Hamamatsu S5378-02), an energy degrader, and a rotating irradiation sample holder were installed in the chamber. The energy and profile of the RI beam were measured using the PSD. The energy of the ^{7}Be beam was 4.16 MeV/A, and the beam spot size was 4.8×8.1 mm in FWHM when the momentum spread was set to $\pm$3.1 %. The relatively large beam-spot size seems related to a halo of the beam spot at the gas target. The implantation rate of the ^{7}Be beam was approximately 60 kBq/h, according to a gamma-ray measurement after the implantation.

The ^{22}Na beam was produced via the H(^{22}Ne,^{22}Na)n reaction. A 6.1 MeV/A $^{22}Ne^{7+}$ beam with an average intensity of 0.25 pμA was introduced to the H_2 gas target at 400 Torr and 90 K. The energy and size of the $^{22}Na^{11+}$ beam at F2 was 3.67 MeV/A and 4.7×4.3 mm in FWHM, respectively, with a momentum spread of $\pm$3.1 %. The implantation rate was approximately 0.3 kBq/h.

For wear-loss diagnostics, the depth profile of implanted RI should be controlled and characterized accurately. The depth profile was controlled using a rotating energy degrader that had eight foils of different thicknesses. The foils were circularly placed on a wheel of diameter 14 cm rotating at 12 rpm so that they cross the RI beam path one by one. An additional degrader foil can be mounted on a beam collimator with a diameter of 10 mm placed downstream of the wheel.

To study the implantation-depth profile, we first irradiated a stack of 2-μm-thick Al foils with the RI beams, and measured the radioactivity of each foil with a Ge detector. Then we obtained the beam-energy spectra by the PSD, and calculated the range distribution of the ions in Al with the SRIM code[3]. Figure 1 shows a case of a ^{22}Na beam with a narrow momentum distribution of $\pm$1 % implanted to the stack after the rotating degrader with a blank and seven Al foils with thicknesses of 4.9, 7.6, 11.9, 16.9, 23.8, 27.4, and 31.7 μm. The depth profile with the stacked-foil is shown by black circles as relative intensities of the radioactivity in the foils. The horizontal and vertical error bars indicate the thickness and the statistical error for each foil. The dotted line shows the SRIM calculation of the range distribution from the energy spectrum. Below a depth of 5 μm, the corresponding energy spectrum could not be measured as it was below the detector threshold. The triangles indicate normalized fractions of the foils obtained by re-binning the range spectrum according to the stack-foil thicknesses. We multiplied a factor of 0.97 to the stopping power of the SRIM calculation for optimum agreement between the stacked-foil measurement and the calculation.

The conventional stacked-foil method is reliable because it directly measures the implanted RI, but its depth resolution is limited because assembling many thin foils as a stack is hard work. On the other hand, the energy measurement with a Si detector is simpler, but the accuracy of the implantation-depth distribution depends on the range calculation. Here, we combined the two methods with a correction factor for the SRIM calculation results and obtained a continuous implantation-depth profile.

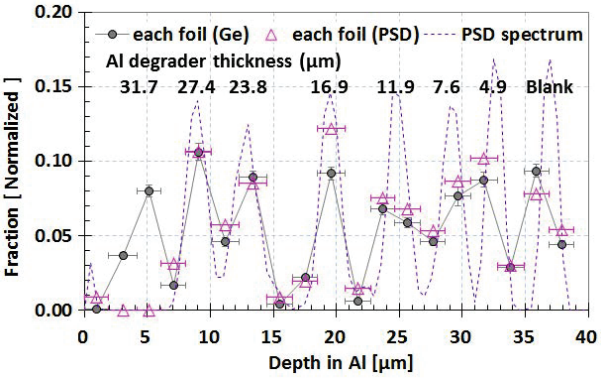

Fig. 1. Implantation-depth profile of ^{22}Na beam in stacked Al foils.

*1 RIKEN Nishina Center
*2 Center for Nuclear Study, Univ. of Tokyo
*3 S.H.I. Examination & Inspection, Ltd.
*4 Sumitomo Heavy Industries, Ltd.

References

1) A. Yoshida et al.: "Operation report of industrial cooperation team", in this report.
2) A. Yoshida et al.: Nucl. Instr. Meth. B 317, 785 (2013).
3) J. F. Ziegler: "The SRIM code, the stopping and range of ions in matter", http://www.srim.org.

Development of a GEM tracker for the J-PARC E16 experiment

W. Nakai[*1,*2] for the J-PARC E16 Collaboration

The main aim of the J-PARC E16 experiment is to measure the mass modification of ϕ mesons in nuclear matter at J-PARC in order to study the origin of hadron mass. The details of this experiment are presented in another article of this report[1].

We employed a tracking detector using the Gas Electron Multiplier (GEM)[2], and have been developing it to be a position-sensitive detector in a magnetic field with a magnitude of 1.8 T at the center of the magnet. Our requirement for this detector is a position resolution of 100 μm up to an incident angle of 30° in a high counting rate environment of up to 5 kHz/mm^2. Our GEM tracker consists of a drift cathode, triple-GEM stack, and readout strip board. We chose a strip pitch of 350 μm to achieve the required position resolution.

For inclined tracks, a hit position of a GEM tracker is determined with a technique called "timing method", where the spatial distribution of a charge cluster generated by a charged track in the drift gap is reconstructed using the arrival timing information of signals from readout strips. As shown in Fig. 1, the distance from ionization electrons to each strip (z) can be calculated by $v_{\rm d} \times t$, where t is the arrival time and $v_{\rm d}$ is the drift velocity. After calculating each z, we fit a straight line to these points and determine the intersection point of the line with the center of drift gap.

In the experiment, a drift gap of 3 mm is desirable to reduce the signal pile-up; however the test experiment was performed using a wider gap. Thus, additional analysis is performed to evaluate performance for a 3 mm gap. The analysis only uses signals that have smaller drift times corresponding to the 3 mm gap.

Results of this analysis are shown in Fig. 2 and Fig. 3. We tested four types of chambers, which are summarized in Table 1. We have achieved a position resolution better than 100 μm and an efficiency of 90% up to an incident angle of 30° for all sizes of GTRs.

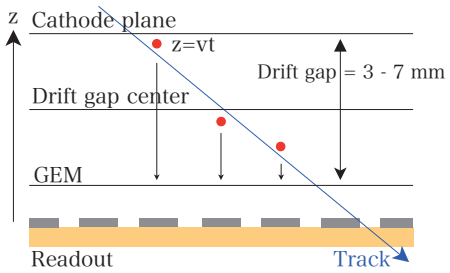

Fig. 1. Positions where ionization electrons are generated can be reconstructed by $v_{\rm d} \times t$.

Table 1. The summary of tested chambers.

Size	Drift gap	Legend in Fig. 2 & 3
100 mm	7 mm	GTR100 A
100 mm	5 mm	GTR100 B
200 mm	7 mm	GTR200
300 mm	7 mm	GTR300

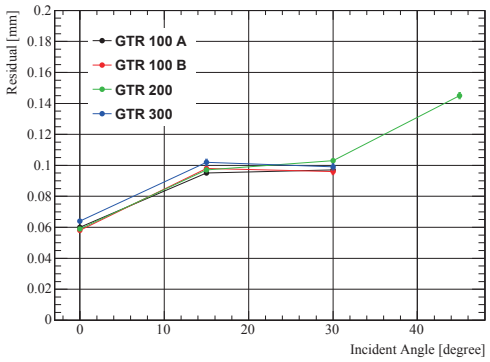

Fig. 2. The result of 3 mm gap equivalent analysis. Standard deviations of residual as functions of incident angle.

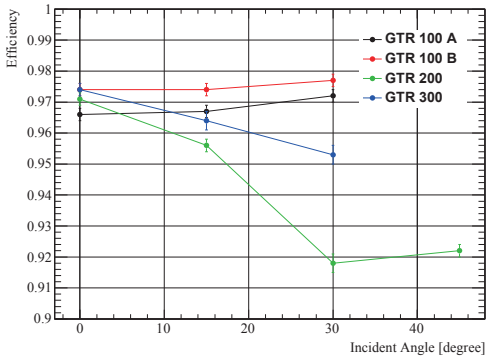

Fig. 3. Detection efficiencies as functions of incident angle.

*1 Department of Physics, The University of Tokyo
*2 RIKEN Nishina Center

References

1) S.Yokkaichi, *et al*, in this report
2) F. Sauli, Nucl. Instrum. Meth. A386 (1997) 531

Preparation status of the J-PARC E16 experiment: measurement of spectral change of vector mesons in nuclei

S. Yokkaichi*1 for the J-PARC E16 Collaboration

We have proposed the experiment E16[1] to measure the vector meson decays in nuclei in order to investigate the chiral symmetry restoration in dense nuclear matter. The experiment will be performed at the J-PARC Hadron Experimental Facility. Scientific ("stage 1") approval was granted to the experiment E16 by PAC in March 2007. For the full approval, we were required to demonstrate the experimental feasibility and show the prospects of acquiring sufficient funds and of beam-line construction. Toward the full approval, the technical design report (TDR) was submitted to PAC held in May 2014, and the TDR is being revised as per the requirements provided by PAC, and the revised TDR will be submitted to the PAC held in July 2015.

The aim of the experiment is to perform a systematic study of the spectral modification of vector mesons, particularly the ϕ meson, in nuclei, using the e^+e^- decay channel with statistics that are two orders larger in magnitude than those of the preceding E325[2] experiment performed at KEK–PS. In other words, the aim is to accumulate 1×10^5 to 2×10^5 events for each nuclear target (H, C, Cu, and Pb) and to deduce the dependence of the modification on the matter size, and the meson momentum. At the same time, the e^+e^- decays of the ρ, ω, and J/ψ mesons can be measured, while the yields depend on the trigger condition required to suppress the background e^+e^- pairs.

For the experiment, we plan to use a 10^{10}-pps, 30-GeV proton beam in the high-momentum beam line, which is being constructed at J-PARC. In order to increase the statistics by a factor of 100, we will construct a large-acceptance spectrometer that can be operated under 10^7 Hz nuclear interactions at the target. In order to cope with such a high-interaction rate, GEM has been adopted for constructing new tracking and PID detectors.

The construction of the high-momentum beam line, where we perform the experiment, has been on-going since 2013 by KEK. The first beam is scheduled around the end of JFY 2016; it was delayed by a year because of the beam stoppage due to the radiation accident at J-PARC in May 2013. The schedule of the spectrometer magnet reconstruction is also delayed, and it is expected to be completed by July 2015. After the completion of the magnet reconstruction, we can begin installing the detectors in the magnet. The target day of the construction is March 2016. Our spectrometer has 26 modules. Owing to the budget limitations, our first goal of the staged construction plan is to construct eight modules, which correspond to approximately one third of the full installation.

The development of the detectors has almost completed, and we are moving to the production phase. For the GEM Tracker (GTR)[3], the production of GEM has been underway since 2013. Six modules (out of eight, as mentioned above) are currently under construction. The production of frames made of CFRP, which is used to install the GEM chambers in the spectrometer, started in 2014. For the HBD[4], which is one of our electron ID detectors, only two modules are currently under construction. The lead-glass (LG) EM Calorimeter, another electron ID detector, utilizes the recycled LG from the TOPAZ experiment. The reshaping of LG blocks, for eight modules (330 blocks), is to be completed at the KEK engineering center within JFY 2014.

The development of the read-out and trigger modules are underway. As a pre-amplifier and front-end module (FEM) of GEM detectors, an APV25 chip and SRS, both are CERN-made, are adopted. We joined the RD51[5] collaboration in CERN in July 2013 to co-develop GEM-related electronics. For HBD, we use the RD51-made APV25 preamp. For GTR, a more smaller preamp using the APV25 chip was fabricated by ourselves and the production started in January 2015. The first version of the FEM for the LG is tested and the revision is on-going.

For the trigger, signals from the GEM foil of GTR and HBD are used. ASICs for the amp-shaper-discriminator to generate the trigger primitive of the two detectors has been produced under the cooperation of the KEK e-sys group. For GTR, the test of the second version is to be started. The test of the first version for HBD is almost completed. To generate a global trigger signal, an FPGA board "UT3"(Belle II collaboration) is used. To transfer the trigger primitives to UT3, we developed another module called "TRG-MRG". The first version of TRG-MRG is already delivered and will be tested at KEK. These tests will be completed by the end of JFY 2014.

*1 RIKEN Nishina Center

References

1) S. Yokkaichi *et al.*: J-PARC proposal No. 16 (`http://j-parc.jp/researcher/Hadron/en/pac_0606/pdf/p16-Yokkaichi_2.pdf`), Lect. Notes Phys. 781 161 (2009).
2) M. Naruki *et al.*: *Phys. Rev. Lett.* 96, 092301 (2006), R. Muto *et al.*: *Phys. Rev. Lett.* 98, 042501 (2007).
3) W. Nakai *et al.*: in this report.
4) K. Kanno *et al.*: in this report.
5) `http://rd51-public.web.cern.ch/RD51-Public/`

Simulation of HBD response in the J-PARC E16 experiment based on test results

K. Kanno[*1,*2] for the J-PARC E16 Collaboration

A hadron blind detector (HBD) has been developed for the J-PARC E16 experiment.[1] The E16 experiment aims to investigate the origin of QCD mass through the spectral change of a ϕ meson in a nucleus. The mass spectrum is reconstructed through electron-positron decays. A detector for electron identification is required. The HBD is utilized in the E16 experiment for this purpose. The HBD identifies electrons by converting Čerenkov photons emitted by an incident electron in a CF_4 radiator into photoelectrons using a CsI photocathode. These photoelectrons are amplified by gas electron multiplier[2] (GEM) foils and are subsequently read out as an electric signal. Other charged particles apart from the electron do not emit Čerenkov photons in the momentum region where we perform the measurement, 0.4–3 GeV/c. With this scheme, the HBD distinguishes electrons from the other charged particles.

We have constructed a prototype of the HBD and performed a test experiment using a positron beam of 1.0 GeV/c at Research Center for Electron Photon Science, Tohoku University. We successfully observed 11 photoelectrons per incident positron with the prototype[3] when the incidence angle to the beam was 0°. This result was consistent with the expected result calculated based on the performance of each detector element. However, only HBD response to an electron was obtained in this beam test, and the response to a pion is also required to determine the pion rejection power for a given electron detection efficiency. We estimated the HBD response to a pion through simulation.

For this simulation, we used the HBD response to a pion that has already been obtained with another prototype. This prototype has a smaller pad readout and longer gap lengths between GEM foils. Taking into account of the differences between the prototype and another prototype, we performed the simulation to evaluate the prototype response to a pion. With this simulation, we estimated an electron detection efficiency of 85% with a pion rejection factor of 50 for 1.0 GeV/c electrons and pions at the threshold of 6.5 e when the incidence angle was 0°. In the actual J-PARC E16 experiment, charged particles including electrons and pions are emitted from a target and the incidence angle of these particles to the HBD is approximately 0–45°. Furthermore, these charged particles move along a curved line because of the magnetic field in the spectrometer used in the experiment, resulting in a larger incidence angle to the HBD.

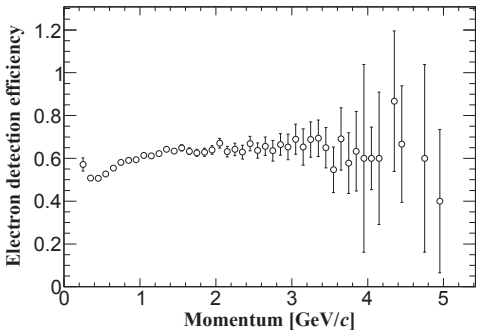

Fig. 1. Electron detection efficiency as a function of electron momentum.

To evaluate the electron detection efficiency in the offline analysis, we performed another simulation by including the possible momentum and incidence angle distribution of electrons from ϕ meson decays. In the simulation, ϕ mesons were generated by a 30 GeV/c proton-induced reaction using the nuclear cascade code JAM.[4] These ϕ mesons decay into electrons and positrons, and then electrons move according to the magnetic field. We assumed pion samples had the same track as the electron samples. The HBD responses to an electron and a pion were estimated based on the result of the beam test and the simulation mentioned in the previous paragraph. The electron detection efficiency as a function of electron momentum with a pion rejection factor of 100 is shown in Fig. 1. The efficiency decreases in the region of 0.4–1.5 GeV/c. This fact reflects that the signal amplitude of a pion increases with decreasing momentum. A pion sample having lower momentum has a larger curvature in a magnetic field and consequently has a larger incidence angle to the HBD, namely, a larger signal amplitude. The large errors in the high-momentum region are due to availability of limited statistics. The overall efficiency is 60% with a pion rejection factor of 100 at the threshold of 7.5 e, which meets the requirement of the experiment.

As the next step, we will measure the response to a pion, which has been simulated, using a pion beam with GEM foils and the readout pad configuration for the production type of HBD.

*1 RIKEN Nishina Center
*2 Department of Physics, Graduate School of Science, The University of Tokyo

References

1) S. Yokkaichi *et al.*: in this report
2) F. Sauli: Nucl. Instr. and Meth. A **386**, 531 (1997)
3) K. Kanno *et al.*: RIKEN. APR. **47**, 226 (2014)
4) Y. Nara *et al.*: Phys. Rev. **C61**, 024901 (1999)

Resistive Plate Chamber (RPC) for BGOegg Experiment†

T. Nam,[*1,*3] N. Tomida,[*2] M. Niiyama,[*2] H. Ohnishi,[*1,*3] C.-Y. Hsieh,[*4] M.-L. Chu,[*4] and W.-C. Chang[*4]

We have developed and installed a time-of-flight system to measure the energy of charged particles, especially protons, for BGOegg experiment. The design of the chamber was based on the RPC chamber for LEPS2 experiment, which we have already reported previously in ref.[1].

BGOegg experiment using LEPS2 beamline to study hadron photoproductions is currently under operation at SPring-8 (**S**uper **P**hoton **ring**-**8** GeV). The main detector is the BGOegg calorimeter which made from 1320 $Bi_4Ge_3O_{12}$ crystals assembled in the shape of an egg (fig. 1). The BGOegg calorimeter can detect high-energy gamma ray coming out from the target in an open angle of 24 to 144 degrees; an energy resolution of 1.3 % at $1\,GeV$ gamma energy was achieved and previously reported at ref [2].

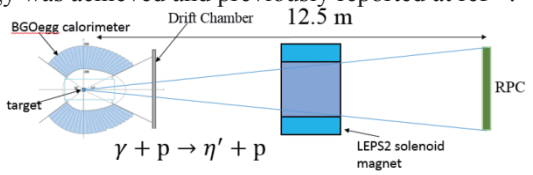

Figure 1: setup of the BGOegg experiment

The RPC is placed $12.5\,m$ downstream from the target, and covers an open-angle of 7^o in the horizontal and 4^o in the vertical. In BGOegg experiment, we are measuring the η' mass modification to study the $U_A(1)$ anomaly problem using a nuclear target with the BGOegg detector system and the LEPS2 high-intensity photon beam. We are looking for the presence of the η' meson in its decay to $\gamma\gamma$, $\pi^0\pi^0\eta$ in the nuclear medium. In addition, the momentum of a forwardly recoiled proton in the A(γ,η') reaction will be measured by the RPC. We use the RF signal as the start signal and the RPC signal as the stop signal, the time resolution must include the contribution of all uncertainty sources such as the amplifier, discriminator, RPC, TDC and the time reference RF.

$$\sigma_{ToF}^2 = \sigma_{RF}^2 + \sigma_{Amp}^2 + \sigma_{Dis}^2 + \sigma_{TDC}^2 + \sigma_{cable}^2 + \sigma_{RPC}^2$$

For the timing measurements, CAEN V1290A TDC modules were used. The resolution of the RF signal is about $4\,ps$. The electron bunch width in the SPring-8 storage ring is ~$15\,ps$. The time resolution of V1290A is $20\,ps$ after the integral non linearity corrections. If we assume that the internal time resolution of RPC is $20ps$[3], then the remaining contributions come from Front-End-Electronics(FEEs) and are considered to be less than $40\,ps$. In total, the resolution of our RPC system is expected to be $50\,ps$.

During the development, we have produced and tested for many aspects of the RPC such as geometry of the pad/strip read-out, width of the gap, number of gap and trigger rate. The $260\,\mu m \times 2$ stacks $\times 5$ gaps $2.5 \times 100\,cm^2$ strip read-out with anode inside geometry reached a time resolution of $50\,ps$ and an efficiency more than 99% above 10 Hz/cm^2[1]. The coverage area is $3.2 \times 2\,m^2$. The wall consists of 32 RPC modules as shown in fig. 2; 2 rows with 16 modules each. The size of an RPC module is 116.2 cm (L) × 24.7 cm (W) × 2.7 cm (H). The active area of an RPC module is 20.75×100 cm^2 and the active area of each RPC module overlaps about 0.3 cm with each other in the horizontal and 0.5 cm in the vertical.

Figure 2: RPC wall

The custom FEEs of our RPC including the amplifier, discriminator and stretcher were developed by Dr. M.-L. Chu. A method for the signal read-out to reduce the total number of TDC and ADC channels by half was applied, and this method is shown in fig. 3.

The special feature of the amplifier is that it is designed to minimize the reflection of the signal. The input impedance of the amplifier is set to $40\,ohm$ and it matches well with the impedance of our RPC, which is about $30-40\,ohm$. The output signal of our custom discriminator has the same width as the input. This width is very narrow, typically around $2\,ns$. And this width is too narrow to be read by V1290A TDC. Therefore, we developed an additional stretcher to be placed after the discriminator to stretch the pulse width to $10\,ns$ so that it can be read by V1290A TDC. For the timing measurement, we use CAEN V1290A TDC modules. For the charge measurement, we use LeCroy Fast Encoding and Readout ADCs (FERAs). The ADC information is used for developing correction parameters and a strip separation method.

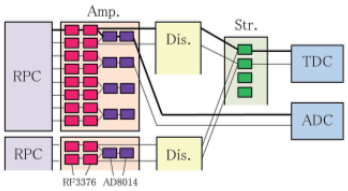

Figure 3: The sketch of FEEs for RPC

BGOegg experiment started acquiring data from April 2014, and the performance of the RPC is being checked against many aspects and the calibrations are under way to ensure the reliability of the RPC's data for physics studies in near future.

† This manuscript summary the results which were reported at *JINST* **9** C10008, 2014.

*1 Research Center for Nuclear Physics, Osaka University.
*2 Physics Department, Kyoto University.
*3 RIKEN Nishina Center
*4 Institute of Physics, Academia Sinica

References

1) N. Tomida, H. Onishi, M. Niiyama, T. Nam, *Large strip RPCs for the LEPS2 TOF system,* Nucl. Instr. Meth. A, 766, 283-287, 2014.
2) T. Ishikawa et al., ELPH Annual Report Vol.1, 61 (2012).
3) C. Williams et al, *A 20 ps timing device-A Multigap Resistive Plate Chamber with 24 gas gaps*, Nucl. Instr. Meth. A, 594, 39–43, 2008.

Quality assurance test of pixel detector ladders for VTX

T. Sumita,[*1] Y. Akiba,[*1] H. Asano,[*1,*2] T. Hachiya,[*1] M. Kurosawa,[*1] T. Moon,[*1,*3] H. Nakagomi,[*1,*4] C. Pancake,[*5] H. Sako,[*1] S. Sato,[*1] A. Taketani,[*1] and the PHENIX VTX group

A silicon vertex tracker (VTX) was installed in the PHENIX detector at the Relativistic Heavy Ion Collider. The VTX detector consists of two inner layers of silicon pixel detectors and two outer layers of silicon strip detectors. A pixel ladder is composed of a mechanical stave, four hybrid sensors[1)], and two readout buses. A hybrid sensor is an assembly consisting of a silicon pixel sensor and four readout chips (ALICE1LHCb[2)]) bump-bonded to the sensor. One ladder has 16 readout chips and one readout chip has 8,192 pixels, with a pixel size of 425 μm $\times$ 50 μm, organized in 32 columns and 256 rows.

We fabricated new spare silicon pixel ladders. In order to ensure correct operation before the assembly of the VTX detector, quality assurance (QA) test of the ladders need to be performed. This report presents the results of the QA test for the ladders.

The QA test system consists of Silicon PIxel Read-Out (SPIRO) modules, Front-End Module (FEM), and NOVEC HFE-7200.[3)] The SPIRO modules provide all electricity, control the readout chip of the sensor module and read out pixel data The FEM is an interface between the SPIRO modules and the data acquisition system. NOVEC HFE-7200 was used to cool the readout chips. The following tests are performed for each ladder.

(1) Current consumption:
The current consumption of the analog and digital circuits of the readout chips are measured.
(2) JTAG functionality:
It is confirmed whether the configuration settings in the chip can be controlled by using Joint Test Action Group (JTAG[4)]) protocol.
(3) Minimum threshold:
For all chips, the minimum threshold in all pixels are determined.
(4) Pulse test:
Pulse test is to check for dead chips and connections. The test pulse from the pulsar inside the chip is transmitted to each pixel cell.
(5) Test using a β-ray source (^{90}Sr):
Faulty bump bonds and the maximum efficiency are evaluated by β-source measurements

The ladder is biased at 10 V during the measurement.

A total of 7 ladders were tested, and correct operation of all the ladders was confirmed except for one ladder. Four chips (one hybrid sensor) of the incorrectly working ladder did not respond to the tests because of a short circuit in the readout bus. A typical result of a readout chip in the source test is shown in Fig. 1. The inefficient area at the bottom of columns 1, 9, 17, and 25 is attributed to the presence of the test pulse signal generator on the readout chips, which affected the readout circuit.

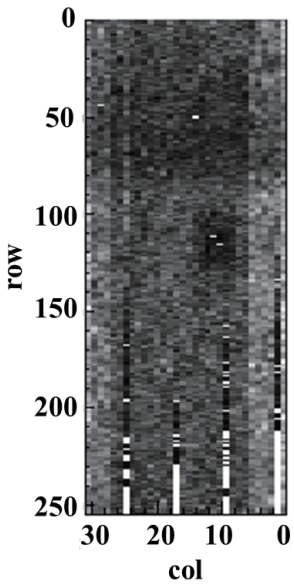

Fig. 1. Typical result of a readout chip in the source test. The horizontal and vertical axes represent pixel position along the column and row directions, respectively. Low gray-levels represents a low number of hits.

In summary, QA tests for the seven new assembled pixel ladders were performed. The results confirmed that six ladders are working properly and that a part of one ladder is not functional. One of functional ladders will be used in the 2015 run.

References

1) T. Sumita et al.: RIKEN Accel. Prog. Rep. **47** 230 (2013).
2) W. Snoeys et al.: Nucl. Instr. Meth. A **466**, 366 (2001).
3) M. Kurosawa et al.: RIKEN Accel. Prog. Rep. **43** 208 (2010).
4) IEEE std 1149.1.

*1 RIKEN Nishina Center
*2 Department of Physics, Kyoto University
*3 Department of Physics, Yonsei University
*4 Department of Physics, University of Tsukuba
*5 Department of Physics, Stony Brook University

Fast clear technique for NEBULA data acquisition for SAMURAI17 experiment

Y. Togano,[*1,*2] Y. Kubota,[*2,*3] H. Baba,[*2] and H. Otsu,[*2] for the SAMURAI17 collaboration

A fast clear technique for NEBULA data acquisition (DAQ) was newly introduced for the ^{132}Sn(p,n) experiment at SAMURAI.[1] The technique enabled the measurement of recoil neutrons and projectile-like neutrons in coincidence. NEBULA DAQ could not work with the main trigger for the (p,n) reaction measurement because the recoil neutrons were slow.

The incoming ^{132}Sn beams were detected by beam tagging detectors: SBT1 and SBT2. We define the signal from SBT1 as "Beam" in this report. Recoil neutrons from the (p,n) reaction were measured using WINDS[2] surrounding a liquid hydrogen target. The charged outgoing particles were analyzed by using the SAMURAI system. The outgoing neutrons from the breakup of reaction products were measured by using NEBULA. The main trigger of the experiment was a coincidence of Beam and WINDS. Because of the slow neutrons from the (p,n) reaction detected by using WINDS, the trigger decision of the experiment was $\sim$ 300 ns slower than the that with the standard SAMURAI setup.[3]

The main trigger for the experiment was controlled by using the GTO module.[4,5] The trigger for NEBULA DAQ was a coincidence of Beam and NEBULA signals ($Beam \times NEBULA$ trigger). The analog and time information of NEBULA was obtained by using CAEN V792 QDC and V775 TDC modules, respectively. The VME module used to interrupt NEBULA DAQ was RPV-130 by REPIC. The fast clear of V792 and V775 could be performed by inputting the fast clear signal to the modules during their data conversion. The dead time of the fast clear was 600 ns. Figure 1 shows the circuit diagram of NEBULA DAQ for the fast clear. The interrupt of NEBULA DAQ was performed by using a 10 μs delayed main trigger signal to allow time for the data conversion of QDC and TDC. If the DAQ system was interrupted when NEBULA data were empty owing to no $Beam \times NEBULA$ trigger or the dead time of fast clear, the NEBULA data were recorded as an empty event. The fast clear signal was generated by anti-coincidence between $Beam \times NEBULA$ (synchronized with DAQ start/stop) and the main trigger. If the main trigger was fired to acquire data during the dead time of fast clear for NEBULA, a fast clear flag was stored by a coincidence register (coin. reg. 1). The NEBULA-accepted trigger was $Beam \times NEBULA$ vetoed by the dead time of NEBULA DAQ and the fast clear of V775/V792. A flag for $Beam \times NEBULA$ was stored by a coincidence register if it was coincident with the main trigger (coin reg. 2). NEBULA DAQ could be switched to the singles mode, in which the trigger was generated by NEBULA itself for calibrations, in B2F experimental area.

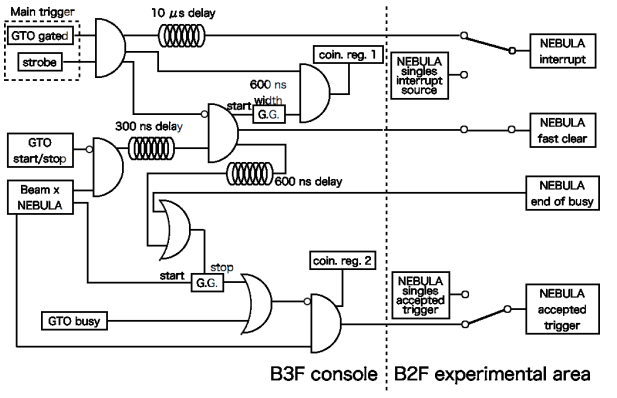

Fig. 1. Circuit diagram for NEBULA DAQ with fast clear.

In the experiment, the typical rate of the main trigger and the $Beam \times NEBULA$ trigger were 2.4 kHz and 1.6 kHz, respectively. Owing to the dead time of the fast clear, $\sim$ 0.7% of NEBULA data could not be collected. Fig. 2 shows the time versus crystal ID plot of NEBULA. The locus at approximately 60 ns corresponds to fast neutrons from the target region indicating that NEBULA DAQ functions effectively. This fast clear technique can be applied to other experiments by adjusting the delay for the $Beam \times NEBULA$ signal (300 ns in this experiment).

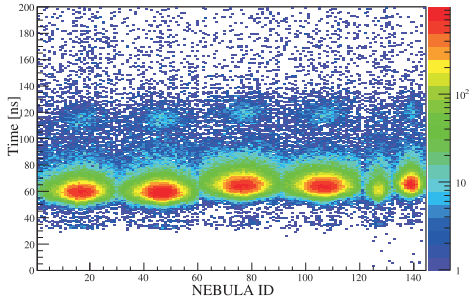

Fig. 2. Time versus crystal ID plot of NEBULA.

*1 Department of Physics, Tokyo Institute of Technology
*2 RIKEN Nishina Center
*3 Center for Nuclear Study, University of Tokyo

References
1) M. Sasano et al.: RIKEN Accel. Prog. Rep. **48** (2015).
2) K. Yako et al.: RIKEN Accel. Prog. Rep. **45**, 137 (2012).
3) T. Kobayashi et al.: Nucl. Instrum. Meth. B **317**, 294 (2013).
4) H. Otsu et al.: RIKEN Accel. Prog. Rep. **46**, 146 (2013).
5) H. Baba et al.: RIKEN Accel. Prog. Rep. **47**, 235 (2014).

Test of the advanced implantation detector array (AIDA) at RIBF

C.J. Griffin,[*1] T. Davinson,[*1] A. Estrade,[*1] D. Braga,[*2] I. Burrows,[*3] P. Coleman-Smith,[*3] T. Grahn,[*4] A. Grant,[*3] L.J. Harkness-Brennan,[*4] M. Kogimtzis,[*3] I. Lazarus,[*3] S. Letts,[*3] Z. Liu,[*1] G. Lorusso,[*5] K. Matsui,[*5,*6] S. Nishimura,[*5] R.D. Page,[*4] M. Prydderch,[*2] V. Pucknell,[*3] S. Rinta-Antila,[*4] O. Roberts,[*7] D. Seddon,[*4] J. Simpson,[*3] J. Strachan,[*3] S.L. Thomas,[*2] and P.J. Woods[*1]

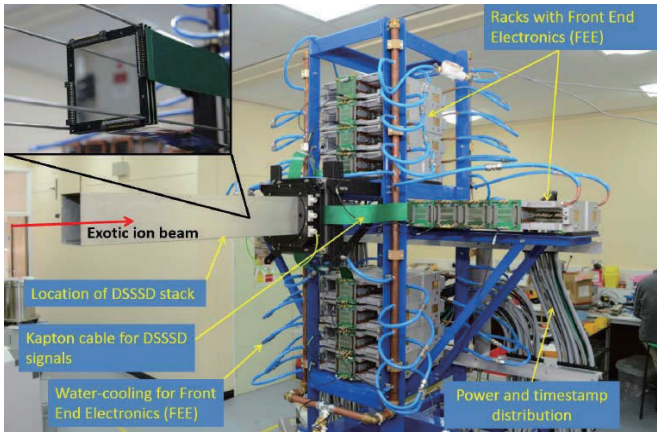

Fig. 1: A photograph of the fully constructed AIDA assembly.

The advanced implantation detector array (AIDA)[1] represents the latest generation of silicon implantation detectors for use in decay spectroscopy measurements of exotic nuclei at fragmentation beam facilities.

Designed to improve upon current generation, the AIDA features high detector pixelation and fast overload recovery (~1 μs), required at modern RI facilities with increasingly high secondary beam intensity and access to isotopes with very short half-lives.

Application specific integrated circuits (ASICs)[2] were specifically designed to meet the above requirements. One ASIC can process 16 data channels, each with two dedicated preamplifiers: one with selectable gain to cover the low and medium energy ranges of up to 1 GeV, and the other, a low-gain amplifier that covers the full dynamic range of 20 GeV. Detector signals are carried via flexible Kapton PCBs to the front end electronics (FEE) cards, which support 64 channels of instrumentation. The FEE cards contain the following: multiple analog-to-digital converters (ADCs) for use in signal processing; a field-programmable gate array (FPGA) for control, signal processing, and event building.

As each FEE card runs a separate data acquisition system (DAQ), reading data from only 64 channels, dead-time is significantly reduced compared to that in current generation detectors dealing with high pixelation. Fig. 1 shows the full AIDA assembly.

To study the response of the AIDA to implantation of heavy ions, an in-beam test was conducted at the Radioactive Ion Beam Factory (RIBF) at RIKEN. The test was conducted parasitically to the first SEASTAR campaign,[3] placing the AIDA at the F11 focal plane. In this test configuration, AIDA comprised one DSSSD type BB18 with a thickness of 1 mm and featuring 128 strips with a 0.625 mm pitch in both the x and y directions. Our test demonstrated the capability of AIDA to detect position and energy of fast fragment beams, as shown in Fig. 2.

With promising progress being made on all fronts, the AIDA is planned for use at the RIBF throughout 2015-2016 with two focuses: β-decay half-life and decay spectroscopy measurements using the EURICA γ-ray detector, and measurements of β-delayed neutron emission probabilities as part of the BRIKEN collaboration.

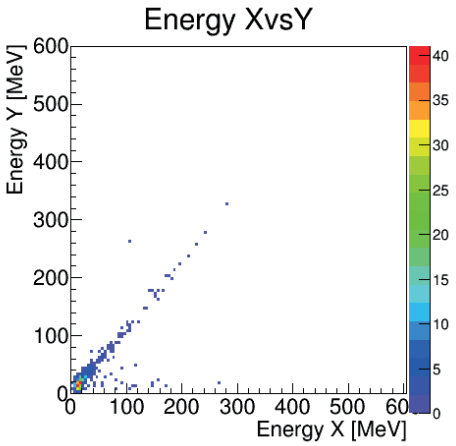

Fig. 2: Spectrum of energy measured using the front and back strips of AIDA's DSSD for fragments around ^{78}Ni, for events in coincidence with a veto scintillator in the front AIDA.

References

1) http://www2.ph.ed.ac.uk/td/AIDA/welcome.html
2) D. Braga, P. J. Coleman-Smith, T. Davinson, I. H. Lazarus, R. Page, S. Thomas: ANIMMA 2nd International Conference Proc., IEEE, (2011), pp. 1–5.
3) In this progress report

† Condensed from the proceeding of XIII Nuclei in the Cosmos, 7-11 July, 2014, Debrecen, Hungary

*1 School of Physics and Astronomy, University of Edinburgh
*2 STFC Rutherford Appleton Laboratory
*3 STFC Daresbury Laboratory
*4 School of Physical Sciences, University of Liverpool
*5 RIKEN Nishina Centre
*6 Department of Physics, University of Tokyo
*7 School of Engineering and Mathematics, University of Brighton

CCJ operations in 2014

S. Yokkaichi,[*1] H. En'yo,[*1] T. Ichihara,[*1] and Y. Watanabe[*1]

1 Overview

The RIKEN Computing Center in Japan (CCJ)[1] commenced operations in June 2000 as the largest offsite computing center for the PHENIX[2] experiment being conducted at the RHIC[3]. Since then, the CCJ has been providing numerous services as a regional computing center in Asia. We have transferred several hundred TBs of raw data files and nDST [a] files from the RHIC Computing Facility (RCF)[4] to the CCJ. The transferred data files are stored in a High Performance Storage System (HPSS)[5]. A joint operation of the CCJ with the RIKEN Integrated Cluster of Clusters (RICC)[6] is continued since July 2009. HPSS and dedicated 20 PC nodes are maintained by them.

Many analysis and simulation projects are being carried out at the CCJ, and these projects are listed on the web page `http://ccjsun.riken.go.jp/ccj/proposals/`. As of December 2014, CCJ has contributed 31 published papers and 40 doctoral theses.

2 Computing hardware and software

In 2014, computing hardware (nodes and RAIDs) and software (OS, batch queuing systems, database engine, and so on) were changed slightly from those described in the previous APR[1]. In summary, we have 28 computing nodes, two login servers, one main server (users home directory, NIS, DNS, NTP), two disk servers and HPSS machines in our machine room, and 20 computing nodes in the RICC room. In total, 524 jobs can be processed simultaneously by these computing nodes.

One database (postgreSQL[7]) server and one AFS[8] server are operated in order to share the PHENIX computing environment (the other database server retired in 2014). Sharing of the Scientific Linux[9] 4 (SL4) environment was stopped in April 2014, and now only the SL5 environment is shared by the computing nodes, which have approximately 0.9 TB of library files. We have four data-transfer servers on which the grid environment[10] is installed for the data transfer to/from RCF. Two servers out of the four retired in Jan. 2015.

Disk failure occurred in March 2014, during a reboot after a planned power outage. File system of an users work disk became corrupt and about 1.5 TB of data were lost in spite of adopting VxFS, a journaling file system. Another trouble, namely, power outage at the RAID due to the power failure on Wako Campus in February, is thought to be an underlying cause of the corruption of the file system. This has been the most serious accident at the CCJ so far, although it is declared that there are no backup of the disk.

Table 1 lists the numbers of malfunctioning SATA or SAS disks in the HP servers, namely, computing nodes and NFS/AFS servers.

Table 1. Number of malfunctioning HDDs in 2011-2014

Type	Size	Total	2014	2013	2012	2011
SATA	1 TB	192	11	16	20	9
	2 TB	120	0	2	5	4
SAS	146 GB	38	2	0	1	1
	300 GB	24	1	0	0	1

2.1 HPSS

The amount of data archived in the HPSS were approximately 1.73 PB (1.53 PiB) in 2.15 million files, as of December 2014, not so changed in 2014. No new data file has been transferred in 2014, and therefore, the data list in the previous APR[1] is still effective.

RICC will be upgraded to the "HOKUSAI" system, a new RIKEN computing cluster launched in April 2015, and HPSS will retire around August 2015. Data migration to the new archiving system was performed in Jan. 19 - Mar. 16 2015. The 863 TB (785 TiB) of data in 1.66 million files out of 1.73 PB were migrated to the new archiving system, because the raw data of PHENIX, which were transferred for DST production and already served out, were not migrated.

3 Prospect

The replacement of the main RAID and server is on-going, and should be completed in May 2015. The batteries of the four UPSs have expired and should be replaced in 2015. Regarding to the upgrade from RICC to HOKUSAI, configuration changes in the network and job submitting environment are planned in the first half of 2015.

References

1) Y. Ikeda et al.: RIKEN Accel. Prog. Rep. **47**, 237 (2014).
2) `http://www.phenix.bnl.gov/`
3) `http://www.bnl.gov/rhic/`
4) `https://www.racf.bnl.gov/`
5) `http://www.hpss-collaboration.org/`
6) `http://accc.riken.jp/ricc/`
7) `http://www.postgresql.org/`
8) `http://www.openafs.org/`
9) `http://www.scientificlinux.org/`
10) `http://www.globus.org/toolkit/docs/latest-stable/gridftp/`

[*1] RIKEN Nishina Center

[a] term for a type of summary data files in PHENIX

Computing and network environment at the RIKEN Nishina Center

T. Ichihara,*1 Y. Watanabe,*1 and H. Baba*1

We are operating the Linux/Unix NIS/NFS cluster systems[1,2] at the RIKEN Nishina Center (RNC).

Figure 1 shows the current configuration of the Linux/Unix servers at the RNC. We have adopted Scientific Linux (SL), which is a clone of Red Hat Enterprise Linux (RHEL), as the operation system.

The host *RIBF.RIKEN.JP* is used as the mail server, NFS server of the user home directory /rarf/u/, and the NIS master server. This is the core server for the RNC Linux/Unix cluster with approximately 600 registered user accounts. The hosts *RIBF00/RIBF01* are used as SSH login servers to provide access to external users, and as general-purpose computational servers, printer servers, and gateways to the RIBF intranet.

An HP PloLiant DL-585 server was installed in 2006 as *RIBF00* and this was replaced by DL-320e G8 in January 2015. At the same time, the OS of *RIBF00* was upgraded from SL 5.11 to SL 6.6.

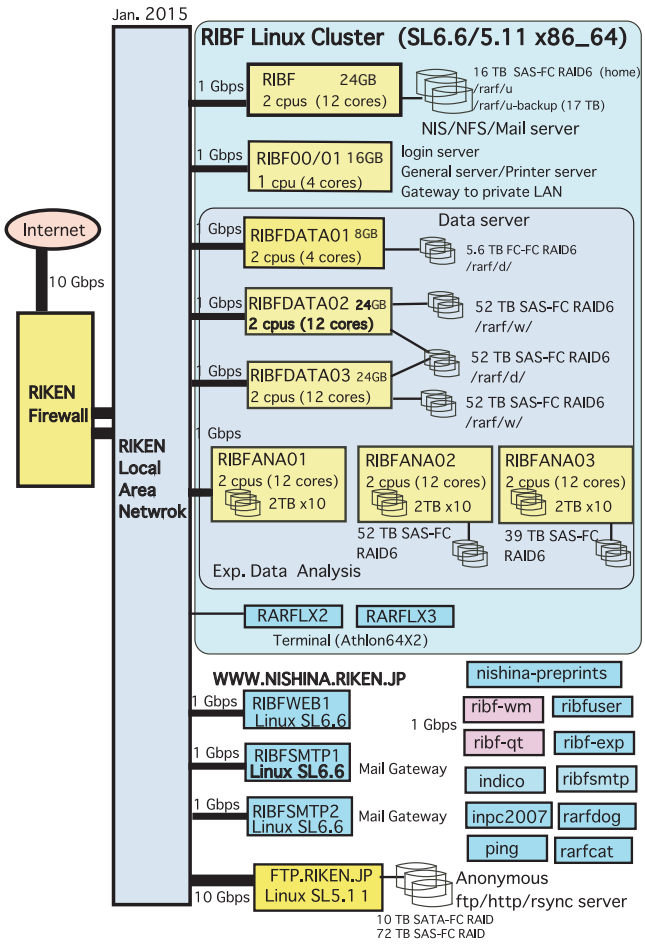

Fig. 1. Configuration of the RIBF Linux cluster.

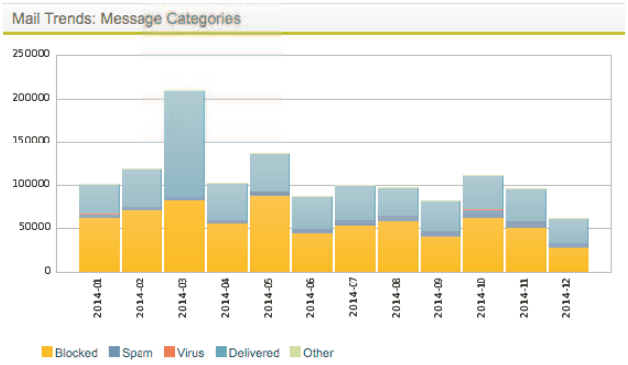

Fig. 2. Mail Trends: Message categories by PMX.

The data servers *RIBFDATA02/03* and analysis servers *RIBFANA01/02/03* are mostly used to store and analyze experimental data at RIBF. We have a 156 TB RAID system to store the experimental data as /rarf/w and /rarf/d/, which is connected to *RIBFDATA02/03*. A 52 TB SAS-FC RAID was added to *RIBFANA02* for data analysis for the SAMURAI experiment in October 2014.

A new Web server *RIBFWEB1* was installed in April 2014 as the official Web server of RNC *WWW.NISHINA.RIKEN.JP* to replace the old Web server *RARFWWW*, which was installed in 2005. The *RIBFWEB1* also serves another Web service with using a virtual host function of the Apache http server[3].

The hosts *RIBFSMTP1/2* are the mail front-end servers, and they are used for tagging spam mails and isolating virus-infected mails. The latest version of the Sophos Email Protection-Advanced (PMX 6.2.1) has been installed on these. Figure 2 shows the Mail Trends by the PMX over 12 months in 2014. The orange bar indicates the number of spam mails blocked by the IP blocker; approximately 55 % of the incoming mails are blocked.

An anonymous ftp server, *FTP.RIKEN.JP*, is managed and operated at the RNC. Major Linux distributions, including Scientific Linux, Ubuntu, Debian, CentOS etc., are mirrored daily at the ftp server for the convenience of their users and for facilitating high-speed access. A new 72 TB RAID, which is capable of performing 1.3 M IO per second (IOPS), was installed in August 2014 to replace previous RAID to ensure the high performance and high reliability of the operation.

References

1) http://ribf.riken.jp/comp/
2) T. Ichihara et al.: RIKEN Accel. Prog. Rep. 47, 236 (2014).
3) http://httpd.apache.org/docs/2.2/en/vhosts/

*1 RIKEN Nishina Center

III. RESEARCH ACTIVITIES II
(Material Science and Biology)

1. Atomic and Solid State Physics (Ion)

Hyperfine structure measurement of ^{133}Cs atoms in superfluid helium

K. Imamura,[*1,*2] T. Furukawa,[*3] X. F. Yang,[*4] Y. Mitsuya,[*2] T. Fujita,[*5] M. Hayasaka,[*6] T. Kobayashi,[*7] A. Hatakeyama,[*8] H. Ueno,[*1] H. Odashima,[*2] and Y. Matsuo[*9]

The study of nuclear structure via laser spectroscopy techniques has contributed to significant progress in nuclear physics[1]. To extend the applicability of laser spectroscopy techniques for the study of low-yield exotic nuclei whose production rate is less than 100 pps, we have been developing OROCHI (Optical RI-atom Observation in Condensed Helium as Ion-catcher)[2]. OROCHI is based on a combination of superfluid helium (He II) as an effective stopper for high-energetic ion beams and in situ laser spectroscopy of atoms. In OROCHI, an energetic ion beam produced at an accelerator facility is directly injected into He II. The injected ions are neutralized during the stopping process and are trapped as isolated atoms. The trapped atoms are subjected to a circularly polarized laser light and driven to the spin polarized state. The Zeeman/hyperfine splittings (ZMS/HFS) of atoms are measured using a laser-RF/MW (radio-frequency/microwave) double resonance method to deduce nuclear spins and moments. So far, a series of experiments using the $^{84\text{-}87}$Rb ion beam have been performed at the RIKEN Nishina Center. The feasibility of the principle of OROCHI has been successfully demonstrated by measuring the ZMS of $^{84\text{-}87}$Rb[3]. For further development of OROCHI, it is indispensable to ensure the applicability of OROCHI for the measurement of HFS of atoms in He II. In particular, the following two issues have to be confirmed i) How the He II environment affects the HFS of an introduced atom, and ii) What is the highest level of measurement accuracy that can be achieved. To investigate the above mentioned issues, we conducted an experiment using ^{133}Cs atoms that are introduced into He II using the laser ablation technique.

The experimental setup is similar to the one in ref.[4]. An open-topped quartz cubic cell (70 × 70 × 70 mm^3) filled with He II liquid was placed inside the cryostat. A solid CsCl was placed approximately 1 cm above the liquid surface. In this experiment, Cs atoms were introduced into He II using two pulsed lasers[4]. The introduced Cs atoms were pumped into the spin polarized state using circularly polarized laser tuned to the D1 transition line of Cs atoms in He II (876 nm)[5]. In this experiment, several gauss of static magnetic field was applied to the trapped atoms using a pair of Helmholtz coils to maintain spin polarization. To observe HFS resonance of Cs atoms, MW was irradiated to the spin polarized Cs atoms and its frequency was scanned. The emitted laser induced fluorescence (LIF) during the scanning of MW frequencies was detected using a photomultiplier tube. To suppress stray light from the laser beam, the wavelength of LIF (892 nm)[5] was selected using a monochromator. Figure 1 shows the obtained spectra in this experiment. We can clearly observe the resonance peaks in the figure. Since the resonance frequencies are shifted by ZMS owing to the applied magnetic field, the resonance frequencies are measured for both cases i.e., using σ^+ and σ^- polarized lasers. The HFS of Cs atoms in He II is calculated by averaging the two measured resonance frequencies. We obtain the preliminary value of 9 250.58(2) MHz as the HFS of Cs atoms in He II. This result shows that the HFS of Cs atoms in He II is approximately 0.63(2) % larger than that in vacuum owing to the effect of the surrounding helium. The achieved measurement accuracy is 6 digits in the current system. Since the accuracy of the HFS of Cs atoms in He II is limited owing to the fluctuation in the intensity of the applied magnetic field, it can be improved by one or two orders of magnitude by installing stabilized power supply for the magnetic field. In the near feature, we will conduct systematic measurement of HFS using $^{84\text{-}87}$Rb to demonstrate the feasibility of OROCHI for the study of low-yield exotic nuclei.

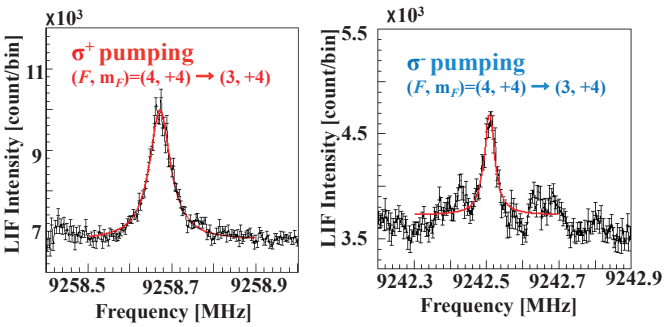

Fig. 1. Observed spectra in this experiment. (a) when using the σ^+ pumping laser. (b) when using the σ^- pumping laser.

*1 RIKEN Nishina Center
*2 Department of Physics, Meiji University
*3 Department of Physics, Tokyo Metropolitan University
*4 School of Physics, Peking University
*5 Department of Physics, Osaka University
*6 Department of Physics, Tokyo Gakugei University
*7 RIKEN Center for Advanced Photonics
*8 Department of Applied Physics, Tokyo University of Agriculture and technology
*9 Department of Advanced Sciences, Hosei University

References

1) B. Cheal and K. T. Flanagan: J. Phys. G Nucl. Partic. 37, 113101 (2010).
2) T. Furukawa et al.: Hyp. Interact. 196, 191 (2010).
3) X. F. Yang et al.: Phys. Rev. A 90, 052516 (2014).
4) T. Furukawa et al.: Phys. Rev. Lett. 96, 095301 (2006).
5) T. Kinoshita et al.: Phys. Rev. B 49, 3648 (1994).

Lattice location and density distribution of hydrogen in β_1-V_2H†

E. Yagi,[*1,*2] T. Hayashi,[*2] T. Yoshida,[*2] S. Koike,[*3] N. Higami,[*2] K. Hirabayashi,[*2] A. Takebayashi,[*2] H. Matsuba,[*2] and K. Ogiwara[*1]

On the atomistic state of hydrogen in V_2H, it has been reported that hydrogen atoms are distributed randomly at tetrahedral (T) sites in the α-phase with a bcc crystal structure at high temperatures above about 470 K, whereas in the low-temperature β_1-phase below about 450 K, they occupy specific octahedral (O_z) sites with an ordered arrangement.[1] The β_1-V_2H has two different crystal structures, a body-centred tetragonal (bct) structure, and a body-centred monoclinic one (bcm) with slight inclination of the c-axis ($\alpha_0 \approx 90.3\text{-}91^\circ$) (a pseudo-tetragonal structure),[1] both of which have an axial ratio between a-and c-axes $c_0/a_0 \approx 1.1$, depending on the condition for crystal growth.[1] When tensile stress is applied along the [001] axis during transformation from the α to β_1-phases, the V_2H crystallizes into the bct structure, while without tensile stress it crystallizes into the bcm structure. The O_z sites are octahedral (O) sites between two adjacent V atoms aligned along the c-axis (z-axis) (Fig.1). The change of hydrogen site from T to O_z sites implies that the O_z-site occupancy is stabilized by elongation of the c-axis, which, conversely, has been induced by forces exerted by hydrogen atoms on neighbouring V atoms. The mechanism of occurrence of the bct structure and the O_z-site occupancy in the β_1-phase was theoretically studied for the uniform elongation of the c-axis under the condition of constant volume, and it was proposed that the elongation of the c-axis is effective for the O_z-site occupancy.[2] Therefore, to examine this effectiveness, in the present study, the site occupancy of hydrogen in both tetragonal β_1-V_2H and monoclinic β_1-V_2H is to be investigated in detail.

Another fundamental problem on hydrogen is the density distribution of hydrogen around its occupation site. This problem is related to the extent of wave function of hydrogen. Experimental values hitherto reported by a neutron diffraction method for the tetragonal β_1-V_2H are larger than the theoretically calculated values and, therefore, there has been a large discrepancy between them.[3,4]

In order to clarify the site occupancy and the spatial density distribution of hydrogen, the channelling method is very useful. In the present study, the channelling method utilizing a nuclear reaction $^1H(^{11}B, \alpha)\alpha\alpha$ with a ^{11}B beam of an energy of about 2 MeV, which had been developed to locate hydrogen dissolved in Ta and V,[5,6] is applied.

The lattice location of hydrogen and its density distribution in the tetragonal β_1-V_2H single crystal prepared under tensile stress and the monoclinic β_1-$V_2H_{1.1}$ single crystal prepared without tensile stress have been studied at room temperature. The following results have been obtained. In these crystals, H atoms are located at octahedral (O) sites with different distributions over O_x, O_y, and O_z sites. In the tetragonal β_1-V_2H, about 80% of the H atoms are located at O_z sites, about 10% of them at O_y sites and about 10% of them at O_x sites. In the monoclinic β_1-$V_2H_{1.1}$, about 65% of the H atoms are located at O_z sites, about 20% of them at O_y sites and about 15% of them at O_x sites. These results support the theoretical prediction that hydrogen preferentially occupies O_z sites under tensile stress along the z-axis (c-axis).

In both crystals, the HWHM of the density distribution of hydrogen is about 0.35 Å in the [100] direction, whereas it is less than 0.13 Å in the [001] direction on the assumption of the Gaussian distribution. The HWHM in the [110] direction has been measured only in the tetragonal crystal to be about 0.35 Å. These values are much smaller than those hitherto obtained by the neutron diffraction method, and close to the values theoretically calculated for the ground state (~0.28 Å for the [100] direction and ~0.093 Å for the [001] direction).

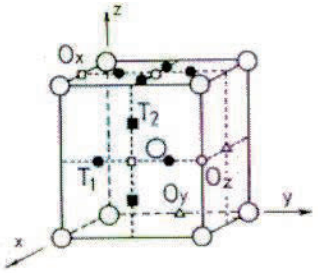

Fig.1. Two kinds of T sites, T_1 and T_2, and three kinds of O sites, O_x. O_y and O_z, in the bct structure. For each type of site, only some of equivalent sites are indicated.

References

1) For example: J. Wanagel, S. L. Sass, and B. W. Batterman: Phys. Stat. Solidi A **10**, 49 (1972); H. Asano, Y. Abe, and M. Hirabayashi: J. Phys. Soc. Jpn. **41**, 974 (1976); Y. Noda, K. Masumoto, S. Koike T. Suzuki, and S. Sato: Acta Crystallogr., Sect. B**42**, 529 (1986).
2) H. Sugimoto: J. Phys. Soc. Jpn. **53**, 2592 (1984).
3) T. Kajitani and M. Hirabayashi: Z. Phys. Chem. NF **145**, 27 (1985).
4) H. Sugimoto and Y. Fukai: J. Phys. Soc. Jpn. **51**, 2554 (1982).
5) E. Yagi, T. Kobayashi, S. Nakamura, Y. Fukai, and K. Watanabe: J. Phys. Soc. Jpn. **52**, 3441 (1983).
6) E. Yagi, T. Kobayashi, S. Nakamura, Y. Fukai, and K. Watanabe: Phys. Rev. B **31**, 1640 (1985).

† Condensed from the article in J. Phys. Soc. Jpn. **81**, 044602 (2012)

*1 RIKEN Nishina Centre
*2 School of Science and Engineering, Waseda University
*3 Department of Physics II, Tokyo University of Science

Observation of the FFLO-like nodal planes in the Au layer of Nb/Au/Fe trilayers by neutron reflectivity measurements

H. Yamazaki,[*1] M. Kubota,[*2] N. Miyata,[*3] and M. Takeda[*2]

From the study of Nb/Au/Fe and Nb/Au/Co trilayers,[1, 2] it was suggested that the superconducting order parameter Δ shows an FFLO-like oscillation with a period of Λ~2.1 nm in the Au layer probably due to the existence of strong spin-orbit coupling. In order to observe the oscillation in Δ, we carried out neutron reflectivity measurements on a trilayer of Nb(28.8nm)/Au(10.4nm)/Fe(12.6nm) with a cap of Au(4.4nm). For a review on the FFLO (or LOFF) states, please see ref. 3.

The Nb layer shows superconductivity below T_c~8.0 K, whereas the Fe layer is ferromagnetic. Below T_c, the Au layer is supposed to be in a superconducting state due to a proximity effect of the Nb layer. For the observation of possible FFLO-like nodal planes, where paramagnetic moments will appear when a magnetic field is applied perpendicular to the planes,[4] neutron reflectivity measurements were performed for $0.07<Q<6$ nm^{-1} at BL17 (Sharaku) in J-PARC/MLF. Measurements were first carried out at [10 K, 0 kOe], and then the sample was cooled to 2.3 K under zero magnetic field ($|H|<0.1$ Oe) to achieve a superconducting state. Measurements were carried out in sequence as shown in Fig. 1: [2.3 K, 0 kOe]→[2.3 K, 2 kOe]→[10 K, 2 kOe]. The data were obtained under four different conditions: (N, H=0) a normal state without field, (S, H=0) a superconducting state without field, (S, $H\neq0$) a superconducting state with an applied field, and (N, $H\neq0$) a normal state with an applied field.

The reflectivity obtained as a function of Q was in excellent agreement with previous results (Project No. 2012B0139). In the present experiment, we were particularly interested in the reflectivity at high Q's. To improve the S/N ratio, the signal was accumulated for a larger number of counts than in the previous measurements.

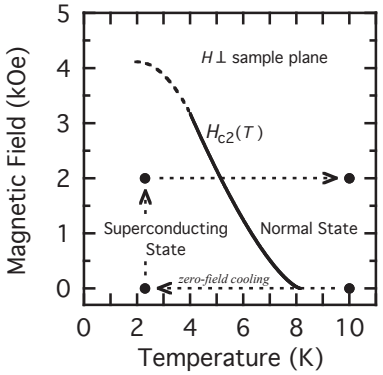

Fig. 1. Conditions for the measurements.

In order to clearly show the changes in reflectivity when measurement conditions were changed, the reflectivity ratios $\log(R_1/R_2)$ were plotted as a function of Q in Fig. 2: [R(2.3 K, 2 kOe)/R(2.3 K, 0 kOe)], [R(2.3 K, 2 kOe)/R(10 K, 2 kOe)], [R(2.3 K, 0 kOe)/R(10 K, 0 kOe)], and [R(10 K, 2 kOe)/R(10 K, 0 kOe)] for (1) (S, $H\neq0$)←(S, H=0), (2) (S, $H\neq0$)←(N, $H\neq0$), (3) (S, H=0)←(N, H=0), and (4) (N, $H\neq0$)←(N, H=0), respectively. The base lines are shifted arbitrarily for clarity of comparison. The variations in $\log(R_1/R_2)$ are qualitatively the same as those obtained in the previous measurements.

At high Q's in Fig. 2, regular and periodic peaks are observed particularly for (1) and (2) with an interval of 0.4 nm^{-1} (shown as broken lines). This interval corresponds to a period of 15.7 nm in real space. Low-noise data acquired in this experiment allow for the resolution of these peaks. At present, the origin of the 15.7 nm period is not clear. The thickness of the Fe layer is 12.6 nm, and we can observe a peak at 0.5 nm^{-1} that corresponds to a thickness of 12.57 nm, reflecting a magnetic change in the Fe layer. For more elaborate analysis, we have to carry out reflectivity simulation based on an appropriate multilayer model, including magnetic components not only in Fe but also in Au. The intense peak at 3.2 nm^{-1} for (1) and (2), however, may prove the existence of the FFLO-like nodal planes in the Au layer.

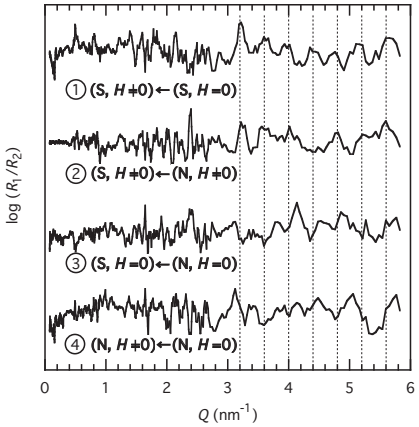

Fig. 2. Changes in neutron reflectivity.

References

1) H. Yamazaki, N. Shannon and H. Takagi: Phy. Rev. B **73**, 094507 (2006).
2) H. Yamazaki, N. Shannon and H. Takagi: Phy. Rev. B **81**, 094503 (2010).
3) R. Casalbuoni and G. Nardulli: Rev. Mod. Phys. **76**, 263 (2004).
4) Y. Matsuda and H. Shimahara: J. Phys. Soc. Jpn. **76**, 051005 (2007).

*1 RIKEN Nishina Center
*2 JAEA
*3 CROSS

Response of polyimide films to U ion beams as etched-track detectors

T. Yamauchi,[*1] T. Kusumoto,[*1] K. Matsukawa,[*1] Y. Mori,[*1] M. Kanasaki,[*1] K. Oda,[*1] S. Kodaira,[*2] K. Yoshida,[*3] Y. Yanagisawa,[*3] T. Kambara,[*3] and A. Yoshida[*3]

The polyimide Kapton retains its excellent physical, electrical, and mechanical properties over a wide temperature range between 4 and 673 K, and hence, it is considered an attractive candidate for a nuclear track membrane. Size-controllable nuclear pores on the sub-micron scale have been fabricated in the polyimide films by chemical etching, subsequent to irradiation with heavy ions.[1-3] Such nuclear membranes have been used in nanopore membranes, templates for metallic nanowires, aerosol filters, and gas separation films.[4-6] Applicability of the polyimide films as etched-track detectors for research on ultra-heavy cosmic rays has also been suggested; in this case, relatively long etchings are performed prior to the surface observations on the micron-scale under optical microscopes.[7] Few studies have been carried out, however, on the response of the polyimide for U ions, even as fundamental studies,[8,9] different from that on polyethylene terephthalate.[10] In this report, we describe the first result on the detection threshold and sensitivity of Kapton for U ions.

Commercially available Kapton films (from Nilaco) with a thickness of 125 μm were stacked and exposed to 345 MeV/n U-238 beams in air at the port of BigRIPS(F12), covering the stopping powers up to 20,000 keV/μm. After the exposure, the films were etched in a sodium hypochlorite solution kept at 55˚C.

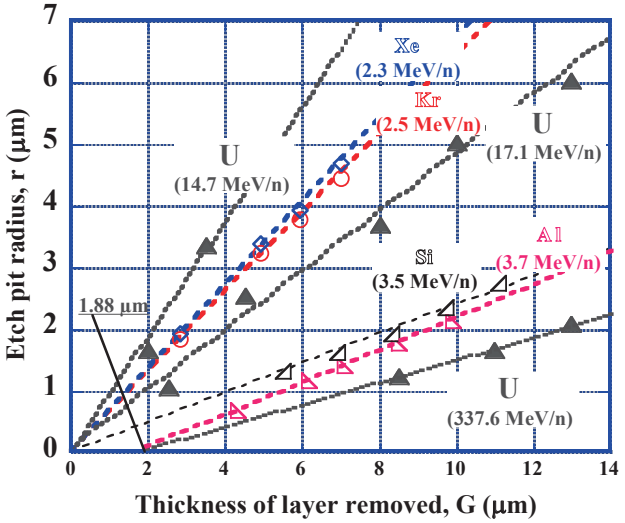

Fig. 1. Etch pit growth curves for U ions (14.7, 17.1 and 337.6 MeV/n), Xe ions (2.3 MeV/n), Kr ions (2.5 MeV/n), Si ions (3.5 MeV/n), and Al ions (3.7 MeV/n). Each energy for other indicating ions is close to that of the Bragg peaks.

*1 Graduate School of Maritime Sciences, Kobe University
*2 National Institute of Radiological Sciences
*3 RIKEN Nishina Center

Figure 1 shows typical growth curves of etch pit radius r against the thickness of layer removed G for U ions and other indicating heavy ions. During the etching, the films were reduced in thickness by $2G$. With increasing energy of U ions, the fitted slope for each data set decreases. The observed linear relation allowed us to use the conical assumption in evaluating the etch rate ratio V, which is the ratio of the track etch rate V_t to the bulk etch rate V_b.[7] The etch rate ratio was assessed by the following relation:

$$V=\{1+(dr/dG)^2\}/\{1-(dr/dG)^2\} \quad (1)$$

where (dr/dG) is the slope of the fitted line. The sensitivity of etch pit formation is defined as V-1. Figure 2 indicates the sensitivity of U ions, as well as other heavy ions, as a function of the stopping power. The threshold of U ions for etch pit formation is 3,439 keV/μm, which is higher than that of other heavy ions. The threshold is also observed in the growth curve (Fig. 1), as the intersect of the fitted line for 337.6 MeV/n U ions with a depth of 1.88 μm.

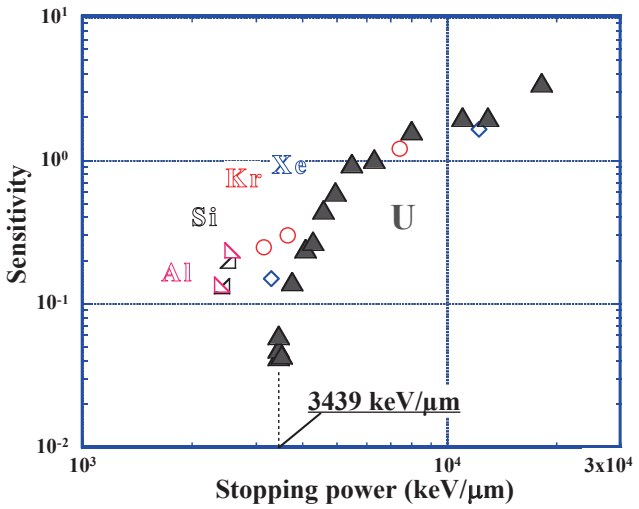

Fig. 2. Sensitivity of Kapton for U ions and other heavy ions against the stopping power.

References

1) P. Vater: Nucl. Tracks Radiat. Meas. **15**, 743 (1988).
2) C. Trautmann et al.: Nucl. Instr. Meth. B **111**, 70 (1996).
3) R. Sudowe et al.: Nucl. Instr. Meth. B **175-177**, 564 (2001).
4) W. Ensinger et al.: Radiat. Meas. **40**, 642 (2005).
5) W. Ensinger et al.: Surf. Coatings Technol. **201**, 8442 (2007).
6) W. Ensinger et al.: Radiat. Phys. Chem. **79**, 204 (2010).
7) T. Yamauchi et al.: Appl. Phys. Exp. **6**, 046401 (2013).
8) C. Trautmann et al.: Nucl. Instr. Meth. B **116**, 429 (1996).
9) S. A. Saleh and Y. Eyal: Nucl. Instr. Meth. B **208**, 137 (2003).
10) D. Drach et al.: Nucl. Instr. Meth. B **28**, 46 (1987).

High-density *n*-type doping of diamond by nitrogen beam implantation

H. Ueno,[*1] R. Kato,[*2] H.M. Yamamoto,[*2,*3] A. Yoshimi,[*1,*4] K. Morimoto,[*1] Y. Ichikawa,[*1] Y. Ishibashi,[*1,*5] Y. Ohtomo,[*1,*6] and T. Suzuki[*1,*6]

After the discovery of the superconductivity of boron-doped (*p*-type) diamond in 2004[1], studies have been extensively conducted to raise the T_c of diamond superconductivity. These studies have indicated that a high doping concentration of boron is favorable for increasing the T_c of superconductivity. High doping concentration can be introduced by the chemical-vapor-deposition (CVD) method[2,3]. Based on this technique, T_c has so far reached 11.4 K[4] at doping concentration ρ =8.4×10^{21} cm^{-3}. Theoretically, it has been predicted that a very high critical temperature $T_c \geq 100$ K is possible for doped diamond[5], because the high phonon frequency of diamond is favorable for increasing the T_c of superconductivity.

Unfortunately, the doping concentration achievable by CVD is limited to less than $\rho = 10^{22}$ cm^{-3} for boron and, more seriously, $\rho = 10^{20}$ cm^{-3} for phosphorus (*n*-type). With higher concentration, the dopants are known to form dimers, causing localization of the doped carriers, and thus cannot be used for electric conduction. In view of electronic applications, both *p*-type and *n*-type dopings are necessary. From an analogy to other superconductors such as high-T_c cuprates, it is natural to expect *n*-type superconductivity in diamond. To date, however, high-density doping of *n*-type carrier has not been achieved.

A new approach expected to realize high-density doping is heavy-ion implantation, because i) a sharp fall-off at the distal edge in the stopping range (i.e., Bragg peak), which becomes remarkable for heavy-ion beams, is favorable for the purpose of high doping concentration, and ii) dopant dimerization should not occur very frequently because of the high randomness of the implanted atoms. Taking these advantages, we have been conducting doped-diamond studies in order to realize an *n*-type diamond superconductivity with T_c as high as possible. Furthermore, it is also important to reproduce the increase in T_c in boron-doped *p*-type region, in particular, outside the CVD limit, under the scheme of heavy-ion implantation utilizing the high beam current of various heavy ions available at the RIBF facility. In parallel, the optimization of conditions for heavy-ion implantation including an annealing process to make the diamond lattice as clean as possible should be also investigated.

In the present work, we report on the first nitrogen-ion implantation experiment at RIBF[a] to investigate a possible onset of *n*-type superconductivity of diamond. A beam of $^{14}N^{3+}$ delivered at energy E/A = 450 keV from the RILAC accelerator at RIBF was implanted into (100)-faceted single crystals of type Ib diamond[6]. This beam energy was set to be much lower than the Coulomb barrier to avoid the radioactivaion of samples. The crystals were prepared in the form of 4 mm × 4 mm × 0.3 mm(t), and mounted on a Cu ladder placed in the center of the GARIS target chamber. The implantation was carried out at room temperature at beam current $I = 3 \sim 10$ μA.

The density $\rho(^{14}N)$ of the implanted ^{14}N particles was simply calculated by

$$\rho(^{14}\mathrm{N}) = \frac{I \cdot T}{q \cdot S \cdot \Delta R}, \quad (1)$$

where I is the beam current, T is the irradiation time, $q = 3^+$ is the charge state of the beam, $S \simeq \pi$×4 mm×6.5 mm is the beam spot size, and ΔR is the stopping-range distribution of the beam in the crystal. Taking a value of $\Delta R \simeq 0.2$ μm at the mean stopping range $R \simeq 2.5$ μm, calculated with the simulation code SRIM[7], we determined $\rho(^{14}N)$ of five nitrogen-implanted diamond crystals, ranging from $\rho = 7.8 \times 10^{20}$ to 1.9×10^{22} cm^{-3}. These densities are approximately the same as the reported CVD-doped boron densities at which superconductivity of diamond has been observed[1,4,8]. Offline resistivity measurements of the obtained nitrogen-doped crystals as a function of temperature are in progress.

References

1) E.A. Ekimov et al.: Nature **428**, 542 (2004).
2) B.V. Spitsyn et al.: J. Cryst. Growth **52**, 219 (1981).
3) M. Kamo et al.: J. Cryst. Growth **62**, 642 (1983).
4) H. Umezawa et al.: cond-mat 0503303 (2005).
5) T. Shirakawa et al.: J. Phys. Soc. Jpn. **76**, 014711 (2007).
6) Sumicrystal: Sumitomo Electric Industries, Ltd., Osaka, Japan.
7) J. Ziegler: SRIM—The stopping and range of ions in matter, http://www.srim.org/ (2008).
8) E. Bustarret et al.: Phys. Rev. Lett. **93**, 237005 (2004).

*1 RIKEN Nishina Center
*2 Condensed Molecular Materials Laboratory, RIKEN
*3 Research Center of Integrative Molecular Systems (CIMoS), Institute for Molecular Science
*4 Research Core for Extreme Quantum World, Okayama University
*5 Institute of Physics, University of Tsukuba
*6 Department of Physics, Tokyo Institute of Technology

a) The experiment was performed under the Experimental Program ML1006-LINAC29.

2. Atomic and Solid State Physics (Muon)

μSR study of the magnetism and superconductivity in the multi-layered Bi-2223 high-T_c superconductor

T. Adachi,[*1,*2] M. A. Baqiya,[*3] K. M. Suzuki,[*1,*4] K. Tsutsumi,[*4] M. Fujita,[*1,*4] S. Adachi,[*5] T. Watanabe,[*5] I. Watanabe,[*1] and Y. Koike[*1,*3]

In the research of high-T_c cuprate superconductors, the relationship between the magnetism and superconductivity has been a central issue. Nuclear-magnetic-resonance (NMR) experiments in the so-called multi-layered Hg-based cuprate Hg-1245 with 5 CuO_2 planes in the unit cell have revealed that the hole concentration per Cu, p, in the CuO_2 plane is larger in the outer planes (OP's) than in the inner planes (IP's) due to the difference in the coordination number of Cu between OP's and IP's.[1] Moreover, it has been suggested that both antiferromagnetic (AF) order and superconductivity coexist homogeneously in a CuO_2 plane with a small p value. In the optimally doped Hg-1245 cuprate, it has been reported from zero-field (ZF) μSR measurements that a muon-spin precession is observed at low temperatures, suggesting the coexistence of AF order and superconductivity.[2]

Fujii et al. have succeeded in growing sizable single-crystals of a tri-layered Bi-based cuprate $Bi_2Sr_2Ca_2Cu_3O_{10+\delta}$ (Bi-2223) with $T_c = 110$ K.[3] Recently, we have performed ZF-μSR measurements of the underdoped Bi-2223 single-crystals with $T_c = 87$ K, obtained through the reduction annealing. It has been found that the depolarization rate of muon spins, λ, increases with decreasing temperature and exhibits a local maximum at 10 K, followed by an increase below 5 K. This suggests the existence of two distinct Cu-spin correlations in a crystal probably originating from IP and OP's. However, the development of the Cu-spin correlation is weak even at 0.3 K, preventing us from investigating the detailed magnetic state in Bi-2223 cuprates. Based on the results, we have performed μSR measurements of Bi-2223 in the heavily underdoped (HUD) regime with $T_c = 40 - 60$ K, obtained through the further reduction-annealing. The ZF and longitudinal-field μSR measurements were carried out using a fly-past HELIOX cryostat at temperatures down to 0.3 K at RIKEN-RAL.

Figure 1 shows ZF spectra of the HUD Bi-2223. At 250 K, the spectrum shows a slow depolarization of muon spins, indicating that Cu spins fluctuate fast beyond the μSR frequency range. With decreasing temperature, it is found that the depolarization becomes fast gradually and an exponential-like depolarization is observed at 0.3 K, indicating the development of the Cu-spin correlation. The λ at 0.3 K is more significant than that observed in the underdoped crystals at 0.3 K. Moreover, the temperature dependence of λ exhibits local maxima at 40 K and 1 K probably corresponding to the development of the Cu-spin correlation in IP and OP's, respectively. The temperatures are higher than those observed in the underdoped crystals, respectively. These results suggest that the Cu-spin correlation is more developed in the HUD crystals than in the underdoped crystals, although no muon-spin precession due to the formation of a magnetic order is observed even at 0.3 K. Accordingly, the p value of IP in the HUD Bi-2223 cuprate may reside in the vicinity of the boundary between the AF and superconducting (SC) phases in the phase diagram.

In summary, we have found two distinct developments of the Cu-spin correlations probably originating from IP and OP's in the HUD Bi-2223 crystals. The p value of IP probably resides in the vicinity of the boundary between the AF and SC phases in the phase diagram, suggesting that the Bi-2223 crystals with T_c lower than ~ 40 K exhibit an AF ground state.

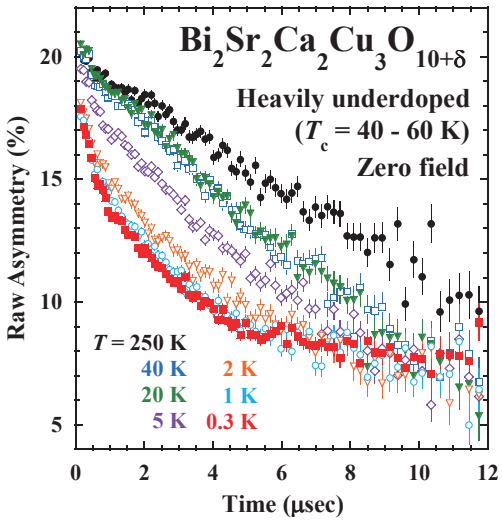

Fig. 1. Zero-field μSR time spectra of the heavily underdoped $Bi_2Sr_2Ca_2Cu_3O_{10+\delta}$ single crystals with $T_c = 40 - 60$ K.

*1 RIKEN Nishina Center
*2 Department of Engineering and Applied Sciences, Sophia University
*3 Department of Applied Physics, Tohoku University
*4 Institute for Materials Research, Tohoku University
*5 Graduate School of Science and Technology, Hirosaki University

References

1) H. Mukuda et al.: J. Phys. Soc. Jpn. **77**, 124706 (2008).
2) K. Tokiwa et al.: Physica C **460-462**, 892 (2007).
3) T. Fujii et al.: J. Cryst. Growth **223**, 175 (2001).

μSR study of the Al-induced magnetic order in $La_{2-x}Sr_xCu_{1-y}Al_yO_4$

K. M. Suzuki,[*1,*2] T. Adachi,[*1,*3] M. A. Baqiya,[*4] M. Abdel-Jawad,[*1] S. Yoon,[*1] I. Watanabe,[*1] and Y. Koike[*1,*4]

The so-called stripe correlation of spins and holes has been studied intensively in order to clarify its relationship with the appearance of superconductivity in the high-T_c cuprates. Nevertheless, the details of the stripes have not yet been clarified to date. One of the reasons is that the frequencies of the dynamical stripes are faster than the μSR frequency range in a wide range of the hole-concentration per Cu, p, where the superconductivity appears. For this reason, impurity substitution is one of crucial ways to study the stripe correlation, because substituted impurities tend to slow down the spin fluctuations, leading to the formation of the static stripe order. Formerly, we have found from the zero-field (ZF) μSR that the magnetic impurity Fe^{3+} tends to stabilize a magnetic order in the whole superconducting regime of $La_{2-x}Sr_xCu_{1-y}Fe_yO_4$ (LSCFO).[1,2] Intriguing is that double successive magnetic transitions are observed in the overdoped regime of LSCFO, indicating that the stripe order induced by the Fe substitution persists up to $p \sim 0.30$ and terminates there. As for effects of non-magnetic Zn^{2+} substitution, weakness of the develpment of the Cu-spin correlation by the Zn substitution prevents us from understanding the nature of the Cu-spin correlation especially in the overdoped regime.[3] Recently, we have observed unexpected behavior in non-magnetic Al^{3+}-substituted $La_{2-x}Sr_xCu_{1-y}Al_yO_4$ (LSCAO) by the μSR measurements, namely, a static magnetic state is induced by 3% Al-substitution in the overdoped regime. It is expected that effects of non-magnetic impurities on the Cu-spin correlation will be clarified even in the overdoped regime.

Therefore, in order to investigate the magnetism induced by the Al substitution, we have performed ZF-μSR experiments for LSCAO with $x = 0.11 - 0.30$ and $y = 0.03$. The polycrystalline samples were prepared by the ordinary solid-state reaction method. ZF-μSR measurements were carried out using a Variox, a Heliox and a Janis cryostats at temperatures down to 0.3 K at RIKEN-RAL.

Figure 1(a) shows the ZF-μSR time spectra of LSCAO with $x = 0.30$ and $y = 0.03$. At 5.0 K, the spectral shows the Gaussian-type relaxation due to the randomly-oriented nuclear dipole field, indicating electron spins fluctuate fast beyond the μSR time window. With decreasing temperature, the muon-spin depolarization becomes fast progressively down to 0.8 K and finally a nearly-static magnetic order is formed at 0.3 K, suggesting a remarkable effect of the Al-substitution on the development of the Cu-spin correlation even in the heavily-doped regime. Figure 1(b) shows the p dependence of the magnetic transition temperature, T_N, defined as the midpoint of the change in the initial asymmetry of the magnetic component in an analytical function. It is found that T_N decreases monotoniously with increasing p, suggesting that the stripe order is induced also in the overdoped regime. Moreover, T_N disappears at $p \sim 0.30$ as observed in LSCFO[2] and LSCZO.[3] Therefore, it has been concluded that, regardless of the type of impurities, the development of the stripe correlation is observed up to $p \sim 0.30$, suggesting an intimate relationship between the stripe correlation and the appearance of the high-T_c superconductivity. Considering the difference between the results of Fe^{3+}, Zn^{2+} and Al^{3+}, charge disorder as well as large magnetic moments may play an important role in the stabilization of the stripe correlation.

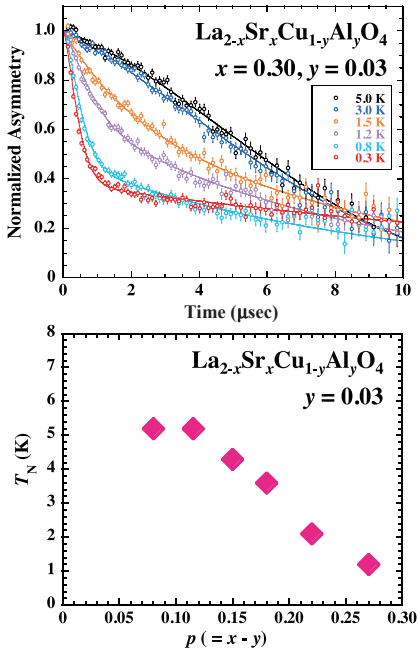

Fig. 1. (a) Zero-field μSR time spectra of $La_{2-x}Sr_xCu_{1-y}Al_yO_4$ (LSCAO) with $x = 0.30$ and $y = 0.03$. (b) Temperature dependence of the magnetic transition temperature, T_N, of LSCAO with $y = 0.03$.

*1 RIKEN Nishina Center
*2 Institute for Materials Research, Tohoku University
*3 Department of Engineering and Applied Sciences, Sophia University
*4 Department of Applied Physics, Tohoku University

References

1) K. M. Suzuki *et al.*, Phys. Rev. B **86**, 014522 (2012).
2) K. M. Suzuki *et al.*, in preparation.
3) Risdiana, *et al.*, Phys. Rev. B **77**, 054516 (2008).

μSR study of cluster-glass state in $Sr_{1-x}La_xRuO_3$

I. Kawasaki,[*1,*2] M. Yokoyama,[*3] K. Fujimura,[*3] and I. Watanabe[*2]

Strontium ruthenate shows various types of physical properties attributed to the itinerant feature of Ru 4*d* electrons and the strong mixing between Ru 4*d* and O 2*p* electrons.[1,2] $SrRuO_3$ crystallizes into a distorted perovskite structure and is a ferromagnet with a Curie temperature of about 160 K.[3] Photoemission experiments showed that the density of states at Fermi level is dominated by the Ru 4*d* state.[4] Therefore, itinerant Ru 4*d* electrons are considered to be responsible for the magnetic properties. It is also argued that the development of the incoherent component in the density of states reflects the electronic correlation effects. In addition, this system shows "bad metal" behavior in transport at high temperatures: the electrical resistivity continues to increase with increasing temperature, even though the Boltzmann mean free path becomes smaller than the lattice constants, indicating that the itinerant quasi-particle description is no longer available in the high temperature range.[5] These experimental findings suggest that the physical properties are strongly influenced by the correlation of the Ru 4*d* electrons, and the Ru 4*d* states have a duality of itinerant and localized natures.

We have studied the Sr site-substituted system $Sr_{1-x}La_xRuO_3$.[6] Substituting La for Sr suppress the Ferromagnetism.[7] In addition, the Ru-O distance increases with increasing x, suggesting that doping La may enhance the role of the electronic interaction. Recent our studies suggest that for $x \geq 0.3$, disorder plays an important role and this system shows a short range ferromagnetic ordering (cluster formation), and with further decreasing temperature these clusters freeze into a cluster-glass state.

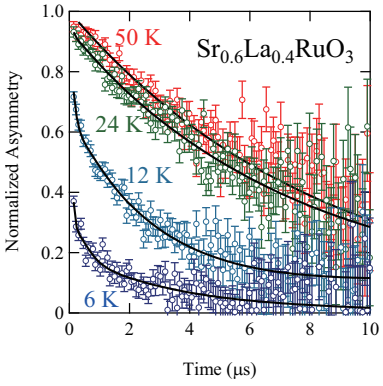

Fig. 1. Zero-field μSR spectra.

*1 Graduate School of Material Science, University of Hyogo
*2 RIKEN Nishina Center
*3 Faculty of Science, Ibaraki University

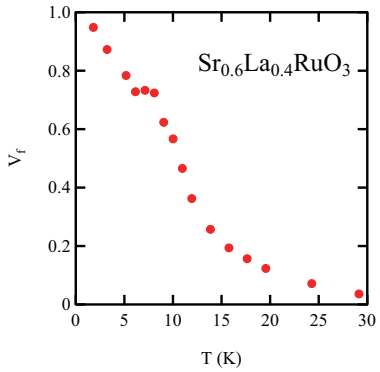

Fig. 2. Temperature dependence of the volume fraction.

In the present study, we performed μSR experiments on polycrystalline sample of $Sr_{1-x}La_xRuO_3$ to further investigate the cluster-glass state of this system. The μSR experiments were carried out at the RIKEN RAL Muon Facility in the UK, where an intense pulsed muon beam is available.

Figure 1 shows the zero-field spectra for $x = 0.4$ measured at various temperatures. Below 30 K, the relaxation rate develops and a loss of initial asymmetry is observed, indicating a development of magnetic clusters. The ZF-spectra are well fitted by the following function, which assumes a presence of two components:

$$P(t) = A_1[\frac{1}{3}e^{-\lambda_1 t} + \frac{2}{3}(1-\Delta_1 t)e^{-\Delta_1 t}] + A_2[\frac{1}{3}e^{-\lambda_2 t} + \frac{2}{3}(1-\Delta_2 t)e^{-\Delta_2 t}],$$

where A_1 and A_2 represent the paramagnetic and ordered volume fractions respectively. The temperature dependence of the volume fraction of the magnetic ordered region is shown in Fig. 2. The volume fraction exhibits a rapid increase at around 10 K, where the magnetic susceptibility shows a peak,[6] and reaches nearly 100% at the lowest temperature. The presence of the magnetic ground state with the volume fraction of 100% inevitably indicates the itinerant nature of the Ru 4*d* electrons in this system.

References

1) S. A. Grigera et al.: Science **294**, 329 (2001).
2) Y. Maeno et al.: Nature **372**, 532 (1994).
3) A. Callaghan et al.: Inorg. Chem. **5**, 1572 (1966).
4) J. Okamoto et al.: Phys. Rev. B **60**, 2281 (1999).
5) P. B. Allen et al.: Phys. Rev. B **53**, 4393 (1996).
6) I. Kawasaki et al.: J. Phys. Soc. Jpn. **83**, 064712 (2014).]
7) H. Nakatsugawa et al.: J. Phys.: Condens. Matter **14**, 415 (2002).

Investigation of magnetic ground states in mixed kagome systems $(Rb_{1-x}Cs_x)_2Cu_3SnF_{12}$ by μSR

T. Suzuki,[*1,*4] K. Katayama,[*2] H. Tanaka,[*2] T. Goto,[*3] and I. Watanabe[*4]

The Heisenberg kagome antiferromagnet (HKAF) has attracted much attention in magnetism, because several frustration and quantum effects have been indicated by theories. For example, in the classical spin model case for HKAF, the $q = 0$ or $\sqrt{3} \times \sqrt{3}$ magnetic structure is stabilized when the next-nearest-neighbor interaction is considered. In the case of $S = 1/2$ kagome lattice, exotic magnetic ground states have been theoretically predicted. For example, numerical calculations revealed that the ground state is a magnetically disordered spin liquid. In the ground state, triplet excitations are gapped, and there exists the continuum of low-lying singlet states below the triplet gap[1]. Valence-bond crystal by a periodic arrangement of singlet dimers has also been proposed as the magnetic ground state of $S = 1/2$ HKAF[2]. Experimentally, many kinds of HKAF have been investigated as the candidate for the ideal kagome spin lattice material.

Another new candidate for the ideal kagome lattice with an exotic magnetic ground state was reported by Ono *et al.* The cupric compound $A_2Cu_3SnF_{12}$ (A = Cs, Rb), which is the subject of this study, is a newly synthesized family of $S = 1/2$ HKAF[3,4]. For $Cs_2Cu_3SnF_{12}$, the weak-ferromagnetic behavior is observed below $T_N = 20$ K, and it is suggested that the antiferromagnetic ordered state appears[4]. On the other hand, for $Rb_2Cu_3SnF_{12}$, the first realization of the "pinwheel" valence bond solid (VBS) ground state in the $S = 1/2$ HKAF are confirmed by inelastic neutron measurements[5]. Quite recently, mixed kagome systems $(Rb_{1-x}Cs_x)_2Cu_3SnF_{12}$ have been prepared[6]. By magnetic susceptibility and specific heat measurements on single crystals, they reported a phase diagram, which shows the existence of the quantum phase transition from the VBS to the AF phase at $x_c = 0.53$. In this concentration, the spin gap vanishes and the ordered state disappears from the view point of magnetization results.

We carried out LF-μSR measurements in $x = 0.53$ single crystal to investigate dynamical magnetic properties microscopically. Figure 1 (a) shows LF-μSR time spectra in 200 gauss at various temperatures. It is emphasized that no disappearance of the initial asymmetry is observed. Below 3 K, time spectra are well fitted by the two component function as follows: $A(t) = A_1 \exp(-\lambda_1 t) + A_2 \exp(-\lambda_2 t)$. Here, $A_1 = 0.58$, $A_2 = 0.42$. As shown in Fig. 1 (b), λ_1 increases with decreasing temperature. LF-dependence of time spectra at 0.27 K is shown in Fig. 1 (c), and LF-dependence of relaxation rates is shown in (d). Muon spin relaxation rates are inversely proportional to LF, and such change indicates "white" frequency spectra, which means the spectra are described by summation of continuously distributed frequencies using the Redfield formula. These results suggest that the internal fields fluctuate, and are consistent with reported macroscopic results at least down to 0.27 K.

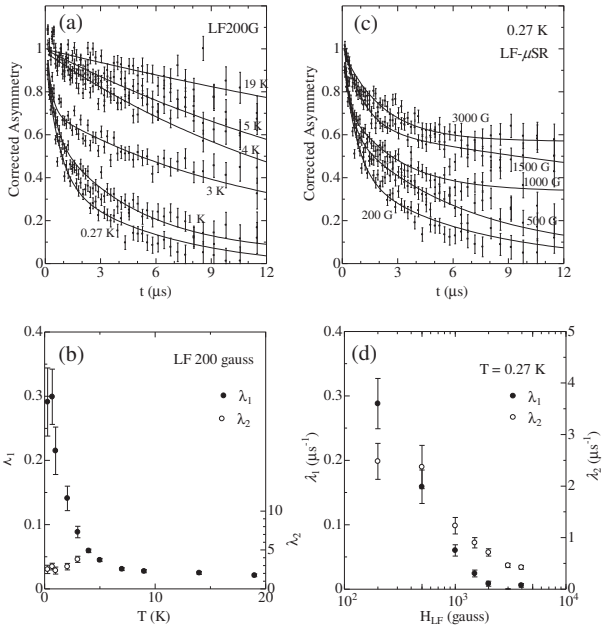

Fig. 1. (a)Temperature dependence of the time spectra in the LF of 200 gauss. (b) Temperature dependence of the muon spin relaxation rate in LF 200 gauss. (c) LF-μSR time spectra above 200 gauss up to 3000 gauss at 0.27 K. (d) LF dependence of the muon spin relaxation rate at 0.27 K.

References

1) H. C. Jiang et al.: Phys. Rev. Lett. **101**, 117203 (2008).
2) R. R. P. Singh et al.: Phys. Rev. B **77**, 144415 (2008).
3) M. Muller et al.: Z. Anorg. Allg. Chem. **621**, 993 (1995).
4) T. Ono et al., Phys. Rev. B **79**, 174407 (2009).
5) K. Matan et al., Nature Phys. **6**, 865 (2010).
6) K. Katayama et al.: arXive:1412.5770v1 [cond-matt.str-el].

*1 College of Engineering, Shibaura Institute of Technology
*2 Department of Physics, Tokyo Institute of Technology
*3 Department of Physics, Sophia University
*4 RIKEN Nishina Center

High pressure μSR study of quantum phase transition in CeNiAsO

H. Guo,[*1,*2] Y. Luo,[*1] I. Watanabe,[*2] and Z. Xu[*1]

The discovery of superconductivity in $LaFeAsO_{1-y}F_y$ systems[1] triggers not only a new search of the iron-based superconductors, but also studies of the Kondo effect when La is replaced by magnetic ions such as Ce. The Fe 3*d* electrons in such systems usually undergo a spin-density-wave (SDW) transition at about 140 K on top of the much lower temperature where the 4*f* electrons become magnetically ordered.[2] In order to study the 4*f* electronic properties, we therefore focused on a Ni-based compound, namely, CeONiAs, instead of Fe-based compounds since the Ni ions are not long-ranged magnetically ordered in these compounds, as observed by experiments and theoretical calculations.[3]

Our previous studies including magnetic susceptibility, transport, and thermal dynamic measurements show that CeONiAs undergoes two successive magnetic transitions at $T_1 = 9.3$ K and $T_2 = 7.3$ K, respectively, and these two transitions can be suppressed both by hydrostatic and chemical pressures (P). When $P > 4$ kbar, T_1 can be hardly seen, while T_2 is continuously suppressed with a critical value of $P_c \sim 6.3$ kbar. Resistivity measurements indicate that there is a quantum phase transition at P_c. In order to reveal the role of magnetic correlations around the quantum critical point (QCP), and the evolution of magnetic structure with pressure, we have performed μSR experiments with gas pressures up to 6.1 kbar on $CeONiAs_{0.9}P_{0.1}$, where the substitution of As by P is expected to reduce P_c.

During the high pressure μSR measurement, most of the muons are stopped at the pressure cell made of Cu, and therefore, muon spin precession is hardly observed even when magnetic ordering appears in the sample, which limits our analyses of the evolution of the magnetic structure with pressure from the observation of muon spin precession in the zero field (ZF) measurement. Alternatively, we performed transverse field (TF) measurements and the spectra were fitted using the following function:

$$A(t) = A_{\rm ini}\cos(\gamma_\mu B t + \varphi)\exp(-\lambda t) \quad (1)$$

where $A_{\rm int}$ is the initial asymmetry, γ_μ is the muon gyromagnetic ratio, B is the magnetic field, and λ is the muon spin relaxation rate.

Figure 1(a) shows the temperature dependence of the initial asymmetry, $A_{\rm ini}$ at ambient pressure (A.P.) and $P = 6.1$ kbar. At A.P., $A_{\rm ini}$ is nearly temperature independent at high temperatures, and decreases sharply below approximately 10 K. No further significant change is observed below 10 K due to the low signal-to-background ratio. The transition temperature is suppressed to approximately 6 K when $P = 6.1$ kbar. Fig. 1(b) shows the temperature dependence of the muon spin relaxation rate λ. The substantial increase of λ below about 10 K and 6 K, respectively, at A.P. and $P = 6.1$ kbar is consistent with the results of the temperature dependence of $A_{\rm ini}$. The appearance of the internal field will increase the internal field distribution width at the muon site, thus enhancing the muon spin relaxation rate. Owing to the usage of a pulsed muon source, the increase in muon spin relaxation rate will usually lead to a decrease in the initial asymmetry. Thus, our current results confirm the magnetic ordering from the microscopic view point. The application of high pressures up to 6.1 kbar also confirms that the magnetic ordering is suppressed by pressure. Unfortunately, valuable information about the evolution of the internal field with the pressure cannot be obtained since we cannot observe the muon spin precession directly as mentioned above.

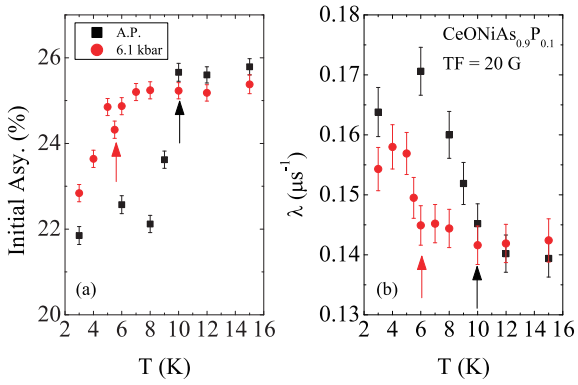

Fig. 1. Temperature dependence of the extracted parameters. (a) The initial asymmetry. (b) The muon spin relaxation rate, λ. The arrows indicate the magnetic transition temperatures.

References
1) Y. Kamihara, H. Hiramatsu, M. Hirano, R. Kawamura, H. Yanagi, T. Kamiya, and H. Hosono, J. Am. Chem. Soc. 128, 10012 (2006).
2) J. Zhao, Q. Huang, C. de la Cruz, S. Li, J. W. Lynn, Y. Chen, M. A. Green, G. F. Chen, G. Li, Z. Li, J. L. Luo, N. L. Wang, and P. Dai, Nature Materials 7, 953 (2008).
3) T. M. McQueen, T. Klimczuk, A. J. Williams, Q. Huang, and R. J. Cava, Phys. Rev. B 79, 172502 (2009).

*1 Department of Physics, Zhejiang University
*2 RIKEN Nishina Center

Investigation of hydrogen dynamics in hydroxyl salts $Co_2(OD)_3Cl$

X.L. Xu,[*1] X.G. Zheng,[*1] H.J. Guo,[*2] and I. Watanabe[*2]

Hydroxyl salts of the type $M_2(OH)_3X$ (X = Cl, Br, or I) have been known for a long time. These compounds containing magnetic ions are magnetic materials. However, only in recent years their magnetic properties have been clarified as a result of our research [1,2] and they are known as "frustrated magnets". Our latest finding is universal strong magnetic--dielectric--lattice coupling in all such compounds. Measurements of dielectric constants and lattice parameters revealed simultaneous changes at the respective T_N for all hydroxyl salts, which indicate strong magnetic--dielectric--lattice coupling. Moreover, we found that for $Co_2(OH)_3Cl$ and $Co_2(OH)_3Br$, which have the highest crystal symmetry in the hydroxyl salt series shown in Fig. 1, the corresponding deuterated compounds $Co_2(OD)_3Cl$ [Br] clearly exhibited a ferroelectric response at exceptionally high temperatures. Sharp peaks were observed at 229 K in both dielectric constants measured at 100 kHz for $Co_2(OD)_3Cl$.[3] Similar behaviors were observed in $Co_2(OD)_3Br$ (T_E = 224 K at 100 kHz).

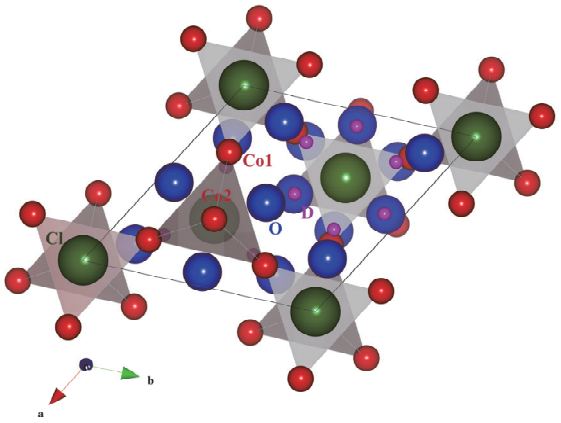

Fig. 1. High crystal symmetry of $Co_2(OD)_3Cl$.

Therefore, we performed μSR experiments on $Co_2(OD)_3Cl$ to reveal the mechanism of this unconventional ferroelectric response, using the muon facilities at RIEKN-RAL. We observed a change in the dynamics of D atoms in $Co_2(OD)_3Cl$ through the nuclear dipolar field of D (Fig. 2).

The asymmetry $a(t)$ of muon-spin-relaxation can be approximately expressed by a combination of the dynamic Kubo-Toyabe function and an exponential function.

The dynamic Kubo-Toyabe function represents the contribution from the nuclear dipolar field of D atoms, and the exponential one accounts for magnetic relaxation.

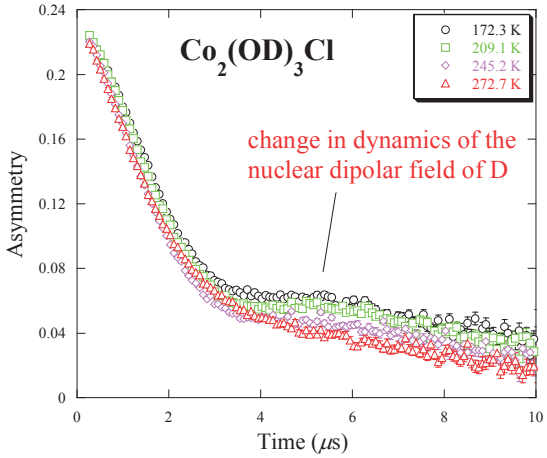

Fig. 2. Muon-spin-relaxation spectra indicating a change in the dynamics of D atoms in $Co_2(OD)_3Cl$.

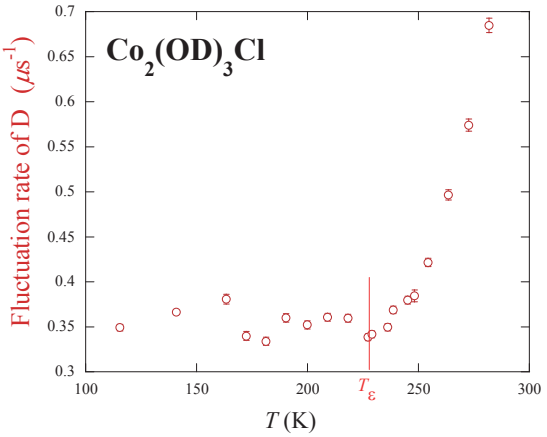

Fig.3. The analyzed fluctuation rate of the nuclear dipolar field of the D atoms in $Co_2(OD)_3Cl$.

The analyzed fluctuation rate of the nuclear dipolar field of the D atoms in $Co_2(OD)_3Cl$ shows an abrupt change around the ferroelectric transition temperature T_E = 230 K (Fig. 3), suggesting that the hydrogen (D) dynamics plays a critical role in the ferroelectric response of $Co_2(OD)_3Cl$.

References

1) X.G. Zheng et al.: Phys. Rev. B **71**, 052409 (2005).
2) X.G. Zheng et al.: Phys. Rev. Lett. **95**, 057201 (2005).
3) X.G. Zheng et al.: Phys. Rev. B 87, 174102 (2013).

[*1] Department of Physics, Saga University
[*2] RIKEN Nishina Center

Partial magnetic order in the quantum spin system NH_4CuCl_3

T. Goto,[*1] K. Matsui,[*1] T. Suzuki,[*2] H. Guo,[*4] A. Oosawa,[*1] M. Fujisawa,[*3] H. Tanaka,[*3] I. Watanabe[*4]

The ground states of boson systems with randomness have been a puzzle for a long time. In a uniform system consisting of mobile bosons, the ground state is the Bose-Einstein condensed fluid. When the mobility of particles is reduced by introducing randomness or frustration, the system becomes solid-like, that is, the Bose glass or the Wigner crystal, details of which, however, are still unknown[1]. For studying the property of the boson system, NH_4CuCl_3 is suitable model compound, where both the density and mobility of the field-induced magnons can be tuned by the magnitude of applied field and the state of non-centrosymmetric NH_4 molecules, respectively.

The quantum spin magnet NH_4CuCl_3 is an S =1/2 three-dimensional dimer system with the crystal structure isomorphic to $TlCuCl_3$, which is a spin-gapped system and is known for the Bose-Einstein condensation of field-induced magnons. The ground state of NH_4CuCl_3, however, is different from that of $TlCuCl_3$, that is, gapless in zero field, showing a magnetic order at T_N = 1.25 K. When a high magnetic field is applied, two-step magnetization plateaus are observed[2]. The mechanism of the two-step plateaus attracts much interest, for it is related to the fundamental property of the field-induced magnons.

One of the models[3] proposed so far is the localized three sublattice dimer model that claims an existence of the three inequivalent dimers A, B and C with different critical fields H_c, one of which *i.e.* H_c^A is zero. This model elegantly explains the two-step plateaus: the two plateaus appear in the field regions where the dimer A and B saturates, and the net magnetization saturates when all three saturate. According to this model, only dimer A magnetically orders at zero field, indicating the partial magnetic order.

The elastic neutron scattering experiment[4] confirms the doubling of the unit cell along *b*, supporting the existence of three inequivalent dimers in an elongated unit cell. However, recent high-field NMR observation[5] disproves this model. That is, in the high field of the second plateau region, the two of the three inequivalent dimers are saturated and only C is paramagnetic, and hence the NMR signal corresponding to C is expected to be observed at nearly zero-shift position. However, in the high-field NMR spectra, a signal corresponding to either A or B is also observed with that for C. This contradiction gives us a good motivation to propose carrying out the μSR experiment on this compound. If the model is correct, one expects that only one site possesses a large hyperfine field while the other three quarter sites are expected to remain in the paramagnetic state, or that when the interaction among inequivalent three dimers is appreciable, three different hyperfine fields will appear at each dimer, similar to the case of $SrCu_2(BO_3)_2$.

So far, zero field (ZF) - μSR measurements on single crystals of NH_4CuCl_3 were carried out at the Riken-RAL Muon Facility using a pulsed surface-muon beam with a momentum of 27 MeV/c. In the ordered state below T_N, a clear muon spin rotation is observed at zero-field. At the lowest temperature 0.31 K, one can see in the depolarization curve a clear beat with two different frequencies and also an extremely fast term that monotonically decreases with time. This leads us to choose reasonably the three-component function $G_{KT}(\Delta;\tau)\cdot(A_1e^{-\lambda_1\tau}+A_2e^{-\lambda_2\tau}\cos\omega_2\tau+A_3e^{-\lambda_3\tau}\cos\omega_3\tau)$ to fit the data below T_N. Above T_N, the depolarization curves simply consist of one component, that is, the first term in the above function. Figure 1 shows the typical depolarization curves with the fitted function at various temperatures. The two hyperfine fields ω_1/γ and ω_2/γ increased monotonically below T_N and reached 150 and 90 Oe. The volume fraction of each component for A_1, A_2 and A_3 were 25, 70 and 5 % at 0.3 K.

Although the observed data clearly demonstrate that the ordered state consists of three different parts, the fraction of each part is not in accord with the model, which declares that A_1, A_2 and A_3 should be in the ratio 1:2:1. For further quantitative comparison of this result with the three-sublattice model, the detailed knowledge of the muon stopping site in the unit cell is indispensable. [6]

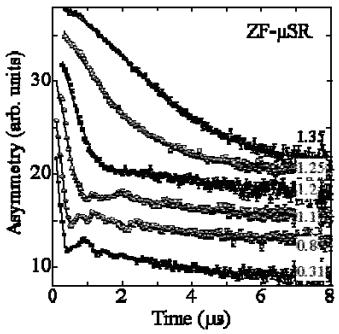

Fig. 1. Muon spin depolarization curves at various temperatures below and above T_N=1.25 K. Solid curves are fitted function with three components $G_{KT}(\Delta;\tau)\cdot(A_1e^{-\lambda_1\tau}+A_2e^{-\lambda_2\tau}\cos\omega_2\tau+A_3e^{-\lambda_3\tau}\cos\omega_3\tau)$.

References

1) K. Kodama, Science 298, 395 (2002).
2) W. Shiramura et al., J. Phys. Soc. Jpn. 67, 1548 (1998).
3) M. Matsumoto, Phys. Rev. B 68, 180403 (2003).
4) Ch. Rüegg et al., Phys. Rev. Lett. 93, 037207 (2004).
5) H. Inoue et al., Phys. Rev. B 79, 174418 (2009).
6) K. Matsui et al. J. Phys.: Conf. Ser. 551 012007 (2014).

*1 Department of Physics, Sophia University
*2 Department of Physics, Shibaura institute of Technology
*3 Department of Physics, Tokyo Institute of Technology
*4 RIKEN Nishina Center

Zn-substitution effects on distorted tetrahedral spin-chain system $Cu_3Mo_2O_9$†

H. Kuroe,*1,*2 T. Sekine,*1 I. Kawasaki,*2 I. Watanabe,*2 and M. Hase*3

The Zn-substitution effects on $Cu_3Mo_2O_9$ were studied. This compound has a quasi one-dimensional distorted tetrahedral spin system made of S = 1/2 Cu^{2+} ions.[1] The multiferroic properties below the Néel temperature T_N = 8 K has been reported based on macroscopic measurements.[2] The substituted Zn ions cut the magnetic chain directly and reduce the magnetic order. We have reported a novel magnetic ground state based on some macroscopic measurements for the heavily (5.0%) Zn-substituted sample.[3] To obtain a microscopic viewpoint of the Zn-substitution effects on $Cu_3Mo_2O_9$, we measured muon spin rotation/relaxation spectra in $(Cu,Zn)_3Mo_2O_9$ with ARGUS spectrometer at Port 2. We prepared single crystals of lightly (0.5%) and heavily (5.0%) Zn substituted $Cu_3Mo_2O_9$ through continuous solid-state crystalization.[4] The sliced single crystals are placed in the Variox cryostat with the ^{3}He sorption refrigerator. We measured the backward-forward asymmetry spectrum $A_{BF}(t)$ defined as

$$A_{BF}(t) = [A_B(t) - \alpha A_F(t)]/[A_B(t) + \alpha A_F(t)] \quad , \qquad (1)$$

where $A_B(t)$ and $A_F(t)$ are the signal from the backward and the forward counters, respectively. A parameter $\alpha \sim 1$ is introduced to correct the small misalignment of the system. The signals from the muons stopping at the Ag foil on the crystals are removed using the comparison of $A_{BF}(t)$ under the transverse magnetic field of 20 G at temperatures below and above T_N. We found that approximately 75% of the implanted muons are stopped at the crystal.

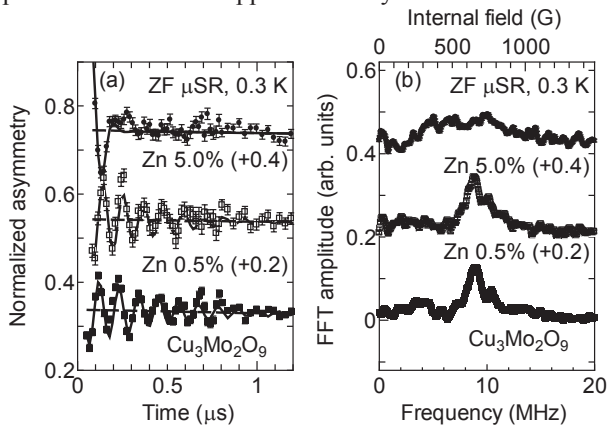

Fig. 1. Normalized asymmetry spectra at 0.3 K in $(Cu,Zn)_3Mo_2O_9$ in (a) and their fast Fourier transformation in (b). The upper scale in (b) denotes the internal field working on the muon stopping site(s).

† Condensed from the article in JPS Conf. Proc. **2**, 010206 (2014)

*1 Physics Division, Sophia University
*2 RIKEN Nishina Center
*3 Natuional Institute for Material Science (NIMS)

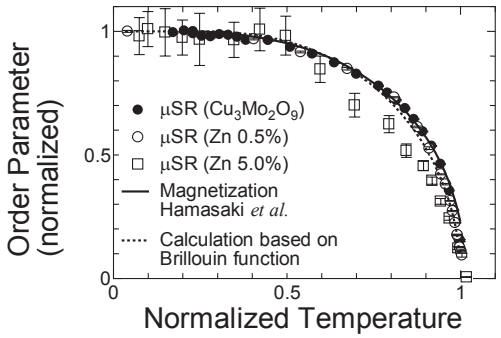

Fig. 2. Normalized internal fields in $(Cu,Zn)_3Mo_2O_9$, the magnetization taken from ref. 1, and the saturation magnetization calculated based on the Brillouin function as functions of the temperature normalized by T_N.

Figures 1(a) and 1(b) show the μSR time spectra and their fast Fourier transformations, respectively. In pure $Cu_3Mo_2O_9$ and the Zn-0.5% sample, the signals are very similar, indicating the same magnetic ground states. The oscillation frequencies of the μSR time spectra in Fig. 1(a) correspond to the dominating components in the frequency-domain spectra of Fig. 1(b) due to the muon precession around the internal field of 650 G. The beat on the oscillating spectrum at approximately 0.7 μs in Fig. 1(a) and the weak peak at 750 G in Fig. 1(b) indicate the two kinds of internal magnetic fields. In the Zn-5.0% sample, the rapidly decaying oscillation in the time-domain spectrum and the widely distributed frequency-domain spectrum were observed as shown in Figs. 1(a) and 1(b), respectively. We conclude that the magnetic ground state of the Zn-5.0% sample is different from the ones in pure $Cu_3Mo_2O_9$ and the Zn-0.5% sample.

In Fig. 2, we show the normalized amplitudes of the dominating internal field in $Cu_3Mo_2O_9$ and the Zn-0.5% sample and that of the averaged internal field in the Zn-5.0% sample as functions of temperature normalized by T_N. These normalized amplitudes have similar temperature dependences with the normalized magnetization because of the weak ferromagnetic component of the spin moment in pure $Cu_3Mo_2O_9$[1] as well as the temperature variation of the saturation magnetization in a ferromagnet calculated based on the Brillouin function. These facts indicate that the order parameter of this multiferroic phase transition is the sublattice magnetization.

References

1) T. Hamasaki *et al.*: Phys. Rev. B 77, 134419 (2008).
2) H. Kuroe *et al.*: J. Phys. Soc. Jpn. 80, 083705 (2011).
3) H. Kuroe *et al.*: J. Kor. Phys. Soc. 63, 542 (2013).
4) K. Oka *et al.*: J. Cryst. Growth 334, 108 (2011).

Magnetic ground state of Cu_6O_8MCl (M = Y, Pb) with a caged structure

K. Kawashima,[*1,*2] H. Takeda,[*1] S. Yasuda,[*1] S. Igarashi,[*1] W. Ito,[*1] I. Kawasaki,[*2] I. Watanabe,[*2] and J. Akimitsu[*1]

Cu_6O_8MCl (M=cation) compound has a Cu_6O_8 cage which forms a three-dimensional Cu-O network by connecting their faces in its crystal structure [1]. The formal Cu valence in the Cu_6O_8 cage is +2.15 for M = Pb^{4+} and +2.33 for M = Y^{3+}, suggesting the existence of Cu^{+} ($3d^{10}$), Cu^{2+} ($3d^{9}$) with S = 1/2 spin, and Cu^{3+} ($3d^{8}$) [2]. If there is partial existence of S = 1/2 spins on the Cu site in the Cu_6O_8 cage, the static magnetic ordered state is expected in the square-lattice and the dynamical spin fluctuation in the triangular-lattice i.e., the magnetic competition state is expected in the magnetic ground state of Cu_6O_8MCl. To elucidate the detailed physical properties of Cu_6O_8MCl, we focused on clarifying the magnetic ground states of Cu_6O_8PbCl, which is the semiconducting material, and compared the observed data with the based material of Cu_6O_8YCl, which is the metallic compound with paramagnetic behavior.

μSR experiments were performed at the RIKEN-RAL Muon facility at the Rutherford-Appleton Laboratory, UK. Fig. 1 shows the zero field (ZF) μSR spectra of Cu_6O_8MCl (M=Y, Pb) at various temperatures. With the decrease in the temperature, the initial asymmetry of Cu_6O_8PbCl rapidly decreased below 20 K (Fig. 1(b)). On the other hand, clear decreasing behavior of the initial asymmetry was not observed in the ZF-μSR spectra of Cu_6O_8YCl down to 0.3 K, indicating that there is no magnetic ordered state in this system (Fig. 1(a)). The ZF-μSR spectra in Fig. 1 were analyzed using the following function,

$$P(t) = A\exp(-\lambda t)G_{KT}(\Delta,t)+A_B \quad (1),$$

where A is the initial asymmetry at t = 0, λ is relaxation ratio of the muon spin, and A_B is the background signal. $G_{KT}(\Delta,t)$ is the static Kubo-Toyabe function with a half-width of Δ, describing the distribution of the nuclear-dipole field at the muon site [3]. Results of the best-fit of eq. 1 are indicated by the solid line in Fig. 1, and the observed adjusted parameters A, λ, and Δ of Cu_6O_8MCl (M=Y, Pb) as functions of temperature are shown in Fig. 2. A (a-relaxing) of Cu_6O_8YCl slightly decreases with the decrease in the temperature (Fig. 2), whereas λ and Δ of Cu_6O_8YCl are almost constant, being temperature independent. These facts indicate that there is no change of spin dynamic and long range magnetic ordered state in Cu_6O_8YCl, which is a metallic compound with paramagnetic behavior. For Cu_6O_8PbCl, the temperature dependence of a-relaxing, λ, and Δ change below 20 K, indicating the change in the magnetic spin state (Fig. 2). However, clear precession signal is not confirmed in the ZF-μSR spectra below 20 K. The Cu_6O_8 cage has a square-lattice and triangular-lattice on its surface, and the Cu sites in the Cu_6O_8 cage are occupied by various valences of Cu^{+}, Cu^{2+}, and Cu^{3+} [2]. These conditions encumber the formation of the completely static magnetic ordered state in Cu_6O_8PbCl. The observed behavior of ZF-μSR spectra and Fig. 2 data of Cu_6O_8PbCl indicate the growth of the short-range magnetic interaction between S = 1/2 spins below 20 K. Consequently, the magnetic ground state of Cu_6O_8PbCl does not have a static long range magnetic ordered state such as an antiferromagnetic state in high-T_c cuprate. There is possibility that the short range interaction of Cu_6O_8PbCl forms the spin glass state below 20 K like under-doping material in high-T_c cuprate. The magnetic ground state of Cu_6O_8MCl compound depends on the valence state of the M site ion.

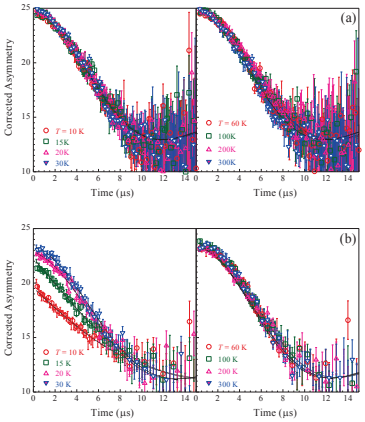

Fig. 1 ZF-μSR time spectra of Cu_6O_8MCl ((a) M = Y, (b) M = Pb) at various temperatures. Solid lines indicate the fitting results of eq. (1).

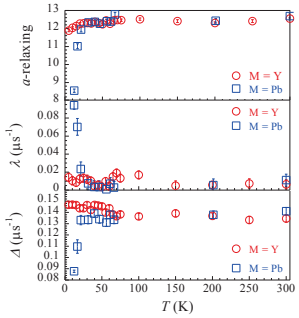

Fig. 2 Temperature dependence of the initial asymmetry A (a-relaxing), relaxation ratio λ, and Δ of Cu_6O_8MCl (M = Y, Pb) defined by the results of fitting for the Fig. 1 data.

References

1) I. Yazawa, R. Sugise, N. Terada, M. Jo, K. Oka, and H. Ihara, Jpn. J. Appl. Phys. **29** L1693 (1990).
2) G. Zouganel, K. Bushida, I. Yazawa N. Terada, M. Jo, H. Hayakawa, and H. Ihara, Sol. St. Comm. **80** 709 (1991).
3) Y. J. Uemura, T. Yamazaki, D. R. Harshman, M. Senba, and E. J. Ansaldo, Phys. Rev. B **31** 546 (1985).

*1 Department of Physics and Mathematics, Aoyama Gakuin University.
*2 RIKEN-RAL, Nishina Center

μSR studies on antiferromagnet RRu_2Al_{10} (R = Sm, Gd)

H. Tanida,[*1,*3] H. Guo,[*1,*2] I. Kawasaki,[*1] M. Sera,[*3] T. Nishioka,[*4] M. Matsumura,[*4] I. Watanabe, [*1] and Z. Xu [*2]

The Kondo semiconductor CeT_2Al_{10} (T = Ru, Os) with an orthorhombic-type structure shows a unique antiferromagnetic (AFM) order at $T_0 \sim 30$ K.[1,2] This compound exhibits numerous unusual electronic properties that can be ascribed to the strong electron correlation between conduction and localized $4f$ electrons, namely, the $c-f$ hybridization effect, by which a renormalized quasi-particle state with heavy effective electron mass is formed in the case of many Ce- or Yb-based intermetallic compounds. However, in the class of materials known as the Kondo semiconductors or insulators, a temperature-dependent energy gap is formed instead. One of the most salient features of this system is magnetic anisotropy in the AFM ordered state. Since the magnetic susceptibility shows a large anisotropy of $\chi_a \gg \chi_c \gg \chi_b$, an AFM ordered moment (m_{AF}) is expected to be parallel to the a-axis in the AFM ordered state. However, $m_{AF} \| c$ is realized, as was revealed by neutron scattering and ^{27}Al NMR/NQR studies.[3–5] The AFM structure is not robust and is easily tuned by magnetic field[4], pressure[6], or chemical doping.[7–9] This indicates that magnetic exchange interactions are not a key parameter for this magnetic ordering, but there could be an unknown parameter related to the strong $c-f$ hybridization effect, which must be related to the extraordinary high transition temperature of $T_0 \sim$30 K.

We previously performed μSR experiments on the above undoped and Rh-doped $CeRu_2Al_{10}$. The results have been published elsewhere.[9] One of the residual problems is the serious inconsistency in the temperature dependence of internal fields (H_{int}) between two muon sites, that is, one component shows a usual mean-field behavior, but the other does not. To address this problem, we planned to perform zero-field μSR on related antiferromagnets with more localized $4f$-electron character, RRu_2Al_{10} (R = Nd, Sm, and Gd). These compounds are worthy of investigation for their AFM ordered state; for instance, in the sample R = Gd, m_{AF} is suggested to be parallel to the [011] direction, although a simple dipole-field calculation suggests that m_{AF} prefers the a-axis direction.[10] In ref. 9, a possible origin of this discrepancy was suggested to be the zig-zag chain structure of Gd sites along the c-axis direction.

Figure 1 shows the zero-field time spectra of $GdRu_2Al_{10}$ at T = 20 K and 15 K; the data were recorded under double-pulse-beam condition. We found that the initial asymmetry is reduced when the temperature is lowered below the AFM transition temperature of T_N = 17 K. This is clear evidence for magnetic ordering. Since H_{int} is expected to be large because of the large magnetic moment of Gd-$4f$ electrons, we should use single-pulse condition with much greater time resolution than that of the double-pulse condition. However, we had to use the double-pulse condition within our beam time because we could not break the extrinsic noise resulting from the kicker operation. Within the present resolution, we could not identify any muon-spin precession behavior, and thus, from the zero field measurement, we could not obtain quantitative information on H_{int}.

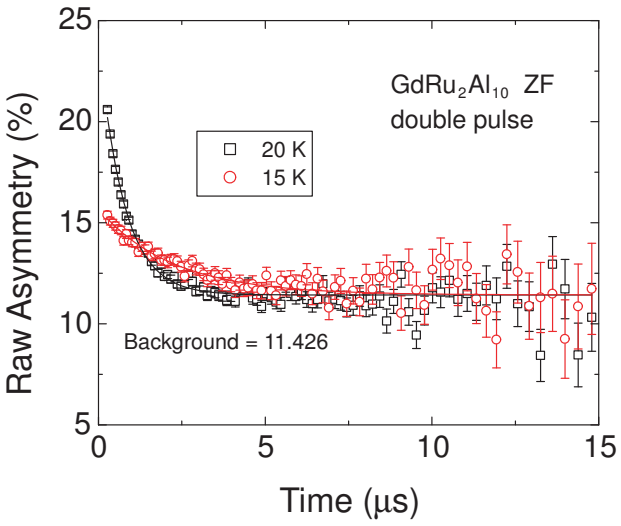

Fig. 1. Zero-field time spectra of $GdRu_2Al_{10}$ at T = 20 and 15 K under double-pulse-beam condition.

*1 RIKEN Nishina Center
*2 Department of Physics and State Key Laboratory of Silicon Materials, Zhejian University
*3 AdSM, Hiroshima University
*4 Graduate school of Integrated Arts and Science, Kochi University

References
1) A. M. Strydom: Physica B **404**, 2981 (2009).
2) T. Nishioka *et al.*: J. Phys. Soc. Jpn. **78**, 123705 (2009).
3) D. D. Khalyavin *et al.*: Phys. Rev. B **82**, 100405(R) (2010).
4) H. Tanida *et al.*: Phys. Rev. B **84**, 233202 (2011).
5) M. Matsumura *et al.*: J. Phys. Soc. Jpn. **78** 123713 (2009).
6) H. Tanida *et al.*: Phys. Rev. B **88**, 045135 (2013).
7) A. Kondo *et al.*: J. Phys. Soc. Jpn. **82**, 054709 (2013).
8) R. Kobayashi *et al.*: J. Phys. Soc. Jpn. **82**, 093702 (2013).
9) H. Guo *et al.*: Phys. Rev. B **88**, 115206 (2013).
10) M. Sera *et al.*: Phys. Rev. B **88**, 100404(R) (2013).

Determination of muon sites on metal-organic hybrids of $(C_6H_5CH_2CH_2NH_3)_2CuCl_4$ and $(C_2H_5NH_3)_2CuCl_4$†

E. Suprayoga,[*1,*2] A. A. Nugroho,[*2] A. O. Polyakov,[*3] T. T. M. Palstra,[*3] and I. Watanabe[*1]

Hybrid materials consisting of metal and organic components have recently attracted considerable attention because they have lots of possibilities for tailoring their functionalities and physical properties by adjusting their metal and/or organic building blocks [1]. The organic component can be used not only to bind the metal components but also to control the connectivity between the metal components and to manipulate their dimensionality [2]. One of the interesting type of hybrid materials is the magnetic hybrid with perovskite-type transition metal salt with a chemical formula such as $(C_2H_5NH_3)_2CuCl_4$ (EA) and $(C_6H_5CH_2CH_2NH_3)_2CuCl_4$ (PEA) [3]. We have carried out μSR measurements on both materials at the RIKEN-RAL muon facilities. The results revealed the appearance of clear muon spin precession under the zero-field condition in magnetically ordered states. This observation provided evidence of the formation of long-range magnetic ordering of Cu spins. The internal field at the muon site was determined from the muon-spin precession frequency to be approximately 200 G at 4 K in both systems. In the case of PEA, a fast-depolarized component in an earlier time region was observed from room temperature down to 4 K. This fast depolarized component was not decoupled even in fields of a couple of Tesla, showing the existence of a possible muon state that is strongly coupled with the surrounding electrons via radical formation. Such a state was not observed in EA. The dipole-dipole interaction is too weak to trigger the 3D magnetic ordered state because of the large distance between the $CuCl_6$ layers.

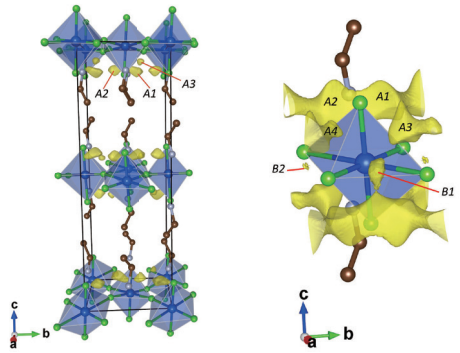

Fig. 1. Crystal structure of EA is shown with Cu ions represented by blue balls and Cl ions by green balls. The isosurface of the electrostatic potential for 455 meV (right) represents the localization volume for muon site positions.

† Condensed from the article in Journal of Physics: Conference Series **551**, 012054 (2014)

*1 RIKEN Nishina Center
*2 FMIPA, Institut Teknologi Bandung
*3 Solid State Chemistry, Rijkuniversiteit Groningen

In order to gain an understanding of the magnetic properties of EA and PEA, we are now attempting to reveal the muon positions. We determine the spin alignment by comparing the experimental results with the muon positions estimated using the computational techniques on the basis of the assumption that internal fields at the muon site are caused by dipole fields from surrounding magnetic moments. We present the results of the first trial to apply density functional theory (DFT) method [4] to EA and PEA in order to reveal the minimum energy positions that could facilitate muon injection. The estimation of the potential minimum positions was carried within the DFT framework as implemented in the Vienna ab-initio simulation package (VASP) [5] using the RICC supercomputer.

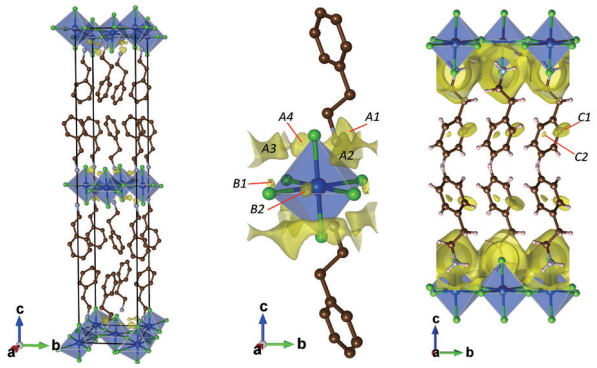

Fig. 2. Crystal structure (left) and DFT calculation results on PEA. The isosurfaces of the electrostatic potentials for 425 meV (center) and 1.025 meV (right) show possible muon sites.

We found six potential minimum positions around $CuCl_6$ in EA as well as in PEA, as shown in Figs. 1 and 2. Four of them (A1 - 4) were around the apical Cl^- ions and two of them (B1 and 2) were in between in-plane Cl^- ions on the $CuCl_4$ plane. These muon positions can be candidates to show muon-spin precession behavior under the zero-field condition in magnetically ordered states in both EA and PEA. Two more minimum potential positions (C1 and 2) were found in PEA in and on the phenyl ring of the organic part, causing possible muon states bound with the surrounding electrons via radical formation with large hyperfine fields.

References

1) C. N. R. Rao et al.: J. Phys. Cond. Matter **20**, 15980 (2008).
2) C. R. Kagan et al.: Science **286**, 945 (1999).
3) A. O. Polyakov et al: Chem. Mater **24**, 133 (2012).
4) W. Kohn and L. J. Sham: Phys. Rev. A **140**, 1133 (1965).
5) G. Kresse and J. Furthmuller: Phys. Rev. **54**, 11169 (1996).

Investigation of muon sites in $YBa_2Cu_3O_6$ using density functional theory†

S.S. Mohd-Tajudin,[*1,*2] S.N.A. Ahmad,[*1] D.F. Hasan-Baseri,[*1] E. Suprayoga,[*2,*3] N. Adam,[*1,*2] A.F. Rozlan,[*1] S. Sulaiman,[*1] M.I. Mohamed-Ibrahim,[*1] and I. Watanabe[*2]

Since the discovery of the Cu-based high-*Tc* superconducting oxides, both theoretical and experimental investigations have been carried out to understand their magnetism, electronic properties, and superconducting mechanism. But the mechanism of high-*Tc* superconductivity is still unclear and further investigations are required. The Muon Spin Relaxation (μSR) technique is one of the effective approaches for these investigations. The μSR technique can give us valuable information on high-*Tc* superconductivity, electronic states, spin structures, and hyperfine fields. Additional information on muon sites can also give us more options to quantitatively discuss these properties. Unfortunately, successful determination of muon sites from μSR experimental data has been possible only for few cases in the past. Thus, we have been trying to establish a way to estimate muon sites from a computational view point by using the density functional theory (DFT). We have already tested our method on La_2CuO_4 (LCO) because this system has been well investigated by μSR. There are a lot of experimental data related to the antiferromagnetically ordered state in LCO and we can compare the data with our calculation results to successfully obtain new results in terms of muon sites in LCO.[1] The similar anitiferromagneticlally ordered state has also been reported in $YBa_2Cu_3O_{6+x}$ (YBCO) and we can apply our computational method to the $YBa_2Cu_3O_6$ as well as the case of LCO.[2-4]

The hole concentration of YBCO can be controlled by changing the oxygen content, x, from 0 to 1. The system changes from antiferromagnetic state (x = 0) to superconducting state (x = 1). [2-4] The anti-ferromagnetic transition temperature, T_N, is approximately 350 K at x = 0. Several components of muon–spin precession have been clearly observed below T_N. This indicates that there are some muon sites in YBCO.[6] In order to optimize the exchange correlation function, we first calculated the density of the state of each electronic orbital of $YBa_2Cu_3O_6$. After optimizing the electronic correlation function, we calculated the electrostatic potential as implemented in Vienna Ab-initio Simulation Package (VASP) by using RIKEN Integrated Cluster of Clusters (RICC) and found six local minimum potential positions. These minimum potential positions can be regarded as initial stopping positions of the injected muons. Three are close to the apical oxygen of the CuO_5 tetrahedra (marked as M1-M3) and one is close to the planar oxygen (marked as M4). [2,6] The M5 site is close to the Cu(I) site in the Cu-O chain, while the M6 site is between the CuO_2 planes. M5 and M6 are new and different from view point of the well-known argument on the muon-binding state with oxygen because muons prefer to associate with oxygen to form the hydrogen binding state that lowers its potential energy.[5] According to the following procedure, we estimate the final state of the muon. We put μ^+ on the minimum potential position and recalculate the μ^+ position in the 3x3x3 supercell taking into account the relaxations of the muon and all atomic positions so as to minimize the total energy of the supercell.

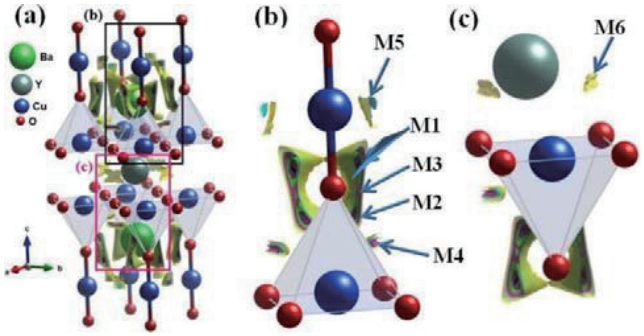

Figure 1. Crystal structure of YBCO with x = 0. Cu(II) in the CuO_2 plane is surrounded by five oxygen atoms and has a spin half. The Cu(II) rules the antiferromagnetically ordered state, while the Cu(I) which is in the Cu-O chain is non-magnetic with a zero spin. We found six local minimum potential positions (M1 to M6) from the calculation by the DFT method. The positions were drawn by the isosurfaces in different colors.

We will carry out precise μSR measurement on YBCO with x = 0 to verify our method for the estimation of muon sites. Then, we will compare the electronic structures, hyperfine fields, and spin structures with the experimental results in terms of insulating YBCO.

References

1) B. Adiperdana *et al.,* Phys. Procedia **30** 109-112 (2012).
2) N. Nishida *et al.,* Jpn. J. appl. Phys. **26** L1856 (1987).
3) S. Sanna *et al.,* Phys. Rev. Lett. **93** 207001 (2004).
4) M. Akoshima et al., Phys. Rev. B **62** 6761 (2000).
5) S.S. Mohd-Tajudin *et al.,* Phys. J.: Conf Ser **551** 012054 (2014).
6) M. Pinkpank *et al.,* Physica C **317-318** 299 (1999).

† Condensed from the article in Physics Procedia **30** 109-112 (2012)

*1 School of Distance Education, Universiti Sains Malaysia
*2 RIKEN Nishina Center
*3 Physics Department, Institut Teknologi Bandung

Muon sites in Ce(Ru, Rh)2Al10 investigated using Density Functional Theory from the perspective of electronic potential†

N. Adam,[*1,*2] E. Suprayoga,[*1,*3] B. Adiperdana,[*4] H. Guo,[*5] H. Tanida,[*6] S.S Mohd-Tajudin,[*2] R. Kobayashi,[*7,*8] M.Sera,[*6] T. Nishioka,[*9] M. Matsumura,[*9] S. Sulaiman,[*2] M.I Mohamed-Ibrahim,[*2] and I. Watanabe[*1,*2,*3,*4,*5]

$CeRu_2Al_{10}$ has the orthorhombic $YbFe_2Al_{10}$-type structure with space group Cmcm.[1] Ce atoms control the magnetism of this system and are surrounded by Al atoms forming a cage-like structure which is suggested to form a two-dimensional plane structure stacking along the *b*-axis.[2,3] Despite having the nearest neighbour distance, approximately 5.2Å between Ce ions, $CeRu_2Al_{10}$ exhibits an antiferromagnetic transition at $T_0 = 27.3$ K which cannot be explained by taking only RKKY interaction into account. [4] The magnetic susceptibility is largely anisotropic whereas the direction of magnetic moment is along the *c*-axis and is expected to flip to the *a*-axis when a small concentration of Ru atoms are substituted by Rh atoms.[5] In addition, from the μSR results of a Rh-doped system, Guo et al. reported drastic changes in internal fields at muon sites which were related to the spin-flop caused by doping of 3% Rh atoms in $CeRu_2Al_{10}$.[6]

A number of investigations of muon sites in Ce-based Kondo semiconductors, $CeRu_2Al_{10}$ and $Ce(Ru, Rh)_2Al_{10}$ were carried out by using Density Functional Theory (DFT) to understand the magnetic properties. From the calculation of electrostatic potential, we found all muon sites previously suggested by Kambe et al.[7] and Khalyavin et al.[8] as shown in Figure 1. Because they were not crystallographically identical, muon sites in $CeRu_2Al_{10}$ are still undefined and the hyperfine interactions cannot be discussed in detail.

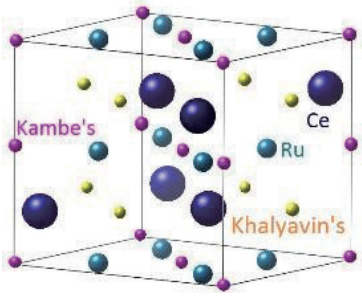

Fig. 1. Muon sites in $CeRu_2Al_{10}$ suggested by Kambe et al.[7] and Khalyavin et al. [8]

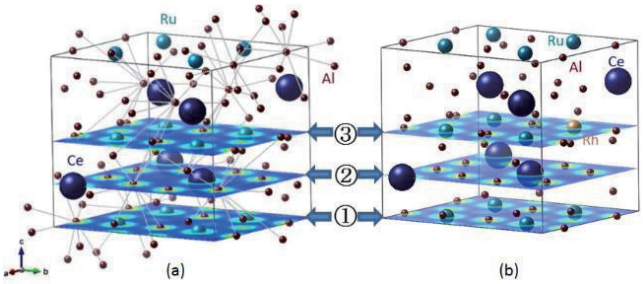

Fig. 2. Three planes that differentiate $CeRu_2Al_{10}$ (a) and $Ce(Ru, Rh)_2Al_{10}$ (b). Planes (1) and (3) contain the muon sites suggested by Kambe et al., whereas the plane (2) contains the muon sites suggested by Khalyavin et al. In plane (3), one Ru atom is substituted by one Rh atom.

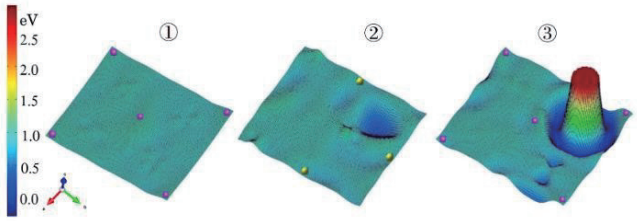

Fig. 3. Potential differences between non-doped and doped systems in planes (1), (2) and (3). The purple and yellow points on the planes indicate the positions of suggested muon sites.

The potential energies calculated for the plane in the non-doped system were subtracted from those of corresponding plane in the doped system to investigate the potential differences. Large differences are seen in plane (3) where a Ru atom was substituted by a Rh atom. Because of this change at the Rh atom in plane (3), the potential energy in plane (2) is also slightly deformed around the position underneath the Rh atom. The large potential difference at the substituted Rh atom in plane (3) may have been because of the difference in valence configuration from that of Ru atom.

However, the potential energy at the suggested muon sites did not exhibit much difference even though the Rh doping concentration in the $CeRu_2Al_{10}$ was increased to 12.5%.

† Condensed from the article in J. Phys.: Conf. Ser. **551** 012053 (2014)

*1 RIKEN Nishina Center
*2 Computational Chemistry and Physics Laboratory, Universiti Sains Malaysia
*3 Physics Department, Institut Teknologi Bandung
*4 Physics Department, Universitas Padjajaran
*5 Department of Physics and State Key Laboratory of Silicon Material, Zhejiang University
*6 Department of Quantum Matter, Hiroshima University
*7 Quantum Condensed Matter Division, Oak Ridge National Laboratory
*8 Neutron Science Laboratory, University of Tokyo
*9 Graduate School of Integrated Arts and Science, Kochi University

References

1) V. M. Thiede et al.: J. Mater. Chem. **8**, 125 (1998).
2) H. Tanida et al.: Phys. Rev. B **84**, 115128 (2011).
3) M. Sera et al.: J. Phys. Soc. Jpn. **82**, 024603 (2013).
4) T. Nishioka et al.: J. Phys. Soc. Jpn. **78** 123705 (2009).
5) A. Kondo et al.: J. Phys. Soc. Jpn. **82** 054709 (2013).
6) H. Guo et al.: Phys. Rev. B **88** 115206 (2013).
7) S. Kambe et al.: J. Phys. Soc. Jpn. **79**, 053708 (2010).
8) D. D. Khalyavin et al.: Phys. Rev. B **82** 100405 (2010).

μSR study of the density wave state in α-(BEDT-TTF)$_2$MHg(SCN)$_4$ (M=K, Rb)

K. Ichimura,[*1,*2] K. Katono,[*2] and I. Watanabe[*1]

Charge density wave (CDW) and spin density wave (SDW) are well-known ground states in low-dimensional conductors and are based on different interactions. The former is due to electron-phonon interaction and the latter is due to on-site Coulomb interaction. Although manifests of CDW and SDW have been discussed separately, the coexistence of CDW and SDW is still an open problem.

In terms of the mixture of CDW and SDW, we focus on the low-dimensional organic conductor α-(BEDT-TTF)$_2$MHg(SCN)$_4$ (M=K, Rb). The compounds undergo the density wave state at T_{DW}= 8 and 12 K for K and Rb-salt, respectively, as a consequence of the nesting of Fermi surfaces. Commonly, organic conductors have too little carrier density to screen the Coulomb interaction. SDW was suggested by anisotropy of the magnetic susceptibility[1]. On the other hand, CDW was suggested by NMR[2], in which no magnetic order was observed. Accordingly, no clear evidence for the ground state of α-(BEDT-TTF)$_2$MHg(SCN)$_4$ has been obtained as yet. We believe that this lack of evidence comes from the coexistence of CDW and SDW. Such a mixture of CDW and SDW forms a new ground state in low-dimensional conductors, and is interesting in terms of g-ology[3], which is a theoretical approach to ground states in one-dimensional system. The present system is expected to be located at the boundary between CDW and SDW. To the best of our knowledge, no study thus far has been able to determine whether CDW and SDW coexist or compete with each other.

For K-salt, Pratt *et al.*[4] performed a zero-field μSR measurement at a temperature range from 5 to 16 K. They reported SDW ordering with an amplitude of 3×10^{-3} μ_B. However, this suggested value of the magnetic moment is extremely smaller than that of conventional SDW, for which the amplitude is in the order of 0.1 μ_B. In order to re-examine the density wave state in α-(BEDT-TTF)$_2$MHg(SCN)$_4$, we performed a μSR experiment at a lower temperature with higher statistics.

Small flakes of single crystals of α-(BEDT-TTF)$_2$MHg(SCN)$_4$ (M=K, Rb) were grown by a standard electrochemical method with deuterated BEDT-TTF molecules to eliminate the nuclear spin of protons. In this experiment, we concentrated on Rb-salt, which has a higher T_{DW} than K-salt. The transition temperature was determined as T_{DW}= 12 K based on the temperature dependence of the static magnetic susceptibility. The powdered sample was mounted as a fly-past setup for a ^{3}He refrigerator. The μSR measurement was performed down to 0.3 K.

*1 RIKEN Nishina Center
*2 Department of Applied Physics, Hokkaido University

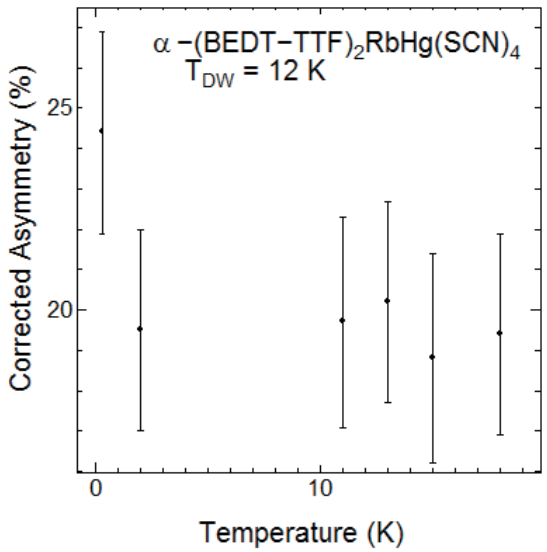

Fig. 1. Temperature dependence of asymmetry for deuterated α-(BEDT-TTF)$_2$RbHg(SCN)$_4$.

Figure 1 shows the temperature dependence of the muon-spin precession component along the longitudinal-field (LF) of 20 G applied along the initial spin-polarization of the injected muon. This component reflects the existence of a static component obtained from internal fields at the muon site in deuterated α-(BEDT-TTF)$_2$RbHg(SCN)$_4$. No drastic change was observed in the local field at T_{DW}= 12 K. This tendency is qualitatively consistent with that obtained by Pratt *et al.*[4]. At present, data accuracy is not considerably higher than that of Pratt *et al.* with large error bars. We will try to improve the accuracy by collecting more muon events in the next trial. This is expected to reduce the upper limit of the expected magnetic moment which has been suggested by Pratt *et al.* to be 3×10^{-3} μ_B following the same logic[4]. On the other hand, we found an unusual increase in the asymmetry below 2 K. This might be an indication of some degree of freedom or subphases[5] in the density wave phase.

References

1) T. Sasaki, H. Sato and N. Toyota: Synth. Met. **41**, 2211 (1991).
2) K. Miyagawa, A. Kawamoto and K. Kanoda: Phys. Rev. B **56**, 14 (1997).
3) J. Solyom: Adv. Phys. **28**, 201 (1979).
4) F. L. Pratt, T. Sasaki, N. Toyota and K. Nagamine: Phys. Rev. Lett. **74**, 3892 (1995).
5) A. Hoshikawa, K. Nomura, S. Takasaki, J. Yamada, S. Nakatsuji, H. Anzai, M. Tokumoto and N. Kinoshita: J. Phys. Soc. Jpn. **69**, 1457 (2000).

Study of coupling between electron conduction and spin fluctuation in novel organic charge transfer complexes with TANC

M. Enomoto,[*1,*2] Y. Furuya,[*1] K. Isoda,[*1] M. Tadokoro,[*1] and I. Watanabe[*2]

We have succeeded to synthesize organic conductors with a novel electron acceptor, 5,6,11,12-tetraazanaphthacene (TANC; see Figure 1). The TANC molecule forms highly conductive compounds in various combinations with metal ions. In particular, several Cu-TANC systems are highly attractive complexes in terms of formation of both π-electron conductive bands and coordinating structure between the acceptor molecule and copper spin sites. Employing these properties is an important approach to construct π-d interaction systems, such as the $(DCNQI)_2Cu$ system,[1] where DCNQI denotes *N*,*N*'-dicyanoquinodiimine.

In the case of $[Cu^{1.5+}(TANC)](NO_3)_{0.5}$, Cu ions and TANC radicals are alternately linked through coordinate interaction between Cu-N atoms along the *b*-axis, as shown in Fig. 2(a). These flat-ribbon structures stack with each other to form 2D layers in the *ab*-plane, while NO_3 anion layers are segregated from each Cu-TANC layers (see Figs. 1(b) and (c)). While the conductivity of this complex shows semiconducting behavior, the single crystal exhibits a high conductivity of 50 S cm^{-1} at 300 K along the *a*-axis, which is the stacking direction of the TANC molecules. Moreover, conductivity shows highly anisotropic behavior, that is, σ||a / σ||b ~ 8.3, which corresponds to the segregated stacked structure of Cu-TANC 2D layers. Interestingly, X-ray photoelectron spectroscopy results indicate the coexistence of Cu^+ and the Cu^{2+} at a 1 : 1 ratio in the Cu-TANC layers. Moreover, the infrared reflectivity measurement reveals that electrons fluctuate between these two valence states at copper ion sites in both the directions of stacking (*a*-axis) and flat-ribbon (*b*-axis) structures.

On the other hand, the TANC complex family, Ag(TANC), also forms a similar conductive layer without a counter anion layer, such as the NO_3 layer in $[Cu^{1.5+}(TANC)](NO_3)_{0.5}$. The anisotropic conductivity measurement for the Ag complex at room temperature shows that σ||a / σ||b ~ 13, which reflects the low-dimensional character of the Ag complex compared with the Cu one. Infrared reflectivity study supports this observation. The reflectivity component, which is normal to the stacking direction, is negligible, while the parallel component can be observed similar to that in the Cu complex.

To understand how electron conduction occurs in the TANC complexes, we carried out μSR measurements on $[Cu^{1.5+}(TANC)](NO_3)_{0.5}$. We found that the depolarization rate at 300 K is proportional to $H^{-1/2}$, which suggests the existence of the 1D diffusion behavior of spin-excited states

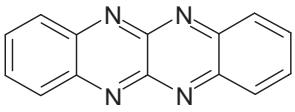

Figure 1

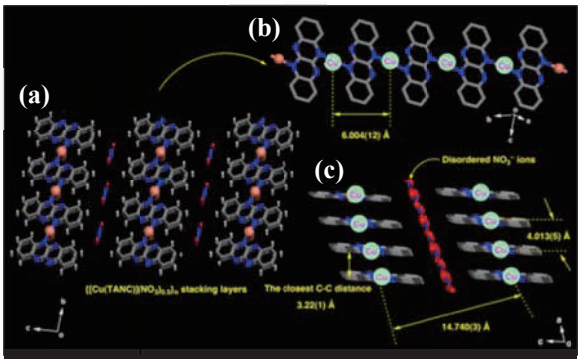

Fig. 2. Crystal structures of $\{[Cu(TANC)](NO_3)_{0.5}\}_n$

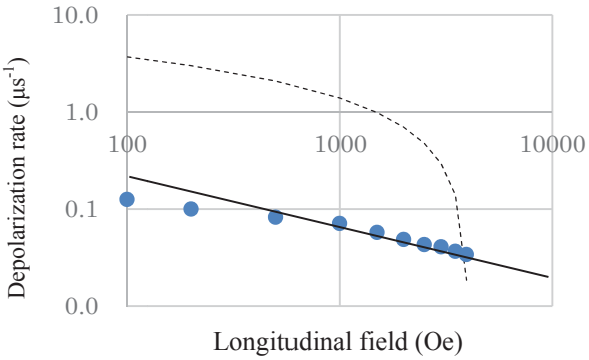

Fig. 3. The field dependence of the depolarization rate at 300 K.

(the solid line in Fig. 2) rather than 2D diffusion (the broken line in Fig. 2). This behavior was also observed at 200 and 100 K. Since we have predicted from our previous light experiments that electrons are conductive in these high-temperature regions, the present μSR results support our prediction. At this moment, we are not sure whether this 1D diffusion behavior occurs in the line of the Cu^+ and Cu^{2+} connection or in the direction of TANC stacking. Comparison between the μSR data of the Cu and Ag complexes will answer this question.

*1 Department of Chemistry, Tokyo University of Science
*2 RIKEN Nishina Center

References

1) A. Aumüller et al.: Angew. Chem., Int. Ed. Engl. 25, 740 (1986).
2) F. L. Pratt et al.: Synth. Met., 85, 1747 (1997).
3) F. L. Pratt et al.: Hyperfine Interact., 104, 357 (1997).
4) N. Kojima et al.: Solid State Commun., 120, 165 (2001).
5) N. Kida et al.: Phys. Rev. B, 77, 14427 (2008).

Study of charge carrier transport in active layer P3HT:ZnO:PCBM hybrid solar cells measured by muon spin relaxation†

L. Safriani,[*1] Risdiana,[*1] A. Bahtiar,[*1] A. Aprilia,[*1] and I. Watanabe[*2]

Recently, many researchers have been making an effort to obtain high performance of solar cells by modifying the active material of the solar cell. Conjugated polymers are promising active materials. Much attention has been paid to polythiophene and its derivatives owing to their chemical and thermal stability in addition to their potential to absorb the solar spectrum in solar cells. Poly(3-hexylthiophene) (P3HT), a derivative of poly(3-alkylthiophene), presents the highest hole mobility,[1] thus attracting researchers'attention.

Hybrid solar cells that combine organic and inorganic materials have been developed to increase the performance of solar cells. P3HT having the highest hole mobility, when combined with inorganic materials with the highest electron mobility, shows promise for better performance. Zinc oxide (ZnO) is an inorganic material that has high electron mobility and is easy to prepare. In bulk heterojunction systems of solar cells, ZnO behaves as an electron acceptor to dissociate excitons formed in P3HT. For practical application to solar cells, ZnO nanoparticles are prepared to resolve the problem associated with the small diffusion range of P3HT.[2] Fullerene and its derivative [6,6]-phenyl C61 butyric acid methyl ester (PCBM) are well-known acceptor materials for polymer solar cells owing to their ability to transfer excitons from polymers within 45 fs.[3]

In previous studies, ZF- and longitudinal-field (LF)-μSR measurements were performed on samples of P3HT[4] and P3HT:ZnO.[5] For both the samples, it was found that charge carrier transport changes from intra-chain to inter-chain diffusion. For P3HT:ZnO, one-dimensional intra-chain diffusion was observed at low temperatures, while three-dimensional inter-chain diffusion was observed at high temperatures.[5] The addition of PCBM into the P3HT:ZnO blend increased the charge transfer from P3HT to ZnO and also reduced the aggregation of ZnO nanoparticles.

To clarify the charge carrier dynamics in a bulk ternary system of hybrid materials, we measured charge carrier transport using LF-μSR in the P3HT:ZnO blend by adding a fullerene derivative (PCBM).

Figure 1 shows the LF dependence of the raw asymmetry at 15 K and 25 K. The initial asymmetry increases with increasing LF field owing to the repolarization of the muonium state.[6] The raw asymmetries at 15 K and 25 K show a clear dependence on field and temperature.

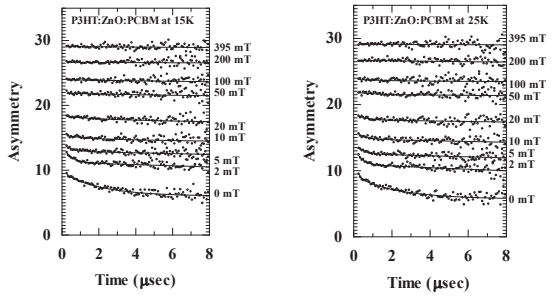

Fig. 1. The asymmetry data of P3HT:ZnO:PCBM at 15 K and 25 K for various longitudinal magnetic fields.

Figure 2 shows the LF dependence of λ_1 in P3HT:ZnO:PCBM, where λ_1 is the depolarization rate associated with the fast component. At 15K, the relationship $\lambda \sim H^{-0.5}$ is observed clearly, which indicate that one-dimensional intra-chain diffusion occurs in this system. Compared with the μSR data for P3HT that show a dimensional crossover at 25K,[3] the data for P3HT:ZnO:PCBM show the dimensional crossover from one-dimensional to three-dimensional apparently at a lower temperature. We cannot explain the experimental results immediately, but they are likely related to the advantageous properties of ZnO nanoparticles that facilitate electron transfer.

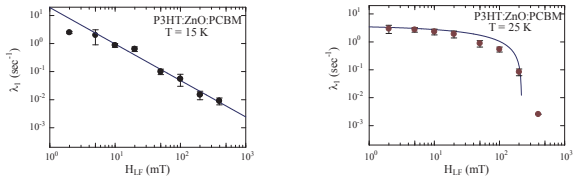

Fig. 2. The longitudinal-field dependence of the relaxation rate λ_1 of P3HT:ZnO:PCBM at 15 K and 25 K.

With increasing temperature, the charge carrier transfer changes from intra-chain to inter-chain diffusion. One-dimensional intra-chain diffusion is observed in the samples at temperatures below 15K, while three-dimensional inter-chain diffusion is observed at temperatures above 25 K.

References

1) W. Ma et al.: Adv. Funct. Mater. 15, 1617-1622 (2005)
2) L. W. Ji et al.: J Matter Sci. 45, 3266-3269 (2010)
3) G. Zerza et al.: Synth. Metals 119, 637 (2001)
4) R. Risdiana, et al.: Journal of Physics Conf. Series 200, 052024-052027 (2010)
5) L. Safriani et al.: Adv. Mater. Res. 896, 477-480 (2014)
6) F. L. Pratt: Philos.Mag. Lett. 75, 371-380 (1997)

† Condensed from the article submitted to Materials Science Forum

*1 Department of Physics, Padjadjaran University
*2 RIKEN Nishina Center

μSR study on antiferromagnetism in K-Rb alloy and Rb clusters in sodalite

T. Nakano,[*1,*2] K. Tanibe,[*1] L. M. Kien,[*1] S. Yoon,[*2,*3] M. Abdel-Jawad,[*2] F. L. Pratt,[*4] I. Watanabe,[*2] and Y. Nozue[*1]

Porous crystals of zeolites make it possible to generate periodically arrayed alkali-metal nanoclusters. Various kinds of magnetically ordered states have been observed in these systems, although they do not contain any magnetic elements. Sodalite is a kind of aluminosilicate zeolites where the β cages with an inner diameter of $\simeq$ 7 Å are arrayed in a bcc structure as shown in Fig. 1 (a). The chemical formula is given by $A_3Al_3Si_3O_{12}$ per β cage where A indicates an alkali cation. By the loading of guest alkali atoms into dehydrated sodalite, an A_4^{3+} cluster is formed in the β cage as schematically shown in Fig. 1 (b), where an s-electron is shared by four A^+ ions and is confined in the cage. When Na_4^{3+} clusters are formed in all the β cages, antiferromagnetic (AFM) ordering occurs below the Néel temperature of $T_N = 48\,K$[1–3] because of the exchange coupling between the adjacent clusters. The material is assigned to a Mott insulator. When heavier alkali cations are substituted for Na^+, T_N systematically increases: 72, 80, and 90-100 K for clusters with average chemical compositions of K_4^{3+}, $(K_3Rb)^{3+}$, and $(K_{1.5}Rb_{2.5})^{3+}$, respectively.[4,5] However, a recent work has revealed that Rb_4^{3+} does not show AFM ordering and shows metallic behavior. In the present work, we investigate in detail the magnetic properties of this system in the vicinity of the insulator-to-metal (I-M) transition by utilizing μSR. The experiments were performed at the RIKEN-RAL Muon Facility using the CHRONUS spectrometer.

Figure 2 (a) shows the zero-field μSR spectra of K-Rb alloy clusters ($(K_{1.7}Rb_{2.3})^{3+}$). At 5 K, a muon-spin precession signal with a large amplitude is clearly observed. This result indicates that the AFM order is robust in the major volume of the sample even just before the I-M transition. The internal field at the muon site is estimated to be 166 Oe. This is stronger than that in Na_4^{3+} (92 Oe)[2], K_4^{3+} (142 Oe), and $(K_3Rb)^{3+}$ (155 Oe)[4]. A systematic increase in the size of the s-electron wave function in the heavier alkali metals, which is the origin of the enhancement of AFM exchange interaction, is expected to provide a stronger Fermi contact between muon and s-electron. T_N is estimated to be $\simeq$ 90 K from the temperature dependence of the internal field. In contrast, the pure Rb clusters (Rb_4^{3+}) only show very slow relaxation even at 2 K as shown in Fig. 2 (b). This result confirms that a non-magnetic state is realized in the metallic phase after the I-M transition.

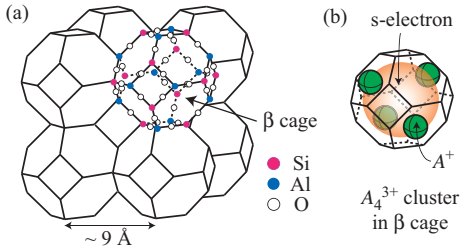

Fig. 1. Schematic illustrations of (a) the crystal structure of sodalite and (b) the A_4^{3+} cluster formed in the β cage, where A indicates an alkali element.

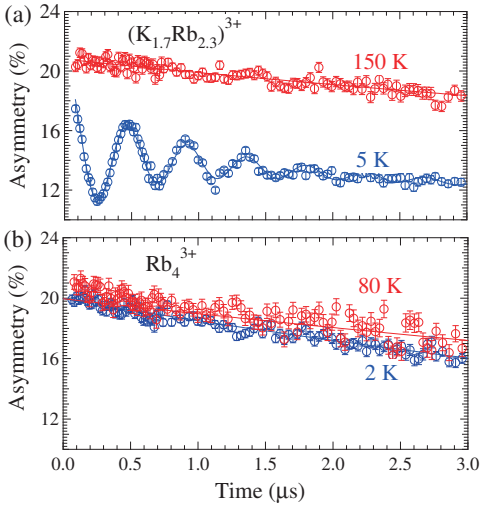

Fig. 2. Zero-field μSR spectra of (a) K-Rb alloy clusters and (b) Rb clusters in sodalite.

*1 Department of Physics, Osaka University
*2 RIKEN Nishina Center
*3 Department of Physics, The Catholic University of Korea
*4 ISIS, Rutherford Appleton Laboratory

References

1) V. I. Srdanov, G. D. Stucky, E. Lippmaa, and G. Engelhardt: Phys. Rev. Lett. **80**, 2449 (1998).
2) R. Scheuermann, E. Roduner, G. Engelhardt, H.-H. Klauss, and D. Herlach: Phys. Rev. B **66**, 144429 (2002).
3) T. Nakano, M. Matsuura, A. Hanazawa, K. Hirota, and Y. Nozue: Phys. Rev. Lett. **109**, 167208 (2012).
4) T. Nakano, R. Suehiro, A. Hanazawa, K. Watanabe, I. Watanabe, A. Amato, F. L. Pratt, and Y. Nozue: J. Phys. Soc. Jpn. **79**, 073707 (2010).
5) T. Nakano, Y. Ishida, A. Hanazawa, and Y. Nozue: J. Kor. Phys. Soc. **62**, 2197 (2013).

Li-ion diffusion in Li_xFePO_4 with $x = 0$, 0.25 and 0.5

I. Umegaki,[*1] M. Månsson,[*2] H. Nozaki,[*1] G. Kobayashi,[*3] R. Kanno,[*4] H. Guo,[*5] K. Ishida,[*5] I. Watanabe,[*5] and J. Sugiyama[*1]

Lithium iron phosphate, $LiFePO_4$, is used as a cathode material in Li-ion batteries. A comparison with the conventional cathode materials such as $LiCoO_2$, $LiNiO_2$, and $LiMn_2O_4$ showed that $LiFePO_4$ has a special advantage over because of its high stability during the lithium extraction/intercalation reaction at medium temperatures (around 400 K).

Based on electrochemical[1,2] and structural analyses,[3] the lithium extraction reaction from $LiFePO_4$ is represented as follows: $LiFePO_4$ - xLi $\rightarrow (1-x)LiFePO_4 + xFePO_4$. Both $LiFePO_4$ and $FePO_4$ phases coexist in Li_xFePO_4, and single phase samples of Li_xFePO_4 have not been obtained so far. Following upon the μ^+SR work on $LiFePO_4$,[4] we have measured μ^+SR spectra on Li_xFePO_4 ($x = 0$, 0.25, and 0.5) in order to understand the diffusive property shown in Li_xFePO_4 sample consisting of the two phases.

Powder samples of Li_xFePO_4 were prepared from $LiFePO_4$ by reacting it with NO_2BF_2 in acetonitrile. Then, the Li-deficient powder sample was sealed into a titanium cell with a gold o-ring. The window of the cell was made of a Kapton film of 50 μm thickness. The cell was mounted onto the Cu plate of a liquid-He flow-type cryostat in the temperature range between 10 and 400 K.

Figure 1 shows the temperature dependence of zero field (ZF-) and longitudinal field (LF-) μ^+SR spectra for $FePO_4$. Since there is no crucial change with temperature, the implanted muons are static up to 250 K. In fact, the spectra were fitted by a combination of a dynamic Kubo-Toyabe (KT) signal and a time-independent background signal from a powder cell. The field distribution width (Δ) and the field fluctuation (ν) were found to be independent of temperature; $\Delta_{FePO4} = 7.1 \times 10^4$ s^{-1} and $\nu_{FePO4} = 2.6 \times 10^4$ s^{-1}.

On the other hand, dynamic behavior was clearly observed for $Li_{0.25}FePO_4$ and $Li_{0.5}FePO_4$. The μ^+SR spectra were well fitted by a combination of two KT signals and a background signal. The two KT signals came from the muons stopped in the $LiFePO_4$ phase and those in the $FePO_4$ phase. Therefore, we used the same values of Δ_{FePO4} and ν_{FePO4} for the KT signal from the $FePO_4$ phase. Figure 2 shows the temperature dependence of Δ and ν for the three samples. As expected, the result is very consistent with that obtained for $LiFePO_4$. Assuming that the Li-ion jump to

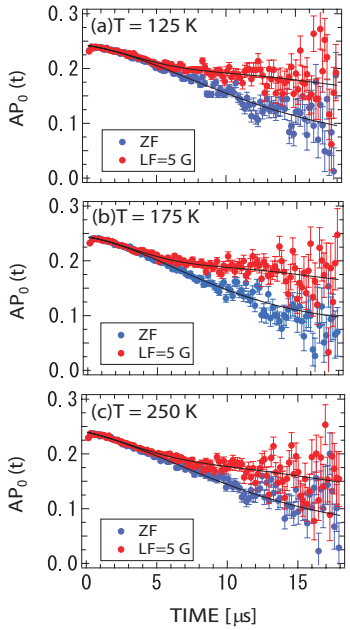

Fig. 1. ZF- and LF-μ^+SR spectra on $FePO_4$ at (a) 125 K, (b) 175 K, and (c) 250 K.

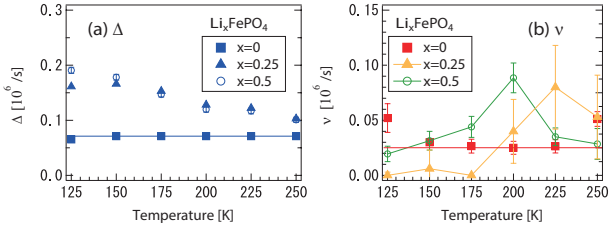

Fig. 2. Temperature dependence of (a) Δ and (b) ν obtained for $FePO_4$, $Li_{0.25}FePO_4$, and $Li_{0.5}FePO_4$.

interstitial sites,[4] we obtained the diffusion coefficient as: $D_{Li} = 5.8 \times 10^{-11}$ cm^2/s at 200 K for $Li_{0.5}FePO_4$ and $D_{Li} = 1.3 \times 10^{-11}$ cm^2/s for $Li_{0.25}FePO_4$. These values are smaller than D_{Li} for $LiFePO_4$,[4] implying the effect of Li-ion diffusion between the $LiFePO_4$ and $FePO_4$ phases. Such interphase diffusion is believed to be the most interesting process shown in the $LiFePO_4$ cathode. In order to understand the interphase Li-ion diffusion, however, we need to study the relationship between D_{Li} and x in Li_xFePO_4 in more detail.

*1 Toyota Central Research and Development Labs., Inc.
*2 Material Physics, Royal Institute of Technology
*3 Institute for Molecular Science
*4 Department of Electronic Chemistry, Tokyo Institute of Technology
*5 RIKEN Nishina Center

References
1) A. K. Pahdi et al.: J. Electrochem. Soc. 144, 1188 (1997).
2) W. -J. Zhang.: J. Power Sources, 196, 2962 (2011).
3) A. Yamada et al.: J. Electrochem. Socl. 148, A224 (2001).
4) J. Sugiyama et al.: Phys. Rev. Lett. 103, 147601 (2009).

Investigations of defects in TiO_2 rutile crystal by muon and muonium

H. Ariga,[*1*2] K. Asakura,[*1] K. Shimomura,[*3] K. Ishida,[*2] F. Platt,[*4] W. Higemoto,[*5] E. Torikai,[*6] A. D. Pant,[*6] K. Yokoyama,[*7] B. Ohtani,[*1] and K. Nagamine[*8]

Metal oxides play a key role in the field of environmental science, heterogeneous catalysis, electrochemistry, biology, chemical sensors, magnetism, and other chemical processes. It is well known that the existence of defect sites drastically changes the chemical and physical properties of metal oxides. TiO_2 is the one of the most studied material among metal oxides. The defect sites in TiO_2 affect the catalytic and photocatalytic properties. The structure of defect site on surface is well known by scanning probe microscope (STM, AFM and so on) observations. The major defect on the surface is oxygen vacancy. However, the microscopic insight of bulk defect sites has not been established yet. Although oxygen vacancy is believed to be a typical defect site in TiO_2, no direct evidence has been reported to characterize the defect structure, and its properties have not been revealed because of the difficulty in detecting defects directly. In order to establish a charge balance, Ti^{3+} is assumed in the nearest neighbor of the bulk oxygen vacancy. Thus, oxygen vacancy has been discussed by measuring Ti^{3+} species, which have one d electron and are characterized with ESR or NMR techniques. However, since Ti^{3+} species do not only exist next to the oxygen vacancies but also at other sites such as interstitial Ti, planar defects, CS planes and so on, it is necessary to obtain information including the adjacent morphology of Ti^{3+}. It is suggested that hydrogen stabilizes at an oxygen vacancy as hydrid (H^-) in TiO_2 through density functional calculations. As Muon is regarded as an isotope of hydrogen, μSR has potential to be the probe of oxygen vacancy.

Our recent preliminary TF μSR measurements at the RIKEN-RAL suggested the existence of a large fraction of a diamagnetic component ($\mu^+ or Mu^-$) and some normal muonium at room temperature in TiO_2 with an oxygen vacancy. The purpose of the present work is to clarify whether negative muonium ions exist in TiO_2 with an oxygen vacancy by laser irradiation and also to determine a further detailed state of μ^+.

We have performed both zero-field (ZF) measurements and "Pump and probe" measurements by laser irradiation at various temperatures. The μSR measurements were performed at the RIKEN-RAL Muon Facility. The mirror-polished rutile TiO_2 single crystals (25 x 25 x 0.5 mm^3, Crystal Base, Japan) oriented to the (110) plane were used. The sample was calcined at 1073 K for 6 h in air followed by reduction at 1173 K for 2 h under an ultra-high vacuum environment (0.5 x 10^{-8} Pa). The color of sample became blue after the reduction procedure. Laser was irradiated from the opposite side of muon through a quartz glass by utilizing the sample cell developed by Prof. Torikai's group.

The ZF muon spin relaxation spectra with and without oxygen vacancies are obtained at various temperatures from 15 K to room temperature. The difference between two samples are observed at a temperature lower than 50 K. The spectra at 15 K are shown in Fig. 1. The relaxation of spectra without an oxygen vacancy is predictable to be derived from nuclear spins of Ti (^{47}Ti and ^{49}Ti) because of the absence of electronic spin. We expected a Gaussian field profile and fitted the plot with a Kubo-Toyabe relaxation function. The spectra without the oxygen vacancy was well fitted with $\Delta = 0.30$ MHz (Gaussian distribution: 0.71 mT), which is a typical value for nuclear spins. The Kubo-Toyabe relaxation function for a Lorentzian field distribution was added for fitting the relaxation of spectra with the oxygen vacancy. The Δ value and the Lorentzian distribution were 0.38 MHz and 1.9 mT, respectively.

We have also preformed pump and probe measurements to examine the existence of Mu^-. The "pump" laser irradiation is intended to remove one electron from the negative muonium ion, which makes the ion detectable by a transverse-field measurement. However, we could not detect obvious differences in the results obtained with and without laser irradiation. The remaining issue is to simulate the dynamics of Mu^- by laser irradiation and determine an approach to detect Mu^-.

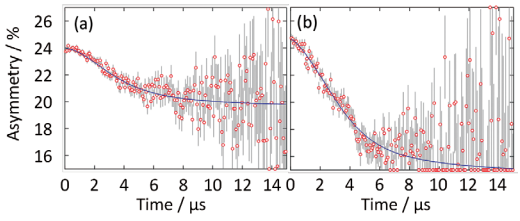

Fig. 1. Zero field μSR spectrum of rutile TiO_2 (a) with and (b) without oxygen vacancy at 15 K.

*1 Catalysis Research Center, Hokkaido University
*2 RIKEN Nishina Center
*3 Insittue of Material Structure Science, KEK
*4 ISIS Science and Technology Facilities Council, Rutherford Appleton Laboratory
*5 Advanced Science Research Center, Japan Atomic Energy Agency
*6 Department of Research Interdisciplinary Graduate School of Medicine and Engineering, University of Yamanashi
*7 ISIS/Qween Marry Univeersity
*8 UC-Riverside

Response of muonium to oxygen contents in hemoglobin and other biological aqueous solutions for cancer research

K. Nagamine,[*1, *2, *3] A.D. Pant,[*4] I. Shiraki,[*4] E. Torikai,[*4] K.Shimomura,[*3] F.L. Pratt,[*5] H. Ariga,[*6] K. Ishida,[*7] and J.S. Schultz[*7]

Hypoxia, or low oxygenation, is known as an important factor in tumor biology; in cancer patients, an accurate measurement of O_2 concentration ($c(O_2)$) or partial pressure in specific regions is critical[1] therefore, improved methods for detecting O_2 are required. Several trials that employ PET, MRI and EPR have been conducted[1].

We have proposed the use of μ^+ as a new sensitive method to probe the existence of paramagnetic O_2 in cancer tumors in the human body. The μ^+ in water is known to take the states of diamagnetic μ^+ such as μ^+OH (60%), paramagnetic muonium (Mu, $\mu^+ + e^-$) (20%), and a missing fraction (20%). In Mu, 50% fraction becomes an ortho state with spin 1, providing a spin rotation signal with a precession pattern (1.39 MHz/G) that is 100 times faster than that of diamagnetic μ^+. Some experimental studies have been conducted on the oxygen-dissolving effects of the spin relaxation rate (λ_{Mu}) of paramagnetic Mu in pure water due to electron spin exchange interactions with paramagnetic O_2 in water; the rate change of λ_{Mu} against $c(O_2)$ is $(1.8 \pm 0.1) \times 10^{10}$ (L/mol)/s [2]. A problem that remains to be solved is the effect of other magnetic molecules, which is the objective of the present study.

Experiment was conducted at Port 2 of RIKEN-RAL using 60 MeV/c decay μ^+. Spin rotation and relaxation were detected under 2.2 G transverse fields at room temperature.

The biological samples used were as follows: 1) Albumin**;** Bovin serum (plasma) albumin 2) Serum**;** Donor horse serum 3) Hemoglobin (Hb); Polymerized hemoglobin of bovine origin in a lactated Ringer's solution at 13% concentration in the form of deoxy-Hb.

Before measuring the O_2 dependence of λ_{Mu}, its dependence on the concentration of each biological molecule was systematically measured. The increasing rates of λ_{Mu} were obtained as 25 μs^{-1}/(g/L) for albumin, 1 μs^{-1}/(vol.%) for serum and 3.1 μs^{-1}/(g/L) for Hb.

Then, by determining the relevant concentration for each molecule, the O_2 dependence of λ_{Mu} was measured. In these biological aqueous solutions, λ_{Mu} showed an almost similar change in relaxation against increasing O_2 concentration as that for pure water.

For higher Hb concentrations, by introducing O_2, a part of deoxy-Hb (magnetic) becomes oxy-Hb (non-magnetic) so that the O_2 dependence of λ_{Mu} becomes non-linear.

Measurements were made upto 2.0 g/L c(Hb) and 20% $c(O_2)$ (Fig. 1). The O_2 dependence of λ_{Mu} at higher Hb concentrations was predicted by assuming the following relation[3]: $\lambda_{Mu} = R_{Hb}(Mu) + R_{O2}(Mu)$. There, $R_{Hb}(Mu)$ is the relaxation rate due to the amount of deoxy-Hb obtained by solving the Hill's equation for the total Hb amount and $c(O_2)$ [4], while $R_{O2}(Mu)$ is the relaxation rate due to the free molecular O_2 in solution obtained by the O_2 dependence data of the pure water and by the amount of free O_2 which is estimated by subtracting the O_2 amount used for oxy-Hb formation obtained by the Hill's equation. As summarized in Fig. 1, λ_{Mu} increases with increasing Hb at any fixed $c(O_2)$; slower increasing rate at Hb higher than 1 g/L due to oxy-Hb formation. The λ_{Mu} becomes undetectably large ($\geq$ 10 μs^{-1}) at $c(O_2)$ lower than 6% at higher c(Hb) of 100 g/L expected for human body.

Before carrying out the clinical application of the proposed method to studies on hypoxia, it is important to conduct further systematic studies on the behavior of O_2 in various other biological aqueous systems, especially with high-concentration Hb. Significant features of the present muon method can be summarized as follows: a) non-invasive nature, b) no need of a high magnetic field and c) sub-mm probing region confinement by the advanced beam method.[5]

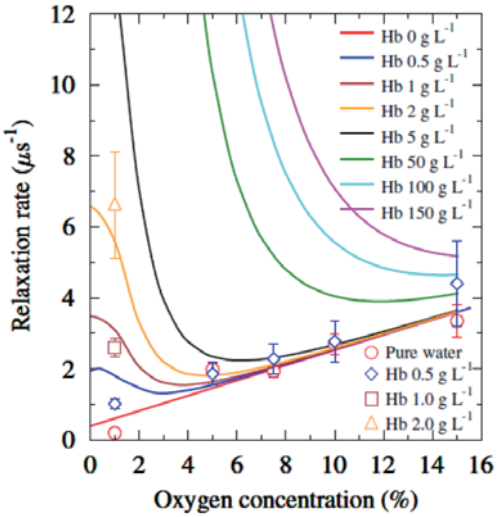

Fig. 1 Summary of dependence on O_2 concentration of muonium relaxation rates in Hb aqueous solution; experimental data upto 2.0 g/L and predictions upto 150 g/L by the method described in the text.

[*1] Atomic Physics Laboratory, RIKEN
[*2] Physics & Astronomy, University of California, Riverside
[*3] Muon Science Laboratory, IMSS, KEK
[*4] Medicine and Engineering, University of Yamanashi
[*5] ISIS, Rutherford Appleton Laboratory
[*6] Catalysis Research Center, Hokkaido University
[*7] RIKEN Nishina Center
[*8] Bio-Engineering, University of California, Riverside

References

1) J.L. Tatum et al., Int. J. Radiat. Biol., 82, 699 (2006).
2) E. Roduner et al., J. Chem. Faraday Trans., 91, 1935 (1995).
3) A.D. Pant et al., J. Phys.: Conf. Series, 551, (2014) 012043.
4) M. Samaja et al., Clin. Chem., 20, 110 (1983).
5) K. Nagamine, JPS Conf. Proc., 2, 010001 (2014).

Development of gas system for MuSEUM experiment

K. S. Tanaka*1,*2 on behalf of J-PARC MuSEUM Collaboration

We are planning to measure the energy of ground state hyperfine structure (HFS) of muonium at J-PARC/MLF. Muonium is a hydrogen-like bound state that consists only leptons, and its HFS is a good probe for testing the QED theory. The latest experiment at LAMPF obtained the following value:[1)]

$$\Delta HFS_{\mathrm{M}}^{\mathrm{ex}} = 4.463302765(53)\ \mathrm{GHz}\ (12\ \mathrm{ppb})\ . \qquad (1)$$

The total uncertainties were determined using the statistical uncertainties. We will achieve an accuracy more than 10 times greater than that of the latest experiment by using the H-line at J-PARC.

Muons polarized in the revese direction of momentum enter the bore of a large superconducting solenoid magnet from the J-PARC/MLF muon beamline. A RF cavity is located at the center of the magnet containing pure Kr gas. Muons stop by collisions in the gas, and polarized muoniums are formed by the electron capture process.

In a magnetic field the ground state splits into four substates. ν_{12} and ν_{34} are obtained by the microwave magnetic resonance technique. High-momentum decay positrons are emitted preferentially in the direction of the muon spin. By driving the transitions with an applied microwave magnetic field perpendicular to the static magnetic field, the muon spin can be reversed and the angular distribution of high-momentum positrons changes from predominantly upstream to downstream with respect to the beam direction. The cavity was designed to be resonant simultaneously in the TM110 mode at the ν_{12} transition frequency and in the TM210 mode at the ν_{34} frequency[2)]. The muonium HFS ($\Delta\nu$) is obtained by summing ν_{12} and ν_{34}.

A Gas chamber surrounds the RF cavity to seal in the Kr gas. The chamber consists of only aluminum and its upstream foil is thin enough (100 μm) for muons to pass through. We performed gas introduction tests in the chamber. The gas pressure is monitored at the 0.02 % level by a silicon pressure transducer. The gas in this system is sampled regularly by small cylinders. Since spin-exchange collisions occur between muonium and paramagnetic contaminant particular oxygen, we intend to determine the purity of a gas at the parts per million level using Q-mass. We studied the performance of the gas panel without gas sampling and precise gas pressure monitoring on November 2014 (Fig. 1). In this test, we measured muonium distributions under several gas pressures (Fig. 2). The gas pressure in the chamber maintain a steady at sub Torr level during this measurement.

*1 RIKEN Nishina Center
*2 Graduate School of Arts and Sciences, University of Tokyo

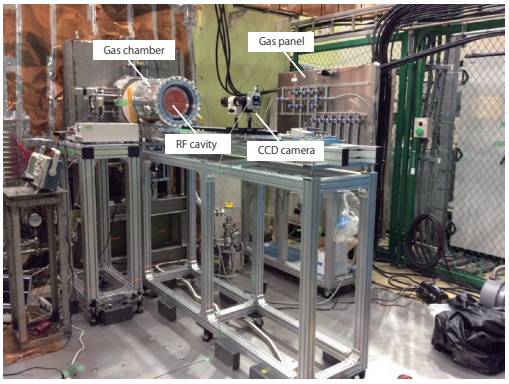

Fig. 1. Experimental setup at 2014A beamtest. The gas chamber is mounted on the support rail. The gas panel is behind the gas chamber.

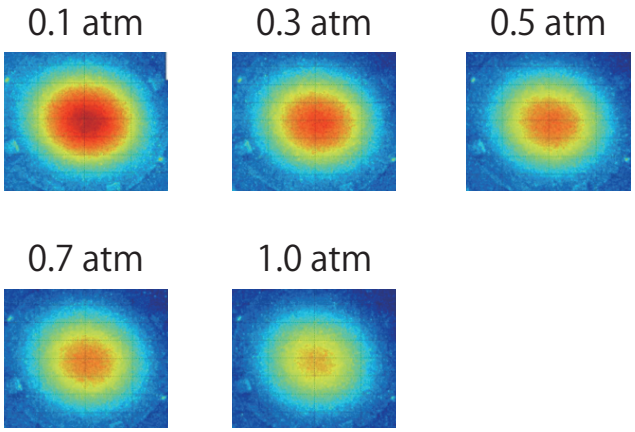

Fig. 2. Muonium distributions at the center of the chamber for different gas pressures.

References

1) W. Liu *et al.*: Phys. Rev. Lett. 82, 711 (1999)
2) K. S. Tanaka on behalf of MuSEUM Collaboration K. S. Tanaka et al.:, JPS Conf. Proc. 2, 010405 (2014)

Development of online muon beam profile monitor for the MuSEUM experiment

S. Kanda[*1,*2] for the MuSEUM Collaboration

Muonium is the bound state of a positive muon and an electron. Because neither muon nor electron has an internal structure, muonium ground state hyperfine splitting (MuHFS) can be the most precise probe for the test of the bound state QED and for the determination of muon mass via the ratio of magnetic moments of a muon and a proton. At J-PARC, we plan to perform a precision measurement of the MuHFS by microwave spectroscopy of muonium. Spectroscopy of the energy states is performed by measurement of positron asymmetry from muonium decays. Our goal is to improve the precision by an order of magnitude compared with that of the most recent experiment. In order to achieve the goal, we utilize J-PARC's highest-intensity pulsed muon beam[2], highly segmented positron detector with Silicon PhotoMultiplier(SiPM)[3], and an online/offline muon beam profile monitor.

The online muon beam profile monitor analyses the muon beam from the aspect of beam shape and relative intensity. Requirements for the beam profile monitor are minimum destruction and high reconfigurability of the beam. We utilize thin plastic scintillation fiber and SiPM. Figure 1 shows the conceptual design of the muon beam profile monitor. The detector consists of an one dimensional array of thin plastic scintillation fiber with a 100 μm diameter. The fibers are bound into a bundle and connected to a SiPM. For a front-end electronics, EASIROC front-end chip[4] was utilized as an ASD (amplifier, shaper, and discriminator). The pulse height is digitized by an external peak holding ADC.

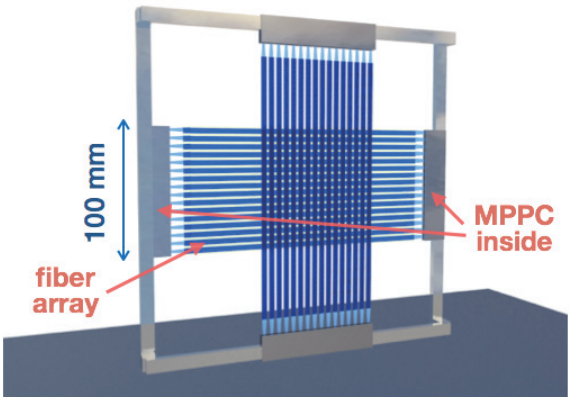

Fig. 1. Conceptual design of the online muon beam profile monitor

*1 Department of Physics, University of Tokyo
*2 RIKEN Nishina Center

Figure 2 shows the developed prototype and its cross-sectional view. The fibers were arrayed on a polyimide film of 25 μm thickness and bonded by epoxy resin. Forty fibers were bound into one band of 4 mm width. Two bands were arrayed with a 2 mm gap.

In November 2014, a beam test was performed at

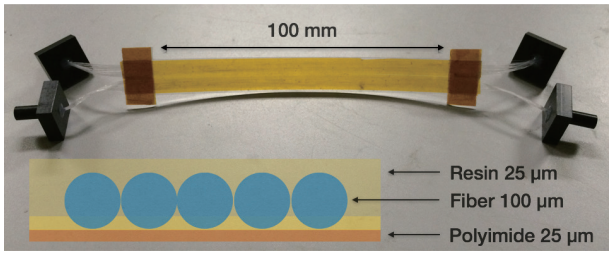

Fig. 2. Developed prototype of the online muon beam profile monitor

J-PARC MLF MUSE D2 beam line. Figure 3 shows the measured photon yield as a function of total muon beam intensity. Saturation in higher intensity region is caused by the limited number of SiPM pixels (in case of this prototype, number of pixels was 667). The beam intensity was controlled by movable slits and measured by an offline beam profile monitor[5], which consists of a gated image intensifier and a cooled CCD. The movable slits only change beam density and keep beam profile unchanged. Based on the result of the beam test, the design of a full-scale detector is in progress. SiPM with narrower pixel pitch will be used and process of fiber bonding will be optimized for uniform thickness.

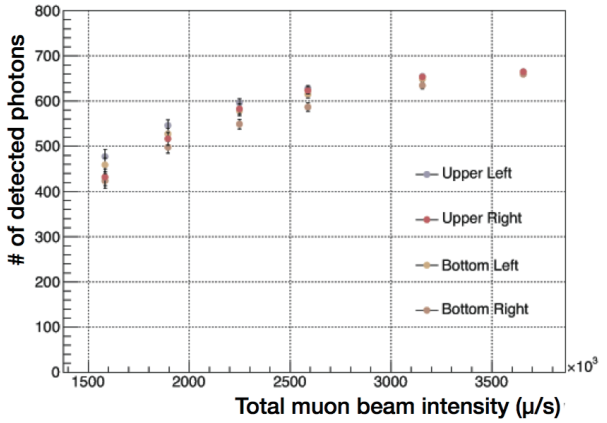

Fig. 3. Measured photon yield

References

1) W. Liu *et al.*: Phys. Rev. Lett. **82** (1999) 711
2) A. Toyoda *et al.*: J. Phys. Conf. Ser. **408** (2013) 012073
3) S. Kanda *et al.*: JPS Conf. Proc. **2** (2014) 010404
4) S. Callier *et al.*: Physics Procedia **37** (2012) 1569
5) T. U. Ito *et al.*: NIM A **754** (2014)

3. Radiochemistry and Nuclear Chemistry

Reversed-phase extraction behavior of the 105th element, Db, with tributyl phosphate

M. Murakami,[*1,*2] S. Tsuto,[*1] K. Ooe,[*1] S. Goto,[*1] D. Sato,[*1] N. Goto,[*1] T. Koyama,[*1] T. Nagaoka,[*1] R. Motoyama,[*1] H. Haba,[*2] Y. Komori,[*2] A. Toyoshima,[*3] A. Mitsukai,[*3,*4] Y. Kitayama,[*5] Y. Fukuda,[*5] and H. Kudo[*1]

Our group has investigated the extraction behavior of Nb and Ta, homologs of the 105th element Db, from HF solutions with tributyl phosphate (TBP) by the batchwise and on-line column chromatographic methods.[1,2] In the on-line column experiment with a 62 wt% TBP resin,[2] the obtained distribution coefficients (K_d) of Ta were in agreement with those obtained by the batch experiment, indicating that the studied system can be applicable to the column chromatographic experiment with the short-lived ^{262}Db ($T_{1/2}$ = 33.8 s). In this work, the extraction behavior of Db was studied to discuss the chemical form of Db in HF media by comparing the behavior of Nb and Ta.

The isotopes ^{262}Db and ^{170}Ta ($T_{1/2}$ = 6.76 min) were simultaneously produced in the bombardment of a ^{19}F beam on the mixed ^{248}Cm/^{nat}Gd target. The ^{19}F beam was delivered from the AVF cyclotron, and its energy was 105.3 MeV at the center of the target. The typical beam intensity was 700 particle-nA. The reaction products were transported with a He/KCl gas-jet system to a chemistry laboratory and were deposited on a collection site in Automated Rapid Chemistry Apparatus (ARCA[3]) for 80 s. Then, the products were dissolved in 140 μL of 1.0 M HF and were loaded onto a column (1.6 mm i.d. × 7.0 mm height) filled with the 62 wt% TBP resin. The flow rate of the eluent was 1.0 mL/min. The effluent was collected in a Ta dish as Fraction 1. The remaining products in the column were stripped with 140 μL of 10 M HF at a flow rate of 1.0 mL/min, and the effluent was collected in another Ta dish as Fraction 2. Both effluent fractions in the Ta dishes were evaporated to dryness and subjected to α spectrometry using an automated rapid α/SF detection system.[4] The α-particle measurement was started at 43 s and 57 s after the collection of the products for Fractions 1 and 2, respectively. The counting duration was 259 s and 248 s for Fractions 1 and 2, respectively. After the α-particle measurement, every third or fifth pair of Ta dishes was subjected to γ-ray spectrometry to monitor the behavior of ^{170}Ta and its chemical yield.

In total, 820 cycles of chromatographic separation were conducted. In the α energy region (E_α = 8.42–8.74 MeV) for ^{262}Db and its α-decay daughter ^{258}Lr ($T_{1/2}$ = 3.9 s), 16 and 2 events were observed in Fractions 1 and 2, respectively, including one time-corelated α pair in Fraction 1. The chemical yield of ^{170}Ta, including deposition and dissolution efficiencies of the aerosols, was 44 ± 13%.

Percent extraction (%Ext) values were evaluated using the equation

$$\%\mathrm{Ext} = \frac{100A_2}{A_1 + A_2}, \quad (1)$$

where A_1 and A_2 are the radioactivities in Fractions 1 and 2, respectively. The correction for the radioactive decay was considered for A_1 and A_2. In Fig. 1, the obtained %Ext values of ^{262}Db and ^{170}Ta are shown as closed symbols, together with those of ^{90g}Nb and ^{178a}Ta (open symbols) obtained in the separate experiment,[2] as a function of the initial HF concentration, $[HF]_{ini}$. Because of the small number of the ^{262}Db events in Fraction 2, an upper-limit %Ext value of ≤ 25% was evaluated for ^{262}Db. The evaluated %Ext value for ^{170}Ta was 93 ± 5%, which was in agreement with the previous result for ^{178a}Ta (%Ext = 94 ± 4%[2]). This suggests that Db would not form a Ta-like fluoride complex $[DbF_6]^-$ in 1.0 M HF, where Ta forms an extractable species, $[HTaF_6(TBP)_3]$.[5]

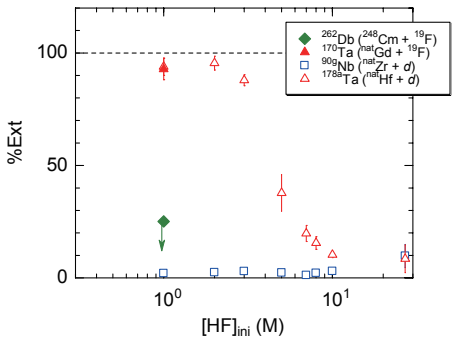

Fig. 1. Dependence of %Ext values of Nb, Ta, and Db on $[HF]_{ini}$.

*1 Department of Chemistry, Niigata University
*2 RIKEN Nishina Center
*3 Advanced Science Research Center, Japan Atomic Energy Agency
*4 Faculty of Science, Ibaraki University
*5 Graduate School of Natural Science and Technology, Kanazawa University

References
1) S. Tsuto et al.: RIKEN Accel. Prog. Rep. **47**, 270 (2014).
2) M. Murakami et al.: In this report.
3) Y. Nagame et al.: Radiochim. Acta **93**, 519 (2005).
4) H. Haba et al.: RIKEN Accel. Prog. Rep. **45**, 204 (2012).
5) Z. Zhu and C. Y. Cheng: Hydrometallurgy **107**, 1 (2011).

Solid-liquid extraction of ^{261}Rf from hydrochloric acid with Aliquat 336 resin

T. Yokokita,[*1,*2] Y. Kasamatsu,[*2] Y. Shigekawa,[*1,*2] Y. Yasuda,[*1,*2] K. Nakamura,[*1,*2] H. Haba,[*1] Y. Komori,[*1] M. Murakami,[*1] and A. Shinohara[*1,*2]

The chemical properties of transactinide elements (atomic numbers $Z \geq 104$) are considered to differ from those of its homologues because of the increasingly strong relativistic effects on the valence shell electrons of heavy atoms. The transactinide nuclei are produced at accelerators using heavy-ion-induced nuclear reactions. These nuclei have low production rates and short half-lives ($T_{1/2} \leq \sim$1 min). Therefore, the chemical experiments of transactinides must be carried out rapidly on one-atom-at-a-time basis using nuclear reaction products transported from the target chamber by a He/KCl gas-jet system. The chemical properties of transactinides have so far been investigated mainly by a partition method based on a comparison of their chemical behavior with those of lighter homologous elements.

Solution chemistry experiments have been often conducted on element 104, rutherfordium (Rf). Anion- and cation-exchange experiments of Rf in HF and HF/HNO_3 were successfully performed under conditions such that the distribution behaviors in equilibria were observed for the homologues of Rf. Clearly different behavior of Rf from its homologues Zr and Hf was reported.[1] On the other hand, in the cation exchange in H_2SO_4/HNO_3, the K_d values of Hf in the online experiment were in good agreement with those in the offline batch experiment, whereas the K_d values of Zr in the online experiment were not.[2] Therefore, it is important to investigate the time dependence of the distribution behaviors of transactinides to obtain their equilibrated data because the time required to reach distribution equilibrium would be different among homologues. Thus, we developed a batch-type solid-liquid extraction apparatus to evaluate the time dependence of the distribution behavior of Rf and to obtain the equilibrated K_d values.[3] To determine the experimental condition and obtain comparison data for Rf, we also performed solid-liquid extraction of Zr and Hf and Th (pseudo homologue) with a quaternary ammonium chloride, Aliquat 336, from HCl.[4] In this work, we performed an online solid-liquid extraction experiment on ^{261}Rf and ^{169}Hf using the developed apparatus at RIKEN.

The ^{261}Rf ($T_{1/2}$ = 68 s) and ^{169}Hf ($T_{1/2}$ = 3.25 min) nuclides were produced in the ^{248}Cm(^{18}O,5n)^{261}Rf and ^{nat}Gd(^{18}O,xn)^{169}Hf reactions, respectively, by the RIKEN K70 AVF cyclotron. The nuclear reaction products that recoiled out from the target were caught by KCl aerosols in He gas and were transported by the gas-jet system to the chemistry laboratory. In the solid-liquid extraction experiments, the reaction products in the gas-jet were deposited on a collection site on a dissolution apparatus. Then, the deposited sample was dissolved in about 0.25 mL of 7.9 and 9.0 M HCl. The solution sample entered the chemical reaction container containing the 28 wt% Aliquat 336 resin (1.11–1.62 mg). After shaking the container with a vortex mixer for 10–60 s, only the solution phase was pushed out of the container by compressed air and collected on the Ta dish. Then the solution sample was evaporated to dryness with hot He gas and a halogen lamp to prepare a sample for α-spectrometry. Subsequently, the Ta dish was transferred to a Si PIN photodiode detector, and α-particle measurement was performed. After the measurement, the γ-ray activity of ^{169}Hf was monitored using a Ge detector to determine its K_d value and chemical yield.

In Fig. 1, the K_d values of Zr, Hf, and Th with the 28wt% Aliquat 336 resin[4] are shown as a function of the HCl concentration. The K_d values of Hf in this work were consistent with those in the offline batch experiment (≥4 h of shaking), indicating that the K_d values of Hf in equilibria could be obtained using batch-type solid-liquid extraction apparatus. The 24 and 3 α events were observed in the experiments at 7.9 M HCl (38 extractions, chemical yield: 56%) and at 9.0 M HCl (68 extractions, chemical yield: 47%), respectively, in the α energy region of ^{261}Rf and its daughter ^{257}No. The detected α counts for eluent clearly decreased with an increase in the HCl concentration. This suggests that Rf forms anionic chloride complexes with Cl^- ions, similar to the case of Zr and Hf and different from the case of Th. The present results are consistent with the previous report.[5] We will report the K_d values of Rf in the present experiment in the future.

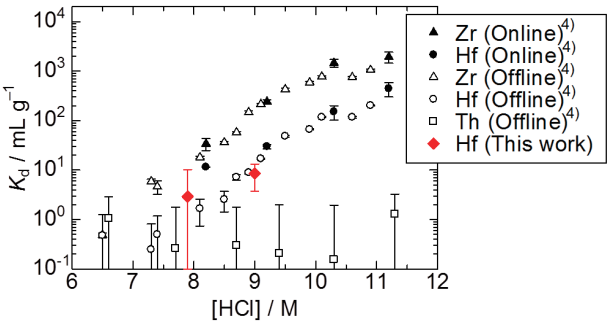

Fig. 1. The K_d values of Zr, Hf, and Th as a function of the HCl concentration with 28 wt% Aliquat 336 resin.

*1 RIKEN Nishina Center
*2 Graduate School of Science, Osaka University

References

1) Y. Ishii et al.: Bull. Chem. Soc. Jpn. **84**, 903 (2011).
2) Z. J. Li et al.: Radiochim. Acta **100**, 157 (2012).
3) A. Kino et al.: RIKEN Accel. Prog. Rep. **46**, 241 (2013).
4) T. Yokokita et al.: 6th International Conference of Ion Exchange, Ginowan, November 12 (2014).
5) H. Haba et al.: J. Nucl. Radiochem. Sci. **3**, 143 (2002).

Extraction behavior of rutherfordium as a cationic fluoride complex with a 2-thenoyltrifluoroacetone chelate extractant from HF/HNO_3 acidic solutions

Y. Kitayama,[*1] Y. Fukuda,[*1] H. Haba,[*2] K. Tsukada,[*3] A. Toyoshima,[*3] H. Kikunaga,[*4] M. Murakami,[*2, *5] Y. Komori,[*2] M. H. Huang,[*2] T. Taniguchi,[*1] S. Ueno,[*1] K. Hayashi,[*1] Y. Yatsu,[*1] I. Chiyonishio,[*6] K. Murakami,[*6] and A. Yokoyama[*6]

Recently, we developed a reversed-phase-chromatography technique with 2-thenoyltrifluoroacetone (TTA) as a chelate extractant to clarify chemical properties of a cationic fluoride complex of a superheavy element, rutherfordium (Rf). The resin containing a TTA *n*-octanol soluiton has been prepared for that purpose [1]. In this study, we have investigated chromatographic behavior of Rf with this technique in various HF/HNO_3 solutions.

Both of batch and on-line experiments were performed with Zr and Hf to determine experimental conditions suitable for Rf. For batch experiments, non-carrier tracers of Zr and Hf were used to examine distribution coefficient (K_d) values. As for on-line experiments, reversed-phase chromatography of the short-lived nuclides $^{89m, 85}$Zr and ^{169}Hf was performed with a micro-column in the same way as Rf experiment to obtain elution curves and percent adsorption values (%ads) as defined below.

In Rf experiments, nuclides of ^{261}Rf with a half-life of 68 s and ^{169}Hf were simultaneously produced in the ^{248}Cm(^{18}O, 5*n*)^{261}Rf and ^{nat}Gd(^{18}O, x*n*)^{169}Hf reactions, respectively, with 109.3 MeV ^{18}O beam at the RIKEN K70 AVF cyclotron. The reaction products were rapidly transported with a KCl/He gas-jet system to the chemistry laboratory and were deposited on the collection site of the on-line Automated Rapid Chemistry-Apparatus (ARCA) for chromatography experiments. The products were dissolved in HF/0.01 M HNO_3 solutions and were fed onto the micro-column (1.6 mmφ×7 mm) of ARCA at a flow rate of 0.1 mL/min. The resin containing 25 wt.% of TTA was filled in the column. The effluent from the column was collected on a Ta-disk as fraction 1. The remaining products in the column were then stripped with a 0.1 M HF/0.1 M HNO_3 solution and were collected on another Ta disk as fraction 2. These disks were then separately evaporated to dryness with a halogen heat lamp and heated He gas. The samples were assayed with a rapid α/SF detection system for studying the aqueous chemistry of superheavy elements at RIKEN.

The K_d values of Zr and Hf in the batch and on-line experiments were determined and compared in the wide range of F^- equilibrium concentration ($[F^-]_{eq}$) as shown in Fig. 1. The values of both Zr and Hf show sudden decreases in the range of $[F^-]_{eq} > 4 \times 10^{-5}$ M in both the batch and on-line experiments. This indicates that fluoride complexation of Zr and Hf consecutively proceeds to form neutral or anionic species from cationic ones with the increase in $[F^-]_{eq}$. Therefore, differences in the formation of fluoride species between Rf and its homologues can be observed in these $[F^-]_{eq}$.

As a preliminary result, 160 α events including 21 time-correlated α-particle pairs (8.00-8.40 MeV) from ^{261}Rf and its daughter nuclide ^{257}No were observed in 1001 cycles of the chromatography experiment. The %ads values of Rf were evaluated by using the following equation:

$$\%\text{ads} = \frac{100 \times Fr2}{Fr1 + Fr2},$$

where Fr1 and Fr2 are the radioactivities observed in the fractions 1 and 2, respectively. The %ads values of Rf were constant at around 60% in the $[F^-]_{eq}$ range up to 5×10^{-4} M and then steeply decreased at $[F^-]_{eq} = 9\times10^{-4}$ M while those of Hf decreased significantly from 100% to a few percent around $[F^-]_{eq} = 1\times10^{-4}$ M. The latter data reproduced the results for Hf for the on-line experiments shown in Fig. 1. This suggests that the cationic fluoride complexes of Rf exist more stably than those of Hf at $[F^-]_{eq} > 1\times10^{-4}$ M.

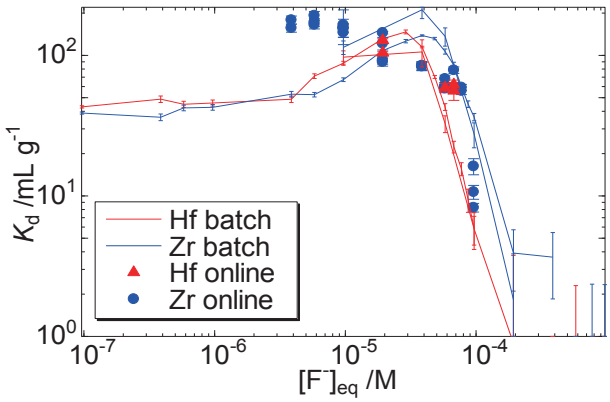

Fig. 1 Distribution coefficients, K_d, of Zr and Hf plotted as a function of $[F^-]_{eq}$ assayed by batch (solid lines) and on-line (closed symbols) experiments.

*1 Graduate School of Natural Science and Technology, Kanazawa University
*2 RIKEN Nishina Center
*3 Advanced Science Research Center, Japan Atomic Energy Agency
*4 Research Center for Electron Photon Science, Tohoku University
*5 Graduate School of Science and Technology, Niigata University
*6 Institute and College of Science and Engineering, Kanazawa University

Reference

1) M. Araki, T. Nanri., Y. Takeda, M. Nishio, M. Nishikawa, Y. Kasamatsu, Y. Ezaki, Y. Kudou, H. Haba, and A. Yokoyama: RIKEN Accel. Prog. Rep. **43**, 271 (2010).

Thermal stability of the group 6 hexacarbonyl complexes

I. Usoltsev,[*1,*2] M. Asai,[*3] H. Brand,[*4] A. Di Nitto,[*5] Ch.E. Düllmann,[*4,*5,*6] R. Eichler,[*1,*2] J. Even,[*5] F. Fangli,[*7] H. Haba,[*8] W. Hartmann,[*4] M. Huang,[*8] E. Jäger,[*4] D. Kaji,[*8] J. Kanaya,[*8] Y. Kaneya,[*8] J. Khuyagbaatar,[*5] B. Kindler,[*4] J.V. Kratz,[*6] J.Krier,[*4] Y. Kudou,[*8] N. Kurz,[*4] B. Lommel,[*4] S. Miyashita,[*3,*9] K. Morimoto,[*8] K. Morita,[*8,*10] M. Murakami,[*8,*11] Y. Nagame,[*3] H. Nitsche,[*12,*13] K. Ooe,[*11] T.K. Sato,[*3] M. Schädel,[*3] J. Steiner,[*4] P. Steinegger,[*1,*2] T. Sumita,[*8] M. Takeyama,[*8] K. Tanaka,[*8] A. Toyoshima,[*3] K. Tsukada,[*3] A. Türler,[*1,*2] Y. Wakabayashi,[*8] Y. Wang,[*7] N. Wiehl,[*3,*6] S. Yamaki,[*8,*1,*4] A. Yakushev,[*4] Q. Zhi[*7]

Recently, the on-line production of $Sg(CO)_6$ was achieved.[1] The Sg-CO bond in the $Sg(CO)_6$ complex was predicted to be slightly more stable than the corresponding bond in the complex of its lighter homolog $W(CO)_6$.[2] In this work, we aim to design the experimental setup to verify this prediction. Alpha-decaying isotopes ^{163}W and ^{164}W were produced in fusion-evaporation reactions $^{144}Sm(^{24}Mg,xn)^{163\text{-}164}W$ at RIKEN Linear Accelerator (RILAC). Therefore, a ^{144}Sm target was bombarded with a 0.66 μA_{part} ^{24}Mg beam, at a center-of-target energy of 136 MeV. The Gas-filled Recoil Ion Separator (GARIS) allowed for efficient separation of the desired evaporation residues from the beam and from multinucleon transfer products. The separated isotopes were thermalized in a gas mixture of CO and He 1:1 by volume. The formed $^{163\text{-}164}W(CO)_6$ complexes were transported to the decomposition setup through PFA Teflon capillaries. The decomposition setup consisted of a *decomposition column*[3], covered inside by silver foil, and a bypass column of the same size made of PFA Teflon. Because of the high inertness toward carbonyl complexes the Teflon bypass was implemented to quantify the actual production yield of the carbonyl complexes. The yields of the carbonyl complex able to pass this decomposition setup were determined by means of total trapping of the volatile complexes in the cryo online thermochromatography detector array COMPACT.[1] The primary result of a complete decomposition experiment is given in a form of a decomposition curve, which pictures the survival probability for a complex as a function of decomposition temperature. The results of the model experiments with ^{104}Mo obtained from the ^{252}Cf spontaneous fission source "Miss Piggy" at the University of Bern [3] are presented together with the current results obtained for $^{163,164}W$ in Fig. 1. The difference of 23 kJ/mol in (FBDEs) of Mo-CO (169 kJ/mol) and W-CO (192 kJ/mol) leads to a decomposition temperature shift of about 100°C. The figure suggests that the experiment can be sensitive to a small difference in FBDE i.e., 10 kJ/mol.

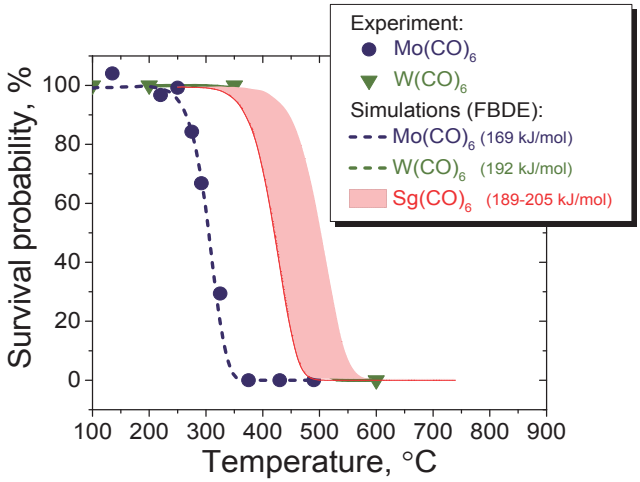

Fig. 1: $^{104}Mo(CO)_6$ and $^{163\text{-}164}W(CO)_6$ experimental decomposition curves (symbols) and simulated curves considering the relevant FBDE's (dashed lines). The predicted interval[2] for $^{265}Sg(CO)_6$ is indicated (red area).

We developed a Monte-Carlo based two-step reversible adsorption-irreversible decomposition model[3] for describing the heterogeneous decomposition process. This model successfully reproduced the experimental results for $Mo(CO)_6$ and $W(CO)_6$ (Fig. 1, dashed lines) and could be used for designing and evaluating data of the future decomposition experiments with $Sg(CO)_6$ (Fig. 1, red interval of FBDE= 197±8 kJ/mol). Thus, a complete method for the experimental verification of the prediction [2] was elaborated.

To conclude, we successfully tested a fast and efficient approach for assessing the thermal stability of group 6 carbonyl complexes. The dissociation energy of the Sg-CO bond can be therefore experimentally investigated and directly compared with the related properties of lighter homologs.

References

1) J. Even et al.: Science 345, 6203 (2014).
2) C. S. Nash: J. Am. Chem. Soc. 121, 10830 (1999).
3) I. Usoltsev: PHD Thesis Univ. Bern (2014).

*1 University of Bern
*2 Paul Scherrer Institute
*3 Advanced Science Research Center
*4 GSI Helmholtzzentrum für Schwerionenforschung
*5 Helmholtz-Institut Mainz
*6 Johannes Gutenberg-Universität Mainz
*7 Institute of Modern Physics Lanzhou
*8 Nishina Center for Accelerator-Based Science
*9 Hiroshima University
*10 Kyushu University
*11 Niigata University
*12 University of California
*13 Lawrence Berkeley National Laboratory
*14 Saitama University

Extraction behavior of Mo and W from H_2SO_4 using amine-extractant (Aliquat336) as homologs of seaborgium

A. Toyoshima,[*1] A. Mitsukai,[*1,*2] A. Vascon,[*1] Y. Kaneya,[*1,*3] M. Murakami,[*4,*5] K. Ooe,[*4] N. Goto,[*4] D. Sato,[*4] Y. Komori,[*5] H. Haba,[*5] K. Tsukada,[*1] M. Asai,[*1] T. K. Sato,[*1] Y. Nagame,[*1] and M. Schädel[*1,*6]

Recently, we began to study the aqueous chemistry of a group-6 transactinide element, Sg. At present, we focus on the formation of anionic sulfate complexes of Mo and W, which are lighter homologs of Sg, by means of amine-extraction in H_2SO_4 as a preparatory experiment for Sg. Previously, we have found that the group-4 transactinide, Rf, has a weaker preference to form a sulfate complex than its lighter homologs, Zr and Hf.[1)] This is consistent with its predicted, larger ionic radius compared to the measured radii of Zr and Hf; moreover, this is in good agreement with a theoretical prediction[2)] that the stability of Rf complexes is lower because of the smaller ionic contribution to the chemical bond. The investigation of sulfate complex formation of Sg is, therefore, expected to provide valuable information on its ionic radius and chemical bonding.

This paper reports on the extraction behavior of the carrier-free radioisotopes ^{93m}Mo and ^{181}W from aqueous H_2SO_4 solution using an amine extractant, Aliquat336, by a batch method to ensure that the chemical behavior of mononuclear complexes of these homologs is retained. First, the extraction kinetics of these radioisotopes in 0.1, 4.3 and 8.6 M H_2SO_4 with 0.2 M Aliquat336 were studied. Then, extraction probabilities were investigated as a function of H_2SO_4 concentration, $[H_2SO_4]$.

In the experiments of Mo, ^{93m}Mo was produced in the ^{nat}Zr(α, xn) reaction at the RIKEN K70 AVF cyclotron. Nuclear reaction products transported by a KCl/He gas-jet at a flow rate of 2.5 L/min were deposited on a small piece of plastic (Naflon®, ~2 cm × 1.5 cm) for 3 min. KCl aerosols were produced by sublimation at 640°C. Then, the deposited products were dissolved win 100 μL of 0.1 – 8.6 M H_2SO_4 solution. The solution was then added to 600 μL of H_2SO_4 solution with the same concentration in a plastic vial. Subsequently, 700 μL of the toluene solution of Aliquat336 was added. After shaking with a Vortex mixer for 360 s, the mixed sample was centrifuged for 30 s. From both the phases, 500 μL solutions were collected separately in 2 vials. These 2 samples were then subjected to γ-ray spectrometry with a Ge detector. The distribution ratio, D, was evaluated with the equation, $D = (A_{org} / V_{org}) / (A_{aq} / V_{aq})$, where A_{org} and A_{aq} are the radioactivities in organic and aqueous phases, respectively, and V_{org} and V_{aq} are the volumes of the organic and aqueous phases, respectively.

In the experiments of W, ^{181}W was produced in the ^{181}Ta(d, xn)^{181}W reaction at the RIKEN K70 AVF cyclotron. After the chemical separation of ^{181}W from a Ta target material through an ion-exchange, carrier-free ^{181}W was stocked in H_2SO_4 solutions. The procedure of the subsequent batch experiment was the same as that for ^{93m}Mo described above.

Results of kinetics experiments showed that the extraction equilibrium of ^{93m}Mo was reached within 5 s in the range of 0.1 M < $[H_2SO_4]$ < 8.6 M, while that of W was dependent on $[H_2SO_4]$; the equilibrium was attained within 40 s at $[H_2SO_4]$ < 1 M and within 2 min at 1 M < $[H_2SO_4]$ < 8.6 M. In Fig. 1, the D values of Mo and W under equilibrated conditions are shown as a function of $[H_2SO_4]$. The D values of Mo and W decrease up to 3 M and 2 M, respectively, with increasing $[H_2SO_4]$. This is probably due to protonation reactions of hydrolyzed Mo and W species. On the other hand, when $[H_2SO_4]$ > 3 M and > 4 M, the D values of W and Mo, respectively, show a sharp increase. This clearly indicates the formation of anionic sulfate complexes of Mo and W. Sulfate complexation of Sg under the present experimental conditions will be clarified in our future experiments.

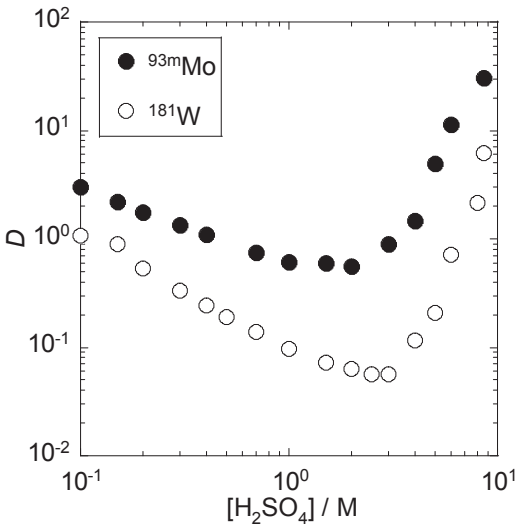

Fig. 1. Variation of D value of Mo and W as a function of H_2SO_4 concentration, $[H_2SO_4]$.

*1 Advanced Science Research Center, Japan Atomic Energy Agency
*2 Faculty of Science, Ibaraki University
*3 Graduate School of Science and Engineering, Ibaraki University
*4 Graduate School of Science and Technology, Niigata University
*5 RIKEN Nishina Center
*6 GSI Helmholtzzentrum für Schwerionenforschung GmbH

References

1) Z. J. Li et al.: Radiochim. Acta **100**, 157 (2012).
2) V. Pershina et al.: Radiochim. Acta **94**, 407 (2006).

Solvent extraction of short-lived radioisotopes of Mo and W from oxalic acid solution with Aliquat 336 for chemical studies of seaborgium (Sg)

N. Goto,[*1] K. Ooe,[*1] A. Toyoshima,[*2] M. Murakami,[*1,*3] Y. Komori,[*3] H. Haba,[*3] S. Goto,[*1] and H. Kudo[*4]

Thus far, few studies of seaborgium (Sg) in an aqueous phase have been reported, where only a few events of Sg were detected after batch-wise cation-exchange chromatography.[1,2] There have been few chemical studies of Sg owing to the experimental difficulties caused by its extremely low production yield and short half-life. To overcome the difficulties, we are developing a new rapid continuous chemistry apparatus based on the solvent extraction technique. We have been also studying solvent extraction behavior and extracted species of molybdenum (Mo) and tungsten (W), which are lighter homologs of Sg, to apply obtained results to development of the new apparatus and to compare extraction behavior among the homologs including Sg. Because it is well-known that Mo and W form polyoxometalate complexes, Mo and W should be extracted on a tracer scale for comparison of extraction behavior of their mononuclear complexes with that of Sg, which can exist only as single atoms. In a previous report, the solvent extraction of W from oxalic acid solution into toluene with Aliquat 336 was carried out with long-lived radiotracer, ^{181}W ($T_{1/2}$ = 121.2 d).[3] In this paper, we report on the extraction behavior of Mo using short-lived radioisotope along with W. The extracted species of these two elements will be discussed.

Short-lived radiotracers ^{93m}Mo ($T_{1/2}$ = 6.85 h) and ^{177}W ($T_{1/2}$ = 2.25 h) were produced in the irradiation with a 50-MeV α beam supplied from the RIKEN K70 AVF cyclotron on a metallic ^{nat}Zr and ^{nat}Hf target foils. Nuclear reaction products recoiling out of the targets were transported by a KCl/He gas-jet method at a He gas flow rate of 2.0 L/min. The transported products were deposited on a small plastic piece (Naflon®) for 1min. Then, the deposited products were dissolved with 100 μL of 0.01 M $H_2C_2O_4$ (oxalic acid)/0.1 M HCl/0.9 M LiCl solution. The solution was then pipetted to a plastic tube in which 600 μL of aqueous solution and 700 μL of Aliquat 336 in toluene had been added. After shaking with a Vortex mixer for 5 min, the mixed sample was centrifuged for 30 s. From both the phases, 500 μL of aliquots were separately taken into two vials. These two samples were then subjected to γ-ray spectrometry with a Ge detector. The distribution ratio (D) of ^{93m}Mo and ^{177}W was calculated using the equation of $D = (A_{org} / V_{org}) / (A_{aq} / V_{aq})$, where A_{org} and A_{aq} are the radioactivities in organic and aqueous phases, respectively, and V_{org} and V_{aq} are the volumes of organic and aqueous phases, respectively.

*1 Graduate School of Science and Technology, Niigata University
*2 Advanced Science Research Center, Japan Atomic Energy Agency
*3 RIKEN Nishina Center
*4 Department of Chemistry, Faculty of Science, Niigata University

Dependence of the D values of ^{93m}Mo and ^{177}W on the Aliquat 336 concentration with a 0.01 M oxalic acid/ 0.1 M HCl/0.9 M LiCl solution is shown in Fig. 1. Results previously obtained with ^{181}W are also plotted in the same figure. The D values of Mo and W increase with increasing concentration of Aliquat 336. The slopes of the D value vs. [Aliquat 336] plot on logarithmic scales are evaluated to be 2.08 ± 0.03 for Mo and 1.33 ± 0.02 for W with a weighted least-squares fitting. This indicates that extracted anionic oxalate complex of Mo is associated with two molecules of Aliquat 336, while that of W is with one molecule. On a macro scale, it was reported that Mo and W are extracted as $(R_3NH)_2MO_2(C_2O_4)_2$ from oxalic acid solution, where R_3N shows a trioctylamine (TOA) molecule and M shows Mo or W.[4,5] The present result for Mo corresponds to the reported Mo oxalate complex. On the other hand, it seems that W forms a different complex from the Mo one. Under the present experimental condition, chloride ions of 1 M are present contrary to the experiment in the reference.[5] Therefore, the extracted W complex might contain one oxalate ion and one chloride ion. To obtain further information on the extracted species of W, we need to investigate the variation in the distribution ratio as a function of the concentration of chloride ions. Based on the extraction behavior of Mo and W obtained in these studies, oxalate complex formation of Sg will be investigated.

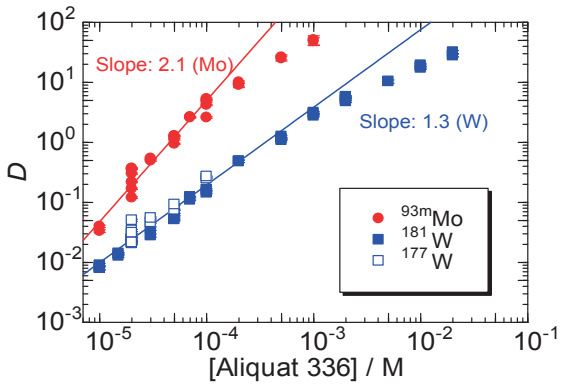

Fig. 1. Variation in the distribution ratio of ^{93m}Mo, ^{177}W and ^{181}W from 1.0 × 10^{-2} M oxalic acid with 0.1 M HCl/0.9 M LiCl as a function of the concentration of Aliquat 336.

References

1) M. Schädel et al.: Radiochim. Acta **77**, 149 (1997).
2) M. Schädel et al.: Radiochim. Acta **83**, 163 (1998).
3) N. Goto et al.: RIKEN Accel. Prog Rep. **47**, 269 (2014).
4) K. Yakabe and S. Minami: Nippon Kagaku Kaishi 1045 (1983).
5) K. Yakabe, K. Iwamoto and S. Minami: Nippon Kagaku Kaishi 714 (1985).

Reversed-phase chromatography of Nb and Ta with TBP for conducting a chemical experiment on the 105th element, Db

M. Murakami,[*1,*2] S. Tsuto,[*1] K. Ooe,[*1] S. Goto,[*1] D. Sato,[*1] N. Goto,[*1] T. Koyama,[*1] T. Nagaoka,[*1] R. Motoyama,[*1] H. Haba,[*2] Y. Komori,[*2] A. Toyoshima,[*3] A. Mitsukai,[*3,*4] Y. Kitayama,[*5] Y. Fukuda,[*5] and H. Kudo[*1]

Detailed chemical properties of superheavy elements (SHEs) have not been elucidated owing to the difficulty in conducting chemical experiments because of their short half-lives and extremely low production rates. For investigating the chemical properties of the 105th element, Db, we studied the extraction behavior of the group-5 homolog elements Nb and Ta from HF media with tributyl phosphate (TBP), which is used in the industrial separation of Nb and Ta. In our previous study using batchwise solvent extraction,[1] we observed the differences between the ^{95g}Nb and ^{179}Ta extraction behaviors; the distribution ratios of ^{179}Ta reach a maximum at the initial HF concentration, $[HF]_{ini} = 0.27$ M, whereas those of ^{95g}Nb increase with increasing $[HF]_{ini}$. To examine the applicability of this extraction system to the short-lived ^{262}Db with $T_{1/2} = 33.8$ s, we performed an on-line reversed-phase chromatographic experiment on Nb and Ta using Automated Rapid Chemistry Apparatus (ARCA).[2]

The nuclides ^{90g}Nb ($T_{1/2}$ = 14.6 h) and ^{178a}Ta ($T_{1/2}$ = 2.45 h) were produced via the ^{nat}Zr(d,xn) and ^{nat}Hf(d,xn) reactions, respectively, with a 24-MeV deuteron beam supplied from the RIKEN AVF cyclotron. The nuclides produced were transported with a He/KCl gas-jet system and were deposited on a collection site in ARCA for 60 s. Then, the products were dissolved in 1–10 M HF solutions and were loaded onto a column (1.6 mm i.d. × 7.0 mm height) filled with a 62-wt% TBP-laden resin, which was prepared in the procedure described in Ref. 3. The flow rate of the eluent was 1.0 mL/min. The effluent fractions were consecutively collected in 7 polypropylene (PP) tubes. The remaining products in the column were stripped with 330 μL of 10 M HF at a flow rate of 1.0 mL/min, and the effluent was collected in another PP tube. Each fraction was subjected to γ-ray spectrometry with a Ge detector.

Figure 1 shows the elution curves of ^{90g}Nb and ^{178a}Ta in 1.0 M HF as an example, in which correction for a dead volume of ARCA (40 μL) was made for the effluent volume. ^{90g}Nb was eluted immediately, whereas ^{178a}Ta showed a broad peak around 770 μL with a small leakage in the first effluent (less than 5% of the total activity of ^{178a}Ta). Similar elution behavior of ^{90g}Nb was also observed at higher $[HF]_{ini}$. The peak volume of the elution curves of ^{178a}Ta gradually decreased, corresponding to the decreasing distribution coefficient (K_d) of ^{178a}Ta on the TBP resin. In Fig. 1, the elution curve of ^{178a}Ta was fitted by the Glückauf formula of chromatography[4] except for the first leakage fraction. The K_d values are described as $K_d = v_p/m_r$, where v_p and m_r are the peak volume and mass of dry resin (6.31 mg), respectively. The evaluated K_d values of ^{178a}Ta are shown in Fig. 2 together with those of ^{179}Ta previously obtained by the batch experiments.[1] The good agreement between the on-line and off-line results indicates that the extraction equilibrium is reached in the present column experiment. Recently, we performed an extraction experiment of Db with the studied system.[5]

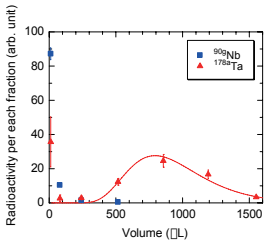

Fig. 1. Elution curves of ^{90g}Nb and ^{178a}Ta in 1.0 M HF on the column of 62 wt%TBP resin.

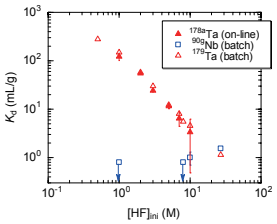

Fig. 2. Variation in K_d values of ^{178a}Ta as a function of $[HF]_{ini}$ (closed symbols). The K_d values of ^{95g}Nb and ^{179}Ta obtained by the batch experiment[1] are also shown as open symbols.

*1 Department of Chemistry, Niigata University
*2 RIKEN Nishina Center
*3 Advanced Science Research Center, Japan Atomic Energy Agency
*4 Faculty of Science, Ibaraki University
*5 Graduate School of Natural Science and Technology, Kanazawa University

References

1) S. Tsuto et al.: RIKEN Accel. Prog. Rep. **47**, 270 (2014).
2) Y. Nagame et al.: Radiochim. Acta **93**, 519 (2005).
3) H. Haba et al.: Radiochim. Acta **95**, 1 (2007).
4) E. Glückauf: Trans. Faraday Soc. **51**, 34 (1955).
5) M. Murakami et al.: In this report.

Liquid-liquid extraction of Nb and Ta with Aliquat 336 from 0.27 M HF solution

D. Sato,[*1,*2] M. Murakami,[*1,*2] K. Ooe,[*1] H. Haba,[*2] H. Kikunaga,[*3] S. Goto,[*1] and H. Kudo[*4]

The elements with atomic numbers ≥ 104 are called transactinide elements. Their chemical properties are greatly interesting because it is expected that chemical behavior of these elements would deviate from that of lighter homologs by strong relativistic effects on valence electrons[1]. Therefore, it is very important to study the chemical behavior of transactinide elements comparing with that of lighter homologs.

Among the transactinide elements, we are interested in the chemical properties of 105th element Db, especially, for complex formation with a fluoride ion which is a strong complexing reagent for group 5 elements. Anionic fluoride complex formation of Db has been investigated through anion exchange study from HF solution[2]. The result of this experiment showed that the K_d value of Db in 13.9 M HF was smaller than that of Nb and Ta, which are lighter homologs of Db. However, the chemical form of Db was not yet determined in this condition. Therefore, for investigation of fluoride complex formation of Db in detail, we have been studying the liquid-liquid extraction behavior of Nb and Ta from HF solutions with quaternary ammonium salt, Aliquat 336. So far, a clear difference of the extraction behavior between Nb and Ta in 10^{-2}-27 M HF was observed. While distribution ratios (D) of Nb were decreased with increasing HF concentration, those of Ta were a maximum at around 0.3 M HF[3]. Since linear relations with slope ≈ 1 for both elements were observed from log D vs. log [Aliquat 336] plots, it was suggested that univalent anionic fluoride complex of $NbOF_4^-$ and TaF_6^- were extracted by Aliquat 336 in 2.7 M and 10 M HF. However, in previous study, we have not obtained information of chemical species in 0.27 M which those of Ta are most extracted. Therefore, in the present work, variation of D values of ^{95g}Nb and ^{179}Ta vs. concentration of Aliquat 336 in 0.27 M HF was studied.

Long-lived radiotracers, ^{95g}Nb ($T_{1/2}$ = 34.97 d) and ^{179}Ta ($T_{1/2}$ = 665 d), were produced during deuteron irradiation of Zr and Hf metallic foil targets with natural isotopic abundances, respectively, using the RIKEN K70 AVF Cyclotron. These radiotracers in the targets were chemically isolated by ion-exchange separation. The tracers were dissolved in 600 μL of 0.27 M HF and then mixed with the same volume of 10^{-8}-10^{-1} M Aliquat 336/1,2-dichloroethane solutions in a polypropylene tube. After shaking of the solutions for 5 min, followed by centrifugation, the two phases were separately pipetted into sample tubes. The radioactivities of the two samples were measured with a Ge detector. D values of Nb and Ta were obtained from the ratio of the radioactivities of the two phases.

The dependences of the distribution ratios of ^{95g}Nb and ^{179}Ta in 0.27 M HF on the concentrations of Aliquat 336 are shown in Fig. 1. The results show a linear relation with a slope of ≈1 for both Nb ([Aliquat 336] = 10^{-5}-10^{-1} M) and Ta ([Aliquat 336] = 10^{-8}-10^{-7} M), which indicates that univalent anionic fluoride complexes are extracted by Aliquat 336. Therefore, it is suggested that $NbOF_4^-$ and TaF_6^- were also extracted by Aliquat 336 in 0.27 M HF along with 2.7M and 10 M HF.

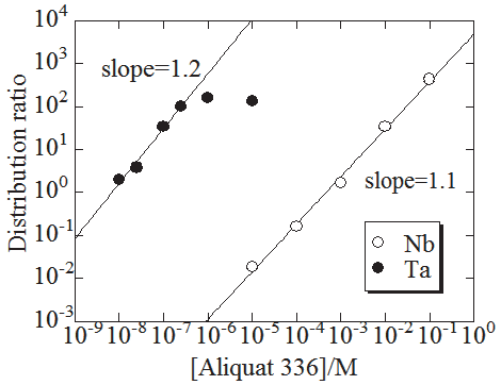

Fig. 1: Variation of the distribution ratio D of ^{95g}Nb and ^{179}Ta vs. concentration of Aliquat 336 in 0.27 M HF.

From the obtained results and reference [4-5], it is assumed that the chemical species of Nb and Ta change from $NbOF_4^-$ to $NbOF_5^{2-}$ and from TaF_6^- to TaF_7^{2-}, respectively, with increasing HF concentration in the range of 0.27-10 M, expressed as following equations:

$$NbOF_4^- + F^- \leftrightarrow NbOF_5^{2-} \quad (1)$$

$$TaF_6^- + F^- \leftrightarrow TaF_7^{2-} \quad (2)$$

In the near future, dependence of D values of ^{95g}Nb and ^{179}Ta on concentration of Aliquat 336 in HF solution lower than 0.27 M will be investigated for further study of fluoride complex formation of group 5 elements.

References

1) P. Pyykko: Chem. Rev. **88**, 563 (1988)
2) K. Tsukada *et al.*:,Radiochim. Acta **97**, 83 (2009).
3) D. Sato *et al.*: Accel. Prog. Rep. **47** 271 (2014).
4) F. Monroy Guzman *et al.*: J. Radioanal. Nucl. Chem. **208**, 461 (1996).
5) A. Agulyansky: The Chemistry of Tantalum and Niobium Fluoride Compounds, 125-134

[*1] Graduate School of Science and Technology, Niigata University
[*2] RIKEN Nishina Center
[*3] Research Center for Electron Photon Science, Tohoku University
[*4] Department of Chemistry, Faculty of Science, Niigata University

Coprecipitation Behaviors of Zr, Hf, and Th with Sm Hydroxide for Chemical Study of Element 104, Rf†

Y. Kasamatsu,[*1] K. Toyomura,[*1] N. Shiohara,[*1] T. Yokokita,[*1] Y. Komori,[*1,*2] A. Kino,[*1] T. Yoshimura,[*3] N. Takahashi,[*1] H. Haba,[*2] Y. Kudou,[*2] H. Kikunaga,[*2,*4] T. Mitsugashira,[*5] T. Ohtsuki,[*6] K. Takamiya,[*6] and A. Shinohara[*1]

Owning to significant relativistic effects on electron orbital shells for heavy elements, the chemical properties of the superheavy elements are expected to deviate from the characteristic periodicity of the lighter homologues in the periodic table, and their chemical studies have attracted much attention. However, experimental evaluation of these species is fraught with difficulties. Because of the extremely low production rates and short half-lives (within a few min) of these heavy nuclides, chemical evaluations of the superheavy elements must be rapidly conducted on a one-atom-at-a-time basis. Thus, simple chemistry employing partition methods such as solvent extraction and ion-exchange chromatography have been utilized and the chemical separations were repeated hundreds or thousands of times under identical conditions. This approach requires a rapid chemistry apparatus. Additionally, for unambiguous identification of superheavy nuclides, it is necessary to measure the energies and lifetimes of α or sometimes spontaneous fission decays.

The purpose of the present study is to establish a new experimental methodology for investigating the chemical properties of superheavy elements, specifically, the coprecipitation properties of ^{261}Rf ($T_{1/2}$ = 68 s) by the formation of hydroxide and ammine complexes. Herein, we applied a simple coprecipitation method with Sm hydroxide, which facilitates α spectrometry with high energy resolution,[1] to the investigation of the coprecipitation behaviors of the homologues of Rf: Zr, Hf, and Th. In addition, a semiautomatic apparatus for repetitive preparation of precipitate samples was developed and tested using the gas-jet transport system of nuclear products.

We used ^{88}Zr, ^{175}Hf, and ^{228}Th radiotracers to prepare coprecipitated samples with Sm hydroxide. A 20 μL aliquot of the Sm standard solution (Sm 1000 ppm, 1 M HNO_3) was added into 220 μL of an aqueous solution (~0.4 M HCl) containing the radiotracers in a polypropylene (PP) beaker. The solution was stirred and 2 mL of the basic solution (dilute and concentrated aqueous NH_3 and 0.1, 1.0, 6.0, and 12.0 M NaOH solutions) was then added to produce the precipitate. After aging the precipitate for 10 s or 10 min at 25 ºC, the precipitate sample was subjected to suction filtration with a PP membrane filter (eichrom, Resolve® Filters 0.1 μm). The obtained sample was dried on a heater at 100 ºC, and was subjected to γ-ray and α-particle measurements. The radioactivities of the filtrate and PP beakers used were also measured. We determined precipitation yields, Y, and the percent adsorption on the PP beaker, R_{ad}, from the radioactivities.

A computer-controlled suction filtration apparatus for the preparation of precipitated samples of heavy elements was developed. The online experiment using the apparatus was performed with relatively short-lived nuclides ^{89m,g}Zr (4.2 min and 78.4 h) and ^{173}Hf (23.6 h) produced using the AVF cyclotron at RCNP. These nuclides were rapidly and continuously transported from the nuclear reaction chamber to the chemistry laboratory using the He/KCl gas-jet system. Using the apparatus, the products were dissolved by 200 μL of dilute HCl and the precipitate samples were prepared at room temperature in a manner similar to that used in the above tracer experiment with stirring for 10 s.

The R_{ad} values of Zr, Hf, and Th for samples aged for 10 s was generally less than 3%, which suggests that physical adsorption of these group 4 elements during coprecipitation with Sm hydroxide was small enough to be negligible in the determination of the coprecipitation yields. The Y values of Zr, Hf, and Th obtained with 10-min and 10-s aging are in good agreement with each other. This suggests that the chemical reactions during coprecipitation of these elements are fast, and the present conditions are suitable for evaluating the coprecipitation behavior of 68-s ^{261}Rf. Almost complete coprecipitation of Zr and Hf with Sm hydroxide was achieved when aqueous NH_3 solutions and 0.1 M NaOH were used. These results are consistent with the well-known properties of these elements, i.e., hydroxide precipitation in basic solutions. With the use of more highly concentrated NaOH solutions, these yields decreased, whereas the Th yields were constant at ca. 100%. This is attributed to the fact that Zr and Hf form hydroxide complex ions in high [OH^-] solutions.

The Y values obtained in the online experiments and their dependence on the composition of the added basic solution are consistent with those in offline experiment. This suggests that the present experimental method using the apparatus under the present conditions should be applicable to the coprecipitation experiment of Rf.

† Condensed from the article in J. Nucl. Radiochem. Sci. **14**, 7 (2014).

*1 Graduate School of Science, Osaka University
*2 RIKEN Nishina Center
*3 Radioisotope Research Center, Osaka University
*4 Research Center for Electron Photon Science, Tohoku University
*5 Institute for Material Research, Tohoku University
*6 Research Reactor Institute, Kyoto University

Reference

1) H. Kikunaga et al., Appl. Radiat. Isot. **67**, 539 (2008).

Liquid-liquid extraction of zirconium and hafnium with 2-thenoyltrifluoroacetone for chemical studies of element 104, rutherfordium

A. Tanaka,[*1] K. Ooe,[*1] H. Kikunaga,[*2] M. Murakami,[*1,*3] Y. Komori,[*3] H. Haba,[*3] S. Goto,[*1] and H. Kudo[*4]

Chemical studies of element 104, rutherfordium (Rf), in aqueous solutions have been carried out mainly using column chromatography.[1),2)] In these column chromatographic experiments, inorganic ligands such as fluoride and chloride ions were used, and inorganic complex formation of Rf was investigated. However, little has been reported regarding the complex formation of Rf with organic ligands such as a chelating agent. In the present study, liquid-liquid extraction of zirconium (Zr) and hafnium (Hf), which are lighter homologs of Rf, was performed to find suitable experimental conditions for complexation studies of Rf with organic ligands. 2-thenoyltrifluoroacetone (TTA), which is often used as a chelate extractant in analytical chemistry and separation techniques, was applied in this experiment.

Radiotracers of ^{88}Zr ($T_{1/2}$ = 83.4 d) and ^{175}Hf ($T_{1/2}$ = 70 d) were produced in the ^{89}Y(d, 3n) and ^{175}Lu(d, 2n) reactions, respectively, using the RIKEN K70 AVF cyclotron. Metal foils of Y (150 μm thickness) and Lu (100 μm thickness) were used as targets. Incident energy of the deuteron beam was 24 MeV. The produced radiotracers were chemically separated from the target materials through the anion exchange method and stored in 3 M HNO_3 solution. Aqueous solution of 3 M HNO_3 (600 μL) containing ^{88}Zr and ^{175}Hf radiotracers was mixed with an equal volume of TTA in toluene solution in a polypropylene tube, and the mixture was mechanically shaken for 15 hours at 25 ºC. After equilibration, the mixture was centrifuged for 30 seconds, and a 420 μL aliquot from each phase was separately transferred into a polypropylene tube. The radioactivity of each phase was measured by a Ge detector, and the distribution ratio (D) was calculated by the following equation:

$$D = A_o/A_a , \qquad (1)$$

where A_a and A_o denote the radioactivities of either of ^{88}Zr and ^{175}Hf in aqueous and organic phases, respectively.

Figure 1 shows the dependence of D values of ^{88}Zr and ^{175}Hf from 3 M HNO_3 on the TTA concentration in toluene. The D value of ^{88}Zr was approximately 10 times that of ^{175}Hf. It is well-known that the chemical behavior of Zr is remarkably similar to that of Hf and mutual separation between these two elements is very difficult. Therefore, the present result shows that TTA has extraction selectivity for Zr, and it is very interesting to investigate extraction behavior of Rf with TTA.

In the extraction of tetravalent metal ions (M^{4+}) with TTA, the extraction reaction is usually described by the following equation:

$$M^{4+} + 4HTTA_{(o)} \rightleftarrows M(TTA)_{4(o)} + 4H^+ . \qquad (2)$$

From eq. (2), it is expected that the log D vs. log [TTA] plot shows linear relation with the slope of 4 and the value of the slope indicates the number of TTA molecules involved in the extraction reaction. A least-squares fit to the present data showed a straight line with a slope of 3.8 for ^{88}Zr and 3.9 for ^{175}Hf. Therefore, this result suggests that the main extracted species of Zr and Hf would be $Zr(TTA)_4$ and $Hf(TTA)_4$ from 3 M HNO_3. The slope value of the log D vs. log [TTA] plot was closer to 3 for both Zr and Hf, in not greater than 2 M HNO_3. This might be caused by the effect of hydrolysis of Zr and Hf: formation of $ZrOH^{3+}$ and $HfOH^{3+}$. Thus, an experimental condition suitable for extraction of $Rf(TTA)_4$ is determined to be 3 M HNO_3 solution.

In the future, liquid-liquid extraction experiments of Zr and Hf with a rapid extraction apparatus using flow injection analysis (FIA) technique[3)] will be performed for the Rf experiment.

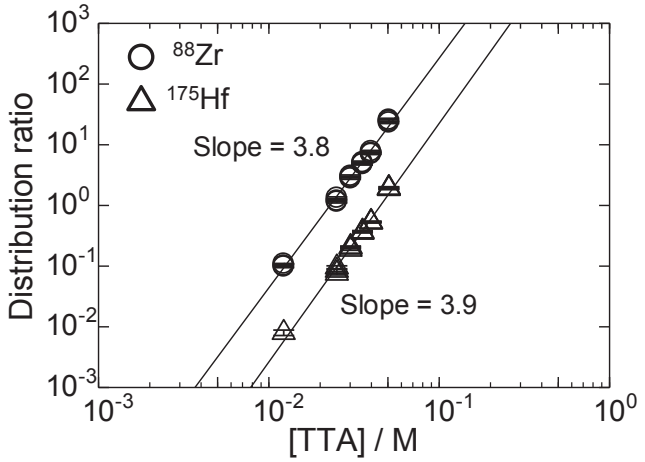

Fig. 1. Dependence of distribution ratios of ^{88}Zr and ^{175}Hf from 3 M HNO_3 on TTA concentration in toluene.

References

1) H. Haba et al.: J. Nucl. Radiochem. Sci. **3**, 143 (2002).
2) H. Haba et al.: J. Am. Chem. Soc. **126**, 5219 (2004).
3) T. Koyama et al.: 5th Asia-Pacific Symposium on Radiochemistry'13 (APSORC 13), "*Development of a rapid solvent extraction technique with flow injection analysis for superheavy element chemistry*" 25-NCP-05.

*1 Institute of Science and Technology, Niigata University
*2 Research Center for Electron Photon Science, Tohoku University
*3 RIKEN Nishina Center
*4 Faculty of Science, Niigata University

Production of platinum radiotracer for Gamma-Ray Emission Imaging

S. Komoto,[*1] M. Munekane,[*1] T. Fukuchi,[*2] H. Haba,[*3] K. Higashikawa,[*1] M. Ueda,[*1] S. Motomura,[*2] and S. Enomoto[*1,*2]

Platinum drugs such as cis-diammine dichloro platinum(Ⅱ) (cisplatin) have been used for a long time as a first-choice drug for several types of tumors. The efficacy of these types of drugs has been certainly approved however the disadvantages are the strong toxic side effects including nephrotoxicity, nausea, and neurotoxicity. These side effects are considered as dose-limitation factors. Further, in treatment, the tumor gradually develops resistance to these drugs. There are some mechanisms of resistance such as "Decreased uptake" and "Increased efflux." [1)]

To investigate potential side effects and drug efficacy, we are developing noninvasive and quantitative distribution analysis methods that can determine the concentration of platinum drugs in normal tissues/organs and tumors. We have propose using a new nuclear medicine imaging technology called GREI (Gamma-Ray Emission Imaging), to visualize the distribution of platinum drugs labeled with platinum radionuclides. GREI comprises a Compton camera composed of two planar germanium (Ge) detectors developed in our laboratory.[2)] GREI has a wide detectable energy range (200-2000 keV) which is different from the conventional imaging modalities, namely single photon emission computed tomography (SPECT) and positron emission tomography (PET). Next, a variety of nuclides that were difficult to image can now be used because of GREI.

For the GREI experiment, platinum radionuclides with optimum half-lives and emitting γ-rays are required. Some useful radionuclides for the GREI are listed in Table 1. In this study, we investigated the production of radio-platinum nuclides that are suitable for GREI experiments via the ^{nat}Os(α,xn) reactions.

For the radio-platinum production, we used metallic ^{nat}Os powder (chemical purity: 99.99 %) as the target material. Approximately 500 mg of osmium powder was pressed by 3 t at 1 min, and molded into a pellet (φ 15 mm). The pellet was covered with a 10-μm Al foil (chemical purity: 99.999%). The osmium target was irradiated by the 30-MeV α-beam supplied by RIKEN AVF cyclotron for 1.5 h. The beam intensity was 1 particle μA. The γ-ray spectrum of the irradiated target is shown in Fig. 1. This spectrum shows that ^{189}Pt and ^{191}Pt were produced, and fewer quantities of other impurities such as radio-osmium and radio-iridium were produced. After the irradiation, the following separation steps were performed to remove the target osmium from the radio-platinum as reported by M. Bonardi, et al.[3)] First, for removing osmium, the irradiated target was dissolved in 10 mL conc. HNO_3 and heated at the 200 ℃. In this step, osmium was distilled and trapped in 4.7 N NaOH. After almost all of the liquid was evaporated, another 10 mL of conc. HNO_3 was added and heated until dryness was achieved. After this step, the process of adding 5 mL of conc. HCl and drying up was repeated thrice. The reaction vessel was washed with 5 mL of 3 M HCl and the solution containing radio-platinum was transferred to a vial. After the chemical separation, the radioactivities of ^{189}Pt and ^{191}Pt were 0.48 and 1.0 MBq, respectively, and the chemical yield was over 90 %.

GREI can detect γ-rays of various energies that are emitted from ^{189}Pt and ^{191}Pt. This allows us to use both of these radio-platinum as radio tracers for imaging. In future, we will synthesize cisplatin with radio-platinum, administer it to a tumor-bearing mouse, and perform imaging experiments.

Table. 1. Useful platinum radionuclides for GREI.

Nuclide	Half-lives	γ-ray enegies and intensities (keV (%))
^{188}Pt	10.2 d	187.6 (19.4) 195.1 (18.6) 381.4 (7.5) 423.3 (4.4) 140.4 (2.3)
^{189}Pt	10.9 h	721.4 (9.3) 94.3 (7.6) 568.8 (7.1) 243.4 (7.0) 544.9 (5.8)
^{191}Pt	2.8 d	538.9 (13.7) 409.4 (8.0) 359.9 (6.0) 82.4 (4.9) 172.2 (3.5)

Data from IAEA

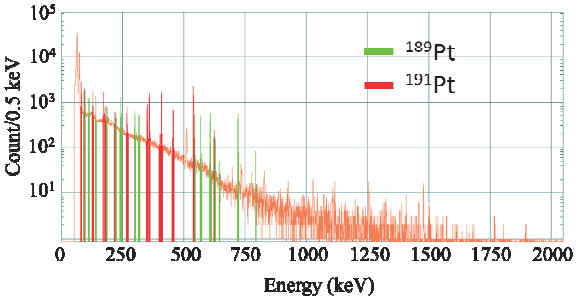

Fig. 1. Gamma-ray spectrum of produced nuclides in irradiated target.

References

1) S. Motomura et al.: J. Anal. At. Spectrom. **28** (6), 934 (2013).
2) M. Kartalou et al.: Mutat. Res.-Fund. Mol. M. **478**.1, 23 (2001).
3) M. Bonardi et al.: J. Radioanal. Nucl. Chem. **236**.1-2, 159, (1998).

[*1] Graduate school of Medicine, Dentistry, and Pharmaceutical Sciences, Okayama University
[*2] RIKEN Center for Life Science Technologies
[*3] RIKEN Nishina Center

Production of ^{88}Y for gamma-ray emission imaging

K. Higashikawa,[*1,*2] A. Morioka,[*1] H. Haba,[*3] M. Ueda,[*1] T. Fukuchi,[*4] and S. Enomoto[*1,*4]

Radioimmunotherapy (RIT) is an internal radiation therapy that uses radiolabeled drugs, in particular particularly in monoclonal antibodies (mAbs) or peptides. ^{90}Y emits highly cytotoxic β^- ray and is thus a promising radionuclide for use in RIT. However, ^{90}Y cannot be readily imaged by nuclear medicine imaging modalities, because ^{90}Y is a pure β^- emitter.[1] On the other hand, ^{86}Y emits β^+ rays, which can be detected by PET.[1-3] In addition, ^{86}Y-labeled drugs (mAbs or peptides) display identical biodistributions to ^{90}Y-labeled drugs because ^{86}Y is chemically identical to ^{90}Y.[1] Therefore, in recent years, ^{86}Y has attracted attention as an attractive surrogate for studying ^{90}Y-labeled drugs. However, the physical half-life of ^{86}Y ($T_{1/2}$ = 14.7 h) is shorter compared to that of ^{90}Y ($T_{1/2}$ = 64.1 h), and thus, it is not suitable as a surrogate for investigating serial biodistribution of RIT drugs with long biological half-lives, such as mAb, which remain circulating in vivo for weeks.[4] A chemically identical surrogate with a longer half-life is desirable for development phases of ^{90}Y-labeled drugs.

^{88}Y is chemically identical to ^{90}Y and has a long half-life of $T_{1/2}$ = 106.6 d. Moreover, ^{88}Y emits γ rays with energies of 898 and 1836 keV, which can be detected using semiconductor Compton cameras through gamma-ray emission imaging (GREI).[5] Therefore, the imaging of ^{88}Y-labeled drugs with GREI has the potential ability to investigate the serial biodistribution of ^{90}Y-labeled drugs with a long biological half-life, in particular, in preclinical studies. The final purpose of our study is to develop an imaging method for ^{88}Y-labeled drugs through GREI. In this study, we produced ^{88}Y for the GREI experiment.

^{88}Y was produced by the ^{nat}Sr(d,x)^{88}Y reactions. To prepare a ^{nat}SrO pellet target with a diameter of 10 mm, approximately 400 mg of $^{nat}SrCO_3$ (Wako Pure Chemical Industries, Ltd., chemical purity: 99.99%) was heated for 2 h at 1000˚C and pressed at 1.6 t. The pellet was covered with a 10-μm Al foil (chemical purity: 99.999%). The target was irradiated with a 24-MeV deuteron beam supplied from the RIKEN AVF cyclotron. The irradiation was performed for 5 h at a beam current of approximately 1.5 particle μA.

Thirty-nine days after the irradiations, ^{88}Y was chemically isolated from the ^{nat}SrO target by extraction chromatography using Ln-resin (Eichrom Technologies, Inc., particle size: 50-100 μm) filled in a Muromac column (Muromachi Technos Co., Ltd., internal diameter: 5 mm, height: 50 mm). The Ln-resin column was washed in advance with 3 mL of water, 10 mL of 10 M HNO_3, and then 4 mL of water, and was pre-equilibrated with 2 mL of 1 M HNO_3. The irradiated ^{nat}SrO target was dissolved in 1 M HCl and evaporated to dryness on a hot plate and under a heat lamp. The residue was dissolved in 5 mL of 1 M HNO_3, and was evaporated to dryness. Subsequently, the residue was dissolved in 5 mL of water and 2 mL of 1 M HNO_3, and was evaporated to dryness. Then, the residue was dissolved in 2 mL of 1 M HNO_3 and loaded onto the Ln-resin column. The resin was then washed with 16 mL of 1 M HNO_3. ^{88}Y was eluted from the resin with 10 mL of 10 M HNO_3. The eluted solution was heated to dryness, and 2 M HCl was added to the residue.

The γ-ray spectrum of the final purified product is shown in Fig. 1. Approximately 10 MBq of ^{88}Y was obtained. The radiochemical yield of ^{88}Y in the chemical isolation process was approximately 80%. In the next experiment, we plan to synthesize ^{88}Y-labeled drugs and try to visualize their biodistirbution using GREI.

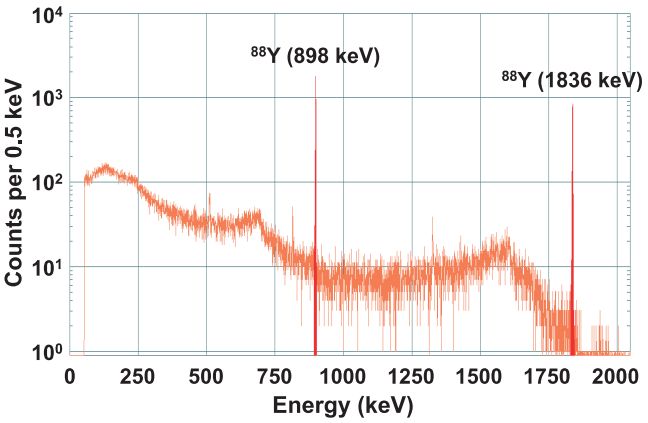

Fig. 1. Gamma-ray spectrum of ^{88}Y after the chemical isolation.

References

1) T. K. Nayak et al.: Med. Chem. **7**(5), 380 (2011).
2) S. Palm et al.: J. Nucl. Med. **44**(7), 1148 (2003).
3) T. K. Nayak et al.: Eur. J. Nucl. Med. Mol. Imaging. **37**, 1368 (2010).
4) D. R. Mould et al.: Curr. Opin. Drug Discov. Devel. **10**(1), 84 (2007).
5) S. Motomura et al.: J. Anal. At. Spectrom. **23**, 1089 (2008).

*1 Department of Pharmaceutical Analytical Chemistry, Graduate school of Medicine, Dentistry, and Pharmaceutical Sciences, Okayama University
*2 Japan Society for the Promotion of Science
*3 RIKEN Nishina Center
*4 Next-Generation Imaging Team, RIKEN

^{99}Ru Mössbauer spectroscopy of Na-ion butteries of Na_2RuO_3 (I)

Y. Kobayashi,[*1,*2] M. Okubo,[*3] H. Haba,[*1] and A. Yamada[*3]

Sodium-ion batteries have attracted considerable attention recently, because of their potential for large-scale applications: higher power and less expensive batteries compared to Li-ion batteries can be realized by utilizing abundant and polarizable sodium ion as a mobile charge carrier. One of the main obstacles to realizing high performance sodium-ion batteries is the low specific capacity of the electrode materials. Thus, it is particularly important to develop novel Na-ion cathode materials with a high capacity as well as a high operating potential.

Our group has recently reported the electrochemical properties of Na excess transition metal oxide $Na[Na_{1/3}Ru_{2/3}]O_2$, where the cation arrangement in the $[Na_{1/3}Ru_{2/3}]$ layer is controlled between the ordered and disordered states by synthetic conditions. Importantly, the ordered and disordered $Na[Na_{1/3}Ru_{2/3}]O_2$ exhibit significant differences in the electrochemical properties[1]. In this work, we conducted Ru Mössbauer spectroscopy for the ordered and disordered $Na[Na_{1/3}Ru_{2/3}]O_2$ to clarify the valence states of Ru ions during desodiation/sodiation.

The source nuclide, ^{99}Rh ($T_{1/2}$=15.0 d) for ^{99}Ru Mössbauer spectroscopy was produced via the ^{99}Ru (p,n) ^{99}Rh reaction. The 96%-enriched ^{99}Ru metal powder was irradiated by protons with E = 12 MeV and I = 10 μA at the AVF Cyclotron. The ^{99}Ru metal powder was packed into an Al holder, which was tightly fixed to the irradiation equipment for cooling by He gas flow and water flow during the irradiation. After irradiation for about 24 hours, the target was used as a ^{99}Rh Mössbauer source without being subjected to annealing or chemical treatment[2].

^{99}Ru absorption Mössbauer spectra of $Na[Na_{1/3}Ru_{2/3}]O_2$ samples were obtained using a conventional Mössbauer spectrometer. Owing to the relatively high energy of the Mössbauer γ-ray (89.8 keV), both the source and the absorbers were maintained at liquid-helium temperature in a cryostat.

The obtained spectra are shown in Fig. 1 and 2. The Mössbauer spectrum for the disordered $Na[Na_{1/3}Ru_{2/3}]O_2$ (Fig. 1 (a)) shows a broad singlet with isomer shift (δ) of −0.30 mm/s and linewidth (Γ) of 0.95 mm/s. The δ value is typical of Ru^{IV}, although the large linewidth suggests structural disorder around Ru. The Mössbauer spectrum for the ordered $Na[Na_{1/3}Ru_{2/3}]O_2$ (Fig. 1 (b)) shows a singlet with δ = −0.27 mm/s and Γ = 0.63 mm/s, indicating Ru^{IV}. Thus, regardless of the synthetic conditions, the valence states of Ru in both compounds are the same. However, the linewidth for the ordered compound is much smaller than that of the disordered one, most likely due to the ordered honeycomb arrangement of Na and Ru in the $[Na_{1/3}Ru_{2/3}]$ layer.

On charging the ordered compound, the Mössbauer spectrum, as shown in Fig.2, cannot determine the electronic structure accurately, in part due to the small amounts of the obtained sample. However, a preliminary result indicates oxidation of Ru from tetravalent to pentavalent, from the obtained δ value of +0.21 mm/s with a small quadrupole splitting of 0.60 mm/s. Further experiments with a larger amount of samples are now in progress to reveal the reaction mechanism of $Na[Na_{1/3}Ru_{2/3}]O_2$.

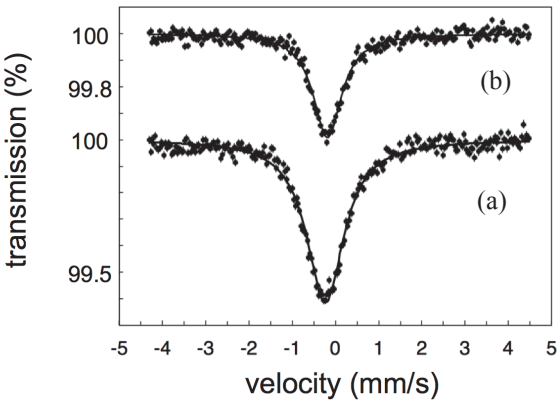

Fig. 1. ^{99}Ru Mössbauer spectra of (a) disordered and (b) ordered $Na[Na_{1/3}Ru_{2/3}]O_2$ at 4.2 K.

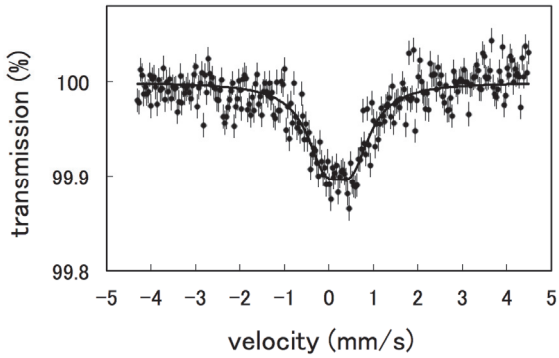

Fig. 2. ^{99}Ru Mössbauer spectra at 4.2 K of the ordered $Na[Na_{1/3}Ru_{2/3}]O_2$ after electric charge.

*1 RIKEN Nishina Center
*2 University of Electro-Commun.
*3 University of Tokyo

References

1) M. Tamaru, et al., Electrochem. Commun. **33**, 23 (2013).
2) Y. Kobayashi et al., J. Phys. **217**, 012023 (2010).

Production of ^{262,263}Db in the ^{248}Cm(^{19}F,xn)$^{267-x}$Db reactions at E_{lab} = 96 MeV

M. Murakami,[*1,*2] S. Goto,[*1] K. Ooe,[*1] D. Sato,[*1] S. Tsuto,[*1] N. Goto,[*1] T. Koyama,[*1] R. Aono,[*1] H. Haba,[*2] M. Huang,[*2] and H. Kudo[*1]

The isotope ^{262}Db ($T_{1/2}$ = 33.8 s[1)]) is often used in the chemical studies of element 105, Db. At RIKEN, the decay properties of ^{262}Db produced in the ^{248}Cm(^{19}F,5n)^{262}Db reaction were recently studied with a gas-jet transport system coupled to the gas-filled recoil ion separator GARIS.[1)] In this study, however, ^{263}Db produced in the 4n channel was not observed at 97.4 MeV and 103.1 MeV. The upper-limit cross sections of ^{263}Db were rather smaller than those predicted by the HIVAP code, which reproduced the 5n channel fairly well. Therefore, in this work, we investigated the production of Db isotopes at a lower energy of 96 MeV, at which the predicted excitation function for ^{263}Db exhibits the maximum.

A $^{248}Cm_2O_3$ target of 460 μg/cm^2 thickness was prepared by electrodeposition onto a Be backing foil of 1.8-mg/cm^2 thickness. $^{nat}Gd_2O_3$ of 23-μg/cm^2 thickness was admixed with the target material to simultaneously produce ^{170}Ta ($T_{1/2}$ = 6.76 min) via the ^{nat}Gd(^{19}F,xn)^{170}Ta reaction. A $^{19}F^{7+}$ beam was supplied by the AVF cyclotron. The beam energy at the middle of the target was 96.2 MeV, and the energy degradation in the target was estimated to be 1.0 MeV. The average beam intensity was 450 pnA.

The reaction products recoiling out of the target were continuously transported by a He/KCl gas-jet system to the rotating wheel detection system MANON. The transport efficiency was estimated to be 74%. Other details of the measurement were similar to those in our previous study.[2)]

We searched for time-correlated α-α event pairs at the α-energy range of 8.0 $\leq E_\alpha \leq$ 9.0 MeV. On setting the time window to 25 s, 16 α-α correlations were found. Figure 1(a) shows the two-dimensional arrays of these α-α correlations. In Fig. 1(a), 74 α-α correlations assigned to the decay chain ^{262}Db $\xrightarrow{\alpha}$ ^{258}Lr $\xrightarrow{\alpha}$ in the previous experiment[1)] are compared. The α-particle spectra of the parent and daughter nuclides are shown in Figs. 1(b) and (c), respectively. For the parent α spectrum, the 8.46-MeV α line of ^{262}Db is seen, while the 8.68-MeV α line was not very clear owing to the low counting statistics. On the other hand, the α lines of ^{258}Lr were clearly found in the daughter α spectrum.

In Fig. 1(a), a solid box indicates the gated α-energy range of the parent ^{262}Db (8.26–8.83 MeV) and the daughter ^{258}Lr (8.36–8.80 MeV). Fourteen events are found in this energy region. The deduced half-life of the daughter nuclide, $T_{1/2} = 4.5^{+1.7}_{-1.0}$ s, is in agreement with the reported half-life of ^{258}Lr, $T_{1/2}$ = 3.9 s.[3)] Thus, these events are attributed to the α decay chain ^{262}Db $\xrightarrow{\alpha}$ ^{258}Lr $\xrightarrow{\alpha}$. The expected number of random correlations was evaluated to be 0.3 in this energy region. Regarding all 14 events as true ones, the production cross section of ^{262}Db is derived as $\sigma = 0.25^{+0.08}_{-0.07}$ nb. This cross section is consistent with the previously reported one, $\sigma = 0.23^{+0.18}_{-0.11}$ nb at 97.4 MeV.[1)]

Only one α-α correlation was found around the energy regions of ^{263}Db and its α-decay daughter ^{259}Lr, as shown by an arrow in Fig. 1(a). Although this number of the event, one, is comparable with the expected number of random events, the deduced half-life of the daughter nucleus, $T_{1/2} = 3.1^{+14.8}_{-1.4}$ s, is consistent with the reported half-life of ^{259}Lr ($T_{1/2}$ = 6.2 s[3)]). If this event is regarded as a true one, the cross section of ^{263}Db is deduced to be $\sigma = 0.031^{+0.072}_{-0.026}$ nb, which is one order of magnitude smaller than that of ^{262}Db as well as the HIVAP predictions.[1)]

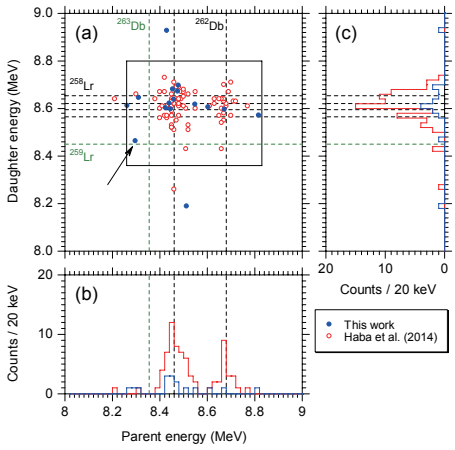

Fig. 1. (a) Two-dimensional representation of time-correlated events. (b) α spectrum of parent nuclei. (c) α spectrum of daughter nuclei.

References

1) H. Haba et al.: Phys. Rev. C **89**, 024618 (2014).
2) M. Murakami et al.: RIKEN Accel. Prog. Rep. **47**, 265 (2014)
3) R. B. Firestone and V. S. Shirley: *Table of Isotopes, 8th ed.* (John Wiley & Sons, 1996).

*1 Department of Chemistry, Niigata University
*2 RIKEN Nishina Center

Production of ^{174}Re in the ^{nat}Gd(^{23}Na,*xn*) reactions for future studies on Bh chemistry using GARIS

H. Haba,[*1] R. Aono,[*2] D. Kaji,[*1] Y. Kasamatsu,[*3] H. Kikunaga,[*4] Y. Komori,[*1] H. Kudo,[*2] K. Morimoto,[*1] K. Morita,[*1] M. Murakami,[*1] K. Nishio,[*5] A. Shinohara,[*3] M. Takeyama,[*1] T. Tanaka,[*1] S. Tsuto,[*2] Y. Wakabayashi,[*1] S. Yamaki,[*1] and T. Yokokita[*3]

We have been developing a gas-jet transport system coupled to GARIS as a novel technique for superheavy element (SHE) chemistry.[1)] So far, isotopes of ^{261}Rf (atomic number Z = 104), ^{262}Db (Z = 105), and ^{265}Sg (Z = 106) have been produced in the ^{248}Cm(^{18}O,5*n*), ^{248}Cm(^{19}F,5*n*), and ^{248}Cm(^{22}Ne,5*n*) reactions, respectively, and the production and decay properties of these isotopes have been investigated for chemical studies.[1–3)] Recently, the chemical synthesis and gas-chromatographic analysis of Sg(CO)$_6$ were successfully conducted with ^{265}Sg.[4)] We plan to obtain a heavier element, Bh (Z = 107), by investigating production conditions of ^{266,267}Bh in the ^{248}Cm(^{23}Na,*xn*) reactions. In this work, as the first step, we optimized setting parameters of the GARIS gas-jet system using ^{174}Re produced in the ^{nat}Gd(^{23}Na,*xn*) reactions. Since Re is a homologous element of Bh in the periodic table, the Re isotopes would be useful in fundamental experiments on Bh chemistry in the future.

The ^{nat}Gd$_2$O$_3$ target with a thickness of 340 μg cm^{-2} was prepared by electrodeposition onto a 2-μm Ti foil. The ^{23}Na^{7+} ion beam was extracted from RILAC. The beam energy was 130.6 MeV at the middle of the target, and the typical beam intensity was 1.4 particle μA. The evaporation residues (ERs) were separated by GARIS. Several magnetic rigidities were investigated ($B\rho$ = 1.58–1.94 Tm) at a He pressure of 33 Pa. Then, the ERs were guided into a gas-jet chamber of 100-mm depth through a 0.7-μm Mylar window. The ERs were transported by a He/KCl gas-jet to a chemistry laboratory. The He flow rate was 5 L min^{-1}, and the chamber pressure was 78 kPa. The KCl aerosols were then collected on a glass filter for 60 s and subjected to γ-ray spectrometry with a Ge detector after a cooling time of 60 s. A 20-μm Al foil was placed at the entrance of the gas-jet chamber to evaluate the gas-jet transport efficiency.

Figure 1 shows a typical γ-ray spectrum observed in the ^{nat}Gd(^{23}Na,*xn*) reactions. In this work, the γ-rays of $^{172–177}$Re and ^{172,173}W were identified in the spectra. The decay curve of the 243.4-keV γ-ray of ^{174}Re is shown in the inset of Fig. 1. The half-life of ^{174}Re was determined to be $T_{1/2}$ = 2.40 ± 0.04 min, which agreed with that in the literature.[5)] Figure 2 shows the variation in the yield of ^{174}Re as a function of magnetic rigidity. The dashed curve represents the result of the least-squares fitting with the Gaussian curve with a maximum yield at $B\rho$ = 1.74 ± 0.01 Tm and a resolution of $\Delta B\rho/B\rho$ = 10.0 ± 0.4%. This optimum $B\rho$ agrees well with that ($B\rho$ = 1.78 ± 0.05 Tm) deduced from our systematic trend for the low-energy recoil ions.[6)] The gas-jet transport efficiency was about 80%. The radioactivity of ^{174}Re available at the chemistry laboratory is 55 ± 2 kBq pμA^{-1} after the 60-s aerosol collection. This yield is high enough to allow development of chemistry apparatuses and investigation of chemical systems for the study of Bh chemistry in the future.

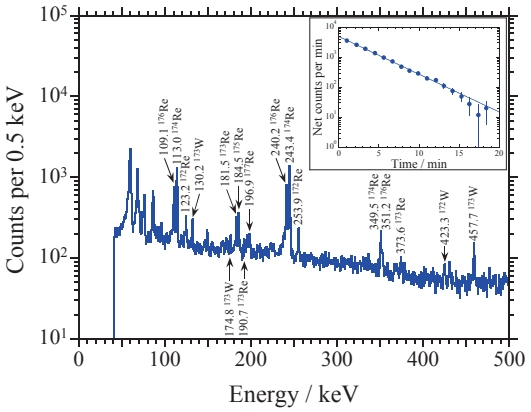

Fig. 1. Typical γ-ray spectrum observed in the ^{nat}Gd(^{23}Na,*xn*) reactions at $B\rho$ = 1.74 Tm.

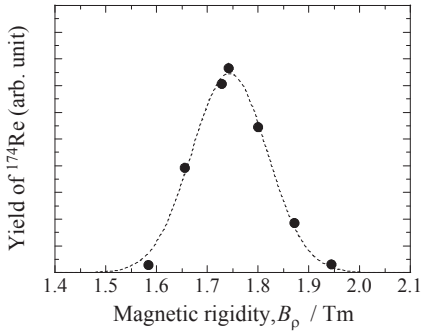

Fig. 2. The yield of ^{174}Re as a function of magnetic rigidity.

*1 RIKEN Nishina Center
*2 Department of Chemistry, Niigata University
*3 Graduate School of Science, Osaka University
*4 Research Center for Electron Photon Science, Tohoku University
*5 Advanced Science Research Center, JAEA

References

1) H. Haba et al.: Chem. Lett. **38**, 426 (2009).
2) H. Haba et al.: Phys. Rev. C **85**, 024611 (2012).
3) H. Haba et al.: Phys. Rev. C **89**, 024618 (2014).
4) J. Even et al.: Science **345**, 1491 (2014).
5) R. B. Firestone and V. S. Shirley: *Table of Isotopes, 8th ed.* (John Wiley & Sons, New York, 1996).
6) D. Kaji et al.: Proc. Radiochim. Acta **1**, 105 (2011).

Excitation function of the ^{nat}Hf(α,x)^{182g}Ta reaction: Cyclotron production of a long-lived γ-ray emitter ^{182g}Ta

M. Murakami,[*1,*2] H. Haba,[*1] and H. Kudo[*2]

We previously investigated the production of ^{179}Ta ($T_{1/2}$ = 1.82 y) in the proton- and deuteron-induced reactions on ^{nat}Hf[1,2] for basic chemical studies of the 105th element Db, which must be conducted at a single-atom scale. Although the long half-life of ^{179}Ta is convenient for such the chemical experiments, the decay characteristics of ^{179}Ta are less suitable: ^{179}Ta does not emit any γ ray in its EC decay, and it must be traced by measuring the characteristic X rays of Hf, which are often interfared by X or γ rays of other nuclides.

Another long-lived Ta isotope, ^{182g}Ta ($T_{1/2}$ = 114.74 d), is a γ-emitting isotope, and it has also been used as a radiotracer to explore the chemical behavior of Ta. ^{182g}Ta is usually produced by the ^{181}Ta(n_{th},γ) reaction with a high cross section of 20.5 ± 0.5 b.[3] However, the ^{182g}Ta radiotracer produced in this way is undesirable for basic studies of Db, because it is obtained with a macro amount of the target material of Ta.

Very recently, Tárkányi et al. measured the cross sections of W, Ta, and Hf isotopes in the ^{nat}Hf(α,x) reactions up to 40 MeV.[4] As shown in Fig. 1, they reported that the excitation function for the ^{nat}Hf(α,x)^{182g}Ta reaction increased with the beam energy. Because the ^{182g}Ta tracer with high specific radioactivity can be obtained with this reaction, we further studied the production of ^{182g}Ta in this reaction.

The excitation functions were measured by a stacked-foil activation technique. 11 pairs of thin metallic foils of ^{nat}Hf (97% chemical purity, 23 μm thickness) and ^{nat}Cu (99.9% chemical purity, 9 μm thickness) were stacked in an alternating sequence. The ^{nat}Cu foils were used for monitoring the beam current and energy by measuring the well-established ^{nat}Cu(α,x)^{67}Ga excitation function.[5] The size of the all foils was 15 × 15 mm^2. The stack was bombarded by a 50-MeV α beam supplied by the AVF cyclotron for 31 min. The beam was collimated within 9 mm in diameter and the average beam current was 0.23 μA. After the bombardment and the proper cooling duration, each foil was subjected to γ-ray spectrometry with a Ge detector.

The production cross sections were derived by the well-known activation formula.[6] The beam energies in the individual target foils were calculated with the SRIM-2008 program.[7] The experimental cross sections were compared with the calculated ones by the TALYS-1.6 code.[8]

In this work, independent cross sections were obtained for the ^{nat}Hf(α,x)^{176,177,178}W, ^{178,183}Ta, ^{179m2,181}Hf reactions, while cumulative ones were obtained for ^{nat}Hf(α,x)^{175,176,177,182g}Ta, ^{175}Hf. The measured cross sections of the ^{nat}Hf(α,x)^{182g}Ta reaction are shown in Fig. 1 along with the calculated ones. The cross sections in the energy range of 41–50 MeV were measured for the first time. The excitation function exhibits the maximum cross section of 8.3 ± 0.3 mb at 41.5 ± 1.2 MeV. The data of Tárkányi et al.[4] are consistent with the present data at ≥30.7 MeV, while that at 27.6 ± 0.7 MeV (0.2 ± 0.3 mb) is much smaller than the present one of 1.60 ± 0.08 mb at 27.2 ± 1.6 MeV. The cross sections calculated by the TALYS-1.6 code[8] show systematically lower values with a similar shape of the excitation function.

The physical thick-target yield was deduced from the measured cross sections and the calculated stopping power by the SRIM-2008 program.[7] The deduced yield of ^{182g}Ta was 5.2 kBq/μAh at 50 MeV.

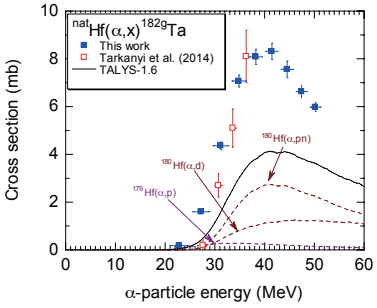

Fig. 1. Excitation function of the ^{nat}Hf(α,x)^{182g}Ta reaction. Dashed curves indicate the individual reaction channels evaluated by the TALYS-1.6 code.[8]

*1 RIKEN Nishina Center
*2 Department of Chemistry, Niigata University

References
1) M. Murakami et al.: Appl. Radiat. Isot. **90**, 149 (2014).
2) M. Murakami et al.: RIKEN Accel. Prog. Rep. **47**,266 (2014)
3) S. F. Mughabghab: in *Atlas of neuteron resonances* (Elsevier Science, 2006).
4) F. Tárkányi et al.: Appl. Radiat. Isot. **91**, 114 (2014).
5) IAEA report IAEA-TECDOC-1211 (2007).
6) M. S. Uddin et al.: Nucl. Instrum. Methods Phys. Res. B **258**, 313 (2007).
7) J. F. Ziegler et al.: Nucl. Instrum. Methods Phys. Res. B **268**, 1818 (2010).
8) A. J. Koning et al.: in *Proceedings of the International Conference on Nuclear Data for Science and Technology*, edited by O. Bersillon et al. (EDP Sciences, 2008), p. 211.

Production cross sections of (*d,x*) reactions on natural ytterbium†

M. U. Khandaker*1,*2 and H. Haba*2

The method for obtaining accurate information of light-charged-particle-induced reaction cross sections has generated significant interest in the nuclear data community because these reactions are being increasingly used in nuclear medicine, accelerator and nuclear technology, and the testing of nuclear reaction theories. Recently, we investigated deuteron-induced reaction cross sections from various target elements because measured data of the (*d,x*) processes are limited compared to those of (*p,x*) processes. A survey of literature shows that several investigations have been conducted for the ^{nat}Yb(*d,x*) reactions leading to various applications. As an example, the production of the ^{177}Lu radionuclide via the ^{nat}Yb(*d,x*) reaction finds applications in internal radiotheraphy and imaging procedures [1,2]. Its half-life is long enough to allow sophisticated preparation (e.g., shipping, labelling, purification etc.) for use without any significant loss of activity. ^{177}Lu can be produced in principle in several ways. Currently, a large scale production of ^{177}Lu is in practice by using only the high flux nuclear reactor via the direct ^{176}Lu(n,γ)^{177}Lu or indirect ^{176}Yb(n,γ)^{177}Yb→^{177}Lu routes followed by a complex separation procedure of ^{177}Lu from the Yb isotopes [3]. On the other hand, the carrier-free ^{177}Lu is available in the charged-particle irradiations on various targets, though its activity is relatively lower than those in the reactor productions. However, it may be possible to overcome this deficiency with recent high-power accelerator technologies, which enable large scale and on-site productions of ^{177}Lu leading to its various practical applications.

The objective of the present study was to report the latest cross sections of the ^{nat}Yb(*d,x*)^{169,170,171,172,173,174m,174,176m,177g}Lu and ^{169,175,177}Yb reactions that were measured with a high precision over the energy range of 2–24 MeV using the AVF cyclotron facility of the RIKEN RI Beam Factory, Wako, Japan. Details on the irradiation technique, radioactivity determination, and data evaluation procedures are available in Ref.[4]. Owing to the space limitation of this report, we present only the ^{nat}Yb(*d,x*)^{177g}Lu cross sections and the deduced yield in Figs. 1 and 2, respectively. Measured cross sections with an overall uncertainty of about 12.8% are listed in Ref.[4]. The cross-sections were normalized by using the ^{nat}Ti(*d,x*)^{48}V monitor cross sections recommended by IAEA. Measured data were critically compared with the available literature data, and an overall good agreement was found. However, only partial agreements were obtained with the data extracted from the TENDL-2013 library based on the TALYS code.

The deduced thick-target yields indicate that a low amount of no-carrier-added radioactivity of ^{177g}Lu (2.4 MBq/μA-h) could be obtained by irradiating an enriched ^{176}Yb target with 11-MeV deuteron energy from a cyclotron.

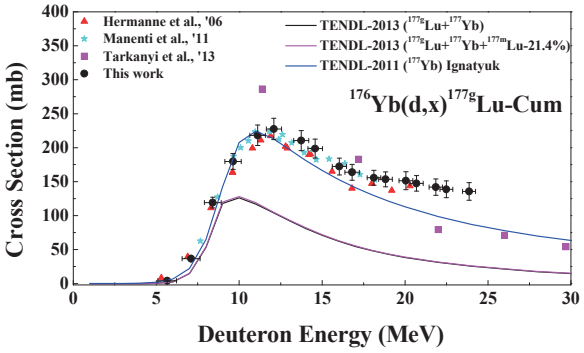

Fig. 1. Excitation function of the ^{nat}Yb(*d,x*)^{177g}Lu reaction.

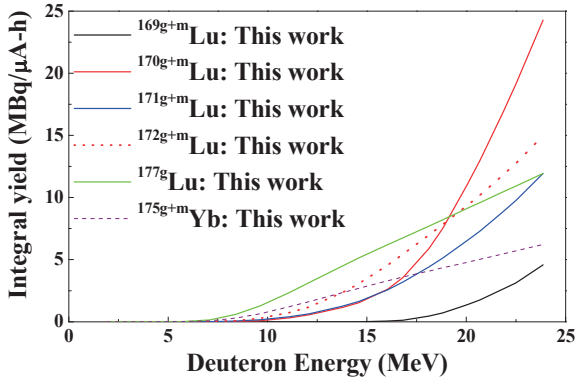

Fig. 2. Physical thick target yields for the $^{169g+m,170g+m,171g+m,172g+m,177g}$Lu and $^{175g+m}$Yb radionuclides.

References

1) J. J. Teunissen, D. J. Kwekkeboom, E. P. Krenning: J. Clin. Oncol. **22**, 2724 (2004).
2) M. R. A. Pillai, S. Chakraborty et al.: Appl. Radiat. Isot. **59**, 109 (2003).
3) E. P. Horwitz, D. R. McAlister et al.: Appl. Radiat. Isot. **63**, 23 (2005).
4) M. U. Khandaker, H. Haba et al.: Nucl. Instrum. Meths Phys. Res. B **335**, 8 (2014).

† Condensed from the article in Nucl. Inst. Meths. B. **335**, 8 (2014).

*1 Department of Physics, University of Malaya
*2 RIKEN Nishina Center

Measurement of production cross sections of Tc isotopes in the ^{nat}Mo(d,x) reactions

Y. Komori,[*1] M. Murakami,[*1] and H. Haba[*1]

Chemical characterization of superheavy elements is one of the important and challenging subjects in the field of nuclear chemistry. We plan to conduct model experiments for chemical studies of element 107, Bh using radiotracers of its homologs, Tc and Re. Relatively long-lived isotopes, ^{95m}Tc ($T_{1/2}$ = 61 d) and ^{184g}Re ($T_{1/2}$ = 35.4 d) are useful for tracer experiments. In the field of nuclear medicine, the isotope ^{99m}Tc, the daughter nuclide of ^{99}Mo, is the most widely used for diagnostic imaging. Recently, the direct production of ^{99}Mo/^{99m}Tc using an accelerator has attracted much attention. In this work, production cross sections of deuteron-induced nuclear reactions on ^{nat}Mo (nat: natural isotopic abundance) have been measured up to 24 MeV for the quantitative production of Tc isotopes. The results are discussed by referring to previously reported data and the theoretical model code TALYS.[1)]

The production cross sections were measured using a stacked-foil technique. Seventeen ^{nat}Mo foils (99.95% purity, 20.9 mg/cm^2 thickness), sixteen ^{nat}Ti foils (99.5% purity, 9.2 mg/cm^2 thickness), and sixteen ^{nat}Ta foils (99.95% purity,16.1 mg/cm^2 thickness) were stacked in the order ofMo/Ti/Ta. The Ti foils were used to calibrate the beam current and the incident energy via the monitor reaction ^{nat}Ti(d,x)^{48}V.[2)] The Ta foils were used to attenuate the beam energy. The size of all foils was 15 × 15 mm^2. The target stack of the Mo/Ti/Ta foils was irradiated for 1 h with a 24-MeV deuteron beam supplied from the RIKEN AVF cyclotron. The average beam current was 0.17 μA. After the irradiation, each foil was subjected to γ-ray spectrometry with a Ge detector.

The excitation functions were measured for the ^{nat}Mo(d,x)^{93m,93g,94m,94g,95m,95g,96m,96g,97m,99m}Tc, ^{93m,99,101}Mo, ^{90g,92m,95m,95g,96g}Nb, and ^{89g}Zr reactions. Figure 1 shows the excitation function of the ^{nat}Mo(d,x)^{95m}Tc reaction. Our results are in good agreement with the previously reported data.[3–5)] It can be seen that the TALYS code (TENDL-2013) underestimates the cross sections at deuteron energies exceeding 10 MeV. For the other reactions, most of our results are in good agreement with those of previous studies. We measured the production cross section of ^{97m}Tc ($T_{1/2}$ = 91 d) in the deuteron energy range of 14–24 MeV for the first time. It was found that the TALYS code qualitatively reproduces the shape of these excitation functions, though there is little agreement between the experimental cross sections and the theoretical values.

Thick-target yields for all the investigated Tc, Mo, Nb, and Zr isotopes were deduced from the measured production cross sections. Figure 2 shows the thick-target yields of the Tc isotopes as a function of the deuteron energy. The deduced yield of ^{95m}Tc at 23.7 MeV is 0.36 MBq/μA·h. For ^{99}Mo and ^{99m}Tc, the deduced yields at 23.7 MeV are 9.6 and 40 MBq/μA·h, respectively. To increase the production yields of ^{99}Mo/^{99m}Tc and to reduce radioactivities from by-reaction products, the use of enriched ^{98}Mo and ^{100}Mo targets is favorable. Based on the present results, we will produce ^{95m}Tc for the model experiments on Bh chemistry. We will also develop a simple and efficient chemical separation scheme to obtain no-carrier-added Tc tracer from the Mo target.

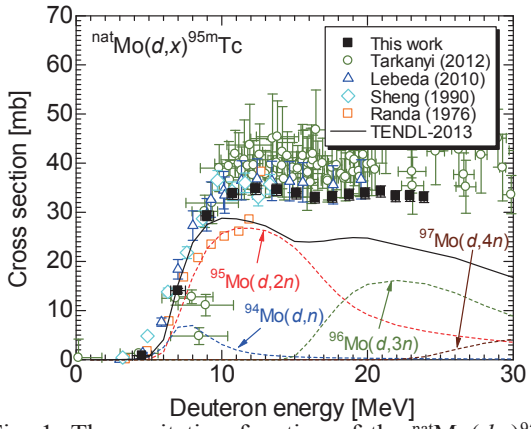

Fig. 1. The excitation function of the ^{nat}Mo(d,x)^{95m}Tc reaction.

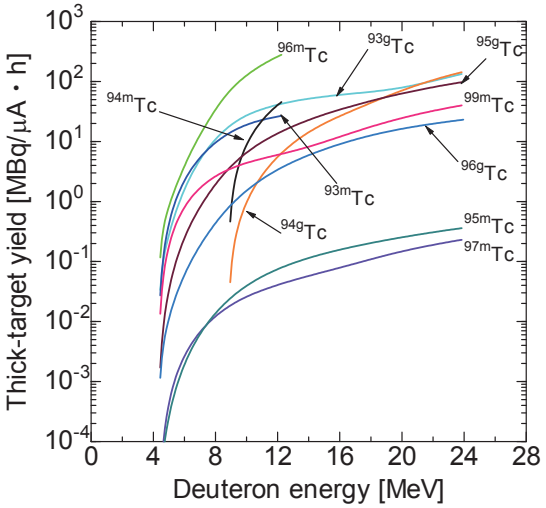

Fig. 2. Thick-target yields of the Tc isotopes expressed as radioactivities after 1-h irradiation with 1 μA.

References

1) A. J. Koning et al.: TENDL-2013: TALYS-based Evaluated Nuclear Data Library, 2013.
2) IAEA: IAEA report IAEA-TECDOC-1211, 2007.
3) W. Sheng et al.: Inst. Nucl. Sci. Technol. Sichuan Univ. Rep., NST-004 (1990).
4) O. Lebeda et al.: Appl. Radiat. Isot. 68, 2425 (2010).
5) F. Tárkányi et al.: Nucl. Instrum. Meth. B 274, 1 (2012)

*1 RIKEN Nishina Center

Measurements of alpha-induced cross section for ^{48}Cr and ^{49}Cr up to 50 MeV

H. Kikunaga,[*1,*2] M. Murakami,[*3,*2] Y. Komori,[*2] and H. Haba[*2]

Chromium is one of the essential trace elements in some animals but it also can be toxic in high concentrations. Understanding the behavior of chromium in animals, plants, and the environment is important and influential on the various fields such as biological sciences.

The radioactive tracer technique has been widely recognized as a powerful tool for behavior analysis of elements in trace amounts. The isotopes ^{48}Cr ($T_{1/2}$ = 21.6 h), ^{49}Cr ($T_{1/2}$ = 42.3 m), and ^{51}Cr ($T_{1/2}$ = 27.7 d) have potential as tracers because of their suitable half-lives. In this work, the cross sections for the reactions ^{nat}Ti(α, X)^{48}Cr and ^{nat}Ti(α, X)^{49}Cr up to 50 MeV were measured to produce these isotopes efficiently.

The excitation functions of these reactions were measured by the stacked-foil technique. The target stack containing 20 natural Ti foils (99.5% pure) with thickness of 20 and 40 μm were irradiated with a α-particle beam delivered from the RIKEN K70 AVF Cyclotron for 30 min. The cyclotron was operated at a beam energy of 50.4 MeV, which was confirmed by TOF measurement, with a mean current of around 0.4 μA.

After the irradiation, the target foils were enclosed in a polyethylene film separately and were subjected to γ-ray spectrometry using a high-purity germanium detector. The incident beam energy and flux were determined by activation of the monitor foil technique using the ^{nat}Ti(α, X)^{51}Cr reaction. The reference data were obtained from the IAEA Reference Data[1]. The energy loss in each foil was calculated using the TRIM code[2].

A γ-ray spectrum of a Ti foil sample at an effective energy of around 50 MeV is shown in Fig. 1. The γ-peaks of scandium, vanadium, and chromium are observed in the spectrum. During the tracer preparation, it is necessary to separate chromium from titanium and the other elements.

The cross sections for the ^{nat}Ti(α, X)^{48}Cr and ^{nat}Ti(α, X)^{49}Cr reaction obtained in this work are shown in Fig. 2. For comparison, the earlier experimental data[3–6] of the ^{nat}Ti(α, X)^{48}Cr reaction and the values calculated using the Talys 1.6 code[7] with default parameters are included in Fig. 1. The cross sections of ^{48}Cr obtained in this work is in good agreement with the earlier experimental data. The calculated values with the Talys code reproduce the experimental values of ^{48}Cr and ^{49}Cr with a reasonable accuracy although each peak position of the excitation functions is deviated slightly.

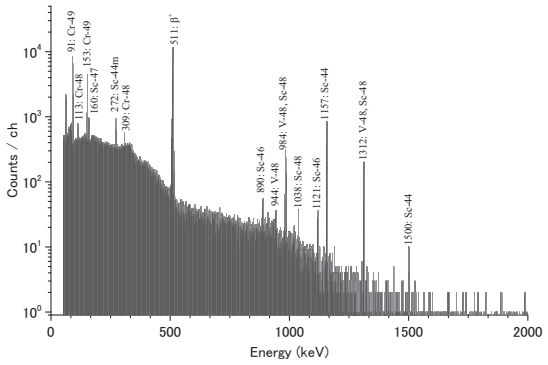

Fig. 1. A γ-ray spectrum of a Ti foil sample at an effective energy of around 50 MeV.

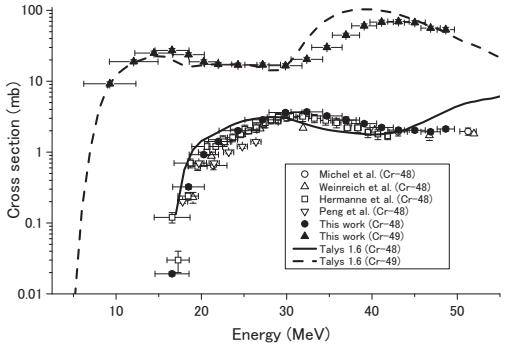

Fig. 2. Cross sections for the ^{nat}Ti(α, X)^{48}Cr and ^{nat}Ti(α, X)^{49}Cr reactions.

References

1) IAEA-Tecdoc-1211 2001 Charged particle cross section database for medical radioisotope production: diagnostic radiosotopes and monitor reactions (IAEA, Vienna, 2001).
2) J. F. Ziegler et al.: The stopping and range of ions in solids (Pergamon Press, New York, 1985).
3) R. Michel et al.: Radiochim. Acta **32**, 173 (1983).
4) R. Weinreich et al.: Appl. Radiat. Isot. **31**, 223 (1980).
5) A. Hermanne et al.: Nucl. Instrum. Meth. B **152**, 187 (1999).
6) X. Peng et al.: Nucl. Instrum. Meth. B **140**, 9 (1998).
7) A. J. Koning et al.: "TALYS-1.0", Proc.. Int. Conf. Nucl. Data Sci. Technol. ND2007, Nice, France, 2007-04 (EDP Sciences, 2008) p.211.

*1 Research Center for Electron Photon Science, Tohoku University
*2 RIKEN Nishina Center
*3 Graduate School of Science and Technology, Niigata University

Improvement in the chemical yield of purified ^{109}Cd for fee-based distribution at the RIKEN AVF cyclotron

Y. Wakitani,[*1] S.Yano,[*1] T.Yamada,[*1] H. Haba,[*2] S. Shibata,[*2] and K. Takahashi[*2]

Since October 2007, we have distributed fee-based ^{109}Cd ($T_{1/2}$ = 469.4d) ,produced via the ^{109}Ag(d,2n)^{109}Cd reaction using the RIKEN AVF cyclotron, to the general public.[1] After irradiation, ^{109}Cd was chemically separated from the Ag target and reaction byproducts. We have employed a separation method involving AgCl precipitate and anion exchange in HCl.[2] However, a considerable percentage of the produced ^{109}Cd tends to be lost by inclusion and adsorption on the AgCl precipitate in this method. F. W. E. Strelow[3] and M. K. Das[4] applied another technique using hydrobromic acid (HBr) for ^{109}Cd separation. Better chemical yield could be expected because the precipitation step was not required in this method. In order to improve the chemical yield for ^{109}Cd separation, we studied a similar technique using anion exchange in HBr without AgCl precipitation for the chemical separation of ^{109}Cd from the irradiated target in the present work.

Cadmium-109 was produced by irradiating a silver plate in natural isotopic abundance (chemical purity: >99.99%; size: ø15 mm; thickness: 0.6 mm) using a 24-MeV deuteron beam from the RIKEN AVF cyclotron. The irradiation time was 37 h, and the average beam intensity was 9 μA. During the irradiation, the target was continuously cooled with helium gas and water.

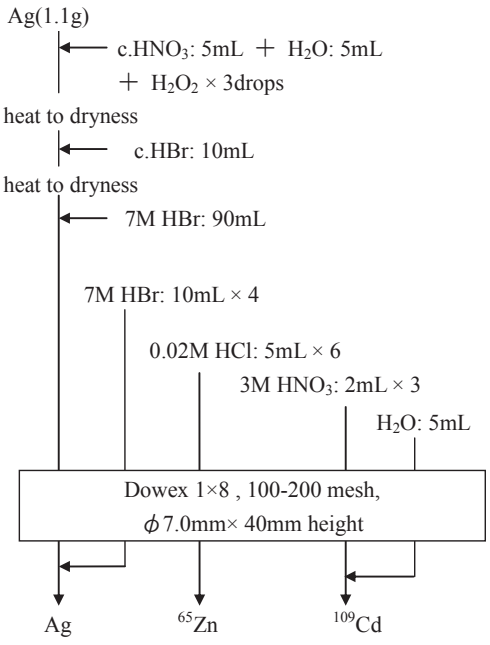

Fig. 1. Chemical separation scheme for ^{109}Cd.

After the irradiation, ^{109}Cd was chemically separated from the Ag target according to the procedure shown in Fig. 1.

The Ag target was dissolved in 5 mL of concentrated nitric acid, 5 mL of water, and three drops of hydrogen peroxide solution. The solution was evaporated to dryness. The residue was dissolved in 10mL of c. HBr. This solution was also evaporated to dryness. The residue was dissolved in 90 mL of 7 M HBr. This 7 M HBr solution was passed through the anion-exchange column (ø7 mm × 40 mm height) packed with Dowex 1X8 (100–200 mesh, Cl^- form). ^{109}Cd was adsorbed on the resin, and Ag was eluted. Then the column was washed with 7 M HBr and 0.02 M HCl. ^{109}Cd was adsorbed on the resin and the unwanted ^{65}Zn was eluted. Finally, ^{109}Cd was eluted with 3 M HNO_3 and H_2O.

The present results are shown in Table 1,together with those obtained in our previous study. The specific radioactivity and radionuclide purity were measured by γ-ray spectrometry using a Ge detector. The chemical impurity was also estimated by ICP-MS for a control sample treated using the same chemical process as the irradiated Ag target. Chemical impurities were found to be 57 ppm for S and 87 ppm for Ca. The others were below 10 ppm. As shown in Table 1, the chemical yield obtained in the present work was significantly improved from 80% to 98%.

Table1. Comparison of the results of the ^{109}Cd purification between our previous[2] and the present work.

	Our previous work	This work
Chemical yield (%)	80	98
Specific radioactivity[*1] (MBq/μg)	94	93
Decontamination factor of Ag	3×10^6	7.6×10^6
Radionuclidic purity	>99.9%	>99.9%

*1 (Beam intensity :10 μA, irradiation time: 48 h)

References

1) T. Kambara et al.: RIKEN Accel. Prog. Rep. **42**, 295 (2008).
2) J. Kanaya et al.: RIKEN Accel. Prog. Rep. **45**, 203 (2012).
3) F. W. E. Strelow et al.: Anal. Chem. **40**, 2021 (1968).
4) M. K. Das et al.: The Third International Conference on Application of RadiotraCers and Energetic Beams in Sciences (ARCEBS-14), January, 2014, Kolkata, India.

*1 Japan Radioisotope Association
*2 RIKEN Nishina Center

Preparation of no-carrier-added ^{85}Sr using the ^{nat}Rb(d,x)^{85}Sr reaction

S. Yano,[*1,*2] Y. Wakitani,[*1] T. Yamada,[*1] H. Haba[*2], S. Shibata,[*2] and K. Takahashi[*2]

Since 2007, we have distributed purified radioisotopes such as ^{65}Zn, ^{88}Y, and ^{109}Cd produced at the RIKEN AVF cyclotron to the general public.[1] After the Fukushima Dai-ichi Nuclear Power Plant accident in 2011, distribution of ^{85}Sr solutions having high specific radioactivity was required to develop analysis techniques for discharged radio-strontium. In response to these demands, we intended to produce ^{85}Sr via the ^{nat}Rb(d,x)^{85}Sr reaction using a 24-MeV deuteron beam from the RIKEN AVF cyclotron. We also studied a chemical separation procedure to obtain a purified ^{85}Sr solution using a no-carrier-added technique. In the previous study,[2] we successfully produced a ^{85}Sr solution having high radionuclidic purity. To estimate specific radioactivity, however, chemical purity should be estimated carefully. In the present study, we therefore evaluated chemical impurities in the prepared solution and assessed the applicability of the ^{nat}Rb(d,xn)^{85}Sr reaction and the no-carrier-added technique to the larger-scale production of the ^{85}Sr solution for distribution.

The ^{85}Sr isotope used in this work was produced by irradiating a RbCl disk (Sigma-Aldrich; chemical purity: > 99.99%; thickness: 500 mg cm^{-2}) of natural isotopic abundance with 24-MeV deuterons. The average beam intensity was 159 nA. The irradiation time was 17 min. ^{85}Sr was chemically separated in accordance with the scheme using a two-step chromatographic separation technique that we had reported.[2] The chemical impurities in 5.0 mL of this purified solution was evaluated using ICP-MS (Agilent Technologies; Model 7700) for a control sample, which was treated using the same procedure as that for the irradiated sample.

The production yield of ^{85}Sr was estimated to be approximately 3.90 MBq·μA^{-1} h^{-1} under the present experimental condition. The chemical yield reached as high as 94%. As shown in Table 1, the Rb target material was successfully removed and the decontamination factor of Rb reached 10^6. The strontium content required for the determination of specific radioactivity was measured to be 0.1 ppm (equivalent to 614 ng) in this analysis. However, the Sr impurities originate from not only the environment but also nuclear reactions. To estimate stable Sr isotopes produced by nuclear reactions, we calculated the expected Sr impurities by comparing the production yield obtained in the present experiment with that simulated by the TALYS code.[3]

Fig. 1 shows the simulated cross sections of ^{85}Sr and other stable Sr isotopes. The production yield of ^{85}Sr was 4.37 MBq·μA^{-1} h^{-1}. To estimate the production yields for other Sr isotopes, the calculated production yields for the stable Sr isotopes were normalized by the calculated rate for ^{85}Sr and the one obtained in the present experiment. As a result, the amount of Sr impurities from irradiation to be 346 ng under 3μA irradiation for 24 h.

The amount of Sr isotopes produced by the nuclear reaction depends on the deuteron beam dose. To apply the present technique to a larger-scale production, we estimated the expected specific radioactivity for the distribution shown in Fig. 2. According to the present result, the purified ^{85}Sr solution having a high specific radioactivity of 124 MBq μg^{-1} could be produced under 3μA irradiation for 24 h using the present chemical separation scheme. We are planning to launch the purified ^{85}Sr solution with a high specific radioactivity prepared using these studied techniques in response to customers' request.

Table 1. Measured principal chemical impurities in the ^{85}Sr solution after the purification process.

Element	Na	Al	Si	S	K
Concentration (ppm)	12.8	4.6	19.5	110.0	4.2
Element	Ca	Ba	Rb	Sr	
Concentration (ppm)	231.8	19.8	0.1	0.1	

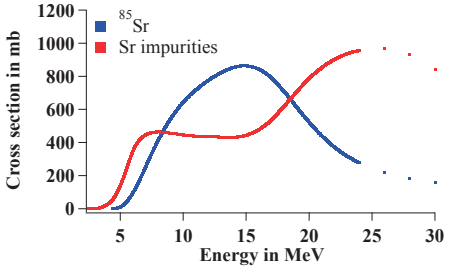

Fig 1. Cross sections for ^{85}Sr and other stable Sr isotopes calculated using the TALYS code.

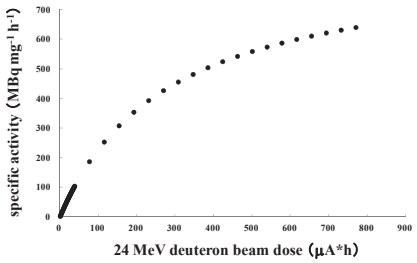

Fig 2. Calculated specific radioactivity for distribution of the purified ^{85}Sr solution as a function of the deuteron beam dose.

References

1) T. Kambara et al.: RIKEN Accel. Prog. Rep. **42**, 295 (2008).
2) S. Yano et al.: In this report.
3) A.J. Koning et al.: ND2007, (2007), p.211-214

[*1] Japan Radioisotope Association
[*2] RIKEN Nishina Center

4. Radiation Chemistry and Biology

Localization of Rad51 and phosphorylated DNA-PKsc after heavy-ion irradiation in mammalian cells

M. Izumi[*1] and T. Abe[*1]

Accelerated heavy-ion particles with high linear energy transfer (LET) induce complex clustered DNA damage, which is considered an obstacle to efficient repair and causes different biological effects compared with low-LET radiation such as X-ray. However, the biological effects of heavy-ion irradiation are not fully understood at the molecular level. To analyze the repair mechanism for DNA double-strand breaks (DSBs) caused by heavy ions, we have investigated cell sensitivity to heavy ions using the wild-type CHO-AA8 cells and two CHO mutant lines deficient in homologous recombination (HR)[1] or non-homologous end-joining (NHEJ)[2] in a previous study[3] and found that HR, but not NHEJ, is primarily involved in the repair pathway induced by high-LET ionizing radiation.

In this study, we investigated the localization of Rad51 and the phosphorylated form of the catalytic subunit of the DNA-dependent kinase (DNA-PKcs) in CHO cells after X-ray or heavy-ion irradiation with immunoflorescence staining. Rad51 is essential for HR and is involved in strand transfer during homologous pairing,[4] whereas DNA-PKcs is involved in NHEJ and phosphorylated upon DNA damage on threonin-2609.[5]

One hour after X-ray irradiation, hundreds of Rad51 or phosphorylated DNA-PKcs foci were observed in nuclei (Fig. 1A), although they were not colocalized with each other. The number of foci started to decrease 4 h after irradiation and fractions of Rad51 and phosphorylated DNA-PKcs foci were colocalized. A small fraction of DSBs was not repaired within 24 h (data not shown), and the foci remaining at 16 h after irradiation contained both Rad51 and phosphorylated DNA-PKcs, suggesting that irreparable DSBs recruite repair proteins of the NHEJ and HR pathways.

On the other hand, large fractions of Rad51 and phosphorylated DNA-PKcs foci were colocalized 1 h after iron-ion irradiation (LET = 1000 keV/μm) (Fig. 1B), suggesting that the majority of DSBs have different structures in nature. Although our previous results suggest that NHEJ is not involved in the repair pathway after heavy-ion irradiation,[3] we observed that phosphorylated DNA-PKcs was recruited to DSBs. These results suggest that repair proteins of both pathways are recruited to DSBs induced by heavy ions, and finally HR is selected for damage repair.

Currently, we are investigating how the cell cycle and LET affect the repair kinetics and colocalization of Rad51 and phosphorylated DNA-PKcs. We are also planning to examine the localization of 53BP1 and Rif1 after heavy-ion irradiation, which are involved in the selection of repair pathways for DSB repair.[6,7]

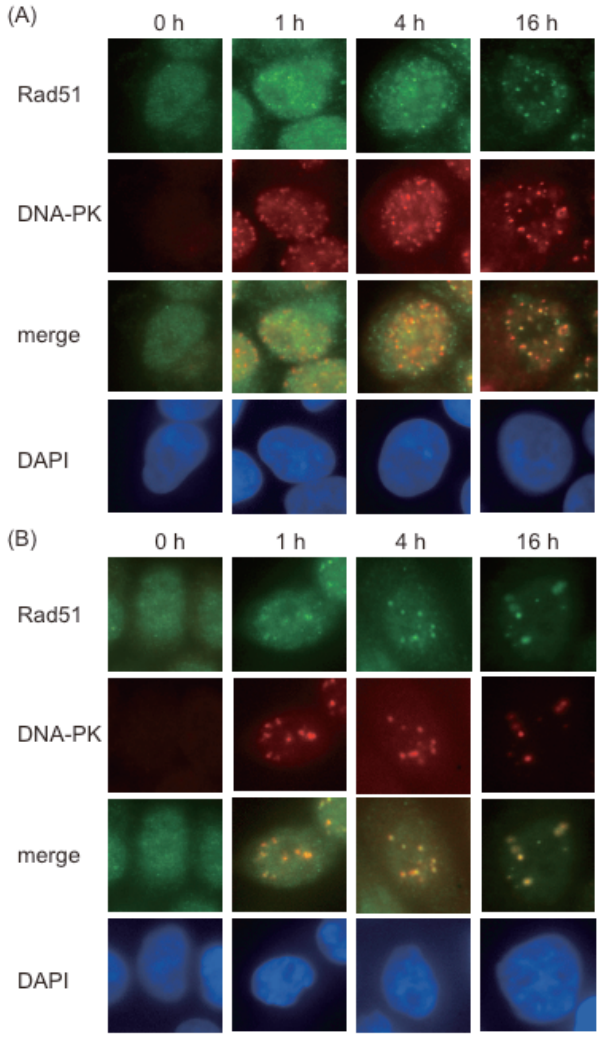

Fig. 1 Representative images of CHO nuclei (blue) with Rad51 (green) and phosphorylated DNA-PKsc (red) foci. The cells were irradiated with 5 Gy of X-ray (A) or iron ions (B) and fixed with 4% paraformaldehyde at indicated time points after irradiation. Foci formation of Rad51 and phosphorylated DNA-PKcs was detected by immunofluorescence staining.

References

1) R.S. Tebbs et al.: Proc. Natl. Acad. Sci. USA **92,** 6354 (1995)
2) S.R. Peterson et al.: Proc. Natl. Acad. Sci. USA **92,** 3171 (1995)
3) M. Izumi and T. Abe.: RIKEN Accel. Prog. Rep. **47,** in press (2014)
4) A. Shinohara et al: **69,** 457 (1992)
5) P. Douglas et al.: Biochem. J. **368,** 243 (2002).
6) C. Escribano-Diaz et al.: Mol. Cell **49**, 872 (2013)
7) J. R. Chapman et al.: Mol. Cell **49,** 858 (2013)

*1 RIKEN Nishina Center

Low-dose high-LET heavy ion-induced bystander signaling

M. Tomita,[*1,*2] T. Tsukada,[*1] and M. Izumi[*1]

The radiation-induced bystander response (RIBR) is a cellular response induced in nonirradiated cells that receive bystander signals from directly irradiated cells within an irradiated cell population.[1)] The RIBR induced by low doses of high-LET radiations is an important issue concerning the health of astronauts and in heavy-ion radiation cancer therapy. Here, we investigated the molecular mechanisms underlying and biological implications of the RIBR induced by such low doses of high-LET radiations.

Figure 1 shows the clonogenic survival curve of normal human fibroblast WI-38 cells irradiated with Fe ions (1000 keV/μm). Cells were harvested from the cell culture flask immediately (0 h) or 16–24 h after irradiation, and the surviving fraction was determined by using a colony formation assay. At doses below 0.2 Gy, the surviving fractions of the cells harvested 16-24 h after exposure to Fe ions were much lower than those extrapolated from higher doses above 0.1 Gy using the linear-quadratic model (LQ model).[2)] On the other hand, the cells harvested immediately after exposure did not show such a high cell killing effect at lower doses. These results suggest that an adequate incubation period is necessary for the bystander signal induction and transfer.

Previously, we have reported that reactive oxygen species (ROS), gap-junction intercellular communication (GJIC), and cyclooxygenase-2 (COX-2) protein as well as nitric oxide (NO) may be involved in high-LET radiation-induced bystander signal transfer.[3)] Here, we show the progress of results reflecting new data [Fig. 2]. Lindane and NS-398 (an inhibitor of GJIC and COX-2, respectively) were dissolved in DMSO (a scavenger of ROS). DMSO did not significantly suppress the bystander cell killing effect. In contrast, lindane, NS-398, and c-PTIO (a scavenger of NO) significantly suppressed cell death to similar levels. Cells pretreated with both c-PTIO and lindane did not show significantly higher surviving fraction than those pretreated with lindane or c-PITO alone. These results suggest that bystander signaling through GJIC and the cell culture medium induces the bystander cell killing effect in a coordinated manner.

Currently, we are examining the role of the NF-κB/Cox-2/prostaglandin E2 and NF-κB/iNOS/NO pathways,[4)] which may be activated in bystander cells.

*1 RIKEN Nishina Center
*2 Radiation Safety Research Center, Central Research Institute of Electric Power Industry

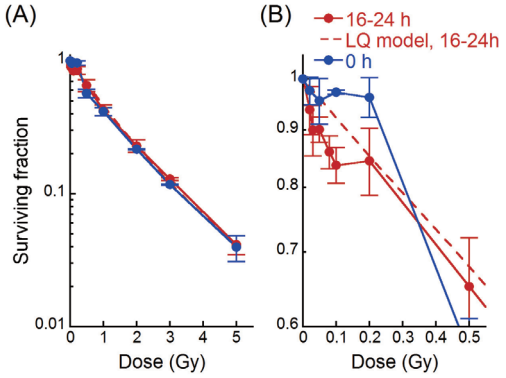

Fig. 1. Survival curves of WI-38 cells. Confluent monolayers of WI-38 cells were irradiated with 90 MeV/u Fe ions (1000 keV/μm) and the cells were harvested immediately (0 h) or 16–24 h after irradiation. The surviving fraction was determined by using a colony forming assay. Panel A shows all data obtained in this study. Panel B shows surviving fractions at doses below 0.5 Gy. The error bars represent the standard deviations.

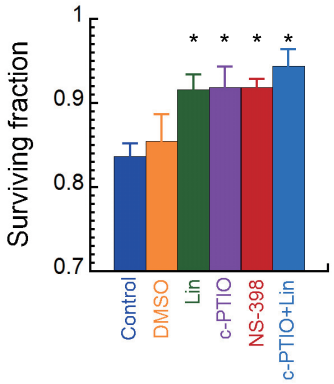

Fig. 2. Effect of inhibitors or scavengers. DMSO (0.1%), lindane (Lin, 50 μM), c-PTIO (20 μM), or NS-398 (50 μM) was added to the medium 2 h before irradiation.[5)] WI-38 cells were irradiated with 0.1 Gy Fe ions. The error bars represent the standard errors of the mean (SEM) (n=3–4).*$P < 0.05$, for comparison with irradiated control cultures.

References

1) M. Tomita and M. Maeda: J. Radiat. Res. **56**, 205 (2015).
2) M. Tomita et al.: RIKEN Accel. Prog. Rep. **42**, 276 (2009).
3) M. Tomita et al.: RIKEN Accel. Prog. Rep. **47**, in press.
4) T. K. Hei et al.: Curr. Mol. Pharmacol. **4**, 96 (2011).
5) M. Tomita et al.: Radiat. Res. **179**, 200 (2013).

Effect of days after irradiation on lethal rate of F3 progeny in the fruit fly mutation isolation system

K. Tsuneizumi[*1] and T. Abe[*1]

Heavy-ion beam mutagenesis is generally recognized as an effective method for mutation breeding[1, 2]. Although this method was greatly successful with a plant, its application is still limited for animals. We therefore plan to acquire more basic data to set up optimal conditions for the irradiation system by heavy-ion beam using *Drosophila melanogaster* (fruit fly) as a useful model.

In a previous study, we have developed and improved a stable mutant isolation system using fruit flies by employing carbon-ion beam irradiation. In the system, we prepared a useful genetic tool, called balancer chromosome, to prevent genomic recombination. We also prepared small commercial cuvettes with a plane surface to apply heavy-ion beam equally to overcome unstable results[3]. Then, we could observe a linear correlation between a number of F1 progeny and an irradiation dose when the males were irradiated with a carbon-ion beam[3].

In this report, we introduced a new machine to improve the mutant isolation system [Fig. 1a]. If fruit flies are put in empty cuvettes for irradiation, they die because of dryness. So, it is necessary to put fly foods in the cuvettes to avoid dryness. However, it was difficult to prepare many samples without polluting the irradiated surface because the food was stuffed manually. The machine made it possible to dispense fly foods to many cuvettes without polluting the side surface of the cuvettes.

We prepared powdered fly foods for the machine, because it is easy to use and is commercially available. We considered using a needle tip for dispensing viscous fly foods to many cuvettes continuously [Fig. 1b]. Then we optimized the water-to- powder ratio for injection. Next, we set parameters for the dispensing machine using a program, such that the surface of fly foods was slanted in a cuvette [Fig. 1c]. As a result of these examinations, we were able to prepare more than 300 cuvettes in 2 hours.

To optimize the conditions for the mutant isolation system, we estimated the suitable state of F1 progeny that includes a possibility of chromosome damages. Various developmental cells are intermingled in testis of irradiated fruit fly. The repair mechanism to DNA damages and the sensitivity to irradiation are different in each cell[4]. So, it is important to know when flies with high probability of DNA damage are born. Because DNA damages to important genes for survival can be judged by the homozygotes born in F3 progeny, we measured a frequency of lethal rate of F3 progeny [Fig. 2]. The progeny being born 4 days after irradiation at 10 Gy dose levels recorded the maximum frequency of lethal rate [Fig. 2]. These data will be helpful for optimizing the irradiation system in the future.

*1 RIKEN Nishina Center

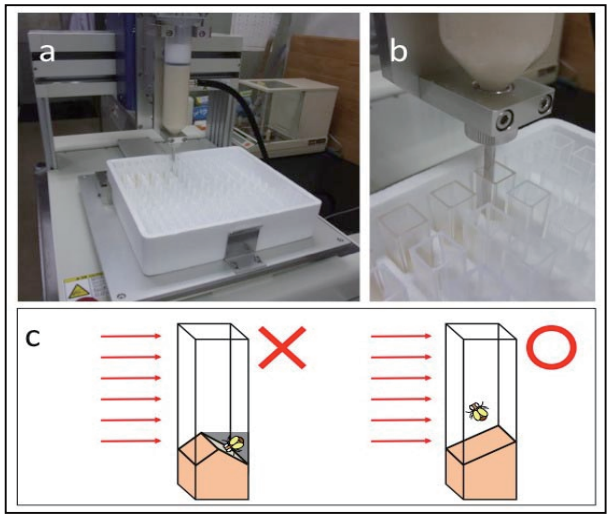

Fig. 1. a) A photograph of a micro dispensing machine (Shopmaster 300DS made by Musashi engineering, Inc.). b) A photograph of magnified view of dispensing fly foods into cuvettes. c) A diagram of a comparison of a surface of fly foods in the cuvettes. A dispensing program has been tuned so that a shadow does not form in the cuvettes by fly foods. The left figure shows a failure caused by fly food shadow. The right figure shows appropriate placement of fly food. Heavy-ion beams are indicated as red arrows.

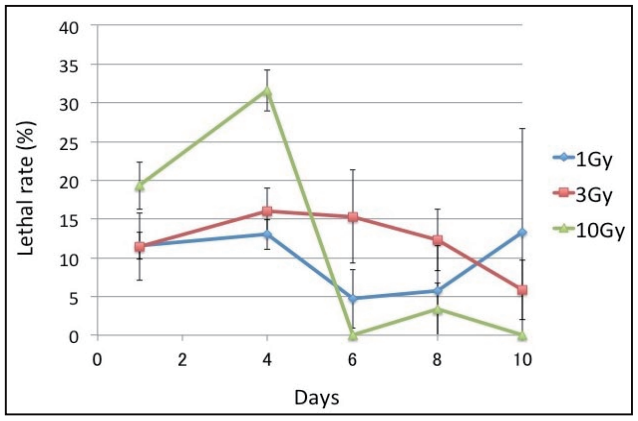

Fig. 2. A change in frequency of lethal rate of F3 progeny. Parental male flies were irradiated with a carbon-ion beam with linear energy transfer values of 80keV/μm. F: filial generation.

References

1) T. Abe et al.: in *Plant Mutation Breeding and Biotechnology*, edited by Q. Y. Shu et al. (CABI, Oxfordshire, 2012), p.99**.**
2) A. Tanaka et al.: J. Radiat. Res. **51**, 223 (2010).
3) K. Tsuneizumi et al.: RIKEN Accel. Prog. Rep. **46**, 255 (2013).
4) M. Ashburner et al.: *Drosophila a Laboratory Handbook* (CSHL Press, New York, 2005).

Extra-early-flowering wheat mutants produced by heavy-ion-beam mutagenesis†

A. Nishiura,[*1] Y. Kazama,[*2] T. Abe,[*2] N. Mizuno,[*3] S. Nasuda,[*3] and K. Murai[*1]

To avoid harvesting in the rainy season, early flowering or early heading is one of the most important characteristics for bread wheat (*Triticum aestivum*) in East Asia, including Japan. A detailed understanding of the flowering mechanism in wheat plants is of value not only for wheat breeding but also for basic scientific research. From the large scale mutant panel of diploid einkorn wheat (*Triticum monococcum*) strain KU104-1 developed by heavy-ion-beam irradiation[1], we identified four extra early-flowering mutants, named *extra-early-flowering1* (*exe1*), *exe2*, *exe3*, and *exe4*. The four *exe* mutants fell into two groups, namely Type I (moderately extra-early-flowering type; *exe1* and *exe3*) and Type II (extremely extra-early-flowering type; *exe2* and *exe4*), based on a field experiment.

In a growth chamber, leaf-emergence timing in wild-type (WT) and *exe* mutant plants was examined under long-day (LD) or short-day (SD) conditions. Under LD conditions, WT plants averaged about 180 days from sowing to flag-leaf unfolding. In contrast, Type I *exe* mutants took about 65 days and Type II about 50 days. WT plants transited from the vegetative to reproductive growth phase at the 9-leaf stage, while *exe* mutants showed earlier phase transition: at the 5-leaf stage for *exe1* and *exe3* (Type I) and the 4-leaf stage for *exe2* and *exe4* (Type II). In WT plants, the flag leaf occurred at the 18-leaf stage, while in *exe1*, *exe2*, *exe3*, and *exe4*, the flag leaf appeared at the 9-leaf, 8-leaf, 9-leaf, and 7-leaf stages, respectively. Under SD conditions, WT plants transited from the vegetative to reproductive growth phase at the 13-leaf stage. In contrast, *exe1* and *exe3* mutants (Type I) transited at the 8-leaf stage, while *exe2* and *exe4* mutants (Type II) transited at the 4-leaf stage. Interestingly, the phase transition was early (at the 4-leaf stage) in Type II *exe* mutants under both SD and LD conditions. Comparing Type I *exe* mutants between SD and LD conditions indicates that these mutants retained photoperiodic sensitivity. However, Type II *exe* mutants had lost almost all photoperiodic sensitivity.

exe

Fig. 1. *Extra-early-flowering* (*exe*) mutant plants grown in the field.

In wheat, it was found that three genes mainly control the flowering, namely *VERNALIZATION 1* (*VRN1*), *VRN2* and *VRN3*. The analysis of *VRN1*, a flowering-promoter gene, showed that it was more highly expressed in seedlings at the early developmental stages in Type II mutants than in Type I mutants. The up-regulation of *VRN1* expression in *exe* mutants was associated with earliness in flowering under LD conditions. The extremely extra-early flowering in Type II mutants was associated with a more rapid up-regulation of *VRN1* expression than in Type I mutants. It is notable that a similar level of *VRN1* expression was observed at the phase transition in each *exe* mutant: at the 5-leaf stage for Type I mutants and at the 4-leaf stage for Type II mutants. This finding suggests that the level of *VRN1* expression is correlated with the phase transition from vegetative to reproductive growth and may act as a threshold for flowering competency in wheat plants.

The original KU104-1 is an einkorn wheat strain that carries a null allele of the *VRN2* gene, a repressor of flowering. Thus, our results indicate that the level of *VRN1* expression controls earliness in flowering in *exe* mutants independently of *VRN2*. In bread wheat, it has been known that winter cultivar quantitatively requires prolonged cold temperature to yield vernalization saturation. Some winter cultivars require 2-4 weeks of low temperature to reach the maximum vernalization effect on heading, and others require more than 4 weeks. Positional cloning of the gene was performed for the duration required for vernalization, and the results demonstrated that this trait is controlled by the recessive *VRN1* gene on the A genome at the protein level[2]. A previous study also revealed that the binding ability of the VRN1 protein to TaHOX1 was associated with the requirement of low-temperature duration to reach vernalization saturation. These findings, together with the present *exe* study, support our model of gene network for flowering: *VRN1* plays a central role in the flowering pathway[3].

† Condensed from the article in Breeding Science **64**, 213 (2014)

*1 Department of Bioscience, Fukui Prefectural University
*2 RIKEN Nishina Center
*3 Graduate School of Agriculture, Kyoto University

References

1) K. Murai et al.: Nucl. Instr. Meth. Phys. Res. B 314, 59 (2013).
2) G. Li et al.: Plant J. 76, 742 (2013).
3) S. Shimada et al.: Plant J. 58, 668 (2009).

Heredity analysis of radiation induced semidwarf mutants in Tartary buckwheat (*Fagopyrum tataricum* Gaertn.)

T. Morishita, [*1, *2] Y. Hayashi,[*2] and T. Abe[*2]

Recently, heavy-ion beams have been regarded as a good mutagen for plant breeding, and as such various varieties have been developed by using heavy-ion beams. We previously reported the biological effects and mutation induction by ion beams in Tartary buckwheat[1) 2)]. We obtained semidwarf mutants named IRBFT-45, 63, 67 and 77. The semidwarf type is important for improving the lodging resistance and yielding ability in buckwheat breeding. These semidwarf mutants were obtained by irradiating dry seeds of Tartary buckwheat (var. Rotundatum) with 40 Gy of carbon (^{23} keV/μm, $^{12}C^{6+}$), 100 Gy of carbon (^{39} keV/μm, $^{12}C^{6+}$), 30 Gy of iron (624 keV/μm, $^{56}Fe^{24+}$) and 20 Gy of argon (280 keV/μm, $^{40}Ar^{17+}$) ions[3)]. On the other hand, we obtained similar semidwarf lines named IRBFT-6 and 20 by irradiating dry seeds with 50 and 500 Gy of gamma rays (^{60}Co, 44.4TBq) at the Institute of Radiation Breeding, and IRBFT-38 by irradiating dry seeds with 40 Gy of helium ions (^{16} keV/μm, $^{4}He^{2+}$) at JAEA. The plant height of all of these semidwarf lines was 50-60% of the original varieties. We performed heredity analysis on these semidwarf mutants.

All of the F_1 plants obtained by crossing among IRBFT-6, 20, 45 and their original varieties showed wild type like phenotype. The phenotypes in the populations of F_2 were segregated into wild type like and semidwarf, and the appropriate segregation ratio was found to be 3:1 by a chi square test (Table 1). This suggests that the trait of semidwarf in IRBFT-6, 20, and 45 was controlled by a nuclear single recessive gene.

To classify these semidwarf lines, a half diallel cross was performed (Fig. 1). When F_1 plants showed a semidwarf phenotype, the causal gene of the parents was considered to be the same. When F_1 plants showed wild-type like phenotype, the causal genes of the parents were considered to be different. From the phenotype in F_1, it was estimated that these 7 lines were classified into 2 groups. One consisted of IRBFT-6, 20 and 45, which had a common semidwarf gene termed *sdA*. The other consisted of IRBFT-38, 63, 67 and 77, which had another semidwarf gene termed *sdB*.

Because a crossing test with original varieties was not performed in *sdB* lines (IRBFT-38, 63, 67 and 77), the number of *sdB* gene(s) was not determined. Instead, we investigated the segregation ratios in the F_2 plants generated by crossing *sdB* lines with IRBFT-20 (*sdA*) (Table 2). The phenotypes in the populations of F_2 were segregated into wild type like and semidwarf. Their segregation ratios were then fitted to the two recessive gene model (Table 2). These results indicated that *sdB* was controlled by a single recessive gene different from *sdA*.

Table 1. Segregation patterns of plant type crossing between semidwarf lines and the original variety in the F_2 population

Cross combination	No. of plants		χ^2	p
	Wild type	Semidwarf	3:1	
Pontivy×IRBFT-6	21	9	0.4	0.53
Hokkai T8×IRBFT-20	54	17	0.04	0.84
Rotundatum×IRBFT-45	60	13	2.01	0.16

♀ \ ♂	IRBFT-20	IRBFT-38	IRBFT-45	IRBFT-63	IRBFT-67	IRBFT-77
IRBFT-6	SD 6	WT 3	SD 4	WT 5	WT 4	WT 4
IRBFT-20		WT 4 (SD 1)	SD 5	WT 4	WT 7	WT 5
IRBFT-38			WT 2 (SD 1)	SD 5	SD 3	SD 1
IRBFT-45				WT 3	WT 4	WT 4
IRBFT-63					SD 17	SD 14
IRBFT-67						SD 16

Fig. 1. Phenotypes of F_1 plants by a half diallel cross. SD means semidwarf type, and WT means wild-type like. Numbers in parentheses are the numbers of research plants.

Table 2. Segregation patterns of plant type crossing between semidwarf lines in the F_2 population

Cross combination	No. of plants		χ^2	p
	Wild type	Semidwarf	9:7	
IRBFT-20×IRBFT-38	109	85	0.01	0.99
IRBFT-20×IRBFT-63	64	56	0.41	0.52
IRBFT-20×IRBFT-67	137	103	0.07	0.79
IRBFT-20×IRBFT-77	130	109	0.33	0.56

References

1) T. Morishita et al.: RIKEN Accel. Prog. Rep. 36, 137 (2003)
2) T. Morishita et al.: RIKEN Accel. Prog. Rep. 40, 255 (2007)
3) T. Morishita et al.: RIKEN Accel. Prog. Rep. 41, 232 (2008)

*1 NARO Hokkaido Agricultural Research Center
*2 RIKEN Nishina Center

Effects of Ar-ion beam irradiation on inducing mutations in chrysanthemum and sweetpotato

Y. Tanokashira,[*1] J. Nagai,[*1] S. Nagayoshi,[*1] and T. Abe[*2]

It is expected that heavy-ion beam irradiation will be useful in inducing mutations for plant breeding in agriculture[1), 2)]. However, effects of Ar-ion beam irradiation on many plant species remain unexplained. Therefore, effects of Ar-ion beam irradiation on chrysanthemum and sweetpotato, which are major crops in Kagoshima Prefecture, was investigated and compared with C-ion beams in this study.

At first, we investigated effects of Ar-ion beam irradiation on regeneration of chrysanthemum. Leaf blades of the spray-mum cultivar "Southern Chelsea", which was developed in Kagoshima Prefecture, were irradiated by Ar-ion beams (LET: 280 keV/μm) at doses of 0.1, 0.3, 0.5, 1, 2, and 3 Gy, and C-ion beams (LET: 23 keV/μm) at doses of 1, 2, and 3 Gy. After irradiation, these tissues were cultured in vitro, and the number of directly regenerated plants from adventitious shoots[1)] were counted. The relative regeneration rates of Ar ions were lower than that of C ions at the same dose, and the proportion between relative regeneration rates of Ar ions and C ions (Ar/C) became lower according to increasing of irradiation doses (Fig. 1). In addition, the relative regeneration rate of Ar ions became higher according to decreasing of irradiation doses; 37.8%, 65.9%, and 90.9% at doses of 1, 0.5, and 0.3 Gy, respectively (Fig. 1). From past findings, the optimal dose for inducing mutations in chrysanthemum will be at the dose when the relative regeneration rate has declined considerably, and this optimal dose of C ions will be 2 Gy[3)]. Consequently, the optimal dose of Ar ions is estimated to be 0.5 Gy assuming that the relative regeneration rate of Ar ions for optimal dose is at the same level with C ions.

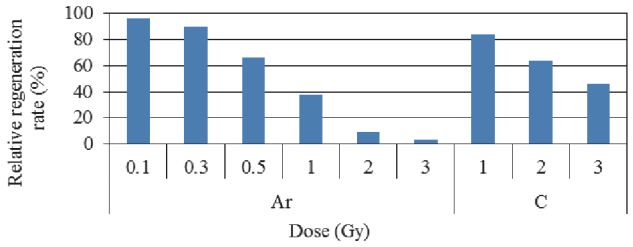

Fig. 1. Comparison of the relative regeneration rate by the Ar-ion and C-ion beam irradiation in "Southern Chelsea". The relative regeneration rate means the rate of regenerated shoots after ion beam irradiation to radiationless regenerated shoots, which were directly developed from adventitious shoots[1)].

Next, we investigated the effects of Ar-ion beam irradiation on inducing mutations for sweetpotato. Axillary shoots of in vitro-grown stems of cultivar "Konamizuki" were irradiated by Ar-ion beams (LET: 280 keV/μm) at doses of 1, 2, and 3 Gy, and C-ion beams (LET: 23 keV/μm) at doses of 10 and 15 Gy. After irradiation, these tissues were cultured for about 10 weeks, and the growth and morphological mutations of in vitro plants were observed. In Fig. 2, mortality rate, stunting rate, and mutation rate mean the rate of samples that died without germination, samples whose stem lengths were less than 2 cm, and samples whose leaves have one or more incisions, respectively, to investigated samples. The original leaf of cultivar "Konamizuki" is cordate. Under the experimental condition used in this study, the mortality rates of both Ar ions and C ions were relatively low (Fig. 2) . In contrast, the stunting rate at 3 Gy Ar ions was about 4.7 times and about 1.8 times higher than those at 10 Gy and 15 Gy C ions, respectively (Fig. 2). This fact suggests that the dose of Ar ions that strongly influences the growth of sweetpotato will be lower than that of C ions. Furthermore, the morphological mutation rate at 2 Gy Ar ions was 25.7% (Fig. 2). This rate was highest under all irradiation conditions. Because many morphological mutations can be detected at the mature stage, the reason that the mutation rate at 2 Gy Ar ions is higer than that at 3 Gy Ar ions could be the high stunting rate at 3 Gy Ar ions. Moreover, some of the mutations leading to the incision of leaves were the results of spontaneous mutation; however, the mutation rate under heavy-ion beam irradiation was clearly higher than that observed under non-irradiation. These morphological mutants are chimera plants generated from multicellular tissues. Therefore, we tried to separate mutation sites by cutting out mutation tissues. On the basis of these results, it is supposed that a low dose of Ar-ion beams strongly affects on the growth and morphological mutation of sweetpotato.

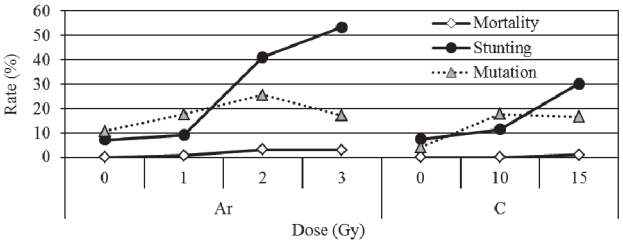

Fig. 2. Effects of heavy-ion beam irradiation on sweetpotato cultivar "Konamizuki". The period and times of irradiation and the number of samples (from 96 to 187) were different based on the line class and doses.

[*1] Kagoshima Prefectural Institute for Agricultural Development
[*2] RIKEN Nishina Center

References
1) K. Ueno et al.: Hot. Res. (Japan) 12, 245 (2013)
2) T. Abe et al.: Breed. Res. 16, 67 (2014)
3) K. Ueno et al.: Breed. Res. 3(Separate Vol. 2), 62 (2001)

Rapid screening of heavy-ion-induced large deletion mutants by using quantitative real-time PCR in *Arabidopsis thaliana*

Y. Kazama,[*1] T. Hirano,[*1,*2] K. Ishii,[*1] M. Yamada,[*1] Y. Shirakawa,[*1] S. Ohbu,[*1] and T. Abe[*1]

In heavy-ion irradiation, the size of deletions can be varied according to different values of linear energy transfer (LET). In irradiation experiments on *Arabidopsis thaliana*, we previously found that beams with LET of 30 keV/μm induced small deletions (1 to 51 bp) with high frequency, and this size is appropriate for disrupting a single gene.[1] Thus, 30-keV/μm beams are suitable for use in mutation breeding as well as in reverse genetics to find single gene disruption lines in conjunction with SNP detection systems. On the other hand, beams with LET of 290 keV/μm caused larger deletions (1 kbp to several hundred kbp).[2] Such high-LET beams can be used for generating mutants lacking tandemly arrayed genes (TAGs) that have functions similar to one another, allowing us to investigate the function of TAGs. Thus, we are now developing a deletion-mutant correction by screening them from M_3 generations after being irradiated with 100-, 200-, or 290-keV/μm beams. The screening is performed using array-CGH designed for all TAGs of *A. thaliana*. Researchers will be able to screen deletion mutants of interest from our stock of over 10,000 of 290-keV/μm irradiated M_2 lines.

However, screening deletion mutants is time-consuming. Conventionally, it was performed by PCR in the M_2 generation, in which only homozygous deletions (HomDels) could be detected unless primers were designed to have deletions placed between them (Table 1). In case that the HomDel mutant of interest is lethal, no candidate would be obtained. By contrast, heterozygous deletions (HetDels) can be inherited over generations, and are found in the M_2 generation with about two times frequency compared with HomDels (Fig.1). If a HetDel is easily detected in the M_2 generation (See Fig. 1), the screening pool size can be reduced. Herein, we tested the quantitative real time PCR (qPCR) for detection of a HetDel.

For our test, we selected an *Arabidopsis* line (C200-84-N2) from our stock induced by carbon-ion beam irradiation (135 MeV/nucleon, 200 keV/μm) at a dose of 75 Gy. This line has a 3.5-kbp deletion at the 2762232-2765771 position on chromosome 4. The 3.5-kbp deletion is harbored as a HetDel in the M_2 generation. Thus, four individual progenies of the M_3 plants of C200-84-N2 were used for qPCR, since some of them would have a 3.5-kbp deletion as the HetDel.

qPCR was performed by using LightCycler and the Universal Probe Library detection format (Roche Diagnostics, Penzberg, Germany). Relative amplification ratios between the 3.5-kbp deleted and non-deleted regions were calculated by using the ΔΔCp method. Sample A showed the same relative amplification ratio as wild-type (Fig. 2). Samples B and C showed about half-level of the ratio as compared to wild-type, indicating that they contain HetDels. Sample D showed no amplification. These results indicate that large deletions can be detected even if they are heterozygous. Our irradiated M_2 seed stocks in conjunction with this method will prove a powerful tool for analyzing the functions of TAGs.

Table1. Features of Hom and Het deletions

	Detection by normal PCR	Incidence in M_2 generation
HomDel	Possible	Low
HetDel	Impossible	High

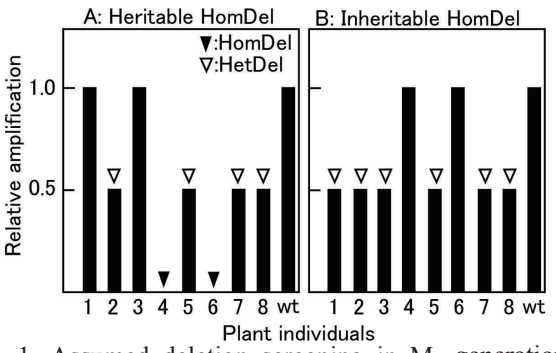

Fig. 1. Assumed deletion screening in M_2 generation by qPCR. HetDels are detected more frequently than HomDels for heritable (A) and inheritable (B) cases. No symbol indicates individuals that have no deletion.

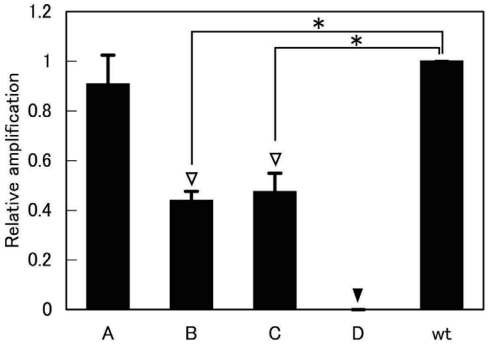

Fig. 2. qPCR in four M_3 plants (A to D). Data are expressed as fold changes compared with values in wild-type (wt). Error bars indicate ±SD. N=3 in each plant. White arrowheads and a black arrowhead indicate HetDel and HomDel, respectively. *, $p < 0.01$ compared to wild-type.

*1 RIKEN Nishina Center
*2 Faculty of Agriculture, University of Miyazaki

References

1) Y. Kazama et al.: BMC Plant Biol. **11**, 161 (2011).
2) T. Hirano et al.: Mutat. Res. **735**, 19 (2012).

LET-dependent effect on mutation induction DNA repair-deficient background in *Arabidopsis thaliana*

K. Ishii,*[1] Y. Kazama,*[1] Y. Shirakawa,*[1] S. Ohbu,*[1] and T. Abe*[1]

A previous study on the effect of LET on inducing mutation revealed that the most effective value of LET (LETmax) on dried seeds of *Arabidopsis thaliana* was 30.0 keVμm^{-1}, within a range 22.5 to 640 keVμm^{-1}.[1)] LET is therefore an important factor in mutation induction. In the mutagenesis process, the DNA double-strand break (DSB) repair system is concerned with the production of mutations. There are two major DSB repair pathways: non-homologous end joining (NHEJ) and homologous recombination repair (HRR) function in eukaryotic cells.[2)] NHEJ and HRR are independent pathways. HRR is a relatively error-free pathway because it utilizes the homologous region of a sister chromatid to repair the damaged strand, whereas the NHEJ pathway is relatively error-prone.

To determine whether DSB repair pathways are involved in the LET-dependent effect on mutation induction, we intended to investigate the effect of LET in the DSB repair-deficient background. We planned to measure the mutation rates after heavy-ion beam irradiation with LET values 22.5 and 30 keVμm^{-1} in the three mutant lines: 1) the HRR pathway-deficient mutant line, 2) the NHEJ pathway-deficient mutant line, and 3) both HRR and NHEJ pathway-deficient mutant line. Here, we report the mutation rates of the *Rad54*-deficient mutant as the HRR pathway-deficient mutant line.

Seeds of the *APG3*$^{(+/-)}$ mutant (CS16118) and the *AtRad54*$^{(-/-)}$ mutant (SALK_038057) were obtained from the Arabidopsis Biological Resource Center (ABRC, Ohio State University) and the European Arabidopsis Stock Centre (NASC, the University of Nottingham), respectively. The *APG3*$^{(+/-)}$ mutant carries BASTA-resistance at the *APG3*-disrupted allele, and a uniformly heterozygous population can be selected as photosynthetic and BASTA-resistant seedlings.[3)] The uniformly heterozygous population facilitates investigation of the mutation frequency in the irradiated (M_1) generation by calculating the proportion of the number of plants with white sectors on true leaves to that of total plants with true leaves (Fig. 1). The *AtRad54*$^{(-/-)}$ mutant carries a kanamycin resistance. The *APG3*$^{(+/-)}$ plants were crossed with the *AtRad54*$^{(-/-)}$ plants. The F_1 seeds were germinated in the presence of BASTA (2 μg/mL) and kanamycin (50 μg/mL), and the germinated plants were replanted to pots. F_2 seeds were collected from the self-pollinated F_1 plants. In the F_2 generation, the photosynthetic and both BASTA- and kanamycin-resistant plants were screened. The second screening of the *APG3*$^{(+/-)}$/*AtRad54*$^{(-/-)}$ plants were conducted by PCR. A sufficient number of seeds were collected from progenies of the identified *APG3*$^{(+/-)}$/*AtRad54*$^{(-/-)}$ plants.

Heavy-ion beam irradiation was conducted as previously described[3)] with some modifications. The seeds of the *APG3*$^{(+/-)}$/*AtRad54*$^{(-/-)}$ and *APG3*$^{(+/-)}$/*AtRad54*$^{(+/+)}$ plants were irradiated with $^{12}C^{6+}$ ions with LETs of 22.5 or 30.0 keVμm^{-1} at a dose of 300 Gy.

The mutation frequencies were obtained as previously described.[3)] The mutation frequencies of *AtRad54*$^{(+/+)}$ plants were 3.0 and 6.6% when the LET values were 22.5 and 30.0 keVμm^{-1}, respectively, and they are significantly different (Table 1; $p<0.05$ with chi-square test). The mutation frequency of 22.5 keVμm^{-1}-irradiated *AtRad54*$^{(-/-)}$ plants was 5.6%, which was at the same level as that of 30.0-keVμm^{-1} irradiated control ($p\geq0.05$). It is assumed that because the HRR pathway is disabled, the error-prone NHEJ pathway mainly functioned to repair DSB. The mutation frequency of 30.0-keVμm^{-1} irradiated *AtRad54*$^{(-/-)}$ plants, however, was still 6.8%, which was at the same level as that of the control ($p\geq0.05$). This result proposed a hypothesis: in the case of the 30.0-keVμm^{-1} irradiation, in contrast to the 22.5-keVμm^{-1} irradiation, DSBs occur beyond the capacity of the HRR pathway functions and are repaired mainly by the NHEJ pathway, leading to a high mutation frequency. Further analysis on other DNA repair gene-deficient mutants is in progress.

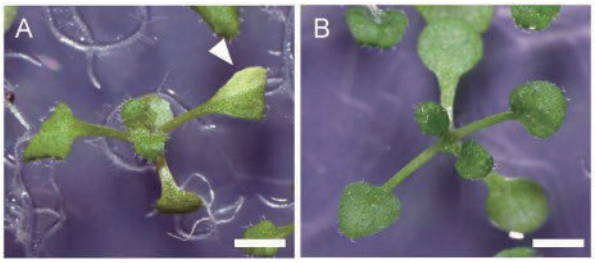

Fig. 1. Sector mutation caused by heavy-ion beam irradiation on the *APG3*$^{(+/-)}$ mutant. (A) A plant showing sector mutation. The leaf exhibiting mutation is indicated by the white arrowhead. (B) A plant not showing abnormal phenotype. Bars = 2 mm.

Table 1. LET-dependent effect on inducing mutation.

LET (keVμm^{-1})	Mutation frequency (%)	
	AtRad54$^{(-/-)}$	*AtRad54*$^{(+/+)}$
22.5	5.6 (916)	3.0* (2,241)
30.0	6.8 (857)	6.6* (2,118)

Numbers in parentheses indicate numbers of samples. *Kazama et al. (2012).

References

1) Y. Kazama et al.: Plant Biotechnol. 25: 113-117 (2008).
2) L. H. Thompson: Mutat. Res. 751: 158-246 (2012).
3) Y. Kazama et al.: Plant Biotechnol. 29: 441-445 (2012).

*1 RIKEN Nishina Center

Characterization of isolates derived from heavy-ion-beam irradiated cells in the unicellular green alga *Parachlorella kessleri*

T. Yamazaki,[*1,*2] Y. Yamashita,[*1] S. Ota,[*1,*2] T. Takeshita,[*1] Y. Kazama,[*3] T. Abe,[*3] and S. Kawano[*1,*2]

Parachlorella kessleri is a unicellular microalga relatived to the *Chlorella* species that belong to the class of Trebouxiophyceae in the Chlorophyta and accumulates starch followed by lipids after suffering sulfur-starvation. [1] A *P. kessleri* strain (NIES-2152) exhibits the highest biomass productivity under continuous high-light conditions among the strains that are relative algal species. [2] The properties of *P. kessleri* such as the ability to produce biomaterials including starch and lipids, and high biomass productivity qualify this strain as the most desired candidate in industrial production.

To improve the productivity of biomass or biomaterials in algal cells, we have been developing a breeding system for microalgae using *P. kessleri* as a model case. Our previous report demonstrated that the isolates from heavy-ion-beam irradiated *P. kessleri* cells exhibit a broad spectrum of phenotypes, which are different from the wild type strain. [3] Another case study demonstrated that the heavy-ion-beam irradiation could disrupt gene(s) responsible for a metabolic pathway to assimilate extracellular nitrates by transporting and oxidizing them to ammonium. [4] These findings suggest that the breeding system based on the heavy-ion-beam will modify a specific metabolic pathway to produce biomaterials.

Wild type *P. kesseleri* cells were grown in the wells of a 384-well plate using a tris-acetate-phosphate (TAP) medium containing inorganic nutrients sufficient for healthy growth under continuous-light conditions. Optical density at 595 nm (OD_{595}) and the emission of a lipophilic fluorescence stain, Nile Red, in each well were measured as an index of cell density and accumulation of neutral lipids in cells, respectively (Fig. 1). The median of OD_{595} for wild type *P. kessleri* cells reached to approximately 1.11 at 12th day of culture after inoculation into a fresh TAP medium. Although the individual values were scattered, they exhibited a constant range of scatter in replications. The wild type cells were grown in nutrient-limited media (dSTAP for sulfur starvation; dNTAP for nitrogen starvation; dPTAP for phosphorus starvation). Among the three conditions, nitrogen starvation suppressed the increase of OD_{595} after inoculation most effectively. In addition, the values in individual wells exhibited also a constant range of scatter. The Nile Red fluorescence values for the three nutrient-limited culture media were almost the same, and they were higher than that for the TAP-medium, suggesting that the neutral lipids accumulate in those cells in high and

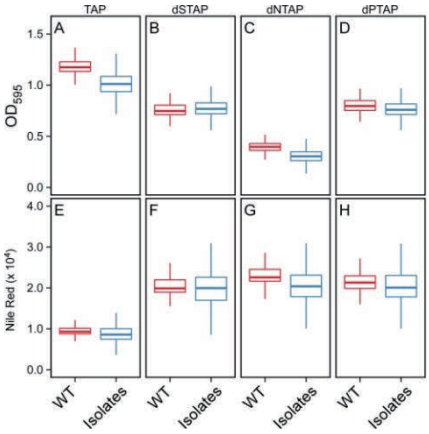

Fig. 1. Boxplots of OD_{595} values and Nile Red emissions in replications for the wild type strain and isolates from heavy−ion−beam irradiated *P. kessleri* cells.

isolates using this method should consider the scatter between wells.

The *P. kessleri* cells were irradiated by heavy-ion beams of different doses and nuclear species (Fe and Ar ions at 25 Gy and 50 Gy). These cells were grown on plates containing a solid TAP medium, and the obtained colonies were defined as isolates. The individual isolates were inoculated in the wells of 384-well plates containing a fresh TAP medium. Four thousand six hundred and eight isolates were grown for 12 days. OD_{595} values and Nile Red emissions for these wells were measured at the 12th day of culture after inoculation (Fig. 1). The distribution of OD_{595} values differed from the expected pattern with the constant range of the scatter spreading around the median calculated for the wild type replications. Although the exact scatter of individual isolates was unclear because the value was measured only once, this result indicates that the population contains heterogeneous isolates with different genetic backgrounds. Under sulfur and phosphorus starvations, the scatters were consistent with that for the wild type replications; however, under nitrogen starvation the median was lower than that for the in the case of wild type. These inconsistencies with the expected result were observed in the constant range of scatter for Nile Red emission except in the case of sulfur starvation. These data suggest that a certain group of isolates from heavy-ion-beam irradiated algal cells alters the genetic background responsible for cell proliferation and metabolism.

This study was supported by JST, CREST (to SK).

[*1] Department of Integrated Biosciences, Graduate School of Frontier Sciences, University of Tokyo
[*2] JST, CREST
[*3] RIKEN Nishina Center

References

1) Mizuno et al. : Bioresour Technol. **129**, 150–155 (2013)
2) Takeshita et al. : Bioresour Technol. **158**, 127-134 (2014)
3) Ota et al. : Bioresour Technol. **149**, 432-438 (2013)
4) Yamazaki et al. : Riken Accel. Prog. Rep. **47**, 301 (2014)

Effects of Ar-ion beam irradiation on survival rate of *Aurantiochytrium* sp.

K. Ikeda,*1 R. Kose,*1 T. Okuda,*1 Y. Sakakura,*1 K. Kaya,*1 Y. Kazama,*2 and T. Abe*2

The organisms that belong to the *Aurantiochytrium* sp. are heterotrophic marine thraustochytrids with a high growth rate. They produce many bioactive compounds such as squalene, docosahexanoic acid (DHA, $C_{22:6n-3}$) and odd-numbered fatty acids, and they are being improved in terms of their cellular cell functions for industrial utilization[1,2].

To introduce novel cell functions, irradiation with a swift, heavy-ion beam to induce mutations is an effective method[3]. At RIKEN RI Beam Factory (RIBF), microbial cells and plant seeds are irradiated with heavy-ion beams such as of carbon and argon (Ar).

In this study, *Aurantiochytrium* spp.NB6-3 and SYLR6#3 were selected because of their short lag times and industrial usage. The strains were exposed to accelerated Ar ions with a dose range of 20 Gy to 80 Gy. After irradiation, cells were cultured on GTY medium (2% glucose, 1% Tryptone, 0.5% yeast extract and 1.8% Red Sea Salt)-containing agar plates (ϕ90 mm) at 25°C for 48 h. The colonies were counted using the colony forming unit (CFU) to estimate their survival rates and were isolated for mutant screening. Values were expressed as averages of duplicate CFU experiments. Survival rate was obtained using the formula:

Survival rate (%) = (number of colonies) / (cell number before irradiation) x 100

The survival rates of both strains rapidly decreased with a dose of 20 Gy (Fig.1). The colony-forming cells were isolated from the agar plates and suspended in the sterilized GTY medium. The cell suspension was transferred to the cell-culture plates with 96 wells for primary screening. Cell density was measured using the iMark Microplate Reader (BIO RAD) at 650 nm. During the primary screening, based on the colony color and a higher growth rate, mutant cells were selected and transferred to test tubes for secondary screening. The colonies of *Aurantiochytrium* with high lipid contents showed cells also show orange to brown color. Therefore, to select mutants with high lipid contents, dark orange to brown colonies were picked out from the various mutated colonies.

During the secondary screening, the selected cells were cultured in test tubes with reciprocal shaking at 25°C for 48 h. The cell growth rate was measured using packed cell volume (PCV, %) and was converted to cell number.

Growth rate was calculated using the following equation:

$$\text{Growth rate (hour}^{-1}\text{)} = \ln(X_1 / X_0) / (t_1 - t_0)$$

where X_1 and X_0 are cell densities (cells/mL) at times t_1 and t_0, respectively. During the primary screening, 22 and 12 mutants were selected from the SYLR6#3 and NB6-3 strains, respectively. However, the characteristic features of the selected mutants in terms of their colors and high growth rates completely disappeared.

The effects of other heavy-ion beams on cells are being investigated.

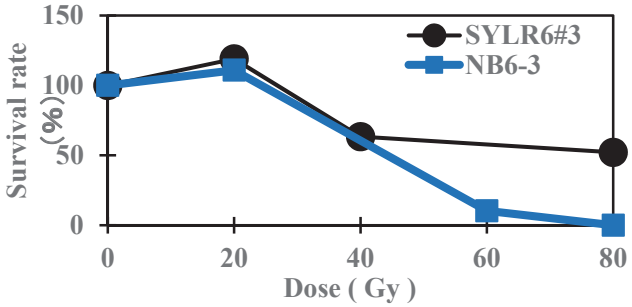

Fig.1 Survival curves of *Aurantiochytrium* sp.

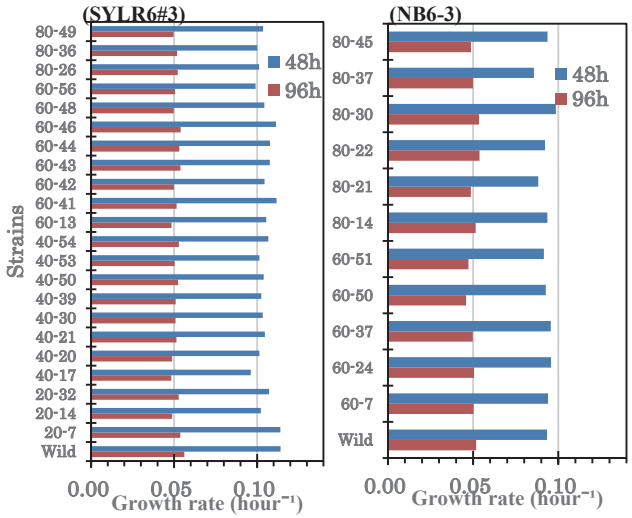

Fig.2 Growth rates of isolated strains estimated during the secondary screening

*1 Sea Act Co. Ltd.
*2 RIKEN Nishina Center

References

1) A. N. Jakobsen et al. : Appl Microbiol Biotechnol. 80 297-306 (2008).
2) Q. Li et al. : Agric. Food Chem., 57, 4267-4272 (2009)
3) A. Tanaka et al. : J. Radiat. Res., 51, 223-233 (2010)

Analysis of DNA breakpoint detected from rice exome sequencing data

R. Morita,[*1] K. Ishii,[*1] S. Kogure,[*1] K. Ichinose,[*1] Y. Hayashi,[*1] and T. Abe[*1]

We have performed exome sequencing analysis to reveal mutations induced by heavy-ion beams in rice. We used three software packages, GATK, Pindel, and BEDTools, to detect mutations from exome sequencing data. Among them, Pindel finds DNA breakpoints, decides the types of mutations such as deletion, insertion, inversion, and tandem duplication[1]. When Pindel cannot determine types of mutations, the mutation is called an "unassigned breakpoint". We found homozygous mutations called unassigned breakpoints from the rice mutant (Mutant-1) induced by Ne-ion beam irradiation. This mutant possessed three unassigned breakpoints. Two of these were located in the same chromosome, suggesting that they were breakpoints derived from an inversion.

We confirmed the candidate inversion by polymerase chain reaction (PCR) analysis. First, we estimated the position of two breakpoints, namely, breakpoint A and breakpoint B by using Integrative Genomic viewer[2]. Then, we designed primer F1 having the sequences in the upstream region of the breakpoint A (Fig. 1). We created primer R1 corresponding to the downstream region of this breakpoint. Similarly, primers F2 and R2 were synthesized on both sides of the breakpoint B. When PCR was carried out with primer sets F1R1 or F2R2 using wild-type genomic DNA as the template, DNA amplification was observed (Fig. 1). On the other hand, when PCR was carried out using Mutant-1 DNA as the template, no amplification of these DNA fragments should be observed (Fig. 1). When we attempted to amplify a DNA fragment with primer sets F1F2 and R1R2 using Mutant-1 DNA, DNA amplification should be observed (Fig. 1).

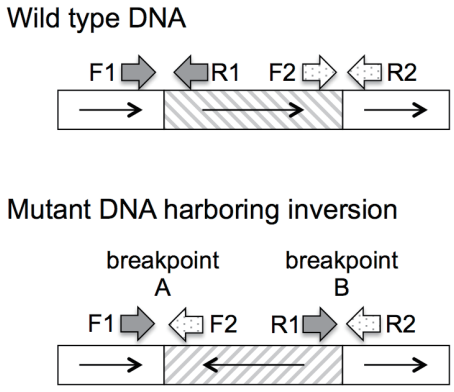

Fig. 1. Experimental design for detecting an inversion by PCR. Bold arrows indicate the annealing site of each primer. Thin arrows indicate the direction of the DNA. Boxes indicate chromosome.

[*1] RIKEN Nishina Center

We investigated the existence of the inversion from DNA amplification pattern in this way.

In the PCR experiment, DNA amplification was observed when we used primer sets F1F2 or R1R2 using mutant 1 genomic DNA as the template (Fig. 2). No amplification of these DNA fragments was observed when we used wild-type DNA as the template (Fig. 2). These results demonstrated that homozygous inversion existed in the Mutant-1 plant as we expected. Sequencing analysis using PCR products of the Mutant-1 plant revealed that 2-bp deletion occurred at breakpoint A and 5-bp deletion occurred at breakpoint B (Fig. 3). The distance from breakpoint A to B was 298.6 kb, and we found a new mutant gene disrupted by breakpoint B (Fig. 3). Our findings suggest that we can identify new mutated gene from a mutation that is called an "unassigned breakpoint" by using Pindel. PCR analysis of "unassigned breakpoint" mutations generated in other mutants is in progress.

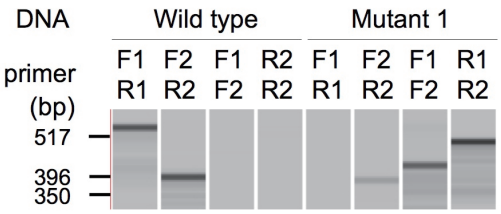

Fig. 2. Detecting an inversion generated in mutant-1. DNA amplification is detected by MCE-202 MultiNA (Shimadzu). The names of the genomic DNAs and primers are displayed above the gel image. DNA size markers are shown on the left side.

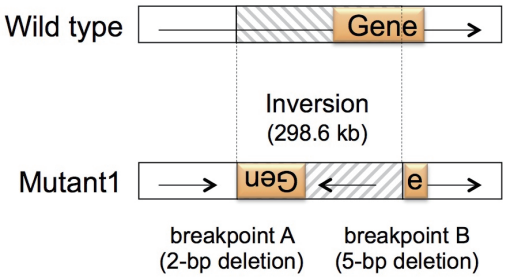

Fig. 3. Structure of inversion determined in this study. Thin arrows indicate the direction of the DNA. The gene disrupted by the inversion is shown as the yellow box.

References

1) K. Ye et al.: Bioinformatics. **25**, 2865 (2009).
2) J. T. Robinson et al.: Nature Genet. **29**, 24 (2011).

Establishment of rice transformation systems to study gene functions

R. Morita,[*1] K. Ichinose,[*1] Y. Shirakawa,[*1] and T. Abe[*1]

We have screened a large number of rice mutants induced by heavy-ion beam. To identify the causal gene for each mutant, a complementation test is needed. The complementation test is the experiment used to determine whether a gene is a causal gene for a mutant. The Recovery of a specific phenotype of a mutant is observed when an intact causal gene is introduced to a mutant (Fig. 1).[1)] To clarify the causal gene for the rice mutant of interest, we used a reliable Agrobacterium-mediated transformation system.[2, 3)] In the Agrobacterium-mediated method, a DNA region termed "T-DNA" transfers from a circular DNA in Agrobacterium into plant chromosomes (Fig. 2). We introduce both the gene of interest and the marker gene for a selection reagent, such as antibiotics or herbicides, into the T-DNA region. Plant cells that have accepted T-DNA will only survive on a medium containing a selection reagent. The Agrobacterium-mediated method is a good means to obtain a transgenic plant with high efficiency and a low copy number.

For a pilot experiment, we introduced the hygromycin phosphotransferase (HPT) gene in rice. The HPT gene confers hygromycin-resistance to rice cells and is one of the most frequently used marker gene in transformation experiments of rice. We obtained more than 20 plantlets from the calluses induced from 100 rice seeds (Fig. 3).

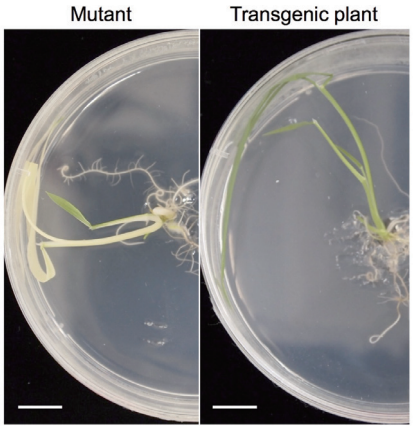

Fig. 1. Complementation test performed in the study of a rice virescent mutant. The virescent mutant generates white leaves when they are grown at 20 °C (left). Mutant plants that contain T-DNA including the intact causal gene show green leaves under the same condition (right). Rice plants are grown in the Murashige and Skoog medium. Bar = 1 cm.

[*1] RIKEN Nishina Center

The transformation efficiency of our experiment (over 20%) was equivalent to the efficiency reported by Toki et al. (2006). Using this technique, we will determine the causal gene for a rice mutant exhibiting an interesting phenotype.

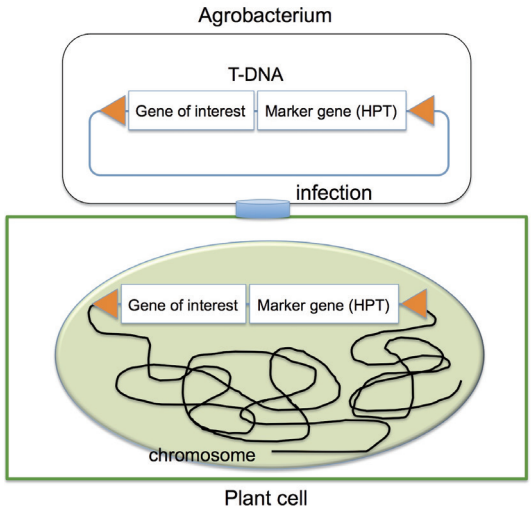

Fig. 2. Schematic representation of the Agrobacterium-mediated plant transformation system.

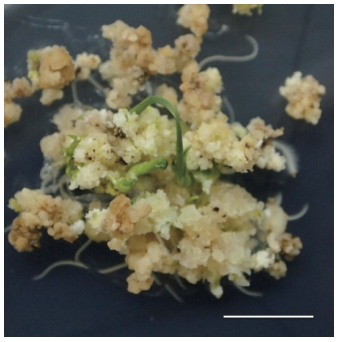

Fig. 3. Regenerated plant from the hygromycin-resistant callus. Bar = 1 cm.

References

1) R. Morita et al.: RIKEN Accel. Prog. Rep. **46**, 259 (2013)
2) S. Toki et al.: Plant J. **47**, 969 (2006)
3) H. Saika et al.: Transgenic Plants: Methods and Protocols **3**, 67 (2012)

Functional analysis of a new *virescent* mutant in rice induced by heavy-ion beam irradiation

H. Abe,[*1] R. Morita,[*1] S. Kogure,[*1] K. Ichinose,[*1] Y. Hayashi,[*1] and T. Abe[*1]

It is evident that heavy-ion beam irradiation effectively produced many phenotypic mutants in rice (*Oryza sativa* L. cv. Nipponbare)[1, 2]; thus, the method has been applied to rice breeding as a new technology. Although many rice mutants have been isolated to date, the functions of a number of their causative genes have not been completely elucidated. One such mutant, 22-4Y in rice, has been obtained as a *virescent* mutant by irradiating seeds with a carbon-ion beam (20 Gy, LET: 22.5 keV/μm)[3]. *virescent* is a chlorotic mutant of higher plants that reduces the chlorophyll content in young leaves, but the chlorophyll content of the leaves recover as the plants grow[4]. Certain classes of the *virescent* mutants are low-temperature conditional[4]; the 22-4Y mutant also shows chlorotic leaves phenotype when grown at 20 °C but not at 30 °C during the early growth stages[3]. As the 22-4Y functions are related with chlorophyll synthesis and/or chloroplast development, both of which are important for crop production, we decided to investigate the 22-4Y gene and to analyze its functions.

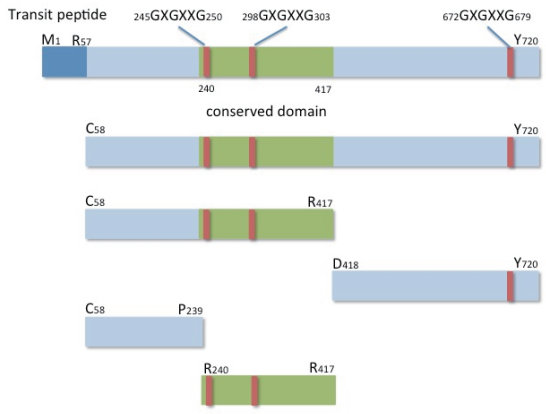

Fig. 1. Schematic representation of the 22-4Y protein and its fragments expressed in *E. coli*.

The predicted 22-4Y protein (the upper line) has 720 amino acids (M1-Y720) with a calculated molecular mass of 78.2 kDa. Each fragment of 22-4Y(C58-Y720), (C58-R417), (D418-Y720), (C58-P239) and (R240-R417) is shown. Positions of the FAD/NAD(P)-binding motif (GXGXXG) are shown in red bars. A region with homology to pyridine nucleotide-disulfide oxidoreductase family enzymes is shown in green. The predicted chloroplast transit peptide is shown in dark blue.

[*1] RIKEN Nishina Center

Genetic analysis of the 22-4Y mutant revealed that gene LOC_Os05g34040 on the long arm of chromosome 5 showed a deletion of 13095 bp[3]. Morita et al.[3] confirmed by using a genetic complementation test that the causative gene of 22-4Y is LOC_05g34040.

In order to know the gene functions, in many cases, it is most important and necessary to reveal the functions of the protein encoding to the corresponding gene. BLAST searches of the complete *Oryza sativa* sequence revealed that only one copy of the 22-4Y gene is present in the nuclear genome, which encodes a putative polypeptide of 720 amino acids with a calculated molecular mass of 78.2 kDa (Fig.1, the upper line). Pfam search predicted that the 22-4Y protein had a putative conserved FAD/NAD(P)-binding motif (GXGXXG) (Fig.1, red bars) and a homology to pyridine nucleotide-disulfide oxidoreductase family enzymes (Fig1, green region). This means that 22-4Y is a new class of VIRECENT protein among so far identified[4] (V1, chloroplast-localized RNA-binding protein; V2, guanylate kinase; V3, large subunit of ribonucleotide reductase). TargetP program predicted that the N-terminal 57 amino acids sequence of the 22-4Y protein was a chloroplast transit peptide. Actually, when the N-terminal 76 amino acids sequence of the 22-4Y protein was fused to cyan fluorescent protein (CFP) and transiently expressed in an onion epidermal cell, the fusion protein was localized to chloroplast. Thus, the N-terminal sequence of the 22-4Y protein was functional as a chloroplast targeting peptide. Electron microscopic observation revealed that chloroplast development was arrested when 22-4Y mutant was grown at 20 °C but not at 30 °C during the early growth stages. These results suggest that the 22-4Y protein was functional in chloroplast and had some important regulatory functions in chloroplast development.

To further reveal and analyze the protein function of 22-4Y, we decided to purify some recombinant proteins of 22-4Y by using an *E. coli* expression system (Fig. 1). It is important to demonstrate the enzymatic activity of the 22-4Y protein, as well as to identify the target (substrate) protein(s) to reveal the regulatory functions of the 22-4Y protein during chloroplast development.

References

1) Y. Hayashi et al.: RIKEN Accel. Prog. Rep. 43, 282 (2010).
2) Y. Hayashi et al.: RIKEN Accel. Prog. Rep. 46, xxiv (2013).
3) R. Morita et al.: RIKEN Accel. Prog. Rep. 46, 259 (2013).
4) K. Kusumi and K. Iba: Front Plant Sci. 5, 386 (2014).

Tracking alleles linked with Fusarium head blight resistance QTLs in wheat (*Triticum aestivum*) released in Kyushu region

S. Niwa,[*1,*2] Y. Kazama,[*1,*2] M. Alagu,[*2] T. Abe,[*1] and T. Ban[*2]

Fusarium head blight (FHB) is a plant diseaseoccuring in small grains such as wheat, barley and maize. In Japan, the FHB of wheat is one of the most destructive diseases because of its coincidence with the flowering to grain-filling period of wheat which provides a fungus-favorable condition. In addition, FHB decreases the yield and the quality of wheat.

The Kyushu region is one of the main wheat production areas in Japan. After the FHB epidemics in 1963, an intensive breeding program for FHB resistance has been conducted in Kyushu as a national breeding program. Similar to the general breeding program, FHB resistance breeding has been performed by crossing a cultivar of interest with another resistant cultivar. Then, progenies having appropriate traits are selected. Through this process, feasible alleles (feasible one of a number of alternative forms of the same gene) would be selected, which implies that the alleles linked to loci related to an unfavorable agronomic trait may also be excluded. Because of the annual variation in rainfall, FHB disease pressure fluctuates, causing rendering the evaluation of FHB resistance lines laborious and uncertain. By investigating the alleles related to the FHB resistance through the breeding linage, information on alleles contributing to the FHB resistance in the breeding program can be obtained.

As a first step, thirteen representative cultivars bred from 1920s to 2010s were selected. The seeds of the cultivars were sown on petri dishes and refrigerated at 4°C for four days; subsequently, they were germinated in a 25°C chamber. The germinated plantlets were transplanted to pots and grown in a glasshouse at 25°C. Leaves were harvested 18 days after sowing and used for DNA extraction. Of the 21 wheat chromosomes, DNA markers linked to the alleles related to FHB resistance were reported in the short arm of chromosomes 2D (2DS), long arm of 2D (2DL), 3BS, 5AS, and 6BS.1-4) By conducting PCR using these markers, types of alleles related to FHB resistance (resistant, susceptible, or other) in individual cultivars were determined. The fragment, after amplification with a DNA marker *UMN10* at 3BS was analyzed by sequencing. The PCR products of the other markers were electrophoresed using MultiNA (Shimadzu, Kyoto, Japan).

The results are listed in Table 1. Resistant alleles on 3BS and 5AS were retained after 'Shinchunaga' was bred. The resistant allele on 2DL was fixed in the linage after 'Asakazekomugi' was bred. In contrast, resistant alleles on 2DS and 6BS were excluded from the lineage for cultivars released after the 1940s released cultivars, when 'Shinchunaga' had contributed as their frequent crossing parent. Interestingly, the susceptible alleles from 'Shinchunaga' had been selected for 2DS, and the resistance alleles on 6BS were selected alternatively from the counter parents of 'Shinchunaga.' It can be expected that some alleles responsible for unfavorable agronomic trait(s) on 6BS from 'Shinchunaga' may be linked to these regions. 'Shinchunaga' has favorable allele (s) such as *rht8* thatdetermins plant height and was selected even linked with the susceptible allele for FHB. In the same manner, other alleles detected in modern cultivars might contribute to FHB resistance rather than the ones detected in old cultivars as new linkage disequilibrium. Further investigation of the alleles related to FHB resistance in every generation of lineages is in progress.

Table1 Types of FHB resistance-related alleles in Kyushu linages

Release		2DS	2DL	3BS	5AS		6BS	
year	Cultivar	TaMRP-D1	Xgwm539	UMN10	Xgwm293	Xgwm304	Xwmc398	Xgwm644
1923	Eshimashinriki	R	o	o	R	R	nd	nd
1931	Norin 5	R	R	o	R	R	o	R
1933	Shinchunaga	S	o	R	R	R	R	R
1936	Norin 20	R	o	R	R	R	R	R
1943	Norin 52	S	o	R	R	R	o	o
1956	Shirasagikomugi	S	o	R	o	S	o	o
1957	Junreikomugi	S	o	R	R	R	o	o
1978	Asakazekomugi	S	R	R	R	R	o	o
1986	Wheat Norin PL-4	S	R	R	R	R	R	nd
1986	Saikai 165	S	R	R	R	R	o	o
1994	Chikugoizumi	S	R	R	R	S	o	o
2006	Towaizumi	S	R	R	nd	R	o	o
2011	Wheat Norin PL-9	S	R	R	o	S	o	o

R: resistant allele, S: susceptible allele, o: other allele (resistant type unknown), nd: not determined

*1 RIKEN Nishina Center
*2 Kihara Institute for Biological Research, Yokohama City University

References
1) P. Cuthbert et al.: Theor. Appl. Genet. **114**: 429 (2007).
2) S. Liu et al.: Cereal Res. Commun. **36**: 195 (2008).
3) H. Buerstmayr et al.: Plant Breed. **128**: 1 (2009).
4) T. Suzuki et al.: Breed Sci. **62**: 11 (2012).

Ion track observation in cell nucleus irradiated by 3 MeV He ion microbeams produced with glass capillaries

T. Ikeda,[*1] M. Izumi,[*1] V. Mäckel,[*2] T. Kobayashi,[*2] R. J. Bereczky,[*1] T. Hirano,[*1] Y. Yamazaki,[*2] and T. Abe[*1]

Microbeam irradiation of cultured single cells using tapered glass capillaries with outlet diameters of the order of 1 μm has been performed employing RIKEN Pelletron accelerator. Apparatus with a 3-μm outlet diameter is reported in elsewhere[1]. Microbeam is a unique scheme [2] that can actively select an irradiation volume of ~μm^3. When a microbeam of He ions of a few MeV hits a target, e.g., a biological cell, the ions will stop at the depth corresponding to their range (10~20 μm). Any other parts downstream of the stopping volume will not be damaged. This is one of advantages of employing beams of a few MeV. The glass capillaries with thin end-windows play an important role in delivering the ions directly to the cells in solution.

At RIKEN, we have developed a unique technology for mutation breeding using high-energy heavy-ion beams from RIKEN Ring Cyclotron. Such high linear energy transfer (LET) ions produce clustered DNA damage that cannot be repaired by the cell itself, leading to cell death, or can only be repaired incompletely by the cell, which induces mutations. In order to investigate both the lethality and the effectiveness of mutation induction, the position selectivity of the microbeam will be needed because hitting of different parts may cause unwanted effect. Here we demonstrate the DNA damages along ion tracks in a cell nucleus using a microbeam with relatively high LET.

A 3-MeV He ion microbeam was used for the irradiation of the nucleus of human cells (HeLa cells) because it is known that there is a similarity in the radiation response between plant and animal cells. The ions were generated by the Pelletron and transported to the cell irradiation port[1]. A 5-cm-long glass capillary optics with a 4-μm-thick end-window whose diameter was 3 μm and with an inlet diameter of 0.8 mm was installed at the beam port with an angle of 45° with respect to the horizontal plane so that widely-used petri dish filled with liquid solution can be used. The LET of a 3-MeV He ion is 150 keV/μm in water. The range of the ions is only 12 μm in water after the end-window. In order to adjust the dose of the irradiation to each cell, a beam chopper consisting of an electrostatic beam deflector was employed so that a few to ten ions were included in a short pulse of 0.8 μs. The pulse was repeated 100-1000 times according to the number of the required ions to the target.

It took approximately 12 min to irradiate about 40 cells in one dish, and totally 168 cells in 4 dishes were irradiated. After the irradiation, the Double Strand Breaks (DSBs) at DNAs were fluorescent-labeled as follows. The time for the repair process based on an enzymatic reaction was 20 min after the irradiation, and then the cells were washed three times with ice-cold phosphate-buffered saline (PBS) and fixed with 4% formaldehyde in PBS at 4°C for 20 min. Then, the cells were permeabilized with 0.5% Nonidet P-40 in PBS at 4°C for 5 min, and phosphorylated histone H2AX was detected by using rabbit antibody (Millipore) and an Alexa488-conjugated donkey anti-rabbit IgG (Jackson ImmunoResearch Laboratories).

Figures 1(a) and (b) are the cross-sectional and bottom views of the irradiated cells, respectively, reconstructed from the photos taken by changing the focus position along the z-axis (vertical axis). Cell nuclei are identified as bean-shaped blue regions with a width of ~15 μm and have fluorescence from a stain DAPI binding to A-T rich regions in DNA. The outlines of the cells are not seen. The DSBs are detected as bright points with green color from Alexa488. Even without irradiation, DSBs can take place as an activity of a living cell. However, the concentration of DSB bright points along a line is an evidence of artificial lesion. The ion track with the angle of 45° is clearly seen as a fluorescent line in Fig. 1(a). We succeeded in observation of a visible track for MeV ions inside a cell nucleus. It is confirmed that MeV-ion irradiation made DSB lesions in the DNA, which may cause gene defects. Further experiments considering other conditions, e.g., LET, control of cell cycle, and so on are needed as well as the number of ions necessary to form a track.

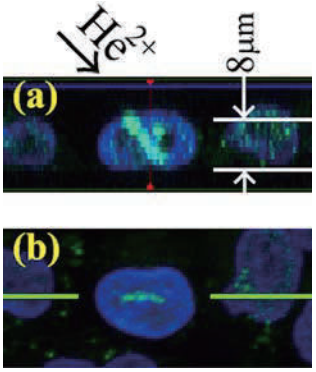

Fig. 1. Fluorescent lines corresponding to the ion track in a human cell nucleus. (a) Cross-sectional view of the irradiated cells at the horizontal line in the bottom view. (b) Bottom view of the cell.

References

1) V. Mäckel et al.: Rev. Sci. Instrum. **85**, 014302 (2014).
2) Y. Iwai et al.: Appl. Phys. Lett. **92**, 023509 (2008).

[*1] RIKEN Nishina Center
[*2] Atomic Physics Laboratory, RIKEN

Estimation method of microbeam divergence from glass capillaries for biological use

R.J. Bereczky,[*1] T. Ikeda,[*1] T. Kobayashi,[*2] M. Utsugi,[*3,*1] T. Hirano,[*4,*1] Y. Sakai,[*3] and T. Abe[*1]

Ion microbeams can be used in various fields such as basic research, or for many different technical applications such as in radiobiology. When an ion beam with energy on the order of megaelectron volts is transmitted through a tapered glass microcapillary, the extracted beam can be used as a ion microbeam for cell irradiation. Moreover, the ions can be directly guided to the cell using a capillary with a thin-end window. At RIKEN, we have developed a unique technology for mutation breeding using high-energy heavy-ion beams. Heavy-ion beams at relatively low doses induce mutations at a high rate without severely inhibiting growth. Densely ionizing radiation produces clusters of DNA damage that cannot be repaired by the cell, leading to cell death, or can only be repaired incompletely by the cell, which induces mutations. The effects of heavy-ion beams on both the lethality and effectiveness of mutation induction should be investigated in more detail in future studies. An ion microbeam is a useful tool for DNA damage or repair process research. The regions relevant to mutations in a living cell are not distributed uniformly, but concentrated into a small region. A well-defined microbeam is required to irradiate these small regions.

The purpose of our work is the development of microbeam irradiation for human cells, in which it is easy to observe DNA damages. Through these investigations, we provide an estimation method to define the beam divergence in a tapered glass capillary. Our studies have been performed both experimentally and theoretically. In the case of thinner capillaries, i.e., on the order of 1 micron, the divergence of the transmitted beam has been investigated, and similar experiments with a 200 μm diameter capillary without a thin end-window were also reported[1]. No study has yet reported on capillaries with outlet diameters in the 10 μm range and with thin end-windows, a size at which the application for cell irradiation is not obvious anymore.

The result of our first SRIM simulations[2] showed discrepancy from the experimental ones (see procedure below). When we changed the divergence of the beam inside the capillary from 0 to a nonzero value, i.e, 2.5°, the results of the simulation and the experiment were in good agreement (Fig. 1).

We measured the beam distribution extracted in air as a function of the distance between the exit of the capillary and a piece of CR-39, using He ions with the energy of 4.5 MeV produced by the RIKEN pelletron accelerator.

*1 RIKEN Nishina Center
*2 Atomic Physics Laboratory, RIKEN
*3 Toho University, Department of Physics
*4 University of Miyazaki, Faculty of Agriculture

The ions were transmitted through a tapered glass capillary (pulled from injection needle), set at the end of the beam line.
The inlet diameter of the capillary was 800 μm, the outlet diameter was 4 μm, and it had a thin end-window made of plastic with a thickness of 8 μm[3]. The length of the capillary was ~ 65 mm. The profile of the extracted beam was measured with CR-39 (Fig. 2). The average rate of the ions was 14 counts/s during the measurement. To avoid the overlap of the ion tracks on the CR-39 surface, the number of transmitted ions was chosen once as 200, and as 600 in the other cases.

Further systematic studies will be performed in the near future that will contribute to the development of microbeam irradiation of human cells.

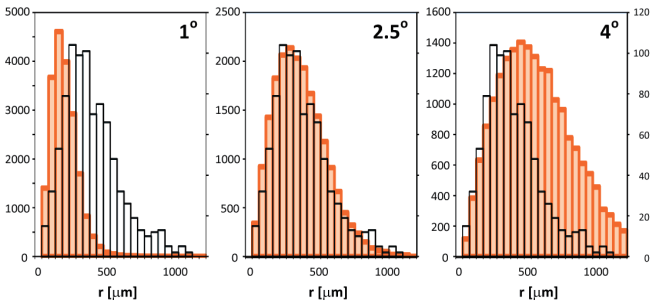

Fig.1. Comparison of the beam profile of the experiments (black) and SRIM simulations (orange). The horizontal axis shows the distance of the ion tracks from the center of the beam. The values of the beam divergence inside the capillary are shown in each figures. The distance between the exit of the capillary and the CR-39 was 6 mm.

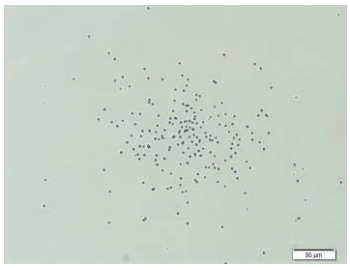

Fig.2. Profile of the extracted beam, when the distance between the exit of the capillary and the CR-39 was 2 mm. The scale corresponds to 50 μm.

References
1) N. Fujita et al.: NIMB **315**, 332-335 (2013).
2) SRIM-2013: http://www.srim.org/.
3) Y. Iwai et al.: Appl. Phys. Lett. **92**, 023509 (2008).

Fricke nanocomposite gel dosimeter for heavy ion beam irradiation

T. Maeyama,[*1] N. Fukunishi,[*1] K. L. Ishikawa,[*1,*2] K. Fukasaku,[*3,*4] and S. Fukuda[*5]

In advanced radiotherapy with energetic heavy ions such as pencil beam scanning treatment, a very complex dose distribution is applied to a desired target volume. A real 3D verification dosimeter is needed. Gel dosimetry has been proposed as a possible method for the 3D verification dosimeter in radiotherapy. One drawback of gel dosimetry is the decrease in radiation detection sensitivity with the increase in linear energy transfer (LET), which hinders absolute dose determination when used for ion beams. Thus, we have started developing new nanocomposite gel dosimeters based on the liquid radiation chemical dosimeter and diffusion suppression technique using adsorption properties of nano-clay. In our previous report, we presented the nanocomposite dichromate gel dosimeter with radiation-induced reduction reactions, which showed sensitivity degradation with increase in LET. [1] On the other hand, nanocomposite Fricke gel (NC-FG) with radiation-induced oxidation reactions exhibited the response almost independent of LET. These observations indicated a different LET dependence from that of the liquid radiation chemistry study, and therefore, more detail investigations were required. In this study, detailed radiological properties of NC-FG under various preparation conditions were investigated under argon and carbon beam irradiation covering an LET range from 10 to 3000 eV/nm. Details of the chemical compositions of gel dosimeters are summarized in Table 1. Irradiations were performed with 290 MeV/nucleon $^{12}C^{6+}$ or 500 MeV/nucleon $^{40}Ar^{18+}$ ion beams accelerated by the HIMAC. Measurements of the relaxation rates ($R_1 = 1/T_1$) were performed using a 1.5-T MRI (Philips).

Figures 1(a) and 1(b) show the R_1 ($1/T_1$) distributions measured for the normal NC-FG sample (composition was 1 wt% Laponite, 3 wt% gelatin, 1 mM ammonium iron (II) sulfate, and 50 mM perchloric acid, as shown in our previous report [2]) irradiated with 290 MeV/nucleon carbon ion beams and 500 MeV/nucleon argon ion beams, respectively. The dose dependence of R_1 near the entrance surface (square symbol, 5 mm depth) and near the Bragg Peak (circle symbol, 79 mm for carbon beam, 105 mm for argon beam) was shown in Figs. 1(c) and 1(d). Although the peak positions of each irradiated sample was adjusted within 1 pixel of the MRI resolution (0.78 mm) to ensure overlapping, a good linearity was confirmed at every position. The rate of R_1 incensement per unit of entrance surface dose was calculated and is plotted in Figs. 1(e) and 1(f) to compare it with the dose distribution obtained by the ionization chamber (right vertical axis in Fig. 1). The δR_1 distribution of NC-FG faithfully reproduces the dose distribution including the peak of argon ion beam. Surprisingly, the radiation sensitivity of NC-FG does not change even at very high LET (3000 eV/nm) at the Bragg peak region of argon ion beam. This is a unique property because all gel and solid type dosimeters such as film, scintillation, and semiconductor dosimeters have LET dependence.

By varying the concentration of the nano-clay, Fe^{2+} and perchloric acid from the standard composition described in our previous report, we have obtained the following features.

1. NC-FG works not only in an acidic, but also in a neutral condition.
2. The concentration of ferrous ions affects radiation sensitivity.
3. Radiation sensitivity is lost at nano-clay concentration below 0.1 wt%.

The first two features were completely different from those of conventional Fricke gel dosimeters. The third feature suggested that nano-clay in NC-FG is essential for radiation induced reactions, and that ferrous ions oxidize by a new mechanism that completely different from the previous one.

Table 1 Chemical composition.

Gelatin	Laponite	$HClO_4$	Fe^{2+}	Degassing
3 wt%	0.1 – 1 wt%	0 - 150 mM	0.2 - 5 mM	Ar

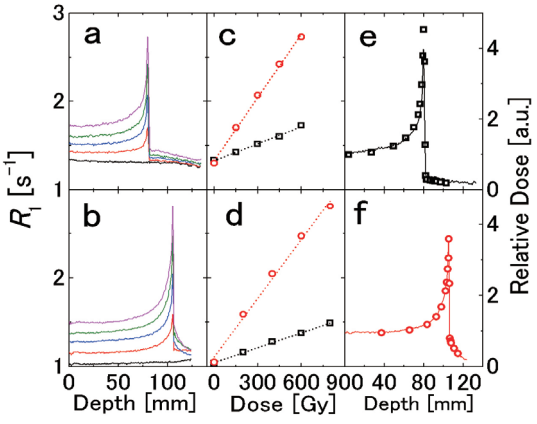

Fig. 1. Dose dependence of R_1 distribution with different ion beam irradiation.

*1 RIKEN Nishina Center
*2 Dept. of Nucl. Eng. & Management, Grad. Sch. Eng., Univ. of Tokyo
*3 RIKEN Advanced Center for Computing and Communication
*4 Dept. of neurosurgery, Himon'ya Hospital
*5 NIRS Research Center for Charged Particle Therapy

References

1) T. Maeyama et al.: J. Phys. Conf. Ser. 444, 012033 (2013).
2) T. Maeyama et al.: Radiat. Phys. Chem. 96, p.92 (2014).

IV. OPERATION RECORDS

Program Advisory Committee meetings for nuclear physics and for material and life science

K. Yoneda, [*1] K. Ishida, [*1] H. Yamazaki, [*1] N. Imai, [*2] K. Yako, [*2] H. Ueno, [*1] and H. Sakai[*1]

The Program Advisory Committees (PAC) is in charge of reviewing scientific proposals submitted for use of the accelerator facility of RIKEN Nishina Center (RNC). In Fiscal Year 2014, three PAC meetings were held; two for proposals of nuclear physics (NP-PAC), and one for proposals of material and life science (ML-PAC). The NP-PAC meetings were co-organized by RNC and the Center for Nuclear Study (CNS), the University of Tokyo. The NP-PAC reviewed experimental proposals at RIBF, whereas the ML-PAC reviewed proposals at Rutherford Appleton Laboratory (RAL) and RIBF.

NP-PAC

The 14th and 15th NP-PAC meetings were held on June 27 and 28, 2014, and December 12 and 13, 2014, respectively[1)]. In the 14th (15th) NP-PAC meeting, 23 (20) proposals were reviewed, and 11 (14) proposals were approved as grade S or A. The outcome of these NP-PAC meetings is summarized in Table 1.

Before the 14th NP-PAC meeting, one of the PAC members resigned, and no new member was added. Consequently, the number of the PAC members became sixteen.

The PAC members of the 14th and 15th NP-PAC meetings are as follows:
M.N. Harakeh (KVI, the chair), R.F. Casten (Yale Univ.), H. Emling (GSI), H. Iwasaki (Michigan State Univ.), W. Loveland (Oregon State Univ.), S. Nakamura (Tohoku Univ.), T. Nakatsukasa (RNC), T. Nilsson (Chalmers Univ. of Technology), C. Scheidenberger (GSI), B. Sherrill (FRIB Lab.), O. Sorlin (GANIL), A. Tamii (RCNP, Osaka Univ.), F.-K. Thielemann (Univ. of Basel), Y. Utsuno (JAEA), M. Yahiro (Kyushu Univ.), and Y. Ye (Peking Univ.).

Table 1. Summary of the outcome of the 14th and 15th NP-PAC meetings. The proposals ranked with S and A are treated as the "approved" proposals.

14th NP-PAC (June 27 – 28, 2014)	requested proposals (days)	approved proposals (days)
GARIS (RILAC)	1 (26)	1 (26)
CRIB (AVF)	3 (37)	1 (18)
RIPS (RRC)	3 (38)	3 (16.5)
BigRIPS/ZDS	9 (88)	3 (20.5)
SHARAQ	1 (5.5)	0 (0)
SAMURAI	6 (50.5)	3 (21)
Construction	0 (-)	0 (-)
Total	23 (245)	11 (102)

15th NP-PAC (December 12 – 13, 2014)	requested proposals (days)	approved proposals (days)
GARIS (RILAC)	0 (0)	0 (0)
CRIB (AVF)	3 (19.333)	3 (19.333)
RIPS (RRC)	0 (0)	0 (0)
BigRIPS/ZDS	12 (91.5)	7 (34)
SHARAQ	0 (0)	0 (0)
SAMURAI	5 (40.5)	4 (12.5)
Construction	0 (-)	0 (-)
Total	20 (151.333)	14 (65.833)

ML-PAC

The 11th ML-PAC meeting was held on January 8 and 9, 2015[2)]. In this meeting, 31 RAL proposals and 8 RIBF proposals were reviewed. The summary of the outcome of the meeting is given in Table 2.

Table 2. Summary of the outcome of the 11th ML-PAC meeting.

11th ML-PAC (January 8 – 9, 2015)	requested proposals (days)	approved proposals (days)
RAL	31 (208)	30 (123)
RIBF	8 (66)	7 (50)
Total	39 (274)	37 (173)

The 11th ML-PAC members are as follows:
J.-M. Poutissou (TRIUMF, the chair), A. Amato (PSI), T. Azuma (RIKEN), A. Hiller (ISIS, RAL), R. Kadono (KEK), A. Kawamoto (Hokkaido Univ.), N. Kojima (Univ. of Tokyo), K. Kubo (ICU), D.E. MacLaughlin (UC Riverside), S. Maekawa (JAEA), P. Mendels (Univ. Paris, Orsay), H. Yamase (NIMS), S. Yoshida (Thera Projects Associates), and X.G. Zheng (Saga Univ.).

References
1) http://www.nishina.riken.jp/RIBF/NP-PAC/index.html
2) http://www.nishina.riken.jp/RIBF/ML-PAC/index.html

*1 RIKEN Nishina Center
*2 Center for Nuclear Study, the University of Tokyo

Beam-time statistics of RIBF experiments

K. Yoneda,[*1] H. Ueno,[*1] and H. Sakai[*1]

This report describes the statistics of the beam times (BTs) at the RIBF facility in Fiscal Year (FY) 2014. In the following, the BTs are categorized into two groups: high-energy-mode and low-energy-mode BTs. In the former mode, the beams were delivered in the acceleration scheme of AVF, RILAC, or RILAC2 → RRC → (fRC → IRC →) SRC, where the accelerators in parentheses can be skipped in the cascade acceleration, depending on the beam species used. In the latter mode, the acceleration scheme is AVF or RILAC (→ RRC).

BTs in the high-energy mode were scheduled from April to July, from October to December 2014, and in the latter half of March 2015, considering the restriction of utility-power use, budgetary constraints, maintenance schedule of the accelerator system and co-generation system, as well as other constraints. In the series of experiments in spring, the primary beams of ^{238}U, ^{70}Zn, ^{2}H, and ^{16}O were provided to users, and in the autumn series, the primary beams of ^{238}U and ^{48}Ca were provided. The beam time in March 2015 was used only for the nuclear transmutation program which was carried out as a Nishina Center mission program, i.e. as an experiment other than what the RIBF Program Advisory Committees[1)] (PAC) was approved. 13 experiments approved by the PAC with the approved beam time of 70.4 days were conducted in total. 7.3 days were used for the facility development programs, defined as machine study (MS) experiments. Other than these, three new isotope search experiments and two transmutation experiments were conducted as the Nishina Center mission programs.

The data summary of the high-energy-mode BTs in FY2014 is given in Fig. 1 as a bar chart. Compared to the beam time in FY2013, the user time increased, as the beam time operation in FY2013 was in spring only. Including the Nishina Center mission beam time, the total amount of beam time available in FY2014 was recovered to the level of FY2012.

The data summary for the low-energy mode is shown in Fig. 2. Here the BTs are classified by the accelerator operation modes, AVF, RILAC, and RRC. In FY2014, most of the low-energy-mode experiments after December had to be cancelled, due to the restriction of the operation budget. Despite of this cancellation, the total amount was almost the same as in FY2013. The fraction of the RILAC stand-alone beam time increased, as a long experiment approved as the S grade was conducted.

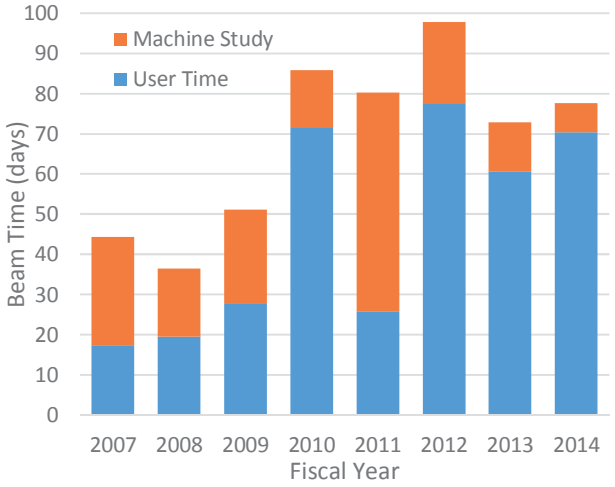

Fig. 1. Bar chart showing the BT statistics for high-energy-mode experiments from FY2007 to FY2014. The accelerator tuning time and Nishina Center mission time are not included.

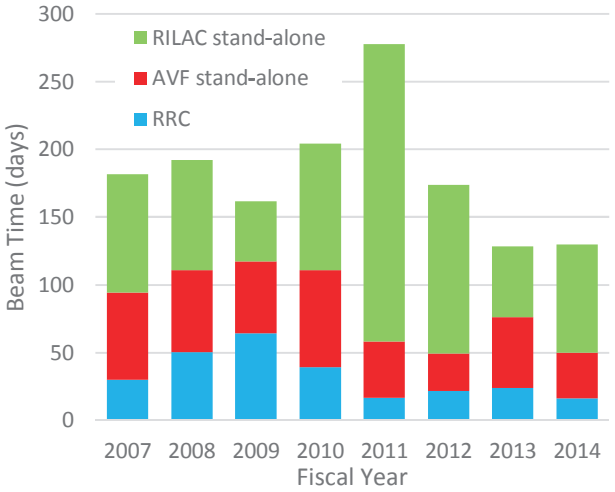

Fig. 2. Bar chart showing the BT statistics for low-energy-mode experiments from FY2007 to FY2014.

References

1) K. Yoneda, K. Ishida, H. Yamazaki, N. Imai, K. Yako, H. Ueno, and H. Sakai: In this report.

*1 RIKEN Nishina Center

Operation report of the industrial cooperation team

A. Yoshida,[*1] T. Kambara,[*1] H. Takeichi,[*1] H. Haba,[*1] S. Shibata,[*1] K. Takahashi,[*1] S. Yanou,[*2] and Y. Wakitani[*2]

In 2014, the industrial cooperation team was engaged in collaboration research for industrial application of RI beam, fee-based utilization of heavy-ion beams to industry, and fee-based distribution of radioisotopes. These activities are summarized below.

Under a collaborative research agreement entitled "Development and application of wear diagnosis method with RI beams" between RIKEN, University of Tokyo, and two private companies, we develop a method for wear diagnostics of industrial materials using RI beams as tracers. Compared with conventional methods where tracer RIs are produced in the materials by ion-beam irradiations, our method employs RI-beam implantation for the materials, which results in less radiation damage in the materials. We had two beamtimes, IC13-01-01 in February and IC13-01-02 in March 2014, at E7A beamline of the AVF cyclotron. Beams of RI nuclei ^{7}Be ($T_{1/2}$ = 53 days) with intensities up to 10^{8} ions/s and ^{22}Na ($T_{1/2}$ = 2.6 years) with intensities up to 10^{7} ions/s were provided by CNS RI beam separator (CRIB) and implanted near the surface of metallic machine parts, whose wear-loss was evaluated through radioactivity measurements. Another article in this report describes technical details on the preparation and characterization of the RI beams.[1] Concerning this research, two patents have been applied for.[2]

RIKEN Nishina Center opened the AVF cyclotron, RILAC, and RIKEN Ring Cyclotron (RRC) for industrial utilizations.[3] The first proposal of fee-based utilization was submitted by private companies in June and was reviewed and approved by the Industrial Program Advisory Committee (InPAC) in August (proposal number IC14-01). The beamtime was performed in October with a 70-MeV/A ^{84}Kr beam at the E5A beamline of the RIKEN Ring Cyclotron. Another article in this report describes technical details of the beam preparation and characterization according to the customers' requests.[4]

Since 2007, RIKEN distributes radioisotopes (RIs) produced at RIBF to users in Japan for a fee in collaboration with the Japan Radioisotope Association[5] (JRIA). According to a material transfer agreement (MTA) drawn between JRIA and RIKEN, JRIA mediates the transaction of the RIs and distributes them to users. The distributed RIs are ^{65}Zn ($T_{1/2}$ = 244 days), ^{109}Cd ($T_{1/2}$ = 463 days), and ^{88}Y ($T_{1/2}$ = 107 days). The RIs are produced by the RI Applications Team at the AVF cyclotron. ^{65}Zn, ^{109}Cd, and ^{88}Y are produced with a 24-MeV deuteron beam through ^{65}Cu(d,2n)^{65}Zn, ^{109}Ag(d,2n)^{109}Cd, and ^{nat}Sr(d,xn)^{88}Y reactions, respectively.

In 2014, we delivered three shipments of ^{109}Cd with a total activity of 22 MBq, seven shipments of ^{65}Zn with a total activity of 44 MBq, and one shipment of ^{88}Y with an activity of 1 MBq. The final recipients of the RIs were five universities, one research institute, and two hospitals. Figure 1 shows the yearly trends in the number of orders and the amounts of the distributed RIs.

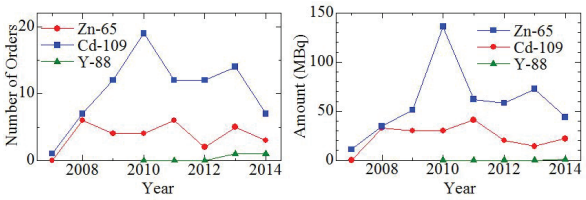

Fig. 1. Number of orders (left) and amount (right) of the RIs distributed yearly from 2007 to 2014. The distribution of ^{88}Y started in 2010.

Information on the RIs can be obtained from JRIA through their dedicated website (https://www.j-ram.net/jram/DispatchTopPage.do; in Japanese) or FAX (03-5395-8055).

References

1) A. Yoshida et al.: in this report.
2) A. Yoshida et al.: Japanese Patent No. 2014-4555 and T. Kambara, A. Yoshida and H. Takeichi: Japanese Patent No. 2014-34417.
3) http://ribf.riken.jp/sisetu-kyoyo/ (Japanese).
4) T. Kambara et al.: in this report.
5) http://www.jrias.or.jp/ (Japanese), http://www.jrias.or.jp/e/ (English).

*1 RIKEN Nishina Center
*2 Japan Radioisotope Association

Electric power condition of Wako campus in 2014

E. Ikezawa, *[1] M. Kato, *[1] H. Yamazawa, *[1] and M. Kase*[1]

The monthly electrical power consumption data for RIKEN Wako campus (Wako) and RIKEN Nishina Center (RNC), and the energy supply by the cogeneration systems (CGSs) are shown in Fig. 1. The hourly average electrical power consumption at RNC for each day in 2014 is shown in Fig. 2. The annual data of electrical power consumption and energy supply in 2014 is listed in Table 1. The total electrical power consumption of Wako in 2014 was 157,943 MWh, which was 10% higher than that in 2013. On the other hand, the total electrical power consumption of RNC in 2014 was 72,724 MWh, which was 30% higher than that in 2013. When the RI Beam Factory (RIBF) experiments using the uranium (^{238}U) beam were conducted, the maximum electrical power supply to Wako from Tokyo electric power corporation (TEPCO) reached 22.0 MW with a CGS output of 3.5 MW on April 9, 2014, whereas the maximum electrical power consumption of RNC reached 17.1 MW on October 21, 2014.

A complete overhaul of the gas turbine of the CGS #1 after 8,000 h of operation was carried out in September 2014.

We experienced the following problems during the reporting period. The CGS #1 stopped on May 25, 2014, and again, on October 21, 2014, because of control equipment failure. We had an interruption in power supply on February 15, 2014, due to a snow storm. Earth leakages also occurred 9 times. However, the origin of most of those leakages were unexplained.

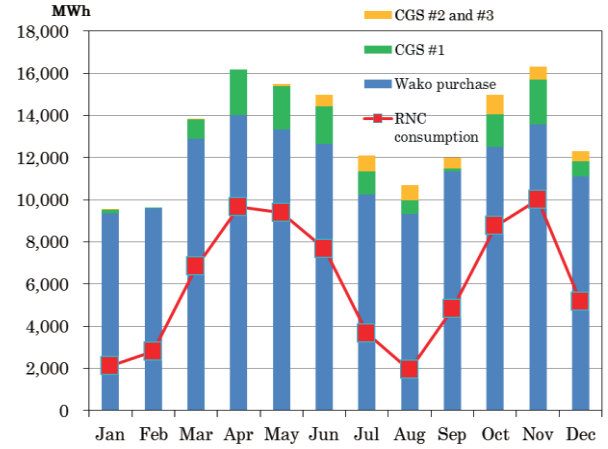

Fig.1 Monthly electrical power consumption and energy supply by CGSs in 2014.

Fig.2 Hourly average electrical power consumption at RNC for each day in 2014.

Table 1 Annual data of electrical power consumption and energy supply in 2014.

	Total	Unit	Note	% of 2013
Wako purchase	139,851	MWh	Total electrical power supply to Wako from TEPCO	111%
Wako consumption	157,943	MWh	Wako electrical power consumption (CGSs + TEPCO)	110%
RNC purchase	59,319	MWh	Total electrical power supply to RNC from TEPCO	137%
CGS #1	13,405	MWh	CGS #1 total electrical power output	107%
RNC consumption	72,724	MWh	RNC total electrical power consumption	130%

*[1] RIKEN Nishina Center

Radiation safety management at RIBF

K. Tanaka,*1 Y. Uwamino,*1 H. Sakamoto,*1 R. Hirunuma-Higurashi,*1 H. Mukai,*2 A. Akashio,*1 T. Okayasu,*1
R. Suzuki,*3 M. Takekoshi,*3 Y. Yamauchi,*3 S. Fujita,*1 H. Aiso,*1 K. Igarashi,*1 S. Iizuka,*1 and N. Usudate*1

Residual radioactivity at the cyclotron deflectors was measured just before maintenance works were carried out in the summer of 2014. The same measurement has been performed regularly since 1986, and the variations in the dose rates are shown in Fig. 1. Considering that the dose rate depends on the beam intensity and the cooling time, the trend has not changed considerably since 2006, when RIBF operation started.

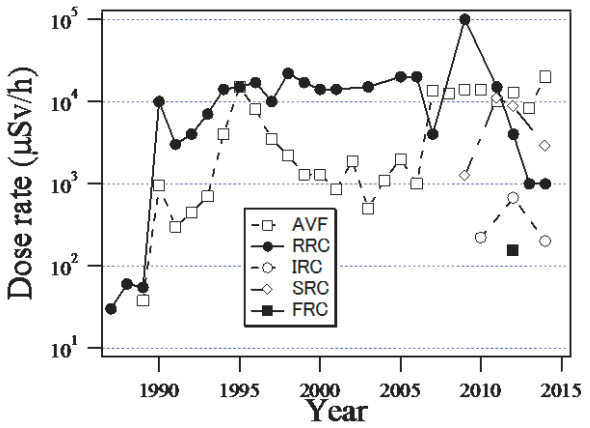

Fig. 1. Dose rates of residual radioactivity at the deflectors of five cyclotrons.

The residual radioactivity was measured along the beam lines after almost every experiment. Points 1–26, marked with solid circles in Fig. 2, are locations where high-residual dose rates were usually observed. Table 1 lists these dose rates and the measurement dates, beam conditions, and the decay periods after the end of operation. The conditions for the data are chosen to be maximum doses among the measured data at each points. The maximum dose rate was found to be 17 mSv/h at point 13, which is the neighbor of the G01 Faraday cup.

We continuously monitor the radiation in and around the RIBF facility by using neutron and gamma area monitors. In 2014, the annual dose at the site boundary were less than the detection limit of the monitors after background correction. The neutron dose had been lower than the detection limit of 2 μSv/y and the γ-ray dose had been lower than the detection limit of 8 μSv/y. Therefore, the annual total dose in 2014 was less than 10 μSv/y, which was considerably lower than the legal limit of 1 mSv/y.

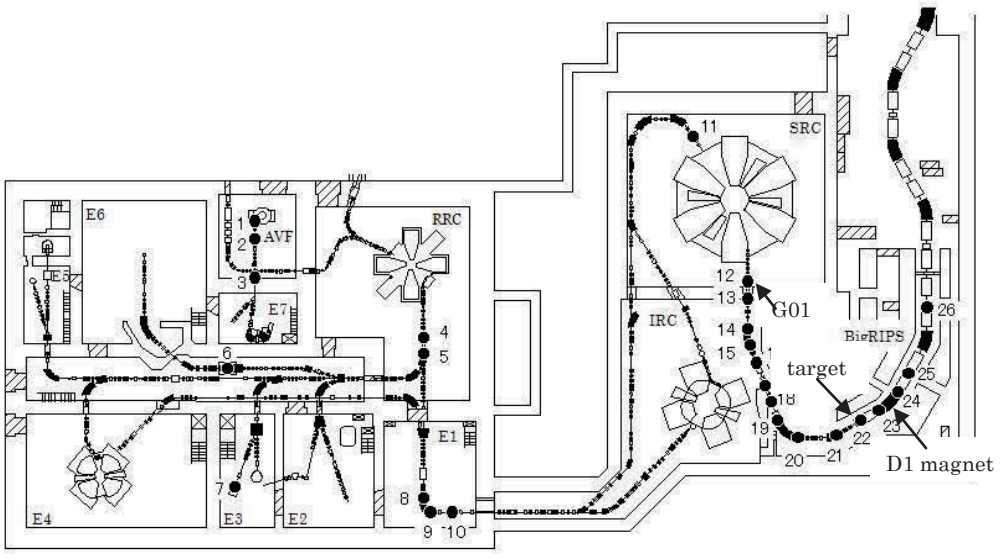

Fig. 2. Layout of beam lines at RIBF. Locations listed in Table 1 are indicated. G01, the target, and D1 magnet are also shown.

*1 RIKEN Nishina Center
*2 Japan Environment Research Corporation
*3 Daiwa Atomic Engineering Corporation

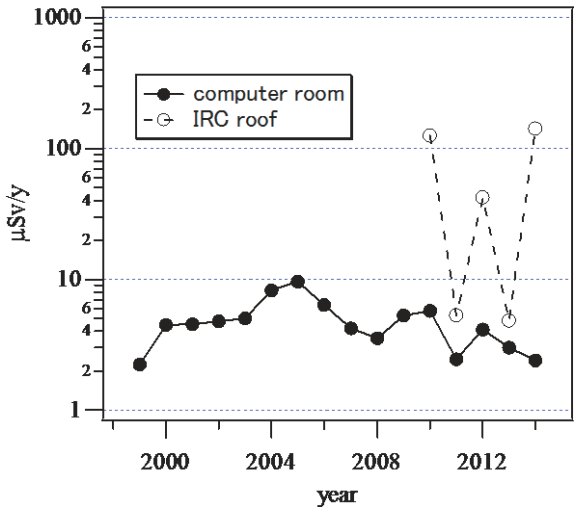

Fig. 3. Accumulated leakage radiation at the boundary of the radiation-controlled area.

The dose rates at the radiation-controlled area in 2014 have been monitored. Three monitors are placed at the boundary of the radiation-controlled area. One is in the computer room of the Nishina building, and the other two are on the roofs of the IRC and BigRIPS. The highest observed value was 142 μSv/y at the IRC roof as a result of beam loss at the transport line between SRC and BigRIPS. Figure 3 shows the annual neutron dose at these locations since 1999. These were considerably lower than the legal limit of 1.3 mSv/3 month. The dose on the BigRIPS roof was below the detection limit of 3 μSv/y for neutrons.

The water in closed cooling systems at BigRIPS was sampled after the 2014 operation of RIBF. A 345-MeV/u 20 particle nA, on average, ^{238}U beam was provided during April and May, and during October and November. A ^{70}Zn 75 particle nA was provided in May and June. A 400 particle nA ^{48}Ca beam was in November and December. Radionuclide concentrations were measured by using a liquid-scintillation counter and a Ge detector to compare them with the legal limit. The results are shown in Table 2. After operation with the intense ^{48}Ca beam, the summation of the ratios of the concentrations to the legal limits for the drain water of all the radionuclides at the BigRIPS became approximately 1/4, and the water was transferred into the drain tank before the next operation. This is to prevent contamination of the room in case of a water leakage. The water in the drain tank, which contains drain water from other places, is released after the concentration of radionuclides is confirmed to be lower than the legal limit. This water circulates in the closed system with ion exchange resins. Thus, the nuclides in waters listed in Table 2, with the exception of tritium, are already filtered values. However, tritium accumulates in the water because the nuclide has a long half life of 12.3 year and is difficult to remove with filters. At the measurement before beam irradiation in 2014, the concentration of tritium in water in all systems was approximately 3 Bq/cm^3.

Table 1. Dose rates measured at beam lines in 2014. Points 1−26 indicate the measured locations shown in Fig. 2.

Point	Dose rate (μSv/h)	Date (M/D)	Particle	Energy (MeV/u)	Intensity (pnA)	Decay period (h)
1	55	7/23	α	12.5	400	54
2	650	7/23	α	12.5	400	54
3	450	7/23	α	12.5	400	54
4	100	10/8	Kr-84	70	0.07	19
5	1000	11/14	U-238	10.75	1430	13
6	190	12/16	Ca-48	63	200	2215
7	80	7/23	N-14	135	500	15621
8	1300	12/16	Ca-48	45.4	938	113
9	2000	7/23	O-18	88	51	534
10	70	7/23	O-18	88	51	534
11	170	12/16	Ca-48	345	530	110
12	5000	12/16	Ca-48	345	530	110
13	17000	12/16	Ca-48	345	530	110
14	550	12/16	Ca-48	345	530	110
15	700	12/16	Ca-48	345	530	110
16	100	12/16	Ca-48	345	530	110
17	400	12/16	Ca-48	345	530	110
18	750	12/16	Ca-48	345	530	113
19	100	12/16	Ca-48	345	530	113
20	150	12/16	Ca-48	345	530	113
21	1500	12/16	Ca-48	345	530	113
22	3000	12/16	Ca-48	345	530	113
23	7000	12/16	Ca-48	345	530	113
24	2800	12/16	Ca-48	345	530	113
25	325	12/16	Ca-48	345	530	113
26	150	12/16	Ca-48	345	530	113

In 2014, the primary beam mode was newly mounted on the safety management system of RIBF by considering the high radiation dose risk due to the intense beam. The target intensity of the primary beam in RIBF is 6×10^{12} particle/second on the production target of BigRIPS. Then, a secondary beam of low intensity is generated via a nuclear reaction and separation through BigRIPS. However, in the experimental rooms located downward from BigRIPS, the permitted beam intensity is 10^7 particle/second both for primary and secondary beams. In RIBF operation, faint primary beams are sometimes derived to the experimental rooms directly. If intense primary beams more than the permission derived to the experimental rooms owing to accelerator trouble etc., the interlock system work in a moment and stop the beam automatically. However, a delay of few seconds is necessary before a beam is stopped by the interlock system operation. There may be a serious risk of radiation exposure to workers even in the neighbor rooms that are outside the irradiated area. Therefore, the safety

management system was improved to inhibit the unexpected radiation exposure.

The primary beam mode in the radiation control system affects the restriction area, accelerator operation, and beam transport operation. When the primary beam mode is started, the entry-forbidden area is first expanded to the neighbor experimental rooms of the beam delivered area. Secondly, a combination of the attenuation devices of the accelerator, which control the beam intensity, is limited to regulate the beam intensity less than permitted limit. Additionally, while the primary beam mode is off, the magnetic field of the D1 magnet of BigRIPS, which determines whether the primary or secondary beam is transported to the experimental rooms, is always monitored. Moreover, if the value corresponds to a primary beam transportation, the safety management system does not permit beam irradiation until the primary beam mode is on, which means no-entry allowed to the neighbor experimental rooms. With these improvements, radiation exposure risk due to unexpected intense beams is mitigated.

Table 2. Radionuclide concentrations in cooling water of BigRIPS, the allowable legal limits for drain water, and the ratio of the concentration to the allowable limit.

Cooling water	Nuclide	Concentration[a] (Bq/cm^3)	Limit[b] (Bq/cm^3)	Ratio to limit [a/b]
BigRIPS F0 target	H-3	14	60	0.23
	Be-7	1.5e-3	30	4.9e-3[1)]
	Co-58	8.2e-4	1	8.2e-4
	Mn-54	6.4e-4	1	6.4e-4
			summation	0.23
BigRIPS exit beam dump	H-3	12	60	0.2
	Be-7	1.7e-2	30	5.7e-4
	Co-57	1.2e-3	4	2.9e-4
	Co-58	3.7e-3	1	3.7e-3
	Mn-54	9.7e-4	1	9.7e-4
			summation	0.21
BigRIPS side-wall beam dump	H-3	11	60	0.18
	Be-7	0.14	30	4.7e-3
	Co-58	1.3e-3	1	1.3e-3
			summation	0.19

1) read as 4.9×10^{-3}

RILAC operation

E. Ikezawa,*1 T. Ohki,*2 M. Kase,*1 T. Nakagawa,*1 N. Sakamoto,*1 H. Okuno,*1 N. Fukunishi,*1
M. Komiyama,*1 A. Uchiyama,*1 T. Maie,*1 M. Nagase,*1 M. Fujimaki,*1 T. Watanabe,*1 H. Hasebe,*1
H. Imao,*1 H. Kuboki,*1 K. Ozeki,*1 K. Suda,*1 Y. Higurashi,*1 K. Yamada,*1 Y. Watanabe,*1 S. Watanabe,*1
T. Nagatomo,*1 T. Aihara,*2 H. Yamauchi,*2 K. Oyamada,*2 M. Tamura,*2 A. Yusa,*2 K. Kaneko,*2 and O. Kamigaito*1

The RIKEN heavy-ion linac (RILAC) has operated steadily throughout the reporting period and has supplied various ion beams for different experiments. Some statistics regarding the RILAC operation from January 1 to December 31, 2014, are given in Table 1. The total beam service time of the RILAC accounted for 84.5% of its operation time. The two operation modes of the RILAC, the standalone mode and the injection mode, in which the beam is injected into the RIKEN Ring Cyclotron (RRC), accounted for 53.1% and 46.9% of the total beam service time of the RILAC, respectively. For beam experiments and machine study of the RI Beam Factory (RIBF), a 2.650-MeV/nucleon ^{70}Zn-ion beam and a 2.675-MeV/nucleon ^{48}Ca-ion beam accelerated by the RILAC were injected into the RRC from May 12 to June 7 and from November 12 to December 11 2014, respectively. Table 2 lists the beam service times in the standalone mode of the RILAC allotted to each beam course in the RILAC target rooms in 2014. The e2 beam course in target room no. 1 was used in experiments using the GARIS2. The e3 beam course in target room no. 1 was used in experiments using the GARIS. The e6 beam course in target room no. 2 was used in the analysis of trace elements. Table 3 lists the operation time of the 18-GHz ECR ion source (18G-ECRIS) in 2014.

We carried out the following improvements and overhauls during the reporting period.

1) In the RF systems, the DC high-voltage power supplies were subjected to annual inspection. The major components of mechanical parts were subjected to simple inspection. The contact fingers for the trimmer of CSM cavities were replaced with new ones.
2) Two water pumps were overhauled. The other water pumps were subjected to simple inspection. All cooling towers were subjected to monthly inspection and annual cleaning.
3) All the turbomolecular pumps were subjected to annual inspection. Cryogenic pumps used for the no. 1 and no. 2 cavities of RILAC and the A5 and A6 cavities of CSM were overhauled. A compressor unit of the cryogenic pump used for the no. 5 RILAC cavity was repaired.

We faced the following mechanical problems during the reporting period.

1) A section of the cooling pipe of an earth ring for the lower stem in the FC-RFQ cavity had a vacuum leak. We repaired the pipes with a repair material as a stopgap measure.
2) Water was found to have splashed in the rf power feeder of the no.1 RILAC cavity because of leakage from a cooling pipe for the coaxial conductor. We replaced it with new ones.
3) Water was found to have splashed in the CSM A4 cavity because of leakage from a cooling pipe of the end drift tube. We repaired the pipes with a repair material as a stopgap measure.

Table 1. Statistics of RILAC operation from January 1 to December 31, 2014.

Operation time of RILAC	2960.0	h
Mechanical problems	153.1	h
Standalone RILAC	1327.3	h
Injection into RRC	1172.6	h
Total beam service time of RILAC	2499.9	h

Table 2. Beam service time of the standalone RILAC allotted to each beam course in target rooms no. 1 and no. 2 in 2014.

Beam course	Total time (h)	%
e2	419.7	31.6
e3	878.0	66.1
e6	29.7	2.2
Total	1327.3	100.0

Table 3. Operation time of the 18G-ECRIS in 2014.

Ion	Mass	Charge state	Total time (h)
N	14	3	62.3
N	15	3	105.7
Na	23	7	504.0
Al	27	6	216.0
Ar	40	11	144.0
Ca	48	10,11	1487.6
Zn	70	15	609.2
Kr	82	18	216.0
Kr	86	18	120.0
	Total		3464.7

*1 RIKEN Nishina Center
*2 SHI Accelerator Service Ltd.

AVF operations in 2014

N. Tsukiori,[*2] M. Fujimaki,[*1] T. Fujinawa,[*1] N. Fukunishi,[*1] S. Fukuzawa,[*2] M. Hamanaka,[*2] H. Hasebe,[*1] Y. Higurashi,[*1] E. Ikezawa,[*1] H. Imao,[*1] S. Ishikawa,[*2] T. Kageyama,[*1] O. Kamigaito,[*1] M. Kase,[*1] M. Kidera,[*1] K. Kobayashi,[*2] M. Komiyama,[*1] Y. Kotaka,[*3] R. Koyama,[*2] H. Kuboki,[*1] K. Kumagai,[*1] T. Maie,[*1] M. Nagase,[*1] T. Nagatomo,[*1] T. Nakagawa,[*1] M. Nakamura,[*1] T. Nakamura,[*2] M. Nishida,[*2] M. Nishimura,[*2] J. Ohnishi,[*1] Y. Ohshiro,[*3] H. Okuno,[*1] K. Ozeki,[*1] N. Sakamoto,[*1] J. Shibata,[*2] K. Suda,[*1] A. Uchiyama,[*1] T. Watanabe,[*1] Y. Watanabe,[*1] K. Yadomi,[*2] K. Yamada,[*1] and S. Yamaka[*3]

In 2014, the total annual operation time of the K70 AVF cyclotron (denoted as AVF hereafter) was 2942 hours as shown in Table 1. This was increased by 311 hours compared with that in 2013. In this duration, the time for beam tuning was 1240 hours, which was 274 hours longer than that in 2013. Most of the increased time (311 hours) was spent on beam tuning because the time for beam tuning for "Injection to RRC-SRC" was increased to two to three times longer than usual, and it took considerable time to recover from problems. On the other hand, the total beam supply time was 1702 hours, which was classified into three categories: "Injection to RRC", "Injection to RRC-SRC", and "AVF standalone". The operation times for these three categories are listed in Table 1.

All of the beams accelerated by the AVF in 2014 are listed in Table 2. In this table, the following beams were accelerated for the first time in 2014: ^{16}O (4.9 MeV/u), ^{84}Kr (3.97 MeV/u), α (12.5 MeV/u), ^{11}B (5.0 MeV/u), ^{19}F (6.08 and 6.768 MeV/u), and α (7.5 MeV/u). The supplied courses were as follows (in order of the supplied time): RI production, RRC-SRC, CRIB, RRC-E5, Student Ex, and E7B.

Table 1. AVF operation statistics in 2014.

	2013	2014
Total operation time (hr)	2631	2942
Beam tuning	966	1240
Injection to RRC	738	208
Injection to RRC-SRC	118	455
AVF standalone	809	1039
Beam course (AVF standalone) (hr)		
E7A	480	335
E7B	18	58
C03	311	646

The total fault time was 118 hours. The main faults are listed in Table 3, in descending order of time spent on restoration, and details are indicated below.

Table 2. AVF beam list in 2014.

Particle	*E* (MeV/u)	Course
p	12.0	RI production
d	12.0	RI production
d	4.9	RRC-SRC
α	6.5	Student Ex.
α	7.5	RI production
α	12.5	RI production
^{6}Li	11.2	CRIB
^{7}Li	5.6	CRIB
^{7}Li	8.6	E7B
^{11}B	5.0	CRIB
^{12}C	7.0	RRC-E5
^{16}O	4.9	RRC-SRC
^{18}O	6.07	RI production
^{19}F	6.08	RI production
^{19}F	6.768	RI production
^{22}Ne	6.1	CRIB
^{40}Ar	5.2	RRC-E5
^{56}Fe	5.0	RRC-E5
^{84}Kr	3.97	RRC-E5

(1) During ^{40}Ar beam tuning, the beam stopped unexpectedly at RRC. This was due to an incorrect arrangement of the readout-cable of baffle slits, which cut across the beam trajectory in the chamber of the RRC.

(2) During ^{6}Li beam supply, the beam current decreased at the ion source. To investigate the cause, the ion source was disassembled. Consequently, some contaminations were observed and lack of ^{6}Li metal was found.

(3) During ^{12}C beam tuning, one of the hollow conductors from the magnetic channel of the AVF cracked and cooling water sprayed out from that crack. The crack was temporarily caulked by putty because it was difficult to close the crack by weld. The beam tuning was restarted without any problems.

Table 3. Main faults in 2014. See text for details.

	Date	Time for restoration (hr)
(1)	6th September	22
(2)	13th May	18
(3)	16th September	17

*1 RIKEN Nishina Center
*2 SHI Accelerator Service Ltd.
*3 Center for Nuclear Study, the university of Tokyo

Present status of the liquid-helium supply and recovery system†

T. Dantsuka,*1 H. Okuno,*1 M. Nakamura,*1 M. Kase,*1 S. Tsuruma,*1
M. Ohshima,*2 H. Miura,*2 H. Shiraki,*2 H. Hirai,*2 H. Hazama,*2 and H. Shiba*2

The liquid-helium supply and recovery system[1], which can produce liquid helium at a liquefaction rate of 200 L/h from pure helium gas, has been under stable operation since the beginning of April 2001. The volumes of liquid helium supplied each year from 2001 to 2013 are shown in Fig. 1. The volume gradually increased from 2001 to 2008 but sharply increased in 2010, before decreasing sharply in 2011, and again sharply increasing in 2012.

We improved our recovery system in 2014. A new recovery line was connected to the existing line of the Nanoscience Joint Laboratory at the Emergent Matter Research Facilities.

The purity of helium gas recovered from laboratories gradually improved once the construction of the system was completed. Currently, the impurity concentration in the recovered gas rarely exceeds 200 ppm. The volume of helium gas recovered from each building in the Wako campus and the volume transported to the liquid helium supply and recovery system were measured. The recovery efficiency, which is defined as the ratio of the amount of recovered helium gas to the amount of supplied liquid helium, was calculated. The recovery efficiency for the buildings on the south side of the Wako campus, such as the Cooperation Center building of the Advanced Device Laboratory, the Chemistry and Material Physics building, and the Nanoscience Joint Laboratory building, increased to more than 90%.

However, the system experienced malfunctioning at the end of September 2014. The motor of helium compressor failed and we could not supply liquid helium for a period of two and a half months. One cause of motor failure was deterioration due to age. We updated the inverter of the helium compressor in March 2014.

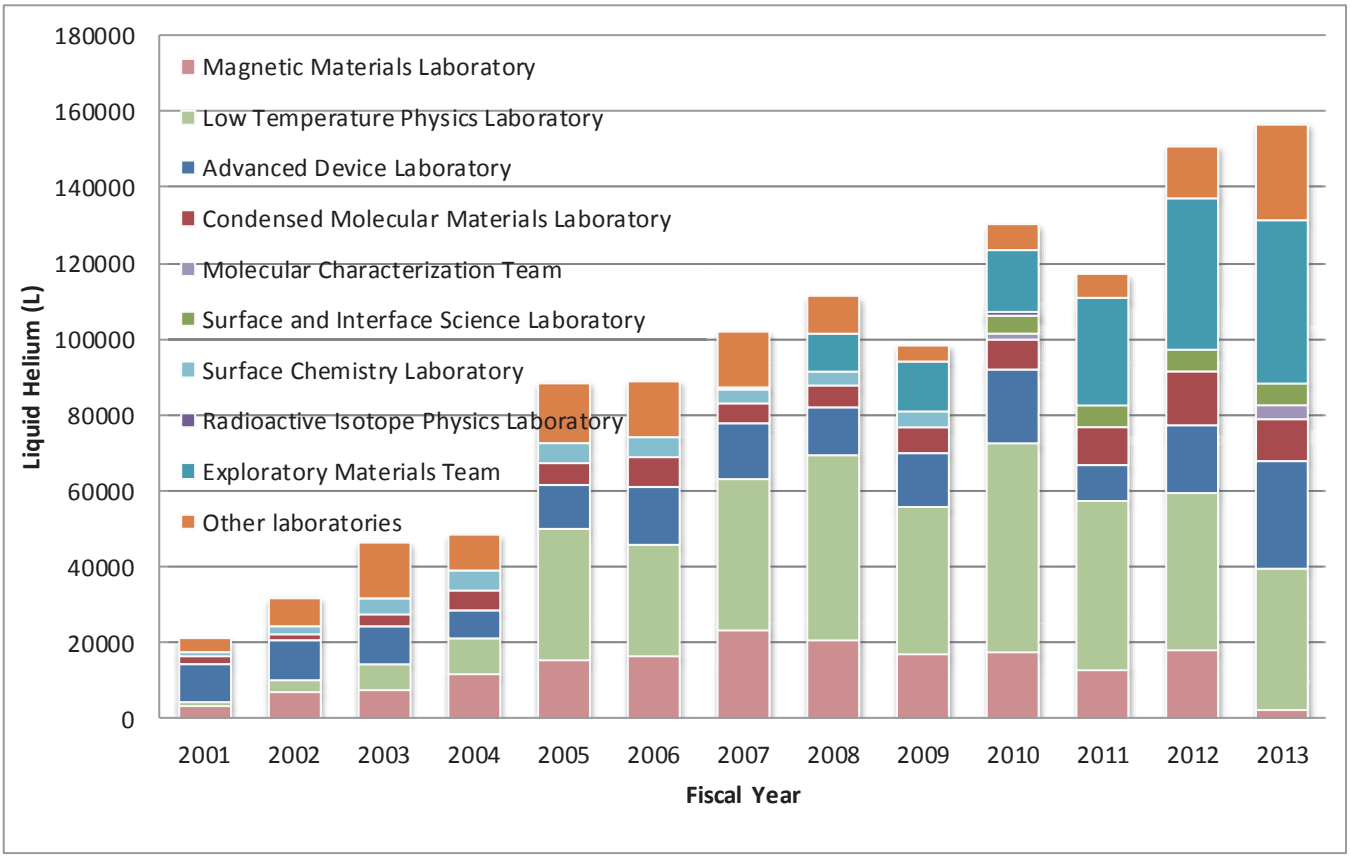

Fig.1. Volumes of liquid helium supplied to laboratories for each fiscal year from 2001 to 2013

† Condensed from the article in Phys. Rev. Lett. **85**, 1827 (2000)

*1 RIKEN Nishina Center
*2 Nippon Air Conditioning Service K.K

References

1) K. Ikegami et al.: RIKEN Accel. Prog. Rep. 34, 349 (2001).

Operation of the superconducting ring cyclotron cryogenic system

H. Okuno,[*1] T. Dantsuka,[*1] M. Ohshima,[*2] H. Shiraki,[*2] H. Hazama,[*2] A. Mikami,[*2] H. Miura,[*2] H. Shiba,[*2] M. Kubota,[*2] H. Hirai,[*2] and M Haneda[*2]

The SRC (Superconducting Ring Cyclotron) cryogenic system, which consists of three compressors, a He refrigerator, and four He buffer tanks for cooling the 240-MJ superconducting magnets used for the SRC, has a cooling capacity of approximately 1 kW at 4.5 K and an inventory of 5000 L of liquid He. The cooling system was operated for approximately nine months in 2014, with a three-month maintenance shutdown in summer (July–August) and a shutdown to conserve electrical power in January.

We experienced some problems with in the operations, some of which required us to stop the operation of the He refrigerator and the compressor. The problems are listed in Table 1. We stopped the operation of the helium compressor during the He purification process on February 19, 2014 because heavy snow on that day stopped the fan in the cooling tower for cooling water. Some improvements were carried out to prevent the fans from stopping due to heavy snow. A temperature sensor in the He refrigerator also demonstrated unusual , and we presume that this was because the attachment between the pipe and sensor became loose. Unfortunately this sensor plays a role in the interlock logic, but we let it go because we had to open the cold box to improve the attachment. On October 29 the second and third turbines tripped suddenly due to the high speed of the third turbine. However, we could find no sign of their high speed from the trend graph. We suspect that this was caused by the noise of the control system. We will check the rotation speed monitor system using a signal generator during the next summer maintenance.

During the operation from April to June, the helium flow rate of the cooling channel for a small power lead gradually degraded. This suggests trapping of some impurity that decreased the flow rate. On November 22 the interlock system for the superconducting magnet required that the power supply of all the superconducting trim coils be shut down. We could find no signs of an increase in temperature. Thus we suspect that this comes from the noise of the control system. On December 25, the flow rate of the cooling channel for one small power lead suddenly increased: we suspect that the impurity dropped or a control valve in the line. We believe that we need to monitor the impurity and aging of the control system regulary.

Table 1. Lists of problems that occured in the He cooling system in 2014.

Subsystem	Date	Problems
He compressor	February 19	Fans in the cooling stopped working due to heavy snow
He refrigerator	April – June	A temperature sensor behaved unusually
	October 12	Mishandling of the pre-cooling valve (warm gas injection)
	October 29	Trip of the second and third turbines.
Sc. magnet	April – June	Gradual decrease of the flow rate for small current power leads
	November. 22	Discharge of the superconducting trim coils
	October 29	Sudden increase of the flow rate for a small current power lead

*1 RIKEN Nishina Center
*2 Nippon Kucho Service Co., Ltd

Present status of the BigRIPS cryogenic plant

K. Kusaka,[*1] M. Ohtake,[*1] T. Kubo,[*1] K. Yoshida,[*1] M. Ohshima,[*2] A. Mikami,[*2] H. Shiba,[*2] H. Hazama,[*2] H. Miura,[*2] H. Shiraki,[*2] H. Hirai,[*2] M. Haneda,[*2] M. Kubota,[*2] M. Noguchi,[*3] and N. Suzuki[*3]

In addition to periodic calibration of pressure and temperature sensors, maintaining the oil-removal module in the helium compressor unit is crucial to ensure long-term continuous operations of BigRIPS[1]. The oil-removal module comprises an oil vessel with a demister (1SP), three coalescer vessels (2SP, 3SP, and, 3.5SP), and two adsorbent vessels (4SP and 5SP). We replaced the activated charcoal and molecular sieves in 4SP every year and the activated charcoal in 5SP every 2 years to ensure low oil contamination in helium gas at the exit of the oil-removal module.

Before the adsorbent vessels, oil in the helium gas is separated by coalescer filters in three coalescer vessels. The drain oil separated from the helium gas is sent to the compressor via a drain line with solenoid valves, depending on the oil level in the coalesce vessel. By measuring the operation interval of the solenoid valves, the oil contamination level of the helium gas at the entrance of the second and the third coalesce vessel can be evaluated. The expected oil contamination levels at the entrance of the coalescer vessels are 15-50 and 0.75-1.25 wt. ppm for 3SP and 3.5SP, respectively. The oil contamination level can also be easily measured with an oil check kit[2].

Each coalescer vessel contains four coalescer filters, manufactured by Domnick Hunter[3], and all the filters were replaced every 2 years, since 2008. However, the filters used for 6 years were discontinued and replaced with the successive product of Domnick Hunter in 2014.

Figure 1 shows an estimate of the oil contamination level at the entrance of 3SP as a function of the coalescer filter operation time from the oil drain from the 3SP. The navy blue, green, and, yellow diamonds represent the estimates for the 2008-2009, 2010-2011, and 2012-2013 operations, respectively. The estimate for the 2014 operation with new coalescer filters is shown as pink diamonds. The estimates increase to 50~75 wt. ppm up to an operation time of 2000 hours for the period of 2008-2009 and 2010-2011 and then stays constant. The estimate for the 2014 operation shows similar behavior. On the other hand, the estimate for the period of 2012-2013 scatters largely and shows monotonous increasing tendency. The oil check kit values are also shown as open symbols in Fig. 1. The open triangles, squares, circles, and diamonds represent results for the 2008-2009, 2010-2011, 2012-2013, and 2014 operations, respectively.

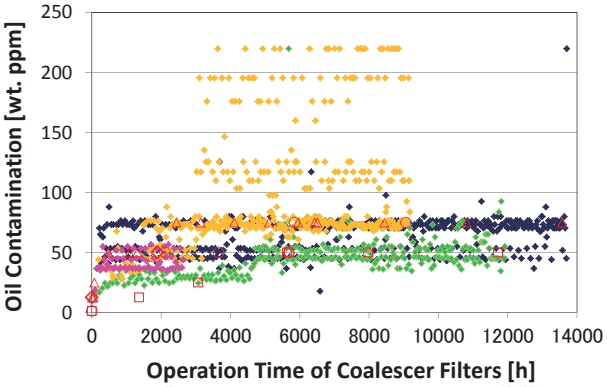

Fig. 1. Oil contamination at the entrance of the second coalescer vessel (3SP).

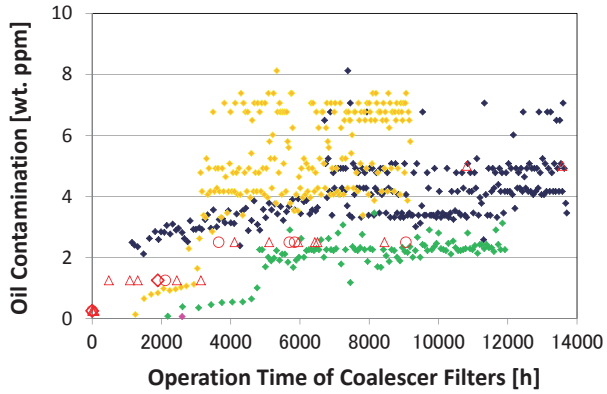

Fig. 2. Oil contamination at the entrance of the third coalescer vessel (3.5SP).

In Fig. 2, we show a similar analysis of the oil contamination at the entrance of 3.5SP. Symbols and colors used in Fig. 2 are same as those in Fig. 1. A gradual increasing tendency of the oil contamination is seen in all operation periods. Following the large oil contamination at the entrance of the 3SP, the results for the period of 2012-2013 are approximately twice of that for the other period. Since the solenoid valve of 3.5SP was operated only once since Sept. 2014, only one pink symbol is plotted in Fig. 2. Although the performance efficiency of the new filter elements seem to be similar to that of discontinued ones, we shall continue observations and investigate oil-removal modules carefully in the coming maintenance period.

*1 RIKEN Nishina Center
*2 Nippon Kucho Service Co., Ltd.
*2 Mayekawa Mfg. Co., Ltd.

References

1) K. Kusaka et al.: RIKEN Accel. Prog. Rep. **41**, 244 (2008).
2) K. Kusaka et al.: RIKEN Accel. Prog. Rep. **43**, 309 (2010).
3) http://www.parker.com/

Operation report on the ring-cyclotrons in the RIBF accelerator complex

S. Fukuzawa,[*3] N. Sakamoto,[*1] T. Dantsuka,[*1] M. Fujimaki,[*1] N. Fukunishi,[*1] T. Fujinawa,[*1]M. Hamanaka,[*3] H. Hasebe,[*1] Y. Higurashi,[*1] E. Ikezaw,a[*1] H. Imao,[*1] S. Ishikawa,[*3] M. Kase,[*1] T. Kageyama,[*1] O. Kamigaito,[*1] M. Kidera,[*1] K. Kumagai,[*1] H. Kuboki,[*1] K. Kobayashi,[*3] Y. Kotaka,[*2] M. Komiyama,[*1] R. Koyama,[*3] T. Maie,[*1] M. Nagase,[*1] T. Nagatomo,[*1] T. Nakagawa,[*1] M. Nakamura,[*1] T. Nakamura,[*3] M. Nishida,[*3] M. Nishimura,[*3] J. Ohnishi,[*1] Y. Ohshiro,[*2] H. Okuno,[*1] K. Ozeki,[*1] J. Shibata,[*3] K. Suda,[*1] N. Tsukiori,[*3] A. Uchiyama,[*1] T. Watanabe,[*1] Y. Watanabe,[*1] S. Watanabe,[*1] K. Yadomi,[*3] S. Yamaka,[*2] K. Yamada,[*1] and H. Yamasawa[*1]

The operation of ring-cyclotrons (RRC, fRC, IRC, and SRC) in the RIBF accelerator complex in 2014 is reported. Table 1 summarizes the accelerated beams provided for users. The scheduled beam service time was 3192.3 h. The delivered beam service time was 2967.1 h. Note that 82% of the beam service time was distributed to the experiments that utilize beams accelerated by SRC and the remaining 18% was distributed to the experiments in which the beams extracted from RRC are used by the users. Beam availability, which is the most important parameter indicating the stability of operation, was 92.9%.

In March 2014, the campaign-type experiments utilizing the ^{238}U 345 MeV/u beam were performed. In the beginning of the beam tuning procedure, we experienced a hardware fault related to the main differential probe (MDP) of the fRC twice, which resulted in 4.5-day delay of the beam start time. Once the beam service started on March 27, five experiment programs were performed without any issue with accelerators. After an 8.3 -day break of the IRC and SRC operations scheduled for the 28-GHz ECR ion source, the beam service of uranium ions was resumed and it finished on May 13. Three experimental programs were performed after the break.

From May 16, we started a beam service of a 345-MeV/u ^{70}Zn beam. During the beam service, a hardware fault with the control system of the gas cogeneration system that supplies backup electricity to the helium refrigerator used for SRC occurred, which resulted in an 8-day beam service interruption in total.

After the problem was fixed, the beam was stably delivered until June 7. Owing to the beam current upgrade in the 18-GHz ECR ion source, the beam intensity increased to 123 particle nA, which corresponds to 120% of the intensity recorded during the beam service performed in 2012.

Since June 9, deuteron and ^{18}O beams (250 MeV/u) are provided for RIBF experiments. In these beam services, low -emittance high beams with stability were strongly required by the users to realize high resolution measurements. The operation parameters of the accelerators used were finely tuned and the purity of single-turn extraction was 0.2%. This high-quality operation was maintained by fine tuning as necessary ,throughout these beam services.

After a shutdown scheduled for a routine maintenance in summer, the ^{238}U (345 MeV/u) beams were delivered for six RIBF experiments from October 20 to November 18. The maximum beam intensity of 27.9 particle nA was recorded during this beam service.

Next, from November 18 to December 11, ^{48}Ca (345 MeV/u) beams were delivered for four RIBF experiments. During these beam services, the operational total acceleration voltage of the SRC RF system was upgraded to 2.4 MV/turn and a voltage applied to the electric deflection channel of SRC was 128 kV. These parameters are close to their maximum capability and essential in producing a low-beam-loss operation required for high-power beams. In addition to an ion-source improvement, the maximum beam intensity recorded in the beam service ,0.53 particle μA, was obtained. This corresponds to the beam power of 8.8 kW which is the power record of the beams obtained in RIBF.

In addition to the biological experiments at E5B, the beam services of ^{48}Ca for RIPS (E6) and 136Xe for KISS (E2B) were performed.

Table 1. Summary of the accelerated beams in 2014

Ions	Energy (MeV/u)	Accelerators	Beam Course	Beam Current(particle nA) requested	Beam Current(particle nA) Max	Scheduled time (h)	Delivered time (h)*	Downtime (h)**	Total time (h)	Availability (%)***
^{12}C	135	AVF-RRC	E5B(Biology+MS)	1	393	71	71	0	71	100
^{40}Ar	95		E5B(Biology)	1	91.2	32	32	0	32	100
^{56}Fe	90		E5B(Biology)	1	2.8	20	20	0	20	100
^{48}Ca	63	RILAC-RRC	E6(RIPS)	200	235.3	108	103.1	1.2	104.3	95.4
^{84}Kr	70		E5B(Industry)	1	0.1	85	72.9	9.8	82.8	85.8
^{136}Xe	10.75	RILAC2-RRC	E2B(KEK/KISS)	10	405	96	100.5	2.8	103.4	104.7
$^{238(235)}$U	10.75		A02,D(MS)	N/A	1428	121	121	0	121	100
^{238}U	50	RILAC2-RRC-fRC	H course(MS)	N/A	125	15	15	0	15	100
d	250	AVF-RRC-SRC	BigRIPS	10	510	252	268.1	42.7	310.8	106.4
^{16}O	250		SHARAQ(CNS)	10	41.8	108	125.4	18.6	144	116.1
^{48}Ca	345	RILAC-RRC-IRC-SRC	BigRIPS, ZDS SAMURAI	500	530	492.2	474.1	18.1	492.2	96.3
^{70}Zn(1st)	345		SHARAQ(CNS)	75	123	216	200.2	39.1	239.3	92.7
^{70}Zn(2nd)	345		SHARAQ(CNS)	75	116.6	96	93.1	2.9	96	97
^{238}U(1st)	345	RILAC2-RRC-fRC-IRC-SRC	BigRIPS, ZDS,SAMURAI	10	22.1	540	384.4	159.6	544.1	71.2
^{238}U(2nd)	345		BigRIPS,ZDS	10	25	408	385.2	94.8	480.1	94.4
^{238}U(3rd)	345		BigRIPS,ZDS,SAMURAI, EURICA	15	27.9	532.1	501	31.1	532.1	94.2

*Delivered time = Supply time for Beam users.

**Down time = Supply stop time caused by accelerator issues.

***Availability =Delivered time/scheduled time.

*1 RIKEN Nishina Center
*2 Center for Nuclear Study, the University of Tokyo
*3 SHI Accelerator Service Ltd.

V. EVENTS

ARIS2014 - 2nd Conference on Advances in Radioactive Isotope Science

T. Motobayashi*1

The second conference on Advances in Radioactive Isotope Science (ARIS 2014) was held at the Ito International Research Center in Tokyo on June 1-6, 2014. It was jointly organized by the RIKEN Nishina Center and CNS, the University of Tokyo, sponsored by IUPAP (International Union of Pure and Applied Physcs), and supported by several Japanese institutions and societies. The first ARIS conference was held in 2011 in Leuven, Belgium, by merging the two meetings, ENAM (International Conference on Exotic Nuclei and Atomic Masses) and RNB (International Conference on Radioactive Nuclear Beam). In a joint assembly of the advisory committees of the two meetings, the ultimate goal of ARIS was set to create the "flagship conference" series on the science of radioactive isotopes, including the physics of exotic nuclei and studies with RI beams. Since the Nishina Center and the CNS have extensively studied on radioactive isotopes with excellent RI-beam facilities and their significant contributions in the near futre are foreseen, the second conference in Japan was very well-timed.

The scientific scope of ARIS 2014 was of the following subjects, taking over the ones of the first conference with some modifications: 1)nuclear structure, 2)nuclear astrophysics, 3)fundamental symmetries and interactions, 4)nuclear reactions and responses, 5)nuclear properties including atomic masses and fundamental constants, nuclear moments and radii, rare decay modes, and nuclei at the driplines, 6)nuclear EOS and its implications, 7)heaviest elements and fission, 8)radioactive isotope production and developments of experimental devices, 9)computational developments, 10)applications, and 11)other related issues.

On Sunday June 1, public lectures attracted a large audience of about 300 people including high school students. The conference started on Monday with the welcome address by the Conference Chair, Hideto En'yo. In the first scientific session chaired by the Conference Co-chair, Takaharu Otsuka, Robert Janssens gave the keynote talk addressing "big" questions in the field and providing an overview of the new and important developments after the first conference.

The number of registrants turned out to be 407 from 27 countries. Thus the higly optimistic goal set by the organizers was reached, reflecting the considerble interest and amount of work done in this the research field. The conference photo shown below (Fig. 1) delivers the lively atmosphere of the conference.

There were 48 plenary talks and 82 oral presentations in three parallel sessions held on June 3 and 6 afternoons. Recent highlights from RIBF, the new neutron magic number 34 experimentally confirmed for the neutron-rich nucleus ^{54}Ca and first life-time measurements for a number of nuclei in the r-process path, for example, attracted much attention as well as new results from world facilities. Among 239 papers presented in poster sessions, seven posters presented by young scientists were selected as "Best Posters", and the awarding ceremony took place in the closing session. Angela Bracco summarized the conference by selecting major aspects from numerous presentations and emphasizing the bright future of the field.

The conference proceedings will be published electronically in the JPS Conference Proceedings Volume 6 (2015). The next ARIS conference will be jointly hosted by NSCL and TRIUMF.

Fig. 1. Conference photo taken in the session hall.

*1 Scientific Secretary of ARIS2014, RIKEN Nishina Center

The 8th Nishina School

T. Kishida*1 and H. Ueno*1

The RIKEN Nishina Center (RNC) has commenced Nishina School to enhance international research relationship in the Asian Region through human-resource development in the field of nuclear physics. In this program, undergraduate students are being accepted by the RNC from Peking University since 2008 and from Seoul National University since 2012 for two weeks every summer. Both the programs have been merged since 2013.

The 8th Nishina School was held from July 28 to August 8, 2014. The curriculum of the School was designed to introduce the pleasure of nuclear physics into the undergraduate students from Peking University (5 students) and Seoul National University (5 students). The first week, program consisted of lectures and basic experimental trainings. In the second week they performed a real-beam experiment using the RIKEN Pelletron accelerator, starting from its planning and followed by the analyses and the discussions. On the last day of the School, the presentation session by the students was held. The program timetable in 2014 is shown in Fig. 1.

In response to a request for improving the management of the Nishina School proposed by the people in charge of the Nishina School held in the last year, the RNC director convened a preparatory meeting on December 25, 2013, to discuss the development of an organizational management system of the Nishina School and the improvement of transparency in the decision-making process. For this purpose, it was determined at the meeting to newly set up the Nishina School Steering Committee. The Committee is composed of Ueno (Chair), En'yo, Sakurai, and Sakai. The Committee Meetings were held four times on March 3, April 23, May 26, and July 15, 2014. Kishida, principle of the Nishina School, also attended all these Meetings as an observer. Their meeting minutes were reported at the second, fourth, and fifth RNC Coordination Committee Meetings held in 2014.

In order to enhance the experimental training, the Committee determined to incorporate accelerator experimental training into the curriculum. In this year, cross-section measurements were conducted for the ^{12}C(p,γ)^{13}N reaction utilizing a proton beam at E_p = 1600–1850 keV delivered from the RIKEN Pelletron accelerator. Technical instructions of the experimental training were provided by Research Scientists in Nuclear Spectroscopy Lab., Spin Isospin Lab., and RI Physics Lab. They were technically assisted by IPA and JRA researchers of these laboratories.

The Committee also considered that enhancement of working-level dialogue among the persons in charge of, e.g., the entire program, experimental trainings, and office procedures is an important subject. This year, three working-level meetings, including an on-site meeting at the Pelletron, were held on July 4, 10, and 18. Despite such a gradual improvement, the situation can be further improved.

All the students had a good experience and enjoyed the School and life at the RNC. Figure 2 shows a photograph taken at the opening ceremony on July 28.

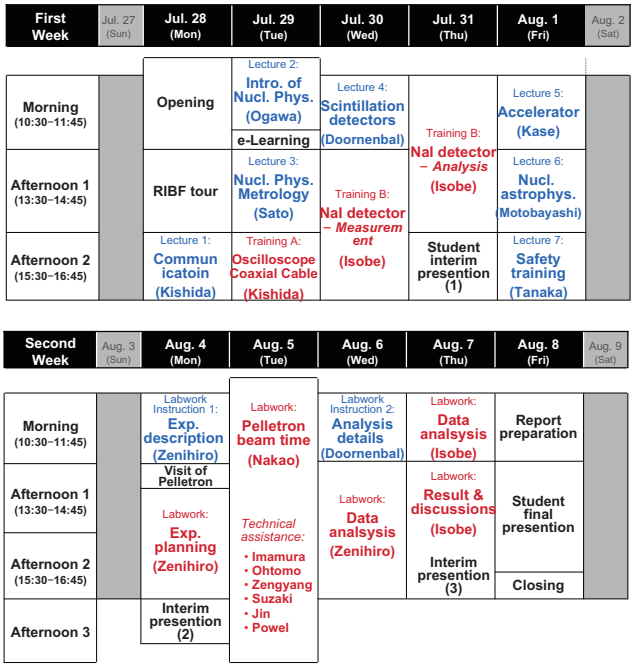

Fig. 1. The curriculum and timetable of Nishina School 2014. The lectures and experimental trainings are indicated in blue and red, respectively.

Fig. 2. Photograph of Nishina School 2014.

*1 RIKEN Nishina Center

The 27th World Conference of the International Nuclear Target Development Society (INTDS2014)

H. Okuno,[*1] H. Hasebe,[*1] H. Kuboki,[*1] H. Imao,[*1] A. Yoshida,[*1]
K. Morimoto,[*1] D. Kaji,[*1] K. Yoshida,[*1] and K. Sakuma[*1]

The 27th World Conference of the International Nuclear Target Development Society (INTDS 2014) was held from August 31th to September 5th, 2014 at the National Museum of Emerging Science and Innovation (Miraikan) in Odaiba Tokyo, Japan with special emphasis on targets for accelerator-based research. INTDS 2012 was organized by the RIKEN Nishina Center for Accelerator-based Science, Saitama.

The series of INTDS conferences dates back to 1963 when the "First Symposium on Research Materials for Nuclear Measurements" was held sponsored by the Central Bureau for Nuclear Measurements (CBNM; recently, IRMM, -Institute for Reference Materials and Measurements) in Belgium. Since then, researchers involved in target preparation shared their experience and discussed related problems during biennial conferences hosted alternatively in Europe, North America, and Asia (www.intds.org). The 23rd INTDS conference was held in Tsukuba, Japan in 2006. It was delightful to meet again in Japan on the occasion of the 27th International INTDS conference.

More than 77 participating scientists from 17 countries (Belgium, Canada, China, France, Germany, India, Italy, Japan, Korea, Pakistan, Poland, Romania, Russia, South Africa, Switzerland, UK, USA), met in Tokyo to present over 67 scientific contributions covering the wide field of "State-of-the-art Technologies for Nuclear Target and Charge Stripper". A laboratory tour of the RIKEN RI Beam Factory was included in the scientific program to introduce the institution and laboratories. The conference comprised eleven different sessions titled ,"Targets and strippers for RIBF", "Classical accelerator targets", "RI beams", "Gas strippers", "Liquid strippers", "Production targets", "Medical and industrial applications", "Radioactive targets", "Target characterization", "Liquid and gas targets", "Radioactive targets", and "Laser-related targets". The sessions included many activities such as the discussion of exciting new developments or methods, reports on improvements of established techniques, presentation of scientific results by young scientists, and the introduction of new groups and laboratories in the society.

Fig. 1: Photo of conference attendees

*1 RIKEN Nishina Center for Accelerator-Based Science

The 6th International Conference on Trapped Charged Particles and Fundamental Physics

M. Wada,[*1] P. Schury,[*1] Y. Ichikawa,[*1] and Y. Ito[*1]

The 6th International Conference on Trapped Charged Particles and Fundamental Physics (TCP2014) was held from 1st to 5th December, 2014 at the Takamatsu International Conference Hall. Prior to the conference, a preschool (TCP school) for young researchers was organized from 28th to 29th November at the Nishina Hall of RIKEN where inspiring lectures were given by S. Ulmer, R. Thompson, R. Hayano, H. Katori, V. Dzuba, Yu. Litvinov, W. Nörtershäuser. About 60 participants enrolled in the school and half of them went to Takamatsu.

During the conference, a variety of scientific programs using stored particles were actively discussed. Anti-Hydrogens are routinely synthesized and precision spectroscopy of them is being actively pursued. Multi-reflection time-of-flight (MRTOF) mass spectrographs were put online at three different laboratories at almost the same time at ISOLDE, RIKEN and GSI, and are also under preparation at TRIUMF, MSU, ANL, and IBS in Korea. Advanced resonance detection methods in Penning trap mass spectrometers were discussed. Several fundamental symmetry studies using molecular ions, neutral atoms and highly charged ions (HCI) were discussed. The highlight of the conference was a sympathetically cooled HCI crystal in a linear Paul trap by Heidelberg-Aarhus collaboration. It can be a next-generation frequency standard, but also provides a platform for research in physics beyond the standard model such as time variation of the fine structure constant. An Australian theorist suggests that Cf^{16+} is the best candidate for such research at present.

A total of 107 registered participants attended and 63% of them were from abroad. We invited 47 speakers. Of them, 45 accepted the invitation, 2 of whom later cancelled. We accepted 23 oral presentations and 26 posters; additionally, 3 oral contributions included posters.

An international workshop, NNP2014, was held at the same time and location, hence joint sessions and social events were held.

In the international organization committee meeting, it was decided that TCP2018 will be held in USA and organized by G. Bollen of MSU.

Fig. 2 An atraction during the banquet.

Fig. 1 Participants of TCP2014 in Takamatsu

*1 RIKEN Nishina Center

VI. ORGANIZATION AND ACTIVITIES OF RIKEN NISHINA CENTER (Activities and Members)

1. Organization

1.1 Organization Chart as of March 31, 2015

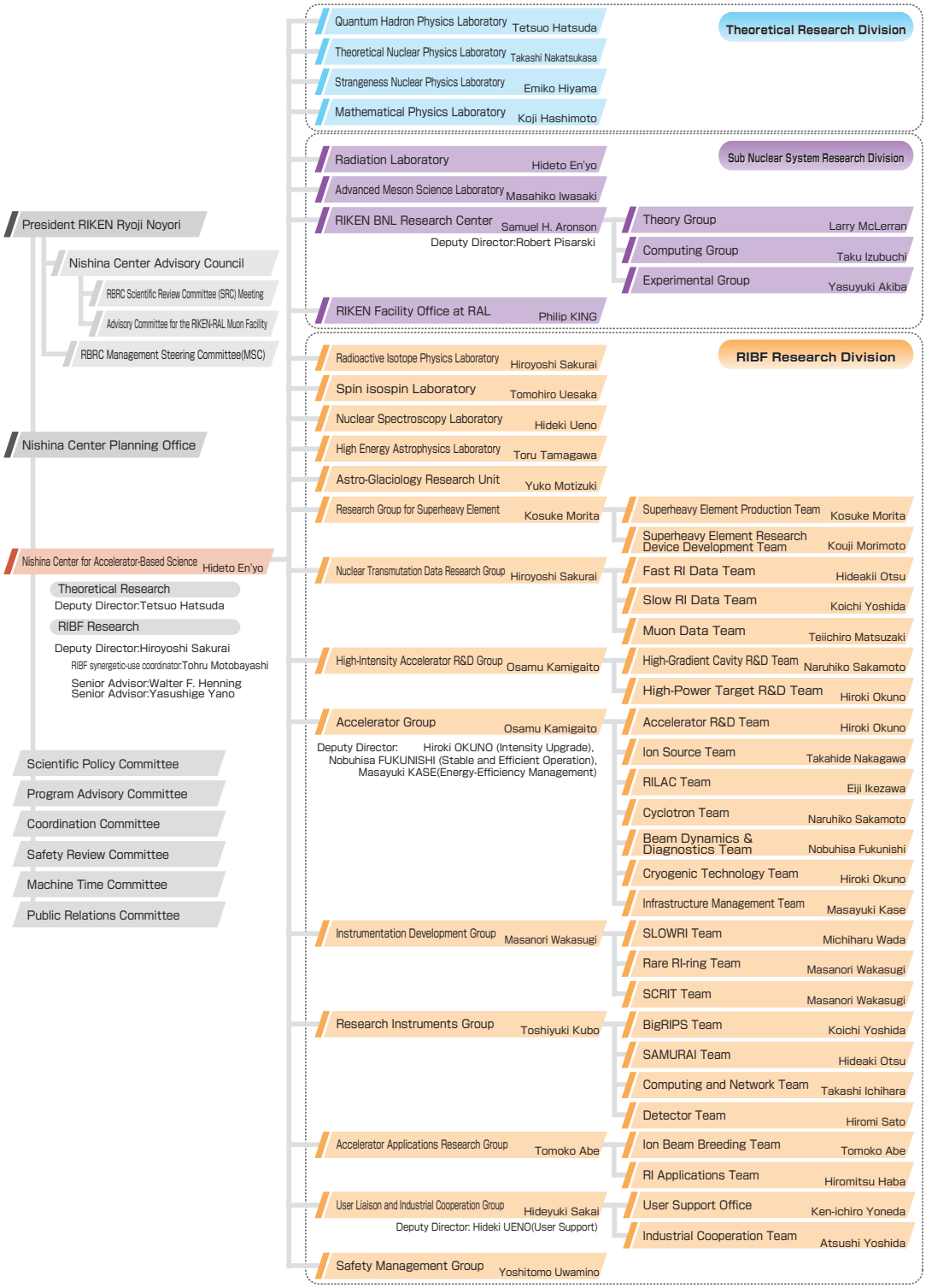

1.2 Topics in FY2014

In fiscal year 2014, RNC launched several interdisciplinary innovation programs as yet another new challenge for its researchers. One such example is RNC's participation in the ImPACT program which aims to significantly reduce and resource recycle high-level radioactive waste. To achieve this goal, the organizational structure required to develop key technology for effective nuclear transmutation has been revised so that the nuclear reaction data of the long-life fission products can be obtained. RNC also participates in the Strategic Innovation Program (SIP) in cooperation with eighteen other institutes in Japan to undertake the task of building a system for strategic omics breeding technology.

With President's Discretionary Fund providing the financial support of 450 million yen for international research collaboration, RNC was able to execute approximately five months of RIBF operation in total. Accordingly, user time also reached its record-high 2597 hours.

Oct. 1, 2014	Start of Nuclear Transmutation Data Research Group associated with following three teams Fast RI Data Team Slow RI Data Team Muon Data Team
	Start of High-Intensity Accelerator R&D Group associated with following two teams High-Gradient Cavity R&D Team High-Power Target R&D Team
Mar. 31, 2015	End of Mathematical Physics Laboratory

2. Finances

As mentioned in "1. Administrative Topic in FY2014", RNC executed approximately five months of RIBF operation. Breakdown expenses of the RNC FY2014 budget and a transition for the past five years are shown in following graphs.

[Correction: In the 2013 edition, the FY2014 budget was shown erroneously instead of that of FY2013. The budget of FY 2014 has been reprinted with the revised external funding.].

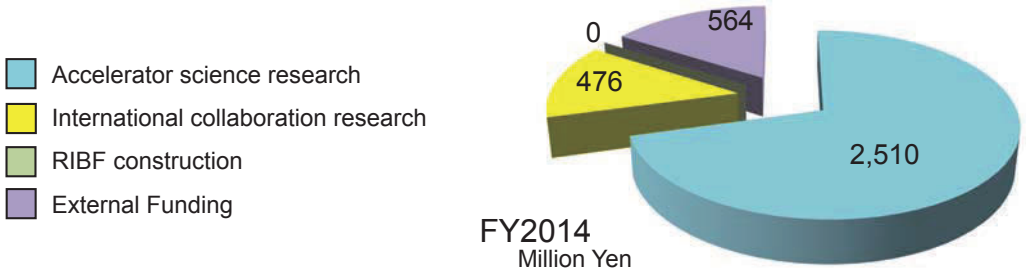

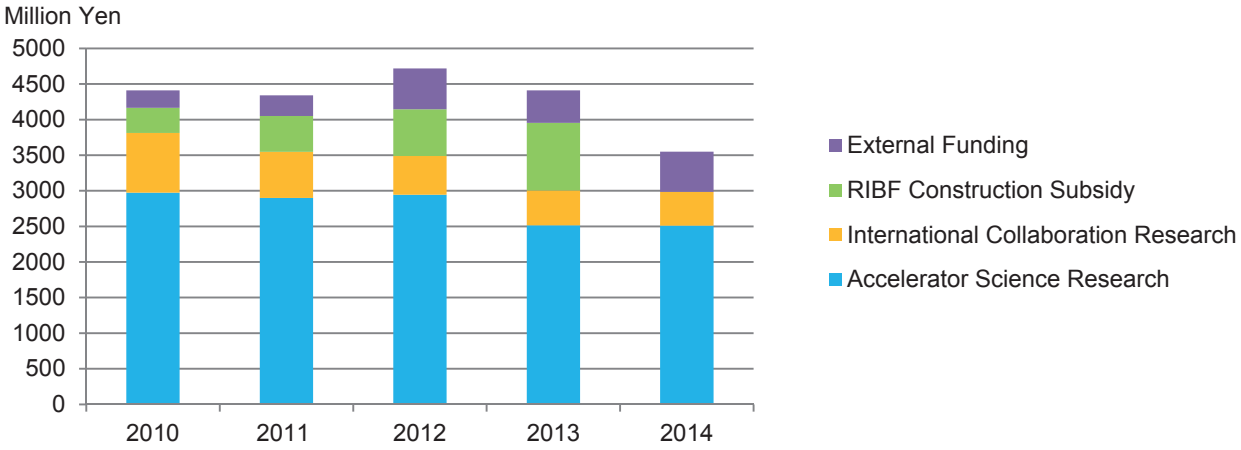

3. Staffing

At the start of FY 2014, April 1 2014, there were 246 personnel affiliated with RNC and 347 researchers visiting RNC for research purpose. The following graphs show a breakdown of personnel into seven categories as of April 2014, and a transition of the number of each category. In the transition graph, researchers associated with the BNL collaboration in 2014 are counted as Contract Researcher.

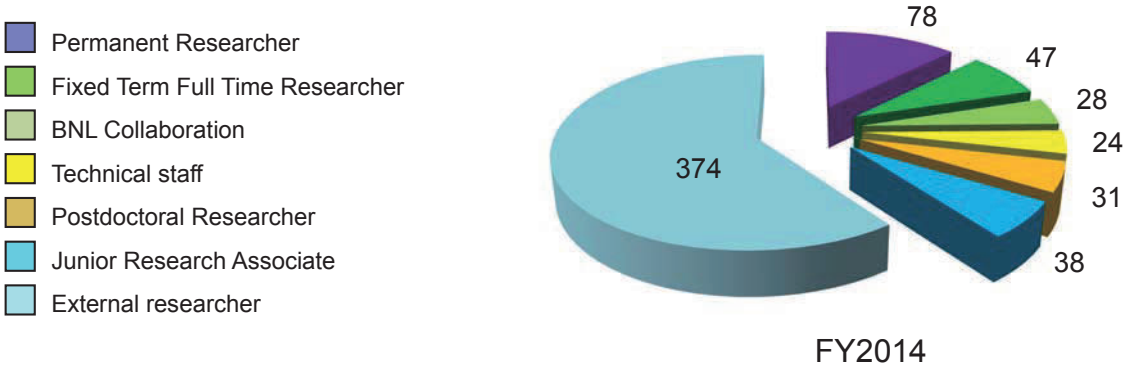

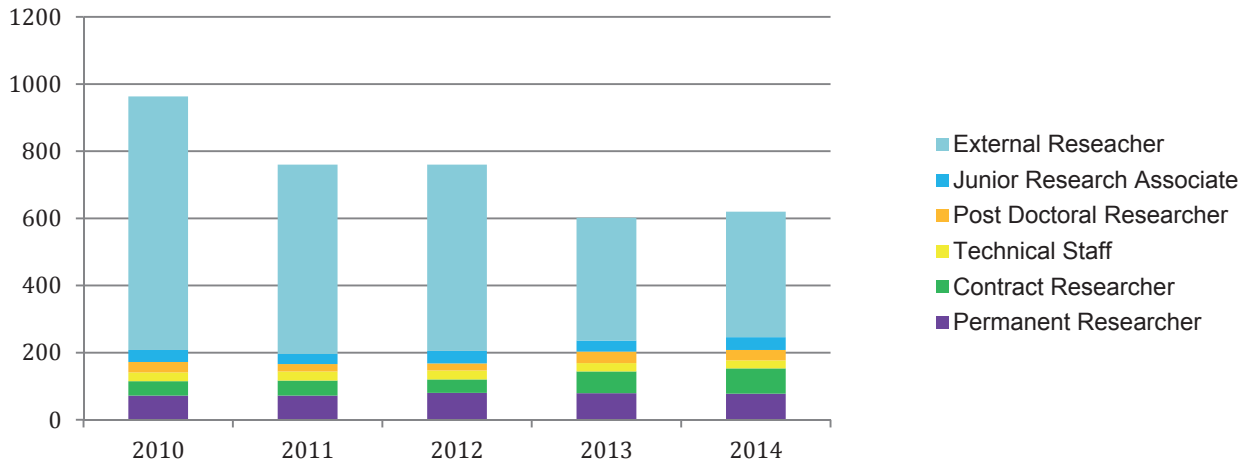

4. Research publication

Research results published in 2014 are roughly split into two categories, i.e., papers published in journals and oral presentations. A transition of the number of the past five years is shown in the following graph.

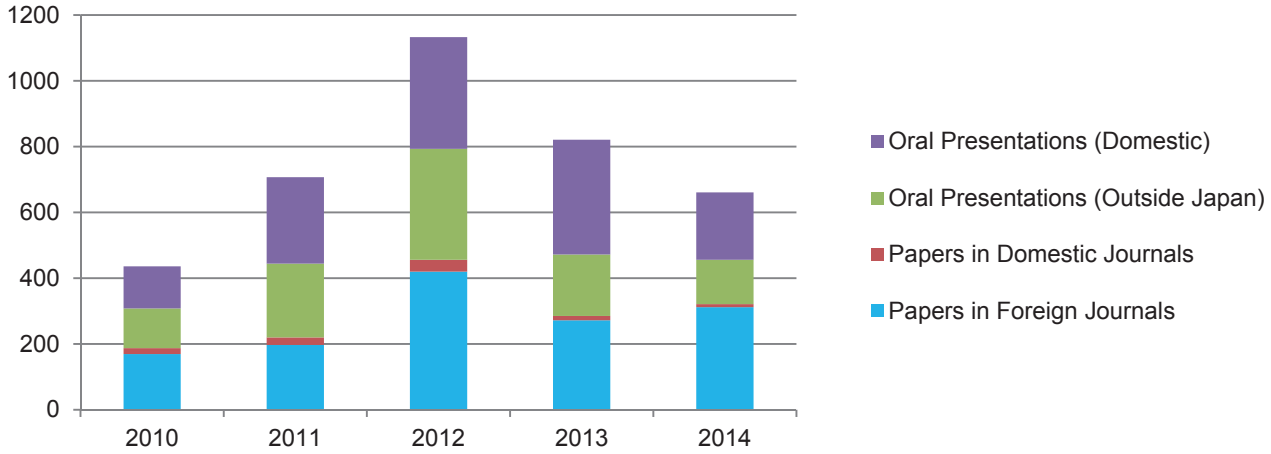

5. Management

Headed by the RNC Director Hideto En'yo, the RIKEN Nishina Center for Accelerator-Based Science (RNC) consists of:

10 Laboratories
1 Research unit
9 Groups with 25 Teams
2 overseas research center with 3 Groups

as of the latter half of FY2014. There are also three 'Partner Institutes' which conduct research in the laboratories set up in RNC.

RNC is managed by its Director who takes into consideration the majority decision of the RNC Coordination Committee. The Nishina Center Planning Office under the auspices of President of RIKEN is responsible for administrative matters of RNC.

The management of RNC is supported by the following committees:

Scientific Policy Committee
Program Advisory Committee
Safety Review Committee
RIBF Machine Time Committee
Public Relations Committee

There are also committees to support the President of RIKEN and/or the Director of RNC such as:

RBRC Management Steering Committee (MSC) and Nishina Center Advisory Council with two subcommittees,
RBRC Management Steering Committee (MSC) and
Nishina Center Advisory Council with two subcommittees,
RBRC Scientific Review Committee (SRC) and
Advisory Committee for the RIKEN-RAL Muon Facility

Nishina Center for Accelerator-based Science

Executive Members (as of March 31, 2015)

Hideto EN'YO	Director RNC; Chief Scientist, Director of Radiation Laboratory
Tetsuo HATSUDA	Deputy Director (Theoretical Research), RNC; Chief Scientist, Director of Quantum Hadron Physics Laboratory
Hiroyoshi SAKURAI	Deputy Director (RIBF Research), RNC; Chief Scientist, Director of Radioactive Isotope Physics Laboratory; Group Director, Nuclear Transmutation Data Research Group
Tohru MOTOBAYASHI	RIBF Synergetic-Use Coordinator
Walter F. HENNING	Senior Advisor
Yasushige YANO	Senior Advisor
Minami IMANISHI	Assistant

RNC Coordination Committee

The following subjects relevant to the RNC management are deliberated under the chairmanship of the RNC Director:

Establishment of the new organization or reorganization in RNC
Personnel management of RNC researchers
Research themes and research budget
Approval of the Partner Institutes
Evaluation of the management of RNC and the response to the recommendations by external evaluation

The RNC Coordination Committee is held monthly.

Members (as of March 31, 2015)

Hideto EN'YO	Director, RNC; Chief Scientist, Director of Radiation Laboratory
Hiroyoshi SAKURAI	Deputy Director, RNC; Chief Scientist, Director of Radioactive Isotope Physics Laboratory; Group Director, Nuclear Transmutation Data Research Group
Tetsuo HATSUDA	Deputy Director, RNC; Chief Scientist, Director of Quantum Hadron Physics Laboratory
Tohru MOTOBAYASHI	RIBF Synergetic-Use Coordinator
Walter F. HENNING	Senior Advisor
Yasushige YANO	Senior Advisor
Masahiko IWASAKI	Chief Scientist, Director of Advanced Meson Science Laboratory
Tomohiro UESAKA	Chief Scientist, Director of Spin isospin Laboratory
Hideki UENO	Chief Scientist, Director of Nuclear Spectroscopy Laboratory; Deputy Group Director, User Liaison and Industrial Cooperation Group
Toru TAMAGAWA	Associate Chief Scientist, Director of High Energy Astrophysics Laboratory
Takashi NAKATSUKASA	Associate Chief Scientist, Director of Theoretical Nuclear Physics Laboratory
Emiko HIYAMA	Associate Chief Scientist, Director of Strangeness Nuclear Physics Laboratory
Koji HASHIMOTO	Associate Chief Scientist, Director of Mathematical Physics Laboratory
Kosuke MORITA	Group Director, Research Group for Superheavy Element; Team Leader, Superheavy Element Production Team
Osamu KAMIGAITO	Group Director, Accelerator Group; Group Director, High-Intensity Accelerator E&D Group

Hideyuki SAKAI	Group Director, User Liaison and Industrial Cooperation Group
Hiroki OKUNO	Deputy Group Director, Accelerator Group; Team Leader, Accelerator R&D Team; Team Leader, Cryogenic Technology Team; Team Leader, High-Power Target R&D Team
Nobuhisa FUKUNISHI	Deputy Group Director, Accelerator Group; Team Leader, Beam Dynamics & Diagnostics Team
Masayuki KASE	Deputy Group Director, Accelerator Group; Team Leader, Infrastructure Management Team
Tomoko ABE	Group Director, Accelerator Applications Research Group; Team Leader, Radiation Biology Team
Yoshitomo UWAMINO	Group Director, Safety Management Group
Toshiyuki KUBO	Group Director, Research Instruments Group; Team Leader, Detector Team
Masanori WAKASUGI	Group Director, Instrumentation Development Group; Team Leader, Rare RI-ring Team; Team Leader, SCRIT Team
Eiji IKEZAWA	Team Leader, RILAC Team
Takashi ICHIHARA	Team Leader, Computing and Network Team
Naruhiko SAKAMOTO	Team Leader, Cyclotron Team; Team Leader, High-Gradient Cavity R&D Team
Hiromi SATO	Team Leader, Detector Team
Takahide NAKAGAWA	Team Leader, Ion Source Team
Hiromitsu HABA	Team Leader, RI Applications Team
Koji MORIMOTO	Team Leader, Superheavy Element Device Development Team
Atsushi YOSHIDA	Team Leader, Industrial Cooperation Team
Koichi YOSHIDA	Team Leader, BigRIPS Team; Team Leader, Slow RI Data Team
Ken-ichiro YONEDA	Team Leader, User Support Office
Michiharu WADA	Team Leader, SLOWRI Team
Hideaki OTSU	Team Leader, SAMURAI Team; Team Leader, Fast RI Data Team
Teiichiro MATSUZAKI	Team Leader, Muon Data Team
Yasuyuki AKIBA	Vice Chief Scientist; Group Leader, Experimental Group, RIKEN BNL Research Center
Katsuhiko ISHIDA	Vice Chief Scientist, Advanced Meson Science Laboratory
Tsukasa TADA	Vice Chief Scientist, Quantum Hadron Physics Laboratory
Yuko MOTIZUKI	Research Unit Leader, Astro-Glaciology Research Unit
Mitsuru KISHIMOTO	Deputy Director, Nishina Center Planning Office

Nishina Center Planning Office

The Nishina Center Planning Office is responsible for the following:

- Planning and coordination of RNC's research program and system
- Planning and management of RNC's use of budget
- Public relations activities

Members (as of March 31, 2015)

Hiroshi TSUBOI	Executive Director; Director, Head of Nishina Center Planning Office
Mitsuru KISHIMOTO	Deputy Director, Nishina Center Planning Office; Administration Manager, RBRC; Administration Manager, RIKEN Facility Office at RAL
Kazunori MABUCHI	Deputy Manager, Nishina Center Planning Office
Yasutaka AKAI	Administrative Officer of Nishina Center Planning Office; Deputy Administration Manager, RBRC
Yukari ONISHI	Chief, Nishina Center Planning Office
Kumiko SUGITA	Special Administrative Employee
Yuko OKADA	Task-Specific Employee
Yukiko SATO	Task-Specific Employee
Kyoji YAMADA	Special Temporary Employee
Yoshio OKUIZUMI	Temporary Employee
Masatoshi MORIYAMA	Consultant for Advisory Committee, Research Review, etc.
Rie KUWANA	Temporary Staff

Scientific Policy Committee

The Scientific Policy Committee deliberates on the following:

- Research measures and policies of RNC
- Administration of research facilities under RNC's management

The Committee members are selected among professionals within and outside RNC. The members were not chosen nor the Committee held in FY2014.

Program Advisory Committee

The Program Advisory Committee reviews experimental proposals submitted by researchers and reports the approval/disapproval of the proposals to the RNC Director. The Committee also reports to the RNC Director the available days of operation at RIBF or the Muon Facility at RAL allocated to researchers.

The Committee is divided into three categories according to the research field.

(1) Nuclear Physics Experiments at RIBF (NP-PAC): academic research in nuclear physics

(2) Materials and Life Science Researches at RNC (ML-PAC): academic research in materials science and life science
(3) Industrial Program Advisory Committee (In-PAC): non-academic research

Program Advisory Committee for Nuclear Physics Experiments at RI Beam Factory (NP-PAC)

Members (as of March 31, 2015)

Muhsin N. HARAKEH (Chair)	Prof., KVI (Kernfysisch Versneller Instituut), University of Groningen, Netherlands
Yanlin YE	Prof., State Key Lab. of Nucl. Phys. and Tech., School of Physics, Peking University, China
Christoph SCHEIDENBERGER	Head, NuSTAR/ENNA Department, GSI, Germany
Friedrich-K. THIELEMANN	Prof., Department of Physics, University of Basel, Switzerland
Rick F. CASTEN	Prof., Department of Physics, Yale University, USA
Christopher J. (KIM) LISTER	Prof., Department of Physics and Applied Physics, University of Massachusetts, Lowell, USA
Hans EMLING	Prof. Dr., GSI, Germany
Hironori IWASAKI	Assistant Prof., National Superconducting Cyclotron Laboratory, Michigan State University, USA
Walter D. LOVELAND	Full Prof., Department of Chemistry, Oregon State University, USA
Thomas NILSSON	Prof., Chalmers Univ. of Technology, Sweden; Chair of BFC (Board of FAIR Collaborations)
Bradley. M.SHERRILL	FRIB Associate Laboratory Director for Users, Michigan State University, USA
Olivier SORLIN	GANIL (Grand Accélérateur National d'Ions Lourds), France
Satoshi N. NAKAMURA	Prof. Nuclear Experiment Group, Faculty of Science, Tohoku University, Japan
Atsushi TAMII	Associate Prof., Research Center for Nuclear Physics, Osaka University, Japan
Yutaka UTSUNO	Senior Scientist, Advanced Science Research Center, JAEA, Japan
Masanobu YAHIRO	Prof., Faculty of Sciences, Kyushu University, Japan
Takashi NAKATSUKASA	Associate Chief Scientist, Theoretical Nuclear Physics Laboratory, RNC, Japan

Program Advisory Committee for Materials and Life Science Researches at RIKEN Nishina Center (ML-PAC)

Members (as of March 31, 2015)

Jean-Michel POUTISSOU (Chair)	Senior research scientist Emeritus, TRIUMF, Canada
Alex AMATO	Bulk μSR Group Head, GPS Scientist, Laboratory for Muon Spin Spectroscopy, PSI, Switzerland
Douglas E. MACLAUGHLIN	Prof., Emeritus, University of California, Riverside, USA
Sadamichi MAEKAWA	Director General, Advanced Science Research Center, JAEA, Japan
Kenya KUBO	Prof., Department of Material Science, International Christian University, Japan
Adrian HILLIER	ISIS, RAL, UK
Philippe MENDELS	Prof., Laboratorie de Physique des Solides, Universite Paris-SUD, France
Xu-Guang ZHENG	Prof., Department of Physics Faculty of Science and Engineering, Saga University, Japan
Hiroyuki YAMASE	Senior Researcher, National Institute for Materials Science, Japan
Ryosuke KADONO	Prof., Division Head, Muon Science Laboratory, Institute of Materials Structure Science, KEK, Japan
Norimichi KOJIMA	Prof., Department of Basic Science, Graduate School of Arts and Sciences, University of Tokyo, Japan
Toshiyuki AZUMA	Chief Scientist, Atomic, Molecular & Optical Physics Laboratory, RIKEN, Japan
Atsushi KAWAMOTO	Prof., Graduate School of Science, Hokkaido University, JAPAN
Shigeo YOSHIDA	Research Consultant, RIKEN Center for Sustainable Resource Science, RIKEN, Japan

Industrial Program Advisory Committee (In-PAC)

Members (as of March 31, 2015)

Akihiro IWASE (Chair)	Prof., Graduate School of Engineering, Osaka Prefecture University, Japan
Kenya KUBO	Prof., The College of Liberal Arts, International Christian University, Japan
Hitoshi NAKAGAWA	Auditor, Japan International Research Center for Agricultural Sciences, Japan
Nobuhiko NISHIDA	Full time research fellow, Toyota Physical and Chemical Research Institute, Japan
Toshinori MITSUMOTO	Chief Engineer, Quantum Equipment Division, Sumitomo Heavy Industries, Ltd, Japan
Toshiyuki AZUMA	Chief Scientist, Atomic, Molecular & Optical Physics Laboratory, RIKEN, Japan

Safety Review Committee

The Safety Review Committee is composed of two sub committees, the Safety Review Committee for Accelerator Experiments and the Hot-Lab Safety Review Committee. These Committees review the safety regarding the usage of radiation generating equipment based on the proposal submitted to RNC Director from the spokesperson of the approved experiment.

Safety Review Committee for Accelerator Experiments

Members (as of March 31, 2015)

Takashi KISHIDA (Chair)	Senior Research Scientist, Radioactive Isotope Physics Laboratory
Kouji MORIMOTO	Team Leader, Superheavy Element Device Development Team
Eiji IKEZAWA	Team Leader, RILAC Team
Hiromitsu HABA	Team Leader, RI Applications Team
Shinichiro MICHIMASA	Assistant Prof., Center for Nuclear Study, University of Tokyo
Hidetoshi YAMAGUCHI	Lecturer, Center for Nuclear Study, University of Tokyo
Hiroshi WATANABE	Lecturer, Radioactive Nuclear Beam Group, IPNS, KEK

Hiromi SATO	Team Leader, Detector Team
Atsushi YOSHIDA	Team Leader, Industrial Cooperation Team
Koichi YOSHIDA	Team Leader, BigRIPS Team
Naoki FUKUDA	Nishina Center Research Scientist, BigRIPS Team
Naruhiko SAKAMOTO	Team Leader, Cyclotron Team
Ex officio members	
Yoshitomo UWAMINO	Group Director, Safety Management Group
Kanenobu TANAKA	Deputy Group Director, Management Group
Hisao SAKAMOTO	Nishina Center Technical Scientist, Safety Management Group

Hot-Lab Safety Review Committee

Members (as of March 31, 2015)

Masako IZUMI (Chair)	Senior Research Scientist, Radiation Biology Team
Hiromitsu HABA	Team Leader, RI Applications Team
Yoshitomo UWAMINO	Group Director, Safety Management Group
Kanenobu TANAKA	Deputy Group Director, Safety Management Group
Hisao SAKAMOTO	Nishina Center Technical Scientist, Safety Management Group
Hiroki MUKAI	Assigned Employee, Safety Management Group

RIBF Machine Time Committee

Upon request of the RNC Director, the RIBF Machine Time Committee deliberates on the machine time schedule of RIBF, and reports the results to him.

Members (as of March 31, 2015)

Hideyuki SAKAI (Chair)	Group Director, User Liaison and Industrial Cooperation Group
Tomoko ABE	Group Director, Accelerator Applications Research Group
Nobuhisa FUKUNISHI	Deputy Group Director, Accelerator Group
Osamu KAMIGAITO	Group Director, Accelerator Group
Masayuki KASE	Deputy Group Director, Accelerator Group
Toshiyuki KUBO	Group Director, Research Instruments Group
Kouji MORIMOTO	Team Leader, Superheavy Element Research Device Development Team
Hiroki OKUNO	Deputy Group Director, Accelerator Group
Hiroyoshi SAKURAI	Chief Scientist, Radioactive Isotope Physics Laboratory
Hideki UENO	Chief Scientist, Nuclear Spectroscopy Laboratory
Tomohiro UESAKA	Chief Scientist, Spin isospin Laboratory
Yoshitomo UWAMINO	Group Director, Safety Management Group
Masanori WAKASUGI	Group Director, Instrumentation Development Group
Ken-ichiro YONEDA	Team Leader, User Support Office
Susumu SHIMOURA	Professor, Center for Nuclear Study, University of Tokyo
Hidetoshi YAMAGUCHI	Lecturer, Center for Nuclear Study, University of Tokyo
Hiroari MIYATAKE	Professor, Radioactive Nuclear Beam Group, IPNS, KEK

Observers (as of March 31, 2015)

Hideto EN'YO	Director, RNC
Nobuaki IMAI	Chair, RIBF-UEC, Associate Prof. Center for Nuclear Study, University of Tokyo
Hiromitsu HABA	Team Leader, RI Applications Team
Kosuke MORITA	Group Director, Research Group for Superheavy Element
Tohru MOTOBAYASHI	RIBF Synergetic-Use Coordinator
Koichi YOSHIDA	Team Leader, BigRIPS Team; Team Leader, Slow RI Data Team
Kanenobu TANAKA	Deputy Group Director, Safety Management Group
Mitsuru KISHIMOTO	Deputy Director, Nishina Center Planning Office

Public Relations Committee

Upon request of the RNC Director, the Public Relations Committee deliberates and coordinates the following matters:

(1) Creating public relations system for the RNC

(2) Prioritization of the public relations activities for the RNC

(3) Other general and important matters concerning the public relations of RNC

Members (as of March 31, 2015)

Hiroshi TSUBOI	Executive Director; Director, Head of Nishina Center Planning Office
Hiroyoshi SAKURAI	Deputy Director, RNC; Chief Scientist, Radioactive Isotope Physics Laboratory
Tetsuo HATSUDA	Deputy Director, RNC; Chief Scientist, Quantum Hadron Physics Laboratory
Tohru MOTOBAYASHI	RIBF synergetic-use coordinator
Walter F. HENNING	Senior Advisor
Yasushige YANO	Senior Advisor

Masahiko IWASAKI	Chief Scientist, Advanced Meson Science Laboratory
Tomohiro UESAKA	Chief Scientist, Spin isospin Laboratory
Hideki UENO	Chief Scientist, Nuclear Spectroscopy Laboratory
Toru TAMAGAWA	Associate Chief Scientist, High Energy Astrophysics Laboratory
Takashi NAKATSUKASA	Associate Chief Scientist, Theoretical Nuclear Physics Laboratory
Emiko HIYAMA	Associate Chief Scientist, Strangeness Nuclear Physics Laboratory
Koji HASHIMOTO	Associate Chief Scientist, Mathematical Physics Laboratory
Kosuke MORITA	Group Director, Research Group for Superheavy Element
Osamu KAMIGAITO	Group Director, Accelerator Group
Hideyuki SAKAI	Group Director, User Liaison and Industrial Cooperation Group

RBRC Management Steering Committee (MSC)

RBRC MSC is set up according to the Memorandum of Understanding between RIKEN and BNL concerning the collaboration on the Spin Physics Program at the Relativistic Heavy Ion Collider (RHIC).

Members (as of March 31, 2015)

Maki KAWAI	Executive Director, RIKEN
Shoji NAGAMIYA	Science Advisor, RIKEN
Hideto EN'YO	Director, RNC
Berndt MUELLER	Associate Laboratory Director for Nuclear and Particle Physics, BNL
David LISSAUER	Deputy Chair, Physics Department, BNL
Satoshi OZAKI	Senior Advisor, BNL

Nishina Center Advisory Council

The agenda to be deliberated by NCAC are set by the Terms of Reference presented by the RNC Director on the fundamental issues regarding research activities and administrative matters. NCAC submits its report to the President of RIKEN, and to the Director of Nishina Center if necessary. The members of NCAC are recommended by the Director of the Nishina Center to the President of RIKEN and selected from among highly knowledgeable individuals and experts worldwide. NCAC has two sub-councils for the RBRC and the RAL Muon Facility, respectively.

Members (as of March 31, 2015)

Robert TRIBBLE (Chair)	Deputy Director for Science and Technology, BNL, USA
Hirokazu TAMURA	Prof., Department of Physics, Graduate School of Science, Tohoku University, Japan
Muhsin N. HARAKEH	Prof., Emeritus, KVI (Kernfysisch Versneller Instituut), University of Groningen, Netherlands; *Chair, NP-PAC*
Jean-Michel POUTISSOU	Senior research scientist Emeritus, TRIUMF, Canada; *Chair, ML-PAC*
Richard MILNER	Prof., Director, Laboratory for Nuclear Science, MIT, USA; *Chair, RBRC-SRC*
Andrew TAYLOR	Executive Director, STFC National Laboratories, UK; *Chair, RAL-IAC*
Juha ÄYSTÖ	Director of Helsinki Institute of Physics, Finland
Angela BRACCO	Prof., Department of Physics, the University of Milan, Italy
Masaki FUKUSHIMA	Prof., Institute for Cosmic Ray Research, University of Tokyo, Japan
Ken'ichi IMAI	Group Leader, Research Group for Hadron Physics, Advanced Science Research Center, JAEA, Japan
Marek LEWITOWICZ	Deputy Director, GANIL (Grand Accélérateur National d'Ions Lourds), France
Lia MERMINGA	Head, Accelerator Division, TRIUMF, Canada
Witold NAZAREWICZ	Prof., Department of Physics and Astronomy, the University of Tennessee, USA
Susumu SHIMOURA	Prof., Center for Nuclear Study (CNS), University of Tokyo, Japan
Matthias SCHÄDEL	Group Leader, Research Group for Superheavy Elements, Advanced Science Research Center, JAEA. , Japan
Jun SUGIYAMA	Principal Research Scientist, Toyota Central R&D Labs., INC, Japan
Wolfram WEISE	Director, European Center for Theoretical Studies in Nuclear Physic and Related Areas, Italy
GuoQing XIAO	Director, Institute of Modern Physics, Chinese Academy of Sciences, China
Akira YAMAMOTO	Head, Linear Collider Project Office, Department of Advanced Accelerator Technologies, KEK, Japan

RBRC Scientific Review Committee (SRC)

Members (as of March 31, 2015)

Richard MILNER (Chair)	Prof., Director, Laboratory for Nuclear Science, MIT, USA
Shinya AOKI	Prof., Yukawa Institute for Theoretical Physics, Kyoto University, Japan
Ken'ich IMAI	Group Leader, Research Group for Hadron Physics, Advanced Science Research Center, JAEA, Japan
Tetsuo MATSUI	Prof., Department of Basic Science, Graduate School of Arts and Sciences, Komaba, University of Tokyo, Japan
Alfred MUELLER	Prof., Department of Physics, Columbia University, USA
Peter Braun-MUNZINGER	Prof., Dr. GSI Helmholtzzentrum für Schwerionenforschung, Germany
Charles PRESCOTT	Prof., Stanford Linear Accelerator Center, USA
Akira UKAWA	Prof., Graduate School of Pure and Applied Science, University of Tsukuba, Japan

Advisory Committee for the RIKEN-RAL Muon Facility

Members (as of March 31, 2015)

Andrew D TAYLOR (Chair)	Executive Director, STFC National Laboratories, UK
Jean-Michel POUTISSOU	Senior research scientist Emeritus, TRIUMF, Canada
Klaus P. JUNGMANN	Prof., University of Groningen, Netherlands
Roberto De RENZI	Prof., Department of Physics and Earth Sciences, University of Parma, Italy
Yasuyuki MATSUDA	Assoc. Prof., Graduate School of Arts and Sciences, the University of Tokyo, Japan
Jun SUGIYAMA	Principal Research Scientist, Toyota Central R&D Labs., INC, Japan

6. International Collaboration

Country	Partner Institute	Objects	RNC contact person
Austria	Stefan Meyer Institute for Subatomic Physics	Experimental and theoretical hadron physics, especially in exotic hadronic atoms and meson and baryon nuclear bound states	Masahiko IWASAKI, Chief Scientist, Director of Advanced Meson Science Laboratory
Belgium	Katholieke Universiteit te Leuven	Framework	Michiharu WADA, Team Leader, SLOWRI Team
Bulgaria	The Institute for Nuclear Research and Nuclear Energy (INRNE)	Framework	Hedeki UENO, Chief Scientist, Nuclear Spectroscopy Laboratory
Canada	TRIUMF	Accelerator-based Science	Hiroyoshi SAKURAI, Deputy Director, Chief Scientist, Radioactive Isotope Physics Laboratory
China	China Nuclear Physics Society	Creation of the council for China -Japan research collaboration on nuclear physics	Hiroyoshi SAKURAI, Deputy Director, Chief Scientist, Radioactive Isotope Physics Laboratory
	Peking University	Nuclear Science	Hiroyoshi SAKURAI, Deputy Director, Chief Scientist, Radioactive Isotope Physics Laboratory
		Strategic cooperation (Nishina School)	Hiroyoshi SAKURAI, Deputy Director, Chief Scientist, Radioactive Isotope Physics Laboratory
	Shanghai Jiao Tong University	International Joint Graduate School Program	Takashi NAKATSUKASA, Associate chief scientist, Theoretical Nuclear Physics Laboratory
	ZHEJIANG University	International Joint Graduate School Program	Isao WATANABE, Advanced Meson Science Laboratoy
	Institute of Modern Physics, Chinese Academy of Science	Physics of heavy ions	Hiroyoshi SAKURAI, Deputy Director, Chief Scientist, Radioactive Isotope Physics Laboratory
	School of Nuclear Science and Technology, Lanzhou University	Framework	Yue MA, Advanced Meson Science Laboratory
	School of Physics, Nanjing University	Framework	Emiko HIYAMA, Associate chief scientist, Strangeness Nuclear Physics Laboratory
EU	European Gamma-Ray Spectroscopy Pool Owners Committee	The use of Euroball ditector at RIKEN	Shunji NISHIMURA, Radioactive Isotope Physics Laboratory
	European Center for Theoretical Studies in Nuclear Physics and Related Areas (ECT*)	Theoretical physics	Tetsuo HATSUDA, Deputy Director, Chief Scientist, Quantum Hadron Physics Laboratory
	CERN	Framework	Satoshi YOKKAICHI, Senior Research Scientist, Radiation Laboratory
		RD-51:R&D programme for micro-pattern gas detectors (MPGD)	Satoshi YOKKAICHI, Senior Research Scientist, Radiation Laboratory
	ALICE Collaboration	Development of Gas Electron Multiplier, Silicon Detectors, etc.	Satoshi YOKKAICHI, Senior Research Scientist, Radiation Laboratory
	GSI & Reaction with Relativistic Radioactive Beams (R3B) Collaboration	To unravel structure of nuclei in the vicinity of and beyond the neutron dripline through experiments with the NeuLAND detector combined with the SAMURAI magnetic spectrometer at the RIBF	Tomohiro UESAKA, Chief Scientist, Spin Isospin Laboratory
Finland	University of Jyvaskyla	Basic nuclear physics and related instrumentation	Michiharu WADA, Team Leader, SLOWRI Team
France	National Institute of Nuclear Physics and Particle Physics (IN2P3)	Physics of heavy ions	Tohru MOTOBAYASHI, RIBF synergetic-use coordinator
	CNRS, CEA,GANIL, Université Paris Sud, etc.	Creation of an International Associated Laboratory (LIA) French-Japanese International Associated Laboratory for Nuclear Structure Problems	Tohru MOTOBAYASHI, RIBF synergetic-use coordinator
	IRFU CEA-Saclay DSM/IRFU, IPNO CNRS IN2P3, GANIL	The preparation and realization for the MUST2 campaign of experiments at RIKEN	Hiroyoshi SAKURAI, Deputy Director, Chief Scientist, Radioactive Isotope Physics Laboratory
	CEA-DSM	The use of MINOS device at RIKEN	Tomohiro UESAKA, Chief Scientist, Spin Isospin Laboratory
	SIMEM Graduate School, Department of Physics, Caen University	Framework	Tomohiro UESAKA, Chief Scientist, Spin Isospin Laboratory
	Université de Caen Basse Normandie	International Joint Graduate School Program	Tomohiro UESAKA, Chief Scientist, Spin Isospin Laboratory

Country	Partner Institute	Objects	RNC contact person
Germany	Technische Universität München	Nuclear physics, hadron physics, nuclear astrophysics	Emiko HIYAMA, Associate chief scientist, Strangeness Nuclear Physics Laboratory
	Max-Planck Gesellschaft	Comprehensive agreement	Hiroyoshi SAKURAI, Deputy Director, Chief Scientist, Radioactive Isotope Physics Laboratory
	GSI	Physics of heavey ions and accelerator	Hiroyoshi SAKURAI, Deputy Director, Chief Scientist, Radioactive Isotope Physics Laboratory
Hungary	The Institute of Nuclear Research of the Hungarian Academy of Sciences (ATOMKI)	Nuclear physics, Atomic Physics	Tomohiro UESAKA, Chief Scientist, Spin Isospin Laboratory
Indonesia	ITB, UNPAD, ITS, UGM	Material science using muons at the RIKEN-RAL muon facility	Isao WATANABE, Advanced Meson Science Laboratoy
	UNPAD	International Joint Graduate School Program	Isao WATANABE, Advanced Meson Science Laboratoy
	Institut Teknologi Bandung (ITB)	International Joint Graduate School Program	Isao WATANABE, Advanced Meson Science Laboratoy
	Universitas Hasanuddin	Agricultural science and related fields involving heavy-ion beam mutagenesis using Indonesian crops	Tomoko ABE, Group Director, Accelerator Applications Research Group
Italy	National Institute of Nuclear Physics (INFN)	Physics of heavy ions	Tohru MOTOBAYASHI, RIBF synergetic-use coordinator
	Applied Physics Division, National Institute for New Technologies, Energy and Environment (ENEA)	Framework	Tohru MOTOBAYASHI, RIBF synergetic-use coordinator
Korea	Seoul National University	Nishina School	Hiroyoshi SAKURAI, Deputy Director, Chief Scientist, Radioactive Isotope Physics Laboratory
		International Joint Graduate School Program	Itaru NAKAGAWA, Radiation Laboratory
	Institute of Basic Science, Rare Isotope Science Project	Rare ion accelerator and related fields	Hiroyoshi SAKURAI, Shunji NISHIMURA
	Department of Physics, Kyungpook National University	Framework	Tomohiro UESAKA, Chief Scientist, Spin Isospin Laboratory
	College of Natural Sciences of Kyungpook National University	International Joint Graduate School Program	Tomohiro UESAKA, Chief Scientist, Spin Isospin Laboratory
	College of Science, Yonsei University	Framework	Tomohiro UESAKA, Chief Scientist, Spin Isospin Laboratory
	Department of Physics, Yonsei University	International Joint Graduate School Program	Yasuyuki AKIBA, Radiation Laboratory
	Department of Physics, Korea University	Framework	Yuji GOTO, Radiation Laboratory
	College of Natural Science, Ewha Women's University	Framework	Tomohiro UESAKA, Chief Scientist, Spin Isospin Laboratory
Malaysia	Universiti Sains Malaysia	Framework on Muon Science	Isao WATANABE, Advanced Meson Science Laboratoy
Poland	the Henryk Niewodniczanski Institute of Nuclear Physics, Polish Academy of Sciences(IFJ PAN)	Framework	Hiroyoshi SAKURAI, Deputy Director, Chief Scientist, Radioactive Isotope Physics Laboratory
Romania	"Horia Hulubei" National Institute of Physics and Nuclear Engineering Bucharest-Magurele, Romania	Framework	Tomohiro UESAKA, Chief Scientist, Spin Isospin Laboratory
Russia	Joint Institute for Nuclear Research (JINR)	Framework	Tomohiro UESAKA, Chief Scientist, Spin Isospin Laboratory
	Russian Research Center "Kurchatov Institute"	Framework	Hiroyoshi SAKURAI, Tomohiro UESAKA, Osamu KAMIGAITO, Masanori WAKASUGI
Switzerland	Paul Scherrer Institute	Improve the performance and reliability of accelerator systems	Osamu KAMIGAITO, Director, Chief Scientist, Accelerator Group
UK	The Science and Technology Facilities Council	Muon science using the ISIS Facility at the Rutherford Appleton Laboratory	Philip KING, Director of RIKEN-RAL muon facility
	University of Liverpool	International Joint Graduate School Program	Hiroyoshi SAKURAI, Deputy Director, Chief Scientist, Radioactive Isotope Physics Laboratory
USA	BNL	The Spin Physics Program at the Relativistic Heavy Ion Collider(RHIC)	Hideto EN'YO, Director of RNC
	Columbia University	The development of QCDCQ	Taku IZUBUCHI, Group Leader, Computing Group, RBRC
	Michigan State University	Framework	Tomohiro UESAKA, Chief Scientist, Spin Isospin Laboratory
		TPC(Time Projection Chamber)	Hiroyoshi SAKURAI, Deputy Director, Chief Scientist, Radioactive Isotope Physics Laboratory & Tadaaki ISOBE, Radioactive Isotope Physics Laboratory
Vietnam	Vietnam Atomic Energy Commission	Framework	Tohru MOTOBAYASHI, RIBF synergetic-use coordinator
	Hanoi University of Science	International Joint Graduate School Program	Hiroyoshi SAKURAI, Deputy Director, Chief Scientist, Radioactive Isotope Physics Laboratory
	Institute of Physics, Vietnam Academy of Science and Technology	Framework	Hiroyoshi SAKURAI, Deputy Director, Chief Scientist, Radioactive Isotope Physics Laboratory

7. Awards

Awardee, Laboratory / Team	Award	Organization	Date
Tetsuo HATSUDA, Quantum Hadron Physics Laboratory Shinya AOKI (Visiting Scientist), Quantum Hadron Physics Laboratory Noriyoshi ISHII (Visiting Scientist), Radiation Laboratory	The Prizes for Science and Technology in Research Category, in the FY2015 Commendation for Science and Technology	The Minister of Education, culture, Sports, Science and Technology (MEXT)	Apr. 15
Tomonari HIRANO, Ion Beam Breeding Team Yusuke KAZAMA, Ion Beam Breeding Team Kotaro ISHII, Ion Beam Breeding Team Sumie OHBU, Ion Beam Breeding Team Yuki SHIRAKAWA, Ion Beam Breeding Team Tomoko ABE, Ion Beam Breeding Team	The Outstanding Presentation Award for their research at the 125th Meeting of the Japanese Society of Breeding	Japanese Society of Breeding	May 14
Maeyama TAKUYA, Beam Dynamics & Diagnostics Team	Young Scientist Award	The 5th Asia Pacific Symposium on Radiation Chemistry (APSRC2014)	Sep. 11
Yuko MOTIZUKI, the Astro-Glaciology Research Unit	NIceSTEP Award	National Institute of Science and Technology Policy	Dec. 19
Kimiko SEKIGUCHI (Visiting Scientist) , Spin Isospin Laboratory	The silver prize of the 2nd Yuasa Prize	Ochanomizu University	Dec. 24
Yoichi IKEDA, Quantum Hadron Physics Laboratory Toru SATO (Visiting Scientist), Strangeness Nuclear Physics Laboratory	The 20th Best Paper Award	The Physical Society of Japan	Mar. 23
Aiko TAKAMINE (Visiting Scientist) , SLOWRI Team	The 9th Young Scientist Award in the field of experimental nuclear physics	The Physical Society of Japan	Mar. 21
Abhay DESHPANDE, RBRC experimental group	Appointment as an APS Fellow	The American Physical Society	Mar. 13

8. Brief overview of the RI Beam Factory

Intensity of Primary Beams

Achieved beam intensities (as of March 2015)

^{238}U	28 pnA	(345 MeV/u, Oct. 2014)
^{124}Xe	38 pnA	(345 MeV/u, Jun. 2013)
^{86}Kr	30 pnA	(345 MeV/u, Nov. 2007)
^{70}Zn	123 pnA	(345 MeV/u, Jun. 2014)
^{48}Ca	530 pnA	(345 MeV/u, Nov. 2014)
^{18}O	1,000 pnA	(345 MeV/u, Jun. 2010)
^{14}N	400 pnA	(250 MeV/u, Oct. 2010)
^{4}He	1,000 pnA	(250 MeV/u, Oct. 2009)
d	1,000 pnA	(250 MeV/u, Oct. 2010)
pol. d	1,000 pnA	(250 MeV/u, Apr. 2009)

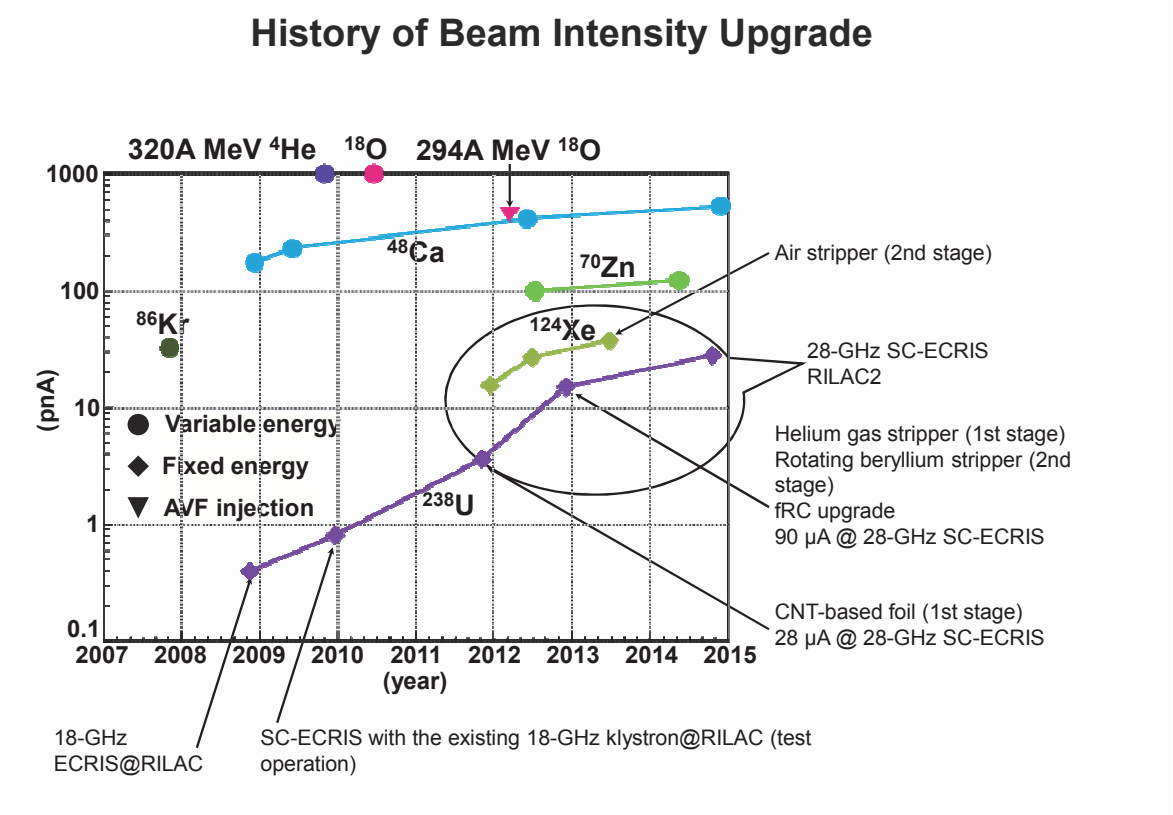

Total beam time for experiments

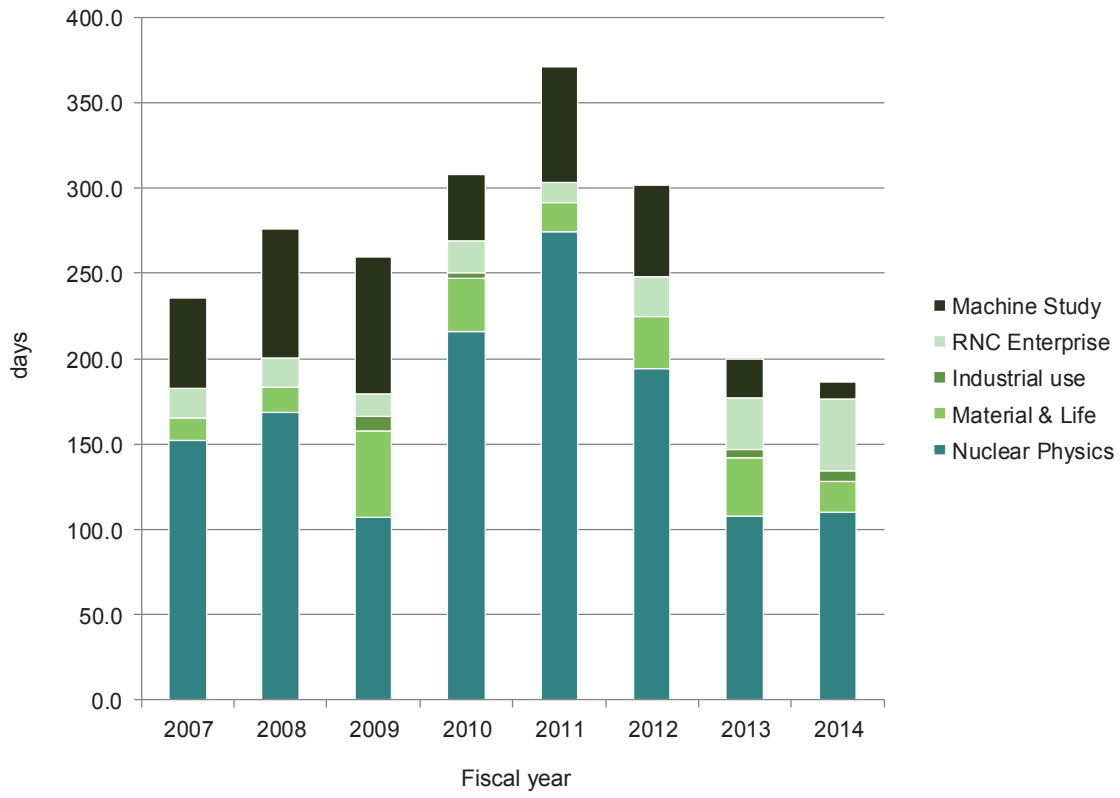

Breakdown of Nucl. Phys. Expts.

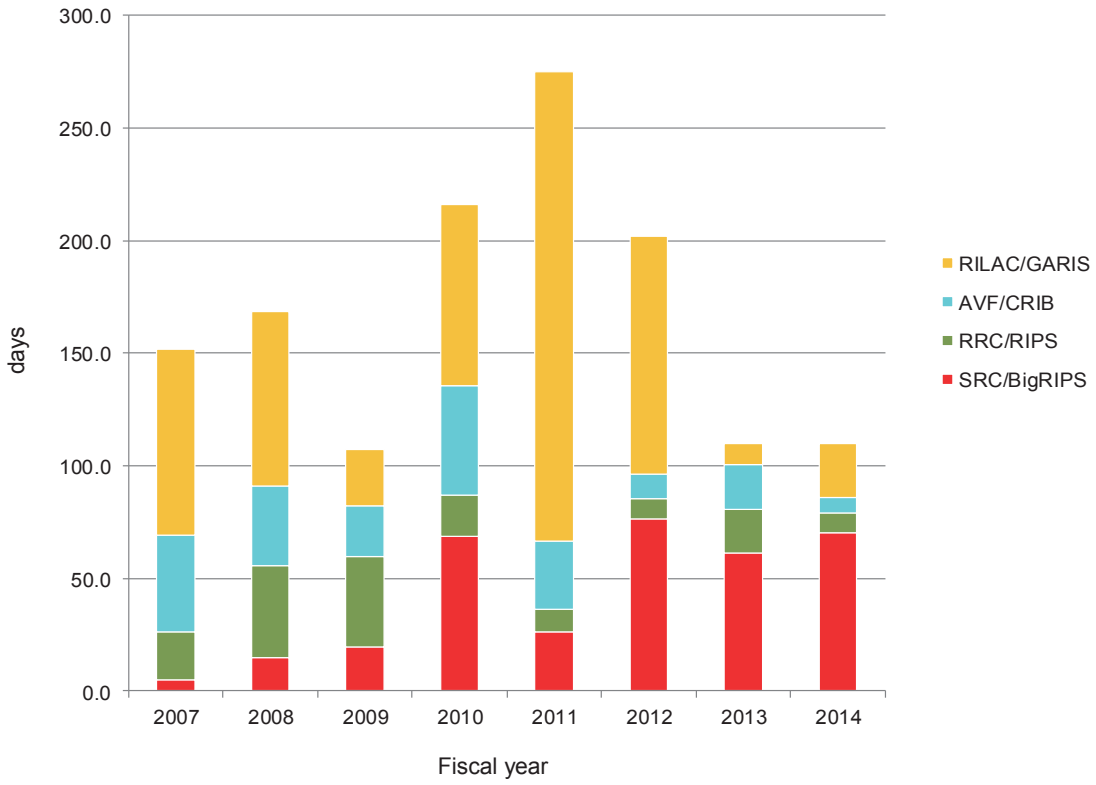

Total beam time allocated to BigRIPS experiments

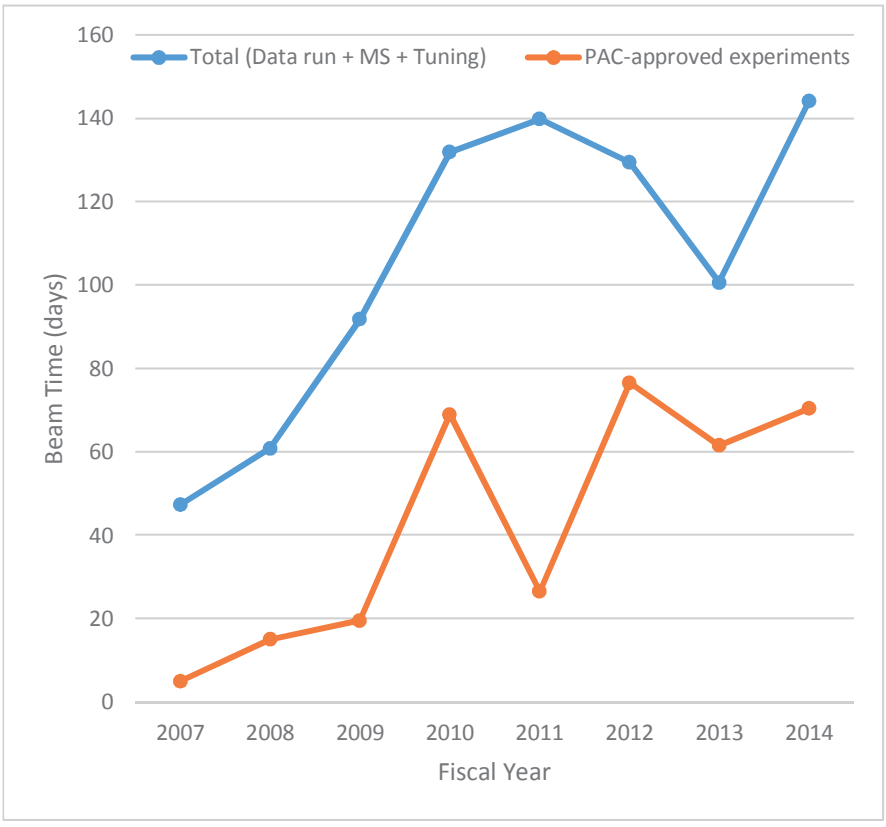

Theoretical Research Division
Quantum Hadron Physics Laboratory

1. Abstract

Atomic nuclei are made of protons and neutrons bound by the exchange of Yukawa's pion and other mesons. Also, protons and neutrons are made of quarks bound by the exchange of gluons. These strong interactions are governed by the non-Abelian gauge theory called the quantum chromodynamics (QCD). On the basis of theoretical and numerical analyses of QCD, we study the interactions between the nucleons, properties of the dense quark matter realized at the center of neutron stars, and properties of the hot quark-gluon plasma realized in the early Universe. Strong correlations common in QCD and cold atoms are also studied theoretically to unravel the universal features of the strongly interacting many-body systems. Developing perturbative and non-perturbative techniques in quantum field theory and string theory are of great importance not only to solve gauge theories such as QED and QCD, but also to find the theories beyond the standard model of elementary particles. Various theoretical approaches along this line have been attempted.

2. Major Research Subjects

(1) Improving the tenth-order QED contribution to the electron $g-2$
(2) Physics of particles with resonant interactions
(3) String duality and Sine-Square Deformation of Conformal Field Theory
(4) Theory of spontaneous symmetry breaking
(5) QCD under extreme conditions
(6) Lattice baryon forces

3. Summary of Research Activity

(1) Improving the tenth-order QED contribution to the electron $g-2$

The preliminary value of the tenth-order of the perturbation theory of QED contribution to the electron anomalous magnetic moment ($g-2$) was reported by us in 2012. Since then, we have been involved in improving and establishing its accuracy. To carry out it, we reevaluated the most difficult and large set of the Feynman diagrams by using the advanced technique of numerical calculation especially suitable to RIKEN's supercomputer. As a result, we have obtained more reliable and more precise values for the eighth- and tenth-order terms. Together with the Harvard experiment of the electron $g-2$, it leads to the world-best value of the fine-structure constant α that will be used to determine a next CODATA recommended value of α.

(2) Physics of particles with resonant interactions

Some particles, such as nucleons, can only weakly or nearly bind by pair. As a result, their pairwise interaction is resonant. Resonant interactions induce universal few-body phenomena, such as the Efimov effect. These phenomena lead to the existence of universal three-body bound states, that can be easily investigated with ultra-cold atoms. After analysing these experiments and clarifying these few-body phenomena for the past few years, we have now started to explore their consequences at the many-body level, by first looking at mixtures of resonantly interacting heavy and light particles. The near-resonant interaction induces a phase made of trimers of two heavy and one light particles. We have characterized this phase by carrying out for the first time a six-body calculation of the effective interaction between two universal trimers.

(3) String duality and Sine-Square Deformation of Conformal Field Theory

String duality is the concept that has been leading us to better understandings of the dynamics of string theory. One of such dualities is the open-closed duality, which suggests relation between gauge theories and the theory of gravity, thus could be behind another duality, AdS/CFT correspondence. Since the difference between open string and closed string is the difference of the boundary condition of the worldsheet of string, of particular interest is the recently found phenomenon called Sine-Square Deformation (SSD) in which certain quantum systems exhibit the change from the closed-boundary vacuums to open-boundary ones through the spatial modulation of the couplings. We investigated SSD in the context of Conformal Field Theory (CFT) in particular and found continuous Virasoro algebra, suggesting that CFT would acquire a continuous energy spectrum under SSD.

(4) Theory of spontaneous symmetry breaking

(4-1) Dispersion relations of Nambu-Goldstone modes at finite temperature and density

We discussed the dispersion relations of Nambu-Goldstone (NG) modes associated with spontaneous breaking of internal symmetries at finite temperature and/or density. We showed that the dispersion relations of type-A (I) and type-B (II) NG modes are linear and quadratic in momentum, whose imaginary parts are quadratic and quartic, respectively. In both cases, the real parts of the dispersion relations are larger than the imaginary parts when the momentum is small, so that the NG modes can propagate far away. We derived the gap formula for NG modes in the presence of a small explicit breaking term. We also discussed the gapped partners of type-B NG modes, when type-A and type-B NG modes coexisted.

(4-2) Effective field theory for spacetime symmetry breaking

We discussed the effective field theory for spacetime symmetry breaking from the local symmetry point of view. By gauging spacetime symmetries, the identification of Nambu-Goldstone (NG) fields and the construction of the effective action were performed based on the breaking pattern of diffeomorphism, local Lorentz, and (an)isotropic Weyl symmetries as well as the internal symmetries including possible central extensions in nonrelativistic systems. Such a local picture distinguishes, e.g., whether the symmetry breaking condensations have spins and provides a correct identification of the physical NG fields, while the standard coset construction based on global symmetry breaking does not. We illustrated that the local picture becomes important in particular when we took into account

massive modes associated with symmetry breaking, whose masses were not necessarily high. We also revisited the coset construction for spacetime symmetry breaking. Based on the relation between the Maurer-Cartan one form and connections for spacetime symmetries, we classified the physical meanings of the inverse Higgs constraints by the coordinate dimension of broken symmetries. Inverse Higgs constraints for spacetime symmetries with a higher dimension remove the redundant NG fields, whereas those for dimensionless symmetries can be further classified by the local symmetry breaking pattern.

(5) QCD under extreme conditions

(5-1) Production and Elliptic Flow of Dileptons and Photons in the semi-Quark Gluon Plasma

We considered the thermal production of dileptons and photons at temperatures above the critical temperature in QCD. We used a model where color excitations are suppressed by a small value of the Polyakov loop, the semi Quark-Gluon Plasma (QGP). Comparing the semi-QGP to the perturbative QGP, we found a mild enhancement of thermal dileptons. In contrast, to leading logarithmic order in weak coupling there are far fewer hard photons from the semi-QGP than the usual QGP. To illustrate the possible effects on photon and dileptons production in heavy ion collisions, we integrated the rate with a realistic hydrodynamic simulation. Dileptons uniformly exhibit a small flow, but the strong suppression of photons in the semi-QGP tends to bias the elliptical flow of photons to that generated in the hadronic phase.

(5-2) Relativistic hydrodynamics from quantum field theory on the basis of the generalized Gibbs ensemble method

We derived relativistic hydrodynamics from quantum field theories by assuming that the density operator is given by a local Gibbs distribution at initial time. We decomposed the energy-momentum tensor and particle current into nondissipative and dissipative parts, and analyzed their time-evolution in detail. Performing the path-integral formulation of the local Gibbs distribution, we microscopically derived the generating functional for the nondissipative hydrodynamics. We also constructed a basis to study dissipative corrections. In particular, we derived the first-order dissipative hydrodynamic equations without choice of frame such as the Landau-Lifshitz or Eckart frame.

(6) Lattice baryon forces

One of the most important subjects in nuclear physics is to determine nuclear forces and hyperon forces, or generalized baryon forces, directly based on the fundamental theory, QCD. In HAL QCD Collaboration, we have been developing a novel lattice QCD formulation and performing first-principles numerical simulations to determine baryon forces. Spin-orbit forces have been calculated for the first time, and attraction in 3P2 channel is observed, which is related to the P-wave neutron pairing in neutron stars. The calculation of the N-Omega interaction shows that the system is bound in 5S2 channel. Three-nucleon forces have been calculated at several heavy quark masses, and quark mass dependence is found to be small. The lattice calculations are extended to the the exotic tetraquark systems as Tcc and Tcs, and the phenomenological diquark picture in these systems is studied as well. As an application, properties of medium-heavy nuclei have been calculated based on lattice nuclear forces, and so-called "mass-formula" is obtained.

Members

Chief Scientist (Lab. Head)

Tetsuo HATSUDA (Deputy Director, RNC)

Vice Chief Scientist

Tsukasa TADA

Research & Technical Scientists

Takumi DOI (Senior Research Scientist)
Yoshimasa HIDAKA (Senior Research Scientist)
Pascal Raphaël Gabriel NAIDON (Research Scientist)

Nishina Center Research Scientist

Makiko NIO

Special Postdoctoral Researchers

Arata YAMAMOTO (– Mar. 31, 2014)
Kanabu NAWA (– Mar. 31, 2015)
Yuji SAKAI (– Apr. 30, 2014)
Takashi SANO (– Mar. 31, 2015)
Kazuhiko KAMIKADO
Noriaki OGAWA (Apr. 1, 2014 –)

Foreign Postdoctoral Researchers

Gergely Peter FEJOES
Vojtech KREJCIRIK (Apr. 1, 2014 –)

Postdoctoral Researchers

Yoichi IKEDA
Koich HATTORI (Feb. 1, 2014 –)
Taichi KAWANAI (– Sep. 30, 2014)
Shinsuke YOSHIDA (– Mar. 31, 2015)
Daisuke SATO (– Sep. 30, 2014)

Junior Research Associate

Masaru HONGO (Univ. of Tokyo)

International Program Associate

Robert Friedrich LANG (– Feb. 12, 2012)

Visiting Scientists

Noriyoshi ISHII (Osaka Univ.)
Yoshitaka HATTA (Kyoto Univ.)
Motoi TACHIBANA (Saga Univ.)
Masashi HAYAKAWA (Nagoya Univ.)
Toichiro KINOSHITA (Cornell Univ.)
Kenji SAKAI (Univ. of Tsukuba)
Shinya AOKI (Kyoto Univ.)
Hiroshi SUZUKI (Kyushu Univ.)
Keiko MURANO (Osaka Univ.)
Daisuke KADOH (KEK)
Yuji HIRONO (Univ. of Tokyo)
Tatsuyuki TAKATSUKA (Iwate Univ.)
Hong MAO (Hangzhou Normal Univ.)
Arata YAMAMOTO (Univ. of Tokyo)
Sho OZAKI (KEK)
Takashi OKA (Univ. of Tokyo)
Keitaro NAGATA (KEK)
Takashi INOUE (Nihon Univ.)
Kazuyuki KANAYA (Univ. of Tsukuba)
Sachiko TAKEUCHI (Japan College of Social Work)
Takayuki MATSUKI (Tokyo Kasei Univ.)
Takumi IRITANI (Kyoto Univ.)
Hiroshi TOKI (Osaka Univ.)
Tetsuo MATSUI (Univ. of Tokyo)
Makoto TAKIZAWA (Showa Pharm. Univ.)
Teiji KUNIHIRO (Kyoto Univ.)
Shoichi SASAKI (Tohoku Univ.)
Masahito UEDA (Univ. of Tokyo)

Student Trainees

Bruno CHARRON (Univ. of Tokyo)
Shimpei ENDO (Univ. of Tokyo)
Yusuke HAMA (Univ. of Tokyo)
Yasuki TACHIBANA (Univ. of Tokyo)
Tomoya HAYATA (Univ. of Tokyo)
Koichi MURASE (Univ. of Tokyo)
Yuya TANIZAKI (Univ. of Tokyo)
Ryuichi KURITA (Univ. of Tokyo)
Kota MASUDA (Univ. of Tokyo)
Masanori YAMADA (Univ. of Tsukuba)
Terukazu ICHIHARA (Kyoto Univ.)
Yuta KIKUCHI (Kyoto Univ.)
Shoichiro TSUTSUI (Kyoto Univ.)

Part-time Workers

Yuki MINAMI (Oct. 1, 2014 – Mar. 31, 2015)
Kayo YAMAJI

Theoretical Research Division
Theoretical Nuclear Physics Laboratory

1. Abstract

Nuclei are finite many-particle systems composed of protons and neutrons. They are self-bound in femto-scale (10^{-15}m) by the strong interaction (nuclear force) whose study was pioneered by Hideki Yukawa. Uncommon properties of the nuclear force (repulsive core, spin-isospin dependence, tensor force, etc.) prevent complete microscopic studies of nuclear structure. There exist number of unsolved problems even at present. In addition, radioactive beam facilities reveal novel aspects of unstable nuclei. We are tackling these old problems and new issues in theoretical nuclear physics, developing new models and pursuing large-scale calculations of quantum many-body systems. We are also strongly involved in research on other quantum many-body systems, to resolve mysteries in the quantum physics.

2. Major Research Subjects

(1) Nuclear structure and quantum reaction theories
(2) First-principle calculations with the density functional theory for many Fermion systems
(3) Computational nuclear physics

3. Summary of Research Activity

(1) Systematic calculation of $T = 1$ triplets with proton-neutron-mixed energy density functionals

We have performed a systematic calculation for the $T = 1$ isobaric analog states (IASs) based on the Skyrme energy density functionals (EDFs) including protons-neutron (*p*-*n*) mixing. The IASs are calculated using the isocranking method. First we performed a systematic calculation for the energies of the $T = 1$ triplets in the $A = 10 \sim 66$ region with several Skyrme parameter sets. We used the isoscalar *p*-*n* mixed Skyrme EDFs, which are invariant under rotation in the isospin space, together with the Coulomb energy functional. The calculated results show a systematic underestimation from the experimental data, which may be related to violation of the charge symmetry and the charge independence of the nucleon-nucleon interaction and may imply that we need to further extend the energy functionals including isospin breaking terms. Recently, we have started a calculation including the isospin breaking interactions.

(2) Three dimensional mesh calculations for covariant density functional theory

The covariant density functional theory has some numerical difficulties, such as variational collapse and the fermion doubling. Because of these problems, the three-dimensional (3D) mesh calculation was impossible for a long time. In order to realize such calculations for the first time, we proposed in a novel and practical method to solve Dirac equations in the 3D coordinate space. The variational collapse is prevented by employing a method based on the variational principle for the inverse of a single-particle Hamiltonian, while for the fermion doubling, we have extended the method of Wilson fermion, which has been widely employed in lattice QCD calculations.

Using ^{16}O as an example, we have confirmed that our strategy provides accurate solutions for self-consistent mean-field calculations without the influence of the negative-energy spectrum and the spurious solutions of a discretized Dirac equation. We have also shown with ^{24}Mg and ^{28}Si that this method is applicable to deformed solutions in the (β, γ) deformation plane. This development enables us, e.g., i) to study any complicated structure of nuclei with a single numerical code, ii) to compare directly the results of the relativistic models to those of 3D mesh calculations with the non-relativistic models, and iii) to provide reliable theoretical predictions with the relativistic models for unknown nuclei allowing symmetry-breaking solutions. It also allows a straightforward extension of the finite amplitude method within the relativistic framework for a study of nuclear excitations in deformed nuclei.

(3) Microscopic description of fusion hindrance in heavy systems

We investigate fusion hindrance in heavy systems, where the fusion probability is strongly hindered compared with that in light- and medium-mass systems, to understand the origin of the fusion hindrance from a microscopic point of view. We employ microscopic time-dependent Hartree-Fock (TDHF) model for the analysis. In TDHF simulations, we reasonably reproduce the extra-push energies estimated from experimental data for heavy systems. Then, we extract nucleus-nucleus potential and energy dissipation by combining TDHF simulations for fusion reactions with Newton equation including a dissipation term. Extracted potentials in heavy systems show monotonic increase as the relative distance of two nuclei decreases and the disappearance of an ordinary barrier structure, which are different from lighter systems. Using these properties, we analyze the origin of the extra-push energy and find that the contribution to extra-push energy from the increase in potential is larger than that from dissipated energy in most systems. We conclude from our analysis that the main origin of the fusion hindrance is dynamical increase in potential.

(4) Hidden pseudo-spin and spin symmetries and their origins in atomic nuclei

Pseudo-spin symmetry (PSS) was introduced to explain the near degeneracy between pairs of nuclear single-particle states with the quantum numbers (n-1, l+2, j=l+3/2) and (n, l, j=l+1/2). We have written a review article [arXiv:1411.6774, *Phys. Rep.* in press], and intended to provide a comprehensive overview on the recent progress of pseudo-spin and spin symmetries in a systematic way. These symmetries were discussed in various systems and potentials: from stable nuclei to exotic nuclei, from non-confining to confining potentials, from local to non-local potentials, from central to tensor potentials, from bound states to resonant states, from nucleon spectra to

anti-nucleon spectra, from nucleon spectra to hyperon spectra, from spherical nuclei to deformed nuclei.

Furthermore, three of the open issues in this field were selected and discussed in detail, i.e., the perturbative nature of PSS, the puzzle of intruder states, and the supersymmetric (SUSY) representation of PSS. For the perturbative nature of PSS, we emphasized that whether or not the symmetry breaking behaves perturbatively depends on whether an appropriate symmetry limit is chosen and an appropriate symmetry-breaking term is identified. As long as an appropriate symmetry limit is chosen, the nature of PSS is indeed perturbative. For the puzzle of intruder states, we showed several different features about this puzzle. By doing that a number of "contradicting" results in the literature for the spin (pseudo-spin) partners have been clarified in an explicit way. For the SUSY representation of PSS, we pointed out one of the promising ways for understanding the PSS and its symmetry breaking, by combining the similarity renormalization group, the SUSY quantum mechanics, and the perturbation theory. Meanwhile, how to apply the SUSY technique directly to the Dirac equations, which have non-trivial scalar and vector potentials, remains an interesting and open question.

(5) "Hybrid Kurotama model" for total reaction cross sections

We have developed a new general-purpose-total-reaction-cross-section model/subroutine called ``Hybrid Kurotama". The model has been tested and compared with available data for *p*+He, *p*+nucleus, and nucleus+nucleus total reaction cross sections. The overall agreement has been found better than former published models. This model is therefore very suitable to be used in any deterministic or Monte Carlo particle and heavy ion transport code.

(6) Improved parametrization of the transparency parameter in Kox and Shen models of total reaction cross sections

The total reaction cross section is an essential quantity in particle and heavy-ion transport codes when determining the mean-free path of a transported particle. Many transport codes determine the distance a particle is transported before it collides with the target or is stopped in the target material, with the Monte Carlo (MC) method using semiempirical parametrization models for the total reaction cross sections. In order to improve the well-known Kox and Shen models of total reaction cross sections and allow the models to be used at energies below 30 MeV/nucleon, we have proposed a modified parametrization of the transparency parameter. We have also reported that the Kox and Shen models have a projectile-target asymmetry and should be used so that the lighter nucleus is always treated as the projectile.

(7) Energy and mass number dependence of total reaction cross sections of nuclei

We have systematically analyzed nuclear reaction data that are sensitive to nuclear size, namely, proton-nucleus total reaction cross sections and differential elastic cross sections, using a phenomenological black-sphere approximation of nuclei that we are developing. In this framework, the radius of the black sphere is found to be a useful length scale that simultaneously accounts for the observed proton-nucleus total reaction cross section and first diffraction peak in the proton elastic differential cross section. This framework is expected to be applicable to any kind of projectile that is strongly attenuated in the nucleus. On the basis of a cross-section formula constructed within this framework, we find that a less familiar $A^{1/6}$ dependence plays a crucial role in describing the energy dependence of proton-nucleus total reaction cross sections.

(8) Probing the critical behavior in the evolution of GDR width at very low temperatures in $A \sim 100$ mass region

The influence of giant dipole resonance (GDR) induced quadrupole moment on GDR width at low temperatures is investigated experimentally by measuring the GDR width systematically in the unexplored temperature range T = 0.8-1.5 MeV, for the first time, in $A \sim$ 100 mass region. The measured GDR width, using alpha induced fusion reaction, for ^{97}Tc confirms that the GDR width remains constant at the ground state value up to a critical temperature and increases sharply thereafter with the increase in T. The data have been compared with the adiabatic thermal shape fluctuation model (TSFM), phenomenological critical temperature fluctuation model (CTFM) and microscopic phonon damping model (PDM). Interestingly, the CTFM and PDM give the similar results and agree with the data, whereas the TSFM differs significantly even after incorporating the shell effects indicating towards the inclusion of GDR-GQR coupling in the TSFM.

(9) Giant dipole resonance in highly excited nuclei

The evolution of the giant dipole resonance's (GDR) width and shape at finite temperature T and angular momentum J is described within the framework of the phonon damping model (PDM). The PDM description is compared with the established experimental systematics obtained from heavy-ion fusion and inelastic scattering of light particles on heavy target nuclei, as well as with predictions by other theoretical approaches. Extended to include the effect of angular momentum J, its strength functions have been averaged over the probability distributions of T and J for the heavy-ion fusion evaporation reaction, which forms the compound nucleus ^{88}Mo at high T and J. The results of theoretical predictions are found in excellent agreement with the experimental data. The predictions by PDM and the heavy-ion fusion data are also employed to predict the viscosity of hot medium and heavy nuclei.

We also explore an approach that includes temperature-dependent shell effects and fluctuations of the pairing field in the thermal shape fluctuation model (TSFM). We apply this approach to study the width of GDR in ^{120}Sn, ^{179}Au and ^{208}Pb. Our results demonstrate that the TSFM that includes pairing fluctuations can explain the recently observed quenching in the GDR width.

(10) Reentrance phenomenon of superfluid pairing in hot rotating nuclei

When a nucleus rotates (total angular momentum J and/or rotational frequency ω are not zero), the nucleon (proton and neutron) pairs located around the Fermi surface will scatter to the empty levels nearby and lead to the decreasing of pairing correlation. When the J or ω is sufficiently high, i.e., equal to the critical value J_c or ω_c, the scattered nucleons completely block the single-particle levels around the Fermi surface. Consequently, pairing correlation disappears. However, when J is slightly higher than J_c (or $\omega > \omega_c$), the increase of temperature T will relax the particles scattered around the Fermi surface and causes some levels become partially unoccupied, making them available for scattered pairs. As a result, the pairing correlation reappears at some critical value T_1. As T goes higher, e.g., at $T_2 > T_1$, the newly created pairs will be eventually broken down again. This phenomenon is called the pairing reentrance. The recently developed

FTBCS1 theory that includes the effect due to quasiparticle-number fluctuations in the pairing field and angular momentum z projection at $T \neq 0$ has predicted the pairing reentrance effect in some realistic nuclei. The shell-model Monte Carlo calculations have suggested that the pairing reentrance effect can be observed in the nuclear level density in a form of a local maximum at low T (or excitation energy E^*) and high J (or ω). Recently, an enhancement of level density of ^{104}Pd at low E^* and high J has been experimentally reported. This work demonstrates that the enhancement observed in the extracted level density of ^{104}Pd is the first evidence of pairing reentrance phenomenon in atomic nuclei.

Members

Associate Chief Scientist (Lab. Head)
Takashi NAKATSUKASA

Research & Technical Scientist
Akihisa KOHAMA (Senior Research Scientist)

Nishina Center Research Scientist
Dang Dinh NGUYEN

Special Postdoctoral Researchers
Kohei WASHIYAMA (– Mar. 31, 2015)
Koichi SATO

Foreign Postdoctoral Researcher
Haozhao LIANG (– Mar. 31, 2015)

Research Consultants
Akitsu IKEDA
Kenichi MATSUYANAGI

Visiting Scientists
Kazuhiro OYAMATSU (Aichi Shukutoku Univ.)
Takashi ABE (Univ. of Tokyo)
Kei IIDA (Kochi Univ.)
Naoyuki ITAGAKI (Kyoto Univ.)
Yasuyuki SUZUKI (Niigata Univ.)
Kazuko TANABE (Otsuma Women's Univ.)
Nguyen Quang HUNG (Tan Tao Univ.)
Kaori KAKI (Shizuoka Univ.)
Kazuyuki OGATA (Osaka Univ.)
Kiyomi IKEDA (Niigata Univ.)

Student Trainees
Rhine Kumar Arayakkandi Keechiprath
(Indian Inst. of Tech. Roorkee)

Part-time Workers
Kiyomi ARAI
Yoko OZAWA (– Mar. 31, 2014)
Noriko OKAYASU
Kahori SHIMADA (– Sep. 30, 2014)
Tsuneyo SUZUKI
Mie DOI (Oct. 1, 2014 –)
Miki KANOU
Naomi MURAKAMI (Jan. 1, 2015–)

Theoretical Research Division
Strangeness Nuclear Physics Laboratory

1. Abstract

We proposed accurate calculation method called 'Gaussian Expansion Method using infinitesimally shifted Gaussian lobe basis function'. When one proceeds to four-body systems, calculation of the Hamiltonian matrix elements becomes much laborious. In order to make the four-body calculation tractable even for complicated interactions, the infinitesimally-shifted Gaussian lobe basis function has been proposed. The GEM with the technique of infinitesimally-shifted Gaussians has been applied to various three-, four- and five-body calculations in hypernuclei, the four-nucleon systems, and cold-atom systems. As results, we succeeded in extracting new understandings in various fields.

2. Major Research Subjects

(1) Hypernuclear structure from the view point of few-body problem
(2) Structure of exotic hadron system
(3) Baryon-baryon interaction based on lattice QCD
(4) Structure of three- and four-body ^{4}He atom systems

3. Summary of Research Activity

(1) Recently, we observed of neutron-rich system nnΛ as a bound state. To investigate this system, we performed nnΛ+Nn Σ three-body coupled channel calculation. Using YN interaction to reproduce observed binding energies for $^4_\Lambda$H, $^4_\Lambda$He, and $^3_\Lambda$H, we do not find any bound state for nnΛ system which is inconsistent with the data. Now, we propose the experimentalists to perform a search experiment of nnΛ system again.
(2) It is interesting to study the structure of Ar isotope, since we have some superdeformed states (SD) in this Isotope. Within the framework of AMD method, we investigate the structure of SD states. In addition, we study the structure of Ar Λ hypernuclei. Then, we found that Λ-separation energy was dependent on the degree of deformation of core nuclei.
(3) Using several realistic ^{4}He atomic potential, we calculate Efimov spectra of trimer and tetramer systems of 4He. Our result shows an extension of the universality in Efimov trimers that the appearance of the repulsive barrier at the three-body hyperradius $R_3 \approx 2\ W_{rvd}$ makes the critical scattering lengths independent of the short-range details of the interactions as reported in the literature and also in the present work for the 4He trimer with the realistic potentials.

Members

Associate Chief Scientist (Lab. Head)
Emiko HIYAMA

Contract Researcher
Yasuro FUNAKI

Research Scientists
Hiroya SUNO (Research Scientist, concurrent : Strangeness Nuclear Physics Laboratory, Main: Field Theory Research Team)

Special Postdoctoral Researcher
Masahiro ISAKA

Foreign Postdoctoral Researcher
Philipp GUBLER (– Oct. 31, 2014)

Postdoctoral Researcher
Hajime TOGASHI (Apr. 1, 2014 –)

Research Consultants
Yasuo YAMAMOTO (– Mar. 31, 2014)
Toshio MOTOBA (– Mar. 31, 2014)
Yoshikazu FUJIWARA (Apr. 1, 2014 –)

Junior Research Associates
Tetsuya YOSHIDA (Apr. 1, 2014 –)
Saori MAEDA (Apr. 1, 2014 –)
Shota OHNISHI

Visiting Researchers

Naoyuki Sakumichi (JSPS)
Christiane SCHMICKLER (JSPS, Apr. 1, 2014 – Mar. 31, 2015)

Visiting Scientists

Takayuki MYO (Osaka Inst. of Tech.)
Hidekatsu NEMURA (Univ. of Tsukuba)
Masakiyo KITAZAWA (Osaka Univ.)
Taiichi YAMADA (Kanto Gakuin Univ.)
Takenori FURUMOTO (Ichinoseki Nat'l College of Tech.)
Yasuo YAMAMOTO (Tsuru Univ.) (Apr. 1, 2014 –)
Makoto OKA (Tokyo Tech.)
Atsushi UMEYA (Nihon Inst. of Tech.)
Tetsuo HYODO (Kyoto Univ.)
Daisuke JIDO (Tokyo Met. Univ.)
Soichi ISHIKAWA (Hosei Univ.)
Thomas Adriaan RIJKEN (Radboud Univ. Nijmegen)
Atsushi HOSAKA (Osaka Univ.)
Shoji SHINMURA (Gifu Univ.)
Akinobu DOTE (KEK)
Kazuma NAKAZAWA (Gifu Univ.)
Toru SATO (Osaka Univ.)
Jinniu HU (Peking Univ.)
Philipp GUBLER (ECT*)
Wolfram WEISE (TUM)
Yoshikazu FUJIWARA (Kyoto Univ.) (– Mar. 31, 2014)
Toshio MOTOBA (Osaka Elec.-Com. Univ.) (Apr. 1, 2014 –)
Shuichi GOJUKI (SGI Japan Ltd.)
Javier ROCAMAZA (Univ. of Milan)
Hyun-Chul KIM (Inha Univ.)
Xian-Rong ZHOU (Xiamen Univ.)
Satoshi NAKAMURA (Tohoku Univ.)
Satoru HIRENZAKI (Nara Women's Univ.)
Tomokazu FUKUDA (Osaka Elec.-Com. Univ.)
Kiyomi IKEDA (Niigata Univ.) (Jul. 1, 2014 –)

Student Trainees

Akira YOKOTA (Tokyo Tech.)
Saori MAEDA (Tokyo Tech.) (– Mar. 31, 2014)
Tetsuya YOSHIDA (Tokyo Tech.) (– Mar. 31, 2014)
Yongwoo CHOI (Kyungpook Nat'l Univ.) (– Feb. 31, 2015)
Hana GIL (Kyungpook Nat'l Univ.) (– Feb. 31, 2014)

Theoretical Research Division
Mathematical Physics Laboratory

1. Abstract

The aim of mathematical physics laboratory is to apply mathematical scheme to resolve long-standing issues in various subjects of physics. Mathematics, in particular that originates in superstring theory, has universal feature which is common to wide range of physics. This covers elementary particle physics, hadron physics, nuclear physics, cosmology, general relativity and condensed matter physics. We apply mathematical scheme such as superstring theory, D-branes, AdS/CFT correspondence, solitons, statistical mechanics and integrable systems. Topics which the laboratory covers currently include non-perturbative analysis of quantum chromo-dynamics, superstrings, and models beyond the standard model of particle physics, and soliton physics.

2. Major Research Subjects

(1) Application of Superstring Theory
(2) Non-perturbative analyses of strongly-coupled gauge theories
(3) Physics of Black Holes and Cosmology
(4) Solitons physics
(5) Mathematical physics
(6) Lattice gauge theory

3. Summary of Research Activity

Interplay between mathematics and physics is indispensable, as any physics law is described in terms of mathematics. However, the present status of various theoretical physics does not fully appreciate the usefulness of mathematics, as each topics goes into details and has less interaction with other subjects even nearby. We integrate various subjects of physics, by applying recent development of mathematics and mathematical physics, to solve long-standing issues in physics. In particular, mathematical methods in superstring theory has been developed and is mature enough to be applied to other physics. We put efforts on the application as described below, in addition to some other mathematical techniques such as numerical simulations, solitons and integrable systems.

(1) Application of superstring theory

1) Magnetic instability in AdS/CFT : Schwinger effect and Euler-Heisenberg Lagrangian of Super- symmetric QCD

To reveal the Schwinger effect for quarks, i.e., pair creation process of quarks and antiquarks, we derive the vacuum decay rate at strong coupling using AdS/CFT correspondence. Magnetic fields, in addition to the electric field responsible for the pair creation, causes prominent effects on the rate, and is important also in experiments such as RHIC/LHC heavy ion collisions. In this paper, through the gravity dual we obtain the full Euler-Heisenberg Lagrangian of N=2 supersymmetric QCD and study the Schwinger mechanism with not only a constant electric field but also a constant magnetic field as external fields. We determine the quark mass and temperature dependence of the Lagrangian. In sharp contrast with the zero magnetic field case, we find that the imaginary part, and thus the vacuum decay rate, diverges in the massless zero-temperature limit. This may be related to a strong instability of the QCD vacuum in strong magnetic fields. The real part of the Lagrangian serves as a generating function for non-linear electro-magnetic responses, and is found such that the Cotton-Mouton effect vanishes. Interestingly, our results of the Schwinger / Cotton-Mouton effects coincide precisely with those of N=2 supersymmetric QED.

2) Electric Field Quench in AdS/CFT

An electric field quench, a suddenly applied electric field, can induce nontrivial dynamics in confining systems which may lead to thermalization as well as a deconfinement transition. In order to analyze this nonequilibrium transitions,we use the AdS/CFT correspondence for N=2 supersymmetric QCD that has a confining meson sector. We find that the electric field quench causes the deconfinement transition even when the magnitude of the applied electric field is smaller than the critical value for the static case (which is the QCD Schwinger limit for quark-antiquark pair creation). The time dependence is crucial for this phenomenon, and the gravity dual explains it as an oscillation of a D-brane in the bulk AdS spacetime. Interestingly, the deconfinement time takes only discrete values as a function of the magnitude of the electric field. We advocate that the new deconfinement phenomenon is analogous to the exciton Mott transition.

3) Entropic destruction of heavy quarkonium in non-Abelian plasma from holography

Lattice QCD indicates a large amount of entropy associated with the heavy quark-antiquark pair immersed in the quark-gluon plasma. This entropy grows as a function of the inter-quark distance giving rise to an entropic force that can be very effective in dissociating the bound quarkonium states. In addition, the lattice data show a very sharp peak in the heavy quark-antiquark en- tropy at the deconfinement transition. Since the quark-gluon plasma around the deconfinement transition is strongly coupled, we employ the holographic correspondence to study the entropy as- sociated with the heavy quark-antiquark pair in two theories: i) N=4 supersymmetric Yang-Mills and ii) a confining Yang-Mills theory obtained by compactification on a Kaluza-Klein circle. In both cases we find the entropy growing with the inter-quark distance and evaluate the effect of the corresponding entropic forces. In the

case ii), we find a sharp peak in the entropy near the de- confinement transition, in agreement with the lattice QCD results. This peak in our holographic description arises because the heavy quark pair acts as an eyewitness of the black hole formation in the bulk ? the process that describes the deconfinement transition. In terms of the boundary theory, this entropy likely emerges from the entanglement of a ”long string” connecting the quark and antiquark with the rest of the system.

(2) Cosmology

1) Dynamical breaking of shift-symmetry in supergravity-based inflation

Shift-symmetry is essential to protect the flatness of the potential, even beyond the super- Planckian vacuum expectation value (VEV) for an inflaton field. The breaking of the shift- symmetry can yield potentials suitable for super-Planckian excursion of the inflaton. The aim of this paper is to illustrate that it is indeed possible to break the shift-symmetry dynamically within 4 dimensional supergravity prior to a long phase of inflation. Thanks to the shift-symmetry, the leading contribu- tion to the inflaton potential is free from the dangerous exponential factor even after its breaking, which is the main obstacle to realizing the super-Planckian inflation in super- gravity. But, in our simple model, the resulting inflaton potential is a cosine type potential rather than the power-law one and it is difficult to realize a super-Planckian breaking scale unfortunately.

2) Effective gravitational interactions of dark matter axions

We investigate the structure of gravitational self-interactions of coherently oscillating axions in the general relativistic framework. A generic action for a massive scalar field in the Friedmann- Robertson-Walker background is first introduced based on the effective field theory approach to cosmological perturbations. Using the obtained setup, we evaluate the effective gravitational inter- action of the massive scalar field, i.e. scalar quartic interactions mediated by metric perturbations. Applying the results to the system of dark matter axions, we estimate their self-interaction rate and discuss its implications for the axion Bose-Einstein condensate dark matter scenario. Leading contributions for the gravitational interactions of axions are given by the process mediated by the dynamical graviton field, which is essentially the Newtonian potential induced by fluctuations of the background fluids. We find that it leads to the same order of magnitude for the interaction rate of dark matter axions in the condensed regime, compared with the results of previous studies using the Newtonian approximation.

(3) Condensed matter physics

1) Current Reflection and Transmission at Conformal Defects: Applying BCFT to Transport Process

We study reflection/transmission process at conformal defects by introducing new transport co- efficients for conserved currents. These coefficients are defined by using BCFT techniques thanks to the folding trick, which turns the conformal defect into the boundary. With this definition, exact computations are demonstrated to describe reflection/transmission process for a class of conformal defects. We also compute the boundary entropy based on the boundary state.

2) Bulk angular momentum and Hall viscosity in chiral superconductors

We establish the Berry-phase formulas for the angular momentum (AM) and the Hall viscosity (HV) to investigate chiral superconductors (SCs) in two and three dimensions. The AM is defined by the temporal integral of the anti-symmetric momentum current induced by an adiabatic defor- mation, while the HV is defined by the symmetric momentum current induced by the symmetric torsional electric field. Without suffering from the system size or geometry, we obtain the macro- scopic AM Lz = (h/2pi) m N0/2 at zero temperature in full-gap chiral SCs, where m is the magnetic quantum number and N0 is the total number of electrons. We also find that the HV is equal to half the AM at zero temperature not only in full-gap chiral SCs as is well-known but also in nodal ones, but its behavior at finite temperature is different in the two cases.

(4) Mathematical physics

1) Duality and integrability of supermatrix model with external source

We study the Hermitian supermatrix model involving an external source. We derive the deter- minantal formula for the supermatrix partition function, and also for the expectation value of the characteristic polynomial ratio, which yields the duality between the characteristic polyno- mial and the external source with an arbitrary matrix potential function. We also show that the supermatrix integral satisfies the one and two dimensional Toda lattice equations as well as the ordinary matrix model.

2) Laplace operators on Sasaki-Einstein manifold

We decompose the de Rham Laplacian on Sasaki-Einstein manifolds as a sum over mostly positive definite terms. An immediate consequence are lower bounds on its spectrum. These bounds constitute a supergravity equivalent of the unitarity bounds in dual superconformal field theories. The proof uses a generalization of Kahler identities to the Sasaki-Einstein case.

3) Non-Lagrangian Theories from Brane Junctions

We use 5-brane junctions to study the 5D TN SCFTs corresponding to the 5D N=1 uplift of the 4D N=2 strongly coupled gauge theories, which are obtained by compactifying N M5 branes on a sphere with three full punctures. Even though these theories have no Lagrangian description, by using the 5-brane junctions proposed by Benini, Benvenuti and Tachikawa, we are able to derive their Seiberg-Witten curves and Nekrasov partition functions. We cross-check our results with the 5D superconformal index proposed by Kim, Kim and Lee. Through the AGTW correspondence, we discuss the relations between 5D superconformal indices and n-point functions of the q-deformed WN Toda theories.

4) From the Berkovits formulation to the Witten formulation in open superstring field theory

The Berkovits formulation of open superstring field theory is based on the large Hilbert space of the superconformal ghost sector. We discuss its relation to the Witten formulation based on the small Hilbert space. We introduce a one-parameter family of conditions

for partial gauge fixing of the Berkovits formulation such that the cubic interaction of the theory under the partial gauge fixing reduces to that of the Witten formulation in a singular limit. The local picture-changing operator at the open-string midpoint in the Witten formulation is regularized in our approach, and the divergence in on-shell four-point amplitudes coming from collision of picture-changing operators is resolved. The quartic interaction inherited from the Berkovits formulation plays a role of adjusting different behaviors of the picture-changing operators in the s channel and in the t channel of Feynman diagrams with two cubic vertices, and correct amplitudes in the world-sheet theory are reproduced. While gauge invariance at the second order in the coupling constant is obscured in the Witten formulation by collision of picture-changing operators, it is well defined in our approach and is recovered by including the quartic interaction inherited from the Berkovits formulation.

5) Duality of topological branes

We show a duality of branes in the topological B-model by inserting two kinds of the non-compact branes simultaneously. We explicitly derive the integral formula for the matrix model partition function describing this situation, which correspondingly includes both of the characteristic poly- nomial and the external source. We show that these two descriptions are dual to each other through the Fourier transformation, and the brane partition function satisfies integrable equa- tions in one and two dimensions.

Members

Associate Chief Scientist (Lab. Head)
Koji HASHIMOTO

Contract Researcher
Shunji MATSUURA (Sep. 1, 2014 –)

Special Postdoctoral Researchers
Masato TAKI (– Apr. 30, 2014)
Shingo TORII (– Mar. 31, 2015)
Toshifumi NOUMI (– Mar. 31, 2015)

Postdoctoral Researchers
Yuki MINAMI (– Mar. 31, 2014)
Yasuhiro YAMAGUCHI (Apr. 1, 2014 –)

Visiting Researcher
Taro KIMURA (JSPS Fellow, – Mar. 31, 2015)

Senior Visiting Scientist
Koichi YAZAKI (Univ. of Tokyo)

Visiting Scientists
Yoshio YAMAGUCHI (Univ. of Tokyo)
Shoichi MIDORIKAWA (Aomori Univ.)
Keiji IGI (Univ. of Tokyo)
Hiroshi ITOYAMA (Osaka City Univ.)
Yuuichirou SHIBUSA (Nagasaki Inst. of Applied Sci.)
Nobuyuki ISHIBASHI (Univ. of Tsukuba)
Asato TSUCHIYA (Shizuoka Univ.)
Tatsumi AOYAMA (Nagoya Univ.)
Kazutoshi OHTA (Meiji Gakuin Univ.)
Takeo INAMI (Chuo Univ.)
Masanori HANADA(KEK)
Yu MAEZAWA(Univ. Bielefeld)
Minoru ETO (Yamagata Univ.)
Norisuke SAKAI (Tokyo Women's Christian Univ.)
Makoto SAKAGUCHI (Ibaraki Univ.)
Tetsutaro HIGAKI (KEK)
Keisho HIDAKA (Tokyo Gakugei Univ.)
Kazuo FUJIKAWA (Univ. of Tokyo)

Sub Nuclear System Research Division
Radiation Laboratory

1. Abstract

Nucleons, such as protons and neutrons, are a bound state of constituent quarks glued together with gluons. The detail structure of nucleons, however, is not well understood yet. Especially the mechanism to build up the spin of proton, which is 1/2, is a major problem in physics of the strong force. The research goal of Radiation Laboratory is to solve this fundamental question using the world first polarized-proton collider, realized at RHIC in Brookhaven National Laboratory (BNL) in USA. RHIC stands for Relativistic Heavy Ion Collider, aiming also to create Quark Gluon Plasma, the state of Universe just after the Big Bang. RIKEN-BNL Research Center (RBRC) directed by S. Aronson carries our core team at BNL for those exciting researches using the PHENIX detector. We have found that the proton spin carried by gluons is indeed small. We also identified W bosons in the electron/positron decay channel and in the muon decay channel, with which we are about to conclude how much anti-quarks carry the proton spin. Other than the activities at RHIC we are preparing new experiments at J-PARC and Fermilab to study the nature of hadron. We are also performing technical developments such as novel ion sources, fine-pitch silicon pixel detectors and high-performance trigger electronics.

2. Major Research Subjects

1) Spin physics with relativistic polarized-proton collisions at RHIC
2) Study of nuclear matter at high temperature and/or at high density
3) Technical developments on radiation detectors and accelerators

3. Summary of Research Activity

(1) Experimental study of spin structure of proton using RHIC polarized proton collider

[See also RIKEN-BNL Research Center Experimental Group for the activities at BNL]

In 2014 we have reached a major milestone in determining the gluon spin contribution to the total spin of the nucleon. After initially measuring small asymmetries statistically consistent with zero, we have succeeded to determine non-zero gluon polarization in the recent high statistics runs at 510 GeV. With the valence quark spin contribution already reasonably well known, the contributions from sea quarks and orbital angular momenta remain to be understood. PHENIX has collected data to access the sea quark polarizations via leptonic decays of W bosons. Preliminary results have been obtained using all the data taken so far. While orbital angular momentum cannot be directly accessed at RHIC, several transverse spin phenomena are being accumulated to study the orbital angular momentum and the overall three-dimensional structure of the nucleon.

To further investigate these effects the PHENIX experiment proposes substantial detector upgrades to go along the expected accelerator improvements. The proposed upgrade replaces the present magnet with a solenoid, so that we are considering to build an open-geometry forward spectrometer which can measure hadrons, photons, electrons, muons and jets in the forward rapidity region. Especially the Drell-Yan (quark-antiquark annihilation into lepton pairs) transverse single spin asymmetries are the main goal of these upgrades. As a pilot measurement, some of us are participating in the Fermilab SeaQuest experiment which has been collecting muon pairs using a 120-GeV unpolarized proton at Fermilab. By measuring the unpolarized Drell-Yan process, we can study quark spin-orbit effects which supplement what can be learned in the polarized Drell-Yan process.

(2) Experimental study of quark-gluon plasma using RHIC heavy ion collider

[See also RIKEN-BNL Research Center Experimental Group for the activities at BNL]

We have completed several key measurements in the study of quark-gluon plasma at RHIC. As the top of them, we lead the analysis of the first thermal photon measurement in heavy ion collisions. The measurement indicates that the initial temperature reached in the central Au+Au collision at 200 GeV is about 350MeV, far above the expected transition temperature Tc~170MeV, from hadronic phase to quark-gluon plasma. This work was rewarded by Nishina Memorial Prize in 2011. Using the same “virtual photon” method used in the thermal photon measurement, we measured direct photons in d+Au collisions. The results show that there is little cold nuclear effects in direct photons. This supports that the large enhancement of direct photons observed in Au+Au is indeed due to hot quark-gluon plasma formed in Au+Au collisions.

We also measured the elliptic flow strength, v2, of direct photons in Au+Au collisions. The results show surprisingly large v2, which means the source of those photons expands elliptically. This is one of the most interesting results from RHIC in the last three years. One of the JRA students of Radiation Laboratory led this important analysis. Also, the most recent measurements of high p_T π^0 suppression in Au+Au collisions show that the suppression reduces at very high pT (pT~20GeV).

We lead measurement of heavy quark (charm and bottom) using VTX, a 4 layer silicon vertex tracker which we jointly constructed with US DOE. The detector was installed in PHENIX in 2011. Analysis of heavy quark using the silicon vertex detector is ongoing. The first preliminary results from the 2011 Au+Au run and 2012 p+p run was reported in the Quark Matter 2012 conference. We are now finalizing the results for publication. Analysis of the 2014 Au+Au run is also in progress and we expect the first preliminary results from the 2014 run in this year (2015).

In Wako we are operating a cluster computer system specialized to analyze huge data sets taken with the PHENIX detector. It consists

of 28 nodes (18 old nodes and 10 new nodes) each of which has two CPUs and 10 sets of local disk for data repository (old node: quad-core CPU, 1TB disk, new node: six-core CPU, 2TB disk). There are 264 CPU cores and 380 TB disks in total. This configuration ensures the fastest disk I/O when the jobs are assigned to the nodes where the required data sets are stored. It is also important that this scheme doesn't require an expensive RAID system and network. Through this development we have established a fast and cost-effective solution in analyzing massive data.

We have about 1.7 PB of data produced by the PHENIX experiment. They are stored in the archive system (HPSS) operated by the Advanced Center for Computing and Communication (ACCC). Since ACCC decided to replace HPSS, we have started to transfer the data into the new archive system.

(3) Study of properties of mesons and exotic hadrons with domestic accelerators

Preparation of the experiment E16 at J-PARC 50-GeV PS is underway with the Grant-in-Aid for Scientific Research on Innovative Areas (MEXT). This experiment aims to perform a systematic study of the mass modification of low-mass vector mesons in nuclei to explore the chiral symmetry breaking in dense nuclear matter, namely, the mechanism proposed by Nambu to generate the major part of hadron mass.

Gas Electron Multiplier (GEM) technology is adopted for the two key detectors, GEM Tracker (GTR) and Hadron-blind Cherenkov detector (HBD). With a cooperation with Japanese industries, GEM foils with a world-largest size (30cm x 30cm) are newly developed. Through the beam tests at ELPH, J-PARC, LEPS, and RIKEN RIBF, the followings are achieved and proven; 1) required position resolution of 0.1 mm, and 2) stable operation under the hadron-background environment, typically 30 times higher rate than that expected in the J-PARC experimental area. The design parameters of the GTR and HBD were finalized and the mass-production of GTR GEM started. HBD GEM is under the final tuning to achieve the required stability, efficiency and pion-rejection power.

For the readout electronics of GEM, a preamp using the APV25 ASIC chip is developed and tested. For the digitization and the data transfer, the SRS system developed by CERN is also tested and adopted. Another preamp-ASIC for the trigger signal from GEM foils is also developed and tested. Trigger logic boards, which are developed by Belle II, are tested with the firmware customized for this experiment.

The development phase of the detectors is just over and we are moving to the production phase. For the readout electronics, the mass production will start in a year after some remained tests. The construction of the beam line is finally funded in KEK and started at J-PARC in 2013. It will be completed by March 2016. The spectrometer construction at the beam line is planned to start in March 2015 and the commissioning with a primary beam will be performed in early 2016.

(4) Detector development for PHENIX experiment

After 7 years of hard work, we installed the silicon vertex tracker (VTX) into the PHENIX detector at RHIC in December 2010. VTX is a 4-layer silicon tracker to measure heavy quark (charm and bottom) production in p+p and heavy ion collisions at RHIC. The detector was funded by RIKEN and the US DOE. We and RIKEN BNL Research Center are responsible for construction and operation of the inner two pixel detectors. The VTX was successfully commissioned during the 500 GeV p+p run in 2011. Subsequently, we collected 5 billion Au+Au events in the 2011 run, 11/pb of p+p data at 510 GeV, 3/pb of p+p data at 200 GeV, 110/μb of U+U data at 193 GeV, and 2.9/nb of Cu+Au at 200 GeV. We are now analyzing those datasets to study the interaction between heavy quarks and the quark-gluon plasma.

During the 2011 run, part of the pixel detector was damaged due to thermal stress on the detector. We repaired the damaged pixel detectors in 2012 to 2013, and the tracker was re-installed in PHENIX before the 2014 run and has been successfully re-commissioned. The 2014 run is a major heavy quark run of RHIC and the VTX detector worked very well during the run. PHENIX recorded about 20 billion Au+Au collision events with VTX. This dataset is effectively more than 10 times of that of 2011 data. We expect definitive results on heavy quark measurements from the 2014 run.

Sea quark polarization measurement via W-boson production is one of the highlight of PHENIX spin program. In order to detect high momentum muons from W-decay, we developed the momentum-sensitive trigger system for the PHENIX forward muon arms with collaborators from KEK, Kyoto and Rikkyo University. Together with new hadron absorber, W-boson measurement was successfully carried out using the new high momentum trigger. We accumulated high-integrated luminosity of about $250pb^{-1}$ in Run13 and almost achieved our goal. The intensive analysis is underway towards the publication. Preliminary results were released in October 2014 and the analysis is at the final stage towards the publication. Besides W detection, the trigger system has been also operated for heavy flavor meson detection in conjunction with a forward vertex (FVTX) detector.

(5) Development of beam source

Under the collaboration with Brookhaven National Laboratory, we are developing various techniques for a laser ion source (LIS) to provide high quality heavy-ion beams to the accelerators at present or in the future. In 2014, we installed a new LIS which provides various species of singly charged ions to the RHIC-AGS complex. The commissioning was very successful and we have delivered C, Al, Ti, Si, Ta and Au ions. We also demonstrated fast switching of ion species within one second. At this moment, we are upgrading this LIS to provide gold beam and other lighter ion beams simultaneously. Once this upgrade is completed, all the ion beams except proton and uranium will be supplied by the LIS at the RHIC-AGS complex with much enhanced versatility. Besides, we are studying the highly charged ionization and magnetic field confinement of laser ablation plasma, and testing a linear accelerator model which selectively accelerates charge states.

Members

Chief Scientist (Lab. Head)
Hideto EN'YO (Director, RNC)

Vice Chief Scientist
Yasuyuki AKIBA

Research & Technical Scientists
Yasushi WATANABE (Senior Research Scientist)
Yuji GOTO (Senior Research Scientist)
Itaru NAKAGAWA (Senior Research Scientist)
Satoshi YOKKAICHI (Senior Research Scientist)
Ralf SEIDL (Senior Research Scientist)
Hiroaki ONISHI (Senior Research Scientist, concurrent; Advanced Meson Science Lab.)

Contract Researchers
Takashi HACHIYA (– Mar. 31, 2015)
Maki Kurosawa (– Sep. 30, 2014)
Hisayuki TORII (– Mar. 31, 2014)

Postdoctoral Researchers
Yoki ARAMAKI (– Mar. 31, 2014)
Yuhei MORINO (– Jul. 31, 2014)
Tomonori TAKAHASHI (– Mar. 31, 2014)
Takayuki SUMITA
Yoshimasa IKEDA (– Mar. 31, 2014)

Junior Research Associates
Yusuke KOMATSU (Univ. of Tokyo, – Mar. 31, 2014)
Shinichi HAYASHI (Univ. of Tokyo, –Mar. 31, 2015)
Yuko SEKIGUCHI (Univ. of Tokyo)
Koki KANNO (Univ. of Tokyo)
Wataru NAKAI (Univ. of Tokyo)
Megumi SEKINE (Tokyo Tech., – Mar. 31, 2014)
Sanshiro MIZUNO (Univ. of Tsukuba, – Mar. 31, 2015)
Tomoya TSUJI (Univ. of Tokyo, – Mar. 31, 2015)
Tomoya HOSHINO (Hiroshima Univ.)
Shunsuke Ikeda (Tokyo Tech.)
Masafumi KUMAKI (Waseda Univ.)
Hiroshi NAKAGOMI (Univ. of Tsukuba)
Yasuhiro FUWA (Kyoto Univ., – Mar. 31, 2015)
Satoshi YANO (Hiroshima Univ.)
Daisuke WATANABE (Univ. of Tsukuba)
Kohei TERASAKI (Univ. of Tokyo)

International Program Associates
Sanghwa PARK (Seoul Nat'l Univ., – Feb. 26, 2015)
Inseok YOON (Seoul Nat'l Univ.)
Minjung KIM (Seoul Nat'l Univ.)
Taebong MOON (Yonsei Univ.)
Chong KIM (Korea Univ., – Dec. 9, 2014)
Se Young HAN (Ewha Womans Univ., Oct. 1, 2014 –)

Visiting Researcher
Daisuke KAWAMA (JSPS Fellow, – Mar. 31, 2015)

Senior Visiting Scientists
Toshiaki SHIBATA (Tokyo Tech.)
Takashi NAKANO (Osaka Univ.)

Visiting Scientists
Kyoichiro OZAWA (KEK)
Noriyoshi ISHII (Univ. of Tsukuba)
Susumu SATO (JAEA)
Megumi NARUKI (KEK)
Akitomo ENOKIZONO (Rikkyo Univ.)
Yoshinori FUKAO (KEK)
Michiko SEKIMOTO (KEK)
Kiyoshi TANIDA (Seoul Nat'l Univ.)
Hirotsugu KASHIWAGI (JAEA)
Taku GUNJI (Univ. of Tokyo)
Junpei TAKANO (KEK)
Kazuya AOKI (KEK)
Masashi KANETA (Tohoku Univ.)
Munehisa OHTANI (Kyorin Univ.)
Yorito YAMAGUCHI (Univ. of Tokyo)
Youngil KWON (Yonsei Univ.)
Kenichi NAKANO (Tokyo Tech.)
Maya SHIMOMURA (Iowa State Univ.)
Noriyosu HAYASHIZAKI (Tokyo Tech.)
Yuhei MORINO (KEK)
Kenji FUKUSHIMA (Keio Univ.)
Atsushi NAKAMURA (Hiroshima Univ.)
Ryo ICHIMIYA (KEK)
Tomohiro NISHITANI (Nagoya Univ.)
Tomonori TAKAHASHI (Osaka Univ.)
Tsutomu MIBE (KEK)
Makoto KUWAHARA (Nagoya Univ.)
Masahiro OKAMURA (BNL)
Shunzo KUMANO (KEK)
Bentz WOLFGANG (Tokai Univ.)
Alexander BAZILEVSKY (BNL)
Shin-ya SAWADA (KEK)
Ryotaro MUTO (KEK)
Masanori HIRAI (Tokyo Univ. of Sci.)

Student Trainees

Yusuke KOMATSU (Univ. of Tokyo)
Shoichiro NISHIMURA (Univ. of Tokyo)
Takuya SHIBUKAWA (Univ. of Tokyo)
Yuki OBARA (Univ. of Tokyo)
Yusuke OYA (Hiroshima Univ.)
Kazuya NAGASHIMA (Hiroshima Univ.)
Hikari MURAKAMI (Univ. of Tokyo)
Yosuke UEDA (Hiroshima Univ.)
Key NAGAI (Tokyo Tech.)

Interns

Hidemitsu ASANO (Kyoto Univ.)
Chong KIM (Korea Univ.)
Sarah CAUSSIN
Kotoko SHUKUTANI (Rikkyo Univ.)
Yomei FUKUSHIMA (Rikkyo Univ.)
Junsang PARK (Seoul Nat'l Univ.)

Part-time Workers

Maki KUROSAWA (Oct. 1, 2014 –)
Kimiaki HASHIMOTO (Rikkyo Univ., – Mar. 31, 2014)
Ryoji AKIMOTO (Univ. of Tokyo, – Mar. 31, 2014)
Takeru IGURI (Rikkyo Univ., – Mar. 31, 2014)
Wataru SAITO (Rikkyo Univ., – Mar. 31, 2014)
Toru NAGASHIMA
Hikari MURAKAMI (Univ. of Tokyo)

Assistants

Keiko SUZUKI
Mitsue YAMAMOTO

Sub Nuclear System Research Division
Advanced Meson Science Laboratory

1. Abstract

Particles like muons, pions, and kaons have finite life times, so they do not exist in natural nuclei or matters. By implanting these particles into nuclei/matters, exotic phenomena in various objects can be studied from new point of view.

Kaon is the second lightest meson having "strange"-quark as a constituent quark, which also does not exist in natural nuclei. It is expected that if one embed mesons into nuclei, the sizes of the nuclei become smaller and one can form a high density object beyond the normal nuclear density. Study of this object could lead to better understanding of the origin of the mass of the matter, and may reveal the quark degree of freedom beyond the quark-confinement. The other example is the weak interaction in nuclear matter. It can only be studied by the weak decay of hypernuclei, which have Lambda particle in the nuclei.

Muon provides even wider scope of studies, covering condensed matter physics as well as nuclear and atomic physics, and we are trying to extend the application field further into chemical and biological studies. For instance, stopping positively charged muon in a material, we obtain information on the magnetic properties or the local field at the muon trapped site (μSR). Injecting negatively charged muon to hydrogen gas, muonic hydrogen atom (μp) is formed. We are planning to measure μp hyperfine splitting energy to measure proton magnetic radius, which is complementary quantity to the proton charge radius and its puzzle lately attracts strong interest. We are also interested in precision measurement of muon property itself, such as muon anomalous magnetic moment (g-2) to study physics beyond the standard model.

In our research, we introduce different kind of impurities into nuclei / matters, and study new states of matter, new phenomena, or the object properties.

2. Major Research Subjects

(1) Study of meson property and interaction in nuclei
(2) Origin of matter mass / quark degree of freedom in nuclei
(3) Condensed matter and material studies with muon
(4) Nuclear and particle physics studies via muonic hydrogen
(5) Development of ultra cold muon beam, and its application from material science to particle physics

3. Summary of Research Activity

(1) Hadron physics at J-PARC, RIKEN-RIBF, GSI and SPring-8

Kaon and pion will shed a new insight to the nuclear physics. The discovery of deeply bound pionic atom enables us to investigate the properties of mesons in nuclear matter. At RIKEN-RIBF, we are preparing precise experimental study of the pionic atom. We have also started next generation kaon experiments (E15 and E31) at J-PARC. In these experiments, we are aiming at precise determination of the $K^{bar}N$ interaction, and clarify the nature of kaon in nuclei and the nature of Λ(1405), which could be K^-p bound state. At Spring-8 and at GSI, we are also aiming to study omega and η' nuclei. By these experiments, we aim to be a world-leading scientific research group using these light meta-stable particles.

(1-A) Deeply bound kaonic nuclei

We have performed experimental exploration of theoretically predicted deeply bound kaonic nuclear states, such as the $<K^-pp>$ bound state. One of the most interesting features of the kaonic nucleus is the strong attraction of the $K^{bar}N$ interaction. Because of this strong attraction, the kaon in nucleus will attract surrounding nucleons, resulting in extremely high-density object, which is several times larger than normal nuclear density. Measurement of the kaon properties at such high energy density will provide precious information on the origin of hadron masses and the chiral symmetry breaking and its partial restoration.

The experiment J-PARC E15 aims to identify the nature of the $<K^-pp>$ bound state by the in-flight $^3He(K^-, n)$ reaction, which allows us to investigate such state both in the formation via the missing-mass spectroscopy using the emitted neutron, and in its decay via the invariant-mass spectroscopy by detecting decay particles from $<K^-pp>$. For the experiment, we constructed a dedicated spectrometer system at the secondary beam-line, K1.8BR, in the hadron hall of J-PARC.

The first physics data-taking was carried out in March and May, 2013 with $6x10^9$ kaons on ^3He target, corresponding to a ~1% of the approved proposal. We successfully obtained semi-inclusive $^3He(K^-, n)$ X missing-mass spectrum, and found a tail structure just below the mass threshold of $(K^- + p + p)$ which cannot be explained by well-known processes and backgrounds. We also demonstrated an exclusive analysis by reconstructing $^3He(K^-, \Lambda p)$ n events. To derive more information on the $K^{bar}N$ interaction by the exclusive measurement, we are planning to perform the second physics-run, in which 10 times more data will be accumulated.

(1-B) Precision X-ray measurement of kaonic atom

Simultaneously, with the above experiment (1), we have performed an X-ray spectroscopy of atomic $3d \rightarrow 2p$ transition of negatively charged K mesons captured by helium atoms (J-PARC E17). However, the energy resolution of the conventional semiconductor spectrometers is insufficient to see the K^- - nucleus potential observed by atomic levels at zero energy. This is closely related to the problem on the existence of deeply bound kaonic states in nuclei, well below the atomic levels, and this is one of the biggest problems in strangeness

nuclear physics. Aiming to provide a breakthrough from atomic level observation, we will perform high-resolution X-ray spectroscopy of kaonic atoms at a J-PARC hadron beam line using a novel cryogenic X-ray spectrometer: an array of superconducting transition-edge-sensor (TES) micro-calorimeters. The spectrometer offers unprecedented energy resolution, which is about two orders of magnitude better than that of conventional semiconductor detectors. A spectrometer array of 240 pixels will have an effective area of about 20 mm^2. Very recently, we have performed a proof-of-principle experiment by measuring pionic-atom X rays with a TES array at the PiM1 beam line at the Paul Scherrer Institut (PSI), and successfully demonstrated the feasibility of TES-based exotic-atom x-ray spectroscopy in a hadron-beam environment. Based on the results, we are preparing for the kaonic-atom experiment at J-PARC.

Another important X-ray measurement of kaonic atom would be $2p \rightarrow 1s$ transition of kaonic deuteron. We have measured same transition of kaonic hydrogen, but the width and shift from electro-magnetic (EM) value reflect only isospin average of the $K^{bar}N$ interaction. We can resolve isospin dependence of the strong interaction by the measurement. We submitted a proposal to J-PARC PAC to measure kaonic deuteron X-ray and got stage-one approval.

(1-C) Deeply bound pionic atoms and η' mesic nuclei

We have been working on precision spectroscopy of pionic atoms systematically, that leads to understanding of the origin of hadron mass. The precision data set stringent constraints on the chiral condensate at nuclear medium. We are presently preparing for the precision measurement at RIBF. The first measurement is aiming at ^{121}Sn as the first step for the systematic spectroscopy. A pilot experiment was performed in 2010, and showed a very good performance of the system. We have been analyzing the data to improve experimental setup of the pionic atom spectroscopy at the RIBF in RIKEN. We expect to achieve better experimental resolution with much reduced systematic errors.

We are also working on spectroscopy of η' mesic nuclei in GSI/FAIR. Theoretically, peculiarly large mass of η' is attributed to UA(1) symmetry and chiral symmetry breaking. As a result, large binding energy is expected for η' meson bound states in nuclei (η'-mesic nuclei). From this measurement, we can access information about partial restoration of chiral symmetry in nuclear media via the binding energy and decay width of η'-nuclear bound state.

(1-D) Hadron physics at SPring-8/LEPS2

Photo-production of meson in nuclei is known to be a powerful tool to investigate property of the hadron in nuclear media. For this study, we started a new experimental project named LEPS2 (Laser Electron Photon at SPring-8 II) in this RIKEN Mid-term. The experimental hutch for LEPS2 at SPring-8 was constructed in March 2011, lead by RIKEN. The Large solenoid spectrometer magnet (2.96 m inner diameter x 2.22 m length) was successfully transported from BNL (US) to SPring-8 and installed into LEPS2 hutch in 2011.

One of the first physics programs is photo-production of η' in nuclei. Especially (γ, p) is most important reaction channel, where we can perform missing mass spectroscopy by detecting forward going proton. One of the big advantage of photo-production reaction is that the initial reaction is expected to be much cleaner than the hadron channel.

Detector construction for the first physics program is in progress. The 4π Electro-Magnetic calorimeter has been constructed and proton counter to detect forward going proton produced via (γ, p) reaction was installed in November 2013. Engineering run for the first experiment was performed in December 2013 to confirm performance of our detector system. Full set of the detector will be installed by mid April 2014 and we are planning to perform first physics data taking run starting from mid April 2014 to end of July 2014.

(2) Muon science at RIKEN-RAL branch

The research area ranges over particle physics, condensed matter studies, chemistry and life science. Our core activities are based on the RIKEN-RAL Muon Facility located at the Rutherford-Appleton Laboratory (UK), which provides intense pulsed-muon beams. We have variety of important research activities such as particle / nuclear physics studies with muon's spin and condensed matter physics by muon spin rotation / relaxation / resonance (μSR).

(2-A) Condensed matter/materials studies with μSR

We have opened the new μSR spectrometer named CHRONUS to collaborative experiments from the May-June cycle in 2014. To have higher affinity on μSR studies with the ISIS muon facility, common data acquisition (DAQ) system with the ISIS standard DAQ (DAEIII) and the front-end control system (SECI) have been installed and optimized along with other equipment in Port-4. The same DAQ and control systems will be installed in Port-2 as well. Thus, we can perform two independent μSR experiments in Port-2 and 4 at the same time, switching double-pulse to share beam between the two.

Among our scientific activities on μSR studies from year 2012 to 2014, following five subjects of material sciences are most important achievements at the RIKEN-RAL muon facility:

1) A static ordering of small Ir moments in the pyrochlore iridate, $Nd_2Ir_2O_7$, was examined. We found that this system is located close to the quantum critical point.
2) A static ordering of Yb moment in pyrochlore structure of $Yb_2Ti_2O_7$ crystal has been confirmed. This ordering can be explained by the Higgs mechanism.
3) Spontaneous small static internal fields in the superconducting state of URu_2Si_2 have been measured. From the data and its crystal structure, we obtained a scenario to explain superconducting mechanism of this system.
4) The universality class of the Mott transition in $EtMe_3P[Pd(dmit)_2]_2$ has been confirmed by pressure dependences of transportation properties.
5) A novel coexisting state between Fe spin-glass and Cu stripe ordered states have been found in the doverdoped regime of $La_{2-x}Sr_xCu_{1-y}Fe_yO_4$.

(2-B) Nuclear and particle physics studies via ultra cold muon beam and muonic atoms

If we can improve muon beam-emittance, beam-timing and energy-dispersion (*so-called* "ultra-slow muon"), then the capability of μSR study will be drastically improved. The ultra-slow muon beam can be stopped in thin foil, multi-layered materials and artificial lattices and we can apply the μSR techniques to surface and interface science. The development of ultra-slow muon beam is also very important as the source of ultra-cold (pencil-like small emittance) muon beam for muon g-2 measurement. Therefore, we have been working on R&D study.

We had been working on the "ultra-slow muon" generation based on the following technique, namely, positive muon beam with thermal energy has been produced by laser ionization of muoniums in vacuum (bound system of μ^+ and electron) emitted from the hot tungsten surface by stopping "surface muon beam" at Port-3. However, the muon yield and obtained emittance was far from satisfactory, and remained to be far from any kind of realistic application.

Therefore, in this mid-term, we are developing two key components first, namely high efficiency muonium generator at room temperature and high intensity ionization laser. The study of muonium generator has been done in collaboration with TRIUMF. In 2013, we demonstrated tremendous increase of the muonium emission efficiency by fabricating fine laser drill-holes on the surface of silica aerogel. We also developed a high power Lyman-α laser in collaboration with laser group at RIKEN. In this laser development, we succeeded to synthesize novel laser crystal Nd:YGAG, which has an ideal wave-length property for laser amplification to generate Lyman-α by four wave mixing in Kr gas cell. The developed new laser will ionize muoniums 100 times more efficiently for slow muon beam generation. In order to fully apply these new developments to slow muon generation, we designed and manufactured a new beam line based on microscope optics. Its installation and beam test is planned in the first half of 2015.

Concerning the muonic atom, we are planning a new precise measurement of proton radius. A large discrepancy was found recently in the proton charge radius between the new precise value from muonic hydrogen atom and those from normal hydrogen spectroscopy and e-p scattering. We propose a precise measurement of Zemach radius (with charge and magnetic distributions combined) using the laser spectroscopy of hyperfine splitting energy in the muonic hydrogen atom**.** Preparation of the hydrogen target, mid-infrared laser and muon spin polarization detectors is in progress.

Members

Chief Scientist (Lab. Head)
Masahiko IWASAKI

Vice Chief Scientist
Katsuhiko ISHIDA

Research & Technical Scientists
Isao WATANABE (Senior Research Scientist)
Kenta ITAHASHI (Senior Research Scientist)
Haruhiko OUTA (Senior Research Scientist)
Hiroaki OHNISHI (Senior Research Scientist)
Fuminori SAKUMA (Senior Research Scientist)
Yue MA (Research Scientist)

Contract Researchers
Yu OISHI
Shinji OKADA
Masaharu SATO
Majed ABEDL JAWAD (– Sep. 30, 2014)
Teiichiro MATSUZAKI (Main; Team Leader, Muon Data Team, Dec. 1, 2014 -)

Special Postdoctoral Researchers
Tadashi HASHIMOTO (Apr. 1, 2014 -)
Ikuto KAWASAKI (– Sep. 30, 2014)

Special Temporary Employees
Teiichiro MATSUZAKI (– Nov. 30, 2014)

Research Consultants
Yoshinori AKAISHI
Hironari MIYAZAWA
Masayasu KAMIMURA

Junior Research Associates
Kazuo TANAKA (Univ. of Tokyo) (Apr. 1, 2014-)
Yuki NOZAWA (Kyoto Univ) (– Mar. 31, 2015)
Sohtaro KANDA (Univ. of Tokyo) (– Mar. 31, 2014)
Takuya SHIBUKAWA (Univ. of Tokyo) (Apr. 1, 2014-)
Hirotomo HAMANO (Osaka Univ.)
Nam TRAN (Osaka Univ.) (Apr. 1, 2014-)

International Program Associates
Edi SUPRAYOGA (Bandung Inst. Tech.)
Zhang QI (Lanzhou Univ.)
Noraina ADAM (USM, Feb. 15, 2014 –)
Sungwon YOON (Catholic Univ. of Korea, Nov. 25, 2014 –)

Senior Visiting Scientist

Kazuhiro TANAKA (KEK)

Visiting Scientists

Toshimitsu YAMAZAKI (Univ. of Tokyo)
Mototsugu MIHARA (Osaka Univ.)
Donald George FLEMING (Univ. of British Columbia/TRIUMF)
Yasuo NOZUE (Osaka Univ.)
Takehito NAKANO (Osaka Univ.)
Tadashi ADACHI (Tohoku Univ.)
Zyun Francis EZAWA (Tohoku Univ.)
Jin NAKAMURA (Univ. of Elec.-Com.)
Yasuyuki ISHII (Tokyo Med. Univ.)
Johann ZMESKAL (SMI)
Risdiana (UNPAD)
Norimichi KOJIMA (Univ. of Tokyo)
Satoshi TSUTSUI (JASRI)
Takao SUZUKI (Shibaura Inst. of Tech.)
Masami IIO (KEK)
Georg Peter BERG (Univ. of Notre Dame)
Takayuki GOTO (Sophia Univ.)
Masaya ENOMOTO (Tokyo Univ. of Sci.)
Hiroyuki FUJIOKA (Kyoto Univ.)
Takayuki KAWAMATA (Tohoku Univ.)
Lee CHOW (UCF)
Helmut WEICK (GSI)
Harry W. K. TOM (UC Riverside)
Agustinus NUGROHO (ITB)
Kawakami Kenji ROLAND (Univ. of California, Riverside)
Ichiro SHIRAKI (Univ. of Yamanashi)
Kensuke SUZUKI (Tohoku Univ.)
Kyosuke ISODA (Tokyo Univ. of Sci.)
Ken SUZUKI (SMI)
Irwan DHARMAWAN (UNPAD)
Koji YOKOYAMA (Queen Marry Univ.)
Kazuki UENO (KEK)
Lusy SAFRIANI (UNPAD)
Hiroyuki NOUMI (Osaka Univ.)
Zhuan XU (Zhejiang Univ.)
Hiroshi TANIDA (Hiroshima Univ.)
Kenji KOJIMA (KEK)
Atsushi OKAZAWA (Univ. of Tokyo)
Tobat Parasian Irianto SARAGI (Univ. of Kassel)
Katsuhiko NISHIMURA (Univ. of Toyama)
Kenji MATSUDA (Univ. of Toyama)
Hexi SHI (Univ. of Tokyo)
Mohamed Ismail MOHAMED IBRAHIM (USM)
Shukri SULAIMAN (USM)
Kenji KAWASHIMA (Aoyama Gakuin Univ.)
Ayi BAHTIAR (UNPAD)
Koichi ICHIMURA (Hokkaido Univ.)
Youichi IGARASHI (KEK)
Makoto YOKOYAMA (Ibaraki Univ.)
Ichihiro YAMAUCHI (KEK)
KwangYong CHOI (Chung-Ang Univ.)
Peklan TOH (Univ. Sains Malaysia)
Emma HAETTNER (GSI)
Andrea VACCHI (INFN)
Eiichi YAGI (Waseda Univ.)
Yoshio KOBAYASHI (Univ. of Elec.-Com.)
Naohito SAITO (KEK)
Jun MIYAZAKI (Nihon Univ.)
Kouichirou SHIMOMURA (KEK)
Eiko TORIKAI (Univ. of Yamanashi)
Wataru HIGEMOTO (JAEA)
Yoji KOIKE (Tohoku Univ.)
Kazuhiko SATO (Saitama Univ.)
Masaru YOSOI (Osaka Univ.)
Dai TOMONO (Kyoto Univ.)
Kazuki OHISHI (Comprehensive Res. Org. for Sci. and Soc.)
Yasuhiro MIYAKE (KEK)
Prasad Tara DAS (SUNY)
Yasuhiro YAMADA (Tokyo Univ. of Sci.)
Kenya KUBO (ICU)
Tsutomu MIBE (KEK)
Hiroko ARIGA (Hokkaido Univ.)
Satoru HIRENZAKI (Nara Women's Univ.)
Yasuaki EINAGA (Keio Univ.)
Ryousuke KADONO (KEK)

Visiting Technicians

Yuya FUJIWARA (Univ. of Tokyo)
Kazuo OOYAMA (JOHO com.)
Dita PUSPITA SARI (Inst. Teknologi Sepuluh Nopember)
Retno ASIH (Insti. Teknologi Sepuluh Nopember)

Research Fellows

Yuta SADA (Kyoto Univ.)
Shun ENOMOTO (Osaka Univ.)

Student Trainees

Kensuke SUZUKI (Tohoku Univ.)
Tadashi HASHIMOTO (Univ. of Tokyo) (-Mar. 31, 2014)
Takahiro NISHI (Univ. of Tokyo)
Natsuki TOMIDA (Kyoto Univ.)
Ryo SHIMIZU (Tokyo Univ. of Sci.)
Sohtaro KANDA (Univ. of Tokyo) (Apr. 1, 2014-)
Kentaro INOUE (Osaka Univ.)
Yoshiki TANAKA (Univ. of Tokyo)
Hanjie GUO (Zhejiang Univ.)
Yohei MURAKAMI (Univ. of Tokyo)
Hiroyuki YAMADA (Univ. of Tokyo)
Ryo MIYATANI (Tokyo Univ. of Sci.)
Kazuma SHIGA (Tokyo Univ. of Sci.)
Anba Datt PANT (Yamanashi Univ.)
Yuni WATANABE (Univ. of Tokyo)
Hiroaki KOBAYASHI (Univ. of Tokyo)
Xingliang Xu (Saga Univ.)
Masato SUZUKI (Univ. of Elec.-Com.)
Yukiko SATO (Univ. of Elec.-Com.)
Shotaro TANIGAWA (Univ. of Elec.-Com.)
Daiki NATORI (Univ. of Elec.-Com.)
Kenichi TANABE (Tokyo Univ. of Sci.)
Miho SATO (Tokyo Univ. of Sci.)
Takafumi TABATA (Tokyo Univ. of Sci.)
Malik Anjelh BAQIYA (Tohoku Univ.)
Hiroki YAMAKAMI (Kyoto Univ.)
Shinji OGAWA (Univ. of Tokyo)
Shingo KAWASAKI (Osaka Univ.)
Sajjad MARI (IUT)
Ryo KITAMURA (Univ. of Tokyo)
Fuminao HOSOMI (Univ. of Tokyo)
Kenji FUJIMURA (Ibaraki Univ.)
Taehyung KIM (Tokyo Tech.)
Shingo YASADA (Aoyama Gakuin Univ.)

Wataru ITO (Aoyama Gakuin Univ.)
Kazuki MATSUI (Sophia Univ.)
Ruidong ZHU (Univ. of Tokyo)
Ainul Fauzeeha Binti ROZLAN (Univ. Saints Malaysia)
Saidah Sakinah Binti MOHD TAJUDIN (Univ. Saints Malaysia)
Sungwon YOON (Catholic Univ., Korea)
(Feb. 10, 2014 – Sep. 30, 2014)
Yoshiyuki FURUYA (Tokyo Univ. of Sci.)
Go MISHIMA (Univ. of Tokyo)
Kazuhiro KATONO (Hokkaido Univ.)
Shu AIKAWA (Tokyo Tech.)
Takumi YAMAGA (Osaka Univ.)
Hiroshi HORII (Univ. of Tokyo)
Kenji TANIBE (Osaka Univ.)
Kien LUU (Osaka Univ.)
Kazuya KATAYAMA (Tokyo Tech.)
Koshi KURASHIMA (Tohoku Univ.)

Part-time Workers

Makoto TOKUDA (Tokyo Tech.)
Abdel Jawad MAJED (Oct. 1, 2014 -)
Taehyung KIM (Tokyo Tech.)
Yuta SADA (Kyoto Univ.) (- Mar. 31, 2014)

Assistants

Yuri TSUBURAI(- Apr. 30, 2014)
Mitsue YAMAMOTO (May 1, 2014-)
Yoko FUJITA

Sub Nuclear System Research Division
RIKEN-BNL Research Center

1. Abstract

The RIKEN BNL Research Center was established in April 1997 at Brookhaven National Laboratory with Professor T. D. Lee of Columbia University as its initial Director. It is funded by the Rikagaku Kenkyusho (RIKEN, The Institute of Physical and Chemical Research) of Japan. The Center is dedicated to the study of strong interactions, including spin physics, lattice QCD and RHIC physics through the nurturing of a new generation of young physicists. Professor Lee was succeed by BNL Distinguished Scientist, N. P. Samios, who served until 2013. The current director is Dr. S. H. Aronson. Support for RBRC was initially for five years and has been renewed three times, and presently extends to 2018. The Center is located in the Physics Department. The RBRC Theory Group activities are closely and intimately related to those of the Nuclear Theory, High Energy Theory, and Lattice Gauge Theory Groups at BNL. The RBRC Experimental Group works closely with the DOE RHIC Spin Group, the RIKEN Spin Group at BNL, and the PHENIX heavy ion groups. BNL provides office space, management, and administrative support. In addition, the Computer Science Center (CS) and Information Technology Division (ITD) at BNL provides support for computing, particularly the operation and technical support for the RBRC 400 Teraflop QCDCQ (QCD Chiral Quark) lattice gauge theory computer. The Deputy Director of RBRC is R. Pisarski (BNL). L. McLerran (BNL) is leader of the Theory Group. Y. Akiba (RIKEN) is Experimental Group leader with A. Deshpande (Stony Brook) deputy. T. Izubuchi (BNL) is Computing Group leader.

2. Major Research Subjects

Major research subjects of the theory group are
(1) Heavy Ion Collision
(2) Perturbative QCD
(3) Phenomenological QCD

Major research subjects of the computing group are
(1) Search for new law of physics through tests for Standard Model of particle and nuclear physics
(2) Dynamics of QCD and related theories
(3) Theoretical and algorithmic development for lattice field theories, QCD machine design

Major research subject of the experimental group are
(1) Experimental Studies of the Spin Structure of the Nucleon
(2) Study of Quark-Gluon Plasma at RHIC
(3) PHENIX detector upgrades

3. Summary of Research Activity

Summary of Research Activities of the three groups of the Center are given in the sections of each group.

Members

Director
Samuel H. ARONSON

Deputy Director
Robert PISARSKI

Administrative Staff
Mituru KISHIMOTO (Administration Manager, Nishina Center Planning Office)
Kazunori MABUCHI (Deputy Administration Manager, Nishina Center Planning Office, – Dec. 31, 2014)
Yasutaka AKAI (Deputy Administration Manager, Nishina Center Planning Office, Jan. 1, 2015 –)
Colleen MICHAEL (Administrative Assistant)
Pamela ESPOSITO (Administrative Assistant)
Taeko ITO (Administrative Assistant)

Sub Nuclear System Research Division
RIKEN-BNL Research Center
Theory Group

1. Abstract

The efforts of the RBRC theory group are concentrated on the major topics of interest in High Energy Nuclear Physics. This includes: understanding of the Quark-Gluon Plasma; the nature of dense quark matter; the initial state in high energy collisions, the Color Glass Condensate; its evolution through a Glasma; spin physics, as is relevant for polarized hadronic collisions; physics relevant to electron-hadron collisions.

Theory Group hosted many joint tenure track positions with universities in U.S. and Japan.

2. Major Research Subjects

(1) Heavy Ion Collision
(2) Perturbative QCD
(3) Phenomenological QCD

3. Summary of Research Activity

(1) Spin Physics

The experimental program at RBRC is strongly focused on determining the origin of spin in the proton and neutron. To extract the spin content of nucleon requires both precise data and precise computation. Dr. Jianwei Qiu of the Nuclear Theory group is one of the world's leading theorists in perturbative QCD, and leading the effort at BNL in spin physics. Their effort will continue to concentrate on computing perturbative QCD effects to sufficient precision that one can reliably extract information from the evolving experimental program. In addition they are developing ideas which might be tested in an electron-hadron collider, such as the one proposed to be built by adding an electron ring to RHIC.

(2) Matter at High Energy Density

The RHIC experimental heavy ion program is designed to study the properties of matter at energy densities much greater than that of atomic nuclei. This includes the initial state of nucleus-nucleus collisions, the Color Glass Condensate, the intermediate state to which it evolves, the Glasma, and lastly the thermal state to which it evolves, the Quark-Gluon Plasma. Theorists at the RBRC have made important contributions to all of these subjects.

Matter at high temperature has been studied by a variety of techniques involving both numerical and analytic methods. Much of the high precision work on numerical simulations of lattice QCD at nonzero temperature and density such matter have been done by members of the Lattice Gauge Theory Group at BNL, including Frithjof Karsch, Peter Petreczsky, Swagato Mukherjee, and postdoctoral assistants. These groups, along with collaborators at Columbia University, the University of Bielefeld, and other groups, have computed numerous properties of QCD in thermodynamic equilibrium. This includes the equation of state for physical quark masses, susceptibilies with respect to quark chemical potentials, and transport coefficients.

Phenomenological theories of the Quark-Gluon Plasma, based upon results from lattice simulations, have been developed by R. Pisarski of the Nuclear Theory Group, in collaboration with Dr. Y. Hidaka (previously of RBRC/BNL, and now a permanent member at RIKEN in Waco), Shu Lin, Daisuke Sato, and other postdoctoral research assistants at RBRC/BNL.

The theory of the Color Glass Condensate and Glasma was largely developed by RBRC scientists. This theory has been successfully applied to a wide variety of experimental results involving high energy collisions of hadrons, electrons and nuclei. There is recent data on heavy ion collisions that are naturally explained by such matter, including data on proton (or deuteron) nucleus collisions. Much of the effort here will be aimed towards excluding or verifying the Color Glass Condensate and Glasma hypothesis in RHIC and LHC experiments.

Thermal matter at high temperature and baryon density has been traditionally conjectured to be of two phases: confined and deconfined, with a direct correlation between deconfinement and the restoration of chiral symmetry. RBRC scientists have recently conjectured a third phase, of quarkyonic matter. This is baryonic matter at energy densities very high compared to the QCD scale. It has a pressure and energy density typical of quarks, yet it is confined. The name arises because it shares properties of confined baryonic matter with unconfined quark matter. This hypothesis is new and predicts new classes of phenomena that might be observed in collisions of nuclei of relatively low energy at RHIC. There are a number of first principle theoretical issues also to be understood.

Efforts on RHIC phenomenology proceed on a broad front. Recent efforts include improving hydrodynamic computations using state of the art equations of state derived from lattice gauge theory. Understanding the nature of matter at high baryon number density has generated the idea of Quarkyonic Matter, that may have implications for an upcoming low energy run at RHIC and eventual experiments in the future at FAIR and NICA. An issue being studied is the nature of mass generation and the breaking of translational invariance. A central focus of work at RBRC, the Color Glass Condensate and the Glasma, matter that controls the high energy limit of QCD, is being realized in experiments at RHIC. Much activity focuses on the relation between observations at LHC and the implications made at RHIC.

Members

Group Leader (Lab. Head)
Larry McLERRAN

Deputy Group Leader
Robert PISARSKI (concurrent : Deputy Director, RBRC)

RHIC Physics Fellows
Fedor BEZRUKOV
Jinfeng LIAO
Ho-Ung YEE

Research Associates
Adam BZDAK (– Apr. 30, 2014)
Daniel PITONYAK

Special Postdoctoral Researchers
Kouji KASHIWA (– Mar. 31, 2014)
Akihiko MONNAI

Foreign Postdoctoral Researchers
Shu LIN
Sergey SYRITSYN

Visiting Scientists
Testufumi HIRANO (Univ. of Tokyo)
Feng YUAN (LBNL)
Edward SHURYAK (State Univ. New York, Stony Brook)
Miklos GYULASSY (Columbia Univ.)
Robert L. JAFFE (MIT)
Thomas BLUM (Univ. of Connecticut)
Taku IZUBUCHI (concurrent; Computing Gr.)

Sub Nuclear System Research Division
RIKEN-BNL Research Center
Computing Group

1. Abstract

The computing group founded in 2011 as a part of the RIKEN BNL Research Center established at Brookhaven National Laboratory in New York, USA, and dedicated to conduct researches and developments for large scale physics computations important for particle and nuclear physics. The group was forked from the RBRC Theory Group.

The main mission of the group is to provide important numerical information that is indispensable for theoretical interpretation of experimental data using the theories of particle and nuclear physics. Their primary area of research is lattice quantum chromodynamics (QCD), which describes the sub-atomic structures of hadrons, which allow us the ab-initio investigation for strongly interacting quantum field theories beyond pertrubative analysis.

The RBRC group and its collaborators have emphasized the necessity and importance of precision calculations, which will precisely check the current understandings of nature, and will have a potential to find a physics beyond the current standard model of fundamental physics. We have therefore adopted techniques that aim to control and reduce any systematic errors. This approach has yielded many reliable results.

The areas of the major activities are R&D for high performance computers, developments for computing algorithms, and researches of particle, nuclear, and lattice theories. Since the inception of RBRC, many breakthroughs and pioneering works has carried out in computational forefronts. These are the use of the domain-wall fermions, which preserve chiral symmetry, a key symmetry for understanding nature of particle nuclear physics, the three generations of QCD devoted supercomputers, pioneering works for QCD calculation for Cabibbo-Kobayashi-Maskawa theory, QCD+QED simulation for isospin breaking, novel algorithm for error reduction in general lattice calculation. Now the chiral quark simulation is performed at the physical up, down quark mass, the precision for many basic quantities reached to accuracy of sub-percent, and the group is aiming for further important and challenging calculations, such as the full and complete calaution for $K \rightarrow \pi\pi$ decay, ε'/ε, or hadronic contributions go muon's anomalous magnetic moment, or Nucleon's shape and structures.

2. Major Research Subjects

(1) Search for new law of physics through tests for Standard Model of particle and nuclear physics, especially in the framework of the Cabibbo–Kobayashi–Maskawa (CKM), hadronic contributions to the muon's anomalous magnetic moment (g-2).
(2) Dynamics of QCD and related theories, including study for the structures of nucleons
(3) Theoretical and algorithmic development for lattice field theories, QCD machine design

3. Summary of Research Activity

In 2011, QCD with Chiral Quarks (QCDCQ), a third-generation lattice QCD computer that is a pre-commercial version of IBM's Blue Gene/Q, was installed as an in-house computing resource at the RBRC. The computer was developed by collaboration among RBRC, Columbia University, the University of Edinburgh, and IBM. Two racks of QCDCQ having a peak computing power of 2×200 TFLOPS are in operation at the RBRC. In addition to the RBRC machine, one rack of QCDCQ is owned by BNL for wider use for scientific computing. In 2013, 1/2 rack of Blue Gene/Q is also installed by US-wide lattice QCD collaboration, USQCD. The group has also used the IBM Blue Gene supercomputers located at Argonne National Laboratory and BNL (NY Blue), and RICC, the cluster computers at RIKEN (Japan), Fermi National Accelerator Laboratory, the Jefferson Lab, and others.

Such computing power enables the group to perform precise calculations using up, down, and strange quark flavors with proper handling of the important symmetry, called chiral symmetry, that quarks have. Several projects are ongoing: flavor physics in the framework of the CKM theory for kaons and B mesons; the electromagnetic properties of hadrons; hadronic contributions to the muon's anomalous magnetic moment; the proton's and neutron's electric dipole moments; proton decay; nucleon form factors, which are related to the proton spin problem; and QCD thermodynamics in finite temperature/density systems such as those produced in heavy-ion collisions at the Relativistic Heavy Ion Collider. Major breakthroughs on important problems such as the direct CP violation process ($K \rightarrow \pi\pi$, ε'/ε) will be attempted using this computer.

The RBRC group and its collaborators have emphasized the necessity and importance of precision calculations, which will precisely check the current understandings of nature, and will have a potential to find physics beyond the current standard model of fundamental physics. We have therefore adopted techniques that aim to control and reduce any systematic errors. This approach has yielded many reliable results.

The group also delivers an algorithmic breakthrough, which speed up generic lattice gauge theory computation typically by a factor of 20 or more. In this novel technique called All Mode Averaging (AMA), the whole calculation is divided into frequent approximated calculations, and infrequent expensive and accurate calculation using lattice symmetries.

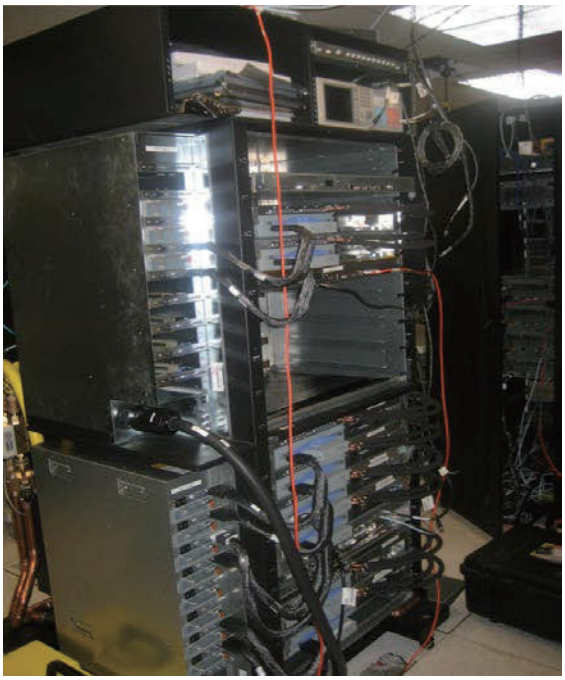

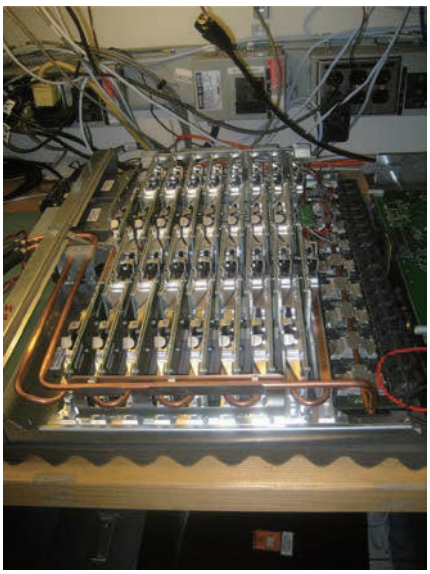

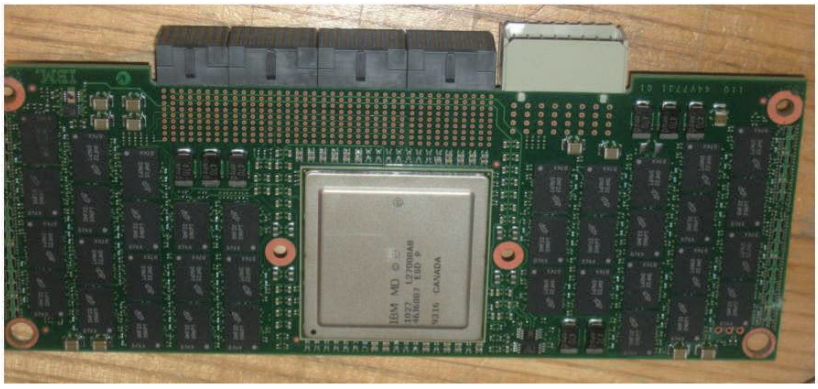

Fig. The rack, motherboard, and chips of QCDCQ

Members

Group Leader (Lab. Head)
Taku IZUBUCHI

RIKEN BNL Fellow
Tomomi ISHIKAWA (concurrent; Visiting Scientist, Univ. of Connecticut)

RHIC Physics Fellows
Brian TIBURZI
Ethan NEIL
Stefan MEINEL

Foreign Postdoctoral Researcher
Christopher KELLY

Visiting Senior Scientist
Robert MAWHINNEY (Columbia Univ.)

Visiting Scientists
Shigemi OHTA (KEK)
Yasumichi AOKI (Nagoya Univ.)
Thomas BLUM (Univ. of Connecticut)
Chulwoo JUNG (BNL)
Christoph LEHNER (BNL)
Meifeng LIN (Yale Univ.)
Eigo SHINTANI (Inst. fur Kernphysik Johannes Gutenberg-Univ. at Mainz)
Takeshi YAMAZAKI (Nagoya Univ.)
Hyung-Jin KIM (BNL)

Sub Nuclear System Research Division
RIKEN-BNL Research Center
Experimental Group

1. Abstract

RIKEN BNL Research Center (RBRC) Experimental Group studies the strong interactions (QCD) using RHIC accelerator at Brookhaven National Laboratory, the world first heavy ion collider and polarized p+p collider. We have three major activities: Spin Physics at RHIC, Heavy ion physics at RHIC, and detector upgrades of PHENIX experiment at RHIC. We study the spin structure of the proton using the polarized proton-proton collisions at RHIC. This program has been promoted by RIKEN's leadership. The first focus of the research is to measure the gluon spin contribution to the proton spin. Our recent data analysis has shown that the proton spin carried by the gluons is small, which is a very striking finding beyond our expectations. The aim of Heavy ion physics at RHIC is to re-create Quark Gluon Plasma (QGP), the state of Universe just after the Big Bang. Two important discoveries, jet quenching effect and strong elliptic flows, have established that new state of dense matter is indeed produced in heavy ion collisions at RHIC. We are now studying the property of the matter. Recently, we have measured direct photons in Au+Au collisions for $1<p_T<3$ GeV/c, where thermal radiation from hot QGP is expected to dominate. The comparison between the data and theory calculations indicates that the initial temperature of 300 MeV to 600 MeV is achieved. These values are well above the transition temperature to QGP, which is calculated to be approximately 160 MeV by lattice QCD calculations.

We have major roles in detector upgrades of PHENIX experiment, namely, the silicon vertex tracker (VTX) and muon trigger upgrades. Both of the upgrade is now complete. VTX detector was installed in PHENIX in 2011 and we are taking data since then. Muon trigger was complete and it was essential for W→μ measurement in 2013.

2. Major Research Subjects

(1) Experimental Studies of the Spin Structure of the Nucleon
(2) Study of Quark-Gluon Plasma at RHIC
(3) PHENIX detector upgrades

3. Summary of Research Activity

We study the strong interactions (QCD) using the RHIC accelerator at Brookhaven National Laboratory, the world first heavy ion collider and polarized p+p collider. We have three major activities: Spin Physics at RHIC, Heavy ion physics at RHIC, and detector upgrades of PHENIX experiment.

(1) Experimental study of spin structure of proton using RHIC polarized proton collider

How is the spin of proton formed with 3 quarks and gluons? This is a very fundamental question in Quantum Chromodynamics (QCD), the theory of the strong nuclear forces. The RHIC Spin Project has been established as an international collaboration between RIKEN and Brookhaven National Laboratory (BNL) to solve this problem by colliding two polarized protons for the first time in history. This project also has extended the physics capabilities of RHIC.

The first goal of the Spin Physics program at RHIC is to determine the gluon contribution to proton spin. It is known that the spin of quark accounts for only 25% of proton spin. The remaining 75% should be carried either by the spin of gluons or the orbital angular momentum of quarks and gluons. One of the main goals of the RHIC spin program has been to determine the gluon spin contribution. Before the start of RHIC, there was little experimental constraint on the gluon polarization, ΔG.

PHENIX measures the double helicity asymmetry (A_{LL}) of π^0 production to determine the gluon polarization. Our publication from 2006 run has shown that the gluon polarization in the proton is small and only about half of proton spin can be accounted by gluon spin in the measured region of gluon momentum in proton. Figure 1 shows our most recent results of π^0 ALL measurement, which has just submitted to Physical Review D. The figure shows the combined results of RUN5, RUN6, and RUN9. The new data give even stronger constraint on the gluon spin. RBRC exp. G led the gluon spin analysis in PHENIX. K. Bolye, a fellow of RBRC experimental group has a major role in this paper.

RHIC achieved polarized p+p collisions at 500 GeV in 2009. The collision energy increased to 510 GeV in 2012 and 2013. We have recorded The main goal of these high energy p+p run is to measure anti-quark polarization via single spin asymmetry AL of the W boson production. We have published the first results on W→e measurement at mid-rapidty from 2009 dataset in 2011. We upgraded the muon trigger system to measure W→m decays in the forward direction. With the measurement of W→ e and W→μ, we can cover a wide kinematic range in anti-quark polarization measurement. The 2013 run is the main spin run at 510 GeV. PHENIX has recorded more than 150/pb of data in the run. Combined with the datasets in 2009 (8.6/pb), 2011(18/pb), and 2012(~30/pb), we will have a definite measurement of anti-quark spin.

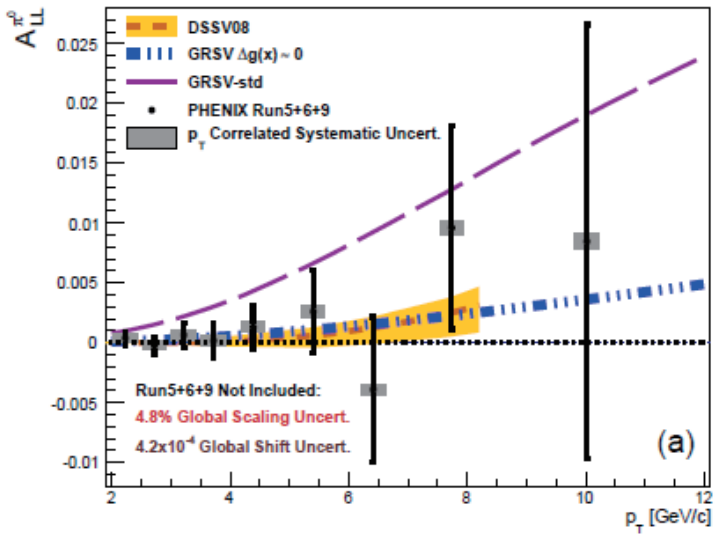

Figure 1 Double spin asymmetry ALL in π^0 production as function of transverse momentum pT compared with expectations for different gluon polarization ΔG(x). Published in Physical Review D90,012007 (2014)

(2) Experimental study of Quark-Gluon Plasma using RHIC heavy-ion collider

The goal of high energy heavy ion physics at RHIC is study of QCD in extreme conditions i.e. at very high temperature and at very high energy density. Experimental results from RHIC have established that dense partonic matter is formed in Au+Au collisions at RHIC. **The matter is very dense and opaque, and it has almost no viscosity and behaves like a perfect fluid. These conclusions are primarily based on the following two discoveries:**

- **Strong suppression of high transverse momentum hadrons in central Au+Au collisions (jet quenching)**
- **Strong elliptic flow**

These results are summarized in PHENIX White paper, which has over 1900 citations to date.

The focus of the research in heavy ion physics at RHIC is now to investigate the properties of the matter. RBRC have played the leading roles in some of the most important results from PHENIX in the study of the matter properties. These include (1) measurements of heavy quark production from the single electrons from heavy flavor decay (2) measurements of J/Psi production (3) measurements of di-electron continuum and (4) measurements of direct photons.

The most important recent result is the measurement of direct photons for $1<p_T<5$ GeV/c in p+p and Au+Au through their internal conversion to e+e- pairs. **If the dense partonic matter formed at RHIC is thermalized, it should emit thermal photons. Observation of thermal photon is direct evidence of early thermalization, and we can determine the initial temperature of the matter. It is predicted that thermal photons from QGP phase is the dominant source of direct photons for $1<p_T<3$ GeV/c at the RHIC energy. We measured the direct photon in this p_T region from measurements of quasi-real virtual photons that decays into low-mass e+e- pairs. Strong enhancement of direct photon yield in Au+Au over the scaled p+p data has been observed. Several hydrodynamical models can reproduce the central Au+A data within a factor of two. These models assume formation of a hot system with initial temperature of Tinit = 300 MeV to 600 MeV. This is the first measurement of initial temperature of quark gluon plasma formed at RHIC. These results are recently published in Physical Review Letters. Y. Akiba is the leading person of the analysis and the main author of the paper.** He received 2011 Nishina memorial Prize mainly based on this work.

(3) PHENIX detector upgrade

The group has major roles in several PHENIX detector upgrades, namely, the silicon vertex tracker (VTX) and muon trigger upgrades.

VTX is a high precision charged particle tracker made of 4 layers of silicon detectors. It is jointly funded by RIKEN and the US DOE. The inner two layers are silicon pixel detectors and the outer two layers are silicon strip detectors. Y. Akiba is the project manager and A. Deshpande is the strip system manager. The VTX detector was completed in November 2010 and subsequently installed in PHENIX. The detector started taking data in the 2011 run. With the new detector, we are measuring heavy quark (charm and bottom) production in p+p, A+A collisions to study the properties of quark-gluon plasma. We have recorded 20 billion Au+Au collisions in the 2014 run. The large dataset will produce definitive results on heavy quark production at RHIC.

Muon trigger upgrades are needed for W→μ measurement at 500 GeV. New trigger electronics (Muon Trigger FEE) and new Muon

trigger detectors using RPC technology were installed in PHENIX muon arms. Additional hadron absorbers were installed in front of the muon arms to reduce the background. These upgrades were essential for the high statistic W→μ measurement in 2013 run. Over 150/pb of data was recorded in the run. I. Nakagawa is the leading person of the installation of the Muon Trigger FEE, and R. Seidl have major role in the RPC project. He is also leading the W→μ analysis.

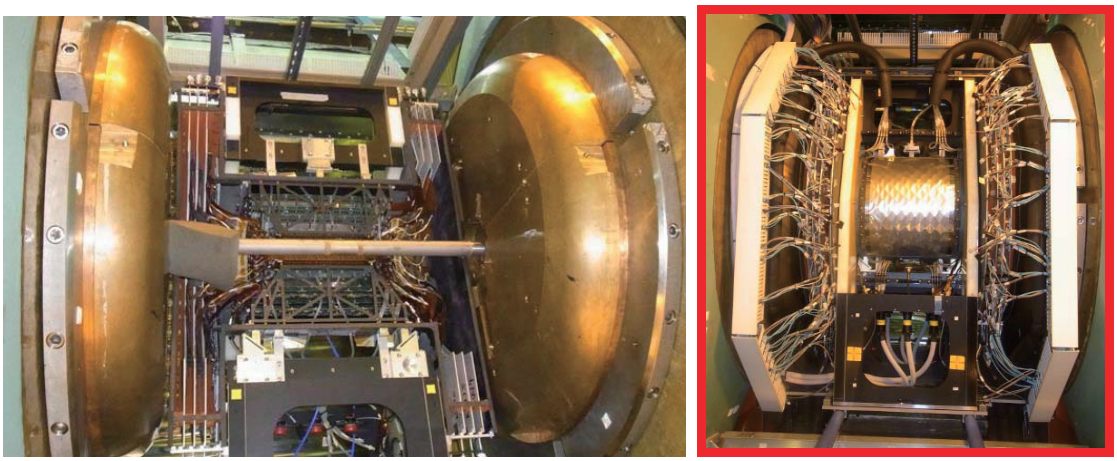

Figure 2 Left: a picture of West half of VTX detector installed in PHENIX experiment. The interior of the detector can be seen. Right: The VTX detector completed with all cables, cooling tubes and dry gas connections.

(4) Other data analysis in PHENIX

PHENIX experiment has a very good capability of low mass electron pair measurement. Recently we used this capability for search for "dark photon", a hypothetical particle in Beyond Standard Model theories. Many experiments looked for this particle since it can provide a simultaneous explanation of the 3.6σ deviation of the measured value of muon anomalous magnetic moment (g-2) from its theoretically calculated value and the positron excess observed by PAMELLA, FERMI, and AMS-2 experiments. If dark photon exists, it decays into an electron-positron pair, and thus it can be observed as a narrow peak in e^+e^- mass spectrum. We looked for this signal of dark photon in a large sample of electron pairs measured by PHENIX experiment. We observed no significant signal of dark photon and then set the upper limit of the dark photon – ordinary photon mixing parameter as function of mass. The result is shown in Fig. 3 below. Combined with other experimental limits, the parameter space of dark photon as the explanation of muon g-2 anomaly was almost completely ruled out.

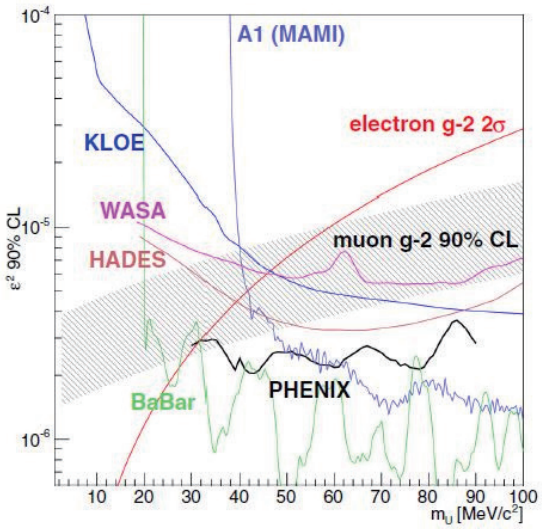

Figure 3 90% CL limit of photon-dark photon mixing parameter as a function of mass. The shaded band show the parameter space favored by the muon g-2 anomaly. Accepted in Physical Review C.

Members

Group Leader (Lab. Head)

Yasuyuki AKIBA (Deputy Chief Scientist)

Deputy Group Leader
Abhay DESHPANDE

RIKEN Spin Program Researchers
Yasushi WATANABE (concurrent: Radiation Lab.)
Yuji GOTO (concurrent: Radiation Lab.)
Itaru NAKAGAWA (concurrent: Radiation Lab.)
Takashi ICHIHARA (concurrent: RI Physics Lab.)
Atsushi TAKETANI (concurrent: Neutoron Beam Technology Team, Advanced Photonics Technology development Group, RAP)
Satoshi YOKKAICHI (concurrent: Radiation Lab.)

RIKEN BNL Fellows
Josef SEELE (– Feb. 7, 2014)
Kieran BOYLE

RHIC Physics Fellows
Xiaorong WANG
Stefan BATHE (– Jan. 31, 2015)

Special Postdoctoral Researcher
Maki KUROSAWA (– Mar. 31, 2014)

Research Associates
Chin-Hao CHEN (– Aug. 29, 2014)

RBRC Collaborating Scientists
Rachid NOUICER
Ady HERSHCOVITCH (BNL)

Visiting Scientists
Akio OGAWA (BNL)
Zheng LI
Masahiro OKAMURA (concurrent: BNL)

Sub Nuclear System Research Division
RIKEN Facility Office at RAL

1. Abstract

Our core activities are based on the RIKEN-RAL Muon Facility located at the Rutherford Appleton Laboratory (UK), which provides intense pulsed-muon beams. Muons have their own spins with 100% polarization, and can detect very precisely local magnetic fields and their fluctuations at muon stopping sites. The method to study characteristic of materials by observing time-dependent changes of muon spin polarization is called "Muon Spin Rotation, Relaxation and Resonance (μSR method), and is applied to studies of electro-magnetic properties of insulating, metallic, magnetic, superconducting systems. Muons reveal static and dynamic properties of electronic state of materials in the zero-field condition, which is the ideal magnetic condition for researches on the magnetism. μSR is applied to those systems. As one example of those researches, we have carried out μSR investigations on frustrated pyrochlore systems, which have variety of exotic ground state of magnetic spins. We are approaching to achieve the first evidence of the appearance of a quasi-monopole state in the pyrochlore system.

We have been working on producing ultra-slow muon beam, which has a momentum spread as small as thermal energy. Our method of the beam generation is based on the laser ionization of muoniums (bound system of μ^+ and electron), which emitted from hot tungsten surface by stopping low-momentum muon beam at Port-3. The ultra-slow muon beam can be stopped in thin foils, multi-layered materials and artificial lattices and we can apply the μSR techniques to surface and interface science. The development of ultra-slow muon beam is also very important as the source of ultra-cold (pencil-like small emittance) muon beam for muon g-2/EDM measurement. We have been developing muonium generators to create more muoniums in vacuum even at room temperature. Very recently, we demonstrated tremendous increase of the muonium emission efficiency by fabricating fine laser drill-holes on the surface of silica aerogel. We also developed a high power Lyman-alpha laser in collaboration with the Advanced Photonics group at RIKEN. The new laser will ionize muoniums 100 times more efficiently for slow muon beam generation.

2. Major Research Subjects

(1) Materials science by muon-spin-relaxation method
(2) Hyperfine interactions at muon sites studied by the computation science
(3) Nuclear and particle physics studies via muonic atoms and ultra-cold muon beam

3. Summary of Research Activity

(1) Material Science at the RIKEN-RAL Muon Facility

Muons with their own spin polarization enable us to conduct (1) material studies under external zero-field condition, (2) magnetism studies with samples without nuclear spins, and (3) measurements of muon spin relaxation changes at wide temperature range with same detection sensitivity. The detection time range of local field fluctuations by μSR is 10^{-6} to 10^{-11} second, which is an intermediate region between neutron scattering method (10^{-10}-10^{-12} second) and Nuclear Magnetic Resonance (NMR) (longer than 10^{-6} second). At Port-2 and 4 of the RIKEN-RAL Muon Facility, we have been performing μSR researches on newly fabricated strong correlated-electron systems, organic molecules and biological samples to study electron structures, superconductivity, magnetism, molecular structures and crystal structures.

In the period from 2012 to 2014, we have obtained excellent results, and the highlights are listed in the following,

1) A static ordering of small Ir moments in the pyrochlore iridate; $Nd_2Ir_2O_7$ is close to a quantum critical point.
2) A static ordering of Yb moment on the corner of the pyrochlore structure of $Yb_2Ti_2O_7$ can be explained by the Higgs mechanism.
3) Spontaneous formation of small static internal fields in the superconducting state of URu_2Si_2 was observed, which indicate appearance of an exotic superconducting state in this material.
4) Universality class of the Mott transition is confirmed in $EtMe_3P[Pd(dmit)_2]_2$.
5) Finding new muon sites in La_2CuO_4, which can only be explained by taking into account the spatial distribution of Cu spin.
6) A novel coexisting state between Fe spin-glass and Cu stripe ordered states in the over-doped regime of $La_{2-x}Sr_xCu_{1-y}Fe_yO_4$.
7) International collaborations to organize new μSR experiments and to develop a group to work on muon-site calculations by using computational technique.

Solid observations of a static magnetically ordered state of corner-shared magnetic moments on pyrochlore systems gave us new interpretation to understand exotic phenomena, like the quantum criticality of magnetic moments and a quasi-magnetic monopole state (result-1 and 2). We measured an increase of static internal fields at the muon site in the zero-field condition just below the superconducting transition temperature of URu_2Si_2. This could shed a light on the mechanism of the superconductivity, which has been a long-standing problem of this system (result-3). We have been developing gas-pressurized high-pressure apparatus, which can be used not only for μSR but also for other purposes. We have applied this pressure system to $EtMe_3P[Pd(dmit)_2]_2$ and have found that pressure dependent resistivity and thermoelectric coefficient measurements have shown that the Mott transition belongs to the Ising universality

class even in two-dimensional states (result-4). Well-known and deeply investigated La_2CuO_4 has opened a new scheme of the Cu spin. Taking into account the effect of the spatial distribution of Cu spin, we have succeeded to explain newly found muon sites and hyperfine fields at those sites (result-5). Fe spins form a spin glass state through the RKKY interaction in the over-doped regime in $La_{2-x}Sr_xCu_{1-y}Fe_yO_4$. This spin glass state is expected to co-exist with the stripe ordered state at lower temperatures (result-6).

We have been very keen to develop muon activities in Asian countries. We have formed MOU with Universiti Sains Malaysia (USM) in order to develop activities on the muon-site calculation. We have newly started to collaborate in μSR experiments on strongly correlated systems with researchers from Taiwan and Korea including graduate students (result-7).

A new μSR spectrometer "Chronus" which has finely multi-segmented forward and backward μ-e counter arrays (304 counters each) is now used for real μSR experiments in Port-4 in parallel with ARGUS in Port-2. Software systems, which control the data acquisition and experimental conditions, are renewed based on the ISIS frontend so as to have common data format with the other ISIS muon facilities (DAE with SECI), so as to have more affinity with the ISIS facility and its analysis platform.

(2) Ultra Slow (low energy) Muon Beam Generation and Applications

We are performing R&D to realize efficient generation of ultra-slow muon beam having energy dispersion below thermal energy utilizing laser ionization of muoniums at Port-3. To study magnetism at surface and interface, and to realize new high-precision muon g-2/EDM measurement, it is essential to increase the slow muon beam production efficiency by more than 100 times. There are three key techniques in ultra-slow muon generation: production of thermal muonium, high intensity Lyman-alpha laser and the ultra-slow muon beam line.

In the period from 2011 to 2014, we developed a high power Lyman-alpha laser in collaboration with the Advanced Photonics group at RIKEN. The new laser will ionize muoniums 100 times more efficiently for slow muon beam generation. This development was funded mostly by the Grant-in-Aid for Scientific Research on Innovative Areas "Frontier in Materials, Life and Particle Science Explored by Ultra Slow Muon Microscope". This Grant-in-Aid research group is a complex of research institutions from universities together with J-PARC muon group and RIKEN. The new laser system was installed to J-PARC slow muon beam line and is being tested. In this development, we succeeded to synthesize novel ceramic-based Nd:YGAG crystal, and this crystal can also be applicable to the flash-lamp based Lyman-alpha laser system of RIKEN-RAL to realize substantial improvement of the laser power at a much reduced cost based on the experiences.

Another plan in 2011-2014 was to realize drastic improvements on the ultra-slow muon source with much reduced emittance. We have been developing muonium generators to create more muoniums in vacuum even at room temperature. In 2013, we demonstrated tremendous increase of the muonium emission efficiency by fabricating fine laser drill-holes on the surface of silica aerogel. The measurement was carried out at TRIUMF in collaboration with J-PARC muon g-2/EDM group. We believe that the better efficiency and beam quality can be achieved in ultra-slow muon generation by using this new muonium source.

Based on these two new key components, we are planning to feed these new techniques to RIKEN-RAL ultra-slow muon beam line to realize further development of ultra-slow muon technology. The present muonium production target section, which had been designed with hot tungsten, was rebuilt to use advantage of the new room temperature target, such as no need of thermal shielding etc. Also, we adopted an all-cylindrical beam-transport design, because of its simpler optics and better manufacture precision, which will contribute to the ultimate cold muon source required for muon g-2/EDM. We plan the testing with the muon beam to be started in middle 2015.

(3) Other topics

Muon catalyzed fusion has been one of the main subject of studies since the start of the RIKEN-RAL Muon Facility. It has produced many new results by using the advantage of the high-intensity pulsed muon beam and the advanced tritium handling facility as was reported in previous RIKEN-RAL IACs. Even though, huge increase of the catalysis rate that is enough for energy production is yet difficult to achieve. Considering the limited budget and human resources maintaining the tritium facility, we had discussions with RAL on the safe closure of the tritium facility. The decommissioning was completed in March 2015.

New demand is emerging on utilizing the muon beam for electronics chips radiation effect studies. Recent progress of semiconductor devices has produced electronics chips with very fine structure. It is concerned that the single memory upset by the ionization effect of single muon may result in malfunction or errors of advanced electronics. Muon is the main component of the cosmic ray in our ordinal life and difficult to be removed. We have started measurement at RIKEN-RAL in 2013 to measure such an error rate and observed an effect that is correlated with the muon energy deposit rate. Further measurements were performed in 2014.

A new proposal was submitted to measure the proton radius by using the hyperfine splitting of the 1S states of muonic hydrogen. This is in contrast to the recent measurement at PSI using energy splitting between 2S-2P levels. The hyperfine transition measurement needs a high intensity laser so it needs to be matched with pulsed muon beam. A new laser system was designed in collaboration with RIKEN's advanced photonics group based on their experience on the commissioning of a laser of similar type. We are also preparing the target chamber and detectors for this measurement.

Members

Director
Philip KING

Research & Technical Scientist
Isao WATANABE (concurrent: Advanced Meson Science Lab.)

Administration Manager
Mitsuru KISHIMOTO (concurrent: Nishina Center Planning Office)

RIBF Research Division
Radioactive Isotope Physics Laboratory

1. Abstract

This laboratory explores exotic nuclear structures and dynamics in exotic nuclei that have never been investigated before, such as those with largely imbalanced proton and neutron numbers. Our aim is to develop new experimental techniques utilizing fast RI beams to discover new phenomena and properties in exotic nuclei. Another important subject is the equation-of-state in asymmetric nuclear matter, and its association with the origin of elements and with neutron stars. For instance, we are making attempts to the better understand underlying mechanism for exotic stability-enhancements of very neutron-rich fluorine isotopes, the large deformation of the nucleus Mg-34 with N=22 in spite of its vicinity to the N=20 magic neutron number and anomalous collectivity in C-16. We are further extending these studies to medium- and heavy-mass regions by developing facilities, detectors and unique methods at RIBF, thereby leading on the challenging task to find new exotic phenomena. We also perform numerical simulations of nucleosynthesis under the environment of core-collapse supernovae, and moreover quest for footprints of supernovae and solar activities in the past, embedded in Antarctic ice core.

2. Major Research Subjects

(1) Study of structure and dynamics of exotic nuclei through developments of new tools in terms of reaction- and technique-based methodology
(2) Research on EOS in asymmetric nuclear matter via heavy-ion induced reactions
(3) Detector developments for spectroscopy and reaction studies

3. Summary of Research Activity

(1) In-beam gamma spectroscopy

In the medium and heavy mass region explored at RIBF, collective natures of nuclei are one of important subjects, which are obtained through production and observation of high excited and high spin states. To populate such states, heavy-ion induced reactions such as fragmentation, fission are useful. So far, we have developed two-step fragmentation method as an efficient method to identify and populate excited states, and lifetime measurements to deduce transition strength.

Devices utilized for the in-beam gamma spectroscopy are ZeroDegree Spectrometer (ZDS) and a NaI array DALI2. Since the end of 2008, the first spectroscopy on nuclei island-of-inversion region was performed, we have explored step-by-step new and unknown regions in the nuclear chart. The second campaign in 2009 was organized to study background components originating from atomic processes in a heavy target. Neutron-rich nuclei at N=20 to 28 were studied in 2010. In 2011-2013, we conducted experiment programs for Ca-54, Ni-78, neutron-rich nuclei at N=82 and neutron-deficient nuclei at Z=50.

A multitude of data obtained with inelastic, nucleon knock-out, fragmentation channels have been analyzed and published. In 2011-2013, collective natures of Mg-36, 38 and Si-42 were both published in PRL. Excited states firstly observed in Ca-54 were reported in Nature to demonstrate a new nuclear magic number of 34. Fragmentation reaction has been found efficient for nuclei with A>100 and low-lying excited state in Pd-126 has been successfully observed and reported in PRC.

To further strengthen the in-beam gamma spectroscopy at RIBF, we have proposed a new setup of MINOS + DALI2 to search for the 1^{st} excited states in even-even neutron-rich nuclei with Z~20 to 40. The program was submitted to the PAC 2013 as a new category "proposal for scientific program" and was S-ranked. A dedicated collaboration "SEASTAR" has been established as a subset of in-beam gamma collaboration "SUNFLOWER". The two campaigns were organized in 2014 and 2015 to study very neutron-rich isotopes.

Concerning a next generation detector, a construction proposal of a LaBr3 array "SHOGUN", was submitted to the PAC 2009, and an international workshop was organized in Feb. 2011 to form the SHOGUN collaboration. A technical development with small sized crystals is now in progress.

(2) Decay spectroscopy

Beta- and isomer-spectroscopy is an efficient method for studying nuclear structure, especially for non-yrast levels. We had accumulated experimental techniques at the RIPS facility to investigate nuclear structure in light mass region via beta-gamma and beta-p coincidence. Concerning the medium and heavy mass region available at RIBF, we have developed two position-sensitive active-stoppers, strip-silicon detectors and a cylindrical active stopper called CAITEN, to achieve a low-background measurement by taking correlation between heavy ion stop position and beta-ray emission position. A site of decay-spectroscopy at the new facility of RIBF is the final focal plane of ZDS, where high precision of TOF in particle identification is obtained due to a long flight path from BigRIPS to ZDS.

At the end of 2009, the first decay spectroscopy was organized with a minimum setup of four clover gamma detectors and silicon strip detectors, to study neutron-rich nuclei with A~110. The first campaign was found successful and efficient to publish four letter articles in 2011, two PRL's and two PLB's. One of the PRL papers is associated to the r-process path where half-lives for 18 neutron-rich nuclei were determined for the first time. The other PRL paper reported a finding of deformed magic number 64 in the Zr isotopes.

The success of the first decay-spectroscopy campaign stimulated to form a new large-scale collaboration "EURICA", where a twelve Euroball cluster array is coupled with the silicon-strip detectors to enhance gamma efficiency by a factor of 10. A construction proposal of "EURICA" was approved in the PAC 2011, and the commissioning was successfully organized in spring 2012. Since then, physics runs have been conducted for programs approved to survey nuclei of interest as many as possible, such as Ni-78, Pd-128, Sn-100. So far, 10 papers including 7 PRL's were published. One of the highlights is discovery of a seniority isomer in Pd-128, of which cascade gamma decay gives the energy of 1^{st} excited state and robustness of N=82 magic number.

Beta-delayed neutron emission probability of medium and heavy neutron-rich nuclei is important to understand nuclear structure and the r-process path. In 2013, a new collaboration "BRIKEN" has been established to form a He-3 detector array. A present design of the

array has neutron efficiency as high as 70% up to 3 MeV. The array will be coupled with the AIDA silicon strip system. A construction proposal was approved at the PAC 2013 and two physics proposals have been approved at PAC 2014.

The CAITEN detector was successfully tested with fragments produced with a Ca-48 beam in 2010.

(3) Equation-of-state via heavy-ion central collisions

Equation-of-state in asymmetric nuclear matter is one of major subjects in physics of exotic nuclei. Pi-plus and pi-minus yields in central heavy ion collisions at the RIBF energy are considered as one of EOS sensitive observables at the RIBF energy. To observe charged pions, a TPC for the SAMURAI spectrometer is being constructed under an international collaboration "SπRIT". Construction proposal was submitted at the PAC 2012, and physics proposals were approved at the PAC 2012 and 2013. Physics runs are scheduled in 2016.

An international symposium "NuSYM" on nuclear symmetry energy was organized at RIKEN July 2010 to invite researchers in three sub-fields, nuclear structure, nuclear reaction and nuclear astrophysics, and to discuss nuclear symmetry energy together. Since then, the symposium series have been held every year and been useful to encourage theoretical works and to strengthen the collaboration.

(4) Nucleon correlation and cluster in nuclei

Nucleon correlation and cluster in nuclei are matters of central focus in a "beyond mean-field" picture. The relevant programs with in-beam gamma and missing-mass techniques are to depict nucleon condensations and correlations in nuclear media as a function of density as well as temperature. Neutron-halo and –skin nuclei are objects to study dilute neutron matter at the surface. By changing excitation energies in neutron-rich nuclei, clustering phenomena and role of neutrons are to be investigated.

In 2013, two programs were conducted at the SAMURAI spectrometer. One is related to proton-neutron correlation in the C-12 nucleus via p-n knockout reaction with a carbon target. The other is to search for a cluster state in C-16, which was populated via inelastic alpha scattering. The data is being analyzed.

(5) Nuclear data for nuclear waste of long-lived fission products

The nuclear waste problem is an inevitable subject in nuclear physics and nuclear engineering communities. Since the Chicago Pile was established in 1942, nuclear energy has become one of major sources of energy. However, nowadays the nuclear waste produced at nuclear power plants has caused social problems. Minor actinide components of the waste have been studied well as a fuel in fast breeder reactors or ADS. Long-lived fission products in waste, on the other hand, have not been studied extensively. A deep geological disposal has been a policy of several governments, but it is difficult to find out location of the disposal station in terms of security, sociology and politics. To solve the social problem, a scientific effort is necessary for nuclear physics community to find out efficient methods for reduction of nuclear waste radioactivity.

In 2013, we have started up a new project to take nuclear data for transmutation of long-lived fission products to obtain cross section data needed for designing a nuclear waste treatment system. In 2014, we made the first attempt to obtain fragmentation reaction data with Cs-137 and Sr-90 beams at 200A MeV.

Since 2014, this activity has been intensively organized as one of the ImPACT projects by the Nuclear Transmutation Data Research Group.

Members

Chief Scientist (Lab. Head)

Hiroyoshi SAKURAI (Deputy Director,RNC)

Vice Chief Scientist

Takashi ICHIHARA

Research & Technical Scientists

Yoichi NAKAI (Senior Research Scientist)
Takashi KISHIDA (Senior Research Scientist)
Shunji NISHIMURA (Senior Research Scientist)
Hideaki OTSU (Senior Research Scientist)
Tadaaki ISOBE (Research Scientist)
Hiu Ching LEE (Research Scientist)
Pieter Christiaan DOORNENBAL (Research Scientist)

Contract Researchers

Satoshi TAKEUCHI
Mizuki NISHIMURA

Postdoctoral Researchers

He WANG
Paer-Anders SOEDERSTROEM (– Jan. 31, 2014)

Foreign Postdoctoral Researchers

Giuseppe LORUSSO (– Dec. 31, 2014)
Paer-Anders SOEDERSTROEM

Research Associate

Mizuki NISHIMURA (– Mar. 31, 2014)

Research Consultants

Masayasu ISHIHARA
Hiroyuki MURAKAMI

Consultant
Takeaki TORII (– May 2014)

International Program Associates
Xiaofei YANG (Peking Univ.)
Hongna LIU (Peking Univ.)
Jin WU (Peking Univ.)
William Barry POWELL (Univ. of Liverpool)
Sidong CHEN (Peking Univ.)

Junior Research Associates
Shintaro GO (Univ. of Tokyo)
Yoshiaki SHIGA (Rikkyo Univ.)
Noritsugu NAKATSUKA (Kyoto Univ.)
Keishi MATSUI (Univ. of Tokyo)

Part-time Worker
Zhengyu XU (Univ. of Tokyo, – Mar. 31, 2014)

Visiting Researchers
Gabor KISS (JSPS)
David STEPPENBECK (JSPS)
Ann-Kathrin PERREVOORT (DFG/JSPS)

Senior Visiting Scientists
Kengo OGAWA (Chiba Univ.)
Shigeru KUBONO (Univ. of Tokyo)

Visiting Scientists
Toshiyuki SUMIKAMA (Tohoku Univ.)
Hooi Jing ONG (RCNP)
Megumi NIIKURA (Univ. of Tokyo)
Silivio CHERUBINI (Univ. of Catania)
Hyo Soon JUNG (Univ. of Notre Dame)
Daiki NISHIMURA (Tokyo Univ. of Sci.)
Nobuyuki KOBAYASHI (Univ. of Tokyo)
Naohiko OTSUKA (Intl. Atomic Energy Agency, Austria)
Giuseppe LORUSSO (National Physics Lab., UK)
Hiu Ching LEE (Univ. of Hong Kong)
Zhengyu XU (Univ. of Hong Kong)
Indranil MAZUMDAR (GSI)
Alessia Pietro DI (INFN Catania)
Pierpaolo FIGUERA (INFN Catania)
Byungsik HONG (Korea Univ.)
Prabhakar PALNI (MSU)
Rebecca SHANE (MSU)
Alan MCINTOSH (Texas A & M Univ.)
Michael YOUNG (Texas A & M Univ.)
Thomas DAVINSON (Univ. of Edinburgh)
Yassid AYYAD (Osaka Univ.)
Kathrin WIMMER (Univ. of Tokyo)
Tetsuya MURAKAMI (Kyoto Univ.)
Kazuo IEKI (Rikkyo Univ.)
Mitsunori FUKUDA (Osaka Univ.)
Nori AOI (RCNP)
Le Hong KHIEM (Vietnam Academy of Sci. and Tech.)
Evgueni NIKOLSKI (RRC Kurchatov Inst.)
Alexey OGLOBLIN (RRC Kurchatov Inst.)
Hiroshi WATANABE (Beihang Univ.)

Visiting Technicians
Ivan KOJOUHAROV (GSI)

Student Trainees
Kenta YOSHINAGA (Tokyo Univ. of Sci.)
Masayuki NAGASHIMA (Niigata Univ.)
Jongwon HWANG (Seoul Nat'l Univ.)
Sunji KIM (Seoul Nat'l Univ.)
Zhengyu XU (Tokyo Univ.)
Yosuke MITSUYA (Meiji Univ.)
Yusuke MORITA (Osaka Univ.)
Junichi OHNO (Osaka Univ.)
Yasuto KAMISHOU (Osaka Univ.)
Hiroki NISHIBATA (Osaka Univ.)
Yifan ZHU (Tokyo Univ. of Sci.)
Hisaya HOTAKA (Tohoku Univ.)
Kotomi MUTO (Tohoku Univ.)
Tetsuya YAMAMOTO (Osaka Univ.)
Noritsugu NAKATSUKA (Kyoto Univ.)
Ayumi YAGI (Osaka Univ.)
Kazuma KOBAYASHI (Rikkyo Univ.)
Ryo TANIUCHI (Univ. of Tokyo)
Tomomi FUJITA (Osaka Univ.)
Takamasa YOSHIDA (Rikkyo Univ.)
Takumi USUKURA (Rikkyo Univ.)
Shunpei KINNO (Tokyo Univ. of Sci.)
Daisuke WATANABE (Univ. of Tsukuba)
Yifan FANG (Osaka Univ.)
Jin-hee CHANG (Korea Univ.)
Tomoki ISHIGAKI (Osaka Univ.)
Rie DAIDO (Osaka Univ.)
Shouta MORIMOTO (Osaka Univ.)
Keisuke TASHIRO (Niigata Univ.)
Akira HOMMA (Niigata Univ.)
Daiki MUROOKA (Niigata Univ.)
Akihiro KOJIMA (Tohoku Univ.)
Tadashi TAKO (Tohoku Univ.)
Ippei NISHIZUKA (Tohoku Univ.)
Takuya MIYAZAKI (Univ. of Tokyo)
Satoru MOMIYAMA (Univ. of Tokyo)
Mana TANAKA (Osaka Univ.)
Shintaro YAMAOKA (Osaka Univ.)
Kouta WATANABE (Osaka Univ.)
Justin Brian ESTEE (MSU)
Masanori KANEKO (Kyoto Univ.)
Hideyuki MATSUZAWA (Rikkyo Univ.)
Schrock PHILIPP (TU Darmstadt)
Hirotaka SUZUKI (Osaka Univ.)
Suwat TANGWANCHAROEN (MSU)
JungWoo LEE (Korea Univ.)
Takashi ANDO (Univ. of Tokyo)
Shunpei KOYAMA (Univ. of Tokyo)
Yuki YAMAGUCHI (Rikkyo Univ.)
Hiroyasu NAGAKURA (Rikkyo Univ.)

Hang DU (Osaka Univ.)
Yutaro TANAKA (Osaka Univ.)
Jiro SHIMAYA (Osaka Univ.)
Jonathan BARNEY (MSU)
Hiroyuki OIKAWA (Tokyo Univ. of Sci.)
Yoshimasa TAGUCHI (Tokyo Univ. of Sci.)
Naoya KAMBARA (Tokyo Univ. of Sci.)
Toshiki YOSHINOBU (Tokyo Univ. of Sci.)
Atsushi MIZUKAMI (Tokyo Univ. of Sci.)
Yuki KANKE (Tokyo Univ. of Sci.)
Junya NAGUMO (Tokyo Univ. of Sci.)
Matthew CHAPMAN (Texas A&M Univ.)
Rensheng WANG (Tsinghua Univ.)
Phong VI (Hanoi Univ. of Sci.)
Jiajian LIU (Univ. of Hong Kong)
Joachim TSCHEUSCHNER (TU Darmstadt)
Shinnosuke YOSHIDA (Osaka Univ.)
Hiroshi KANAOKA (Osaka Univ.)
Shoichiro MASUOKA (Rikkyo Univ.)
Yan ZHANG (Tsinghua Univ.)

Interns

Ilias AROUEL (Universite Paris Sud XI)
Yuito AWATAGUCHI (Tokyo Met. College of Ind. Tech.)
Jonathan BARNEY (MSU)

RIBF Research Division
Spin isospin Laboratory

1. Abstract

The Spin Isospin Laboratory pursues research activities putting primary focus on interplay of spin and isospin in exotic nuclei. Investigations on isospin dependences of nuclear equation of state, spin-isospin responses of exotic nuclei, occurrence of various correlations at low-densities, evolution of spin-orbit coupling are main subjects along the line. One of our goals is to elucidate a variety of nuclear phenomena in terms of interplay of spin and isospin.

Establishment of storage-ring science in Japan is another big goal of our laboratory. We are leading, in collaboration with the Wakasugi group, the Rare RI Ring project to achieve precision mass measurement of r-process nuclei.

2. Major Research Subjects

(1) Direct reaction studies of neutron-matter equation of state
(2) Study of spin-isospin responses with RI-beams
(3) Production of spin polarized protons and its application to RI-beam experiments
(4) R-process nucleosynthesis study with heavy-ion storage ring
(5) Development of special targets for RI-beam experiments

3. Summary of Research Activity

(1) Direct reaction studies of neutron matter equation of state

Direct reactions induced by light-ions serve as powerful tools to investigate various aspects of nuclei. We are advancing experimental programs to explore equation of state of neutron matter, via light-ion induced reactions with RI-beams.

(1-a) Determination of a neutron skin thickness by proton elastic scattering

A neutron skin thickness is known to have strong relevance to asymmetry terms of nuclear equation of state, especially to a term proportional to density. The ESPRI project aims at determining density distributions in exotic nuclei precisely by proton elastic scattering at 200−300 MeV/nucleon. An experiment for ^{132}Sn that is a flagship in this project is planned to be performed in 2015. Prior to the ^{132}Sn experiment, we have applied the ESPRI setup that consists of a solid hydrogen target and recoil proton detectors to ^{16}C in 2012.

(1-b) Asymmetry terms in nuclear incompressibility

Nuclear incompressibility represents stiffness of nuclear matter. Incompressibility of symmetric nuclear matter is determined to be 230±20 MeV, but its isospin dependence still has a large uncertainty at present. A direct approach to the incompressibility of asymmetric nuclear matter is an experimental determination of energies of isoscalar giant monopole resonances (GMR) in heavy nuclei. We have developed, in close collaboration with Center for Nuclear Study (CNS) of University of Tokyo, an active gas target for deuteron inelastic scattering experiments to determine GMR energies. The active gas target has been already tested with oxygen and xenon beams at HIMAC and will be applied to a ^{132}Sn experiment in 2015.

(1-c) Multi-neutron andα-cluster correlations at low densities

Occurrences of multi-neutron andα-cluster correlations are other interesting aspects of nuclear matter and define its low-density behavior. The multi-neutron andα-cluster correlations can be investigated with the large-acceptance SAMURAI spectrometer. The SAMURAI has been already applied to experiments to explore light neutron-rich nuclei close to the dripline. We plan to reinforce experimental capabilities of the SAMURAI by introducing advanced devices such as MINOS (Saclay) and NeuLAND (GSI).

(1-d) Fission barrier heights in neutron-rich heavy nuclei

The symmetry energy has a strong influence on fission barrier heights in neutron-rich nuclei. Knowledge on the fission barrier heights, which is quite poor at present, is quite important for our proper understanding on termination of the r-process. We are planning to perform, in collaboration with the TU Munich group, (p,2p)-delayed fission experiments at the SAMURAI to determine the fission barrier heights in neutron-rich nuclei in Pb region.

(2) Study of spin-isospin responses with RI-beams

The study of spin-isospin responses in nuclei forms one of the important cores of nuclear physics. A variety of collective states, for example isovector giant dipole resonances, isobaric analogue states, Gamow-Teller resonances, have been extensively studied by use of electromagnetic and hadronic reactions from stable targets.

The research opportunities can be largely enhanced with light of availabilities of radioactive isotope (RI) beams and of physics of unstable nuclei. There are three possible directions to proceed. The first direction is studies of spin-isospin responses of unstable nuclei via inverse-kinematics charge exchange reactions. A neutron-detector array WINDS has been constructed, under a collaboration of CNS, Tokyo and RIKEN, for inverse kinematics (p,n) experiments at the RI Beam Factory. We have already applied WINDS to the (p,n) experiments for ^{12}Be, ^{132}Sn and plan to extend this kind of study to other exotic nuclei.

The second direction is studies with RI-beam induced charge exchange reaction. RI-beam induced reactions have unique properties which are missing in stable-beam induced reactions and can be used to reach the yet-to-be-discovered states. We have constructed the SHARAQ spectrometer and the high-resolution beam-line at the RI Beam Factory to pursue the capabilities of RI-beam induced reactions as new probes to nuclei. One of the highlights is an observation of β^+ type isovector spin monopole resonances (IVSMR) in ^{208}Pb and ^{90}Zr via the (t, ^{3}He) reaction at 300 MeV/nucleon.

The third direction is studies of neutron- and proton-rich nuclei via stable-beam induced charge exchange reactions, which is conducted under collaboration with Research Center for Nuclear Physics (RCNP), Osaka University. We have performed the double charge exchange ^{12}C(^{18}O, ^{18}Ne)^{12}Be reaction at 80 MeV/nucleon to investigate structure of a neutron-rich ^{12}Be nucleus. Peaks corresponding to

ground and excited levels in ^{12}Be have been clearly observed.

(3) Production of spin-polarized protons and its application to RI-beam experiments

Recent experimental and theoretical studies have revealed that spin degrees of freedom play a vital role in exotic nuclei. Tensor force effects on the evolution of shell and possible occurrence of p-n pairing in the proton-rich region are good examples of manifestations of spin degrees of freedom.

In exploring the spin effects in exotic nuclei, scattering with polarized protons should be a powerful tool. We have constructed a novel polarized proton solid target aiming to shed light of polarization on the physics of exotic nuclei. A distinguished feature of the target system is that it works under a low magnetic field of 0.1 T and temperature higher than 100 K, which exhibits a striking contrast to standard DNP targets working in extreme conditions of several Tesla and sub-Kelvin. It should be noted that we have recently achieved a proton polarization of 40% at room temperature in a pentacene-d_{14} doped p-terphenyl crystal.

The polarized proton target was applied, for the first time, to measurement of vector analyzing power in the proton elastic scattering of neutron-rich ^{6,8}He nuclei at 71 MeV/nucleon at RIPS, RIKEN. At RI Beam Factory, a hole-state spectroscopy via the (p, 2p) knockout reaction from unstable oxygen isotopes was performed with the polarized target.

(4) R-process nucleosynthesis study with heavy-ion storage ring

Most of the r-process nuclei become within reach of experimental studies for the first time at RI Beam Factory at RIKEN. The Rare RI Ring at RIBF is the unique facility with which we can perform mass measurements of r-process nuclei. Construction of the Rare RI Ring started in FY2012 in collaboration with Tsukuba and Saitama Universities. A major part of the ring has been completed and the commissioning run is planned in FY2014.

We are planning to start precise mass measurements of r-process nuclei in 2015. A series of experiments will start with nuclei in the A=80 region and will be extended to heavier region.

(5) Development of special targets for RI-beam experiments

For the research activities shown above, we are developing and hosting special targets for RI-beam experiments listed below:

a) Polarized proton target
b) Thin solid hydrogen target
c) MINOS (developed at Saclay and hosted by the Spin Isospin Laboratory)

Members

Chief Scientist (Lab. Head)

Tomohiro UESAKA

Research & Technical Scientists

Ken-ichiro YONEDA (Senior Research Scientist, concurrent ; Team Leader, User Support Office)
Masaki SASANO (Research Scientist)
Juzo ZENIHIRO (Research Scientist)
Sarah NAIMI (Research Scientist, Apr. 1, 2014 –)

Contract Researcher

Daisuke NAGAE (Jan. 1, 2015 –)

Special Postdoctoral Researchers

Masami SAKO
Yuma KIKUCHI

Postdoctoral Researchers

Masanori DOZONO (– Mar. 31, 2014)
Kenichiro TATEISHI (Apr. 1, 2014 –)
Valerii PANIN

Research Associate

Kenichiro TATEISHI (– Mar. 31, 2014)

Junior Research Associates

CheongSoo LEE (Univ. of Tokyo)
Fumi SUZAKI (Saitama Univ.)
Keiichi KISAMORI (Univ. of Tokyo)
Yuki KUBOTA (Univ. of Tokyo)

International Program Associates

Zhengyang TIAN (Peking Univ., Apr. 15, 2014 – Oct. 14, 2014)
Chao WEN (Peking Univ.)
Sergey CHEBOTARYOV (Kyungpook Nat'l Univ.)
Evgeniy Vladimirovich MILMAN (Kyungpook Nat'l Univ.)
Clementine Angelique Marie SANTAMARIA (Univ. Paris Sud XI, – Sep. 30, 2014)
Sebastian Benedict REICHERT (TUM, Aug. 1, 2014 – Nov 10, 2014)
Dahee KIM (Ewha Womans Univ., Oct. 1, 2014 –)

Part-time Worker

Tomomi KAWAHARA (– Jul. 31, 2014)

Research Consultant

Harutaka SAKAGUCHI

Visiting Researchers

Alexandre OBERTELLI (CEA Saclay, – May 1, 2014)
Dennis MUECHER (JSPS Fellow, Apr. 1, 2014 – Jun. 6, 2014)
Stuhl LASZLO (JSPS Fellow, Apr. 15, 2014 –)

Senior Visiting Scientists

Didier BEAUMEL (IPN)
Hiroyuki SAGAWA (Aizu Univ.)

Visiting Scientists

Didier BEAUMEL (IPN)
Yosuke KONDO (Tokyo Tech.)
Elekes ZOLTAN (Atomki)
Hidetoshi AKIMUNE (Konan Univ.)
Yohei MATSUDA (Osaka Univ.)
Yasuhiro TOGANO (Tokyo Tech.)
Satoshi SAKAGUCHI (Kyusyu Univ.)
Kenjiro MIKI (Osaka Univ.)
Valerie LAPOUX (CEA Saclay)
Alexandre OBERTELLI (CEA Saclay)
Alain GILLIBERT (CEA Saclay)
Emanuel POLLACCO (CEA Saclay)
Anna CORSI (CEA Saclay)
Dennis MUECHER (TUM)
Yury LITVINOV (GSI)
Yuhu ZHANG (CAS)
Igor GASPARIC (Ruder Boskovic Inst. Zagreb Croatia)
Hans Toshihide TOERNQVIST (TU Darmstadt)
Christoph CAESAR (GSI)
Haik SIMON (GSI)
Matthias HOLL (TU Darmstadt)
Takayuki YAMAGUCHI (Saitama Univ.)
Takashi NAKAMURA (Tokyo Tech.)
Atsushi TAMII (Osaka Univ.)
Attila KRASZNAHORKAY (ATOMKI)
Takashi WAKUI (Tohoku Univ.)
Kimiko SAKAGUCHI (Tohoku Univ.)

Visiting Technicians

Tomomi KAWAHARA (Toho Univ.)
Gilles AUTHELET (CEA Saclay)
Jean-Marc GHELLER (CEA Saclay)
Cedric PERON (CEA Saclay)
Jean-Yves ROUSSE (CEA Saclay)
Denis CALVET (CEA Saclay)
Alan PEYAUD (CEA Saclay)
Alain DELBART (CEA Saclay)
Frederic CHATEAU (CEA Saclay)
Caroline LAHONDE-HAMDOUN (CEA Saclay)
Arnaud GIGANON (CEA Saclay)
Daniel KOERPER (GSI)

Student Trainees

Shota FUKUOKA (Univ. of Tsukuba)
Zhengyang TIAN (Peking Univ.)
Ryogo MINAKATA (Tokyo Tech.)
Yasunori WADA (Tohoku Univ.)
Takahiro TAGUCHI (Tohoku Univ.)
Shun OGOSHI (Tokyo Tech.)
Tatsuya FURUNO (Kyoto Univ.)
Tatsuo BABA (Kyoto Univ.)
Miho TSUMURA (Kyoto Univ.)
Jumpei YASUDA (Kyushu Univ.)
Taku FUKUNAGA (Kyushu Univ.)
Naruki INABA (Univ. of Tsukuba)
Yuuta SHIOKAWA (Tohoku Univ.)
Shuhei GOTANDA (Univ. of Miyazaki)
Yoshihisa KANAYA (Univ. of Miyazaki)
Junpei KOUNO (Saitama Univ.)
Satoshi MATSUNAGA (Saitama Univ.)
Yuki ISHII (Kyoto Univ.)
Mizuki SHIKATA (Tokyo Tech.)
Junichi TSUBOTA (Tokyo Tech.)
Miduki ONO (Saitama Univ.)
Chihiro SHIMURA (Saitama Univ.)
Yuuki TAKEUCHI (Saitama Univ.)
Syunichirou OHMIKA (Saitama Univ.)
Hiroshi MIURA (Saitama Univ.)
Takuma NISHIMURA (Saitama Univ.)
Motoki MURATA (Kyoto Univ.)
Kazuki SAWAHATA (Tokyo Tech.)
Clementine Angelique Marie SANTAMARIA (Univ.Paris Sud XI)
Syunsuke KAWAKAMI (Miyazaki Univ.)
Daijiro ETO (Tohoku Univ.)
Junki TANAKA (Osaka Univ.)
Sebastian Benedikt REICHERT (TU Munchen)
Tomoyuki OZAKI (Tokyo Tech.)
Atsumi SAITO (Tokyo Tech.)
Yasutaka NISHIO (Kyushu Univ.)
Yusuke SHINDO (Kyushu Univ.)
Munemi TABATA (Kyushu Univ.)
Atomu WATANABE (Tohoku Univ.)
Ayaka OHKURA (Kyushu Univ.)
Yukina ICHIKAWA (Univ. of Tsukuba)
Xiangcheng CHEN (Univ. of Heidelberg)
Kotaro YAMADA (Toho Univ.)
Tomoaki KANEKO (Toho Univ.)
Julian KAHLBOW (TU Darmstadt)
Robert KISSEL (TU Darmstadt)
Gregor DENTINGER (TU Darmstadt)
Taras LOKOTKO (Univ. of Hong Kong)

Interns

Raphael SAISEAU (Univ. Paris Sud XI)
Zhuang GE (IMP, CAS)
Lily SIEGENBERG (Univ. of Surrey)

Assistants

Emiko ISOGAI
Yu NAYA
Yuri TSUBURAI

RIBF Research Division
Nuclear Spectroscopy Laboratory

1. Abstract

The research group has conducted nuclear-physics studies utilizing stopped/slowed-down radioactive-isotope (RI) beams mainly at the RIBF facility. These studies are based on the technique of nuclear spectroscopy such as β-ray-detected NMR, γ-PAD (Perturbed Angular Distribution), laser, and Mössbauer among other methods that takes advantage of intrinsic nuclear properties such as nuclear spins, electromagnetic moments, and decay modes. In particular, techniques and devices for the production of spin-controlled RI beams have been developed and combined to the spectroscopic studies, which enable high-sensitivity measurements of spin precessions/resonances through a change in the angular distribution of radiations. Anomalous nuclear structures and properties of far unstable nuclei are investigated from thus determined spin-related observables. The group also aim to apply such techniques to interdisciplinary fields such as fundamental physics and materials science by exploiting nuclear probes.

2. Major Research Subjects

(1) Nuclear spectroscopy with stopped/slowed-down RI beams
(2) R&D studies on the production of spin-oriented RI beam
(3) Application of RI probes
(4) Fundamental physics: Study of symmetry

3. Summary of Research Activity

(1) Nuclear spectroscopy with stopped/slowed-down RI beams

Measurements of static electromagnetic nuclear moments over a substantial region of the nuclear chart have been conducted for structure studies on the nuclei far from the β-decay stability. Utilizing nuclear spin orientation phenomena of RIs created in the projectile-fragmentation reaction, ground- and excited-state nuclear moments of nuclei far from the stability have been determined by means of the β-ray-detected nuclear magnetic resonance (β-NMR) and the γ-ray time differential perturbed angular distribution (γ-TDPAD) methods. To extend these observations to extremely rare RIs, a new method has been developed based on the laser spectroscopy which makes use of characteristic atomic properties of RIs surrounded by liquid helium.

(2) R&D studies on the production of spin-oriented RI beams

A new method has been developed for controlling spin in a system of rare RIs, taking advantage of the mechanism of the two-step projectile fragmentation reaction combined with the momentum-dispersion matching technique. This success allows us to utilize spin-controlled world's highest intensity rare RIBs delivered from BigRIPS for researches on the nuclear structure of species situated outside the traditional region of the nuclear chart. In parallel with this work, the development of a new apparatus to produce highly spin-polarized RI beams will be conducted by extending the atomic beam resonance method to fragmentation-based RI beams.

(3) Application of RI probes

The application of RI and heavy ion beams as a probe for condensed matter studies is also conducted by the group. The microscopic material dynamics and properties have been investigated through the deduced internal local fields and the spin relaxation of RI probes based on various spectroscopies utilizing RI probes such as the β-NMR/nuclear quadrupole resonance (NQR) methods, in-beam Mössbauer spectroscopy and the γ-ray time differential perturbed angular correlation (γ-TDPAC) spectroscopy.

(4) Fundamental physics: Study of symmetry

The nuclear spins of stable and unstable isotopes sometimes play important roles in fundamental physics research. New experimental methods and devices have been developed for studies of the violation of time reversal symmetry (*T*-violation) using spin-polarized nuclei. These experiments aim to detect the small frequency shift in the spin precession arising from new mechanisms beyond the Standard Model.

Members

Chief Scientist (Lab. Head)
Hideki UENO

Research & Technical Scientists
Aiko NAKAO (Senior Research Scientist)
Yuichi ICHIKAWA (Research Scientist)
Hiroki YAMAZAKI (Senior Research Scientist)

Research Consultant
Takuya OKADA

Junior Research Associates
Yoko ISHIBASHI (Univ. of Tsukuba, – Mar. 31, 2014)
Kei IMAMURA (Meiji Univ.)

Yuichi OHTOMO (TIT, – Feb. 28, 2015)

Part-time Worker

Yoko ISHIBASHI (Univ. of Tsukuba, Sep. 1, 2014 –)

Senior Visiting Scientist

Yukari MATSUO (Hosei Univ.)

Visiting Scientists

Wataru SATO (Kanazawa Univ.)
Kensaku MATSUTA (Osaka Univ.)
Jin NAKAMURA (Univ. of Elec.-Com.)
Atsushi HATAKEYAMA (Tokyo Univ. of Agric. and Tech.)
Takeshi FURUKAWA (Tokyo Met. Univ.)
Satoshi TSUTSUI (JASRI)
Takamasa MOMOSE (Kyoto Univ.)
Jean-Michel DAUGAS (CEA)
Xiaolong WANG (Kyoto Univ.)
Yoshio KOBAYASHI (Univ. of Elec.-Com.)
Jiro MURATA (Rikkyo Univ.)
Koichiro ASAHI (TIT)
Jun MIYAZAKI (Tokyo Univ. of Agric. and Tech.)
Yasuhiro YAMADA (Tokyo Univ. of Sci.)
Kenya KUBO (ICU)
Akihiro YOSHIMI (Okayama Univ.)
Yukari MATSUO (Hosei Univ.)
Yasuaki EINAGA (Keio Univ.)

Student Trainees

Yoko ISHIBASHI (Univ. of Tsukuba)
Masato TSUCHIYA (Tokyo Tech.)
Hazuki SHIRAI (Tokyo Tech.)
Miki HAYASAKA (Tokyo Gakugei Univ.)
Ryo MIYATANI (Tokyo Univ. of Sci.)
Kazuma SHIGA (Tokyo Univ. of Sci.)
Tomomi FUJITA (Osaka Univ.)
Yuichi OHTOMO (Tokyo Tech)
Takahiro SUZUKI (Tokyo Tech)
Masaomi TANAKA (Osaka Univ.)
Ryosuke KANBE (Osaka Univ.)
Yu SAKAMOTO (Tokyo Tech)
Yukiko SATO (Univ. of Elec.-Com.)
Shotaro TANIGAWA (Univ. of Elec.-Com.)
Daiki NATORI (Univ. of Elec.-Com.)
Kenichi TANABE (Tokyo Univ. of Sci.)
Miho SATO (Tokyo Univ. of Sci.)
Takafumi TABATA (Tokyo Univ. of Sci.)
Tsubasa SAGAYAMA (Tokyo Gakugei Univ.)
Shota KISHI (Tokyo Gakugei Univ.)
Yuki KANNO (Tokyo Tech.)
Shuichiro KOJIMA (Tokyo Tech.)
Tomoya SATO (Tokyo Tech.)
Aleksey GLADKOV (Kyungpook Nat'l Univ.)
Yonggeun SEON (Kyungpook Nat'l Univ.)
Daiki TOMINAGA (Hosei Univ.)
Syouhei OOSIRO (Tokyo Gakugei Univ.)
Miku MATSUMOTO (Tokyo Gakugei Univ.)
Ryo OGAWA (Univ. of Elec.-Com.)
Yusuke HAMABE (Univ. of Elec.-Com.)
Ippei KUBONO (Tokyo Univ. of Sci.)
Shota AMAGASA (Tokyo Univ. of Sci.)
Chikako FUNAYAMA (Tokyo Tech)
Chika HIRAO (Tokyo Tech)
Taro KOMINE (Tokyo Tech)
Tsuyoshi EGAMI (Hosei Univ.)
Takafumi KAWAGUCHI (Hosei Univ.)

Interns

ZheWei YIN (Peking Univ.)
Hoi Io KONG (Peking Univ.)
Jing MA (Peking Univ.)
Zong Hao LI (Peking Univ.)
Bo WANG (Peking Univ.)
Hyunsuk CHOI (Seoul Nat'l Univ.)
Hangil CHOI (Seoul Nat'l Univ.)
Sangbaek LEE (Seoul Nat'l Univ.)
Honggi JEON (Seoul Nat'l Univ.)
Hakrim KIM (Seoul Nat'l Univ.)

RIBF Research Division
High Energy Astrophysics Laboratory

1. Abstract

In the immediate aftermath of the Big Bang, the beginning of our universe, only hydrogen and helium existed. However, nuclear fusion in the interior of stars and the explosion of supernovae in the universe over the course of 13.8 billion years led to the evolution of a world brimming with the many different elements we have today. By using man-made satellites to observe X-rays and gamma-rays emitted from celestial objects, we are observing the synthesis of the elements at their actual source. Our goal is to comprehensively elucidate the scenarios for the formation of the elements in the universe, together with our research on sub-atomic physics through the use of an accelerator.

2. Major Research Subjects

(1) Nucleosynthesis in Stars and Supernovae
(2) Particle Acceleration Mechanism in Astronomical Objects
(3) Physics in Extremely Strong Magnetism and Gravity
(4) Research and Development of Innovative X-ray and Gamma-ray detectors

3. Summary of Research Activity

High Energy Astrophysics Laboratory started on April 2010. The goal of our research is to reveal the mechanism of nucleosynthesis in the universe, and to observe exotic physical phenomena in extremely strong magnetic and/or gravitational field. We have observed supernova remnants, strongly magnetized neutron stars, pulsars, black holes and galaxies with X-ray astronomical satellites.

We showed that the expansion of ejecta in Tycho's supernova remnant was consistent with a spherically symmetric shell, based on Suzaku (Japanese X-ray observatory) measurements of the Doppler broadened X-ray emission lines. This is the first direct measurement of the expansion velocity of the elements produced in the thermonuclear expansion supernova. This information tells us the stratified structure of the elements, implying that the heavier elements such as Fe are produced deeper interior of the explosion.

We discovered the emission line of aluminum in supernova remnant G344.7-0.1 for the first time. Aluminum is produced in the neutron rich environment of supernova explosions. We also found manganese, which is enriched in the environment of neutron excess, in some supernova remnants. A systematic study of those lines emitted from the neutron rich elements will be a good tool to explore the nucleosynthesis in the interior of star explosions.

High-energy X-rays from radioactive Ti-44, which is a direct tracer of the supernova blast, was first imaged with the focusing telescope, NuSTAR. The map of Ti-44 in Cassiopeia A does not show spherical or axial symmetry, but asymmetry, supporting a mildly asymmetric explosion model with low-mode convection. This is the first astronomical image with nuclear gamma-rays and new observational evidence to understand the mechanism of supernova explosion and nucleosynthesis.

Gamma-ray emission up to 10 MeV was detected from thundercloud, suggesting that the detected gamma-rays were produced by relativistic electrons via bremsstrahlung. Those relativistic electrons are probably accelerated through an electrical potential difference in the thundercloud. This observation gives us a hint of the particle acceleration probably occurred near the neutron stars.

We continue to construct the Gravity and Extreme Magnetism Small Explorer (GEMS) under the collaboration with NASA Goddard Space Flight Center (USA). GEMS is the first dedicated satellite for the X-ray polarimetry, which is opening a new field in Astrophysics and Astronomy. The construction of an engineering model and basic performance studies of an X-ray polarimeter were carried out in FY2010, and the semiflight model of the detector was built in FY2012 and tested in FY2013. Unfortunately, NASA stops the GEMS project due to an expected cost overrun in 2012, but we will repropose the mission in 2014 with some modification. RIKEN will become a co-principal investigator institute and takes more responsibility on the X-ray polarimeter system and science.

Members

Associate Chief Scientist (Lab. Head)
Toru TAMAGAWA

Contract Researcher
Goro SATO (– Mar. 31, 2014)
Yuki OKURA (Jun. 1, 2014 –)

Special Postdoctoral Researchers
Asami HAYATO
Satoru KATSUDA (– Mar. 31, 2014)
Shin'ya YAMADA (– Mar. 31, 2014)
Kumi ISHIKAWA
Hirofumi NODA (Apr. 1, 2014 –)
Takayuki YUASA (Apr. 1, 2014 –)

Postdoctoral Researcher
Takao KITAGUCHI

Part-time Workers
Fumi ASAMI (– Jul. 31, 2014)
Rie YOSHII

Megu KUBOTA
Shigeru ENDO (– Feb. 28, 2014)

Visiting Researchers

Wataru IWAKIRI (JSPS Fellow, Saitama Univ.)
Teruaki ENOTO (JSPS Fellow, Stanford Univ.)

Visiting Scientists

Yukikatsu TERADA (Saitama Univ.)
Yujin NAKAGAWA (Waseda Univ.)
Masaki WAKABAYASHI (Jakulin Commercial Company LC)
Aya BAMBA (JAXA)
Naohisa INADA (Univ. of Tokyo)
Rohta TAKAHASHI (Tomakomai Nat'l College of Tech.)
Toru MISAWA (Shinshu Univ.)
Hiroya YAMAGUCHI (Harvard Univ.)
Satoru KATSUDA (JAXA)
Shin'ya YAMADA (Tokyo Met. Univ.)
Takao KITAGUCHI (Hiroshima Univ.)
Harufumi TSUCHIYA (JAEA)

Student Trainees

Rie YOSHII (Tokyo Univ. of Sci.)
Fumi ASAMI (Tokyo Univ. of Sci.)
Akifumi YOSHIKAWA (Tokyo Univ. of Sci.)
Yoko TAKEUCHI (Tokyo Univ. of Sci.)
Kenta KANEKO (Kogakuin Univ.)
Megu KUBOTA (Tokyo Univ. of Sci.)
Kazuki NISHIDA (Tokyo Univ. of Sci.)

RIBF Research Division
Astro-Glaciology Research Unit

Our Astro-Glaciology Research Unit promotes both theoretical and experimental studies to open up a new interdisciplinary research field between astrophysics and glaciology. On the theoretical side, we numerically simulate:

(1) Changes in the chemical composition of the stratosphere induced by high-energy photons and/or particles emitted from explosive astronomical phenomena, such as solar proton events and galactic supernovae, and

(2) The explosive nucleosynthesis, including the rapid neutron capture process (the r-process) for the creation of the elements heavier than iron, arising in the environment of core-collapse supernova explosions.

Subjects (1) and (2) themselves are very important in solar–terrestrial research and nuclear astrophysics, respectively; furthermore, the items (1) and (2) are intended to be coupled with experimental studies described below.

On the experimental side, we analyze ice cores drilled at the Dome Fuji station in Antarctica in collaboration with National Institute of Polar Research, Tokyo. These ice cores correspond to time capsules of the past. In particular, the ice cores obtained at Dome Fuji are known to be unique because they contain much more information on conditions in the stratosphere than any other ice cores recovered from other locations in either hemisphere. This means that the Dome Fuji ice cores may have an original advantage to study astronomical phenomena of the past, since gamma-rays and high-energy protons emitted from astronomical events affect the chemical and isotopic compositions in the stratosphere and not those in the troposphere. Accordingly, we measure:

(3) Variations in the nitrate ion (NO_3^-) concentrations in the ice cores, in order to seek the proxy of past solar activity and the footprints of supernovae in our galaxy,

(4) Variations in the water isotopes (^{18}O and ^{2}H) in the ice cores, in order to reconstruct past temperature changes on the earth, and

(5) Variations in the nitrate isotope (^{15}N) in the ice cores, in order to investigate the possibility of this isotope becoming a new and a more stable proxy for solar activity and/or galactic supernovae.

Items (3), (4), and (5) have been analyzed with Dome Fuji ice cores with a temporal resolution of about 1 year. By comparing the results for items (3) and (4), we aim to understand the correlation between solar activity and climate changes in the past on the millennium scale. The basis for item (4) is already established in glaciology. Item (5) will be the one of very first measurements taken in ice cores. The theoretical studies related to items (1) and (2) will provide a background for distinguishing the characteristics of the astronomical events from meteorological noise that usually appears in the ice core data. Finally, we note that the supernova rate in our galaxy is crucial to understand the r-process nucleosynthesis but yet remains unknown. Our item (3) is also intended to diagnose the galactic supernova rate ultimately.

Members

Research Unit Leader (Lab. Head)

Yuko MOTIZUKI

Research & Technical Scientists

Kazuya TAKAHASHI (Concurrent: Senior Research Scientist)
Yoichi NAKAI (Concurrent: Senior Research Scientist)

Postdoctoral Researcher

Sachiko OKAMOTO

Part-time Workers

Ai SHIMADA (TANEICHI) (– May 31, 2014)
Keiko FUKUSHIMA (WATANABE) (– Nov. 30, 2014)
Manami MARUYAMA
Yuma HASEBE (Saitama Univ., Nov. 1, 2014 –)

Visiting Scientists

Akira HORI (Kitami Inst. of Tech.)
Hideharu AKIYOSHI (Nat'l Inst. for Environ. Studies)
Hideki MADOKORO (Mitsubishi Heavy Ind., Ltd.)

Student Trainees

Yuma HASEBE (Saitama Univ.)

RIBF Research Division
Research Group for Superheavy Element

1. Abstract

The elements with their atomic number Z>103 are called as trans-actinide or superheavy elements. The chemical properties of those elements have not yet been studied in detail. Those elements do not exist in nature. Therefore, they must be produced by artificially for the scientific study of those elements. In our laboratory, we have been studying the physical and chemical properties of the superheavy elements utilizing the accelerators in RIKEN and various methods of efficient production of the superheavy elements.

2. Major Research Subjects

(1) Search for new superheavy elements
(2) Decay spectroscopy of the heaviest nuclei
(3) Study of the chemical properties of the heaviest elements
(4) Study of the reaction mechanism of the fusion process (theory)

3. Summary of Research Activity

(1) Searching for new elements

To expand the periodic table of elements and the nuclear chart, we will search for new elements.

(2) Spectroscopic study of the nucleus of heavy elements

Using the high sensitivity system for detecting the heaviest element, we plan to perform a spectroscopic study of nuclei of the heavy elements.

(3) Chemistry of superheavy elements

Study of chemistry of the trans-actinide (superheavy element) has just started world-wide, making it a new frontier in the field of chemistry. Relativistic effects in chemical property are predicted by many theoretical studies. We will try to develop this new field.

(4) Study of a reaction mechanism for fusion process

Superheavy elements have been produced by complete fusion reaction of two heavy nuclei. However, the reaction mechanism of the fusion process is still not well understood theoretically. When we design an experiment to synthesize nuclei of the superheavy elements, we need to determine a beam-target combination and the most appropriate reaction energy. This is when the theory becomes important. We will try to develop a reaction theory useful in designing an experiment by collaborating with the theorists.

(5) Research Highlight

The discovery of a new element is one of the exciting topics both for nuclear physicists and nuclear chemists. The elements with their atomic number Z>103 are called as trans-actinides or superheavy elements. The chemical properties of those elements have not yet been studied in detail. Since those elements do not exist in nature, they must be produced by artificially, by using nuclear reactions for the study of those elements. Because the production rate of atoms of those elements is extremely small, an efficient production and collection are key issues of the superheavy research. In our laboratory, we have been trying to produce new elements, studying the physical and chemical properties of the superheavy elements utilizing the accelerators in RIKEN.

Although the Research Group for Superheavy element has started at April 2013, the Group is a renewal of the Superheay Element Laboratory started at April 2006, based on a research group which belonged to the RIKEN accelerator research facility (RARF), and had studied the productions of the heaviest elements. The main experimental apparatus is a gas-filled recoil ion separator GARIS. The heaviest elements with their atomic numbers, 107 (Bohrium), 108 (Hassium), 109 (Meitnerium), 110 (Darmstadtium), 111 (Roentogenium), and 112 (not yet named) were discovered as new elements at Helmholtzzentrum für Schwerionenforschung GmbH (GSI), Germany by using ^{208}Pb or ^{209}Bi based complete fusion reactions, so called “cold fusion” reactions. We have made independent confirmations of the productions of isotopes of 108th, 110th, 111th, and 112th elements by using the same reactions performed at GSI. After these work, we observed an isotope of the 113th element, ^{278}113, in July 2004, in April, 2005, and in August 2012. The isotope, ^{278}113, has both the largest atomic number, (Z = 113) and atomic mass number (A = 278) which have determined experimentally among the isotopes which have been produced by cold fusion reactions. We could show the world highest sensitivity for production and detection of the superheavy elements by these observations.

We decided to make one more recoil separator GARIS-II, which has an acceptance twice as large as existing GARIS, in order to realize higher sensitivity. The design of GARIS-II has finished in 2008. All fabrication of the separator will be finished at the end of fiscal year 2008. It will be ready for operation in fiscal year 2009 after some commissioning works.

Preparatory work for the study of the chemical properties of the superheavy elements has started by using the gas-jet transport system coupled to GARIS. The experiment was quite successful. The background radioactivity of unwanted reaction products has been highly suppressed. Without using the recoil separator upstream the gas-jet transport system, large amount of unwanted radioactivity strongly prevents the unique identification of the event of our interest. This new technique makes clean and clear studies of chemistry of the heaviest elements promising.

The spectroscopic study of the heaviest elements has started by using alpha spectrometry. New isotope, ^{263}Hs (Z=108), which has the smallest atomic mass number ever observed among the Hassium isotopes, had discovered in the study. New spectroscopic information for ^{264}Hs and its daughters have obtained also. The spectroscopic study of Rutherfordium isotope ^{261}Rf (Z=104) has done and 1.9-s isomeric state has directly produced for the first time.

Preparatory works for the study of the new superheavy elements with atomic number 119 and 120 have started in 2013. We measured the reaction products of the ^{248}Cm(^{48}Ca, xn)$^{296-x}$Lv(Z=116) previously studied by Frelov Laboratory of Nuclear Reaction, Russia, and GSI.

We observed 5 isotopes in total which tentatively assigned to ^{293}Lv, and ^{292}Lv.

Members

Group Director
Kosuke MORITA

International Program Associate
Christian BERNER (TUM, Aug. 1, 2014 – Nov. 10, 2014)

Visiting Scientist
Kunihiro FUJITA (Kyushu Univ.)

Student Trainees
Shoya YAMAMOTO (Kyushu Univ.)
Taiki TANAKA (Kyushu Univ.)
Yoshihiro NARIKIYO (Kyushu Univ.)
Reii KAKU (Kyushu Univ.)

RIBF Research Division
Research Group for Superheavy Element
Superheavy Element Production Team

For this year, see the section of Research Group for Superheavy Element.

Members

Team Leader
Kosuke MORITA (concurrent; Group Director, Research Group for Superheavy Element)

Research & Technical Scientist
Kouji MORIMOTO (Senior Research Scientist, concurrent; Team Leader, Superheavy Element Device Development Team)

Nishina Center Technical Scientists
Akira YONEDA
Daiya KAJI (concurrent; Superheavy Element Device Development Team)

Special Postdoctoral Researcher
Yasuo WAKABAYASHI (Univ. of Tokyo)

Research Consultant
Kenji KATORI

Junior Research Associate
Mirei TAKEYAMA (Yamagata Univ.)

Part-time Worker
Kengo TANAKA (Tokyo Univ. of Sci.)

Visiting Scientists
Hiroyuki KOURA (JAEA)
Marc ASFARI (Institut Pluridisciplinaire Hubert Curien)
Benoit Jean-Paul GALL (Strasbourg Univ.)

Student Trainees
Yukiko KOMORI (Osaka Univ.)
Kengo TANAKA (Tokyo Univ. of Sci.)
Takuya YOKOKITA (Osaka Univ.)

RIBF Research Division
Research Group for Superheavy Element
Superheavy Element Research Device Development Team

1. Abstract

A gas-filled recoil ion separator has been used as a main experimental device for the study of superheavy elements. This team is in charge of maintain, improve, develop and operate the separators and rerated devices. There are two gas-filled recoil ion separators installed at RILAC experimental hall. One is GARIS that is designed for symmetric reaction such as cold-fusion reaction, and the other is newly developed GARIS-II that is designed for asymmetric reaction such as hot-fusion reaction. New element ^{278}113 were produced by ^{70}Zn + ^{209}Bi reaction using GARIS. Further the new element search Z > 118 are preparing by using GARIS-II.

2. Major Research Subjects

(1) Maintenance of GARIS and development of new gas-filled recoil ion separator GARIS-II.
(2) Maintenance and development of detector and DAQ system for GARIS and GARIS-II.
(3) Maintenance and development of target system for GARIS and GARIS-II.

3. Summary of Research Activity

The GARIS-II is newly developed which has an acceptance twice as large as existing GARIS, in order to realize higher sensitivity. It will be ready for operation in fiscal year 2014 after some commissioning works. We will also offer user-support if a researcher wishes to use the devices for his/her own research program.

Members

Team Leader
Kouji MORIMOTO

Nishina Center Research Scientist
Daiya KAJI

Nishina Center Technical Scientist
Akira YONEDA (concurrent; Superheavy Element Production Team)

Junior Research Associate
Sayaka YAMAKI (Saitama Univ., Apr. 1, 2014 –)

Part-time Worker
Sayaka YAMAKI (– Mar. 31, 2014)

Visiting Scientists
Fuyuki TOKANAI (Yamagata Univ.)
Sayaka YAMAKI (Saitama Univ.)

RIBF Research Division
Nuclear Transmutation Data Research Group

1. Abstract

The disposal of high-level radioactive wastes from nuclear power plants is a problem considered to be one of the most important issues at both national and international levels. As a fundamental solution to the problem, the establishment of nuclear transmutation technology where long-lived nuclides can be changed to short-lived or stable ones will be vital. Progress in R & D in the transmutation of long-lived fission products (LLFP) in the nuclear wastes however, has been slow. Our group aims to obtain reaction data of LLFP at RIBF and other facilities which may lead to a new discovery and invention for peaceful use of nuclear power and the welfare of humanity.

2. Major Research Subjects

The Group is formed by three research teams. The first two Teams, “Fast RI Data Team” and “Slow RI Data Team”, are in charge of proton- and deuteron-induced reaction data of LLFP in inverse kinematics at RIBF. The third Team “Muon Data Team” is to obtain muon capture data of LLFP at muon facilities. All of the teams are focusing to obtain high-quality data which are essentially necessary to establish reliable reaction models. Each team has its own subjects and promotes LLFP reaction programs based on their large experiences, techniques and skills.

3. Summary of Research Activity

In 2014, all the teams polished up experimental strategies, formed collaboration and prepared experiments.

Members

Group Director

Hiroyoshi SAKURAI (concurrent: Chief Scientist, RI Physics Lab.)

RIBF Research Division
Nuclear Transmutation Data Research Group
Fast RI Data Team

1. Abstract

Fast RI team aims at obtaining and accumulating the cross section data for long lived fission products (LLFPs) in order to explore the possibility of using accelerator for nuclear transmutation.

LLFPs as nuclear waste have been generated continuously in nuclear power plants for wealth for human lives, while people noticed the way of disposal has not necessarily been established, especially after the Fukushima Daiichi power plant disaster. One of the ways to reduce the amount of LLFP or to recover them as recycled resources is nuclear transmutation technique.

RIBF facility has a property to generate such LLFP as a secondary beam and the beam species are identified by event by event. Utilizing the property, absolute values of the cross section of various reactions on LLFPs are measured and accumulated as database.

2. Major Research Subjects

1) Measurement of reaction products by the interaction of LLFPs with proton, deuteron, and photon to explore candidate reactions for transmutation of LLFPs.
2) Evaluation of the cross section data for the neutron induced reactions from the obtained data.

3. Summary of Research Activity

1) Acting as collaboration hub on many groups which plan to take data using fast RI beam in RIBF facility.
2) Concentrating on take data for proton and deuteron induced spallation reactions with inverse kinematics.
3) Accumulating the cross section data and evaluating them as evaluated nuclear data.
4) Evaluating cross section of neutron induced reaction on LLFP by collaborating with the nuclear model calculation and evaluation group.

Members

Team Leader

Hideaki OTSU (Oct. 1, 2014−, concurrent: Team Leader, SAMURAI Team)

Technical Staff I

Nobuyuki CHIGA (Jan. 1, 2015−)

Student Trainees

Shouhei ARAKI (Kyushu Univ.)

Tatsuya YAMAMOTO (Miyazaki Univ.)

RIBF Research Division
Nuclear Transmutation Data Research Group
Slow RI Data Team

1. Abstract

This team is in charge of the development of low-energy RI beams of long-lived fission fragments (LLFP) from the ^{238}U by means of degrading the energy of beams produced by the BigRIPS fragment separator.

2. Major Research Subjects

Studies of the energy degradation and purification of RI beams are the main subjects of the team. Developments of devices used for the energy degradation of RI beams are also an important subject.

3. Summary of Research Activity

1) Study and development of the energy degradation methods for LLFP.
2) Development of the devices used for the energy degradation.
3) Operation of the BigRIPS separator and supply the low energy LLFP beam to the experiment in which the cross sections of LLFP are measured at the low energy.

Members

Team Leader

Koichi YOSHIDA (concurrent: BigRIPS Team)

RIBF Research Division
Nuclear Transmutation Data Research Group
Muon Data Team

1. Abstract

Dr. Yoshio Nishina observed muons in cosmic rays in 1937. The muon is an elementary particle belonging to electron group, and is 207 times as heavy as electron. The muon has positive or negative electric charge, and the lifetime is 2.2 μsec. The negative muon is caught by a nucleus (atomic number: Z) in materials to form a muonic atom, and is then captured by the nucleus. The negative muon is combined with a proton to form a neutron and a neutrino to create an excited state of the nucleus with the atomic number of Z-1, followed by emissions of neutrons and gamma rays. The muon nuclear capture reaction produces the isotopes of the (Z-1) nucleus. However, the reaction mechanism is not yet well clarified. The research team aims at obtaining the experimental data to understand the mechanism of muon nuclear capture reactions as well as at establishing the reaction theory.

2. Major Research Subjects

(1) Experimental clarification on reaction mechanism of nuclear muon-capture
(2) Establishment of reaction theory on nuclear muon-capture
(3) Interdisciplinary applications of nuclear muon-capture reactions

3. Summary of Research Activity

Members

Team Leader

Hiroyoshi SAKURAI (Oct. 1, 2014 – Nov. 30, 2014, concurrent: Chief Scientist, RI Physics Lab.)
Teiichiro MATSUZAKI (Dec. 1, 2014 –)

RIBF Research Division
High-Intensity Accelerator R&D Group

1. Abstract

The R&D group, consisting of two teams, develops elemental technology of high-power accelerators and high-power targets, aiming at future applications to nuclear transmutations of long-lived fission product into short-lived nuclides. The research subjects are superconducting rf cavities for low-velocity ions, design of high-power accelerators, high-power target systems and related technologies.

2. Major Research Subjects

(1) R&D of elemental technology of high-power accelerators and high-power targets

3. Summary of Research Activity

(1) Based on the discussion with other research groups, R&D study of various accelerator components and elements is under progress.

Members

Group Director

Osamu KAMIGAITO (concurrent: Chief Scientist, Group Director, Accelerator Gr.)

RIBF Research Division
High-Intensity Accelerator R&D Group
High-Gradient Cavity R&D Team

Members

Team Leader
Naruhiko SAKAMOTO (concurrent: Cyclotron Team)

Research & Technical Scientists
Kazunari YAMADA (Senior Technical Scientist, concurrent: Beam Dynamics & Diagnostics Team)
Kazutaka OHZEKI (Technical Scientist, concurrent: Cyclotron Team)

RIBF Research Division
High-Intensity Accelerator R&D Group
High-Power Target R&D Team

Members

Team Leader

Hiroki OKUNO (concurrent: Deputy Group Director, Accelerator Gr.)

RIBF Research Division
Accelerator Group

1. Abstract

The accelerator group, consisting of seven teams, pursues various upgrade programs of the world-leading heavy-ion accelerator facility, RI-Beam Factory (RIBF), to enhance the accelerator performance and operation efficiency. The programs include the R&D of superconducting ECR ion source, charge stripping systems, beam diagnostic devices, radiofrequency systems, control systems, and beam simulation studies. We are also maintaining the large infrastructure to realize effective operation of the RIBF, and are actively promoting the applications of the facility to a variety of research fields.

Our primary mission is to supply intense, stable heavy-ion beams for the users through effective operation, maintenance, and upgrade of the RIBF accelerators and related infrastructure. The director members shown below govern the development programs that are not dealt with by a single group, such as intensity upgrade and effective operation. We also promote the future plans of the RIBF accelerators along with other laboratories belonging to the RIBF research division.

2. Major Research Subjects

(1) Intensity upgrade of RIBF accelerators (Okuno)
(2) Effective and stable operation of RIBF accelerators (Fukunishi)
(3) Operation and maintenance of infrastructures for RIBF (Kase)
(4) Promotion of the future plan (Kamigaito, Fukunishi, Okuno)

3. Summary of Activity

(1) The maximum intensity of the calcium beam reached 530 pnA at 345 MeV/u, which corresponds to 8.8 kW.
(2) The maximum intensity of the uranium beam reached 28 pnA at 345 MeV/u.
(3) The overall beam availability for the RIBF experiments in 2014 reached 92 %.
(4) The large infrastructure was properly maintained based on a well-organized cooperation among the related sections.
(5) An intensity-upgrade plan of the RIBF has been further investigated, mainly on the design of a new superconducting linac.

Members

Group Director
Osamu KAMIGAITO

Deputy Group Directors
Hiroki OKUNO (Intensity upgrade)
Nobuhisa FUKUNISHI (Stable and efficient operation)
Masayuki KASE (Energy-efficiency management)

Research Consultant
Tadashi FUJINAWA (– Mar. 31, 2015)

International Program Associate
Vasileios TZOGANIS (Univ. of Liverpool)

Visiting Researchers
Akira GOTO (Yamagata Univ.)
Toshiyuki HATTORI (Tokyo Tech.)

Assistant
Karen SAKUMA

RIBF Research Division
Accelerator Group
Accelerator R&D Team

1. Abstract

We are developing the key hardware in upgrading the RIBF accelerator complex. Our primary focus and research is charge stripper which plays an essential role in the RIBF accelerator complex. Charge strippers remove many electrons in ions and realize efficient acceleration of heavy ions by greatly enhancing charge state. The intensity of uranium beams is limited by the lifetime of the carbon foil stripper conventionally installed in the acceleration chain. The improvement of stripper lifetimes is essential to increase beam power towards the final goal of RIBF in the future. We are developing the low-Z gas stripper. In general gas stripper is free from the lifetime related problems but gives low equilibrium charge state because of the lack of density effect. Low-Z gas stripper, however, can give as high equilibrium charge state as that in carbon foil because of the suppression of the electron capture process. Another our focus is the upgrade of the world's first superconducting ring cyclotron.

2. Major Research Subjects

(1) Development of charge strippers for high power beams (foil, low-Z gas)
(2) Upgrade of the superconducting ring cyclotron
(3) Maintenance and R&D of the electrostatic deflection/inflection channels for the beam extraction/injection

3. Summary of Research Activity

(1) Development of charge strippers for high power beams (foil, low-Z gas)

(Hasebe, H., Imao, H. Okuno., H.)

We are developing the charge strippers for high intensity heavy ion beams. We are focusing on the developments on carbon or berrilium foils and gas strippers including He gas stripper.

(2) Upgrade of the superconducting ring cyclotron

(Ohnishi, J., Okuno, H.)

We are focusing on the upgrade of the superconducting ring cyclotron.

(3) Maintenance and R&D of the electrostatic deflection/inflection channels for the beam extraction/injection

(Ohnishi, J., Okuno, H.)

We are developing high-performance electrostatic channels for high power beam injection and extraction.

Members

Team Leader

Hiroki OKUNO (concurrent: Deputy Group Director, Accelerator Gr.)

Research & Technical Scientists

Hiroshi IMAO (Senior Research Scientist)
Jun-ichi OHNISHI (Senior Technical Scientist)

Nishina Center Technical Scientist

Hiroo HASEBE

Special Postdoctoral Researcher

Hironori KUBOKI (– Mar. 31, 2013)

Visiting Scientists

Andreas ADELMANN (PSI)
Noriyosu HAYASHIZAKI (Tokyo Tech.)
Hironori KUBOKI (KEK)

RIBF Research Division
Accelerator Group
Ion Source Team

1. Abstract

Our aim is to operate and develop the ECR ion sources for the accelerator-complex system of the RI Beam Factory. We focus on further upgrading the performance of the RI Beam Factory through the design and fabrication of a superconducting ECR ion source for production of high-intensity uranium ions.

2. Major Research Subjects

(1) Operation and development of the ECR ion sources
(2) Development of a superconducting ECR heavy-ion source for production of high-intensity uranium ion beams

3. Summary of Research Activity

(1) Operation and development of ECR ion sources

(T. Nakagawa, M. Kidera, Y. Higurashi, K. Ozeki, T. Nagatomo, H. Haba, and T. Kageyama)

We routinely produce and supply various kinds of heavy ions such as zinc and calcium ions for the super-heavy element search experiment as well as uranium ions for RIBF experiments. We also perform R&D's to meet the requirements for stable supply of high-intensity heavy ion beams.

(2) Development of a superconducting ECR ion source for use in production of a high-intensity uranium ion beam

(T. Nakagawa, J. Ohnishi, M. Kidera, Y. Higurashi, K. Ozeki and T. Nagatomo)

The RIBF is required to supply uranium ion beams with very high intensity so as to produce RI's. We have designed and are fabricating an ECR ion source with high magnetic field and high microwave- frequency, since the existing ECR ion sources have their limits in beam intensity. The coils of this ion source are designed to be superconducting for the production of high magnetic field. We are also designing the low-energy beam transport line of the superconducting ECR ion source.

Members

Team Leader
Takahide NAKAGAWA

Research & Technical Scientist
Takashi NAGATOMO (Technical Scientist)

Nishina Center Research Scientists
Masanori KIDERA
Yoshihide HIGURASHI

Contract Researcher
Kazutaka OHZEKI (– Sept. 30, 2014)

Special Postdoctoral Researcher
Tatsuya URABE (Apr. 1, 2014 –)

Postdoctoral Researcher
Tatsuya URABE (– Mar. 31, 2014)

Research Consultant
Tadashi KAGEYAMA (Apr. 1, 2014 –)

Temporary Employee
Tadashi KAGEYAMA (– Mar. 31, 2014)

Part-time Worker
Yumi KURAMITSU

RIBF Research Division
Accelerator Group
RILAC Team

1. Abstract

The operation and maintenance of the RIKEN Heavy-ion Linac (RILAC) have been carried out. There are two operation modes: one is the stand-alone mode operation and the other is the injection mode operation. The RILAC has been used especially as an injector for the RIKEN RI- Beam Factory accelerator complex. The RILAC is composed of the ECR ion source, the frequency-variable RFQ linac, six frequency-variable main linac cavities, and six energy booster cavities (CSM).

2. Major Research Subjects

(1) The long term high stability of the RILAC operation.
(2) Improvement of high efficiency of the RILAC operation.

3. Summary of Research Activity

The RILAC was started to supply ion beams for experiments in 1981. Thousands hours are spent in a year for delivering many kinds of heavy-ion beams to various experiments.

The RILAC has two operation modes: one is the stand-alone mode operation delivering low-energy beams directly to experiments and the other is the injection mode operation injecting beams into the RRC. In the first mode, the RILAC supplies a very important beam to the nuclear physics experiment of “the research of super heavy elements”. In the second mode, the RILAC plays a very important role as upstream end of the RIBF accelerator complex.

The maintenance of these devices is extremely important in order to keep the log-term high stability and high efficiency of the RILAC beams. Therefore, improvements are always carried out for the purpose of more stable and more efficient operation.

Members

Team Leader
Eiji IKEZAWA

Research & Technical Scientist
Yutaka WATANABE (Senior Technical Scientist)

Research Consultants
Masatake HEMMI
Toshiya CHIBA

RIBF Research Division
Accelerator Group
Cyclotron Team

1. Abstract

Together with other teams of Nishina Center accelerator division, maintaining and improving the RIBF cyclotron complex. The accelerator provides high intensity heavy ions. Our mission is to have stable operation of cyclotrons for high power beam operation. Recently stabilization of the rf system is a key issue to provide 10 kW heavy ion beam.

2. Major Research Subjects

(1) RF technology for Cyclotrons
(2) Operation of RIBF cyclotron complex
(3) Maintenance and improvement of RIBF cyclotrons
(4) Single turn operation for polarized deuteron beams
(5) Development of superconducting cavity

3. Summary of Research Activity

Development of the rf system for a reliable operation
Development of highly stabilized low level rf system
Development of superconducting cavity
Development of the intermediate-energy polarized deuteron beams.

Members

Team Leader
Naruhiko SAKAMOTO

Research & Technical Scientist
Kazutaka OHZEKI (Technical Scientist)

Nishina Center Research Scientist
Kenji SUDA

Research Consultant
Yoshiaki CHIBA

Visiting Technician
Yan CONG (IMP, CAS)

RIBF Research Division
Accelerator Group
Beam Dynamics & Diagnostics Team

1. Abstract

The cascaded cyclotrons used in RIKEN RI Beam Factory (RIBF) requires not only strict matching of operation parameters but also high stability of all the accelerator components in order to establish stable operation of the world's most intense heavy-ion beams. Beam Dynamics and Diagnostics Team is responsible for power supplies, beam instrumentation, computer control and beam dynamic of the RIBF accelerator complex and strongly contributes to the performance upgrade of the RIBF.

2. Major Research Subjects

(1) Seeking the best operation method of the RIBF accelerator complex based on the beam dynamics study.
(2) Maintenance and development of the beam instrumentation, especially non-destructive monitors.
(3) Upgrade of the computer control system of the RIBF accelerator complex.
(4) Maintenance and improvements of the magnets and power supplies.
(5) Developments of beam interlock system suited to high-power cyclotron complex.

3. Summary of Research Activity

(1) The world-first beam current monitor with a high-Tc current sensor and SQUID has been developed.
(2) The bending power of the fixed-frequency Ring Cyclotron has been upgraded to 700 MeV. It enables us to accelerate $^{238}U^{64+}$ ions obtained by the helium gas stripper and contributes to stable and high-intensity operation of RIBF.
(3) An EPICS-based control system and a homemade beam interlock system have been stably working. Replacement of the existing legacy control system used in the old half of our facility is ongoing. Construction of the new control system for the new injector RILAC2 was successfully completed, where the embedded EPICS system running on F3RP61-2L CPU module, developed by KEK and RIKEN control group, was used.
(4) We replaced some dated power supplies of RIKEN Ring Cyclotron by new ones, which have better long-term stability than the old ones. The other existing power supplies (~900) are stably operated owing to elaborate maintenance work.
(5) We have contributed to RILAC2 construction, especially in its beam diagnosis, control system, magnet power supplies, vacuum system, high-energy beam transport system etc.

Members

Team Leader
Nobuhisa FUKUNISHI (concurrent; Deputy Group Director, Accelerator Gr.)

Research & Technical Scientists
Masaki FUJIMAKI (Senior Technical Scientist)
Keiko KUMAGAI (Senior Technical Scientist)
Tamaki WATANABE (Senior Technical Scientist)
Kazunari YAMADA (Senior Technical Scientist)

Nishina Center Technical Scientists
Misaki KOMIYAMA
Akito UCHIYAMA

Special Postdoctoral Researcher
Takuya MAEYAMA

Temporary Employee

Part-time Workers
Yuki SHIRAISHI
Makoto NAGASE

Visiting Scientists
Kenichi ISHIKAWA (Univ. of Tokyo)
Shin-ichiro Hayashi (Hiroshima Int'l Univ.)
Hiromichi RYUTO (Kyoto Univ.)

Visiting Technician
Jun-ichi ODAGIRI (KEK)

RIBF Research Division
Accelerator Group
Cryogenic Technology Team

1. Abstract

We are operating the cryogenic system for the superconducting ring cyclotron in RIBF. We are operating the helium cryogenic system in the south area of RIKEN Wako campus and delivering the liquid helium to users in RIKEN. We are trying to collect efficiently gas helium after usage of liquid helium.

2. Major Research Subjects

(1) Operation of the cryogenic system for the superconducting ring cyclotron in RIBF
(2) Operation of the helium cryogenic plant in the south area of Wako campus and delivering the liquid helium to users in Wako campus.

3. Summary of Research Activity

(1) Operation of the cryogenic system for the superconducting ring cyclotron in RIBF
(Okuno, H., Dantsuka, T., Nakamura, M., Maie, T.,)
(2) Operation of the helium cryogenic plant in the south area of Wako campus and delivering the liquid helium to users in Wako campus.
(Dantsuka, T., Tsuruma, S., Okuno, H.).

Members

Team Leader
Hiroki OKUNO (concurrent: Deputy Group Director, Accelerator Gr.)

Research & Technical Scientist
Masato NAKAMURA (Senior Technical Scientist)

Nishina Center Technical Scientist
Takeshi MAIE

Technical Staff I
Tomoyuki DANTSUKA

Temporary Employee
Kumio IKEGAMI (– Mar. 31, 2014)

Research Consultant
Kumio IKEGAMI (Apr. 1, 2014 –)

Part-time Worker
Shizuho TSURUMA

RIBF Research Division
Accelerator Group
Infrastructure Management Team

1. Abstract

The RIBF facility is consisting of many accelerators and its infrastructure is very important in order to make an efficient operation of RIBF project. We are maintaining the infrastructure of the whole system and to support the accelerator operation with high performance. We are also concerning the contracts of gas- and electricity-supply companies according to the annual operation plan. The contracts should be reasonable and also flexible against a possible change of operations. And we are searching the sources of inefficiency in the operation and trying to solve them for the high-stable machine operation.

2. Major Research Subjects

(1) Operation and maintenance of infrastructure for RIBF accelerators.
(2) Renewal of the old equipment for the efficient operation.
(3) Support of accelerator operations.

Members

Team Leader
Masayuki KASE (concurrent; Deputy Group Director, Accelerator Gr.)

Research & Technical Scientists
Shu WATANABE (Senior Technical Scientist)
Hideyuki YAMASAWA (Manager)

Temporary Employee
Tadashi FUJINAWA (– Mar. 31, 2014)

Research Consultant
Shin-ichi WATANABE

Visiting Scientist
Hideshi MUTO (Tokyo Univ. of Sci. Suwa)

RIBF Research Division
Instrumentation Development Group

1. Abstract

This group develops core experimental installations at the RI Beam factory. Experimental installations currently under setting up include common elements enabling multiple-use (SLOWRI), as well as others that are highly program specific (SCRIT and Rare-RI Ring). All were designed to maximize the research potential of the world's most intense RI beams, made possible by the exclusive equipment available at the RI Beam Factory. Beam manipulation techniques, such as a beam accumulation and a beam cooling, will be able to provide opportunities of new experimental challenges and the foundation for future developments of RIBF.

2. Major Research Subjects

(1) SCRIT Project
(2) SLOWRI Project
(3) Rear RI Ring Project

3. Summary of Research Activity

We are developing beam manipulation technology in carrying out above listed project. They are the high-quality slow RI beam production (SCRIT and SLOWRI), the beam cooling and stopping (SCRIT and SLOWRI), and the beam accumulation technology (Rare RI Ring). The technological knowhow accumulated in our projects will play a significant role in the next generation RIBF. Status and future plan for each project is described in subsections. SCRIT is now under finalizing the experimental setup for electron scattering off unstable nuclei, and the comprehensive test will be soon. The first experiment will be planed in 2015. Rare RI Ring construction has been almost completed. Test experiments using alpha particle for evaluating the ring performance were successfully performed, and the isochronism in the order of 10^{-5} was confirmed in ten-turns circulation. The first commissioning experiment is planed in June 2015. Construction of the SLOWRI system was completed in 2014, and it is now under setting up for the first commissioning in 2015.

Members

Group Director
Masanori WAKASUGI

Senior Visiting Scientist
Akira OZAWA (Univ. of Tsukuba)

Student Trainees
Mamoru TOGASAKI (Rikkyo Univ.)
Yohei SUMI (Rikkyo Univ.)
Saki MATSUO (Rikkyo Univ.)
Kohei YAMADA (Rikkyo Univ.)

RIBF Research Division
Instrumentation Development Group
SLOWRI Team

1. Abstract

Construction of a next-generation stopped and low-energy radioactive ion beam facility (SLOWRI) which will provide low-energy, high-purity and small emittance ion beams of all elements has been started in FY2013 as one of the principal facilities at the RIKEN RI-beam factory (RIBF). High-energy radioactive ion beams from the projectile fragment separator BigRIPS are thermalized in a large He gas catcher cell (RFC cell) or in a small Ar gas catcher cell (PALIS cell). In the RFC cell, thermalized ions in buffer gas are guided and extracted to a vacuum environment by a combination of dc electric fields and inhomogeneous rf fields (rf carpet ion guide). The PALIS cell will be placed in the vicinity of the second focal plane slits of BigRIPS and can be used continuously during other experiments. From these gas cells, the low-energy ion beams will be delivered via mass separators and switchyards to various devices: such as an ion trap, a collinear fast beam apparatus, and a multi-reflection time of flight mass spectrograph. In the R&D works at the present ring cyclotron facility, an extraction efficiency of 33% for a 100A MeV ^{8}Li ion beam from the projectile fragment separator RIPS was achieved and the dependence of the efficiency on the ion beam intensity was investigated.

First spectroscopy experiment at the prototype SLOWI was performed on Be isotopes. Energetic ions of ^{7,10,11}Be from the RIPS were trapped and laser cooled in a linear rf trap and precision spectroscopy was performed. The evaluated ion temperature of <10 mK demonstrates that a reduction of more than 15 orders of magnitude for the kinetic energy of radioactive Be was achieved online. The ground state hyperfine constants of all Be isotopes have been measured precisely by laser and microwave. These precision measurements will be used to confirm the anomalous mean radius of the valence neutron of the so called neutron halo nucleus. Other laser spectroscopy experiments using the slow RI-beams are also under progress in off-line setups. A collinear fast beam apparatus for nuclear charge-radii measurements was build and tested with stable Ar^{+} ion beams.

A multi-reflection time-of-flight mass spectrograph (MRTOF) has been developed and tested online for radioactive lithium isotope, ^{8}Li. A high mass resolving power of 170,000 has been obtained for an isobaric doublet of ^{40}K and ^{40}Ca with a very short flight time of 2 ms. This performance allowed accurate mass determination of $<10^{-7}$ accuracy by a single isobaric reference. Two mass measurement projects using MRTOF mass spectrographs have been started: one is for trans uranium elements at the GARIS facility and the other is for r-process nuclides at SLOWRI facility.

Resonance ionization spectroscopy has been tested during the offline development of PALIS gas cell. Stable isotopes of Co, Cu, Fe, Ni, Ti, Nb, Sn, In, and Pd were resonantly ionized by excimer pumped dye lasers or Nd:YAG laser pumped Ti:Sapphire lasers with the prototype gas cell setup. The resonance spectra are in many cases sufficient to resolve the hyperfine structures. Nuclear spins and magnetic moments will be determined for various isotopes obtained during other experiments.

2. Major Research Subjects

(1) Construction of stopped and low-energy RI-beam facility, SLOWRI.
(2) Laser spectroscopy of trapped radioactive Beryllium isotopes.
(3) Development of a multi-reflection time-of-flight mass spectrograph for precision mass measurements of short-lived nuclei.
(4) Development of parasitic slow RI-beam production method using resonance laser ionization.
(5) Development of ion-surfing gas cell.

3. Summary of Research Activity

(1) Construction of stopped and low-energy RI-beam facility (SLOWRI)

(WADA, Michiharu, SONODA, Tetsu, KATAYAMA, Ichiro, SCHURY, Peter, ITO, Yuta, ARAI, Fumiya, ARAI, Shigeaki, KUBO, Toshiyuki, KUSAKA, Kensuke, FUJINAWA Tadashi, MAIE Takeshi, YAMASAWA Hideyuki, WOLLNIK, Hermann,)

Installation of SLOWRI has been started in FY2013. It consists of two gas catchers (RF Carpet gas cell and PALIS gas cell), mass separators a 50-m beam transport line, a beam cooler-buncher, an isobar separator, and a laser system. The RFCarpet gas cell will be installed at the exit of the D5 dipole magnet of BigRIPS. The gas catcher contains a large cryogenic He gas cell with a large traveling wave rf-carpet. It will convert main beams of BigRIPS to low-energy, low-emittance beams without any restrictions on the chemical properties of the elements. The PALIS gas cell will be installed in the vicinity of the second focal plane slit of BigRIPS. It will provide parasitic RI-beams from those ions lost in the slits during other experiments. In this gas catcher, thermalized RI ions quickly become neutral and will be re-ionized by resonant laser radiations. These gas catchers will be tested off-line in FY2014. The 50 m beam transport line consists of four dipole magnets (SD1 to SD4), two focal plane chambers, 62 electrostatic quadrupole singlets, 11 electrostatic quadrupole quartets (EQQ1 to EQQ11) and 7 beam profile monitors (BPM). SD1 and SD2, located right after the gas catchers will be used for isotope separation. After eliminating contaminant ions at the focal plane chamber, the low energy beam will be transported by FODO lattice structure with phase space matching using EQQs. The EQQs have multipole elements made of 16 rods on which various potentials can be applied to produce 6-pole and 8 pole fields, simultaneously, for compensation of ion optical aberrations. This multipole element can also produce dipole fields for steering and scanning the beam. The BPM have a classical cross-wire beam monitor as well as a channel electron multiplier with a pinhole collimator. Combining the scanning capability of the EQQs and the pinhole detector, we can observe a beam profile even for a very low-intensity RI-beams. Off- and on-line commissioning will take place in FY2014 and the low-energy RI-beams will be provided for users in FY2015.

(2) Laser spectroscopy of trapped radioactive beryllium isotope ions

(WADA, Michiharu, TAKAMINE, Aiko, SCHURY Peter, SONODA Tetsu, OKADA, Kunihiro, KANAI, Yasuyuki, YOSHIDA, Atsushi, KUBO, Toshiyuki, WOLLNIK, Hermann, SCHUESSLER, Hans, Shunsuke, KATAYAMA Ichiro)

As a first application of the prototype SLOWRI setup, we applied hyperfine structure spectroscopy to the beryllium isotopes to determine in particular the anomalous radius of the valence neutron of the neutron halo nucleus ^{11}Be, and to determine the charge radii of these beryllium isotopes through laser-laser double resonance spectroscopy of laser-cooled ions. Laser cooling is an essential prerequisite for these planned experiments. The first laser spectroscopy experiments for beryllium isotopes were performed to measure the resonance frequencies of 2s $^2S_{1/2}$ - 2p $^2P_{3/2}$ transition of ^{7}Be+, ^{9}Be+, ^{10}Be$^+$ and ^{10}Be+ ions and the nuclear charge radii of these isotopes were determined. The hyperfine structures of ^{11}Be$^+$ and ^{7}Be$^+$ ions using the laser-microwave double resonance spectroscopy were also performed and the magnetic hyperfine constants of ^{7}Be$^+$ and ^{11}Be$^+$ ions were determined with accuracies of better than10^{-7}.

(3) Development of a multi-reflection TOF mass spectrograph for short-lived nuclei

(WADA, Michiharu, SCHURY Peter, ITO, Yuta, ARAI Fumiya, SONODA Tetsu, WOLLNIK, Hermann, MORIMOTO, Koji, KAJI, Daiya, HABA, Hiromitsu, KOURA, Hiroyuki)

The atomic mass is one of the most important quantities of a nucleus and has been studied in various methods since the early days of physics. Among many methods we chose a multi-reflection time-of-flight (MR-TOF) mass spectrometer. Slow RI beams extracted from the RF ion-guide are bunch injected into the spectrometer with a repetition rate of ~100 Hz. The spectrometer consists of two electrostatic mirrors between which the ions travel back and forth repeatedly. These mirrors are designed such that energy-isochrononicity in the flight time is guaranteed during the multiple reflections while the flight time varies with the masses of ions. A mass-resolving power of 170,000 has been obtained with a 2 ms flight time for 40K and 40Ca isobaric doublet. This mass-resolving power should allow us to determine ion masses with an accuracy of 10^{-7}. An online mass measurement for radioactive lithium isotope has been carried out at the prototype SLOWRI setup.

The MR-TOF mass spectrograph has been placed under the GARIS-II separator aiming at direct mass measurements of trans-uranium elements. A small cryogenic gas catcher cell will be placed at the focal plane box of GARIS-II and a bunched low-energy heavy ion beam can be transported to the trap of MR-TOF. An online commissioning experiment is planned in FY2014.

(4) Development of collinear fast beam apparatus for nuclear charge radii measurements

(WADA, Michiharu, SCHUESSLER, Hans, IIMURA, Hideki, SONODA, Tetsu, SCHURY, Peter, TAKAMINE, Aiko, OKADA, Kunihiro, WOLLNIK, Hermann)

The root-mean-square charge radii of unstable nuclei have been determined exclusively by isotope shift measurements of the optical transitions of singly-charged ions or neutral atoms by laser spectroscopy. Many isotopes of alkaline, alkaline-earth, noble-gases and several other elements have been measured by collinear laser spectroscopy since these ions have all good optical transitions and are available at conventional ISOL facilities. However, isotopes of other elements especially refractory and short-lived ones have not been investigated so far.

In SLOWRI, isotopes of all atomic elements will be provided as well collimated mono-energetic beams. This should expand the range of applicable nuclides of laser spectroscopy. In the first years of the RIBF project, Ni and its vicinities, such as Ni, Co, Fe, Cr, Cu, Ga, Ge are planned to be investigated. They all have possible optical transitions in the ground states of neutral atoms with presently available laser systems. Some of them have so called recycle transitions which enhance the detection probabilities noticeably. Also the multistep resonance ionization (RIS) method can be applied to the isotopes of Ni as well as those of some other elements. The required minimum intensity for this method can be as low as 10 atoms per second.

We have built an off-line mass separator and a collinear fast beam apparatus with a large solid-angle fluorescence detector. A 617 nm transition of the metastable Ar+ ion at 20 keV was measured with both collinear and anti-collinear geometry that allowed us to determine the absolute resonant frequency of the transition at rest with more than 10^{-8} accuracy. Such high accuracy measurements for Ti and Ni isotopes are in progress.

(5) Development of parasitic slow RI-beam production scheme using resonance laser ionization

(SONODA Tetsu, IIMURA Hideki, WADA Michiharu, KATAYAMA Ichiou, ADACHI Yoshitaka, NOTO Takuma, TAKATSUKA Takaaki, TOMITA Hideki, WENDT Klaus, ARAI Fumiya, ITOU Yuta, SCHURY Peter, FUKUDA Naoki, INABE Naohito, KUBO Toshiyuki, KUSAKA Kensuke, TAKEDA Hiroyuki, SUZUKI H., WAKASUGI Masanori, YOSHIDA Koichi)

More than 99.9% of RI ions produced in projectile fission or fragmentation are simply dumped in the first dipole magnet and the slits. A new scheme, named PALIS, to rescue such dumped precious RI using a compact gas catcher cell and resonance laser ionization was proposed as a part of SLOWRI. The thermalized RI ions in a cell filled with Ar gas can be quickly neutralized and transported to the exit of the cell by gas flow. Irradiation of resonance lasers at the exit ionizes neutral RI atoms efficiently and selectively. The ionized RI ions can be further selected by a magnetic mass separator and transported to SLOWRI experimental area for various experiment. The resonance ionization scheme itself can also be a useful method to perform hyperfine structure spectroscopy of RI of many elements.

A prototype setup has been tested for resonance ionization scheme of several elements, extraction from the cell, and transport to a high vacuum chamber. An online setup, which will be placed at the second focal plane (F2) of BigRIPS, has been fabricated in FY2013 and commissioning is scheduled in FY2014.

Members

Team Leader
Michiharu WADA

Research & Technical Scientist
Hideyuki YAMASAWA (concurrent; Infrastructure Management Team)

Nishina Center Research Scientists
Tetsu SONODA
Kensuke KUSAKA (concurrent; BigRIPS Team)

Nishina Center Technical Scientist
Takeshi MAIE (concurrent; Cryogenic Technology Team)

Contract Researcher
Peter Henry SCHURY

Special Postdoctoral Researcher
Yuta ITO (Apr. 1, 2014 –)

Research Associate
Yuta ITO (– Mar. 31, 2014)

Temporary Employee
Tadashi FUJINAWA (concurrent, – Mar. 30, 2014)

Part-time Workers
Shigeaki ARAI
Ichiro KATAYAMA

Research Consultant
Hirokane KAWAKAMI

Visiting Researcher
Mikael REPONEN (JSPS, Aug. 4, 2014 –)

Visiting Scientists
Hans A SCHUESSLER (Texas A&M Univ.)
Hermann WOLLNIK (Univ. of Giessen)
Aiko TAKAMINE (Aoyama Gakuin Univ.)
Hideki IIMURA (JAEA)
Hideki TOMITA (Nagoya Univ.)
Klaus WENDT (Johannes Gutenberg Univ. Mainz)
Kunihiro OKADA (Sophia Univ.)

Student Trainees
Takuma NOTO (Nagoya Univ.)
Takaaki TAKATSUKA (Nagoya Univ.)
Fumiya ARAI (Univ. of Tsukuba)
Yoshitaka ADACHI (Nagoya Univ.)
Takahide TAKAMATSU (Nagoya Univ.)

RIBF Research Division
Instrumentation Development Group
Rare RI-ring Team

1. Abstract

Mass measurement is one of the most important contributions to a nuclear property research especially for short-lived unstable nuclei far from the beta-stability line. In particular, a high-precision mass measurement for nuclei located around the r-process pass (rare-RI) is required in nucleosynthesis point of view. We chose a method of isochronous mass spectrometry (IMS) to make a measurement time shorter than 1 ms. Heavy-ion storage ring named "Rare-RI Ring (R3)" has been constructed until end of 2013 and is now under preparation for the first commissioning experiment. Our target performance in the mass determination is to achieve accuracy of the order of 10^{-6} (~100 keV) even if we get only one event. Since an isochronism in R3 is established over a wide range of the momentum, rare-RIs with a large momentum spread, $\Delta p/p=\pm 0.5$ %, are acceptable. Another significant feature of the R3 system is an individual injection scheme in which a produced rare-RI itself triggers the injection kicker. Design study for R3 has been continued from more than ten years ago, and it was constructed in 2012 and 2013. In 2014, we demonstrated the R3 performances in test experiments using alpha particle. We are now setting up and testing all equipments including the power supplies, the control system, the vacuum system, and so on, toward the first commissioning planed in 2015.

2. Major Research Subjects

Developments of isochronous storage ring to measure mass of rare RI.

3. Summary of Research Activity

Since the lattice design of R3 is based on the cyclotron motion, it can provide an isochronism in a wide range of the momentum. We expect a great improvement in mass resolution in IMS as long as the isochronous field is precisely formed in R3. Therefore, IMS using R3 is capable of both a high-precision measurement and a fast measurement. All the devices in R3 was designed under the assumption that an incoming beam has an energy of 200 MeV/u and a charge to mass ratio, m/q, of less than 3. The ring structure was designed with a similar concept of a separate-sector ring cyclotron. It consists of six sectors and 4.02-m straight sections, and each sector consists of four rectangular bending magnets. A radially homogeneous magnetic field is produced in the magnet, and a magnetic rigidity is 6.5 Tm at maximum. Main coils of all the bending magnets are connected in series, and the current of 3000 A is required for rare-RIs, for instance, ^{78}Ni with the magnetic rigidity of 5.96 Tm. Two magnets at both ends of each sector are additionally equipped with ten trim coils to form an precise isochronous magnetic field. For $\Delta p=0$ particle, the circumference is 60.35 m and the betatron tunes are $\nu x=1.21$ and $\nu y=0.84$ in horizontal and vertical directions, respectively. The momentum acceptance is $\Delta p/p=\pm 0.5$ %, and the transverse acceptances are 20π mmmrad and 10π mmmrad in horizontal and vertical directions, respectively. Although the transverse acceptances of the R3 itself are actually larger than these values, they are limited by that of the injection beam line. Of special note is that the isochronism is precisely fulfilled in a wide range of momentum (full width 1 %) due to a cyclotron-motion based lattice design.

Another performance required for R3 is to efficiently seize hold of an opportunity of the measurement for rare-RIs produced unpredictably. We adopted an individual injection scheme in which the produced rare-RI itself triggers the injection kicker magnets. Full activation of the kicker magnetic field have to be completed within the flight time of the rare-RI from an originating point (F3 focal point in BigRIPS) of the trigger signal to the kicker position in R3. Development of an ultra-fast response kicker system is a key issue for establishing the individual injection scheme. Performances required for the kicker system are an ultra-fast response, a fast charging, and a full-time charging.

We provided ordinary beam diagnostic devices such as a screen monitor and a beam position monitor based on triangle pickup electrodes. Although five sets of these monitors distributed along the orbit in R3 are useful in a machine tuning process using a high-intensity primary beam. They, however, are incapable for rare-RIs because of the poor sensitivity. Therefore, we inserted high-sensitive monitors, which are applicable even for a single particle circulation. One of them is a cavity type of Schottky pick-up. A resonance frequency is designed to be 171 MHz, which corresponds to the harmonic number of 56, and a measured quality factor is about 1900 and shunt impedance is 170 kΩ. We can detect single ion circulation of $^{78}Ni^{28+}$ with only a few ms measurement. Another is a timing monitor, which detects secondary electrons emitted from thin carbon foil placed on the accumulation orbit. The thickness of the foil will be 50 μg/cm^2. The rare-RI with the energy of 200 MeV/u survives only for first 1000 turns because of an energy loss at the foil.

In test experiments using alpha particles emitted from an ^{241}Am source performed in 2014, we succeeded in the individual injection of the single particle, beam accumulation and the beam extraction. We successfully measured the TOF for 1~10 turns circulation of alpha particles, and the isochronism in R3 in the order of 10^{-5} was confirmed. R2 is now under preparation for the first commissioning experiment using heavy ion beam from accelerators.

Members

Team Leader
Masanori WAKASUGI (concurrent; Group Director, Instrumentations Development Gr.)

Research & Technical Scientists
Yoshiyuki YANAGISAWA (Senior Research Scientist, concurrent; BigRIPS Team)
Tamaki WATANABE (Senior Technical Scientist, concurrent; Beam Dynamics and Diagnostics Team)
Yutaka WATANABE (Senior Technical Scientist, concurrent; RILAC team)
Naohito INABE (Senior Technical Scientist, concurrent; BigRIPS Team)
Hideyuki YAMASAWA (concurrent; Infrastructure Management Team)

Nishina Center Research Scientist
Yoshitaka YAMAGUCHI

Nishina Center Technical Scientists
Takeshi MAIE (concurrent; Cryogenic Technology Team)
Misaki KOMIYAMA (concurrent; Beam Dynamics and Diagnostics Team)

Research Consultant
Akira NODA (– Mar. 31, 2014)

Junior Research Associate
Yasushi ABE (Univ. of Tsukuba)

Temporary Employee
Tadashi FUJINAWA (concurrent, – Mar. 30, 2014)

Visiting Scientist
Daisuke NAGAE (Univ. of Tsukuba)

Student Trainees
Yuta SAITO (Univ. of Tsukuba)
Shunsuke OKADA (Univ. of Tsukuba)
Ayano ENOMOTO (Saitama Univ.)

RIBF Research Division
Instrumentation Development Group
SCRIT Team

1. Abstract

The SCRIT Electron Scattering Facility is now under construction at RIKEN RIBF. This aims at investigation of internal nuclear structure for short-lived unstable nuclei by means of electron scattering. SCRIT (Self-Confining RI Ion Target) is a novel method to form internal targets in an electron storage ring. This technique has made electron scattering experiments for unstable nuclei possible. Construction of the facility has been started in 2009. This facility consists of an electron accelerator (RTM), a SCRIT-equipped electron storage ring (SR2), an electron-beam-driven RI separator (ERIS), and a detector system for scattered electrons. Operation of accelerators, RTM and SR2, was started in 2010, performance test of the SCRIT system using stable isotopes, ^{133}Cs and ^{132}Xe, was successfully done in 2011 and 2012. Construction of ERIS was started in 2011 and it was commissioned in 2012. The first RI beams from ERIS were supplied in 2013, and the extraction efficiency was improved by a factor more than ten in 2014. The detector system consisting of a high-resolution magnetic spectrometer, drift chambers, trigger scintillators, and luminosity monitors were installed. The commissioning using tungsten wire target resulted the energy resolution of 10^{-3}. We are going to perform the first experiment of electron scattering from unstable nuclei within a fiscal year 2015.

2. Major Research Subjects

Development of SCRIT electron scattering technique and construction of the SCRIT electron scattering facility.

3. Summary of Research Activity

Development of an electron scattering experimental system for short-lived unstable nuclei using a novel internal target of unstable nuclei (SCRIT).

(Wakasugi, Ohnishi, Kurita, Suda, Tsukada, Tamae, Enokizono, Hori, Hara, Ichikawa)

SCRIT is novel technique to form internal target in an electron storage ring. Positive ions are confined in the electron beam axis by transverse focusing force given by the circulating electron beam. This is well known "ion trapping" phenomenon. The created ion cloud in which RI ions injected from outside are confined works as a target of electron scattering.

In 2010, we successfully commissioned electron accelerators RTM and SR2. Current of electron beams stored in SR2 and its storage lifetime have been reached to 300 mA and 2 hours, respectively, in the energy range of 150-300 MeV that is required in electron scattering experiments. In test experiments of the SCRIT system performed in 2011 and 2012, we used stable isotopes, ^{133}Cs and ^{132}Xe, and revealed many details of the SCRIT performance. The luminosity of 10^{27} /(cm^{2}s) was obtained in case of the number of injected ions of 10^8. The lifetime of the ion confinement was obtained to be over 1 s. They are performances satisfactory to the electron scattering experiment. In fact, we succeeded in measurements of angular distributions of scattered electrons from the target ions trapped in the SCRIT device.

Development of ERIS is one of the most important issue in the facility construction. RIs are generated by photo-fission process of ^{238}U, which is driven by the 150-MeVelectron beams from RTM. ERIS consists of a target ion source including UCx targets and a mass separation system. ERIS was constructed in 2011 and performances such as the extraction efficiency of 21 % and the mass resolving power of 1660 were obtained in the commissioning in 2011. We developed production method of UCx targets by ourselves. The first RI production was succeeded in last year, and $^{126\text{-}132}$Sn and $^{138\text{-}141}$Xe isotopes were extracted. The extraction efficiency was improved in 2014, and the overall efficiencies for ^{137}Xe and ^{132}Sn reached to 14% and 2%, respectively. The yield of ^{137}Xe isotopes exceeded 10^7 pps with 10-W driver power. A cooler buncher system based on a RFQ linear trap connected to the ERIS beam line is indispensable, because the continuous beam from ERIS has to be converted to pulsed beam for ion injection to the SCRIT device. The offline test experiments resulted more than 10% bunching efficiency for heavy ion beam, and the cooler buncher was installed in the ion beam line from ERIS.

The new detector system consists of a high-resolution magnetic spectrometer, a beam tracking system using drift chambers, trigger scintillators, and a luminosity monitor. This has a solid angle of 100 msr, energy resolution of 10^{-3}, and the scattering angle coverage of 30-60 degrees. A wide range of momentum transfer, 80-300 MeV/c, is covered by changing the electron beam energy from 150 to 300 MeV. In last year, the new detector system was successfully commissioned by means of electron scattering from a tungsten wire target.

Members

Team Leader

Masanori WAKASUGI (concurrent; Group Director, Instrumentations Development Gr.)

Research & Technical Scientists

Masamitsu WATANABE (Senior Research Scientist)

Tetsuya OHNISHI (Senior Technical Scientist)

Research Consultants

Tadaaki TAMAE
Shin-ichi ICHIKAWA
Masahiro HARA
Takashi EMOTO

Senior Visiting Scientist
Toshitada HORI (Hiroshima Univ.)

Visiting Scientists
Shuo WANG (Tohoku Univ.)
Kyo TSUKADA (Tohoku Univ.)
Toshimi SUDA (Tohoku Univ.)

Part-time Worker
Shunpei YONEYAMA

Student Trainees
Takaya MIYAMOTO (Tohoku Univ.)
Yuto SHIMAKURA (Rikkyo Univ.)
Yuji HARAGUCHI (Nagaoka Univ. of Tech.)
Shunpei YONEYAMA (Tohoku Univ.)
Teruaki TSURU (Tohoku Univ.)
Yosuke MORIYA (Tohoku Univ.)

Intern
Ryota TOBA (Nagaoka Univ. of Tech.)

RIBF Research Division
Research Instruments Group

1. Abstract

The research instruments group is the driving force at RI Beam Factory (RIBF) for continuous enhancement of activities and competitiveness of experimental research. Consisting of four teams, we are in charge of the construction, operation and improvement of the core research instruments at RIBF, such as BigRIPS in-flight separator, ZeroDegree spectrometer and SAMURAI spectrometer, and the related infrastructure and equipment. We are also in charge of the production and delivery of RI beams using the BigRIPS separator. The group also conducts related experimental research as well as R&D studies on the research instruments.

2. Major Research Subjects

Design, construction, operation and improvement of the core research instruments at RIBF and related R&D studies. Experimental studies on exotic nuclei.

3. Summary of Research Activity

The current research subjects are summarized as follows:

(1) Production and delivery of RI beams and related research
(2) Design, construction, operation and improvement of the core research instruments at RIBF and their related infrastructure and equipment
(3) R&D studies on the core research instruments and their related equipment at RIBF
(4) Experimental research on exotic nuclei using the core research instruments at RIBF

Members

Group Director
Toshiyuki KUBO

Junior Research Associates
Daichi MURAI (Rikkyo Univ.)
Momo MUKAI (Tsukuba Univ.)

Part-time Worker
Meiko UESAKA

Senior Visiting Scientist
Toshio KOBAYASHI (Tohoku Univ.)

RIBF Research Division
Research Instruments Group
BigRIPS Team

1. Abstract

This team is in charge of design, construction, development and operation of BigRIPS in-flight separator and its related research instruments at RI beam factory (RIBF). They are employed not only for the production of RI beams but also the experimental studies using RI beams.

2. Major Research Subjects

Design, construction, development and operation of BigRIPS in-flight separator, RI-beam transport lines, and their related research instruments

3. Summary of Research Activity

This team is in charge of design, construction, development and operation of BigRIPS in-flight separator, RI-beam transport lines, and their related research instruments such as ZeroDegree spectrometer at RI beam factory (RIBF). They are employed not only for the production of RI beams but also various kinds of experimental studies using RI beams.

The research subjects may be summarized as follows:

(1) General studies on RI-beam production using in-flight scheme.
(2) Studies on ion-optics of in-flight separators, including particle identification of RI beams
(3) Simulation and optimization of RI-beam production.
(4) Development of beam-line detectors and their data acquisition system.
(5) Experimental studies on production reactions and unstable nuclei.
(6) Experimental studies of the limits of nuclear binding.
(7) Development of superconducting magnets and their helium cryogenic systems.
(8) Development of a high-power production target system.
(9) Development of a high-power beam dump system.
(10) Development of a remote maintenance and remote handling systems.
(11) Operation, maintenance and improvement of BigRIPS separator system, RI-beam transport lines, and their related research instruments such as ZeroDegree spectrometer and so on.
(12) Experimental research using RI beams.

Members

Team Leader
Koichi YOSHIDA

Research & Technical Scientists
Yoshiyuki YANAGISAWA (Senior Research Scientist)
Naohito INABE (Senior Technical Scientist)
Masao OHTAKE (Senior Technical Scientist)
Kanenobu TANAKA (Technical Scientist, concurrent; Deputy Group Director, Safety Management Gr.)

Nishina Center Research Scientists
Hiroyuki TAKEDA
Kensuke KUSAKA
Naoki FUKUDA

Contract Researcher
Daisuke KAMEDA (– Aug. 31, 2014)

Postdoctoral Researchers
Hiroshi SUZUKI
Deuk Soon AHN

Part-time Worker
Hidekazu KUMAGAI (– Mar. 31, 2014)

Research Consultant
Hidekazu KUMAGAI (Apr. 1, 2014 –)

Senior Visiting Scientist

Jerry NOLEN (Argonne National Lab.)

Visiting Scientists

Daisuke KAMEDA (TOSHIBA Corp.)
Michael A. FAMIANO (Western Michigan Univ.)
Daniel Pierre BAZIN (NSCL, MSU)
Oleg Borisovich TARASOV (NSCL, MSU)
Hans GEISSEL (GSI)
David Joseph MORRISSEY (NSCL, MSU)
Bradley Marc SHERRILL (NSCL, MSU)
Martin Alfred WINKLER (GSI)
Mauricio PORTILLO (NSCL, MSU)
Dogyun KIM (IBS)
Eunhee KIM (IBS)
Alan Matthew AMTHOR (Bucknell Univ.)
Yutaka MIZOI (Osaka Elec.-Com. Univ.)
Naohito IWASA (Tohoku Univ.)
Sadao MOMOTA (Kochi Univ. of Tech.)
Kazuo IEKI (Rikkyo Univ.)

Student Trainees

Yohei OHKODA (Tohoku Univ.)
Kousei ASADA (Tohoku Univ.)

RIBF Research Division
Research Instruments Group
SAMURAI Team

1. Abstract

In collaboration with research groups in and outside RIKEN, the team designs, develops and constructs the SAMURAI spectrometer and relevant equipment that are and will be used for reaction experiments using RI beams at RI Beam Factory. The SAMURAI spectrometer consists of a large superconducting dipole magnet and a variety of detectors to measure charged particles and neutrons. After the commissioning experiment in March 2012, the team prepared and conducted, in collaboration with researchers in individual experimental groups, the first series of experiments with SAMURAI in May 2012. Then, several numbers of experiments were well performed until now utilizing the property of SAMURAI. The team also provides basis for research activities by, for example, organizing collaboration workshops by researchers who are interested in studies or plan to perform experiments with the SAMURAI spectrometer.

2. Major Research Subjects

Design, operation, maintenance and improvement of the SAMURAI spectrometer and its related research instruments. Help and management for SAMURAI-based research programs.

3. Summary of Research Activity

The current research subjects are summarized as follows:

(1) Operation, maintenance and improvement of a large superconducting dipole magnet that is the main component of the SAMURAI spectrometer
(2) Design, development and construction of various detectors that are used for nuclear reaction experiments using the SAMURAI spectrometer.
(3) Preparation for planning experiments using SAMURAI spectrometer.
(4) Maintenance and improvement of the SAMURAI beam line.
(5) Formation of a collaboration platform called "SAMURAI collaboration"

Members

Team Leader
Hiromi SATO (− Mar. 31, 2014)
Hideaki OTSU (Apr. 1, 2014 −)

Deputy Team Leader
Ken-ichiro YONEDA (− Mar. 31, 2014, concurrent; Team Leader, User Support Office)

Research Associate
Yohei SHIMIZU(− Dec. 31, 2014)

Visiting Scientist
Bertis Charles RASCO (Louisiana State Univ.)

Visiting Technician
Nobuyuki CHIGA (Tohoku Univ.)

Student Trainee
Kunihiko HASEGAWA (Tohoku Univ.)

RIBF Research Division
Research Instruments Group
Computing and Network Team

1. Abstract

This team is in charge of development, management and operation of the computing and network environment, mail and information servers and data acquisition system and management of the information security of the RIKEN Nishina Center.

2. Major Research Subjects

(1) Development, management and operation of the general computing servers
(2) Development, management and operation of the mail and information servers
(3) Development, management and operation of the data acquisition system
(4) Development, management and operation of the network environment
(5) Management of the information security

3. Summary of Research Activity

This team is in charge of development, management and operation of the computing and network environment, mail and information servers and data acquisition system and management of the information security. The details are described elsewhere in this progress report.

(1) Development, management and operation of the general computing servers

We are operating Linux/Unix NIS/NFS cluster system for the data analysis of the experiments and general computing. This cluster system consists of eight computing servers with 64 CPU cores and totally 200 TB RAID of highly-reliable Fibre-channel interconnection. Approximately 600 user accounts are registered on this cluster system. We are adopting the latest version of the Scientific Linux (X86_64) as the primary operating system, which is widely used in the accelerator research facilities, nuclear physics and high-energy physics communities in the world. We have added a 52 TB RAID for the data analysis in the autumn of 2014 and replaced the ssh login server (RIBF00) in the winter of 2015.

(2) Development, management and operation of the mail and information servers

We are operating RIBF.RIKEN.JP server as a mail/NFS/NIS server. This server is a core server of RIBF Linux cluster system. Postfix has been used for mail transport software and dovecot has been used for imap and pop services. These software packages enable secure and reliable mail delivery. Sophos Email Security and Control (PMX) installed on the mail front-end servers tags spam mails and isolates virus-infected mails. The probability to identify the spam is approximately 95-99%. We are operating several information servers such as Web servers, Integrated Digital Conference (INDICO) server, Wiki servers, Groupware servers, Windows Media and Quick Time streaming servers, and an anonymous FTP server (FTP.RIKEN.JP). A new Web server has been installed in April 2014 as an official Web server of RNC to replace the old Web server installed in 2005. A new 72 TB RAID was installed to replace the old RAID to the anonymous FTP server in August 2014.

(3) Development, management and operation of the data acquisition system

We have developed the standard data-acquisition system named as RIBFDAQ. This system can process up to 40 MB/s data. By using parallel readout from front-end systems, the dead time could be small. To synchronize the independent DAQ systems, the time stamping system has been developed. The resolution and depth of the time stamp are 10 ns and 48 bit, respectively. This time stamping system is very useful for beta decay experiments such as EURICA and BRIKEN projects. The current main task is the DAQ coupling, because detector systems with dedicated DAQ systems are transported to RIBF from foreign facilities. In case of SAMURAI Silicon (NSCL/TUM/WUSTL), the readout system is integrated into RIBFDAQ. The projects of MUST2 (GANIL), MINOS (CEA Saclay), and NeuLAND (GSI) cases, data taken by their DAQ systems are transferred to RIBFDAQ. For SPIRIT (RIKEN/GANIL/CEA Saclay/NSCL), RIBFDAQ data are sent to GET system that is a large-scale signal processing system for the time projection chamber. These cases, data are merged in online. On the other hand, EURICA (GSI) and BRIKEN (GSI/Univ. Liverpool/IFIC) projects, we adopt the time stamping system to use individual trigger for each detector system. In this case, data are merged in offline. In addition to the development DAQ system, we are developing intelligent circuits based on FPGA. Mountable Controller (MOCO) is a very fast readout controller for VME modules. General Trigger Operator (GTO) is an intelligent triggering NIM module. Functions of “common trigger management”, “gate and delay generator”, “scaler” are successfully implemented on GTO.

(4) Development, management and operation of the network environment

We have been managing the network environment collaborating with Advanced Center for Computing and Communications (ACCC). All the Ethernet ports of the information wall sockets are capable of the Gigabit Ethernet connection (10/100/1000BT). In addition, a 10 Gbps network port has been introduced to the RIBF Experimental area in for the high speed data transfer of RIBF experiment to ACCC in near future. Approximately 60 units of wireless LAN access points have been installed to cover the almost entire area of Nishina Center.

(5) Management of the information security

It is essential to take proper information security measures for information assets.

We are managing the information security of Nishina Center collaborating with ACCC.

Members

Team Leader
Takashi ICHIHARA (concurrent; Vice Chief Scientist, RI Physics Lab.)

Research & Technical Scientist
Yasushi WATANABE (concurrent; Senior Research Scientist, Radiation Lab.)

Nishina Center Research Scientist
Hidetada BABA

Student Trainee
Ryousuke TANUMA (Rikkyo Univ.)

RIBF Research Division
Research Instruments Group
Detector Team

1. Abstract

This team is in charge of development, fabrication, and operation of various detectors used for nuclear physics experiments at RIBF. Our current main mission is maintenance and improvement of beam-line detectors which are used at BigRIPS separator and its succeeding beam lines for beam diagnosis and particle identification of RI beams. We are also engaged in research and development of new detectors that can be used for higher-intensity RI beams.

2. Major Research Subjects

Development, fabrication, and operation of various detectors for nuclear physics experiments, including beam-line detectors which are used for the production and delivery of RI beams (beam diagnosis and particle identification).

3. Summary of Research Activity

The current research subjects are summarized as follows:

(1) Maintenance and improvement of the beam-line detectors which are used at BigRIPS separator and its succeeding beam lines.
(2) Development of new beam-line detectors with radiation hardness and tolerance for higher counting rates
(3) Development of a high dynamic range preamplifier for silicon strip detectors

Members

Team Leader
Toshiyuki KUBO (concurrent; Group Director, Research Instruments Gr., – Mar. 31, 2014)
Hiromi SATO (Apr. 1, 2014 –)

Special Postdoctoral Researcher
Yuki SATO

Research Consultant
Hiroyuki MURAKAMI

Visiting Scientist
Kohei FUJIWARA (Tokyo Met. Ind. Tech. Res. Inst.)

RIBF Research Division
Accelerator Applications Research Group

1. Abstract

This group promotes various applications of ion beams from RI Beam Factory (RIBF). Radiation Biology Team studies various biological effects of fast heavy ions and develops new technology to breed plants and microbials by heavy-ion irradiations. RI Applications Team studies production and application of radioisotopes for various research fields, development of trace element analysis and its application, and development of chemical materials for ECR ion sources of RIBF accelerators.

2. Major Research Subjects

Research and development in biology, chemistry and materials science utilizing heavy-ion beams from RI Beam Factory.

3. Summary of Research Activity

(1) Biological effects of fast heavy ions.
(2) Development of heavy-ion breeding.
(3) Production and application of radioisotopes.
(4) Developments of trace elements analyses.
(5) Development of chemical materials for ECR ion sources of RIBF accelerators.

Members

Group Director
Tomoko ABE

RIBF Research Division
Accelerator Applications Research Group
Ion Beam Breeding Team

1. Abstract

Ion beam breeding team studies various biological effects of fast heavy ions. It also develops new technique to breed plants by heavy-ion irradiations. Fast heavy ions can produce dense and localized ionizations in matters along their tracks, in contrast to photons (X rays and gamma rays) which produce randomly distributed isolated ionizations. These localized and dense ionization can cause double-strand breaks of DNA which are not easily repaired and result in mutation more effectively than single-strand breaks. A unique feature of our experimental facility at the RIKEN Ring Cyclotron (RRC) is that we can irradiate living tissues in atmosphere since the delivered heavy-ion beams have energies high enough to penetrate deep in matter. This team utilizes a dedicated beam line (E5B) of the RRC to irradiate microbes, plants and animals with beams ranging from carbon to iron. Its research subjects cover physiological study of DNA repair, genome analyses of mutation, and development of mutation breeding of plants by heavy-ion irradiation. Some new cultivars have already been brought to the market.

2. Major Research Subjects

(1) Study on the biological effects by heavy-ion irradiation
(2) Studies on ion-beam breeding and genome analysis
(3) Innovative application of heavy-ion beams

3. Summary of Research Activity

We study biological effects of fast heavy ions from the RIKEN Ring Cyclotron using 135A MeV C, N, Ne ions, 95A MeV Ar ions and 90A MeV Fe ions. We also develop breeding technology of microbes and plants. Main subjects are:

(1) Study on the biological effects by heavy-ion irradiation

Heavy-ion beam deposits a concentrated amount of dose at just before stop with severely changing the LET. The peak of LET is achieved at the stopping point and known at the Bragg peak (BP). It is well know to be good for cancer therapy to adjust the BP to target malignant cells. On the other hand, a uniform dose distribution is a key to the systematic study, and thus to the improvement of the mutation efficiency. Therefore plants and microbes are treated using ions with stable LET. We investigated the effect of LET ranging from 22.5 to 640 keV/μm, on mutation induction using the model plant *Arabidopsis thaliana*. The most effective LET (LETmax) was 30.0 keV/μm. In the case of microbe (*Mesorhizobium lothi*), the results showed a higher incidence of deletion mutations for Fe ions at 640 KeV/μm than for C ions at 23-40 keV/μm. Thus, the LET of ion beams seems to be an important factor affecting mutagenesis.

(2) Study on ion-beam breeding and genome analysis

In contrast to X rays and gamma rays, fast heavy ions are found to be useful for plant breeding since they only cause localized damage on DNA and can induce mutations more effectively with lower dosage. Our team utilizes beams of fast heavy ions from the RRC to develop heavy-ion breeding techniques. LETmax is effective for breeding because of its very high mutation frequency. Since most mutations are small deletions, these are sufficient to disrupt a single gene. Thus, irradiation can efficiently generate knockout mutants of a target gene, and can be applied to reverse genetics. Higher LET (> 290 keV/μm) was shown to efficiently generate large deletions ranging from several to several tens of kbp. Many genes in the *Arabidopsis* genome (> 10%) are composed of tandem duplicated genes that share functions. Previous studies demonstrated that large deletions were required to knockout tandem arrayed genes, and the appropriate deletion size was estimated to be approximately 5–10 kbp, based on gene density in *Arabidopsis*. No method is currently available to efficiently generate deletion mutants of this size. As such, higher LET irradiation is promising as a new mutagen suitable for the functional analysis of tandem duplicated genes.

(3) Innovative application of heavy-ion beams

We have formed a consortium for ion-beam breeding. It consisted of 24 groups in 1999, in 2014, it consisted of 168 groups from Japan and 18 from overseas. Breeding was performed previously using mainly flowers and ornamental plants. We have recently put a new Japanese barnyard millet cultivar with low amylose content and short culm, ‘Nebarikko No. 2’ on the market. Beneficial variants have been grown for various plant species, such as high yield rice, semi-dwarf early rice, semi-dwarf buckwheat, semi-dwarf barley, hypoallergenic peanut, spineless oranges, non-flowering Eucalyptus and lipids-hyperaccumulating unicellular alga. We also successfully isolated 4 salt-resistant lines of rice from 325 progeny lines. We collaborate with Miyagi prefecture and Tohoku University to breed salt-resistant lines in the more delicious commercial rice varieties, ‘Hitomebore’ and ‘Manamusume’, that will grow normally and retain their good taste in saline paddy fields affected by the recent tsunami. The target of heavy-ion breeding is extended from flowers to crops like grains so that it will contribute to solve the global problems of food and environment.

Members

Team Leader

Tomoko ABE (concurrent: Group Director, Accelerator Applications Research Gr.)

Research & Technical Scientist

Kazuhide TSUNEIZUMI (Senior Research Scientist)
Masako IZUMI (Senior Research Scientist)
Tokihiro IKEDA (Senior Research Scientist)
Teruyo TSUKADA (Senior Research Scientist)
Katsunori ICHINOSE (Senior Technical Scientist)
Hiroshi ABE (Senior Technical Scientist)
Ryouhei MORITA (Technical Scientist)

Contract Researchers

Hiroyuki ICHIDA (Feb.,1., 2015)
Yusuke KAZAMA
Tomonari HIRANO (– Nov. 30, 2014)

Postdoctoral Researcher

Koutaro ISHII

Technical Staff I

Yoriko HAYASHI
Sachiko KOGURE (– Mar. 31, 2014)
Motoko MURAKAMI (Apr. 1, 2014 –)

Technical Staff II

Sumie OHBU

Foreign Postdoctoral Researcher

Reka BERECZKY

Research Consultants

Tadashi SATO
Masahiro MII

Part-time Workers

Hideo TOKAIRIN
Yuki SHIRAKAWA
Sachiko KOGURE (Apr. 15, 2014 –)
Taeko WAKANA
Sayaka NIWA (May 7, 2-14 – Nov. 30, 2014)
Mieko YAMADA
Satoko YASUDA
Haruka WATANABE (Aug. 11, 2014 – Sep. 12, 2014)
Anju MATSNAGA (Aug. 4, 2014 – Sep. 30, 2014)
Honami OOHASHI (– Sep. 5, 2014)

Visiting Scientist

Makoto FUJIWARA (Univ. of Tokyo)
Masao WATANABE (Tohoku Univ.)
Hisashi TSUJIMOTO (Tottori Univ.)
Yutaka MIYAZAWA (Tohoku Univ.)
Toshinari GODO (Botanic Gardens Toyama)
Masanori TOMITA (CRIEPI)
Toshikazu MORISHITA (Nat'l. Inst. Agric. Res.)
Hiroyuki ICHIDA (Stanford Univ.)
Koji MURAI (Fukui Pref. Univ.)
Hinako TAKEHISA (Nat'l. Inst. Agric. Sci.)
Akiko HOKURA (Tokyo Denki Univ.)
Norihiro OHTSUBO (Natl. Inst. Floricult. Sci.)
Eitaro FUKATSU (Forestry and Forest Products Res. Inst.)
Tomonari HIRANO (Univ. of Miyazaki)
Yoichi SATO (Riken Food Co., Ltd.)
Ali FERJANI (Tokyo Gakugei Univ.)
In-Ja SONG (Jeju Nat'l University)
Katsutomo SASAKI (Nat'l Agric. and Food Res. Org.)
Kunio SUZUKI (Technoflora, Co., Ltd.)
Kazumitsu MIYOSHI (Akita Pref. Univ.)
Makoto UBUKATA (Hokkaido Univ.)
Akihiro IWASE (Osaka Pref. Univ.)

Visiting Technicians

Takuji YOSHIDA (Takii Seed Co., Ltd.)
Tomojirou KOIDE (Riken Vitamin Co., Ltd.)
Yutaka ITOH (Riken Food Co., Ltd.)

Research Fellows

Naoji WAKITA (Wadomari Cho Agr. Exp. Station)
Kyousuke NIWA (Hyogo Pref. Res. Inst.)
Miyuki NISHI (Saga Agric. Experiment Station)
Tadahito OOTUBO (Wadomari Cho Agr. Exp. Station)
Shunsuke IMANISHI (Natl. Inst.Veg. and Tea Sci.)
Takeya ICHIKI (Wadomari Cho)
Tomihiro TAKESHITA (Wadomari Cho)
Humio SUGAMURA (Wadomari Cho)

Student Trainees

Fumitaka YAMAGISHI (Tokyo Denki Univ.)
Fumitaka TAMEZAWA (Tokyo Denki Univ.)
Kentaro FUJITA (Tokyo Denki Univ.)
Kana MIYOSHI (Tokyo Univ. of Sci.)
Takuto TAKAHASHI (Tokyo Denki Univ.)
Hiroki KAWAMOTO (Univ. of Tokyo)
Megumi UTSUGI (Toho Univ.)
Yu IMAMURA (Tokyo Denki Univ.)
Hiroki ISHIKAWA (Sophia Univ.)
Mao SUZUKI (Sophia Univ.)
Shun SASAKI (Sophia Univ.)

RIBF Research Division
Accelerator Applications Research Group
RI Applications Team

1. Abstract

The RI Applications Team develops production technologies of radioisotopes (RIs) at RIKEN RI Beam Factory (RIBF) for application studies in the fields of physics, chemistry, biology, medicine, pharmaceutical and environmental sciences. We use the RIs mainly for nuclear and radiochemical studies such as RI production and superheavy element chemistry. The purified RIs such as ^{65}Zn and ^{109}Cd are delivered to universities and institutes through Japan Radioisotope Association. We also develop new technologies of mass spectrometry for the trace-element analyses using accelerator technology and apply them to the research fields such as cosmochemistry, environmental science, archaeology and so on. We also develop chemical materials for ECR ion sources of the RIBF accelerators.

2. Major Research Subjects

(1) Research and development of RI production technology at RIBF
(2) RI application researches
(3) Development of trace element and isotope analyses using accelerator techniques and its applications to geoscience and environmental science
(4) Development of chemical materials for ECR ion sources of RIBF accelerators

3. Summary of Research Activity

RI Applications Team utilizes RIBF heavy-ion accelerators for following research subjects:

(1) Research and development of RI production technology at RIBF and RI application studies

Due to its high sensitivity, the radioactive tracer technique has been successfully applied for investigations of the behavior of elements in the fields of chemistry, biology, medicine, engineering, and environmental sciences. We have been developing production technologies of useful radiotracers at RIBF and conducted their application studies in collaboration with many researchers in various fields. With 14-MeV proton, 24-MeV deuteron, and 50-MeV alpha beams from the AVF cyclotron, we presently produce about 30 radiotracers from ^{7}Be to ^{206}Bi. Among them, ^{65}Zn, ^{85}Sr, ^{88}Y, and ^{109}Cd are delivered to Japan Radioisotope Association for fee-based distribution to the general public in Japan. On the other hand, radionuclides of a large number of elements are simultaneously produced from metallic targets such as ^{nat}Ti, ^{nat}Ag, ^{nat}Hf, and ^{197}Au irradiated with a 135-MeV nucl.$^{-1}$ ^{14}N beam from the RIKEN Ring Cyclotron. These multitracers are also supplied to universities and institutes as collaborative researches.

In 2014, we developed production technologies of radioisotopes such as ^{28}Mg, ^{48,51}Cr, ^{67}Cu, ^{95m}Tc, ^{183,184m,184g}Re, and ^{191}Pt which were strongly demanded but lack supply sources in Japan. We also investigated the excitation functions for the ^{nat}Ti(α,x), ^{nat}Ge(α,x), ^{nat}Zr(α,x), ^{nat}Mo(d,x), ^{nat}Cd(α,x), ^{116}Cd(α,x), ^{nat}Sm(d,x), ^{nat}Ho(α,x), ^{nat}W(d,x), and ^{nat}Pt(d,x) reactions to produce useful RIs. We produced ^{65}Zn, ^{109}Cd, and ^{88}Y for our scientific researches on a regular schedule and supplied the surpluses through Japan Radioisotope Association to the general public. In 2014, we have accepted 5 orders of ^{65}Zn with a total activity of 33 MBq, 3 orders of ^{109}Cd with 21 MBq, and 2 orders of ^{88}Y with 2 MBq.

(2) Superheavy element chemistry

Chemical characterization of newly-discovered superheavy elements (SHEs, atomic numbers $Z \geq 104$) is an extremely interesting and challenging subject in modern nuclear and radiochemistry. We are developing SHE production systems as well as rapid single-atom chemistry apparatuses at RIBF. Using heavy-ion beams from RILAC and AVF, long-lived ^{261}Rf (Z = 104), ^{262}Db (Z = 105), and ^{265}Sg (Z = 106) are produced in the ^{248}Cm(^{18}O,5n)^{261}Rf, ^{248}Cm(^{19}F,5n)^{262}Db, and ^{248}Cm(^{22}Ne,5n)^{265}Sg reactions, respectively, and their chemical properties are investigated.

We have been developing a gas-jet transport system at the focal plane of the gas-filled recoil ion separator GARIS at RILAC. This system is a promising approach for exploring new frontiers in SHE chemistry: (i) the background radioactivities of unwanted reaction products are strongly suppressed, (ii) the intense beam is absent in the gas-jet chamber and hence high gas-jet efficiency is achieved, and (iii) the beam-free condition also allows for investigations of new chemical systems. In 2014, the isotope of element 107 ^{266}Bh was produced in the ^{248}Cm(^{23}Na,5n)^{266}Bh reaction, and its decay properties were investigated using the rotating wheel apparatus MANON for α/SF spectrometry. Toward the SHE chemistry behind GARIS, we developed a gas-chromatograph apparatus directly coupled to GARIS, which enabled in-situ complexation and gas-chromatographic separation of a large variety of volatile compounds of SHEs. Toward aqueous chemistry of the heaviest elements such as Sg and Bh, we also started to develop a new rapid chemistry apparatus which consisted of a continuous dissolution apparatus Membrane DeGasser (MDG), a flow liquid-liquid extraction apparatus, and a flow liquid scintillation detector for α/SF-spectrometry.

At the AVF cyclotron, the distribution coefficients (K_d) of ^{261}Rf on the Aliquat 336 resin were measured in HCl with the AutoMated Batch-type solid-liquid Extraction apparatus for Repetitive experiments of transactinides (AMBER) in collaboration with Osaka Univ. The extraction behavior of ^{89m}Zr and ^{173}Hf in the Aliquat 336/HCl system was investigated for Rf chemistry with the flow-type liquid-liquid extraction apparatus. The reversed-phase TTA extraction chromatography of ^{261}Rf and its homologues ^{85}Zr and ^{169}Hf was conducted in HF/HNO_3 using the Automated Rapid Chemistry Apparatus (ARCA) in collaboration with Kanazawa Univ., Niigata Univ., and JAEA. The reversed-phase extraction chromatography of ^{90g}Nb and ^{178a}Ta in Aliquat 336/HF and the anion-exchange chromatography of ^{90g}Nb and ^{178a}Ta in HF/HNO_3 were also conducted with ARCA for chemical studies of Db. For Sg chemistry, we investigated the extraction behavior of ^{93m}Mo and ^{177,179m}W in H_2SO_4 and $H_2C_2O_4$ solutions with Aliquat 336.

(3) Development of trace element analysis using accelerator techniques and its application to geoscience and environmental science

We developed new mass spectrometry technologies for trace element analyses as an application of accelerator technology to various fields such as cosmochemistry, environmental science, and archaeology. ECRIS-AMS is a new type of accelerator mass spectrometry at RILAC equipped with an ECR ion source. This system is available for measuring trace elements (10^{-14}–10^{-15} level) and is expected to be especially effective for measurements of low-electron-affinity elements such as ^{26}Al, ^{41}Ca, and ^{53}Mn. In 2014, we have renovated the detection system and examined the sensitivity and mass resolution power. We also attempted to develop another technology by customizing a mass spectrometer equipped with a stand-alone ECR ion source for analyses of elemental and isotopic abundances. Especially, we equipped laser-ablation system with ion source to achieve high-resolution analysis. Furthermore, we analyzed sulfur and lead isotope ratios for cinnabar samples from ancient tombs in Japan to elucidate the origin of cinnabar. In 2014, we showed that the lead isotopes in cinnabar ore exhibited clear local characteristics and the origin of the cinnabar ore could be distinguished from the lead isotope compositions.

(4) Development of chemical materials for ECR ion sources of RIBF

In 2014, we investigated production methods of $^{238}U(C_8H_8)_2$ and metallic ^{50}Ti powder for the ECR ion source of RIBF. We also prepared metallic ^{238}U and $^{238}UO_2$ on a regular schedule.

Members

Team Leader
Hiromitsu HABA

Research & Technical Scientist
Kazuya TAKAHASHI (Senior Research Scientist)

Postdoctoral Researchers
Minghui HUANG (– Mar. 31, 2014)
Yukiko KOMORI

Technical Staff I
Jumpei KANAYA

Research Consultant
Seiichi SHIBATA

Junior Research Associate
Masashi MURAKAMI (Niigata Univ.)

Part-time Workers
Michiko KITAGAWA
Yu Vin SAHOO

Visiting Scientists
Akihiko YOKOYAMA (Kanazawa Univ.)
Kazuhiko AKIYAMA (Tokyo Met. Univ.)
Kazuhiro OOE (Niigata Univ.)
Hidetoshi KIKUNAGA (Tohoku Univ.)
Masayoshi TODA (Tokyo Univ. Marine Sci. and Tech.)
Mayeen Uddin KHANDAKER (Univ. Malaya)
Takahiro YAMADA (Japan Rad. Assoc.)
Miho TAKAHASHI (Tokyo Univ. Marine Sci. and Tech.)
Hiroshi SHIMIZU (Rissho Univ.)

Visiting Technicians
Yuichiro WAKITANI (Japan Rad. Assoc.)
Shinya YANOU (Japan Rad. Assoc.)

Student Trainees
Junichi HIRATA (Tokyo Univ. Marine Sci. and Tech.)
Yuuki SHIGEYOSHI (Kanazawa Univ.)
Yuuta KITAYAMA (Kanazawa Univ.)
Hajime KIMURA (Kanazawa Univ.)
Eita MAEDA (Kanazawa Univ.)
Keigo TOYOMURA (Osaka Univ.)
Kouhei NAKAMURA (Osaka Univ.)
Yuri OBI (Tokyo Univ. Marine Sci. and Tech.)
Yoshiki FUKUDA (Kanazawa Univ.)
Yudai SHIGEKAWA (Osaka Univ.)
Shingo UENO (Kanazawa Univ.)
Kazunori HAYASHI (Kanazawa Univ.)
Takumi TANIGUCHI (Kanazawa Univ.)
Naoya GOTO (Niigata Univ.)
Takumi KOYAMA (Niigata Univ.)
Shohei TSUTO (Niigata Univ.)
Ryuji AONO (Niigata Univ.)
Daisuke SATO (Niigata Univ.)
Akira TANAKA (Niigata Univ.)
Tetuya NAGAOKA (Niigata Univ.)
Iori CHIYONISHIO (Kanazawa Univ.)
Ahmed USMAN (Univ. of Malaya)
Kento MURAKAMI (Kanazawa Univ.)
Teruyoshi FUJISAWA (Kanazawa Univ.)
Yukari YATSU (Kanazawa Univ.)
Yuki YASUDA (Osaka Univ.)
Yoshihiko HAYASHI (Osaka Univ.)
Risa MOTOYAMA (Niigata Univ.)

RIBF Research Division
User Liaison and Industrial Cooperation Group

1. Abstract

The essential mission of the “User Liaison and Industrial Cooperation (ULIC) Group” is to maximize the research activities of RIBF by attracting users in various fields with a wide scope.

The ULIC Group consists of two teams.

The User Support Team provides various supports to visiting RIBF users through the User’s Office. The Industrial Cooperation Team supports potential users in industries who use the beams for application purposes or for accelerator related technologies other than basic research. Production of various radioisotopes by the AVF cyclotron is also one of the important mission. The produced radioisotopes are distributed to researchers in Japan for a charge through the Japan Radioisotope Association.

In addition the ULIC Group takes care of laboratory tours for RIBF visitors from public. The numbers of visitors amounts to 2,300 per year.

Members

Group Director
Hideyuki SAKAI

Deputy Group Director
Hideki UENO (concurrent: Chief Scientist, Nuclear Spectroscopy Lab.)

Research & Technical Scientist
Mieko KOGURE (Technical Assistant, – Mar. 31, 2014)

Special Temporary Employee
Tadashi KAMBARA

Senior Visiting Scientists
Ikuko HAMAMOTO (Lund Univ.)
Munetake ICHIMURA (Univ. of Tokyo)

Assistants
Katsura IWAI
Noriko KIYAMA
Tomoko IWANAMI

RIBF Research Division
User Liaison and Industrial Cooperation Group
User Support Office

1. Abstract

To enhance synergetic common use of the world-class accelerator facility, the Radioisotope Beam Factory (RIBF), it is necessary to promote a broad range of applications and to maximize the facility's importance. The facilitation and promotion of the RIBF are important missions charged to the team. Important operational activities of the team include: i) the organization of international Program Advisory Committee (PAC) meetings to review experimental proposals submitted by RIBF users, ii) RIBF beam-time operation management, and iii) promotion of facility use by hosting outside users through the RIBF Independent Users program, which is a new-user registration program begun in FY2010 at the RIKEN Nishina Center (RNC) to enhance the synergetic common use of the RIBF. The team opened the RIBF Users Office in the RIBF building in 2010, which is the main point of contact for Independent Users and provides a wide range of services and information.

2. Major Research Subjects

(1) Facilitation of the use of the RIBF
(2) Promotion of the RIBF to interested researchers

3. Summary of Research Activity

(1) Facilitation of the use of the RIBF

The RIBF Users Office, formed by the team in 2010, is a point of contact for user registration through the RIBF Independent User program. This activity includes:

- registration of users as RIBF Independent Users,
- registration of radiation workers at the RIKEN Wako Institute,
- provision of an RIBF User Card (a regular entry permit) and an optically stimulated luminescence dosimeter for each RIBF Independent User, and
- provision of safety training for new registrants regarding working around radiation, accelerator use at the RIBF facility, and information security, which must be completed before they begin RIBF research.

The RIBF Users Office is also a point of contact for users regarding RIBF beam-time-related paperwork, which includes:

- contact for beam-time scheduling and safety review of experiments by the In-House Safety Committee,
- preparation of annual Accelerator Progress Reports, and
- maintaining the above information in a beam-time record database.

In addition, the RIBF Users Office assists RIBF Independent Users with matters related to their visit, such as invitation procedures, visa applications, and the reservation of on-campus accommodation.

(2) Promotion of the RIBF to interested researchers

- The team has organized an international PAC for RIBF experiments; it consists of leading scientists worldwide and reviews proposals in the field of nuclear physics (NP) purely on the basis of their scientific merit and feasibility. The team also assists another PAC meeting for material and life sciences (ML) organized by the RNC Advanced Meson Laboratory. The NP and ML PAC meetings are organized twice a year.
- The team coordinates beam times for PAC-approved experiments and other development activities. It manages the operating schedule of the RIBF accelerator complex according to the decisions arrived at by the RIBF Machine Time Committee.
- To promote research activities at RIBF, proposals for User Liaison and Industrial Cooperation Group symposia/mini-workshops are solicited broadly both inside and outside of the RNC. The RIBF Users Office assists in the related paperwork.
- The team is the point of contact for the RIBF users' association. It arranges meetings at RNC headquarters for the RIBF User Executive Committee of the users' association.
- The Team conducts publicity activities, such as arranging for RIBF tours, development and improvement of the RNC official web site, and delivery of RNC news via email and the web.

Members

Team Leader
Ken-ichiro YONEDA

Deputy Team Leader
Yasushi WATANABE (concurrent: Senior Research Scientist, Radiation Lab.)

Technical Staff I
Narumasa MIYAUCHI

RIBF Research Division
User Liaison and Industrial Cooperation Group
Industrial Cooperation Team

1. Abstract

Industrial cooperation team handles non-academic activities at RIBF corresponding to industries and to general public.

2. Major Research Subjects

(1) Fee-based distribution of radioisotopes produced at RIKEN AVF Cyclotron
(2) Support of industrial application using the RIBF accelerator beam and its related technologies including novel industrial applications.
(3) Development of real-time wear diagnostics of industrial material using RI beams

3. Summary of Research Activity

(1) Fee-based distribution of radioisotopes

This team handles fee-based distribution of radioisotopes Zn-65, Y-88 and Cd-109 from 2007, which are produced by the RI application team at the AVF cyclotron, to nonaffiliated users under a Material Transfer Agreement between Japan Radioisotope Association and RIKEN. In 2014, we delivered 3 shipments of Cd-109 with a total activity of 22 MBq, 7 shipments of Zn-65 with a total activity of 44 MBq and one shipment of Y-88 with an activity of 1 MBq. The final recipients of the RIs were five universities, one research institutes and two hospitals.

(2) Support of Industrial application using RIBF

In November 2009, RNC started a new project “Promotion of applications of high-energy heavy ions and RI beams” as a grant-in-aid program of MEXT “Sharing Advanced Facilities for Common Use Program”. In this project, RNC opens the old part of the RIBF facility, which includes the AVF cyclotron, RILAC, RIKEN Ring Cyclotron and experimental instruments like RIPS, to non-academic proposals from users including private companies. This MEXT program was terminated in September 2010, but RNC succeed and promote this facility sharing program after that. The proposals are reviewed by a program advisory committee, industrial PAC. The proposals which have been approved by the industrial PAC are allocated with beam times and the users pay RIKEN the beam time fee. The intellectual properties obtained by the use of RIBF belong to the users. In order to encourage the use of RIBF by those who are not familiar with utilization of ion beams, the first two beam times of each proposal can be assigned to trial uses which are free of beam time fee.

The fourth industrial PAC meeting held in August 2014 reviewed two fee-based proposals from private companies and approved them. The first proposal of fee-based utilization was performed in October with a 70-MeV/A 84Kr beam at the E5A beamline of the RIKEN Ring Cyclotron.

(3) Development of real-time wear diagnostics using RI beams

We are promoting a method for real-time wear diagnostics of industrial material using RI beams as tracers. For that purpose, very intense RI beams of 7Be (T1/2=52 days) at 4.1 MeV/u and 22Na (T1/2=2.6 years) at 3.7 MeV/u were produced via the (p,n) reaction at the CRIB separator using beams from the AVF cyclotron. As we can provide RI beams of different nuclides and control the implantation depth, we have developed a novel method of wear diagnostics.

Under a collaborative research agreement entitled “Development and application of wear diagnosis method with RI beams" between RIKEN, University of Tokyo and two private companies, we had two beam-times in February and in March 2014, at E7A beam-line of the AVF cyclotron. Beams of RI nuclei 7Be and 22Na were provided by CRIB and implanted near surface of metallic machine parts, whose wear-loss rate was evaluated through measurements of the radio-activities.

We are also developing a new method to determine the spatial distribution of positron-emitting RIs on periodically-moving objects in a closed system, which can be used for real-time evaluation of wear loss in a running machine. This is based on the same principle as the medical PET systems but is simpler and less expensive.

Members

Team Leader
Atsushi YOSHIDA

Research & Technical Scientist
Hiroshige TAKEICHI (Senior Research Scientist, –Jun. 30, 2014)

Visiting Technicians
Shuhei TATEMICHI (Fuji Electric Systems)
Masanori INOUE (Fuji Electric Systems)

RIBF Research Division
Safety Management Group

1. Abstract

The RIKEN Nishina Center for Accelerator-Based Science possesses one of the largest accelerator facilities in the world, which consists of two heavy-ion linear accelerators and five cyclotrons. This is the only site in Japan where uranium ions are accelerated. The center also has electron accelerators of microtron and synchrotron storage ring. Our function is to keep the radiation level in and around the facility below the allowable limit and to keep the exposure of workers as low as reasonably achievable. We are also involved in the safety management of the Radioisotope Center, where many types of experiments are performed with sealed and unsealed radioisotopes.

2. Major Research Subjects

(1) Safety management at radiation facilities of Nishina Center for Accelerator-Based Science
(2) Safety management at Radioisotope Center
(3) Radiation shielding design and development of accelerator safety systems

3. Summary of Research Activity

Our most important task is to keep the personnel exposure as low as reasonably achievable, and to prevent an accident. Therefore, we daily patrol the facility, measure the ambient dose rates, maintain the survey meters, shield doors and facilities of exhaust air and wastewater, replenish the protective supplies, and manage the radioactive waste. Advice, supervision and assistance at major accelerator maintenance works are also our task.

We revised the safety interlock system of RIBF building to prevent excess exposures due to unexpected high-intensity beam transport through the BigRIPS. When the primary beam is transported through BigRIPS, rooms adjacent to and in the vicinity of the room where the beam is transported are evacuated. If the magnetic fields of the two dipole magnets before and after the BigRIPS target position were set very closely, the interlock system recognizes the primary beam is transported through the BigRIPS. The primary beam mode can be also set manually. In the primary beam mode, some attenuators of accelerators cannot be taken out not to deliver a high-intensity beam to BigRIPS by human error.

Members

Group Director
Yoshitomo UWAMINO

Deputy Group Director
Kanenobu TANAKA (Apr. 1, 2014 –)

Nishina Center Technical Scientists
Rieko HIGURASHI
Hisao SAKAMOTO
Takeshi MAIE (concurrent; Cryogenic Technology Team)

Technical Staff I
Atsuko AKASHIO
Tomoyuki DANTSUKA (concurrent; Cryogenic Technology Team)

Research Consultant
Masaharu OKANO (Japan Radiation Res. Soc.)

Visiting Scientists
Hee Seock LEE (POSTECH)
Joo-Hee OH (POSTECH))
Nam-Suk JUNG (POSTECH)
Takashi NAKAMURA (Shimizu Corp.)
Noriaki NAKAO (Shimizu Corp.)
Koji OHISHI (Shimizu Corp.)

Assigned Employee
Hiroki MUKAI

Temporary Staffing
Ryuji SUZUKI
Hiroyuki FUKUDA

Part-time Workers
Hiroshi KATO
Satomi IIZUKA
Kimie IGARASHI
Hiroko AISO
Naoko USUDATE
Shin FUJITA
Kazushiro NAKANO

Assistant
Tomomi OKAYASU

Partner Institution

The Nishina Center established the research partnership system in 2008. This system permits an external institute to develop its own projects at the RIKEN Wako campus in equal partnership with the Nishina Center. At present, three institutes, Center for Nuclear Study of the University of Tokyo (CNS), Institute of Particle and Nuclear Studies of KEK (KEK), and Department of Physics, Niigata University (Niigata) are conducting research activities under the research partnership system.

CNS and the Nishina Center signed the partnership agreement in 2008. Until then, CNS had collaborated in joint programs with RIKEN under the "Research Collaboration Agreement on Heavy Ion Physics" (collaboration agreement) signed in 1998. The partnership agreement redefines procedures related to the joint programs while keeping the spirit of the collaboration agreement. The joint programs include experimental nuclear physics activities using CRIB, SHARAQ, GRAPE at RIBF, theoretical nuclear physics activities with ALPHLEET, accelerator development, and activities at RHIC PHENIX.

The partnership agreement with the Niigata University was signed in 2010. The activity includes theoretical and experimental nuclear physics, and nuclear chemistry.

KEK started low-energy nuclear physics activity at RIBF in 2011 under the research partnership system. The newly constructed isotope separator KISS will be available for the users in near future.

The activities of CNS, Niigata, and KEK are reported in the following pages.

Partner Institution
Center for Nuclear Study, Graduate School of Science
The University of Tokyo

1. Abstract

The Center for Nuclear Study (CNS) aims to elucidate the nature of nuclear system by producing the characteristic states where the Isospin, Spin and Quark degrees of freedom play central roles. These researches in CNS lead to the understanding of the matter based on common natures of many-body systems in various phases. We also aim at elucidating the explosion phenomena and the evolution of the universe by the direct measurements simulating nuclear reactions in the universe. In order to advance the nuclear science with heavy-ion reactions, we develop AVF upgrade, CRIB and SHARAQ facilities in the large-scale accelerators laboratories RIBF. We started a new project OEDO for a new energy-degrading scheme, where a RF deflector system is introduced to obtain a good quality of low-energy beam. We promote collaboration programs at RIBF as well as RHIC-PHENIX and ALICE-LHC with scientists in the world, and host international meetings and conferences. We also provide educational opportunities to young scientists in the heavy-ion science through the graduate course as a member of the department of physics in the University of Tokyo and through hosting the international summer school.

2. Major Research Subjects

(1) Accelerator Physics
(2) Nuclear Astrophysics
(3) Nuclear spectroscopy of exotic nuclei
(4) Quark physics
(5) Nuclear Theory
(6) OEDO/SHARAQ project
(7) Exotic Nuclear Reaction
(8) Active Target Development

3. Summary of Research Activity

(1) Accelerator Physics

One of the major tasks of the accelerator group is the AVF upgrade project that includes development of ion sources, upgrading the AVF cyclotron of RIKEN and the beam line to CRIB. Development of ECR heavy ion sources is to provide new HI beams, higher and stable beams of metallic ions, and to improve the control system. The Hyper ECR and the Super ECR sources provide all the beams for the AVF cyclotron and support not only CRIB experiments but also a large number of RIBF experiments. Injection beam monitoring and control are being developed and studied. Detailed study of the optics from the ion sources are expected to improve transmission and qualities of beams for the RIBF facility.

(2) Nuclear Astrophysics

The nuclear astrophysics group in CNS is working for experimental researches using the low-energy RI beam separator CRIB.
The call for proposals for the NP-PAC now includes proposals for CRIB again, and 3 new proposals have been approved in the NP-PAC meetings in the fiscal year 2014. In May 2014, a measurement of the elastic scattering of ^{8}B+Pb was performed in collaboration with INFN-LNL (Padova). It was made possible by the special development of intense and energy-enhanced ^{6}Li beam. A unique beam of ^{8}B at 50 MeV and 10^{4} pps was produced, and the measurement was successfully completed.

(3) Nuclear structure of exotic nuclei

The NUSPEQ (NUclear SPectroscopy for Extreme Quantum system) group studies exotic structures in high-isospin and/or high-spin states in nuclei. The CNS GRAPE (Gamma-Ray detector Array with Position and Energy sensitivity) is a major apparatus for high-resolution in-beam gamma-ray spectroscopy. Missing mass spectroscopy using the SHARAQ is used for another approach on exotic nuclei. In 2014, the following progress has been made.

Experimental data taken in 2013 under the EURICA collaboration are being analyzed for studying octupole deformation in neutron-rich nuclei. Gamow-Teller transitions of ^{8}He were studied by the (p,n) reaction in inverse kinematics, where a prominent sharp peak at Ex~8 MeV was found to be the Gamow-Teller resonance. Exothemic charge exchange reactions (^{8}He,^{8}Li*(1+)) on ^{4}He are being analyzed for studying spin-dipole response of few-body system on the photon line. The tetra-neutron system was studied by the ^{4}He(^{8}He,^{8}Be)4n reaction, which shows a candidate of the ground state of the tetra neutrons just above the 4n threshold as well as continuum at higher excitation energy.

The readout system of 14 detectors of the CNS GRAPE was upgraded, where digital pulse data taken by sampling ADCs are analyzed by FPGAs on boards.

(4) Quark Physics

Main goal of the quark physics group is to understand the properties of hot and dense nuclear matter created by colliding heavy nuclei at relativistic energies. The group has been involved in the PHENIX experiment at Relativistic Heavy Ion Collider (RHIC) at Brookhaven National Laboratory, and the ALICE experiment at Large Hadron Collider (LHC) at CERN.

As for PHENIX, the group has been concentrating on the physics analysis involving leptons and photons; dielectron measurement in Au+Au collisions, dark photon searches in low mass Dalitz decays, and J/ψ production in ultra-peripheral Au+Au collisions.

As for ALICE, the group has involved in the data analyses, which include the neutral pion production in Pb+Pb collisions, and measurement of low-mass lepton pairs in Pb+Pb and p+Pb collisions. The group has involved in the ALICE-TPC upgrade using a Gas Electron Multiplier (GEM). Performance evaluation of the MicroMegas + GEM systems for the upgrade is performed.

R&D of GEM and related techniques has been continuing. Development of Teflon GEM has been progressing in collaboration with the Tamagawa group of RIKEN.

(5) Nuclear Theory

The nuclear theory group has been promoting the CNS-RIKEN collaboration project on large-scale nuclear structure calculations since 2001 and maintaining its PC cluster. In order to review and promote this collaboration further, an international workshop "Progress in nuclear shell-model calculations in CNS-RIKEN collaboration" was held on Nov. 26-28, 2014.
This group has revealed that the 4^{+}_{1} of ^{44}S is high-K isomer, and discussed the deformation properties of the high-spin states of neutron-rich Cr and Fe isotopes utilizing shell-model calculations. A memorandum of understanding on this collaboration has been made between CNS and RIKEN in March 2014. In parallel, this group participated in activities of HPCI Strategic Programs for Innovative Research (SPIRE) Field 5 “The origin of matter and universe” since 2011.

(6) OEDO/SHARAQ project

The OEDO/SHARAQ group promoted high-resolution experimental studies of RI beams by using the high-resolution beamline and SHARAQ spectrometer. The mass measurement by TOF-Bρ technique was performed for very neutron-rich calcium isotopes around N=34. For the experiment, we introduced new detector devices into the experiment. Diamond detectors, which were developed as timing counters with extreme resolution, were installed for measuring time of flight at the first and final foci of the beam line. Clover-type Ge detectors were installed at the final focal plane of the SHARAQ spectrometer for the first time, enabling particle identification of RI beams by probing delayed gamma rays from known isomeric states of specific nuclei.

We have started ion optical development for achievement of high-quality RI beams with energies lower than 100 MeV/u. This project was named OEDO (Optimized Energy-Degrading Optics for RI beam) and the basic magnet arrangement and ion optics was discussed based on the existing high-resolution beamline and SHARAQ spectrometer.

(7) Exotic Nuclear Reaction

The Exotic Nuclear Reaction group studies various exotic reactions induced by beams of unstable nuclei.
In 2014, a parity transfer probe of the (^{16}O, ^{16}F(g.s)) reaction was demonstrated on ^{12}C at SHARAQ. The proton from the subsequent instant decay of ^{16}F(g.s.) → ^{15}F+p was detected by a MWDC newly introduced. The kinematical reconstruction of ^{16}F was successful. At SAMURAI, a measurement of knockout reactions from Borromean nuclei, ^{11}Li and ^{14}Be was performed to study the two-neutron correlation. Analysis of the ^{22,24}O(p,2p) reaction data obtained in 2012 was almost finished and the spin-orbit splitting of proton 0p orbitals in ^{22}O was derived.

(8) Active Target Development

In a project of active target development launched as an intergroup collaboration in 2009, two types of active target, called GEM-MSTPC and CAT, respectively, have been developed. The (α,p) reactions on ^{18}Ne, ^{22}Mg and ^{30}S, and the alpha emission following the beta decay of ^{16}N have been measured using GEM-MSTPC and data analyses are on going. The deuteron inelastic scattering off ^{132}Xe was measured by using the CAT with 10^{6}-particles-per-spill ^{132}Xe beam at HIMAC accelerator facility in Chiba.

Members

Director

Takaharu OTSUKA

Scientific Staff

Susumu SHIMOURA (Professor)
Hideki HAMAGAKI (Professor)
Kentaro YAKO (Associate Professor)
Nobuaki IMAI (Associate Professor, June 2014 –)
Noritaka SHIMIZU (Project Associate Professor)
Hidetoshi YAMAGUCHI (Lecturer)
Shin'ichiro MICHIMASA (Assistant Professor)
Taku GUNJI (Assistant Professor)
Shinsuke OTA (Assistant Professor)

Guest Scientists

Hiroaki UTSUNOMIYA (Guest Professor)
Yutaka UTSUNO (Guest Associate Professor)

Technical Staff

Norio YAMAZAKI (–Mar. 2014)
Yukimitsu OHSHIRO

Techinical Assistants

Hiroshi KUREI
Takehiko SENOO (–Mar. 2014)
Akira YOSHINO (Jun. 2014–)

Shoichi YAMAKA
Kazuyuki YOSHIMURA
Masahiko TANAKA (Jun. 2014–)
Mamoru KATAYANAGI (Apr. 2014–)

Project Research Associates

Tooru YOSHIDA
Yoritaka IWATA

Post Doctoral Associates

Masanori DOZONO (Apr. 2014 –)
Yorito YAMAGUCHI (– May 2014)
Taro NANAO (– Mar. 2014)
Reiko KOJIMA (– Mar. 2014)
David STEPPENBECK (– Oct. 2014)
Tomoaki TOGASHI
Naofumi KADOTA (Apr. 2014–)
Masafumi MATSUSHITA
Yoki ARAMAKI (– Oct. 2014)
Yosuke WATANABE (Apr. 2014–)
Seiya HAYAKAWA (Aug. 2014–)

Graduate Students

David. M KAHL
Akihisa TAKAHARA (–Mar. 2014)
Hiroyuki MIYA
Ryoji AKIMOTO (–Mar. 2014)
Hiroshi TOKIEDA
Tomoya TSUJI
Shintaro GO (–Mar. 2014)
Shoichiro KAWASE
ShinIchi HAYASHI
KeiIchi KISAMORI
Motonobu TAKAKI
Tang T. LEUNG (–Mar. 2014)
Yuko SEKIGUCHI
Rin YOKOYAMA
Yuki KUBOTA
CheongSoo LEE
Kohei TERASAKI
Motoki KOBAYASHI
Kentaro YUKAWA
Yuji SAKAGUCHI
Yu KIYOKAWA

Administration Staff

Hiroshi YOSHIMURA
Ikuko YAMAMOTO
Takako ENDO
Yukino KISHI
Toshiko ITAGAKI
Yuko SOMA

Partner Institution
Center for Radioactive Ion Beam Sciences
Institute of Natural Science and Technology, Niigata University

1. Abstract

The Center for Radioactive Ion Beam Sciences, Niigata University, aims at uncovering the properties of atomic nuclei and heavy elements and their roles in the synthesis of elements, with use of the advanced techniques of heavy ion and radioactive ion beam experiments as well as the theoretical methods. Main research subjects include the measurements of various reaction cross sections and moments of neutron- or proton-rich nuclei, synthesis of super-heavy elements and radio-chemical studies of heavy nuclei, and theoretical studies of exotic nuclei based on quantum many-body methods and various nuclear models. In addition, we promote interdisciplinary researches related to the radioactive ion beam sciences, such as applications of radioactive isotopes and radiation techniques to material sciences, nuclear engineering and medicine. Many of them are performed in collaboration with RIKEN Nishina Center and with use of the RIBF facilities. The center emphasizes also its function of graduate education in corporation with the Graduate School of Science and Technology, Niigata University, which invites three researchers in RIKEN Nishina Center as visiting professors.

2. Major Research Subjects

(1) Reaction cross section and radii of neutron-rich nuclei
(2) Production of superheavy nuclei and radiochemistry of heavy elements
(3) Nuclear theory

3. Summary of Research Activity

(1) Reaction cross section and radii of neutron-rich nuclei

The experimental nuclear physics group has studied nuclear structure with the RI beam. One of our main interests is the interaction/reaction cross section measurements. They are good probes to investigate nuclear matter radii and nuclear matter distributions including halo or skin structure. Recently we have measured the interaction sections of Ne, Na, Mg and Al isotopes from stable region to neutron drip line with BigRIPS in RIBF. We found a large enhancement of cross section at ^{31}Ne. It suggests that ^{31}Ne nucleus has a neutron halo. It is consistent with the soft E1 excitation measurement. We also found an enhancement at ^{37}Mg. For odd-*Z* nuclei, Na and Al, we did not find such a large enhancement from neighbor isotopes. The systematics of observed interaction/reaction cross sections shows the changing of nuclear structure from stable region to neutron drip line via island of inversion.

(2) Production of superheavy nuclei and radiochemistry of heavy elements

The nuclear chemistry group has been investigating decay properties of super-heavy nuclei, measured the excitation functions of rutherfordium isotopes, and clarified the ambiguity of the assignment of a few-second spontaneously fissioning isotope of ^{261}Rf. The new equipment designed for measurement of short-lived alpha emitters is under development.
For the chemistry research of super-heavy elements, preparatory experiments, such as solvent extraction for the group 4, 5, and 6th elements and gaseous phase chemistry for group-4 elements, have been performed using radioisotopes of corresponding homolog elements.

(4) Nuclear theory

One of the main activities of the nuclear theory group concerns with developments of the nuclear density functional theory and exploration of novel correlations and excitations in exotic nuclei. A fully selfconsistent scheme of the quasiparticle random phase approximation (QRPA) on top of the Skyrme-Hartree-Fock-Bogoliubov mean-field for deformed nuclei has been developed in the group. The versatility of this method to describe the deformation splitting of the giant resonances associated with the onset of deformation has been demonstrated for the first time by the intensive numerical calculation performed for Nd and Sm isotopes. The same method is further extended to describe the spin-isospin modes of excitation in deformed neutron-rich nuclei. A successful description of the Gamov-Teller beta-decay transition rate in the neutron-rich Zr isotopes is achieved with this method. Another correlation of interest in neutron-rich nuclei is the pair correlation, for which the spatial di-neutron correlation has been a key topic. Applying the continuum QRPA to the pairing modes of excitation in neutron-rich Sn isotopes, we predict the emergence of an anomalous pair vibration for isotopes with A>132. Furthermore the new mode is predicted to exhibits the di-neutron character. In addition to these studies, activities related to the proton-neutron pairing, the di-neutron correlation in the asymptotic tail in drip-line nuclei, the quasiparticle resonances in unbound odd-N nuclei are under way. Cluster structure and the ab initio studies of light nuclei are also important research subjects of the theory group.

Members

Director

Masayuki MATSUO (Professor)

Scientific Staff

Hisaaki KUDO (Professor)
Takashi OHTSUBO (Associate Professor)
Shin-ichi GOTO (Associate Professor)
Shigeyoshi AOYAMA (Associate Professor)
Takuji IZUMIKAWA (Associate Professor)
Kenichi YOSHIDA (Assistant Professor)

Kazuhiro OOE (Assistant Professor)
Jun GOTO (Assistant Professor)
Maya TAKECHI (Assistant Professor)

Post Doctoral Associates

Hirotaka SHIMOYAMA

Graduate Students

Kazuya HIROKAWA
Yoshihiko KOBAYASHI
Junpei ANZAI
Sho KANESAWA

Partner Institution
Radioactive Nuclear Beam Group, IPNS (Institute for Particle and Nuclear Studies)
KEK (High Energy Accelerator Research Organization)

1. Abstract

The KEK Isotope Separation System (KISS) has been constructed to experimentally study the β-decay properties of unknown neutron-rich nuclei with around neutron magic numbers N = 126 for astrophysical interest. In FY2014, first radioactive nuclear beam of ^{199}Pt, which was produced by ^{136}Xe + ^{198}Pt reaction, collected by an Ar gas cell, selectively ionized by a resonant ionization technique and mass-separated, has been successfully extracted from KISS. The measured half-life of extracted ^{199}Pt was good agreement with the reported value.

2. Major Research Subjects

(1) Radioactive isotope beam production and manipulation for nuclear experiments.
(2) Explosive nucleosyhnthesis (r- and rp-process).
(3) Heavy ion reaction mechanism for producing heavy neutron-rich nuclei.
(4) Single particle states of neutron-rich nuclei by isobaric analog resonances.
(5) Development of RNB probes for materials science applications.

3. Summary of Research Activity

The KISS is an element-selective isotope separator using a magnetic mass separator combined with in-gas-cell resonant laser ionization. The gas cell filled with argon gas of 50 kPa is a central component of the KISS for extracting only the element of interest as ion beam for subsequent mass separation. In the cell, the element primarily produced by low-energy heavy ion reactions is stopped (thermalization and neutralization), transported by buffer gas (argon gas-flow of ~50 kPa in the present case), and then re-ionized by laser irradiation just before the exit. The gas cell was fabricated to efficiently correct the reaction products produced by the multi-nucleon transfer reaction of ^{136}Xe +^{198}Pt system. For the first extraction of the reaction products, the ^{136}Xe beam energy and ^{198}Pt target thickness were set at 10.8 MeV/u and 6 mg/cm^2, respectively. In FY2014, for the half-life measurement, β-ray telescopes and a tape transport system were installed at the focal point of KISS. The β-ray telescopes were composed of three double-layered thin plastic scintillators; thickness of the first layer and second one were 0.5 and 1 mm, respectively. In order to reduce the background, they were surrounded with low-activity lead blocks and a veto counter system consisting of plastic scintillator bars. The background rate of the present β-ray telescopes was measured to be 0.7 counts per second. After the installation of the detection system, we have successfully extracted laser-ionized ^{199}Pt which mainly formed ^{199}PtAr$_2^+$ molecular ions and was transported with the mass separator as the molecular ions. The measured half-life of ^{199}Pt was $t_{1/2}$ = 33(4) min. which was good agreement with the reported value of 30.8(2) min.

Also, we investigated the extraction efficiency of ions from KISS, using ^{198}Pt elastic scattered particles. The ^{198}Pt was also extracted as ^{199}PtAr$_2^+$ molecule. The extraction efficiency was measured to be about 0.2 % which was independent of the ^{136}Xe primary beam intensities. The obtained selectivity and purity were higher than 300 and 99.7 %, respectively, at the maximum primary beam intensity of 20 pnA. In order to improve the extraction efficiency, we have started to install a new sextupole ion-guide (SPIG) at the exit of the gas cell with lager angular acceptance, which is divided into two parts with different apertures of 8 and 3 mm diameters, respectively. At the off-line test for the newly installed SPIG, we have clearly observed the dissociation of molecular ions of laser-ionized iridium, by applying DC voltage between first and second parts of the SPIG. We can expect to improve the extraction efficiency, at least, by a factor of 1.5. In FY2015, we will perform the on-line test for the new SPIG to measure the improved extraction efficiency.

For measurements of half-lives of unknown neutron-rich nuclei on N = 126, the present background rate of β-rays telescopes is not low enough. We have constructed a new β-rays telescopes in which ΔE plastic scintillator would be exchanged to a smaller one. We can expect to reduce the background rate by several factors. Further, we have started to develop a gas counter as a ΔE counter to realize the background rate of our goal, several counts per hour or less.

As a continuing effort for search for effective laser ionization scheme of elements of our interest (Z<82), a reference cell was fabricated, and is currently being used to search for auto ionizing states in Ta, W, and etc…

In order to investigate the feasibility of the multi-nucleon transfer (MNT) in the reaction system of ^{136}Xe on ^{198}Pt for producing heavy neutron-rich isotopes around the mass number of 200 with the neutron magic number of 126, We performed the cross section measurement at GANIL in 2012 and the analysis of the data has been almost completed. The cross sections of target-like fragments around N =126 were comparable to those estimated using the GRAZING code, and they appear to be mainly contributed by the reactions with low total energy loss with the weak N/Z equilibration and particle evaporation. This suggests the promising use of the MNT reactions with a heavy projectile at the energies above the Coulomb barrier for production of the neutron-rich isotopes around N = 126.

The diffusion coefficient of lithium in solid materials used in secondary Li-ion batteries is one of key parameters that determine how fast a battery can be charged. The reported Li diffusion coefficients in solid battery materials are largely scattered over several order of magnitudes. We have developed an in-situ nanoscale diffusion measurement method using α-emitting radioactive ^{8}Li tracer. In the method, while implanting a pulsed ^{8}Li beam of 8 keV, the alpha particles emitted at a small angle ($\theta = 10 \pm 1^\circ$) relative to a sample surface were detected as a function of time. We can obtain Li diffusion coefficient from the time dependent yields of the α particles, whose energy loss can be converted to nanometer-scale position information of diffusing ^{8}Li. The method has been successfully applied to measure the lithium diffusion coefficients for an amorphous Li_4SiO_4 - Li_3VO_4 (LVSO) which was used as a solid electrotype in a solid-state Li thin film battery, well

demonstrating that the present method has the sensitivity to the diffusion coefficients down to a value of 10^{-12} cm^2/s, corresponding with nanoscale Li diffusion. From FY2014, we have started to measure Li diffusion coefficients in a spinel type Li compound of $LiMn_2O_4$ (LMO), which is used as a positive electrode of a Li battery in an electric vehicle. We have observed a significant change on the time dependent yields of the α particles at the sample temperature of around 623 K and will continue the measurements to obtain temperature dependency of Li diffusion coefficients in LMO.

Members

Group Leader

Hiroari MIYATAKE

Members

Yoshikazu HIRAYAMA
Nobuaki Imai
Yutaka WATANABE
Hironobu ISHIYAMA
Sunchan JEONG
Michihiro OYAIZU
Hyo-Soon Jung
Yung-Hee KIM (PhD. Student, Seoul National Univ.)
Momo MUKAI (PhD. Student, Tsukuba Univ.)
Sota KIMURA (PhD. Student, Tsukuba Univ.)

Events (April 2014 - March 2015)

RIKEN

Apr. 10 - 11	The 3rd EURICA Workshop
Apr. 19	Wako Open campus
Jun. 1 - 6	The 2nd Conference on "Advances in Radioactive Isotope Science" (ARIS2014) http://ribf.riken.jp/ARIS2014/
Jun. 27 - 28	The 14th NP-PAC
Jul. 1 - 3	Nishina Center Advisory Council
Jul. 28 – Aug. 8	Nishina School
Aug. 7	The 4th In-PAC
Aug. 31 - Sep. 5	The 27th International Conference of the International Nuclear Target Development Society (INTDS-2014) http://ribf.riken.jp/intds2014/
Oct. 1	Start of Nuclear Transmutation Data Research Group associated with following three teams Fast RI Data Team, Slow RI Data Team and Muon Data Team Start of High-Intensity Accelerator R&D Group associated with following two teams High-Gradient Cavity R&D Team and High-Power Target R&D Team
Dec. 1-5	The 6th International Conference on Trapped Charged Particles and Fundamental Physics (TCP2014) http://indico2.riken.jp/indico/conferenceDisplay.py?confId=1395
Dec. 10	Effect of MOU between Universitas Hasanuddin, Indonesia and RNC
Dec. 12 - 13	The 15th NP-PAC
Jan. 5	Effect of MOU between RNC and Peking University
Jan. 8 - 9	The 11th ML-PAC
Mar. 31	End of Mathematical Physics Laboratory led by associate chief scientist Koji Hashimoto

CNS

Aug. 28 - Sep. 03	The 12th CNS international Summer School (CNSS13) http://indico.cns.s.u-tokyo.ac.jp/conferenceDisplay.py?confId=81

Niigata Univ.

	not held in FY2014

KEK

Aug, 21-28	KEK Summer Challenge 2014 http://www2.kek.jp/ksc/8th_2014/index.html

Press Releases (April 2014 - March 2015)

RNC

Apr. 11	Elucidation of exotic structures in very neutron-rich nuclei -a unified picture for neutron-halo, magicity-loss and large deformation-	Joint PR: Released from Tokyo Tech.
Apr. 24	Hyperfine structure constant of the single neutron halo nucleus 11Be+ has been precisely measured to be A= -2677.302988±0.000072 MHz using laser microwave double resonance spectroscopy.	Michiharu WADA (SLOWRI Team)
Jun. 18	Neutron Halo Appears in a Neutron-rich Magnesium Isotope ---Suggesting that neutron halo is a more common feature of heavier, extremely neutron-rich nuclei---	Joint PR: Released from Tokyo Tech.
Jul. 22	Rewriting the history of volcanic forcing during the past 2000 years ---A year-by-year record of volcanic eruptions from a comprehensive Antarctic ice core array---	Yuko MOTIZUKI (Astro-Glaciology Research Unit) Joint PR with Desert Research Institute
Aug. 29	Nickel-78 has been confirmed to be a 'doubly magic' isotope -- Precise beta-decay half-life measurement of ^{78}Ni --	Z. Y. Xu & Shunji Nishimura (Radioactive Isotope Physics Lab.) Joint PR with the Univ. of Tokyo
Sep. 18	SUZAKU studies of the central engine in the typical Type I seyfert NGC 3227: Detection of multiple primary X-ray continua with distinct properties	Hirofumi Noda (High Energy Astrophysics Lab.) Joint PR with the Univ. of Tokyo
Sep. 18	Efficient production of muonium at room temperature--- Stringent survey of deviation from the standard model of particle physics comes closer to reality in Japan---	Katsuhiko Ishida (Advanced Meson Science Lab.) Joint PR: Released from KEK
Sep. 19	Synthesis of a carbonyl complex of element 106, seaborgium (Sg) ---Sg shows chemical properties characteristic to the group-6 elements in the periodic table---	Hiromitsu Haba (RI Applications Team) Joint PR with JAEA
Feb. 13	Muonium in Stishovite: Implications for the Possible Existence of Neutral Atomic Hydrogen in the Earth's Deep Mantle	Dai Tomono & Teiichiro MATSUZAKI (Muon Data Team) Released from the University of Tokyo
Mar. 9	Ensuring food safety using space technology ---technology originally designed for use in outer space to create a new system, called LANFOS, which can inexpensively and non-destructively detect radioactive cesium contamination in food---	Hiromitsu Haba (RI Applications Team) Joint PR with GTEC

VII. LIST OF PUBLICATIONS & PRESENTATIONS

RIKEN Nishina Center for Accelerator-Based Science

Publications

[**Book · Proceedings**]

(Proceedings)

Enyo H.: "RIKEN Radio Isotope Beam Factory:Japanese Flagship for Nuclear Science", Proceedings of the first international African Symposium on Exotic Nuclei (IASEN-2013), (iThemba LABS), Cape Town, South Africa, pp. 43–52 (2014).

Oral Presentations

(International Conference etc.)

Enyo H.: "Status and Prospect of J-PARC E16", Hadron Physics Symposium, (Nagoya University), Nagoya, Japan, April. (2014).

Motobayashi T.: "Coulomb dissociation for studies of astrophysical reactions - achievements and perspectives", Workshop on Indirect Measurement Methods of Nuclear Astrophysics Reaction Cross Sections, (Anhui University), Hefei, China, May. (2014).

Motobayashi T.: "Nuclear astrophysics studies at RIKEN RIBF", Carpathian Summer School for Physics 2014, ("Horia Hulubei" National Institute for Physics and Nuclear Engineering, Bucharest), Sinaia, Romania, July. (2014).

Motobayashi T.: "Coulomb dissociation for astrophysics studies", PKU-CUSTIPEN Nuclear Reaction Workshop, (Pekin University), Beijing, China, Aug. (2014).

Enyo H.: "RIKEN RI Beam Factory", The VII International Symposium on Exotic Nuclei (EXON-2014), (Immanuel Kant Baltic Federal University), Kaliningrad, Russia, Sep. (2014).

Motobayashi T.: "Roles of simulation in spectroscopy with RI Beams", The International Workshop on Nuclear Science and Simulation in Fundamental and Applied Researches (IWNSS), (Ton Doc Thang University), Ho Chi Minh City, Vietnam, Oct.-Nov. (2014).

Motobayashi T.: "Nuclear astrophysics studies with fast RI beams at RIKEN RIBF", The International Symposium on Physics of Unstable Nuclei 2014 (ISPUN14), (INST, Hanoi), Ho Chi Minh City, Vietnam, Nov. (2014).

Motobayashi T.: "Experimental Studies with Magnetic Devices at RIBF", NUSTAR Annual Meeting, (GSI), Darmstadt, Germany, Mar. (2015).

Quantum Hadron Physics Laboratory

Publications

[**Journal**]

(Original Papers) *Subject to Peer Review

Tanizaki Y.: "Lefschetz-thimble techniques for path integral of zero-dimensional $O(n)$ sigma models", Phys. Rev. D **91**, 036002 (2015)*.

Tanizaki Y. and Koike T.: "Real-time Feynman path integral with Picard–Lefschetz theory and its applications to quantum tunneling", Annals of Physics **351**, 250 (2014)*.

Tanizaki Y.: "Many-body composite bosons from the viewpoint of functional renormalization", Bulg. J. Phys. **41**, no.2, 180 (2014)*.

Kashiwa K., and Tanizaki Y.: "Phase structure of $SU(3)$ gauge-Higgs unification models at finite temperature", Phys. Rev. D **89**, 116013 (2014)*.

Naidon P., Endo S., and Ueda M. :"Physical origin of the universal three-body parameter in atomic Efimov physics ",Phys. Rev. A**90**, 022106(2014)*.

Naidon P., Endo S., and Ueda M. :"Microscopic Origin and Universality Classes of the Efimov Three-Body Parameter ",Phys. Rev. Lett**112**, 105301(2014)*.

Cho S., Hattori K., Lee S. H., Morita K., and Ozaki S.: "Charmonium Spectroscopy in Strong Magnetic Fields by QCD Sum Rules: S-Wave Ground States", Phys.Rev. D **91**, 045025 (2015)*.

Cho S., Hattori K., Lee S. H., Morita K., and Ozaki S.: "QCD Sum Rules for Magnetically Induced Mixing between η_c and J/ψ", Phys.Rev. Lett. **113**, 172301 (2014)*.

Fejos G., Patkos A, and Szep Z: "Renormalized O(N) model at next-to-leading order of the 1/N expansion: Effects of the Landau pole", Phys. Rev. D**90**,016014(2014)*.

Fejos G.: "Fluctuation induced first order phase transition in U(n)xU(n) models using chiral invariant expansion of functional renormalization group flows", Phys. Rev. D**90**,096011(2014)*.

Fejos G.: "Renormalization of the 2PI-Hartree approximation in a broken phase with nonzero superflow", Phys. Rev. D**90**,116001(2014)*.

Misumi T. and Kanazawa T. :"Adjoint QCD on $R^3 \times S^1$ with twisted fermionic boundary conditions ", JHEP**06**, 181 (2014)*.

Kanazawa T. and Wettig T. :"Stressed Cooper pairing in QCD at high isospin density: effective Lagrangian and random matrix theory ", JHEP**10**, 055(2014)*.

Kamikado K. and Kanazawa T. :"Magnetic susceptibility of a strongly interacting thermal medium with 2+1 quark flavors ", JHEP**01**, 129(2015)*.

Kanazawa T. and Yamamoto A. : "Asymptotically free lattice gauge theory in five dimensions ", Phys. Rev. D**91**, 074508(2015)*.

Kanazawa T. and Tanizaki Y. : "Structure of Lefschetz thimbles in simple fermionic systems ", JHEP**03**, 044(2015)*.

Tachibana Y., and Hirano T. :"Momentum transport away from a jet in an expanding nuclear medium ",Phys. Rev. C**90**, 021902(R) (2014)*.

Hirono Y., Hongo M., and Hirano T. :"Estimation of the electric conductivity of the quark gluon plasma via asymmetric heavy-ion collisions ",Phys. Rev. C**90**, 021903(R) (2014)*.

Aoyama T., Hayakawa M., Kinoshita T., and Nio M. :"Tenth-order electron anomalous magnetic moment: Contribution of diagrams without closed lepton loops ",Phys. Rev. D**91**, 033006 (2015)*.

Baym G., Hatsuda T.: "Polarization of Direct Photons from Gluon Anisotropy in Ultrarelativistic Heavy Ion Collisions", PTEP**2015**,031D01 (2015)*.

Asakawa M., Hatsuda T., Itou E, Kitazawa M., Suzuki H. (FlowQCD Collaboration): "Thermodynamics of SU(3) gauge theory from gradient flow on the lattice", Phys. Rev. D**90**,011501(R) (2015)*.

Inoue T., Aoki S., Charron B., Doi T., Hatsuda T., Ikeda Y., Ishii N., Murano K., Nemura H., and Sasaki K. (HAL QCD Collaboration) :"Medium-Heavy Nuclei from Nucleon-Nucleon Interactions in Lattice QCD ",Phys. Rev. C**91**,011001(R) (2015)*.

Deka M., Doi T., Yang Y.B, Chakraborty B., Dong S.J., Draper T., Glatzmaier M., Gong M., Lin H.W., Liu K.F., Mankame D., Mathur N., and Streuer T. (χQCD Collaboration) :"A Lattice Study of Quark and Glue Momenta and Angular Momenta in the Nucleon ",Phys. Rev. D**91**,014505 (2015)*.

Etminan F., Nemura H., Aoki S., Doi T., Hatsuda T., Ikeda Y., Inoue T., Ishii N., Murano K., and Sasaki K. (HAL QCD Collaboration) :"Spin-2 $N\Omega$ Dibaryon from Lattice QCD ",Nucl. Phys. A**928**,89 (2014)*.

Murano K., Ishii N., Aoki S., Doi T., Hatsuda T., Ikeda Y., Inoue T., Nemura H., and Sasaki K. (HAL QCD Collaboration) :"Spin-Orbit Force from Lattice QCD ",Phys. Lett. B**735**,19 (2014)*.

Gale C., Hidaka Y., Jeon S., Lin S., Paquet J. -F., Pisarski R. D., Satow V. V., and Vujanovic G. :"Production and Elliptic Flow of Dileptons and Photons in the semi-Quark Gluon Plasma", Phys. Rev. Lett.**114**, 072301 (2015)*.

Hayata T. and Hidaka Y. :"Dispersion relations of Nambu-Goldstone modes at finite temperature and density", Phys. Rev. D**91**, 056006 (2015)*.

Anzaki R., Fukushima K., Hidaka Y., and Oka T. :"Restricted phase-space approximation in real-time stochastic quantization", Ann. Phys**353**, 107 (2015)*.

Hayata T., Hidaka Y., and Yamamoto A.: "Temporal Chiral Spiral in Strong Magnetic Fields", Phys. Rev. D**89**, 085011 (2014)*.

Hayata T. and Hidaka Y. :"Broken spacetime symmetries

and elastic variables", Phys. Lett. B**735**, 195 (2014)*.
(Review)
土井琢身, "格子 QCD シミュレーションによるハドロン間相互作用の解明", 原子核研究第 58 巻 1 号, 109 (2013)*
土井琢身, "格子 QCD シミュレーションで解き明かす核力の謎", 日本シミュレーション学会誌第 32 巻 1 号, 16 (2013)*

[**Book・Proceedings**]

(Original Papers) *Subject to Peer Review

Tachibana Y., and Hirano T. :"Di-jet asymmetric momentum transported by QGP fluid", Nucl. Phys. A**932**, 387–391 (2014)*.

Krejcirik V. :"Nucleon-nucleon scattering in the large N_c limit ",submitted to JPS Conference Proceedings.*

Oral Presentations

(International Conference etc.)

Tachibana Y., and Hirano T. : "Collective dynamics in dijet+QGP-fluid system", Fourth Joint Meeting of the Nuclear Physics Divisions of the American Physical Society and the Physical Society of Japan-Waikoloa,Hawaii,October(2014).

Tachibana Y., and Hirano T. : "Momentum Transport in Dijet+QGP-fluid", Quadrangle2014, High Energy Strong Interactions: A School for Young Asian ScientistsCentral China Normal University,Wuhan,China,September(2014).

Tachibana Y., and Hirano T. : "Momentum flow in dijet+QGP-fluid system", ATHIC 2014,Osaka University,Osaka,August(2014).

Tachibana Y., and Hirano T. : "Collective flow induced by energetic partons in heavy-ion collisions", The 26th Heavy Ion Cafe,The University of Tokyo,Tokyo,July(2014).

Hongo M., Hayata T., Yoshimasa H., Minami Y., and Noumi T. : "Derivation of anomalous hydrodynamics from quantum field theory", Fourth Joint Meeting of the Nuclear Physics Divisions of the American Physical Society and the Physical Society of Japan-Waikoloa,Hawaii,October(2014).

Hongo M., Hirono Y., and Hirano T. "Anomaly-induced transport in heavy-ion collisions", ATHIC 2014,Osaka University,Osaka,August(2014).

Kanazawa T.: "Matrix model for high-density QCD with mismatched chemical potentials", Workshop on QCD under extreme conditions (XQCD2014) New York,USA,June(2014).

Kanazawa T.: "Matrix model for high-density QCD with mismatched chemical potentials", High Energy Strong Interactions: A School for Young Asian Scientists Wuhan,China,Sep.(2014).

Fejos G.: "Finite temperature chiral symmetry restoration with functional renormalization group methods", Theoretical physics seminar at Wigner RCPBudapest,Hungary, January(2015).

Hidaka Y, "Magnetic Catalysis vs. Magnetic Inhibition", QCD Chirality Workshop 2015, Los Angeles, USA, Jan. (2015).

Hidaka Y, Hayata T,: Hongo M,: Minami Y,: Noumi T.: "Relativistic hydrodynamic equations and effective Lagrangian from quantum field theory", 4th Joint Meeting of the APS Division of Nuclear Physics and the Physical Society of Japan, Hawaii, USA, Oct. (2014).

Hidaka Y. "Spontaneous symmetry breaking and Nambu-Goldstone modes in QCD matter", XIth Quark Confinement and the Hadron Spectrum, Saint Petersburg, Russia, Sep. (2014).

Hidaka Y. "Dispersion relation of Nambu-Goldstone modes at finite temperature and density", The international workshop "Higgs Modes in Condensed Matter and Quantum Gases", Kyoto, Japan, Jun. (2014).

Tanizaki Y.: "Lefschetz-thimble Path Integral and Spontaneous Symmetry Breaking of Matrix Models", Frontiers of Hadron PhysicsBrookhaven National Laboratory, USA, Feb.(2015).

Tanizaki Y.: "Functional renormalization group approach for composite-particle excitations", Algebraic Methods in Quantum Field Theory, Sofia, Bulgaria, July(2014).

Yoshida S.: "Perturbative Matching of the Quasi-PDFs in Continuum Space and Lattice Space", The 21st International Symposium on Spin Physics, Beijing, China, Oct. (2014).

Nio M.: "QED tenth-order contribution to the electron g-2 and a new value of the fine structure constant", Fundamental Constants Meeting 2015, Eltville, Germany, Feb. (2015).

Krejcirik V.: "Effective model for $\bar{K}N$ interactions including the $L = 1$ partial wave", Hadrons and Hadron Interactions in QCD – Effective theories and Lattice, YITP, Japan, Mar. (2015).

Krejcirik V.: "Effective model for $\bar{K}N$ interactions including the $L = 1$ partial wave", Workshop on Progress on J-PARC hadron physics, Tokai, Japan, Nov. (2014).

Krejcirik V.: "Nucleon-nucleon scattering in the large N_c limit", The 2nd International Symposium on Science at J-PARC (J-PARC 2014), Tsukuba, Japan, Jul. (2014).

Kota Masuda,Muneto Nitta: "Effects of Magnetic Field and Rotation on $^3P_2$ Superfluidity in Neutron Stars", Hawaii 2014 Waikoloa, Hawaii, USA, Oct. (2014).

Kurita R.: "Entropy fluctuation from Hydrodynamic noise" The 5th Asian Triangle Heavy Ion Conference 2014 Osaka,Japan, Aug.(2014).

Kurita R.: "Fluctuation theorem in Bjoreken expansion" 4th Joint Meeting of the Nuclear Physics Divisons of the APS and JPS Hawaii,USA Oct.(2014).

Hatsuda T.: "SU(3) Thermodynamics from Yang-Mills Gradient Flow", Hadrons and Hadron Interactions in QCD – Effective theories and Lattice – (HHIQCD2015), YITP, Japan, March 2-6 (2015).

Hatsuda T.: "Z_c and T_{cc} from Lattice QCD with HAL QCD method", KEK Flavor Factory Workshop / Belle

II Theory Interface Platform Meeting, KEK, Japan, Oct. 31 (2014).

Hatsuda T.: "From QCD to Compact Stars", Advances and Perspectives in Computational Nuclear Physics Hawaii, USA, Oct. 6, (2014).

Hatsuda T.: "Physics with Hadrons at J-PARC", 2nd International Symposium on Science at J-PARC (J-PARC 2014) , Tsukuba, Japan, July 12-16, (2014).

Hatsuda T.: "New Approach to Lattice QCD Thermodynamics from Yang-Mills Gradient Flow", Quark Matter 2014, Darmstadt, Germany, May 19-24, (2014).

Hatsuda T.: "Hadron Physics at Finite Density", Hadron Physics Symposium, Nagoya, Japan, April 19, (2014).

Doi T.: "Three-Nucleon Forces from Lattice QCD", Hadrons and Hadron Interactions in QCD – Effective theories and Lattice – (HHIQCD2015), YITP, Japan, Feb.-Mar. (2015).

Doi T.: "HAL QCD method for hadron interactions on the lattice", Multi-Hadron and Nonlocal Matrix Elements in Lattice QCD (MNME 2015), BNL, USA, Feb. (2015).

Doi T.: "Charmed Tetra-quark states in Lattice QCD – Interactions from HAL QCD method–", The International Workshop on Heavy Quarkonium 2014 (Quarkonium 2014) CERN, Switzerland, Nov., (2014).

Doi T.: "Recent development in Lattice QCD studies for Three-Nucleon Forces", Fourth Joint Meeting of the Nuclear Physics Divisions of the APS and JPS (Hawaii 2014), Hawaii, USA, Oct., (2014).

Doi T.: "Quark mass dependence of three-nucleon forces in lattice QCD", The 32nd International Symposium on Lattice Field Theory (Lattice 2014), New York, USA, Jun., (2014).

Ogawa N.: "Entanglement Entropy of de Sitter Space α-Vacua", YITP workshop "Holographic vistas on Gravity and Strings",YITP,Kyoto,Japan,May,(2014).

Ogawa N.:, "Entanglement Entropy of de-Sitter Space α-Vacua", YITP workshop "Strings and Fields", YITP,Kyoto,Japan,July,(2014).

Ogawa N.: "Statistical Mechanics of Cell Mosaic Patterns in Fish Eyes", RIKEN-Osaka-OIST-Taiwan mathphys workshop,OIST,Okinawa,Japan,March,(2015).

Ogawa N.: "Entanglement Entropy of de Sitter Space α-Vacua", Strings Conference 2014, Poster session, Princeton,USA,June(2014).

(Domestic Conference)

Hongo M., Hayata T., Yoshimasa H., Minami Y., and Noumi T. : "Derivation of second order relativistic hydrodynamics from quantum field theory", Spring Meeting of Physical Society of Japan 2015Waseda University,Tokyo,March(2015).

Hongo M., Hirono Y., and Hirano T. "Chiral magnetic wave and charge-dependent elliptic flow from relativistic hydrodynamic model", Autumn Meeting of Physical Society of Japan 2014,Tokai University,Kanagawa,September(2014).

金澤拓也, "Exotic QCD on compactified spacetime", 基研研究会 素粒子物理学の進展 2014 京都, 日本,7 月 (2014).

金澤拓也, 山本新: "格子上の Lifshitz 型ゲージ理論の研究", 日本物理学会 第 70 回年次大会東京, 日本,3 月 (2015).

Fejos G.: "Chiral symmetry restoration with functional renormalization group methods", Workshop on J-Parc hadron physics in 2014Tokai, Japan ,December(2014).

Hattori K.: "Charmonium spectroscopy in strong magnetic fields by QCD sum rules", Hadrons and Hadron Interactions in QCD – Effective theories and Lattice – (HHIQCD2015), YITP, Kyoto Univ., Japan, Mar. (2015).

Hattori K.: "Photon propagation in strong magnetic fields", QCD Chirality Workshop 2015, UCLA, USA, Jan. (2015).

Cho S., Hattori K., Lee S. H., Morita K., and Ozaki S., "Charmonium spectroscopy in strong magnetic fields by QCD sum rules", Fourth Joint Meeting of the Nuclear Physics Divisions of the American Physical Society and The Physical Society of Japan, Hawaii, USA, Oct. (2014).

多田司, "On the infinite circumference limit of CFT", 日本物理学会年会早稲田大学, 3 月 (2015).

日高 義将: "QGP の基礎的性質概観（粘性など）", チュートリアル研究会「重イオン衝突の物理：基礎から最先端まで」和光, 日本, 3 月 (2015).

日高 義将, 早田智也, 本郷優, 南佑樹, 野海俊文: "相対論的流体の有効ラグランジアンと自発的対称性の破れ", 日本物理学会第 70 回年次大会東京, 日本, 3 月 (2015).

日高 義将: "自発的対称性と南部ゴールドストーンモード", 理研研究会「これからの弦理論 – 橋本研 closing 研究会 –」和光, 日本, 2 月 (2015).

日高 義将: "自発的対称性の破れと南部-Goldstone モード", 理研シンポジウム・iTHES 研究会 「熱場の量子論とその応用」和光, 日本, 9 月 (2014).

谷崎 佑弥, 小池貴之: "実時間経路積分への Lefschetz thimble 法の応用とトンネル効果", 日本物理学会年会早稲田大学, 東京,3 月 (2015).

益田晃太, 新田宗土: "中性子 $^3P_2$ 超流動体における磁場と回転の効果 (I)", 日本物理学会第 70 回年次大会 早稲田大学, 日本, 3 月 (2015).

土井 琢身: "Lattice QCD approach for Three-Nucleon Forces", Workshop on Nuclear many-body physics based on QCD RCNP, 日本, 12 月 (2014).

土井 琢身: "Lattice QCD approach for Three-Nucleon Forces", Workshop on Nuclear many-body physics based on QCD RCNP, 日本, 12 月 (2014).

土井琢身: "Calculation of Nucleon Spin in Lattice QCD", Workshop on High-energy QCD and nucleon structure Tokyo Institute of Technology, 日本, 5 月 (2014).

小川軌明, 飯塚則浩, 野海俊文: "Entanglement Entropy of de-Sitter Space α-Vacua", 日本物理学会秋季大会, 佐賀大学,9 月,(2014).

小川軌明: "時間発展系のエンタングルメントとホログラフィー", 理研研究会「これからの弦理論 –橋本研 closing

研究会–」 理化学研究所, 和光,2 月,(2015).
小川軌明, 橋本幸士, 山口康宏: “ホログラフィック模型による重クォーコニウムのスペクトラムとスピン縮退”, 日本物理学会年次大会, 早稲田大学,3 月,(2015).

Theoretical Nuclear Physics Laboratory

Publications

[Journal]

(Original Papers) *Subject to Peer Review

Nakatsukasa T.: "Finite amplitude method in linear response TDDFT calculations", Journal of Physics: Conference Series **533**, 012054 (2014). *

Matsuo M., Hinohara N., Sato K., Matsuyanagi K., Nakatsukasa T., and Yoshida K.: "Quadrupole shape dynamics from the viewpoint of a theory of large-amplitude collective motion", Phys. Scr. **89**, 054020 (2014). *

Inakura T., Horiuchi W., Suzuki Y., and Nakatsukasa T.: "Mean-field analysis of ground state and low-lying electric dipole strength in ^{22}C", Phys. Rev. C **89**, 064316 (2014). *

Ebata S., Nakatsukasa T., and Inakura T., : "Systematic investigation of low-lying dipole modes using the canonical-basis time-dependent Hartree-Fock-Bogoliubov theory", Phys. Rev. C **90**, 024303 (2014). *

Sihver L., Kohama A., Iida K., Oyamatsu K., Hashimoto S., Iwase H., and Niita K.: "Current status of the "Hybrid Kurotama model" for total reaction cross sections", Nucl. Instrum. Meth. **B 334**, 34–39 (2014). *

Sihver L., Lantz M., Kohama A., "Improved parametrization of the transparency parameter in Kox and Shen models of total reaction cross sections", Phys. Rev. C **89**, 067602-1–067602-4 (2014). *

Dinh Dang N.: "Thermal pairing and giant dipole resonance in highly excited nuclei", J. Phys.: Conf. Series **580**, 01205-1–01205-6 (2015). *

Dinh Dang N.: "Viscosity: From air to hot nuclei", Pramana - journal of physics **83**, 683–693 (2014). *

Rhine Kumar A.K., Arumugam P., Dinh Dang N.: "Pairing effect in thermal shape fluctuation model on the width of giant dipole resonance", Phys. Rev. C **90**, 044308-1 – 044308-6 (2014). *

Washiyama K.: "Fusion and quasi-fission in heavy systems with the microscopic time-dependent energy density functional theory", EPJ Web Conf. **86** 00062-1-00062-4 (2015).*

Van Giai N., Liang H.Z., Gu H.-Q., Long W.H., and Meng J.: "Treating Coulomb exchange contributions in relativistic mean field calculations: why and how", Phys. Scr. **89** 054008 (2014) *.

Liang H.Z., Nakatsukasa T., Niu Z.M., and Meng J.: "Finite-amplitude method: an extension to the covariant density functionals", Phys. Scr. **89**, 054018 (2014) *.

Liang H.Z., Meng J., Shen S.H., Van Giai N., Zhang S.Q., Zhang Y., and Zhao P.W.: "Pseudospin symmetry: Recent progress with supersymmetric quantum mechanics", Journal of Physics: Conference Series **533**, 012020 (2014).

Sheikh J. A., Hinohara N., Dobaczewski J., Nakatsukasa T., Nazarewicz W., and Sato K.: "Isospin-invariant Skyrme energy-density-functional approach with axial symmetry", Phys. Rev. C **89**, 054317-1–054317-12 (2014). *

Tanabe K., and Sugawara-Tanabe K.: "Nuclear moment of inertia as an indicator of the phase transition", Phys. Rev. C **91**, 034328 (2015). *

Sugawara-Tanabe K., Tanabe K., and Yoshinaga N.: "Analysis of the triaxial, strongly deformed bands in odd-odd nucleus 164Lu with the tops-on-top model", Progress of Theoretical and Experimental Physics **2014**, 063D0 (2014). *

(Review)

Liang H.Z., Meng J., and Zhou S.-G.: "Hidden pseudospin and spin symmetries and their origins in atomic nuclei", Physics Reports **570**, pp. 1–84 (2015). *

Oral Presentations

(International Conference etc.)

Nakatsukasa T.: "Mean-field calculations for IoI", RIBF Discussion Plus!: Island of Inversion, (RIKEN), Wako, Apr. (2014).

Nakatsukasa T.: "Nuclear response and equation of state", APCTP Workshop on the intersection of cold-atomic and nuclear physics, (APCTP), Pohang, Korea, May (2014).

Nakatsukasa T.: "Nuclear structure studies with energy density functionals", International workshop on Progress in nuclear shell-model calculations in CNS-RIKEN collaboration, (RIKEN/University of Tokyo), Wako, Nov. (2014).

Nakatsukasa T.: "Isospin invariant energy density functional and isobaric analogue states", International Symposium on Physics of Unstable Nuclei 2014, (Institute for Nuclear Science and Technology), Ho Chi Minh City, Vietnam, Nov. (2014).

Nakatsukasa T.: "Time-dependent density functional calculation of nuclear response functions", International Conference: Nuclear Theory in the Supercomputing Era - 2014, (Pacific National University), Khabarovsk, Russia, June. (2014).

Nakatsukasa T.: "Time-dependent approaches to nuclear many-body dynamics", International Workshop on New Frontier of Numerical Methods for Many-Body Correlations, (University of Tokyo/CMSI), Tokyo, Feb. (2015).

Makinaga A., Ebata S., Aikawa M., Furutachi N., Ichinkhorloo D., Kato K., Odsuren M., Devi V., Otuka N., Kohama A., Otsu H., and Sakurai H.: "Compilation of Nuclear Reaction Data from RIBF", 2nd Conference on Advances in Radioactive Isotope Science (ARIS2014), (RIKEN Nishina Center, CNS), Tokyo, Jun. (2014)

Dinh Dang N.: "Recent achievements in the study of highly excited nuclei: Thermal pairing and giant dipole

resonance", International Symposium on Physics of Unstable Nuclei (ISPUN14), (INST and LIA), HoChiMinh City, Nov. (2014).

Dinh Dang N.: "Effect of thermal fluctuations in the pairing field on the width of giant dipole resonance", International Workshop on Nuclear Science and Simulation in fundamental and applied researches, (TonDucThang University), HoChiMinh City, Oct. - Nov. (2014).

Dinh Dang N.: "Recent achievements in the study of thermal pairing and giant resonances in highly excited nuclei", 2nd International Workshop on Theoretical and Computational Physics, (Institute of Theoretical Physics and Vietnam Physics Society), Buon Ma Thuot, July (2014).

Dinh Dang N.: "Thermal pairing and giant dipole resonance in highly excited nuclei", 11th international spring seminar on nuclear physics, (University of Napoli), Ischia, May (2014).

Washiyama K.: "Microscopic analysis of fusion hindrance in heavy systems", Advances in Radioactive Isotope Science, (RIKEN/University of Tokyo), Tokyo, Japan, Jun. (2014).

Washiyama K.: "Fusion hindrance and extra push in fusion reactions with heavy nuclei", Nuba Conference Series-1: Nuclear Physics and Astrophysics, (Akdeniz University), Antalya, Turkey, Sep. (2014).

Washiyama K..: "Microscopic analysis of fusion hindrance in heavy systems", HAWAII 2014: Fourth Joint Meeting of the Nuclear Physics Divisions of the American Physical Society and The Physical Society of Japan, (APS/JPS), Waikoloa, USA, Oct. (2014).

Washiyama K.: "Fusion hindrance in heavy systems with the time-dependent energy density functional Theory", The International Symposium on Physics of Unstable Nuclei 2014, (Institute for Nuclear Science and Technology), Ho Chi Minh City, Vietnam, Nov. (2014).

Washiyama K.: "Microscopic description of extra-push energy and fusion dynamics in heavy systems", 22nd ASRC International Workshop "Nuclear Fission and Exotic Nuclei", (JAEA), Tokai, Japan, Dec. (2014).

Liang H.Z.: "Pseudospin symmetry in nuclear single-particle spectra", International Workshop: Intersection of Cold-atomic and Nuclear Physics, (Asia Pacific Center for Theoretical Physics), Pohang, South Korea, May (2014).

Liang H.Z.: "Nuclear Spin-Isospin Excitations — Towards exotic deformed nuclei", The 2nd Conference: Advances in Radioactive Isotope Science, (RIKEN), Tokyo, Jun. (2014).

Liang H.Z.: "Nuclear collective excitations in finite amplitude method", Lectures on Covariant Density Functional Theory in Nuclear Physics, (Shandong University), Weihai, China, Jul. (2014).

Liang H.Z.: "Nuclear Spin-Isospin Excitations — Towards exotic deformed nuclei", The 21st International Symposium on Spin Physics, (Peking University), Beijing, China, Oct. (2014).

Liang H.Z.: "Nuclear Spin-Isospin Excitations — Towards exotic deformed nuclei", The 15th Chinese National Conference on Nuclear Structure, (Guangxi Normal University), Guilin, China, Oct. (2014).

Liang H.Z.: "Solving Dirac equations in 3D coordinate space", International Workshop on Nuclear Science and Simulation in fundamental and applied researches, (Ton DucThang University), Ho Chi Minh, Vietnam, Oct. (2014).

Liang H.Z., Meng J., and Zhou S.-G.: "Hidden pseudospin and spin symmetries in nuclei", International Symposium on Physics of Unstable Nuclei, (Institute for Nuclear Science and Technology), Ho Chi Minh, Vietnam, Nov. (2014).

Liang H.Z.: "Nuclear spin and isospin physics in spin-isospin excitations and single-particle spectra", Nuclear Physics Seminar in Tsinghua University, (Tsinghua University), Beijing, China, Oct. (2014).

Liang H.Z.: "Dirac equation in 3D lattice and its application in covariant density functional theory", Seminar in Physics School, (Anhui University), Hefei, China, Mar. (2015).

Liang H.Z.: "Supersymmetry and relativistic symmetry in nuclei'', Seminar in School of Physics, (Peking University), Beijing, China, Apr. (2014).

Liang H.Z.: "Solutions of Dirac equation in 3D lattice'', Seminar in Institute of Theoretical Physics, (Chinese Academy of Sciences), Beijing, China, Apr. (2014).

Sato K., Dobaczewski J., Nakatsukasa T., and Satuła W.: "Isocranking calculation with proton-neutron mixed energy density functionals", Fourth Joint Meeting of the Nuclear Physics Divisions of the American Physical Society and The Physical Society of Japan (HAWAII 2014), (JPS, APS), Hawaii, Oct. (2014).

Sato K., Dobaczewski J., Nakatsukasa T., and Satuła W.: "Mean-field calculation based on proton-neutron mixed energy density functionals", 2nd Conference on Advances in Radioactive Isotope Science (ARIS2014), (CNS, University of Tokyo), Tokyo, Jun. (2014).

(Domestic Conference)

中務孝: "原子核密度汎関数理論の概要", サマースクール「クォークから超新星爆発まで」, (京都大学基礎物理学研究所、計算基礎科学連携拠点、HPCI 戦略プログラム分野 5「物質と宇宙の起源と構造」), 京都, 7 月 (2014).

中務孝: "核励起と核反応の密度汎関数計算", 「長寿命核分裂核廃棄物の核変換データとその戦略」ワークショップ, (理研), 和光, 3 月 (2014).

小濱洋央, 飯田圭, 親松和浩, 小浦寛之: "変形核反応における全反応断面積の角度平均の取り方", 日本物理学会第 70 回年次大会, 東京, 3 月 (2015).

鷲山広平：“重い反応系における核融合阻害現象の微視的解析”，日本物理学会年次大会，（日本物理学会），東京，3 月 (2015).

Liang H.Z.: "Hidden pseudospin and spin symmetries in nuclei'', RCNP Nuclear Physics Colloquium, (Osaka University), Osaka, Dec. (2014).

佐藤弘一, Dobaczewski J., 中務孝, Satuła W.: "陽子—中性子混合を含んだ密度汎関数計算", 千葉大学原子核理論研究室セミナー, (千葉大学原子核理論研究室), 千葉, 5 月 (2014).

佐藤 弘一, Dobaczewski J., 中務 孝, Satuła W.: "Isospin breaking term を入れた陽子—中性子混合密度汎関数計算", 日本物理学会　第 70 回年次大会, (日本物理学会), 東京, 3 月 (2015).

Strangeness Nuclear Physics Laboratory

Publications

[Journal]

(Original Papers) *Subject to Peer Review

Hiyama E., Ohnishi S., Gibson B., Rijken T.,
"Three-body structure of the nn Λ system with ΛN- ΣN coupling", Physical Review C, 89, 061302(R) (2014). *

Zhou B., Funaki Y., Tohsaki H., Horiuchi H., Ren Z.,
"The container picture with two-alpha correlation for the ground state of 12C", Progress of Theoretical and Experimental Physics, 101D01(7pages) (2014). *

Funaki Y., Yamada T., Hiyama E., Zhou B., Ikeda K.,
"The container structure of alpha-alpha-Lambda clusters in 9-Lambda-Beryrium", Progress of Theoretical and Experimental Physics, 113D01(16pages) (2014). *

Roepke G., Schuck P., Funaki Y., Horiuchi H., Ren Z., Tohsaki A., Yamada T., Zhou B.,
"Nuclear clusters bound to doubly magic nuclei: The case of Po-212". Physical Review C, 90, 034304 (2014). *

Lyu M., Ren Z., Zhou B., Funaki Y., Horiuchi H., Roepke G., Schuck P., Tohsaki A., Xu C., Yamada T.,
"Investigation of 9Be from nonlocalized clustering concept", Physical Review C, 014313 (2015). *

Homma H., Isaka M., Kimura M.,
"Parity reversal of 12LambdaBe", Physical Review C, 91, 014314 (2015). *

Sakumichi N., Suganuma H.,
"Perfect Abelian dominance of quark confinement in SU(3) QCD", Physical Review D (Rapid communication), 90, 111501 (2014). *

Ikeda T.N., Sakumichi N., Polkovnikov A.,Ueda M.,
"The second law of thermodynamics under unitary evolution and external operations", Annals of Physics, 354, 338 (2015). *

Lu BN., Hiyama E., Sagawa H., Zhou SG.,
"Superdeformed Λ hypernuclei within relativistic mean field models", Physical Review C, 89, 044307 (2014). *

Hiyama E., Kamimura M.,
"Universality in Efimov-associated tetramers in 4He", Physical Review A, 90, 052514 (2014). *

Schulze HJ., Hiyama E.,
"Skyrme force for light and heavy hypernuclei", Physical Review C, 90, 047301 (2014). *

Hu J., Hiyama E.,Toki H.,
"Effective ΛN potential from relativistic Brueckner-Hartree-Fock theory", Physical Review C, 90, 014309 (2014). *

Suno H., Esry BD.,
"Cold elastic and reactive atom-molecule collisions in helium-helium-alkali-metal triatomic systems", Physical Review A, 89, 052701 (2014). *

Suno H., Suzuki Y., Descouvemont P.,
"Triple-α continuum structure and Hoyle resonance of ^{12}C using the hyperspherical slow variable discretization", Physical Review C, 91, 014004 (2015).

[Book · Proceedings]

(Others) *Subject to Peer Review

Isaka M.,
"Studies of hypernuclei with the AMD method", Chiral Symmetry in Hadrons and Nuclei, 53-56 (2014).

Isaka M.,
"Structure of p-sd shell Lambda hypernuclei studied with AMD", Journal of Physics: Conference Series, 569, 012083 (2014

Ohnishi S., Ikeda Y., Hyodo T., Hiyama E., Weise W.,
"K-d ->πΣn reactions and structure of the Λ(1405)", Journal of Physics: Conference Series, 569, 012077 (2014). *

Togashi H., Takehara Y., Yamamuro S., Nakazato K., Suzuki H., Sumiyoshi K., Takano M.,
"Equation of state for nuclear matter in core-collapse supernovae by the variational method", Journal of Physics: Conference Series, 569, 012058 (2014). *

Togashi H., Takehara Y., Yamamuro S., Nakazato K., Suzuki H., Sumiyoshi K., Takano M.,
"Nuclear equation of state for core-collapse supernovae with realistic nuclear forces", Proceedings of Science, PoS (NIC XIII) 169 (2015). *

Kikuchi Y., Myo T., Kato K., Ikeda K.,
"Mechanism of Coulomb breakup reactions of two-neutron halo nuclei 6He and 11Li", Journal of Physics: Conference Series, 569, 012034 (2014). *

Oral Presentations

(International Conference etc.)

Hiyama E.,
"Structure of light hypernuclei", Sixth Asia-Pacific Conference on Few-Body Problems in Physics APFB 2014, Hahndorf, Australia, Apr.(2014).

Hiyama E.,
"Structure of light Lambda hypernuclei by (e, e'K+) reaction", JLab Workshop on hypernuclear physics "Perspectives of high resolution hypernuclear spectroscopy at Jlab", Newport News, VA, USA, May (2014).

Hiyama E.,
"Structure of α clustering Λ hypernuclei", 3rd International Workshop on "State of the Art in Nuclear Cluster Physics" (SOTANCP3), Yokohama, May(2014).

Hiyama E.,
"Few-body aspects of hypernuclear physics", Present Status of the Nuclear Interaction Theory, Beijing, China, Aug. (2014).

Hiyama E.,
"Structure of neutron-rich Lambda hypernuclei", SPHERE MEETING 2014, Prague, Czech, Sep. (2014).

Hiyama E.,
"Three- and four-body structure of 4He trimer and tetramer system", 11th Asian International Seminar on Atomic and Molecular Physics (AISAMP11), Sendai, Japan, Oct. (2014).

Hiyama E.,
"Structure of few-body hypernuclei", Fourth Joint

Meeting of the Nuclear Physics Divisions of the American Physical Society and The Physical Society of Japan (HAWAII 2014), Waikoloa, Hawaii, USA, Oct. (2014).

Hiyama E.,
"Structure of neutron-rich hypernuclei", Critical Stability 2014, Santos, Brazil, Oct. (2014).

Hiyama E.,
"Structure of neutron rich hypernuclei", Achievements and Perspectives in Low-Energy QCD with Strangeness, ECT*, Trento, Italy, Oct. (2014).

Hiyama E.,
"Structure of neutron-rich Lambda hypernuclei", FUSTIPEN Workshop "New Directions for Nuclear Structure and Reaction Theories", CAEN, France, Mar. (2015).

Funaki Y.,
"Alpha condensates and nonlocalized cluster structures", The 3rd International Workshop on "State of the Art in Nuclear Cluster Physics (SOTANCP3)", Yokohama, Japan, May (2014).

Funaki Y.,
"Alpha condensates and nonlocalized cluster structures", International Workshop on "Multi facets of Eos and Clustering (IWM-EC 2014)", Catania, Italy, May (2014).

Funaki Y.,
"Cluster states and container picture in light nuclei, and triple-alpha reaction rate", Nuba conference Series-1: Nuclear Physics and Astrophysics, Antalya, Turkey, Sep. (2014).

Isaka M.,
"Structure of Lambda hypernuclei with the antisymmetrized molecular dynamics method", Sixth Asia-Pacific Conference on Few-Body Problems in Physics (APFB 2014), Hahndorf, Australia, Apr. (2014).

Isaka M.,
"Deformations of sd and pf shell Lambda hypernuclei with antisymmetrized molecular dynamics", JLab Workshop on hypernuclear physics "Perspectives of high resolution hypernuclear spectroscopy at Jlab", Newport News, VA, USA, May (2014).

Isaka M.,
"Structure of p-sd shell Lambda hypernuclei studied with AMD", 3rd International Workshop on "State of the Art in Nuclear Cluster Physics" (SOTANCP3), Yokohama, May(2014).

Isaka M., Homma H., Kimura M.,
"Structure of single Lambda Hypernuclei", International workshop on 'Future prospect in nuclear physics with strangeness at J-PARC', Wako, Japan, June(2014).

Isaka M.,
"Structure of p-sd shell Lambda hypernuclei with antisymmetrized molecular dynamics", The SPHERE Meeting 2014, Prague, Czech, Sep. (2014).

Isaka M.,
"Structure of Lambda Hypernuclei with Antisymmetrized Molecular Dynamics", Fourth Joint Meeting of the Nuclear Physics Divisions of the American Physical Society and The Physical Society of Japan (HAWAII 2014), Waikoloa, Hawaii, USA, Oct. (2014).

Isaka M., Kimura M., Hiyama E., Sagawa H.,
"Superdeformed states in hypernuclei with antisymmetrized molecular dynamics", Fourth Joint Meeting of the Nuclear Physics Divisions of the American Physical Society and The Physical Society of Japan (HAWAII 2014), Waikoloa, Hawaii, USA, Oct. (2014).

Isaka M.,
"Superdeformed states in hypernuclei with antisymmetrized molecular dynamics", Strangeness Nuclear Physics 2014, Changsha, China, Dec. (2014).

Isaka M.,
"Triaxial deformation of 27LambdaMg with antisymmetrized molecular dynamics", International workshop on 'Hypernuclear physics with Electromagnetic Probes', Wako, Japan, Jan. (2015).

Ohnishi S., Ikeda Y., Hyodo T., Hiyama E., Weise W.,
"K-d scattering and structure of Λ(1405)", Sixth Asia-Pacific Conference on Few-Body Problems in Physics (APFB2014), Hahndorf, Australia, Apr. (2014).

Ohnishi S., Ikeda Y., Hyodo T., Hiyama E., Weise W.,
"K- scattering on deuteron target and structure of Λ (1405)", 3rd International Workshop on "State of the Art in Nuclear Cluster Physics" (SOTANCP3), Yokohama, Japan, May(2014).

Ohnishi S., Ikeda Y., Hyodo T., Hiyama E., Weise W.,
" Λ (1405) resonance in K-d scattering reaction", International Conference on Exotic Atoms and Related Topics (EXA2014), Wien, Austria, Sep. (2014).

Togashi H., Takehara Y., Yamamuro S., Nakazato K., Suzuki H., Sumiyoshi K., Takano M.,
"Equation of state for nuclear matter in core-collapse supernovae by the variational method", 3rd International Workshop on "State of the Art in Nuclear Cluster Physics" (SOTANCP3), Yokohama, Japan, May(2014).

Togashi H., Takehara Y., Yamamuro S., Nakazato K., Suzuki H., Sumiyoshi K., Takano M.,
"Variational study of the supernova equation of state with realistic nuclear forces", Fourth Joint Meeting of the Nuclear Physics Divisions of the American Physical Society and The Physical Society of Japan (HAWAII 2014), Waikoloa, Hawaii, USA, Oct. (2014).

Togashi H., Hiyama E., Takano M., Yamamoto Y.,
"Cluster variational method for nuclear matter with hyperons", Strangeness Nuclear Physics 2014, Changsha, China, Dec. (2014).

Togashi H., Hiyama E., Takano M., Yamamoto Y.,
"Equation of state for hyperonic nuclear matter with the cluster variational method", HPCI and iTHES workshop on "Study of Neutron stars and Core-Collapse Supernovae", Wako, Japan, Dec. (2014).

Togashi H., Hiyama E., Takano M., Yamamoto Y.,

"Variational study of nuclear equation of state for core-collapse supernovae and hyperonic neutron stars", International Workshop on NEUTRINO PHYSICS and ASTROPHYSICS, Istanbul, Turkey, March(2015).

Maeda S., Yokota A., Hiyama E., Oka M., Liu YR., Fukukawa K.,
"Scattering length of YcN 2 body potential and Lambda_c NN 3 body calculation with angular momentum", Fourth Joint Meeting of the Nuclear Physics Divisions of the American Physical Society and The Physical Society of Japan (HAWAII 2014), Waikoloa, Hawaii, USA, Oct. (2014).

Yoshida T., Oka M., Hosaka A., Hiyama E., Sadato K.,
"P-wave heavy baryons with the constituent quark model", Fourth Joint Meeting of the Nuclear Physics Divisions of the American Physical Society and The Physical Society of Japan (HAWAII 2014), Waikoloa, Hawaii, USA, Oct. (2014).

Yoshida T., Oka M., Hosaka A., Hiyama E., Sadato K.,
"Charmed baryon with constituent quark model", Workshop "Charm Hadron and Nuclear Physics", Tokyo, Japan, Nov. (2014).

Yoshida T., Oka M., Hosaka A., Hiyama E., Sadato K.,
"Charmed baryon spectroscopy in a quark model", Mini workshop on "Structure and productions of charmed baryonsⅡ", Ibaraki, Tokai, Japan, Aug. (2014).

(Domestic Conference)

肥山詠美子: "変分法の一般論と無限小変位ガウスローブ基底関数展開法, 少数核子系、及び不安定核物理への応用, ハドロン物理への応用, ハイパー核物理の応用と J-PARC を視野に入れた将来の展望", 少数多体系物理の最前線, 大阪, 11 月(2014).

肥山詠美子: "ミクロな世界の 3 体・4 体問題へのいざない", 理化学研究所 科学講演会 2014, 東京, 11 月 (2014).

肥山詠美子: "厳密少数多体系計算法の確立とその展開", 第 922 回九大原子核セミナー, 福岡, 1 月(2015).

井坂政裕: "ＡＭＤ, ｈｙｐｅｒ核理論 ～ＡＭＤによるハイパー核の構造研究～", ストレンジネスを含む原子核に関わる研究会 －－課題と挑戦－－, 和光, 6 月(2014).

井坂政裕, 福川賢治, 木村真明, 肥山詠美子, 佐川弘幸, 山本安夫: "反対称化分子動力学よるＡ～４０ のΛハイパー核の超変形状態", ダブルストレンジネス核物理研究会, 岐阜, 9 月(2014).

井坂政裕: "ＡＭＤ による ｓｄ－ｐｆ 殻Λハイパー核の変形状態の研究", 「ストレンジネスを含む原子核の最近の展開」研究会, 静岡, 9 月(2014).

井坂政裕, 木村真明, 肥山詠美子, 佐川弘幸: "AMD による Ar ハイパー核の超変形状態の研究", 日本物理学会 第 70 回年次大会(2015 年), 東京, 3 月(2015).

大西祥太, 池田陽一, 兵藤哲雄, 肥山詠美子, Wolfram Weise: "3 体散乱方程式に基づく Lambda(1405)共鳴生成反応の研究", ELPH 研究会 C009「光生成反応によるハドロン間相互作用の研究の進展」, 仙台, 11 月(2014).

富樫甫, 肥山詠美子, 鷹野正利: "変分法によるハイペロン物質状態方程式の研究", 「ストレンジネスを含む原子核の最近の展開」研究会, 静岡, 9 月(2014).

富樫甫, 肥山詠美子, 鷹野正利, 山本安夫: "変分法によるハイペロン混合を考慮した核物質状態方程式", 新学術領域研究会「中性子星核物質」, 京都, 3 月(2015).

富樫甫, 肥山詠美子, 鷹野正利, 山本安夫: "一様ハイペロン物質に対するクラスター変分法の研究", 日本物理学会 第 70 回年次大会(2015 年), 東京, 3 月(2015).

数納広哉, 作道直幸, 肥山詠美子: "超球座標を用いた 2 次元ヘリウム原子 3 体系の理論研究", 日本物理学会 2014 年秋季大会, 春日井, 9 月(2014).

山中長閑: "Nuclear electric dipole moment of 3-body systems in the Gaussian expansion method", KEK 研究会「Flavor of New Physics」, 東海村, 3 月(2015).

山中長閑: "Nuclear electric dipole moment of 3-body systems in the Gaussian expansion method", RIBF Seminar, 和光, 3 月(2015).

山中長閑: "Nuclear electric dipole moment of 3-body systems in the Gaussian expansion method", 日本物理学会 第 70 回年次大会(2015 年), 東京, 3 月(2015).

吉田哲也, 岡真, 保坂淳, 肥山詠美子, 定藤克法: "P-wave heavy baryons in the constituent quark model", Hadron Spectroscopy Café（東京工業大学), 東京, 5 月(2014).

吉田哲也, 岡真, 保坂淳, 肥山詠美子, 定藤克法: "チャームバリオンのスペクトルとその構造の研究", 「ストレンジネスを含む原子核の最近の展開」研究会, 静岡, 9 月(2014).

Mathematical Physics Laboratory

Publications

[**Journal**]

(Original Papers) *Subject to Peer Review

Kimura T., Murata M.: "Current Reflection and Transmission at Conformal Defects: Applying BCFT to Transport Process", Nucl. Phys. **B885**, 266-279 (2014). *

Shitade A., Kimura T.: "Bulk Angular Momentum and Hall Viscosity in Chiral Superconductors", Phys.Rev. **B90**, 134510 (2014). *

Kimura T.: "Note on a duality of topological branes", Prog. Theor. Exp. Phys. **2014**, 103B04 (2014). *

Kimura T.: "Hofstadter problem in higher dimensions", Prog. Theor. Exp. Phys. **2014**, 103B05 (2014). *

Kimura T.: "Duality and integrability of a supermatrix model with an external source", Prog. Theor. Exp. Phys. **2014**, 123A01 (2014). *

Hashimoto K.: "Possibility of ferromagnetic neutron matter", Phys.Rev. **D91**, 085013 (2015). *

Inami T., Koyama Y., Nakayama Y., Suzuki M.: "Is cosmological constant screened in Liouville gravity with matter? ", Prog. Theor. Exp. Phys. **2015**, 053B05 (2015). *

Hashimoto K., Kharzeev D.: "Entropic destruction of heavy quarkonium in non-Abelian plasma from holography", Phys. Rev. **D90**, 125012 (2014). *

Hashimoto K., Kinoshita S., Murata K., Oka T.: "Turbulent meson condensation in quark deconfinement", Phys. Lett. **B746**, 311-314 (2015). *

Hashimoto K., Kinoshita S., Murata K., Oka T.: "Electric Field Quench in AdS/CFT", JHEP **1409**, 126 (2014). *

Mazumdar A., Noumi T., Yamaguchi M.: "Dynamical breaking of shift-symmetry in supergravity-based inflation", Phys. Rev. **D90**, 043519 (2014) *

Hashimoto K., Oka T., Sonoda A.: "Magnetic instability in AdS/CFT: Schwinger effect and Euler-Heisenberg Lagrangian of supersymmetric QCD", JHEP **1406**, 085 (2014). *

Oral Presentations

(International Conference etc.)

Kimura T., "Towards $U(N|M)$ knot invariant from ABJM theory", 6th Bethe Center Workshop: Topological String and Applications, (Bethe Center for Theoretical Physics, Physikalisches Institut, Universität Bonn), Bonn, Germany, Oct. (2014).

Kimura T., "Wilson loop as a source in matrix model", チェコ科学アカデミー物理学教室セミナー, (チェコ チェコ科学アカデミー物理学教室), プラハ, チェコ, Oct. (2014).

Kimura T., "FQH/CFT and its deformation" University of Crete HEP seminar, (Crete Center for Theoretical Physics, University of Crete), イラクリオン, ギリシャ, Nov. (2014).

Kimura T., "Introduction to ABJM theory", S?minaire de Laboratoire de Physique Theorique d'Orsay, (Laboratoire de Physique Theorique d'Orsay, Universit? de Paris-Sud), オルセー, フランス, Jan. (2015).

木村太郎："ランダム行列のお話", 在仏若手研究者交流セミナー, (フランス 在仏若手研究者有志), パリ, Jan. (2015).

Kimura T.: "ゼータ関数の統計力学と深リーマン予想 ", 2nd Cross-disciplinary Meeting of Japanese Young Scientists in Europe, (在欧若手日本人研究者有志), リューデスハイム、ドイツ, Jul. (2014).

Hashimoto K.: "Electric quench in holography", APCTP focus week on holography, (APCTP), Pohang, Korea, July (2014).

Hashimoto K.: "Turbulent meson condensation at quark deconfinement", Workshop on strong dynamics beyond QCD from the lattice and string theory (NCTS Taiwan), Shinchu, Taiwan, Dec. (2014).

Hashimoto K.: "Turbulent meson condensation at quark deconfinement", KEK 理論研究会 (KEK), Tsukuba, Japan, Jan. (2015).

Hashimoto K.: "Hadron and string theory", NEW HADRON PHYSICS SYMPOSIUM, (Nagoya university), Nagoya, Japan, Apr. (2014).

(Domestic Conference)

木下俊一郎, 村田佳樹, 橋本幸士, 岡隆史, "ホログラフィック QCD における時間依存電場への応答", 日本物理学会, 佐賀大学, 9 月 (2014).

木下俊一郎, 村田佳樹, 橋本幸士, 岡隆史, "強相関絶縁体におけるシュィンガー機構の実現とゲージ重力対応による理論の比較", 日本物理学会, 早稲田大学, 3 月 (2015).

木下俊一郎, 村田佳樹, 橋本幸士, 岡隆史, "Turbulent meson condensation in quark deconfinement", 日本物理学会, 早稲田大学, 3 月 (2015).

山口康宏, 小川軌明, 橋本幸士, "ホログラフィック模型による重クォーコニウム・スペクトラムとスピン縮退", 日本物理学会, 早稲田大学, 3 月 (2015).

橋本幸士, 杉下宗太郎, 寺嶋靖治, "Ramond-Ramond couplings of D-branes", 日本物理学会, 早稲田大学, 3 月 (2015).

Radiation Laboratory

Publications

[Journal]

(Original Papers) *Subject to Peer Review

Adare A., *et al.* PHENIX Collaboration, "Heavy-flavor electron-muon correlations in p+p and d+Au collisions at $\sqrt{s}$ = 200 GeV", Phys. Rev. C **89**, 034915 (2015). *

Adler S. S., *et al.* PHENIX Collaboration, "Transverse-energy distributions at midrapidity in p+p, d+Au, and Au+Au collisions at $\sqrt{s_{NN}}$=62.4 - 200 GeV and implications for particle-production models", Phys. Rev. C **89**, 044805 (2014). *

Adare A., *et al.* PHENIX Collaboration, "Azimuthal-angle dependence of charged-pion-interferometry measurements with respect to 2nd and 3rd-order event plane in Au+Au collisions at $\sqrt{s_{NN}}$ = 200 GeV", Phys. Rev. Lett. **112**, 222301 (2014). *

Adare A., *et al.* PHENIX Collaboration, "Cold nuclear-matter effects on heavy-quark production at forward and backward rapidities in d+Au collisions at $\sqrt{s_{NN}}$=200 GeV", Phys. Rev. Lett. **112**, 252301 (2014). *

Adare A., *et al.* PHENIX Collaboration, "Measurement of transverse-single-spin asymmetries for midrapidity and forward-rapidity production of hadrons in polarized p+p collisions at $\sqrt{s}$ = 200 and 62 GeV", Phys. Rev. D **90**, 012006 (2014). *

Adare A., *et al.* PHENIX Collaboration, "Inclusive Double-Helicity Asymmetries in Neutral-Pion and Eta-Meson Production in p+p Collisions at $\sqrt{s}$ = 200 GeV", Phys. Rev. D **90**, 012007 (2014). *

Adare A., *et al.* PHENIX Collaboration, "System-size dependence of open-heavy-flavor production in nucleus-nucleus collisions at $\sqrt{s_{NN}}$=200 GeV", Phys. Rev. C **90**, 034903 (2014). *

Adare A., *et al.* PHENIX Collaboration, "Centrality Categorization for $R_p(d)$ + A in high-energy collisions", Phys. Rev. C **90**, 034902 (2014). *

Adare A., *et al.* PHENIX Collaboration, "Low-Mass Vector-Mesons Production at forward rapidity in p+p Collisions at $\sqrt{s}$ = 200 GeV", Phys. Rev. D **90**, 052002 (2014). *

Adare A., *et al.* PHENIX Collaboration, "Cross Section and Transverse Single-Spin Asymmetry of η Mesons in $p^{\uparrow}+p$ collisions at $\sqrt{s}$ = 200 GeV at Forward Rapidity", Phys. Rev. D **90**, 072008 (2014). *

Adare A., *et al.* PHENIX Collaboration, "Measurement of K^0_S and K^{*0} in p+p, d+Au and Cu+Cu collisions at $\sqrt{s_{NN}}$= 200 GeV", Phys. Rev. C **90**, 054905 (2014). *

Adare A., *et al.* PHENIX Collaboration, "Nuclear matter effects on J/psi production in asymmetric Cu+Au collisions at $\sqrt{s_{NN}}$ =200GeV", Phys. Rev. C **90**, 064908 (2014). *

Adare A., *et al.* PHENIX Collaboration, "Cross-section for *barb* production via dielectrons in d+Au collisions at $\sqrt{s_{NN}}$ =200 GeV", Phys. Rev. C **91**, 014907 (2015). *

Adare A., *et al.* PHENIX Collaboration, "Charged-pion cross sections and double-helicity asymmetries in polarized p+p collisions at $\sqrt{s}$ = 200 GeV", Phys. Rev. D **91**, 032001 (2015). *

Adare A., *et al.* PHENIX Collaboration, "Measurement of the Upsilon(1S+2S+3S) production in p+p and Au+Au collisions at $\sqrt{s_{NN}}$ = 200 GeV", Phys. Rev. C **91**, 024913 (2015). *

Adare A., *et al.* PHENIX Collaboration, "Search for dark photons from neutral meson decays in p+p and d+Au collisions at $\sqrt{s_{NN}}$ = 200 GeV", Phys. Rev. C **91**, 031901 (2015). *

Seidel R, PHENIX W to mu measurements in polarized proton-proton collisions, PoS DIS2014(2014) 205, 2014/07/16

Kanesue T, Fuwa Y, Kondo K, Okamura M, "Laser ion source with solenoid field", APPLIED PHYSICS LETTERS, 105, 193506 (2014) *

Okamura M, Sekine M, Ikeda S, Kanesue T, Kumaki M, Fuwa Y, "Preliminary result of rapid solenoid for controlling heavy-ion beam parameters of laser ion source", Laser and Particle Beams, doi:10.1017/S026303461500004X (2015) *

(Review) *Subject to Peer Review

Akiba Y, "Quest for the quark-gluon plasma — hard and electromagnetic probles", Progress of theoretical and experimental physics 03A105(2015), 2015/01/12 *

[Book・Proceedings]

(Original Papers)

Kanesue T, *et al.* "THE COMMISSIONING OF THE LASER ION SOURCE FOR RHIC EBIS", Proceedings of IPAC 2014 (ISBN 978-3-95450-132-8), p1890-1892

Munemoto N, *et al.*, "LASER ABLATION ION SOURCE FOR THE KEK DIGITAL ACCELERATOR", Proceedings of IPAC 2014 (ISBN 978-3-95450-132-8), p598-600

Ikeda S, *et al.*, "Control of Plasma Flux with Pulsed Solenoid for Laser Ion Source", Proceedings of IPAC 2014, (ISBN 978-3-95450-132-8), p601-603

Fuwa Y, *et al.*, "Beam dynamics of multi charge state ions in RFQ linac", Proceedings of LINAC 2014 (ISBN 978-3-95450-142-7), p317-319

Okamura M, *et al.*, "Low Charge Laser Ion Source for the EBIS injector", Proceedings of LINAC 2014 (ISBN 978-3-95450-142-7), p64-66

(Review)

秋葉康之, クォーク・グルーオン・プラズマの物理 (共立出版), ISBN 978-4-320-03523-2, 2014/4/15

Oral Presentations

(International Conference etc.)

Yasuyuki Akiba, "Future plan at BNL", Hadron physics symposium (科研費新学術領域「新ハドロン」), Nagoya, Japan, 2014/4/18

Yasuyuki Akiba, "Electromagnetic probes and heavy flavor from RHIC and LHC", Hawaii 2014 (Fourth Joint Meeting of the Nuclear Physics Division of the American Physical Society and the Physical Society of Japan) (APS/JPS), Waikoloa Village, HI, USA, 2014/10/7

Ralf Seidl, "W to mu measurements at PHENIX", Conference on Deep inelastic scattering and related topics , Warsaw, Poland, 2014/05/29

Ralf Seidl, "Three-Dimensional Imaging and Spin - from Valence Quarks to the Sea", Hawaii 2014 (Fourth Joint Meeting of the Nuclear Physics Division of the American Physical Society and the Physical Society of Japan) (APS/JPS), Waikoloa Village, HI, USA, 2014/10/7

T. Kanesue, "THE COMMISSIONING OF THE LASER ION SOURCE FOR RHIC EBIS", 5th International Particle Accelerator Conference (Cockcroft Inst. and U. Liverpool), Dresden, Germany, 2014/06/15-16

Y. Fuwa, "Charge-State Selective Ion Beam Acceleration with RFQ Linac", 20th International Symposium on Heavy-Ion Inertial Fusion (IMP), Lanzhou, China, 2014/08/11-15

T. Kanesue, "Stable operation of Laser Ion Source for low charge state ion production", 20th International Symposium on Heavy-Ion Inertial Fusion (IMP), Lanzhou, China, 2014/08/11-15

Shunsuke Ikeda, "Control of plasma flux with pulsed solenoid for laser ion source", 5th International Particle Accelerator Conference (Cockcroft Inst. and U. Liverpool), Dresden, Germany, 2014/06/15-16

N. Munemoto, "LASER ABLATION ION SOURCE FOR THE KEK DIGITAL ACCELERATOR", 5th International Particle Accelerator Conference (Cockcroft Inst. and U. Liverpool), Dresden Germany, 2014/06/15-20

M. Okamura, "Preliminary result of rapid solenoid for controlling heavy-ion beam parameters of laser ion source", 20th International Symposium on Heavy-Ion Inertial Fusion (IMP), Lanzhou, China, 2014/08/11-15

Y. Fuwa, "Beam dynamics of multi charge state ions in RFQ linac", 27th Linear Accelerator Conference (CERN), Geneva, Switzerland, 2014/08/31-09/05

M. Okamura, "Low Charge Laser Ion Source for the EBIS injector", 27th Linear Accelerator Conference (CERN), Geneva, Switzerland, 2014/08/31-09/05

Shunsuke Ikeda, "Influence of solenoidal magnetic field on laser ablation plasma", 5th Euro-Asian Pulsed Power Conference (Kumamoto Univ.), Kumamoto, Japan, 2014/09/11

Masafumi Kumaki, "Proton beam generation using Au-coated plastic target from Laser Ion Source" 19th International Conference on Ion Beam Modification of Materials, Leuven, Belgium, 2014/09/14-19

Yusuke Komatsu, "Development of a Tracking and Electron Identification System Using GEM for the J-PARC E16 Experiment", IEEE NUCLEAR SCIENCE SYMPOSIUM 2014 (IEEE), Seattle, USA, 2014/11/08-15

Satoshi Yokkaichi, "Measurement of vector mesons in nuclei at J-PARC E16 experiment" , Hadrons and Hadron Interactions in QCD 2015 (YITP), Kyoto, Japan 2015/03/05

(Domestic Conference etc.)

Ralf Seidl, "Experimental overview: Nucleon spin structure" , APS Division of Nuclear Physics (APS) Temple University, Philadelphia, PA, USA 2014/9/13,

Ralf Seidl, "Belle 実験における di-hadron の破砕関数", 日本物理学会第 70 回年次大会早稲田大学、東京, 2015/3/21-24

秋葉康之, "RHIC PHENIX 実験とその将来計画", 第 1 回 CiRfSE ワークショップ (筑波大学数理物質融合科学センター), 筑波大学、つくば市, 2015/3/12

Kotaro KONDO 大電流レーザーイオン源にむけた重金属標的を用いたレーザーアブレーションプラズマの価数分析日本原子力学会　2014 年秋の大会京都大学、京都 2014/09/08-10

池田峻輔, " レーザーアブレーションプラズマに対するパルス磁場の影響", 日本物理学会第 70 回年次大会, 早稲田大学、東京, 2015/3/21-24

熊木雅史" ピコ秒レーザーを用いたレーザーイオン源開発" 日本物理学会第 70 回年次大会早稲田大学、東京 2015/3/21-24

村上ひかり, "チェレンコフ検出器用 CsI GEM の開発", 第 11 回 MPGD 研究会 (東北大学), 東北大学、仙台, 2014/12/20

中井　恒, "J-PARC E16 実験における GEM 検出器の開発状況", 第 11 回 MPGD 研究会 (東北大学), 東北大学、仙台, 2014/12/20

Advanced Meson Science Laboratory

Publications

[Journal]

Abdel-Jawad M., Watanabe I., Tajima N., Ishii Y., and Kato R., "Universality Class of the Mott-Hubbard Transition", Phys. Rev. Lett. 114, 106401-1-5 (2015).

Adam N., Suprayoga E., Adiperdana B., Guo H., Tanida K., Mohd-Tajudin S.S., Kobayashi R., Sera M., Nishioka T., Matsumura M., Sulaiman S., Mohamed Ibrahim M.I., and Watanabe I, "Muon sites in $Ce(Ru,Rh)_2Al_{10}$ investigated by using Density Functional Theory from the view point of electronic potential" J. Phys. Conf. Ser. **551**, 012053 (2014).

Adare A., Ohnishi H. et al. (PHENIX Collaboration) "Measurement of K^0_S and K^{*0} in p+p, d+Au, and Cu+Cu collisions at $\sqrt{S_{NN}}$=200 GeV", Phys. Rev. C90 (2014) 5, 054905

Adare A., Ohnishi H. *et al.* (PHENIX Collaboration) "System-size dependence of open-heavy-flavor production in nucleus-nucleus collisions at $\sqrt{S_{NN}}$=200 GeV" ,Phys.Rev. C90 (2014) 034903

Adiperdana B., Suprayoga E., Adam N., Mohm-Tajudin S.S., Rozlan A.F., Sulaiman S., Mohamed-Ibrahim M.I., Kawamata T., Adachi T., Dharmawan I.A. , Siregar R.E., Koike Y., and Watanabe I., "An Effect of the Super-Cell Calculation on Muon Positions and Local Deformations of Crystal Structure in La2CuO4", J. Phys. Conf. Ser. 551, 012051 (2014).

Adler S.S., Ohnishi H. *et al.* (PHENIX Collaboration) "Transverse-energy distributions at midrapidity in p+p , d+Au , and Au+Au collisions at$\sqrt{S_{NN}}$= 62.4-200 GeV and implications for particle-production models", Phys.Rev. C89 (2014) 044905

Agnello H., Outa H., FINUDA collaboration, "First determination of the one-proton induced Non-Mesonic Weak Decay width of p-shell Λ-Hypernuclei", Phys. Lett. B738 (2014) 499-504*

Ariga H., Shimomura K., Ishida K., Pratt F., Yoshizawa, Wataru K., Higemoto W., Torikai E., Asakura K., "Detection of Oxygen Vacancy in Rutile TiO_2 Single Crystal by μSR Measurement", JPS Conference Proceedings (2014) 010307

Bakule P., Sukhorukov O., Ishida K., Pratt F., Fleming D., Momose T., Matsuda Y., and Torikai E., "First accurate experimental study of Mu reactivity from a state-selected reactant in the gas phase: the Mu + H2{1} reaction rate at 300 K", J. Phys. B: At. Mol. Opt. Phys. 48 (2015) 045204

Bazzi M., Iwasaki M., SIDDHARTA collaboration, "L-series X-ray yields of kaonic 3He and 4He atoms in gaseous targets", Eur. Phys. J. A50 (2014) 91*

Beer G.A., Fujiwara Y., Hirota S., Ishida K., Iwasaki M., Kanda S., Kawai H., Kawamura N., Kitamura R., Lee S., Lee W., Marshall G.M., Mibe T., Miyake Y., Okada S., Olchanski K., Olin A., Ohnishi H., Oishi Y., Otani M., Saito N., Shimomura K., Strasser P., Tabata M., Tomono D., Ueno K., Won E., and Yokoyama K., "Enhancement of Muonium Emission Rate from Silica Aerogel with a Laser-Ablated Surface", Prog. Theor. Exp. Phys. 091C01 (2014).

Cargnello M., Iwasaki M., SIDDHARTA collaboration, "X-ray spectroscopy of kaonic atoms at SIDDHARTA", EPJ Web Conf. 73 (2014) 05008*

Chang L. –J., Lees M.R., Watanabe I., Hillier A.D., Yasui Y., and Onoda S., "Static Magnetic Moments Revealed by Muon Spin Relaxation and Thermodynamic Measurements in Quantum Spin Ice $Yb_2Ti_2O_7$", Phys. Rev. B 89, 184416-1-5 (2014)*

Curceanu C., Iwasaki M., Okada S. *et al.* (SIDDHARTA Collaborarion), "Unveiling the strangeness secrets: low-energy kaon-nucleon/nuclei interactions studies at DAΦNE", EPJ Web Conf. 66 (2014) 09004

Enomoto S., Hashimoto T., Itahashi K., Iwasaki M., Ma. Y., Okada S., Ohnishi H., Outa H., Sakuma. F., Sato M., Tokuda M., Yamazaki T. (J-PARC E15 collaboration), "Search for deeply-bound Kbar-nuclear states via the 3He(inflight-K-,n) reaction at J-PARC", Proceedings of XV International Conference on Hadron Spectroscopy (Hadron 2013), Proceedings of Science (Hadron 2013) 182 (2014)

Funamori N., Kojima K.M., Wakabayashi D., Sato T., Taniguchi T,, Nishiyama N., Irifune T., Tomono D., Matsuzaki T., Miyazaki M., Hiraishi M., Koda A., and Kadono R., "Muonium in Stishovite: Implications for the Possible Existence of Neutral Atomic Hydrogen in the Earth's Deep Mantle", Scientific Report 5, 8437-1-5 (2015).

Fujihala M., Xu-Guang Zheng, Norodomi H., Kawae T., Matsuo A., Kindo K., and Watanabe I., "Unconventional Spin Freezing in the Highly Two-Dimensional Spin-1/2 Kagome Antiferromagnet $Cd_2Cu_3(OH)_6(SO_4)_2 \cdot 4H_2O$: Evidence of Partial Order and Coexisting Spin Singlet State on a Distorted Kagome Lattice", Phys. Rev. B 89, 100401(R)-1-5 (2014)*

Fujioka H., Brinkmann K.T., Friedrich S., Geissel H.,Hayano R.S., Hirenzaki S., Itahashi K., Itoh S., Jido D., Metag V., Nagahiro H., Nanova M., Nishi T., Okochi K., Outa H., Suzuki K., Suzuki T.,Tanaka Y.K., Watanabe Y.N., Weick H., "Spectroscopy of eta-prime Mesic Nuclei via Semi-Exclusive Measurement at FAIR", EPJ Web Conf. 66 (2014) 09006

Goto T., Suzuki T., Watanabe I., Manaka H., Luetkens H., and Amato A., "Ground State of Bond-Disordered Quasi-One-Dimensional Spin System $(CH_3)_2CHNH_3Cu(Cl_xBr_{1-x})_3$ with x=0, 0.025 and 0.3", J. Phys. Soc. Conf. Proc. 2, 010207-1-5 (2014).

Guo H., Xing H., Tong J., Tao Q., Watanabe I., and Zhu-an Xu, "Possible Spin Frustration in $Nd_2Ti_2O_7$ Probed by Muon Spin Relaxation", Journal of Physics: Condens. Matter. 26, 436002 (2014).

Hashimoto T. *et al.* (J-PARC E15 collaboration),

"A search for the K-pp bound state in the 3He(K- in-f light, n) reaction at J-PARC", Proceedings of the 25th International Nuclear Physics Conference (INPC 2013), EPJ Web of Conferences 66, 09008 (2014)

Iliescu M., Iwasaki M., Okada S., Tatsuno H. *et al.* (SIDDHARTA, SIDDHARTA-2 and AMADEUS Collaboration), " Progress and perspectives in the low-energy kaon-nucleon/nuclei interaction studies at the DAΦNE collider", J. Phys. Conf. Ser. 556 (2014) 012004

Ikedo Y., Miyake Y., Shimomura K., Strasser P., Kawamura N., Nishiyama K., Makimura S., Fujimori H., Koda A., Nakamura J., Nagatomo T., Kobayashi Y., Adachi T., Pant A.D., Ogitsu T., Nakamoto T,, Sasaki K., Ohhata H., Okada R., Yamamoto A., Makida Y., Yoshida M., Okamura T., Ohkubo R., Higemoto W., Ito T.U., Nakahara K., Ishida K., "U-Line at MLF/J-PARC for Ultra Slow Muon Microscopy", JPS Conference Proceedings 2 (2014) 010103

Ishiwatari T., Iwasaki M., Okada S. *et al.* (SIDDHARTA Collaborarion), " Kaonic Atoms - Results of the SIDDHARTA Experiment", Acta Phys. Polon. B45 (2014) 787

Ishiwatari T., Iwasaki M., OkadaS. *et al.* (SIDDHARTA Collaborarion), "New precision era of experiments on strong interaction with strangeness at DAFNE/LNF-INFN ", EPJ Web Conf. 66 (2014) 05016

Itahashi K., "Meson Bound States Spectroscopy in Nuclei: Pionic Atoms at RIBF and η '-Mesic Nuclei at GSI/FAIR", Acta Phys. Polon. B45 (2014) 773*

Kanda S., Fujimori H., Fukao Y., Ikedo Y., Ishida K., Iwasaki M., Kawamura N., Kojima K.M., Lee M., Makimura S., Mibe T., Miyake Y., Nakamura J., Nagashima Y., Nagatomo T., Nagumo K., Nishimura S., Okada S., Saito N., Shimomura K., T. Suzuki, Strasser P., Ueno K., Won E., "Development of High-Rate Positron Tracker for the Muonium Production Experiment at J-PARC", JPS Conference Proceedings 2 (2014) 010404

Kawasaki I., Watanabe I., Hillier A.D., and Aoki D., "Evidence for Time-Reversal Symmetry Breaking in Both the Hidden Order and Superconducting States of URu_2Si_2", J. Phys. Soc. Jpn. 83, 094720-1-5 (2014)*

Kuroe H., Aoki K., Sato T., Kino R., Kuwahara H., Sekine T., Hase M., Kawasaki I., Kawamata T., Suzuki T., Watanabe I., Oka K., Ito T., and Eisaki H., "Muon spin Spectroscopy in Multiferroic $(Cu,Zn)_3Mo_2O_9$" J. Phys. Soc. Conf. Proc. 2, 010206-1-8 (2014).

Månsson M., Umegaki I., Nozaki H., Higuchi, Kawasaki I., Watanabe I., Sakurai H., and Sugiyama J., "Na-Ion Dynamics in Quasi-1D Compound NaV_2O_4" J. Phys. Conf. Ser. 551, 012035 (2014).

Månsson M., Nozaki H., Wikberg J.M., Prsa K., Sassa Y., Dahbi M., Kamazawa K., Sedlak K., Watanabe I., and Sugiyama J., "Lithium Diffusion and Magnetism in Battery Cathode Material $Li_xNi_{1/3}Co_{1/3}Mn_{1/3}O_2$", J. Phys. Conf. Ser. 551, 012037 (2014).

Miyazaki K., Saito N., Okamura K., Oishi Y., Louchev O.A., Iwasaki M. and Wada S., "Tunable 820.65 nm Light Source by Injection-Seeded Optical Parametric Oscillator and Amplifier for Muonium Lyman-Alpha Generation", JPS Conference Proceedings 2 (2014) 010107

Matsuzaki T., Ishida K., Iwasaki M., "High-pressure solid hydrogen target for muon catalyzed fusion", Journal of Radioanalytical and Nuclear Chemistry, DOI 10.1007/s10967-015-4080-y

Mohd-Tajudin S.S., Ahmad S.N.A., Hasan-Baseri D.F., Suprayoga E., Adam N., Rozlan A.F., Sulaiman S., Mohamed-Ibrahim M.I., and Watanabe I., "An Investigation of Muon Sites in YBa2Cu3O6 by Using Density Functional Theory", J. Phys. Conf. Ser. 551, 012052 (2014).

Moritsu M., Itahashi K., J-PARC E19 collaboration, "High-resolution search for the Θ+ pentaquark via a pion-induced reaction at J-PARC ", Phys.Rev. C90 (2014) 035205*

Mukai K., Aoki Y., Andreica D., Amato A., Watanabe I., Giblin S.R., and Sugiyama J., "Spin Fluctuation above 100K in Stoichiometric $LiCoO_2$", J. Phys. Conf. Ser. 551, 012008 (2014).

Mukai K., Aoki Y., Andreica D., Amato A., Watanabe I., Giblin S.R., and Sugiyama J., "Thermally Activated Spin Fluctuations in Stoichiometric LiCoO2 Clarified by Electron Paramagnetic Resonance and Muon-Spin Rotation and Relaxation Measurements", Phys. Rev. B 89, 094406-1-11 (2014)*

Nakamura J., Nagatomo T., Oishi Y., Ikedo Y., Strasser P., Saito N., Miyazaki K., Yokoyama K., Okamura K., Miyake Y., Makimura S., Nishiyama K., Shimomura K., Kawamura N., Koda A., Higemoto W., Wada S., Iwasaki M., Torikai E., "Ultra Slow Muon Microscope at MUSE / J-PARC", J.Phys.Conf.Ser. 502 (2014) 012042*

Nakamura J., Oishi Y., Saito N., Miyazaki K., Yokoyama K., Okamura K,, Makimura S., Miyake Y., Nagatomo T., Strasser P., Ikedo Y., Tomono D., Shimomura K., Wada S., Kawamura N., Koda A. and Nishiyama K., ,"Transport of Coherent VUV Radiation to Muon U-Line for Ultra Slow Muon Microscope", JPS Conference Proceedings 2 (2014) 010108

Nishi T., Berg G.P.A., Dozono M., Fujioka H., Fukuda M., Furuno T., Geissel H., Hayano R.S., Inabe N., Itahashi K., Itoh S., Kameda D., Kubo T., Matsubara H., Michimasa S., Miki K., Miya H., Murakami Y., Nakamura M., Nakatsuka M., Noji S., Okochi K., Ota S., Suzuki H., Suzuki K., Takaki M., Takeda H., Tanaka Y.K., Todoroki K.,Tsukada K., Uesaka T., Watanabe Y.N., Weick H., Yamada H., Yoshida K., "The first precision measurement of deeply bound pionic states in ^{121}Sn", EPJ Web Conf. 66 (2014) 09014

Nishimura K., Matsuda K., Komaki Y., Nunomura N., Wenner S., Holmestad R., Matsuzaki T., Watanabe I., Pratt F.L., and Marioara C.D., "μSR Study of Al-0.67%

Mg-0.77%Si Alloy", J. Phys. Conf. Ser. 551, 012031 (2014).

Nozaki H., Harada M., Ohta S., Asaoka T., Watanabe I., Pomjakshin V., kedo Y., Miyake Y., Jaralvo N.H., Mamontov E., and Sugiyama J., "Diffusive Behavior of Li Ions in Garnet $Li_{5+x}La_3Zr_xNb_{2-x}O_{12}$ Studied with both QENS and μ SR", Solid State Ionics 262, 585-588 (2014).

Ohnishi H., Iwasaki M., Sakuma F., Yokkaichi S., Bühler P., Hartmann O., Ishiwatari T., Marton J., Suzuki K., Widmann E., Zmeskal J. Curceanu C., Guaraldo C., Okada S., Vidal A.R., Sirghi D., Sirghi F., Vazquez Doce O., Hicks K., Muto R., Naruki M., Sawada S., Niiyama M., Noumi H., Sakaguchi A., Tsukada K., "A Search for φ Meson Nucleus Bound State Using Antiproton Annihilation on Nucleus", Acta Phys.Polon. B45 (2014) 819-826*

Oishi Y., Okamura K., Miyazaki K., Saito N., Iwasaki M., Wada S., "All-solid-state laser amplifiers for intense Lyman-α generation" Proceedings of the International Symposium on Science Explored by Ultra Slow Muon. Vol.2, 010105-1～5 (2014)

Okada Y., Yagi E., Matsuba H., Sugi C., Koike S., Nakamura S., Sugawara T., Shishido T. and Ogiwara K., "Site occupancy of hydrogen in Ta-rich Ta-Nb alloys as observed by the channelling method", J. Phys. Soc. Jpn. 83 (2014) 064602-1–9.

Okamura K., Saito N., Miyazaki K., Oishi Y., Louchev O,, Iwasaki M. and Wada S., "Temporally Resolved Spectral Structure of 821 nm Broad-Area Laser Diode Seeder for Muonium Lyman-Alpha Generation", JPS Conference Proceedings 2 (2014) 010106

Pant A.D., Nagamine K., Shiraki I., Torikai E., Shimomura K., Pratt F.L., Ariga H., Ishida K., and Schultz J.S., "Muonium Responses to Oxygen Content in Biological Aqueous Solutions for Cancer Research", J. Phys. Conf. Ser. 551, 012043 (2014)

Risdiana, Safriani L., Somantri W.A., Saragi T., Adachi T., Kawasaki I., Watanabe I., and Koike Y.,"Impurity-Induced Magnetic Order in Electron-Doped Superconducting Cuprates $Eu_{1.85}Ce_{0.15}Cu_{1-y}Ni_yO_{4+\alpha-\delta}$ Studied by Muon-Spin-Relaxation", Advanced Materials Research **896**, 354-357 (2014)*

Sada Y., Hashimoto T., Itahashi K., Ma Y., Iwasaki M., Ohnishi H., Okada S., Outa H., Sakuma F., Sato M., Tokuda M., Tomono D., Yamazaki T., Zhang Q. *et al.* (J-PARC E15 Collaboration),"A Search for Deeply-bound Kaonic Nuclear States by In-flight $^3He(K^-,n)$ Reaction at J-PARC", EPJ Web Conf. 81 (2014) 02016

Safriani L., Risdiana, Bahtiar A., Aprilia A., Siregar R.E., Hidayat R., Saragi T.P.I, Kawasaki I., and Watanabe I., "Charge Carrier Dynamics of Active Material Solar Cell P3HT: ZnO Nanoparticles Studied by Muon Spin Relaxation (μSR)", Advanced Materials Research 896, 477-480 (2014)*

Sakuma F., Hashimoto T., Itahashi K., Iwasaki M., Ma. Y., Okada S., Ohnishi H., Outa H., Sato M., Tokuda M., Yamazaki T. (J-PARC E15 collaboration), "A Search for Deeply-bound Kaonic Nuclear States by In-flight 3He(K-,n) Reaction at J-PARC", Proceedings of the Second International Symposium on Mesic Nuclei, Acta Phys. Pol. B45, 767 (2014)*

Shi H., Iwasaki M., Okada S. *et al.* (SIDDHARTA Collaborarion), "The yield of kaonic hydrogen X-rays in the SIDDHARTA experiment", EPJ Web Conf. 66 (2014) 09016

Sierawski B.D., Bhuva B., Reed R., Ishida K., Tam N., Hillier A., Narasimham B., Trinczek M., Blackmore E., Wen Shi-Jie, and Wong R., "Bias Dependence of Muon-Induced Single Event Upsets in 28 nm Static Random Access Memories", Reliability Physics Symposium, 2014 IEEE International , vol., no., pp.2B.2.1,2B.2.5, 1-5 June 2014, doi: 10.1109/IRPS.2014.6860585

Suprayoga E., Nugroho A.A., Polyakov A,O., Palstra T.T.M. , and Watanabe I.,"Search for Potential Minimum Positions in Metal-Organic Hybrids, $(C_2H_5NH_3)_2CuCl_4$ and $(C_6H_5CH_2CH_2NH_3)_2CuCl_4$, by Using Density Functional Theory", J. Phys. Conf. Ser. 551, 012054 (2014).

Suzuki T., Watanabe I., Yamada F., Ishii Y., Ohishi K., Goto T., and Tanaka H.,"Gradual Evolution in Spin Dynamics of $TlCu^{1-x}Mg_xCl_3$ Probed by Mon-Spin-Relaxation (μSR) Technique", Journal of Physics: Conference Series **502**, 012041-1-14 (2014).

Tanabe Y., Adachi T., Suzuki K. , Akoshima M., Kawamata T., Ishii Y., Suzuki T., Watanabe I., and Koike Y., "Development of Spatial Inhomogeneity of Internal Magnetic Field above T_C in$Bi_2Sr_2Ca_{1-x}Y_xCu_2O_8$ Observed by Longitudinal-Field Muon-Spin-Relaxation" J. Phys. Soc. Jpn. **83**, 074707-1-5 (2014)*

Tanaka K.S., Aoki M., Iinuma H., Ikedo Y., Ishida K., Iwasaki M., Ueno Y., Ohkubo R., Ogitsu T., Kadono R., Kamigaito O., Kawamura N., Kawall D., Kanda S., Kubo K., Kume T., Koda A., Kojima K., Saito N., Sakamoto N., Sasaki K., Shimomura K., Sugano M., Tomono D., Toyoda A., Torii H.A., Torikai E., Nagamine K., Nishiyama K., Strasser P., Fukao Y., Fujiwara Y., Matsuda Y., Mibe T., Miyake Y., Yoshida M., "Measurement of Muonium Hyperfine Splitting at J-PARC", JPS Conference Proceedings 2 (2014) 010405

Tanaka Y.K., Brinkmann K.T., Friedrich S., Fujioka H., Geissel H.,Hayano R.S., Hirenzaki S., Itahashi K., Itoh S., Jido D., Metag V., Nagahiro H., Nanova M., Nishi T., Okochi K., Outa H., Suzuki K., Suzuki T., Watanabe Y.N., Weick H., "Missing Mass Spectroscopy of η' Mesic Nuclei with the (p,d) Reaction at GSI", EPJ Web Conf. 66 (2014) 09019

Tomida N., Niiyama M., Ohnishi H., Tran M., Hsieh C.-Y., Chu M.-L., Chang W.-C., Chen J.-Y., "Large strip RPCs for the LEPS2 TOF system", Nucl. Instrum. Meth. A766 (2014) 283-287*

Watanabe Y.N., Berg G.P.A, Dozono M., Fujioka H., Fukuda N., Furuno T., Geissel H., Hayano R.S., Inabe N., Itahashi K., Itoh S., Kameda D., Kubo T., Matsubara H., Michimasa S., Miki K., Miya H.,

Murakami Y., Nakamura M., Nakatsuka N., Nishi T., Noji S., Okochi K., Ota S., Suzuki H., Suzuki K., Takaki M., Takeda H., Tanaka Y.K., Todoroki K., Tsukada K., Uesaka T., Weick H., Yamada H., Yamakami H., Yoshida K., "Status and future plan of the spectroscopy of pionic atoms",
J.Phys.Conf.Ser. 503 (2014) 012037

Oral Presentations

(International Conference etc.)

Hashimoto T., Itahashi K., Iwasaki M., Ma. Y., Okada S., Ohnishi H., Outa H., Sakuma. F., Sato M., Yamazaki T. (J-PARC E15 collaboration), "Search for the K-pp bound state via the 3He(K-,n) reaction at 1 GeV/c", 3rd International Workshop on "State of the Art in Nuclear Cluster Physics" (SOTANCP3), KGU Kannai Media Center, Kanto Gakuin University, Yokohama, Japan., May(2014)

Hashimoto T., Itahashi K., Iwasaki M., Ma. Y., Okada S., Ohnishi H., Outa H., Sakuma. F., Sato M., Yamazaki T. (J-PARC E15 collaboration), "Search for the K-pp bound state via the infight-kaon reaction on helium-3", 20th Particles and Nuclei International Conference 2014 (PANIC2014), Hamburg, Germany, Aug.(2014)

Itahashi K., "Experimental spectroscopy of pionic atoms and eta'-mesic nuclei", HHIQCD14, Kyoto, Mar. (2015)

Itahashi K., "Precision measurement of deeply bound pionic Sn atoms in RIBF", EXA14, Vienna, Sep. (2014)

Itahashi K., "High precision systematic measurement of deeply bound pionic atoms", 4th Joint Meeting of the APS Division of Nuclear Physics and the Physical Society of Japan, Hawaii, Oct. (2014)

K., Hashimoto T., Itahashi K., Iwasaki M., Ma. Y., Okada S., Ohnishi H., Outa H., Sakuma. F., Sato M., Yamazaki T., (J-PARC E15 collaboration), "A Search forDeeply-bound Kaonic nuclear states", The 3rd Korea-Japan Workshop on Nuclear and Hadron Physics at J-PARC, Inha University, Korea, Mar.(2014)

Kawasaki S.,Hashimoto T., Itahashi K., Iwasaki M., Ma. Y., Okada S., Ohnishi H., Outa H., Sakuma. F., Sato M., Yamazaki T. (J-PARC E15 collaboration), "Experimental search for K-pp deeply bound statevia in-flight 3He(K-,n) reaction at J-PARC K1.8BR", The 2nd International Symposium on Science at J-PARC 2014, Tsukuba, Japan, Jul.(2014)

Okada S., Bennett D. A., Doriese. W. B., Fowler. J. W., Irwin. K. D., Ishimoto S., Sato M., Schmidt. D. R., Swetz. D. S., Tatsuno H., Ullom. J. N., Yamada S., "Study of strong interaction between anti-kaon and nucleus via high-resolution kaonic-atom x-ray spectroscopy with superconducting transition-edge-sensor microcalorimeters", Suzaku-MAXI 2014 (Expanding the Frontiers of the X-ray Universe), Matsuyama, Feb. (2014).

Sada Y., Hashimoto T., Itahashi K., Iwasaki M., Ma. Y., Okada S., Ohnishi H., Outa H., Sakuma. F., Sato M., Yamazaki T. (J-PARC E15 collaboration), "Search for the K-pp bound state via the in-flight 3He(K-,n) reaction", 13th International Workshop on Meson Production, Properties and Interaction (MESON2014), Krakow, Poland, Jun.(2014)

Sakuma F., Hashimoto T., Itahashi K., Iwasaki M., Ma. Y., Okada S., Ohnishi H., Outa H., Sato M., Yamazaki T. (J-PARC E15 collaboration), "Recent results and future prospects of the KbarNN search via the (K-,N) reaction at J-PARC", Achievements and Perspectives in Low-Energy QCD with Strangeness, ECT*, Italy, Oct.(2014)

Tanaka Y.K.,
"Search for η mesic nuclei with (p,d) reaction at GSI", 4th Joint Meeting of the APS Division of Nuclear Physics and the Physical Society of Japan, Hawaii, Oct. (2014)

Tanaka Y.K.,
"Eta' mesic nucleus spectroscopy with (p,d) reaction at GSI" , 20th Particles and Nuclei International Conference (PANIC2014), 25-29, August, 2014, Hamburg, Germany

足立匡, 高橋晶, 鈴木謙介, Baqiya M.A. , 今野巧也, 高松智寿, 加藤雅恒, 渡邊功雄, 幸田章宏, 宮崎正範, 門野良典, 小池洋二, "Novel Coexistence of Superconductivity with Short-Range Magnetic Order in Electron-Doped High-T_C T'-Cuprates",The 2nd International Symposium on Science at J-APRC, J-PARC, 東海村. 茨城県, 2014 年 7 月

足立匡, 高橋晶, 鈴木謙介, Baqiya M.A., 今野巧也, 高松智寿, 加藤雅恒, 渡邊功雄, 幸田章宏, 宮崎正範, 門野良典, 小池洋二, "Novel Coexistence of Superconductivity with Short-Range Magnetic Order in High-T_C T'-Cuprates Observed by Muon Spin Relaxation", Superstripes 2014, Erice, Sicily, イタリア, 2014 年 7 月

渡邊功雄, 松平和之, 川崎郁斗, 分島亮, 日夏幸雄, Zhu-an Xu
"μSR Sudies of Spin Ground States in the Pyrochlore Iridate $Nd_2Ir_2O_7$", 2014 Collaborative Conference 3D and Materials Researchs (CC3DMR2014) 韓国仁川, 2014 年 6 月

渡邊功雄
"Muon Site Estimation in La_2CuO_4 by the Density Functional Theory", 2nd International Conference on Functional Material Science 2014, Lombok, インドネシア, 2014 年 11 月

Abdel-Jawad M.M., 渡邊功雄, 石井康之, 田嶋尚也, 加藤礼三, "Universality Class Of The Mott Transition In $EtMe_3P[Pd(dmit)_2]_2$",Internaional Conference on Synthetic Metals ICSM2014, Turku, フィンランド、2014 年 6 月

Lees M.R., Chang L.-J.,渡邊功雄, Hillier A.D.,安井幸夫, 小野田茂樹, Balakrishnan G., Lhotel E., Giblin S.R.,
"Studies of Magnetic Order in $Yb_2Ti_2O_7$"
International Conference on Highly Frustrated Magnetism 2014 (HFM2014), Cambridge, 英国, 2014 年 7 月

小池洋二, 鈴木謙介, 足立匡, 佐藤輔, 渡邊功雄

"Novel Fe-Induced Magnetism in the Overdoped Regime of the La-214 High-TC Curate: Implication for Dtripe Fluctuation", 27th International Conference on Low Temperature Physics(LT27), Buenos Aires, 2014 年 8 月

(Domestic Conference)

足立匡, 高橋晶, 鈴木謙介, M.A. Baqiya, 渡邊功雄, 幸田章宏, 宮崎正範, 門野良典, 小池洋二: "μSR からみた電子型 T'-214 高温超伝導体における Cu スピン相関とノンドープ超伝導", 第 2 回物構研サイエンスフェスタ, KEK, 茨城県つくば市, 1 月(2014)

足立匡, 高橋晶, 鈴木謙介, Baqiya M.A., 今野巧也, 高松智寿、加藤雅恒, 渡邊功雄, 幸田章宏, 宮崎正範, 門野良典小池洋二, "電子型 T'-214 高温超伝導体における超伝導と短距離磁気秩序の新奇な共存", 日本物理学会秋の大会, 中部大学, 名古屋, 2014 年 9 月

足立匡, 高橋晶, 鈴木謙介, Baqiya M.A., 今野巧也, 高松智寿, 加藤雅恒, 渡邊功雄, 幸田章宏, 宮崎正範, 門野良典, 小池洋二, "電子型 T' 高温超伝導体における超伝導と短距離磁気秩序の新奇な共存", 新学術領域「超低速ミュオン顕微鏡」第 3 回領域会議, 東北大学、仙台市、2014 年 9 月

上原友敬, 伊藤美穂, 谷口浩三, 佐藤和彦, 石井康之, 渡邊功雄, "μSR Study of κ-(h8-BEDT-TTF)$_2$Cu[N(CN)$_2$]Cl and Discussion of Muon Site Using Relaxation Signal from Deuterated κ-(d8-BEDT-TTF)$_2$Cu[N(CN)$_2$]Br" 1st RIKEN-Sophia Joint Syposium Recent Progresses on the Muon-Site Estimation, 上智大学, 四谷, 東京, 2014 年 12 月

板橋健太, "η 中間子原子核分光実験の検討", ELPH 研究会 C009「光生成反応によるハドロン間相互作用の研究の進展」, 仙台, 11 月 (2014)

應田治彦, 板橋健太, 岩崎雅彦, Ma Y, 岡田信二,大西宏明, 佐久間史典, 佐藤将春, 山崎敏光, E15 collaborator : "E15 experiment on K-pp", KEK theory center workshop on J-PARC hadron physics in 2014, つくば市, 2 月(2014).

應田治彦 (for J-PARC E15 Collaboration) "Status of kaonic nucleus search experiment (E15) at J-PARC",新学術研究領域「実験と観測で解き明かす中性子星の核物質」 研究会,熱川ハイツ, 2014 年 9 月

岡田信二, 石田勝彦, 岩崎雅彦, 上野一樹, Eunil Won, 大石裕, Art Olin, 河合秀幸, 河村成肇, 神田聡太郎, 北村遼, 齊藤直人, 下村浩一郎, Patrick Strasser, 田端誠, 友野大, 西村昇一郎, Pavel Bakule, George Beer, 藤原裕也, Glen Marshall, 松田恭幸, 三部勉, 三宅康博, 横山幸司, Woodo Lee: "超低速ミュオン生成のための室温ミュオニウム真空放出源の開発" 日本物理学会第 69 回年次大会, 平塚市, 3 月(2014).

川崎郁斗, 横山淳, 藤村健司, 渡邊功雄, 天谷健一 "ミュオンスピン緩和法からみた $Sr_{1-x}La_xRuO_3$ における不均一強磁性クラスターの形成",日本物理学会秋の大会, 中部大学, 名古屋, 2014 年 9 月

北村遼, 深尾祥紀, 石田勝彦, 河村成肇, 近藤恭弘, 三部勉, 三宅康博, 大谷将士, Patrick Strasser, 齊藤直人, 下村浩一郎 他 J-PARC muon g-2/EDM コラボレーション, "J-PARC ミューオン g-2/EDM 精密測定実験のためのミューオン再加速試験に向けた低速ミューオン源開発の準備状況", 日本物理学会第 70 回年次大会, 早稲田大学,東京, 3 月(2015)

後藤貴行, 松井一樹, 足立匡, 大槻東巳, 田邉洋一, 渡邊功雄, "トポロジカル絶縁体におけるスピンロック現象 μSR 検出", 新学術領域「超低速ミュオン顕微鏡」第 3 回領域会議, 東北大学、仙台市、2014 年 9 月

小林弘明, 岡澤厚, 小島憲道, 川崎郁斗, 渡邊功雄: "スピン平衡を示すスピンクロスオーバー鉄 (II) 錯体におけるメスバウアー分光とミュオン分光からみた動的挙動", メスバウアー分光研究会, 東大本郷キャンパス, 3 月(2014)

今野巧也, 足立匡, 扇太郎, 高橋晶, 加藤雅恒, 渡邊功雄, 小黒英俊, 淡路智, 小池洋二, "電子ドープ型超伝導体 $Pr_{1.3-x}La_{0.7}Ce_xCuO_{4+\delta}$} (x≦0.1)単結晶における還元アニール効果と電子状態", 日本物理学会春の大会, 早稲田大学, 東京, 2015 年 3 月

佐久間史典 (for J-PARC E15 collaboration), "J-PARC E15 実験における K 中間子原子核探索の最近の進展",新学術研究領域「実験と観測で解き明かす中性子星の核物質」 研究会,熱川ハイツ, 2014 年 9 月

佐久間史典 (for J-PARC E15 collaboration), "Recent results and future prospects of the KbarNN search @ J-PARC E15", 原子核媒質中のハドロン研究 II, J-PARC, 2014 年 10 月

佐田優太, 板橋健太, 岩崎雅彦, 應田治彦, 岡田信二, 大西宏明, 佐藤将春, 佐久間史典, 徳田真, 橋本直, 山崎敏光, Ma Yue (J-PARC E15 実験): "J-PARC K1.8BR における 3He(K-,Λpn)反応を用いての K-多核子吸収の研究",日本物理学会第 69 回年次大会, 東海大学, 神奈川, 3 月(2014)

鈴木謙介, 足立匡, Hanjie Guo, 川崎郁斗, 渡邊功雄, 小池洋二 : "$La_{2-x}Sr_xCu_{1-y}Al_yO_4$ のオーバードープ領域における Al 誘起磁気秩序",日本物理学会大 69 回年次大会, 東海大学湘南キャンパス, 神奈川県, 3 月(2014)

鈴木謙介, 足立匡, Baqiya M.A.,Guo H., 川崎郁斗、今野巧也、Jawad M.A., Yoon S., 渡邊功雄, 小池洋二, "Impurity substitution effects on magnetic correlation in $La_{2-x}Sr_xCu_{1-y}M_yO_4$ (M = Fe, Al)", Research Frontier of Transition-metal Compounds Opened by Advanced Spectroscopies, 東北大, 仙台, 2014 年 9 月

鈴木栄男, Hanjie Guo, 川崎郁斗, 渡邊功雄, 片山和哉, 後藤貴行, 田中秀数: "ミュオンスピン緩和でみたボースグラス相 Tl$_{1-x}$K$_x$CuCl$_3$ のゼロ磁場極限における磁気的基底状態", 日本物理学会大 69 回年次大会, 東海大学湘南キャンパス, 神奈川県, 3 月(2014)

高尾健太, 劉鐘昇, 宇治克俊, 太田寛人, 和氣剛、田畑吉計, 渡邊功雄, 中村裕之, "Cr 系逆ペロフスカイト型窒化物の磁性", 日本物理学会春の大会, 早稲田大学, 東京, 2015 年 3 月

田中良樹, "(p,d)反応の分光による η′ 中間子原子核の探索", 日本物理学会第７０回年会、早稲田、３月(2015)

渡辺珠以, "逆運動学によるパイ中間子原子分光のための重水素ガスドリフトチェンバーの開発", 日本物理学会第７０回年会、早稲田、３月(2015)

中野岳仁, Gayan Prasad Hettiarachchi, 石井康之, 渡邊功雄, 野末泰夫: "ゼオライト LSX 中の Na-K 合金クラスターが示すフェリ磁性の He による圧力効果", 日本物理

学会大 69 回年次大会, 東海大学湘南キャンパス, 神奈川県, 3 月(2014)

中野岳仁, Hettiarachchi G.P., 岸本亮三, 石井康之, 渡邊功雄, 野末泰夫, “ゼオライト LSX 中の Na-K 合金クラスターが示すフェリ磁性の He による圧力効果 II”, 日本物理学会秋の大会, 中部大学, 名古屋, 2014 年 9 月

中野岳仁, 谷辺健志, Kien L.M., Yoon S., Majed Abdel-Jawad, Pratt F.L., 渡邊功雄, 野末泰夫, “ソーダライト中の K-Rb 合金および Rb クラスターの μSR“, 日本物理学会春の大会, 早稲田大学, 東京, 2015 年 3 月

劉鐘昇、宇治克俊、和氣剛、田畑吉計、中村裕之、渡邊功雄 “Cr_3GeN の構造と磁性“, 粉体粉末冶金協会春季大会、早稲田大学、東京都、2014 年 6 月

渡邊功雄, “Applications of a DC Muon Source to the Muon to Material Science”, RISP scientific Seminar, RISP, 太田市, 韓国 1 月(2014)

渡邊功雄: “Applications of Pulsed Muon Beam to Material Science at the RIKEN-RAL Muon Facility”, NTNU Science Seminar, NTNU, Trondheim, ノルウェー, 1 月(2014)

渡邊功雄: “μSR から見たパイロクロア酸化物 $Yb_2Ti_2O_7$ のスピンダイナミクス”, 三機関連携による量子複雑現象研究会, 理研、埼玉県和光市, 1 月(2014)

渡邉功雄, ”Applications of the Pulsed Muon Beam at the RIKEN-RAL Muon Facility”, 3rd Workshop for Light/Quantum Beam Science Promotion, Tohoku University New insight into materials and life sciences using light/quantum beams (III) ---Introduction of overseas facilities and cooperation with Tohoku University---, 宮城県仙台市, 東北大学金研, 3 月(2014)

渡邊功雄, “Muon Site Estimation in La_2CuO_4 by the Density Functional Theory”, RIKEN Symposium: 1st RIKEN-Sophia Joint Syposium “Recent Progresses on the Muon-Site Estimation”,上智大学, 四谷, 東京, 2014 年 12 月

渡邊功雄, “ミュオン位置計算法の最近の進展”, 第 8 回 三機関連携「量子複雑現象」研究会, SPring-8, 西播磨, 兵庫県, 2015 年 1 月

渡辺珠以, "逆運動学によるパイ中間子原子分光のための重水素ガスドリフトチェンバーの開発”, 日本物理学会第７０回年会、早稲田、３月(2015)

Adam M., Suprayoga E., Mohd Tajudin S.S., 谷田博司,世良正文, Sulaiman S., Mohamed Ismail M.I., 渡邊功雄 “The Electronic Structures of $CeRu_2Al_{10}$ and Muon Sites Studied by DFT” 日本物理学会春の大会, 早稲田大学, 東京、2015 年 3 月

Adam A., Adiperdana B., Suprayoga E., Sakinah Mohd-Tajudin S., A. Fauzeeha Rozlan, Slaiman S., Mohamed-Ibraham M.I., Guo H., 谷田博司, 世良正文, 西岡孝, 松村政博, 渡邊功雄,“$Ce(Ru,Rh)_2Al_{10}$ におけるミュオン位置計算と磁気モーメント構造および超微細場に関する考察”, 日本物理学会大 69 回年次大会, 東海大学湘南キャンパス, 神奈川県, 3 月(2014)

Budi Adiperdana, Edi Suprayoga, Aina Adam, Irwan A. Dharmawan, Rustam Siregr, Saidah Sakinah Mohd-Tajudin, Ainul Fauzeeha Rozlan, Shukri Slaiman, Mohamad Ismail Mohamed-Ibraham, 川股隆行, 足立匡, 小池洋二, Pabitra Kumar, Alex Amato, 渡邊功雄, “La_2CuO_4 におけるミュオン位置計算およびミュオンから見た Cu モーメントの状態”, 日本物理学会大 69 回年次大会, 東海大学湘南キャンパス, 神奈川県, 3 月(2014)

Rozlan A.F., Sulaiman S., Mohamed-Ibrahim M.I.,渡邊功雄, “Electronic Structure and Hyperfine Interaction of Muonated La_2CuO_4”,1st RIKEN-Sophia Joint Syposium Recent Progresses on the Muon-Site Estimation, 上智大学, 四谷, 東京, 2014 年 12 月

Mohd-Tajudin S.S., Adam M., Suprayoga E., Sulaiman S., Mohamed-Ibrahim M.I., 渡邊功雄,“First-Principles Calculation of Electronic Structure and Muon Sites in $YBa_2Cu_3O_6$”,日本物理学会春の大会, 早稲田大学, 東京, 2015 年 3 月

Suprayoga E., Adiperdana B., Adam A., Mohd-Tajudin S.S., Rozlan A.F., Slaiman S., Mohamed-Ibraham M.I., Guo H., 谷田博司, 世良正文, 西岡孝, 松村政博, Nugroho A.A., 渡邊功雄, “Study on the Hyperfine Fields and Muon Site Calculation in $CeRu_2Al_{10}$ Kondo-Semiconductor”, 日本物理学会大 69 回年次大会, 東海大学湘南キャンパス, 神奈川県, 3 月(2014)

Suprayoga E., Nugroho A.A., Polyakov A.O. Palstra T.T,M., 渡邊功雄,“Electronic Structure of $(C_6H_5CH_2CH_2NH_3)_2CuCl_4$ and $(C_2H_5NH_3)_2CuCl_4$ Organic-Inorganic Hybrid Materials”, 日本物理学会春の大会, 早稲田大学, 東京, 2015 年 3 月

Zhang Q., “Kalman Filter for E15 Experiment at J-PARC”,日本物理学会春の大会, 早稲田大学, 東京, 2014 年 3 月

RBRC Theory Group

Publications

[**Journal**]

(Original Papers) *Subject to Peer Review

Bezrukov F, Gorbunov D, : "Relic Gravity Waves and 7 keV Dark Matter from a GeV scale inflaton", Phys.Lett. B Volume 736 Page 494-498, 2014/09/07 *

Bezrukov F, Shaposhnikov M, : " Higgs inflation at the critical point ", Phys.Lett. B Volume 734 Page 249-254, 2014/06/27 *

Cho S., Hattori K., Lee S. H., Morita K., and Ozaki S.: "Charmonium Spectroscopy in Strong Magnetic Fields by QCD Sum Rules: S-Wave Ground States", Phys.Rev. D **91**, 045025 (2015)*

Cho S., Hattori K., Lee S. H., Morita K., and Ozaki S.: "QCD Sum Rules for Magnetically Induced Mixing between η_c and J/ψ", Phys.Rev. Lett. **113**, 172301 (2014)*

Xu J, Liao J, Gyulassy M, : Consistency of perfect fluidity and jet quenching in semi-quark-gluon monopole plasmas", arXiv:1411.3673[hep-ph]

Jiang Y, Huang X-G, Liao J, : "Chiral electric separation effect in the quark-gluon plasma", Physical Review D Volume 91 Issue 4 Article 045001, 2015 *

Shi S, Liao J, Zhuang P, : Ripples on a relativistically expanding fluid", Physical Review C Volume 90 Issue 6 Article 064912, 2014 *

Huang X-G, Liao J, : Kinetic evolution of the glasma and thermalization in heavy ion collisions", International Journal of Modern Physics E Volume 23 Article 1430003, 2014 *

Liao J, : Anomalous transport effects and possible environmental symmetry violation in heavy-ion collisions", Pramana Volume 84 Issue 5 Article 901, 2015 *

Li D, Liao J, Huang M, : Enhancement of jet quenching around phase transition: result from the dynamical holographic model", Physical Review D Volume 89 Issue 12 Article 126006, 2014 *

Bloczynski, Huang X-G, Zhuang X, Liao J, : Charge-dependent azimuthal correlations from AuAu to UU collisions", Nuclear Physics A Volume 939 Article 85, 2015 *

Lin, S, Robert D. Pisarski, Vladimir V. Skokov: "Collisional energy loss above the critical temperature in QCD", Physics Letter B Volume 730, Pages 236242, 2014/03/07 *

K. Kashiwa, A. Monnai: "Quark contribution for center domain in heavy ion collisions", Physical Review D Rapid Communications Volume 89 Issue 1 Article 011501 Page 1-5, 2014/01/07 *

A. Monnai : "Thermal photon v_2 with slow quark chemical equilibration", Physical Review C Rapid Communications Volume 90 Issue 2 Article 021901 Page 1-5, 2014/08/11 *

Gamberg L, Kang Z-B, Metz A, Pitonyak D, Prokudin A, : Left-right spin asymmetry in $\ell N^{\uparrow} \to hX$, Physical Review D Volume 90 Issue 7 Article 074012 Page 1-12, 2014/10/01 *

Kanazawa K, Koike Y, Metz A, Pitonyak D, : Towards an explanation of transverse single-spin asymmetries in proton-proton collisions: the role of fragmentation in collinear factorization, Physical Review D Volume 89 Issue 11 Article 111501(R) Page 1-5, 2014/06/01 *

Pitonyak D, Schlegel M, Metz A, : Polarized hadron pair production from electron-positron annihilation, Physical Review D Volume 89 Issue 5 Article 054032 Page 1-20, 2014/03/01 *

Yee H.-U, Yin Y, : "Realistic Implementation of Chiral Magnetic Wave in Heavy Ion Collisions", Physical Review C Volume 89 Issue 4 Article 044909 Page 1-11, 2014/04/28 *

Chen J, Son D, Stephanov M, Yee H.-U, Yin Y, : "Lorentz Invariance in Chiral Kinetic Theory", Physical Review Letters Volume 113 Issue 18 Article 182302 Page 1-5, 2014/10/30 *

Satow D, Yee H.-U, : "Chiral Magnetic Effect at Weak Coupling with Relaxation Dynamics", Physical Review D Volume 90 Issue 1 Article 014027 Page 1-12, 2014/07/17 *

Yee H.-U, : "Chiral Magnetic and Vortical Effects in Higher Dimensions at Weak Coupling", Physical Review D Volume 90 Issue 6 Article 065021 Page 1-24, 2014/09/16 *

[**Book, Proceedings**]

(Books)

A. Monnai : "Relativistic Dissipative Hydrodynamic Description of the Quark-Gluon Plasma", Springer Theses ISBN 978-4-431-54797-6 Page 1-127, 2014/01/30 *

(Original Papers)

Fedor Bezrukov: "The Planck and LHC results and particle physics", PoS EPS-HEP2013 (2013) 476 .

Jean-Paul Blaizot, Jinfeng Liao, Larry McLerran: Gluon transport equation in the small angle approximation and the onset of Bose-Einstein condensation", Nuclear Physics A 931(2014)359 .

Jinfeng Liao: The extraordinary glow", Nuclear Physics A 928(2014)247 .

Lin, S, Yoshimasa Hidaka, Robert D. Pisarski, Daisuke Satow, Vladimir D. Skokov: "Production of dilepton/photon in semi-quark gluon plasma", Nucl.Phys. A931 (2014) 681-685 .

A. Monnai : "Effects of quark chemical equilibration on thermal photon elliptic flow", Journal of Physics: Conference Series Volume 612 Article 012026 Pages 1-4 2015/05/19 *

Oral Presentations

(International Conference etc.)

Bezrukov F: "Higgs Inflation – relating particle physics

and cosmology", The 4th KIAS Workshop on Particle Physics and Cosmology Seoul, South Korea, 2014/11/30.

Bezrukov F: "Vacuum stability and the Higgs boson", SUSY-2014 Manchester, England, 2014/07/24.

Bezrukov F: "Models of keV scale sterile neutrino Dark Matter", MIAPP workshop Munich, Germany, 2014/07/10.

Bezrukov F: "Higgs inflation and large gravity waves – status and predictivity", QUARKS-2014 Suzdal, Russia, 2014/06/05.

Hattori K.: "Charmonium spectroscopy in strong magnetic fields by QCD sum rules", Hadrons and Hadron Interactions in QCD – Effective theories and Lattice – (HHIQCD2015), YITP, Kyoto Univ., Japan, Mar. (2015).

Hattori K.: "Photon propagation in strong magnetic fields", QCD Chirality Workshop 2015, UCLA, USA, Jan. (2015).

Cho S., Hattori K., Lee S. H., Morita K., and Ozaki S., "Charmonium spectroscopy in strong magnetic fields by QCD sum rules", Fourth Joint Meeting of the Nuclear Physics Divisions of the American Physical Society and The Physical Society of Japan, Hawaii, USA, Oct. (2014).

Liao, J: Condensed Matter Physics of Strong Interaction", Six Lectures for Advanced Summer Course Physics Department, Fudan University, Shanghai, China, 2014/07/28.

Liao, J: Pre-Equilibrium Physics in Heavy Ion Collisions", Lecture at "2014 Berkeley Summer School on Collective Dynamics" Berkeley, California, USA, 2014/06/09.

Liao, J: Geometry & Physics of Jet Quenching, and What We Can Learn from Heavy Flavor", The 1st HFT+ Meeting of STAR Collaboration UIC, Chicago, Illinois, USA, 2014/12/01.

Liao, J: Chiral Effects and Anomalous Transport in the Extreme Matter", The 2nd Workshop on "QCD Vacuum and Matter under Strong Magnetic Field" IHEP, Beijing, China, 2014/10/17.

Liao, J: Theoretical Summary on QGP at RHIC and LHC and Future", Joint JPA/APS DNP Annual Fall Meeting 2014 Big Island, Hawaii, USA, 2014/10/07.

Liao, J: Chiral Effects under Extreme Conditions", BES II Workshop 2014 Berkeley, California, USA, 2014/09/28.

Liao, J: Ripples on Relativistically Expanding Fluid", WPCF 2014 Gyongyos, Hungary, 2014/08/25.

Liao, J: Jet Tomography of Fluctuating Initial Conditions and the Opaqueness Evolution from RHIC to LHC", Plenary Talk at ATHIC 2014 Osaka, Japan, 2014/08/06.

Liao, J: Probing QCD Physics with QED Fields", XQCD 2014 Stony Brook, New York, USA, 2014/06/21.

Liao, J: In Search of Anomalous Transport Effects in Heavy Ion Collisions", Simons Center Workshop on "Quantum Anomaly & Hydrodynamics" Stony Brook, New York, USA, 2014/02/18.

Liao, J: The Initial Conditions in Heavy Ion Collisions", Plenary Session of STAR Collaboration Meeting at Feb 2014 BNL, New York, USA, 2014/02/13.

Lin, S: "Photon suppression and dilepton enhancement in semi-QGP", Quark Matter 2014 Darmstadt, Germany, 2014/05/19.

Lin, S: "Photon suppression and dilepton enhancement in semi-QGP", RBRC workshop: Thermal Photons and Dileptons in Heavy-Ion Collisions Brookhaven National Laboratory, Upton, NY, USA, 2014/08/22.

A. Monnai, B. Mueller: "Collinear parton splittings for early thermal and chemical equilibration", Frontiers of Hadronic Physics: Brains Recirculate Two Brookhaven National Laboratory, New York, USA, 2014/03/13.

A. Monnai: "Effects of quark chemical equilibration on thermal photon v_2", Extreme QCD 2014 Stony Brook University, New York, USA, 2014/06/21.

A. Monnai: "Thermal photons from chemically non-equilibrated QCD medium", Strong and Electroweak Matter 2014 EPFL, Lausanne, Switzerland, 2014/07/17.

A. Monnai: "Quark chemical equilibration for thermal photon elliptic flow", Thermal Photons and Dileptons in Heavy-Ion Collisions Brookhaven National Laboratory, New York, USA, 2014/08/21.

A. Monnai: "Elliptic flow of thermal photons in chemically non-equilibrated QCD medium", Particles and Nuclei International Conference 2014 Hamburg University, Hamburg, Germany, 2014/08/25.

A. Monnai: "Quark chemical equilibration and thermal photons in heavy-ion collisions", RIKEN Symposium/iTHES Workshop "Thermal Quantum Field Theory and Their Applications" RIKEN, Wako, Japan, 2014/09/05.

A. Monnai: "Effects of quark chemical equilibration on thermal photon elliptic flow", Hot Quarks 2014 Almeria, Andalucia, Spain, 2014/09/26.

Pitonyak, D: A_N in proton-proton collisions and the role of twist-3 fragmentation, Transversity Workshop Cagliari, Italy, 2014/06/11.

Pitonyak, D: Transverse single-spin asymmetries in proton-proton collisions within collinear factorization, QCD Evolution Workshop Santa Fe, NM, 2014/13/05.

Pitonyak, D: Towards an understanding of transverse single-spin asymmetries in proton-proton collisions, RBRC Brain Workshop BNL, Upton, NY, 2014/13/03.

Yee, H.-U: "Status of Chiral Magnetic Wave in Heavy Ion Collisions", RHIC & AGS Users Meeting Brookhaven National Laboratory, Upton New York, USA, 2014/06/17

Yee, H.-U: "Chiral Magnetic and Vortical Effects at Weak Coupling", Extreme QCD (XQCD) Stony Brook University, New York, USA, 2014/06/19

Yee, H.-U: "Interplay of QCD with Electromagnetism in Heavy-ion Collisions", QCD Long Range Plan Town

Hall Meeting Temple University, Philadelphia, Pennsylvania USA, 2014/09/15

Yee, H.-U: "Aspects of Chiral Magnetic and Vortical Effects at Weak Coupling", BNL Nuclear Seminars Brookhaven National Laboratory, Upton New York, USA, 2014/10/17

RBRC Computing Group

Publications

[Journal]

(Original Papers) *Subject to Peer Review

Thomas Blum, Masashi Hayakawa, and Taku Izubuchi, : "Hadronic light-by-light scattering contribution to the muon anomalous magnetic moment from lattice QCD", Physical Review Letters Volume 114 Issue 1 Article 012001, 2014/07/10 *

Thomas Blum P.A. Boyle, N.H. Christ, J. Frison, N. Garron, R.J. Hudspith, T. Izubuchi, T. Janowski, C. Jung, A. Juettner, C. Kelly, R.D. Kenway, C. Lehner, M. Marinkovic, R.D. Mawhinney, G. McGlynn, D.J. Murphy, S. Ohta, A. Portelli, C.T. Sachrajda, A. Soni: "Domain Wall QCD with Physical Quark Mass", submitted for publication in Physical Review D :, 2014/11/25

Norman H. Christ, Jonathan M. Flynn, Taku Izubuchi, Taichi Kawanai, Christoph Lehner, Amarjit Soni, Ruth S. Van de Water, Oliver Witzel, *"B-meson decay constants from 2+1-flavor lattice QCD with domain-wall light quarks and relativistic heavy quarks"*, Phys. Rev. D91:054502, 2015 (arXiv:1404.4670 [hep-lat])*.

Z. Bai, N.Y. Christ, T. Izubuchi, C.T. Sachrajda, and A. Soni and J. Yu, *"$K_L - K_S$ Mass Difference from Lattice QCD"*, Phys. Rev. Lett., 113, 2014, 112003 (arXiv:1406.0916 [hep-lat])*.

Y. Aoki, T. Ishikawa, T. Izubuchi, C. Lehner and A. Soni, "Neutral B meson mixings and B meson decay constants with static heavy and domain-wall light quarks," Phys. Rev. D **91**, no. 11, 114505 (2015) [arXiv:1406.6192 [hep-lat]].*

T. Bhattacharya, M. I. Buchoff, N. H. Christ, H.-T. Ding, R. Gupta, C. Jung, F. Karsch and Z. Lin *et al.*, "The QCD phase transition with physical-mass, chiral quarks" Phys. Rev. Lett. **113**, 082001 (2014) [arXiv:1402.5175 [hep-lat]]*.

Jung,C *et al.*, SWME Collaboration: "Improved determination of B_K with staggered quarks" Phys. Rev. **D89**, 074504 (2014) arXiv:1402.0048 [hep-lat]*.

M. I. Buchoff, M. Cheng, N. H. Christ, H.-T. Ding, C. Jung, F. Karsch, Z. Lin and R. D. Mawhinney *et al.*, "The QCD chiral transition, $u(1)_A$ symmetry and the Dirac spectrum using domain wall fermions" Phys. Rev. D **89**, 054514 (2014) [arXiv:1309.4149 [hep-lat]]*.

Z. S. Brown, W. Detmold, S. Meinel, K. Orginos: "Charmed bottom baryon spectroscopy from lattice QCD", Physical Review D Volume 90 Issue 9 Article 094507 Page 1-31, 2014/11/19 *

Ethan Neil, Thomas Appelquist et al. (LSD Collaboration): "Two-color gauge theory with novel infrared behavior", Physical Review Letters Vol. 112, no. 11, 111601 2014/03/18 *

Ethan Neil, Alexei Bazavov et al. (Fermilab Lattice and MILC Collaborations): "Determination of $|V_{us}|$ from a lattice-QCD calculation of the $K \to \pi\ell\nu$ semileptonic form factor with physical quark masses", Physical Review Letters Vol. 112, no. 11, 112001 2014/03/17 *

Ethan Neil, Thomas Appelquist et al. (LSD Collaboration): "Composite bosonic baryon dark matter on the lattice: SU(4) baryon spectrum and the effective Higgs interaction", Physical Review D Vol. 89, no. 9, 094508 2014/05/28 *

Ethan Neil, Jon A. Bailey et al. (Fermilab Lattice and MILC Collaborations): "Update of $|V_{cb}|$ from the $\bar{B} \to D^*\ell\bar{\nu}$ form factor at zero recoil with three-flavor lattice QCD", Physical Review D Vol. 89, no. 11, 114504 2014/06/19 *

Ethan Neil, Richard C. Brower et al. (LSD Collaboration): "Maximum-Likelihood Approach to Topological Charge Fluctuations in Lattice Gauge Theory", Physical Review D Vol. 90, no. 1, 014503 2014/07/09 *

Ethan Neil, Alexei Bazavov et al. (LSD Collaboration): "Charmed and light pseudoscalar meson decay constants from four-flavor lattice QCD with physical light quarks", Physical Review D Vol. 90, no. 7, 074509 2014/10/30 *

Ethan Neil, Thomas Appelquist et al. (LSD Collaboration): "Lattice simulations with eight flavors of domain wall fermions in SU(3) gauge theory", Physical Review D Vol. 90, no. 11, 114502 2014/12/12 *

E. Shintani, R. Arthur, T. Blum, T. Izubuchi, C. Jung and C. Lehner, "Covariant approximation averaging,", arXiv:1402.0244 [hep-lat], accepted by Physical Review D*

J. Green, S. Meinel, M. Engelhardt, S. Krieg, J. Laeuchli, J. Negele, K. Orginos, A. Pochinsky, S. Syritsyn: "High-precision calculation of the strange nucleon electromagnetic form factors", submitted to Physical Review D arXiv:1505.01803, 2015/05/07

J.R. Green, M. Engelhardt, S. Krieg, J.W. Negele, A.V. Pochinsky, S.N. Syritsyn: "Nucleon Structure from Lattice QCD Using a Nearly Physical Pion Mass", Physical Letters B Volume 734 Pages 290-295, 2012/06/27 *

J.R. Green, J.W. Negele, A.V. Pochinsky, S.N. Syritsyn, M. Engelhardt, S. Krieg: "Nucleon electromagnetic form factors from lattice QCD using a nearly physical pion mass", Physical Review D Volume 90 Article 074507, 2014/04/15 *

Lee, J-W, Tiburzi, B: "Background electromagnetic fields and nonrelativistic QED matching: Scalar case", Physical Review D Volume 89 Issue 5 Article 054017 Page 1-15, 2014/03/17 *

Tiburzi, B, : "Neutron in a strong magnetic field: Finite volume effects", Physical Review D Volume 89 Issue 7 Article 074019 Page 1-22, 2014/04/08 *

Tiburzi, B, : "Finite volume effects on the extraction of form factors at zero momentum", Physical Review D Volume 90 Issue 5 Article 054508 Page 1-15, 2014/09/23 *

Lee, J-W, Tiburzi, B: "Reconciling the lattice background field method with nonrelativistic QED: Spinor case", Physical Review D Volume 90 Issue 7 Article 074036 Page 1-16, 2014/10/29 *

Beane, S, Change, E, Cohen, S, Detmold, W, Lin, H-W, Orginos, K, Parreno, A, Savage, M, Tiburzi, B: "Magnetic moments of light nuclei from lattice quantum chromodynamics", Physical Review Letters Volume 113 Issue 25 Article 252001 Page 1-5, 2014/12/16 *

[Book, Proceedings]

(Original Papers)

Tom Blum, et al.: "Hadronic contributions to the muon anomalous magnetic moment Workshop. $(g-2)_\mu$: Quo vadis? Workshop. Mini proceedings", arXiv:1407.4021.

N. Christ *et al.* [RBC and UKQCD Collaborations], "Calculating the $K_L - K_S$ mass difference and ϵ_K to subpercent accuracy," PoS LATTICE **2013**, 397 (2014)

Norman H. Christ, *"Weak interactions of kaons from lattice QCD"*, Proceedings, 11th International Conference on Hyperons, Charm and Beauty Hadrons (BEACH 2014) Birmingham, UK, July 21-26, 2014, J.Phys.Conf.Ser. 556, 012005, 2014.

Tomomi Ishikawa, Yasumichi Aoki, Taku Izubuchi, Christoph Lehner, Amarjit Soni: "Neutral B meson mixing with static heavy and domain-wall light quarks", PoS LATTICE2013 (2014) 410 .

E. Shintani, H. J. Kim, T. Blum and T. Izubuchi, "Vacuum polarization function in $N_f = 2 + 1$ domain-wall fermion," PoS LATTICE **2013**, 487 (2014).

T. Blum, M. Hayakawa and T. Izubuchi, "Update on the hadronic light-by-light contribution to the muon $g - 2$ and inclusion of dynamically charged sea quarks," PoS LATTICE **2013**, 439 (2014).

T. Blum *et al.* [RBC and UKQCD Collaborations], "Weak Decay Measurements from 2+1 flavor DWF Ensembles," PoS LATTICE **2013**, 404 (2014).

E. Shintani, T. Blum, A. Soni and T. Izubuchi, "Neutron and proton EDM with $N_f = 2+1$ domain-wall fermion," PoS LATTICE **2013**, 298 (2014).

H. J. Kim and T. Izubuchi, "Möbius domain wall fermion method on QUDA," PoS LATTICE **2013**, 033 (2014).

S. Drury, T. Blum, M. Hayakawa, T. Izubuchi, C. Sachrajda, R. Zhou "Non-degenerate light quark masses from 2+1f lattice QCD+QED ", PoS LATTICE2013 (2014) 268 .

Christopher Kelly, Daiqian Zhang: "Lattice Measurement of the Delta I=1/2 Contribution to Standard Model Direct CP-Violation in K→pi pi Decays at Physical Kinematics: Part I ", PoS(LATTICE2014)365 .

Christopher Kelly, Daiqian Zhang: "Lattice Measurement of the Delta I=1/2 Contribution to Standard Model Direct CP-Violation in K→pi pi Decays at Physical Kinematics: Part II ", PoS(LATTICE2014)366 .

Lin,M: "Nucleon Form Factors with 2+1 Flavors of Domain Wall Fermions and All-Mode-Averaging" PoS LATTICE2013 (2014) 275.

Lin,M *et. al*: "Accelerating Ab Initio Nucleon Structure Calculations with All-Mode-Averaging on Gordon" XSEDE2014 proceedings

R. R. Horgan, Z. Liu, S. Meinel, M. Wingate: "Rare B decays using lattice QCD form factors", PoS LATTICE2014, 372 (2014).

Ethan Neil, Alexei Bazavov et al. (Fermilab Lattice and MILC Collaborations): "The D_s, D^+, B_s and B decay constants from 2+1 flavor lattice QCD", PoS LATTICE **2013**, 394 (2014) .

Ethan Neil, Elvira Gamiz et al. (Fermilab Lattice and MILC Collaborations): "Kaon semileptonic form factors with $N_f = 2 + 1 + 1$ HISQ fermions and physical light quark masses", PoS LATTICE **2013**, 395 (2014) .

Ethan Neil, Alexei Bazavov et al. (Fermilab Lattice and MILC Collaborations): "Charmed and strange pseudoscalar meson decay constants from HISQ simulations", PoS LATTICE **2013**, 405 (2014) .

Ethan Neil, Yuzhi Liu et al. (Fermilab Lattice and MILC Collaborations): "Heavy-meson semileptonic decays for the Standard Model and beyond", PoS LATTICE **2013**, 386 (2014) .

Ethan Neil, George Fleming: "From Lattice Strong Dynamics to Phenomenology", Proceedings of the KMI-GCOE Workshop on Strong Coupling Gauge Theories in the LHC Perspective (SCGT 12), p. 58 (2014) .

Ethan Neil, Alexei Bazavov et al. (Fermilab Lattice and MILC Collaborations): "Charmed and light pseudoscalar meson decay constants from HISQ simulations", PoS LATTICE **2014**, 382 (2014) .

Ethan Neil, Jon A. Bailey et al. (Fermilab Lattice and MILC Collaborations): "$B \to \pi\ell\nu$ semileptonic form factors from unquenched lattice QCD and determination of $|V_{ub}|$", PoS LATTICE **2014**, 385 (2014) .

Ethan Neil, Thomas DeGrand, Yuzhi Liu, Yigal Shamir, Benjamin Svetitsky: "Spectroscopy of SU(4) lattice gauge theory with fermions in the two index antisymmetric representation", PoS LATTICE **2014**, 275 (2014) .

Ohta, S, "Systematics analyses on nucleon isovector observables in 2+1-flavor dynamical domain-wall lattice QCD near physical mass", PoS LATTICE2014 (2015) 149

M. Engelhardt, Bernhard Musch, T. Bhattacharya, R. Gupta, Ph. Hagler, J. Negele, A. Pochinsky, A. Schafer, S. Syritsyn, B. Yoon: "Nucleon transverse momentum-dependent parton distributions from domain wall fermion calculations at 297 MeV pion mass", PoS LATTICE2014 (2014) 167 .

S. Syritsyn, T. Blum, M. Engelhardt, J. Green, T. Izubuchi, C. Jung, S. Krieg, M. Lin, S. Meinel, J. Negele: "Initial nucleon structure results with chiral quarks at the physical point", PoS LATTICE2014 (2015) 134 .

Sergey Syritsyn: "Review of Hadron Structure Calculations on a Lattice", PoS LATTICE2013 (2014) 009 .

Tiburzi, B, : "Volume effects on the method of extracting form factors at zero momentum", PoS LATTICE2014 (2015) 132

Lee, J-W, Tiburzi, B: "Background field method and nonrelativistic QED matching", PoS LATTICE2014 (2015) 155

Oral Presentations

(International Conference etc.)

Blum, T: "Hadronic contributions to the muon g-2", Confinement XI (St. Petersburg) St. Petersburg, Russia, 2014/09/13.

Blum, T: "Lattice calculation on the nucleon EDM", BNL HET lunch seminar BNL, USA, 2014/08/8.

Blum, T: "Lattice calculations of the Hadronic contributions to the muon g-2", 5th International Symposium on LEPTON MOMENTS Cape Cod, MA, USA, 2014/07/24.

Blum, T: "Fundamental Parameters I: Quark Masses", FLAG-Mad, Instituto de Física Teórica UAM/CSIC Madrid, Spain, 2014/05/24.

Blum, T: "Summary and Perspectives of Lattice QCD", Hadronic contributions to the muon anomalous magnetic moment: strategies for improvements of the accuracy of the theoretical prediction UITP, Walthhausen Castle, Mainz, Germany, 2014/04/05.

Christ, N: "Chiral fermions and precision lattice field theory", PPCM 2014, Boston University, May 8-10, 2014 http://blogs.bu.edu/ppcm/

Christ, N: "Computing K → pipi decay and the KL KS mass difference using lattice QCD", Southampton University, July 18, 2014.

Christ, N: "Computing K → pipi decay and the KL KS mass difference using lattice QCD, the University of Maryland, May 12, 2014.

Ishikawa, T: "B meson decay constants and Delta B=2 matrix elements with static heavy and doma in-wall light quarks", 32nd International Symposium on Lattice Field Theory (Lattice 2014) New York, USA, 2014/06/23-28.

Izubuchi, T: *"Supercomputing Fundamental Particle & Nuclear Physics"* BNL Lecture BNL, Upton, NY September 2014

Izubuchi, T: *"Lattice QCD calculations for particle physics"* XXVI IUPAP Conference on Computational Physics Boston University,Boston, MA 2014/08/11-14.

Izubuchi, T: *"Hadronic Light-by-Light: What can lattice QCD achieve?"*
Hadronic contributions to the muon anomalous magnetic moment: strategies for improvements of the accuracy of the theoretical prediction Waldthausen Castle near Mainz, Germany 2014/04/02.

Izubuchi, T: *"Hadronic Vacuum Polarization for muon g-2"* Lattice QCD Meets Experiment 2014 Fermi National Laboratory, Batavia, IL 2014/03/08.

Christopher Kelly: "Light hadronic physics from lattice QCD at the physical point", RBRC lunch seminar BNL, Upton, NY, USA, 2014/01/31.

Christopher Kelly: "New horizons in kaon physics on the lattice", USQCD all-hands meeting presentation JLAB, Newport News, VA, USA, 2014/04/18.

Christopher Kelly: "Lattice Measurement of the Delta I=1/2 Contribution to Standard Model Direct CP-Violation in K→pi pi Decays at Physical Kinematics: Part I", Lattice 2014 parallel talk Columbia University, NY, USA, 2014/06/23.

Christopher Kelly: "Lattice Measurement of the Delta I=1/2 Contribution to Standard Model Direct CP-Violation in K→pi pi Decays at Physical Kinematics", Seminar University of Edinburgh, Edinburgh, UK, 2014/09/29.

Lehner, C "Perspectives in lattice B physics" HET/RIKEN Lunch Seminar BNL, Upton, NY 2014/02/07

Lehner, C "Towards the large volume limit" Lattice 2014 New York, NY 2014/06/27

Lehner, C "Analytic Methods for Precise Predictions" Lattice Meets Continuum Siegen, Germany 2014/10/01

Lehner, C "Bloch's theorem and QCD+QED simulations" HET lunch seminar BNL,Upton, NY 2014/11/21

Lin, M "Nucleon structure on the lattice: Approaching the physical limit" High Energy Theory/RIKEN Lunch Seminar BNL,Upton,NY 2014/03/28

Lin, M "Computational Issues in BSM Theories Past, Present and Future" Field Theoretic Computer Simulations for Particle Physics and Condensed Matter Boston University Center for Computational Science Boston, MA 2014/05/08

Lin, M Multigrid HMC" The Eighth International Workshop on Numerical Analysis and Lattice QFT Yale University, Yale, CT. 2014/06/20

Lin, M "Application of Adaptive Multigrid Algorithm in Hybrid Monte Carlo Simulations" The 32nd International Symposium on Lattice Field TheoryColumbia University, NY 2014/06/23

S. Meinel: "Lattice QCD and the search for new physics using beauty quarks", APS Four Corners Section Meeting, Utah Valley University, Utah, 2014/10/18.

Ethan Neil: "Bayesian Methods for Parameter Estimation from LAttice Simulations", Eighth International Workshop on Numerical Analysis and Lattice QFT, Yale University, New Haven, CT 2014/06/21

Ethan Neil: "Leptonic B and D decay constants with 2+1 flavor asqtad fermions", XXXII International Symposium on Lattice Field Theory, Columbia University, New York, NY 2014/06/25

Shintani,E "Accurate calulation of nucleon form factor in lattice QCD" the 4th Joint Meeting of the APS Division

of Nuclear Physics and the Physical Society of JapanOctober 7-11, 2014 Waikoloa, Hawaii.

Shintani,E "Symmetry on honeycomb lattice formulation", 11th Quark confinement and Hadron spectrum XI, 7-12 September 2014, St. Petersburg.

Shintani,E "Progress of lattice calculation of light-by-light contribution to muon g-2", 37th international conference on high energy physics, 2 - 9 July 2014, Valencia, Spain.

Shintani,E "Hadronic contributions to the muon anomalous magnetic moment: strategies for improvements of the accuracy of the theoretical prediction", Working group in lattice QCD, MITP workshop, 1-5 April 2014, Waldthausen Castle near Mainz.

Shintani,E "α_s from the lattice", High precision fundamental constants at the TeV scale, March 10-21, 2014, JGU Campus Mainz.

Shintani,E "Lattice calculation of nucleon EDM", Hirschegg 2014, Hadrons from Quarks and Gluons, International Workshop XLII on Gross Properties of Nuclei and Nuclear Excitations, Hirschegg, Kleinwalsertal, Austria, January 12 - 18, 2014.

S. Syritsyn: "Nucleon Matrix Elements From Lattice QCD", INT Workshop INT-14-57W "Nuclear Aspects of Dark Matter Searches" USA, Seattle, University of Washington, 2014/12/10-12.

S. Syritsyn: "Nucleon Structure and Spin From Lattice QCD: Review", 4th Joint Meeting APS & JPS Nuclear Physics Divisions USA, Hawaii, 2014/10/7-11.

S. Syritsyn: "Nucleon Structure on a Lattice at the Physical Point", CCP 2014 USA, Boston, Boston University, 2014/08/11-14.

S. Syritsyn: "Initial Nucleon Structure Results with Chiral Quarks at the Physical Point", Lattice 2014 USA, New York, Columbia University, 2014/06/23-28.

S. Syritsyn: "Nucleon Structure on a Lattice : Present and Future Computing Requirements", Large Scale Computing and Storage Requirements for Nuclear Physics : Target 2017 USA, Bethesda, MD, 2014/04/29.

S. Syritsyn: "QCD on a Lattice : Nucleon Structure and Beyond", High Energy/Nuclear Seminar USA, East Lansing, Michigan State University, 2014/04/30.

Tiburzi, B:, "Neutron in a strong magnetic field and effects from finite volume", Theory seminar Maryland Center for Fundamental Physics, College Park, Maryland USA 2014/03/13

Tiburzi, B:, "Neutron in a strong magnetic field and effects from finite volume", Theory seminar College of William and Mary, Williamsburg, Virginial USA 2014/03/13

Tiburzi, B:, "A smaller size for the proton?", Physics department colloquium Amherst College, Amherst, Massachusetts USA 2014/04/03

Tiburzi, B:, "Four lectures on effective field theories", National nuclear physics summer school College of William and Mary, Williamsburg, Virginia USA 2014/06/09

Tiburzi, B:, "Towards exploring parity violation with lattice QCD", Workshop on Bound states and resonances in effective field theories and lattice QCD calculations Centro de Ciencias de Benasque Pedro Pascual, Benasque, Spain 2014/07/30

Tiburzi, B:, "The prospects for two-photon physics with lattice QCD", Town Hall Meeting, American Physical Society, Division of Nuclear Physics Temple University, Philadelphia, Pennsylvania USA 2014/09/14

(Domestic Conference etc.)

Izubuchi, T: *"Study of the nucleon structure by lattice QCD"* Physical Society of Japan Joint symposium among experimental nuclear, theoretical nuclear , experimental particle, and theoretical particle physics, Latest results and future programs on the nucleon structure - Toward an understanding of the nucleon spin - JPS Symposium Tokai University, Kanagawa, Japan 2014/03/30

Poster Presentations

(International Conference etc.)

Shintani, E "Precise lattice calculation of nucleon form factor with all-mode-averaging", 11th Quark confinement and Hadron spectrum XI, 7-12 September 2014, St. Petersburg.

Shintani, E "Improved statistics of proton decay matrix element", the 32st International Symposium on Lattice Field Theory 23-28 June 2014, Columbia University, NY

Shintani, E "Error reduction with all-mode-averaging in Wilson fermion", the 32st International Symposium on Lattice Field Theory, 23-28 June 2014, Columbia University, NY.

T.Blum T. Izubuchi (for USQCD Collaboration), *"All mode averaging and calculations of the muon anomalous magnetic moment,* $(g-2)_\mu$*"*, SciDAC PI meeting, September 2014, Washington D.C., MD

RBRC Experimental Group

Publications

[Journal]

(Original Papers) *Subject to Peer Review

Adare A., *et al.* PHENIX Collaboration, "Heavy-flavor electron-muon correlations in p+p and d+Au collisions at $\sqrt{s}$ = 200 GeV", Phys. Rev. C **89**, 034915 (2015). *

Adler S. S., *et al.* PHENIX Collaboration, "Transverse-energy distributions at midrapidity in p+p, d+Au, and Au+Au collisions at $\sqrt{s_{NN}}$=62.4 - 200 GeV and implications for particle-production models", Phys. Rev. C **89**, 044805 (2014). *

Adare A., *et al.* PHENIX Collaboration, "Azimuthal-angle dependence of charged-pion-interferometry measurements with respect to 2nd and 3rd-order event plane in Au+Au collisions at $\sqrt{s_{NN}}$ = 200 GeV", Phys. Rev. Lett. **112**, 222301 (2014). *

Adare A., *et al.* PHENIX Collaboration, "Cold nuclear-matter effects on heavy-quark production at forward and backward rapidities in d+Au collisions at $\sqrt{s_{NN}}$=200 GeV", Phys. Rev. Lett. **112**, 252301 (2014). *

Adare A., *et al.* PHENIX Collaboration, "Measurement of transverse-single-spin asymmetries for midrapidity and forward-rapidity production of hadrons in polarized p+p collisions at $\sqrt{s}$ = 200 and 62 GeV", Phys. Rev. D **90**, 012006 (2014). *

Adare A., *et al.* PHENIX Collaboration, "Inclusive Double-Helicity Asymmetries in Neutral-Pion and Eta-Meson Production in p+p Collisions at $\sqrt{s}$ = 200 GeV", Phys. Rev. D **90**, 012007 (2014). *

Adare A., *et al.* PHENIX Collaboration, "System-size dependence of open-heavy-flavor production in nucleus-nucleus collisions at $\sqrt{s_{NN}}$=200 GeV", Phys. Rev. C **90**, 034903 (2014). *

Adare A., *et al.* PHENIX Collaboration, "Centrality Categorization for $R_p(d) + A$ in high-energy collisions", Phys. Rev. C **90**, 034902 (2014). *

Adare A., *et al.* PHENIX Collaboration, "Low-Mass Vector-Mesons Production at forward rapidity in p+p Collisions at $\sqrt{s}$ = 200 GeV", Phys. Rev. D **90**, 052002 (2014). *

Adare A., *et al.* PHENIX Collaboration, "Cross Section and Transverse Single-Spin Asymmetry of η Mesons in $p^{\uparrow} + p$ collisions at $\sqrt{s}$ = 200 GeV at Forward Rapidity", Phys. Rev. D **90**, 072008 (2014). *

Adare A., *et al.* PHENIX Collaboration, "Measurement of K^0_S and K^{*0} in p+p, d+Au and Cu+Cu collisions at $\sqrt{s_{NN}}$= 200 GeV", Phys. Rev. C **90**, 054905 (2014). *

Adare A., *et al.* PHENIX Collaboration, "Nuclear matter effects on J/psi production in asymmetric Cu+Au collisions at $\sqrt{s_{NN}}$ =200GeV", Phys. Rev. C **90**, 064908 (2014). *

Adare A., *et al.* PHENIX Collaboration, "Cross-section for *barb* production via dielectrons in d+Au collisions at $\sqrt{s_{NN}}$ =200 GeV", Phys. Rev. C **91**, 014907 (2015). *

Adare A., *et al.* PHENIX Collaboration, "Charged-pion cross sections and double-helicity asymmetries in polarized p+p collisions at $\sqrt{s}$ = 200 GeV", Phys. Rev. D **91**, 032001 (2015). *

Adare A., *et al.* PHENIX Collaboration, "Measurement of the Upsilon(1S+2S+3S) production in p+p and Au+Au collisions at $\sqrt{s_{NN}}$ = 200 GeV", Phys. Rev. C **91**, 024913 (2015). *

Adare A., *et al.* PHENIX Collaboration, "Search for dark photons from neutral meson decays in p+p and d+Au collisions at $\sqrt{s_{NN}}$ = 200 GeV", Phys. Rev. C **91**, 031901 (2015). *

E.C Aschenauer, K. Boyle, *et al.* "eRHIC Design Study: An Electron-Ion Collider at BNL", arXiv:1409.1633.

Chin-Hao Chen "Studying the Early Universe via Quark-Gluon Plasma", Nucl. Phys. Proc. Suppl. 246-247 (2014) 38-41.

A.Bzdak, V. Sokov and S. Bathe "Centrality dependence of high energy jets in p+Pb collisions at the LHC", arXiv:1408.3156.

C.Aidala, *et al.* "The PHENIX Forward Silicon Vertex Detector", Nucl. Instrum. Meth. A755 (2014) 44.*

Seidel R, PHENIX W to mu measurements in polarized proton-proton collisions, PoS DIS2014(2014) 205, 2014/07/16

Kanesue T, Fuwa Y, Kondo K, Okamura M, "Laser ion source with solenoid field", APPLIED PHYSICS LETTERS, 105, 193506 (2014) *

Okamura M, Sekine M, Ikeda S, Kanesue T, Kumaki M, Fuwa Y, "Preliminary result of rapid solenoid for controlling heavy-ion beam parameters of laser ion source", Laser and Particle Beams, doi:10.1017/S026303461500004X (2015) *

(Review) *Subject to Peer Review

Akiba Y, "Quest for the quark-gluon plasma — hard and electromagnetic probles", Progress of theoretical and experimental physics 03A105(2015), 2015/01/12 *

[Book・Proceedings]

(Original Papers)

Kanesue T, *et al.* "THE COMMISSIONING OF THE LASER ION SOURCE FOR RHIC EBIS", Proceedings of IPAC 2014 (ISBN 978-3-95450-132-8), p1890-1892

Ikeda S, *et al.*, "Control of Plasma Flux with Pulsed Solenoid for Laser Ion Source", Proceedings of IPAC 2014, (ISBN 978-3-95450-132-8), p601-603

Fuwa Y, *et al.*, "Beam dynamics of multi charge state ions in RFQ linac", Proceedings of LINAC 2014 (ISBN 978-3-95450-142-7), p317-319

Okamura M, *et al.*, "Low Charge Laser Ion Source for the EBIS injector", Proceedings of LINAC 2014 (ISBN 978-3-95450-142-7), p64-66

(Review)
秋葉康之, クォーク・グルーオン・プラズマの物理 (共立出版), ISBN 978-4-320-03523-2, 2014/4/15

Oral Presentations

(International Conference etc.)
Yasuyuki Akiba, "Future plan at BNL", Hadron physics symposium (科研費新学術領域「新ハドロン」), Nagoya, Japan, 2014/4/18
Yasuyuki Akiba, "Electromagnetic probes and heavy flavor from RHIC and LHC", Hawaii 2014 (Fourth Joint Meeting of the Nuclear Physics Division of the American Physical Society and the Physical Society of Japan) (APS/JPS), Waikoloa Village, HI, USA, 2014/10/7
Ralf Seidl, "W to mu measurements at PHENIX", Conference on Deep inelastic scattering and related topics , Warsaw, Poland, 2014/05/29
T. Kanesue, "THE COMMISSIONING OF THE LASER ION SOURCE FOR RHIC EBIS", 5th International Particle Accelerator Conference (Cockcroft Inst. and U. Liverpool), Dresden, Germany, 2014/06/15-16
Y. Fuwa, "Charge-State Selective Ion Beam Acceleration with RFQ Linac", 20th International Symposium on Heavy-Ion Inertial Fusion (IMP), Lanzhou, China, 2014/08/11-15
T. Kanesue, "Stable operation of Laser Ion Source for low charge state ion production", 20th International Symposium on Heavy-Ion Inertial Fusion (IMP), Lanzhou, China, 2014/08/11-15
Shunsuke Ikeda, "Control of plasma flux with pulsed solenoid for laser ion source", 5th International Particle Accelerator Conference (Cockcroft Inst. and U. Liverpool), Dresden, Germany, 2014/06/15-16
M. Okamura, "Preliminary result of rapid solenoid for controlling heavy-ion beam parameters of laser ion source", 20th International Symposium on Heavy-Ion Inertial Fusion (IMP), Lanzhou, China, 2014/08/11-15
Y. Fuwa, "Beam dynamics of multi charge state ions in RFQ linac", 27th Linear Accelerator Conference (CERN), Geneva, Switzerland, 2014/08/31-09/05
M. Okamura, "Low Charge Laser Ion Source for the EBIS injector", 27th Linear Accelerator Conference (CERN), Geneva, Switzerland, 2014/08/31-09/05
Shunsuke Ikeda, "Influence of solenoidal magnetic field on laser ablation plasma", 5th Euro-Asian Pulsed Power Conference (Kumamoto Univ.), Kumamoto, Japan, 2014/09/11
Masafumi Kumaki, "Proton beam generation using Au-coated plastic target from Laser Ion Source" 19th International Conference on Ion Beam Modification of Materials, Leuven, Belgium, 2014/09/14-19
Yusuke Komatsu, "Development of a Tracking and Electron Identification System Using GEM for the J-PARC E16 Experiment", IEEE NUCLEAR SCIENCE SYMPOSIUM 2014 (IEEE), Seattle, USA, 2014/11/08-15

(Domestic Conference etc.)
秋葉康之, "RHIC PHENIX 実験とその将来計画", 第 1 回 CiRfSE ワークショップ (筑波大学数理物質融合科学センター), 筑波大学、つくば市, 2015/3/12
池田峻輔, " レーザーアブレーションプラズマに対するパルス磁場の影響", 日本物理学会第 70 回年次大会, 早稲田大学、東京, 2015/3/21-24
熊木雅史" ピコ秒レーザーを用いたレーザーイオン源開発" 日本物理学会第 70 回年次大会早稲田大学、東京 2015/3/21-24

Radioactive Isotope Physics Laboratory

Publications

[Journal]

(Original Papers) *Subject to Peer Review

Takechi M., Suzuki S., Nishimura D., Fukuda M., Ohtsubo T., Nagashima M., Suzuki T., Yamaguchi T., Ozawa A., Moriguchi T., Ohishi H., Sumikama T., Geissel H., Aoi N., Chen Rui-Jiu Fang De-Qing Fukuda N., Fukuoka S., Furuki H., Inabe N., Ishibashi Y., Itoh T., Izumikawa T., Kameda D., Kubo T., Lantz M., Lee C., S., Ma Yu-Gang Matsuta K., Mihara M., Momota S., Nagae D., Nishikiori R., Niwa T., Ohnishi T., Okumura K., Ohtake M., Ogura T., Sakurai H., Sato K., Shimbara Y., Suzuki H., Takeda H., Takeuchi S., Tanaka K., Tanaka M., Uenishi H., Winkler M., Yanagisawa Y., Watanabe S., Minomo K., Tagami S., Shimada M., Kimura M., Matsumoto T., Shimizu Y., R., Yahiro M.: "Evidence of halo structure in Mg-37 observed via reaction cross sections and intruder orbitals beyond the island of inversion", Phys. Rev. C **90**. **61305** (2014).

Patel Z., Soederstroem P.-A., Podolyak Zs., Regan P. H., Walker P. M., Watanabe H., Ideguchi E., Simpson G. S., Liu H. L., Nishimura S., Wu Q., Xu F. R., Browne F., Doornenbal P., Lorusso G., Rice S., Sinclair L., Sumikama T., Wu J., Xu Z. Y., Aoi N., Baba H., Garrote F. L., Bello Benzoni G., Daido R., Fang Y., Fukuda N., Gey G., Go S., Gottardo A., Inabe N., Isobe T., Kameda D., Kobayashi K., Kobayashi M., Komatsubara T., Kojouharov I., Kubo T., Kurz N., Kuti I., Li Z., Matsushita M., Michimasa S., Moon C. -B., Nishibata H., Nishizuka I., Odahara A., Sahin E., Sakurai H., Schaffner H., Suzuki H., Takeda H., Tanaka M., Taprogge J., Vajta Zs., Yagi A., Yokoyama R.: "Isomer Decay Spectroscopy of Sm-164 and Gd-166: Midshell Collectivity Around N=100", Phys. Rev. Lett. **113**, 262502 (2014).

Doornenbal P., Takeuchi S., Aoi N., Matsushita M., Obertelli A., Steppenbeck D., Wang H., Audirac L., Baba H., Bednarczyk P., Boissinot S., Ciemala M., Corsi A., Furumoto T., Isobe T., Jungclaus A., Lapoux V., Lee J., Matsui K., Motobayashi T., Nishimura D., Ota S., Pollacco E. C., Sakurai H., Santamaria C., Shiga Y., Sohler D., Taniuchi R.: "Intermediate-energy Coulomb excitation of Sn-104: Moderate E2 strength decrease approaching Sn-100", Phys. Rev. C. **90**, 61302 (2014).

Tshoo K., Satou Y., Bertulani C. A., Bhang H., Choi S., Nakamura T., Kondo Y., Deguchi S., Kawada Y., Nakayama Y., Tanaka K. N., Tanaka N., Togano Y., Kobayashi N., Aoi N., Ishihara M., Motobayashi T., Otsu H., Sakurai H., Takeuchi S., Yoneda K., Delaunay F., Gibelin J., Marques F., M., Orr N., A., Honda T., Kobayashi T., Sumikama T., Miyashita Y., Yoshinaga K., Matsushita M., Shimoura S., Sohler D., Hwang J. W., Zheng T., Li Z. H., Cao Z. X. :
"Neutron occupancy of the 0d(5/2) orbital and the N=16 shell closure in O-24", Phys. Lett.B **739**, 19-22 (2014).

Yang Xiaofei, Furukawa Takeshi, Wakui Takashi, Fujita Tomomi, Imamura Kei, Mitsuya Yosuke, Hayasaka Miki, Ichikawa Yuichi, Ishibashi Yoko, Shirai Hazuki, Suzuki Takahiro, Ebara Yuta, Hatakeyama Atsushi, Wada Michiharu, Sonoda Tetsu, Ito Yuta, Kobayashi Tohr,u Nishimura Shunji, Kurata-Nishimura Mizuki, Kondo Yosuke, Yoneda Ken-Ichiro, Kubono Shigeru, Ohshiro Yoshimitsu, Ueno Hideki, Shinozuka Tsutomu, Shimoda Tadashi, Asahi Koichiro, Matsuo Yukari: "Laser-radio-frequency double-resonance spectroscopy of Rb84-87 isotopes trapped in superfluid helium", Phys. Rev. A **90** **52516** (2014).

Taprogge J., Jungclaus A., Grawe H., Nishimura S., Xu Z., Y., Doornenbal P., Lorusso G., Nacher E., Simpson G. S., Soederstroem P. -A., Sumikama T., Baba H., Browne F., Fukuda N., Gernhauser R., Gey G., Inabe N., Isobe T., Jung H. S., Kameda D., Kim G. D., Kim Y. -K., Kojouharov I., Kubo T., Kurz N., Kwon Y. K., Lin Z., Sakurai H., Schaffner H., Steiger K., Suzuki H., Takeda H., Vajta Zs., Watanabe H., Wu J., Yagi A., Yoshinaga K., Benzoni G., Boenig S., Chae K. Y., Coraggio L., Covello A., Daugas J. -M., Drouet F., Gadea A., Gargano A., Ilieva S., Kondev F. G., Kroell T., Lane G. J., Montaner-Piza A., Moschner K., Muecher D., Naqvi F., Niikura M., Nishibata H., Odahara A., Orlandi R., Patel Z., Podolyak Zs., Wendt A.: "Identification of a millisecond isomeric state in Cd-129(81) via the detection of internal conversion and Compton electrons", Phys. Lett.B **738** **223-227** (2014).

Wendt A., Taprogge J., Reiter P., Golubev P., Grawe H., Pietri S., Boutachkov P., Algora A., Ameil F., Bentley M. A., Blazhev A., Bloor D., Bondili N. S., Bowry M., Bracco A., Braun N., Camera F., Cederkall J., Crespi F., de la Salle A., DiJulio D., Doornenbal P., Geibel K., Gellanki J., Gerl J., Grebosz J., Guastalla G., Habermann T., Hackstein M., Hoischen R., Jungclaus A., Merchan E., Million B., Morales A., Moschner K., Podolyak Zs., Pietralla N., Ralet D., Reese M., Rudolph D., Scruton L., Siebeck B., Warr N., Wieland O., Wollersheim H. J.:, "Isospin symmetry in the sd shell: Transition strengths in the neutron-deficient sd shell nucleus Ar-33", Phys. Rev. C 90 54301 (2014).

Simpson G. S., Gey G., Jungclaus A., Taprogge J., Nishimura S., Sieja K., Doornenbal P., Lorusso G., Soederstroem P. -A., Sumikama T., Xu Z.Y., Baba H., Browne F., Fukuda N., Inabe N., Isobe T., Jung H.S., Kameda D., Kim G. D., Kim Y. -K., Kojouharov I., Kubo T., Kurz N., Kwon Y. K., Li Z., Sakurai H., Schaffner H., Shimizu Y., Suzuki H., Takeda H., Vajta Z., Watanabe H., Wu J., Yagi A., Yoshinaga K., Boenig S., Daugas J. -M., Drouet F., Gernhaeuser R., Ilieva S., Kroell T., Montaner-Piza A., Moschner K., Muecher D., Naidja H., Nishibata H., Nowacki F., Odahara A., Orlandi R., Steiger K., Wendt A.: "Yrast 6(+) Seniority Isomers of Sn-136,Sn-138", Phys. Rev. Lett. **113**, 132502 (2014).

Jung H. S., Lee C. S., Kwon Y. K., Moon J. Y., Lee J. H.,

Yun C. C., Kim M. J., Hashimoto T., Yamaguchi H., Kahl D., Kubono S., Wakabayashi Y., Togano Y., Choi Seonho, Kim Y. H., Kim Y. K., Park J. S., Kim E. J., Moon C. -B., Teranishi T., Iwasa N., Yamada T., Kato S., Cherubini S., Hayakawa S., Rapisarda G. G.: "Elastic scattering of Al-25 + p to explore the resonance structure in Si-26", Phys. Rev. C **90**, 35805 (2014).

Lee Jenny, Pang Dan-Yang, Han Yin-Lu, Tsang, M. B.: "Proton Spectroscopic Factors Deduced from Helium-3 Global Phenomenological and Microscopic Optical Model Potentials", Chin. Phys. Lett. **31**, 92103 (2014).

Watanabe H., Lorusso G., Nishimura S., Otsuka T., Ogawa K., Xu Z.Y., Sumikama T., Soederstroem P. -A., Doornenbal P., Li Z., Browne F., Gey G., Jung H. S., Taprogge J., Vajta Zs., Wu J., Yagi A., Baba H., Benzoni G., Chae K. Y., Crespi F. C. L., Fukuda N., Gernhaeuser R., Inabe N., Isobe T., Jungclaus A., Kameda D., Kim G. D., Kim Y. K., Kojouharov I., Kondev F. G., Kubo T., Kurz N., Kwon Y. K., Lane G. J., Moon C. -B., Montaner-Piza A., Moschner K., Naqvi F., Niikura M., Nishibata H., Nishimura D., Odahara A., Orlandi R., Patel Z., Podolyak Zs., Sakurai H., Schaffner H., Simpson G. S., Steiger K., Suzuki H., Takeda H., Wendt A., Yoshinaga K.: Monopole-Driven Shell Evolution below the Doubly Magic Nucleus Sn-132 Explored with the Long-Lived Isomer in Pd-126", Phys. Rev. Lett. **113** 042502 (2014).

Xu Z. Y., Nishimura S., Lorusso G., Browne F., Doornenbal P., Gey G., Jung, H. -S., Li Z., Niikura M., Soederstroem P. -A., Sumikama T., Taprogge J., Vajta Zs., Watanabe H., Wu J., Yagi A., Yoshinaga K., Baba H., Franchoo S., Isobe T., John P. R., Kojouharov I., Kubono S., Kurz N., Matea I., Matsui K., Mengoni D., Morfouace P., Napoli D. R., Naqvi F., Nishibata H., Odahara A., Sahin E., Sakurai H., Schaffner H., Stefan I. G., Suzuki D., Taniuchi R., Werner V.: "beta-Decay Half-Lives of Co-76,Co-77, Ni-79,Ni- 80, and Cu-81: Experimental Indication of a Doubly Magic Ni-78", Phys. Rev. Lett. 113 32505 (2014).

Kobayashi N., Nakamura T., Kondo Y., Tostevin J. A., Utsuno Y., Aoi N., Baba H., Barthelemy R., Famiano M. A., Fukuda N., Inabe N., Ishihara M., Kanungo R., Kim S., Kubo T., Lee G. S., Lee H. S., Matsushita M., Motobayashi T., Ohnishi T., Orr N. A., Otsu H., Otsuka T., Sako T., Sakurai H., Satou Y., Sumikama T., Takeda H., Takeuchi S., Tanaka R., Togano Y., Yoneda K.: "Observation of a p-Wave One-Neutron Halo Configuration in Mg-37", Phys. Rev. Lett. **112**, 242501 (2014).

Michimasa S., Yanagisawa Y., Inafuku K., Aoi N., Elekes Z., Fueloep Zs., Ichikawa Y., Iwasa N., Kurita K., Kurokawa M., Machida T., Motobayashi T., Nakamura T., Nakabayashi T., Notani M., Ong H., J., Onishi T., K., Otsu H., Sakurai H., Shinohara M., Sumikama T., Takeuchi S., Tanaka K., Togano Y., Yamada K., Yamaguchi M., Yoneda K.: "Quadrupole collectivity in island-of-inversion nuclei Ne-28,Ne-30 and Mg-34,Mg-36", Phys. Rev. C **89**, 54307 (2014).

Doornenbal P., Scheit H., Takeuchi S., Utsuno Y., Aoi N., Li K., Matsushita M., Steppenbeck D., Wang H., Baba H., Ideguchi E., Kobayashi N., Kondo Y., Lee J., Michimasa S., Motobayashi T., Otsuka T., Sakurai H., Takechi M., Togano Y., Yoneda K.: "Rotational level structure of sodium isotopes inside the island of inversion", Progr. Theor. Exp. Phys. **053D01** (2014).

Crawford H. L., Fallon P., Macchiavelli A. O., Clark R. M., Brown B. A., Tostevin J. A., Bazin D., Aoi N., Doornenbal P., Matsushita M., Scheit H., Steppenbeck D., Takeuchi S., Baba H., Campbell C. M., Cromaz M., Ideguchi E., Kobayashi N., Kondo Y., Lee G., Lee I. Y., Lee J., Li K., Michimasa S., Motobayashi T., Nakamura T., Ota S., Paschalis S., Petri M., Sako T., Sakurai H., Shimoura S., Takechi M., Togano Y., Wang H., Yoneda K.: "Shell and shape evolution at N=28: The Mg-40 ground state", Phys. Rev. C **89**, 41303 (2014).

Yang Z. H., Ye Y. L., Li Z. H., Lou J. L., Wang J. S., Jiang D. X., Ge Y. C., Li Q. T., Hua H., Li X. Q., Xu F. R., Pei J. C., Qiao R., You H. B., Wang H., Tian Z. Y., Li K. A., Sun Y. L., Liu H. N., Chen J., Wu J., Li J., Jiang W., Wen C., Yang B., Yang Y. Y., Ma P., Ma J. B., Jin S. L., Han J. L., Lee J.: " Observation of Enhanced Monopole Strength and Clustering in Be-12 ", Phys. Rev. Lett. **112**, 162501 (2014).

Nakamura T., Kobayashi N., Kondo Y., Satou Y., Tostevin J., A., Utsuno Y., Aoi N., Baba H., Fukuda N., Gibelin J., Inabe N., Ishihara M., Kameda D., Kubo T., Motobayashi T., Ohnishi T., Orr N., A., Otsu H., Otsuka T., Sakurai H., Sumikama T., Takeda H., Takeshita E., Takechi M., Takeuchi S., Togano Y., Yoneda K.: "Deformation-Driven p-Wave Halos at the Drip Line: Ne-31", Phys. Rev. Lett. **112,** 142501 (2014)

Taprogge J., Jungclaus A., Grawe H., Nishimura S., Doornenbal P., Lorusso G., Simpson G., S., Soederstroem P., -A., Sumikama T., Xu Z., Y., Baba H., Browne F., Fukuda N., Gernhaeuser R., Gey G., Inabe N., Isobe T., Jung H., S., Kameda D., Kim G., D., Kim Y., -K., Kojouharov I., Kubo T., Kurz N., Kwon Y., K., Li Z., Sakurai H., Schaffner H., Steiger K., Suzuki H., Takeda H., Vajta Zs., Watanabe H., Wu J., Yagi A., Yoshinaga K., Benzoni G., Boenig S., Chae K., Y., Coraggio L., Covello A., Daugas J., -M., Drouet F., Gadea A., Gargano A., Ilieva S., Kondev F., G., Kroell T., Lane G., J., Montaner-Piza A., Moschner K., Muecher D., Naqvi F., Niikura M., Nishibata H., Odahara A., Orlandi R., Patel Z., Podolyak Zs., Wendt A.: "1p(3/2) Proton-Hole State in Sn-132 and the Shell Structure Along N=82", Phys. Rev. Lett.**112**, 132501 (2014).

Wang He, Aoi Nori, Takeuchi Satoshi, Matsushita Masafumi, Doornenbal Pieter, Motobayashi Tohru, Steppenbeck David, Yoneda Kenichiro, Baba Hidetada, Dombradi Zsolt, Kobayashi Kota, Kondo Yosuke, Lee Jenny, Liu Hong-Na, Minakata Ryogo, Nishimura Daiki, Otsu Hideaki, Sakurai Hiroyoshi, Sohler Dora, Sun Ye-Lei, Tian Zheng-Yang, Tanaka Ryuki, Vajta Zsolt, Yang Zai-Hong, Yamamoto Tetsuya, Ye Yan-Lin, Yokoyama

Rin: " Structure of Sn-136 and the Z=50 magicity ", Progr. Theor. Exp. Phys., 023D02 (2014).
Danielewicz Pawel, Lee Jenny : "Symmetry energy II: Isobaric analog states", Nucl. Phys. A **922,** 1-70 (2014).
Obertelli A., Delbart A., Anvar S., Audirac L., Authelet G., Baba H., Bruyneel B., Calvet D., Chateau F., Corsi A., Doornenbal P., Gheller J. -M., Giganon A., Lahonde-Hamdoun C., Leboeuf D., Loiseau D., Mohamed A., Mols J. -Ph., Otsu H., Peron C., Peyaud A., Pollacco E. C., Prono G., Rousse J. -Y., Santamaria C., Uesaka T.: "MINOS: A vertex tracker coupled to a thick liquid-hydrogen target for in-beam spectroscopy of exotic nuclei", Eur. Phys. J. A **50** 8 (2014).
Satou Y., Hwang J. W., Kim S., Tshoo K., Choi S., Nakamura T., Kondo Y., Matsui N., Hashimoto Y., Nakabayashi T., Okumura T., Shinohara M., Fukuda N., Sugimoto T., Otsu H., Togano Y., Motobayashi T., Sakurai H., Yanagisawa Y., Aoi N., Takeuchi S., Gomi T., Ishihara M., Kawai S., Ong H. J., Onishi T. K., Shimoura S., Tamaki M., Kobayashi T., Matsuda Y., Endo N., Kitayama M.: "One-neutron knockout reaction of C-17 on a hydrogen target at 70 MeV/nucleon", Phys. Lett. B **728** 462-466 (2014).
Patel Z., Browne F., Bruce A.M., Chiga N., Daido R., et al.: "Commissioning of a LaBr3(Ce) array with EURICA at RIBF" RIKEN Accel. Prog. Rep. 47, 13 (2014)
Yagi A. et al.:
"Search for isomers in neutron-rich Cs isotopes"
RIKEN Accel. Prog. Rep. 47 in print (2014)
M. Kurata-Nishimura, H. Otsu and T. Isobe:
"Development of Multiple-Particle Tracking Algorithm for Forward Drift Chamber in SAMURAI"
RIKEN Accel. Prog. Rep. 47 (2014)

[Book ・Proceedings]

(Original Papers) *Subject to Peer Review

Wu J., Nishimura S., Lorusso G., Xu Z.Y., Ideguchi E. et al.: "Beta-decay of neutron-rich nuclei with Z~60: The origin of rare-earth elements" In Proceedings of XIII Nuclei in the Cosmos, PoS (NIC XIII), page 016. Sissa, (2014).
Jungclaus A., Taprogge J., Simpson G. S., Gey G., Nishimura S. et al.: "Beta decay and isomer spectroscopy in the 132Sn region: New results from EURICA"
J. Phys. Conf. Ser. 533, 012045 (2014)
Shunji Nishimura:
"β-decay spectroscopy for the r-process nucleosynthesis"
AIP Conf. Proc. 1595, 144 (2014)
Wu J., Nishimura S., Lorusso G., Xu Z. Y., Baba H., et al.: "β-decay of neutron-rich Z ~ 60 nuclei and the origin of Rare Earth Elements" AIP Conf. Proc. 1594, 388 (2014)
Lorusso G., Nishimura S., Baba H., Browne F., Daido R., et al.: "β-decay spectroscopy at RIBF: the EURICA project" AIP Conf. Proc. 1594, 370 (2014)
Jungclaus A., Simpson G.S., Gey G., Taprogge J., Nishimura S., et al.:
"Isomer and beta decay spectroscopy in the 132Sn region with EURICA" EPJ Web Conf. 66, 02040 (2014)
Söderström P.-A, Nishimura S., Baba H., Browne F., Daido R. , et al.: "Status of the EURICA Project After One Year at RIKEN" JPS Conf. Proc. 1, 013046 (2014)
Xu Z. Y, Nishimura S., Lorusso G., Doornenbal P., Sumikama T., et al.: "Systematic Study of β-Decay Half-Lives in the Vicinity of 78Ni" JPS Conf. Proc. 1, 013035 (2014)
Warr N., Blazhev A. and Moschner K.: "Simulations of the SIMBA array towards the determination of Qβ values" EPJ Web Conf. 93, 07008 (2015)
Söderström P.-A., Nishimura S., Doornenbal P., Lorusso G., Sumikama T., et al.: "Installation and Commissioning of EURICA -- Euroball-RIKEN Cluster Array"
Nucl. Inst. Meth. B, 317, 649 (2013)
Wang H. et al., "Structural Evolution of the Pd Isotopes Towards N = 82", Proceedings of the 12th Asia Pacific Physics Conference (APPC12), JPS Conf. Proc. Volume 1 (2015)
Wang H. et al., "Collectivity in the neutron-rich Pd isotopes toward N = 82", Proceedings of 2nd conference on Advances in Radioactive Isotope Science (ARIS2014), JPS Conf. Proc. Volume 6 (2015)
Wang H., "In-beam gamma-ray spectroscopy and cross section measurement strategy for long-lived fission products at RIBF", Proceedings of the 2014 Symposium on Nuclear Data(*Subject to Peer Review)
M. Kurata-Nishimura, H. Otsu and T. Isobe
"Development of Multiple-Particle Tracking Algorithm for Forward Drift Chamber in SAMURAI"
RIKEN Accel. Prog. Rep. 47 (2014)

Oral Presentations

(International Conference etc.)

H. Sakurai : "Emergence of Exotic Phenomena in Unstable Nuclei -how to observe them", International School of Nuclear Physics in Eriche, Sicily, Italy, September (2014) *Invited Talk*

H. Sakurai : "Physics of Exotic Nuclei at RIBF", APS-JPS Joint Nuclear Physics Meeting, Hawaii, USA, October (2014) *Invited Talk*

H. Sakurai : "Physics Programs at RIBF"
International Symposium on Physics of Unstable Nuclei 2014, Ho Chi Minh City, Vietnam, November (2014) *Invited Talk*

Nishimura S.: "Survey of decay properties nad perspective at RIBF", Workshop on Nuclear Astrophysics, Beihang Univ., China January 21-23 (2015) *Invited Talk*

Nishimura S.: "Decay properties of exotic nuclei relevant to r-process nucleosynthesis", APS-JPS Meeting 2014, Hawaii, USA, October 7-11 (2014).

Nishimura S.: "Study of R-process Nucleosynthesis via Decay Spectroscopy at RIBF", International nuclear physics conference (NUBA2014), Adrasan-Antalya, Turkey, September 15-22 (2014). *Invited Talk*

Nishimura S.: Decay spectroscopy of exotic nuclei with EURICA spectrometer at RIBF", Fifteenth International

Symposium on Capture Gamma-Ray Spectroscopy and Related Topics (CGS2014), Dresden, Germany, August 25-29 (2014). *Invited Talk*

Nishimura S.: "Decay Properties of Exotic Nuclei with the EURICA", 4th European Gamma and Ancillary detectors network (EGAN2014), Darmstadt, Germany, June 23-26 (2014). *Invited Talk*

Nishimura S.: "Decay Properties of Exotic Nuclei and their Impacts to the r-process Nucleosynthesis" International Conference for Advances in Radioactive Isotope Science (ARIS2014), Tokyo, Japan, June 1-6 (2014). *Invited Talk*

Nishimura S.: "Decay spectroscopy of EURICA at RIBF", 11th International Spring Seminar on Nuclear Physics, Ischia, Italy, May 12-16 (2014). *Invited Talk*

Nishimura S.: "Decay spectroscopy of Ni isotopes", The structure of 68Ni: Current knowledge and open questions, Leuven, Belgium, April 23-24 (2014). *Invited Talk*

Pieter Doornenbal: "Perspectives for In-Beam Gamma-Ray Spectroscopy at the RIBF", Invited talk at the JPS Spring Meeting, Waseda Univ., Japan, March (2015)

Pieter Doornenbal: "Overview of SUNFLOWER", Invited talk at the Progress in Nuclear Shell-Model Calculations Workshop, Wako, Japan, November 26-28 (2014)

Pieter Doornenbal: "In-Beam Gamma-Ray Spectroscopy with Fast Beams Around the `Island of Inversion`", Invited talk at ISPUN14, Ho Chi Minh City, Vietnam, November 3th -- 8th (2014)

Pieter Doornenbal: "In-Beam Gamma-Ray Spectroscopy of Fast Exotic Beams at the RIBF", Invited talk at the 4th Joint APS--JPS Meeting, Hawaii, USA, October 7th -- 11th (2014)

Pieter Doornenbal: "Overview of In-Beam Gamma-Ray Spectroscopy at the RIBF", Invited talk at CGS15, Dresden, Germany, August 25th -- 29th (2014)

Pieter Doornenbal: " Overview of In-Beam Gamma-Ray Spectroscopy at the RIBF", Invited talk at the Zakopane Conference on Nuclear Physics, Poland, August 31st -- September 7th (2014)

Pieter Doornenbal: "Spectroscopy of Exotic Nuclei with EURICA", Invited talk at Nuclear Structure 2014, Vancouver, Canada, July 21st -- 25th (2014)

Pieter Doornenbal: "AGATA@RIBF",Oral Presentation at the 4th EGAN Workshop, Darmstadt, Germany, June 23rd -- 26th (2014)

Par-Anders Soderstrom, "Recent work of decay spectroscopy at RIBF", Fourth Joint Meeting of the Nuclear Physics Divisions of the American Physical Society and The Physical Society of Japan, Waikoloa, Hawai'i, USA, 8 Oct 2014.

Isobe T., "SPiRIT project for the study of density dependent symmetry energy of high dense matter with Heavy RI collisions at RIBF", 4th International Symposium on the Nuclear Symmetry Energy NuSYM14, University of Liverpool, UK, 7-9 July 2014.

Isobe T., "Readout System for SPiRIT experiment" , SAMURAI International Collaboration Workshop 2014, Tohoku University, 2014 8th -9th Sep. 2014

Isobe T., "GET for SPiRIT project", GET collaboration meeting 2014, Saint Avit Loisirs, France, 22-25 Sep. 2014.

Isobe T., "Development of SPYBOX for the calibration of GET clock synchronization", GET collaboration meeting 2014, Saint Avit Loisirs, France, 22-25 Sep. 2014.

Isobe T., "SPiRIT-TPC with GET readout electronics for the study of density dependent symmetry energy of high dense matter with Heavy RI collisions", APS/DNP 4th joint meeting @HAWAII, Hawaii, USA, 7-11 Oct. 2014.

Shiga Y., K. Yoneda, D. Steppenbeck, N. Aoi, P. Doornenbal, J. Lee, H. Liu, M. Matushita, S. Takeuchi, H. Wang, H. Baba, P. Bednarczyk, Zs. Dombradi, Zs. Fulop, S. Go, T. Hashimoto, E. Ideguchi, K. Ieki, K. Kobayashi, Y. Kondo , et al., "Shell structure studies in the vicinity of the doubly-magic ^78 Ni by in-beam γ-ray spectroscopy", FOURTH JOINT MEETING OF THE NUCLEAR PHYSICS DIVISIONS OF THE AMERICAN PHYSICAL SOCIETY and The PHYSICAL SOCIETY OF JAPAN , HAWAII ISLAND, 7th-11th Oct. 2014.

Nakai Y., Hidaka H., Watanabe N., Kojima T. M., "Ionic cluster formation using an ion drift-tube with selected-ion injection - Measurement of thermodynamic quantities for H3O+ Hydrate", The 17th International Symposium on Small Particles and Inorganic Clusters, Fukuoka, Sep. (2014).

Hidaka H., Nakai Y., Kojima T. M., Watanabe N., "Drift time measurements of H3O+ hydrate formed by NO+ injection into drift tube filled with H2O/buffer gas at low temperatures", The 17th International Symposium on Small Particles and Inorganic Clusters, Fukuoka, Sep. (2014).

Nakai Y., Hidaka H., Watanabe N., Kojima T. M.: "Experiments for ionic cluster formation using an ion drift-tube with selected-ion injection", Workshop on interstellar Matter 2014, Sapporo, Oct. (2014).

Hidaka H., Nakai Y., Kojima T. M., Watanabe N., "Formation of H3O+ hydrate by NO+ injection into drift tube filled with H2O/buffer gases: separation between the contributions of two formation pathways by the drift time measurements", Workshop on interstellar Matter 2014, Sapporo, Oct. (2014).

(Domestic Conference)

H. Sakurai, "Current Status and Future of RIBF My Very Personal Perspectives" (招待講演),
RIBF Theory Forum Workshop, Wako, August (2014)

H. Sakurai, "Status of RIBF and Strategy of Operation"(招待講演),
SAMURAI International Collaboration Workshop, Tohoku University, Sendai, September (2014)

櫻井博儀,"長寿命核分裂廃棄物の核変換データとその戦略"(招待講演)、原子力学会、京都、2014 年 9 月

H. Sakurai, "Nuclear Transmutation Programs at SAMURAI", SAMURAI International Collaboration Workshop, Sendai, Japan, Sept., 2014

櫻井博儀,"長寿命核分裂廃棄物の核変換データとその戦略"

原子力システム成果報告会、東京、2015 年 1 月

M. Kurata-Nishimura: “Status Of the SPiRIT Time Projection Chamber”
SAMURAI International Collaboration Workshop 2014 , Tohoku Univ., Sendai Japan, September (2014)

Par-Anders Soderstrom, “Gamma-ray spectroscopy results from the EURICA experiment”, Progress in nuclear shell-model calculations in CNS-RIKEN collaboration, RIKEN, Wako, Japan, 28th Nov 2014.

磯部忠昭, “理研 RIBF における重 RI 衝突を用いた対称エネルギー密度依存性の研究”,「宇宙核物理実験の現状と将来」研究会, 大阪大学核物理研究センター,7th-8th Aug. 2014

磯部忠昭, “理研 RIBF での低エネルギー非対称重イオン衝突を用いた原子核状態方程式の研究”,「J-PARC における重イオン衝突実験が拓く新しい物理」研究会, KEK, 26th-27th Nov. 2014

磯部忠昭, “ビームタイム一週間の加速器実験に求められるフレキシブルな計算機環境～RIKEN-RIBF でのコンピューティング ～”, 第 70 回年次大会、シンポジウム「実験のための最先端コンピューティング」, 早稲田大, 21st-24th Mar. 2015

磯部忠昭, “自由自在にモノ（物質）を変えられるとしたら、何を何に変えたいですか？”, 日本科学未来館 サイエンティスト・クエスト, 日本科学未来館, 27 Mar. 2015
http://www.miraikan.jst.go.jp/event/1503031418003.html

Y. Shiga, K. Yoneda, D. Steppenbeck, N. Aoi, P. Doornenbal, J. Lee, H. Liu, M. Matushita,S. Takeuchi, H. Wang, H. Baba, P. Bednarczyk, Zs. Dombradi, Zs. Fulop, S. Go, T. Hashimoto, E. Ideguchi, K. Ieki, K. Kobayashi, Y. Kondo, et al., “Persistence of /N/ = 50 shell closure in the vicinity of ^78 Ni studied by in-beam γ -ray spectroscopy”, The 2nd Conference on "Advances in Radioactive Isotope Science(ARIS2014)", Tokyo University, 1st-6th Jun. 2014,

岸田隆, “核変換技術の科学コミュニケーション”, 第一回「長寿命核分裂核廃棄物の核変換データとその戦略」ワークショップ, 和光, 3 月(2014)

岸田隆, “３つの循環と文明論の科学”, 西宮サイエンス談話会, 西宮, 12 月(2014)

岸田隆, “静かな革命へ向かう覚悟 -- 文明論的視座からのバックキャスティング -“, 自由民主党「国家戦略本部」講演会, 東京, 3 月(2015)

岸田隆, “３つの循環と文明論の科学”, 鳥居薬品外部講師講演会, 東京, 3 月(2015)

中井陽一, 日高宏, 渡部直樹, 小島隆夫, “イオン打ち込み移動管を用いた水和クラスターイオンの生成実験の現状 4”, 日本物理学会第 69 回年次大会, (日本物理学会), 平塚, 3 月(2014)

日高宏, 中井陽一, 小島隆夫, 渡部直樹, “NO+による水クラスターイオン生成 : 準安定 NO+による影響”, 日本物理学会第 69 回年次大会, (日本物理学会), 平塚, 3 月(2014)

渡部直樹, 日高宏, 中井陽一, 小島隆夫, “イオン誘起微粒子核生成 I : 装置開発とねらい”, 日本地球惑星科学連合大会 2014 年大会, 横浜, 5 月(2014)

日高宏, 中井陽一, 小島隆夫, 渡部直樹, “イオン誘起微粒子核生成 II : 水クラスターイオンの自由エネルギー”, 日本地球惑星科学連合大会 2014 年大会, 横浜, 5 月(2014)

Wang H., “Total kinetic energy detector” (invited talk), BigRIPS data analysis workshop, RIKEN Nishina Center, 11th Sep., 2014

Wang H., “Status of RIBF-31 experiment: Structure study of the neutron-rich nuclei beyond 132Sn” (invited talk), 3rd SUNFLOWER workshop, University of Tokyo, 15th -16th Sep., 2014

Wang H., “Cross section measurement strategy for long-lived fission product and in-beam gamma-ray spectroscopy at RIBF” (invited talk), 2014 Symposium on Nuclear Data, Hokkaido University Conference hall, Nov. 27-28, 2014

(Other Seminars)

櫻井博儀："科学するこころ -対象、思索、実行-"
不動岡高校、加須市、2014 年 6 月

櫻井博儀："経験、知識、知恵 -実生活から研究活動までの三つのキーワード-", 大宮高校、さいたま市、2014 年 11 月

Spin Isospin Laboratory

Publications

[Journal]

(Original Papers) *Subject to Peer Review

Bai, C. L. and Sagawa, H. and Colo, G. and Fujita, Y. and Zhang, H. Q. and Zhang, X. Z. and Xu, F. R.: "Low-energy collective Gamow-Teller states and isoscalar pairing interaction", Physical Review C **90**, 054335 (2014).*

Bohm, C. and Borgmann, C. and Audi, G. and Beck, D. and Blaum, K. and Breitenfeldt, M. and Cakirli, R. B. and Cocolios, T. E. and Eliseev, S. and George, S. and Herfurth, F. and Herlert, A. and Kowalska, M. and Kreim, S. and Lunney, D. and Manea, V. and Ramirez, E. M. and Naimi, S. and Neidherr, D. and Rosenbusch, M. and Schweikhard, L. and Stanja, J. and Wang, M. and Wolf, R. N. and Zuber, K.: "Evolution of nuclear ground-state properties of neutron-deficient isotopes around Z=82 from precision mass measurements", Physical Review C **90**, 044307 (2014).*

Cao, L. G. and Colo, G. and Sagawa, H. and Bortignon, P. F.: "Properties of single-particle states in a fully self-consistent particle-vibration coupling approach", Physical Review C **89**, 044314(2014).*

Colo, G. and Garg, U. and Sagawa, H.: "Symmetry energy from the nuclear collective motion: constraints from dipole, quadrupole, monopole and spin-dipole resonances", European Physical Journal A **50**, 26(2014).*

Fujita, Y. and Fujita, H. and Adachi, T. and Bai, C. L. and Algora, A. and Berg, G. P. A. and von Brentano, P. and Colo, G. and Csatlos, M. and Deaven, J. M. and Estevez-Aguado, E. and Fransen, C. and De Frenne, D. and Fujita, K. and Ganioglu, E. and Guess, C. J. and Gulyas, J. and Hatanaka, K. and Hirota, K. and Honma, M. and Ishikawa, D. and Jacobs, E. and Krasznahorkay, A. and Matsubara, H. and Matsuyanagi, K. and Meharchand, R. and Molina, F. and Muto, K. and Nakanishi, K. and Negret, A. and Okamura, H. and Ong, H. J. and Otsuka, T. and Pietralla, N. and Perdikakis, G. and Popescu, L. and Rubio, B. and Sagawa, H. and Sarriguren, P. and Scholl, C. and Shimbara, Y. and Shimizu, Y. and Susoy, G. and Suzuki, T. and Tameshige, Y. and Tamii, A. and Thies, J. H. and Uchida, M. and Wakasa, T. and Yosoi, M. and Zegers, R. G. T. and Zell, K. O. and Zenihiro, J.: "Observation of Low- and High-Energy Gamow-Teller Phonon Excitations in Nuclei", Physical Review Letters, **112**, 112502(2014).*

Hagino, K. and Sagawa, H.: "Three-body model calculation of the 2(+) state in O-26", Physical Review C, **90**, 027303(2014).*

Hagino, K. and Sagawa, H.: "Correlated two-neutron emission in the decay of the unbound nucleus O-26", Physical Review C, **89**, 014331(2014).*

Hamamoto, I. and Sagawa, H.: "Self-consistent Hartree-Fock and RPA Green's function method indicate no pygmy resonance in the monopole response of neutron-rich Ni isotopes", Physical Review C, **90**, 031302(2014).*

Isaka, M. and Fukukawa, K. and Kimura, M. and Hiyama, E. and Sagawa, H. and Yamamoto, Y.: "Superdeformed Lambda hypernuclei with antisymmetrized molecular dynamics", Physical Review C, **89**, 024310(2014).*

Karakoc, M. and Zegers, R. G. T. and Brown, B. A. and Fujita, Y. and Adachi, T. and Boztosun, I. and Fujita, H. and Csatlos, M. and Deaven, J. M. and Guess, C. J. and Gulyas, J. and Hatanaka, K. and Hirota, K. and Ishikawa, D. and Krasznahorkay, A. and Matsubara, H. and Meharchand, R. and Molina, F. and Okamura, H. and Ong, H. J. and Perdikakis, G. and Scholl, C. and Shimbara, Y. and Susoy, G. and Suzuki, T. and Tamii, A. and Thies, J. H. and Zenihiro, J.: "Gamow-Teller transitions in the A=40 isoquintet of relevance for neutrino captures in Ar-40", Physical Review C, **89**, 064313(2014).*

Kreim, S. and Beck, D. and Blaum, K. and Borgmann, C. and Breitenfeldt, M. and Cocolios, T. E. and Gottberg, A. and Herfurth, F. and Kowalska, M. and Litvinov, Y. A. and Lunney, D. and Manea, V. and Mendonca, T. M. and Naimi, S. and Neidherr, D. and Rosenbusch, M. and Schweikhard, L. and Stora, T. and Wienholtz, F. and Wolf, R. N. and Zuber, K.: "Competition between pairing correlations and deformation from the odd-even mass staggering of francium and radium isotopes", Physical Review C, **90**, 024301(2014).*

Ladygin, V. P. and Uesaka, T. and Glagolev, V. V. and Gurchin, Y. V. and Isupov, A. Y. and Itoh, K. and Janek, M. and Karachuk, J. T. and Kawabata, T. and Khrenov, A. N. and Kiselev, A. S. and Krasnov, V. A. and Kurepin, A. B. and Kurilkin, A. K. and Kurilkin, P. K. and Ladygina, N. B. and Lipchinski, D. and Maeda, Y. and Malakhov, A. I. and Martinska, G. and Nedev, S. and Piyadin, S. M. and Popovichi, J. and Rangelov, S. and Reznikov, S. G. and Rukoyatkin, P. A. and Sakaguchi, S. and Sakai, H. and Sekiguchi, K. and Shikhalev, M. A. and Suda, K. and Terekhin, A. A. and Trpisova, B. and Urban, J. and Vasiliev, T. A. and Vnukov, I. E. and Witala, H.: "Spin physics in few body systems at Nuclotron", Physics of Particles and Nuclei, **45**, 327-329(2014).*

Lu, B. N. and Hiyama, E. and Sagawa, H. and Zhou, S. G.: "Superdeformed Lambda hypernuclei within relativistic mean field models", Physical Review C, **89**, 044307(2014).*

Maeda, Y. and Saito, T. and Miyasako, H. and Uesaka, T. and Ota, S. and Kawase, S. and Kikuchi, T. and Tokieda, H. and Kawabata, T. and Yako, K. and Wakasa, T. and Sakaguchi, S. and Chen, R. and Sakaguchi, H. and Shima, T. and Suzuki, T. and Tamii, A.: "Measurement of the H-2(p, n) Breakup Reaction at 170 MeV and the Three-Nucleon Force Effects", Few-Body Systems, **55**, 729-732(2014).*

Myo, T. and Kikuchi, Y. and Mosui, H. and Kato, K.: "Recent development of complex scaling method for many-body resonances and continua in light nuclei", Progress in Particle and Nuclear Physics, **79**, 1-56(2014).*

Obertelli, A. and Delbart, A. and Anvar, S. and Audirac, L. and Authelet, G. and Baba, H. and Bruyneel, B. and Calvet, D. and Chateau, F. and Corsi, A. and Doornenbal, P. and Gheller, J. M. and Giganon, A. and Lahonde-Hamdoun, C. and Leboeuf, D. and Loiseau, D. and Mohamed, A. and Mols, J. P. and Otsu, H. and Peron, C. and Peyaud, A. and Pollacco, E. C. and Prono, G. and Rousse, J. Y. and Santamaria, C. and Uesaka, T.: "MINOS: A vertex tracker coupled to a thick liquid-hydrogen target for in-beam spectroscopy of exotic nuclei", European Physical Journal A, **50**, 8(2014).*

Oishi, T. and Hagino, K. and Sagawa, H.: "Role of diproton correlation in two-proton-emission decay of the Be-6 nucleus", Physical Review C, **90**, 034303(2014).*

Sagawa, H. and Colo, G.: "Tensor interaction in mean-field and density functional theory approaches to nuclear structure", Progress in Particle and Nuclear Physics, **76**, 76-115(2014).*

Schury, P. and Wada, M. and Ito, Y. and Arai, F. and Naimi, S. and Sonoda, T. and Wollnik, H. and Shchepunov, V. A. and Smorra, C. and Yuan, C.: "A high-resolution multi-reflection time-of-flight mass spectrograph for precision mass measurements at RIKEN/SLOWRI", Nuclear Instruments and Methods in Physics Research Section B-Beam Interactions with Materials and Atoms, **335**, 39-53(2014).*

Scott, M. and Shimbara, Y. and Austin, S. M. and Bazin, D. and Brown, B. A. and Deaven, J. M. and Fujita, Y. and Guess, C. J. and Gupta, S. and Hitt, G. W. and Koeppe, D. and Meharchand, R. and Nagashima, M. and Perdikakis, G. and Prinke, A. and Sasano, M. and Sullivan, C. and Valdez, L. and Zegers, R. G. T.: "Gamow-Teller transition strengths from Fe-56 extracted from the Fe-56(t,He-3) reaction", Physical Review C, **90**, 025801(2014).*

Sekiguchi, K. and Okamura, H. and Wada, Y. and Miyazaki, J. and Taguchi, T. and Gebauer, U. and Dozono, M. and Kawase, S. and Kubota, Y. and Lee, C. S. and Maeda, Y. and Mashiko, T. and Miki, K. and Sakaguchi, S. and Sakai, H. and Sakamoto, N. and Sasano, M. and Shimizu, Y. and Takahashi, K. and Tang, R. and Uesaka, T. and Wakasa, T. and Yako, K.: "Complete Set of Deuteron Analyzing Powers for dp Elastic Scattering at Intermediate Energies and Three Nucleon Forces" Few-Body Systems, **55**, 717-719(2014).*

Sekiguchi, K. and Okamura, H. and Wada, Y. and Miyazaki, J. and Taguchi, T. and Gebauer, U. and Dozono, M. and Kawase, S. and Kubota, Y. and Lee, C. S. and Maeda, Y. and Mashiko, T. and Miki, K. and Sakaguchi, S. and Sakai, H. and Sakamoto, N. and Sasano, M. and Shimizu, Y. and Takahashi, K. and Tang, R. and Uesaka, T. and Wakasa, T. and Yako, K.: "Complete set of deuteron analyzing powers for dp elastic scattering at intermediate energies", Physics of Particles and Nuclei, **45**, 190-192(2014).*

Sekiguchi, K. and Wada, Y. and Miyazaki, J. and Witala, H. and Dozono, M. and Gebauer, U. and Golak, J. and Kamada, H. and Kawase, S. and Kubota, Y. and Lee, C. S. and Maeda, Y. and Mashiko, T. and Miki, K. and Nogga, A. and Okamura, H. and Saito, T. and Sakai, H. and Sakaguchi, S. and Sakamoto, N. and Sasano, M. and Shimizu, Y. and Skibinski, R. and Suzuki, H. and Taguchi, T. and Takahashi, K. and Tang, T. L. and Uesaka, T. and Wakasa, T. and Yako, K.: "Complete set of deuteron analyzing powers for dp elastic scattering at 250-294 MeV/nucleon and the three-nucleon force", Physical Review C, **89**, 064007(2014).*

Stuhl, L. and Krasznahorkay, A. and Csatlos, M. and Algora, A. and Gulyas, J. and Kalinka, G. and Timar, J. and Kalantar-Nayestanaki, N. and Rigollet, C. and Bagchi, S. and Najafi, M. A.: "A neutron spectrometer for studying giant resonances with (p,n) reactions in inverse kinematics", Nuclear Instruments and Methods in Physics Research Section a-Accelerators Spectrometers Detectors and Associated Equipment, **736**, 1-9(2014).*

Tanimura, Y. and Sagawa, H. and Hagino, K.: "Three-body model calculations for N = Z odd-odd nuclei with T=0 and T=1 pairing correlations" Progress of Theoretical and Experimental Physics, 5, 053D02(2014).*

Wen, P. W. and Cao, L. G. and Margueron, J. and Sagawa, H.: "Spin-isospin response in finite nuclei from an extended Skyrme interaction", Physical Review C, **89**, 044311(2014).*

Nuclear Spectroscopy Laboratory

Publications

[Journal]

(Original Papers) *Subject to Peer Review

Asahi K., Ichikawa Y., Chikamori M., Ohtomo Y., Hikota E., Suzuki T., Inoue T., Furukawa T., Yoshimi A., Suzuki K., Nanao T., Miyatake H., Tsuchiya M., Yoshida N., Shirai H., Ino T., Ueno H., Matsuo Y., and Fukuyama T.: "Search for Electric Dipole Moment in ^{129}Xe Atom Using a Nuclear Spin Oscillator" Phys. Part. Nucl. **45**, 199–201 (2014). ∗

Yang X. F., Furukawa T., Wakui T., Fujita T., Imamura K., Mitsuya Y., Hayasaka M., Ichikawa Y., Ishibashi Y., Shirai H., Suzuki T., Ebara Y., Hatakeyama A., Wada M., Sonoda T., Ito Y., Kobayashi T., Nishimura S., Nishimura M., Kondo Y., Yoneda K., Kubono S., Ohshiro Y., Ueno H., Shinozuka T., Shimoda T., Asahi K., and Matsuo Y.: "Laser-radio-frequency double resonance spectroscopy of $^{84-87}$Rb isotopes trapped in superflid helium", Phys. Rev. A **90**, 052516 (2014). ∗

Michimasa S., Yanagisawa Y., Inafuku K., Aoi N., Elekes Z., Fulop Zs., Ichikawa Y., Iwasa N., Kurita K., Kurokawa M., Machida T., Motobayashi T., Nakamura T., Nakabayashi T., Notani M., Ong H. J., Onishi T. K., Otsu H., Sakurai H., Shinohara M., Sumikama T., Takeuchi S., Tanaka K., Togano Y., Yamada K., Yamaguchi M., and Yoneda K.: "Quadrupole collectivity in island-of-inversion nuclei ^{28,30}Ne and ^{34,36}Mg", Phys. Rev. C **89**, 054307 (2014). ∗

(Review)

上野秀樹："理研 RI ビームファクトリー施設と利用研究", 応用物理学会放射線分科会会誌 放射線 **40**, 85–91 (2014).

市川雄一："スピン操作した RI ビームの生成", 原子核研究 **59**, 29–39 (2014).

[Book・Proceedings]

(Original Papers) *Subject to Peer Review

Kubo M. K., Kobayashi Y., Yamada Y., Mihara M., Nagatomo T., Sato W., Miyazaki J., Sato S., and Kitagawa A.: "In-beam Mössbauer spectroscopy of ^{57}Fe/^{57}Mn in MgO and NaF at Heavy-Ion Medical Accelerator in Chiba" Rev. Sci. Instrum. **85** 02C310 (2014).

Ichikawa Y., Sato T., Ohtomo Y., Sakamoto Y., Kojima S., Suzuki T., Chikamori M., Hikota E., Miyatake H., Nanao T., Suzuki K., Tsuchiya M., Inoue T., Furukawa T., Yoshimi A., Bidinosti C. P., Ino T., Ueno H., Matsuo Y., Fukuyama T., and Asahi K.: "Search for EDM in ^{129}Xe using active spin maser", Proceedings of 7th International Workshop on Fundamental Physics Using Atoms (FPUA2014), Tokyo, 2014–3, pp. 37–44 (2015).

Sato T., Ichikawa Y., Ohtomo Y., Sakamoto Y., Kojima S., Suzuki T., Chikamori M., Hikota E., Miyatake H., Nanao T., Suzuki K., Tsuchiya M., Inoue T., Furukawa T., Yoshimi A., Bidinosti C. P., Ino T., Ueno H., Matsuo Y., Fukuyama T., and Asahi K.: "Co-magnetometry with ^{129}Xe/^{3}He dual active spin maser technique", Proceedings of 7th International Workshop on Fundamental Physics Using Atoms (FPUA2014), Tokyo, 2014–3, pp. 80–83 (2015).

Sakamoto Y., Bidinosti C. P., Ichikawa Y., Sato T., Ohtomo Y., Kojima S., Suzuki T., Chikamori M., Hikota E., Miyatake H., Nanao T., Suzuki K., Tsuchiya M., Inoue T., Furukawa T., Yoshimi A., Ino T., Ueno H., Matsuo Y., Fukuyama T., and Asahi K.: "Performance test of improved magnetic-field system for ^{129}Xe EDM measurement", Proceedings of 7th International Workshop on Fundamental Physics Using Atoms (FPUA2014), Tokyo, 2014–3, pp. 84–87 (2015).

Ohtomo Y., Ichikawa Y., Sato T., Sakamoto Y., Kojima S., Suzuki T., Chikamori M., Hikota E., Miyatake H., Nanao T., Suzuki K., Tsuchiya M., Inoue T., Furukawa T., Yoshimi A., Bidinosti C. P., Ino T., Ueno H., Matsuo Y., Fukuyama T., and Asahi K.: "Study of EDM cell with coexisting ^{129}Xe/^{3}He", Proceedings of 7th International Workshop on Fundamental Physics Using Atoms (FPUA2014), Tokyo, 2014–3, pp. 88–91 (2015).

Kojima S., Sato T., Ichikawa Y., Ohtomo Y., Sakamoto Y., Suzuki T., Chikamori M., Hikota E., Miyatake H., Nanao T., Suzuki K., Tsuchiya M., Inoue T., Furukawa T., Yoshimi A., Bidinosti C. P., Ino T., Ueno H., Matsuo Y., Fukuyama T., and Asahi K.: "Digital feedback system for active spin maser", Proceedings of 7th International Workshop on Fundamental Physics Using Atoms (FPUA2014), Tokyo, 2014–3, pp. 92–95 (2015).

Oral Presentations

(International Conference etc.)

Ueno H.: "Polarized beams?", 3rd EURICA Workshop, (RIKEN Nishina Center), Wako, Japan, Apr. (2014).

Ueno H.: "Ground state structure study around the island of inversion", RIBF Discussion Plus! –Island of inversion, (RIKEN Nishina Center), Wako, Japan, Apr. (2014).

Ueno H.: "Nuclear Moments and Structure of Unstable Nuclei", The 2nd Conference on advances in Radioactive Isotope Science (ARIS2014), (RIKEN Nishina Center and the Center for Nuclear Study, the University of Tokyo), Tokyo, Japan, Jun. (2014).

Yang X. F., Furukawa T., Wakui T., Fujita T., Imamura K., Mitsuya Y., Hayasaka M., Ichikawa Y., Ishibashi Y., Shirai H., Suzuki T., Ebara Y., Hatakeyama A., Wada M., Sonoda T., Ito Y., Kobayashi T., Nishimura S., Nishimura M., Kondo Y., Yoneda K., Kubono S., Ohshiro Y., Ueno H., Shinozuka T., Shimoda T., Asahi K., and Matsuo Y.: "A laser spectroscopy method using superfluid helium for measurements of spins and electromagnetic moments in exotuc nuclei", The 2nd Conference on advances in Radioactive Isotope Science (ARIS2014), (RIKEN Nishina Center and the Center for

Nuclear Study, the University of Tokyo), Tokyo, Japan, Jun. (2014).

Sato T., Ichikawa Y., Ohtomo Y., Sakamoto Y., Kojima S., Suzuki T., Shirai H., Chikamori M., Hikota E., Miyatake H., Nanao T., Suzuki K., Tsuchiya M., Inoue T., Furukawa T., Yoshimi A., Bidinosti C. P., Ino T., Ueno H., Matsuo Y., Fukuyama T., and Asahi K.: "^{129}Xe EDM Search Experiment Using Active Nuclear Spin Maser", The 2nd Conference on advances in Radioactive Isotope Science (ARIS2014), (RIKEN Nishina Center and the Center for Nuclear Study, the University of Tokyo), Tokyo, Japan, Jun. (2014).

Imamura K., Furukawa T., Yang X. F., Mitsuya Y., Fujita T., Hayasaka M., Kobayashi T., Hatakeyama A., Ueno H., and Asahi K.: "Measurement of the hyperfine splitting of ^{133}Cs atoms in superfluid helium", The 5th Joint International Conference on Hyperfine Interactions and Symposium on Nuclear Quadrupole Interactions (HFI/NQI 2014), (University of New South Wales and Australian National University), Canberra, Australia, Sep. (2014).

Sato T., Ichikawa Y., Ohtomo Y., Sakamoto Y., Kojima S., Funayama C., Suzuki T., Chikamori M., Hikota E., Tsuchiya M., Furukawa T., Yoshimi A., Bidinosti C. P., Ino T., Ueno H., Matsuo Y., Fukuyama T., and Asahi K.: "EDM measmrement in ^{129}Xe atom using dual active feedback nuclear spin maser", The 5th Joint International Conference on Hyperfine Interactions and Symposium on Nuclear Quadrupole Interactions (HFI/NQI 2014), (University of New South Wales and Australian National University), Canberra, Australia, Sep. (2014).

Sakamoto Y., Bidinosti C. P., Ichikawa Y., Sato T., Ohtomo Y., Kojima S., Funayama C., Suzuki T., Tsuchiya M., Furukawa T., Yoshimi A., Ueno H., Matsuo Y., Fukuyama T., and Asahi K.: "Development of high-homogeneity magnetic field coil for ^{129}Xe EDM experiment", The 5th Joint International Conference on Hyperfine Interactions and Symposium on Nuclear Quadrupole Interactions (HFI/NQI 2014), (University of New South Wales and Australian National University), Canberra, Australia, Sep. (2014).

Ueno H.: "Scientific opportunities and plans for RIBF", 4th Joint Meeting of the Nuclear Physics Division of the American Physical Society and The Physical Society of Japan (HAWAII 2014), (the American Physical Society and The Physical Society of Japan), Waikoloa, Hawaii, USA, Oct. (2014).

Furukawa T., "OROCHI experiment: Laser spectroscopy of RI atoms in superfluid helium for measurements of nuclear spins and electromagnetic moments", 4th Joint Meeting of the Nuclear Physics Division of the American Physical Society and The Physical Society of Japan (HAWAII 2014), (the American Physical Society and The Physical Society of Japan), Waikoloa, Hawaii, USA, Oct. (2014).

Ichikawa Y., Sato T., Ohtomo Y., Sakamoto Y., Kojima S., Funayama C., Hirao C., Suzuki T., Chikamori M., Hikota E., Miyatake H., Nanao T., Suzuki K., Tsuchiya M., Inoue T., Furukawa T., Yoshimi A., Bidinosti C. P., Ino T., Ueno H., Matsuo Y., Fukuyama T., and Asahi K.: "Experimental search for EDM in diamagnetic atom ^{129}Xe using active nuclear spin maser" 4th Joint Meeting of the Nuclear Physics Division of the American Physical Society and The Physical Society of Japan (HAWAII 2014), (the American Physical Society and The Physical Society of Japan), Waikoloa, Hawaii, USA, Oct. (2014).

Sato T., Ichikawa Y., Ohtomo Y., Sakamoto Y., Kojima S., Funayama C., Suzuki T., Chikamori M., Hikota E., Tsuchiya M., Furukawa T., Yoshimi A., Bidinosti C. P., Ino T., Ueno H., Matsuo Y., Fukuyama T., and Asahi K.: "Progress of the ^{129}Xe EDM search using active feedback nuclear spin maser", 4th Joint Meeting of the Nuclear Physics Division of the American Physical Society and The Physical Society of Japan (HAWAII 2014), (the American Physical Society and The Physical Society of Japan), Waikoloa, Hawaii, USA, Oct. (2014).

Kojima S., Sato T., Ichikawa Y., Ohtomo Y., Sakamoto Y., Funayama C., Suzuki T., Chikamori M., Hikota E., Tsuchiya M., Furukawa T., Yoshimi A., Bidinosti C. P., Ino T., Ueno H., Matsuo Y., Fukuyama T., and Asahi K.: "Performance of active nuclear spin maser with double-cell geometry", 4th Joint Meeting of the Nuclear Physics Division of the American Physical Society and The Physical Society of Japan (HAWAII 2014), (the American Physical Society and The Physical Society of Japan), Waikoloa, Hawaii, USA, Oct. (2014).

Sakamoto Y., Bidinosti C. P., Ichikawa Y., Sato T., Ohtomo Y., Kojima S., Funayama C., Suzuki T., Tsuchiya M., Furukawa T., Yoshimi A., Ino T., Ueno H., Matsuo Y., Fukuyama T., and Asahi K.: "Performance check of cell with newly designed electrode for ^{129}Xe EDM measurement", 4th Joint Meeting of the Nuclear Physics Division of the American Physical Society and The Physical Society of Japan (HAWAII 2014), (the American Physical Society and The Physical Society of Japan), Waikoloa, Hawaii, USA, Oct. (2014).

Funayama C., Furukawa T., Sato T., Ichikawa Y., Ohtomo Y., Sakamoto Y., Kojima S., Suzuki T., Chikamori M., Hikota E., Tsuchiya M., Yoshimi A., Bidinosti C. P., Ino T., Ueno H., Matsuo Y., Fukuyama T., and Asahi K.: "Development of a high intensity laser for effecient spin exchange optical pumping in a spin maser measurement of the ^{129}Xe EDM", 4th Joint Meeting of the Nuclear Physics Division of the American Physical Society and The Physical Society of Japan (HAWAII 2014), (the American Physical Society and The Physical Society of Japan), Waikoloa, Hawaii, USA, Oct. (2014).

Ohtomo Y., Ichikawa Y., Shirai H., Ueno H., Ishibashi Y., Suzuki T., Furukawa T., Yoshimi A., Abe Y., Asahi K., Daugas J. M., Fujita T., Hayasaka M., Imamura K.,

Kishi S., Kojima S., Nagae D., Nakao A., Sagayama T., Sakamoto Y., Sato Y.: "Ground-state nuclear-moment measurement of neutron-rich sulfur isotopes", 4th Joint Meeting of the Nuclear Physics Division of the American Physical Society and The Physical Society of Japan (HAWAII 2014), (the American Physical Society and The Physical Society of Japan), Waikoloa, Hawaii, USA, Oct. (2014).

Imamura K., Furukawa T., Yang X. F., Fujita T., Wakui T., Mitsuya Y., Hayasaka M., Ichikawa Y., Hatakeyama A., Kobayashi T., Odashima H., Ueno H., and Matsuo Y.: "Hyperfine structure measurement of ^{87}Rb atoms injected into superfluid helium as highly energetic ion beam", 4th Joint Meeting of the Nuclear Physics Division of the American Physical Society and The Physical Society of Japan (HAWAII 2014), (the American Physical Society and The Physical Society of Japan), Waikoloa, Hawaii, USA, Oct. (2014).

Hayasaka M., Furukawa T., Tomita H., Takamatsu T., Imamura K., Fujita T., Kobayashi T., Uematsu H., Ueno H., and Matsuo Y.: "Effective production of spin polarization of atoms in superfluid helium using pulsed lasers", 4th Joint Meeting of the Nuclear Physics Division of the American Physical Society and The Physical Society of Japan (HAWAII 2014), (the American Physical Society and The Physical Society of Japan), Waikoloa, Hawaii, USA, Oct. (2014).

Fujita T., Furukawa T., Imamura K., Yang X. F., Mitsuya Y., Hayasaka M., Sagayama T., Kishi S., Kobayashi T., Ueno H., Shimoda T., and Matsuo Y.: "Sublevel laser spectroscopy of ^{197}Au atom in superfluid helium", 4th Joint Meeting of the Nuclear Physics Division of the American Physical Society and The Physical Society of Japan (HAWAII 2014), (the American Physical Society and The Physical Society of Japan), Waikoloa, Hawaii, USA, Oct. (2014).

Kinbara S., Nakazawa K., Ichikawa Y., Ueno H., Yoshida J., Khin T. T., Myint K. S., Mishina A., Ito H., Endo Y., and Kobayashi H.: "Isotope Identification in Nuclear Emulsion Plate", 4th Joint Meeting of the Nuclear Physics Division of the American Physical Society and The Physical Society of Japan (HAWAII 2014), (the American Physical Society and The Physical Society of Japan), Waikoloa, Hawaii, USA, Oct. (2014).

Ueno H.: "Production of High Nuclear Spin Alignment of Radioactive Ion Beams", The 21st International Symposium on Spin Physics (SPIN2014), (Peking University), Beijing, China, Oct. (2014).

Furukawa T., Yang X. F., Imamura K., Fujita T., Wakui T., Mitsuya Y., Hayasaka M., Ichikawa Y., Ishibashi Y., Shirai H., Suzuki T., Sato T., Ohtomo Y., Kojima S., Ebara Y., Kishi S., Sagayama T., Wada M., Sonoda T., Ito Y., Kobayashi T., Nishimura S., Nishimura M., Kondo Y., Yoneda K., Kubono S., Ohshiro Y., Hatakeyama A., Ueno H., Shinozuka T., Shimoda T., Asahi K., and Matsuo Y.: "Spin polarization of radioisotope atoms with optical pumping in superfluid helium for the measurement of nuclear spins and electromagnetic moments", The 21st International Symposium on Spin Physics (SPIN2014), (Peking University), Beijing, China, Oct. (2014).

Ueno H.: "Research Activities at RIBF", Internaional Workshop on Progress in nuclear shell-model calculations in CNS-RIKEN collaboration, (Center for Nuclear Study, the University of Tokyo and RIKEN Nishina Center), Wako, Japan, nov. (2014).

Yamazaki H., and Shannon N.: "Superconducting Proximity Effects in Nb/rare-earth Bilayers", The 9th International Symposium on Intrinsic Josephson Effects and THz Plasma Oscillations in High-Tc Superconductors (THz-Plasma 2014), Kyoto, Japan, Nov.–Dec. (2014).

Fujita T., Furukawa T., Imamura K., Yang X. F., Wakui T., Mitsuya Y., Hayasaka M., Ichikawa Y., Ishibashi Y., Shirai H., Suzuki T., Sato T., Ohtomo Y., Kojima S., Ebara Y., Kishi S., Sagayama T., Hatakeyama A., Kobayashi T., Ueno H., Asahi K., Shimoda T., and Matsuo Y.: "Leaser spectroscopy of atoms in superfluid helium for the measurement of nuclear spins and electromagnetic moments of radioisotope atoms", 6th International Conference on Trapped Charged Particles and Fundamental Physics (TCP2014), (RIKEN Nishina Center), Takamatsu, Japan, Dec. (2014).

(Domestic Conference)

上野秀樹："理研 RI ビームファクトリーと最近の研究成果", 明治大学 科学技術研究所講師招聘講演会物理学系セミナー, (明治大学), 神奈川県川崎市, 7 月 (2014).

今村慧 , 古川武 , YangXiaofei , 三津谷洋助 , 藤田朋美 , 早坂美希 , 小林徹 , 畠山温 , 上野秀樹 , 松尾由賀利："超流動ヘリウム中に植えこまれた Cs 原始の超微細構造間隔", 日本物理学会 2014 年秋季大会, (日本物理学会), 愛知県春日井市, 9 月 (2014).

市川雄一："RI を用いた原子 EDM 探索に向けて", RCNP 研究会 "CP violation in elementary particles and composite systems", (大阪大学核物理研究センター), 大阪府吹田市, 11 月 (2014).

佐藤智哉："能動帰還型スピンメーザーによる ^{129}Xe 原子 EDM 探索実験", RCNP 研究会 "CP violation in elementary particles and composite systems", (大阪大学核物理研究センター), 大阪府吹田市, 11 月 (2014).

旭耕一郎："EDM の実験的探索の現状", 日本物理学会第 70 回年次大会, (日本物理学会), 東京都新宿区, 3 月 (2015).

舟山智歌子 , 古川武 , 佐藤智哉 , 市川雄一 , 大友祐一 , 坂本雄 , 小島修一郎 , 平尾千佳 , 菅野雄揮 , 小峰太郎 , 鈴木貴大 , 近森正敏 , 彦田絵里 , 土屋真人 , 吉見彰洋 , Bidinosti C. P., 猪野隆 , 上野秀樹 , 松尾由賀利 , 福山武志 , 旭耕一郎："^{129}Xe/^{3}He 同時メーザー発振のためのポンピングレーザーシステムの開発", 日本物理学会第 70 回年次大会, (日本物理学会), 東京都新宿区, 3 月 (2015).

坂本雄 , Bidinosti C. P., 市川雄一 , 佐藤智哉 , 大友祐一 , 小島修一郎 , 舟山智歌子 , 平尾千佳 , 菅野雄揮 , 小峰太郎

, 鈴木貴大 , 近森正敏 , 彦田絵里 , 土屋真人 , 古川武 , 吉見彰洋 , 猪野隆 , 上野秀樹 , 松尾由賀利 , 福山武志 , 旭耕一郎 : “一様磁場環境下での ^{129}Xe/^{3}He 同時メーザー発振”, 日本物理学会第 70 回年次大会, (日本物理学会), 東京都新宿区, 3 月 (2015).

小島修一郎 , 佐藤智哉 , 市川雄一 , 大友祐一 , 坂本雄 , 舟山智歌子 , 平尾千佳 , 菅野雄揮 , 小峰太郎 , 鈴木貴大 , 近森正敏 , 彦田絵里 , 土屋真人 , 古川武 , 吉見彰洋 , Bidinosti C. P., 猪野 隆 , 上野 秀樹 , 松尾 由賀利 , 福山 武志 , 旭耕一郎 : “ダブルセルにおける ^{129}Xe/^{3}He 核スピンメーザーの周波数特性”, 日本物理学会第 70 回年次大会, (日本物理学会), 東京都新宿区, 3 月 (2015).

佐藤智哉 , 市川雄一 , 大友祐一 , 坂本雄 , 小島修一郎 , 舟山智歌子 , 平尾千佳 , 菅野雄揮 , 小峰太郎 , 鈴木貴大 , 近森正敏 , 彦田絵里 , 土屋真人 , 古川武 , 吉見彰洋 , Bidinosti C. P., 猪野 隆 , 上野 秀樹 , 松尾 由賀利 , 福山 武志 , 旭耕一郎 : “^{3}He 共存磁力計の導入による ^{129}Xe 原子 EDM 測定実験 IV”, 日本物理学会第 70 回年次大会, (日本物理学会), 東京都新宿区, 3 月 (2015).

西村太樹 , 金野峻平 , 田口義眞 , 千葉順成 , 藤田佳孝 , 阿部康介 , 馬場秀忠 , 福田茂一 , 本間彰 , 保高寿也 , 市川雄一 , 泉川卓司 , 神戸峻輔 , 菊川直樹 , 北川淳志 , 小島拓実 , 小島和佳 , 古浦新司 , 劉斌 , 松多健策 , 三原基嗣 , 水上淳 , 森田祐介 , 室岡大樹 , 長島正幸 , 大野淳一 , 大坪隆 , 鈴木伸司 , 佐藤眞司 , 田中聖臣 , 田代圭佑 , 若林優 , 渡邉大 , 吉永健太 , 朱易帆 : “超許容ベータ崩壊核 ^{34}Ar の精密分岐比測定 III”, 日本物理学会第 70 回年次大会, (日本物理学会), 東京都新宿区, 3 月 (2015).

大友祐一 , 市川雄一 , 石橋陽子 , 鈴木貴大 , 上野秀樹 , 今村慧 , 藤田朋美 , 早坂美希 , 富永大樹 , 松本未来 , 江上魁 , 古川武 , 佐藤智哉 , 坂本雄 , 小島修一郎 , 舟山智歌子 , 平尾千佳 , 菅野雄揮 , 小峰太郎 , 旭耕一郎 : “中性子過剰核 S 同位体の偏極度および磁気モーメント測定”, 日本物理学会第 70 回年次大会, (日本物理学会), 東京都新宿区, 3 月 (2015).

今村慧 , 古川武 , 涌井崇志 , 藤田朋美 , 早坂美希 , 松本未来 , 江上魁 , 富永大樹 , 小田島仁司 , 上野秀樹 , 松尾由賀利 : “低収量原子核の核構造研究へ向けたレーザー・RF/MW 二重共鳴信号の高強度化”, 日本物理学会第 70 回年次大会, (日本物理学会), 東京都新宿区, 3 月 (2015).

金原 慎二 , 仲澤 和馬 , 上野 秀樹 , 市川 雄一 , 吉田 純也 , KhinThanTint , MyintKyawSoe , AyeMohMohTheint , 三品旭弘 , 伊藤宏紀 , 遠藤陽子 , 小林秀隆 : “原子核乾板を用いた荷電粒子識別法の開発”, 日本物理学会第 70 回年次大会, (日本物理学会), 東京都新宿区, 3 月 (2015).

High Energy Astrophysics Laboratory

Publications

[Journal]

(Original Papers) *Subject to Peer Review

Noda, Hirofumi; Makishima, Kazuo; Yamada, Shin'ya; Nakazawa, Kazuhiro; Sakurai, Soki; Miyake, Katsuma: "Suzaku Studies of the Central Engine in the Typical Type I Seyfert NGC 3227: Detection of Multiple Primary X-Ray Continua with Distinct Properties" The Astrophysical Journal, 794, 2 (2014). *

Yoshikawa, A., Yamada, S., Nakahira, S., Matsuoka, M., Negoro, H., Mihara, T., Tamagawa, T.: "Repeated short-term spectral softening in the low/hard state of the Galactic black hole candidate Swift J1753.5-0127" Publications of the Astronomical Society of Japan, 67, 11 (2015). *

Asami, Fumi; Enoto, Teruaki; Iwakiri, Wataru; Yamada, Shin'ya; Tamagawa, Toru; Mihara, Tatehiro; Nagase, Fumiaki: "Broad-band spectroscopy of Hercules X-1 with Suzaku" Publications of the Astronomical Society of Japan, 66, 44 (2014). *

Hamaguchi, Kenji; Corcoran, Michael F.; Takahashi, Hiromitsu; Yuasa, Takayuki; Ishida, Manabu; Gull, Theodore R.; Pittard, Julian M.; Russell, Christopher M. P.; Madura, Thomas I.: "Suzaku Monitoring of Hard X-Ray Emission from η Carinae over a Single Binary Orbital Cycle" The Astrophysical Journal, 795, 119 (2014). *

Suwa, Y., Enoto, T.: "Anisotropic neutrino effect on magnetar spin: constraint on inner toroidal field" Monthly Notices of the Royal Astronomical Society 443, 3586 (2014). *

Makishima, K., Enoto, T., Hiraga, J. S., Nakano, T., Nakazawa, K., Sakurai, S., Sasano, M., Murakami, H.: "Possible Evidence for Free Precession of a Strongly Magnetized Neutron Star in the Magnetar 4U 0142+61" Physical Review Letters 112, 171102 (2014). *

Konami, S., Matsushita, K., Nagino, R., Tamagawa, T.: "Abundance Patterns in the Interstellar Medium of Early-type Galaxies Observed with Suzaku" Astrophysical Journal 783, 8 (2014). *

Sasano, M., Makishima, K., Sakurai, S., Zhang, Z., Enoto, T.: "Suzaku view of the neutron star in the dipping source 4U 1822-37" Publications of the Astronomical Society of Japan 66, 35 (2014) *

Yamaguchi, H., Badenes, C., Petre, R., Nakano, T., Castro, D., Enoto, T., Hiraga, J. S., Hughes, J. P., Maeda, Y., Nobukawa, M., Safi-Harb, S., Slane, P. O., Smith, R. K., Uchida, H.: "Discriminating the Progenitor Type of Supernova Remnants with Iron K-shell Emission" Astrophysical Journal Letter 785, L27 (2014). *

Wik, D. R., Hornstrup, A., Molendi, S., Madejski, G., Harrison, F. A., Zoglauer, A., Grefenstette, B. W., Gastaldello, F., Madsen, K. K., Westergaard, N. J., Ferreira, D. D. M., Kitaguchi, T., Pedersen, K., Boggs, S. E., Christensen, F. E., Craig, W. W., Hailey, C. J., Stern, D., Zhang, W. W.: "NuSTAR Observations of the Bullet Cluster: Constraints on Inverse Compton Emission" Astrophysical Journal 792, 48 (2014). *

Grefenstette, B. W., Harrison, F. A., Boggs, S. E., Reynolds, S. P., Fryer, C. L., Madsen, K. K., Wik, D. R., Zoglauer, A., Ellinger, C. I., Alexander, D. M., An, H., Barret, D., Christensen, F. E, Craig, W. W., Forster, K., Giommi, P., Hailey, C. J., Hornstrup, A., Kaspi, V. M., Kitaguchi, T., Koglin, J. E., Mao, P. H., Miyasaka, H., Mori, K., Perri, M., Pivovaroff, M. J., Puccetti, S., Rana, V., Stern, D., Westergaard, N. J., Zhang, W. W.: "Asymmetries in core-collapse supernovae from maps of radioactive ^{44}Ti in Cassiopeia A" Nature 506, 339-342 (2014). *

Kitaguchi, T., An, H., Beloborodov, A. M., Gotthelf, E. V., Hayashi, T., Kaspi, V. M., Rana, V. R., Boggs, S. E., Christensen, F. E., Craig, W. W., Hailey, C. J., Harrison, F. A., Stern, D., Zhang, W. W.: "NuSTAR and Swift Observations of the Fast Rotating Magnetized White Dwarf AE Aquarii" Astrophysical Journal 782, 3 (2014). *

Grefenstette, Brian W.; Reynolds, Stephen P.; Harrison, Fiona A.; Humensky, T. Brian; Boggs, Steven E.; Fryer, Chris L.; DeLaney, Tracey; Madsen, Kristin K.; Miyasaka, Hiromasa; Wik, Daniel R.; Zoglauer, Andreas; Forster, Karl; Kitaguchi, Takao; Lopez, Laura; Nynka, Melania; Christensen, Finn E.; Craig, William W.; Hailey, Charles J.; Stern, Daniel; Zhang, William W.: "Locating the Most Energetic Electrons in Cassiopeia A" The Astrophysical Journal, 802, 15 (2015). *

Wik, Daniel R.; Hornstrup, A.; Molendi, S.; Madejski, G.; Harrison, F. A.; Zoglauer, A.; Grefenstette, B. W.; Gastaldello, F.; Madsen, K. K.; Westergaard, N. J.; Ferreira, D. D. M.; Kitaguchi, T.; Pedersen, K.; Boggs, S. E.; Christensen, F. E.; Craig, W. W.; Hailey, C. J.; Stern, D.; Zhang, W. W. "NuSTAR Observations of the Bullet Cluster: Constraints on Inverse Compton Emission" The Astrophysical Journal,792,48(2014). *

Maeda, Keiichi; Katsuda, Satoru; Bamba, Aya; Terada, Yukikatsu; Fukazawa, Yasushi: "Long-lasting X-Ray Emission from Type IIb Supernova 2011dh and Mass-loss History of the Yellow Supergiant Progenitor" The Astrophysical Journal, 785, 95 (2014). *

Serino, Motoko; Sakamoto, Takanori; Kawai, Nobuyuki; Yoshida, Atsumasa; Ohno, Masanori; Ogawa, Yuji; Nishimura, Yasunori; Fukushima, Kosuke; Higa, Masaya; Ishikawa, Kazuto; Ishikawa, Masaki; Kawamuro, Taiki; Kimura, Masashi; Matsuoka, Masaru; Mihara, Tatehiro; Morii, Mikio; Nakagawa, Yujin E.; Nakahira, Satoshi; Nakajima, Motoki; Nakano, Yuki; Negoro, Hitoshi; Onodera, Takuya; Sasaki, Masayuki; Shidatsu, Megumi; Sugimoto, Juri; Sugizaki, Mutsumi;

Suwa, Fumitoshi; Suzuki, Kazuhiko; Tachibana, Yutaro; Takagi, Toshihiro; Toizumi, Takahiro; Tomida, Hiroshi; Tsuboi, Yohko; Tsunemi, Hiroshi; Ueda, Yoshihiro; Ueno, Shiro; Usui, Ryuichi; Yamada, Hisaki; Yamamoto, Takayuki; Yamaoka, Kazutaka; Yamauchi, Makoto; Yoshidome, Koshiro; Yoshii, Taketoshi: "MAXI observations of gamma-ray bursts" Publications of the Astronomical Society of Japan,66,8714(2014) *

Broersen, Sjors; Chiotellis, Alexandros; Vink, Jacco; Bamba, Aya: "The many sides of RCW 86: a Type Ia supernova remnant evolving in its progenitor's wind bubble" Monthly Notices of the Royal Astronomical Society,441,3040(2014) *

Tanaka, Y. T.; Stawarz, .; Finke, J.; Cheung, C. C.; Dermer, C. D.; Kataoka, J.; Bamba, A.; Dubus, G.; De Naurois, M.; Wagner, S. J.; Fukazawa, Y.; Thompson, D. J.: "Extreme Blazars Studied with Fermi-LAT and Suzaku: 1ES 0347-121 and Blazar Candidate HESS J1943+213" The Astrophysical Journal,787,155(2014). *

Misawa, Toru; Inada, Naohisa; Oguri, Masamune; Gandhi, Poshak; Horiuchi, Takashi; Koyamada, Suzuka; Okamoto, Rina: "Resolving the Clumpy Structure of the Outflow Winds in the Gravitationally Lensed Quasar SDSS J1029+2623" The Astrophysical Journal Letters,794,L20(2014). *

"Discovery of Four Doubly Imaged Quasar Lenses from the Sloan Digital Sky Survey" Inada, Naohisa; Oguri, Masamune; Rusu, Cristian E.; Kayo, Issha; Morokuma, Tomoki: The Astronomical Journal,147,153(2014). *

Tsuchiya, Harufumi: "Surrounding material effect on measurement of thunderstorm-related neutrons" Astroparticle Physics,57,33(2014). *

[Book・Proceedings]

(Original Papers) *Subject to Peer Review

Wakabayashi, M., Komiya, K., Tamagawa, T., Takeuchi, Y., Aoki, K., Taketani, A., Hamagaki, H.: "Development of a Diehard GEM using PTFE insulator substrate" Journal of Instrumentation 9, C3043 (2014). *

Takeuchi, Y., Tamagawa, T., Kitagushi, T., Yamada, S., Iwakiri, W., Asami, F., Yoshikawa, A., Kaneko, K., Enoto, T., Hayato, A., Kohmura, T.: "Property of LCP-GEM in Pure Dimethl Ether at Low Pressure" Journal of Instrumentation C01002 (2014). *

Hill, Joanne E.; Black, J. Kevin; Emmett, Thomas J.; Enoto, Teruaki; Jahoda, Keith M.; Kaaret, Philip; Nolan, David S.; Tamagawa, Toru: "Design improvements and x-ray performance of a time projection chamber polarimeter for persistent astronomical sources" Proceedings of the SPIE, 9144, 91441N (2014).

Jahoda, Keith M.; Black, J. Kevin; Hill, Joanne E.; Kallman, Timothy R.; Kaaret, Philip E.; Markwardt, Craig B.; Okajima, Takashi; Petre, Robert; Soong, Yang; Strohmayer, Tod E.; Tamagawa, Toru; Tawara, Yuzuru: "X-ray polarization capabilities of a small explorer mission" Proceedings of the SPIE, 9144, 91440N (2014).

Hayashida, Kiyoshi; Yonetoku, Daisuke; Gunji, Shuichi; Tamagawa, Toru; Mihara, Tatehiro; Mizuno, Tsunefumi; Takahashi, Hiromitsu; Dotani, Tadayasu; Kubo, Hidetoshi; Yatsu, Yoichi; Tokanai, Fuyuku; Nakamori, Takeshi; Shibata, Shinpei; Hayato, Asami; Furuzawa, Akihiro; Kishimoto, Yuji; Kitamoto, Shunji; Toma, Kenji; Sadamoto, Masaaki; Yoshinaga, Keigo; Kim, Juyong; Ide, Shunichiro; Kamitsukasa, Fumiyoshi; Anabuki, Naohisa; Tsunemi, Hiroshi; Katagiri, Jun; Sugimoto, Juri: "X-ray gamma-ray polarimetry small satellite PolariS" Proceedings of the SPIE, 9144, 91440K (2014).

Nakazawa, Kazuhiro; Takahashi, Tadayuki; Watanabe, Shin; Ichinohe, Yuto; Takeda, Shin'ichiro; Enoto, Teruaki; Fukazawa, Yasushi; Kamae, Tuneyoshi; Kokubun, Motohide; Makishima, Kazuo; Mitani, Takefumi; Mizuno, Tsunefumi; Nomachi, Masaharu; Tajima, Hiroyasu; Takashima, Takeshi; Tamagawa, Toru; Terada, Yukikatsu; Tashiro, Makoto; Uchiyama, Yasunobu; Yoshimitsu, Tetsuo: "Sub-MeV all sky survey with a compact Si/CdTe Compton telescope" Proceedings of the SPIE, 9144, 91440J (2014).

Kitaguchi, T., Tamagawa, T., Hayato, A., Enoto, T., Yoshikawa, A., Kaneko, K., Takeuchi, Y., Black, K., Hill, J., Jahoda, K., Krizmanic, J., Sturner, S., Griffiths, S., Kaaret, P., Marlowe, H.: "Monte-Carlo estimation of the inflight performance of the GEMS satellite x-ray polarimeter" Society of Photo-Optical Instrumentation Engineers (SPIE) Conference Series, p.91444L (2014)

Takeuchi, Y., Kitaguchi, T., Hayato, A., Tamagawa, T., Iwakiri, W., Asami, F., Yoshikawa, A., Kaneko, K., Enoto, T., Black, K., Hill, J., Jahoda, K.: "Properties of the flight model gas electron multiplier for the GEMS mission" Society of Photo-Optical Instrumentation Engineers (SPIE) Conference Series, p.91444N (2014)

Enoto, T., Black, J. K., Kitaguchi, T., Hayato, A., Hill, J. E., Jahoda, K., Tamagawa, T., Kaneko, K., Takeuchi, Y., Yoshikawa, A., Marlowe, H., Griffiths, S., Kaaret, P. E., Kenward, D., Khalid, S.: "Performance verification of the Gravity and Extreme Magnetism Small explorer (GEMS) x-ray polarimeter" Society of Photo-Optical Instrumentation Engineers (SPIE) Conference Series, p.91444M (2014)

Hill, J. E., Black, J. K., Emmett, T. J., Enoto, T., Jahoda, K. M., Kaaret, P., Nolan, D. S., Tamagawa, T.: "Design improvements and x-ray performance of a time projection chamber polarimeter for persistent astronomical sources" Society of Photo-Optical Instrumentation Engineers (SPIE) Conference Series, p.91441N (2014)

Jahoda, K. M., Black, J. K., Hill, J. E., Kallman, T. R., Kaaret, P. E., Markwardt, C. B., Okajima, T., Petre, R., Soong, Y., Strohmayer, T. E., Tamagawa, T., Tawara, Y.: "X-ray polarization capabilities of a small explorer mission" Society of Photo-Optical Instrumentation Engineers (SPIE) Conference Series, p.91440N (2014)

Oral Presentations

(International Conference etc.)

Takayuki Yuasa, "A SPACEWIRE ROUTER ARCHITECTURE WITH NON-BLOCKING PACKET TRANSFER MECHANISM", International Space Wire Conference, Athens, Greece, September (2014).

Takayuki Yuasa, "The origin of the Galactic Ridge X-ray Emission", East Asian Core Observatories Association 2015, Taipei, Taiwan, February (2015).

Hirofumi Noda, "Understanding X-ray Spectral and Timing Characteristics of Active Galactic Nuclei by Novel Picture with Multiple Primary Emission" The X-ray Universe 2014, Dublin, Ireland, June (2014).

Hirofumi Noda, "A Novel Picture of the AGN Central Engine Derived with X-ray and Optical Simultaneous Observations" COSPAR 2014, Moscow, Russia, August (2014).

Hirofumi Noda, "Novel Picuture of the AGN Central Engine Established by X-ray and Optical Simultaneous Stuies" APRIM 2014, Deajeon, Koria, August (2014).

Toru Tamagawa, "GEM Production in Japan", Invited seminar, (National institute of nuclear and particle physics (IN2P3)), Paris, France, August (2014).

Wataru B. Iwakiri, "Cosmic X-ray Study of the Physics in Strong Magnetic Field and Expectation for Ground Experiments", PLASMA 2014 (invited), Niigata, Japan, November (2014).

Teruaki Enoto, "Astrophysical Observations and Future Projects of Neutron Stars and Magnetars" 4th Joint Meeting of the Nuclear Physics Divisions of the American Physical Society and the Physical Society of Japan, Hawaii, USA, October (2014).

Teruaki Enoto, "Status Report Spectral Analysis Cookbook" ASTRO-H Science Meeting 12, Paris, France, July (2014).

Teruaki Enoto, "Are Magnetars in X-ray Binaries? The Slowest Rotating Accreting Neutron Star 4U 1954+319" EWASS2014, Geneva, Switzerland, June (2014).

(Domestic Conference)

吉川瑛文, 山田真也, 野田博文, 玉川徹: "「すざく」衛星を用いたブラックホール連星 Cygnus X-1 の high/soft 状態のハード成分の詳細解析" 日本天文学会 2014 年秋季年会, (日本天文学会), 山形, 9 月 (2014).

榎戸輝揚, 笹野理, 山田真也, 玉川徹, 牧島一夫ほか: "自転周期のきわめて遅いX線パルサー 4U 1954+319 のすざく観測" 日本天文学会 2014 年秋季年会, (日本天文学会), 山形, 9 月 (2014).

勝田哲, 森浩二, 大平豊, 常深博, 小山勝二, 中嶋大, 内田裕之, 上司文善, 馬場彩, 山崎了, 澤田真理, 坪根義雄, Petre Robert, 玉川徹: "「チャンドラ」衛星による超新星残骸 RCW 86 南西端の再観測" 日本天文学会 2014 年秋季年会, (日本天文学会), 山形, 9 月 (2014).

山崎典子, 満田和久, 竹井洋, 辻本匡弘, 小川美奈, 杉田寛之, 佐藤洋一, 篠崎慶亮, 岡本篤, 藤本龍一, 大橋隆哉, 石崎欣尚, 江副祐一郎, 山田真也, 小波さおり, 田代信, 寺田幸功, 瀬田裕美, 北本俊二, 星野晶夫, 玉川徹, 石川久美, 野田博文, 佐藤浩介, 太田直美, 澤田真理, 三石郁之, 村上正秀, 村上弘志, 伊豫本直子, R.L. Kelley, C.A. Kilbourne, F.S. Porter, K.R. Boyce, M. E. Eckart, M. P. Chiao, M. A. Leutenegger, G.V. Brown, D. McCammon, A. Szymkowiak, J.-W. den Herder, D. Haas, C. de Vries, E. Costantini, H. Akamatsu, S.Paltani, 他 ASTRO-H SXS チーム: "ASTRO-H 搭載精密軟 X 線分光装置 SXS の開発の現状 XII" 日本天文学会 2014 年秋季年会, (日本天文学会), 山形, 9 月 (2014).

岩切渉, 早藤麻美, 武内陽子, 玉川徹, 北口貴雄, 榎戸輝揚, 吉川瑛文, 金子健太, 窪田恵, 西田和樹, Keith Gendreau: "小型かつ変調型の X 線発生装置 Modulated X-ray Source(MXS) の製作と性能評価" 日本天文学会 2014 年秋季年会, (日本天文学会), 山形, 9 月 (2014).

林田清, 吉永圭吾, キムジュヨン, 井出舜一郎, 上司文善, 穴吹直久, 常深博, 郡司修一, 柴田晋平, 片桐惇, 中森健之, 米徳大輔, 三原建弘, 玉川徹, 早藤麻美, 杉本樹梨, 高木利紘, 水野恒史, 高橋弘充, 谷津陽一, 堂谷忠靖, 斎藤芳隆, 古澤彰浩, 窪秀利, 當真賢二, 岸本祐二, Keith Jahoda, Joe Hill, ほか PolariS-WG: "X 線ガンマ線偏光観測小型衛星 PolariS：開発の現状 2014" 日本天文学会 2014 年秋季年会, (日本天文学会), 山形, 9 月 (2014).

武内陽子, 玉川徹, 北口貴雄, 早藤麻美, 榎戸輝揚, 岩切渉, 吉川瑛文, 金子健太, 窪田恵, 西田和樹: "光電子追跡型 X 線偏光計の製作および基礎性能評価" 日本天文学会 2014 年秋季年会, (日本天文学会), 山形, 9 月 (2014).

湯浅孝行, 林多佳由, 石田学, 寺田幸功: "強磁場激変星 V1223 Sgr の鉄 Kα 輝線構造の時間変動解析" 日本天文学会 2014 年秋季年会, (日本天文学会), 山形, 9 月 (2014).

桑原啓介, 山田真也, 大橋隆哉, 野田博文: "狭輝線 1 型セイファート銀河 PG1244+026 の X 線時間変動解析" 日本天文学会 2014 年秋季年会, (日本天文学会), 山形, 9 月 (2014).

河口賢至, 深沢泰司, 田中康之, 伊藤亮介, 川端弘治, 植村誠, 秋田谷洋, 神田優花, 峰崎岳夫, 野田博文, かなたチーム: "かなた望遠鏡による活動銀河核の可視光・X 線・ガンマ線での相関の探査" 日本天文学会 2014 年秋季年会, (日本天文学会), 山形, 9 月 (2014).

野田博文, 牧島一夫, 山田真也, 中澤知洋, 三宅克馬: "セイファート NGC 3227 が示す巨大ブラックホールへの降着流の状態遷移" 日本天文学会 2014 年秋季年会, (日本天文学会), 山形, 9 月 (2014).

笹野理, 榎戸輝揚, 牧島一夫, 堂谷忠靖, 岩井將親: "「すざく」による特異な低質量星と中性子星の連星 GRO J1744-28 の観測" 日本天文学会 2014 年秋季年会, (日本天文学会), 山形, 9 月 (2014).

牧島一夫, 榎戸輝揚, 中澤知洋, 平賀純子, 中野俊男, 笹野理, 櫻井壮希, 村上浩章: "マグネター 4U 0142+61 における自由歳差運動の徴候 II" 日本天文学会 2014 年秋季年会, (日本天文学会), 山形, 9 月 (2014).

安田哲也, 田代信, 寺田幸功, 神頭知美, 岩切渉, 榎戸輝揚, 中川友進, 馬場彩, 浦田裕次, 柴田晋平, 牧島一夫, すざく WAM チーム: "すざく衛星搭載 WAM 検出器による AXP 1E1547.0-5408 の硬 X 線バーストの観測 (II)" 日本天文学

会 2014 年秋季年会, (日本天文学会), 山形, 9 月 (2014).

寺田幸功, 前田啓一, 玉川徹, 馬場彩, 高橋忠幸, 深沢泰司, 榎戸輝揚, 勝田哲: “「すざく」を用いた Ia 型超新星 SN2014J の硬エックス線観測” 日本天文学会 2015 年春季年会, (日本天文学会), 大阪, 3 月 (2015).

辻本匡弘, 満田和久, 山崎典子, 竹井洋, 小川美奈, 杉田寛之, 佐藤洋一, 篠崎慶亮, 岡本篤, 藤本龍一, 大橋隆哉, 石崎欣尚, 江副祐一郎, 山田真也, 小波さおり, 田代信, 寺田幸功, 瀬田裕美, 北本俊二, 星野晶夫, 玉川徹, 石川久美, 野田博文, 佐藤浩介, 太田直美, 澤田真理, 三石郁之, 村上正秀, 村上弘志, 伊豫本直子, R. L. Kelley, C. A. Kilbourne, F. S. Porter, K. R. Boyce, M. E. Eckart, M. P. Chiao, M. A. Leutenegger, G.V. Brown, D. McCammon, A. Szymkowiak, J.-W. den Herder, D. Haas, C. de Vries, E. Costantini, H. Akamatsu, S.Paltani, ほか ASTRO-H SXS チーム: “ASTRO-H 搭載精密軟 X 線分光装置 SXS の開発の現状 XIII” 日本天文学会 2015 年春季年会, (日本天文学会), 大阪, 3 月 (2015).

玉川徹, 早藤麻美, 北口貴雄, 榎戸輝揚, 岩切渉, 吉川瑛文, 武内陽子, 窪田恵, 西田和樹, 田原譲, 幅良統, 林田清, 水野恒史, Keith Jahoda, Joanne Hill, ほか PRAXyS 衛星チーム: “X 線偏光観測衛星 PRAXyS” 日本天文学会 2015 年春季年会, (日本天文学会), 大阪, 3 月 (2015).

窪田めぐ, 武内陽子, 西田和樹, 吉川瑛文, 金子健太, 榎戸輝揚, 早藤麻美, 北口貴雄, 岩切渉, 玉川徹, Keith M. Jahoda, Joanne E. Hill, Kevin Black: “PRAXyS 衛星搭載に向けた光電効果型ガス偏光計の性能評価” 日本天文学会 2015 年春季年会, (日本天文学会), 大阪, 3 月 (2015).

北口貴雄, 玉川徹, 早藤麻美, 岩切渉, 窪田恵, 西田和樹, 武内陽子, 榎戸輝揚, 武井大, 高山裕貴: “SPring-8 によるマイクロパターンガス偏光計の詳細な性能評価” 日本天文学会 2015 年春季年会, (日本天文学会), 大阪, 3 月 (2015).

中澤知洋, 国分紀秀, 佐藤悟朗, 川原田円, 佐藤理江, 渡辺伸, 高橋忠幸, 太田方之, 小高裕和, 武田伸一郎, 原山淳, 斉藤新也, 湯浅孝行, 谷津陽一, 内山秀樹, 田島宏康, 山岡和貴, 深沢泰司, 水野恒史, 大野雅功, 高橋弘充, 勝田隼一郎, 寺田幸功, 牧島一夫, 片岡淳, 野田博文, 榎戸輝揚, 田中孝明, 内山泰伸, 中森健之, Olivier Limousin, Philippe Laurent, Francois Lebrun, 櫻井壮希, 笹野理, 中野俊男, 小林翔悟, 村上浩章, 小野光, 加藤佑一, 三宅克馬, 古田禄大, 室田優紀, 萩野浩一, 桂川美穂, 古井俊也, 枝廣育実: “ASTRO-H 衛星搭載硬 X 線撮像検出器 (HXI) の現状 FM の完成” 日本天文学会 2015 年春季年会, (日本天文学会), 大阪, 3 月 (2015).

桑原啓介, 山田真也, 大橋隆哉, 野田博文: “狭輝線 1 型セイファート銀河の X 線時間変動に対する特徴付けとその比較” 日本天文学会 2015 年春季年会, (日本天文学会), 大阪, 3 月 (2015).

野田博文, 峰崎岳夫, 牧島一夫, 中澤知洋, 諸隈智貴, 小久保充, 土居守, 河口賢至, 伊藤亮介, 川端弘治, 深沢泰司, 中尾光, 渡辺誠, 森鼻久美子, 伊藤洋一, 斉藤嘉彦, 山田真也: “セイファート NGC 3516 の X 線と可視光の間に見られた光度変動の遅延” 日本天文学会 2015 年春季年会, (日本天文学会), 大阪, 3 月 (2015).

宮崎直人, 山田真也, 榎戸輝揚, 大橋隆哉: “「すざく」データを用いた微弱な輝線や吸収線の統計的評価方法” 日本天文学会 2015 年春季年会, (日本天文学会), 大阪, 3 月 (2015).

村上浩章, 牧島一夫, 榎戸輝揚, 古田禄大, 笹野理, 中野俊男, 櫻井壮希, 中澤知洋: “マグネター 4U 0142+61 における自由歳差運動の徴候 IV” 日本天文学会 2015 年春季年会, (日本天文学会), 大阪, 3 月 (2015).

牧島一夫, 榎戸輝揚, 村上浩章, 古田禄大, 笹野理, 中野俊男, 中澤知洋: “マグネター歳差運動の二例目：「すざく」による 1E1547.0 − 5408 の結果” 日本天文学会 2015 年春季年会, (日本天文学会), 大阪, 3 月 (2015).

中野俊男, 村上浩章, 古田禄大, 平賀純子, 牧島一夫, 金田英宏, 内山秀樹, 榎戸輝揚: “マグネター 1E 2259+586 と付随する超新星残骸 CTB109 の親星質量” 日本天文学会 2015 年春季年会, (日本天文学会), 大阪, 3 月 (2015).

宮武広直, Steve Bickerton, Alexie Leauthaud, Surhud More, 岡部信広, 高田昌広, 大栗真宗, 浜名崇, 宮崎聡, Bob Armstrong, Jim Bosch, Robert Lupton, Paul Price, 梅津敬一, Rachel Mandelbaum, Melanie Simet, 内海洋輔, 西澤淳, 大倉悠貴, ほか HSC weak lensing analysis team: “Hyper Suprime-Cam における銀河形状測定の系統誤差の評価” 日本天文学会 2015 年春季年会, (日本天文学会), 大阪, 3 月 (2015).

北口貴雄, 玉川徹, 早藤麻美, 榎戸輝揚, 岩切渉, 吉川瑛文, 金子健太, 武内陽子, 窪田恵, 西田和樹: “X 線の直線偏光・分光・到達時間を測定できるマイクロパターンガス検出器の開発”, 日本物理学会 2014 年秋季大会, (日本物理学会), 佐賀, 9 月 (2014).

窪田恵, 早藤麻美, 北口貴雄, 武内陽子, 榎戸輝揚, 岩切渉, 金子健太, 西田和樹, 吉川瑛文, 玉川徹: “変調型 X 線源を用いたジメチルエーテル中での電子輸送特性の測定” 日本物理学会 2014 年秋季大会, (日本物理学会), 佐賀, 9 月 (2014).

小宮一毅, 藤原康平, 小林丈士, 若林正毅, 玉川徹, 武内陽子, 浜垣秀樹: “新しい絶縁材料を用いた GEM の開発” 日本物理学会 2014 年秋季大会, (日本物理学会), 佐賀, 9 月 (2014).

牧島一夫, 榎戸輝揚, 村上浩章, 平賀純子, 中野俊男, 中澤知洋, 櫻井壮希, 笹野理: “「すざく」で探るマグネター 4U 0142+61 における中性子星の自由歳差運動と磁気変形 II” 日本物理学会 2014 年秋季大会, (日本物理学会), 佐賀, 9 月 (2014).

楳本大悟, 土屋晴文, 榎戸輝揚, 湯浅孝行, 山田真也, 中澤知洋, 牧島一夫: “GROWTH 実験で 2012 年に検出された北陸冬季雷雲からの対消滅線” 日本物理学会 2014 年秋季大会, (日本物理学会), 佐賀, 9 月 (2014).

早藤麻美, 北口貴雄, 岩切渉, 玉川徹, 武内陽子, 窪田恵, 西田和樹, 榎戸輝揚: “宇宙観測を目的とした TPC 型 X 線偏光計の性能評価試験” 日本物理学会第 70 回年次大会, (日本物理学会), 早稲田, 3 月 (2015).

岩切渉, 北口貴雄, 早藤麻美, 玉川徹, 武内陽子, 窪田恵, 西田和樹, 榎戸輝揚, Keith M. Jahoda, Joanne E. Hill, J. Kevin Black: “PRAXYS 衛星搭載 X 線偏光計のシンクロトロン放射光を用いた性能評価” 日本物理学会第 70 回年次大会, (日本物理学会), 早稲田, 3 月 (2015).

石崎欣尚, 満田和久, 山崎典子, 竹井洋, 辻本匡弘, 小川美奈, 杉田寛之, 佐藤洋一, 篠崎慶亮, 岡本篤, 藤本龍一,

大橋隆哉, 江副祐一郎, 山田真也, 小波さおり, 田代信, 寺田幸功, 瀬田裕美, 北本俊二, 星野晶夫, 玉川徹, 石川久美, 野田博文, 佐藤浩介, 太田直美, 澤田真理, 三石郁之, 村上正秀, 村上弘志, 伊豫本直子, R.L. Kelley, C.A. Kilbourne, F.S. Porter, K.R. Boyce, M. E. Eckart, M. P. Chiao, M. A. Leutenegger, G.V. Brown, D. McCammon, A. Szymkowiak, J.-W. den Herder, D. Haas, C. de Vries, E. Costantini, H. Akamatsu, S.Paltani, 他 ASTRO-H SXS チーム: “ASTRO-H 搭載 精密軟 X 線分光装置 SXS の開発の現状 (VI)” 日本物理学会第 70 回年次大会, (日本物理学会), 早稲田, 3 月 (2015).

楳本大悟, 土屋晴文, 湯浅孝行, 中澤知洋, 榎戸輝揚, 古田録大, 山田真也, 牧島一夫: “GROWTH 実験 1：2014 年末に新規設置した雷雲ガンマ線検出器と初期成果” 日本物理学会第 70 回年次大会, (日本物理学会), 早稲田, 3 月 (2015).

古田禄大, 楳本大悟, 土屋晴文, 湯浅孝行, 中澤知洋, 榎戸輝揚, 山田真也, 牧島一夫: “GROWTH 実験 2：2014-2015 冬に観測された雷由来ガンマ線の詳細解析” 日本物理学会第 70 回年次大会, (日本物理学会), 早稲田, 3 月 (2015).

橋本直, D.A. Bennett, C. Curceanu, W.B Doriese, J.W. Fowler, J. Gard, F.P. Gustafsson, 早野龍五, 施赫將, M. Iliescu, 石元茂, 板橋健太, 岩崎雅彦, 桑原啓介, J. Marton, 野田博文, G.C. O ’ Neil, 岡田信二, 應田治彦, C.D. Reintsema, 佐藤将春, D.R. Schmidt, 鈴木謙, 鈴木隆敏, D.S. Swetz, 竜野秀行, F，J. Uhlig, J.N. Ullom, E. Widmann, 山田真也, J. ZmeskalH: “K 中間子原子 X 線分光に向けた超伝導遷移端マイクロカロリメータの π-ビーム試験” 日本物理学会第 70 回年次大会, (日本物理学会), 早稲田, 3 月 (2015).

竜野秀行, D.A. Bennett, C. Curceanu, W.B Doriese, J.W. Fowler, J. Gard, F.P. Gustafsson, 橋本直, 早野龍五, 施赫將, M. Iliescu, 石元茂, 板橋健太, 岩崎雅彦, 桑原啓介, J. Marton, 野田博文, G.C. O ’ Neil, 岡田信二, 應田治彦, C.D. Reintsema, 佐藤将春, D.R. Schmidt, A. Scordo, 鈴木謙, 鈴木隆敏, D.S. Swetz, J. Uhlig, J.N. Ullom, E. Widmann, 山田真也, J. Zmeskal: “荷電粒子ビーム環境における超伝導遷移端マイクロカロリメータ X 線検出器の性能評価” 日本物理学会第 70 回年次大会, (日本物理学会), 早稲田, 3 月 (2015).

岡田信二, D.A. Bennett, C. Curceanu, W.B Doriese, J.W. Fowler, J. Gard, F.P. Gustafsson, 橋本直, 早野龍五, 施赫將, M. Iliescu, 石元茂, 板橋健太, 岩崎雅彦, 桑原啓介, J. Marton, 野田博文, G.C. O ’ Neil, 應田治彦, C.D. Reintsema, 佐藤将春, D.R. Schmidt, 鈴木謙, 鈴木隆敏, D.S. Swetz, 竜野秀行, F，J. Uhlig, J.N. Ullom, E. Widmann, 山田真也, J. Zmeskal: “超伝導遷移端マイクロカロリメータを用いた K 中間子原子 X 線精密分光実験” 日本物理学会第 70 回年次大会, (日本物理学会), 早稲田, 3 月 (2015).

田島宏康, 深沢泰司, 渡辺伸, 内山秀樹, 内山泰伸, 榎戸輝揚, 太田方之, 大野雅功, 小高裕和, 片岡淳, 川原田円, 国分紀秀, 佐藤悟朗, 佐藤理江, 高橋忠幸, 高橋弘充, 武田伸一郎, 田代信, 田中孝明, 寺田幸功, 中澤知洋, 中森健之, 林克洋, 原山淳, Roger Blandford, 牧島一夫, Grzegorz Madejski, 水野恒史, 森國城, 谷津陽一, 山岡和貴, 山田真也, 湯浅孝行, 米徳大輔, Philippe Laurent, Olivier Limousin, Fran ois Lebrun, ほか ASTRO-H SGD チーム: “ASTRO-H 衛星搭載軟ガンマ線検出器の衛星搭載器試験結果” 日本物理学会第 70 回年次大会, (日本物理学会), 早稲田, 3 月 (2015).

玉川 徹, 早藤麻美, 北口貴雄, 榎戸輝揚, 岩切渉, 林田 清, 水野恒史, 吉川瑛文, 武内陽子, 窪田恵, 西田和樹, Keith Jahoda, Joanne Hill, 田原譲, 幅良統, ほか PRAXyS チーム: “X 線偏光観測衛星 PRAXYS の提案” 宇宙科学シンポジウム, (宇宙航空研究開発機構 宇宙科学研究所), 相模原, 1 月 (2015).

石川久美, “瞳再配置法高コントラスト干渉計イメージング” 地球型惑星観測装置ワークショップ, 定山渓, 2 月 (2014).

石川久美, “「すざく」XIS による地球外圏からの軟 X 線放射の系統探査” 全天軟 X 線放射研究会, (理化学研究所), 和光市, 5 月 (2014).

石川久美, “X 線観測レビュー” 地球磁気圏 X 線可視化に関する研究会, (首都大学東京), 東京, 11 月 (2014)

榎戸輝揚, “マグネターの時期活動と X 線観測” 第二回 DTA シンポジウム (招待講演), (国立天文台), 三鷹, 10 月 (2014)

榎戸輝揚, “マグネターと将来の突発天体観測” 高宇連将来計画シンポジウム, (宇宙科学研究所), 淵野辺, 8 月 (2014)

榎戸輝揚, “中性子星・バイナリー等の MeV 放射: 100 keV–100 MeV の話題” 高宇連将来計画シンポジウム, (宇宙科学研究所), 淵野辺, 8 月 (2014)

玉川 徹, “今後 20 年間の X 線・ガンマ線偏光観測ミッションと準備状況” 高宇連将来計画シンポジウム, (宇宙科学研究所), 淵野辺, 8 月 (2014)

Astro-Glaciology Research Unit

Publications

[Journal]

(Original Papers) *Subject to Peer Review

Sigl M., McConnell J., Toohey M., Curran M., Das S., Edwards R., Isaksson E., Kawamura K., Kipfstuhl S., Krüger K., Layman L., Maselli O., Motizuki Y., Motoyama H., Pasteris D., Severi M.: "Insights from Antarctica on volcanic forcing during the Common Era", Nature Climate Change, 4, 693–697,(2014). *

Okamoto S., Takahashi K., Nakai Y., Motizuki Y., Makabe A., Koba K., Motoyama H.: "Measurement of nitrogen and oxygen isotope ratios in considerably low nitrate concentration ice core samples", RIKEN Accel. Prog. Rep. 47, 139, (2014).*

Miyake F., Suzuki A., Masuda K., Horiuchi K., Motoyama H., Matsuzaki H., Motizuki Y., Takahashi K., Nakai Y.: "Cosmic ray event of AD 774-775 shown in quasi-annual 10Be data from the Antarctic Dome Fuji ice core", Geophysical Research Letters, 42, 84-89, (2015).*

Oral Presentations

(International Conference etc.)

Motizuki Y., Motoyama H., Nakai Y., Suzuki K., Iizuka Y., Takahashi K.: "Chemical composition and uniquecharacteristics of shallow ice core samples from a Dome Fuji core (Antarctica) drilled in 2001" (A poster presentation), The 38th International Symposium on Environmental Analytical Chemistry, Lausannne, Switzerland, June.(2014).

(Domestic Conference)

田邊健茲, 望月優子 : "共生星 R Aquarii の 1073/1074 年新星爆発に対する地質学的痕跡", 日本天文学会 2014 年秋季年会, 山形, 9 月(2014).

三宅芙沙, 鈴木麻未, 増田公明, 堀内一穂, 本山秀明, 松崎浩之, 望月優子, 高橋和也, 中井陽一.: "南極アイスコア中 10Be 濃度を用いた西暦 774-775 年宇宙線イベントの調査", 日本物理学会 2014 年秋季大会, 佐賀, 9 月(2014).

藤田秀二, 東久美子, 飯塚芳徳, 平林幹啓, 堀 彰, 望月優子, 本山秀明.: "東南極ドームふじ近傍で掘削された複数の浅層コアのフィルンの生成・変態・変形", 雪氷研究大会, 八戸, 9 月(2014).

望月優子 : "アイスコアと宇宙からのシグナル", 総研大・学融合「生命概念の普遍化ー宇宙の生命」第 6 回研究会, 三浦郡, 12 月(2014).

望月優子: "DF01 浅層コアの硝酸イオンプロファイルと宇宙からのシグナル", ドームふじアイスコアコンソーシアム ICC 研究集会, 立川, 3 月(2014).

高橋和也, 望月優子, 中井陽一.: "ドームふじ浅層コアのイオン及び硝酸同位体の詳細解析の現状と今後について", ドームふじアイスコアコンソーシアム ICC 研究集会, 立川, 3 月(2014).

Superheavy Element Production Team

Publications

[Journal]

(Original Papers) *Subject to Peer Review

J. Even, A. Yakushev, Ch. E. Düllmann, H. Haba, M. Asai, T. K. Sato, H. Brand, A. Di Nitto, R. Eichler, F. L. Fan, W. Hartmann, M. Huang, E. Jäger, D. Kaji, J. Kanaya, Y. Kaneya, J. Khuyagbaatar, B. Kindler, J. V. Kratz, J. Krier, Y. Kudou, N. Kurz, B. Lommel, S. Miyashita, K. Morimoto, K. Morita, M. Murakami, Y. Nagame, H. Nitsche, K. Ooe, Z. Qin, M. Schädel, J. Steiner, T. Sumita, M. Takeyama, K. Tanaka, A. Toyoshima, K. Tsukada, A. Türler, I. Usoltsev, Y. Wakabayashi, Y. Wang, N. Wiehl, S. Yamaki, "Synthesis and detection of a seaborgium carbonyl complex",Science 345, 1491 (2014).

D. Kaji, K. Morimoto, F. Tokanai
"Beam intensity monitor based on gas scintillation emitted from helium gas molecules in a gas-filled recoil ion separator", Nucl. Instr. and Meth. B317, 311 (2014),

M. Huang, H. Haba, M. Murakami, M. Asai, D. Kaji, J. Kanaya, Y. Kasamatsu, H. Kikunaga, Y. Kikutani, Y. Komori, H. Kudo, Y. Kudou, K. Morimoto, K. Morita, K. Nakamura, K. Ozeki, R. Sakai, A. Shinohara, T. Sumita, K. Tanaka, A. Toyoshima, K. Tsukada, Y. Wakabayashi, and A. Yoneda , "Production of ^{88}Nb and ^{170}Ta for chemical studies of element 105, Db, using the GARIS gas-jet system", J. Radioanal. Nucl. Chem., 304 845-849, (2015).

H. Haba, M. Huang, D. Kaji, J. Kanaya, Y. Kudou, K. Morimoto, K. Morita, M. Murakami, K. Ozeki, R. Sakai, T. Sumita, Y. Wakabayashi, A. Yoneda, Y. Kasamatsu, Y. Kikutani, Y. Komori, K. Nakamura, A. Shinohara, H. Kikunaga, H. Kudo, K. Nishio, A. Toyoshima, and T. Tsukada, "Production of ^{262}Db in the ^{248}Cm(^{19}F,5n)^{262}Db reaction and decay properties of ^{262}Db and ^{258}Lr", Phys. Rev. C, 89, 024618/1-11, 2014

[Book ・Proceedings]

(Original Papers) *Subject to Peer Review

D. Kaji, K. Morimoto, H. Haba, Y. Wakabayashi, Y. Kudou, M. Huang, S. Goto, M. Murakami, N. Goto, T. Koyama, N. Tamura, S. Tsuto, T. Sumita, K. Tanaka, M. Takeyama, S. Yamaki, K. Morita, "Startup of a new gas-filled recoil separator GARIS-II", J. Radioanal. Nucl. Chem., (2014) 303: 1523-1525

Daiya KAJI, Kouji MORIMOTO, Hiromitsu HABA, Yasuo WAKABAYASHI, Yuki KUDOU, Minghui HUANG, Shin-ichi GOTO, Masashi MURAKAMI, Naoya GOTO, Takumi KOYAMA, Nobuyuki TAMURA, Shouhei TSUTO, Takayuki SUMITA, Kengo TANAKA, Mirei TAKEYAMA, Sayaka YAMAKI, and Kosuke MORITA "Research and development of a new gas-filled recoil separator GARIS-II", JPS Conf. Proc., 013051 (2014)

Oral Presentations

(International Conference etc.)

D. Kaji, NUSTAR meeting 2014, "SHE experiments with GARIS-I/-II at RIKEN", (Invited talk)

K. Morita, 2nd Conference on Advances in Redioactive Isotope Science (ARIS2014), (Invited talk), June 4, 2014, Tokyo, Japan, 'Research of Superheavy Elements at RIKEN - Present Status and Perspective –'

K. Morita, Zakopane Conference on Nuclear Physics, Invited talk Sep. 3, 2014, Zakopane, Poland, 'Research on Superheavy Element at RIKEN

K. Morita, K. Morimoto, D. Kaji, H. Haba, K. Ozeki, Y. Kudou, Y. Wakabayashi, A. Yoneda, A. Yoshida, T. Ohnishi, Y. Kasamatsu, H. Hasebe, M.-H. Huang, J. Kanaya, R. Kanungo, K. Katori, T. Sumita, K. Tanaka, T. Yamaguchi, T. Akiyama, R. Sakai, S. Yamaki, H. Kudo, S. Goto, M. Murakami, Y. Kariya, H.-S. Xu , T. H. Huang, Z. Gan, L. Ma, E. Ideguchi, T. Suda, H. Kikunaga, N. Sato, H. Koura, S. Mitsuoka, M. Asai, F. Tokanai, T. Moritani, K. Mayama, M. Takeyama, S. Namai, A. Mashiko, A. Ozawa, K. Sueki, Y.-L. Zhao, H. Geissel, S. Hofmann, Y. Maurer, K. Fujita, Y. Narikiyo, T. Tanaka, and S. Yamamoto, JPS-APS Joint meeting on Nuclear Physics Division, Oct. 9, 2014, Hawaii, U.S.A.

D. Kaji, "Performance of New Gas-filled Recoil Ion Separator GARIS-II for Asymmetric Fusion Reaction", Tokyo, June, 2014, ARIS2014

D. Kaji, "The first α -γ spectroscopic study by using a Si-Ge detector array installed at the focal plane of GARIS", Tokyo, June, 2014, ARIS 2014,

D. Kaji, "Present status of superheavy element production target for gas-filled recoil separators GARIS and GARIS-II", Tokyo, Aug. 2014, INTD2014

Yamaki S., Morimoto K., Kaji D., Wakabayashi Y., et al., "Pulse Shape Analysis Using Flash-ADC for Short-lived Decay of Super Heavy Elements", ARIS2014, Tokyo, June (2014).

(Domestic Conference)

山木さやか: "Flash-ADC により取得したプリアンプ波形のための解析アルゴリズムの開発", 日本物理学会第 69 回年次大会, (日本物理学会), 平塚市、東海大学, 3 月(2014)

加治大哉, "GARIS-II commissioning #3"、 平塚市、東海大学, 3 月(2014), 第 69 回 日本物理学会

新井郁也, 和田道治, Peter Schury, 伊藤由太, 片山一郎, 園田哲, Mikael Reponen, 高峰愛子, 加治大哉, 森本幸司, 羽場宏光, 森田浩介, Hermann Wollnik, "理研 GARIS-IIにおけるイオンサーフィン型RFカーペットガスセルの性能評価", 第70回年次大回 日本物理学会 早稲田大学 2015年3月

加治大哉, "GARISを用いたホットフュージョン反応 ^{248}Cm+^{48}Ca→^{296}Lv* に関する研究", 名古屋、2014 年 9 月, 第 58 回放射化学討論会,

加治大哉, "気体充填型反跳分離装置 GARIS-II の非対称系反応に対する性能試験", 名古屋、2014 年 9 月, 第 58 回放射化学討論会,

加治大哉, "GARIS を用いた 113 番元素研究の総括", 名古屋、2014 年 9 月, 第 58 回放射化学討論会,

加治大哉, "超重核研究のための焦点面検出器の開発", 名古屋、2014 年 9 月, 第 58 回放射化学討論会,

森本幸司: ”加速器を用いた新元素探索の最前線”, 第 23 理化学研究所里庄セミナー、岡山県、８月(2014)

一般向け講演会

森田浩介、大阪大学理学部物理学科セミナー　2014 年 7 月 25 日　豊中市‘新元素の探索－現代の錬金術－’

森田浩介、日本耳鼻咽喉科学会学術講演会　2014 年 5 月 16 日　福岡市　‘113 番元素発見への道のり’

森田浩介、福岡県高校理科部会夏季研修会講演会　2014 年 8 月 20 日　　福岡市‘113 番新元素の探索’

森田浩介、科学を語る会講演会　2014 年 11 月 8 日　福岡市　‘新元素の探索－現代の錬金術－’

森田浩介、理化学研究所、研究員幹事会総会講演会　2015 年 3 月 6 日　和光市　‘113 番新元素の探索

Superheavy Element Research Device Development Team

Publications

[Journal]

(Original Papers) *Subject to Peer Review

J. Even, A. Yakushev, Ch. E. Düllmann, H. Haba, M. Asai, T. K. Sato, H. Brand, A. Di Nitto, R. Eichler, F. L. Fan, W. Hartmann, M. Huang, E. Jäger, D. Kaji, J. Kanaya, Y. Kaneya, J. Khuyagbaatar, B. Kindler, J. V. Kratz, J. Krier, Y. Kudou, N. Kurz, B. Lommel, S. Miyashita, K. Morimoto, K. Morita, M. Murakami, Y. Nagame, H. Nitsche, K. Ooe, Z. Qin, M. Schädel, J. Steiner, T. Sumita, M. Takeyama, K. Tanaka, A. Toyoshima, K. Tsukada, A. Türler, I. Usoltsev, Y. Wakabayashi, Y. Wang, N. Wiehl, S. Yamaki, "Synthesis and detection of a seaborgium carbonyl complex",Science 345, 1491 (2014).

D. Kaji, K. Morimoto, F. Tokanai
"Beam intensity monitor based on gas scintillation emitted from helium gas molecules in a gas-filled recoil ion separator", Nucl. Instr. and Meth. B317, 311 (2014),

M. Huang, H. Haba, M. Murakami, M. Asai, D. Kaji, J. Kanaya, Y. Kasamatsu, H. Kikunaga, Y. Kikutani, Y. Komori, H. Kudo, Y. Kudou, K. Morimoto, K. Morita, K. Nakamura, K. Ozeki, R. Sakai, A. Shinohara, T. Sumita, K. Tanaka, A. Toyoshima, K. Tsukada, Y. Wakabayashi, and A. Yoneda, "Production of ^{88}Nb and ^{170}Ta for chemical studies of element 105, Db, using the GARIS gas-jet system", J. Radioanal. Nucl. Chem., 304 845-849, (2015).

H. Haba, M. Huang, D. Kaji, J. Kanaya, Y. Kudou, K. Morimoto, K. Morita, M. Murakami, K. Ozeki, R. Sakai, T. Sumita, Y. Wakabayashi, A. Yoneda, Y. Kasamatsu, Y. Kikutani, Y. Komori, K. Nakamura, A. Shinohara, H. Kikunaga, H. Kudo, K. Nishio, A. Toyoshima, and T. Tsukada, "Production of ^{262}Db in the ^{248}Cm(^{19}F,5n)^{262}Db reaction and decay properties of ^{262}Db and ^{258}Lr", Phys. Rev. C, 89, 024618/1-11, 2014

[Book ・Proceedings]

(Original Papers) *Subject to Peer Review

D. Kaji, K. Morimoto, H. Haba, Y. Wakabayashi, Y. Kudou, M. Huang, S. Goto, M. Murakami, N. Goto, T. Koyama, N. Tamura, S. Tsuto, T. Sumita, K. Tanaka, M. Takeyama, S. Yamaki, K. Morita, "Startup of a new gas-filled recoil separator GARIS-II", J. Radioanal. Nucl. Chem., (2014) 303: 1523-1525

Daiya KAJI, Kouji MORIMOTO, Hiromitsu HABA, Yasuo WAKABAYASHI, Yuki KUDOU, Minghui HUANG, Shin-ichi GOTO, Masashi MURAKAMI, Naoya GOTO, Takumi KOYAMA, Nobuyuki TAMURA, Shouhei TSUTO, Takayuki SUMITA, Kengo TANAKA, Mirei TAKEYAMA, Sayaka YAMAKI, and Kosuke MORITA "Research and development of a new gas-filled recoil separator GARIS-II", JPS Conf. Proc., 013051 (2014)

Oral Presentations

(International Conference etc.)

D. Kaji, NUSTAR meeting 2014, "SHE experiments with GARIS-I/-II at RIKEN", (Invited talk)

K. Morita, K. Morimoto, D. Kaji, H. Haba, K. Ozeki, Y. Kudou, Y. Wakabayashi, A. Yoneda, A. Yoshida, T. Ohnishi, Y. Kasamatsu, H. Hasebe, M.-H. Huang, J. Kanaya, R. Kanungo, K. Katori, T. Sumita, K. Tanaka, T. Yamaguchi, T. Akiyama, R. Sakai, S. Yamaki, H. Kudo, S. Goto, M. Murakami, Y. Kariya, H.-S. Xu , T. H. Huang, Z. Gan, L. Ma, E. Ideguchi, T. Suda, H. Kikunaga, N. Sato, H. Koura, S. Mitsuoka, M. Asai, F. Tokanai, T. Moritani, K. Mayama, M. Takeyama, S. Namai, A. Mashiko, A. Ozawa, K. Sueki, Y.-L. Zhao, H. Geissel, S. Hofmann, Y. Maurer, K. Fujita, Y. Narikiyo, T. Tanaka, and S. Yamamoto, JPS-APS Joint meeting on Nuclear Physics Division, Oct. 9, 2014, Hawaii, U.S.A.

D. Kaji, "Performance of New Gas-filled Recoil Ion Separator GARIS-II for Asymmetric Fusion Reaction", Tokyo, June, 2014, ARIS2014

D. Kaji, "The first α -γ spectroscopic study by using a Si-Ge detector array installed at the focal plane of GARIS", Tokyo, June, 2014, ARIS 2014,

D. Kaji, "Present status of superheavy element production target for gas-filled recoil separators GARIS and GARIS-II", Tokyo, Aug. 2014, INTD2014

S. Yamaki, K. Morimoto, D. Kaji,Y. Wakabayashi, et al., "Pulse Shape Analysis Using Flash-ADC for Short-lived Decay of Super Heavy Elements", ARIS2014, Tokyo, June (2014).

(Domestic Conference)

山木さやか: "Flash-ADC により取得したプリアンプ波形のための解析アルゴリズムの開発", 日本物理学会第 69 回年次大会, (日本物理学会), 平塚市、東海大学, 3 月(2014)

加治大哉, "GARIS-II commissioning #3"、 平塚市、東海大学, 3 月(2014), 第 69 回 日本物理学会

新井郁也, 和田道治, Peter Schury, 伊藤由太, 片山一郎, 園田哲, Mikael Reponen, 高峰愛子, 加治大哉, 森本幸司, 羽場宏光, 森田浩介, Hermann Wollnik, "理研GARIS-IIにおけるイオンサーフィン型RFカーペットガスセルの性能評価", 第70回年次大回 日本物理学会 早稲田大学 2015年3月

加治大哉, "GARISを用いたホットフュージョン反応 ^{248}Cm+^{48}Ca→^{296}Lv* に関する研究", 名古屋、2014 年 9 月, 第 58 回放射化学討論会,

加治大哉, "気体充填型反跳分離装置 GARIS-II の非対称系反応に対する性能試験", 名古屋、2014 年 9 月, 第 58 回放射化学討論会,

加治大哉, "GARIS を用いた 113 番元素研究の総括", 名古屋、2014 年 9 月, 第 58 回放射化学討論会,

加治大哉, "超重核研究のための焦点面検出器の開発", 名古屋、2014 年 9 月, 第 58 回放射化学討論会,

森本幸司: "加速器を用いた新元素探索の最前線", 第 23 理化学研究所里庄セミナー、岡山県、8 月(2014)

Accelerator Group

Publications

[**Journal**]

（Original Papers） *Subject to Peer Review

Kuboki H., Okuno H., Hasebe H., Fukunishi N., Ikezawa E., Imao H., Kamigaito O., and Kase M.: "Charge state distribution of ^{86}Kr in hydrogen and helium gas charge strippers at 2.7 MeV/nucleon", Phys. Rev. ST Accel. Beams **17**, 123501 (2014). ∗

Ohnishi J., Okuno H., Nakamura M.: "Support Structure of Cold-Mass for Superconducting Ring Cyclotron and Electromagnetic Force Measurements with Strain Gauges", IEEE Trans. Applied Superconductivity **24**, 4000504 (2014). ∗

Ozeki K., Higurashi Y., Kidera M., and Nakagawa T.: "Note: Effect of hot liner in producing ^{40,48}Ca beam from RIKEN 18-GHz electron cyclotron resonance ions source", Rev. Sci. Instrum. **86**, 016114 (2015). ∗

Maeyama T., Fukunishi N., Ishikawa K.L., Furuta T., Fukasaku K., Takagi S., Noda S., Himeno R., and Fukuda S.: "Radiological characteristics of MRI-based VIP polymer gel under carbon beam irradiation", Radiation Physics and Chemistry **107**, p. 7–11 (2015).

（Others） *Subject to Peer Review

前山拓哉, 福西暢尚, 石川顕一, 古田琢哉, 深作和明, 高木周, 野田茂穂, 姫野龍太郎, 福田茂一: "VIP ポリマーゲル線量計による炭素線線量分布評価手法の検討", 放射線化学 **98**, p. 11–15 (2014).

[**Book · Proceedings**]

（Original Papers） *Subject to Peer Review

Lu L., Kamigaito O., Sakamoto N., Suda K., Yamada K.: "Design of a Triple-Spoke Cavity as a Rebuncher for RIKEN RI-Beam Factory", Proceedings of the 16th International Conference on RF Superconductivity (SRF2013), p. 988–990 (2014).

Ohnishi J., Okuno H., Nakamura M.: "Design of New Superconducting Ring Cyclotron for the RIBF", Proceedings of the 20th International Conference on Cyclotrons and their Applications (Cyclotrons'13), p. 79 (2014).

Sakamoto N., Fujimaki M., Fukunishi N., Higurashi Y., Kamigaito O., Okuno H., Suda K., Watanabe T., Watanabe Y., Yamada K., Koyama R.: "Performance of New Injector RILAC2 for RIKEN RI-Beam Factory", Proceedings of the 27th Linear Accelerator Conference (LINAC14), p. 1123–1126 (2015).

Suda K., Ikezawa E., Kamigaito O., Sakamoto N., Yamada K., Touchi Y.: "Construction of the New Amplifiers for the RIKEN-LINAC", Proceedings of the 27th Linear Accelerator Conference (LINAC14), p. 339–341 (2015).

Watanabe T., Fukunishi N., Kase M., Kamigaito O., Inamori S., Kon K.: "Improvements of Beam Current Monitor by using a High Tc Current Sensor and SQUID at the RIBF", Journal of Physics: Conf. Series **507**, 042047 (2014).

Yamada K., Kamigaito O., Sakamoto N., Suda K.: "Conceptual Design of SC Linac for RIBF-Upgrade Plan", Proceedings of the 16th International Conference on RF Superconductivity (SRF2013), p. 137–139 (2014).

Yamada K., Suda K., Sakamoto N., Kamigaito O.: "Design of a New Superconducting Linac for the RIBF Upgrade", Proceedings of the 27th Linear Accelerator Conference (LINAC14), p. 1127–1130 (2015).

池沢英二, 小山田和幸, 大木智則, 山内啓資, 田村匡史, 遊佐陽, 金子健太, 渡邉裕, 坂本成彦, 須田健嗣, 山田一成, 加瀬昌之, 上垣外修一: "理研重イオンリニアックの現状報告", Proceedings of the 11th Annual Meeting of Particle Accelerator Society of Japan, p. 398–400 (2014).

内山暁仁, 込山美咲, 福西暢尚: "RIBF におけるビームサービス時間可視化システムの実装", Proceedings of the 11th Annual Meeting of Particle Accelerator Society of Japan, p. 767–770 (2014).

大関和貴, 日暮祥英, 中川孝秀: "理研 RILAC のための新しい 18-GHz ECR イオン源の導入", Proceedings of the 11th Annual Meeting of Particle Accelerator Society of Japan, p. 544–547 (2014).

小高康照, 石川盛, 小林清志, 小山亮, 柴田順翔, 月居憲俊, 仲村武志, 西田稔, 西村誠, 濱仲誠, 福沢聖児, 矢冨一慎, 坂本成彦, 内山暁仁, 奥野広樹, 影山正, 加瀬昌之, 上垣外修一, 熊谷桂子, 込山美咲, 須田健嗣, 中川孝秀, 長瀬誠, 長友傑, 福西暢尚, 藤巻正樹, 真家武士, 山田一成, 渡邉環, 渡邉裕, 山家捷一, 大城幸光: "理研 AVF サイクロトロン運転の現状報告", Proceedings of the 11th Annual Meeting of Particle Accelerator Society of Japan, p. 364–368 (2014).

福沢聖児, 濱仲誠, 石川盛, 小高康照, 小林清志, 小山亮, 仲村武志, 西田稔, 西村誠, 柴田順翔, 月居憲俊, 矢冨一慎, 須田健嗣, 段塚知志, 藤巻正樹, 福西暢尚, 藤縄雅, 長谷部裕雄, 日暮祥英, 池沢英二, 今尾浩士, 加瀬昌之, 影山正, 上垣外修一, 木寺正憲, 熊谷桂子, 久保木浩功, 込山美咲, 真家武士, 長瀬誠, 中川孝秀, 中村仁音, 大西純一, 奥野広樹, 大関和貴, 坂本成彦, 内山暁仁, 渡邉環, 渡邉裕, 渡部秀, 山田一成, 山澤秀行: "理研 RIBF におけるリングサイクロトロンの運転報告", Proceedings of the 11th Annual Meeting of Particle Accelerator Society of Japan, p. 401–405 (2014).

山口由高, 若杉昌徳, 阿部康志, 洲嵜ふみ, 藤縄雅, 加瀬昌之, 込山美咲, 熊谷桂子, 眞家武士, 長江大輔, 大西純一, 小沢顕, 上坂友洋, 渡邉裕, 山口貴之, 山澤秀行, 柳澤善行, 銭廣十三, 矢野安重: "理研 RIBF における稀少 RI リングの現状", Proceedings of the 11th Annual Meeting of Particle Accelerator Society of Japan, p. 1381–1385 (2014).

山田一成, 須田健嗣, 坂本成彦, 奥野広樹, 上垣外修一: "RIBF 大強度化計画用重イオン超伝導線形加速器の概念設計", Proceedings of the 11th Annual Meeting of Particle Accelerator Society of Japan, pp. 457–462 (2014).

渡邉環, 福西暢尚, 加瀬昌之, 稲森聡, 今康一: "HTc-SQUID ビーム電流モニターの実用化", Proceedings of the

11th Annual Meeting of Particle Accelerator Society of Japan, p. 292–295 (2014).

Oral Presentations

(International Conference etc.)

Fukunishi N.: “Heavy-ion Cyclotron Gymnastics and Associated Beam Dynamics Issues”, 54th ICFA Advanced Beam Dynamics Workshop on High Intensity, High Brightness and High Power Hadron Beams (HB2014), Michigan State University, East Lansing, USA, Nov. (2014).

Higurashi Y., Nakagawa T., Ohnishi J., Ozeki K.: “Emittance Measurements for RIKEN 28 GHz SC-ECRIS”, The 21st international workshop on ECR Ion Sources (ECRIS2014), Nizhny Novgorod, Russia, Aug. (2014).

Maeyama T., Fukunishi N., Ishikawa K.L., Furuta T., Fukasaku K., Takagi S., Noda S., Himeno R., and Fukuda S.: “Preliminary Result of Nanocomposite Fricke Gel Dosimeter”, The 5th Asia Pacific Symposium on Radiation Chemistry, Tokyo, Japan, Sep. (2014).

Okuno H.: “Experience with Stripping of Heavy Ion Beams”, 54th ICFA Advanced Beam Dynamics Workshop on High Intensity, High Brightness and High Power Hadron Beams (HB2014), Michigan State University, East Lansing, USA, Nov. (2014).

Sakamoto N.: “Present Performance of the RF System for the RIBF Accelerator Complex and their Upgrade Plan”, Science with Rare Ion Beams (SCRIBE-2014), (Variable Energy Cyclotron Centre and TRIUMF), Variable Energy Cyclotron Centre, Kolkata, India, Nov. (2014).

Uchiyama A.: “Current Status of Web Application for RIBF Accelerator Operations”, Workshop on Accelerator Operations (WAO2014), Mainz, Germany, Oct. (2014).

(Domestic Conference)

前山拓哉, 福西暢尚, 石川顕一, 古田琢哉, 深作和明, 高木周, 野田茂穂, 姫野龍太郎, 福田茂一: “LET 依存性のないナノクレイ添加フリッケゲル線量計の開発”, 第 107 回日本医学物理学会学術大会, 日本医学物理学会横浜, 4 月 (2014).

前山拓哉, 福西暢尚, 石川顕一, 深作和明, 古田琢哉, 高木周, 野田茂穂, 姫野龍太郎, 福田茂一: “LET に依存しない三次元線量計”, 第 15 回放射線プロセスシンポジウム, 東京, 6 月 (2014).

前山拓哉, 福西暢尚, 石川顕一, 深作和明, 福田茂一: “LET 依存性のないゲル線量計の開発”, 先端放射線化学シンポジウム, 日本放射線化学会東京, 3 月 (2015).

渡邉環, 福西暢尚, 加瀬昌之, 稲森聡, 今康一: “HTc-SQUID ビーム電流モニターの実用化”, 第 11 回日本加速器学会年会, 青森, 8 月 (2014).

渡邉環: “理研 RIBF における高温超伝導 SQUID ビーム電流モニターの実用化”, 日本物理学会第 70 回年次大会, 東京, 3 月 (2015).

（Others）

Watanabe T.: “Development of beam current monitor with High-Tc SQUID at RIBF”, Institute of Modern Physics Colloquium, Lanzhou, China, (2015).

前山拓哉, 福西暢尚, 石川顕一, 深作和明, 古田琢哉, 高木周, 野田茂穂, 姫野龍太郎, 福田茂一: “LET 依存性のないゲル線量計の開発”, 平成 25 年度 HIMAC 共同利用研究成果発表会, 放射線医学総合研究所千葉, 4 月 (2014).

前山拓哉: “粒子線治療計画の三次元検証ツールとしてのナノコンポジットゲル線量計”, 平成 26 年度第 3 回重粒子線医工学連携セミナー, 群馬大学群馬, 6 月 (2014).

前山拓哉: “粒子線治療計画の三次元検証ツールとしてのナノコンポジットゲル線量計”, 理化学研究所新技術説明会, 理化学研究所, 埼玉, 6 月 (2014).

前山拓哉, 福西暢尚, 石川顕一, 深作和明, 福田茂一: “ナノコンポジットフリッケゲル線量計の組成条件の検討”, 第 3 回 3D ゲル線量計研究会, 名古屋, 11 月 (2014).

渡邉環: “理研 AVF サイクロトロンのエネルギー測定”, 第 10 回 AVF 合同打合せ, 高崎, 7 月 (2014).

渡邉環: “HTc-SQUID ビーム電流計”, 日新イオン機器株式会社講演会, 京都, 11 月 (2014).

SLOWRI Team

Publications

[**Journal**]

(Original Papers) *Subject to Peer Review

Schury P., Ito Y., Wada M., and Wollnik H.: "Wide-band mass measurements with a multi-reflection time-of-flight mass spectrograph", Int. J. Mass Spectrom. **359**, 19–25 (2014). *

Arai F., Ito Y., Wada M., Schury P., Sonoda T., and Mita H.: "Investigation of the ion surfing transport method with a circular rf carpet", Int. J. Mass Spectrom. **362**, 56–58 (2014). *

Schury P., Wada M., Ito Y., Arai F., Naimi S., Sonoda T., Wollnik H., Shchepunov V.A., Smorra C., and Yuan C.: "A high-resolution multi-reflection time-of-flight mass spectrograph for precision mass measurements at RIKEN/SLOWRI", Inst. Meth. In Phys. Res. B **335**, 39–53 (2014). *

Hirayama Y., Mukai M., Watanabe Y., Imai N., Ishiyama H., Jeong S., Miyatake H., Oyaizu M., Matsuo Y., Sonoda T., and Wada M.: "Ionization cross section measurements for autoionizing states of iridium and rhenium", J. Phys. B: At. Mol. Opt. Phys. **47**, 075201 (2014). *

Yang X., Furukawa T., Wakui T., Fujita T., Imamura K., Mitsuya Y., Hayasaka M., Ichikawa Y., Ishibashi Y., Shirai H., Suzuki T., Ebara Y., Hatakeyama A., Wada M., Sonoda T., Ito Y., Kobayashi T., Nishimura S., Kurata-Nishimura M., Kondo Y., Yoneda K.I., Kubono S., Ohshiro Y., Ueno H., Shinozuka T., Shimada T., Asahi K., and Matsuo Y.: "Laser-radio-frequency double-resonance spectroscopy of $^{84-87}$Rb isotopes trapped in superfluid helium", Phys. Rev. A **90**, 052516 (2014). *

Takamine A., Wada M., Okada K., Sonoda T., Schury P., Nakamura T., Yamazaki Y., Kanai Y., Kojima T.M., Kubo T., Katayama I., Ohtani S., Wollnik H., and Schuessler H.A.: "The hyperfine structure constant of Neutron Halo Nucleus $^{11}Be^{+}$", Phys. Rev. Lett. **112**, 162502 (2014). *

Okada K., Suganuma T., Furukawa T., Takayanagi T., Wada M., and Schuessler H.A.: "Cold ion-polar-molecule reactions studied with a combined Stark-velocity-filter-ion-trap apparatus", Phys. Rev. A **87**, 043427 (2013). *

Oral Presentations

(International Conference etc.)

Ito Y.: "Gas-cell beam cooler-buncher for low-energy experiments at SLOWRI", 6th international conference on Trapped Charged Particles and Fundamental Physics (TCP2014), Takamatsu, Japan, Dec. (2014).

Arai F.: "Performance of ion surfing rf-carpets for RI beam gas catcher", 4th Joint Meeting of the APS Division of Nuclear Physics and the Physical Society of Japan, Hawaii, US, Oct. (2014).

Ito Y.: "A windowless gas-cell cooler-buncher at RIKEN/SLOWRI", 4th Joint Meeting of the APS Division of Nuclear Physics and the Physical Society of Japan, Hawaii, US, Oct. (2014).

Ito Y.: "MRTOF for high-precision mass measurements at RIKEN", 4th Joint Meeting of the APS Division of Nuclear Physics and the Physical Society of Japan, Hawaii, US, Oct. (2014).

Schury P.: "Towards Identification of Super Heavy Elements by Means of Mass Spectroscopy", 4th Joint Meeting of the APS Division of Nuclear Physics and the Physical Society of Japan, Hawaii, US, Oct. (2014).

Wada M.: "SLOWRI: a Universal Low-Energy RI-Beam Facility at RIKEN RIBF", 2nd Conference on Advances in Radioactive Isotope Science (ARIS2014), Tokyo, Japan, June (2014).

(Domestic Conference)

Tomita H., Takamatsu T., Furuta Y., Noto T., Wendt K., Sonnenschein V., Nakamura A., Iguchi T., Kron T., Sonoda T., and Wada M.: "Development of High Resolution Resonance Ionization Spectroscopy for radionuclide analysis", The 75th Japan Society of Applied Physics, Sapporo, Japan, Sept. (2014).

Rare RI-ring Team

Oral Presentations

(International Conference etc.)

Wakasugi M., and rare-RI ring collaboration: "The Rare-RI Ring Facility at RIKEN RI Beam Factory", 2nd Conference on Advances in Radioactive Isotope Science (ARIS2014), Tokyo, Japan, June (2014).

Yamaguchi Y., and rare-RI ring collaboration: "Rare-RI Ring at RIKEN RI Beam Factory", The sixth international conference on Trapped Charged Particles and Fundamental Physics (TCP2014), Takamatsu, Japan, Desember (2014).

Abe Y., Yamaguchi Y., Wakasugi M., Uesaka T., Ozawa A., Suzaki F., Miura H., Yamaguchi T., and Yano Y.: "Isochronous study of the Rare-RI Ring", 9th International Conference on Nuclear Physics at Storage Rings (STORI2014), St. Goar, Germany, September (2014).

Ozawa A.: "Mass measurement with Rare-RI Ring", Science and Next Generation Experiments at FRIB and RIBF, Hawaii, USA, October (2014).

Abe Y.: "Mass measurement of RI with Rare-RI Ring at RIKEN", Post-TCP PMM Workshop, Wako, Japan, December (2014).

Suzaki F., Zenihiro J., Ozawa A., Suzuki T., Uesaka T., Wakasugi M., Yamada K., Yamaguchi T., Abe Y., and Yamaguchi Y.: "Performance of a resonant Schottky pick-up for Rare-RI Ring project", 2nd Conference on Advances in Radioactive Isotope Science (ARIS2014), Tokyo, Japan, June (2014).

Yamaguchi Y., Miura H., Wakasugi M., Abe Y., Ozawa A., Suzaki F., Tokuchi A., Uesaka T., Yamaguchi T., and Yano Y.: "Fast-kicker system for Rare-RI Ring", 9th International Conference on Nuclear Physics at Storage Rings (STORI2014), St. Goar, Germany, September (2014).

Suzaki F., Zenihiro J., Ozawa A., Suzuki T., Uesaka T., Wakasugi M., Yamada K., Yamaguchi T., Abe Y., and Yamaguchi Y.: "A resonant Schottky pick-up for Rare-RI Ring at RIKEN", 9th International Conference on Nuclear Physics at Storage Rings (STORI2014), St. Goar, Germany, September (2014).

(Domestic Conference)

洲嵜ふみ, 阿部康志, NaimiSarah, 三浦宙, 小沢顕, 鈴木健, 上坂友洋, 若杉昌徳, 山田一成, 山口貴之, 山口由高, 銭廣十三, ChenXiangcheng: "稀少 RI リングの共鳴ショットキーピックアップのオフライン性能試験", 日本物理学会第 70 回年次大会, (日本物理学会), 東京, 3 月 (2015).

三浦宙, 山口由高, 若杉昌徳, 阿部康志, 小沢顕, 洲嵜ふみ, 徳地明, 上坂友洋, 山口貴之, 長江大輔, 柳澤善行, 鈴木健: "稀少 RI リングのためのキッカーマグネットの開発", 日本物理学会　第 70 回年次大会, (日本物理学会), 東京, 3 月 (2015).

山口由高, 若杉昌徳, 阿部康志, 洲嵜ふみ, 藤縄雅, 加瀬昌之, 込山美咲, 熊谷桂子, 眞家武士, 長江大輔, 大西純一, 小沢顕, 上坂友洋, 山口貴之, 山澤秀行, 柳澤善行, 銭廣十三, 矢野安重: "理研 RIBF における稀少 RI リングの現状", 第 11 回日本加速器学会年会, (日本加速器学会), 青森市, 8 月 (2014).

SCRIT Team

Oral Presentations

(International Conference etc.)

Wakasugi M., and SCRIT collaboration : "The SCRIT electron scattering facility at the RIKEN RI Beam Factory", 5th EURISOL Topical Meeting, (York University), York, UK, Jul. (2014).

Suda T. : "SCRIT Electron Scattering Facility", 59th Annual Conference of the SA Institute of Physics, (South African Institute of Physics), Johannesburg, South Africa, Jul. (2014).

Ohnishi T., and SCRIT collaboration : "The SCRIT electron scattering facility project at RIKEN RI Beam Factory", 9th International conference on Nuclear Physics at Storage Rings (STORI14), (GSI Helmholtz Centre for Heavy Ion Research), St Goar, Germany, Oct. (2014).

Wakasugi M., and SCRIT collaboration : "The SCRIT electron scattering facility", 6th Trapped Charged Particleand Fundamental Physics, (RIKEN), Takamatsu, Kagawa, Japan, Dec. (2014).

Suda T. : "Electron Scattering for Exotic Nuclei", 38th Symposium on Nuclear Physics, (Universidad Nacional Autónoma de México), Cocoyoc, Mexico, Jan. (2015).

(Domestic Conference)

榎園昭智, 市川進一, 大西哲哉, 栗田和好, 須田利美, 玉江忠明, 塚田暁, 水流輝明, 戸ヶ崎衛, 原雅弘, 原口祐司, 堀利匡, 松尾咲希, 米山俊平, 若杉昌徳,WANG Shou : "Development of the electron spectrometer for the SCRIT experiment", 4th Joint Meeting of the Nuclear Physics Divisions of the American Physics Society and the Physical Society of Japan , (日本物理学会, アメリカ物理学会), Hawaii, USA, 10 月 (2014).

塚田暁, 宮本嵩也, 須田利美, 玉江忠明, 水流輝明, 米山俊平, 原雅弘, 市川進一, 大西哲哉, 若杉昌徳, 榎園昭智, 栗田和好, 松尾咲希, 戸ケ崎衛, 原口祐司,Wang Shuo : "SCRIT electron scattering facility", 4th Joint Meeting of the Nuclear Physics Divisions of the American Physics Society and the Physical Society of Japan , (日本物理学会, アメリカ物理学会), Hawaii, USA, 10 月 (2014).

松尾咲希, 市川進一, 榎園昭智, 大西哲哉, 栗田和好, 須田利美, 玉江忠明, 塚田暁, 水流輝明, 戸ヶ崎衛, 原雅弘, 原口祐司, 堀利匡, 米山俊平, 若杉昌徳,WANG Shou : "Development of the scattererd electron spectrometer for the SCRIT experiment", 第 70 回日本物理学会年次大会, (日本物理学会), 新宿, 日本, 3 月 (2015).

塚田暁, 須田利美, 玉江忠明, 水流輝明, 米山俊平, 松田一衛, 森谷洋祐, 原雅弘, 市川進一, 大西哲哉, 若杉昌徳, 榎園昭智, 栗田和好, 松尾咲希, 戸ケ崎衛, 堀利匡 : "SCRIT 電子スペクトロメータの運動量分解能とアクセプタンス評価", 第 70 回日本物理学会年次大会, (日本物理学会), 新宿, 日本, 3 月 (2015).

米山俊平, 須田利美, 玉江忠明, 塚田暁, 水流輝明, 松田一衛, 森谷洋祐, 大西哲哉, 若杉昌徳, 榎園昭智, 栗田和好, 戸ヶ崎衛, 松尾咲希 : "制動輻射を利用した SCRIT 実験用ルミノシティモニタ", 第 70 回日本物理学会年次大会, (日本物理学会), 新宿, 日本, 3 月 (2015).

BigRIPS Team

Publications

[**Journal**]

(Original Papers) *Subject to Peer Review

Watanabe H., Lorusso G., Nishimura S., Otsuka T., Ogawa K., Xu Z.Y., Sumikama T., Söderström P.-A., Doornenbal P., Li Z., Browne F., Gey G. Jung H. S.. Taprogge J., Vajta Zs., Wu J., Yagi A., Baba H., Benzoni G., Chae K. Y.. Crespi F.C. L., Fukuda N., Gernhäuser R., Inabe N., Isobe T., Jungclaus A., Kameda D., Kim J. D., Kim Y. K., Kojouharov I., Kondev F. G., Kubo T., Kurz N., Kwon Y. K., Lane G. J., Moon C.-B., Montaner-Pizá A., Moschner K., Naqvi F., Niikura M., Nishibata H., Nishimura D., Odahara A., Orlandi R., Patel Z., Podolyák Zs., Sakurai H., Schaffner H., Simpson G. S., Steiger K., Suzuki H., Takeda H., Wendt A., and Yoshinaga K.: "Monopole-Driven Shell Evolution below the Doubly Magic Nucleus ^{132}Sn Explored with the Long-Lived Isomer in ^{126}Pd", Phys. Rev. Lett. **113**, 042502 (2014). *

Taprogge J., Jungclaus A., Grawe H., Nishimura3 S., Doornenbal P., Lorusso G., Simpson G. S., Söderström P.-A., Sumikama T., Xu Z. Y., Baba H., Browne F., Fukuda N., Gernhäuser R., Gey G., Inabe N., Isobe T., Jung H. S., Kameda D., Kim G. D., Kim Y.-K., Kojouharov I., Kubo T., Kurz N., Kwon Y. K., Li Z., Sakurai H., Schaffner H., Steiger K., Suzuki H., Takeda H., Vajta Zs., Watanabe H., Wu J., Yagi A., Yoshinaga K., Benzoni G., Bönig S., Chae K. Y., Coraggio L., Covello A., Daugas J.-M., Drouet F., Gadea A., Gargano A., Ilieva S., Kondev F. G., Kröll T., Lane G. J., Montaner-Pizá A., Moschner K., Mücher D., Naqvi F., Niikura M., Nishibata H., Odahara A., Orlandi R., Patel Z., Podolyák Zs., and Wendt A.: "$1p_{3/2}$ Proton-Hole State in ^{132}Sn and the Shell Structure Along N = 82", Phys. Rev. Lett. **112**, 132501 (2014). *

Taprogge J., Jungclaus A., Grawed H., Nishimura S., Xu Z.Y., Doornenbal P., Lorusso G., Nácher E., Simpson G. S., Söderström P.-A., Sumikama T., Baba H., Browne F., Fukuda N., Gernhäuser R., Gey G., Inabe N., Isobe T., Jung H. S., Kameda D., Kim G. D., Kim Y.-K., Kojouharov I., Kubo T., Kurz N., Kwon Y. K., Li Z., Sakurai H., Schaffner H., Steiger K., Suzuki H., Takeda H., Vajta Zs., Watanabe H., Wu J., Yagi A., Yoshinaga K., Benzoni G., Bönig S., Chae K. Y., Coraggio L., Covello A., Daugas J.-M., Drouet F., Gadea A., Gargano A., Ilieva S., Kondev F. G., Kröll T., Lane G. J., Montaner-Pizá A., Moschner K., Mücher D., Naqvi F., Niikura M., Nishibata H., Odahara A., Orlandi R., Patel Z., Podolyák Zs., and Wendt A.: "Identification of a millisecond isomeric state in ^{129}Cd$_{81}$ via the detection of internal conversion and Compton electrons", Phys. Lett. **B 738**, 223–227 (2014). *

Simpson G. S., Gey G., Jungclaus A., Taprogge J., Nishimura S., Sieja K., Doornenbal P., Lorusso G., Söderström P.-A., Sumikama T., Xu Z. Y., Baba H., Browne F., Fukuda N., Inabe N., Isobe T., Jung H. S., Kameda D., Kim G. D., Kim Y.-K., Kojouharov I., Kubo T., Kurz N., Kwon Y. K., Li Z., Sakurai H., Schaffner H., Shimizu Y., Suzuki H., Takeda H., Vajta Z., Watanabe H., Wu J., Yagi A., Yoshinaga K., Bönig S., Daugas J.-M., Drouet F., Gernhäuser R., Ilieva S., Kröll T., Montaner-Pizá A., Moschner K., Mücher D., Naïdja H., Nishibata H., Nowacki F., Odahara A., Orlandi R., Steiger K., and Wendt A.: "Yrast 6^+ Seniority Isomers of ^{136,138}Sn", Phys. Rev. Lett. **113**, 132502 (2014). *

Kobayashi N., Nakamura T., Kondo Y., Tostevin J. A., Utsuno Y., Aoi N., Baba H., Barthelemy R., Famiano M. A., Fukuda N., Inabe N., Ishihara M., Kanungo R ., Kim S., Kubo T., Lee G. S., Lee H. S., Matsushita M., Motobayashi T., Ohnishi T., Orr N. A., Otsu H., Otsuka T., Sako T., Sakurai H., Satou Y., Sumikama T., Takeda H., Takeuchi S., Tanaka R., Togano Y., and Yoneda K.: "Observation of a p-Wave One-Neutron Halo Configuration in ^{37}Mg", Phys. Rev. Lett. **112**, 242501 (2014). *

Nakamura T., Kobayashi N., Kondo Y., Satou Y., Tostevin J. A., Utsuno Y., Aoi N., Baba H., Fukuda N., Gibelin J., Inabe N., Ishihara M., Kameda D., Kubo T., Motobayashi T., Ohnishi T., Orr N. A., Otsu H., Otsuka T., Sakurai H., Sumikama T., Takeda H., Takeshita E., Takechi M., Takeuchi S., Togano Y., and Yoneda K.: "Monopole-Driven Shell Evolution below the Doubly Magic Nucleus ^{132}Sn Explored with the Long-Lived Isomer in ^{126}Pd", Phys. Rev. Lett. **113**, 042502 (2014). *

Ozawa A., Moriguchi T., Ohtsubo T., Aoi N., Fang D. Q., Fukuda N., Fukuda M., Geissel H., Hachiuma I., Inabe N., Ishibashi Y., Ishimoto S., Ito Y., Izumikawa T., Kameda D., Kubo T., Kuboki T., Kusaka K., Lantz M., Ma Y. G., Mihara M., Miyashita Y., Momota S., Nagae D., Namihira K., Nishimura D., Ooishi H., Ohkuma Y., Ohnishi T., Ohtake M., Ogawa K., Shimbara Y., Suda T., Sumikama T., Suzuki H., Suzuki S., Suzuki T., Takechi M., Takeda H., Tanaka K., Watanabe R., Winkler M., Yamaguchi T., Yanagisawa Y., Yasuda Y., Yoshinaga K., Yoshida A., and Yoshida K.: "Charge-changing cross sections of ^{30}Ne, ^{32,33}Na with a proton target", Phys. Rev. C **89**, 044602 (2014). *

Oral Presentations

(International Conference etc.)

Fukuda N., Kameda D., Takeda H., Suzuki H., Ahn D. S., Shimizu Y., Inabe N., and Kubo T.: "Performance of the Fragment Separator BigRIPS and Perspectives on In-flight RI Beam Production", Advances in Radioactive Isotope Science (ARIS2014), (RIKEN and University of Tokyo), Tokyo, Japan, June (2014).

Sato Y., Fukuda N., Takeda H., Kameda D., Suzuki H., Shimizu Y., Ahn D.S., Murai D., Inabe N., Shimaoka T., Tsubota M., Kaneko J., Chayahara A., Umezawa H., Shikata S., Kumagai H., Murakami H., Yoshida K., Kubo T.: "Status of Beam Line Detectors for the BigRIPS Fragment Separator at RIKEN RI Beam Factory: Issues on High Rates and Resolution", The 2nd Conference on "Advances in Radioactive Isotope Science 2014" (ARIS 2014), (RIKEN and University of Tokyo), Tokyo, Japan, June (2014).

Fukuda N., Kameda D., Takeda H., Suzuki H., Ahn D. S., Shimizu Y., Murai D., Inabe N., and Kubo T. "Production of rare isotopes at RIKEN RI Beam Factory: summary of search for neutron-rich new isotopes", Forth joint meeting of the nuclear physics divisions of the American Physical Society and the Physical Society of Japan, (American Physical Society and the Physical Society of Japan), Hawaii, USA, Oct. (2014).

Shimizu Y., Kubo T., Fukuda N., Ahn D. S., Inabe N., Kameda D., Sato H., Suzuki H., Takeda H., Yoshida K., and EURICA collaboration: "Identification of 25 new neutron-rich isotopes produced in the EURICA uranium beam campaign at RIKEN RIBF", 4th Joint Meeting of the APS Division of Nuclear Physics and the Physical Society of Japan, (American Physical Society and the Physical Society of Japan), Hawaii, USA, October (2014).

Kameda D., Kubo T., and the BigRIPS new isotope collaboration: "Observation of new K isomers among neutron-rich rare earth nuclei produced by in-flight fission of 345 MeV/nucleon ^{238}U", Forth joint meeting of the nuclear physics divisions of the American Physical Society and the Physical Society of Japan, (American Physical Society and the Physical Society of Japan), Hawaii, USA, Oct. (2014).

Murai D. Ieki K., Kubo T., Inabe N., Kameda D., Fukuda N., Takeda H., Suzuki H., Yoshida K., and BigRIPS collabration: "Measurement of production yield for neutron-rich nuclei around Z=60 from in-flight fission of a ^{238}U beam at 345 MeV/nucleon", Forth joint meeting of the nuclear physics divisions of the American Physical Society and the Physical Society of Japan, (The American Physical Society and the Physical Society of Japan), Hawaii, USA, Oct.

Suzuki H., Kubo T., Fukuda N., Inabe N., Kameda D., Takeda H., Sato H., Shimizu Y., Ahn D. S., Ohkoda Y., Iwasa N., Murai D., and BigRIPS collaboration: "Production cross section of radioactive isotopes produced from a ^{124}Xe beam at 345 MeV/u by the BigRIPS separator at RIKEN RI Beam Factory", Forth joint meeting of the nuclear physics divisions of the American Physical Society and the Physical Society of Japan, (The American Physical Society and the Physical Society of Japan), Hawaii, USA, Oct. (2014).

(Domestic Conference)

木佐森慶一, 下浦享, 李清秀, 井手口栄治, 稲辺尚人, 伊藤正俊, 上坂友洋, 大田晋輔, 亀田大輔, 川畑貴裕, 川瀬頌一郎, 菊地陽介, 久保敏幸, 久保田悠樹, 郷慎太郎, 小林幹, 近藤洋介, 坂口聡志, 酒井英行, 笹本良子, 笹野匡紀, 佐藤広海, 清水陽平, 鈴木宏, 高木基伸, 民井淳, 竹田浩之, 武内聡, 津村美保, 時枝紘史, 西隆博, 西村美月, 野地俊平, 馬場秀忠, 馬場辰彦, 堂園昌伯, 福田直樹, 藤井俊彦, 前田幸重, 松原礼明, 三木謙二郎, 道正新一郎, 宮裕之, 柳沢善行, 矢向謙太郎, 横山輪, 吉田光一, M. Assie, D. Beaumel, F. Hammache, A. Stolz: "発熱型二重荷電交換反応 ^{4}He(^{8}He,^{8}Be)4n による 4 中性子系の研究", 日本物理学会第 70 回年次大会, (早稲田大学), 東京, 3 月 (2015).

小山俊平, 大津秀暁, 清水陽平, 米田健一郎, 佐藤広海, 本林透, 西村美月, 銭廣十三, 櫻井博儀, 武内聡, 磯部忠昭, 馬場秀忠, 日下健祐, 大西純一, 笹野匡紀, P. Doornenbal, 福田直樹, 小林俊雄, 炭竈聡之, 松田洋平, 佐藤義輝, J. Hwang, 近藤洋介, 中村隆司, 栂野泰宏, 南方亮吾, 生越駿, 村上哲也, 中塚徳継, J. Gibelin, L. Sylvain, 新倉潤, 小林信之, H. Liu, J. Lee, E. Nikolskii, 坂口聡志, D. Beaumel: "^{16}C クラスター準位探索実験", 日本物理学会第 70 回年次大会, (早稲田大学), 東京, 3 月 (2015).

齊藤敦美, 近藤洋介, 中村隆司, Nadia Lynda Achouri, Thomas Aumann, 馬場秀忠, Franck Delaunay, Pieter Doornenbal, 福田直樹, Julien Gibelin, Jongwon Huang, 稲辺尚人, 磯部忠昭, 亀田大輔, 簡野大輝, Sunji Kim, 小林信之, 小林俊雄, 久保敏幸, Sylvain Leblond, Jenny Lee, Miguel Marques, 南方亮吾, 本林透, 村井大地, 村上哲也, 武藤琴美, 中嶋丈嘉, 中塚徳継, Alahari Navin, 西征爾郎, 生越駿, Nigel Andrew Orr, 大津秀暁, 佐藤広海, 佐藤義輝, 清水陽平, 鈴木宏, 高橋賢人, 竹田浩之, 武内聡, 田中隆己, 栂野泰宏, Adam Garry Tuff Marine Vandebrouck, 米田健一郎: "中性子過剰 ^{19}B の相互作用断面積", 日本物理学会第 70 回年次大会, (早稲田大学), 東京, 3 月 (2015).

栂野泰宏, 南方亮吾, 生越駿, 中村隆司, 磯部忠昭, 稲辺尚人, 大津秀暁, 亀田大輔, 簡野大輝, 久保敏幸, 小林俊雄, 小林信之, 近藤洋介, 佐藤広海, 佐藤義輝, 清水陽平, 鈴木宏, 高橋賢人, 武内聡, 竹田浩之, 田中隆己, 中嶋丈嘉, 中塚徳継, 西征爾郎, 福田直樹, 馬場秀忠, 武藤琴美, 村井大地, 村上哲也, 本林透, 米田健一郎, N. L. Achouri, A. G. Tuff, T. Aumann, F. Delaunay, J. Gibelin, J. Hwangy, S. Kim, J. Lee, M. Marques, A.Navin, N. A. Orr, P. Doornenbal, S. Leblond, M. Vandebrouck: "^{19,20,22}C の反応断面積", 日本物理学会第 70 回年次大会, (早稲田大学), 東京, 3 月 (2015).

SAMURAI Team

Publications

[**Journal**]

(Original Papers) *Subject to Peer Review

N. Kobayashi, T. Nakamura, Y. Kondo, J. A. Tostevin, Y. Utsuno, N. Aoi, H. Baba, R. Barthelemy, M. A. Famiano, N. Fukuda, N. Inabe, M. Ishihara, R. Kanungo, S. Kim, T. Kubo, G. S. Lee, H. S. Lee, M. Matsushita, T. Motobayashi, T. Ohnishi, N. A. Orr, H. Otsu, T. Otsuka, T. Sako, H. Sakurai, Y. Satou, T. Sumikama, H. Takeda, S. Takeuchi, R. Tanaka, Y. Togano, K. Yoneda.:
"Observation of a p-Wave One-Neutron Halo Configuration in ^{37}Mg", Phys.Rev.Lett. 112, 242501 (2014).

S. Michimasa, Y. Yanagisawa, K. Inafuku, N. Aoi, Z. Elekes, Zs. Fulop, Y. Ichikawa, N. Iwasa, K. Kurita, M. Kurokawa, T. Machida, T. Motobayashi, T. Nakamura, T. Nakabayashi, M. Notani, H. J. Ong, T. K. Onishi, H. Otsu, H. Sakurai, M. Shinohara, T. Sumikama, S. Takeuchi, K. Tanaka, Y. Togano, K. Yamada, M. Yamaguchi, K. Yoneda.:
"Quadrupole collectivity in island-of-inversion nuclei ^{28,30}Ne and ^{34,36}Mg", Phys.Rev. C 89, 054307 (2014).

T. Nakamura, N. Kobayashi, Y. Kondo, Y. Satou, J. A. Tostevin, Y. Utsuno, N. Aoi, H. Baba, N. Fukuda, J. Gibelin, N. Inabe, M. Ishihara, D. Kameda, T. Kubo, T. Motobayashi, T. Ohnishi, N. A. Orr, H. Otsu, T. Otsuka, H. Sakurai, T. Sumikama, H. Takeda, E. Takeshita, M. Takechi, S. Takeuchi, Y. Togano, K. Yoneda.:
"Deformation-Driven p-Wave Halos at the Drip Line: ^{31}Ne", Phys.Rev.Lett. 112, 142501 (2014).

A. Obertelli, A. Delbart, S. Anvar, L. Audirac, G. Authelet, H. Baba, B. Bruyneel, D. Calvet, F. Chateau, A. Corsi, P. Doornenbal, J.-M. Gheller, A. Giganon, C. Lahonde-Hamdoun, D. Leboeuf, D. Loiseau, A. Mohamed, J.-Ph. Mols, H. Otsu, C. Peron, A. Peyaud, E. C. Pollacco, G. Prono, J.-Y. Rousse, C. Santamaria, T. Uesaka.:
"MINOS: A vertex tracker coupled to a thick liquid-hydrogen target for in-beam spectroscopy of exotic nuclei", Eur.Phys.J. A 50, 8 (2014).

Y. Satou, J.W. Hwang, S. Kim, K. Tshoo, S. Choi, T. Nakamura, Y. Kondo, N. Matsui, Y. Hashimoto, T. Nakabayashi, T. Okumura, M. Shinohara, N. Fukuda, T. Sugimoto, H. Otsu, Y. Togano, T. Motobayashi, H. Sakurai, Y. Yanagisawa, N. Aoi, S. Takeuchi, T. Gomi, M. Ishihara, S. Kawai, H. J. Ong, T. K. Onishi, S. Shimoura, M. Tamaki, T. Kobayashi, Y. Matsuda, N. Endo, M. Kitayama.:
"One-neutron knockout reaction of ^{17}C on a hydrogen target at 70 MeV/nucleon", Phys. Lett. B 728, 462 (2014).

K. Tshoo, Y. Satou, C. A. Bertulani, H. Bhang, S. Choi, T. Nakamura, Y. Kondo, S. Deguchi, Y. Kawada, Y. Nakayama, K. N. Tanaka, N. Tanaka, Y. Togano, N. Kobayashi, N. Aoi, M. Ishihara, T. Motobayashi, H. Otsu, H. Sakurai, S. Takeuchi, K. Yoneda, F. Delaunay, J. Gibelin, F. M. Marques, N. A. Orr, T. Honda, T. Kobayashi, T. Sumikama, Y. Miyashita, K. Yoshinaga, M. Matsushita, S. Shimoura, D. Sohler, J. W. Hwang, T. Zheng, Z. H. Li, Z. X. Cao.:
"Neutron occupancy of the $0d_{5/2}$ orbital and the N=16 shell closure in ^{24}O", Phys.Lett. B 739, 19 (2014).

R. Shane, A.B. McIntosh, T. Isobe, W.G. Lynch, H. Baba, J. Barney, Z. Chajecki, M. Chartier, J. Estee, M. Famiano, B. Hong, K. Ieki, G. Jhang, R. Lemmon, F. Lu, T. Murakami, N. Nakatsuka, M. Nishimura, R. Olsen, W. Powell, H. Sakurai, A. Taketani, S. Tangwancharoen, M.B. Tsang, T. Usukura, R. Wang,S.J. Yennello, J. Yurkona.:
"SπRIT: A time-projection chamber for symmetry-energy studies", Nuclear Instruments and Methods in Physics Research A 784 (2015) 513–517.

[**Book · Proceedings**]

(Original Papers)

K. Tshoo, Y. Satou, H. Bhang, S. Choi, T. Nakamura, Y. Kondo, S. Deguchi, Y. Kawada, N. Kobayashi, Y. Nakayama, K. N. Tanaka, N. Tanaka, Y. Togano, N. Aoi, M. Ishihara, T. Motobayashi, H. Otsu, H. Sakurai, S. Takeuchi, K. Yoneda, F. Delaunay, J. Gibelin, F. M. Marques, N. A. Orr, T. Honda, M. Matsushita, T. Kobayashi, Y. Miyashita, T. Sumikama, K. Yoshinaga, S. Shimoura, D. Sohler, T. Zheng, Z. X. Cao, Z. H. Li.:
"Neutron occupancy of $0d_{5/2}$ orbital in ^{24}O", Int.Nuclear Physics Conf. 2013, (IUPAP), Firenze, Italy, June 2-7, 2013, S.Lunardi, P.G.Bizzeti, W.S.Kabana, C.Bucci, et al.Eds.p.02103 (2014); EPJ web of Conf.v.66, (2014).

Oral Presentations

(International Conference, etc.)

Y. Kondo.: "Experimental study of neutron-rich nuclei near and beyond drip line with SAMURAI at RIBF", 3rd International Workshop on "State of the Art in Nuclear Cluster Physics"(SOTANCP3), KGU Kannai Media Center, Kanto Gakuin University, Yokohama, Japan. May 26-30, 2014.

Y. Kondo.: "Invariant-mass spectroscopy of extremely neutron-rich nuclei with SAMURAI at RIBF", Advances in Radioactive Isotope Science (ARIS2014), ITO International Research Center, University of Tokyo, Japan, June 1-6, 2014

T. Nakamura.: "Weakly bound and unbound few-body nucleonic systems", Workshop " Few-body universality in atomic and nuclear physics: Recent Experimental and Theoretical Advances, INT, University of Washington, Seattle, USA, May 12–16, 2014.

H. Otsu.: "SAMURAI at RIBF", Workshop on the High-Rigidity Spectrometer for FRIB, (Michigan State University), East Lansing, July (2014).

T. Nakamura.: "Coulomb and nuclear breakup of exotic nuclei near the neutron drip line". ECT* Workshop "Breakup Reactions of Exotic Nuclei and Related Topics", ECT*, Trento, Italy , July 16–18, 2014,

Y. Kondo.: "Experimental studies related to di-neutron correlations", One-day intensive workshop on "di-neutron and alpha-cluster correlations in exotic nuclei", RIKEN, Japan. July 10, 2014.

T. Nakamura.: "Island of Inversion Studied by Coulomb and Nuclear Breakup", PKU-CUSTIPEN Nuclear Reaction Workshop, "Reactions and Spectroscopy of Unstable Nuclei", Peking Univ., Beijing, China, 10–14, Aug. (2014).

Y. Kondo.: "Recent experimental results on unbound oxygen isotopes beyond the drip line", PKU-CUSTIPEN Nuclear Reaction Workshop "Reactions and Spectroscopy of Unstable Nuclei", Peking University, Beijing, China, August 10-14, 2014.

T. Nakamura.: "Nuclear Structure near and beyond the neutron drip line probed by breakup reactions", Int. Symposium on Physics of Unstable Nuclei, Ho Chi Minh City, Vietnam, 3–8, Nov. (2014).

T. Nakamura.: "Study of nuclei near and beyond the neutron drip line at SAMURAI at RIBF", International Workshop on "Critical Stability in Few-body Systems", RIKEN, Wako, 26-30, Jan. (2015).

V. Panin for the HI-p collaboration.: "Investigation of proton-unbound states in neutron-deficient isotopes relevant to the astrophysical rp-process", SAMURAI International Collaboration Workshop 2014, (Tohoku University), Sendai, Sep. (2014).

Y. Kondo, T. Nakamura, N. L. Achouri, T. Aumann, H. Baba, F. Delaunay, P. Doornenbal, N. Fukuda, J. Gibelin, J. Hwang, N. Inabe, T. Isobe, D. Kameda, D. Kanno, S. Kim, N. Kobayashi,T. Kobayashi,T. Kubo,S. Leblond, J. Lee, F. M. Marques, R. Minakata, T. Motobayashi, T. Murakami, K. Muto, T. Nakashima, N. Nakatsuka, A. Navin, S. Nishi, S. Ogoshi, N. A. Orr, H. Otsu, H. Sato,Y. Satou,Y. Shimizu, H. Suzuki, K. Takahashi, H. Takeda, S. Takeuchi, R. Tanaka, Y. Togano, A. G. Tuff, M. Vandebrouck, K. Yoneda.:
"Experimental study of ^{25}O and ^{26}O by using SAMURAI at RIBF", 4th Joint Meeting of the APS Division of Nuclear Physics and the Physical Society of Japan, Waikokoa, Hawaii, USA, Oct. 7-11 (2014).

Y. Togano for SAMURAI collaboration, "Reaction cross section of ^{22}C", 4th Joint Meeting of the APS Division of Nuclear Physics and the Physical Society of Japan, Waikokoa, Hawaii, USA, Oct. 7-11 (2014).

M. Shikata, T. Nakamura, Y. Togano, Y. Kondo.: "Development of the new gamma–ray calorimeter for the measurement of Pigmy Dipole Resonance", 4th Joint Meeting of the APS Division of Nuclear Physics and the Physical Society of Japan, Waikokoa, Hawaii, USA, Oct. 7-11 (2014).

J. Tsubota.: "Simulation of two neutron detection for invariant mass spectroscopy of unstable nuclei", 4th Joint Meeting of the APS Division of Nuclear Physics and the Physical Society of Japan, Waikokoa, Hawaii, USA, Oct. 7-11 (2014).

Y. Kubota.: "Probing multi-neutron correlation via knockout reaction", Critical Stability in Few-Body Systems, Saitama, Japan, January 26–30, 2015.

T. Nakamura: "Nuclear Matter in Neutron Stars by Experimental and Astronomical Observations" Hadrons and Hadron Interactions in QCD 2015 (symposium), YITP, Kyoto University, 2–6, March (2015).

(Domestic Conference)

栂野泰宏, "中性子過剰核の電気双極子応答を用いた対称エネルギーの研究", 実験と観測で解き明かす中性子星の核物質 第 3 回研究会, 静岡県熱川ハイツ, 2015 年 8 月.

栂野泰宏, "中性子過剰核の電気双極子応答と核物質の状態方程式", 宇宙核物理実験の現状と将来, 大阪大学 RCNP, 2014 年 8 月.

近藤洋介: "中性子ドリップライン近傍核における 2 中性子相関", RCNP 研究会 "QCD を基礎とする核子多体系物理の理解", (大阪大学 RCNP), 大阪 12 月 (2014)

小山俊平, 大津秀暁, 清水陽平, 米田健一郎, 佐藤広海, 本林透, 西村美月, 銭廣十三, 櫻井博儀, 武内 聡, 磯部忠昭, 馬場秀忠, 日下健祐, 大西純一, 笹野匡紀, Doornenbal P., 福田直樹, 小林俊雄, 炭竈聡之, 松田洋平, 佐藤義輝, Hwang J., 近藤洋介, 中村隆司, 栂野泰宏, 南方亮吾, 生越駿, 村上哲也, 中塚徳継, Gibelin J., Sylvain L., 新倉潤, 小林信之, Liu H., Lee J., Nikolskii E., 坂口聡志, Beaumel D.:
"^{16}C クラスター準位探索実験", 日本物理学会 70 年次大会, (早稲田大学), 東京, 3 月 (2015).

宮崎卓也, 大津秀暁, Nikolskii E.Y., 志賀慶明, 西村美月, 武内 聡, 佐藤義輝, 黒川明子, 馬場秀忠, Lorusso G., 磯部忠昭, 新倉 潤, Kuzmin E.A., Korsheninnikov A.A., Ogloblin A.A., Krupko S.A., Golovkov M.S., Bezbakh A.A, Slepnev R.S., Fomichev A.S., Sidorchuk S.I., Gorshkov A.V., Knyazev A.G., Papka P., JinØ.H., Kim S. Hwang J., Choi S., Chae H., Kim E., Kim Y., Lubos D., Beaumel D., Soederstroem P.A., 坂口 聡志, 久保野茂, Perrevoort A.K., Milman E., Chebotaryov S., Powell W., 本林透, 米田健一郎, 櫻井博儀.:
"欠損質量核分光による陽子ドリップライン炭素原子核の構造研究", 日本物理学会第 70 回年次大会, (早稲田大学), 東京, 3 月 (2015).

V. Panin and K. Yoneda for the HI-p collaboration.: "Investigation of key nuclear reactions in the astrophysical rp-process using SAMURAI", 日本物理学会第 70 回年次大会, (早稲田大学), 東京, 3 月 (2015).

Stuhl L., Krasznahorkay A., Csatlós A., Algora A., Gulyás J., Kalinka G., Timár J., Kalantar-Nayestanaki N., Rigollet C., Bagchi S., Najafi M.A., Sasano M., Yasuda

J.: “Neutron spectrometer for studying giant resonances with (p,n) reactions in inverse kinematics”, 日本物理学会第 70 会年次大会, (早稲田大学), 東京, 3 月 (2015).

久保田悠樹, Corsi A., 笹野匡紀, 上坂友洋, Obertelli A., Santamaria C., Pollacco E. C., 銭廣十三, 堂園昌伯, 大田晋輔, 時枝紘史, 川瀬頌一郎, Tang T. L., 高木基伸, 木佐森慶一, 李清秀, 矢向謙太郎, 小林幹, 小林俊雄, 長谷川邦彦, 中村隆司, 近藤洋介, 栂野泰宏, 四方瑞紀, 坪田潤一, 齊藤敦美, 米田健一郎, 佐藤広海, 大津秀暁, 清水陽平, 本林透, Doornenbal P., 馬場秀忠, 磯部忠昭, 松下昌史, 安田淳平, 坂口聡, 小林信之, Lapoux V., Gillibert A., 酒向正己, 進藤佑輔, 田端心海, 大倉綾華, Stuhl L., Korkulu Z., 清川裕, Flavigny F., Gibelin J., Orr N. A., Marques F. M., Yang Z., 金谷佳尚, 川上駿介.: “ボロミアン核 (p,pn) 反応を用いた二中性子運動量相関の研究”, 日本物理学会第 70 会年次大会, (早稲田大学), 東京, 3 月 (2015).

四方瑞紀，中村隆司，栂野泰宏，近藤洋介.: “ガンマ線カロリメータ CATANA のシミュレーション”, 日本物理学会第 70 回年次大会, (早稲田大学), 東京, 3 月 (2015).

齊藤敦美，近藤洋介，中村隆司，Nadia Lynda Achouri, Thomas Aumann，馬場秀忠，Franck Delaunay，Pieter Doornenbal，福田直樹，Julien Gibelin，Jongwon Huang，稲辺尚人，磯部忠昭，亀田大輔，簡野大輝，Sunji Kim，小林信之，小林俊雄，久保敏幸，Sylvain Leblond，Jenny Lee，Miguel Marques，南方亮吾，本林透，村井大地，村上哲也，武藤琴美，中嶋丈嘉，中塚徳継，Alahari Navin，西征爾郎，生越駿，Nigel AndrewOrr，大津秀暁，佐藤広海，佐藤義輝，清水陽平，鈴木宏，高橋賢人，竹田浩之，武内聡，田中隆己，栂野泰宏 I，Adam Garry Tuff，Marine Vandebrouck，米田健一郎.: “中性子過剰 ^{19}B の相互作用断面積”, 日本物理学会第 70 回年次大会, (早稲田大学), 東京, 3 月 (2015).

栂野泰宏，南方亮吾，生越駿，中村隆司，磯部忠昭，稲辺尚人，大津秀暁，亀田大輔，簡野大輝，久保敏幸，小林俊雄，小林信之，近藤洋介，佐藤広海，佐藤義輝，清水陽平，鈴木宏，高橋賢人，武内聡，竹田浩之，田中隆己，中嶋丈嘉，中塚徳継，西征爾郎，福田直樹，馬場秀忠，武藤琴美，村井大地，村上哲也，本林透，米田健一郎，N. L. Achouri，A. G. Tuff，T. Aumann，F. Delaunay，J. Gibelin，J. Hwang，S. Kim，J. Lee，M. Marques，A.Navin，N. A. Orr，P. Doornenbal，S. Leblond，M. Vandebrouck.: “$^{19,20,22}C$ の反応断面積”, 日本物理学会第 70 回年次大会, (早稲田大学), 東京, 3 月 (2015).

尾崎友志，中村隆司，栂野泰宏，馬場秀忠，中塚徳継，Oliver Wieland，Thomas Aumann，他 RIBF 51/56/61 collaboration, “ピグミー共鳴測定用 $LaBr_3$ 検出器のエネルギー較正”, 日本物理学会第 70 回年次大会, (早稲田大学), 東京, 3 月 (2015).

栂野 泰宏:, “Symmetry energy and electric dipole response of neutron-rich nuclei”, 新学術領域研究会「中性子星核物質」 2015 年 3 月, 京都大学.

近藤洋介.: “Island of Inversion の南側”, 九大研究会 –中性子過剰領域における弱束縛系の物理– , (九州大学箱崎キャンパス), 福岡 3 月 (2015).

Computing and network Team

Publications

[**Journal**]

（Original Papers） *Subject to Peer Review

Baba H., Ichihara T., Ohnishi T., Takeuchi S., Yoshida K., Watanabe Y., Ota S., Shimoura S., Yoshinaga K.: "Time-stamping system for nuclear physics experiments at RIKEN RIBF", Nucl. Instr. Meth. A **777**, 75–79 (2015). *

Oral Presentations

(International Conference etc.)

Baba H., Ichihara T., Isobe T., Houarner C., Maugeais C., Raine B., Saillant F., Wittwer G., Kurz N., Schaffner H., Gernhäuser R., Anvar S., Calvet D., Château F., Pollacco E.: "DAQ Coupling in RIKEN RIBF", 19th REAL TIME CONFERENCE (RT2014) , (RCNP, RIKEN, KEK), Nara, Japan, May (2014).

Baba H.: "Development of FPGA-based NIM logic circuits", 4th Joint Meeting of the APS Division of Nuclear Physics and the Physical Society of Japan , Waikoloa, Hawaii, October (2014).

(Domestic Conference)

馬場秀忠, 市原卓, 大西哲哉, 武内聡, 渡邊康, 吉田光一, 大田晋介, 下浦享: "モジュールマウント型 VME コントローラの開発", 日本物理学会, (日本物理学会), 平塚, 3 月 (2014).

Detector Team

Publications

[**Journal**]

（Original Papers） *Subject to Peer Review

Sato Y., Shimaoka T., Kaneko J.H., Murakami H., Isobe M., Osakabe M., Tsubota M., Ochiai K., Chayahara A., Umezawa H., Shikata S.: "Radiation hardness of a single crystal CVD diamond detector for MeV energy protons", Nucl. Instr. and Meth. A **784**, 147-150 (2014). ∗

Sato Y., Murakami H., Shimaoka T., Tsubota M., Kaneko J.H.: "Single-crystal CVD diamond detector for high resolution particle spectrometry", Euro. Phys. Let. **108**, 42001 (2014). ∗

Sato Y., Shimaoka T., Kaneko J.H., Murakami H., Miyazaki D., Tsubota M., Chayahara A., Umezawa H., Shikata S.: "Pulse shape distortion of output signals from single-crystal CVD diamond detector in few-GHz broadband amplifiers", Euro. Phys. Let. **106**, 22001 (2014). ∗

Oral Presentations

(International Conference etc.)

Sato Y., Fukuda N., Takeda H., Kameda D., Suzuki H., Shimizu Y., Ahn D.S., Murai D., Inabe N., Shimaoka T., Tsubota M., Kaneko J.H., Chayahara A., Umezawa H., Shikata S., Kumagai H., Murakami H., Yoshida K., Kubo T.: "Status of Beam Line Detectors for the BigRIPS Fragment Separator at RIKEN RI Beam Factory: Issues on High Rates and Resolution", The 2nd Conference on "Advances in Radioactive Isotope Science 2014" (ARIS 2014), (RIKEN, U. Tokyo), Bunkyo, Japan, June (2014).

Sato Y., Shimaoka T., Kaneko J.H., Murakami H., Isobe M., Nagakabe M., Tsubota M., Ochiai K., Chayahara A., Umezawa H., Shikata S.: "Radiation hardness of single crystal CVD diamond detector for MeV energy protons", SORMA XV - 2014 Symposium on Radiation Measurements and Applications, (U. Michigan), Michigan, USA, June (2014).

Shimaoka T., Kaneko J.H., Arikawa Y., Isobe M., Sato Y., Tsubota M., Nagai T., Kojima S., Abe Y., Sakata T., Fujioka S., Nakai M., Shirakami H., Azechi H., Chayahara A., Umezawa H., Shikata S.: "Response measurement of single crystal CVD diamond radiation detector for intense X-rays aiming at burn-history measurement on an inertial confinement fusion with fast ignition", SORMA XV - 2014 Symposium on Radiation Measurements and Applications, (U. Michigan), Michigan, USA, June (2014).

Shimizu Y., Kubo T., Fukuda N., Ahn D.S., Inabe N., Kameda D., Sato H., Suzuki H., Takeda H., Yoshida K.: "Identification of 25 new neutron-rich isotopes produced in the EURICA uranium beam campaign at RIKEN RIBF", 4th Joint Meeting of the APS Division of Nuclear Physics and the Physical Society of Japan, (APS, PSJ), Hawai, USA, October (2014).

Suzuki H., Kubo T., Fukuda N., Inabe N., Kameda D., Takeda H., Sato H., Shimizu Y., Ahn D.S., Ohkoda Y., Iwasa N., Murai D.: "Production cross section of neutron-deficient radioactive isotopes produced from a ^{124}Xe beam at 345 MeV/u by the BigRIPS separator at RIKEN RI Beam Factory", 4th Joint Meeting of the APS Division of Nuclear Physics and the Physical Society of Japan, (APS, PSJ), Hawai, USA, October (2014).

(Domestic Conference)

木佐森慶一, 下浦享, 李清秀, 井手口栄治, 稲辺尚人, 伊藤正俊, 上坂友洋, 大田晋輔, 亀田大輔, 川畑貴裕, 川瀬頌一郎, 菊地陽介, 久保敏幸, 久保田悠樹, 郷慎太郎, 小林幹, 近藤洋介, 坂口聡志, 酒井英行, 笹本良子, 笹野匡紀, 佐藤広海, 清水陽平, 鈴木宏, 高木基伸, 民井淳, 竹田浩之, 武内聡, 津村美保, 時枝紘史, 西隆博, 西村美月, 野地俊平, 馬場秀忠, 馬場辰彦, 堂園昌伯, 福田直樹, 藤井俊彦, 前田幸重, 松原礼明, 三木謙二郎, 道正新一郎, 宮裕之, 柳沢善行, 矢向謙太郎, 横山輪, 吉田光一, M. Assie, D. Beaumel, F. Hammache, A. Stolz: "発熱型二重荷電交換反応 ^{4}He(^{8}He,^{8}Be)4n による 4 中性子系の研究", 日本物理学会第 70 回年次大会, (早稲田大学), 東京, 3 月 (2015).

小山俊平, 大津秀暁, 清水陽平, 米田健一郎, 佐藤広海, 本林透, 西村美月, 銭廣十三, 櫻井博儀, 武内聡, 磯部忠昭, 馬場秀忠, 日下健祐, 大西純一, 笹野匡紀, P. Doornenbal, 福田直樹, 小林俊雄, 炭竈聡之, 松田洋平, 佐藤義輝, J. Hwang, 近藤洋介, 中村隆司, 栂野泰宏, 南方亮吾, 生越駿, 村上哲也, 中塚徳継, J. Gibelin, L. Sylvain, 新倉潤, 小林信之, H. Liu, J. Lee, E. Nikolskii, 坂口聡志, D. Beaumel: "^{16}C クラスター準位探索実験", 日本物理学会第 70 回年次大会, (早稲田大学), 東京, 3 月 (2015).

久保田悠樹, Anna Corsi, 笹野匡紀, 上坂友洋, Alexandre Obertelli, Clementine Santamaria, Emanuel Pollacco, 銭廣十三, 堂園昌伯, 大田晋輔, 時枝紘史, 川瀬頌一郎, Tang Tsz Leung, 高木基伸, 木佐森慶一, 李清秀, 矢向謙太郎, 小林幹, 小林俊雄, 長谷川邦彦, 中村隆司, 近藤洋介, 栂野泰宏, 四方瑞紀, 坪田潤一, 齊藤敦美, 米田健一郎, 佐藤広海, 大津秀暁, 清水陽平, 本林透, Pieter Doornenbal, 馬場秀忠, 磯部忠昭, 松下昌史, 安田淳平, 坂口聡, 小林信之, Valerie Lapoux, Alain Gillibert, 酒向正己, 進藤佑輔, 田端心海, 大倉綾華, Laszlo Stuhl, Zeren Korkulu, 清川裕, Freddy Flavigny, Julien Gibelin, Nigel Orr, Marques Miguel, Zaihong Yang, 金谷佳尚, 川上駿介: "ボロミアン核 (p,pn) 反応を用いた二中性子運動量相関の研究", 日本物理学会第 70 回年次大会, (早稲田大学), 東京, 3 月 (2015).

齊藤敦美, 近藤洋介, 中村隆司, Nadia Lynda Achouri, Thomas Aumann, 馬場秀忠, Franck Delaunay, Pieter Doornenbal, 福田直樹, Julien Gibelin, Jongwon Huang, 稲辺尚人, 磯部忠昭, 亀田大輔, 簡野大輝, Sunji Kim, 小林信之, 小林俊雄, 久保敏幸, Sylvain Leblond, Jenny Lee, Miguel Marques,

南方亮吾, 本林透, 村井大地, 村上哲也, 武藤琴美, 中嶋丈嘉, 中塚徳継, Alahari Navin, 西征爾郎, 生越駿, Nigel Andrew Orr, 大津秀暁, 佐藤広海, 佐藤義輝, 清水陽平, 鈴木宏, 高橋賢人, 竹田浩之, 武内聡, 田中隆己, 栂野泰宏, Adam Garry Tuff Marine Vandebrouck, 米田健一郎: "中性子過剰 ^{19}B の相互作用断面積", 日本物理学会第 70 回年次大会, (早稲田大学), 東京, 3 月 (2015).

栂野泰宏, 南方亮吾, 生越駿, 中村隆司, 磯部忠昭, 稲辺尚人, 大津秀暁, 亀田大輔, 簡野大輝, 久保敏幸, 小林俊雄, 小林信之, 近藤洋介, 佐藤広海, 佐藤義輝, 清水陽平, 鈴木宏, 高橋賢人, 武内聡, 竹田浩之, 田中隆己, 中嶋丈嘉, 中塚徳継, 西征爾郎, 福田直樹, 馬場秀忠, 武藤琴美, 村井大地, 村上哲也, 本林透, 米田健一郎, N. L. Achouri, A. G. Tuff, T. Aumann, F. Delaunay, J. Gibelin, J. Hwangy, S. Kim, J. Lee, M. Marques, A.Navin, N. A. Orr, P. Doornenbal, S. Leblond, M. Vandebrouck: "^{19,20,22}C の反応断面積", 日本物理学会第 70 回年次大会, (早稲田大学), 東京, 3 月 (2015).

Ion Beam Breeding Team

Publications

[Journal]

(Original Papers) *Subject to Peer Review

Inthima P., Otani M., Hirano T., Hayashi Y., Abe T., Nakano M., and Supaibulwatana K.: "Mutagenic effects of heavy-ion beam irradiation on in vitro nodal segments of *Artemisia annua* L.", Plant Cell Tiss. Organ Cult. **119**, 131-139 (2014). *

Nakano M., Yamada T., Masuda Y., Sato Y., Kobayashi H., Ueda H., Morita R., Nishimura M., Kitamura K., and Kusaba M.: "A Green-Cotyledon/Stay-Green Mutant Exemplifies the Ancient Whole-Genome Duplications in Soybean", Plant Cell Physiol. **55**(10), 1763-1771 (2014). *

Nishiura A., Kazama Y., Abe T., Mizuno N., Nasuda S., and Murai K.: "Level of *VERNALIZATION 1* expression is correlated with earliness in extra *early-flowering* mutant wheat lines", Breed Sci. **64**(3), 213-221 (2014). *

Maeda S., Gunji S., Hanai K., Hirano T., Kazama Y., Ohbayashi I., Abe T., Sawa S., Tsukaya S., and A. Ferjani.: "The Conflict between cell proliferation and expansion primarily affects stem organogenesis in Arabidopsis", Plant Cell Physiol. **55**, 1994-2007 (2014). *

Hara T., Kobayashi E., Ohtsubo K., Kumada S., Kanazawa M., Abe T., Itoh R. D., and Fujiwara M. T.: "Organ-level analysis of idioblast patterning in *Egeria densa* Planch. leaves", PLoS ONE **10**, e0118965 (2015).*

Hirano T., Kazama Y., Ishii K., Ohbu S., Shirakawa Y., and Abe T.: "Comprehensive identification of mutations induced by heavy-ion beam irradiation in *Arabidopsis thaliana*", Plant J. **82**, 93-104 (2015). *

(Review)

阿部知子, 風間裕介, 西美友紀, 永吉実孝: "九州ブランドを世界に！―突然変異育種の挑戦―", 育種学研究 **16**, 67-71 (2014).

阿部知子, 福西暢尚: "重イオンビーム照射による農作物の品種改良", 電気評論 **99**, 51-55 (2014).

松田尚大, 竹下毅, 大田修平, 山﨑誠和, 風間裕介, 阿部知子, 平田愛子, 河野重行: "微細藻類への重イオンビーム照射によるバイオ燃料増産株の作出", 生物工学会誌 **92**, 602-606 (2014).

平野智也: "重イオンビームを利用した花弁園芸植物の育種", 花葉 **33**(通巻第 34 号), 2-5 (2014).

[Book・Proceedings]

(Book)

池田時浩: "ガラスキャピラリーオプティクスによる収束と偏向", マイクロビームアナリシス・ハンドブック, 第Ⅰ編 基礎編 第 1 章 分析機器の主要構成 1.2.1 (5) P.71-73 オーム社 (2014).

Shibata F., Kazama Y., Kawano S., Hizume M.: "Chromosome painting and FISH of distal end satellite DNAs in dioecious plants with sex chromosomes" In: Atlas of Plant Cell Structure. Noguchi T., Kawano S., Tsukaya H., Matsunaga S., Sakai A., Karahara I., Hayashi Y. (Eds.), pp14-15, Springer, Berlin/Heidelberg, Germany. (2015).

Oral Presentations

(International Conference etc.)

Ikeda T.: "Cell irradiation with microbeams of MeV heavy ions using glass capillaries", Workshop on Applications of Highly Charged Ions (HCI App), East Lansing, MI, USA, May (2014).

Abe T., Hayashi Y., Endo T., Saeki K., Sato H., Sakai M., and Sato T.: "DEVELOPMENT OF SALT-RESISTANT RICE IN MIYAGI PREFECTURE", 4th International Rice Congress (IRC2014), Bangkok, Thailand, Oct. (2014).

Ishii K., Hirano T., Kazama Y., Hamada M., Ono Y., and Abe T.: "Pipeline for whole-genome analysis of heavy-ion-induced mutants", International Symposium on Genome Science 2015 Expanding Frontiers of Genome Science II, Tokyo, Japan, Jan. (2015).

(Domestic Conference)

常泉和秀, 阿部知子: "重イオンビーム照射によるキイロショウジョウバエ変異系統の樹立系構築", 日本農芸化学会 2014 年度大会, 川崎, 3 月 (2014).

平野智也: "重イオンビーム誘発変異の全ゲノム解析", 植物生存システム 春期研究成果発表会, 千葉, 4 月 (2014).

風間裕介: "ヒロハノマンテマ雄性決定領域の重イオン欠失マッピング", 植物生存システム 春期研究成果発表会, 千葉, 4 月 (2014).

池田時浩: "ガラスキャピラリーによる細胞内組織 3 次元選択的破壊のためのマイクロイオンビーム照射", 植物生存システム 臨時セミナー, 千葉, 5 月 (2014).

石井公太郎: "巡回セールスマン問題に帰着したヒロハノマンテマ組換え抑制領域のマッピング", 植物生存システム 臨時セミナー, 千葉, 5 月 (2014).

阿部知子: "イオンビームはすごいのだ！～いろんな植物で実証されるイオンビームの威力～", 福井県立大学 コムギイオンビーム変異体観察会, 福井, 6 月 (2014).

宇都木萌, 池田時浩, 泉雅子, 平野智也, 小林知洋, 阿部知子, 酒井康弘: "ガラスキャピラリーを使ったマイクロビーム細胞照射法の開発、出射ビーム特性", 第 15 回放射線プロセスシンポジウム, 東京, 6 月 (2014).

阿部知子, 風間裕介, 平野智也: "イオンビーム育種の最近の展開", 第 15 回放射線プロセスシンポジウム, 東京, 6 月 (2014).

池田時浩, 小林知洋, Mäckel V., 泉雅子, 荻原清, 浜垣学, 平野智也, 小島隆夫, Puttaraksa N., 宇都木萌, 酒井康弘, 山崎泰規, 阿部知子: "ガラスキャピラリーを使ったマイクロビーム細胞照射法", 第 15 回放射線プロセスシンポジウム, 東京, 6 月 (2014).

泉雅子: "放射線による DNA 損傷修復機構と細胞応答", 第 51 回アイソトープ・放射線研究発表会, 東京, 7 月 (2014).

阿部知子: "イオンビーム育種研究会 10 年の歩み ―理化学研究所仁科加速器研究センターRI ビームファクトリー（RIBF）―", 第 10 回イオンビーム育種研究会, 水戸, 7 月 (2014).

竹下毅, 太田修平, 山崎誠和, 大島健志朗, 服部正平, 風間裕介, 阿部知子, 河野重行: "重イオンビーム照射によるクロレラの突然変異誘導率と屋外大量培養株の作出", 第 10

回イオンビーム育種研究会, 水戸, 7 月 (2014).
風間裕介, 石井公太郎, 池田時浩, 川元寛章, 河野重行, 阿部知子: “巡回セールスマン問題を応用した重イオンビーム欠失マッピング”, 第 10 回イオンビーム育種研究会, 水戸, 7 月 (2014).
阿部知子: “巨大加速器で発生する重イオンビームで黄色のサクラ、咲きました。”, 第 32 回日本植物細胞分子生物学会(盛岡)大会・シンポジウム, 盛岡, 8 月 (2014).
風間裕介, 平野智也, 阿部知子: “重イオンビーム育種の開発と品種改良ユーザー会”, 平成 26 年度 非破壊検査に関する研究発表会, 大阪, 8 月 (2014).
Ali F., 前田沙織理, 郡司玄, 花井研哉, 平野智也, 風間裕介, 大林祝, 阿部知子, 塚谷裕一: “細胞増殖と細胞伸長の異常が茎の形態形成に及ぼす影響”, 日本植物形態学会第 26 回総会・大会, 川崎, 9 月 (2014).
川元寛章, 石井公太郎, 風間裕介, 阿部知子, 河野重行: “ヒロハノマンテマへの黒穂菌を感染によって生じる葯に Y 染色体の関与はあるか”, 日本植物形態学会第 26 回総会・大会, 川崎, 9 月 (2014).
風間裕介, 石井公太郎, 池田時浩, 川元寛章, 河野重行, 阿部知子: “巡回セールスマン問題を応用したヒロハノマンテマ雄性決定領域の欠失マッピング”, 日本植物学会第 78 回大会, 川崎, 9 月 (2014).
石井公太郎, 風間裕介, 川元寛章, 河野重行, 阿部知子: “Y 染色体遺伝子アレイを用いたヒロハノマンテマ性分化ステージの発現プロファイリング”, 日本植物学会第 78 回大会, 川崎, 9 月 (2014).
川元寛章, 石井公太郎, 風間裕介, 阿部知子, 河野重行: “雌蕊も雄蕊もないヒロハノマンテマの無性花変異体に黒穂菌を感染させると起きる変化”, 日本植物学会第 78 回大会, 川崎, 9 月 (2014).
仁田坂英二, 星野敦, 阿部知子, 中野完: “宇宙種子実験によって得られたアサガオの変異体”, 日本宇宙生物科学会第 28 回大会, 堺, 9 月 (2014).
二羽恭介, 阿部知子, 小檜山篤志: “養殖ノリにおける倍数性育種の可能性 ―スサビノリと隠蔽種の種間交雑実験―”, 平成 26 年日本水産学会秋季大会, 福岡, 9 月 (2014).
風間裕介, 平野智也, 石井公太郎, 森田竜平, 村井耕二, 阿部知子: “Mutagenesis から Mutagenomics へ : 重イオンビームを用いたオンデマンド変異誘発”, 第七回 TRS 研究会, 宮崎, 9 月 (2014).
風間裕介, 石井公太郎, 池田時浩, 川元寛章, 河野重行, 阿部知子: “巨大 Y 染色体との格闘～ヒロハノマンテマの性決定遺伝子の探索～”, 日本育種学会第 126 回講演会, 宮崎, 9 月 (2014).
高原学, 蝦名真澄, 森田竜平, 風間裕介, 阿部知子, 高溝正, 中川仁: “イオンビーム変異体によるアポミクシス遺伝子座乗領域の絞り込み”, 日本育種学会第 126 回講演会, 宮崎, 9 月 (2014).
西浦愛子, 風間裕介, 阿部知子, 水野信之, 那須田周平, 村井耕二: “時計関連遺伝子 *Wheat PHYTOCLOCK 1* の欠失コムギ変異体は短日応答が消失して極早生となる”, 日本育種学会第 126 回講演会, 宮崎, 9 月 (2014).
阿部知子: “突然変異誘発研究は形態変異体の選抜からはじまる”, 第 19 回バイオテンプレート研究懇談会, 東京, 10 月 (2014).
金澤美加子, 小林永実, 原拓也, 大坪昴平, 熊田翔吾, 阿部知子, 伊藤竜一, 藤原誠: “オオカナダモにおける異型細胞形成パターンの解析”, 日本農芸化学会関東支部 2014 年度支部大会, 埼玉, 10 月, (2014).
森田竜平, 石井公太郎, 林依子, 佐藤雅志, 阿部知子: “イネ Exome 解析による重イオンビーム誘発突然変異遺伝子の迅速決定”, 第 12 回先端農学研究センター・サテライトセミナー, 仙台, 10 月 (2014).
佐藤陽一, 平野智也, 鈴木健, 伊藤泰, 阿部知子, 河野重行: “全国 6 産地の養殖ワカメの形態と生理学的特性の比較”, 平成 26 年度日本水産学会東北支部大会, 秋田, 11 月 (2014).
泉雅子, 水野武, 今本尚子, 阿部知子, 花岡文雄: “ヒト Mcm10 と Mcm2-7 複合体の相互作用の解析”, 第 37 回分子生物学会年会, 横浜, 11 月 (2014).
阿部知子: “放射線を用いた品種改良から変異遺伝子同定へ”, 東北エネルギー懇談会　第 59 回技術委員会, 仙台, 3 月 (2015).
村井耕二, 西浦愛子, 水野信之, 那須田周平, 風間裕介, 阿部知子: “コムギにおける生物時計機能は短日応答性に必須である”, 第 56 回日本植物生理学会年会, 東京, 3 月 (2015).
竹下毅, 山下雄一, 大田修平, 山﨑誠和, 大島健志朗, 服部正平, 風間裕介, 阿部知子, 河野重行: “クロレラの重イオンビーム照射による突然変異誘導と屋外大量培養株の作出”, 第 39 回日本藻類学会, 福岡, 3 月 (2015).
佐藤陽一, 平野智也, 二羽恭介, 村上素子, 鈴木健, 伊藤泰, 阿部知子, 河野重行: “全国 6 産地の養殖ワカメの形態と栄養塩吸収特性の比較”, 第 39 回日本藻類学会, 福岡, 3 月 (2015).
石井公太郎, 平野智也, 風間裕介, 浜田道昭, 小野幸輝, 阿部知子: “全ゲノム変異解析のためのパイプラインの構築”, 日本育種学会第 127 回講演会, 町田, 3 月 (2015).
道坂怜生, 増岡千裕, 津山睦, 阿部知子, 田中朋之: “イネ突然変異系統 13-45 における白未熟粒発生機構の解析 第 2 報 : 原因候補遺伝子の同定と発現量の比較”, 日本作物学会第 239 回講演会, 藤沢, 3 月 (2015).
小玉雅晴, 田邊雄太, 平野智也, 阿部知子: “重イオンビーム照射によるアジサイの花色変異体の作出”, 園芸学会 平成 27 年度春季大会, 千葉, 3 月 (2015).
加藤雅博, 正村典也, 正野仁慈, 岡本大作, 阿部知子, 今井真介: “涙の出ない, 辛みのないタマネギの作出と特性解析”, 園芸学会 平成 27 年度春季大会, 千葉, 3 月 (2015).
小林永実, 金澤美加子, 平野智也, 阿部知子, 伊藤竜一, 藤原誠: “オオカナダモ葉緑体欠失細胞における細胞生物学的解析”, 日本農芸化学会 2015 年度大会, 岡山, 3 月, (2015).
石川浩樹, 佐々木駿, 鈴木麻央, 平野智也, 風間裕介, 阿部知子, 伊藤竜一, 藤原誠: “シロイヌナズナ花粉発生過程における色素体増殖の解析”, 日本農芸化学会 2015 年度大会, 岡山, 3 月, (2015).
佐々木駿, 石川浩樹, 加賀谷奨, 風間裕介, 阿部知子, 伊藤竜一, 藤原誠: “シロイヌナズナ葉緑体分裂異常変異体における花粉色素体の解析”, 日本農芸化学会 2015 年度大会, 岡山, 3 月, (2015).

RI Applications Team

Publications

[Journal]

(Original Papers) *Subject to Peer Review

Haba H., Huang M., Kaji D., Kanaya J., Kudou Y., Morimoto K., Morita K., Murakami M., Ozeki K., Sakai R., Sumita T., Wakabayashi Y., Yoneda A., Kasamatsu Y., Kikutani Y., Komori Y., Nakamura K., Shinohara A. Kikunaga H., Kudo H., Nishio K., Toyoshima A., and Tsukada K., "Production of ^{262}Db in the ^{248}Cm(^{19}F,5*n*)^{262}Db Reaction and Decay Properties of ^{262}Db and ^{258}Lr", Phys. Rev. C **89**, 024618 (2014).*

Sato N., Sato T. K., Asai M., Toyoshima A., Tsukada K., Li Z. J., Nishio K., Nagame Y., Schädel M., Haba H., Ichikawa S., and Kikunaga H., "Production of ^{256}Lr in the ^{249,250,251}Cf + ^{11}B, ^{243}Am + ^{18}O, and ^{248}Cm + ^{14}N Reactions", Radiochim. Acta **102**, 211 (2014).*

Murakami M., Haba H., Goto S., Kanaya J., and Kudo H., "Production Cross Sections of Niobium and Tantalum Isotopes in Proton-Induced Reactions on ^{nat}Zr and ^{nat}Hf up to14 MeV", Appl. Radiat. Isot. **90**, 149 (2014).*

Khandaker M. U., Haba H., Otuka N., and Usman A. R., "Investigation of (*d*,*x*) Nuclear Reactions on Natural Ytterbium up to 24 MeV", Nucl. Instr. and Meth. B **335**, 8 (2014).*

Kasamatsu Y., Toyomura K., Shiohara N., Yokokita T., Komori Y., Kino A., Yoshimura T., Takahashi N., Haba H., Kudou Y., Kikunaga H., Mitsugashira T., Ohtsuki T., Takamiya K., and Shinohara A., "Coprecipitation Behaviors of Zr, Hf, and Th with Sm Hydroxide for Chemical Study of Element 104, Rf", J. Nucl. Radiochem. Sci. **14**, 7 (2014).*

Khandaker M. U., Haba H., Murakami M., Otuka N., and Kassim H. A., "Deuteron-Induced Activation Cross-Sections on Natural Copper up to 24 MeV", J. Radioanal. Nucl. Chem. **302**, 759 (2014).*

Even J., Yakushev A., Düllmann Ch. E., Haba H., Asai M., Sato T. K., Brand H., Di Nitto A., Eichler R., Fan F.L., Hartmann W., Huang M., Jäger E., Kaji D., Kanaya J., Kaneya Y., Khuyagbaatar J., Kindler B., Kratz J. V., Krier J., Kudou Y., Kurz N., Lommel B., Miyashita S., Morimoto K., Morita K., Murakami M., Nagame Y., Nitsche H., Ooe K., Qin Z., Schädel M., Steiner J., Sumita T., Takeyama M., Tanaka K., Toyoshima A., Tsukada K., Türler A., Usoltsev I., Wakabayashi Y., Wang Y., Wiehl N., and Yamaki S., "Synthesis and Detection of a Seaborgium Carbonyl Complex", Science **345**, 1491 (2014).*

Kawano M., Takeuchi A., Takahashi K., Imazu S., and Minami T., "Determination of Sources of Vermillion Used in Japanese Burial Mound of Yayoi and Kofun Periods", ISIJ International, **54**, 1155 (2014).*

Urabe T., Takahashi K., Kitagawa M., Sato T., Kondo T., Enomoto S., Kidera M., and Seto Y., "Development of Portable Mass Spectrometer with Electron Cyclotron Resonance Ion Source for Detection of Chemical Warfare Agents in Air", Spectrochim. Acta A: Molec. Biomolec. Spectr., **120**, 437 (2014).*

Toyoshima A., Miyashita S., Ooe K., Lerum H. V., Kitayama Y., Wada A., Asai M., Sato T. K., Kaneya Y., Komori Y., Yokokita T., Kasamatsu Y., Tsukada K., Kitatsuji Y., Nagame Y., Schädel M., Omtvedt J. P., Yokoyama A., Haba H., Shinohara A., and Kratz J. V., "Preparatory On-Line Extraction Experiment of Group-6 Elements Mo and W for a Reduction Study of Sg", JAEA-Review **2013-057**, 33 (2014).

Toyoshima A., Ooe K., Miyashita S., Asai M., Attallah M. F., Goto N., Gupta N. S., Haba H., Huang M., Kanaya J., Kaneya Y., Kasamatsu Y., Kitatsuji Y., Kitayama Y., Koga K., Komori Y., Koyama T., Kratz J. V., Lerum H. V., Oshimi Y., Pershina V., Sato D., Sato T. K., Shigekawa Y., Shinohara A., Tanaka A., Tsukada K., Tsuto S., Yokokita T., Yokoyama A., Omtvedt J. P., Nagame Y., and Schädel M., "Chemical Studies of Mo and W in Preparation of a Seaborgium (Sg) Reduction Experiment Using MDG, FEC, and SISAK", J. Radioanal. Nucl. Chem. **303**, 1169 (2015).*

Ooe K., Attallah M. F., Asai M., Goto N., Gupta N. S., Haba H., Huang M., Kanaya J., Kaneya Y., Kasamatsu Y., Kitatsuji Y., Kitayama Y., Koga K., Komori Y., Koyama T., Kratz J. V., Lerum H. V., Miyashita S., Oshimi Y., Pershina V., Sato D., Sato T. K., Shigekawa Y., Shinohara A., Tanaka A., Toyoshima A., Tsukada K., Tsuto S., Yokokita T., Yokoyama A., Omtvedt J. P., Nagame Y., and Schädel M., "Development of a New Continuous Dissolution Apparatus with a Hydrophobic Membrane for Superheavy Element Chemistry", J. Radioanal. Nucl. Chem. **303**, 1317 (2015).*

Komori Y., Yokokita T., Kasamatsu Y., Haba H., Toyoshima A., Toyomura K., Nakamura K., Kanaya J., Huang M., Kudou Y., Takahashi N., and Shinohara A., "Solid-liquid Extraction of Mo and W by Aliquat 336 from HCl Solutions toward Extraction Chromatography Experiments of Sg", J. Radioanal. Nucl. Chem. **303**, 1385 (2015).*

Kaji D., Morimoto K., Haba H., Wakabayashi Y., Kudou Y., Huang M., Goto S., Murakami M., Goto N., Koyama T., Tamura N., Tsuto S., Sumita T., Tanaka K., Takeyama M., Yamaki S., and Morita K., "Startup of a New Gas-Filled Recoil Separator GARIS-II", J. Radioanal. Nucl. Chem. **303**, 1523 (2015).*

Miyake F., Suzuki A., Masuda K., Horiuchi K., Motoyama H., Matsuzaki H., Motizuki Y., Takahashi K., and Nakai Y., "Cosmic Ray Event of A.D. 774–775 Shown in Quasi-Annual ^{10}Be Data from the Antarctic Dome Fuji Ice Core", Geophys. Res. Lett., **42**, 84 (2015).*

Even J., Ackermann D., Asai M., Block M., Brand H., Di Nitto A., Düllmann Ch. E., Eichler R., Fan F., Haba H., Hartmann W., Hübner A., Heßberger F. P., Huang M., Jäger E., Kaji D., Kanaya J., Kaneya Y., Khuyagbaatar J., Kindler B., Kratz J. V., Krier J., Kudou Y., Kurz N., Laatiaoui M., Lommel B., Maurer J., Miyashita S., Morimoto K., Morita K., Murakami M., Nagame Y.,

Nitsche H., Ooe K., Qin Z., Sato T. K., Schädel M., Steiner J., Sumita T., Takeyama M., Tanaka K., Toyoshima A., Tsukada K., Türler A., Usoltsev I., Wakabayashi Y., Wang Y., Wiehl N., Yakushev A., and Yamaki S., "In-Situ Synthesis of Volatile Carbonyl Complexes with Short-Lived Nuclides", J. Radioanal. Nucl. Chem. **303**, 2457 (2015).*

Khandaker M. U., Haba H., Murakami M., and Otuka N., "Production Cross-Sections of Long-Lived Radionuclides in Deuteron-Induced Reactions on Natural Zinc up to 23 MeV", Nucl. Instr. and Meth. B **346**, 8 (2015).*

Huang M., Haba H., Murakami M., Asai M., Kaji D., Kanaya J., Kasamatsu Y., Kikunaga H., Kikutani Y., Komori Y., Kudo H., Kudou Y., Morimoto K., Morita K., Nakamura K., Ozeki K., Sakai R., Shinohara A., Sumita T., Tanaka K., Toyoshima A., Tsukada K., Wakabayashi Y., and Yoneda A., "Production of ^{88}Nb and ^{170}Ta for Chemical Studies of Element 105, Db, Using the GARIS Gas-Jet System", J. Radioanal. Nucl. Chem. (in press).*

Wang Y., Qin Z., Fan F.L., Haba H., Komori Y., Cao S.W., Wu X.-L., and Tan C.-M., "Gas-Phase Chemistry of Technetium Carbonyl Complexes", Phys. Chem. Chem. Phys. (in press).*

(Review)

羽場宏光, "GARIS が拓く新元素の化学", 放射化学 **30**, 7 (2014).*

[Book ・Proceedings]

(Original Papers) *Subject to Peer Review

Kaji D., Morimoto K., Haba H., Wakabayashi Y., Kudou Y., Huang M., Goto S., Murakami M., Goto N., Koyama T., Tamura N., Tsuto S., Sumita T., Tanaka K., Takeyama M., Yamaki S., and Morita K., "Research and Development of a New Gas-Filled Recoil Separator GARIS-II", Proceedings of the 12th Asia Pacific Physics Conference, JPS Conf. Proc. **1**, 013051 (2014).*

Oral Presentations

(International Conference etc.)

Usoltsev I., Eichler R., Di Nitto A., Düllmann C., Fan F.L., Hartmann W., Huang M., Jäger E., Kaji D., Kanaya J., Kaneya Y., Khuyagbaatar J., Türler A., Kindler B., Kratz J., Krier J., Kudou Y., Kurz N., Lommel B., Miyashita S., Morimoto K., Morita K., Murakami M., Wang Y., Nagame Y., Nitsche H., Ooe K., Schädel M., Steiner J., Sumita T., Takeyama M., Tanaka K., Toyoshima A., Tsukada K., Even J., Wakabayashi Y., Wiehl N., Yamaki S., Qin Z., Yakushev A., Haba H., Asai M., Sato T., Brand H., "Decomposition Studies of W and Mo Carbonyl Complexes and Their Implications for Future Experiments with $Sg(CO)_6$", 17th Radiochemical Conference, (Division of Nuclear and Radiochemistry, European Association for Chemical and Molecular Sciences), Marianske Lazne, Czech Republic, May (2014).

Haba H., Kaji D., Kasamatsu Y., Kikunaga H., Komori Y., Kudo H., Morimoto K., Morita K., Murakami M., Nishio K., Ooe K., Shinohara A., Toyoshima A., Tsukada K., and Wakabayashi Y., "Production of ^{261}Rf, ^{262}Db, and ^{265}Sg for Chemical Studies Using GARIS at RIKEN", 17th Radiochemical Conference, (Division of Nuclear and Radiochemistry, European Association for Chemical and Molecular Sciences), Marianske Lazne, Czech Republic, May (2014).

Murakami M., Goto S., Murayama H., Kojima T., Kaji D., Morimoto K., Haba H., Kudou Y., Sumita T., Sakai R., Yoneda A., Morita K., Kasamatsu Y., Kikunaga H., Sato T., and Kudo H., "Excitation Functions for Production of Rutherfordium Isotopes in the ^{248}Cm + ^{18}O Reaction", 17th Radiochemical Conference, (Division of Nuclear and Radiochemistry, European Association for Chemical and Molecular Sciences), Marianske Lazne, Czech Republic, May (2014).

Attallah M. F., Lerum H. V., Toyoshima A., Ooe K., Miyashita S., Asai M., Goto N., Gupta N. S., Haba H., Huang M., Kanaya J., Kaneya Y., Kasamatsu Y., Kitatsuji Y., Kitayama Y., Koga K., Komori Y., Koyama T., Kratz J. V., Oshimi Y., Pershina V., Sato D., Sato T. K., Shigekawa Y., Shinohara A., Tanaka A., Tsukada K., Tsuto S., Yokokita T., Yokoyama A., Nagame Y., Schädel M., and Omtvedt J. P., "Preliminary Investigations towards the Separation of Hexavalent and Tetravalent Seaborgium - Extraction of Homologs", 17th Radiochemical Conference, (Division of Nuclear and Radiochemistry, European Association for Chemical and Molecular Sciences), Marianske Lazne, Czech Republic, May (2014).

Toyoshima A., Asai M., Attallah M. F., Goto N., Gupta N. S., Haba H., Huang M., Kanaya J., Kaneya Y., Kasamatsu Y., Kitatsuji Y., Kitayama Y., Koga K., Komori Y., Koyama T., Kratz J. V., Lerum H. V., Miyashita S., Ooe K., Oshimi Y., Pershina V., Sato D., Sato T. K., Shigekawa Y., Shinohara A., Tanaka A., Tsukada K., Tsuto S., Yokokita T., Yokoyama A., Omtvedt J. P., Nagame Y., and Schändel M., "Electrolytic Reduction Studies of Mo and W towards the Reduction of Seaborgium", 17th Radiochemical Conference, (Division of Nuclear and Radiochemistry, European Association for Chemical and Molecular Sciences), Marianske Lazne, Czech Republic, May (2014).

Murakami M., Haba H., Goto S., and Kudo H., "Production Cross Sections of Nb and Ta Isotopes in the (p,x) and (d,x) Reactions on ^{nat}Zr and ^{nat}Hf", 17th Radiochemical Conference, (Division of Nuclear and Radiochemistry, European Association for Chemical and Molecular Sciences), Marianske Lazne, Czech Republic, May (2014).

Omtvedt J. P., Koga K., Komori Y., Koyama T., Kratz J. V., Lerum H. V., Miyashita S., Ooe K., Oshimi Y., Pershina V., Sato D., Sato T. K., Shigekawa Y., Shinohara A., Tanaka A., Toyoshima A., Tsukada K., Tsuto S., Yokokita T., Yokoyama A., Nagame Y., Schädel M., Asai M., Attallah M. F., Goto N., Gupta N. S., Haba H., Huang M., Kanaya J., Kaneya Y., Kasamatsu Y., Kitatsuji Y., and Kitayama Y., "Preparations for Redox Studies of Seaborgium with SISAK Coupled to the Flow Electrolytic Column FEC", 17th Radiochemical

Conference, (Division of Nuclear and Radiochemistry, European Association for Chemical and Molecular Sciences), Marianske Lazne, Czech Republic, May (2014).

Haba H., "Production of Radioisotopes for Application Studies at RIKEN", The 27th World Conference of the International Nuclear Target Development Society (INTDS-2014), (RIKEN Nishina Center), Odaiba, Japan, Sep. (2014).

Haba H., "Present Status and Future Plans of SHE Researches at RIKEN", 13th Workshop on Recoil Separator for Superheavy Element Chemistry (TASCA14), Darmstadt, Germany, Oct. (2014).

Haba H., "Productions and Decay Studies of Transactinide Elements for Superheavy Element Chemistry", DAE-BRNS 12th National Symposium on Nuclear and Radiochemistry (NUCAR-2015), (Board of Research in Nuclear Sciences, Department of Atomic Energy; Indian Association of Nuclear Chemists and Allied Scientists), Mumbai, India, Feb. (2015).

Haba H., "Production and Decay Studies of ^{265}Sg for Chemical Studies of Seaborgium Using the Gas-Filled Recoil Ion Separator GARIS at RIKEN", 249th American Chemical Society National Meeting & Exposition, (American Chemical Society), Denver, USA, Mar. (2015).

Takahashi K., Obi Y., and Tanaka M., "The Lead Isotopes of Aeolian Dust Observed at Saitama Area (Japan) and Their Genetic Implications", China-Japan-Korea Symposium for Analytical Chemistry, (Research Center for Analytical Sciences, Northeastern University), Shenyang, China, Aug. (2014).

(Domestic Conference)

羽場宏光, "理研 RIBF における RI 製造応用", 第 24 回金属の関与する生体関連反応シンポジウム (SRM2014), 特別講演 (兼市民講演会), (日本薬学会 物理系薬学部会), 京都市, 6 月 (2014).

加治大哉, 森本幸司, 羽場宏光, 若林泰生, 武山美麗, 山木さやか, 田中謙吾, 長谷部裕雄, M. Huang, 金谷淳平, 村上昌史, 米田 晃 , 吉田 敦, 山口貴之, 門叶冬樹, 吉田友美, Gan Z., Ma L., Geissel H., Hofmann S., Maurer Y., 藤田訓裕, 成清義博, 田中泰貴, 山本翔也, 浅井雅人, 鹿取健二, 森田浩介, "GARIS を用いたホットフュージョン反応 ^{248}Cm+^{48}Ca→^{296}Lv*に関する研究", 2014 日本放射化学会年会・第 58 回放射化学討論会, (日本放射化学会), 名古屋市, 9 月 (2014).

村上昌史, 羽場宏光, 黄 明輝, "^{nat}Zr(d,x), ^{nat}Hf(d,x)反応による Nb, Ta 同位体の励起関数測定", 2014 日本放射化学会年会・第 58 回放射化学討論会, (日本放射化学会), 名古屋市, 9 月 (2014).

笠松良崇, 豊村恵悟, 横北卓也, 重河優大, 高橋成人, 羽場宏光, 小森有希子, 金谷淳平, 黄 明輝, 森田浩介, 村上昌史, 菊永英寿, 三頭聰明, 吉村 崇, 大槻勤, 高宮幸一, 篠原 厚, "104 番元素 Rf の水酸化サマリウム共沈挙動", 2014 日本放射化学会年会・第 58 回放射化学討論会, (日本放射化学会), 名古屋市, 9 月 (2014).

佐藤大輔, 村上昌史, 羽場宏光, 菊永英寿, 大江一弘, 後藤真一, 工藤久昭, "Aliquat 336 を用いた Nb, Ta のフッ化水素酸溶液からの溶媒抽出挙動", 2014 日本放射化学会年会・第 58 回放射化学討論会, (日本放射化学会), 名古屋市, 9 月 (2014).

津藤翔平, 村上昌史, 大江一弘, 後藤真一, 佐藤大輔, 後藤尚哉, 長岡哲也, 羽場宏光, 豊嶋厚史, 工藤久昭, 小山 巧, 本山李沙, 小森有希子, 北山雄太, 福田芳樹, "Db の化学実験に向けた 5 族元素 Nb, Ta のオンライン逆相クロマトグラフィー", 2014 日本放射化学会年会・第 58 回放射化学討論会, (日本放射化学会), 名古屋市, 9 月 (2014).

北山雄太, 福田芳樹, 塚田和明, 豊嶋厚史, 羽場宏光, 菊永英寿, 村上昌史, Huang M.H., 谷口拓海, 上野慎吾, 林 和憲, 横山明彦, "TTA 逆相クロマトグラフィーによる超重元素ラザホージウム(Rf)の吸着挙動", 2014 日本放射化学会年会・第 58 回放射化学討論会, (日本放射化学会), 名古屋市, 9 月 (2014).

加治大哉, 森本幸司, 羽場宏光, 若林泰生, 武山美麗, 山木さやか, 田中謙吾, Huang M., 金谷淳平, 村上昌史, 浅井雅人, 森田浩介, "気体充填型反跳分離装置 GARIS-II の非対称系反応に対する性能試験", 2014 日本放射化学会年会・第 58 回放射化学討論会, (日本放射化学会), 名古屋市, 9 月 (2014).

豊嶋厚史, 大江一弘, 宮下 直, 北山雄太, 小森有希子, 金谷佑亮, 後藤尚哉, 津藤翔平, 浅井雅人, 佐藤哲也, 塚田和明, 北辻章浩, Vascon A., 永目諭一郎, Schaedel M., 佐藤大輔, 押見吉成, 小山 巧, 田中 彰, 横山明彦, 羽場宏光, Huang M., 笠松良崇, 重河優大, 横北卓也, 篠原 厚, 水飼秋菜, 古賀和樹, 金子政志, Lerum H. V., Attallah M. F., Gupta N. S., Omtvedt J. P., Kratz J. V., Pershina V., "超アクチノイド元素シーボーギウム(Sg)の還元に向けた同族元素 Mo と W の電解還元", 2014 日本放射化学会年会・第 58 回放射化学討論会, (日本放射化学会), 名古屋市, 9 月 (2014).

横北卓也, 木野愛子, 重河優大, 豊村恵悟, 中村宏平, 笠松良崇, 高橋成人, 安田勇輝, 吉村 崇, 小森有希子, 羽場宏光, 金谷淳平, 黄 明輝, 村上昌史, 篠原 厚, "104 番元素 Rf 実験に向けた自動抽出装置を用いた Zr と Hf の固液抽出", 2014 日本放射化学会年会・第 58 回放射化学討論会, (日本放射化学会), 名古屋市, 9 月 (2014).

加治大哉, 森本幸司, 羽場宏光, 森田浩介, "GARIS を用いた 113 番元素研究の総括", 2014 日本放射化学会年会・第 58 回放射化学討論会, (日本放射化学会), 名古屋市, 9 月 (2014).

村上昌史, 羽場宏光, 柴田誠一, 工藤久昭, "^{nat}Hf(a,x)反応の励起関数測定", 2014 日本放射化学会年会・第 58 回放射化学討論会, (日本放射化学会), 名古屋市, 9 月 (2014).

小森有希子, 村上昌史, 羽場宏光, 柴田誠一, "^{nat}Mo(d,x)反応による Tc 同位体の生成断面積測定", 2014 日本放射化学会年会・第 58 回放射化学討論会, (日本放射化学会), 名古屋市, 9 月 (2014).

後藤尚哉, 大江一弘, 村上昌史, 後藤真一, 工藤久昭, 塚田和明, 豊嶋厚史, 浅井雅人, 佐藤哲也, 宮下 直, 金谷佑亮, 北山雄太, 羽場宏光, 小森有希子, "Sg の同族元素 Mo, W のシュウ酸水溶液からのイオン対抽出挙動", 2014 日本放射化学会年会・第 58 回放射化学討論会, (日本放射化学会), 名古屋市, 9 月 (2014).

福田芳樹, 北山雄太, 羽場宏光, 塚田和明, 豊嶋厚史, 菊永英寿, Huang M.H., 村上昌史, 小森有希子, 千代西尾伊織, 後藤尚哉, 津藤翔平, 長岡哲也, 大江一弘, 谷口拓海, 上

野慎吾, 林 和憲, 横山明彦, “超重元素ラザホージウム(Rf)の溶液化学実験のための TTA 逆相クロマトグラフィーによる Zr, Hf の吸着挙動”, 2014 日本放射化学会年会・第 58 回放射化学討論会, (日本放射化学会), 名古屋市, 9 月 (2014).

脇谷雄一郎, 矢納慎也, 山田崇裕, 羽場宏光, 柴田誠一, 高橋和也, “理研 AVF サイクロトロンを用いた頒布用 RI の調製(I)^{109}Cd”, 2014 日本放射化学会年会・第 58 回放射化学討論会, (日本放射化学会), 名古屋市, 9 月 (2014).

矢納慎也, 脇谷雄一郎, 山田崇裕, 羽場宏光, 金谷淳平, 柴田誠一, 高橋和也, “理研 AVF サイクロトロンを用いた頒布用 RI の調製(II)^{85}Sr”, 2014 日本放射化学会年会・第 58 回放射化学討論会, (日本放射化学会), 名古屋市, 9 月 (2014).

羽場宏光, “理研における RI 製造応用”, 東北大学電子光理学研究センター研究会「大強度電子ビームとその応用利用」, (東北大学電子光理学研究センター), 仙台市, 3 月 (2015).

横北卓也, 中村宏平, 重河優大, 安田勇輝, 笠松良崇, 高橋成人, 吉村 崇, 羽場宏光, 小森有希子, 村上昌史, 篠原 厚, “104 番元素 Rf の抽出挙動の時間依存性： バッチ型固液抽出装置を用いた Rf の Aliquat336/HCl 系の固液抽出”, 日本化学会第 95 春季年会, (日本化学会), 船橋市, 3 月 (2015).

北山雄太, 福田芳樹, 羽場宏光, 塚田和明, 豊嶋厚史, 菊永英寿, 小森有希子, 村上昌史, 上野慎吾, 谷口拓海, 林 和憲, 谷津由香里, 千代西尾伊織, 村上拳冬, 横山明彦, “TTA 逆相クロマトグラフィーによる超重元素ラザホージウム(Rf)フッ化物錯体逐次形成の評価”, 日本化学会第 95 春季年会, (日本化学会), 船橋市, 3 月 (2015).

Industrial Cooperation Team

Publications

[Book · Proceedings]

吉田敦、神原正、上本龍二, "RI ビーム打込み法を用いた摩耗検査法の開発", 月刊トライボロジー2014-08 No324 pg.16-18,新樹社

吉田敦、神原正, "研究室紹介 No.43 理化学研究所仁科加速器研究センター産業連携チーム", 月刊トライボロジー2015-02 No330 pg.66,新樹社

Oral Presentations

(Domestic Conference)

吉田敦: "理研　RI ビームバラエティ（産業利用まで）", 第 54 回放射線科学研究会(エキゾチックビームシリーズ <12>), 大阪ニュークリアサイエンス協会, 大阪, 7 月 (2014).

Safety Management Group

Publications

[Journal]

(Original Papers)

Mikami S., Maeyama T., Hoshide Y., Sakamoto R., Sato S., Okuda N., Demongeot S., Gurriaran R., Uwamino Y., Kato H., Fujiwara M., Sato T., Takemiya H., Saito K.: "Spatial Distributions of Radionuclides Deposited onto Ground Soil Around the Fukushima Dai-Ichi Nuclear Power Plant and their Temporal Change until December 2012", J. Environmental Radioactivity **139**, 320 (2015).*

[Book · Proceedings]

(Original Papers)

Tanaka K., Inabe N., Yoshida K., Kubo T.: " Evaluation of radiation levels and comparison with PHITS calculations for the BigRIPS separator in Radioactive Isotope Beam Factory", Progress in Nuclear Science and Technology **4**, 201 (2014).*

(Others)

上蓑義朋, 他 日本原子力学会「遮蔽」ハンドブック研究専門委員会,: "放射線遮蔽ハンドブック ―基礎編―", 日本原子力学会 (2015).

Oral Presentations

(International Conference etc.)

Nakao N., Uwamino Y., Tanaka K.: "Measurement of Neutrons Generated by 345 MeV/u 238U Beam at RIKEN RIBF", 5th International Particle Accelerator Conference (IPAC2014), Dresden, June (2014).

(Domestic Conference)

岡野眞治, 加藤博: "スペクトロメトリー解析", 第 51 回アイソトープ・放射線研究発表会, (日本アイソトープ協会), 東京, 7 月(2014).

上蓑義朋, 岡野眞治, 加藤博, 向井弘樹、七沢潔、大森淳郎: "福島原発事故直後ならびに 3 年後の環境放射能推移", 第 51 回アイソトープ・放射線研究発表会, (日本アイソトープ協会), 東京, 7 月(2014).

田中鐘信, 稲辺尚人, 吉田光一, 久保敏幸: "理化学研究所 RI ビームファクトリー重イオン加速器施設における線量評価", 日本原子力学会 2014 年秋の大会(日本原子力学会), 京都, 9 月, (2014).

Center for Nuclear Study (CNS)
Graduate School of Science, the University of Tokyo

Publications

[Journal]

(Original Papers) *Subject to Peer Review

Tshoo K., Satou Y., Bertulani C.A., Bhang H., Choi S., Nakamura T., Kondo Y., Deguchi S., Kawada Y., Nakayama Y., Tanaka K.N., Tanaka N., Togano Y., Kobayashi N., Aoi N., Ishihara M., Motobayashi T., Otsu H., Sakurai H., Takeuchi S., Yoneda K., Delaunay F., Gibelin J., Marques F.M., Orr N.A., Honda T., Kobayashi T., Sumikama T., Miyashita Y., Yoshinaga K., Matsushita M., Shimoura S., Sohler D., Hwang J.W., Zheng T., Li Z.H., and Cao Z.X.: "Neutron occupancy of the $0d_{5/2}$ orbital and the $N = 16$ shell closure in ^{24}O", Phys. Lett. B **739**, 19–22 (2014)

Muto H., Ohshiro Y., Yamaka S., Watanabe S., Oyaizu M., Yamaguchi H., Kobayashi K., Kotaka Y., Nishimura M., Kubono S., Kase M., Hattori T., and Shimoura S.: "Note: ^{6}Li III light intensity observation for $^{6}Li^{3+}$ ion beam operation at Hyper-Electron Cyclotron Resonance ion source", Rev. Sci. Instrum **85**, 126107 (2014)

Crawford H.L., Fallon P., Macchiavelli A.O., Clark R.M., Brown B.A., Tostevin J.A., Bazin D., Aoi N., Doornenbal P., Matsushita M., Scheit H., Steppenbeck D., Takeuchi S., Baba H., Campbell C.M., Cromaz M., Ideguchi E., Kobayashi N., Kondo Y., Lee G., Lee I.Y., Lee J., Li K., Michimasa S., Motobayashi T., Nakamura T., Ota S., Paschalis S., Petri M., Sako T., Sakurai H., Shimoura S., Takechi M., Togano Y., Wang H., and Yoneda K.: "Shell and shape evolution at N=28: The 40Mg ground state", Phys. Rev. C **89**, 41303 (2014)

Patel Z., Soderstrom P.A., Podolyak Zs., Regan P.H., Walker P.M., Watanabe H., Ideguchi E., Simpson G.S., Liu H.L., Nishimura S., Wu Q., Xu F.R., Browne F., Doornenbal P., Lorusso G., Rice S., Sinclair L., Sumikama T., Wu J., Xu Z.Y., Aoi N., Baba H., Bello Garrote F.L., Benzoni G., Daido R., Fang Y., Fukuda N., Gey G., Go S., Gottardo A., Inabe N., Isobe T., Kameda D., Kobayashi K., Kobayashi M., Komatsubara T., Kojouharov I., Kubo T., Kurz N., Kuti I., Li Z., Matsushita M., Michimasa S., Moon C.B., Nishibata H., Nishizuka I., Odahara A., Sahin E., Sakurai H., Schaffner H., Suzuki H., Takeda H., Tanaka M., Taprogge J., Vajta Zs., Yagi A., and Yokoyama R.: "Isomer Decay Spectroscopy of ^{164}Sm and ^{166}Gd: Midshell Collectivity Around $N = 100$", Phys. Rev.Lett. **113** 262502 (2014)

Michimasa S., Yanagisawa Y., Inafuku K., Aoi N., Elekes Z., Fülöp Zs., Ichikawa Y., Iwasa N., Kurita K., Kurokawa M., Machida T., Motobayashi T., Nakamura T., Nakabayashi T., Notani M., Ong H.J., Onishi T., Otsu H., Sakurai H., Shinohara M., Sumikama T., Takeuchi S., Tanaka K., Togano Y., Yamada K., Yamaguchi M., and Yoneda K.: "Quadrupole collectivity in island-of-inversion nuclei ^{28,30}Ne and ^{34,36}Mg", Phys. Rev. C **89**, 054307 (2014)

Doornenbal P., Scheit H., Takeuchi S., Utsuno Y., Aoi N., Li K., Matsushita M., Steppenbeck D., Wang H., Baba H., Ideguchi E., Kobayashi N., Kondo Y., Lee J., Michimasa S., Motobayashi T., Otsuka T., Sakurai H., Takechi M., Togano Y., and Yoneda K.: "Rotational level structure of sodium isotopes inside the "island of inversion", Prog. Theor. Exp. Phys. **2014**, 053D01 (2014)

Kobayashi N., Nakamura T., Kondo Y., Tostevin J.A., Utsuno Y., Aoi N., Baba H., Barthelemy R., Famiano M.A., Fukuda N., Inabe N., Ishihara M., Kanungo R., Kim S., Kubo T., Lee G.S., Lee H.S., Matsushita M., Motobayashi T., Ohnishi T., Orr N.A., Otsu H., Otsuka T., Sako T., Sakurai H., Satou Y., Sumikama T., Takeda H., Takeuchi S., Tanaka R., Togano Y., and Yoneda K.: "Observation of a p-Wave One-Neutron Halo Configuration in ^{3}7Mg", Phys. Rev.Lett. **112** 242501 (2014)

Abelev B.B. *et al.* [ALICE Collaboration]: "Production of charged pions, kaons and protons at large transverse momenta in pp and PbPb collisions at $\sqrt{s_{\rm NN}}$ =2.76 TeV", Phys. Lett. B **736**, 196 (2014)

Adare A. *et al.* [PHENIX Collaboration]: "Azimuthal-angle dependence of charged-pion-interferometry measurements with respect to second- and third-order event planes in Au+Au collisions at $\sqrt{s_{NN}} = 200$ GeV", Phys. Rev. Lett. **112**, no. 22, 222301 (2014)

Abelev B.B. *et al.* [ALICE Collaboration]: "Performance of the ALICE Experiment at the CERN LHC", Int. J. Mod. Phys. A **29**, 1430044 (2014)

Adare A. *et al.* [PHENIX Collaboration]: "Inclusive double-helicity asymmetries in neutral-pion and eta-meson production in $\vec{p}+\vec{p}$ collisions at $\sqrt{s} = 200$ GeV", Phys. Rev. D **90**, no. 1, 012007 (2014)

Abelev B.B. *et al.* [ALICE Collaboration]: "Measurement of quarkonium production at forward rapidity in *pp* collisions at $\sqrt{s} = 7$ TeV", Eur. Phys. J. C **74**, no. 8, 2974 (2014)

Abelev B.B. *et al.* [ALICE Collaboration]: "Freeze-out radii extracted from three-pion cumulants in pp, pPb and PbPb collisions at the LHC", Phys. Lett. B **739**, 139 (2014)

Abelev B.B. *et al.* [ALICE Collaboration]: "Measurement of visible cross sections in proton-lead collisions at $\sqrt{s_{\rm NN}}$ = 5.02 TeV in van der Meer scans with the ALICE detector", JINST **9**, no. 11, P11003 (2014)

Abelev B.B. *et al.* [ALICE Collaboration]: "Azimuthal anisotropy of D meson production in Pb-Pb collisions at $\sqrt{s_{\rm NN}} = 2.76$ TeV", Phys. Rev. C **90**, no. 3, 034904 (2014)

Abelev B.B. *et al.* [ALICE Collaboration]: "Transverse momentum dependence of inclusive primary charged-particle production in p-Pb collisions at $\sqrt{s_{\rm NN}}$ =

5.02 TeV", Eur. Phys. J. C **74**, no. 9, 3054 (2014)

Abelev B.B. *et al.* [ALICE Collaboration]: "Measurement of prompt D-meson production in $p-Pb$ collisions at $\sqrt{s_{NN}} = 5.02$ TeV", Phys. Rev. Lett. **113**, no. 23, 232301 (2014)

Adare A. *et al.* [PHENIX Collaboration]: "Measurement of K^0_S and K^{*0} in $p+p$, $d+Au$, and $Cu+Cu$ collisions at $\sqrt{s_{NN}} = 200$ GeV", Phys. Rev. C **90**, no. 5, 054905 (2014)

Abelev B.B. *et al.* [ALICE Collaboration]: "Neutral pion production at midrapidity in pp and Pb-Pb collisions at $\sqrt{s_{\rm NN}} = 2.76\,$TeV", Eur. Phys. J. C **74**, no. 10, 3108 (2014)

Abelev B.B. *et al.* [ALICE Collaboration]: "Suppression of ψ(2S) production in p-Pb collisions at $\sqrt{s_{NN}} = 5.02$ TeV", JHEP **1412**, 073 (2014)

Adare A. *et al.* [PHENIX Collaboration]: "Low-mass vector-meson production at forward rapidity in p+p collisions at $\sqrt{s} = 200$ GeV", Phys. Rev. D **90**, no. 5, 052002 (2014)

Abelev B.B. *et al.* [ALICE Collaboration]: "Beauty production in pp collisions at $\sqrt{s} = 2.76$ TeV measured via semi-electronic decays", Phys. Lett. B **738**, 97 (2014)

Abelev B.B. *et al.* [ALICE Collaboration]: "Suppression of $\Upsilon(1S)$ at forward rapidity in Pb-Pb collisions at $\sqrt{s_{\rm NN}} = 2.76$ TeV", Phys. Lett. B **738**, 361 (2014)

Abelev B.B. *et al.* [ALICE Collaboration]: "Multiparticle azimuthal correlations in p -Pb and Pb-Pb collisions at the CERN Large Hadron Collider", Phys. Rev. C **90**, no. 5, 054901 (2014)

Adare A. *et al.* [PHENIX Collaboration]: "Cross section and transverse single-spin asymmetry of η mesons in $p^{\uparrow}+p$ collisions at $\sqrt{s} = 200$ GeV at forward rapidity", Phys. Rev. D **90**, no. 7, 072008 (2014)

Abelev B.B. *et al.* [ALICE Collaboration]: "Exclusive J/ψ photoproduction off protons in ultra-peripheral p-Pb collisions at $\sqrt{s_{\rm NN}} = 5.02$ TeV", Phys. Rev. Lett. **113**, no. 23, 232504 (2014)

Abelev B. *et al.* [ALICE Collaboration]: "Upgrade of the ALICE Experiment: Letter Of Intent", J. Phys. G **41**, 087001 (2014)

Abelev B. *et al.* [ALICE Collaboration]: "Technical Design Report for the Upgrade of the ALICE Inner Tracking System", J. Phys. G **41**, 087002 (2014)

Abelev B.B. *et al.* [ALICE Collaboration]: "Event-by-event mean $p_{\rm T}$ fluctuations in pp and Pb-Pb collisions at the LHC", Eur. Phys. J. C **74**, no. 10, 3077 (2014)

Doornenbal P., Takeuchi S., Aoi N., Matsushita M., Obertelli A., Steppenbeck D., Wang H., Audirac L., Baba H., Bednarczyk P., Boissinot S., Ciemala M., Corsi A., Furumoto T., Isobe T., Jungclaus A., Lapoux V., Lee J., Matsui K., Motobayashi T., Nishimura D., Ota S., Pollacco E.C., Sakurai H., Santamaria C., Shiga Y., Sohler D., and Taniuchi R.: "Intermediate-energy Coulomb excitation of Sn-104: Moderate E2 strength decrease approaching Sn-100", Phys. Rev. C **90**, 061302 (2014)

Satou .Y, Hwang. JW, Kim S., Tshoo K., Choi S., Nakamura T., Kondo Y., Matsui M., Hashimoto Y., Nakabayashi T., Okumura T., Shinohara M., Fukuda N., Sugimoto T., Otsu H., Togano Y., Motobayashi T., Sakurai H., Yanagisawa Y., Aoi N., Takeuchi S., Gomi T., Ishihara M., Kawai S., Ong H.J., Onishi T.K., Shimoura S., Tamaki N., Kobayashi T., Matsuda Y., Endo N., Kitayama N.; "One-neutron knockout reaction of 17C on a hydrogen target at 70 MeV/nucleon ", Phys. Lett. B **728** (2014) 462–466.

Muto H., Ohshiro Y., Yamaka S., Watanabe S., Oyaizu M., Kubono S., Yamaguchi H., Kase M., Hattori T., Shimoura S.: "Plasma spectroscopy of metal ions for hyper-electron cyclotron resonance ion source", Rev. Sci. Instrum. **85** (2014) 02A905.

Zhang L.Y., He J.J., Parikh A., Xu S.W., Yamaguchi H., Kahl D., Kubono S., Mohr R., Hu J., Ma P., Chen S.Z., Wakabayashi Y., Wang H.W., Tian W.D., Chen R.F., Guo B., Hashimoto T., Togano Y., Hayakawa S., Teranishi T., Iwasa M., Yamada T., Komatsubara T., Zhang Y.H., Zhou X.H., "Investigation of the thermonuclear ^{18}Ne(α,p)^{21}Na reaction rate via resonant elastic scattering of ^{21}Na+p", Phys. Rev. C **89** (2014) 015804.

Hu J., He J.J., Parikh A., W. S., Yamaguchi H., Kahl D., Ma P., Su J., Wang H.W., Nakao T., Wakabayashi Y., Teranishi T., Hahn K.I., Moon J.Y., Jung H.S., Hashimoto T., Chen A.A., Irvine D., Lee C.S., and Kubono S.: "Examination of the role of the 14O(alpha, p)17F reaction rate in type-I x-ray bursts", Phys. Rev. C **90**, 025803 (2014)

Mcneice E., Setoodehnia K., Singh B., Abe Y., Binh D., Chen A., Chen J., Cherubini S., Fukuoka S., Hashimoto T., Hayakawa T., Ishibashi Y., Ito Y., Kahl D., Komatsubara T., Kubono S., Moriguchi T., Nagae D., Nishikiori R., Niwa T., Ozawa A., Shizuma T., Suzuki H., Yamaguchi H., and Yuasa T.: "In-beam γ-ray spectroscopy of ^{30}P via the ^{28}Si(3He,pγ)^{30}P reaction", Nuclear Data Sheets **120**, 88–90 (2014)

Imai N., Mukai M., Cederkall J., Aghai H., Golubev P., Johansson H.T., Kahl D., Kurcewics J., Teranishi T., and Watanabe Y.X.: "Isobaric analog resonances of ^{31}Mg and the border of the island of inversion", Phys. Rev. C **90**, 011302 (2014)

Komatsubara T., Kubono S., Hayakawa T., Shizuma T., Ozawa A., Ito Y., Ishibashi Y., Moriguchi T., Yamaguchi H., Kahl D., Hayakawa S., Binh D.N., Chen A.A., Chen J., Setoodehnia K., and Kajino T.: "Excited states above the proton threshold in ^{26}Si", Eur. Phys. J. A **50**, 136 (2014)

Spitaleri C., Lamia L., Puglia S.M.R.., Romano S., La Cognata M., Crucilla V., Pizzone R.G., Rapisarda G.G., Sergi M.L., Del Santo M.G., Carlin N., Munhoz M.G., Souza F.A., Szanto de A., Tumino A., Irgaziev

B., Mukhamedzhanov A., Tabacaru G., Burjan V., Kroha V., Hons Z., Mrazek J., Zhou S.H., Li C., Wen Q., Wakabayashi Y., Yamaguchi H., and Somorjai E.: "Measurement of the 10 keV resonance in the ^{10}B(p,α_0)^{7}Be reaction via the trojan horse method", Phys. Rev. C **90**, 035801 (2014)

Jung H.S., Lee C.S., Kwon Y.K., Moon J.Y., Lee J.H., Yun C.C., Kim M.J., Hashimoto T., Yamaguchi H., Kahl D., Kubono S., Wakabayashi Y., Togano Y., Choi S., Kim Y.H., Kim Y.K., Park J.S., Kim E.J., Moon C.B., Teranishi T., Iwasa N., Yamada T., Kato S., Cherubini S., Hayakawa S., and Rapisarda: G.: "Elastic scattering of ^{25}Al+p to explore the resonance structure in ^{26}Si", Phys. Rev. C **90** 035805 (2014)

Y. Tsunoda, T. Otsuka, N. Shimizu, M. Honma, and Y. Utsuno, "Novel shape evolution in exotic Ni isotopes and configuration-dependent shell structure", Physical Review C **89** (2014) 031301(R).

Yuan C., Qi C., Xu F., Suzuki T., and Otsuka T.: "Mirror energy difference and the structure of loosely bound proton-rich nuclei", Phys. Rev. C **89**, 044327 (2014)

Watanabe H. , Lorusso G., Nishimura S., Otsuka T., Ogawa K., Xu Z.Y., Sumikama T., Sderstrm P.A., Doornenbal P., Li Z., Browne F., Gey G., Jung H.S., Taprogge J., Vajta Zs., Wu J., Yagi A., Baba H., Benzoni G., Chae K.Y., Crespi F.C.L., Fukuda N., Gernhuser R., Inabe N., Isobe T., Jungclaus A., Kameda D., Kim G.D., Kim Y.K., Kojouharov I., Kondev F.G., Kubo T., Kurz N., Kwon Y.K., Lane G.J., Moon C.-B., Montaner-Piz A., Moschner K., Naqvi F., Niikura M., Nishibata H., Nishimura D., Odahara A., Orlandi R., Patel Z., Podolyk Zs., Sakurai H., Schaffner H., Simpson G.S., Steiger K., Suzuki H., Takeda H., Wendt A., and Yoshinaga K. : "Monopole-Driven Shell Evolution below the Doubly Magic Nucleus Sn 132 Explored with the Long-Lived Isomer in Pd 126 ". Physical review letters, **113** (4), 042502.

Doornenbal P., Scheit H., Takeuchi S., Utsuno Y., Aoi N., Li K., Matsushita M., Steppenbeck D., Wang H., Baba H., Ideguchi E., Kobayashi N., Kondo Y., Lee J., Michimasa S., Motobayashi T., Otsuka T., Sakurai H., Takechi M., Togano Y., and Yoneda K.: "Rotational level structure of sodium isotopes inside the "island of inversion", Prog. Theor. Exp. Phys. **2014**, 053D01 (2014)

Kobayashi N., Nakamura T., Kondo Y., Tostevin J.A., Utsuno Y., Aoi N., Baba H., Barthelemy R., Famiano M.A., Fukuda N., Inabe N., Ishihara M., Kanungo R., Kim S., Kubo T., Lee G.S., Lee H.S., Matsushita M., Motobayashi T., Ohnishi T., Orr N.A., Otsu H., Otsuka T., Sako T., Sakurai H., Satou Y., Sumikama T., Takeda H., Takeuchi S., Tanaka R., Togano Y., and Yoneda K.: "Observation of a p-Wave One-Neutron Halo Configuration in 37Mg ", Phys. Rev. Lett. **112**, 242501 (2014)

Nakamura T., Kobayashi N., Kondo Y., Satou Y., Tostevin J.A., Utsuno Y., Aoi N., Baba H., Fukuda N., Gibelin J., Inabe N., Ishihara M., Kameda D., Kubo T., Motobayashi T., Ohnishi T., Orr N.A., Otsu H., Otsuka T., Sakurai H., Sumikama T., Takeda H., Takeshita E., Takechi M., Takeuchi S., Togano Y., and Yoneda K.: "Deformation-Driven p-Wave Halos at the Drip Line: 31Ne ", Phys. Rev. Lett. **112**, 142501 (2014)

Sanetullaev A., Tsang M.B., Lynch W.G., Lee Jenny, Bazin D., Chan K.P., Coupland D., Henzl V., Henzlova D., Kilburn M., Rogers A.M., Sun Z.Y., Youngs M., Charity R.J., Sobotka L.G., Famiano M., Hudan S., Shapira D., Peters W.A., Barbieri C., Hjorth-Jensen M., Horoi M., Otsuka T., Suzuki T., Utsuno Y. : "Neutron spectroscopic factors of 55Ni hole-states from image transfer reactions", Phys. Lett. B **736**, 137 (2014)

[Book・Proceedings]

(Original Papers) *Subject to Peer Review

Ajitanand N.N. *et al.* [PHENIX Collaboration]: "Comparison of the space-time extent of the emission source in d+Au and Au+Au collisions at $\sqrt{s_{NN}}$ = 200 GeV", Nucl. Phys. A **931**, 1082 (2014)

Ball M. *et al.* [ALICE TPC Collaboration]: "Ion backflow studies for the ALICE TPC upgrade with GEMs", JINST **9**, C04025 (2014)

Gunji T. [ALICE Collaboration]: "Future Upgrade and Physics Perspectives of the ALICE TPC", Nucl. Phys. A **931**, 1152 (2014)

Sako H., Chujo T., Gunji T., Harada H., Imai K., Kaneta M., Kinsho M. and Liu. Y *et al.*: "Towards the heavy-ion program at J-PARC", Nucl. Phys. A **931**, 1158 (2014)

Maeda Y., Saito T., Miyasako H., Uesaka T., Ota S., Kawase S., Kikuchi T., Tokieda H., Kawabata T., Yako K., Wakasa T., Sakaguchi S., Chen R., Sakaguchi H., Shima T., Suzuki T., and Tamii A.: "Measurement of the H-2(p,n) Breakup Reaction at 170 MeV and the Three-Nucleon Force Effects", Few-Body Systems, 55, 729-732 (2014)

Yamaguchi H., Kahl D., Nakao T., Wakabayashi Y., Kubono S., Hashimoto T., Hayakawa S., Kawabata T., Iwasa N., Teranishi T., Kwon Y.K., Lee P.S., Binh D.N., Khiem L.H., and Duy N.N.: "Studies on alpha-induced astrophysical reactions using the low-energy RI beam separator CRIB" EPJ Web of Conferences **66**, 07027 (2014).

Kobayashi M., Yako K., Shimoura S., Dozono M., Kawase S., Kisamori K., Kubota Y., Lee C.S., Michimasa S., Miya H., Ota S., Sakai H., Sasano M., Takaki M., "Measurement of the ^{8}He$(p,n)^8$Li reaction at intermediate energy in inverse kinematics", Proceedings of the 12th Asia Pacific Physics Conference (APPC12), Jul. 14–19, 2013, Makuhari, Japan, JPS Conf. Proc. 1, 013034 (2014)

Kubota Y., Sasano M., Uesaka T., Dozono M., Itoh M., Kawase S., Kobayashi M., Lee C.S., Matsubara H., Miya

H., Ota S., Sekiguchi K., Taguchi T., Tang T.L., Tokieda H., and Wakui T.; "A new neutron detector with a high position resolution for the study of the (p,pn) reaction on rare isotopes", EPJ Web of Conferences Vol. 66, No. 11022 (2014).

Kahl D., Hashimoto T., Duy N.N., Kubono S., Yamaguchi H., Binh D.N., Chen A.A., Cherubini S., Hayakawa S., He J.J., Ishiyama H., Iwasa N., Khiem L.H., Kwon Y.K., Michimasa S., Nakao T., Ota S., Teranishi T., Tokieda H., Wakabayashi Y., Yamada T., and Zhang L.Y.: "Active target studies of the αp-process at CRIB", AIP Conference Proceedings **1594**, 163–170 (2014)

He J.J., Hu J., Zhang L.Y., Xu S.W., Parikh A., Yamaguchi H., Kahl D., Ma P., Chen S.Z., Su J., Wakabayashi Y., Togano Y., Hayakawa S., Wang H.W., Tian W.D., Chen R.F., Guo B., Nakao T., Teranishi T., Moon J.Y., Jung H.S., Hashimoto T., Chen A.A., Irvine D., Hahn K.I., Iwasa N., Yamada T., Komatsubara T., Lee C.S., Kubono S.: "Astrophysics studies relevant to stellar X-ray bursts", AIP Conference Proceedings **1594**, 176–183 (2014)

Cherubini S., Gulino M., Spitaleri C., La Cognata M., Lamia L., Puglia S., Rapisarda G., Romano S., Kubono S., Yamaguchi H., Binh D., Hayakawa S., Kurihara Y., Wakabayashi Y., Bishop S., Coc A., De Sereville N., and Hammache F.: "First results of trojan horse method using radioactive ion beams: ^{18}F(p,α) at astrophysical energies", AIP Conference Proceedings **1594**, 184–189 (2014)

Yamaguchi H., Kahl D., Nakao T., Wakabayashi Y., Kubano S., Hashimoto T., Hayakawa S., Kawabata T., Iwasa N., Teranishi T., Kwon Y.K., Binh D.N., Khiem L.H., and Duy N.G.: "Alpha resonant scattering for astrophysical reaction studies", AIP Conference Proceedings **1594**, 220–225 (2014)

Yamaguchi H., Kahl D., Nakao T., Wakabayashi Y., Hashimoto T., Hayakawa S., Kawabata T., Teranishi T., Kwon Y.K., Binh D.N., Khiem L.H., Duy N.N., Kubono S., Suhara T., Kanada-En'yo Y., Moon J.Y., Kim A., Iwasa N., Lee P.S., Chae K.Y., Cha S.M., Gwak M.S., Kim D.H., and Milman E.: "Nuclear clusters studied with alpha resonant scatterings using RI beams at CRIB", Journal of Physics: Conference Series **569**, 012019 (2014)

Shimizu N., Abe T., Honma M., Otsuka T., Tsunoda Y., Utsuno Y., and Yoshida T. : "Frontier of nuclear shell-model calculations and high performance computing", accepted, JPS conference proceedings, ARIS2014

Utsuno Y., Otsuka T., Tsunoda Y., Shimizu N., Honma M., Togashi T., and Mizusaki T.: "Recent Advances in Shell Evolution with Shell-Model calculations", arXiv:1409.4506[nucl-th], accepted, JPS conference proceedings, ARIS2014

Togashi T., Shimizu N., Utsuno Y., Abe T., and Otsuka T. : "GPGPU Application to the Computation of Hamiltonian Matrix Elements between Non-orthogonal Slater Determinants in Monte Carlo Shell Model", Proc. Comp. Sci. **29**, 1711 (2014)

Abe T., Maris P., Otsuka T., Shimizu N., Utsuno Y.,and Vary J.P.: "Monte Carlo Shell Model for ab initio nuclear structure", EPJ Web Conf. **66**, 02001 (2014)

Tsunoda Y., Otsuka T., Shimizu N., Honma M., and Utsuno Y. : "Study of nuclei around Z = 28 by large-scale shell model calculations", EPJ Web Conf. **66**, 02105 (2014)

Utsuno Y., Otsuka T., Shimizu N., Honma M., Mizusaki T., Tsunoda Y., and Abe T. : "Recent shell-model results for exotic nuclei", EPJ Web Conf. **66**, 02106 (2014)

Yoshida T., Shimizu N., Abe T., and Otsuka T. : "Density profiles of light nuclei in Monte Carlo shell-model calculation", EPJ Web Conf. **66**, 02113 (2014)

Iwata Y.: "Co-existence of states in quantum systems", J. Phys. Conf. Ser. **569** (2014) 012029

Iwata Y.: "Present Status of Fission Research Based on TDDFT", The proceedings of the 2014 symposium on nuclear data, to appear.

Iwata Y., Shimizu N., Utsuno Y., Honma M., Abe T., and Otsuka T. : "Ingredients of nuclear matrix element for two-neutrino double-beta decay of 48Ca", JPS Conf. Proc. Volume **6** (2015), to appear.

Yoshida T., Shimizu N., Abe T., and Otsuka T. : "Appearance of -cluster structure in Be isotopes based on Monte Carlo shell model", Journal of Physics: Conference Series, **569**, 012063 (2014)

(Others)

大塚孝治："「テンソル力とエキゾチック核の構造進化」", 原子核研究, 59 巻, pp86-100, (2014).

大塚孝治："「^{54}Ca で発見した新しい魔法数」", Isotope News, No.720, 4 月号, 2014 年.

Oral Presentations

(International Conference etc.)

Shimoura S. (invited): "Nuclear responses via inelastic scatterings of exotic nuclei", Advances in Nuclear Structure at Extreme Conditions, Bormio, Italy, Feb. 19–22, 2014

Takaki M.(oral): "New type of spectroscopy via Heavy-Ion Double Charge eXchange reaction", Advances in Nuclear Structure at Extreme Conditions, Bormio, Italy, Feb. 19–22, 2014

Michimasa S., Yanagisawa Y., Inafuku K., Aoi N., Elekes Z., Fulop Zs., Ichikawa Y., Iwasa N., Kurita K., Kurokawa M., Machida T., Motobayashi T., Nakamura T., Nakabayashi T., Notani M., Ong H.J., Onishi T., Otsu H., Sakurai H., Shinohara M., Sumikama T., Takeuchi S., Tanaka K., Togano Y., Yamada K., Yamaguchi M., Yoneda K. (oral): "Proton inelastic scattering on Island-of-inversion nuclei", The 2nd Conference on "Advances in Radioactive Isotope Science"(ARIS2014), Tokyo, Japan, June 1–6, 2014

Kisamori K., Shimoura S., Assie M., Baba H., Baba T., Beaumel D., Dozono M., Fujii T., Fukuda N., Go S., Hammache F., Ideguchi E., Inabe N., Itoh M., Kameda D., Kawase S., Kawabata T., Kobayashi M., Kondo Y., Kubo T., Kubota Y., Kurata-Nishimura M., S. Lee C., Maeda Y., Matsubara H., Michimasa S., Miki K., Miya H., Nishi T., Noji S., Ota S., Sakaguchi S., Sakai H., Sasamoto Y., Sasano M., Sato H., Shimizu Y., Stolz A., Suzuki H., Takaki M., Takeda H., Takeuchi S., Tamii A., Tang L., Tokieda H., Tsumura M., Uesaka T., Yako K., Yanagisawa Y., Yokoyama R. (poster): "Missing-mass Spectroscopy of the 4n System by Exothermic Double-charge Exchange Reaction ^{4}He(^{8}He, ^{8}Be)4n", The 2nd Conference on "Advances in Radioactive Isotope Science"(ARIS2014), Tokyo, Japan, June 1–6, 2014

Yokoyama R., Ideguchi E., Simpson G., Tanaka Mn., Nishimura S., Doornenbal P., Sderstrm P.-A., Lorusso G., Y. Xu Z., Wu J., Sumikama T., Aoi N., Baba H., Bello F., Brown F., Daido R., Fang Y., Fukuda N., Gey G., Go S., Inabe N., Isobe T., Kameda D., Kobayashi K., Kobayashi M., Komatsubara T., Kubo T., Kuti I., Li Z., Matsushita M., Michimasa S., Moon C.B., Nishibata H., Nishizuka I., Odahara A., Patel Z., Rice S., Sahin E., Sinclair L., Suzuki H., Takeda H., Taprogge J., Vajta Zs., Watanabe H., Yagi A. (oral): "Isomers in Pm isotopes on the neutron-rich frontier of largely deformed $Z \sim 60$ region", at the 2nd Conference on Advances in Radioactive Isotope Science, Tokyo, Japan, June 1-6, 2014,

Kisamori K., Shimoura S., Michimasa S., Miya H., Assie M., Baba H., Baba T., Beaumel D., Dozono M., Fujii T., Fukuda N., Go S., Hammache F., Ideguchi E., Inabe N., Itoh M., Kameda D., Kawase S., Kawabata T., Kobayashi M., Kondo Y., Kubo T., Kubota Y., Kurata-Nishimura M., S. Lee C., Maeda Y., Matsubara H., Miki K., Nishi T., Noji S., Ota S., Sakaguchi S., Sakai H., Sasamoto Y., Sasano M., Sato H., Shimizu Y., Stolz A., Suzuki H., Takaki M., Takeda H., Takeuchi S., Tamii A., Tang L., Tokieda H., Tsumura M., Uesaka T., Yako K., Yanagisawa Y., Yokoyama R. (oral): "Missin- mass spectroscopy of the 4n system by exothermic double-charge exchange reaction ^{4}He(^{8}He, ^{8}Be)4n", at the 8th International Workshop on "Direct Reactions with Exotic Beams - DREB2014", Darmstadt, Germany, June 30–July 4, 2014

Kisamori K., Sasano M., Uesaka T., Kikuchi Y. (oral): "Tetra-neutron study via four neutron decay of superheavy hydrogen ^{7}H" SAMURAI international collaboration workshop 2014, Sendai, Japan, September 8–9, 2014

Michimasa S. (oral): "Quadrupole Colletivity in Island-of-Inversion Nuclei ", The 3rd SUNFLOWER Workshop, Tokyo, Japan, September 15–16, 2014

Matsushita M.(oral): "New Energy-Degrading Beamline for Low-Energy Reaction Measurements of RI beam", The 3rd SUNFLOWER Workshop, Tokyo, Japan, September 15–16, 2014

Shimoura S.(invited): "Charge exchange reactions of RI-beams using SHARAQ spectrometer", NUBA Conference Series-1: Nuclear Physics and Astrophysics in Antalya, Adrasan, Turkey, September 15–21, 2014

Dozono M. (oral) : "The (^{16}O,4^{16}F) reaction as a novel probe for studying the spin-dipole excitations in nuclei", Neutrino Nuclear Reponses for Neutrino Studies in Nuclei (NNR14), RCNP, Osaka University, Japan, Nov. 5-6, 2014

Shimoura S. (invited): "Nucleon transfer reactions at intermediate energy to exotic nuclei using inverse kinematics", ECT* Workshop on 'From nuclear structure to particle-transfer reactions and back II', Trento, Italy, November 10–14, 2014

Michimasa M. (invited): "In-beam gamma spectroscopy using direct reactions for probing shell evolution", Progress in nucler shell-model calculations in CNS-RIKEN collaboration, Wako, Saitama, Japan, Nov. 26–28, 2014

Kisamori K., Shimoura S., Assie M., Baba H., Baba T., Beaumel D., Dozono M., Fujii T., Fukuda N., Go S., Hammache F., Ideguchi E., Inabe N., Itoh M., Kameda D., Kawase S., Kawabata T., Kobayashi M., Kondo Y., Kubo T., Kubota Y., Kurata-Nishimura M., Lee C.S., Maeda Y., Matsubara H., Michimasa S., Miki K., Miya H., Nishi T., Noji S., Ota S., Sakaguchi S., Sakai H., Sasamoto Y., Sasano M., Sato H., Shimizu Y., Stolz A., Suzuki H., Takaki M., Takeda H., Takeuchi S., Tamii A., Tang L., Tokieda H., Tsumura M., Uesaka T., Yako K., Yanagisawa Y., Yokoyama R. (oral): "Study of tetra-neutron system via the exothermic double-charge exchange reaction 4He(8He, 8Be)4n" International Workshop on "Critical Stability in Few-Body System", Wako, Saitama, Japan, January 26–30, 2015

Gunji T. for the ALICE Collaboration (oral): "Future upgrade and physics perspectives of the ALICE TPC", XXIV International Conference on Ultrarelativistic Nucleus-Nucleus Collisions (QM2014), Darmstat, Germany, May 19 - 24, 2014

Gunji T. for the ALICE Collaboration (invited): "Dark Photon searches in ALICE for the ALICE Collaboration", International workshop on Dark Interactions: Perspectives from Theory and Experiment, Brookhaven National Laboratory, New York, USA, June 11-13, 2014,

Watanabe Y.(oral): "Measurements of di-electron production in Au+Au collisions at RHIC-PHENIX", The 5th Asian Triangle Heavy Ion Conference (ATHIC2014), Osaka, Japan, August 5-8, 2014

Hayashi S. on behalf of the ALICE Collaboration (poster): "Study of dielectron production in p-Pb collisions at $\sqrt{s_{NN}} = 5.02$ TeV using Transition Radiation Detector triggers with the ALICE detector", XXIV International Conference on Ultrarelativistic Nucleus-Nucleus Collisions (QM2014), Darmstat, Germany, May 19 - 24,

2014

Hayashi S. on behalf of the ALICE Collaboration (oral): "Dielectron measurement in p-Pb collisions at $\sqrt{s_{\rm NN}}$ = 5.02 TeV with the ALICE detector", The 5th Asian Triangle Heavy Ion Conference (ATHIC2014), Osaka, Japan, August 5-8, 2014

Hayashi S. on behalf of the ALICE Collaboration (oral): "Dielectrons production from heavy quark decays in p-Pb collisions at $\sqrt{s_{\rm NN}}$ = 5.02 TeV", High Energy Strong Interactions: A School for Young Asian Scientists, Wuhan, Chaina, September 22-26, 2014

Ota S., Tokieda T., Lee C.S., Watanabe Y.N., for CAT collaboration (invited): "CNS Active Target (CAT) for Missing Mass Spectroscopy with Intense Beams", 27th International Conference of the International Nuclear Target Development Society (INTDS-2014), Tokyo, Japan, Aug. 31 - Sep. 5, 2014

Ota S., Tokieda H., Lee C.S., Kojima R., Watanabe Y.N., Corsi A., Dozono M., Gibelin J., Hashimoto T., Kawabata T., Kawase S., Kubono S., Kubota Y., Maeda Y., Matsubara H., Matsuda Y., Michimasa S., Nakao T., Nishi T., Obertelli A., Otsu H., Santamaria C., Sasano M., Takaki M., Tanaka Y., Leung T., Uesaka T., Yako K., Yamaguchi H., Zenihiro J., Takada E. (poster): "Development of CNS Active Target for Deuteron Induced Reactions with High Intensity Exotic Beam", The 2nd conference on "Advances in Radioactive Isotope Science" (ARIS2014), Tokyo, Japan, Jun. 1-6, 2014

LEE C. OTA S., TOKIEDA H., KOJIMA R., WATANABE Y., SAISEAU R., UESAKA T.(poster): "Property of THGEM in Low-Pressure Deuterium for a Low-Pressure Gaseous Active Target", The 2nd conference on "Advances in Radioactive Isotope Science" (ARIS2014), Tokyo, Japan, Jun. 1-6, 2014

Yamaguchi H. (invited): "Studying alpha-cluster structure using low-energy RI beam", 3rd International Workshop on State of the Art in Nuclear Cluster Physics (SOTANCP3) KGU Kannai Media Center, Kanto Gakuin University, Yokohama, Japan, May 26-30, 2014

Yamaguchi H.(oral): "Proton resonance elastic scattering of 7Be at CRIB", RIBF-ULIC mini workshop: 'The way to evaluate the inelastic channel in the proton resonance elastic scattering', RIKEN Nishina Center, Wako, Saitama, Japan, May 31, 2014,

Yamaguchi H.(invited): "Studies on Nuclear Astrophysics and Exotic Structure at the Low-Energy RI beam Facility CRIB", The 2nd Conference on Advances in Radioactive Isotope Science (ARIS2014) Ito International Center, Tokyo, Japan, June 2-6, 2014

Kahl D.(poster): "^{30}S+alpha Resonant Elastic Scattering with an Active Target", The 2nd Conference on Advances in Radioactive Isotope Science (ARIS2014) Ito International Center, Tokyo, Japan, June 2-6, 2014

Yamaguchi H.(oral): "Studies on Nuclear Astrophysics and Exotic Structure at the Low-Energy RI Beam Facility CRIB", Sicily-East Asia Workshop for Low-energy Nuclear Physics, Catania University, Ortygia island, Siracusa, July 28–31, 2014

Kahl D.(oral): "^{30}S+alpha Resonant Elastic Scattering with an Active Target", Sicily-East Asia Workshop for Low-energy Nuclear Physics, Catania University, Ortygia island, Siracusa, July 28–31, 2014

Yamaguchi H.(oral): "Search for cluster states by measurements of alpha resonant scattering", The 10th RIBF Discussion 'Cluster states probed by reaction experiments', Yukawa institute for theoretical physics, Kyoto Univ., Sep. 25, 2014

H. Yamaguchi (oral), "Recent status and technical aspects of RI Beam separator CRIB", Nuclear physics seminar at RISP, Feb. 28, 2014, IBS, Daejeon, Korea.

Yamaguchi H.(invited): "Nuclear astrophysics, reaction, and structure studies at the low-energy RI beam separator CRIB", The International Symposium on Physics of Unstable Nuclei 2014 (ISPUN14) Hotel New World Saigon, Ho Chi Minh City, Vietnam, November 3–8, 2014

Otsuka T. (invited): "Dual Fermi liquid, critical point and 68Ni", Workshop on "The structure of 68Ni: current knowledge and open questions", Leuven, Belgium, April 23-24, 2014

Otsuka T. (invited): "Shape evolution, shape coexistence and shell evolution in exotic nuclei", 11th INT. SPRING SEMINAR ON NUCLEAR PHYSICS, Ischia, Italy, May 12-16, 2014

Otsuka T. (invited): "Shell model and nuclear shapes", French-US Theory Institute for Physics with Exotic Nuclei (FUSTIPEN) Topical Meeting, GANIL, France, July 19-20, 2014

Otsuka T. (invited): "Shapes of exotic nuclei and quantum liquid picture", Fourth Workshop of the European Gamma and Ancillary Detectors Network, GSI, Germany, July 23-25, 2014

Otsuka T. (invited): "Shapes of exotic nuclei and shell evolution", Fifteenth International Symposium on Capture Gamma-Ray Spectroscopy and Related Topics (CGS15), Dresden, Germany, August 25-29, 2014

Otsuka T. (invited): "Dual quantum liquids and shell evolutions in exotic nuclei", INTERNATIONAL SCHOOL OF NUCLEAR PHYSICS 36th Course, Erice, Italy, September 16-24, 2014

Otsuka T. (invited): "Dual quantum liquids and shell evolution in exotic nuclei", International Symposium on Physics of Unstable Nuclei, Ho Chiming, Vietnam, November 2-8, 2014

Otsuka T. (invited): "Two-neutrino Double Beta Decay from 48Ca calculated with sd and pf shells", EMMI Rapid Reaction Task Force on matrix elements of neutrinoless double beta decay, Darmstadt, Germany, November 10-21, 2014

Shimizu N. (invited), Abe T., Honma M., Mizusaki T., Otsuka T., Togashi T., Tsunoda Y., Utsuno Y., and Yoshida T.: "Frontier of nuclear shell-model calculations and high performance computing", Advances in Radioactive Isotope Science (ARIS2014), Univ. of Tokyo, Tokyo, Japan, Jun. 05, 2014

Utsuno Y. (invited), Otsuka T., Tsunoda Y., Shimizu N., Honma M., Togashi T., Mizusaki T.: "Recent Advances in shell evolution with shell-model calculations", 2nd International Conference "Advances in Radioactive Isotope Science", Tokyo, Japan, Jun. 2-6, 2014

Utsuno Y. (invited), Otsuka T., Shimizu N., Tsunoda Y., Honma M., Abe T., Mizusaki T., Togashi T. and Brown B.A. : "Large-scale shell-model studies for exotic nuclei: probing shell evolution", International Conference "Nuclear Theory in the Supercomputing Era 2014 (NTSE-2014)", Khabarovsk, Russia, Jun. 23-27, 2014

Iwata Y. (invited) : "Present status of fission research based on TDDFT", Symposium on Nuclear Data, Hokkaido University, Japan, Nov 2014

Iwata Y. (invited) : "Nuclear matrix element of 48Ca", NNR14, RCNP, Osaka University, Japan, Nov 2014

Iwata Y. (Poster), Shimizu N., Utsuno Y., Honma M., Abe T., and Otsuka T. : "Large-scale shell model calculations for double beta decay of 48Ca", ARIS 2014, Tokyo, Japan, Jun. 2014

Iwata Y. : "Shape transition induced by rotation", 3rd International Workshop on "State of the Art in Nuclear Cluster Physics" (SOTANCP3), Yokohama, Japan, May 2014

Yoshida T. (Poster), Shimizu N., Abe T., Otsuka T. : "Cluster Structure of Be Isotopes based on Monte Carlo Shell Model", The 2nd Conference on "Advances in Radioactive Isotope Science" (ARIS2014), Tokyo, Japan. Jun. 1-6, 2014

Yoshida T., Shimizu N., Abe T., and Otsuka T. : "Cluster structure of Be isotopes based on Monte Carlo shell model", ICNT workshop "Physics of exotic nuclei: Theoretical advances and challenges", RIKEN Wako Campus, Japan, Jun. 9-13, 2014

Togashi T., Shimizu N., Utsuno Y., Abe T. and Otsuka T.: "GPGPU Application to the Computation of Hamiltonian Matrix Elements between Non-orthogonal Slater Determinants in the Monte Carlo Shell Model", , ICCS2014, Pullman Cairns International, Cairns, Australia, Jun. 11, 2014

Togashi T. (Poster), Shimizu N., Utsuno Y., Otsuka T. and Honma M. : "Shell-model calculation of high-spin states in neutron-rich Cr and Fe isotopes", Advances in Radioactive Isotope Science (ARIS2014), Univ. of Tokyo, Tokyo, Japan, Jun. 05, 2014

Yoshida T., Shimizu N., Abe T., Otsuka T. : "Appearance of alpha-cluster structure in Be isotopes based on Monte Carlo shell model", 3rd International Workshop on " State of the Art in Nuclear Cluster Physics " (SOTANCP3), KGU Kannai Media Center, Kanto Gakuin University, Yokohama, Japan, May 26-30, 2014

Iwata Y. : "Large-scale shell model calculation project for double-beta decay", Workshop on "Progress in nuclear shell-model calculations in CNS-RIKEN collaboration", RIKEN, Japan, Nov. 2014

Tsunoda N. (invited) : "Microscopic description of neutron-rich nuclei from the nuclear force", Progress in nuclear shell-model calculation in CNS-RIKEN collaboration, RIKEN, Wako, Nov. 26-28, 2014

Utsuno Y. (invited) : "Exploring shell evolution with alphleet collaborations", Workshop "Progress in nuclear shell-model calculations in CNS-RIKEN collaboration", Wako, Japan, Nov. 26-28, 2014

Shimizu N. : "Overview of Alphleet collaboration project and Monte Carlo shell model", International workshop on "Progress in nuclear shell-model calculations in CNS-RIKEN collaboration", RIKEN Nishina hall, Wako, Japan, November 26, 2014

Shimizu N. : "Introduction to shell-model code, KSHELL", International workshop on "Progress in nuclear shell-model calculations in CNS-RIKEN collaboration", RIKEN Nishina hall, Wako, Japan, November 27, 2014

(Domestic Conference)

Lee C.S., Ota S., Tokieda H., Kojima R., Watanabe Y., and T. Uesaka: "重水素アクティブ標的の大強度重イオンビーム照射に向けた開発", JPS Spring meeting, Tokai University, Japan, Mar. 27–30, 2014

Kawase S., Uesaka T., Shimoura S., Yako K., Ota S., Michimasa S., Tokieda H., Miya H., Leung T.T., Kisamori K., Takaki M., Kubota Y., Lee C.S., Yokoyama R., Fujii T., Kobayashi M., Sasano M., Zenihiro J., Matsubara H., Dozono M., Lee J., Sakai H., Kubo T., Yoshida K., Inabe N., Yanagisawa Y., Takeda H., Kusaka K., Fukuda N., Kameda D., Suzuki H., Kawahara T., Wakui T., Sakaguchi S., Noro T., Wakasa T., Yasuda J., Fukunaga T., Maeda Y., Kim W., Hwang S., Stepanyan S., Obertelli A., Galind-Uribarri A., Padilla-Rodal E., and Beaumel D.: "準弾性 AO(p,2p) 反応による窒素同位体の陽子一空孔状態の核分光", JPS Spring meeting, Tokai University, Japan, Mar. 27–30, 2014

Ota S., Corsi A., Dozono M., Garg U., Hashimoto T., Ito M., Kawabata T., Kawase S., Kojima R., Kubota Y., Lee C.S., Maeda Y., Matta J., Matsuda Y., Michimasa S., Obertelli A., Otsu H., Patel D., Santamaria C., Sasano M., Takaki M., Terashima T., Tokieda H., Uesaka T., Yamaguchi H., Zenihiro J., and H307 collaboration, "重水素ガスアクティブ標的を用いた錫領域不安定核における巨大単極共鳴の測定計画", JPS Spring meeting, Tokai University, Japan, Mar. 27–30, 2014

Tokieda H., Ota S., Dozono M., Gunji T., Hamagaki H., Hashimoto T., Kawabata T., Kawase S., Kojima R., Kubono S., Kubota Y., Lee C.S., Maeda Y., Matsubara H., Michimasa S., Otsu H., Sako M., Uesaka T.,

Yamaguchi H., and Watanabe Y.: “重水素ガスアクティブ標的の反跳粒子飛跡再構成と性能評価”, JPS Spring meeting, Tokai University, Japan, Mar. 27–30, 2014

Yako K., “Study of nuclear matrix element of the double-beta decay by charge-exchange reactions”, JPS Spring meeting, Tokai University, Japan, Mar. 27–30, 2014

Kubota Y., Sasano M., Uesaka T., Dozono M., Itoh M., Kawase S., Kobayashi M., Lee C.S., Matsubara H., Miki K., Miya H., Ota S., Sekiguchi K., Shima T., Taguchi T., Tamii A., Tang T.L., Tokieda H., Wakasa T., Wakui T., Yasuda J., and Zenihiro J.: “不安定核研究のための高位置分解能ファイバーシンチ中性子検出器の開発”, JPS Spring meeting, Tokai University, Japan, Mar. 27–30, 2014

Gunji. T for the ALICE Collaboration, “R&D status of the ALICE GEM-TPC upgrade”, JPS Spring meeting, Tokai University, Japan, Mar. 27–30, 2014

Yukawa K., Gunji T., Hamagaki H., Terasaki K., “GEM-TPC におけるイオンバックフローの空間電荷依存性の研究”, JPS Spring meeting, Tokai University, Japan, Mar. 27–30, 2014

Kisamori K., Shimoura S., Assie M., Baba H., Baba T., Beaumel D., Dozono M., Fujii T., Fukuda N., Go S., Hammache F., Ideguchi E., Inabe N., Itoh M., Kameda D., Kawase S., Kawabata T., Kobayashi M., Kondo Y., Kubo T., Kubota Y., Kurata-Nishimura M., Lee C.S., Maeda Y., Matsubara H., Michimasa S., Miki K., Miya H., Nishi T., Noji S., Ota S., Sakaguchi S., Sakai H., Sasamoto Y., Sasano M., Sato H., Shimizu Y., Stolz A., Suzuki H., Takaki M., Takeda H., Takeuchi S., Tamii A., Tang L., Tokieda H., Tsumura M., Uesaka T., Yako K., Yanagisawa Y., Yokoyama R. (poster): “Study of tetra-neutron system by the exothermic double-charge exchange reaction ^{4}He(^{8}He, ^{8}Be)4n”, 実験と観測で解き明かす中性子星の核物質第三回研究会, Atagawa, Shizuoka, Japan, September 23-25, 2014

Shimoura S.(invited): “New energy degraded beam project at RIBF OEDO project ”, Fourth Joint Meeting of the Nuclear Physics Divisions of the American Physical Society and The Physical Society of Japan, Waikoloa, Hawaii, USA, October 7–11, 2014

Michimasa S.(invited): “RI-induced reaction studies by new energy-degrading beam line, OEDO”, Fourth Joint Meeting of the Nuclear Physics Divisions of the American Physical Society and The Physical Society of Japan, Waikoloa, Hawaii, USA, October 7–11, 2014

Dozono M.(oral) : “The parity-transfer reaction (^{16}O,^{16}F) for studies of pionic 0^{-} mode”, 4th Joint Meeting of the APS Division of Nuclear Physics and the Physical Society of Japan, Waikoloa, Hawaii, USA, Oct. 7-11, 2014

Kisamori K., Shimoura S., Assie M., Baba H., Baba T., Beaumel D., Dozono M., Fujii T., Fukuda N., Go S., Hammache F., Ideguchi E., Inabe N., Itoh M., Kameda D., Kawase S., Kawabata T., Kobayashi M., Kondo Y., Kubo T., Kubota Y., Kurata-Nishimura M., Lee C.S., Maeda Y., Matsubara H., Michimasa S., Miki K., Miya H., Nishi T., Noji S., Ota S., Sakaguchi S., Sakai H., Sasamoto Y., Sasano M., Sato H., Shimizu Y., Stolz A., Suzuki H., Takaki M., Takeda H., Takeuchi S., Tamii A., Tang L., Tokieda H., Tsumura M., Uesaka T., Yako K., Yanagisawa Y., Yokoyama R. (oral): “Tetra-neutron system studied by exothermic double-charge exchange reaction ^{4}He(^{8}He, ^{8}Be)4n”, The 4th Joint Meeting of the Nuclear Physics Devisions of the APS and JPS, Hawaii, USA, October 7–11, 2014

Kobayashi M., Yako K., Shimoura S., Dozono M., Kawase S., Kisamori K., Kubota Y., Lee C.S., Michimasa S., Miya H., Ota S., Sakai H., Sasano M., and Takaki M. (oral): “Spin-isospin response of neutron-rich nuclei ^{8}He via (p, n) reaction in inverse kinematics”, Fourth Joint Meeting of the Nuclear Physics Divisions of the American Physical Society and The Physical Society of Japan (Hawaii2014), Waikoloa, Hawaii, US, Oct. 7–11, 2014,

Miya H., Shimoura S., Kisamori K., Baba H., Baba T., Dozono M., Fukuda N., Fujii T., Go S., Ideguchi E., Inabe N., Ito M., Kameda D., Kawabata T., Kawase S., Kikuchi Y., Kubo T., Kubota Y., Kobayashi M., Kondo Y., Lee C.S., Maeda Y., Matsubara H., Miki K., Michimasa S., Nishi T., Nishimura M., Ota S., Sakaguchi S., Sakai H., Sasano M., Sato H., Shimizu Y., Suzuki H., Takaki M., Takeda H., Takeuchi S., Tamii A., Tokieda H., Tsumura M., Uesaka T., Yanagisawa Y., Yako K., Yokoyama R., Yoshida K., Assie M., Beaumel D., Fariouz H., and Stolz A.: ”Missing mass spectroscopy of ^{4}H via exothermic charge exchange reaction (^{8}He, ^{8}Liγ)”, The 4th Joint Meeting of the Nuclear Physics Devisions of the APS and JPS, Hawaii, USA, October 7–11, 2014

Lee C.S., Ota S., Aramaki Y., Saiseau R., Tokieda H., and Watanabe Y.: ”Development of a dual-gain multiplication in CNS Active Target for high-intensity heavy-ion beam injection”, The 4th Joint Meeting of the Nuclear Physics Devisions of the APS and JPS, Hawaii, USA, October 7–11, 2014

Ota S.(oral): ”CNS Active Target for deuteron induced reactions with high intensity beams”, The 4th Joint Meeting of the Nuclear Physics Devisions of the APS and JPS, Hawaii, USA, October 7–11, 2014

Imai N., Mukai M., Cederkall J., Aghai H., Golubev P., Johansson H., Kahl D., Kurcewics J., Teranishi T., and Watanabe Y.: ”Small spectroscopic factors of low-lying positive parity states in ^{31}Mg”, The 4th Joint Meeting of the Nuclear Physics Devisions of the APS and JPS, Hawaii, USA, October 7–11, 2014

Gunji T.(invited): “Experimental upgrades at RHIC and LHC”, JPS-DNP at Hawaii2014 Workshop on ”Quark Gluon Plasma and Future Directions in Heavy Ion Physics at RHIC and LHC”, Hawaii 2014, Hawaii, USA, October 7–11

Gunji T. (oral): “LHC-ALICE 実験用 MPGD を用いた TPC 検出器開発の現状”, MicroPattern Gas Detector 研究会, 東北大学, Dec. 19 - 20, 2014

Yukawa K.(oral): “GEM と MICROMEGAS におけるイオンバックフローの研究”, MicroPattern Gas Detector 研究会, 東北大学, Dec. 19 - 20, 2014

Gunji T.(poster): “Future Upgrade and Physics Perspectives of the LHC-ALICE Experiment”, Hadron Physics Symposium, Nagoya University, Japan, April 17-19, 2014

Watanabe Y.(oral): “Measurements of di-electron production in Au+Au collisions at $\sqrt{s_{NN}} = 200$ GeV by RHIC-PHENIX using Hadron Blind Detector”, 4th Joint Meeting of the APS Division of Nuclear Physics and the Physical Society of Japan, Hawaii, USA, Oct. 7 – 11, 2014

Hayashi S. on behalf of the ALICE Collaboration (oral): “Dielectrons from Charm and Bottom meson decays in p-Pb collisions at $\sqrt{s_{\rm NN}} = 5.02$ TeV measured with the ALICE detector”, Fourth Joint Meeting of the Nuclear Physics Divisions of the American Physical Society and The Phsical Society of Japan, Hawaii, USA, Octorber 7-11

Hayshi S.(invited): “Review of Quark Matter 2014(Heavy Flavor)”, Heavy Ion Pub and Heavy Ion Cafe 合同研究会, Nagoya, Japan, June 6

Hayashi S. (invited): ”LHC での p-Pb 衝突における粒子相関”, Heavy Ion Pub, Osaka, Japan, December 5

Sekiguchi Y. for ALICE collaboration (oral): “Long range correlation in p-Pb collisions at $\sqrt{s_{NN}} = 5.02$ TeV with the ALICE detector”, at 4th Joint Meeting of the APS Division of Nuclear Physics and the Physical Society of Japan, Waikoloa, Hawaii, USA, Oct. 7-11, 2014

Terasaki K., Hamagaki H., Gunji T., Yamaguchi Y.(oral): “Performance Evaluation of the COBRA GEM for the Application of the TPC”, at 4th Joint Meeting of the APS Division of Nuclear Physics and the Physical Society of Japan, Waikoloa, Hawaii, USA, Oct. 7-11, 2014

Otsuka T. (invited): “What can we learn from large-scale MCSM calculations?”, Fourth Joint Meeting of the Nuclear Physics Divisions of the American Physical Society and The Physical Society of Japan, Waikoloa, USA, Oct. (2014).

Utsuno Y. (invited): “Shells and shapes in exotic nuclei”, Fourth Joint Meeting of the Nuclear Physics Divisions of the American Physical Society and The Physical Society of Japan, Waikoloa, USA, Oct. (2014).

Shimizu N., Utsuno Y., Togashi T., Otsuka T., and Honma M. : “Shell-model description of E1 excitation”, Fourth Joint Meeting of the Nuclear Physics Divisions of the American Physical Society and The Physical Society of Japan, Waikoloa, USA, Oct. (2014).

Iwata T., Shimizu N., Utsuno Y., Honma M., Abe T., and Otsuka T. : “Large-scale shell model calculations for two-neutrino double-beta decay of 48Ca”, Fourth Joint Meeting of the Nuclear Physics Divisions of the American Physical Society and The Physical Society of Japan, Waikoloa, USA, Oct. (2014).

Yoshida T., Shimizu N., Abe T., and Otsuka T. : “Structure of Be isotopes based on Monte Carlo shell model”, Fourth Joint Meeting of the Nuclear Physics Divisions of the American Physical Society and The Physical Society of Japan, Waikoloa, USA, Oct. (2014).

Tsunoda N.: “Neutron-rich nuclei from the nuclear force a new Many-body perturbation theory with 3N force and its first application”, Fourth Joint Meeting of the Nuclear Physics Divisions of the American Physical Society and The Physical Society of Japan, Waikoloa, USA, Oct. (2014).

Togashi T., Shimizu N., Utsuno Y., Otsuka T. and Honma M. : “Large-scale shell-model calculation of unnatural parity high-spin states in neutron-rich Cr and Fe isotopes”, Fourth Joint Meeting of the Nuclear Physics Divisions of the American Physical Society and The Physical Society of Japan, Waikoloa, USA, Oct. (2014).

富樫智章, 清水則孝, 吉田亨, 宇都野穣, 阿部喬, 大塚孝治 : “モンテカルロ殻模型計算のマルチ GPGPU への適用と開発状況”, 第 6 回「学際計算科学による新たな知の発見・統合・創出」シンポジウム.

(Colloquium) Y. Iwata : “Fission Dynamics of A=240 Nuclei Based on Time-Dependent Density Functional Calculations”, Colloquium at Tokyo Institute of Technology, Sep. (2014).

下浦 享: 「エキゾチック原子核の世界」, Konan University, Kobe, Japan, June 9–11, July 8–9, 2014

Niigata University

Publications

[Journal]

(Original Papers) *Subject to Peer Review

Matsuo M., Hinohara N., Sato K., Matsuyanagi K., Nakatsukasa T., and Yoshida K.: "Quadrupole shape dynamics from the viewpoint of a theory of large amplitude collective motion", Phys. Scr. **89**, 054020(6) (2014). *

Zhang Y., Matsuo M., and Meng J.: "Asymptotic form of neutron Cooper pairs in weakly bound nuclei", Phys. Rev. C **90**, 034313 (2014). *

Takechi M., Suzuki S., Nishimura D., Fukuda M., Ohtsubo T., Nagashima M., Suzuki T., Yamaguchi T., Ozawa A., Moriguchi T., Ohishi H., Sumikama T., Geissel H., Aoi N., Chen Rui-Jiu, Fang De-Qing, Fukuda N., Fukuoka S., Furuki H., Inabe N., Ishibashi Y., Itoh T., Izumikawa T., Kameda D., Kubo T., Lantz M., Lee C. S., Ma Yu-Gang, Matsuta K., Mihara M., Momota S., Nagae D., Nishikiori R., Niwa T., Ohnishi T., Okumura K., Ohtake M., Ogura T., Sakurai H., Sato K., Shimbara Y., Suzuki H., Takeda H., Takeuchi S., Tanaka K., Tanaka M., Uenishi H., Winkler M., Yanagisawa Y., Watanabe S., Minomo K., Tagami S., Shimada M., Kimura M., Matsumoto T., Shimizu Y. R., and Yahiro M.: "Evidence of halo structure in Mg-37 observed via reaction cross sections and intruder orbitals beyond the island of inversion", Phys. Rev. C **90**, 061305 (2014). *

Fan G. W., Fukuda M., Nishimura D., Cai X. L., Fukuda S., Hachiuma I., Ichikawa C., Izumikawa T., Kanazawa M., Kitagawa A., Kuboki T., Lantz M., Mihara M., Nagashima M., Namihira K., Ohkuma Y., Ohtsubo T., Ren Zhongzhou, Sato S., Shen Z. Q., Sugiyama M., Suzuki S., Suzuki T., Takechi M., Yamaguchi T., Xu B. J., and Xu W.: "Structure of Li-8 from a reaction cross-section measurement", Phys. Rev. C **90**, 044321 (2014). *

Moriguchi T., Ozawa A., Ishimoto S., Abe Y., Fukuda M., Hachiuma I., Ishibashi Y., Ito Y., Kuboki T., Lantz M., Nagae D., Namihira K., Nishimura D., Ohtsubo T., Ooishi H., Suda T., Suzuki H., Suzuki T., Takechi M., Tanaka K., and Yamaguchi T.: "Density distribution of Be-14 from reaction cross-section measurements", Nucl. Phys. A **929**, 83–93 (2014). *

Muto S., Stone N. J., Bingham C. R., Stone J. R., Walker P. M., Audi G., Gaulard C., Koester U., Nikolov J., Nishimura K., Ohtsubo T., Podolyak Z., Risegari L., Simpson G. S., Veskovic M., and Walters W. B.: "Magnetic properties of Hf-177 and Hf-180 in the strong-coupling deformed model", Phys. Rev. C **89**, 044309 (2014). *

Ozawa A., Moriguchi T., Ohtsubo T., Aoi N., Fang D. Q., Fukuda N., Fukuda M., Geissel H., Hachiuma I., Inabe N., Ishibashi Y., Ishimoto S., Ito Y., Izumikawa T., Kameda D., Kubo T., Kuboki T., Kusaka K., Lantz M., Ma Y. G., Mihara M., Miyashita Y., Momota S., Nagae D., Namihira K., Nishimura D., Ooishi H., Ohkuma Y., Ohnishi T., Ohtake M., Ogawa K., Shimbara Y., Suda T., Sumikama T., Suzuki H., Suzuki S., Suzuki T., Takechi M., Takeda H., Tanaka K., Watanabe R., Winkler M., Yamaguchi T., Yanagisawa Y., Yasuda Y., and Yoshinaga K.: "Charge-changing cross sections of Ne-30, Na-32,Na-33 with a proton target", Phys. Rev. C **89**, 044602 (2014). *

Estradé A., Kanungo R., Horiuchi W., Ameil F., Atkinson J., Ayyad Y., Cortina-Gil D., Dillmann I., Evdokimov A., Farinon F., Geissel, H., Guastalla G., Janik, R., Kimura M., Knöbel R., Kurcewicz J., Litvinov Yu. A., Marta M., Mostazo M., Mukha I., Nociforo C., Ong H. J., Pietri S., Prochazka A., Scheidenberger C., Sitar B., Strmen P., Suzuki Y., Takechi M., Tanaka J., Tanihata I., Terashima S., Vargas J., Weick H., and Winfield J. S.: "Proton Radii of B12–17 Define a Thick Neutron Surface in B17", Phys. Rev. Lett. **113**, 132501 (2014). *

Crawford H. L., Fallon P., Macchiavelli A. O., Clark R. M., Brown B. A., Tostevin J. A., Bazin D., Aoi N., Doornenbal P., Matsushita M., Scheit H., Steppenbeck D., Takeuchi S., Baba H., Campbell C. M., Cromaz M., Ideguchi E., Kobayashi N., Kondo Y., Lee G., Lee I. Y., Lee J., Li K., Michimasa S., Motobayashi T., Nakamura T., Ota S., Paschalis S., Petri M., Sako T., Sakurai H., Shimoura, S., Takechi M., Togano Y., Wang, H., and Yoneda K.: "Shell and shape evolution at $N = 28$: The Mg40 ground state", Phys. Rev. C **89**, 041303 (2014). *

Watanabe S., Minomo K., Shimada M., Tagami S., Kimura M., Takechi M., Fukuda M., Nishimura D., Suzuki T., Matsumoto T., Shimizu Y. R., and Yahiro M.: "Ground-state properties of neutron-rich Mg isotopes", Phys. Rev. C **89**, 044610 (2014). *

Nakamura T., Kobayashi N., Kondo Y., Satou Y., Tostevin J. A., Utsuno Y., Aoi N., Baba H., Fukuda N., Gibelin J., Inabe N., Ishihara M., Kameda D., Kubo T., Motobayashi T., Ohnishi T., Orr, N. A., Otsu H., Otsuka T., Sakurai H., Sumikama T., Takeda H., Takeshita E., Takechi M., Takeuchi S., Togano Y., and Yoneda K.: "Deformation-Driven p-Wave Halos at the Drip Line: Ne31", Phys. Rev. Lett. **112**, 142501 (2014). *

Caballero-Folch R., Domingo-Pardo C., Cortès G., Taín J. L., Agramunt J., Algora A., Ameil F., Ayyad Y., Benlliure J., Bowry M., Calviño F., Cano-Ott D., Davinson T., Dillmann I., Estrade A., Evdokimov A., Faestermann T., Farinon F., Galaviz D., García-Ríos A., Geissel H., Gelletly W., Gernhäuser R., Gómez-Hornillos M. B., Guerrero C., Heil M., Hinke C., Knöbel R., Kojouharov I., Kurcewicz J., Kurz N., Litvinov Y., Maier L., Marganiec J., Marta M., Martínez T., Montes F., Mukha I., Napoli D. R., Nociforo C.,

Paradela C., Pietri S., Podolyák Zs., Prochazka A., Rice S., Riego A., Rubio, B., Schaffner H., Scheidenberger C., Smithr K., Sokol E., Steiger K., Sun B., Takechi M., Testov D., Weick H., Wilson E., Winfield J. S., Wood R., Woods P. J., and Yeremin A.: "β-decay and β-delayed Neutron Emission Measurements at GSI-FRS Beyond $N = 126$, for r-process Nucleosynthesis', Nucl. Data Sheets **120**, 81–83 (2014). ∗

Shibata Y., Matsuzaki T., Abe K., Fujita Y., Goto J., Itoh T., Kikukawa N., Nagashima M., Nakamura Y., Ogura T., Ohtsubo T., Ohya S., Sakai T., Sera D., Suzuki S., Takeda K., Yajima A., and Yoshikawa T.: "Observation of Muonic X-rays of Cosmic-Ray Muons Stopped in Al and Fe Targets", J. Phys. Soc. Jpn. **84**, 034301 (2015). ∗

Yoshida K.: "Proton-neutron pairing vibrations in $N = Z$ nuclei: Precursory soft mode of isoscalar pairing condensation", Phys. Rev. C **90**, 031303(R) (2014). ∗

Even J., Yakushev A., Düllmann Ch. E., Haba H., Asai M., Sato T. K., Brand H., Nitto A. Di, Eichler R., Fan F. L., Hartmann W., Huang M., Jäger E., Kaji D., Kanaya J., Kaneya Y., Khuyagbaatar J., Kindler B., Kratz J. V., Krier J., Kudou Y., Kurz N., Lommel B., Miyashita S., Morimoto K., Morita K., Murakami M., Nagame Y., Nitsche H., Ooe K., Qin Z., Schädel M., Steiner J., Sumita T., Takeyama M., Tanaka K., Toyoshima A., Tsukada K., Türler A., Usoltsev I., Wakabayashi Y., Wang Y., Wiehl N., and Yamaki S.: "Synthesis and detection of a seaborgium carbonyl complex", Science **345**, 1491–1493 (2014). ∗

Yokokita T., Kasamatsu Y., Ooe K., Yoshimura T., Takahashi N., Komori Y., and Shinohara A.: "Solvent extraction of Mo(V) and Mo(VI) from hydrochloric acid into Aliquat 336 chloroform solution", J. Radioanal. Nucl. Chem. **301**, 751–756 (2014). ∗

Haba H., Huang M., Kaji D., Kanaya J., Kudou Y., Morimoto K., Morita K., Murakami M., Ozeki K., Sakai R., Sumita T., Wakabayashi Y., Yoneda A., Kasamatsu Y., Kikutani Y., Komori Y., Nakamura K., Shinohara A., Kikunaga H., Kudo H., Nishio K., Toyoshima A., and Tsukada K.: "Production of ^{262}Db in the ^{248}Cm(^{19}F, $5n$)^{262}Db reaction and decay properties of ^{262}Db and ^{258}Lr", Phys. Rev. C **89**, 024618(11) (2014). ∗

Murakami M., Haba H., Goto S., Kanaya J., and Kudo H.: "Production corss section of niobium and tantalum isotopes in proton-induced reactions on ^{nat}Zr and ^{nat}Hf up to 14 MeV", Appl. Radiat. Isot. **90**, 149–157 (2014). ∗

Khandaker M. U., Haba H., Murakami M., Otuka N., and Kassim H. A.: "Deuteron-induced activation cross sections on natural copper up to 24 MeV", J. Radioanal. Nucl. Chem. **302**, 759–764 (2014). ∗

Fan G. W., Fukuda M., Nishimura D., Cai X. L., Fukuda S., Hachiuma I., Ichikawa C., Izumikawa T., Kanazawa M., Kitagawa A., Kuboki T., Lantz M., Mihara M., Nagashima M., Namihira K., Ohkuma Y., Ohtsubo T., Ren Z. Z., Sato S., Sheng Z. Q., Sugiyama M., Suzuki S., Takechi M., Yamaguchi T., and Xu W.: "Density distribution of Li-8 and B-8 and capture reaction at low energy", Phys. Rev. C **91**, 014614 (2015). ∗

Takechi M., Suzuki S., Nishimura D., Fukuda M., Ohtsubo T., Nagashima M., Suzuki T., Yamaguchi T., Ozawa A., Moriguchi T., Ohishi H., Sumikama T., Geissel H., Aoi N., Chen R. J., Fang D. Q., Fukuda N., Fukuoka S., Furuki H., Inabe N., Ishibashi Y., Itoh T., Izumikawa T., Kameda D., Kubo T., Lantz M., Lee C. S., Ma Y. G, Matsuta K., Mihara M., Momota S., Nagae D., Nishikiori R., Niwa T., Ohnishi T., Okumura K., Ohtake M., Ogura T., Sakurai H., Sato K., Shimbara Y., Suzuki H., Takeda H., Takeuchi S., Tanaka K., Tanaka M., Uenishi H., Winkler M., Yanagisawa Y., Watanabe S., Minomo K., Tagami S., Shimada M., Kimura M., Matsumoto T., Shimizu Y. R., and Yahiro M.: "Evidence of halo structure in Mg-37 observed via reaction cross sections and intruder orbitals beyond the island of inversion", Phys. Rev. C **90**, 061305 (2014). ∗

（Review）

菖蒲川由郷, 後藤淳: "チーム毘沙門の南相馬市支援活動記録", 新潟県医師会報, **771**, (2014).

[Book · Proceedings]

（Original Papers） *Subject to Peer Review

Ooe K., Attallah M. F., Asai M., Goto N., Gupta N. S., Haba H., Huang M., Kanaya J., Kaneya Y., Kasamatsu Y., Kitatsuji Y., Kitayama Y., Koga K., Komori— Y., Koyama T., Kratz J. V., Lerum H. V., Miyashita S., Oshimi Y., Pershina V., Sato D., Sato T. K., Shigekawa Y., Shinohara A., Tanaka A., Toyoshima A., Tsukada K., Tsuto S., Yokokita T., Yokoyama A., Omtvedt J. P., Nagame Y., and Schädel M.: "Development of a new continuous dissolution apparatus with a hydrophobic membrane for superheavy element chemistry", J. Radioanal. Nucl. Chem., **303**, 1317–1320 (2015). ∗

Oral Presentations

(International Conference etc.)

Yoshida K.: "Low-lying Gamow-Teller Excitations and Beta-Decay Properties of Neutron-Rich Zr Nuclei", The second international Conference on Advances in Radioactive Isotope Science, (University of Tokyo), Tokyo, Japan, Jun. (2014).

Yoshida K.: "Skyrme-EDF for charge-changing excitation modes", ICNT Workshop "Physicics of exotic nuclei: Theoretical advances and challenges", (RIKEN), Wako, Japan, Jun. (2014).

Yoshida K.: "Gamow-Teller excitations and beta-decay properties of deformed neutron-rich Zr isotopes", Nuclear Structure 2014, (TRIUMF, the University of British Columbia), Vancouver, Canada, Jun. (2014).

Yoshida K.: "Giant multi-pole resonances in rare-earth

nuclei with shape changes", International Workshop on Nuclear Science and Simulation in fundamental and applied researchesv, (Ton Duc Thang University), Ho Chi Minh City, Vietnam, Oct. (2014).

Yoshida K.: "Proton-neutron pairing vibrations in $N = Z$ nuclei", The International Symposium on Physics of Unstable Nuclei 2014, Ho Chi Minh City, Vietnam, Nov. (2014).

Takechi M., Suzuki S., Nishimura D., Fukuda M., Ohtsubo T., Nagashima M., Suzuki T., Yamaguchi T., Ozawa A., Moriguchi T., Ooishi H., Sumikawa T., Geissel H., Ishihara M., Aoi N., Chen R. J., Fang D. Q., Fukuda N., Fukuoka S., Furuki H., Inabe N., Ishibashi Y., Ito T., Izumikawa T., Kameda D., Kubo T., Lee C. S., Lantz M., MA Yu-Gang, Matsuta K., Mihara M., Momota S., Nagae D., Nishikiori R., Niwa T., Ohnishi T., Okumura K., Ogura T., Sakurai H., Sato K., Shimbara Y., Suzuki H., Takeda H., Takeuchi S., Tanaka K., Uenishi H., Winkler M., Yanagisawa Y., Watanabe S., Minomo K., Tagami S., Shimada M., Kimura M., Matsumoto T., Shimizu Y., and Yahiro M.: "Deformed halo nuclei observed thorough the reaction cross sections measurements for Ne and Mg isotopes to the vicinity of neutron-drip line", DREB2014 Direct Reactions with Exotic Beams, Darmstadt, Germany, Jun. (2014).

Murakami M., Goto S., Murayama H., Kojima T., Kaji D., Morimoto K., Haba H., Kudou Y., Sumita T., Sakai R., Yoneda A., Morita K., Kasamatsu Y., Kikunaga H., Sato T., and Kudo H.: "Excitation functions for production of rutherfordium isotopes in the ^{248}Cm $+^{18}$ O reaction", 17th Radiochemical Conferencec, Mariánské Lázně, Czech Republic, May (2014).

Murakami M., Haba H., Goto S., and Kudo H.: "Production cross sections of Nb and Ta isotopes in the (p, x) and (d, x) reactions on $^{\mathrm{nat}}$Zr and $^{\mathrm{nat}}$Hf", 17th Radiochemical Conferencec, Mariánské Lázně, Czech Republic, May (2014).

Kudo H., Goto S., and Murakami M. (Poster): "Gas phase chemistry of the volatile chloride compound of Hf isotopes", 17th Radiochemical Conferencec, Mariánské Lázně, Czech Republic, May (2014).

Murakami M.: "Cross section measurements of useful radiotracers for application studies at RIKEN", Seminar at International Atomic Energy Agency, (IAEA), Vienna, Austria, May (2014).

(Domestic Conference)

Goto J., Amaya Y., Hirayama S., Shiiya T., Shobugawa Y., Kawano Y., Izumukawa T., Uematsu K., Katsuragi Y., Takahashi T., Yoshida H., and Naito M. (Oral): "Development of a car-borne directional gamma-ray survey system", 日本原子力学会 2015 年春の年会, (日本原子力学会), 茨城大学 (日立キャンパス), 3 月 (2015).

Yoshida K. (Oral): "中性子ドリップ線近傍核における集団モード", 九大研究会「中性子過剰領域における弱束縛系の物理」, (九州大学), 九州大学 (福岡), 3 月 (2015).

Yoshida K. (Oral): "Proton-neutron pairing vibrations in $N = Z$ nuclei", 日本物理学会　第 70 回年次大会, (日本物理学会), 早稲田大学 (東京), 3 月 (2015).

Murakami M., Haba H., Huang M., Goto S., and Kudo H. (Oral): "$^{\mathrm{nat}}$Zr(d, x), $^{\mathrm{nat}}$Hf(d, x) 反応による Nb，Ta 同位体の励起関数測定", 第 58 回放射化学討論会, (日本放射化学会), 名古屋大学 (東山キャンパス), 9 月 (2014).

Sato D., Murakami M., Haba H., Kikunaga H., Ooe K., Goto S., and Kudo H. (Oral): "Aliquat 336 を用いた Nb，Ta のフッ化水素酸溶液からの溶媒抽出挙動", 第 58 回放射化学討論会, (日本放射化学会), 名古屋大学 (東山キャンパス), 9 月 (2014).

Tsuto S., Murakami M., Ooe K., Goto S., Sato D., Goto N., Nagaoka T., Haba H., Toyoshima A., Kudo H., Koyama T., Motoyama R., Komori Y., Kitayama Y., and Fukuda Y. (Oral): "Db の化学実験に向けた 5 族元素 Nb，Ta のオンライン逆相クロマトグラフィー", 第 58 回放射化学討論会, (日本放射化学会), 名古屋大学 (東山キャンパス), 9 月 (2014).

Tanaka A., Ooe K., Kikunaga H., Goto S., and Kudo H. (Poster): "104 番元素 Rf の同族元素 Zr、Hf のキレート配位子を用いた溶媒抽出挙動の研究", 第 58 回放射化学討論会, (日本放射化学会), 名古屋大学 (東山キャンパス), 9 月 (2014).

Goto N., Ooe K., Murakami M., Goto S., Tsukada K., Toyoshima A., Asai M., Sato T. K., Miyashita S., Kaneya Y., Kitayama Y., Haba H., Komori Y., and Kudo H. (Poster): "Sg の同族元素 Mo, W のシュウ酸水溶液からのイオン対抽出挙動", 第 58 回放射化学討論会, (日本放射化学会), 名古屋大学 (東山キャンパス), 9 月 (2014).

Asai T., Goto S., Ooe K., and Kudo H. (Poster): "$BiCl_3$ の等温ガスクロマトグラフィ挙動に関する研究", 第 58 回放射化学討論会, (日本放射化学会), 名古屋大学 (東山キャンパス), 9 月 (2014).

Murakami M., Haba H., Shibata S., and Kudo H. (Poster): "$^{\mathrm{nat}}$Hf(α, x) 反応の励起関数測定", 第 58 回放射化学討論会, (日本放射化学会), 名古屋大学 (東山キャンパス), 9 月 (2014).

Oshimi Y., Goto S., Ooe K., and Kudo H. (Poster): "Off-line 実験における Zr，Hf 塩化物の等温くガスクロマトグラフィ挙動", 第 58 回放射化学討論会, (日本放射化学会), 名古屋大学 (東山キャンパス), 9 月 (2014).

Tamura N., Nishio K., Hirose K., Nishinaka I., Makii H., Kimura A., Ota S., Andreyev A., Vermeulen M., Gilespire S., Bentley M., Nagayama T., Ooe K., Goto S., and Kudo H. (Poster): "マイナーアクチノイドの中性子誘起核反応断面積の測定法の開発", 第 58 回放射化学討論会, (日本放射化学会), 名古屋大学 (東山キャンパス), 9 月 (2014).

Radioactive nuclear beam group
IPNS (Institute for Particle and Nuclear Studies)
KEK (High Energy Accelerator Research Organization)

Publications

[Journal]

(Original Papers) *Subject to Peer Review

Hirayama Y., Mukai M., Watanabe Y.X., Imai N., Ishiyama H., Jeong S.C., Miyatake H., Oyaizu M., Matsuo Y., Sonoda T., Wada M., "Ionization cross section measurements for autoionizing states of iridium and rhenium", J. Phys. B: At. Mol. Opt. Phys. **47** (2014) 075201, *

Ishiyama H., Jeong S.C., Watanabe Y.X., Hirayama Y., Imai N., Hiroari M., Oyaizu M., Katayama I., Osa A., Otokawa Y., Matsuda M., Nishio K., Makii H., Sato T.K.., Kuwata N., Kawamura J., Nakao A., Ueno H., Kim Y.H., Kimura S., Mukai M., "Nanoscale diffusion tracing by radioactive ^{8}Li tracer", Jpn. J. Appl. Phys **53** (2014) 110303, *

Das S.K., Ishiyama H., Watanabe Y.X., Miyatake H., Hirayama Y., Jeong S.C., Yamaguchi K., "Energy resolution and gas gain of an active-target type Gas counter of GEM-MSTPC", J. Bangla. Aca. Sci. **37** (2014) 139-144, *

Ishiyama H., Jeong S.C., Watanabe Y.X., Hirayama Y., Imai N., Hiroari M., Oyaizu M., Katayama I., Osa A., Otokawa Y., Matsuda M., Nishio K., Makii H., Sato T.K.., Kuwata N., Kawamura J., Nakao A., Ueno H., Kim Y.H., Kimura S., Mukai M., "In situ lithium diffusion measurement in solid ionic conductors using short-lived radiotracer beam of ^{8}Li", Nucl. Instrum. Method B **XX** (2014) XXXXX, *

Mukai M., Hirayama Y., Jeong S.C., Imai N., Ishiyama H., Miyatake H., Oyaizu M., Watanabe Y.X., Kim Y.H., "In-gas-cell laser ion source for KEK isotope separation system", Rev. Sci. Instrum. **85** (2014) 02B906, *

[Book • Proceedings]

(Original Papers) *Subject to Peer Review

Hirayama Y., Jeong S.C., Watanabe Y.X., Imai N., Ishiyama H., Miyatake H., Oyaizu M., Kim Y.H., Mukai M., Sonoda T., Wada M., Huyse M., Kudryavtsev Yu., Van Duppen P., "Present Status of KEK Isotope Separation System", EPJ Web of Conference **66** (2014) 11017,*

Hirayama Y., Watanabe Y.X., Imai N., Ishiyama H., Jeong S.C., Miyatake H., Oyaizu M., Kim Y.H., Mukai M., Kimura S., "β-deacy spectroscopy of r-process nuclei with N = 126 at KISS", AIP Conf. Proc. **1594** (2014) 380-387,*

Kim Y.H., Watanabe Y.X., Hirayama Y., Imai N., Ishiyama H., Jeong S.C., Miyatake H., Oyaizu M., Kimura S., Mukai M., Choi S.H., Song J.S., Clement E., De France G., Navin A., Rejmund M., Schmitt C., Pollarolo G., Corradi L., Fioretto E., Montanari D., Niikura M., Suzuki D., Nishibata H., Takatsu J., "Study of multinucleon transfer reactions of ^{136}Xe + ^{198}Pt for production of exotic heavy nuclei", EPJ Web of Conference **66** (2014) 03044,*

Oral Presentations

(International Conference etc.)

Watanabe Y.X., Hirayama Y., Imai N., Ishiyama H., Jeong S.C., Miyatake H., Oyaizu M., Kimura S., Mukai M., Choi S.H., Kim Y.H., Song J.S., Clement E., De France G., Navin A., Rejmund M., Schmitt C., Pollarolo G., Corradi L., Fioretto E., Montanari D., Niikura M., Suzuki D., Nishibata H., Takatsu J., "Study of multinucleon transfer reactions of ^{136}Xe+^{198}Pt for production of exotic nuclei", VI International Conference FUSION14 February, 2014, New Delhi, India

VIII. LIST OF PREPRINTS

List of Preprints (April 2014 - March 2015)

RIKEN NC-NP

132	Quadrupole shape dynamics in view from a theory of large amplitude collective motion	M. Matsuo, N. Hinohara, K. Sato, K. Matsuyanagi, T. Nakatsukasa, K. Yoshida
133	Isospin-invariant Skyrme energy-density-functional approach with axial symmetry	J.A. Sheikh, N. Hinohara, J. Dobaczewski, T. Nakatsukasa, W. Nazarewicz, K. Sato
134	Systematic investigation of low-lying dipole modes using the canonical-basis time-dependent Haratree-Fock-Bogoliubov theory	S. Ebata, T. Nakatsukasa, T. Inakura
135	Mean-field analysis of ground state and low-lying electric dipole strength in 22C	T. Inakura, W. Horiuchi, Y. Suzuki, T. Nakatsukasa
136	Thermal pairing and giant dipole resonance in highly excited nuclei	N.D. Dang
137	Hidden pseudospin and spin symmetries and their origins in atomic nuclei	H. Liang, J. Meng et al.
138	Pairing effect in thermal shape fluctuation model on the width of giant dipole resonance	A.K. Rhine Kumar, P. Arumugam, N. Dinh Dang
139	Viscosity: From air to hot nuclei	N.D. Dang
140	Possible presence and properties of multi chiral pair-bands in odd-odd nuclei with the same intrinsic	I. Hamamoto
141	Oblate deformation of light neutron-rich even-even nuclei	I. Hamamoto
142	Pigmy resonance in monopole response of neutron-rich Ni isotopes ?	I. Hamamoto, H. Sagawa
143	Energy and mass-number dependence of hadron-nucleus total reaction cross sections	A. Kohama, K. Iida, K. Oyamatsu
144	Microscopic analysis of fusion hindrance in heavy systems	K. Washiyama
145	Repulsive aspects of pairing correlation in nuclear fusion reaction	S. Ebata, T. Nakatsukasa
146	Finite amplitude method in linear response TDDFT calculations	T. Nakatsukasa
147	Mean-field calculation based on proton-neutron mixed energy density functionals	K. Sato, J. Dobaczewski, T. Nakatsukasa, W. Satula
148	Multiple period states of the superfluid fermi gas in an optical lattice	S. Yoon, F. Dalfovo, T. Nakatsukasa, G. Watanabe
149	Hidden pseudospin and spin symmetries and their origins in atomic nuclei	H. Liang, J. Meng, S.G. Zhou
150	Three-dimensional mesh calculations for covariant density functional theory	Y. Tanimura, K. Hagino, H. Z. Liang

RIKEN NC- AC

	Not Applicable	

RIKEN MP

88	Entanglement Entropy of de Sitter Space α-Vacua	N. Iizuka, T. Noumi, N. Ogawa
89	Dynamical breaking of shift-symmetry and super-Planckian inflation	A. Mazumdar, T. Noumi, and M. Yamaguchi
90	Towards U(N|M) knot invariant from ABJM theory	B. Eynard, T. Kimura
91	Electric field quench in QdS/CFT	K. Hashimoto, S. Kinoshita, K. Murata, and T. Oka

92	Bulk Angular Momentum and Hall Viscosity in Chiral Superconductors	A. Shitade and T. Kimura
93	Turbulent Meson Condensation as Quark Deconfinement	K. Hashimoto, S. Kinoshita, K. Murata, and T. Oka
94	Duality and integrability of a supermatrix model with an external source	T. Kimura
95	Entropic destruction of heavy quarkonium in non-Abelian plasma from the holographic correspondence	K. Hashimoto, D.E. Kharzeev
96	Effective field theory for spacetime symmetry breaking	Y. Hidaka, T. Noumi, and G. Shiu
97	Is cosmological constant screened in Liouville gravity with matter?	T. Inami, Y. Koyama, Y. Nakayama, M. Suzuki
98	Meson turbulence at quark deconfinement from AdS/CFT	K. Hashimoto, S. Kinoshita, K. Murata, and T. Oka
99	Electromagnetic instability in holographic QCD	K. Hashimoto, A. Sonoda, T. Oka
100	Holographic heavy quark symmetry	K. Hashimoto, N. Ogawa, and Y. Yamaguchi
101	$h^0 ¥to c ¥bar{c}$ as a test case for quark flavor violation in the MSSM	A. Bartl, H. Eberl, E. Ginina, K. Hidaka, W. Majerotto
102	Higgs boson decay to charm pair at full one-loop level in the MSSM with flavour violation	H. Eberl, A. Bartl, E. Ginina, K. Hidaka, W. Majerotto
103	Ramond-Ramond Couplings of D-branes	K. Hashimoto, S. Sugishita, S. Terashima
104	Possibility of QCD ferromagnetism at high density	K. Hashimoto
105	Holographic Entanglement and Causal Shadow in Time-Dependent Janus Black Hole	Y. Nakaguchi, N. Ogawa, T. Ugajin
106	Conditionally valid uncertainty relations	K. Fujikawa
107	Quantum Discord, CHSH Inequality and Hidden Variables -- Critical reassessment of hidden-variables	K. Fujikawa
108	Aharonov-Bohm effect and geometric phases -- Exact and approximate topology	K. Fujikawa
109	Eigenvalues of the Breit equation	Y. Yoshio, H. Kasari
110	Linking loops in ABJM and refined theory	T. Kimura
111	Relativistic hydrodynamics from quantum field theory on the basis of the generalized Gibbs ensemble method	T. Hayata, Y. Hidaka, M. Hongo, T. Noumi

RIKEN QHP

146	Di-jet asymmetric momentum transported by QGP fluid	Y. Tachibana, T. Hirano
147	Sine-Square Deformation and its Relevance to String Theory	T. Tada
148	Renormalized O(N) model at next-to-leading order of the 1/N expansion: effects of the Landau pole	G. Fejos, A. Patkos, Zs. Szep
149	Entanglement Entropy of de Sitter Space α-Vacua	N. Iizuka, T. Noumi, N. Ogawa
150	Restricted phase-space approximation in real-time stochastic quantization	R. Anzaki, K. Fukushima, Y. Hidaka, and T. Oka
151	Production and Elliptic Flow of Dileptons and Photons in the semi-Quark Gluon Plasma	C. Gale, Y. Hidaka, S. Jeon, S. Lin, J.-F. Paquet, R.D. Pisarski, D. Satow, B. Schenke, V.V. Skokov, G. Vujanovic
152	Adjoint QCD on $R^3 ¥times S^1$ with twisted fermionic boundary conditions	T. Misumi, T. Kanazawa
153	Polarization of Direct Photons from Gluon Anisotropy in Ultrarelativistic Heavy Ion Collisions	G. Baym and T. Hatsuda,
154	Nonlinear electromagnetic response in quark-gluon plasma	D. Satow

155	Production of dileptons and photons in the semi-quark gluon plasma	Y. Hidaka, S. Lin, R.D. Pisarski, D. Satow
156	Real-time Feynman path integral with Picard--Lefschetz theory and its applications to quantum tunneling	Y. Tanizaki, T. Koike
157	Stressed Cooper pairing in dense QCD: effective Lagrangian and random matrix theory	T. Kanazawa, T. Wettig
158	QCD sum rules for magnetically induced mixing between ¥eta_c and J/¥psi	S. Cho, K. Hattori, S.H. Lee, K. Morita and S. Ozaki
159	Dispersion relations of Nambu-Goldstone modes at finite temperature and density	T. Hayata, Y. Hidaka
160	Inhomogeneous Polyakov loop induced by inhomogeneous chiral condensates	T. Hayata, A. Yamamoto
161	Fluctuation induced first order phase transition in U(n)xU(n) models using chiral invariant expansion of FRG	G. Fejos
162	Medium-Heavy Nuclei from Nucleon-Nucleon Interactions in Lattice QCD	T. Inoue, T. Hatsuda et al. (HAL QCD Collaboration)
163	Magnetic susceptibility of strongly interacting matter with $2+1$ quark flavors	K. Kamikado, T. Kanazawa
164	Many-body composite bosons from the viewpoint of functional renormalization	Y. Tanizaki
165	On the origin of the narrow peak and the isospin symmetry breaking of the X(3872)	S. Takeuchi, K. Shimizu, M. Takizawa
166	Lefschetz-thimble techniques for path integral of zero-dimensional O(n) sigma models	Y. Tanizaki
167	Renormalization of the 2PI-Hartree approximation in a broken phase with nonzero superflow	G. Fejos
168	Quasi-instantons in QCD with chiral symmetry restoration	T. Kanazawa, N. Yamamoto
169	Asymptotically free lattice gauge theory in five dimensions	T. Kanazawa, A. Yamamoto
170	Complex Langevin simulation of quantum vortex nucleation in the Bose-Einstein condensate	T. Hayata, A. Yamamoto
171	Effective field theory for spacetime symmetry breaking	Y. Hidaka, T. Noumi, G. Shiu
172	Charmonium Spectroscopy in Strong Magnetic Fields by QCD Sum Rules: (I) S-Wave Ground States	S. Cho, K. Hattori, S.H. Lee, K. Morita, and S. Ozaki
173	Coupled channel approach to strangeness S = -2 baryon-baryon interactions in Lattice QCD	K. Sasaki, S. Aoki, T. Doi, T. Hatsuda, Y. Ikeda, T. Inoue, N. Ishii, K. Murano, H. Nemura (HAL QCD Collaboration)
174	Structure of Lefschetz thimbles in simple fermionic systems	T. Kanazawa, Y. Tanizaki
175	Holographic heavy quark symmetry	K. Hashimoto, N. Ogawa, Y. Yamaguchi
176	Holographic Entanglement and Causal Shadow in Time-Dependent Janus Black Hole	Y. Nakaguchi, N. Ogawa, T. Ugajin
178	Tenth-Order Electron Anomalous Magnetic Moment: Contribution of Diagrams without Closed Lepton Loops	T. Aoyama, M. Hayakawa, T. Kinoshita, and M. Nio
179	Omega-Omega interaction from 2+1 flavor lattice QCD	M. Yamada, K. Sasaki, S. Aoki, T. Doi, T. Hatsuda, Y. Ikeda, T. Inoue, N. Ishii, K. Murano and H. Nemura (HAL QCD Collaboration)
180	Relativistic hydrodynamics from quantum field theory on the basis of the generalized Gibbs ensemble method	T. Hayata, Y. Hidaka, M. Hongo, T. Noumi
181	From quantum to classical dynamics: Dynamic crossover in the relativistic $O(N)$ model at finite	D. Mesterhazy, Y. Tanizaki
182	Jarzynski-type equalities in gambling: role of information in capital growth	Y. Hirono, Y. Hidaka
183	Evading the sign problem through Lefschetz-thimble path integral	Y. Tanizaki, H. Nishimura, K. Kashiwa
184	Accurate Determination of Reference Scales for Wilson Gauge Action from Yang{Mills Gradient Flow	M. Asakawa, T. Hatsuda, T. Iritani, E. Itou, M. Kitazawa, H. Suzuki
185	Phonons, Pions and Quasi-Long-Range Order in Spatially Modulated Chiral Condensates	Y. Hidaka, K. Kamikado, T. Kanazawa and T. Noumi
186	Infinite circumference limit of conformal field theory	N. Ishibashi, T. Tada

CNS-REP		
93	CNS Annual Report 2013	T. Gunji, S.Ota, Y. Kishi

Nishina Center Preprint server (not including Partner Institution) can be found at
http://nishina-preprints.riken.jp/

IX. LIST OF SYMPOSIA & WORKSHOPS

List of Symposia & Workshops (April 2014 - March 2015)

RNC

1	The Approach to Equilibrium in Strongly Interacting Matter http://www.bnl.gov/aesim2014/index.php	BNL	Apr. 2-4
2	4rd Joint ISIS/RIKEN Muon Facility Development Workshop（ISIS/UK）	RAL	Apr. 4
3	The 3rd EURICA workshop http://indico2.riken.jp/indico/conferenceDisplay.py?confId=1429	RIBF Conference Hall	Apr. 10
4	RIBF Discussion Plus! -Island of Inversion http://indico2.riken.jp/indico/conferenceDisplay.py?confId=1462	RIBF Conference Hall	Apr. 25
5	The 3rd International Workshop on “State of the Art in Nuclear Cluster Physics” (SOTANCP3) http://kguramo.kanto-gakuin.ac.jp/sotancp3/	KGU Kannai Media Center	May 26-30
6	ICNT workshop "Physics of exotic nuclei: Theoretical advances and challenges" http://indico2.riken.jp/indico/conferenceDisplay.py?confId=1450	RIKEN Main Research Bldg.	Jun. 9
7	PALIS strategy meeting 2014	RIBF Conference Hall	Jun. 9
8	One-day intensive workshop on “di-neutron and alpha-cluster correlations in exotic nuclei” http://indico2.riken.jp/indico/conferenceDisplay.py?confId=1565	RIBF Bldg. 203	Jul. 10
9	The 9th RIBF Discussion meeting on the spin-isospin excitations in neutron rich nuclei http://indico2.riken.jp/indico/conferenceDisplay.py?confId=1553	Okouchi Hall	Jul. 31
10	RIKEN BNL Research Center Workshop: Thermal Protons & Dilepton in Heavy-Ion Collisions http://www.bnl.gov/tpd2014/	BNL	Aug. 20-22
11	HET-RBRC Symposium: Creutz Fest 2014 -A Celebration of the Career and Accomplishments of Michael Creutz- http://www.bnl.gov/creutzfest/	BNL	Sep. 4-5
12	SAMURAI International Collaboration Workshop 2014 http://indico2.riken.jp/indico/conferenceDisplay.py?confId=1593	Tohoku U.	Sep. 8-9
13	BigRIPS analysis workshop http://indico2.riken.jp/indico/conferenceDisplay.py?confId=1562	RIBF Conference Hall	Sep. 11
14	The 3rd SUNFLOWER Workshop http://indico2.riken.jp/indico/conferenceDisplay.py?confId=1560	U. Tokyo	Sep. 15-16
15	The 10th RIBF discussion meeting on Cluster states probed by reaction experiments http://indico2.riken.jp/indico/conferenceDisplay.py?confId=1577	Kyoto U.	Sep. 25
16	Advances and perspectives in computational nuclear physics http://indico2.riken.jp/indico/conferenceDisplay.py?confId=1534	Hilton Waikoloa Village	Oct. 6
17	The 3rd Japan-Korea PHENIX Collaboration Meeting http://indico2.riken.jp/indico/conferenceDisplay.py?confId=1683	Okouchi Hall	Nov. 27-28
18	The 2nd RIBF Discussion Plus! -basic course of mean field theory http://indico2.riken.jp/indico/conferenceDisplay.py?confId=1722	Nishina Hall	Dec. 24
19	Workshop for development of beam line detectors with high rate capabilities http://indico2.riken.jp/indico/conferenceDisplay.py?confId=1745	RIBF Conference Hall	Jan. 19
21	Workshop on Multi-Hadron and Nonnlocal Matrix Elements in Lattice QCD https://indico.bnl.gov/conferenceDisplay.py?confId=934	BNL	Feb. 5-9
22	理研研究会『これからの弦理論 ～ 橋本研 closing 研究会 ～』 http://indico2.riken.jp/indico/conferenceDisplay.py?confId=1774	Okouchi Hall	Feb. 21-22

23	The 11th RIBF Discussion on Heavy-ion reaction and multi-nucleon transfer http://indico2.riken.jp/indico/conferenceDisplay.py?confId=1754	U. Tsukuba	Mar. 2

CNS

1	Advances in Radioactive Isotope Science (Jointly organized by the RIKEN Nishina Center and the CNS) https://ribf.riken.jp/ARIS2014/index.html	U. Tokyo	June 1-6
2	The first Sicily-East Asia Workshop for Low-energy Nuclear Physics https://agenda.infn.it/conferenceDisplay.py?confId=8300	Sicily, Italy	July 28 - 31
3	Progress in nuclear shell-model calculations in CNS-RIKEN collaboration http://indico.cns.s.u-tokyo.ac.jp/conferenceDisplay.py?confId=180	Nishina Hall, RIBF Conference Hall	Nov. 26-28
4	第一回放射線によるイメージングの展望 http://indico.cns.s.u-tokyo.ac.jp/conferenceDisplay.py?confId=195	U. Tokyo	Nov. 29
5	第二回放射線によるイメージングの展望 http://indico.cns.s.u-tokyo.ac.jp/conferenceDisplay.py?confId=204	U. Tokyo	Jan. 24

KEK

1	「宇宙核物理実験の現状と将来」研究会	RCNP	Aug. 7-8

X. LIST OF SEMINARS

List of Seminars (April 2014 - March 2015)

Nuclear Physics Monthly Colloquium

1	Yasuhiro Okada (KEK), Sachio Komamiya (U. Tokyo) & Kaoru Yokoya (KEK)	International Linear Collider: From Design to Reality http://indico2.riken.jp/indico/conferenceDisplay.py?confId=1651	Nov. 10
2	Koji Hashimoto (RNC)	Quark and superstring http://indico2.riken.jp/indico/conferenceDisplay.py?confId=1711	Dec. 26

RIBF Nuclear Physics Seminar

1	Takehito Hayakawa (JAEA)	Nuclear physics for nuclear security and nonproliferation http://indico2.riken.jp/indico/conferenceDisplay.py?confId=1488	Apr. 22
2	Newcomers to Nishina Center in 2014	New-Comers Seminar in 2014 http://indico2.riken.jp/indico/conferenceDisplay.py?confId=1504	May 14
3	Zhengyu Xu (RNC/U. Hong Kong)	β-Decay properties in the vicinity of 78Ni and their implications on nuclear shell structure far off the b-stability line http://indico2.riken.jp/indico/conferenceDisplay.py?confId=1505	May 30
4	Yuma Kikuchi (RNC)	Two-neutron correlations in the ground and excited states of 6He http://indico2.riken.jp/indico/conferenceDisplay.py?confId=1545	Jul. 8
5	Shinya Wanajo (RIKEN iTHES)	Origin of the r-process elements http://indico2.riken.jp/indico/conferenceDisplay.py?confId=1546	Jul. 15
6	Giuseppe Lorusso (RNC)	Beta-decay half-lives of N~82 nuclei on the r-process path http://indico2.riken.jp/indico/conferenceDisplay.py?confId=1618	Sep. 30
7	Aiko Takamine (Aoyama Gakuin U.)	Measurement of the hyperfine structure constant for laser-cooled Be-11 ions http://indico2.riken.jp/indico/conferenceDisplay.py?confId=1639	Oct. 28
8	Karl-Ludwig Kratz (U. Mainz)	One-day Workshop Program "Recent progress on r-process and nucleosynthesis" http://indico2.riken.jp/indico/conferenceDisplay.py?confId=1650	Nov. 25
9	Wataru Horiuchi (Hokkaido U.)	Correlated basis approach to nuclear five- and six-body problems http://indico2.riken.jp/indico/conferenceDisplay.py?confId=1688	Nov. 25
10	Jean-Michel Daugas (CEA) et al.	Workshop on "Progress in nuclear shell-model calculations in CNS-RIKEN collaboration" http://indico2.riken.jp/indico/conferenceDisplay.py?confId=1684	Nov. 26-28
11	Kathrin Wimmer (U. Tokyo/CNS/RIKEN)	CNS & Nuclear Physics Seminar : In-beam gamma-ray spectroscopy with GRETINA at the NSCL http://indico2.riken.jp/indico/conferenceDisplay.py?confId=1698	Dec. 1
12	Shuichiro Ebata (Hokkaido U.)	Developments of the Canonical-basis Time-dependent Hartree-Fock-Bogoliubov Theory http://indico2.riken.jp/indico/conferenceDisplay.py?confId=1729	Jan. 13
13	Nobuaki Imai (CNS)	Low-energy nuclear physics program at CNS 201 http://indico2.riken.jp/indico/conferenceDisplay.py?confId=1735	Jan. 20
14	Shinsho Oryu (Tokyo U. of Sci.)	A Possibility of the Long Range Nuclear Potential by the NNp Three Body Approach and the Pion-Deuteron Scattering Length http://indico2.riken.jp/indico/conferenceDisplay.py?confId=1769	Feb. 10
15	Yutaka Watanabe (KEK, IPNS)	Present status of KEK isotope separation system (KISS) http://indico2.riken.jp/indico/conferenceDisplay.py?confId=1747	Feb. 17
16	Makoto Ito (Kansai U.)	Studies of the reaction size with the method of the scattering radius http://indico2.riken.jp/indico/conferenceDisplay.py?confId=1748	Feb. 24
17	Nodoka Yamanaka (RIKEN iTHES)	Nuclear electric dipole moment of 3-body systems in the Gaussian expansion method http://indico2.riken.jp/indico/conferenceDisplay.py?confId=1770	Mar. 3

18	John L. Wood (Georgia Inst. of Tech.)	Coexistence in Nuclei http://indico2.riken.jp/indico/conferenceDisplay.py?confId=1777	Mar. 10
19	Takeyasu Ito (LANL)	Development of neutron electric dipole moment experiments at Los Alamos http://indico2.riken.jp/indico/conferenceDisplay.py?confId=1791	Mar. 13
20	Tatsushi Shima (RCNP)	GLOBAL - ultra-low background experiment on the Earth's surface http://indico2.riken.jp/indico/conferenceDisplay.py?confId=1782	Mar. 17
21	Wenlong Zhang (CAS)	ADANES: accelarator driven advance nuclear energy system http://indico2.riken.jp/indico/conferenceDisplay.py?confId=1813	Mar. 27
22	Lei Yang (IMP)	Development of high flux neutron source and ADANES http://indico2.riken.jp/indico/conferenceDisplay.py?confId=1814	Mar. 27

Lecture Series on Nuclear Physics

	not held in FY2014		

Special Seminar

	not held in FY2014		

Seminar by Each Laboratory

Theoretical Research Division

1	Daisuke Sato (RIKEN Low Temperature Physics Lab.)	Strangeness Nuclear Physics Seminar: 2 次元ヘリウム 3 の基底状態	Apr. 18
2	Shunji Matsuura (McGil U.)	Math Phys Seminar: Charged quantum entanglement	Apr. 21
3	Vojtech Krejcirik (RNC)	QHP Seminar: Model-independent form factor relations at large N_c	Apr. 21
4	Akihisa Kohama (RNC)	TNP Internal Seminar: Deformed nuclei in the black-sphere approximation http://indico2.riken.jp/indico/conferenceDisplay.py?confId=1496	Apr. 22
5	Noriaki Ogawa (RNC)	QHP Seminar: Applications of AdS/CFT Correspondence to Real Physics	Apr. 28
6	Xiang Liu (Lanzhou U.)	QHP Seminar: Interpretation of some exotic hadrons via the initial single chiral particle emission mechanism	May 12
7	Shinya Wanajo (RIKEN iTHES) & Yuto Teraki (RIKEN ABB Lab.)	ABB & TNP Joint Group Seminar: The r-process and nuclear physics http://indico2.riken.jp/indico/conferenceDisplay.py?confId=1503	May 19
8	Yuma Kikuchi (RNC)	ABB & TNP Joint Group Seminar: The r-process and nuclear physics	May 20
9	Kazuki Maeda (RNC)	QHP Seminar: Orthogonal polynomials and solutions to the discrete Toda lattice	May 26
10	Sho Ozaki (KEK)	QHP Seminar: QCD vacuum and hadron properties in strong magnetic fields	Jun. 2

11	Kazuya Mameda (U. Tokyo)	QHP Seminar: QCD theta-vacua from the chial limit to the quenched limit	Jun. 9
12	Daisuke Takahashi (RIKEN)	Math Phys Seminar: 南部ゴールドストーンモードの分類と数え上げ：ボゴリューボフ理論による定式化	Jun. 13
13	Takashi Nakatsukasa (RNC)	TNP Internal Seminar: Constraint or cranking?	Jun. 30
14	Yukinao Akamatsu (KMI)	QHP Seminar: Heavy quark master equations in the Lindblad form	Jun. 30
15	Takahiro Nishi (U. Tokyo)	QHP Seminar: Deeply bound-pionic atom and partial restoration of chiral symmetry in nucler medium	Jul. 10
16	Masahiro Nozaki (YITP)	Math Phys Seminar: Quantum Entanglement of Local Operators http://indico2.riken.jp/indico/conferenceDisplay.py?confId=1568	Jul. 11
17	Pablo Morales (U. Tokyo)	QHP Seminar: Spontaneous symmetry breaking and particle production in curved spaces	Jul. 14
18	Koukei Washiyama (RNC)	TNP Internal Seminar: Microscopic analysis of fusion hindrance in heavy systems http://indico2.riken.jp/indico/conferenceDisplay.py?confId=1570	Jul. 15
19	Pablo Soler Gomis (Hong Kong U. of Sci. & Tech.)	Math Phys Seminar: U(1) portals into hidden sectors http://indico2.riken.jp/indico/conferenceDisplay.py?confId=1574	Jul. 18
20	Toshiyuki Gogami (Kyoto U.)	Strangeness Nuclear Physics Seminar: Spectroscopic research of ¥Lambda hypernuclei with high quality electron beam at Jefferson Lab	Jul. 18
21	Yuma Kikuchi (RNC)	ABB & TNP Joint Group Seminar: Search for exotic n-n correlations in weakly-bound nuclei http://indico2.riken.jp/indico/conferenceDisplay.py?confId=1572	Jul. 28
22	Don Warren (North Carolina State U.)	ABB & TNP Joint Group Seminar: Cosmic-Ray Acceleration and Photon Production during the Afterglow Phase of Gamma-ray Bursts http://indico2.riken.jp/indico/conferenceDisplay.py?confId=1572	Jul. 28
23	Alexander Karpov (FLNR)	Nuclear Theory Seminar: Superheavy nuclei: Which regions of nuclear map are accessible in nearest future? http://indico2.riken.jp/indico/conferenceDisplay.py?confId=1573	Jul. 28
24	Takahiro Sasaki (U. Tokyo)	QHP Seminar: Studying the QCD phase diagram with PNJL type effective model	Jul. 28
25	Shin Nakamura (Chuo U.)	Strangeness Nuclear Physics Seminar: AdS/CFT 対応を用いた非平衡統計物理学への挑戦	Aug. 1
26	Pengwei Zhao (Kyoto U.)	Nuclear Theory Seminar: Novel Nuclear Structure from Covariant Density Functional http://indico2.riken.jp/indico/conferenceDisplay.py?confId=1606	Sep. 1
27	Masako Bando (Inst. Fundamental Sci., NPO Sci. Edu. Exchange: EINSTEIN)	放射線の生物影響の統一的考察：動物から植物まで http://indico2.riken.jp/indico/conferenceDisplay.py?confId=1614	Sep. 10
28	Di-Lun Yang (National Taiwan U.)	Math Phys Seminar: Electromagnetic-induced Effects in Strongly Coupled Plasmas http://indico2.riken.jp/indico/conferenceDisplay.py?confId=1620	Sep. 12
29	Daisuke Satow (RIKEN)	QHP Seminar: Nonlinear Electromagnetic Response in Quark-Gluon Plasma	Sep. 17
30	Sho Nagao (Tohoku U.)	Strangeness Nuclear Physics Seminar: Spectroscopy of electro-produced hypernuclei at Mainz Microtron http://indico2.riken.jp/indico/conferenceDisplay.py?confId=1626	Sep. 29
31	Yoshitomo Kamiya (RIKEN iTHES/CMT Lab.)	QHP Seminar: Magnetic Vortex Crystals in Frustrated Mott Insulator	Oct. 15
32	Tomoya Takiwaki (RIKEN ABB Lab.)	ABB-TNP Joing Lunch Time Seminar: Impact of electron capture rate and equation of state on the supernovae explosions http://indico2.riken.jp/indico/conferenceDisplay.py?confId=1640	Oct. 20

33	Hajime Togashi (RNC)	ABB-TNP Joing Lunch Time Seminar: Supernova equation of state with the cluster variational method http://indico2.riken.jp/indico/conferenceDisplay.py?confId=1640	Oct. 20
34	Koichiro Asahi (Tokyo Tech.)	Pioneer project seminar : Search for a Permanent Electric Dipole Moment in Diamagnetic Atom 129Xe http://indico2.riken.jp/indico/conferenceDisplay.py?confId=1645	Oct. 31
35	Guido Cossu (KEK)	QHP Seminar: Magnetic Vortex Crystals in Frustrated Mott Insulator	Nov. 4
36	Akira Shimizu (U. Tokyo)	Math Phys Seminar: Pure state quantum statistical mechanics http://indico2.riken.jp/indico/conferenceDisplay.py?confId=1676	Nov. 10
37	Alexander G. Magner (Inst. for Nuclear Research)	Nuclear Theory Seminar: Semiclassical approaches to the macroscopic and microscopic nuclear dynamics http://indico2.riken.jp/indico/conferenceDisplay.py?confId=1677	Nov. 14
38	Hyun-Chul Kim (Inha U.)	Strangeness Nuclear Physics Seminar: The charge and spin structure of the nucleon and the pion	Nov. 14
39	Seiji Terashima (YITP)	Math Phys Seminar: A Localization Computation in Confining Phase http://ribf.riken.jp/MP/Seminar_semina.html	Nov. 17
40	Sahin Kaya Ozdemir (Washington U., St. Louis)	QHP Seminar: Controlling light at the exceptional points with whispering gallery microresonators	Nov. 17
41	Nguyen Dinh Dang (RNC)	TNP Internal Seminar: Recent achievements in the study of highly excited nuclei: Thermal pairing and giant dipole resonance in not rotating nuclei http://indico2.riken.jp/indico/conferenceDisplay.py?confId=1692	Nov. 18
42	Gordon Baym (U. Illinois – Urbana Champaign)	QHP Seminar: The Superfluid Mass Density and the Landau Criterion for Superfluidity http://indico2.riken.jp/indico/conferenceDisplay.py?confId=1691	Nov. 20
43	Masaki Murata (Academy of Sci. of the Czech Republic)	Math Phys Seminar: 境界のある共形場理論による透過率	Nov. 28
44	Kantaro Ohmori (U. Tokyo)	Math Phys Seminar: Anomaly polynomial of general 6d SCFTs	Dec. 15
45	Yuji Tachikawa (U. Tokyo)	QHP Seminar: Magnetic discrete gauge field in the confining vacua and the supersymmetric index	Dec. 22
46	Hiromichi Nishimura (Bielefeld U.)	QHP Seminar: Complex saddle points in finite-density QCD	Dec. 22
47	Yu Maezawa (Bielefeld U.)	QHP Seminar: Thermal modification of in-medium mesons from screening properties on lattice	Dec. 22
48	Koichi Sato (RNC)	TNP Internal Seminar: Proton-neutron mixing calculation with isospin breaking term	Dec. 24
49	Kazunobu Maruyoshi (Imperial College London)	Math Phys Seminar: 4d N=1 SCFTs from M5-branes	Jan. 16
50	Masafumi Fukuma (Kyoto U.)	QHP Seminar: Entropic formulation of (relativistic) continuum mechanics and a causal completion of relativistic fluid mechanics	Jan. 19
51	Akinori Tanaka (Osaka U.)	Math Phys Seminar: RP2 超共形指数とミラー対称性	Jan. 26
52	Shu Lin (RBRC)	QHP Seminar: Axial charge dynamics in quark gluon plasma	Feb. 5
53	Annop Wongwathanarat (RIKEN ABB Lab.)	ABB-TNP Joint Lunch Time Seminar: Supernova 1987A: neutrino-driven explosions in three dimensions and light curves http://indico2.riken.jp/indico/conferenceDisplay.py?confId=1768	Feb. 9
54	Tohru Motobayashi (RNC)	ABB-TNP Joint Lunch Time Seminar: First access to the r-process path http://indico2.riken.jp/indico/conferenceDisplay.py?confId=1768	Feb. 9

55	Osamu Morimatsu (KEK)	QHP Seminar: Dynamic Critical Exponent from One and Two-Particle Irreducible 1/N Expansion of Effective and Microscopic Theories	Feb. 9
56	Sanjin Benić (U. Tokyo)	QHP Seminar: An effective model for the QCD phase transitions at finite baryon density	Mar. 2
57	Hironori Hoshino (Nagoya U.)	Math Phys Seminar: ホログラフィーによる非平衡密度物質の有限温度の解析	Mar. 9
58	Koji Hashimoto (RNC)	The Associate Chief Scientist Final Report http://indico2.riken.jp/indico/conferenceDisplay.py?confId=1794	Mar. 10
59	Luca Delacretaz (Stanford U.)	Math Phys Seminar: Wess-Zumino terms in theories with spontaneously broken space-time symmetries	Mar. 26
60	Hiroshi Isono (National Tsing Hua U.)	Math Phys Seminar: Note on the self-duality of gauge fields in topologically nontrivial spacetime	Mar. 30

Sub Nuclear System Research Division

1	Kaustubh Agashe (U. Maryland)	Joint HET/YITP/RIKEN Seminar: Using energy-peaks to measure particle (new and old) masses	Apr. 9
2	Adam Ritz (U. Victoria)	High-Energy Physics & RIKEN Theory Seminar: Light dark matter and neutrino beams	Apr. 16
3	Adam Bzdak (RBRC)	RIKEN/BNL Lunch Time Talk	Apr. 17
4	Hong Liu (MIT)	Nuclear Physics & RIKEN Theory Seminar: Renormalized entanglement entropy and RG flows	Apr. 18
5	Michael Endres (MIT)	High-Energy Physics & RIKEN Theory Seminar: Signal/noise enhancement strategies for stochastically estimated correlation functions	Apr. 23
6	Roy Lacey (Stony Brook U.)	RIKEN/BNL Lunch Time Talk	Apr. 24
7	Thomas Mehen (Duke U.)	Nuclear Physics & RIKEN Theory Seminar: Fragmentation Functions and Fragmenting Jet Functions in Quarkonium Production	Apr. 25
8	Daniel Litim (U. Sussex)	Nuclear Physics & RIKEN Theory Seminar: Aspects of functional renormalization	May 2
9	Toru Kojo (U. Illinois – Urbana-Champaign)	Nuclear Physics & RIKEN Theory Seminar: The quark mass gap in strong magnetic fields	May 9
10	Shu Lin (RBRC)	RIKEN/BNL Lunch Time Talk: On the axial charge dynamics at strong coupling	May 15
11	J.D. Vergados (U. Ioannina)	High-Energy Physics & RIKEN Theory Seminar: Relic Neutrinos in Cosmology-The prospects of detecting relic antineutrinos by capturing them in nuclei	May 28
12	Martin Hentschinski (BNL)	RIKEN/BNL Lunch Time Talk	May 29
13	Takumi Doi (RNC) et al.	第 2 回 高エネルギーQCD・核子構造 勉強会 http://indico2.riken.jp/indico/conferenceDisplay.py?confId=1515	May 30
14	Naoto Tanji (RIKEN/BNL)	RIKEN/BNL Lunch Time Talk: Real-time lattice simulations of fermion fields and Quark production in heavy-ion collisions	Jun. 5
15	Ron Longacre (BNL)	Nuclear Physics & RIKEN Theory Seminar: Flow or Flux Tubes or both	Jun. 6

16	Masanori Hanada (YITP)	Nuclear Physics & RIKEN Theory Seminar: Why does black hole describe deconfinement phase?	Jun. 13
17	Thomas Hambye (UCL, Brussel)	High-Energy Physics & RIKEN Theory Seminar: On the possibilities of probing a hidden sector dark matter particle	Jun. 18
18	Sean Bartz (U. Minnesota)	Nuclear Physics & RIKEN Theory Seminar: A Dynamical Three-Field AdS/QCD Model	Jun. 23
19	Masakiyo Kitazawa (Osaka U.)	Nuclear Physics & RIKEN Theory Seminar	Jun. 30
20	Philipp Scior (TU Darmstadt)	RIKEN/BNL Lunch Time Talk: Effective Theories with heavy quarks on the lattice	Jul. 3
21	Ahmed Ismail (ANL & UIC)	High-Energy Physics & RIKEN Theory Seminar: When is a top quark a parton?	Jul. 9
22	Juchien Xu (Columbia U.)	Nuclear Physics & RIKEN Theory Seminar	Jul. 11
23	Yuki Yokokura (Kyoto U.)	素核宇宙融合レクチャーシリーズ第 12 回: ブラックホールの蒸発と情報問題	Jul. 15-16
24	Al Mueller (Columbia U.)	Nuclear Physics & RIKEN Theory Seminar: Fluctuations and geometric scaling in statistical and particle physics	Jul. 18
25	Tigran Kalaydzhyan (Stony Brook U.)	Nuclear Physics & RIKEN Theory Seminar: Interaction of QCD strings and collective phenomena	Jul. 25
26	Masashi Hayakawa (Nagoya U.)	Nuclear Physics & RIKEN Theory Seminar: Upgrade of QED contribution to lepton $g-2$	Aug. 1
27	Terukazu Ichihara (Kyoto U.)	RIKEN/BNL Lunch Time Talk: QCD phase diagram with both fluctuation and finite coupling effects in the strong coupling lattice QCD	Aug. 7
28	Adrian Dumitru (Baruch College)	Nuclear Physics & RIKEN Theory Seminar	Aug. 8
29	Tom Blum (Univ of Connecticut)	High-Energy Physics & RIKEN Theory Seminar: Nucleon Electric Dipole Moments	Aug. 8
30	Koichi Hattori (RIKEN/RBRC)	RIKEN/BNL Lunch Time Talk: Photon propagations and charmonium spectroscopy in strong magnetic fields	Aug. 14
31	Gabriel Denicol (McGill U.)	Nuclear Physics & RIKEN Theory Seminar	Aug. 15
32	Ralf Seidl, Yasuyuki Akiba (RNC) et al.	第 3 回 高エネルギーQCD・核子構造 勉強会 http://indico2.riken.jp/indico/conferenceDisplay.py?confId=1563	
33	Shoichiro Tsutsui (Kyoto U.)	RIKEN/BNL Lunch Time Talk: Parametric instabilities of color magnetic field	Aug. 28
34	Qun Wang	Nuclear Physics & RIKEN Theory Seminar	Aug. 29
35	Chris Korthals Altes (NIKHEF & Centre Physique Theorique au CNRS)	RIKEN/BNL Lunch Time Talk: What causes the instability of the Stefan-Boltzmann plasma?	Sep. 11
36	Bjoern Schenke	Nuclear Physics & RIKEN Theory Seminar	Sep. 12
37	Zhen Liu (U. Pittsburgh)	High-Energy Physics & RIKEN Theory Seminar: Neutralino Dark Matter in the (N)MSSM: Direct/Indirect Detection and Collider Searches	Sep. 17
38	Matthew Buckley (Rutgers, The State U. New Jersey)	High-Energy Physics & RIKEN Theory Seminar: Searching for new scalars and dark matter at the LHC	Sep. 24

39	Stefan Meinel (U. Arizona/RBRC)	RIKEN/BNL Lunch Time Talk: Heavy baryons in lattice QCD	Oct. 2
40	Ayres Freitas (U. Pittsburgh)	High-Energy Physics & RIKEN Theory Seminar: Opening the loops: The muon g-2 at the LHC	Oct. 8
41	Steffen Bass	RHIC & Users' Group Open Forum Meeting	Oct. 9
42	Isao Watanabe, Noraina Adam, Siadah Sakinah, Edi Suprayoga (RNC)	DFT 法によるミュオン位置計算セミナー	Oct. 16
43	Piotr Korcyl (Columbia U.)	RIKEN/BNL Lunch Time Talk: A non-perturbative renormalization scheme in position space: A non-perturbative renormalization scheme in position space	Oct. 16
44	Ho-Ung Yee (U. Illinois – Chicago)	Nuclear Physics & RIKEN Theory Seminar: Aspects of Chiral Magnetic and Vortical Effects at Weak Coupling	Oct. 17
45	Majed Jawad (RNC)	Advanced Meson Science Lab. seminar	Oct. 23
46	David Mesterhazy (U. Illinois – Chicago)	Nuclear Physics & RIKEN Theory Seminar: Dynamics of the chiral phase transition – Universal fluctuations near criticality –	Oct. 24
47	Eugene Levin (Tel Aviv U. & UTFSM)	RIKEN/BNL Lunch Time Talk: Large b behaviour and CGC/saturation approach: the BFKL equation with massive gluon	Oct. 30
48	Yuji Hirono (Stony Brook U.)	Nuclear Physics & RIKEN Theory Seminar: Charge-dependent correlations from event-by-event anomalous hydrodynamics	Oct. 31
49	Itaru Nakagawa (RNC) et al.	第 4 回 高エネルギーQCD・核子構造 勉強会 http://indico2.riken.jp/indico/conferenceDisplay.py?confId=1653	Nov. 1
50	Simone Marzani (MIT)	High-Energy Physics & RIKEN Theory Seminar: The Higgs Cross Section from Analyticity	Nov. 5
51	Alfonso Sastre (Bergische U. Wuppertal)	Joint Riken Lunch/Nuclear Theory/RIKEN Seminar: Some results on Lattice QCD at the physical point: SU(2) chiral perturbation theory and some words about hadron vacuum polarization	Nov. 6
52	Yuta Kikuchi (Kyoto U.)	Nuclear Physics & RIKEN Theory Seminar: Derivation of the Hydrodynamic Equation from the Quantum Transport Equation	Nov. 7
53	Zackaria Chacko (Maryland)	Joint HET/YITP/RIKEN Seminar: Colorless Top Partners, a 125 GeV Higgs and the Limits on Naturalness	Nov. 12
54	Kirill Boguslavski (U. Heidelberg)	RIKEN/BNL Lunch Time Talk	Nov. 13
55	Ismail Zahed (Stony Brook U.)	Nuclear Physics & RIKEN Theory Seminar: Holographic Strings in ep, pp and pA	Nov. 14
56	Kim Maltman (York U.)	High-Energy Physics & RIKEN Theory Seminar: A Hybrid Strategy for the Lattice Evaluation of the LO HVP Contribution to the Muon Anomalous Magnetic Moment	Nov. 19
57	Jacquelyn Noronha-Hostler (Columbia U.)	RIKEN/BNL Lunch Time Talk: Bulk viscosity-driven suppression of shear viscosity effects on the flow harmonics at RHIC	Nov. 20
58	Anna Stasto (Penn State U.)	Nuclear Physics & RIKEN Theory Seminar: Scattering amplitudes and recursion relations in light-front perturbation theory	Nov. 21
59	Nils Strodthoff (Heidelberg U.)	RIKEN/BNL Lunch Time Talk: Exploring the phase structure and the dynamics of QCD	Dec. 4
60	Yachao Qian (Stonybrook U.)	Nuclear Physics & RIKEN Theory Seminar: Spin Asymmetries and P-odd effects through QCD instantons	Dec. 5
61	Sanjay Reddy (U. Washington)	High-Energy Physics & RIKEN Theory Seminar: The transport properties of cold dense matter	Dec. 10

62	Yuki Okura (BNL)	RIKEN/BNL Lunch Time Talk: LSST sensor effect in constraining the cosmological parameter	Dec. 11
63	Sean Fleming (U. Arizona)	Nuclear Physics & RIKEN Theory Seminar: Forward scattering in SCET: Glauber exchange and the BFKL equation	Dec. 12
64	Isao Watanabe, Noraina Adam、Siadah Sakinah、Edi Suprayoga、Sungwan Yoon	RIKEN Seminar: USM-Sophia-Riken International Workshop on Frontiers of Muon Physics Program	Dec. 15-16
65	Toh Pek Lan (U. Sains Malaysia)	Indonesia/Malaysia Seminar: Penyiasatan Teori Fungsi Ketumpatan untuk Struktur Elektronik dan Interaksi Hiperhalus bagi Muonium dalam Terbitan Imidazole	Dec. 17
66	Peter Lepage (Cornell)	High-Energy Physics & RIKEN Theory Seminar: High-Precision QCD Parameters from Lattice QCD	Dec. 17
67	Satri Zulkarnaen Bisri (CEMS)	Indonesia/Malaysia Seminar: Electronic Transport in Nanomaterials	Dec. 18
68	Hans-Peter Schadler (U. Graz)	RIKEN/BNL Lunch Time Talk: Generalized quark number susceptibilities at finite chemical potential from fugacity expansion on the lattice	Dec. 18
69	Toru Kojo (U. Illinois – Urbana-Champaign)	Nuclear Physics & RIKEN Theory Seminar: Phenomenological QCD equation of state for massive neutron stars	Dec. 19
70	Arun Madhav thalapilili (Rutgers)	High-Energy Physics & RIKEN Theory Seminar: The Higgs as a Probe for New Physics : Higgs Portals, Soft Yukawas and Extended Gauge Mediation	Jan. 7
71	Vladimir Skokov (Western Michigan U.)	Nuclear Physics & RIKEN Theory Seminar: Anisotropy of the semi-classical gluon field of a large nucleus at high energy	Jan. 9
72	Yue Zhang (Caltech)	High-Energy Physics & RIKEN Theory Seminar: Exploring Dark Matter and Baryon Asymmetry: Higgs is the Key	Jan. 14
73	Sayantan Sharma (BNL)	RIKEN/BNL Lunch Time Talk: The origin of axial anomaly and the high temperature phase of QCD	Jan. 15
74	Mauricio Martinez Guerrero (Ohio State U.)	Nuclear Physics & RIKEN Theory Seminar: A new exact solution to the Boltzmann equation and its hydrodynamical limit	Jan. 16
75	Julia Angel (Saitama U.)	Indonesia/Malaysia Seminar: Crystal Growth and Magnetism of Layered Antiferromagnet Deuterated κ -(BEDT-TTF)2Cu[N(CN)2]Br	Jan. 23
76	Wilke van der Schee (MIT)	Nuclear Physics & RIKEN Theory Seminar: Strong coupling QGP thermalization with longitudinal dynamics	Jan. 23
77	Grigory Ovanesyan (U. Massachusetts Amherst)	Nuclear Physics & RIKEN Theory Seminar: Regge behavior in effective field theory	Jan. 30
78	Antonin Portelli (U. Southampton)	High-Energy Physics & RIKEN Theory Seminar: Ab initio calculation of the neutron-proton mass difference	Feb. 4
79	Vincenzo Cirigliano (Los Alamos)	High-Energy Physics & RIKEN Theory Seminar: Electric Dipole Moments, New Physics, and (lattice) QCD	Feb. 11
80	Tigran Kalaydzhyan (Stony Brook U.)	Nuclear Physics & RIKEN Theory Seminar: Gravity waves generated by sounds from cosmological phase transitions	Feb. 13
81	Mariengela Lisanti (Princeton)	High-Energy Physics & RIKEN Theory Seminar: The Search for Relic Neutrinos	Feb. 25
82	Marlene Nahrgang	Theory and Modeling for the beam energy scan: From Exploration to Discovery	Feb. 26-27
83	Samuel MacDermott	High-Energy Physics & RIKEN Theory Seminar: The Galactic Center Gamma-ray Excess: Have We Started to See Dark Matter?	Mar. 4

84	Constantin Loizides	Collectivity in small colliding systems with high multiplicity	Mar. 4-6
85	Jorge Noronha (Sao Paulo U.)	Nuclear Physics & RIKEN Theory Seminar: Hydrodynamic transport coefficients for the non-conformal quark-gluon plasma from holography	Mar. 13
86	Luca Vecchi (U. Maryland)	HET/RIKEN Seminar: Spontaneous CP violation and the strong CP problem	Mar. 18
87	Antonio Ortiz Velasquez (National Autonomous U. Mexico)	Nuclear Physics & RIKEN Theory Seminar: Flow like behavior in small systems -- Multi-parton interactions and color reconnection effects at LHC energies	Mar. 20
88	Can Kilic (U. Texas – Austin)	HET/RIKEN Seminar: Flavored Dark Matter with Weak Scale Mediators	Mar. 25

RIBF Research Division

1	Hermann Wollnik (Giessen)	A mass spectrometer for the ROSETTA space-mission to a comet http://indico2.riken.jp/indico/conferenceDisplay.py?confId=1479	Apr. 9
2	Toshiro Shigaki (Papua New Guinea National Agricultural Research Inst.)	パプアニューギニアおよびソロモン諸島におけるサツマイモ並びにアイビカ（トロロアオイ）の遺伝資源管理と品種改良	May 14
3	Hirofumi Noda (RNC)	High Energy Astrophysics Lab. Seminar: X-ray studies of Central Engine in Active Galactic Nuclei http://indico2.riken.jp/indico/conferenceDisplay.py?confId=1525	Jun. 5
4	Claudio Ricci (Kyoto U.)	High Energy Astrophysics Lab. Seminar: X-ray reflection features as a probe of the structure and evolution of circumnuclear material in Active Galactic Nuclei http://indico2.riken.jp/indico/conferenceDisplay.py?confId=1554	Jul. 4
5	Takayuki Yuasa (RNC)	High Energy Astrophysics Lab. Seminar: White dwarf mass estimation method based on X-ray spectral modeling http://indico2.riken.jp/indico/conferenceDisplay.py?confId=1569	Jul. 17
6	Ken Takayama (KEK)	RIBF Accelerator Seminar: Induction microtron and its application http://indico2.riken.jp/indico/conferenceDisplay.py?confId=1580	Jul. 31
7	Renata S. Cumbee (U. Georgia)	Charge Exchange in the Cygnus Loop? http://indico2.riken.jp/indico/conferenceDisplay.py?confId=1586	Aug. 8
8	Hiroyoshi Sakurai & Tomohiro Uesaka (RNC)	Lectures for theory researchers: Current status and future of RIBF experiments (I) http://indico2.riken.jp/indico/conferenceDisplay.py?confId=1600	Aug. 18
9	Yoichi Nagashima (Copenhagen U.) & Hiroshi Ezawa (Gakushuin U.)	Bohr's 8mm film in 1937 http://indico2.riken.jp/indico/conferenceDisplay.py?confId=1643	Oct. 24
10	Yukari Matsuo (Hosei U.)	Nuclear Spectroscopy Laboratory Seminar: 超流動ヘリウム中原子の精密レーザー分光 -OROCHI- http://indico2.riken.jp/indico/conferenceDisplay.py?confId=1657	Oct. 31
11	Tomoko Abe (RNC)	戦略的オミクス育種技術体系の構築	Nov. 21
12	Benoit Gall (Strasbourg U)	How did Earth generate and operate more than 15 Natural Nuclear Reactors? http://indico2.riken.jp/indico/conferenceDisplay.py?confId=1695	Dec. 15
13	Chris Done (Durham U.)	High Energy Astrophysics Lab. Seminar: The disc-spin-jet connection in stellar and supermassive black holes http://indico2.riken.jp/indico/conferenceDisplay.py?confId=1766	Feb. 24
14	Yoshio Kobayashi (U. Electro-Communications)	Nuclear Spectroscopy Laboratory Seminar: 短寿命不安定核を用いたインビーム・メスバウアー分光法の物質科学への応用 http://indico2.riken.jp/indico/conferenceDisplay.py?confId=1797	Mar. 11
15	Shinsuke Fujioka (Osaka U.)	High Energy Astrophysics Laboratory Seminar: Application of laser-generated strong magnetic field to plasma physics research http://indico2.riken.jp/indico/conferenceDisplay.py?confId=1796	Mar. 12
16	Hideki Ueno (RNC)	Lectures for theory researchers: Current status and future of RIBF experiments (II) http://indico2.riken.jp/indico/conferenceDisplay.py?confId=1795	Mar. 20

CNS

1	Kathrin Wimmer (U. Tokyo/CNS)	In-beam gamma-ray spectroscopy with GRETINA at the NSCL	Dec. 1
2	Javier Menendez (U. Tokyo)	From nuclear structure to neutrinos and dark matter	Dec.16
3	Tetsuya Sakurai (U. Tsukuba)	A Scalable Parallel Eigensolver for Large-scale Simulations on Petascale Computing Environment	Jan. 19

Niigata Univ.

1	Yuma Kikuchi (RNC)	Two-neutron correlations in the ground and excited states of 6He	Sep. 18
2	A. G. Magner (Institute for Nuclear Research, Kyiv)	Semiclassical shell-structure moment of inertia within the phase-space approach	Nov. 11
3	Yoshihumi Shimizu (Kyushu U.)	角運動量射影法によるエキゾチックな変形・回転状態の研究	Nov. 27
4	Takayuki Yamaguchi (Saitama U.)	重イオンビーム荷電変化反応による不安定核の陽子分布半径	Jan. 22

AUTHOR INDEX

J

K

L

M

国立研究開発法人理化学研究所
埼玉県　和光市　広沢
RIKEN　2015-047